PROCEEDINGS OF THE

Xth COLLOQUIUM SPECTROSCOPICUM INTERNATIONALE

Edited by

ELLIS R. LIPPINCOTT,
University of Maryland

and

MARVIN MARGOSHES,
National Bureau of Standards

SPARTAN BOOKS
6411 CHILLUM PLACE, N W • WASHINGTON 12, D. C.

IIA Lib.,

Library of Congress Catalog Card No. 57-14964

Copyright © 1963 by Spartan Books

Printed in the United States of America
All rights reserved

This book or parts thereof, may not be reproduced in any
form without permission of the publishers.

TABLE OF CONTENTS

Page

The Role of Spectroscopy in Astrophysics 1
Jesse L. Greenstein

Present Status of Our Knowledge of Atomic Transition Probabilities 37
W. L. Wiese

Recent Developments in Infrared Atomic Emission Spectroscopy in the 1- to 4-Micron Region 57
Curtis J. Humphreys

Isotopic Shifts in the Spectra of Dysprosium and Samarium 73
A. R. Striganov

Absorption Spectra of Gaseous Atoms formed at Flash-Heated Tungsten Surfaces 83
L. S. Nelson and N. A. Kuebler

Critical Review of Methods and Results of Time-Resolved Spectroscopy 91
K. Laqua and W. -D. Hagenah

Atomic Absorption Spectroscopy 127
A. Walsh

Excitation and Related Phenomena in Flames 143
C. Th. J. Alkemade

Chemiluminiscent Flame Spectrophotometry 171
Paul T. Gilbert, Jr.

Extreme Ultraviolet Spectroscopy 217
B. Vodar

A Pulsed Light Source for the Extreme Ultraviolet . . . 247
W. R. Hunter

Sur Quelques Methodes de Spectrometrie X 263
J. Philibert

X-Ray Emission Spectra and Chemical Bond 307
A. Faessler

Spectroscopie X D'elements Radioactifs 321
Y. Cauchois

X-Ray Emission Spectrography at Long Wavelenghts . . 341
P. D. Zemany

Scanning Techniques in Electron Probe Microanalysis, with some Applications in Mineralogy and Biology . . 357
V. E. Cosslett

Page

Quantitative Electron Microprobe Analysis of Radioactive and Irradiated Materials 383
R. Theisen and J. P. Lecoq

High Precision Microprobe Analysis by Thin Metallic Film Calibration 391
R. Theisen and J. Lemaître

Spectroscopic Studies with the Ruby Optical Maser . . . 399
D. P. Stoicheff

The Ruby Optical Maser as a Raman Source 417
S. P. S. Porto

The Emission Mode Patterns of Ruby Lasers 421
E. S. Dayhoff

Recent Developments in Infrared Reflection Spectroscopy Attenuated Total Reflection 437
J. Fahrenfort

Comparative Studies of Infrared and Raman Group Frequencies and Their Applications 461
R. N. Jones, P. J. Krueger, K. Noack, J. J. Elliott, R. A. Ripley, G. A. A. Nonnenmacher and J. B. DiGiorgio

The Origins of Group Frequency Shifts. Part II The Influence of Inductive Effects and of Non-Bonded Interactions on Infrared Group Frequencies 487
L. J. Bellamy

Substituent Effects on the Infrared and Electronic Absorption Spectra of Organic Molecules 505
C. N. R. Rao, R. Venkataraghavan, K. R. Bhaskar and A. Balasubramanian

The Donor Characteristics of the Carbonyl Group III. BF_3 Complexes 539
Denys Cook

Some High Resolution Studies in the Infrared 549
J. H. Jaffe

Infra-red Dispersion Studies 563
W. H. Prichard and W. J. Orville-Thomas

Infra-red Solvent Shifts and Molecular Interactions . . . 569
H. E. Hallam and T. C. Ray

Recording the Infra-red Spectra of Gas-Chromatography Fractions 577
A. R. Philpotts

Optical Spectra of Gaseous Free Radicals 583
D. A. Ramsay

Features and Regularities in Research of Diatomic Molecular Spectra 597
Rafael Grinfeld

Page

The Methodology of the Measurement and Representation of Fluorescence Spectra 605
Giorgio Nebbia
Total Luminescence of Organic Molecules of Petrochemical Interest 631
S. P. McGlynn, B. T. Neely, and W. C. Neely
Chemical Applications of Nuclear Magnetic Resonance 647
R. E. Richards
Recent Applications of High Resolution Nuclear Magnetic Resonance to Chemical Problems 657
J. N. Shoolery
Spin Density Distributions in Conjugated Molecules by NMR Contact Shifts 665
D. R. Eaton, W. D. Phillips, R. E. Benson and A. D. Josey
Unsteady Modes of the Spin Generator 677
K. V. Vladimirsky and B. A. Labzov
The Application of Electron Magnetic Resonance Techniques to the Study of the Phosphorescence of Organic Molecules 681
Clyde A. Hutchison, Jr.
High Resolution Electron Spin Resonance 707
K. H. Hausser
Electron Spin Resonance in Oriented Radicals 719
D. H. Whiffen
Low Frequency to Near Microwave Spectrum Spectroscopy 729
Herbert A. Elion and Louis Shapiro
Correlation of Mass Spectra with Molecular Structure 743
J. H. Beynon
Vacuum Spark Mass Spectrographic Analysis of Solids and Liquids 769
A. J. Ahearn
The Teaching of Spectroscopy 791
A. C. Menzies

Foreword

The Xth Colloquium Spectroscopicum Internationale is the first of the Colloquium series to be held in the western hemisphere. For a considerable number of years spectroscopists in the United States had observed with interest the stimulating and informative spectroscopic Colloquia in Europe and actions were begun to have the United States serve as a host for one of the Colloquia. Following the organization of the national Society for Applied Spectroscopy in 1958, the possibility existed for formal invitation to the Colloquium by a representative body in the U. S. A. With the selection of Washington and the year 1962 for the first National Meeting of SAS, both an appropriate location and time were available for the Society to act as host to the Colloquium. Accordingly an invitation was presented at the IXth Colloquium in Lyon in June, 1961 to hold the next Colloquium in the U. S. A. in 1962. The invitation was accepted by the Colloquium group with the informal expression that the even numbered years might be reserved for infrequent meetings of the Colloquium held outside of Europe. This international conference also was sponsored by the University of Maryland, Department of Chemistry, and by the International Union of Pure and Applied Chemistry, through action initiated by its Commission on Spectrochemical and Other Optical Procedures of Analysis.

The Xth Colloquium was held June 18-22, 1962 at the University of Maryland, College Park, Maryland, U. S. A. More than 170 papers, including 24 invited papers, were presented in 27 sessions during the five days. The registration totaled 944, consisting of 807 full participants, 80 associate, and 57 single session registrants, representing 29 countries. In the plan followed for the program, invited lectures were arranged to be given in the morning and early afternoons to present general surveys of research on currently important themes in basic and applied spectroscopy. These lectures were followed by contributed research papers related to the same themes. The general program of papers with abstracts appeared in Applied Spectroscopy, Vol. 16, No. 2, 1962; abstracts of post-deadline papers will be found in the same journal, Vol. 16, No. 5, 1962.

The question of publication of the Proceedings of the Colloquium received considerable attention in the planning stages. While publication of all papers has much appeal, past experience has shown that considerable delays are encountered in publication of the full program, resulting from the large volume of material and difficulties in collecting the manuscripts. Furthermore, it was the opinion of some advisors that papers dealing with original research should be subject to the usual editorial review and published in the existing journals.

For this Colloquium a compromise was adopted in which the invited papers providing broad surveys of important research in spectroscopy and other selected papers of a general nature were scheduled to be published in the Proceedings, and authors of more specialized research papers were referred to the spectroscopic journals. This plan has the advantage of providing a well-knit assembly of authoritative surveys of current spectroscopic research with a minimum time required for publication. The time feature is especially important because of the ever accelerating pace in research in these fields and the pressing need for more rapid communication.

The Chairman of the Program Committee, Dr. Ellis R. Lippincott, and the Secretary of the Conference, Dr. Marvin Margoshes kindly agreed to serve as editors for this volume. With the prompt response of the authors, the diligence of the editors, and the cooperation of the publisher, publication of the Proceedings within a few months was assured. The Organizing Committee for the Colloquium extends its appreciation to the many individuals who made this publication possible.

National Bureau of Standards
Washington 25, D. C.
September 15, 1962

Bourdon F. Scribner
General Chairman
Xth Colloquium

PROCEEDINGS OF THE
Xth COLLOQUIUM
SPECTROSCOPICUM
INTERNATIONALE

THE ROLE OF SPECTROSCOPY IN ASTROPHYSICS

Jesse L. Greenstein
Mount Wilson and Palomar Observatories
Carnegie Institution of Washington
California Institute of Technology
Pasadena, California, U.S.A.

INTRODUCTION

A large fraction of the observational data of astronomy is obtained by spectroscopic methods, and a similarly large portion of astrophysical theory is devoted to the analysis of spectroscopic data. Any general review of so large a subject must be superficial. The goal of the present review is to describe (1) some of the instrumental problems, and the limitations of the observational techniques, (2) the physical conditions in the sources of the spectra, (3) the peculiarities of the excitation mechanism in various types of astronomical objects, and (4) the chemical composition of the stars, and their relation to nuclear energy generation and the theories of the origins of the chemical elements.

The enormous range of physical conditions in the sources makes astronomy an important branch of applied spectroscopy, notable at one extreme for high temperatures, low pressures, and nearly complete ionization; at another extreme very high pressure phenomena become important; in some problems, the deviations from thermodynamic equilibrium are very large. There are no standard techniques, no calibrated sources—nature plays a difficult game, sometimes an unfair one, with the investigator. But there is no richer road in astronomy—we are so greatly limited in our experimental techniques that we take gladly what information we can, from the slenderest of clues.

It should be remembered that the faintest objects which are studied spectroscopically have a total flux, at the earth, of less than one photon per cm^2 per second; with a spectral resolution of even 10^3, which can be used on so faint an object, the 200-inch reflector gathers only 40 photons/sec per spectral resolving-power unit and the inefficiency of the slit spectrograph and of the photographic process reduces this number to less than one silver grain per second. Thus, astronomical exposures run from several nights at a dispersion of 400 Å/mm, for a distant galaxy or a faint star, up to relatively short exposures at 1 Å/mm for stars of naked-eye brightness, to snapshots at 0.1 Å/mm for the sun. In general, we still employ photographic techniques, although photoelectric scanning of the spectrum of bright stars at high resolution (≈ 50,000), and of faint stars at low resolution (≈ 500), and image-intensifiers for low resolution spectra are now in regular use and under intensive development. Photography and the atmosphere together limit the spectral region observable to $\lambda3100$ to $\lambda8900$.

Infrared scanning of the sun, within the limitations of the transmission of the terrestrial atmosphere, is generally employed to 3μ, and experimental development in the 10μ region is under way. I will omit discussion of far ultraviolet observations from rockets and satellites except to say that spectral emission-line studies of the sun have been carried down to 100Å, in detail, the general intensity distribution charted in the X-ray region, and γ-rays detected from outside the solar system. One very important long wavelength feature is the 21-cm hyperfine transition in the ground states of atomic hydrogen in interstellar space; here the observing techniques are those of radio astronomy. Till now, no other monochromatic radiation has been detected in the long wavelength region, nor are any beyond those of molecular hydrogen expected to be strong; no definite quantitative predictions of the interstellar molecular hydrogen spectrum yet exist.

Among the goals of astronomical spectroscopy are (1) identification of atoms, ions, radicals, and molecules present, (2) the quantitative analysis of stellar atmospheres, (3) the study of the physical conditions in the source of the spectrum, e.g., temperature, electron and gas pressure, magnetic field, state of motion (convection or turbulence) and mass motion. The nature of the excitation process is of the greatest interest; the existence of spectral lines in emission or absorption depends on deviations from complete thermodynamic equilibrium. For example, studies of intensities of the absorption lines across the disk of the sun provide information concerning the temperature gradient in the outer 500 km of the solar atmosphere. The change of the spectrum into emission lines, and the increase of the level of excitation and ionization with height above the solar surface, in the range 10^3 to 10^6 km, reveal the chromosphere and corona, where the temperature ranges from 10^4 to 4×10^6 °K.

THE ASTRONOMICAL BACKGROUND

The variety of densities, temperatures and compositions is so great that one can only say that astrophysics embraces all ranges of density at which spectra can be observed—generally atomic, although molecules dominate the coolest stars, and solids may be responsible for some interstellar bands. A very rough idea of the range of temperature, T, and density, n_H (hydrogen atoms per cm^3) is given in Table 1. The symbols A and E under *Lines* indicate absorption and emission lines. Under *Processes* I list some of the interesting peculiarities in each type of source. The excitation processes will be discussed in detail below, but in general, except for the stellar reversing layers, are dominated by violent deviations from thermodynamic equilibrium. Since hydrogen is dominant in nearly all sources except for planets and comets only its concentration is given. For planets and comets, densities are largely unknown and strongly dependent on which height is being studied. Relative abundances of other elements in interstellar space parallel those in the normal, young stars. The concentration of interstellar compounds is very low, probably about 10^{-6} n_H.

The determination of the composition of the stars will be discussed later; Table 2 gives a recent compilation by Aller [1]. We shall take such a composition as the standard with which peculiar stars are compared. But except in the most abnormal objects, Table 2 shows that the enormous predominance of hydrogen must control the appearance of the spectra of the stars, either by the strength of its lines, or by its continuous opacity which sets the depth of the atmosphere through which one can observe, and therefore the strength of other lines. Along the main sequence the mass above the photosphere (which is located at optical depth near unity) varies from 0.2 gm/cm^2 at 25000° to 4 gm/cm^2 at 5000°, the temperature of the sun. Surface gravity, and therefore the pressure, decreases from main sequence stars to supergiants. The gas pressure is about 10^5 $dynes/cm^2$ in the sun and drops to 10^2 in a supergiant, while in a white dwarf, the gas pressure reaches 10^9 $dynes/cm^2$. Collisions with neutral hydrogen cause line-broadening, although resonance self-broadening occurs for the strong lines of Ca II, Ca I and Na I at very low temperatures. When hydrogen becomes partially ionized, above 7000°K, collisions with ions and electrons dominate line broadening, and the detailed theory of the hydrogen-line broadening itself has been given by Kolb, Griem and Shen [2].

The observability of lines of a given element depends on many factors besides the abundance. The limitation on the observable spectral region, in particular, requires that subordinate

Table 1

Physical Conditions in Astronomical Sources

Source	Lines	T(°K)	n_H/cm^3	Processes
Interstellar gas	A	50 - 120	0.1 - 100	21-cm emission of H. Lines from lowest energy levels of Na, Ti, Fe, Ca II. Degenerated bands CN, CH; diffuse bands connected with dust, solid state, H_2?
Diffuse nebulae	E	10^4	$10 - 10^5$	Recombination spectra H, He; resonance excitation OIII; collisional excitation leading to forbidden lines of [N II], [O II], [O III]. Shock waves?
Stellar envelopes	E	$5000 - 10^6$	$10^3 - 10^8$	Material ejected from stars due to rotation, tidal forces in binaries, radiation pressure, turbulence. Large scale motions and gaseous streams. Recombination, collisional ionization and excitation. Chromosphere and corona.
Stellar envelopes	A	$10^2 - 10^4$	$10^4 - 10^{10}$	Ejected unstable shell. Mass motions. Metastability enhances population of low energy states; ground state absorption; grades into normal atmosphere.

Table 1—Continued

Source	Lines	T(°K)	n_H/cm^3	Processes
Stellar reversing layer	A	2000 - 75000	10^{12} - 10^{18}	Excitation by radiation or by collisions. Stable, or convective motions. Near-local-thermodynamic equilibrium. Magnetic fields, electric microfields due to plasma. Continuous opacity of H, H^-, and possibly molecules in cooler stars. Molecular bands diatomic, some triatomic radicals.
Comets	E	10^2 - 10^3	?	Excitation by resonance fluorescence of sunlight, radicals and molecules derived from heavier unknown parents. C_2, C_3, NH_2, Na, OH, NH in heads; ions in plasma tail, OH^+, CO^+, CO_2^+, N_2^+, CH^+.
Planets	A	100 - 200	?	Molecules absorbing sunlight; CO_2, NH_3, CH_4, ice, H_2.

Table 2

Normal Stellar Composition of Young Stars and Chondritic Meteorites

Element	log N	Element	log N
H	12.0 v	Ga	2.4
He	11.0 v	Ge	3.2
Li	1.0 v	Rb	2.5
Be	2.2 v	Sr	2.7 v
B	2.9 :	Y	2.4 v
C	8.6 v	Zr	2.5 v
N	8.0 v	Nb	2.0 v
O	9.0 v	Mo	1.9 v
F	6.0 :	Ru	1.4 v
Ne	8.7	Rh	0.8
Na	6.3	Pd	1.2
Mg	7.4	Ag	0.2 :
Al	6.2	Cd	1.5
Si	7.5 v	In	1.2 :
P	5.3 v	Sn	1.5
S	7.3 v	Sb	1.9 :
Cl	6.2 :	Ba	2.1 v
A	6.9	La	1.2 v
K	4.8	Ce	1.3 v
Ca	6.2 v	Pr	0.6 v
Sc	2.8 v	Nd	1.3 v
Ti	4.8 v	Sm	0.9 v
V	3.8 v	Eu	0.5 v
Cr	5.4 v	Gd	1.0 v
Mn	5.1 v	Dy	1.1 v
Fe	6.8	Ho	0.4
Co	4.7	Er	0.8
Ni	5.9	Tm	0.1
Cu	4.5	Yb	0.8
Zn	4.6	Lu	0.0
		Pb	1.8

v = deviations from normal abundances suspected in some types of stars.
: = presence or abundance uncertain.
Rare-earths from chondritic meteorites. Schmitt et al.; other elements solar or stellar, modified from Aller.

lines be used, because most resonance lines are in the ultraviolet; for highly ionized atoms this is always true, requiring rocket and satellite spectroscopy. The high excitation potential of observable lines of H, He I, He II (10, 20, 40 ev) make the abundances of these elements uncertain since the Boltzmann factor is very temperature-sensitive. In the sun, the metals are singly ionized, but their low levels are easily observable. Their relative abundances can be well determined, but their ratio to hydrogen is difficult. Elements like C, N, O, also have high excitation potentials, so they are not too well determined. In hot stars, H, He, C, N, O, Ne, Si, are well observed at various stages of ionization, while the metals are too highly ionized.

However, it must be noted that ultraviolet spectra will not be a cure-all. Distant stars are in general unobservable below 1000 A, because of the opacity of the interstellar hydrogen. In addition, in cool stars, the crowding and overlapping of the lines of the metals will make the region below 3000 A almost useless for quantitative purposes, although important for identification and for emission-line study of the hot chromospheres and coronas of the stars. In some ways development of the stellar techniques for high resolution in the near infrared may prove more profitable, because of the comparative simplicity of the atomic spectra and the appearance of new molecular species.

HIGH TEMPERATURE ENVELOPES

Doppler determinations have led to our knowledge of the velocity distribution of the stars, interstellar gas, and distant galaxies, culminating in a value of $cd\lambda/\lambda = 0.46$ for a distant galaxy, the radio source 3C295. But equally important has been the contribution of radial velocities to the determination of stellar masses from the orbits of close spectroscopic binary stars. Less well known, but very significant in the understanding of the high-temperature envelopes of the sun and stars is the existence of convection, "turbulence," stream motions and mass loss in certain types of stars. On the surface of the sun, small, bright, hot granules are observed to rise with speeds near 1 km/sec, in a semi-regular pattern resembling Benard cells. Stars, for which we often observe the integrated result of similar motions on a grander scale, have broadened absorption lines. Loosely described as turbulence, these motions have scales of length up to an appreciable fraction of the stars' radius (macroturbulence) and down to a fraction of the scale height of the reversing layer ($\approx$ 200 km), and velocities from 40 km/sec down to nearly thermal values of 1 to 5 km/sec. They are driven by a convective instability of the stellar plasma. The temperature gradient in most stars is radiative, and depends on the opacity; since hydrogen and metals both contribute to the opacity, the latter is a function of temperature T and pressure P. Given knowledge of the composition of the star and the physics of the opacity, the radiative temperature gradient is found. Convection will occur if

$$\left|\frac{d\ln T}{d\ln P}\right|_{\text{rad.}} > \left|\frac{d\ln T}{d\ln P}\right|_{\text{ad.}} \qquad (1)$$

The ratio of specific heats of the gas, γ, gives the adiabatic temperature gradient

$$\left|\frac{d \ln T}{d \ln P}\right|_{ad.} = \frac{\gamma - 1}{\gamma} . \qquad (2)$$

Therefore, if the radiative gradient is close to the adiabatic one, a change of level of ionization, which will make a substantial change in γ, will drive convection. In stars like the sun, the ionization of hydrogen is responsible, while He and even H_2 ionization zones occur in other types of stars. Such convection may be responsible for stellar light and radius variation such as is found for cepheids and long-period variables.

Energy transport by convection can be computed from the temperature fluctuation in the convective elements, $\Delta T/T$, their velocity and pressure. In the sun, the velocities are subsonic, $\Delta T/T \approx 0.05$, and the energy thus transported as pressure waves is a non-negligible fraction of the solar output. The important fact, however, is that pressure waves, running through the outer low density envelope, gain velocity because of the conservation of energy. As they approach the velocity of sound, i.e., as $M(= v/v_s) \rightarrow 1$, the production of noise becomes important, and most of this sound energy, E_s, is converted into heat. For isotropic turbulence, when M is not large,

$$E_s = 19\rho \langle v^2 \rangle^{3/2} M^5 \text{ erg/cm}^2 \text{ sec}, \qquad (3)$$

where $\langle v^2 \rangle$ is the mean-square turbulent velocity. In the region where solar granulation appears, $\rho \approx 10^{-6}$ gm/cm^3, with $\langle v^2 \rangle^{1/2} \approx 2 \times 10^5$ cm/sec, ($M = 0.2$), we find $E_s \approx 10^6$ erg/cm^2 sec, about 10^{-4} of the radiant energy of the solar photosphere, 10^{10} erg/cm^2 sec. This small fraction, however, is ample to account for the phenomena of solar activity, the chromosphere (10^4 °K) and the low density corona (10^6 °K). Biermann and Lüst [3] give a rough estimate of the energy involved in high-temperature, non-thermal, or particle radiation from the sun, reproduced in Table 3. Violent activity involves large fluxes for short periods, as in solar flares. While these numbers are highly uncertain, they are in the range of the acoustic noise energy, or the transport of energy by the granules, so that they may be different aspects of the same phenomena. Larger units of mass transport have also been suggested, e.g., spicules. Of course, still a different mechanism is present in the form of the moving magnetic fields of the sunspots, flares, prominences and ejected plasma. But the energies in the magnetic fields may

Table 3

Solar Non-Thermal Energies

(ergs/cm^2 sec)

Type	Radiation		Particles	
	U.V.	Radio Freq.	Normal	Relativistic
Average	10^5	10^{-1}	10^5	--
Active Regions	$>10^6$	1 - 10	10^6	--
Flares	$10^8 - 10^{10}$	$10^2 - 10^3$	$10^7 - 10^9$	$10^7 - 10^8$

also have the convective plasma transport as their fundamental energy source, and magnetic lines of force may be merely a coupling mechanism, and provide the locale for particle acceleration.

A non-thermal source of local heating gives a temperature or level of ionization corresponding to about $1 - 4 \times 10^6$ °K in the sun, i.e., about 400 ev. Strong forbidden emission lines of [Fe X], [Fe XIV], [Ca XV] are found in the corona. If all energy densities are in rough equipartition, characteristic values are $U_{mag.} = B^2/8\pi = U_{thermal} = 3/2\, n_H kT = U_{kin.} = 1/2\, n_H m_H v^2$. At typical conditions in the lower solar corona, $n_H = 10^8/cm^3$, $T = 10^6$ °K, $<v^2>^{1/2} = 100$ km/sec (approaching random motions observed) and the magnetic field strength is 1 gauss (not far from the solar general dipole field). Magneto-hydrodynamic velocities are $v_A = B(4\pi\, n_H m_H)^{-1/2} = 300$ km/sec. The spectroscopy of such a source, very far from equilibrium between matter and radiation density, is extremely interesting, and the rocket and satellite results will be of great interest. Ultraviolet permitted lines from high ionization levels have already been detected, and X-ray radiation traced far beyond the energies suggested by the above elementary considerations. Some double stars containing red giants, as well as ordinary novae at certain stages of their evolution, show emission-line spectra similar to that of the solar corona, ranging from [Fe II] to [Fe XIV]. One recurrent nova showed forbidden lines from as low as [O I] (low temperature) to [Ca XV] (very high temperature). Permitted emission lines up to OVI occur near faint, hot stars which are nuclei of planetary nebulae, i.e., which have ejected large quantities of gas with velocities up to 100 km/sec. Thus we often find superposed on the normal and absorption-line spectra of stars, emission-line features as evidence for a hot circumstellar envelope. Since the solar corona is only 10^{-6} as bright as the sun, such objects must display these non-thermal features on an enormously greater scale than does the sun.

IDENTIFICATION OF ATOMS AND MOLECULES

At the present time, the sun provides the most thoroughly explored stellar spectrum. Disregarding the rocket ultraviolet, lines of about 62 elements have been identified, in the absorption spectrum of the reversing layer and in the emission spectrum of the chromosphere and corona. Molecular species like CN, CH, C_2, CO, OH, NH are seen in the normal spectrum, but the sunspots, which are about 900°K, show greatly enhanced molecular lines, many of which are not yet completely identified. Eleven molecules have been identified. The cool layer below the start of the temperature inversion into the chromosphere contains C_2 and CO. Some H_2 may exist but cannot yet be detected. The atomic species in the sun are neutral and singly ionized; an element with ionization potential near 9 ev is approximately half ionized. The neutral elements have lower excitation potentials than do most ions, so that lines of neutral elements dominate in the sun. The elements which have not yet been identified in the sun have low abundance, complex spectra, or no low-lying energy states capable of producing lines in the normal spectral region. No element, anomalously weak, has been noted, if terrestrial and meteoritic abundances are used as guides. A few differences can be easily understood, e.g., the near absence of H and He on the earth, and weakness of D and Li in the sun (easily destroyed by thermonuclear processes).

The comparatively high opacity of the solar atmosphere results in weak lines of metallic ions. The most interesting group of these are the rare earths. These are found more easily in normal red giants than in the sun, and very much more easily in certain peculiar A stars with large general magnetic fields and in heavy-element-rich red giants. However, only one element of particular interest need be mentioned. This is technetium, ^{43}Tc, first collected on earth as a fission product, for which the longest-lived isotope has a half-life of 2.6×10^6 years. It is therefore very overabundant in those peculiar stars in which it is found, and must have been recently synthesized. Elements with high excitation potentials, such as appear only at high temperature, must be added to any list of elements present. Altogether, in stars and nebulae, where forbidden lines become useful, one can add another ten elements to those found in the sun, giving a total of about 70 out of the possible 90 that we may expect. Table 4 contains a list of the stable elements still missing. For many of these the spectroscopic situation is very unfavorable, in that the spectra are very rich, so that no single line has a large transition probability. Others have unfavorable energy-level diagrams; a number of elements in Table 4 will undoubtedly be eventually identified in neutral or first ionized

Table 4

List of Unidentified Elements

Z	El.	Log Estimated Abundance (Si = +6)	Notes	Z	El.	Log Estimated Abundance (Si = +6)	Notes
5	B	+1.4	1	68	Er	-0.7	2
33	As	0.6		69	Tm	-1.4	
34	Se	1.8		73	Ta	-0.7	
35	Br	1.1		75	Re	-0.6	
50	Sn	0.1	2	76	Os	-0.1	
52	Te	+0.5		77	Ir	-0.3	
53	I	-0.2		78	Pt	+0.2	
54	Xe	+0.6		79	Au	-0.8	
65	Tb	-1.2		81	Tl	-0.9	2
67	Ho	-1.1		83	Bi	-1.0	

1 - Possibly identified in hot stars.
2 - Possibly identified in sun.

stages in stars of moderate temperature. The hot stars observed in the ultraviolet will contribute largely to information on the lighter, relatively abundant elements, in higher stages of ionization. However, laboratory doubly and triply ionized spectra are still very poorly known. Among the greatest needs are lists of lines of doubly ionized metals and rare earths, in the region $3500 < \lambda < 7500$ Å, and for this and higher stages of ionization of elements with $Z < 20$, also in the normal spectral region. The high-level transitions for these elements are hardly known at all, and are difficult to produce in the laboratory. For example, even CI is poorly known, since many lines have been found by Keenan and Greenstein in a carbon-rich star, which can be fitted into the known scheme of energy levels, but which had not been observed in laboratory sources. The following are particularly important: CI, CV, N IV-N VI, O IV-OVII, Ne III-Ne VIII, and similar high stages of Si, Mg and the iron-group metals up to 600 ev ionization potential. These will be interesting also for the far ultraviolet, but many of these must be important in the normal spectral regions of such objects as supernovae, in which most lines still remain unidentified.

While the number of elements is satisfactorily large, the difficulty remains that the number of unidentified lines is still very large in peculiar stars. Only this year a very strong line known for the last 25 years in magnetic A stars was identified with Si II, a startlingly late date for so well-known an element. The major number of unidentified lines will be almost certainly singly and doubly ionized metals and rare earths, especially in stars of peculiar composition, with abnormally high abundance of the fifth period. In my own investigation of a sharp-lined star rich in rare earths and in carbon, about 500 lines remain poorly identified; Bidelman of the Lick Observatory has found two stars extraordinarily rich in heavy elements, in which Mo II, Dy II, Nd II are very strong, and elements such as Fe are considerably weakened. At present we can only guess with how much detail ultraviolet spectra of the sun and stars will be obtained. The resonance and other low-lying lines of many stages of ionization are well known already; however, difficulties in laboratory sources make excitation of subordinate lines somewhat selective, with ionic and collisional broadening often shifting and suppressing high levels. Thus it is probable that the strong solar far-ultraviolet lines will be identifiable, but the weaker lines, and the near vacuum ultraviolet will be difficult. This is particularly unfortunate for interpretation of stellar far ultraviolet spectra. The interstellar gas has a Lyman continuous absorption at $\lambda < 912$ Å which is extremely strong, with an optical depth of 10^3 for stars at 100 psc distance. Thus it is the region 1000 Å - 3000 Å which will be most easily observed, and which remains the least well explored in the laboratory, for common elements doubly to about ten-fold ionized.

The determination of relative abundances of the isotopes in the sun and peculiar stars is of especial importance in theories of nucleosynthesis. Astronomical determination of particular physical interest involve the ratios: D^2/H^1, He^3/He^4, Li^6/Li^7, C^{12}/C^{13}, Mg^{24}/Mg^{25}, Ti, Zr. We will discuss nucleosynthesis theory later and the significance of the discovery of He^3 and C^{13} in astronomical sources. D^2 has been searched for, till now, with contradictory results. Molecular bands offer the greatest promise for future work in this field. Stellar sources give largely hydrides or oxides. Bands so far studied are listed in Table 5.

Bands of the hydrides could provide a means of detecting D, but the low terrestrial ratio $D/H = 1.5 \times 10^{-4}$ makes success unlikely. Interstellar $D/H < 0.2$ from interstellar molecular bands of CH, but radio astronomy has reduced D/H to less than 2×10^{-4}, from failure of direct observations of the hyperfine-structure transition of the ground state of atomic D. The bands of CH are very strong in many stars, and failure to observe CD suggests $D/H < 0.003$. A particularly important experiment, not yet carried out, is to attempt to observe MgH (which is present in stars of surface temperature near 4500°K), since the terrestrial isotope ratios (79:10:11) are relatively favorable. In nuclear reactions, Mg^{24} can be synthesized by successive γ-ray captures of alpha particles on C^{12}, while Mg^{25} and Mg^{26}

Table 5

Molecules Detected in Astronomical Sources

Comets	Stars		Interstellar Space
CH	CH	TiO	H^2 ?
NH	NH	VO	CH
NH_2	OH	CrO?	CH^+
OH	MgH	MnO?	CN
C_2	AlH	SrO?	
C_3	SiH	YO	
CN	CaH	ZrO	
CO^+	C_2	NbO	
CO_2^+	C_3	LaO	
N_2^+	CN	SiC_2	
CH^+	CO	SiN	
	MgO?		
	AlO		
	ScO		

can be made only by neutron capture on Mg^{24}. Other interesting groups of isotopes are those of Ti and Zr, easily studied in their oxides, TiO and ZrO, present in stars below about 3500°K.

In the theory of nucleosynthesis no large anomalies are expected in the abundance of Ti, and none are observed in the stars. But Ti^{46} to Ti^{50} (ratios 8:7:74:6:5) are made either by neutron capture, on the slow or fast time scale, or by a very high temperature equilibrium process. As a result, the Ti isotope ratios might be different from those on earth; so far, no gross effects have been found by inspection of the TiO band. On the other hand, Zr is greatly variable in abundance from star to star, built by slow neutron capture processes in red giants. The terrestrial ratios, Zr^{90}, Zr^{91}, Zr^{92}, Zr^{94}, Zr^{96} are 52:11:17:17:3; if a different number of neutrons were added to the parents of the stellar Zr than for terrestrial Zr, these ratios could be drastically altered. The bands of ZrO are strong in certain peculiar stars and it is hoped that further studies will yield the Zr isotope ratios. The particular significance of these stars is that in the ZrO rich objects, the radioactive element Tc is also detected, an element which must have been made by neutron capture within the last few million years.

PHYSICAL CONDITIONS IN THE SOURCES

Once the elements present have been identified, spectroscopy provides several different categories of information about the sources, and it is this subject which has been of the greatest astrophysical importance. I will discuss, therefore, various environments and their physical description, as derived spectroscopically, with increasing degrees of deviation from thermodynamic equilibrium. The interior of a star is hot, with a mean temperature of about 5×10^6 °K, and a mean density of 1 gm/cm^3. Photons are absorbed and re-emitted an enormous number of times as they diffuse outward, and gradually degrade in energy as the temperature drops. The "atmosphere" of a star is that region where a typical photon suffers, on the average, one absorption and re-emission before leaving the star. This absorption, in the space between spectral lines, is regulated by the continuous absorption coefficient, the "opacity," caused largely by H, H^-, He, sometimes by molecular bands, and by scattering by electrons or H. It regulates the depth through which we can look, i.e., the number of atoms capable of producing a spectral line. To a first order, the opacity is quite well known, so that the theory of the continuous spectrum of the stars (between spectral lines) is on a sound basis. If we know τ_ν, the opacity, and if the emission at every optical depth is thermal in character and dominated by the local temperature, the emission is $B_\nu(T)$ (the Planck function) and the emergent flux from the stars is:

$$F_\nu(0) = 2 \int_0^\infty B_\nu\,[T(\tau_\nu)]\,K_2\,(\tau_\nu)\,d\tau_\nu\ , \tag{4}$$

where $T(\tau_\nu)$ is the temperature at optical depth τ_ν and K_2 is the second exponential-integral function. The temperature distribution with height is crucial. It must satisfy an integral equation:

$$B_\nu\,[T(\tau_\nu)] = \frac{1}{2} \int_0^\infty B_\nu\,[T(\tau_\nu)]\,K_1\,(|t_\nu - \tau_\nu|)\,dt_\nu\ , \tag{5}$$

where K_1 is the first exponential-integral function. The solution of this problem for a general τ_ν has to be obtained by very tedious numerical integration, which has been greatly accelerated by the use of large electronic computers. The limited problems when the opacity, κ_ν = constant (the gray-body problem), and when κ_ν varies only slightly with frequency have been solved exactly. Even then, the evaluation $T(\tau_\nu)$ is difficult. However, the strength of spectral lines varies with the temperature gradient in the outer atmosphere, particularly for τ from 0.001 to 0.3, and many small effects must then be included. One of the most obvious is the effect of the spectral lines themselves in "blanketing" the atmosphere, i.e., in re-radiation of photons downwards. Since in many strong lines the line absorption coefficient, l_ν, is 10^2 to 10^4 times the continuous absorption, κ_ν, the blanketing may change the temperature gradient substantially. The gray-body has a temperature contrast of about 20 percent in the optical depth range $\Delta\tau = 1$; this may be increased to nearly 40 percent in non-gray opacity models. Other important parameters are the gas pressure, P_g, and the electron pressure, P_e, which vary with optical depth according to:

$$dP_g = \frac{g}{\bar{\kappa}} d\tau, \tag{6}$$

where g is the surface gravity and $\bar{\kappa}$ the mean opacity. The conditions at a typical point are of some interest. For the sun, at $\tau = 0.2$, a representative point in the atmosphere, $\log P_g = 4.63$, $\log P_e = 0.74$, T = 5350°K. The effective opacity of the gas is such that an average quantum in the continuum penetrates about 0.5 gm/cm^2. The thickness of a layer in which P_e changes by ten is only 200 km. Under these conditions the average metal is about 95 percent ionized, hydrogen is dominantly neutral. Strong lines of the metals are appreciably broadened by collision with neutral hydrogen atoms. The random electric fields of the ions and electrons produces a linear stark effect broadening of the hydrogen lines. The radiation field is quite asymmetric, because of proximity to the boundary of the star, about 2.2 times as strong upwards as downwards. The energy density of radiation is about 0.6 that of a black-body at the "effective temperature" of the sun, 5750°K. Within a strong line the radiation field approaches that of a black-body. Deviations from the Boltzmann distribution in the populations of the levels of an atom depend on details of term structure, the radiation field and collisional excitation; these deviations are probably not larger than a factor of two, but as we approach the surface, i.e., as $\tau \to 0$, the radiation field becomes asymmetric, more dilute, absorption lines appear, and the level population differs considerably from that in local thermodynamic equilibrium. These deviations will be largest when the excitation is purely by radiation. We can write the steady-state condition for a two-level atom connected by a line of energy $h\nu$ (where the statistical weights are taken to be unity)

$$n_2(A_{21} + B_{21} I_\nu) = n_1 B_{12} I_\nu . \tag{7}$$

Here A_{21}, B_{21} and B_{12} are the Einstein transition probabilities, n_2 and n_1 are the populations in the two states, and I_ν the actual radiation field. From the relations between A and B coefficients, we can rewrite the population ratio as

$$\frac{n_2}{n_1} = \frac{1}{1 + \frac{B_\nu(T)}{I_\nu}\,(e^{h\nu/kT} - 1)}, \tag{8}$$

where $B_\nu(T)$ is the Planck function. Note that if we neglect stimulated emission, the population ratio is $I_\nu(2h\nu^3/c^2)^{-1}$, which for large $h\nu/kT$ and small I_ν gives

$$\frac{n_2}{n_1} \approx \frac{I_\nu}{B_\nu(T)}\, e^{-h\nu/kT}\,. \tag{9}$$

Note that equation (9) resembles the Boltzmann equation except that the population is reduced by the ratio of the actual I_ν to the Planck function. This dilution of the radiation field is very common in astronomical sources. For example, an atom in interstellar space is excited by stellar radiation whose distribution with frequency may be close to that of a black body, but which has a low flux because of the small solid angle subtended by the stars. Near the surface of a star the dilution, $I_\nu/B_\nu(T)$, is about 0.5, in interplanetary space it is only 10^{-5} and in interstellar space 10^{-14}. We will expect severe deviations from Boltzmann population of the levels when radiative excitation holds and when the radiation field is very dilute. Other types of deviation occur in gaseous nebulae, when recombination of ions populates the levels, in the solar corona, where collisional ionization holds, and in the chromosphere, where the radiation and kinetic temperatures are very different. Still another interesting set of deviations from normal level population occurs when only collisional excitation populates low metastable levels.

The dilution of radiation in a stellar atmosphere is not the only factor leading to deviations from local thermodynamic equilibrium. Because of the convective transport of energy, the sun and other stars have a temperature inversion in their surrounding envelopes of low gas density. Although the details of the structure of this region are still controversial, its spectrum is one containing strong emission lines and possibly continua far into the X-ray region. In the transition region where the temperature rises in the chromosphere, the density and temperature structure is very inhomogeneous. Hydrogen is largely ionized, the electron density is about 10^{11} to $10^9/\text{cm}^3$, and the temperature rises from 5000°K to 10^6 °K. In the corona, where some estimates suggest temperature fluctuations from 1 to 4 million degrees, the ionization level is very high, the spectrum in the visual region dominated by forbidden lines, and the ultraviolet by X-rays and permitted emission lines with ionization potentials up to 600 ev. In the corona the density is in the range 10^8 to $10^5/\text{cm}^3$. The effect of these ultraviolet emissions on the normal solar reversing layer has not been explored. But the chromospheric emission by hydrogen and the ionized metals undoubtedly affects the central intensities of the absorption lines in the normal regions of the spectrum, and the level of ionization and excitation in the upper layers of the reversing layer. These, and other effects, are important in the present discussions of non-local-thermodynamic equilibrium. The most interesting part of the study of extreme deviations from Boltzmann distribution is the information provided on the nature of the sources themselves, and I will discuss some interesting cases of spectra produced in extreme astrophysical environments.

EXTREME DEVIATIONS FROM EQUILIBRIUM

Perhaps the closest-home example of the effect of the dilution of radiation in a low density source is found in the spectrum of comets. These objects have nuclei (10 km in diameter) of frozen gases and other solids, which emit large quantities of gas under the influence of solar heating, and possibly because of solar plasma bombardment and surface chemical activity. The parent molecules are unknown, but are rich in astrophysically abundant elements such as H, C, N, O, Na and Fe. Comets spend nearly their entire life at distances up to 10^5 astronomical units from the sun; since the black-body temperature is $300°\text{K} \times (1/r)^{1/2}$, where r is the distance in astronomical units, the solids are very cold, until a close approach to the sun, where rapid outgassing occurs. The sun, radius R, seen from a distance of r, subtends $\pi R^2/r^2$ steradians, which is $7 \times 10^{-5}\,(1/r)^2$ where r is again expressed in astronomical units. Thus, since comets are usually observed with $0.1 < r < 5$, the solar radiation is geometrically diluted below a Planck curve of 6000°K by about 10^{-5}. The comet gas has a low temperature, its molecules undergo few or no collisions once they are observable in the head, and even more so in the tail, where they become ionized. The emission-line spectra of the molecules have been observed to give strange and apparently discordant vibrational and rotational temperatures. For example, bands of CN required about 50° to 300°K while the C_2 structure required 3000°K. High-resolution spectroscopic observations on comets are difficult, and only in 1957 was it possible to see the rotational structure of C_2, although CN had been partially resolved before. Spectra of CN in Comet Mrkos, 1957d, and in Comet Seki-Lines, 1962c, are shown in Figure 1, and intensity tracings of Mrkos and the sun in Figure 2. There is no trace of the (1,1) CN band, and the intensity distribution in both the P and R branches is very badly mangled from any smooth envelope that might be drawn. For thermal excitation of an emission band one would expect a smooth distribution of the populations of the rotational levels of the upper states leading to the emission lines - a distribution which would give the "rotational" temperature. The erratic intensity pattern observed shows that the populations of the upper levels is not a smooth function, as it would be if there were collisions exciting the states. In addition, the details of the bands in the two comets are quite different, certain lines being nearly absent in one and not the other. The explanation is simple, and was suggested by McKellar and studied in detail by Swings 20 years ago. The ground electronic state is the only one populated at low radiation density and the low temperature of the comet gases. Absorption of the solar radiation populates the upper

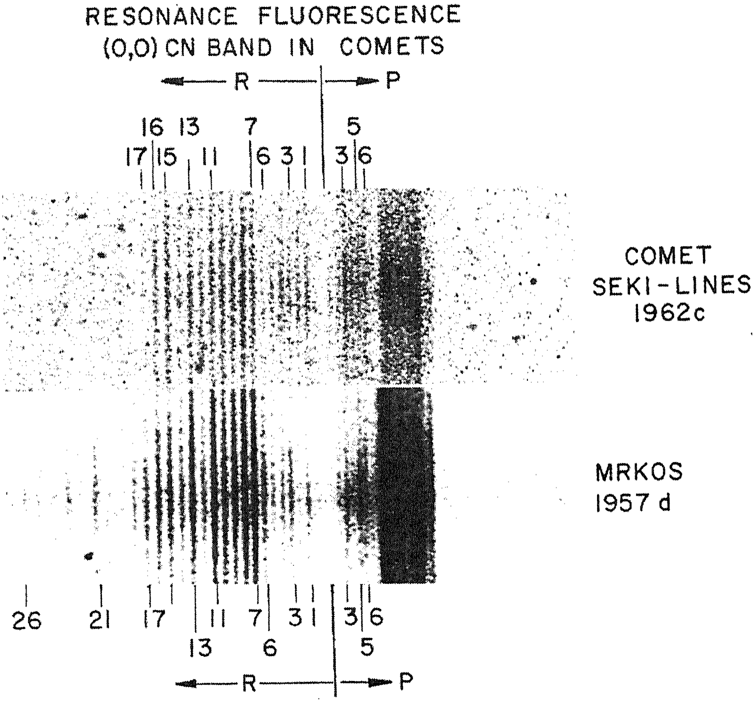

Figure 1. Emission lines of CN, (0,0) band near λ3883, in two comets, excited by resonance fluorescence. Note the erratic intensity distribution among individual rotational lines, and the differences between the two comets.

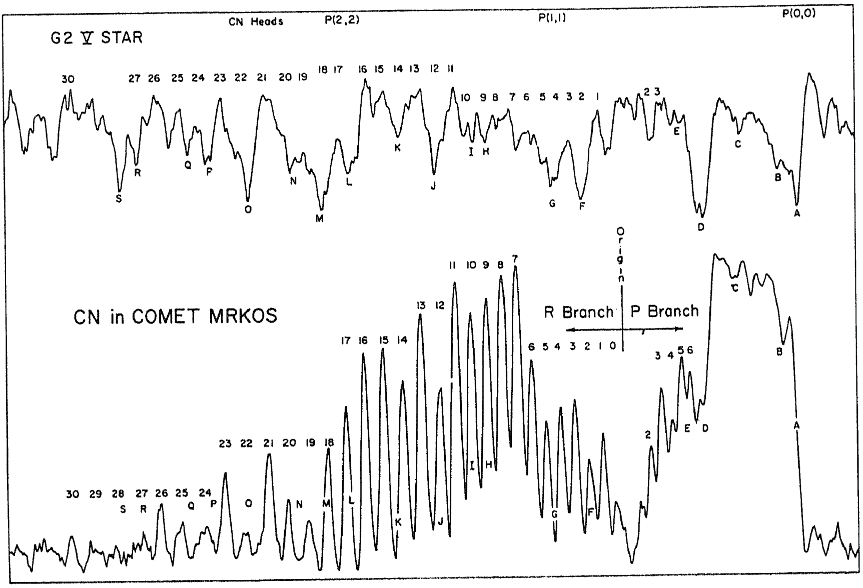

Figure 2. Intensity tracings of the solar spectrum (above) showing strong absorption lines. The CN band is to the same wavelength scale, and prominent solar absorption features are identified by letters. The numbers refer to ordinal number in the P and R branches.

levels, and the emission lines are then produced by spontaneous decay. The population depends on the details of the energy available in the solar spectrum, which is full of absorption lines, and even has strong P(0,0), P(1,1) band heads of CN. The mutilated solar spectrum is seen from the comet with different wavelength shifts dependent on the relative velocity of comet and sun. The two comets illustrated in Figure 1 had very different velocities, so wavelength shifts were nearly one Angstrom. Figure 2 shows how the dips in the solar spectrum are correlated with weakenings of individual CN lines below a smooth intensity profile. The P branch has its long wavelength side destroyed by the weakness of solar radiation in the solar P(0,0) band; the low members of the R branch are in strong solar absorption, and R5, 9, 10, 12, 14, etc., are weakened. Obviously, such resonance fluorescence in a molecule is slightly blurred by populating the upper state from other lower states than that to which the observed emission line goes, but the effect is clearly present and has been studied in full detail now also for C_2. No other excitation mechanisms exist. I have found differences in the intensity anomalies between the two sides of a comet. These are caused by internal motions of only 1 or 2 km/sec, which alter the available solar exciting radiation by Doppler shifts if a solar absorption line closely coincides with a CN transition.

Another, and much more extreme example of distortion of molecular bands by conditions in the source is found in the interstellar absorption by CN, CH and CH^+. It was known that the only atoms producing interstellar absorption lines were those with strong resonance lines in the accessible spectrum, namely Na I (3^2S-4^2P°), K I (4^2S-4^2P°), Ca I (4^1S-4^1P°), Ca II (4^2S-4^2P°), Ti II (a^4F-z^4D°, a^4F-z^4F°, a^4F-z^4G°), Fe I (a^5D-z^5F°, a^5D-z^4D°). In addition, very weak sharp lines were found; four are identified as CH $A^2\Delta$ - $X^2\pi$ and $B^2\Sigma$ - $X^2\pi$, (0,0) band lines; three are CN, $B^2\Sigma$ - $X^2\Sigma^+$, (0,0); three are R(0) lines of CH^+, $A^1\pi$ - $X^1\Sigma^+$, (0,0), (1,0), (2,0). In normal stars several hundred lines of the CH band near λ4300 are found; in interstellar space only one is seen. The dilution of radiation in space is about 10^{-14} and the black-body temperature corresponding to this energy density is about 3°K. The kinetic temperature is about 20°K to 100°K, yielding appreciable excitation only for the upper hyperfine level of H I in the ground state.

In addition to the sharp atomic and molecular lines, about 15 somewhat diffuse band-like structures are found to be almost certainly of interstellar origin. The most conspicuous are at λ4430 (very broad and shallow) and at λ6284 (relatively sharp). Some evidence exists that these bands are associated with the interstellar dust grains rather than with the purely gaseous component. In the solid state at low temperature, diffuse bands are seen in astrophysically abundant elements, and it was early suggested that solid O_2 might produce some of the bands observed. Figure 3 contains spectra obtained by Herbig at the Lick Observatory. The strong interstellar Na I lines are seen, as well as weak, broad absorption and emission features in the stars (which are of early type, with shallow lines caused by high rotation). Eight of the sharper interstellar bands are marked, none of which have been yet identified with certainty. Herbig made the very interesting suggestion that the λ4430 band arises from H_2 in the solid grains. This band reaches 200 A width, is very strong, and must be caused by an astronomically abundant substance. The concentration of H_2 in space is unknown and it can probably be formed from atomic H only in contact with solids. The ground state of H_2 gives lines too far in the ultraviolet to be observed through our atmosphere. Herbig postulates that in a low-temperature solid, metastable H_2 in the $c^3\pi_u$ might exist in appreciable quantity. The (0,0) transitions between $c^3\pi_u$ and $p^3\Sigma_g^+$, $r^3\pi_g$ and $s^3\Delta_g$ are concentrated in the λ4400 region. Based on laboratory intensities corrected to the lower temperature of the interstellar solids, and allowing a wavelength shift of 15 A, the computed band resembles the interstellar feature at λ4430 fairly well. The lifetime of the metastable state at laboratory temperatures is very short; whether

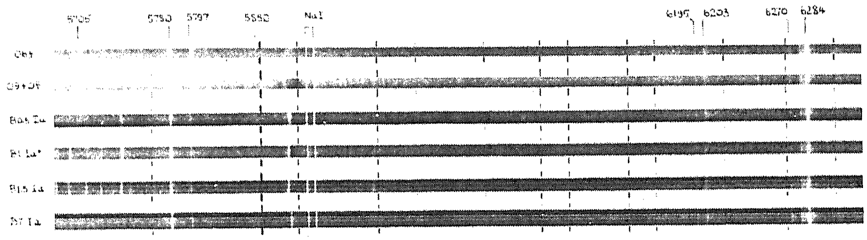

Figure 3. Unidentified interstellar bands marked in six stellar spectra. The emission and absorption feature left of Na I is λ 5876 of He I in the stars. (Herbig, Lick Observatory photograph.)

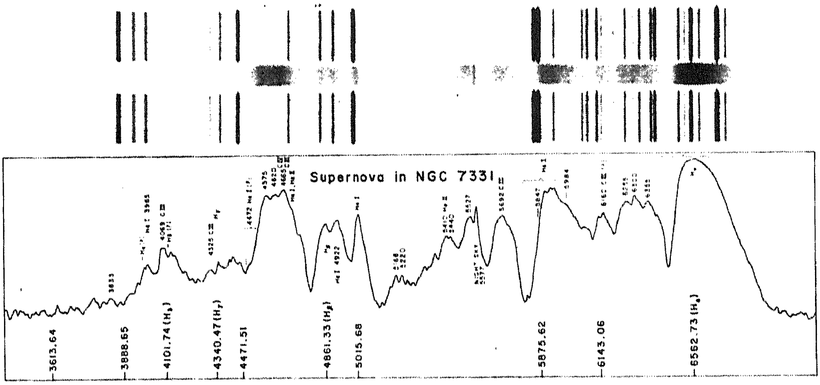

Figure 4. Spectrum of a supernova of type II, 60 days after maximum light. Comparison H, He, Ne; wavelengths of comparison marked at bottom. Tentative identifications on intensity tracing show emission lines of H, He I, He II, C III, C IV. The strong emission lines are accompanied by shortwards—displaced absorption lines from the expanding gases in front of the star.

it can be sufficiently lengthened by low temperature and solid-state effects to be important is not yet known. Herbig requires that the $v = 0$, $K = 1,2$ levels of $c^3\pi_u$ survive to produce the λ4430 band, and suggests that it is possible that interstellar λλ5705, 5850 can also be produced in this way.

The stars show almost any possible grades of deviation from equilibrium excitation processes; dilution of the radiation field results in complex spectroscopic phenomena in shells or envelopes surrounding unstable stars. A hot rotating star may eject gases which become visible at 5 to 100 stellar radii distance from the source. Part of such a cloud produces emission lines, while that part which lies between the observer and the star produces circumstellar absorption lines. The latter arise from either the ground state, or from excited metastable levels, prominent in 2^2S of H I and 2^1S, 2^3S and 2^3P° of He I, as well as in the much lower metastable levels of the ionized metals. One extreme deviation of this type occurs when a star explodes as a supernova. It is generally believed that from 1 to 10 solar masses of gas are ejected with speeds from 10^3 to 10^4 km/sec. In Figure 4 I show a spectrum and an intensity tracing, of the complex spectrum of a supernova (a so-called type II object) in a distant galaxy, NGC 7331. This supernova reached a luminosity 10^{10} times that of the sun, and the spectrum illustrated was taken two months later when the brightness of the star had dropped by a factor of ten. The sharper emission lines are 5000 km/sec in width, and the largest Doppler shifts in the violet-displaced circumstellar absorption, from the quasi-metastable levels of H and He I, reached 10,000 km/sec. The gases shown in Figure 4 are already 5×10^{10} km from the original star, i.e., about 300 times the distance earth to sun. Although the radiation and material density were both high compared to those in shells around normal stars, the excitation and ionization were strange. The star was quite red, the energy density probably near that in an 8000°K black-body, the ionization level very mixed, in that H, He II, C III were all present. But the excitation is very unusual in that only the leading lines of each series were present. The intensity ratios $H\alpha/H\beta/H\gamma$ are exceptionally large in hydrogen; $\lambda 5876$ of He I is very strong and $\lambda 4026$ almost absent in the 2^3P°-n^3D series, etc. Collision may be the source of the excitation and ionization. Not all lines are identifiable. (In passing, I should mention that the broad features in the even more luminous supernovae of type I still defy identification.)

PHYSICAL PROCESSES

Collisional ionization is most clearly studied in a source like the solar corona, although it may occur in stellar explosions, and in shock waves in the interstellar gas and radio sources. The spectroscopic problems here began with that of identification, culminating in the recognition of the strong coronal emissions as forbidden lines of spectra like [Fe X], [Fe XIV], [Ca XV]. These require excellent far-ultraviolet wavelengths for certain identification by the combination principle, and also careful extrapolation of isoelectronic sequences. At present most lines are identified, but the soft X-ray region will undoubtedly bring new problems if the permitted lines of these and possibly higher ionization levels are to be identified. The theory of collisional ionization is moderately good, and it is to be hoped that the use of large electronic computers will permit computation of accurate wave functions for cross-sections for ionization and excitation. The coexistence of a wide range of

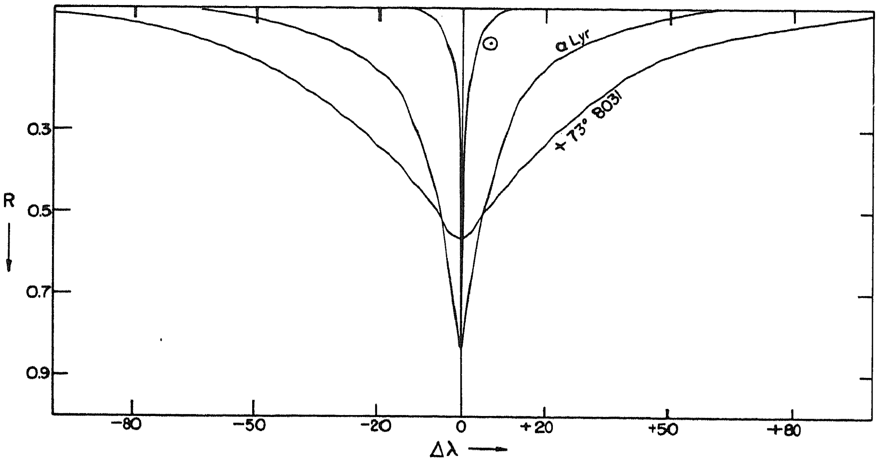

Figure 5. Stark-effect broadening of a hydrogen line in a white dwarf, a normal A star and the sun.

ionization stages in the solar corona is a property both of the collisional process and an important indicator of temperature inhomogeneities in the corona itself. Many peculiar stars show even wider ranges of ionization in larger surrounding gaseous envelopes—for example from [Fe II] to [Ca XV].

Collisions as a source of absorption-line broadening are particularly important for the hydrogen lines, dominating a wide range of stellar temperature, from 25,000° to 5,000°K. The broadening theory was originally based on the work of Holtsmark, in which the distribution of electric field strengths of the neighboring ions was used to compute a statistical Stark broadening. In recent years, the fields of ions and electrons have been included more completely and accurately by Griem, Kolb and Shen [2]. Applications of this theory to stars have been numerous and successful; the strength of the far wings of a Balmer line is quite sensitive to electron pressure. Empirical classification of the stars, according to surface gravity, has long been based on total Balmer line strengths. The total strength also involves the populations of the n=2 level in hydrogen, which is temperature sensitive, and the line-broadening and line-formation theory for the center of the line, which is not yet completely satisfactory. High-dispersion spectra, and photoelectric scan techniques are useful for line wings and provide one accurate means of stellar luminosity classification.

An extreme example of hydrogen-line broadening is found in the white dwarfs. At about 15,000°K, with a surface gravity of 10^8 to 10^9 cm/sec^2, the lines reach 100 Å half-width, and the last member of the Balmer series has an upper quantum number of 7 or at most 8. Figure 5 shows intensity tracings of Hγ in a white dwarf, a normal main-sequence star, and the sun. The analysis of such line profiles has shown that the wing-broadening theory holds quite well. The high surface gravity of the white dwarfs is confirmed; it is also found that the helium/hydrogen ratio may be quite high even when hydrogen lines dominate, and that the metal/hydrogen ratio is quite low.

ABUNDANCE ANALYSES

The composition of the stars is one major problem of astrophysics. The identification of the elements present is only the beginning of the labor. Analysis of composition depends on (1) the development of the theory of stellar atmospheres, (2) availability of the atomic transition probabilities, (3) knowledge of the sources of opacity in the continuous spectrum, (4) determination of the physical parameters of the star (e.g., temperature and pressure), (5) measurement of line intensities, (6) application of either elementary or refined methods from the theory of stellar atmospheres. The spectra available for bright stars have ample resolving power, since line-broadening in the stars is such that resolution above 10^5 are seldom useful. The 100" and 200" coudé spectrographs attain this resolution, but are usually used at much lower dispersions, because of the faintness of the most interesting stars. Because of its brightness and the observability of line intensities across its disk, the sun has been studied in most detail, and is used as the standard of composition for normal stars. Fine analysis methods now used are well outlined in the study of the sun by Goldberg, Müller and Aller [4]. A "model atmosphere" gives the run of temperature and pressure with optical depth. This atmosphere permits machine computation of the continuous opacity, populations of the energy levels, shape of the line-absorption coefficient and what is called the "weighting function." The latter measures the effectiveness of an atom at a given optical depth in producing a line; the thermal re-emission in the continuum by atoms above this optical depth fills in the line, so the weighting function is steeply depth-dependent, approximately equal to $K_3(\tau)$ for a weak line. Atoms with high excitation potential would have level populations increasing inwards, since the temperature rises steeply inwards. The product of the exponential Boltzmann factor and the weight function measures the "contribution function," which has a maximum near $\tau = 0$ for low excitation and at $\tau = 0.5$ to 2.0 for high excitation. This mixture of different levels of origin makes the spectrum of a star somewhat composite (although in general much less so than laboratory arc, spark or plasma sources).

The largest uncertainties in the exact analysis of the sun arise (1) in the details of the model atmosphere adopted, particularly the boundary temperature at $\tau = 0$, (2) from questions as to the importance of deviations from local thermodynamic equilibrium, (3) most importantly, from our ignorance of transition probabilities. Even after very extensive work, Goldberg, Müller and Aller can give abundances for only 42 elements; in my own opinion, half of them are still unreliable. For some abundant elements like C, N, O uncertainties arise from the high excitation of the lines; for rare elements, with weak solar lines, blending in the sun and lack of accurate transition probabilities both contribute to the uncertainty.

All these theoretical difficulties listed above disappear if two similar stars are compared. Main-sequence stars with only small composition differences from the sun should have the same temperature distribution and similar deviations from equilibrium. The transition probabilities cancel out when the ratios of the abundances in the star and the sun are compared. Of course, for stars of widely different temperature and composition this is no longer exactly true, but it is still true that the ratios of abundances of elements in the stars as compared to the sun are surprisingly accurately determinable. For this reason, I will discuss first the evidence on stellar abundances in solar-type stars, and then in more peculiar objects. For such work only a rough analysis method is used; a mean temperature, T, and pressure, P_e, at a standard optical depth is used for both sun and stars. At present, the most accurate temperature determination of a star is obtained from its continuous spectrum. We have fairly good knowledge of the opacity as a function of frequency, given temperature, surface gravity and hydrogen/metal ratio. The temperature stratification in relevant ranges of optical depth has been computed for many model stellar atmospheres, and from these the emergent flux in the continuum obtained. Then observations either of the colors of the star determined between several pairs of wavelengths, or from photoelectric scans of the star's spectrum against absolute standards, permit comparison with theory and the choice of a suitable (T, P_e). Under ideal circumstances the temperature can be determined within ±3 percent.

I can report on several discussions of stars similar to the sun. In one, a résumé of his studies of 34 stars was made by Wallerstein [5] (based also on collaborations with Aller, Greenstein, Helfer and Parker).

Typically, the uncertainty in the logarithm of the abundance ratio of an element i to Fe, in a star as compared to the sun, $[N_i/\mathrm{Fe}]$, is ±0.10 to ±0.30. For ten elements from Na to Ba, the maximum deviation of $[N_i/\mathrm{Fe}]$ is 0.6, which is found for [Mn/Fe], and 0.4 for [Mg/Fe]; only part of this is observational error. Other elements seem to have constant ratio to Fe, within

±0.2 in the logarithm. When the entire group is surveyed statistically, however, a definite trend amounting to 0.3 in the logarithm, is found in the mean ratio of Mg, Si, Ca, Ti to Fe, as a function of the Fe/H abundance. Thus, the general appearance is near constancy of relative metal abundances in these nearly normal, solar-type stars with slightly altered ratios for special stars. Within this group of 31 nearly normal stars, the range in the [Fe/H] ratio is from +0.3 to -0.7, i.e., a factor of 10, and in 3 so-called "subdwarfs" analyzed by Aller and Greenstein, [Fe/H] reaches -2.0.

The major variation observed is in the ratio of metals to hydrogen, and it is found to be correlated with the age of the star and its place of formation in our Galaxy. The subdwarfs are found to have very high velocity with respect to the sun, and highly inclined and eccentric orbits around the center of our Galaxy. They are old, in the sense that they were formed soon after star formation began, and they were formed far from the galactic center and high above the galactic plane. The time since star formation began can be estimated as 12×10^9 years; the sun is 5×10^9 years old, some of the stars of low [Fe/H] ratio studied by Wallerstein et al. are much older than the sun and the subdwarfs may have been formed as little as 10^9 years after star formation began. The rich globular star clusters (often situated high above the galactic plane) are also very old and show low metal abundance, while the galactic clusters, in the plane, are quite young and have essentially the same composition as the sun. Apparently, the ratio of metal to hydrogen increased rapidly in the galactic plane, and stars in our neighborhood formed out of material whose composition has changed only slightly in the last 10 billion years. The ratio of number of hydrogen/metal atoms is about 10^4 in the sun, and may reach 10^6 in the oldest, metal-poor stars. The very important H/He ratio cannot be well determined in the atmospheres of solar-type stars.

A recent, unpublished, elaborate investigation by R. and G. Cayrel has applied the advanced, model-atmosphere methods to the composition of a red giant star. The observation was based on plates of 1 and 2.8 Å/mm dispersion obtained by W. K. Bonsack. The temperature was determined within 3 percent; the H/metal ratio was the same as in the sun ±0.2 in the logarithms, and the $[N_i/Fe]$ ratios for 28 elements were the same as in the sun within the probable error (which was ±0.07 to ±0.30) except possibly for Na, +0.30 ± 0.20. This research involved the ultimate present observational and astrophysical techniques, and resulted mainly in establishing the normalcy of normal stars.

The stars with "peculiar" spectra provide much grosser phenomena, and the number of types of these is at first bewildering. A peculiar spectrum is defined as one in which the intensities of lines present deviate grossly from those in normal stars of approximately the same (T, P_e). Visual inspection, often at low dispersion, has been sufficient to reveal these peculiarities. Table 6 gives a brief description of the best known types of peculiar stars; since many of these are rare or faint, quantitative analyses are difficult, and in addition physical conditions may be quite unusual, e.g., large magnetic fields, or in the cool red giants, strong molecular bands. Only such objects as have elemental abundances abnormal by a factor of 10 or more can be reliably noted at low dispersion, or studied quantitatively at moderate scale.

In Table 7 I give a résumé of almost forty elements noted as peculiar in quantitative work of this more approximate type. They are classified here by the type of nuclear process now supposed to be responsible for their anomalous abundance. We are near the end of our problem, and I would like to review very briefly the current theory of nucleosynthesis in the stars.

Table 6

Common Types of Stars With Peculiar Abundances

Name	Characteristics
DO, sdO	Subluminous hot stars, He/H ratio abnormally high.
Bp	He rich stars of wide range of luminosity.
WC, WN	High-luminosity hot stars, C/N ratio abnormal.
Ap	Large magnetic fields; many types of elements enhanced, e.g., Si, Mn, Sr, rare earths, P, He^3, Be, Ga, etc. Abnormally weak O, N.
Am	Apparent anomalies in Ca, Ti, Mg, Sc.
C	Carbon-rich red giants. C^{12}/H, and sometimes C^{13}/C^{12} high.
Barium	Red giants with fifth-period elements, rare earths and C enhanced.
S	Variable, cool, red giants with fifth-period elements, C and Tc enhanced.
T-Tauri	Unstable, contracting young stars with Li enhanced.
F, G subdwarfs	Solar-type stars with low metal/hydrogen ratio.

THE ORIGIN OF THE ELEMENTS

The overwhelming abundance of hydrogen, especially in the old stars, and an aesthetic desire for simplicity suggested long ago that the elements were built from protons and neutrons. A single-event, high-density early phase of the expanding universe had been suggested by Lemaître and Gamow, but at present the more detailed and plausible hypothesis adopted is that elements are synthesized as a byproduct of thermonuclear energy-producing reactions inside stars. Since a normal main-sequence star like the sun converts H into He at such a rate that in 10^{11} years no H would remain, it is clear that with a galaxy 10^{10} years old, stars of low luminosity like the sun do not yet play an important role. However, stars undergo complex evolutionary changes once 10 percent of their hydrogen is exhausted; they heat up, brighten, expand, become red giants and eventually contract into white dwarfs, or they explode. The time before this evolutionary phase begins, τ_H, is approximately:

$$\tau_H = 10^{10} \frac{M/M_\odot}{L/L_\odot} \approx 10^{10}(M/M_\odot)^{-5/2}, \tag{10}$$

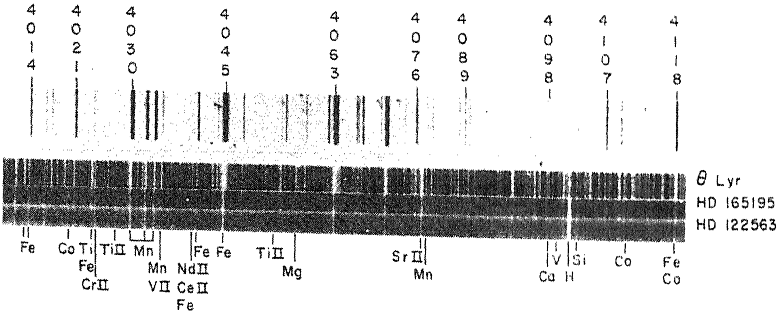

Figure 6. Two very metal-poor, old, red-giant stars are compared with a young, normal red giant θ Lyrae. The stars have nearly the same temperature, 4400°K, and surface gravity, but the metal/hydrogen ratio in HD 165195 and HD 122563 is about 100 times lower than in θ Lyrae. Note the great weakening of Fe, Mn, Sr II, and the great strength and nearly complete absence of Stark effect in λ 4101 of hydrogen.

where mass and luminosity are expressed in solar units and the mass-luminosity law has been used. Note that a star with a mass 10 times the sun will have τ_H of only 3×10^7 years. Massive stars condense out of interstellar gas, conserve their hydrogen and evolve very rapidly, so that they may synthesize new heavy elements and exploding, return them to the interstellar

Table 7

Nuclear Processes Affecting Elements With Abundances Significantly Variable From Star to Star

Thermonuclear Energy Sources	Slow Neutron Capture	Fast Neutron Capture	Alpha Capture	Spallation High Energy	Unknown (Probably High Energy)	Equil. at High Temperature
H^1	S	Eu	C^{12}	He^3	O^{16}	V
He^4	Y^{89}	Gd	Ne	Li	Si	Mn
Li	Zr	--	Mg	Be^9	P^{31}	Fe
Be^9	Nb^{93}	--	Si	--	S	--
C^{12}	Mo	--	Ca	--	Ga^{69}	--
C^{13}	Tc	--	Ti	--	Kr	--
N^{14}	Ba	--	--	--	Hg	--
	La					
	Most rare earths					

gas, in 0.3 percent of the lifetime of a star like the sun. It is therefore the rapidly evolving massive stars that are the major contribution to nucleosynthesis. In 10^8 years after the first massive stars condensed out of what I will assume to be initially pure hydrogen, the interstellar gas is contaminated by nuclear waste products. It takes 10^8 years for a star of 0.8 $M_\odot$ merely to condense from the gas. The early stages of our Galaxy, before matter had largely condensed into stars was the epoch of rapid star formation, during which rapidly evolving massive stars built most (but not all) of the heavier elements. What we see now as peculiar stars are examples where many nuclear processes can now be seen still in operation. They provide therefore strong indications as to the long past, early stages of our system.

The processes [6] that account for the majority of the isotopes of the elements are as follows:

(1) Thermonuclear burning of protons (1 to 15 million degrees) produces D^2, He^3, He^4. D^2 is rapidly destroyed.

(2) Thermonuclear burning of He^4 (200 million degrees) makes C^{12}, O^{16}, Ne^{20} and other integral-alpha nuclei possibly up to Ti^{48}.

(3) Catalysis of proton burning by the presence of C^{12}, O^{16}, Ne^{20} yields He^4 as the main product and C^{13}, O^{17}, Ne^{21}, N^{14}, N^{15}, Ne^{22}, Na^{23} (10-30 million degrees).

(4) Neutrons are released by $C^{13}(\alpha,n)O^{16}$, $O^{17}(\alpha,n)Ne^{20}$, $Ne^{21}(\alpha,n)Mg^{24}$. These neutrons may be captured by elements like Si or Fe and produce essentially all the heavy elements up to Pb; there are two chains of neutron capture, called the s (slow) and r (rapid) processes, depending on the interval between neutron captures relative to the beta-decay lifetimes. The r process is needed to make elements heavier than lead, and some of the isotopes of lighter elements.

(5) The "equilibrium" process appears at very high temperatures, 2 to 4 billion degrees, in collapsing stars that will explode. At these temperatures essentially all nuclear processes occur and only the most stable nuclei, centered on Fe, survive. It is thought that supernova explosions are connected with the e-process, the r-neutron process, and neutrino emission.

(6) Surfaces of stars may act as accelerators, moving magnetic fields causing electro-magnetic discharges (magnetic Ap stars). Protons, or heavier ions, at energies of 0.2 to 1 Bev cause nearly complete disintegration of nuclei of moderate atomic weight. This "spallation" yields such fragments as neutrons, D^2, He^3, He^4, Li^6, Li^7, Be^9, B^{10}, B^{11}. The direct formation of spallation products such as D^2, Li^6---B^{11} is essentially the only method of producing such nuclei, which if formed

in stellar interiors would be immediately consumed. The neutrons released may have secondary effects.

Spectroscopically peculiar stars have been found which display effects of nearly all of these nuclear events. Table 7 has listed a classification by nuclear process of the elements whose abundance has been found to be anomalously high or low. Not all peculiarities need to be real, since complex excitation phenomena often occur in stars. In addition, not all abundance anomalies noted can be explained. Figure 7 shows the evidence for the presence of He^3 in a Bp star (possibly related to the magnetic stars). The wavelength shift between He^3 and He^4 is not large compared to the normal broadening of lines in hot stars, and in addition, pressure shifts of He^4 may occur. However, in this one star (called 3 Centauri A) the correlation of measured wavelengths and the laboratory shifts is quite good, and the He present is largely He^3. No good theory for synthesizing so much He^3 exists; the same star has large excesses of P, Ga, Kr. In Figure 8, some spectra by Searle and Sargent

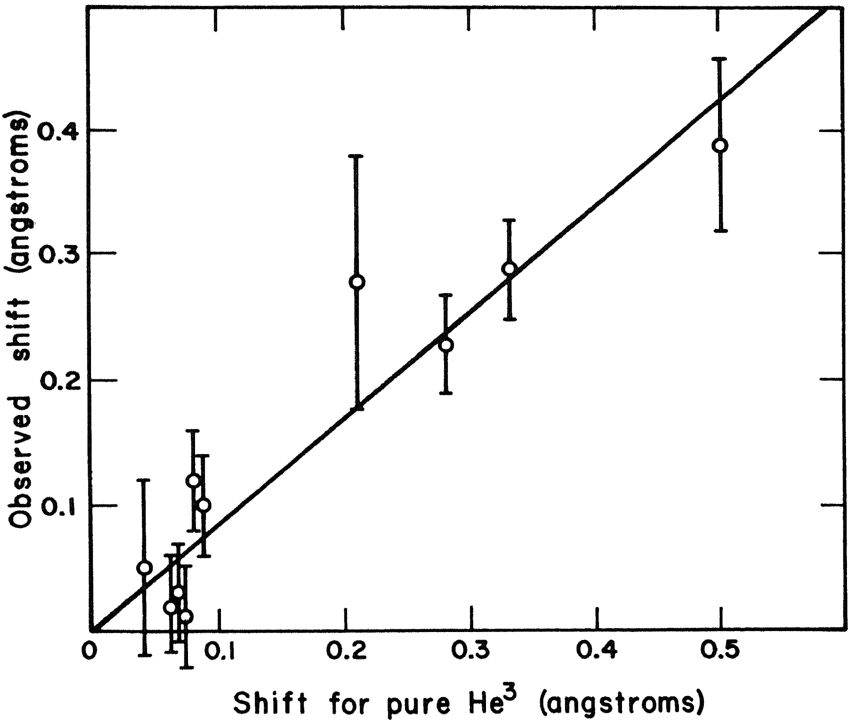

Figure 7. Wavelength shifts of He I lines in the star 3 Centauri A correlated with the isotope shift for He^3 (Sargent and Jugaku).

of magnetic Ap stars are shown, as compared to a normal main-sequence A star at the top. The λ4200 peculiarity involves a strong Si II line; the other stars have Mn, Si, Cr and the rare earths, and Sr excesses. Such objects have surface compositions almost certainly affected by surface reactions with high energy particles. Details have not been explored, but it is likely that r-process neutron reactions occur, together with spallation. Figure 9 shows the wide variations in the Be abundance in magnetic-peculiar stars. The resonance lines of Be II are difficult to observe (near the ozone cutoff) but are sometimes greatly enhanced. Figure 10 shows a section of high dispersion spectra of two Ap stars by Bidelman. In these, normal metallic lines of the comparison spectra are nearly submerged by a very large number of rare-earth and heavy-element lines.

In a very important peculiarity connected with spallation reactions, the element Li is found in newly forming stars, the

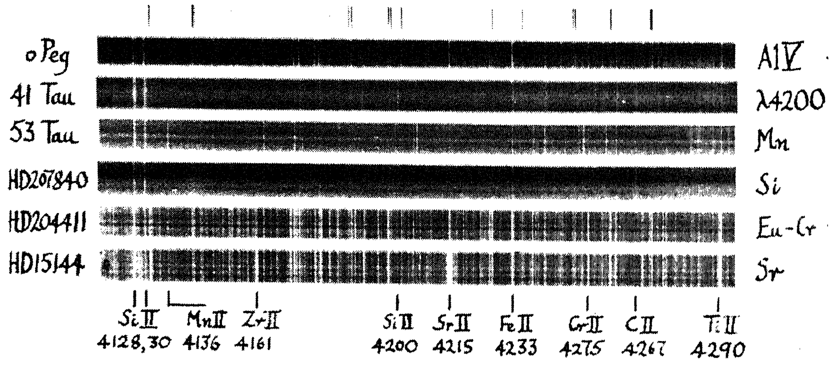

Figure 8. Varieties of magnetic-peculiar stars, near 10,000°K, compared with a normal star (top strip) of similar temperature (Searle and Sargent).

"T Tauri variables." These objects are still immersed in dense dust and gas, have strange spectra, but are the only known group with strong Li I (except for a few cool red giants). It has been conjectured [6] that D^2, Li, Be, B are now being formed around these stars during the contraction process, when the star must dispose of excess magnetic fields and angular momentum—possibly during formation of a planetary system.

Turning to the more normal thermonuclear reactions occurring inside stars during their burning of hydrogen, it can be said that a wide variety of confirmations of the predictions of nuclear astrophysics is provided by study of red giants, old stars and white dwarfs. In the red giants, analyses have shown that in the carbon-rich group, C^{12} (formed from 3 He^4 nuclei) is often greatly overabundant. In some of the carbon-rich stars,

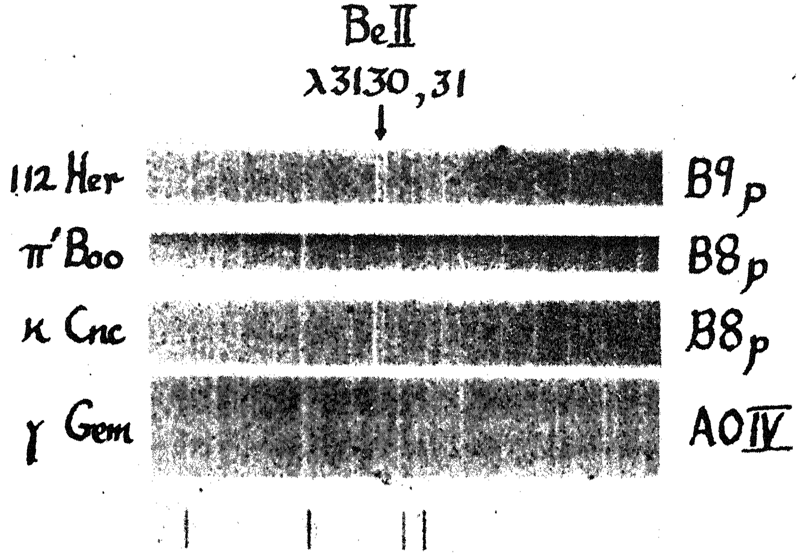

Figure 9. Enhancement of a spallation product, Be, in two magnetic stars (Searle and Sargent).

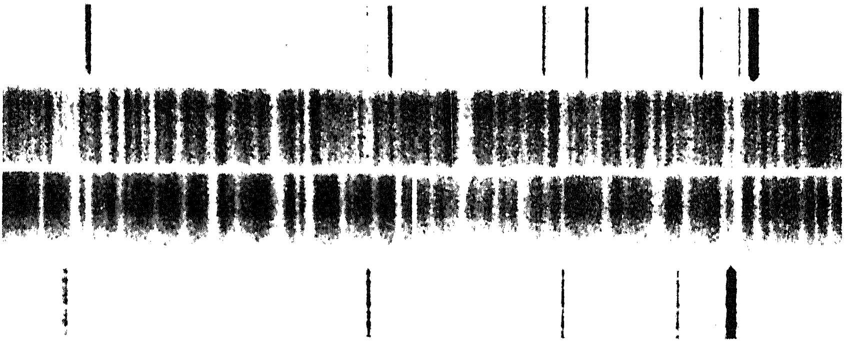

Figure 10. High-dispersion spectra of Ap stars (Bidelman, Lick Observatory) HR 465 (top), HR 4816 (bottom). Very strong lines of Dy II, Nd II and Mo II are present in HR 465.

C^{13}/C^{12} may reach 1/4 instead of 1/90 on the earth. N^{14}/C is greatly increased in certain hot old stars, and possibly in the hot high-luminosity WN stars. Many classes of stars are He rich—some white dwarfs show nothing but He lines in their spectra. Another very strange group of white dwarfs has just been recognized as showing only very diffuse, pressure-broadened bands of C_2. These bands have no trace of the sequences of vibrational heads (the dispersion is too low to show rotational structure) but the (0,0) and (1,0) bands are clearly seen, stretching over 200 Å each. One white dwarf, with Fe I lines, has been found to have a collisional damping constant of 10^{13}, i.e., 10^5 times the classical value. The mean pressure is about 2000 atmospheres. It is probable that pressure shifts are to the violet by about 2 Å. They are of van der Waals type as would arise from Fe + He collisions, according to the laboratory measures of Ch'en [7], since Fe + H collisions give red shifts. The exhaustion of H is essentially complete in very old stars.

The effects of neutron-addition processes are observable in a wide variety of red giants, and are often connected with carbon excess. The neutron flux per initial Si or Fe atom dictates how many atoms of heavy elements are built. Their relative abundances are dictated by the neutron-capture cross sections; an element with a large-capture cross section will be destroyed rapidly once built. Nuclear properties and regularities are well known in the laboratory, although many capture cross sections for 10 kev neutrons are still needed. In general, near the so-called magic number nuclei, there are pronounced minima. In a steady state, as neutrons build and destroy a given nucleus, a smooth curve of the relative abundances of the nuclei is established, with maxima near the magic-number nuclei. Spectroscopically, the consequences of these predictions are most important for elements of the fifth period, which have normal abundances only about 10^{-2} to 10^{-3} those of the fourth period. In the S stars, molecular bands of ZrO, LaO, YO, NbO are strong, while in normal M stars of the same temperature, TiO, VO, ScO are seen. The abundance of the iron-group elements seems to be diminished, while the heavier elements are enhanced. With these come the rare earths built on the s-process, which are all greatly enhanced. Included is technetium, Tc, which is spectroscopically analogous to Mn, i.e., a few strong ground lines from the ground S state. The enhancement of Tc is particularly striking since none exists on the earth because of the short radioactive decay. Tc has about the same abundance as Mo or Ru in the S stars.

It would be pointless to go into further detail about the various nuclear processes that have been confirmed by stellar abundance anomalies, or to list the unexplained anomalies. Serious questions in the overall theory concern the nature of rotationally driven, convective or other types of mixing in the stars, between the hot core where reactions occur and the upper few hundred kilometers of atmosphere where the spectra are observed. Another question is the rate of star formation at different epochs in the early history of our Galaxy, or in different parts of it now. As to the rest of the universe, our knowledge is meager. Other galaxies cannot be studied in much detail; individual stars in galaxies at 10^7 light years distance are observed only at low dispersion. Composite spectra of galaxies show mainly that the abundances of the easily observed elements are approximately the same, in that features due to H, He, Ca, Na, CN, CH, Fe, TiO are seen most prominently. Bright emission nebulae can be seen in the nearer galaxies, and show lines of H,

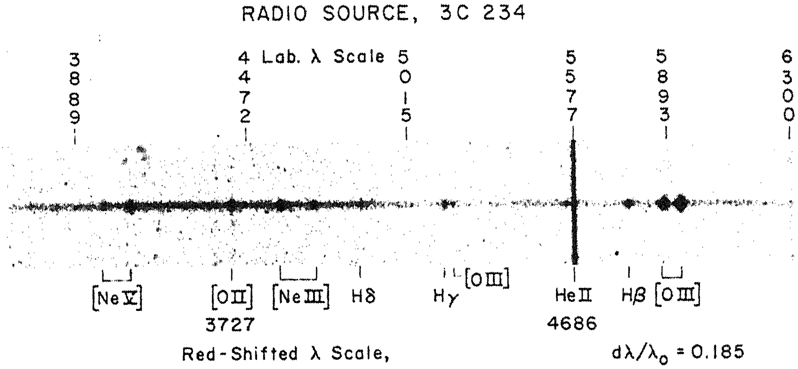

Figure 11. Spectrum of a distant, faint galaxy, the strong radio source 3C234. The night sky lines cross the whole spectrum, the emission lines of the galaxy are concentrated in the central streak. The level of ionization is very high, [Ne V] having an ionization potential of 126 ev. The electron temperature is also very high.

He, N, O, the abundant elements in our own system. Figure 11 shows a spectrum obtained by M. Schmidt, of a very distant object, a radio source 3C234, at a red shift $d\lambda/\lambda_0 = 0.185$, i.e., 56,000 km/sec, about 1.5 to 2 billion light years distant. This extraordinary object has a large fraction of its light in forbidden emission lines of H, He, O and Ne. At least these elements exist at 2 billion light years, and a line of [O II] is seen in the most distant object known, a radio source near 6 billion light years distance. So far, at least, spectroscopy casts some light in the enormous darkness.

BIBLIOGRAPHY

1. Aller, L. H., *The Abundance of the Elements* (New York: Intersci. Pub., Ltd.), 1961; see also, *Stellar Atmospheres*, ed. J. L. Greenstein, 1960 (Chicago: University of Chicago Press), Chaps. 4, 5.
2. Kolb, A. C. and Griem, H., *Phys. Rev.*, *116*, 4 (1959).
3. Biermann, L. and Lüst, R., *Stellar Atmospheres*, ed. J. L. Greenstein, 1960 (Chicago: University of Chicago Press), Chap. 6.

4. Goldberg, L., Müller, E. A. and Aller, L. H., *Astrophys. J. Suppl.*, *5*, 1 (1960).
5. Wallerstein, G., *Astrophy. J. Suppl.*, *6*, 407 (1962), summary review; see also, Astrophys. J., *129*, 347, 720 (1959); *132*, 553 (1960); *133*, 101, 562 (1961).
6. Burbidge, E. M., Burbidge, G. R., Fowler, W. A. and Hoyle, F., *Rev. Mod. Phys.*, *29*, 547 (1957); Fowler, W. A., Greenstein, J. L. and Hoyle, F., *Geophys. J. R. A. S.*, *6*, 148 (1962); Greenstein, J. L., *Mem. soc. roy. sci. Liège*, *14*, 307 (1954); Fowler, W. A. and Greenstein, J. L., *Proc. Nat. Acad. Sci.*, *42*, 173 (1956).
7. Ch'en, S. Y. and Chandrasekharan, V., *Astrophy. J.*, *133*, 1067 (1961).

PRESENT STATUS OF OUR KNOWLEDGE OF ATOMIC TRANSITION PROBABILITIES

W. L. Wiese
National Bureau of Standards
Washington, D. C., U.S.A.

INTRODUCTION

Spectral lines are usually characterized by wavelength and intensity. While the wavelengths of several hundred thousand atomic lines are known to an extremely high accuracy, often to six or more significant figures, the situation is very different for the intensity of the lines. The intensity is, first of all, not an atomic constant like the wavelength, but depends strongly on the mode of excitation of the light source, and is, for example, in a thermal light source a function of temperature and density. Therefore, relative intensities, as given in most spectral line tables, can be used with confidence only if it has been ascertained that the source used is similar in its properties to the one utilized for the tables. The brightness or strength of a line emitted by an optically thin source is determined by its transition probability for spontaneous emission, namely the probability per unit time that a radiative transition from a higher excited atomic level to a lower level occurs. If the emission takes place in a strong radiation field, induced emission and absorption occur. The probabilities for these processes are defined in an analogous fashion, and all three are interrelated. Transition probabilities are sometimes also referred to as Einstein coefficients. The classical equivalent is the oscillator strength, or f-value, and in quantum mechanics the term line strength is frequently used. A table for the mutual conversion of these quantities is given in the appendix (Table 2).

The present status of our knowledge of atomic transition probabilities may briefly be expressed in the following way: Transition probabilities are known only for a small percentage of the lines for which the wavelengths are known, and the accuracy of the available values is, aside from a few special cases, usually poor; even the first significant figure is quite often not reliable.

AVAILABILITY OF TRANSITION PROBABILITIES

The numerical data on transition probabilities are widely scattered in the technical literature. No general exhaustive tabulations of the numerical values are available yet, although there are a few tables of limited scope in the literature.* Therefore, two years ago a data center on atomic transition probabilities was established at the National Bureau of Standards with the objectives to collect and catalogue all relevant literature, to extract and analyze the numerical data, and to prepare and publish bibliographies and general tables of the "best" numerical values. The literature collection is now completely up-to-date, and the current literature including the major abstracting journals is constantly being monitored. A general bibliography on transition probabilities has been prepared and has been published as an NBS Monograph [2]. In this monograph the relevant literature is arranged according to elements and stages of ionization, and for quick orientation the method employed and the class of transitions are indicated behind each reference. All articles on discrete transitions, both permitted and forbidden, regardless of quality, are listed. From the data of the bibliography Table 1 has been assembled which shows the availability of literature for the different elements. The table is arranged with increasing atomic number, which is given in column 3. Column 4 lists all stages of ionization for which references are available (I = neutral atom, II = singly ionized atom, etc.). A subscript f indicates that only material on forbidden (electric quadrupole or magnetic dipole) transitions is known. Hydrogen-like ions, i.e., those atoms with all but one electron stripped off, are not included because their transition probabilities can be obtained from the relations given in Table 2.

In addition, column 5 shows the availability of f-values obtained from the large scale intensity measurements of Meggers, Corliss and Scribner [3]. The derived f-values have been recently published as an NBS Monograph [4]. The arabic numbers in brackets give the number of lines measured. A detailed discussion of this work will be given below.

The table shows clearly the decrease in the amount of material as the atomic number increases, and should be helpful for a first, rough orientation on the availability of literature. The bibliography itself shows that sometimes only one or two articles

---

*Reference 2 contains a comprehensive list of these.

Table 1

Availability of Atomic Transition Probabilities

All stages of ionization (I = neutral atom, II = singly ionized atom, etc.) are listed, for which numerical data exist. A subscript "f" indicates that only data on forbidden lines are available. Hydrogen-like ions are not included. For their relations to hydrogen see the appendix. Column (5) contains the data from the line intensity measurements at NBS (see text). The arabic numbers in brackets give the number of lines measured.

Element (1)	Symbol (2)	Z (3)	Stage of Ionization (4)	Additional Values by Corliss and Bozman (not included in (4)). Stage of Ionization (5)
Hydrogen	H	1	I	
Helium	He	2	I II	
Lithium	Li	3	I II	I[7]
Beryllium	Be	4	I II III	I[17] II[2]
Boron	B	5	I II III IV	I[4]
Carbon	C	6	I II III IV V	I[1]
Nitrogen	N	7	I II III IV V VI	
Oxygen	O	8	I II III IV V VI VII	
Fluorine	F	9	I II III IV V VI VII	
Neon	Ne	10	I II III IV V VI VII VIII IX	
Sodium	Na	11	I II III IV V VI VII VIII IX	I[12]
Magnesium	Mg	12	I II IV V VI VII VIII IX X	I[19] II[6]
Aluminum	Al	13	I II III V VI VII VIII IX X XI	I[16]
Silicon	Si	14	I II III IV VI VII VIII IX X XI XII	I[15]
Phosphorus	P	15	I II III IV V VII VIII IX X XI XII XIII	I[9]

Table 1—Continued

Element (1)	Symbol (2)	Z (3)	Stage of Ionization (4)	Additional Values by Corliss and Bozman (not included in (4)). Stage of Ionization (5)
Sulfur	S	16	I II III IV V VI VIII IX X XI XII XIII_f	
Chlorine	Cl	17	I II III IV V VI VII IX X XI XII XIII XIV_f	
Argon	Ar	18	I II III IV V VI VII VIII X XI XII XIII XIV XV_f	
Potassium	K	19	I III IV V VI VII VIII IX XI XII XIII XIV XV XVI_f	I[8]
Calcium	Ca	20	I II IV V VI VII VIII IX X XII XIII XIV XV XVI_f XVII_f	I[69] II[10]
Scandium	Sc	21	I II V VI VII VIII IX X XI	I[230] II[81]
Titanium	Ti	22	I II VI VII VIII IX X XI XII	I[707] II[178]
Vanadium	V	23	I II VII VIII IX X XI XII XIII	I[795] II[219]
Chromium	Cr	24	I II IV_f VIII IX X XI XII XIII XIV	I[615] II[177]
Manganese	Mn	25	I II V_f IX X XI XII XIII XIV XV	I[290] II[54]
Iron	Fe	26	I II III IV_f V_f VI_f VII_f X XI XII XIII XIV XV XVI	I[671] II[80]
Cobalt	Co	27	I XI XII XIII XIV XV XVI XVII	I[602] II[57]
Nickel	Ni	28	I II III_f XII XIII XIV XV XVI_f XVII XVIII	I[242] II[4]
Copper	Cu	29	I XIX	I[46] II[10]
Zinc	Zn	30	I II	I[18] II[2]

Table 1—Continued

Element (1)	Symbol (2)	Z (3)	Stage of Ionization (4)	Additional Values by Corliss and Bozman (not included in (4)). Stage of Ionization (5)
Gallium	Ga	31	I	I[15]
Germanium	Ge	32	---	I[43]
Arsenic	As	33	---	I[25]
Selenium	Se	34	II	I[5]
Bromine	Br	35	---	
Krypton	Kr	36	I III$_f$	
Rubidium	Rb	37	I II	I[13]
Strontium	Sr	38	I II	I[67] II[9]
Yttrium	Y	39	I II	I[260] II[110]
Zirconium	Zr	40	I II	I[700] II[322]
Niobium	Nb	41	---	I[1062] II[314]
Molybdenum	Mo	42	I	I[1258] II[208]
Technetium	Tc	43	---	
Ruthenium	Ru	44	I	I[915] II[52]
Rhodium	Rh	45	---	I[434] II[25]
Palladium	Pd	46	---	I[76] II[4]
Silver	Ag	47	I	I[11] II[4]
Cadmium	Cd	48	I II	I[20] II[4]
Indium	In	49	I	I[21] II[1]
Tin	Sn	50	I	I[59]
Antimony	Sb	51	---	I[53]
Tellurium	Te	52	---	I[12]
Iodine	I	53	I II	
Xenon	Xe	54	I II$_f$ III$_f$	
Cesium	Cs	55	I	I[19]

Table 1—Continued

Element (1)	Symbol (2)	Z (3)	Stage of Ionization (4)	Additional Values by Corliss and Bozman (not included in (4)). Stage of Ionization (5)
Barium	Ba	56	I II	I[79] II[16]
Lanthanum	La	57	II	I[270] II[272]
Cerium	Ce	58	---	II[1349]
Praseodymium	Pr	59	---	II[232]
Neodymium	Nd	60	---	I[80] II[275]
Promethium	Pm	61	---	
Samarium	Sm	62	---	I[221] II[780]
Europium	Eu	63	---	I[298] II[149]
Gadolinium	Gd	64	---	I[520] II[581]
Terbium	Tb	65	---	I[3]
Dysprosium	Dy	66	---	II[86]
Holmium	Ho	67	---	I[3]
Erbium	Er	68	---	II[78]
Thulium	Tm	69	---	I[62] II[157]
Ytterbium	Yb	70	---	I[53] II[281]
Lutetium	Lu	71	---	I[82] II[81]
Hafnium	Hf	72	---	I[433] II[309]
Tantalum	Ta	73	---	I[789] II[288]
Tungsten	W	74	---	I[1045] II[108]
Rhenium	Re	75	---	I[824] II[48]
Osmium	Os	76	---	I[912] II[35]
Iridium	Ir	77	---	I[511]
Platinum	Pt	78	---	I[161] II[1]
Gold	Au	79	I	I[26]
Mercury	Hg	80	I II III IV	I[19]

Table 1—Continued

Element (1)	Symbol (2)	Z (3)	Stage of Ionization (4)	Additional Values by Corliss and Bozman (not included in (4)). Stage of Ionization (5)
Thallium	Tl	81	I	I[18]
Lead	Pb	82	I	I[38] II[1]
Bismuth	Bi	83	I	I[32]
Polonium	Po	84	---	
Astatine	At	85	---	
Radon	Rn	86	II$_f$	
Francium	Fr	87	---	
Radium	Ra	88	---	
Actimum	Ac	89	---	
Thorium	Th	90	---	I[342] II[789]
Protactinium	Pa	91	---	
Uranium	U	92	---	I[326] II[316]

Appendix to Table 1. Conversion Factors

The numerical factors relating the quantities A_{ki}, f_{ik}, and S are given in the table below, where:

A_{ki} is the transition probability for spontaneous emission (sec^{-1}).
f_{ik} is the absorption oscillator strength (dimensionless).
S is the line strength in atomic units, which are:

For electric dipole transitions (allowed - denoted by E_d):

$$a_o^2 e^2 = 6.459_4 \times 10^{-36} \text{ cm}^2 \text{ esu}^2;$$

for electric quadrupole transitions (forbidden - denoted by E_q):

$$a_o^4 e^2 = 1.808_8 \times 10^{-52} \text{ cm}^4 \text{ esu}^2;$$

for magnetic dipole transitions (forbidden - denoted by M_d):

$$e^2 h^2/16\pi^2 m_e^2 c^2 = 8.599 \times 10^{-41} \text{erg}^2 \text{ gauss}^{-2}.$$

The wavelength λ is given in Angstrom units.

g is the statistical weight.

The factor in each square converts by multiplication the quantity above it into the one at its left. The upper energy level of a transition is denoted by the subscript k, the lower by i. The initial state is written first, i.e., i first means absorption.

Table 2

Conversion Factors

	A_{ki}	f_{ik}	S
A_{ki}	1	$\frac{6.670_2 \times 10^{15}}{\lambda^2} \frac{g_i}{g_k}$	E_d $\frac{2.026_1 \times 10^{18}}{g_k \lambda^3}$ E_q $\frac{1.679_8 \times 10^{18}}{g_k \lambda^5}$ M_d $\frac{2.697_2 \times 10^{13}}{g_k \lambda^3}$
f_{ik}	$1.4992 \times 10^{-16} \lambda^2 \frac{g_k}{g_i}$	1	E_d $\frac{303.7_5}{g_i \lambda}$ E_q $\frac{251.8}{g_i \lambda^3}$ M_d $\frac{4.043_6 \times 10^{-3}}{g_i \lambda}$
S	E_d $4.935_6 \times 10^{-19} g_k \lambda^3$ E_q $5.953 \times 10^{-19} g_k \lambda^5$ M_d $3.707_6 \times 10^{-14} g_k \lambda^3$	E_d $3.292_1 \times 10^{-3} g_i \lambda$ E_q $3.971 \times 10^{-3} g_i \lambda^3$ M_d $247.3_0 g_i \lambda$	1

Appendix to Table 2

Besides the quantities introduced above, the following are also in use and are related to them by:

1. Transition probability of absorption B_{ik}

$$B_{ik} = 6.01\lambda^3 \frac{g_k}{g_i} A_{ki};$$

2. Transition probability of induced emission B_{ki}

$$B_{ki} = 6.01\lambda^3 A_{ki};$$

3. Emission oscillator strength f_{ki}

$$f_{ki} = \frac{g_i}{g_k} f_{ik}.$$

Finally, it should be noted that the line strength S is symmetrical:

$$S = S_{ik} = S_{ki}.$$

Since hydrogen-like ions (with one electron and nuclear charge Z) have intensity quantities which are simply related to hydrogen, papers dealing with these ions are not included in the bibliography. For convenience, the relations are given below:

$$f_Z = f_H \qquad S_Z = Z^{-2} S_H \qquad A_Z = Z^4 A_H.$$

* * *

The numerical values for the natural constants were taken from Cohen, E. R., Crowe, K. M. and Dumond, J. W. M., Fundamental Constants of Physics (Interscience Publishers, Inc., New York, 1957).

are available per element, and only the transition probability for the resonance line may have been determined. But, judging from our experience gained in the data center, it should generally be possible now to obtain reliable transition probabilities for the strongest lines of the important light elements and some metals.

If the transition probability for a particular line has been found in the literature, the question of its accuracy arises. A critical evaluation is very difficult. The theoretical determinations generally cannot give estimations of the size of the errors introduced by the various approximations, and experience shows that in many experimental determinations sources of systematic error have been overlooked. In the following sections the major theoretical and experimental methods are briefly reviewed with the emphasis on discussing their accuracy.

DISCUSSION OF THEORETICAL AND EXPERIMENTAL METHODS

Calculations based on the self-consistent field approximation

Aside from the Coulomb-Approximation, which will be discussed later, this method has found the most general use for the calculation of f-values. It provides a set of wave functions for the atomic electrons, which produces an approximately self-consistent field. The transition probabilities are then determined by integration over the radial parts of these wave-functions. A short outline of the procedure, developed by Hartree and extensively described by him [5], is given below:

It is assumed that the charge density distribution of the atomic system is spherically symmetric, i.e., the potentials of the electrons depend only on their radial positions. Correlations between the electrons are neglected; all are supposed to move independently in the central field, experiencing only the averaged charge distribution of the other electrons and the nucleus. With these simplifications the motions of the individual electrons can be calculated by assuming trial wave-functions for the others, and from the resulting wave-functions the charge density distribution is computed and compared with the initial one obtained with the trial functions. If self-consistency is not achieved, the new, computed wave-functions are used as trial-functions and the procedure is repeated until initial and final charge distributions are identical, i.e., the field is self-consistent.

This basic procedure was improved by Fock, who included exchange effects between electrons of the same spin [6], and by Biermann, Trefftz and others, who also took into account other correlations between the electrons [7] and, in particular, polarization of the core electrons by the excited electron [8] and configuration mixing [9].

The self-consistent field method does not permit an estimation of the errors introduced by the various approximations. However, comparison with experimental results and internal consistency checks applying the "dipole-length" and "dipole-velocity" formulas [7] show that at least for simpler atomic systems accurate transition probabilities with overall uncertainties probably smaller than 20% are obtained, provided the refined procedure including exchange and other correlation effects is applied.

Measurements in Emission

Experimentally, the largest number of f-values so far has been obtained from measurements of the intensities of spectral lines which are emitted from plasmas under well known conditions. The plasma sources are various types of arcs and, to a lesser extent, shock-tubes. Astrophysicists have also utilized the spectra of carefully analyzed stellar atmospheres. The method is briefly as follows: The transition probability for spontaneous emission from state k to state i, A_{ki}, is defined by the relation

$$J_{ki} = \frac{1}{4\pi} A_{ki} \, h\nu \, N_k , \tag{1}$$

where J_{ki} is the total intensity (in ergs sec^{-1} cm^{-3} sr^{-1}) of a line of frequency ν, h is Planck's constant and N_k the density of atoms in the upper state k. A_{ki} may therefore be obtained from the measurement of J_{ki} and the determination of N_k.

The experimental conditions are always chosen so that the plasma is approximately in a state of local thermodynamic equilibrium, because N_k is then a function of temperature and density only and can be determined from the application of equilibrium and conservation equations and measurements of the temperature and electron density. These measurements are mostly done spectroscopically from the determinations of the intensities of lines and continua of known transition probabilities and absorption coefficients or by measuring line profiles and utilizing the results of line broadening theory. This means in practice that hydrogen or helium, for which all the relevant data are rather precisely known, must be added to the plasma. But the introduction of another element complicates the diagnostics of the plasma, since the densities of additional species have to be determined. In arcs one also has to take into account "demixing" effects [10], which make the mixture ratio of cold gas mixtures unreliable for the description of the plasma.

The early arc work was done at Utrecht University starting about 1930. Free burning, unstabilized arcs were used for the determination of a large number of mostly relative transition probabilities for the alkalis, alkaline-earths and refractory metals. Temperatures of 4000-8000°K were reached in the arc column, which sufficed for the excitation of the stronger atomic lines of these elements [11].

In the 1950s high current arcs were developed at Kiel University and axis temperatures up to 50,000°K could be obtained [12]. The arc column was stabilized in its position and constricted by liquids, gases or cooled metallic walls. The wall-stabilized arc, now widely in use, is probably the most stable high temperature source [13]. These arcs have been applied in the last several years to measurements of f-values for numerous lines of several neutral and singly ionized elements, in particular carbon, nitrogen and oxygen.

In recent years the shock tube has gained in importance as a spectroscopic light source. At Michigan University the f-values for several elements were measured with a conventional, diaphragm-type shock-tube [14]. The thermal state of the plasma behind the shock front could be determined simply from the measured shock velocity and application of the equations for conservation of mass, momentum and energy, i.e., the Rankine-Hugoniot equations. A steady state with temperatures in the range from 5000-15,000°K was obtained behind reflected shocks for times as long as 100 μsec. Because of the short time scale no demixing can take place, but now spectroscopic techniques with good time resolution have to be applied, which are more complicated. Very fast pulse techniques are necessary for the recently developed magnetically driven shock tubes with which very high temperature plasmas in the range from 20,000 - 100,000°K may be produced. Here the stationary state behind the shock front lasts only for a time of the order of a microsecond. For magnetically driven shocks, the Rankine-Hugoniot relations may no longer be utilized for the determination of the state of the plasma, and the temperature and electron density have to be determined directly from measurements [15]. With such shock tubes the relative transition probabilities for some helium lines have already been measured [16], and measurements for some 0 III lines are under way [17].

The best absolute f-values obtained from emission experiments are accurate within 15%, but for the bulk of data reported in the literature errors between 20 to 50% must be expected and in some cases they may be even higher. This is especially true for the early arc experiments, which did not take into account the radial temperature and density distribution of the arc column. Only effective temperatures and densities were determined, which introduced some systematic uncertainties.

The state of local thermodynamic equilibrium seems to be always closely approximated, even in the fast, high temperature shock waves. Also, the plasmas have been generally checked for self-absorption. The demixing effect has made unreliable the results of some arc experiments with gas mixtures, in which the mixture ratio was utilized for the analysis. Other significant errors in emission experiments arise from difficulties in determining the continuous background under the lines, from neglecting the contributions of the distant line wings, from uncertainties in the standard light sources and from uncertainties in the high-density corrections due to interaction effects in dense plasmas. Measurements with wall-stabilized arcs should give the most accurate results.

Measurements in Absorption

The determination of f-values from absorption measurements is based on a method which is quite similar to the one used in the emission experiments, since the emission- and absorption-coefficients are proportional over the wavelength range of a line. The transition probability for absorption B_{ik} is introduced, analogous to Eq. (1), by

$$W^* = \frac{1}{4\pi} B_{ik} N_i u_\nu h\nu . \tag{2}$$

W^* is the energy absorbed in a spectral line (in erg sec^{-1} cm^{-3} and sr^{-1}), u_ν the density of the radiation field, and N_i is the population of the lower excited state, which is a function of temperature and total number density if thermal equilibrium exists. Frequently the absorption is expressed in terms of the intensity

$$J = \frac{c}{4\pi} u_\nu$$

of the radiation field as

$$W_\nu = W^*/J_\nu = \int \kappa_\nu \, d\nu = B_{ik} N_i \frac{h\nu}{c} \tag{2a}$$

with κ_ν being the absorption coefficient per cm length. W_ν is often referred to as the "equivalent width" of a line.

In the measurement of the total absorption of lines, the radiation field is produced by a light source giving a continuous spectrum such as the tungsten strip lamp. It then passes through the absorption tube, which is gas filled containing the element to be investigated. The tube has to be at a high temperature to achieve evaporation for the absorbing element, because this must be in the atomic state with sufficient population of excited levels. To do this, R. B. King and A. S. King and collaborators at the California Institute of Technology have used an electric furnace and reached temperatures up to 2600°K [18]. However, even at these temperatures only the lower excited levels of a number of metallic elements are sufficiently populated to produce strong enough absorption lines. Hence, the absorption measurements are confined to lines of refractory metals, alkalis, alkaline-earths, and resonance lines of some other elements.

For the determination of B_{ik}, again temperature and particle density measurements are required, assuming that thermal equilibrium exists. The temperature was generally obtained from pyrometric measurements, and the number density of absorbing atoms was determined from vapor pressure measurements in conjunction with available vapor pressure curves [19]. If vapor pressure curves were not known and only the temperature could be determined, relative f-values were obtained. Since the vapor pressure data at high temperatures are still somewhat unreliable, absolute f-values obtained this way should be treated with caution [20]. A big improvement in the absorption method was achieved by using an atomic beam as the absorber and condensing the atoms on a microbalance built into the chamber. Now the number densities could be determined from the increase of mass per unit time on the microbalance and from the mean velocity of the beam which is proportional to the square-root of the temperature. This method, developed by Kopfermann and Wessel in 1951 [21], has recently been used also at King's laboratory [20].

The major source of systematic errors in the older absorption-tube method are uncertainties in the vapor pressure data. In the case of the iron resonance line at 3070 A, these are probably responsible for the big discrepancy of about a factor of 3 between earlier measurements and the more recent results [20]. The overall uncertainty in atomic beam experiments should be, cautiously estimated, of the order of 20%. The main uncertainties are caused by fluctuations in the beam density, and reflection of a fraction of the atoms from the pan of the microbalance instead of adhering to it.

Lifetime Determinations

The direct measurement of lifetimes of excited atomic states, which are usually in the range from 10^{-7} to 10^{-9} sec, has been attempted for 40 years. Wien and his school produced in a high voltage discharge tube excited atoms and ions, accelerated them in the electric field and let them escape through a hole in the cathode (the "canal") into a high vacuum and observed the decay of light of this "canal ray" photographically [22]. But the canal ray method was still too crude to give reliable results. In the last ten years a number of different methods to study lifetimes of excited states have been devised, which are based mostly on fast counting techniques developed in nuclear physics [23]. The procedure is to excite atoms by radiation or electron impact in short bursts and to observe the subsequent depopulation of excited levels by studying the time decay of the emitted radiation. The population N_k of an excited level k decays according to

$$N_k = N_{o,k}\, e^{-\gamma_k t} \tag{3}$$

where $N_{o,k}$ is the population at time $t = o$. Thus, an exponential decay in the radiation is observed. The lifetime $\tau_k = \gamma_k^{-1}$ of the atomic state is related to the transition probability A_{ki} for spontaneous emission by

$$\tau_k^{-1} = \sum_i A_{ki} - \sum_i B_{ik}\, u(\nu_{ik}) + \sum_p B_{kp}\, u(\nu_{pk}) + Q\ , \qquad (4)$$

neglecting induced emission. Q denotes a term for the collisional population and depopulation rates. In order to obtain A_{ki}, one has to eliminate the collision term Q, and also keep the radiation field u_ν, produced by the decay, so small that the absorption terms (p denotes levels higher than k) are negligible. Both conditions are achieved at very low pressures. Furthermore, generally only the sum of all probabilities for transitions into lower levels i is obtained, and the A_{ki} for a particular transition can be obtained explicitly only in three cases: (a) The sum reduces to a single term, i.e., only transitions to the ground state are possible. This is for example the case for the resonance lines of the alkalis. (b) The sum is dominated by one strong term, e.g., it contains a transition of comparatively very high frequency ν (A_{ki} is proportional to ν^3), or all transitions but one are forbidden, i.e., have very small transition probabilities. (c) The relative transition probabilities contributing to the sum are known.

This method is, therefore, limited to only a few lines per atom, namely those originating from the lowest excited levels. But the results should be very accurate, with uncertainties less than 10 percent, since the method is simple and the instrumentation is by now well developed. The major uncertainties arise from cascading from higher levels, which repopulate the lower ones, and from depopulation by collisions.

Measurement of f-values from the anomalous dispersion at the edges of spectral lines

Rozhdestvenskii obtained as early as 1912 accurate numbers for the relative f-values of the two sodium D-lines from interferometric measurements of their anomalous dispersion [24], and since then a large number of f-values, predominantly relative, were determined in Russian and German laboratories with this method. It is based on the following idea: In the neighborhood of a spectral line the index of refraction n varies according to

$$n - 1 = \frac{e^2 N_i f_{ik}}{4\pi m_e c^2} \frac{\lambda_o^3}{\lambda - \lambda_o} \left(1 - \frac{N_k\, g_i}{N_i\, g_k}\right). \qquad (5)$$

Here g_p denotes the statistical weight of state p; k is the upper state; and e, m_e, c are the usual natural constants. If the gas is in thermal equilibrium, the population of the excited states is governed by the Boltzmann formula, so that usually $N_k \ll N_i$, and $N_k g_i / N_i g_k$ may be neglected. For the determination of $N_i f_{ik}$ the index of refraction n at the wavelength distance $\lambda - \lambda_o$ from the center of the line, λ_o, has to be measured. This can be most precisely done interferometrically with the "hook" method developed by Rozhdestvenskii, and extensively described by him [24]. In this method the gas to be studied fills an absorption tube, which is part of the interferometer. The tube must be at an elevated temperature to achieve evaporation and sufficient population of excited levels, as in the other absorption experiments. The level populations may again be expressed as functions of temperature and total density by using the Boltzmann formula. If only the temperature, but not the density can be measured, relative f-values are obtained. Absolute values were determined sometimes from vapor pressure measurements and, recently, from a combination of the anomalous dispersion and absorption method [25].

The accuracy of transition probabilities obtained with this method should be slightly better than in absorption experiments. While the product $N_i f_{ik}$ can be measured accurately, the major uncertainties come from the determination of the level populations N_i.

Other Methods

In addition to the major methods described above, a number of other theoretical and experimental methods have been employed for the determination of transition probabilities, but have not gained as much importance. Among other theoretical methods, the Wentzel-Kramers-Brillouin procedure [26] and the screening approximation by Layzer [27] and Varsavsky [28] need to be mentioned. The former has found application only in some special cases. The recently developed screening approximation was applied by Varsavsky to a large number of transitions [28]. The initial results do not always compare well with values obtained from other methods. But the theory is promising, and with further refinements good results should soon be forthcoming.

Other experimental methods make use of the magnetorotation, magnetic resonance and other effects. They have been applied only in special cases, but are capable of producing accurate f-values.

COMPREHENSIVE ARTICLES

The available literature is fortunately supplemented by two very comprehensive determinations of transition probabilities: The Coulomb-approximation by Bates and Damgaard [29] and the line intensity measurements at NBS [3,4]. While the latter work gives explicitly the f-values for 25,000 lines of 70 elements, the results of the former are presented in a set of tables, from which the f-values for many lines can be quickly derived.

The Coulomb-Approximation

Under the assumption of Russell-Saunders coupling the line strength S (for its relation to f and A, see table 2) may be expressed as the product of three factors [29]

$$S = \mathcal{S}(M)\ \mathcal{S}(L)\ \sigma^2 .$$

The first two factors represent the strength of the multiplet ($\mathcal{S}(M)$) and the fractional strength of the spectral line within the multiplet ($\mathcal{S}(L)$). The numerical values may be obtained from tables by Goldberg [30] and White and Eliason [31], which are also reproduced by Allen [32].

The difficult problem is the evaluation of the transition integral σ. Bates and Damgaard showed that in general the main contribution to the integral comes from a region in which the deviation of the potential of an atom or ion from its asymptotic Coulomb form is so small that it may be replaced by the latter. Since for the Coulomb potential an analytic solution of the transition integral is known, it is possible to calculate σ^2 as a function of the observed term value and the azimuthal quantum number. Bates and Damgaard have thus compiled tables with numerical values of σ^2 for s-p, p-d and d-f transitions.

The Coulomb approximation is restricted to transitions between levels having the same parent term. It gives the best results if the degree of cancellation in the transition integral is small, i.e., if σ^2 is not too close to zero, and if the upper and lower level of the excited electron is in a shell which contains no other electrons. This is true for the moderately and highly excited levels. But even if the lower level is in a shell which contains other electrons, the results agree fairly well with those obtained by other methods.

Comparison with other theoretical and experimental values shows that for simple atoms or ions, i.e., those with one electron outside closed shells like the alkalis, the agreement is especially good. The deviations are usually smaller than 10%. Also, for many of the more complex atomic systems, in particular for light elements, good agreement is obtained. Larger discrepancies are reported for heavier atoms [33], but here the lack of reliable data makes an assessment of the accuracy of the method difficult.

On the whole, this method has given remarkably good results and has proved to be of great value. It may be confidently used if the conditions as indicated above are met.

The Line Intensity Measurements at NBS

During the last 30 years Meggers, Corliss, and Scribner at NBS have determined relative intensities for 39,000 lines of 70 elements in the wavelength range of 2000-9000 A [3]. They used as their light source a free-burning d.c.-arc with copper electrodes into which 0.1 atomic percent of each element was mixed. The arc column was thus burning in air with an admixture of about 10^{-3} parts of copper and 10^{-6} parts of the element to be measured. In this way the same conditions for all 70 elements were obtained and comparisons on a uniform scale could be made. The line intensities were determined photographically with the following, somewhat simplified method: A relatively broad spectrograph slit was used to insure that all lines have the same width and a uniform intensity over their width. The relationship between measured photographic densities and relative intensities was then obtained in the usual manner using a standard light source in connection with a rotating step sector which produced known intensity steps.

The temperature of the arc was determined by comparing the measured line intensities with known transition probabilities. This could be done for 20 elements and good agreement among the individual determinations was obtained, indicating the general consistency of the data. After the arc temperature was established, the procedure was reversed and a large number of relative f-values for these and the other elements could be derived. These were then converted to an absolute scale as follows: Whenever good absolute f-values were available in the literature, the relative values were normalized against them. For all other elements the normalization factor was determined from the known ratio of the elements against copper. For second spectra the Saha equation was utilized. Altogether, absolute f-values were derived for 25,000 lines of 70 elements. For the other lines the necessary spectroscopic data, in particular the energy levels, were not available. The data have been recently published as an NBS Monograph [4]. In column 5 of table 2 the availability of this material is listed.

Although comparatively large errors in the absolute f-values of the order of a factor 2 may be expected, this work should be very valuable for all applications where high accuracy is not required. The main contributions in the error arise from uncertainties in the temperature and electron density determination, from possible "demixing effects" in the arc column, from statistical errors in the intensity measurements and from neglecting the radial temperature and density distribution in the arc.

In summary it may be said that the present status of our knowledge of atomic transition probabilities is still very far from complete, and much needs to be done. Especially critical is the almost complete lack of accurate f-values for the more complicated atomic systems. Thus one of the most important tasks is to improve the accuracy of the theoretical and experimental determinations.

Furthermore, it is very desirable to have a general tabulation of all numerical data available, as is the case for other atomic data like energy levels, etc. At NBS a critical evaluation of all data for the lightest ten elements and a tabulation of the "best" f-values is under way. This work will probably be completed at the end of this year and will be published as an NBS Monograph. Further tabulations for other elements are planned.

REFERENCES

1. A. Einstein, Physik. Z. 18, 121 (1917).
2. B. M. Glennon and W. L. Wiese, NBS Monograph 50 (1962).
3. W. F. Meggers, C. H. Corliss, and B. F. Scribner, NBS Monograph 32 (1961).
4. C. H. Corliss and W. R. Bozman, NBS Monograph 53 (1962).
5. D. R. Hartree, The Calculation of Atomic Structures, John Wiley and Sons, New York, 1956.
6. V. Fock, Z. Physik 61, 126 (1930).
7. E. Trefftz, A. Schlueter, K. H. Dettmar and K. Joergens, Z. Astrophys. 44, 1 (1957).
8. L. Biermann and E. Trefftz, Z. Astrophys. 26, 213 (1949).
9. E. Trefftz, Z. Astrophys. 26, 240 (1949).
10. F. Mastrup and W. L. Wiese, Z. Astrophys. 44, 259 (1958).
11. For example, J. Terpstra and J. A. Smit, Physica, 24, 937 (1958).
12. W. Lochte-Holtgreven, Reports on Progress in Physics, XXI, 312 (1958).
13. J. B. Shumaker, Rev. Sci. Instr. 32, 65 (1961).
14. O. Laporte and T. D. Wilkerson, J. Opt. Soc. Am. 50, 1293 (1960).
15. W. L. Wiese, H. F. Berg and H. R. Griem, Phys. Rev. 120, 1079 (1960).
16. E. A. McLean, Proc., IV. Symposium on Temperature, Its Measurement and Control, Reinhold Publishing Co., New York, 1962.
17. H. F. Berg (private communication).
18. R. B. King and A. S. King, Astrophys. J. 87, 24 (1938).
19. R. B. King and D. C. Stockbarger, Astrophys. J. 91, 488 (1940).

20. G. D. Bell, M. H. Davis, R. B. King and P. M. Routly, Astrophys. J. 127, 775 (1958).
21. H. Kopfermann and G. Wessel, Z. Physik 130, 100 (1951).
22. W. Wien, Ann. Physik 73, 483 (1924).
23. S. Heron, R. W. P. McWhirter, and E. H. Rhoderick, Proc. Roy. Soc. London A 234, 565 (1956).
24. D. Rozhdestvenskii, An. Physik 39, 307 (1912).
25. Yu. I. Ostrovskii, N. P. Penkin, and L. N. Shabanova, Soviet Phys.—Doklady 3, 538 (1958).
26. H. A. Kramers, Quantum Mechanics, North Holland Publishing Co., Amsterdam (1957).
27. D. Layzer, Am. Phys. 8, 271 (1959).
28. C. M. Varsavsky, Thesis Harvard 1958; and Astrophys J. Suppl. Ser. 6 (No. 53), 75 (1961).
29. D. R. Bates and A. Damgaard, Phil. Trans. Roy. Soc. London A 242, 101 (1949).
30. L. Goldberg, Astrophys. J. 82, 1 (1935) and 84, 11 (1936).
31. H. E. White and A. Y. Eliason, Phys. Rev. 44, 753 (1933).
32. C. W. Allen, Astrophysical Quantities, The Athlone Press, London, 1955.
33. C. W. Allen and A. S. Asaad, Monthly Notices Roy. Astron. Soc. 115, 571 (1955).

RECENT DEVELOPMENTS IN INFRARED ATOMIC EMISSION SPECTROSCOPY IN THE 1- TO 4-MICRON REGION

Curtis J. Humphreys
U. S. Naval Ordnance Laboratory
Corona, California, U.S.A.

INTRODUCTION

The range of spectral response of photographic emulsions has, to a large extent, established the boundaries of the regions of observation of atomic emission spectra. Although the frequency dependence of transition probabilities leads to the expectation that the preponderant energy in most atomic spectra will be emitted within the photographic region, there is abundant evidence that penetration of the artificial curtain near 1.3 μ can lead to the acquisition of material that is highly significant and in some cases indispensable for the complete analysis of spectra.

The author has reviewed the state of progress in the investigation of atomic spectra based on observations in the extra-photographic region in a series of articles [1,2,3] beginning with a presentation at the Rydberg Centennial Conference. In each instance it was noted that activity in this specialty is divided into two distinct periods separated by an interval of more than thirty years. The first period, ending about 1914, is represented almost entirely by the work of Paschen and his pupils, using thermal detectors, and is reported in the monograph by Paschen-Götze [4]. The modern period began with the introduction of photoconductive detectors shortly after the close of World War II.

It is the purpose of this article to emphasize the significance of a number of specific accomplishments rather than to reference all contributions, the latter objective having been realized in the article included in the special issue of the Journal of the Optical Society of America dedicated to Professor H. M. Randall [3].

THE PASCHEN ERA

The observations during the first period were all made upon relatively simple spectra, restricted essentially to the alkalis and alkaline earths. The energy limitation set by the use of thermal detectors—usually linear thermopiles—made it necessary to employ wide slits, something that in turn prevented the resolution of line structures or even the finer details of more complex spectra. This limitation was one of the reasons for the virtual abandonment of this experimental approach. An abbreviated compilation of the outstanding infrared lines associated with elements studied in the first period is displayed in Table 1. This material is introduced mainly because of the significance of some of the results of this early work for current studies. In instances where a term combination leads to a multiplet only the line of a particular category of maximum intensity located in the extra-photographic region is listed with appropriate designation of the levels involved in the transition. A considerable number of less conspicuous lines originating in various Ritz Combinations in the spectra of these elements are listed in the original compilation [4]. The essentially hydrogenic transitions, 4f $^2F^\circ$ - 5g ^2G and 5g ^2G - 6h $^2H^\circ$, at approximately 4.0 and 7.4 μ, observed by Paschen in all alkali spectra, are analogous to the Brackett and Pfund series respectively but actually were observed several years earlier. These lines have never been re-observed.

The wavelengths of the extremely intense, six-line, diffuse series multiplets in Ca I, Sr I, and Ba I, may all be calculated with high precision from interferometric measurements on Ritz Combinations involving the same levels [5]. Unfortunately the same situation does not apply to the infrared principal-series multiplets of zinc, cadmium, and mercury. Consequently the precise evaluation of the levels 5p $^3P^\circ_{0,1,2}$ of Zn I, 6p $^3P^\circ_{0,1,2}$ of Cd I, and 7p $^3P^\circ_{0,1,2}$ of Hg I has had to await modern infrared interferometric measurements, something that has been accomplished in the instance of the latter two spectra [6]. Another problem whose solution has been involved in the transition from old observations to new is the identification of the separate levels of the 5f $^3F^\circ$ term in Hg I [7]. This was accomplished by observation of the resolution of the multiplet 6d ^3D - 5f $^3F^\circ$ into its separate components. Revisions of the original classifications are discussed in the referenced paper.

OUTLINE OF CURRENT PROGRAM

The author's current program emphasizes two essentially distinct areas: observation and description of spectra by high-resolution scanning methods for the purpose of analyzing spectra

Table 1

Leading Lines, Infrared Multiplets, Paschen-Götze

	Transition	σ vac. cm⁻¹ calc.	λ air, Å calc.	λ Å, obs. Paschen
H	$3d\ ^2D_{2½} - 4f\ ^2F^\circ_{3½}$	5331.562	18751.109	18751.35
He I	$2s\ ^3S_1 - 2p\ ^3P^\circ_2$	9230.79	10830.341	10830.32
	$3d\ ^3D - 4f\ ^3F^\circ$	5350.71	18684.01	18683.4
	$3d\ ^1D - 4f\ ^1F^\circ$	5348.02	18693.41	18693.4
	$2s\ ^1S - 2p\ ^1P^\circ$	4857.448	20581.324	20581.312
Li I	$3d\ ^2D_{2½} - 4f\ ^2F^\circ$	5347.08	18696.69	18697.0
Na I	$3d\ ^2D_{2½} - 4f\ ^2F^\circ$	5415.745	18459.64	18459.5
K I	$3d\ ^2D_{2½} - 4f\ ^2F^\circ$	6593.3	15162.8	15166.3
Rb I	$5p\ ^2P^\circ_{1½} - 4d\ ^2D_{2½}$	6538.45	15289.96	15290.3
	$4d\ ^2D_{2½} - 4f\ ^2F^\circ$	7436.97	13442.66	13443.7
	$5p\ ^2P^\circ_{1½} - 6s\ ^2S_{0½}$	7317.0	13663.0	13666.7
Cs I	$6p\ ^2P^\circ_{1½} - 5d\ ^2D_{2½}$	2864.73	34897.78	34892.0
	$6p\ ^2P^\circ_{1½} - 7s\ ^2S_{0½}$	6803.2	14695.0	14694.8
Cu I	$4d\ ^2D_{2½} - 4f\ ^2F^\circ_{3½}$	5484.2	18229.2	18229.5
Ag I	$5d\ ^2D_{2½} - 4f\ ^2F^\circ$	5440.51	18375.61	18382.3
Ca I	$4p\ ^3P^\circ_2 - 3d\ ^3D^\circ_3$	5055.039	19776.842	19777.1
Sr I	$5p\ ^3P^\circ_2 - 4d\ ^3D^\circ_3$	3420.704	29225.776	29225.9
Ba I	$5d\ ^3D_3 - 6p\ ^3P^\circ_2$	3918.187	25515.047	25515.7
Mg I	$4s\ ^3S_1 - 4p\ ^3P^\circ_2$	6654.4	15023.5	15024.3
	$4s\ ^1S - 4p\ ^1P^\circ$	5843.6	17108.0	17108.1
	$3d\ ^3D_3 - 4f\ ^3F^\circ$	6719.34	14878.34	14877.1

Table 1—Continued

	Transition	σ vac. cm^{-1} calc.	λ air, Å calc.	λ Å, obs. Paschen
Zn I	$5s\ ^3S_1 - 5p\ ^3P_2^\circ$	7657.9	13054.8	13054.89
	$5s\ ^1S_0 - 5p\ ^1P_1^\circ$	7120.8	14039.5	14039.5
	$4d\ ^3D_3 - 4f\ ^3F^\circ$	6057.4	16504.2	16498.6
Cd I	$6s\ ^3S_1 - 6p\ ^3P_2^\circ$	7151.904	13978.470*	13979.22
	$6s\ ^1S_0 - 6p\ ^1P_1^\circ$	6597.193	15153.822*	15154.78
	$5d\ ^3D_3 - 4f\ ^3F^\circ$	6065.7	16481.6	16482.2
Hg I	$7s\ ^3S_1 - 7p\ ^3P_2^\circ$	8857.007	11287.406†	11287.15
	$7s\ ^1S_0 - 7p\ ^1P_1^\circ$	7366.872	13570.573†	13570.6
	$6d\ ^3D_3 - 5f\ ^3F_4^\circ$	5855.68	17072.78	17072.67‡
	$6d\ ^1D_2 - 5f\ ^1F_3^\circ$	5909.50	16917.28	16921.0 ‡
Tl I	$6d\ ^2D_{2\frac{1}{2}} - 5f\ ^2F^\circ$	6118.5	16339.4	16340.3

*Recent interferometric measurement.

†Recent interferometric measurement on Hg^{198}.

‡Classified differently by Paschen.

brought under investigation for the first time or extending the analyses of spectra in which the energy levels are incompletely known; and interferometric determinations of wavelength in order to extend the international system of standards into the extra-photographic region.

SELECTED EXAMPLES OF ANALYSIS BASED ON INFRARED EXPERIMENTAL MATERIAL

A limited number of examples, illustrative of the first class of problems, will now be considered. One of the principal incentives to the initiation of the program was a gap in the energy-level scheme of Ca I, namely, the then unknown 3d^2 ^{3}F levels. Dr. Henry Norris Russell had brought this deficiency to the attention of the Director of the National Bureau of Standards along with a special request that observations be undertaken in order to supply the remaining material for a monograph he had in preparation. It turned out eventually, although not completely certain at the beginning of the investigation, that infrared observations beyond the photographic limit were needed to supply the essential experimental material. The discovery of the missing levels, illustrated by the multiplets displayed in Table 2, represented the first conspicuous success of the program in making a significant extension to spectrum analysis [8].

A much more recently studied example of a spectrum requiring extraphotographic infrared observations for completion of the analysis is Cl I. Here the most obvious gap was a fairly wide one comprising 22 levels, namely, the even ^4P and ^2P levels arising from the $s^2p^4 \cdot 5s$ configuration, and the even ^4P, ^4D, ^4F and the ^2P, ^2D, ^2F levels from the $s^2p^4 \cdot 3d$ configuration, all converging to the ^3P limit. All of these missing levels were found on the basis of the infrared observations, and the results are reported in two publications [9]. Table 3 contains a list of the new levels with revisions explained in the immediately following material.

Making use of the same experimental material, together with a photographic description by Corliss which was also used by Humphreys and Paul, Minnhagen [10] was able to interpret 16 unassigned levels found by the previous authors and several additional levels that he found as belonging to the (^3P) 4f, 5f, and 6f configurations. Employing a theoretical procedure involving the evaluation of Slater parameters, Minnhagen was able to identify these levels by means of the energy expressions for the p^4f configuration in pair coupling. All the 4f and 5f levels were identified, and the positions of the 6f levels not actually found were predicted. Furthermore on the basis of material supplied by Avellén, some revisions were made in the assignments proposed by Humphreys and Paul. In one instance, that of the value proposed for 3d $^2F_{2\frac{1}{2}}$, the level was rejected and a substitution made. In other instances there was merely an interchange of assignments. It is emphasized that this ability to make unambiguous assignments, where there is wide departure from ℓs-coupling, is illustrative of the great power inherent in modern theoretical procedures, which can be carried out readily by aid of electronic computers.

Similar infrared observations have been included in recent investigations of I$_\text{I}$[11] and of Br$_\text{I}$, the latter still unpublished.

The spectra of several fourth group elements provide additional examples of the urgent requirement for infrared experimental material. The analysis of Ge I has been brought nearer to completion than that of Sn I or Pb I. The last extensive publication dealing with the analysis of Ge I was that of Andrew and Meissner [12], but this spectrum is still under intensive study.

Table 2

Multiplet Combinations of $3d^2\ ^3F$ in Ca I

	$3d^2\ ^3F_4$ 43508.11	$^3F_3$ 43489.21	$^3F_2$ 43474.89
3d 4p $^3F^\circ_4$ 35896.890	13134.96 (400) 7611.19 7611.22	13167.75 (24) 7592.24 7592.32	
$^3F^\circ_3$ 35818.712	13001.37 (20) 7689.39 7689.40	13033.41 (300) 7670.49 7670.50	13057.82 (20) 7656.15 7656.18
$^3F^\circ_2$ 35730.450	....	12885.21 (15) 7758.71 7758.76	12909.07 (200) 7744.37 7744.44
3d 4p $^1D^\circ_2$ 35835.400	....	13061.84 (8) 7653.79 7653.81	13086.26 (50) 7639.51 7639.49
3d 4p $^3D^\circ_3$ 38259.102	19045.86 (90) 5249.05 5249.01	19114.83 (5) 5230.11 5230.11	.... 5215.79
$^3D^\circ_2$ 38219.094	....	18969.71 (60) 5270.12 5270.12	19021.39 (4) 5255.80 5255.80
$^3D^\circ_1$ 38192.373	....	....	18924.96 (30) 5282.58 5282.52

Table 3

Even Energy Levels of Cl I

Code No.	Assignment		Level value cm^{-1}	Absolute value,* cm^{-1}
	Humphreys & Paul	Avellén		
8	$3d\,^4D_{3\frac{1}{2}}$		87975.13	17015.87
9	$3d\,^4D_{2\frac{1}{2}}$		88075.78	16915.22
10	$3d\,^4D_{1\frac{1}{2}}$		88184.10	16806.90
11	$3d\,^4D_{0\frac{1}{2}}$		88268.35	16722.65
12	$3d\,^4F_{4\frac{1}{2}}$		90189.23	14801.77
13	$3d\,^4F_{3\frac{1}{2}}$		90483.50	14507.50
14	$3d\,^4F_{2\frac{1}{2}}$		90744.95	14246.05
15	$3d\,^4F_{1\frac{1}{2}}$		90944.23	14046.67
16	$3d\,^4P_{2\frac{1}{2}}$		91656.20	13334.80
17	$3d\,^4P_{1\frac{1}{2}}$	$5s\,^4P_{1\frac{1}{2}}$	91676.57	13314.43
18	$3d\,^4P_{0\frac{1}{2}}$	$5s\,^4P_{0\frac{1}{2}}$	92146.98	12844.02
19	$5s\,^4P_{2\frac{1}{2}}$		91122.66	13868.34
20	$5s\,^4P_{1\frac{1}{2}}$	$3d\,^4P_{1\frac{1}{2}}$	91169.15	13821.85
21	$5s\,^4P_{0\frac{1}{2}}$	$3d\,^4P_{0\frac{1}{2}}$	91064.59	13926.41
~~22~~	$3d\,^2F_{2\frac{1}{2}}$	rejected	91304.06	13686.94
22		$3d\,^2P_{1\frac{1}{2}}$	91560.00	13431.00
23	$3d\,^2F_{3\frac{1}{2}}$		91085.10	13905.90
24	$3d\,^2D_{2\frac{1}{2}}$	$3d\,^2F_{2\frac{1}{2}}$	91339.20	13651.80
25	$3d\,^2D_{1\frac{1}{2}}$		91534.18	13456.82
26	$3d\,^2P_{1\frac{1}{2}}$	$3d\,^2D_{2\frac{1}{2}}$	91902.44	13088.56
27	$3d\,^2P_{0\frac{1}{2}}$		92189.74	12801.26
28	$5s\,^2P_{1\frac{1}{2}}$		92135.80	12855.20
29	$5s\,^2P_{0\frac{1}{2}}$		92598.30	12392.70

*Based on Limit, Cl II, 104991 cm^{-1} .

Kaufman and Andrew [13] have made extensive interferometric measurements, both for the purpose of extending the system of wavelength standards and of establishing more precise values of the levels. These in turn support theoretical studies being carried out by Cowan and Andrew [14] that include development of a computer program for determining the values of the Slater parameters which give the best fit between the calculated values—that is, eigenvalues of the Hamiltonian Matrix—and the experimental energy levels of the atom. Computation of matrices of parameter coefficients in ℓs, jj, and jℓ coupling permit determination of the preponderance of a given coupling scheme expressed as a percentage.

As of the time of publication of the article by Andrew and Meissner the even levels of the $4s^2 4p4f$ configuration were subject to considerable uncertainty, both as to the identification and quantum number assignment. In most instances the levels of the 4f category were listed by those authors in parenthesis indicating a single transition as sole evidence. At the suggestion of Dr. Andrew, a cooperative arrangement between him and this author was undertaken to extend the experimental observations into the infrared where transitions were expected that would strengthen or confirm the level assignments, improve the values, and permit identification of missing levels of the 4f configuration, specifically $^3D_1$, $^3F_4$, $^3G_5$, $^3G_3$, and $^1G_4$. All of these objectives have been realized. The first set of infrared observations led to the identification of all the missing levels. Later, when it appeared desirable to establish more precise level values, interferometric observations were undertaken. These led to the precise determination of the wavelengths of 30 lines by means of a vacuum interferometer following the procedure developed and described by the author [15]. These lines included nine described by transitions involving all of the 4f levels requiring supporting measurements. Table 4 is a listing of the latest wavelengths, wave numbers, and classifications of these key combinations. This work has been reported in several presentations and publications [16]. The final joint publication with Dr. Andrew is now in preparation.

A final example of investigations contributing to the energy-level analysis of spectra might also be included as an example in the area of establishment of wavelength standards. This is a very recent interferometric study of the 3d - 4f combinations in Ar I for the purpose of improving the evaluation of the 4f levels and measuring pair differences in the instance of ambiguous transitions. The argon configuration, $3s^2 3p^5 4f$, leads to levels of the same number and quantum description as $4s^2 4p4f$ in Ge I. Consequently the same theoretical procedure and computer program for evaluation of Slater parameters applies. In the instance of

Table 4

Identification of Interferometrically Observed
Combinations of 4f Levels in Ge I

Wavelength, vacuum, A	Coded description*	Conventional description
11920.2705	9° - 25.3	4d $^3F^o_2$ - 4f $^3G_3$
12290.1076	10° - 25.4	4d $^3F^o_3$ - 4f $^3G_4$
12680.0517	6° - 21.4	4d $^3D^o_2$ - 4f $^3F_3$
12684.7471	6° - 20.5	4d $^3D^o_2$ - 4f $^1F_3$
12804.1560	7° - 21.6	4d $^3D^o_1$ - 4f $^3F_2$
12839.8923	10.1° - 26.4	4d $^3F^o_4$ - 4f $^3G_5$
13111.1967	8° - 21.5	4d $^3D^o_3$ - 4f $^3F_4$
14120.5559	11° - 25.5	4d $^3P^o_2$ - 4f $^3D_3$
16703.8522	17° - 26.5	4d $^1F^o_3$ - 4f $^1G_4$

*According to reference [12].

the 4f levels of both spectra the extreme development of $j\ell$ coupling approaches the complete degeneracy of pure pair coupling, in which the pair separations become vanishingly small. Interferometric observations have been completed on the more intense 3d - 4f transitions [17]. The wavelengths are shown in Table 5 and the revised levels, together with pair separations, in Table 6. It develops that, within the limits of resolution available in these experiments, the ambiguous transitions consist entirely of the more intense component. This situation makes these lines available as wavelength standards of absolute accuracy comparable to that of argon lines of different origin discussed in the following section.

INTERFEROMETRIC DETERMINATION OF INFRARED WAVELENGTH STANDARDS

The program of interferometric measurement, intended to make available standard wavelengths of acceptable absolute accuracy in the region beyond the limit of photographic observation, has utilized a scanning technique employing a rotating Fabry-Perot interferometer that has been described in several publications [15]. The program has emphasized measurements of interferometric patterns of lines of the noble atmospheric gases, but

Table 5

Combinations of 4f Levels in Argon I, Interferometrically Observed Transitions

λ, Vacuum (angstroms)	σ, Vacuum (cm^{-1})	Transition
11736.447	8520.466	$3d\ [\tfrac{1}{2}]^{\circ}_{0} - 4f\ [1\tfrac{1}{2}]_{1}$
11947.140*	8370.204	$3d\ [\tfrac{1}{2}]^{\circ}_{1} - 4f\ [1\tfrac{1}{2}]_{1}$
11946.571*	8370.603	$3d\ [\tfrac{1}{2}]^{\circ}_{1} - 4f\ [1\tfrac{1}{2}]_{2}$
12359.678†	8090.826	$3d\ [1\tfrac{1}{2}]^{\circ}_{2} - 4f\ [2\tfrac{1}{2}]_{2,3}$
16441.066	6082.331	$3d\ [1\tfrac{1}{2}]^{\circ}_{1} - 4f\ [2\tfrac{1}{2}]_{2}$
13410.255†	7456.980	$3d\ [3\tfrac{1}{2}]^{\circ}_{4} - 4f\ [4\tfrac{1}{2}]_{4,5}$
13914.360	7186.820	$3d\ [3\tfrac{1}{2}]^{\circ}_{3} - 4f\ [4\tfrac{1}{2}]_{4}$
14260.767	7012.246	$3d'\ [2\tfrac{1}{2}]^{\circ}_{2} - 4f'\ [3\tfrac{1}{2}]_{3}$
14638.414†	6831.341	$3d'\ [2\tfrac{1}{2}]^{\circ}_{3} - 4f'\ [3\tfrac{1}{2}]_{3,4}$
14600.462†	6849.098	$3d'\ [1\tfrac{1}{2}]^{\circ}_{2} - 4f'\ [2\tfrac{1}{2}]_{2,3}$
15904.031	6287.714	$3d'\ [1\tfrac{1}{2}]^{\circ}_{1} - 4f'\ [2\tfrac{1}{2}]_{2}$
14654.353	6823.911	$3d\ [2\tfrac{1}{2}]^{\circ}_{2} - 4f\ [3\tfrac{1}{2}]_{3}$
15306.062†	6533.359	$3d\ [2\tfrac{1}{2}]^{\circ}_{3} - 4f\ [3\tfrac{1}{2}]_{3,4}$

*Pair difference observed; wavelength calculated.
†Only transition associated with $\Delta j = 1$; observed.

some lines of other elements mentioned in the account of work in the earlier period have been included, notably lines of cadmium and mercury, the latter in the form of isotope 198. Ar I is regarded as a particularly good source of standard wavelengths because in the naturally occurring form the element is more than 99 per cent monoisotopic.

The measurement procedure has included intercomparison with the wavelengths of selected lines previously adopted as part of the international system of standards by the International Astronomical Union. Most suitable for this purpose have been the 1s - 2p combinations of Ar I located near 1 micron and the 10139.8Å line of Hg I^{198}. Under favorable conditions an absolute

Table 6

Revised Values of 4f Levels in Argon I

Designation, jℓ Coupling	Designation, Paschen	Level Value, I.A.U. Scale*	Level Value A.E.L. Scale†	Difference
4f [1½]$_1$	X_1	27044.472	120188.274	0.398
4f [1½]$_2$	X_2	27044.871	120188.672	
4f [2½]$_2$	Y_2	27086.303	120230.104	-0.313
4f [2½]$_3$	Y_3	27085.990	120229.791	
4f [3½]$_3$	U_3	27106.116	120249.917	0.038
4f [3½]$_4$	U_4	27106.154	120249.955	
4f [4½]$_4$	V_4	27063.415	120207.216	-0.041
4f [4½]$_5$	V_5	27063.374	120207.175	
4f' [2½]$_2$	Z_2	28510.820	121654.621	-0.346
4f' [2½]$_3$	Z_3	28510.474	121654.275	
4f' [3½]$_3$	W_3	28509.478	121653.279	0.042
4f' [3½]$_4$	W_4	28509.520	121653.321	

*Referred to 4s [1½]$_2^\circ$; that is, 1s$_5$, equal to zero. Derived from observed wave numbers and 3d levels submitted to the 1961 session of the I.A.U.

†Adjusted by reference to the best available recent data. Assumed value 4s [1½]$_1^\circ$, or 1s$_4$, 93750.639 cm^{-1}.

accuracy of about 1 part in 10^7 has been attained with orders of interference in the range of 100,000.

At the meeting of the International Union in 1958 a group of wavelengths in Ar I, measured in connection with the author's program, were adopted as provisional standards. This was the first time in the half-century history of the organization that any infrared wavelength standards beyond the range of photography had been considered.

The lines of noble gases available for interferometric measurement in the region between 1 and 2 microns are for the most part included in the following categories described in the Paschen notation as 2p - 2s and 2p - 3d. At the outset of this program the 2s and 3d levels in the spectra of all the noble gases constituted a gap in terms of precise determination. An exception is the well determined set of 3d levels of Ne I. The 1s, 2p, 3p and in some instances higher members of the s,. p, and d series had been evaluated very accurately from interferometric measurements in the photographic region. The direct interferometric measurement of the noted classes of transitions not only established a considerable number of experimentally determined standards but also made available several hundred additional standards as Ritz Combinations that are equally accurate and at the same time extend the range of standards coverage well beyond the present practical limits of direct spectroscopic observation now somewhere near four microns. Results of the various sets of wavelength determinations under the author's program have been published in a series of reports [18,19], of which the more recent are referenced here. Owing to the rather limited circulation of the referenced articles some of the material of expected greater usefulness for wavelength intercomparisons is included here. Tables 7 and 8, consisting respectively of compilations of vacuum wavelengths and derived energy levels in Ar I, are reproduced with minor revisions from the forthcoming Volume XI, Transactions of the International Astronomical Union.

The fractional parts of the wavelength entries in Table 7 shown in three separate columns represent independent contributions by three different observing teams, in conformity with a rule of the I.A.U. for consideration of material. The methods were also independent. Humphreys and Paul used a rotating interferometer, Littlefield and Rowley a reflection echelon, and Peck a Michelson interferometer with a fringe counting accessory device. With a few exceptions the agreement is excellent. A recent publication by Peck and Khanna [20] indicates slight revisions of the values in the last column. The calculated Ritz Combinations will also appear in Vol. XI, Trans. I.A.U. containing reports of the Berkeley meeting in 1961. A more recent value of level $2s_3$ has been inserted in Table 8. Table 9 contains a set of recently determined wavelengths in the spectrum of natural krypton that have been reported by Paul and Humphreys [21]. It is probable that future measurements on the krypton spectrum will be made using the isotope Kr^{86} since the Kr^{86} line of wavelength 6057.80210_5 A in vacuum has been adopted as the primary standard of length. The usefulness of lines of natural krypton as standards has however been demonstrated, for although both isotopic and hyperfine structure is expected a large proportion of the lines are sharp enough for use as standards in ordinary applications.

A final comment regarding experimental advances is that the range of observation of emission spectra has been extended recently toward longer wavelengths by the use of cooled lead sulfide

Table 7

Vacuum Wavelengths of Ar I in the Infrared

λ_{vac}(Å)	Humphreys and Paul (39a)	Littlefield and Rowley (50)	Peck (69a)
8266.			$.794_5$
9125.			$.471_4$
9227.			.0302
10472.			.922
10676.	.489		.4907
10684.	.698		
11081.	.901		
11671.	.903		
12115.	.639		
12346.	.770		
12406.	.220	$.218_4$	
12442.	.724		
12459.	.523		
12491.	.079	$.079_3$	
12705.	.755		
12806.	.241	.2474	.2406
12936	.734*		
12960.	.203	.2029	.2012
13011.	.822	.8209	
13217.	.606		
13231.	.727		
13276.	.266	.2656	
13316.	.850	.8552	
13370.	.766	.7679	
13507.	.883	.8818	.883
13626.	.383	.3909	.3844
13682.	.290	.2918	
13722.	.327	.3286	.3272
14097.			.4924
16945.	.210	.2129	.2082

*1962 determinations.

detectors. Direct scans have been made as far as 4.0 μ and interferometric observations, as far as 3.5 μ. Energy considerations will probably limit observable features much beyond these wavelengths even with other detectors now available. It is expected that future programming will emphasize spectra of rare earths which constitute the most formidable remaining gap in our knowledge of atomic emission spectra. Illustrative of our work on rare earth spectra is a description of the infrared spectrum of Yb I, including interferometric measurements, that was made in support of a program of the analysis of this spectrum by

Table 8

Argon Levels (in cm^{-1}) Relative to $1s_5 = 0.000$
Based on Interferometric Measurements

Designation	Humphreys and Paul, 1958 as adopted by I.A.U.	Humphreys and Paul, 1959	Littlefield and Rowley	Peck, 1960
$2s_5$	20324.715	.713	.7129	.7125
$2s_4$	20499.501	.500		
$2s_3$	21717.879	.875*		
$2s_2$	21831.261	.259	.2595	
$3d_6$	18524.007	.006		
$3d_5$	18674.269	.268	.2676	.2686
$3d_3$	18995.166	.164	.1635	.1651
$3d_4'$	19606.394	.393	.3925	.3932
$3d_4$	19876.596	.595	.5952	.595
$3d_1''$	20282.206	.205	.1995	.2033
$3d_1'$	20572.796	.795	.7938	
$3d_2$	21003.973	.972	.9737	.9721
$3s_1''''$	21497.234	.232	.2290	
$3s_1''$	21661.376	.375	.3737	
$3s_1'''$	21678.181	.179	.1787	
$3s_1'$	22223.107	.106		

*1962 Determination.

Meggers[22]. Continued observations of this spectrum are contemplated in order to achieve the maximum possible extension into the infrared region.

REFERENCES

1. C. J. Humphreys, Lunds Universitets Årsskrift N.F. Avd. 2, Bd 50, Nr. 21; NOLC Report 146, May 1954.
2. C. J. Humphreys and E. Paul, Jr., NOLC Report 341, October 1956.
3. Curtis J. Humphreys, J. Opt. Soc. Am., 50, 1171 (1960).
4. F. Paschen and R. Götze, Seriengesetze der Linienspektren, Springer, Berlin, 1922.
5. Charlotte E. Moore, Atomic Energy Levels, Circular of the National Bureau of Standards, Vols. I, II, and III, 1949, 1952, 1958.
6. C. J. Humphreys and E. Paul, Jr., NOLC Report 464, September 1959.

Table 9

Interferometric Determinations of Wavelengths in Natural Krypton, 1961

Wavelength in Vac. Angstroms Observed*	Wavelength in Air Angstroms		Wave Number cm-1	
	Observed	Calc.	Observed	Calc.
8931.1443	8928.6930		11196.7735	
9754.4346	9751.7604		10251.7474	
11822.6136	11819.379	.378	8458.3666	.367
12207.8754	12204.536		8191.4335	
12882.3979	12878.875		7762.5300	
13181.0149	13177.411	.411	7586.6692	.669
13626.1413	13622.416	.418	7338.8348	.834
13637.9487	13634.221	.221	7332.4810	.481
13742.6120	13738.856		7276.6371	
14430.7362	14426.793	.794	6929.6534	.653
14738.4687	14734.442	.440	6784.9654	.966
15243.7868	15239.623	.622	6560.0498	.050
15339.1576	15334.968	.967	6519.2628	.263
16789.7178	16785.133	.136	5956.0262	.025
16858.1016	16853.499	.499	5931.8660	.866
16895.0674	16890.454	.452	5918.8873	.888
16901.3800	16896.765		5916.6766	
16940.4393	16935.813	.815	5903.0346	.034
17103.4495	17098.780		5846.7738	
17372.3574	17367.614		5756.2712	
18007.1461	18002.230	.230	5553.3508	.351
18172.2883	18167.327		5502.8843	
21908.5101	21902.532	.534	4564.4364	.436

*Observations made in vacuum with 63-mm etalon.
Standards for 8931 and 9754, Argon (vac.) 9125.4706 and 9660.4346 A.
Standards for all other intercomparisons, Argon (vac.) 13722.327 A.

7. Curtis J. Humphreys, J. Opt. Soc. Am. 43, 1027 (1953).
8. C. J. Humphreys, J. Opt. Soc. Am., 41, 286A(1951); J. Research Natl. Bur. Standards, 47, 262 (1951).
9. Curtis J. Humphreys and Edward Paul, Jr., J. Opt. Soc. Am., 48, 285A (1958); 49, 1180 (1959); NOLC Report 411, May 1958.
10. Lennart Minnhagen, J. Opt. Soc. Am., 51, 298 (1961).
11. C. C. Kiess and C. H. Corliss, J. Research, Natl. Bur. Standards, 63A, 1 (1959).
12. Kenneth L. Andrew and K. W. Meissner, J. Opt. Soc. Am., 49, 146 (1959).
13. Victor Kaufman and Kenneth L. Andrew, J. Opt. Soc. Am., 51, 1465A (1961); J. Opt. Soc. Am. (In Press).

14. Robert D. Cowan and Kenneth L. Andrew, Atomic Spectroscopy Symposium, Argonne National Laboratory, June 1961.
15. C. J. Humphreys, NOLC Report 321, March 1956.
    C. J. Humphreys and E. Paul, Jr., NOLC Reports 341, October 1956; 390, February 1958; A Decade of Basic and Applied Science in the Navy, Office of Naval Research, Washington, D. C., 1957; J. Phys. Radium 19, 424 (1958).
16. Curtis J. Humphreys and Edward Paul, Jr., J. Opt. Soc. Am. 50, 1137A (1960); NOLC Report 533, December 1960; NAVWEPS Report 7214, March 1962.
17. Curtis J. Humphreys and Edward Paul, Jr., J. Opt. Soc. Am. 52, 591A (1962); NAVWEPS Report 7219, June 1962.
18. C. J. Humphreys and E. Paul, Jr., NOLC Reports 429, December 1958; 443, April 1959; 464, September 1959; 503, June 1960; NAVWEPS Reports 7190, September 1961; 7205, December 1961.
19. Report of Commission 14, Trans. I.A.U., Vol. X, 211 (1960); Vol. XI, (1962) (In press).
20. E. R. Peck and B. N. Khanna, J. Opt. Soc. Am., 52, 416 (1962).
21. E. Paul, Jr. and C. J. Humphreys, J. Opt. Soc. Am., 51, 1465A (1961); NAVWEPS Report 7205, December 1961.
22. C. J. Humphreys and E. Paul, Jr., NOLC Report 473, January 1960.

ISOTOPIC SHIFTS IN THE SPECTRA OF DYSPROSIUM AND SAMARIUM

A. R. Striganov
I. V. Kurchatov Atomic Energy Institute
Academy of Sciences
Moscow, U.S.S.R.

INTRODUCTION

The original theory of isotope shift developed by G. Racah, G. Breit and J. E. Rosentahl for heavy elements was based on the liquid-drop model of the nucleus. It follows from this theory that the displacement of the spectral lines of isotopes of a given element should be uniform with respect to mass number. However, it was found experimentally that this did not occur in the spectra of some elements.

An anomalously great shift was found in Nd, Sm, and Gd spectra. In these three cases, a sharp increase in the shift was observed between lines of isotopes with neutron number $N = 88$ and $N = 90$. "Jumps" in the isotopic shift were also found in the Sr, Zr, and Mo spectra between the lines of isotopes with $N = 50$ and $N = 52$, in the Ce spectrum between $N = 82$ and $N = 84$ and in the Pb spectrum between $N = 126$ and $N = 128$. It was also found that the displaced lines were not equidistant in other mass regions, although the effect was not so clear-cut in the latter cases.

"Jumps" in the isotope shift in Sr, Zr, Mo, Ce, and Pb spectra are due to the shell structure of the nucleus. They take place between the lines of even-even isotopes having completely closed shells with neutron numbers of 50, 82 and 126 and the line of the next isotope when the new neutron pair falls into a higher shell. The presence of "jumps" in the isotope shift near "magic" numbers shows that when a new neutron pair is added to a closed shell a relatively great increase occurs in the size of the nucleus. It follows from this that the effective radius of the nucleus depends on peculiarities of neutron shell filling. This is reflected in the isotopic shift. The problem of the relation of isotopic shifts to nuclear shell structure has not yet been considered theoretically.

The anomalous shifts in Nd, Sm and Gd spectra are connected with the transition from spherical to deformed nuclei [1]. The region of deformed nuclei is in the range of N = 90 to N = 116. When a deformed nucleus rotates, there is an increase in effective radius as a result of averaging in all directions. This is displayed in an additional isotope shift, which tends to increase the volume effect. The additional "quadrupole" shift can be substantial, since the deformation of the nucleus with the addition of a neutron pair can vary greatly in going from one isotope to the other. It follows from this that non-equidistance in isotope displacement in the region of deformed nuclei is due to irregular variation of the nuclear deformation of the isotopes of a given element.

Investigation shows that non-equidistance in isotope shift is observed in the case of spherically symmetrical nuclei, too. According to the generalized nuclear model, non-equidistance in the region of spherical even-even nuclei is due to surface vibration in the nucleus, or the so-called zero vibration of the electrical quadrupole moment of the nucleus [2]. The presence of such vibrations results in the "smearing-out" of nuclear boundaries, thus causing an increase in the effective radius of the nucleus. The irregular variation of the amplitude of these vibrations in the nuclei of different isotopes leads to an irregular variation of the effective radius. This is displayed in an additional isotope shift, which we call the vibration effect.

According to Bodmer [3], the isotope shift between levels of two isotopes when an s-electron interacts with the nucleus can be expressed in terms of the effective radius

$$\Delta T = B\psi_s^2(o)\, R_u^{2\gamma}\, \frac{\delta R_u}{R_u} \tag{1}$$

where B is a factor depending on the charge of the nucleus, the fine structure constant, and the large and small components of the Dirac wave function; ψ_s (o) is the electronic wave function and $R_u = \sqrt{5/3}\, \langle r^2 \rangle^{1/2}$ is the effective nuclear radius which is determined by the radius-squared distribution of charge in the ground state $\langle r^2 \rangle^{1/2}$.

For deformed nuclei, the mean square of the radius of proton distribution in the ground state is as follows [4]:

$$\langle r^2 \rangle_q = \frac{3}{5} ZR_o^2 \left(1 + \frac{5}{4\pi} \beta_q^2 + \frac{3}{8\pi} \beta_q^3\right), \tag{2}$$

where β_q is the deformation parameter.

In the case of spherical nuclei, there are surface vibrations about the equilibrium spherical form. The mean square of the radius of proton distribution is [4]

$$\langle r^2 \rangle_v = \frac{3}{5} ZR_o^2 \left(1 + \frac{5}{4\pi} \overline{\beta_v^2}\right), \tag{3}$$

where $\overline{\beta_v^2}$ is the mean square of the amplitude of zero vibration.

If each of these values $\langle r^2 \rangle$ is substituted into formula (1), we shall have the complete isotopic shift, which is the sum of the ordinary volume effect and the additional effect. The latter is responsible for non-equidistance in isotopic shifts.

The relative isotopic shift for any two intervals can be represented by a formula which is also valid for deformed nuclei (ignoring the β_q^3 term) and for spherical nuclei, too

$$\frac{\Delta\nu(A_1 - A_2)}{\Delta\nu(A_3 - A_4)} = \frac{\delta A_{1,2} + \frac{15}{8\pi}\,\frac{A_1 + A_2}{2}\,(\beta^2)_{1,2}}{\delta A_{3,4} + \frac{15}{8\pi}\,\frac{A_3 + A_4}{2}\,(\beta^2)_{3,4}} \tag{4}$$

where A_1, A_2, A_3, and A_4 are mass numbers of four isotopes of the same element, $\delta A_{1,2}$, $\delta A_{3,4}$ are differences of isotopic mass numbers, and $\delta(\beta^2)_{1,2}$, $\delta(\beta^2)_{3,4}$ are the differences of the squares of the nuclear deformation parameter or the differences of the mean squares of the amplitude of zero vibration.

Equation (4) allows us to compare experimental data with values calculated according to known deformation parameters or amplitudes of vibration. Also, by using this formula and measuring the isotope shift between 3 isotopes, the nuclear deformation parameter of one of the isotopes can be found if the parameters of the other two are known. With the aid of the deformation parameter, the inner quadrupole moment Q_o and the probability of electrical quadrupole transition from the ground state of the nucleus to the first excited state $B(E\,2{,}0 \rightarrow 2^+)$ can be calculated.

MEASUREMENTS OF ISOTOPIC SHIFT IN DYSPROSIUM AND SAMARIUM SPECTRA

Enriched isotopes of dysprosium and samarium were used in the form of oxides. Tables 1 and 2 give the isotopic percentage compositions of the samples used.

A discharge tube containing a hollow cathode cooled with liquid nitrogen was used as the light source. Argon was the support gas. To excite spark lines in the samarium spectrum, a

Table 1

The Dysprosium Samples

Samples	156	158	160	161	162	163	164
Natural	0.05	0.09	2.29	18.89	25.53	24.97	28.18
I	0.4	0.4	35.0	8.0	32.7	3.5	20.0
II	19	3	3	19	23	20	13
III	-	25	3	22	20	17	13

Table 2

The Samarium Samples

Samples	144	147	148	149	150	152	154
Natural	3.16	15.07	11.27	13.84	7.47	26.63	22.56
I	29.9	2.7	30.4	3.8	30.9	1.9	0.4
II	31.0	1.8	0.7	1.3	31.0	2.2	32.0
III	30.7	2.4	31.4	3.0	0.3	31.6	0.6

Kr + He mixture was used. The pressure of the support gas in the tube was ≤ 1 mm Hg. The samples were converted to the chloride form with hydrochloric acid before being placed in the cathode cavity.

A Fabry-Perot interferometer with silver and multi-layer coatings was used as the high resolution device. For predispersion, a Steinheil three-prism spectrograph in the case of dysprosium was used and a DFS-3 grating spectrograph in the case of samarium.

The isotopic structure was measured in the 8th to 10th orders on three spectrograms taken with different spacings between interferometer plates.

As an example, a section of the samarium spectrum taken with 15 mm spacing is shown in Figure 1. Even-even isotope lines are well resolved and have almost equal intensity. Even-odd isotope components are absent. This made it possible to avoid systematic errors and obtain high accuracy (errors do not exceed 1-2%).

RESULTS IN THE CASE OF DYSPROSIUM

The isotopic shift was measured for 30 lines of Dy I. For 17 of these lines, the complete isotopic structure between 5 even isotopes was obtained for the first time. Most of the lines have

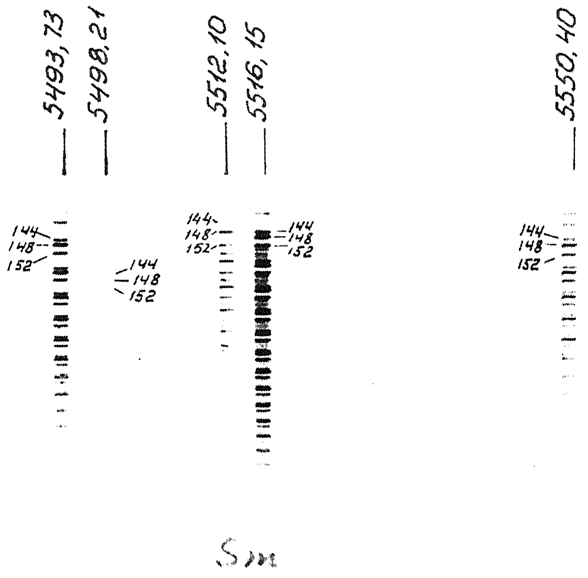

Figure 1. Isotope structure of spectral lines of the three-isotope sample of samarium.

negative shifts (i.e., the component of the heavier isotope is displaced toward smaller wave numbers); 7 lines have a positive shift.

Figure 2 shows the average relative shift of all of the lines. The shifts $\Delta\nu(156 - 158)$ and $\Delta\nu(160 - 162)$ are seen to be 57% and 10% greater, respectively, than the other two intervals. Dysprosium is in the region of deformed nuclei; thus the deviation from equidistance in the position of even-even isotope components is due to uneven variation of the static deformation parameter β. Substituting the available parameters of nuclear deformation into Eq. (4), one can calculate the isotopic shift. Table 3 gives the nuclear deformation parameters of Dy^{160}, Dy^{162}, and Dy^{164}. Using the data of the first column (taken from [5]) one obtains $\Delta\nu(160 - 162)/\Delta\nu(162 - 164) = 0.80$. This result does not agree with the experimental value of the relative isotopic shift (1,10). This is due to errors in the determination of the probabilities of the $B(E2, 0 \rightarrow 2^{+})$ transition which were used to calculate the deformation parameters. The more reliable data in the second column, taken from [6], give $\Delta\nu(160 - 162)/\Delta\nu(162 - 164) = 1.08$, which is in agreement with the experimental data.

Thus isotope displacement can be used to check the correctness of transition probabilities determined by means of the Coulomb excitation method.

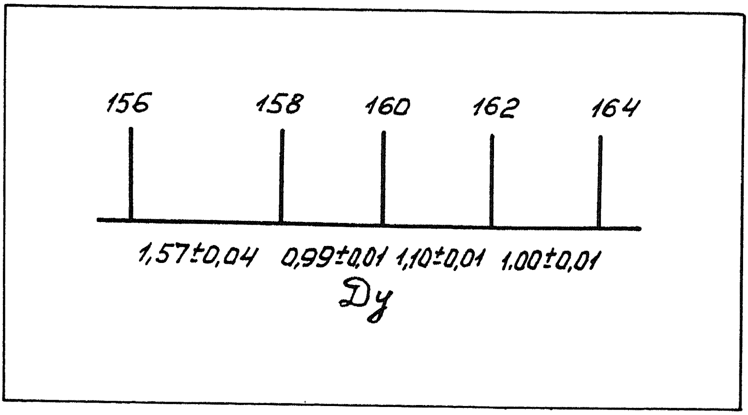

Figure 2. Relative shift in the Dy I spectrum.

Table 3

The Deformation Parameter of Dysprosium Nuclei

Nuclei	[5]	[6]
Dy^{156}	–	0.233 ± 0.061*
Dy^{158}	–	0.285 ± 0.026*
Dy^{160}	0.32	0.301 ± 0.010
Dy^{162}	0.36	0.320 ± 0.005
Dy^{164}	0.41	0.334 ± 0.007

*Our data.

In the case of dysprosium, the deformation parameters are known for only three nuclei (Dy^{160}, Dy^{162}, Dy^{164}). For the nuclei of the rare isotopes Dy^{156} and Dy^{158}, these values have not yet been determined. If one takes the results of [6] for the initial data then the deformation parameters of the Dy^{158} and Dy^{156} nuclei can be calculated from the relative isotopic shift. The results, which are accurate to within about 9% to 26%, respectively, are given in table 3.

RESULTS IN THE CASE OF SAMARIUM

The isotope shift in the spectrum of Sm I was measured for 59 lines, the complete isotope structure for 56 lines having been obtained for the first time [7]. It was found that 31 lines have a negative shift and 28 lines a positive shift. The positive and negative shifts are shown separately in Figure 3.

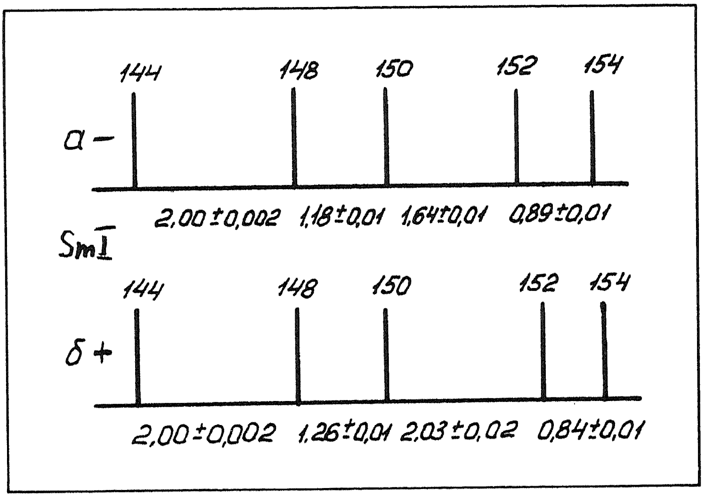

Figure 3. Relative shift in the Sm I spectrum: a) lines with negative shift; b) lines with positive shift.

The results obtained show that besides the known "jump" in isotope shift between the components of the isotope with N = 88 and 90, other intervals also show a non-equidistance which cannot be explained as experimental error. It is known that the non-equidistance in isotope shift for the nuclei with N $\geq$ 90 is due to the change in the static nuclear deformation, and the non-equidistance in the region of the nuclei with N $\geq$ 88 can be explained by surface vibration of the spherical nucleus. Figure 3 indicates that in the spectrum of Sm I, lines with positive and negative shifts have somewhat different shift patterns. On the average, the positive shifts are 0.08 greater for the $\Delta\nu(148 - 150)$ interval and 0.05 smaller for the $\Delta\nu(152 - 154)$ interval than the negative shifts. This difference is 5-6 times greater than the random error of measurement. It is not due to the superposition of the hyperfine structure of the odd isotopes Sm^{147} and Sm^{149}, since there are no additional components on the spectrograms. In case of the interval $\Delta\nu(150 - 152)$, which has a large quadrupole effect, the difference in relative shift as between the lines with positive and negative shift reaches an average value of 0.39, which is 20 times greater than the random error of the average relative shift of the lines with a positive shift. The difference between the positive and negative shifts in the interval $\Delta\nu(150 - 152)$ is so great that the numerical values of the relative shift do not coincide for all 59 of the spectral lines [7].

The same phenomenon was also observed in the Sm II spectrum, where we measured the isotope shift for 12 lines. Figure 4 shows the positive and negative relative shifts. The results

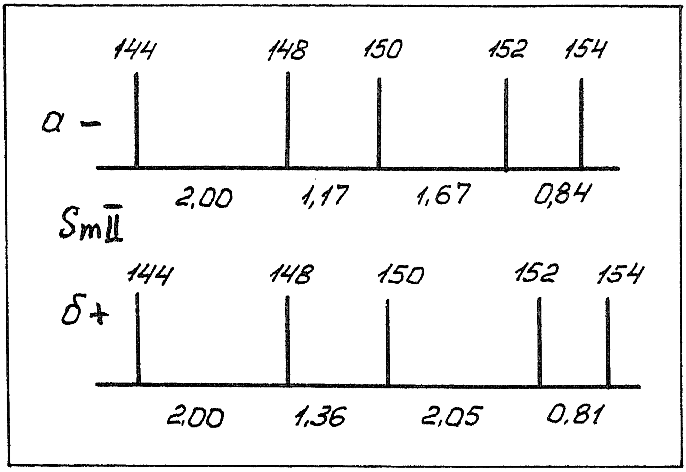

Figure 4. Relative shift in the Sm II spectrum: a) lines with negative shift; b) lines with positive shift.

obtained are in good agreement with the isotopic shifts in the spectrum of Sm I. Here the difference in relative shift in the interval $\Delta\nu$(150 - 152) as between the lines with positive and negative shifts is, on the average, 0.38.

According to the classification of the Sm I spectrum and our data on isotopic shift, all of the lines with negative shift belong to transitions of the type $4f^6 6s6p \rightarrow 4f^6 6s^2$, and the lines with positive shift to those of the type $4f^5 5d6s^2 \rightarrow 4f^6 6s^2$. Since the lower electronic configuration is the same in these transitions the positive shift in the lines is due to a large isotopic displacement of the upper levels belonging to the electron configuration $4f^5 5d6s^2$. The great isotopic shift of these levels can be explained by the reduction in the screening of the two s-electrons when the sixth f-electron enters into the 5d shell, which increases the electron charge density at the nucleus [8]. The same explanation can be offered in connection with the isotopic shift in the Sm II spectrum. In this case, the lines with a negative shift belong to the $4f^6 6p \rightarrow 4f^6 6s$ transitions and the lines with a positive shift, to the $4f^5 5d6s \rightarrow 4f^6 6s$ transitions. The upper levels of the $4f^5 5d6s$ configurations also have a large isotope shift because of the reduction of s-electron screening.

The experimental data of [7] show that the energy levels of the $4f^5 5d6s^2$ electron configuration belonging to the lines with positive shift are in the region 18075-23996 cm^{-1} . They are all mixed in with the levels of the $4f^6 6s6p$ electron configuration lying in the 16112-22632 cm^{-1} region. Therefore it can be assumed that the neighboring levels excite each other. The isotope shift value of such levels depends on the contribution of the perturbing level. If this level belongs to the $4f^6 6s6p$ electron configuration, then the perturbation from the $4f^5 5d6s^2$ level causes an increase in its isotope shift and the shift in the line will decrease. This phenomenon is observed for lines in the short-wavelength region having a negative shift (Table 2 of [7]). Here the shift is approximately the same for all of the long-wavelength lines, but beginning with the line 5157.04 Å it decreases. Similarly, the perturbation of the levels of the $4f^5 5d6s^2$ configuration by the $4f^6 6s6p$ levels should cause a decrease in their isotopic shifts. The isotopic shift will be different for different levels, since the fraction of the wave function perturbing the electron configuration will not be the same. This is observed for the lines with positive shift (Table 3 [7]) where the shifts have various different values.

The data on isotope displacement in the Sm I and Sm II spectra show that in going from a spherical nucleus to a deformed one, in the case of the interval $\Delta\nu(150 - 152)$ the quadrupole effect makes a considerably greater contribution to isotope displacement of levels when the nucleus interacts with the $4f^5 5d6s^2$ and $4f^5 5d6s$ shells. This indicates that in the isotopic displacement of atomic levels, there is a non-linear influence of the deformed nucleus (or the surface vibration of the nucleus) on the wave function of the s-electron. This new phenomenon could be explained either by the perturbing effect of the neighboring levels of the two electron configurations or by the screening effect of the penetrating s-electrons.

However, the first assumption does not agree with our experimental data. The fact is that the characteristic behavior of the relative displacement is the same for lines with both negative and positive shifts, although the upper levels are subject to essentially different degrees of perturbation and the levels belonging to long-wavelength lines with negative shift are not perturbed at all. The second assumption is more probable and indeed follows directly from the experimental data. In fact, experiment shows that the behavior of the relative isotope displacement changes when there is a reduction in the s-electron screening. If one assumes that the wave function $\psi(o)$ is influenced in some way by nuclear deformation, then the screening for a given electron configuration will be different for different intervals of the isotopic structure. It would be interesting to consider this problem theoretically. Apparently, an addition to the formula for isotopic shift in the atomic spectra of heavy elements would be obtained.

The experimental work on the measurement of isotope displacement in the spectrum of dysprosium was carried out by A. F. Golovin and M. P. Gerasimova; the investigation of isotope displacement in the spectrum of samarium was performed by V. A. Katulin, V. V. Eliseyev and H. A. Kulazhenkova.

REFERENCES

1. H. Kopfermann, Kernmomente, 1960.
2. Y. P. Donzov, Opt. i Spect., 8, 446 (1960).
3. A. R. Bodmer, Nuclear Physics, 9, 371 (1959).
4. D. P. Grechuhin, J.E.T.P., 38, 1801 (1960); Nucl. Phys., 24, 576 (1961).
5. T. Huus, J. H. Bjerregaard, B. Elbek, Kgl. Danske Vid. Selsk. Mat. Fys. Medd., 30, No. 17 (1956); A. W. Sunyar, Phys. Rev., 98, 653 (1955).
6. B. Elbek, M. C. Olesen, O. Skilbreid, Nucl. Phys., 19, 534 (1960).
7. A. R. Striganov, V. A. Katulin, V. V. Eliseyev, Opt. i Spect., 12, 171 (1962).
8. P. Brix, H. Kopfermann, Z. Phys., 126, 344 (1949).

ABSORPTION SPECTRA OF GASEOUS ATOMS FORMED AT FLASH-HEATED TUNGSTEN SURFACES

L. S. Nelson and N. A. Kuebler
Bell Telephone Laboratories, Incorporated
Murray Hill, New Jersey, U.S.A.

INTRODUCTION

Gaseous free atoms are of considerable importance in many chemical reactions, both at high and normal temperatures. Studies of these reactions have been limited to relatively few elements, mainly because it is difficult to produce large concentrations of most atoms in the gas phase, especially those of solid elements with high melting points. Jennings [1] has recently reviewed the need for new ways to study atomic reactions.

In this work we describe the use of a flash-heating technique for the thermal production of gaseous atoms from solid elements by vaporization. As a trial material, we used the very refractory metal, tungsten, with boiling point near 6000°C.

Nelson and Lundberg [2] have shown that large concentrations (approximately 10^{-3} mole in 100 cm^3) of gaseous free atoms may be produced by exposing absorbing solids to the flash emission of capacitor discharge lamps. These lamps have been shown [3] to deliver thermal pulses in excess of 30 joules/cm^2/flash in times of about 10^{-3} sec. If the solid absorber has a large surface-to-mass ratio (that is, with at least one dimension below about 100 μ), temperature rises of several thousand degrees can be expected, and have been confirmed semiquantitatively [2].

Flash heating is experimentally similar in many ways to flash photolysis [4], which has been used with great success to prepare large concentrations of short-lived atoms and molecules for kinetic absorption spectroscopy [5]. This similarity prompted us to attempt a thermal instead of photochemical preparation of labile species by flash heating an array of solid bodies in the optical path of a flash-recording spectrograph. We have recently described [6] the method and some preliminary results on several atomic and molecular systems, using grids with fine windings as the array of solid material.

Tungsten wire was the first material used for these studies, because it is easily obtained with diameters below 20 μ, it is quite strong and easy to handle, and it is high-melting. Because of the refractory nature of tungsten, it was expected to offer the greatest difficulty of the metals; that is, if tungsten could be vaporized, we could assume that any other metal might be vaporized this way.

We have produced relatively large quantities of tungsten vapor by flash heating grids wound with fine tungsten wire and have also recorded the absorption spectrum of the vapor at various times during and after the heating flash. Because of the presence of tungsten atoms with thermal energies nearly 22,000 cm^{-1} above the ground state it seems likely that the vapor reaches at least the boiling temperature of tungsten metal.

EXPERIMENTAL

The method and apparatus used have been described recently [6] and shall only be outlined here. About 2 meters of 13-μ-diameter oxide-coated tungsten wire was used to wind each grid on a 25x35 mm rectangular frame made of fused quartz rod. The grids were held in the transparent fused quartz absorption cell so that the beam from the background light source passed through the windings. One grid was sufficient to produce a heavy absorption spectrum when significant vaporization occurred.

A helical flash tube similar to the General Electric Company FT 625 was placed concentrically around the transparent absorption cell; in turn the flash tube was surrounded with a cylindrical polished aluminum reflector. The lamp was powered with an Edgerton, Germeshausen and Grier Company "Sun Flash" photoflash unit, using capacitances up to 1300 μf charged to 4 kv. This produced a maximum radiant energy of 32 joules/cm^2/flash inside the cell, as determined with a graphite radiometer [3]. The heating flash had a duration at half-height of about 1.5 msec at maximum energy.

The background light source was a Lyman end-on discharge of about 20 μsec duration, one flash of which produced suitable film darkening between about 1250 and 4000A. The 2-meter grating spectrograph had an evacuated tank. The ends of the cell were closed with CaF_2 lenses.

The cell could be shielded from electrical effects of the discharge in the heating lamp by wrapping a grounded wire helically around the cell body.

In all experiments described here, the cell containing the tungsten grids was filled with streaming nitrogen at atmospheric pressure, obtained from a cylinder without further purification.

RESULTS

Visual Observations

One flash of the heating lamp at 1300 μf and 4 kv caused complete vaporization of the grid windings, and a thin mirror of tungsten was deposited on the cell wall. Afterward, no tungsten wire remained on the grid frame, nor in the cell. There were no droplets in the cell, either.

At half energy, 650 μf and 4 kv, much less vaporization occurred in the flash, and many windings, although mechanically disturbed, remained on the grid frame. The windings that remained were shiny as a result of removal of surface oxide. Only a small amount of metal was deposited on the cell wall, and, occasionally, metal droplets of about 0.5 mm diameter were found in the cell.

At lower energies per flash, progressively less tungsten was vaporized, and much less surface cleaning occurred.

Absorption Spectra

Several typical absorption spectra of tungsten vapor are shown in Figure 1. Each spectrum was recorded in a separate experiment with a new grid. The flash of the Lyman background source was delayed for various intervals after the start of the heating flash, as indicated at the left. The maximum energy of 1300 μf at 4 kv was used in each heating flash. Many hundreds of absorption lines were recorded over the entire region available to the spectrograph. The similarity of Figure 1 to traditional furnace spectra of an element at various temperatures [7] is very striking.

No banded spectra could be detected.

We have compared in some detail four spectra of tungsten vapor. These were obtained as follows: (1) with an evacuated carbon tube furnace operating at 2800°C, as reported by King [8]; (2) by flash heating four grids at maximum energy (1300 μf at 4kv) and recording after a 900 μsec delay; (3) identical to (2), except with a 2100 μsec delay; and (4) identical to (2), except with half energy (650 μf at 4 kv) and a 750 μsec delay. (Spectra (2) and (3) are longer wavelength portions of the upper and lower spectra in Figure 1, respectively.) The wavelength region studied was between 2831.378A and 2817.480A, the region common to King's spectra and the spectra recorded in this work.

King lists 46 tungsten lines in this wavelength interval. In this same interval, we have observed and measured the wavelengths of 171 absorption lines due to tungsten atoms, and some sensitive lines of impurities in the tungsten, mostly Ca, Zn, Cu,

Table 1

Number of Lines Detected in Spectra of Furnace and Flash-Heated Tungsten

Listed According to Lower Energy Level of Transition
(Wavelength Interval: 2831.378 to 3817.480A)

Lower Energy Level of Transition[a]	Energy[a] (cm $^{-1}$)	Spectrum (1) Furnace[b]	Spectrum (2) Flash[c]	Spectrum (3) Flash[d]	Spectrum (4) Flash[e]	Arc Lines[a]
^5D_o	0.00	3	4	4	2	5
$^5D_1$	1670.27	6	13	10	5	15
$^7S_3$	2951.27	16	23	13	10	29
$^5D_2$	3325.50	5	17	13	5	26
$^5D_3$	4829.99	6	20	11	8	30
$^5D_4$	6219.30	5	19	7	3	30
^3P_o	9528.01		6			9
$^3H_4$	12161.96		8			26
$^3P_1$	13307.09		5			24
$^3G_3$	13348.53		8			41
$^3F_2$	13777.71		2			38
$^3P_2$	14976.17		3			33
$^3H_5$	15069.94	1	4			23
$^3F_3$	15460.00		6			41

$^3G_4$	16431.30		1			29
$^3H_6$	17008.48		-			12
$^3F_4$	17107.01		3			38
-	17701.16		1			41
^3D	18082.84		-			22
$^5G_2$	18116.83		2			28
$^5S_2$	18280.48	1	1			30
$^5G_3$	18974.48		2			32
$^3D_2$	19253.59		3			24
$^5G_4$	19256.22	1	-			26
$^5G_5$	19535.00		3			20
$^5G_6$	19648.48		1			14
$^3G_5$	19826.02		1			20
$^3D_3$	19827.67		2			20
$^7F_2$	21448.66	1	1			3

[a] From reference 9.

[b] Evacuated carbon tube furnace operating at 2800°C, reference 8.

[c] This work, heating lamp fired at 1300 μf, 4 kv, delay 900μ sec after start of heating flash.

[d] This work, same as c except 2150 μ sec delay.

[e] This work, heating lamp fired at 650 μf, 4 kv, delay 750 μsec after start of heating flash.

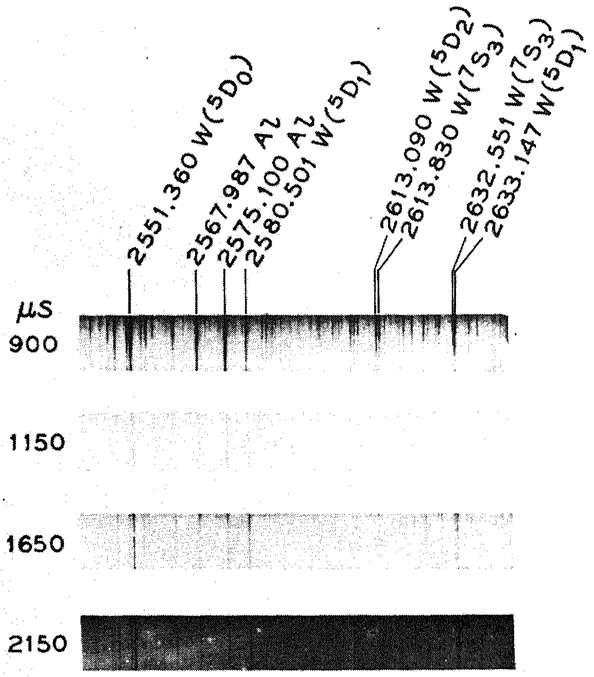

Figure 1. Absorption Spectra of Tungsten Atoms Produced by Flash Heating.

Fe, Mg and Al. Using the tabulation of Laporte and Mack [9], we have identified the lower energy level of each transition in the spectra produced both by furnace and flash heating.

In Table 1 are listed the number of lines identified in each of the four spectra according to the various lower energy states in each transition that forms the line. Also included are the total number of arc lines in the same wavelength interval that terminate in each energy level, according to the listing of Laporte and Mack.

Most of the transitions observed in absorption arose from atoms in the $^5D_0$ ground state, or in the five metastable states, $^5D_1$, $^7S_3$, $^5D_2$, $^5D_3$ and $^5D_4$, lying 1670.27, 2951.27, 3325.50, 4829.99 and 6219.30 cm^{-1} above the ground state, respectively. However, in spectrum (2), atoms were excited thermally to states lying as high as $^7F_2$, which lies 21448.66 cm^{-1} above the ground state. Spectrum (2) was recorded about 200 μsec after the peak of the maximum energy heating flash.

In a few spectra recorded with an unshielded cell under conditions otherwise similar to spectrum (2), a few faint lines corresponding in wavelength to W II could be detected. These were not observed with the shielded cell, however, although their presence did not seem to affect the intensities of the other tungsten lines appreciably.

We have also observed the formation of a slight continuous background absorption that increases with time. This is visible to some extent in Figure 1. It is assumed that this is due to scattering of light from the background source by droplets of tungsten formed as the grids volatilize.

King did not report lines at wavelengths shorter than 2831.387A. With flash heating, however, a very intense, complex absorption spectrum extending to wavelengths as low as about 1600A was recorded. This region below the King region has not been analyzed as yet.

King's exposure times with the furnace were limited by reaction of the tungsten vapor with the carbon tube. In this work, due to the pulse nature of the experiment, hot tungsten was in contact with the cell walls only for a few milliseconds during the flash. The only change in the cell after the flash seemed to be the presence of a thin mirror of tungsten on the wall which could be removed easily by rinsing with dilute hydrofluoric acid.

DISCUSSION

In this work we have shown that flash heating may be used to prepare a concentrated burst of neutral metal atoms in a reaction cell. Since the highly refractory metal, tungsten, vaporizes readily, it seems likely that almost any solid element may be volatilized this way as long as it can be prepared thinner than about 100 μ. Reactions of these atomic vapors alone or with many gases over a wide range of pressures may be studied this way. Photochemical side effects may be minimized by filtering out appropriate spectral regions of the emission from the flash. Side effects that result from metal ions formed electrically by the heating flash may be eliminated by proper shielding of the cell.

The method is quite sensitive. One grid with two meters of 13-μ-diameter tungsten wire, when vaporized, places about 3×10^{-5} gram atoms of gaseous metal in the absorption path of the spectrograph. This produces a very intense absorption spectrum, many lines of which appear completely saturated. Impurities in the tungsten, shown by emission spectrography to be less than 0.001% in the case of aluminum, also appear strongly in absorption in the spectrum, as shown in Figure 1. Thus, in some instances, it is possible to detect as little as 10^{-9} to 10^{-10} gram atoms of a metal. This compares favorably with emission techniques.

As yet, we have not attempted to measure electronic temperatures of the tungsten vapor. However, from the primary thermal population of levels up to about 6200 cm^{-1} in the King furnace at 2800 °C, and over 20,000 cm^{-1} observed in spectrum (2), recorded shortly after the peak of the heating flash fired at maximum energy, it seems reasonable to assume that the absolute temperature of the vapor in spectrum (2) was at least twice that of the furnace, probably near the boiling point of tungsten at 6000 °C. This seems reasonable also because the tungsten does vaporize completely, very probably via a liquid phase. There also is the possibility that the tungsten may have superheated before vaporizing, giving temperatures even higher than the boiling point.

By similar reasoning, the vapor in spectrum (4) produced at half energy probably has a temperature nearer that of the King furnace, while that in spectrum (3), recorded when the heating flash fired at maximum energy has decayed to about 20% of its peak intensity, is probably between the temperatures of spectrum (2) and the spectrum (1), recorded in the furnace.

REFERENCES

1. K. R. Jennings, Quart. Rev. (London) 15, 237 (1961).
2. L. S. Nelson and J. L. Lundberg, J. Phys. Chem. 63, 433 (1959).
3. N. A. Kuebler and L. S. Nelson, J. Opt. Soc. Am. 51, 1411 (1961).
4. G. Porter, Proc. Roy. Soc. (London) A200, 284 (1950).
5. See review by R. G. W. Norrish and B. A. Thrush, Quart. Rev. (London) 10, 149 (1956).
6. L. S. Nelson and N. A. Kuebler, J. Chem. Phys., 37, 47 (1962). (July 1962).
7. For example see A. S. King, Astrophys. J. 60, 282 (1924).
8. A. S. King, Astrophys. J. 75, 379 (1932).
9. O. Laporte and J. E. Mack, Phys. Rev. 63, 246 (1943).

CRITICAL REVIEW OF METHODS AND RESULTS OF TIME-RESOLVED SPECTROSCOPY

K. Laqua and W. -D. Hagenah
Institut fur Spektrochemie und angewandte Spektroskopie
Dortmund, Germany

INTRODUCTION

In some of the spectroscopic light sources, e.g., spark discharges, wire explosions, pulsed arcs and shock tubes, important parameters such as electric current, temperature, etc. change rapidly with time, and hence the radiation is also time-dependent. It is therefore often advantageous to study the radiation of these sources by resolving its spectrum in time. Schuster and Hemsalech [127], in 1900, were probably the first to use time-resolved spectroscopy for their work on the spectra of spark discharges. By moving the photographic film in the focal plane of their spectrograph with speeds as high as 1 m/sec perpendicular to the direction of wavelength dispersion, they attained a time resolution of the order of 10^{-4} sec.

In 1921 Ramsauer and Wolf [115] investigated the afterglow of spectral lines of the alkali and alkaline earth metals, as well as of Cu, Zn, Al, Hg, using Figure 1 a rotating slotted disc S in front of a spectroscope and a switch with a rotating contact K on the same shaft as the disc, for terminating the electric arc periodically. For measuring the duration of the afterglow, the phase of the rotating contact had to be shifted with respect to the slotted disc. Their time-resolution was of the order of 100 μsec at speeds of 5 rps. A time-resolved spectrograph which corresponds almost to modern specifications was described in 1925 by Sinclair Smith [131]. He used rotating mirrors for sweeping the image perpendicular to the direction of wavelength dispersion Figure 2. Particulars of his apparatus are: mirror speed 150 rps, time dispersion 0.5 mm/μsec, spectral resolving power 60,000, spectral range 3000-5000 A. At the same time, Brown and Beams [28] in their paper "The order of appearance of

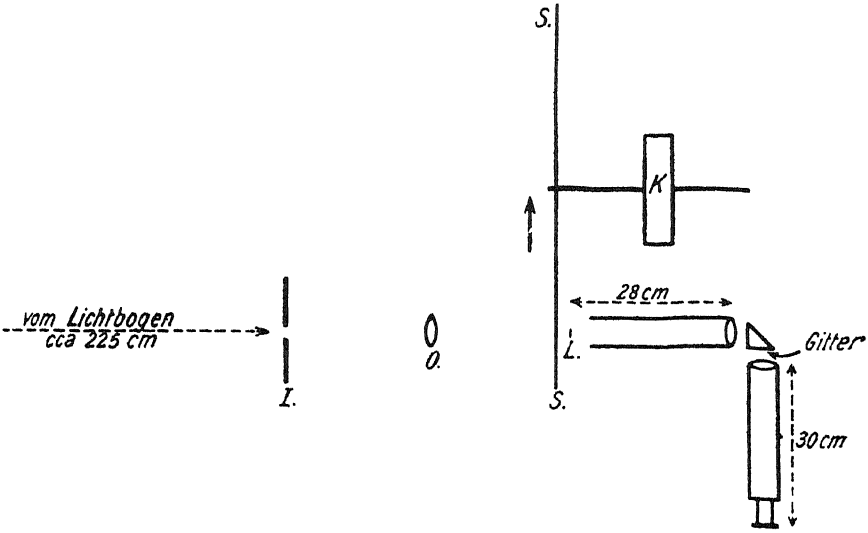

Figure 1. Time-resolved spectroscopy using a slotted disc, [from (115), Courtesy Ann. Phys.].

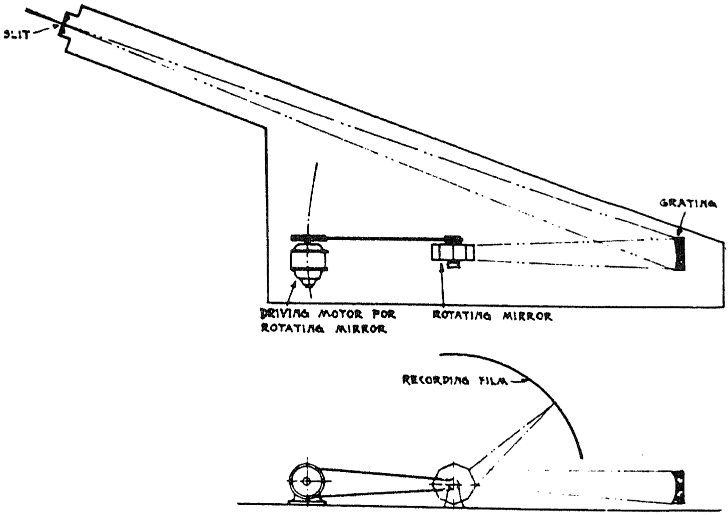

Figure 2. Rotating-mirror spectrograph, [from (131), Courtesy Astrophys. J. Copyright 1925 by the University of Chicago].

certain lines in the spark spectra of cadmium and magnesium'' made use of yet another method, i.e., a Kerr cell electro-optical shutter placed in front of the spectrograph slit. By connecting the Kerr cell in parallel with the spark gap under investigation, they obtained a very accurate synchronization. The use of a delay line between spark gap and shutter enabled them to shift the open period of the shutter with respect to the firing of the spark gap. Very short exposure times were made possible by using this technique (10^{-7} μsec).

In 1926, during their investigations of wire-explosions, Anderson and Sinclair Smith [5] described a magneto-optic shutter, utilising the Faraday effect. As the spark current activated the shutter, a very effective synchronization was achieved. Lawrence and Dunnington [95] used a technique similar to the one described by Brown and Beams [28] in their investigations of the early stages of a spark discharge. Their experimental arrangement is shown in Figure 3. An exposure of 4×10^{-8} sec was obtained. Equally surprising as the variety of these early methods, is the use of widely different methods for triggering and synchronizing. The process under observation is either initiated by the time selecting and resolving device [115] or vice versa [28,95].

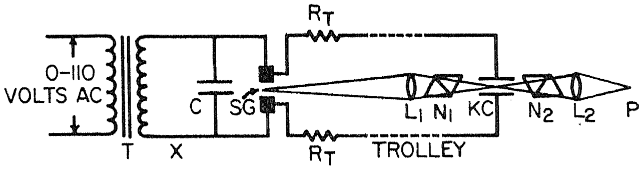

Figure 3. Kerr cell shutter used for time-resolved spectroscopy of sparks, [from (95), Courtesy Phys. Rev.].

The main steps in the further development of time-resolved spectroscopy have been the following:

1. The use of a mirror rotating at high speed (1600 rps) by Beams [20] for studying the time of appearance of spectrum lines in a spark discharge.

2. Deinum and de Boer [49,50] in 1939 superimposed the light of many low power sparks as they are used in spectrochemical analysis. The breakdown of the spark gap was controlled by a contact on the rim of the rotating disc acting as time-resolving shutter. A time resolution of about 10 μsec was obtained.

3. The work by Rawcliffe [117], by Dieke, Crosswhite and co-workers [51,53] by Meek, Craggs and co-workers [107,41,42] on the use of photomultiplier tubes for measuring transient phenomena in spectral lines created the necessary conditions for a further expansion of time-resolved spectroscopy.

4. Orr [110], investigating the spectral properties of spark discharges, made use of such a photoelectric method.

5. Crosswhite, Steinhaus and Dieke [43] investigated the possibilities of using only selected time intervals of the radiation

of spark discharges for spectroscopic and spectrochemical purposes. By pulsing the voltage between two dynodes of a photomultiplier tube, they obtained an off-on ratio of 1:200. They later [133] improved this ratio to 1:10^4 by gating the signal between the photomultiplier tube and the recorder. They proposed using, in a series of spark discharges, only the late arc-like part in each discharge, thus combining the many desirable properties of a spark with the inherent high sensitivity of an arc. An example of such an analysis (0.1 to 1.5% Cr in steel) was given. Figure 4 shows the change with time of a copper spark spectrum taken from one of their publications; Figure 5 shows the reduction in dark current noise by gating the signal.

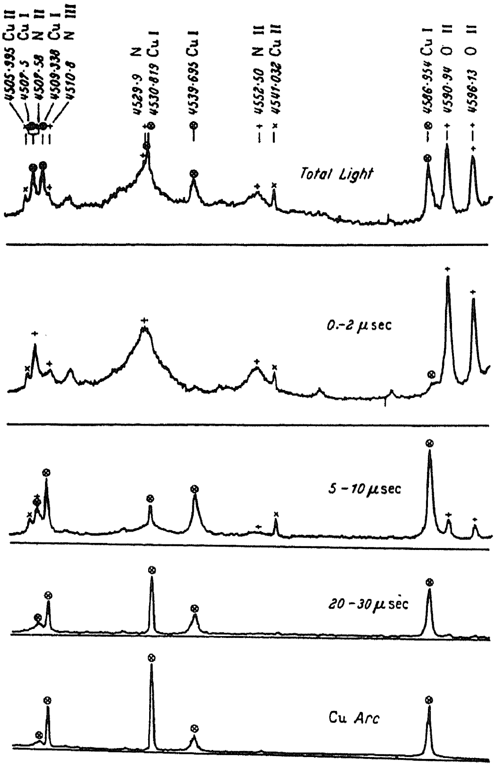

Figure 4. Copper spark spectrum in air at various time intervals after the initiation of the spark discharge, [from (134), Courtesy Spectrochim. Acta].

6. In the meantime Gordon and Cady [74] constructed a photographic time-resolving spectrograph with remarkable properties, using a rotating mirror (600 rps). A time-resolution of 0.5 μsec and a useful time-interval of 10 μsec was obtained. An auxiliary light beam, together with a photomultiplier tube, was employed

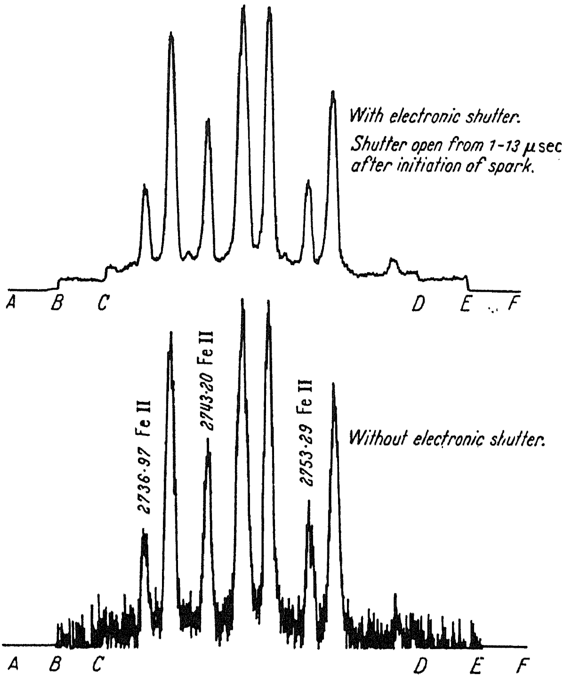

Figure 5. Use of electronic shutter to reduce dark current noise, [from (134), Courtesy Spectrochim. Acta]. A–B and E–F; no voltage on photocell. B–C and D–E; voltage on photocell, no light. C–D; voltage on photocells light, spectrum recorded.

for triggering the spark discharges with low jitter. A similar apparatus was described by Tsui [145].

7. In 1955 Bardocz and Varsanyi [16,17] described a rotating mirror technique with photographic recording of the spectrum, in connection with a high voltage spark generator [10]. An auxiliary light beam, reflected by the rotating mirror, produced an electrical signal for triggering the discharge across one of two auxiliary spark gaps. Figure 6 shows the circuit. The trigger signal is introduced at position y in the figure. As shown later by other authors [77], series-triggering can be used as successfully, instead of the parallel triggering of Bardocz and Varsanyi. Using again the late arc-like part of a spark discharge, a spectrochemical analysis of 0.01% Cu in aluminum was made.

8. The use of image converter and intensifier tubes for producing time-resolved spectra has been explored by Vanyukov and Milov [152]. The sensitivity of these devices is higher than that of any photographic material. The image converter can either be pulsed, acting as light amplifier and shutter at the same time, or the image on its screen can be scanned by other means (e.g.,

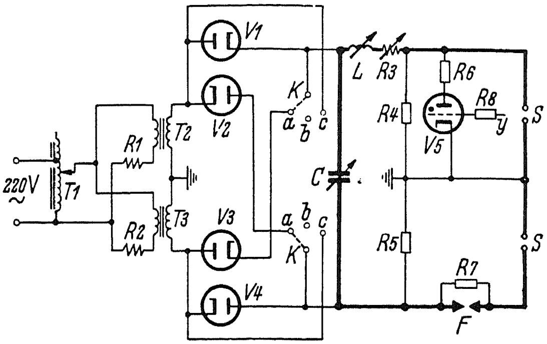

Figure 6. Circuit diagram of electronically controlled high voltage spark generator for spectroscopic purposes,[from (10), Courtesy Z. Angew. Phys.].

rotating mirror). The final time-resolved spectrum can either be obtained on a photographic plate [152,123] or be displayed on the screen of an oscilloscope tube [125]. Figure 7 demonstrates such a scanning system. In Figure 8 a comparison is made between a direct photograph of a spectrum and its photograph taken from the screen of an image converter tube. The gain in intensity can be 10 to 10,000 times depending on the experimental conditions, at the sacrifice of some loss in wavelength resolution.

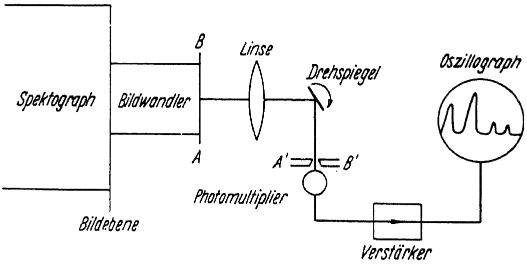

Figure 7. Schematic drawing of scanning and displaying device for time-resolved spectroscopy using an image-converter tube, [from (123), Courtesy North Holland Publishing Company].

9. By having the spectrum focused on the photocathode of a television camera tube, Gloersen [72] used a modern but somewhat unfamiliar method for producing time-resolved spectra on the screen of a cathode ray tube. A rotating slotted disc in front of the spectrograph slit acted in such a way that the spectra belonging to successive slots were displaced vertically on the screen. Figure 9 shows the block diagram of his system, Figure 10 a photograph of a series of spectra taken from the oscilloscope screen.

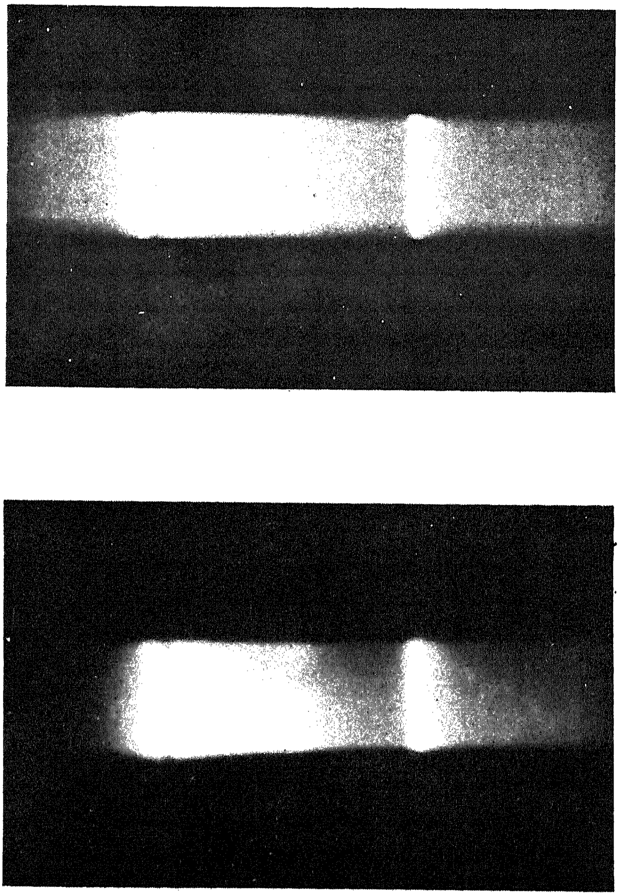

Figure 8. Part of high-pressure mercury vapour spectrum near 6000 A, photographed directly (top) and from the screen of the image converter tube (bottom), [from (123), Courtesy North Holland Publishing Company].

SURVEY OF THE METHODS OF TIME-RESOLVED SPECTROSCOPY

General Considerations

As has been shown so far, many methods can be used for producing time-resolved spectra. Rotating discs and mirrors, a moving photographic film, electro- and magneto-optical shutters placed at suitable positions within the apparatus have all been employed in order to effect the desired time-resolution of the light signal. Photographic materials as well as photoelectric

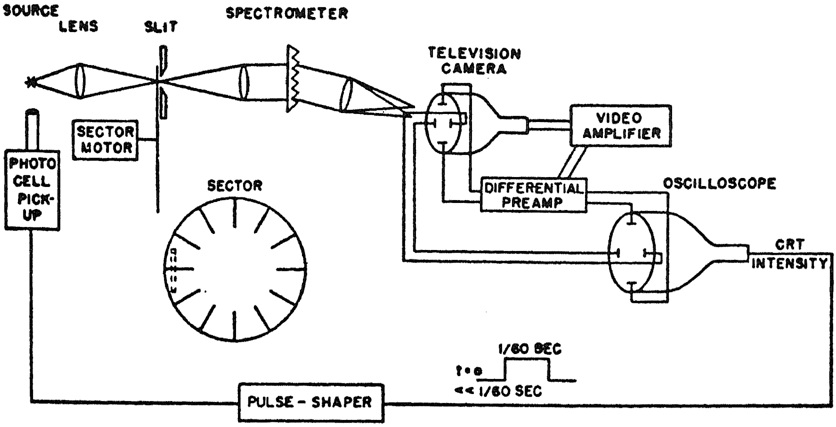

Figure 9. Block diagram of the electronic recording, time-resolving spectrometer using a television camera, [from (72), Courtesy J. Opt. Soc. Amer.].

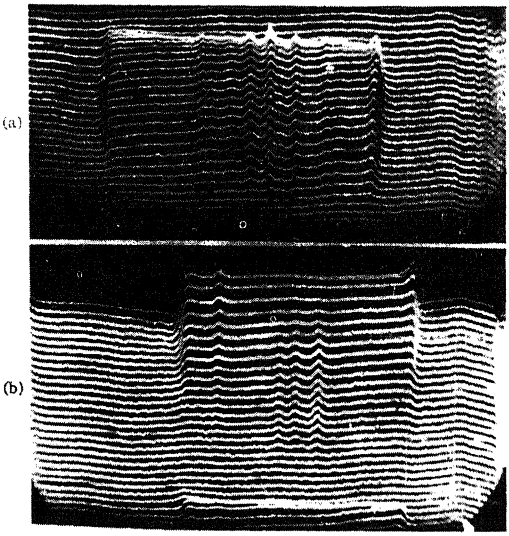

Figure 10. Vidicon records of spectra obtained by using the spectrometer described in Figure 9, [from (72), Courtesy J. Opt. Soc. Amer.].

devices are suitable as radiation receivers, the latter type being able to act as time-resolving element at the same time. In case the optical signal is converted into an electric signal, the latter can be treated in such a way as to produce a resolution in time. All possible kinds of spectral apparatus have been used in conjunction with these time-resolving devices.

As it is not possible to review all these possible combinations, an attempt will now be made to provide a systematic treatment. Intensity measurements in time-resolved spectroscopy can usually be described in the form of

$$I = I\ (x, y, t, \lambda) \tag{1}$$

with x and y the two space coordinates perpendicular to the direction of observation, t the time and λ the wavelength of the radiation. Information regarding the z-coordinate can only be obtained in cases where some assumptions relating to the symmetry of the radiating source under investigation can be made. A full representation of Eq. (1) requires a five dimensional space. In principle the use of digital memory systems is also possible, but has not been reported as far as is known. If, as is often the case in practice, a photographic plate serves as a radiation detector, the intensity is recorded as density, and two other variables of Eq. (1) are represented as coordinates on the plate, while the remaining two variables are used either as parameters or superimposed on two of the other variables. It is also possible to integrate them.

The insertion of an image-converter or image-intensifier between the final image in the measuring apparatus and the photoplate constitutes no fundamental departure from the principle of the experimental arrangement:

A three dimensional recording of measured variables is also obtained if image memory systems with electronic scanning (image orthicons, etc.) are used as far as the mosaic screen is concerned. As the results recorded on the mosaic screen cannot be preserved for a long time, it is necessary either to represent the results on an image screen and have this image photographed (in which case the three dimensional representation is not changed), or have it scanned vertically or horizontally with respect to electric values by a beam of electrons. In the latter case another continuous variable has to be transformed into a discrete parameter.

Most photoelectric methods enable only a two dimensional recording of the results of the measurements.

In Figure 11 some examples of different types of time-resolving spectral apparatus are shown. The top row demonstrates how a perfect optical relay of an information (for example a spark gap) is accomplished. There is a sequence of aperture and image stops with suitable lenses or mirrors at the correct positions, in order to form the corresponding images. The smallest aperture stop determines the f-value, the smallest image stop the field of view. This system can be continued at will. Into this optical system all elements for spectral and time-resolution

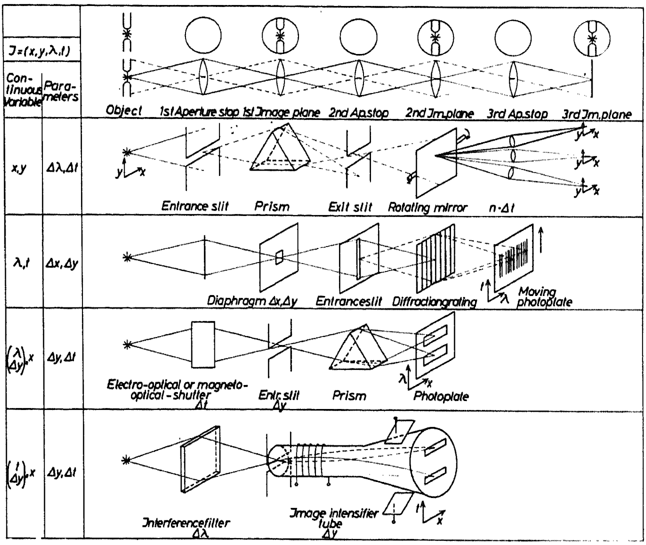

Figure 11. Principles of time-resolving spectroscopic devices.

have to be fitted. In a correctly designed system, all these elements should lie exactly in one of these planes or in some of them, i.e., they should be passed by a parallel beam of light in order to avoid vignetting and other distortions. The selection of the variables of Eq. (1), and their transfer to the coordinates of the receiver are determined by the position of the elements in the optical scheme and relative to each other. In order to demonstrate this scheme, four fundamentally different examples have been chosen. The elements for spectra and time-resolution are always placed in one of the above-mentioned planes. The necessary lenses or mirrors are not indicated in the drawing.

The first example shows the well-known frame-camera or Miller-camera [108] but with spectral resolution. There is a consecutive series of n monochromatic ($\Delta\lambda$) images of the light source (x, y) with an exposure time of Δ t for each image. The next example contains in the first image plane a diaphragm for selecting the desired part of the light source (Δx, Δy) which in turn is imaged on to the grating (second image plane); therefore uniformly illuminated spectrum lines will be recorded in the third aperture stop. If the photographic film or plate is moved perpendicular to the direction of wavelength dispersion (λ) the final record will contain I, λ, t. The next schematic drawing shows a time-resolved spectrograph with an electro-optical or similar shutter (Δt) in the first aperture stop. The width of the horizontal slit of the spectrograph selects the Δy portion of the light source. Continuously recorded on the photographic plate are I, x and λ with Δy superimposed. The last example shows a spectroscopic streak camera, with which I, x and t (superimposed Δy) are being continuously recorded, whereas Δλ and Δy have discrete values.

It is obvious that the properties of any simple combination of spectral and time-resolving means can be deduced from the scheme. Economic considerations play an important part in determining in what sequence the different elements should be used. Even the more sophisticated methods of time-resolved spectroscopy will fit the scheme, e.g., employing a rotating mirror more than once, or having more than one element for either resolution. In Figure 12 a schematic diagram of a complete time-resolved spectrograph is shown [70], the trigger signal being obtained by a contact. In Figure 13 a similar arrangement using a rotating disc and an auxiliary light beam for triggering is demonstrated [77].

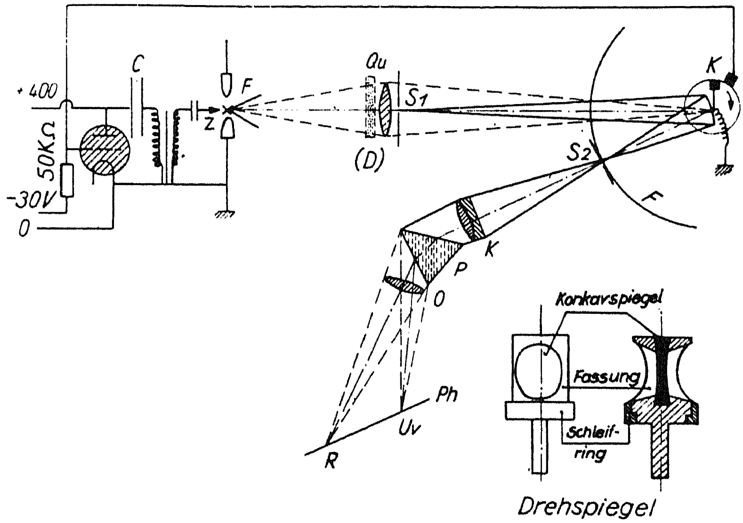

Figure 12. Schematic diagram for time-resolving spectrograph using a rotating mirror, [from (70), Courtesy Optik].

The performance limits of devices for time-resolving spectroscopy

The resolutions in time, wavelength, space and intensity cannot be increased beyond certain limits set by a) the statistical behaviour of the light quanta, b) the mechanical or optical properties of the materials used, c) the wave nature (diffraction) of the light. Whereas a) and c) are of a fundamental nature, improvements of b) may be expected in the course of technical progress.

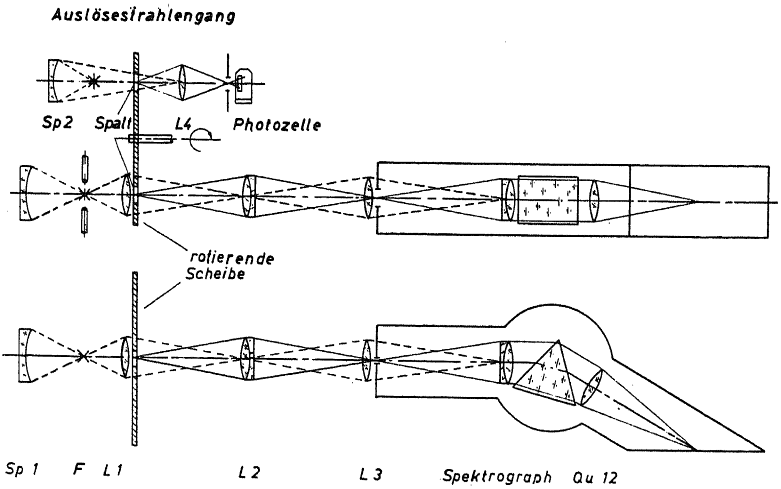

Figure 13. Block diagram of time resolving spectrograph using a rotating disc and an auxiliary light beam which triggers the discharge, [from (77), Courtesy Rev. Universelle Mines].

a. The influence of the statistical nature of the light quanta has been stressed by Zaidel, Malyshev and Shreider [164]. It is useful to define a total resolution A_r (not resolving power!) with respect to the object under investigation for the whole apparatus as follows

$$A_r = A_r(A_I, A_x, A_y, A_t, A_\lambda) \tag{2}$$

with the resolutions of the parameters defined as

$$\text{(2a) } A_I = I/\Delta I, \text{ (2b) } A_x = 1/\Delta x, \text{ (2c) } A_y = 1/\Delta y,$$

$$\text{(2d) } A_t = 1/\Delta t \text{ and (2e) } A_\lambda = \lambda/\Delta\lambda.$$

It will be shown in the appendix that for (2) the following expression can be derived

$$A_r = \eta_{\min} \frac{\lambda^2 E_\lambda \omega}{h\,c} \tag{5a}$$

with $E_\lambda = \dfrac{\text{Radiation energy of the source under observation}}{(\text{cm}^2 \cdot \text{sterad} \cdot \text{sec} \cdot \text{Å})}$

and ω the solid angle into which the utilised radiation is emitted. The meaning of $\eta_{\min}$ should be as follows:

Whereas all considerations so far have been concerned only with the number of quanta emitted from the source, it is now time to consider all processes that lead to a decrease in the actual number of quanta available for the representation of our information. This decrease can be caused by absorption, or by a quantum yield less than 100% at any place in the measuring apparatus where light quanta are being transformed into other kinds of information units, e.g., blackened photographic grains, photoelectrons, etc. In this consideration, η_{min} signifies the ratio of the minimum number of quanta or other information units available at any place inside the apparatus to the original number of quanta available from the source.

b. While Eq. (5a) sets the overall limit for the total resolution, there are additional restrictions limiting the single resolutions, caused by the mechanical properties of rotating mirrors or discs, the coarseness of the photographic grains, the on-off ratio of electro-optical or magneto-optical shutters, the trigger stability etc. In the case of a frame-camera, Schardin [120] has derived a formula for the performance limit of t- and x-resolution caused by the tensile strength of the mirror material and by diffraction. Skinner [130] has expanded this formula by introducing the product of exposure time per frame and frame frequency:

$$\frac{A_t A_x b}{t_f f_w} = \text{const}, \tag{6}$$

where b = image size, t_f = exposure time per frame, and f_w = frame frequency.

In addition it should be mentioned that some time-resolving elements have limitations with respect to wavelength range (e.g., Kerr cell) and most of the radiation receivers have limitations with respect to time-resolution.

The application of time-resolved spectroscopy is usually restricted to a wavelength range where sensitive radiation receivers are available, e.g., from about 100 to 10,000 Å.

c. In optics generally, unavoidable diffraction patterns set a limit to the resolution of images, and they can consequently also be a serious limiting factor in time-resolved spectroscopy. In table 1 an attempt has been made to provide a survey of available data, as published in recent papers. Unfortunately there is hardly any publication in which one can find all the essential data. It should be stressed that only reported values, not calculated limits, are listed. In column 7 reference to papers dealing with the corresponding subject is made. For further information the following review papers should be consulted: [39,65,121,122,123, 98,68,23],

Table 1

Performance Data of Different Devices Used in Time-Resolved Spectroscopy

	I Time-resolution $A_t = \frac{1}{\Delta t} \sec^{-1}$	II On-off ratio of shutter	III Efficiency (transmissivity or quantum yield) of time-resolving apparatus	IV Wavelength range of time-resolving device	V Radiation receiver	VI Quantum yield of receiver	VII Literature
1. Camera with continuous or discontinuous film transport	10^7 (26)	limited by stray-light	1.0	limited by wavelength range of optic	film or photographic plate	10^{-4}	(38,89,142)
2. Mechanical shutter (rotating disc, etc.)	2×10^7 (161)	limited by stray-light	1.0	limited by wavelength range of optic	film or photographic plate	10^{-4}	(13,124)
3. Rotating drum	10^7 (80)	limited by stray-light	1.0	limited by wavelength range of optic	film or photographic plate	10^{-4}	(29,56)
4. Mechano-optical shutter, rotating mirror	10^8 (80,24)	$10^3 \ldots 10^4$	0.8 ... 0.9	limited by wavelength range of optic	film or photographic plate	10^{-4}	(74,8,16,27, 64,25,57)
5. Electro- or magneto-optical shutter Kerr cell Faraday cell	 2×10^8 10^8 (165)	$10^3 \ldots 10^5$ depending on type of polarizer	0.1 ... 0.2	visible spectral range (221)	normally photographic plate or film	10^{-4}	(55,66,75,96, 35,59,34)
6. Electron-optical devices	$10^9 \ldots 10^{10}$ (37,166)	$10^3 \ldots 10^6$	0.05 ... 0.15	0.2 ... 1.2μ	photographic plate or photomultiplier tube	10^{-4} 0.15	(36,44,102, 111,136,3, 125,72)
7. Photomultiplier tube Pulsed multiplier or gated amplifier	3×10^7 (82)	$10^4 \ldots 10^6$	0.15	100 Å ... 10000 Å	--	0.15	(48,41,148, 139,138,61, 43,134)
8. Triggering devices	5×10^8 (165)	--	--	--	--	--	(144,76,47, 12,10,79)

SPECTROSCOPIC MEASUREMENTS USING TIME-RESOLVED SPECTRA

Investigations with the aid of time-resolved spectroscopy can be divided into two groups, e.g., into investigations of single events and into investigations of statistical mean values of many single events. For the former, a minimum amount of light is required, while the latter demands an accurate synchronization as provided by modern electronic techniques. It is therefore not surprising that time-resolved spectroscopy has not been applied for analytical purposes in spectrochemistry before 1951.

It is not the purpose of this paper to give a complete survey of all the work that has been done in this field, but an attempt will be made to single out some typical problems that have been studied by means of time-resolved spectroscopy. As the published literature contains some comprehensive surveys on the use of spectroscopic techniques for diagnostic purposes in hot plasmas, a field in which extensive use has been made of time-resolved spectroscopy [6,163,164,97,109,99,68,23,40] little will be said on this subject here. The most frequent subjects of such investigations have been instabilities of pinched discharges, electron densities, electron temperatures, ion temperatures, degree of ionization, radiation losses and impurities. Measurements of intensities of both individual spectrum lines and continuous radiation as well as determinations of line width and line shift are indispensable in such investigations.

1. A subject of early interest in the history of time-resolved spectroscopy was the order of appearance of different spectrum lines, continuous radiation, band spectra, etc., in transient discharges. Since Schuster and Hemsalech [127] it is known that air lines appear before spark lines and spark lines before arc lines. The dependence on the degree of ionization and excitation potential has been investigated [114,33,22,104,110]. The intensity distribution with time of spectrum lines of different excitation potential and of the continuum has been measured [104,109] and compared with calculations. An example is shown in Figure 14.

2. One of the most discussed subjects in gaseous discharges has always been the temperature of the discharge. By using time-resolution it has now been established that the electron temperature of the channel at the beginning of a spark discharge is as high as 30,000° K or more [71,32,46,103,90,140,101]. This result was obtained with the help of the Ornstein method employing spectral lines of high excitation potential. Lines with an unsufficiently high excitation potential as used previously for temperature determinations have not given the temperature of the core but that of a cooler outer layer (see for instance [22]) as was pointed out by Huldt [84].

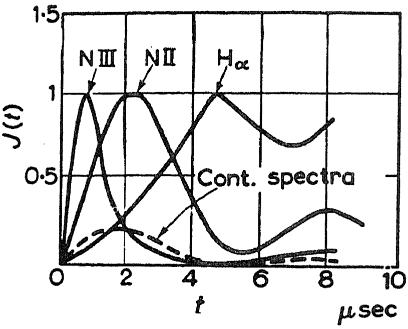

Figure 14. Time-resolved intensities of several lines and of the continuous spectrum, [from (103), Courtesy Spectrochim. Acta]. $C = 0.25\ \mu F$, $L = 10\ \mu H$, $V = 14$ kV.

In cases where the discharge channel has a cylindric symmetry the use of the Abel inversion enables the correct determination of the temperature of other zones than the centre core. It appears impossible to deduce the temperature by the Ornstein method from the relative intensities of two spectrum lines with appreciably different upper level energies inasmuch as they are excited in different discharge zones where the temperatures are different and at different instants in time [90].

The same high temperature has been found independently by applying a hydrodynamic shock theory [1,54] to the expansion of the spark channel [104]. Recently, similar values have been determined by a new method [87] where no transition probabilities or electron densities need be known. If the temperature at which a certain spectrum line reaches its maximum intensity is called "norm temperature" [94] (see Figure 14) it has been shown [132] that in a cylindrically shaped plasma, which is cooling off, the norm temperatures of different lines indicate the temperature of the core at different instants of time. There exists a logarithmic relation between norm temperature and time as is demonstrated in Figure 15. In all these measurements thermodynamic equilibrium is assumed to exist, at least between electrons and ions.

3. As far as the question of thermodynamic equilibrium is concerned, it has been calculated that for an initial temperature of 60,000° K in spark discharges under normal pressure, translatory equilibrium should be reached within 10^{-7} sec [103]. Other authors [167] believe that this time should be somewhat longer (10^{-6} sec). In experiments on the establishment of complete equilibrium in the plasma of an electric discharge, the following results have recently been obtained: All temperatures reach equilibrium within a time smaller than 10^{-6} sec except the vibrational temperature, which takes 20 to 25 μsec [113].

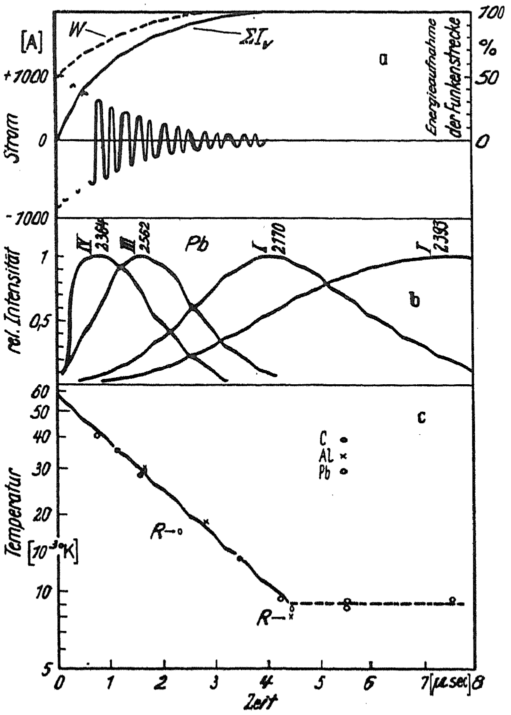

Figure 15. Cooling off of a plasma heated by a short high current pulse. Current and energy (a), light emission of different lines (b), course in time of temperature of the plasma (c), [from (87), Courtesy Z. Physik].

4. The afterglow of electric discharges, also the subject of early investigations [127,115] has been used for classifying spectrum lines in a similar manner as the order of appearance [31, 2,63,169] and recently for calculating coefficients of recombination [155].

In Figure 16 the afterglow of Zn-lines after the spark current has ceased can be seen.

5. From the modulation of the intensity of different spectral lines by a high frequency spark current [49,50] thermodynamic properties of the plasma have recently been calculated [58].

6. Line broadening (see Figure 17) and shifting and their change with time have been used to calculate ion temperature, density of charged particles, the Stark constant and the interatomic fields [22,49,50,21,159,140,15,18,99]. The influence of the upper energy level on shift and width has been stressed [15, 18]. The linear Stark effect (line broadening without shift) in hydrogen has been the subject of considerable interest [99].

7. More work has been done to investigate the properties of the channel of spark discharges and more generally of a plasma.

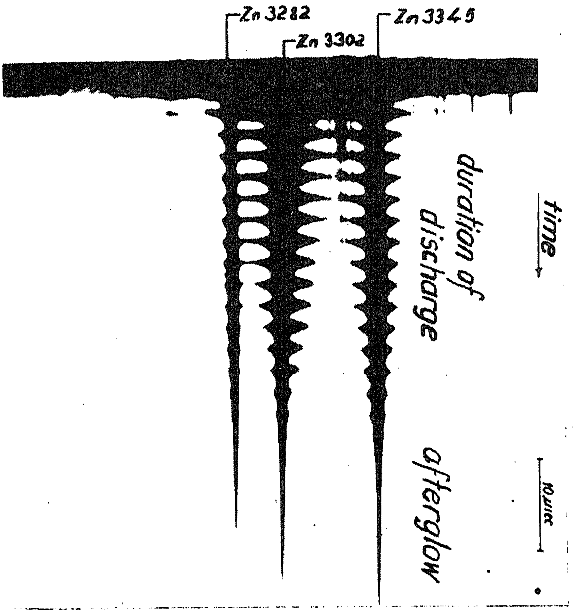

Figure 16. The afterglow of the first triplet of diffuse series of Zn, [from (155), Courtesy Sauerländer u. Co. Aarau/Switzerland].

Figure 18 shows electron density and temperature distribution across a spark channel as determined by time-resolved spectroscopy. The change with time of the diameter of the channel, as well as its dependence on the change of current [147,116,156, 149,135], have been studied. Boltzmann's law for the distribution of atoms among the excitation terms has been tested [147]. The work of Glaser [70,71] covering many aspects of spark discharges should be mentioned. More information on the spectra of the discharge atmospheres, and of the wavelength distribution of line and continuous energy from the ultraviolet to the near infrared has been obtained [116,150,151,118,99]. An example is shown in Figure 19.

8. Wire explosions offering a number of special features e.g., a discharge channel with cylindric symmetry, filled almost completely with the vapor of the wire material instead of the surrounding atmosphere, have been studied for a long time [131, 90]. An interesting result has been reported recently [19]: the channel of the discharge is formed along the wire before the wire has been destroyed by the explosion.

9. Time-resolved spectra and their distribution across the gap of vacuum discharges have been studied using high spark currents [157,128,85]. In these discharges a plasma not influenced

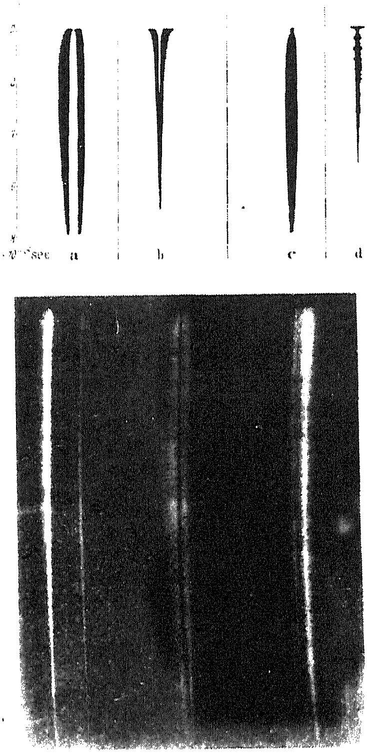

Figure 17. Line shape of time-resolved spectrum lines, [from (50), Courtesy Spectrochim. Acta].

by a discharge atmosphere is obtained in which lines of highly ionized atoms are easily excited [128,85].

10. An object of great interest from many points of view, and for a considerable time, has been the behaviour of the vapor clouds originating from the electrodes. Since Schuster and Hemsalech first measured velocities of such vapor jets [127], extensive studies [86,81,162,45,140,83,105] have been made. With the help of time-resolved spectroscopy, velocities of the vapor jets have been determined by measuring the time of appearance of the spectral lines of the electrode material at certain places in the gap. Values up to 4 km/sec have been recorded, depending on the electrode material and the discharge conditions. The velocity of the anode jet was always higher than that of the cathode jet. No anode vapor jet is found in rare gas atmospheres. This indicates that chemical reactions on the electrode surface are responsible for the production of anode vapor jets in atmosphere other than noble gases. A dependence of the jet velocities on the atomic weight has also been noticed. Further observations

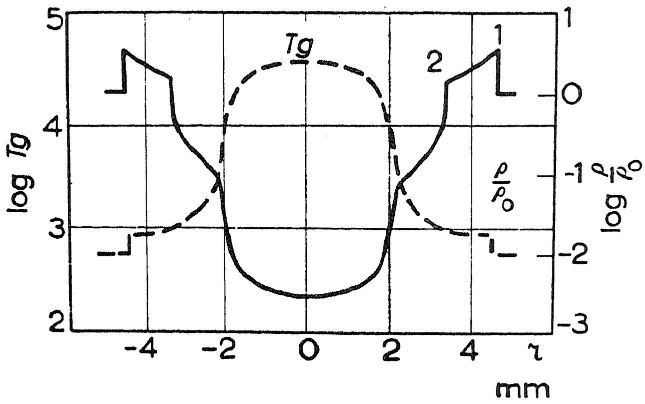

Figure 18. Distribution of electron density and temperature across the channel of a spark discharge 2.9 μsec after breakdown, [from (104), Courtesy Spectrochim. Acta]. t = 2.9 μsec, L = 2 μH, C = 0.25 μF, V = 10 kV. 1 - pressure wave, 2 - channel envelope.

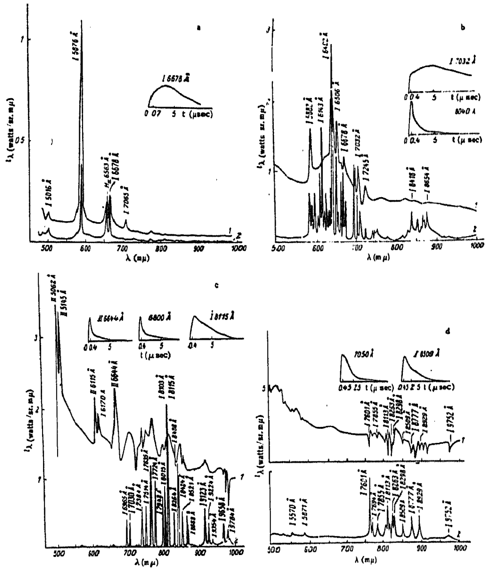

Figure 19. Spectral density of discharges in helium (a), neon (b), argon (c) and krypton (d) recorded at different times, [from (151), Courtesy Opt. Spectry].

revealed that the jets leave the electrodes perpendicular to the surface and that there are pronounced differences in the luminous behaviour of both jets. The kinetic energy of the jet is comparable to that of the mean excitation energy of the spectrum lines. Estimates on the current density have also been made.

11. Following earlier work [95,129,119] the spectrum of spark breakdown has recently been investigated [14,135,158]. In addition to broadened N II and 0 II lines and a strong continuum, a bandspectrum, apparently excited in the colder mantle surrounding the hot channel of the spark, has been detected [14].

12. Sparks as light sources for illumination purposes have been extensively investigated. Radiation density, distribution of radiation energy, and temperatures are of interest in this connection and have been measured [70,71,141,143]. The increase with pressure of the amount of continuous radiation has been carefully studied [70,71]. Sliding sparks for use in high speed cinematography have been investigated along similar lines [67].

13. Few applications of time-resolved spectroscopy to absorption spectroscopy have been reported. The life time of metastable terms in atomic gases has been determined from decay measurements [112]. Experiments have been conducted in which the cooling off of the vapor cloud in a spark discharge was traced, by illuminating the cloud and observing line reversal [31,30]. Figure 20 shows a typical sequence of spectra.

14. Time-resolved spectroscopy has further been applied to research in the following fields: arcs and activated arcs [113,2], diffusion of atoms in an arc [73], long sparks [154,153,135], rapid

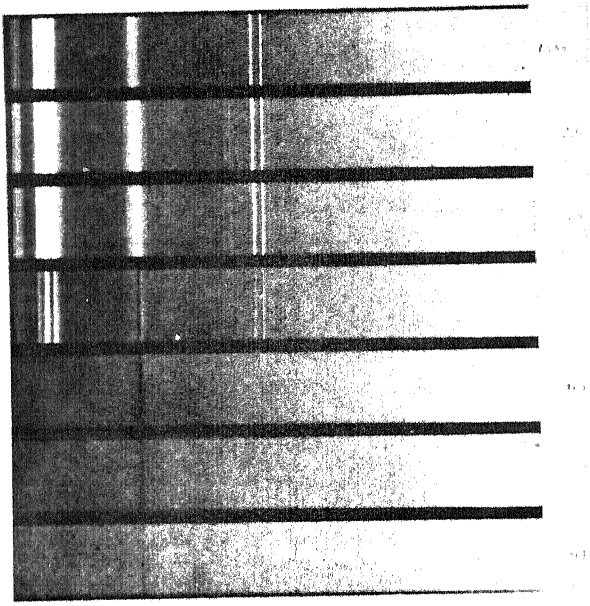

Figure 20. Emission and absorption spectra of the afterglow of a spark discharge between Mg electrodes, time t × 10^{-4} sec. [from (31), Courtesy Z. Naturforsch.].

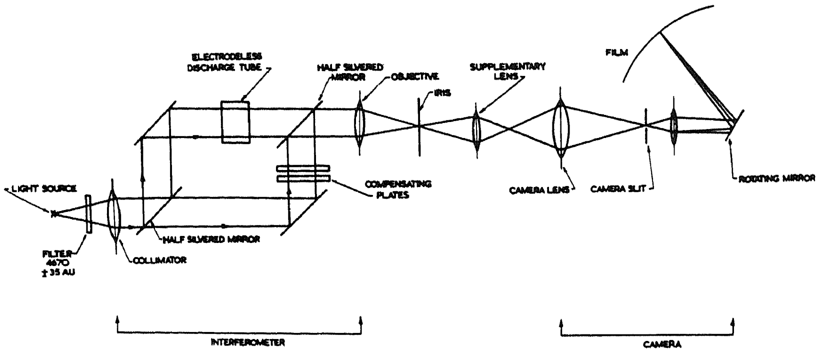

Figure 21. Time-resolved interferometry using a Mach-Zehnder interferometer and a mirror streak camera for measuring electron densities, [from (106), Courtesy North Holland Publishing Company].

chemical reactions [91] pyrotechnics [146], fluorescence [69], interferometry [106], band spectra [160,82], nuclear explosions. A time-resolving interferometer for the determination of the change in electron density in a plasma is shown in Figure 21. An example of a time-resolved band spectrum of high time resolution is demonstrated in Figure 22.

APPLICATIONS OF TIME-RESOLUTION TO SPECTROCHEMISTRY

Light Sources for Spectrochemical Analysis

Electric discharges changing rapidly with time, e.g., spark discharges are widely used as light sources for spectrochemical analysis. It is therefore not surprising that time-resolving devices for studying the properties of spark discharges as spectrochemical light sources have been used in the past with great success [1,86,70,71]. Whereas usually in spectroscopic light sources the plasma of the discharge channel and consequently the properties of the discharge atmosphere are the main subjects of interest, it is obvious that in light sources for spectrochemical applications the vapor clouds originating from the electrodes which are actually used for the analysis, are even more important. The fundamental differences in the behaviour of discharge channel and vapor clouds have first been stressed by Kaiser and Wallraff [86].

Some problems of particular interest to spectrochemists are the following: the rate of evaporation of the sample from the electrodes, the formation of vapor jets and the transport of material into the gap, the distribution and change with time of spectral lines, band spectra and continuous spectra excited in these vapor clouds, the influence of the discharge atmosphere.

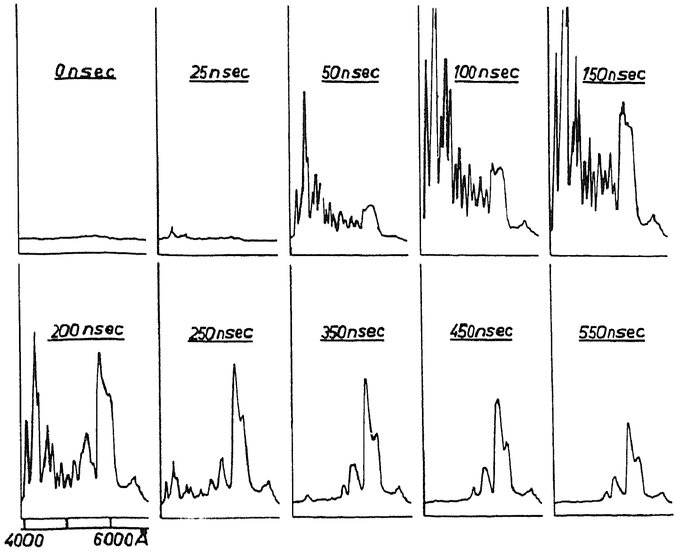

Figure 22. Time-resolved bandspectra ofnitrogen using a pulsedmultiplier, [from (82), Courtesy Philips Tech. Rev.].

Even under carefully controlled electrical conditions there is usually a large variation in light intensity between successive sparks [162,132,88]. Lines of low excitation potential which are easily excited everywhere in the rather cold vapor cloud are subject to much stronger intensity variations than those of high excitation potential which are mostly excited in the hot region near the electrodes. It has been established that the evaporation of the electrode material does not occur continuously during the discharge, but quite irregularly. It is still open to question how the electrode material is liberated from the electrodes. This may happen by purely thermal evaporation [83], or by a process similar to an explosion, in which the vapor clouds are initially relatively cold and then get their excitation energy on passing the hot discharge channel [140].

Using a frame-camera or image converter tubes with spectral resolution it was possible to study the distribution in time, space and wavelength of the radiating vapor cloud, due to the propagation of the initial shock wave and the geometry of the spark gap [9,105]. An example is shown in Figure 23. The behavior of the different kinds of discharges [4,60], i.e., contracted, diffuse and intermediate discharges, especially in rare gas atmosphere, can be seen quite clearly on such photographs. Figure 24. The line structure (line width, self absorption) can be of interest, because this structure may influence the measurements of maximum density of a line, as used for quantitative analysis.

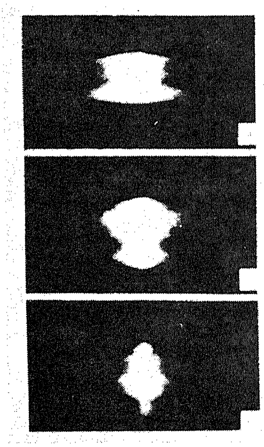

Figure 23. Radiation of the H_α line in a spark discharge in hydrogen, resolved in time and space, [from (9), Courtesy Opt. Spectry]. Exposure time 1 μsec. Time after the beginning of the discharge (in μsec): top – 0, center – 5, bottom – 10.

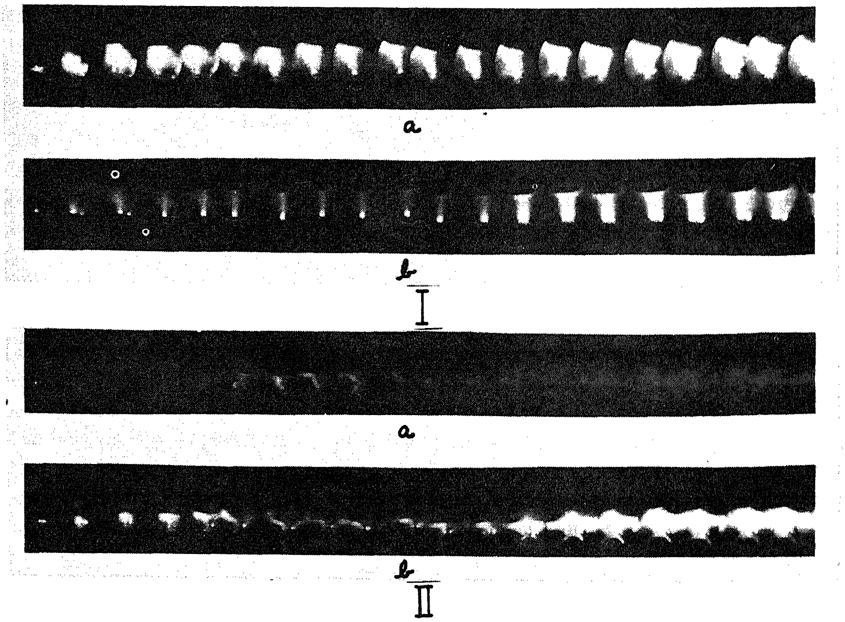

Figure 24. Spark discharges between Ag-electrodes in Ar-atmosphere, resolved in time and space, 10 μsec exposure/frame, current 50/150 Amp, total duration 250 μsec,

I.) contracted discharge: a) Ag 3281 Å, b) Ar 3949 Å
II.) diffuse discharge: a) Ag 3281 Å, b) Ar 3949 Å,

[from (60), Colloquium Spectroscopicum Internationale IX, Lyon, France 1961].

The temperature and other thermodynamic properties of the discharge plasma play an important part insofar as they strongly influence the above-mentioned qualities.

Spectrochemical Analysis Using Time-Resolved Spectroscopy

Whereas the preceding part of this report dealt with the role of time-resolved spectroscopy in the study of rapidly changing parameters of gaseous discharges, quite a different group of problems will now be considered.

In spectrochemical analysis using a spark light source, a property of the sample which is constant in time, e.g., the chemical composition, has to be determined by means of a series of rapidly changing events, e.g., the sparks. Integration over a large number of individual sparks increases the accuracy of the analysis. As was pointed out by Crosswhite, Steinhaus and Dieke [52,43,133,134], the selection of certain temporal parts of a spark discharge for use in spectrochemical analysis enables a higher line to background ratio (and correspondingly a lower detection limit) than could be achieved by using the total light of the discharge. In addition, their results show that interference by air- and spark-lines, which are mostly excited during the initial stage of the spark, can be avoided if for the analysis arc lines in a later part of the discharge are used. As the intensity of the spectrum in the late part of a damped discharge is weak compared to the high intensity of disturbing background and interfering air- or spark-lines excited in the early stage of the discharge, a high on-off ratio of the switch selecting the desired part of the spectrum is necessary. In table 1 obtainable on-off ratios as well as time-resolution are listed.

Photomultiplier tubes as radiation receivers are sensitive, fast and convenient to use and can be combined with an efficient electronic shutter, but it should be emphasized that mechanical, electro-optical and similar shutters can be used in connection with any radiation detector, the main advantage of the photoplate being its ability to record the full time-resolved spectrum, at the expense of its much lower sensitivity.

Using modern electronic methods for synchronizing and triggering, all the above mentioned shutters can be employed with equal success. Values for the jitter in triggering lower than 10^{-7} sec for long times of operation have been reported [126].

There can be no doubt that time-resolved spectroscopy can be a very useful tool for investigations concerned with the improvement of spectrochemical analysis.

In order to employ the possibilities of applying time-resolved spectroscopy *directly* to spectrochemical analysis, more work in this field has been done recently [77,7,138,93,92,126,100]. For the evaluation of this method the following questions should be considered. As there is certainly some additional expense involved in the use of time-resolving mechanisms, the results that can be obtained should justify this expense.

What progress at all should be expected? We think this method, as any new analytical method, should be judged by the answer to the following questions [93]:

a. Is it possible to obtain a definite lowering of the detection limit of traces, compared to customary arc and spark methods?

b. Can the accuracy of the analysis be improved?

c. What other improvements can be achieved?

Before an attempt is made to answer these questions, the following facts should be taken into account:

In all cases where different discharge atmospheres have been used in the course of investigations, comparisons of the respective results can be misleading as these results can be and probably are masked by the very pronounced effects of the different discharge modes possible in different atmospheres [4,60], e.g., a spark between aluminum electrodes in Ar atmosphere will most probably belong to the diffuse type of discharge whereas the same discharge in air may be of the contracted type. For a copper sample conditions could be reversed. With steel, zinc, and other materials there is a choice between three types of discharges. Time-resolved spectra of discharges in different gases can only be compared if produced by the same type of discharge. (See Figure 24).

Now the answers:

a. As the detection limit of an analytical method depends on the line to background ratio, the change in time of this quantity is of paramount importance. A close resemblance of the late time-resolved spark spectrum of fairly low inductance sparks to an arc spectrum in which a high line to background ratio prevails is immediately apparent and was reported as the main advantage of the new method [43,133,134,16,17,11]. Unfortunately, the line to background ratio does not increase indefinitely with time during a spark discharge and in the afterglow, but shows a definite maximum and the detection limit correspondingly a definite minimum which is usually of the same order of magnitude as that obtainable with arclike sparks (high inductance sparks) or slightly better [60]. Figure 25. The obtainable detection limit is almost independent of the kind of spark discharge used for exciting the time-resolved spectrum [60]. In most cases an a.c. arc will yield a lower detection limit. A spark discharge must burn almost as long as the burning period of an a.c. arc and its current must be of the same order of magnitude, if it is desired to attain similar detection limits. This is shown in Figure 26.

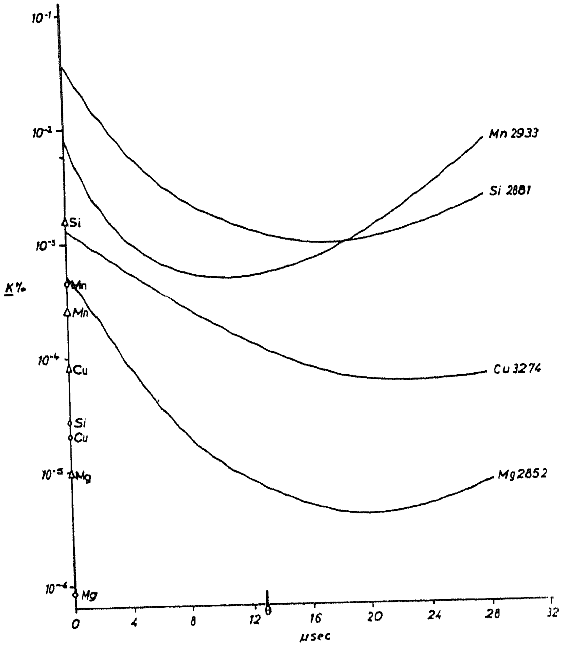

Figure 25. Detection limits of several elements in an Al sample, using a time-resolved spark discharge, [from (93), Courtesy Spectrochim. Acta].

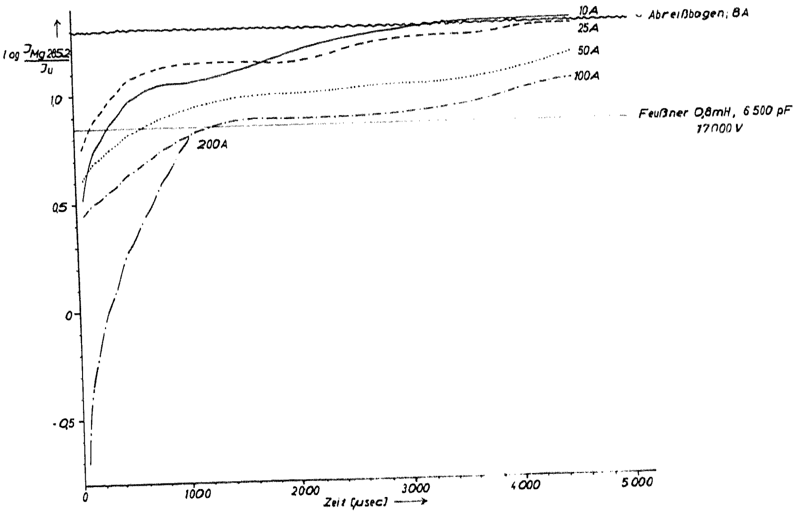

Figure 26. Time resolved line to background ratio of Mg 2852 line in discharges of constant current pulses, compared to the corresponding ratios in unresolved high inductance sparks and a. c. arcs.

b. As there is no marked influence of the parameters of the exciting spark on the obtainable detection limit a discharge can be chosen that will give high accuracy as long as no other contradictory conditions for the choice of discharge parameters are imposed.

c. Conditions for the reduction of third partner effects, optimum evaporation of the sample, etc., can be chosen without sacrificing sensitivity although there might be some decrease in accuracy.

In some cases, where the most sensitive analysis line is masked by an interfering line of different change of intensity with time, the detection limit can be lowered if this line can be used by a suitable adjustment of the time interval [134,60].

In special cases, conditions for a pronounced improvement of the detection limit can be found, e.g., in the case of the copper spark method [60]. Spectral lines normally used for spectrochemical analysis may show up peculiarities that render them unsuitable for analysis with time-resolved methods [126]. To ensure that line pairs employed have nearly identical properties, these lines should have upper energy levels as close together as possible [90]. The low intensity of the most useful late part of a time-resolved spectrum may present difficulties, so that a compromise between line to background ratio and overall intensity must be found.

Time-resolved spectroscopy has also been employed for analytical applications, using an a.c. arc as a light source. Fairly small changes in the spectrum with time have been reported [137].

APPENDIX

The actual resolutions of intensity, space coordinates, time and wavelength will be defined by the equations

(2a) $A_I = I/\Delta I$, (2b) $A_x = 1/\Delta x$, (2c) $A_y = 1/\Delta y$, (2d) $A_t = 1/\Delta t$

and (2e) $A_\lambda = \lambda/\Delta\lambda$, respectively.

With E_λ = Energy/(cm^2 · sterad · sec · Å) it follows for the number of quanta emitted into the solid angle from the source to the first aperture stop:

$$n_{t,x,y,\lambda} = \frac{E_\lambda \, \Delta\lambda \, \Delta t \, \Delta x \, \Delta y \, \omega}{h c/\lambda}, \text{ or rewritten} \tag{3}$$

$$= \frac{E_\lambda \lambda^2 \omega}{h c} \cdot \frac{1}{1/\Delta x} \cdot \frac{1}{1/\Delta y} \cdot \frac{1}{1/\Delta t} \cdot \frac{1}{\lambda/\Delta\lambda} \tag{3a}$$

Hence with (2b) through (2e) it follows,

$$n_{t,x,y,\lambda} = \frac{\lambda^2 E_\lambda \omega}{h c} \cdot \frac{1}{A_x} \frac{1}{A_y} \frac{1}{A_t} \frac{1}{A_\lambda} \cdot \tag{3b}$$

Using the well known relation for the measurement of intensities by counting quanta

$$\frac{\Delta I}{I} = \frac{1}{\sqrt{n_{t,x,y,\lambda}}} \text{, and introducing (2a),} \tag{4}$$

$A_I^2 = n_{t,x,y,\lambda}$ is obtained. Inserting this expression in (3b) it follows (4a)

$$A_r = A_I^2 \; A_\lambda \; A_x \; A_y A_t \le \frac{\lambda^2 E_\lambda \; \omega}{h c} \text{, or} \tag{5}$$

$$A_r = \eta_{min} \frac{\lambda^2 \; E_\lambda \; \omega}{h c} \cdot$$

REFERENCES

1. Abramson, Gegechkori, Drabkina and Mandelshtam, J. Exp. Theoret. Phys. U.S.S.R., 17, 862 (1947).
2. Abramson, I. S. and Mandel'stam, S. L., Bull. Acad. Sci. U.R.S.S. Sér. Phys., 11, 223 (1947).
3. Anderson, A. E., Goetze, G. W., Kanter, H., Proceedings of the Fifth Internation. Congress on High-Speed Photography 1960, 95, New York (1962).
4. Andermann, G. and Kemp, J. W., ASTM Special Technical Publication 259, 23 (1959).
5. Anderson, J. A. and Smith, S., Astrophys. J. 64, 295 (1926).
6. ------------, Atomic Energy, Second International Conference on the Peaceful Uses of; Geneva, Switzerland 1958.
7. Baker, C. A., United Kingdom Atomic Energy Authority, Research Group, Report, Aere - R 2926, 1959.
8. Moore, D. Baker and Crosby, John K., 5th International Congress on High-Speed Photography, Washington 1960, 273, New York (1962).
9. Balashov, I. F., Vanyukov, M. P., Muratov, V. R., Nilov, E. V., Opt. Spectry 10, 279 (1961).
10. Bardócz, Á., Z. Angew. Phys. 9, 82 (1957).
11. Bardócz, Á., Appl. Spectr. 11, 167 (1957).
12. Bardócz, Á., Brit. J. Appl. Phys. 10/7, 310 (1959).
13. Bardócz, Á., Spectrochim. Acta 16, 1173 (1960).
14. Bardócz, Á., IX. Colloquium Spectroscopicum Internationale 1961, Lyon, Paris (1962).

15. Bardócz, Á., Vanyek, U. M. and Voros, T., J. Opt. Soc. Amer., 51, 3, 283 (1961).
16. Bardócz, A. and Varśanyi, F., Z. Naturforsch. 10a, 1031 (1955).
17. Bardócz, Á. and Varśany, F., Nature 177, 222 (1956).
18. Bardócz, Á., Voros, T. and Marta U. Vanyek, Spectrochim. Acta 17, 642 (1961).
19. Bartels, H., Bortfeldt, J., Berg. K.-H., Ionization Phenomena in Gases, Munich 1961, I 1048, Amsterdam (1962).
20. Beams, J. W., Phys. Rev. 33, 1086 (1929).
21. Blitzer, L., J. Opt. Soc. Amer., 45, 564 (1955).
22. Blitzer, L. and Cady, W. M., J. Opt. Soc. Amer., 41, 440 (1951).
23. Bovey, L., Gabriel, A. H., Spectrochim. Acta, 18, 631 (1962).
24. Bortfeldt, J., Ionization Phenomena in Gases, Munich 1961, I, 1931 Amsterdam (1962).
25. Brauer, F. L. and Hansen, D. F., J. Opt. Soc. Amer., 49, 421 (1959).
26. O'Brien, B. and Milne, G., J. Soc. Motion Picture Engrs., 52, 30 (1949).
27. Brixner, B., J. Opt. Soc. Amer., 45, 876 (1955).
28. Brown, F. L. and Beams, Jr., J. W., J. Opt. Soc. Amer., 11, 11 (1925).
29. Cairns, R. W., Industr. Eng. Chem. 36, 79 (1944).
30. Calker, J. van, Naturwiss., 40, 434 (1953).
31. Calker, J. van, Z. Naturforsch. 10 A, 697 (1955).
32. Calker, J. van and Braunisch, H., Z. Naturforsch. 11a, 612 (1956).
33. Calker, J. van and Tacke, E., Z. Naturforsch. 4a, 573, (1949).
34. Coleman, K. R., Kurzzeitphotographie IV. Internationaler Kongress Kōln 1958, 32, Darmstadt and Wien (1959).
35. LeCompte, G. W. and Edgerton, H. E., J. Appl. Phys., 27, 1427 (1956).
36. Courtney-Pratt, J. S., Research. London 2, 287-93 (1949).
37. Courtney-Pratt, J. S., Proc. Roy. Soc. London A, 204, 27 (1950).
38. Courtney-Pratt, J. S., J. Phot. Sci., 1, 21 (1953).
39. Courtney-Pratt, J. S., Rep. Progr. Phys., 379 (1957).
40. Craggs, J. D., Nature, 192, 1032 (1961).
41. Craggs, J. D. and Hopwood, W., Nature, 158, 618 (1946).
42. Craggs, J. D. and Meek, J. M., Proc. Roy. Soc. London A, 186, 241 (1946).
43. Crosswhite, H. M., Steinhaus, D. W. and Dieke, G. H., J. Opt. Soc. Amer., 41, 299 (1951).
44. Cundall, C. M., The British Iron Steel Research Association 1953/54, 1.

45. Cundall, C. M. and Craggs, J. D., Spectrochim. Acta., 7, 149 (1955).

46. Cundall, C. M. and Craggs, J. D., Spectrochim. Acta., 9, 68 (1957).

47. Curzon, F. L. and Greig, J. R., J. Sci. Instr., 38, 239 (1961).

48. Danielsson, A., Instr. and Measurem. Conf. 1956, Spectroscopy, Pap. SP IIc, 1.

49. Deinum, H. W., Diss. 1938, Amsterdam, (Extract in Spectrochim. Acta., 2, 318, (1944).

50. Deinum, H. W. and Boer, F. De, Spectrochim. Acta., 2, 318 (1943).

51. Dieke, G. H. and Crosswhite, H. M., J. Opt. Soc. Amer., 35, 471 (1945).

52. Dieke, G. H., Crosswhite, H. M., J. Opt. Soc. Amer., 36, 192 (1946).

53. Dieke, G. H., Loh, H. Y., Crosswhite, H. M., J. Opt. Soc. Amer., 36, 185 (1946).

54. Drabkina, S. O., Zhur. Eksp. i. Theoret. Fiz. 21, 473 (1951).

55. Dunnington, F. G., Phys. Rev. 38, 1506 (1931).

56. Dyson, J., J. Sci. Instr., 32, 272 (1955).

57. Edels, H., Whittaker, D., J. Sci. Instr., 32, 103 (1955).

58. Eichinger, R., Krempl, H., Z. Angew. Phys., 12, 461 (1960).

59. Elle, D., Z. Angew. Phys., 6, 49 (1954).

60. Ende, H. vom, Hagenah, W.-D., Laqua, K., IX. Colloquium Spectroscopicum Internationale 1961, Lyon; Paris (1962).

61. Ermakov, B. A., Mak, A. A., Pribory i Tekhn. Eksperim. 1959, 3, 94.

62. Feddersen, W., Pgg. Ann. 113, 437 (1961).
116, 132 (1962).

63. Feldkirchner, H., Krempl, H., Arch. Eisenhüttenw. 27, 621 (1956).

64. Filler, A. S., J. Opt. Soc. Amer., 44, 506 (1954).

65. Folkierski, A., Nuclear Instrum. and Methods, 4, 346 (1959).

66. Froome, K. D., Photogr., J. B., 92, 158 (1952).

67. Fünfer, E., Z. Angew. Phys. 1, 295 (1949).

68. Fünfer, E., Lehner, G., Ergebnisse der exakten Naturwissenschaften, Vol. 34, Berlin-Göttingen - Heidelberg (1962).

69. Galanin, M. D., Chizkova, Z. A., Opt. Spectry 11, 143 (1961).

70. Glaser, G., Optik 7, 33 (1950).

71. Glaser, G., Naturforsch. 6a, 706 (1951).

72. Gloersen, Per, J. Opt. Soc. Amer. 48, 712 (1958).

73. Gol'dfarb, B. M., Il'ina, E. V., Opt. Spectry XI, 243 (1961).

74. Gordon, G., Cady, W. M., J. Opt. Soc. Amer. 40, 852 (1950).

75. Goss, W. C., Proceedings of the Fifth Internation. Congress on High-Speed Photography 1960, 135, New York (1962).

76. Greig, J. R., Curzon, F. L., Ionization Phenomena in Gases, Munich 1961, Amsterdam (1962) p. 2027.
77. Hagenah, W.-D., Laqua, K., VII. Inter. Coll. Spectr. Lüttich 1958, Rev. Universelle, Mines, 9, 15, 361 (1959).
78. Hagenah, W.-D., VII^{e} Colloquium Spectroscopicum Internationale, 1958, Rev. Universelle Mines, 9, XV, 369 (1959).
79. Hagenah, W.-D., Laqua, K., Colloquium Spectroscopicum Internat. VIII, 1959, 204, Aarau, (Switzerland 1960).
80. Harrington, F. D., 5th International Congress on High-Speed-Photography, Washington 1960, 277, New York (1962).
81. Haynes, J. R., Phys. Rev., 73, 891 (1948).
82. Hendee, C. F., Brown, W. B., Philips Tech. Rev. 19, 1957/58, 50.
83. Hermoch, V., Czech. J. Phys. 9, 221 (1959).
84. Huldt, L., Spectrochim. Acta, 7, 266 (1955).
85. Jones, H. W., McCormick, W. W., Sawyer, R. A., J. Opt. Soc. Amer., 51, 833 (1961).
86. Kaiser, H., Wallraff, A., Ann. d. Physik, 5. Folge, 34 (1939).
87. Krempl, H., Z. Physik, 167, 302 (1962).
88. Krempl, H., Späth, H., Arch. Eisenhüttenw., 31, 473 (1960).
89. Kühne, J., Kurzzeit-Photographie, 4. Internationaler Kongress, Köln 1958, 179 Darmstadt un Wien (1959).
90. Labuda, A. A., Martinkov, E. G., Nekrashevich, I. G., Izvest. Akad. Nauk S.S.S.R., Ser. Fiz. 22, 720 (1958).
91. Laporte, M., Compt. rend. Paris, 226, 1902 (1948).
92. Laqua, K., Hagenah, W.-D., VIII. Colloquium Spectroscopicum Internationale, Luzern, 1959, 45, Aarau (Switzerland, 1960).
93. Laqua, K., Hagenah, W.-D., Spectrochim. Acta, 18, 183 (1962).
94. Larenz, R. W., Z. Physik 129, 327 (1951).
95. Lawrence, E. O., Dunnington, F. G., Phys. Rev. 35, 396 (1930).
96. Liebing, L., Früngel, F., Proceedings of the Fifth International Congress on High-Speed-Photography 1960, 138, New York (1962).
97. Lochte-Holtgreven, W., Coll. Spectr. Int. VIII, 1959, 9 Aarau (Switzerland 1960).
98. Lunn, G. H., Menzies, E. D., Proceedings of the Fifth International Congress on High-Speed-Photography 1960, 127, New York (1962).
99. Maecker, H. (Editor), Ionization Phenomena in Gases München 1961, Amsterdam 1962.
100. Majkowski, R. F., Joseph, B. W., Spectrochim. Acta 18, 77 (1962).
101. Mak, A. A., Opt. Spectry. VII, 145 (1960).

102. Mandel, L., Proceedings of the Fifth International Congress on High-Speed Photography 1960, 110, New York (1962).
103. Mandelstam, S., Spectrochim. Acta, 15, 255 (1959).
104. Mandelstam, S. L., Spectrochim. Acta, 11, 245 (1957).
105. Martinkov, E. G., Inzh. fiz. Zh, III, 67 (1960).
106. Medford, R. D., Powell, A. L. T., Hunt, A. G., Wright, J. K., Ionization Phenomena in Gases, Munich 1961, II, 2001, Amsterdam (1962).
107. Meek, J. M., Craggs, J. D., Nature, 152, 538 (1943).
108. Miller, C. O., U.S.-Patent 2, 400 887 (1946).
109. McNally, Jr., J. R., J. Opt. Soc. Amer., 49, 328 (1959).
110. Orr, L. W., Microfilm Abst. 10, 189 (1950).
111. Perl, M. L., Jones, L. W., Proceedings of the Fifth Internation. Congress on High-Speed Photography 1960, 98, New York (1962).
112. Phelps, A. V., Pack, J. L., Rev. Sci. Instr., 26, 45 (1955).
113. Prokof'ev, V. K., Gurevich, D. B., Belousova, I. M., Snigirev, Yu. A., Opt. i Spektroskopiya, 7, 14 (1959).
114. Raiskii, S. M., J. Tech. Phys. U.S.S.R. 10, 529 (1947).
115. Ramsauer, C., Wolf, F., Ann. Physik, 66, 395 (1921) IV. Folge, 373.
116. Ravenhill, P., Rept. Brit. Elect. Res. Assoc., Rep. L/T353, 12 (1956).
117. Rawcliffe, R. D., Rev. Sci. Instr. 13, 413 (1942).
118. Reeves, E. M., Parkinson, W. H., Ionization Phenomena in Gases, Munich 1961, I, 1017, Amsterdam (1962).
119. Rimbert, F., Vassy, A., Compt. rend. Paris, 237, 1324 (1953).
120. Schardin, H., 3rd Congress on High Speed Photography, London 1956, 316, Lond. (1957).
121. Schardin, H., Fünfer, E., Z. Angew. Phys., 4, 185 (1952).
122. Schardin, H., Fünfer, E., Z. Angew. Phys., 4, 224 (1952).
123. Schneider, R., Ionization Phenomena in Gases, Munich 1961; Amsterdam (1962), p. 1945.
124. Schneider, R., Mailander, M., Z. Angew. Phys., 12, 521 (1960).
125. Schneider, R., Maisenhälder, F., Kling, M., Z. Angew. Phys., 13, 211 (1961).
126. Schroeder, W. W., Strasheim, A., IX. Colloquium Spectroscopicum Internationale 1961, Lyon, Paris (1962).
127. Schuster, A., Hemsalech, G., Trans. Roy. Soc. (London) 193, 189 (1900).
128. Schwob, J. L., Balloffet, G., J. Phys. Radium, 22, 389 (1961).
129. Shimizu, T., Hirata, M., Sci. Papers Inst. Phys. Chem. Research, Tokyo, 1022, 317 (1941).
130. Skinner, A., Kurzzeitphotographie IV. Internationaler Kongress Köln 1958, 172 Darmstadt und Wien (1959).

131. Smith, S., Astrophys. J. 61, 186 (1925).
132. Späth, H., Krempl. H., Z. Angew. Phys. 12, 8 (1960).
133. Steinhaus, D. W., Crosswhite, H. M., Dieke, G. H., J. Opt. Soc. Amer., 43, 257 (1953).
134. Steinhaus, D. W., Crosswhite, H. M., Dieke, G. H., Spectrochim. Acta, 5, 436 (1953).
135. Stekol'nikov, I. S., Shkilev, A. V., Dokl. Akad. Nauk S.S.S.R., 136, 803 (1961).
136. Stoudenheimer, R. G., Moor, J. C., R.C.A. Rev., 18, 322 (1957).
137. Strasheim, A., Appl. Spectr., 11, 76 (1957).
138. Strasheim, A., Schroeder, W. W., VII^e Colloquium Spectroscopicum Internationale Mai 1959, 1 Rev. Universelle Mines 9^e Serie. 15, 331.
139. Strasheim, A., Schroeder, W. W., IX. Colloquium Spectroscopicum Internationale 1961, Lyon, Paris (1962).
140. Sukhodrev, N. K., Mandel'shtam, S. L., Opt. i Spektroskopiya, 6, 723 (1959).
141. Thackeray, D. P. C., J. Sci. Instr. 35, 206 (1958).
142. Thackeray, D. P. C., J. Sci. Instr. 35, 248 (1958).
143. Thackeray, D. P. C., Kurzzeitphotographie IV. Internation. Kongress Köln 1958, Darmstadt und Wien 1959, 123.
144. Theophanis, G. A., Rev. Sci. Instr., 31, 427 (1960).
145. Tsui, F., Brit. J. Appl. Phys. 3, 139 (1952).
146. Tyroler, J. F., Appl. Spectry 1957/58, 15A.
147. Vainstein, L. A., Leontovich, A. - M., Malyavkin, L. P., Mandelshtam, S. L., J. exptl. theoret. Phys. (A), 24, 326 (1953).
148. Vanyukov, M. P., Ermakov, B. A., Mak, A. A., Muratov, V. R., Vestn. Leningr. Univ. 14, 16, Ser. Fiz. Khim. 3, 25 (1959).
149. Vanyukov, M. P., Isaenko, V. I., Khazov, L. D., Zh. Tekhn Fiz., 25, 1248 (1955).
150. Vanyukov, M. P., Mak, A. A., Muratov, V. R., Opt. i Spektroskopiya 6, 17 (1959).
151. Vanyukov, M. P., Muratov, V. R., Mukhidinova, I. A., Opt. Spectry Vol. 11, 169 (1961).
152. Vanyukov, M. P., Nilov, E. V., Zh. Tekhn Fiz., 24, 1209 (1954).
153. Vassay, A., Compt. Rend. 238, 1398 (1954).
154. Vassy, A., J. Phys. Radium, 16, 292 (1955).
155. Voros, T., VIII. Colloquium Spectroscopicum Internationale 1959, 54, Aarau (Switzerland 1960).
156. Vul'fson, K. S., Chamnaya, F. A., Opt. Spectry, Vol. 11, 296 (1961).
157. Wahr, J. C., McCormick, W. W., Sawyer, R. A., J. Opt. Soc. Amer., 43, 151 (1953).

158. Waters, R. T., Jones, R. E., Ionization Phenomena in Gases, Munich 1961, I 992, Amsterdam (1962).
159. Weniger, S., Herman, L., Herman, R., Coll. Spectr. Int. VI (Amsterdam 1956) Pergamon Press Ltd., London, 333 (1957).
160. White, W. C., Astrophys. J., 121, 271 (1955).
161. Wiese, W. L., Rev. Sci. Instr., 31, 943 (1960).
162. Williams, G. C., Craggs, J. D., Hopwood, W., Proc. Phys. Soc., Lond., B, 62, 49 (1949).
163. Wulff, H., Nuclear Instr. and Methods 4, 352 (1959).
164. Zaidel, A. N., Malyshev, G. M., Shreider, E. Ya., Soviet Phys. Tech. Phys., 6, 93 (1961).
165. Zarem, A. M., Marshall, F. R., Hauser, S. M., Rev. sci. Instrument, 29, 11, 1041 (1958).
166. Zavoiskii, E. K., Fanchenko, S. D., Dokl. Akad. Nauk SSSR, 100, 661 (1955).
167. Weizel, W., Rompe, R., Theorie elektrischer Lichtbögen und Funken, Leipzig (1949).
168. Brixner, B., Rev. Sci. Instr., 30, 1041 (1959).
169. Hovis, W. A., Jr., J. Opt. Soc. Amer. 52, 649, (1962).

ATOMIC ABSORPTION SPECTROSCOPY

A. Walsh
Commonwealth Scientific and Industrial
Research Organization
Melbourne, Australia

One hundred years ago Kirchhoff and Bunsen described their celebrated experiments which showed that atomic spectra, either in emission or absorption, provided a powerful means of chemical analysis. Since that time emission methods of spectrochemical analysis have been steadily developed and during the Second World War culminated in direct reading spectrographs of the type now in widespread use. It is a curious feature of the history of spectrochemical analysis that whilst all these developments in emission methods were taking place, the potentialities of analytical methods based on atomic absorption spectra were almost completely ignored. This neglect is particularly surprising in view of the well known applications of atomic absorption measurements in spectroscopic research work: for example, in studies of furnace spectra; in investigations of hyper-fine structure by means of atomic beams; and in many experiments associated with the measurement of the resonance radiation from atoms. As a purely analytical tool, however, the absorption method has been largely confined to studies of the compositions of the solar and stellar atmospheres, and to the special case of determining the contamination of laboratory atmospheres by mercury vapour.

It is only during the last decade, and particularly during the last four years, that it has been shown that atomic absorption methods of analysis can be applied to a wide variety of analytical problems, and have some important advantages over emission methods. In this review it is proposed to discuss: (a) the basic differences between analytical methods based on atomic emission and on atomic absorption spectra; (b) the methods which have been developed for making the necessary atomic absorption measurements; and (c) the limitations and scope of currently-used analytical methods based on such measurements. Finally the outstanding problems at the present time will be discussed and an outline given of the main directions of current researches. For detailed information of the various analytical methods which have been developed and for a comprehensive bibliography the reader is referred to the numerous review articles [1-9] which have appeared during the past two years.

BASIC DIFFERENCES BETWEEN EMISSION AND ABSORPTION METHODS

Consider first the basic differences between analytical methods based on atomic emission and on atomic absorption measurements. In emission methods, the sample for analysis is atomized and excited (simultaneously, in practice), the emitted radiation dispersed, and the intensitites of selected lines in the emission spectrum measured.

Neglecting self-absorption and induced emission, the integrated intensity of emission of a line is given by

$$\int I_\nu d\nu = C N_j f \qquad (1)$$

where N_j is the number of atoms in the upper state involved in the transition responsible for the line, f is the oscillator strength of the line, and the proportionality constant C depends on the dispersing and detecting systems. Assuming that the atomic vapour is in thermal equilibrium at temperature T, then the number of atoms in an excited state j, of excitation energy E_j, is given by

$$N_j = N_o \frac{P_j}{P_o} e^{-E_j/KT} \qquad (2)$$

where N_o is the number of atoms in the ground state, and P_j and P_o are the statistical weights of the excited and ground states respectively.

From (1) and (2) it can be seen that the emitted intensity depends on T and E_j (which for resonance lines, involving transitions to the ground state, is inversely proportional to the wavelength of the line). Examples of the variation of N_j/N_o with T and E_j (or λ^{-1}) for various elements are given in Table 1.

Consider now the case of absorption of a parallel beam of radiation of intensity $I_{o\nu}$ at frequency ν incident on an atomic gas or vapour of thickness 1 cm. Then if I_ν is the intensity of the transmitted beam, the absorption coefficient K_ν of the vapours at frequency ν is defined by

$$I_\nu = I_{o\nu}\, e^{-K_\nu 1} \qquad (3)$$

Table 1

Values of N_j/N_o for Various Resonance Lines

Resonance Line	Transition	P_j/P_o	N_j/N_o			
			T = 2000°K	T = 3000°K	T = 4000°K	T = 5000°K
Cs 8521 Å	$^2S_{1/2} - {^2P_{3/2}}$	2	4.44×10^{-4}	7.24×10^{-3}	2.98×10^{-2}	6.82×10^{-2}
Na 5890 Å	$^2S_{1/2} - {^2P_{3/2}}$	2	9.86×10^{-6}	5.88×10^{-4}	4.44×10^{-3}	1.51×10^{-2}
Ca 4227 Å	$^1S_o - {^1P_1}$	3	1.21×10^{-7}	3.69×10^{-5}	6.03×10^{-4}	3.33×10^{-3}
Zn 2139 Å	$^1S_o - {^1P_1}$	3	7.29×10^{-15}	5.58×10^{-10}	1.48×10^{-7}	4.32×10^{-6}

the relationship between integrated absorption and concentration is given by

$$\int K_\nu d\nu = \frac{\pi e^2}{m c} N_\nu f \tag{4}$$

where e is the electronic charge, m the electronic mass, c the velocity of light, N_ν the number of atoms per cm³ which are capable of absorbing in the range ν to $\nu + d\nu$. (Equation (4) assumes that the refractive index is of the order of 1 over the breadth of the absorption line and is not applicable to strong absorption lines.)

Now it can be seen from Table 1 that at temperatures up to 5000°K the number of excited atoms is, in most cases, negligible compared with the number of unexcited atoms and thus in equation (4) N_ν can be replaced by N, the total number of atoms per cm³.

It can be seen, therefore, that in contrast to emission intensity, the integrated absorption coefficient for lines originating in the ground state is independent of temperature and of excitation potential, and this is one of the main attractions of the absorption method.

MEASUREMENT OF ABSORPTION BY ATOMIC VAPOURS

Unfortunately, it is not possible in practice to apply equation (4) directly. There is no satisfactory method of determining the integrated absorption coefficient by conventional scanning methods, since the width of atomic absorption lines under the usual conditions of measurement is in the range 0.02-0.1A and the resolution required to record the profiles of such lines is obviously much higher and is beyond the performance of most monochromators. In addition, if it is desired to use photo-electric methods of intensity measurement, then it is scarcely feasible to use a source emitting a continuum, since the energy emitted over such a small spectral range would generally give insufficient signal/noise ratio for satisfactory recording.

The method which has been adopted has been to measure the absorption coefficient at the centre of the line, using an atomic-line source which emits lines having a much smaller half-width than the absorption lines so that, to a good approximation, a measurement can be made of peak absorption. The latter is also linearly proportional to concentration provided the shape and width of the line is independent of concentration.

If such a sharp-line source is used, it is now no longer necessary to use a high resolution monochromator: the function of the monochromator is now simply to isolate the required resonance line from all other lines emitted by the source. Using this technique it is possible to achieve an effective resolution, equal to the half-width of the emitted line, of the order of 0.01A. This high resolution is an essential feature of the absorption technique, and yields an important advantage over emission methods in which the resolution is much lower since it is determined by the optical performance of the monochromator. Thus "radiation interference" effects, which in emission spectroscopy are due to the monochromator being unable to isolate the required line from neighbouring lines or background, have little or no counterpart in absorption methods.

Another feature of the experimental arrangement in the absorption method is the provision of means for compensating for any radiation emitted by the sample at the wavelength at which the absorption measurement is to be made. The simplest method for achieving this is by modulating the radiation from the source before it passes through the atomic vapour and amplifying the output of the detector by an amplifier tuned to this modulation frequency. Thus any radiation emitted by the atomic vapour, which is not modulated, produces no signal at the output of the amplifier. In some cases, such as when using lines below 3000° A, the radiation emitted by the sample is negligible compared to that from the source and D.C. amplification is possible. It is apparent, however, that the modulated system is more generally applicable than a D.C. system.

In a modulated type of atomic absorption spectrophotometer the light source emits, under conditions which ensure the production of extremely sharp lines, the spectrum of the element to be determined and this emitted radiation is modulated, either by modulating the electrical supply to the lamp or by a mechanical chopper in the light beam, before it passes through the atomic vapour of the sample. The monochromator isolates a given line, usually the strongest resonance line, and this falls on to a photoelectric detector. The output from the latter is passed to an amplifier tuned to the same frequency as the light source, and after amplification the signal is rectified, the rectified output being read off on a meter or recorder which indicates the signal with and without the absorbing sample in the radiation path.

APPARATUS

An atomic absorption spectrophotometer [10] typical of those now used in analytical laboratories is shown in Figure 1. The light source is a sealed-off hollow cathode tube, containing a cathode of the element to be determined, and the atomizer is a flame into which is sprayed the sample for analysis. The power

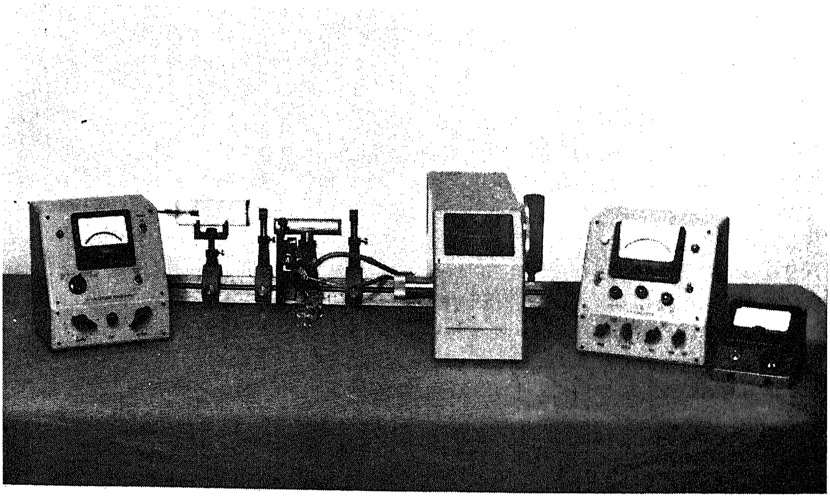

Figure 1. Simple atomic absorption spectrophotometer.

pack on the left supplies the hollow cathode tube with a D.C. supply modulated at 50 or 100 c/s, and the unit on the right contains a regulated power-supply for the photomultiplier tube, A.C. amplifier, rectifier and output meter. The small unit on the extreme right provides scale-expansion. There are, of course, numerous variations of this type of apparatus. For example, for the determination of the alkali metals the usual type of laboratory discharge lamp is satisfactory and the monochromator can be an absorption or interference filter. Figure 2, for example, shows an instrument [11] for the determination of sodium and potassium. The apparatus employs a monitoring system to compensate for fluctuations in the light source and is arranged to give 1 ppm full scale deflection. Similar types of apparatus could obviously be developed for other determinations, but for general analytical work there is at the present time no alternative to a dispersion monochromator. The dispersion and resolution required varies according to the element to be determined, the most stringent demand being in the determination of nickel, where for optimum performance it is necessary to isolate the line at 2320.0Å (which is the most sensitive line in absorption) from the singly-charged ion line at 2319.8Å.

With two exceptions which will be discussed later, all analytical work to date has been restricted to the analysis of solutions which are atomized in a flame, the most commonly used fuel mixtures being air-coal gas, air-propane and air-acetylene. It is usual to employ a burner giving a long (up to 10 cm), narrow flame and, since maximum absorption occurs at different parts of

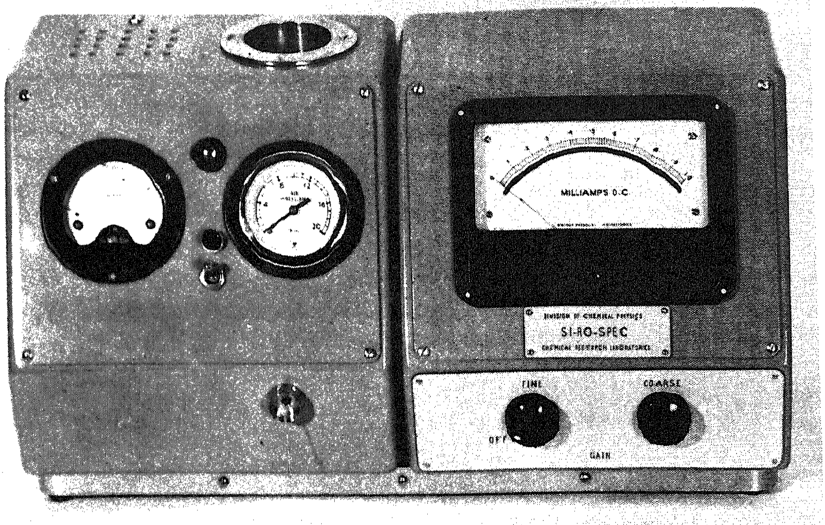

Figure 2. Simple filter instrument for the determination of sodium and potassium.

the flame for different elements, provision must be made for accurate adjustment of burner height.

SCOPE AND LIMITATIONS OF ATOMIC ABSORPTION METHODS

There are now some two hundred laboratories equipped with atomic absorption spectrophotometers and these are being used for analyses of importance in agriculture, pathology, mining, metallurgy and oil refining. The published results are distributed over 70 publications. A list of analyses about which information has been published is given in Table 2. This list by no means embraces all the elements which can be determined and Table 3 includes details of the limits of detection given by Gatehouse and Willis [4] for elements which can be determined by atomic absorption spectroscopy but for some of which no specific analytical applications have yet been published.

From the experience gained with the atomic absorption method to date it seems justifiable to make the following comments:-

1. The advantages to be expected from the fact that absorption is independent of excitation potential (or wavelength of the

Table 2

Summary of Published Applications of Atomic Absorption Spectroscopy

Element	Sample
Na	Plants, soil extracts, blood sera.
K	Soil extracts, blood sera.
Cu	Plants, soils, fertilizers, copper alloys, ore concentrates.
Ag	Lead concentrates.
Mg	Plants, soils, blood sera, urine, milks, aluminium, nickel, steel.
Ca	Plants, soil extracts, blood sera, urine, saliva.
Sr	Plants, soil extracts.
Zn	Plants, soils, fertilizers, urine, brasses.
Cd	Zirconium, urine.
Pb	Urine, copper alloys, steel, wines, petrol.
Bi	Urine.
Mo	Fertilizer, stainless steel.
Mn	Soils, plants.
Fe	Plant ash.
Ni	Leaded brass.

strongest resonance line) have been clearly demonstrated. Zinc (2138 Å) and cadmium (2288 Å), for example, have the same order of detection-limit (0.03 ppm) as sodium (5890.0Å).

2. The relative freedom from radiation interference (due to incomplete isolation of the line it is required to measure) has been demonstrated in several cases. For example, Allan [12] reports that the determination of magnesium in sodium acetate extracts is impracticable by emission methods using a medium spectrograph since the magnesium resonance line at 2852.1Å cannot be isolated from the strong sodium line at 2852.8Å. In absorption, on the other hand, Allan states that the same absorption was obtained from 2 ppm of magnesium in 0.1 N hydrochloric acid as from the same concentration of magnesium in a 10 percent w/v sodium acetate solution.

Another type of radiation interference occurs when the line to be measured lies in a region where there are spectra due to molecular species. For example, in the determination by emission flame photometry of small amounts of sodium in the presence of

Table 3

Limits of Detection of Metal Ions in Solution by a Simple Atomic Absorption Spectrophotometer (See Ref. 4)

Metal	Line (Å)	Concentration (ppm.) Giving 1% Absorption	Metal	Line (Å)	Concentration (ppm.) Giving 1% Absorption
Li	6708	0.03	Ga	2874	250
Na	5890	0.03	Tl	2768	0.8
K	7665	0.03	Sn	2863	5
Rb	7850	0.1	Pb	2833	0.5
Cs	8521	0.15	Sb	2311	1.5
Cu	3248	0.1	Bi	3068	2.
Ag	3281	0.05	Cr	3579	0.15
Au	2428	0.3	Mo	3133	0.5
Mg	2852	0.01	Mn	2795	0.05
Ca	4227	0.08	Fe	2483	0.1
Sr	4607	0.15	Co	2407	0.2
Ba	5536	8	Ni	2320	0.2
Zn	2139	0.03	Rh	3435	0.3
Cd	2288	0.03	Pd	2476	0.8
Hg	2537	10	Pt	2659	5.

large amounts of calcium, the monochromator transmits not only one or both sodium resonance lines of the yellow doublet, but also the molecular band spectra of calcium hydroxide which are emitted in this region. Even when using a spectral slit-width of 1Å the total calcium hydroxide emission may be much greater than that due to sodium. In absorption, on the other hand, Brownell [13] has found the corresponding effects to be extremely small, since the effective spectral slit-width can be reduced to 0.01Å.

Similarly, Zaidel and Korennoi [14] report that "strontium, which interferes seriously in the determination of lithium by the emission method, has no effect on the absorption. The strontium hydroxide formed in the flame emits a molecular band at 6628-6700 A, which overlaps Li 6708 because of the insufficient resolving power of the monochromator. For absorption, the inadequacy of the equipment is not important, because the signal from the unmodulated strontium emission from the flame is not transmitted by the tuned amplifier". (This explanation is not completely correct: another reason for the superiority of the absorption method in this case is due to the high effective resolution and this effect is still operative even if the emission from the atomized sample is negligible compared to that from the light source.)

A further example is in the work of Allan [15] who reports that a solution containing 10 ppm each of iron and manganese, and 3000 ppm potassium, 3000 ppm of calcium, 1000 ppm of sodium, 1000 ppm of magnesium and 500 ppm of phosphorus gave the same iron and manganese absorption readings as a solution containing only 10 ppm each of iron and manganese. Allan points out that "this complete lack of radiation interference is in marked contrast to the situation that occurs in flame emission methods using the most sensitive emission lines, manganese 4030Å and iron 3730Å, which are in a region of the spectrum where there is strong continuous and band emission so that large background corrections are necessary." (Allan has pointed out that the strongest absorption lines of elements having a complex spectra do not necessarily correspond to the strongest emission lines and has described a simple spectrographic method by which they can be determined.)

3. The method has been found suitable for use in routine analytical laboratories. For example, Allan [12] states that magnesium determinations "can be carried out with the same ease as, and probably with greater reliability than, flame photometer determinations of sodium, potassium and calcium."

4. A wide variety of analytical work is possible using equipment which is simple and inexpensive.

5. The outstanding limitations of the absorption method arise from the difficulty in atomizing various elements. The flames which have been used to date are incapable of atomizing elements such as aluminium, silicon, zirconium, etc., which form stable molecules compounds in the flame, and yield virtually no free atoms. Thus the atomic absorption method in its present form is not applicable to the determinations of these elements. Similarly other elements are only partially atomized, thus resulting in loss in sensitivity and the possibility of chemical interference due to variation of the degree of atomization of one element with the concentration of other elements, radicals or compounds in the solution. For example, the alkaline earth elements form compounds with phosphate, sulphate or silicate, and since these are only partially volatilized and/or dissociated their presence lowers the number of free atoms available. This type of interference is present to the same extent in emission and absorption and is responsible for serious limitations in flame methods. Allowance for this type of interference can sometimes be made by using standard solutions which are closely similar in composition to the sample for analysis, but this approach is

obviously of limited application. The more usual method is by: (a) addition of excess amounts of the offending anions or cations; (b) removal of the interfering element; or (c) addition of complexing reagents such as EDTA to prevent the formation of stable or involatile compounds.

When using such methods it may well prove that absorption methods give more scope than emission methods in the choice of suitable additions since the latter may well introduce radiation interference, which as was pointed out earlier, may be much more pronounced in emission than absorption.

6. The absorption method in its present form is not suited to rapid survey work involving the determination of a large number of elements, particularly when only a limited sample is available. There is no counterpart to scanning emission methods and the use of a fixed array of hollow-cathode tubes and an array of photomultiplier tubes at the appropriate points on a focal wave results in an arrangement which is appreciably more complicated than the corresponding arrangement using flame emission methods.

7. There is no counterpart in absorption to flame emission methods based on the use of molecular bands, or to those in which chemiluminescence yields enhanced sensitivity for some lines of some elements.

CURRENT RESEARCH

It seems certain that in the near future the atomic absorption method will be applied to an increasingly wide range of analytical problems by straightforward extension and modification of existing techniques, and much effort will obviously be devoted to the development of the appropriate recipes for specific problems. However, in view of the central importance of the atomization problem it is to be expected that this will be the focus of much research in the future. Whilst there are many variants of the flame which remain to be explored it is highly probable that the most spectacular advances will come from the development of completely new atomizers, although it is difficult to imagine one which is as simple and convenient to operate as a flame.

One promising approach is the cathodic-sputtering technique which my colleagues and I have developed over the past three years [16,17]. In this method, which so far has been restricted to the analysis of metals and alloys, the sample for analysis is in the form of a hollow cylinder and this forms the cathode of a discharge in a rare gas, the pressure of the latter being adjusted to permit formation of a hollow-cathode discharge. In effect then, the sputtering chamber is a hollow-cathode discharge tube which is used as an absorption cell. The impingement of rare gas ions on the inside surface of the cathode results in cathodic sputtering of atoms from the cathode so that in the region enclosed by the cathode there is an appreciable concentration of metal atoms: the absorption of radiation by these atoms, which are predominantly neutral atoms in the ground state, forms the basis of the proposed method.

Experiments to date have been mainly concerned with studying the factors which are important in controlling the sputtering phenomena, and in devising apparatus which will permit rapid conditioning of the tube. Using tank argon and a flow-through system it is now possible to obtain absorption measurements in less than two minutes, and my colleague Mr. J. V. Sullivan has recently obtained promising results for several series of alloys. Figures 3, 4, and 5 show typical calibration curves. Much work remains to be carried out before any assessment of this approach can be made but certainly it has many attractive features. The outstanding advantage over the flame is that the possibility of compound formation is largely obviated since, apart from impurities in the argon and gases liberated from the cathode, the discharge is entirely in a rare gas. Thus the method offers promise of being applicable to a wide range of metallic elements, including those such as aluminium, silicon, etc., which cannot be detected by flame-absorption methods. Similarly, since compound formation is largely avoided there should be smaller effects due

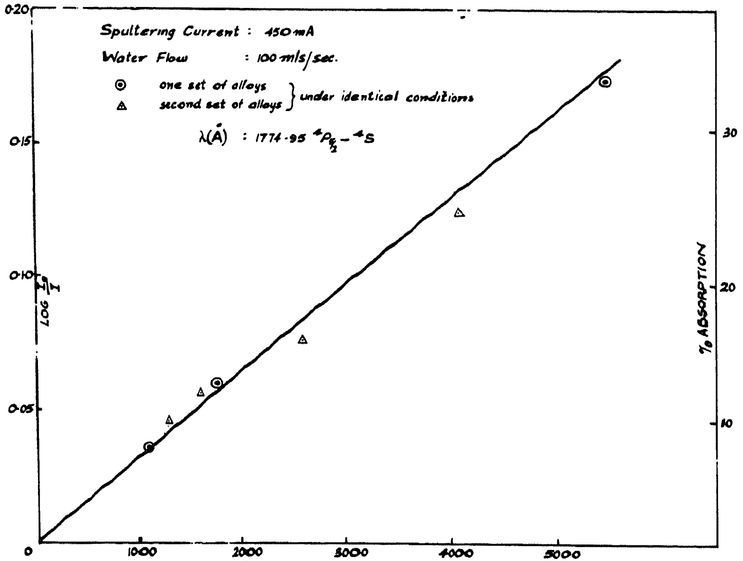

Figure 3. Calibration curve for the determination of phosphorus in copper by the cathodic sputtering method.

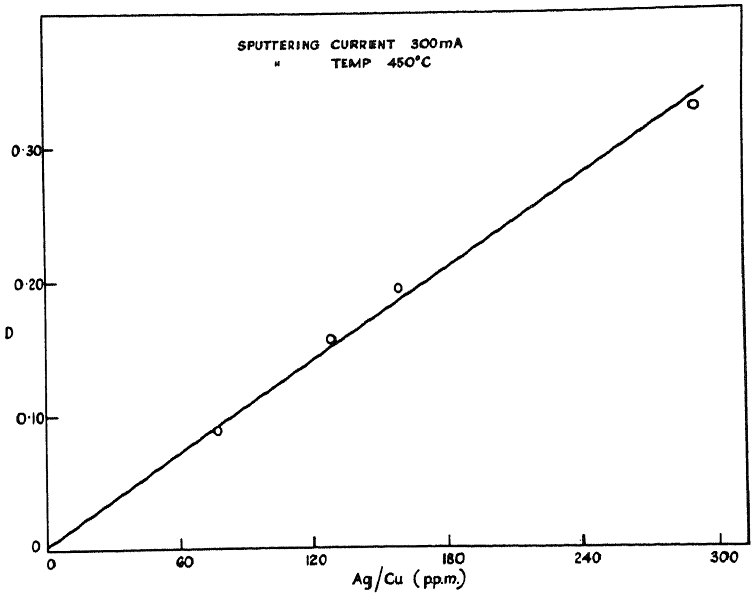

Figure 4. Calibration curve for the determination of silver in copper by the cathodic sputtering method.

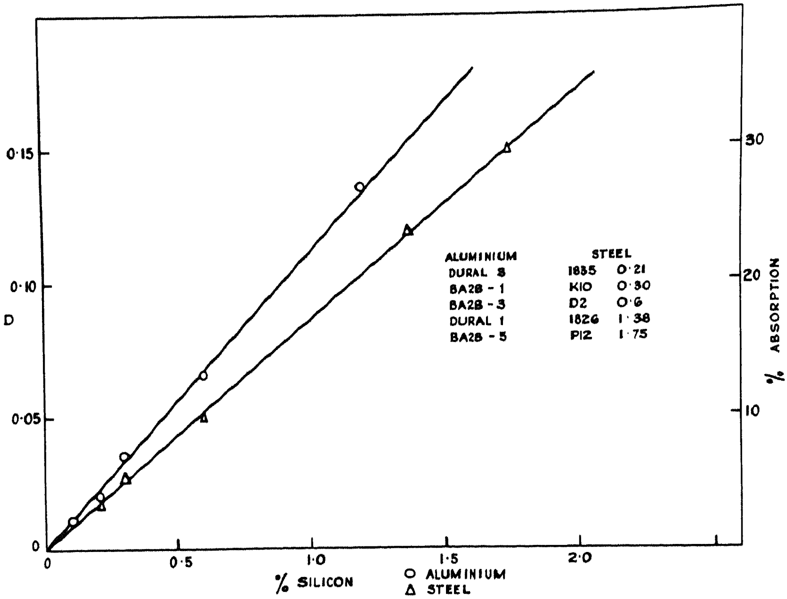

Figure 5. Calibration curves for the determination of silicon in aluminium and in steel by the cathodic sputtering method.

to chemical interference. Other attractive features are the stability of the system and the use of a large surface area of sample, thus minimizing problems due to segregation. It will also be of particular interest to determine whether the absorption by the hollow-cathode discharge is more independent of the effective "temperature" of the discharge than the emission intensity. A further advantage over the flame is that the sputtering technique permits extension of the absorption method to the vacuum ultraviolet region.

Apart from its use as a purely analytical technique, absorption measurements on vapours produced by cathodic sputtering have other important applications, and will obviously prove of great value in fundamental studies of the mechanism of sputtering since previously such studies have been handicapped by lack of a method for determining the concentration of sputtered atoms. Another possible application is in the determination of oscillator strengths, using cathodes made of binary alloys of known composition and determining the ratio of the oscillator strengths of resonance lines of the two elements from absorption measurements on the sputtered vapour. My colleague Mr. J. V. Sullivan is exploring this possibility and in the first place is studying the relationship between the composition of sputtered vapour and that of the binary alloy: other possibilities which suggest themselves are the use of a sputtering chamber as a substitute for a vacuum furnace in many investigations, and the extension of the sputtering technique to the analysis of solutions and liquids.

Another promising approach to the atomizing problem has recently been reported by L'vov [18], who vapourizes the sample completely in a graphite crucible operated in an atmosphere of argon. The substance to be analysed is placed, in solution form, on the end of a carbon electrode, and then evaporated to dryness. The electrode is introduced into an opening in the electrically-heated crucible, the electrode itself being heated by a D.C. arc. Because of the highly reducing conditions existing in the graphite crucible the partial pressures of O and OH which can exist are several orders lower than in a flame. Thus, even the most refractory oxides (BaO, Al, TiO, etc.) and hydroxides (LiOH, CsOH, RbOH, etc.) dissociate almost completely and there are no effects due to chemical interference. The absolute sensitivity is extremely high and for the elements studied lies in the range 10^{-4} to 10^{-5} μg. Using this apparatus L'vov was able to carry out twenty determinations per hour. L'vov's method is obviously of great promise and reports of its further development will be awaited with great interest.

Another aspect of the furnace method is the work of the General Electric Company in the United States, where Vidale [19] has used the atomic absorption method to measure the partial pressures of metallic vapours above heated compounds of various types. From such measurements it has been possible to determine some of the thermo-dynamics of the volatilization process.

The possibility of applying the atomic absorption method to isotopic analysis was pointed out several years ago [20] and recently Zaidel and Korrenoi [14] have successfully determined the isotopic concentration of lithium in solutions. Hollow-cathode discharge tubes containing the purest available lithium isotopes were used as sources and the sample atomized in an air-acetylene flame. The authors report an accuracy of 0.6% and an analysis time of 2-3 minutes. Other workers are investigating the possibility of applying similar methods to other isotopic analyses.

Another aspect of atomic absorption research concerns the measurement of the profiles of the emission and absorption lines involved in the measurement. Recently G. R. Isaak [21], working in the Central Research ICIANZ Laboratories in Melbourne, has developed a method of profile measurement which involves Doppler or Zeeman scanning. Isaak has reported measurements for the sodium resonance lines and my colleague Dr. G. R. Hercus is now attempting to extend the method to other elements.

On the purely instrumental side it is apparent that we can expect the development of improved hollow cathode tubes, double-beam systems employing scale expansion, and instruments for the simultaneous determination of several elements. Much of this work will undoubtedly be carried out by the various instrument manufacturers who are now developing atomic absorption spectrophotometers.

SUMMARY

Atomic absorption measurements are now being applied to a wide range of analytical problems, using equipment which is simple and inexpensive, and many more applications can be expected in the near future. The outstanding problems at the present time are associated with the limitations of the flame as an atomizer and promising new approaches to this problem are now being investigated. In the near future it may be expected that the atomic absorption method will become of increasing value, not simply as a method of analysis, but as an important tool in many physical investigations such as basic studies of phenomena occurring in flames, electrical discharges and plasma.

REFERENCES

1. Allan, J. E., Spectrochim. Acta 18, 605, 1962.

2. David, D. J., Analyst 85, 779 (1960).
3. Elwell, W. T. and Gidley, J. A. F., Atomic Absorption Spectrophotometry, Pergamon Press, London, 1961.
4. Gatehouse, B. M. and Willis, J. B., Spectrochim. Acta 17, 710 (1961).
5. Leithe, W., Angewandte Chemie 73, 488 (1961).
6. Menzies, A. C., Anal. Chem. 32, 898 (1960).
7. Poleutkov, N. S., Zavodskaya Laboratoriya 7, 830 (1961).
8. Robinson, J. W., Anal. Chem. 32, 17A (1960).
9. Walsh, A., Advances in Spectroscopy, Vol. II, Interscience (1961).
10. Box, G. F. and Walsh, A., Spectrochim. Acta 16, 255 (1960).
11. Box, G. F. and Walsh, A., CSIRO Ind. Res. News No. 17 (1959).
12. Allan, J. E., Analyst 83, 466 (1958).
13. Brownell, P., Report of Second Australian Conference, Nature, 184, 1195 (1959).
14. Zaidel, A. H. and Korennoi, E. P., Optics and Spectroscopy, 10, 299 (1961).
15. Allan, J. E., Spectrochim. Acta 15, 800 (1959).
16. Russell, B. J. and Walsh, A., Spectrochim. Acta 15, 883 (1959).
17. Gatehouse, B. M. and Walsh, A., Spectrochim Acta 16, 602 (1960).
18. L'vov, B. V., Spectrochim. Acta 17, 761 (1961).
19. Vidale, G., Technical Information Series Nos. R60SD330, R60SD331, R60SD333, R60SD390, General Electric Company, Philadelphia, U.S.A.
20. Walsh, A., Spectrochim. Acta 7, 108, 1955.
21. Isaak, G. R., Nature 189, 373, 1961.

EXCITATION AND RELATED PHENOMENA IN FLAMES

C. Th. J. Alkemade
Physics Laboratory of the State University
Utrecht, Holland

SECTION 1. INTRODUCTION

The continuous search for new light-sources in spectroscopy which combine the reproducibility and stability of flames with the high temperature attained in arcs, has widely extended the concept of "flame." We may mention, e.g., the attempts made with cyanogen-oxygen, cyanogen-ozone and hydrogen-fluorine gas-mixtures and the "microwave torch" (cf. for general review [16, 17, 22, 24, 25]). Also the "plasma-jet," emerging through a hole in the electrode of a pinched arc, is sometimes referred to as a flame because of its flame-like appearance. In our discussion on flame excitation, however, we shall restrict ourselves to the usual "chemical" flames, such as, e.g., the $H_2 - O_2$ and C_2H_2-air flame, just because these flames are the usual ones in flame spectroscopy and because the excitation processes are better understood here.

The main parameter controlling the flame emission is the temperature. It may then seem most natural to look for special combustion mixtures which may yield higher temperatures, when better excitation is wanted. However, the possibilities of obtaining higher temperatures by using special flames or excitation techniques was already amply discussed by Mavrodineanu at the VIII Colloquium Spectroscopicum in 1959 [cf. 25]. Here we shall only be concerned with the question of which factors control the emission intensity of metal spectra in a flame of normal composition with *given* flame temperature. In particular, we shall discuss under what conditions the excitation in flames is thermal and which deviations from thermal excitation may occur. Of course, we are not only interested in the excitation of metal atoms to states of higher energy, but also in the probability that an excited atom actually emits a photon contributing to the flame emission. Thus we shall also be concerned with the de-activation of excited atoms and with emission losses owing to self-absorption.

For a more general treatment of excitation processes and flame problems the reader may be referred to the literature [5, 8, 11, 12, 19, 20, 23, 26, 32, 36, 37].

SECTION 2. FLAME EQUILIBRIUM AND THERMAL RADIATION OF METAL SPECTRA

A metal atom emits a photon upon transition from an energy state E_i to a lower energy state E_j. The frequency (ν) of the spectral line emitted is determined by the energy balance: $h\nu = E_i - E_j$ (h = Planck's constant). The spectral line is a resonance line for transitions to the ground state with $E_j = 0$, and we then have $h\nu_{res} = E_i$. The total amount of energy radiated per second (J) from a small volume (V) of the flame at frequency (ν) is given by

$$J = AN^* Vh\nu . \qquad (2.1)$$

Here N^* is the number of atoms (per unit volume) in the excited state and A is the Einstein transition probability per sec for the transition $E_i \rightarrow E_j$. (We may disregard stimulated emission when dealing with flames.) The volume V is chosen small enough to neglect self-absorption; i.e., all photons generated inside V will also leave it and thus contribute to its total radiation.

In the above formula for the radiation flux, A and ν are typical constants for the atom considered. However, the occupational number, N^*, of the excited energy state depends not only on the atomic structure, but also on the total number of metal atoms available and on the state of the flame gas. In the case of complete equilibrium this state is uniquely determined by a single macroscopic parameter, i.e., the absolute temperature, T. We then have for N^* according to statistical mechanics

$$N^* = N \cdot \frac{g_i}{g_o} e^{-E_i/kT} . \qquad (2.2)$$

Here N is the number of atoms in the ground state per unit volume; g_i and g_o are the "statistical weight factors" of the excited and ground state, respectively; k is the Boltzmann constant.

Combining Equations (2.1) and (2.2) we find for the radiation flux, J, from a (small) volume V, in the case of a resonance line

$$J = A V N h\nu \frac{g_i}{g_o} \cdot e^{-h\nu/kT} . \qquad (2.3)$$

It should be emphasized that under conditions where self-absorption is negligible, this formula holds irrespective of the particular shape of the spectral line under consideration. So under these conditions, the radiation intensity (integrated over the total line-width) is not influenced by factors affecting the line shape (line-broadening by collisions, Doppler-width).

The total radiational output flux of the *whole* flame may be obtained by dividing the flame into small sub-volumes and by applying (2.3) to each sub-volume separately. In the case of a resonance line we must in general allow for a loss-factor due to self-absorption. A photon emerging at some distance x from the flame surface (see Figure 1) will have some chance of being reabsorbed by other metal atoms in the ground state on its way to the surface. This chance depends not only on the distance x to be traversed, but also on the precise value of the frequency. Here the frequency distribution of the spectral line ("line-shape") enters essentially into the problem.

In computing the spectral radiation intensity, $I(\nu)$, of the flame (i.e., radiation energy emitted per sec and per unit solid angle by a surface element of unit area in a unit frequency-interval) we shall follow the procedure outlined above for a flame with homogeneous composition and temperature; see Figure 1. Let $\alpha(\nu)d\nu$ be the probability that an emitted photon has a frequency between ν and $\nu + d\nu$. ($\alpha(\nu)$ represents the normalized shape of the spectral line when not distorted by self-absorption).

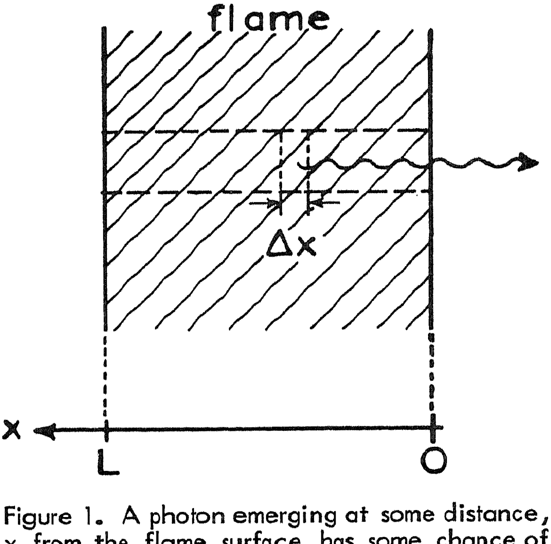

Figure 1. A photon emerging at some distance, x, from the flame surface, has some chance of being re-absorbed before leaving the flame.

Let $\beta(\nu) \cdot N \cdot dx$ be the fractional energy loss owing to reabsorption when the light beam travels over a distance dx through the flame. The contribution to the spectral flame intensity $I(\nu)$ from an element Δx at distance x from the surface is now given by

$$(\Delta I)_x = \left(\frac{g_i}{g_o} \cdot N \exp\left[-\frac{h\nu}{kT}\right]\right) \cdot \left(\frac{A\alpha(\nu)\, h\nu}{4\pi}\right) \left(\exp\left[-\beta(\nu)\, Nx\right]\right) \cdot \Delta x.$$

By integration over the flame-thickness, L, we find for $I(\nu)$

$$I(\nu) = \frac{g_i}{g_o} \exp\left[-\frac{h\nu}{kT}\right] \cdot \frac{A\alpha(\nu)}{\beta(\nu)} \frac{h\nu}{4\pi} \left(1 - \exp\left[-\beta(\nu)\, NL\right]\right). \qquad (2.4)$$

The factor $(1 - \exp[-\beta(\nu)\, NL])$ just equals the absorption factor, $a(\nu)$, of the flame for the particular frequency considered. From the well-known relations in the Einstein theory of radiation [cf., e.g., 26] we find

$$\frac{A \cdot \alpha(\nu)}{4\pi\beta(\nu)/h\nu} = \frac{2h\nu^3}{c^2} \cdot \frac{g_o}{g_i}.$$

Substituting this relation in Equation (2.4) we find:

$$I(\nu) = \frac{2h\nu^3}{c^2} \cdot \exp\left[-\frac{h\nu}{kT}\right] \cdot a(\nu) = P(\nu) \cdot a(\nu), \qquad (2.5)$$

in which, according to Wien's law, $P(\nu)$ represents the spectral radiation intensity emitted by a black body at temperature T. Of course, this result could also have been obtained directly by making use of Kirchhoff's law. However, the derivation given here stresses the close connection between Equations (2.3) and (2.5). Moreover, the general procedure followed above remains also valid in the non-equilibrium case, when, e.g., the number of excited atoms is not given by a Boltzmann factor.

In flame photometry one is usually interested in the line intensity I integrated over the total spectral line width. We find from Equation (2.5)

$$I = \int I(\nu) d\nu = \int P(\nu) a(\nu) d\nu = P(\nu_o) \cdot \int a(\nu) d\nu. \qquad (2.6)$$

In the frequency-interval of interest $P(\nu)$ is virtually constant and equal to $P(\nu_o)$ with ν_o the central frequency of the spectral line considered.

We learn from Equations (2.5) and (2.6):

1. The intensity of the radiation emitted in a *fixed*, small frequency-interval $\Delta\nu$ around ν_o cannot grow indefinitely upon increasing the salt-concentration (N) or the width L of the flame; the maximum intensity to be expected amounts to: $P(\nu_o) \cdot \Delta\nu$, since $a(\nu)$ tends to unity as $N \cdot L$ tends to infinity. Yet the *total*, integrated flame intensity, I, as measured usually in flame photometry, proves to increase indefinitely with increasing flame content ($\sqrt{N}$-law). Apparently, this should be explained by a *broadening* of the total line profile rather than by an increase in central intensity.

2. As the specific absorption coefficient $\beta(\nu)$ does not critically depend on temperature, $a(\nu)$ will likewise not depend critically on T, if N and L are kept constant. It thus follows from Equation (2.6) that the dependence of the integrated intensity I on the temperature is governed by $P(\nu_o)$ only, which involves the Boltzmann factor $\exp[-h\nu/kT]$.

So it appears that the dependence of flame emission on temperature is not much influenced by self-absorption.

It is not our purpose, however, to discuss emission and self-absorption processes as such. We rather wish to insist here on the conditions under which the metal line emission may be "thermal" or not, which will lead us naturally to a consideration of the specific excitation mechanisms.

We may call the flame emission *"thermal"* when the actual occupational number of the excitation level is given by the Boltzmann factor at flame temperature T [cf. Equation (2.2)]. The radiation flux from a small sub-volume of the flame is then given by Equation (2.3), which does *not* contain the *specific* mechanisms responsible for the excitation. This may lead to a paradox. Imagine, we add purposely a molecular compound to the flame gas that is known to be very effective in exciting metal atoms upon collision. Undoubtedly, the rate of excitation (i.e., number of excitations per second and per metal atom) will now be enhanced. But statistical mechanics still tells us that in equilibrium the number of atoms being in the excited state is invariably given by Equation (2.2). This paradox is to be explained by the fact that molecules which are effective in producing excited atoms upon collision (so-called collisions of the first kind), are also effective in de-activating these excited atoms again by collisions (so-called collisions of the second kind). The enhancing effect on the number of excited atoms caused by the increased excitation rate just balances (in equilibrium) the depressing effect caused by the increased de-activation rate. In statistical mechanics this result is more generally expressed by the *"principle of detailed balance"* which, in turn, is based on the "principle of microscopic reversibility." Detailed balance states that in equilibrium the total number of atoms leaving the excited state per second by any process (collision, chemical reaction, radiation, etc.), just equals the number arriving in that state per second by the exact reverse process. It is just this competition of the various excitation and de-activation processes, mutually connected by detailed balance, that guarantees the validity of Equation (2.2) for the population of the excited level, *regardless of the specific composition of the flame gas-mixture.*

The principle of detailed balance is here operative only if the statistical distribution of all other forms of energy of interest is described by a Maxwell-Boltzmann law with the same temperature T as parameter. This implies that the energy should be equally partitioned among the various forms (or "degrees of freedom") that are relevant in the excitation and de-activation of the metal atoms. Where the possible values of energy form a continuous range (e.g., the translational energy), the *equipartition law of energy* states specifically that the average amount of energy per degree of freedom equals 1/2 kT.

But we have now arrived at a real contradiction in the concept of thermal radiation in flames. Radiation is just one of the possible processes in which excited atoms are formed or destroyed. So the number of excited atoms equals its equilibrium value, given by Equation (2.2), only if *also* this process of de-activation is balanced by the reverse process of excitation by photon-absorption. But this balance will not exist, unless the density of the radiation (to be absorbed) in the flame has also reached its equilibrium value at flame temperature. This requires that the flame should fully radiate as a "black-body" at temperature T, at least in that part of the spectrum and in that part of the flame where the atomic line considered is situated. However, in emission-flame photometry the flame intensity measured should just be a *function* of the metal concentration. One sees from Equation (2.6) that this holds only if a(ν), which indeed contains N as parameter, has not yet reached its constant limiting value 1 in the whole spectral range. This again implies that the flame does not fully radiate as a black-body.

Does the concept of "thermal radiation" then still have any sense under the usual conditions in flame photometry? Yes, it does if the following condition is, at least approximately, fulfilled.

The probability that an excited atom returns to the lower state under emission of a photon should be negligibly small compared with the probability of de-activation by all other means, e.g., by collisions or reactions with flame molecules.

For strongly self-absorbed lines this condition may be somewhat weakened. Here the radiation density, at least in the central part of the flame and at the top of the spectral line may fairly well approach its value for a black-body. It should, however, be realized that at the very surface of the flame the radiation *density* equals at most half its black-body value (since the outgoing radiation is here not compensated by an incident radiation flux of equal strength from the surroundings).

In usual flames burning at atmospheric pressure, the above condition is reasonably well fulfilled, so the concept of thermal radiation is meaningful here. Under special circumstances, however, this condition is not met as we shall show in Section 5.

SECTION 3. DEVIATIONS FROM FLAME EQUILIBRIUM

If all processes leading to excitation or de-activation of metal atoms would be perfectly equilibrated at flame temperature T there would be no problem left—and no possibilities of enhancing the metal excitation, at given flame temperature, either!

Deviations from equilibrium, in fact, do exist, as is commonly known, in the first reaction zone (inner cone), where the concept of temperature is even hardly applicable. But also in the burnt gas-mixture beyond this reaction zone (to be called here "flame-body"), less spectacular departures from thermodynamic equilibrium are found.

Some of these deviations may have a bearing upon the excitation of metal spectra. We may distinguish between two kinds of deviations (which are in part mutually connected):

(a) Deviation from general thermodynamic equilibrium occurs insofar as the "temperature" is *locally* different throughout the flame body.
(b) At a given location in the flame the different forms of energy are not equilibrated among each other.

(a) Local differences in "temperature" may be expected, even in pre-mixed laminar flames, since the flame is not truly an adiabatic system and the supply of fuel and oxidant gas may not be quite homogeneous. The flame gases radiate heat to the environment (mainly in the infra-red flame bands of CO_2 and H_2O); entrainment of fresh air at the flame border may cause secondary combustion, but also cooling by convection. Because of these and similar effects a net transport of heat, radiation and mass occurs through the flame. Strictly speaking, there can be no question of general, thermodynamic equilibrium when net transport of energy and mass is found. However, if the rate of transport is comparatively slow with respect to the rate at which the energy is partitioned over its different forms, we still may speak of *local* equilibrium characterized by a *local* temperature T(x). The intensity of a spectral line emitted by the flame might be computed by the same procedure that has led to Equation (2.6) in Section 2. We only have to replace in Equation (2.4), etc., the uniform temperature T by T(x) as defined above. The effect of T(x) on the line-shape may here be neglected to a good approximation. The metal excitation may then again be described by an "effective" or "apparent" temperature, but this value is no longer independent of the metal concentration, line shape, etc.

(b) In discussing the equilibration of the energy at a given locus over the various translational and internal degrees of freedom and of the molecular dissociation and atomic ionization processes, we should realize that the flame gases travel upwards from the reaction zone with considerable speeds of the order 1-10 m/s. In the reaction zone the chemical energy released is primarily carried off by direct reaction products or stabilizing reaction partners. Typical reaction products involve such unstable, highly excited radicals and ions as CH, C_2, HCO^+, H_3O^+, etc. By subsequent collisions this energy will be redistributed among the other species of the flame gases, and the unstable products (ions and radicals) will disappear. The attainment of equilibrium always requires that the particles of the system have suffered a sufficient number of collisions with each other. In flames at atmospheric pressure a flame molecule makes about 10^6 collisions with the surrounding molecules in a time-interval of 1 millisecond. In this time-interval the flame gases travel over a distance of about 1-10 mm onwards from the reaction zone. We shall see now specifically to what extent equilibrium may be attained within this time-interval.

The establishment of a Maxwell equilibrium distribution for the *translational and rotational* energies of the flame molecules requires on the average but 1-10 collisions. It will be reached practically immediately. It should be noted in this connection that the masses of the relevant flame particles are of the same order of magnitude (electrons are of minor importance; cf. below). Thus there is a ready exchange of kinetic energy between all species in the flame.

Experiments with shock-tubes have shown that the equipartition of energy over the *vibrational* degrees of freedom of the molecules is a noticeably slower process. For pure CO gas at atmospheric pressure and at 2,200 °K, time-constants of the order of 150 μ second were reported [cf. 38, also 7, 13, 27]. However, the presence of CO_2 and H_2O molecules (which have shorter relaxation times) have proved to reduce the relaxation time of CO greatly. So a serious lag in the equipartition of the vibrational energy in flames is not to be expected. It may be noted, by the way, that according to theoretical calculations [cf. 33] the *higher* vibrational levels (with energy $\gg$ kT) are "warmed up" at the same rate as the lower levels (with energy $\approx$ kT). So the time-constants mentioned above are also a good measure for the attainment of equilibrium at the higher vibrational levels. This is of interest, since these levels may be of direct importance in exciting metal atoms (cf. next section).

The electronic excitation energy of flame molecules is not expected to be important in the excitation of metal spectra. Exception should be made perhaps for the OH-radical, which is a stable compound under flame conditions. Its strong, slightly self-absorbed UV bands at 3064 Å are a well-known feature of the background flame spectrum. The way in which the electronic excitation of the OH-radical attains its equilibrium value in the course of time, t, is illustrated in Figure 2a. Here the OH-emission at 3060-80 Å is plotted as a function of distance from the first reaction zone in a pre-mixed cylindrical air-acetylene flame, shielded by a cold stream of pure N_2 gas. This shield was necessary to avoid the formation of additional OH radicals by secondary combustion at the flame border. By measuring the (rather homogeneous) rise velocity of the flame gases, the distance scale could be converted into a time scale (see Figure 2). The OH concentration in the ground state is also plotted in relative measure as a function of time after passing the reaction zone (see Figure 2b). The OH concentration could be derived from absorption measurements in which an auxiliary but similar flame was used as background source also radiating the specific OH bands (see Figure 3). By using a synchronous measuring device with periodic light-chopper placed *between* both flames we achieved conditions such that the absorption measurements were not contaminated by the emission of the absorbing flame. The relation between absorption factor and OH content was calibrated by allowing the light from the source flame to pass 1x, 2x and 3x, respectively, through the (same) region of the analysis flame. This was achieved by means of mirrors. From the dependence of OH concentration on distance to the reaction zone and from the flame temperature, which was also measured as a function of distance by reversal of the sodium D-lines (cf. Figure 2c), the OH excitation was calculated if it were to be thermal (see dotted curve in Figure 2a, which was adjusted to the measured excitation curve at great distance, where equilibrium is to be expected). Here it was assumed that reversal of the D-lines yields the true (translational) flame temperature. Allowance was made for the slight effect caused by self-absorption in the calculated excitation curve. These measurements were performed by Mr. P. Zeegers at our laboratory.

It is seen by comparing the solid curve with the dotted curve in Figure 2a that supra-thermal OH radiation persists for some milliseconds beyond the reaction zone. With regard to the

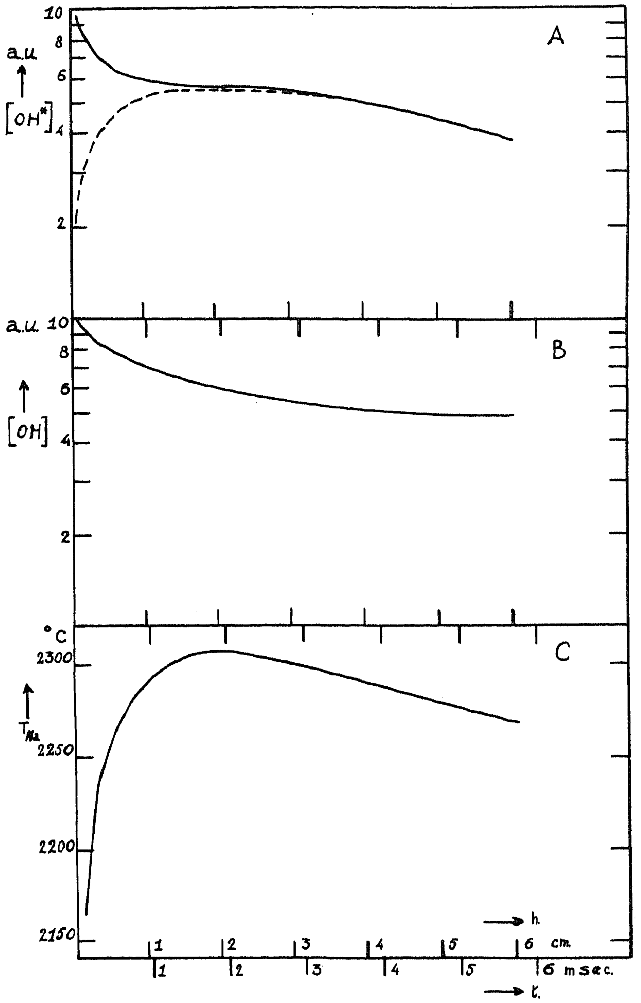

Figure 2. The relative OH-emission measured at 3060-80 Å is plotted in Figure 2a as a function of height, h, above the reaction zone, and of time, t, elapsed since the flame gases passed this zone. A pre-mixed, shielded cylindrical air-acetylene flame was used. The dotted curve shows the (calculated) thermal OH-emission. In Figure 2b the (relative) concentration of OH-radicals in the ground state is plotted as a function of h and t. Figure 2c shows the variation of measured Na-reversal temperature with h and t.

short radiative life-time (about 6.10^{-7} seconds; cf. [2]) of the electronic OH-level considered, this supra-thermal emission cannot be explained as a slow decay of excited OH radicals formed in excess in the reaction zone. We might rather suggest that ex-

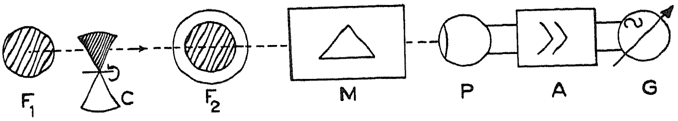

Figure 3. Experimental arrangement for measuring the concentration of OH-radicals in the ground state. F_1 = auxiliary background flame; C = periodic light-chopper; F_2 = shielded analysis flame; M= monochromator; P = phototube; A = a.c. amplifier; G = synchronous meter.

cited OH is formed in excess beyond the reaction zone as a stabilizing reaction partner in:

$$H + OH \text{ (or H)} + OH \rightarrow H_2O \text{ (or } H_2) + OH^* \qquad (3.1)$$

if we assume that [H] and [OH] are in excess of their equilibrium value (cf. below). Indeed, we found $[OH^*]$ to be proportional to $[H][OH]^2$.

This discussion of the formation of excited OH radicals by itself leads us to the question whether deviations from thermodynamic equilibrium are found with respect to molecular *dissociation* beyond the reaction zone. The general agreement found between calculated and theoretical flame temperatures justifies the assumption that the major constituents of the flame gases (such as CO_2, H_2O, O_2, H_2, etc.) are present in equilibrium concentration in the flame. This does not hold, however, for the radicals formed in excess in the reaction zone, which recombine rather slowly to form stable molecules by ternary collision processes, such as [cf. 28].

$$H + H \text{ (or OH)} + M \rightarrow H_2 \text{ (or } H_2O) + M. \qquad (3.2)$$

Here M is the stabilizing collision partner which carries off (part of) the energy released in this exothermic chemical reaction [cf. reaction (3.1)]. The decay of the nonequilibrium concentration of OH with distance from the reaction zone has already been shown in Figure 2b. It appears that often the H concentration decays proportionally to the OH concentration, so that their ratio remains constant. This has been explained by a partial equilibrium brought about by the following rapid binary reaction [cf. 28]:

$$OH + H_2 \rightleftarrows H + H_2O. \qquad (3.3)$$

It is to be noted that the variable (minor) concentrations of H and OH do not really affect the concentrations of H_2 and H_2O, so actually $[OH][H_2]/[H][H_2O]$ is constant (at constant temperature).

The decay in excess H and OH concentration by (rather slow) recombination processes entails an initial rise in flame temperature as a function of distance from the reaction zone which is also seen from the temperature plot in Figure 2c. This rise in temperature may be explained by the energy released gradually when H and OH recombine to H_2 and H_2O. We found that the rise in temperature calculated from the experimental excess concentrations of H and OH agreed within 20 percent with the experimental value.

Finally we shall have to say a few words on the equilibration of the *ionization* in the (pure) flame gases. Not only in the reaction zone, but also in the flame body (interconal gases) of hydrocarbon flames electrons and positive ions have been found in fairly high concentrations. It is reasonable to assume that these excess ionic species were formed originally in the reaction zone and that they decay rather slowly by recombination beyond this zone. But little is known with certainty about this excess ionization and the recombinations of these ions and electrons. It seems that the main ionic species are: HCO^+ and H_3O^+, and that possibly H_3O^+ may be formed from HCO^+ as follows [cf. 6]:

$$HCO^+ + H_2O \rightarrow H_3O^+ + CO.$$

The formation of HCO^+ seems to be essentially limited to carbon-hydrogen flames where CH radicals play an important role. This agrees with the observation that in H-flames ionization is only weak, unless additional acetylene gas is added to the hydrogen flame [cf. 30].

SECTION 4. MECHANISMS OF EXCITATION OF METAL SPECTRA

Before we are able to understand the effect of these deviations on excitation, we first have to consider in detail the various mechanisms that lead to excitation. Again we shall mainly be concerned with the flame body beyond the reaction zone.

All that will be said here on the excitation process is also applicable to the reverse process: the de-activation of the excited metal atoms. Both are linked by the principle of microscopic reversibility (cf. also Section 2); one has just to reverse the argument.

a. *Non-elastic collisions.* These may be distinguished as to the kind of collision partner or as to the form of energy that is consumed in the excitation process.

Collisions with free electrons which are important in arcs, sparks, plasma-jets and gas-discharges in general, do not play an important role in the usual flames, beyond the reaction zone

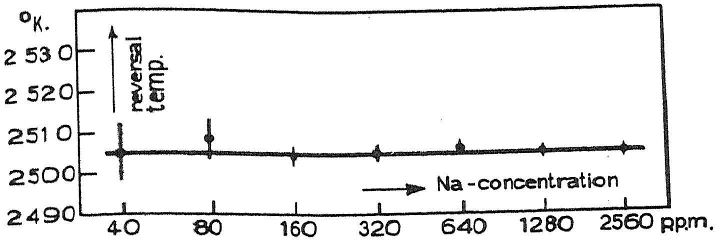

Figure 4. Na-reversal temperature of a shielded air-acetylene flame as a function of the Na-concentration in the sprayed solution.

at least. This may be readily deduced from the fact that the metal excitation is well in accordance with thermal equilibrium even under circumstances where the electron concentration is as low as 10^{10} cm^{-3}. At this low electron concentration a metal atom will have a probability of the order of one percent for meeting an electron during its travel over a distance of 1 cm from the reaction zone. Thus the probability of excitation by electrons is definitely ruled out since, moreover, only a very small fraction of the electrons (having thermal velocities) possess sufficient energy to excite the metal spectra.

For illustration we show Figure 4 in which the sodium line reversal temperature is plotted, for a given flame, as a function of the sodium concentration. Care was taken to avoid self-reversal of the spectral lines by sheathing the flame with a colorless flame mantle. One sees that the measured temperatures, which are in fact a direct indication of the excitation of the sodium atoms, are virtually constant down to sodium concentrations as low as 40 ppm. The calculated free electron concentration at this Na concentration amounts to about 10^{10} - 10^{11} cm^{-3} (cf. above).*

The most likely collision partners are the neutral molecules that form the major constituents of the flame gas-mixture (N_2, O_2, CO_2, H_2O, etc.). The number of collisions with these molecules suffered by an atom when it has covered a distance of 1 cm from the reaction zone, is of the order 10^5 - 10^6. This high value seems promising for establishing an equilibrium population of the excitation level. For example, one calculates from the Maxwell-Boltzmann distribution law that at least one out of 10^5 colliding molecules has an energy of about 3 eV at a temperature of 2000 °K.

---

*These measurements were performed by Mr. Snelleman at our laboratory, who developed a sensitive photoelectric method for measuring line-reversal temperatures [cf. 34].

The interesting question now arises: which specific *form of energy* contained by the molecule is transferred to the excited metal atom in the collision process?

Conversion of *translational* energy of the colliding molecule into electronic energy of the metal atom is not a very probable process, even if the amount of energy available is sufficient. More generally, we may state that when electronic excitation results from a collision process of whatever kind, it will be the less probable the larger the amount of translational energy consumed in the excitation [cf. 26].

The clue to the problem of which other form of energy is then transferred to the excited species is found in the experiments on the reverse process, i.e., quenching of *resonance-fluorescence* by foreign gas molecules. In these experiments, e.g., sodium vapour is excited by absorption of radiation from a sodium discharge lamp. When the pressure is low, the excited Na atoms lose their energy again by emission of light of the same frequency (resonance-fluorescence). When foreign gases such as nitrogen and helium are added, part of the excited atoms are now de-activated upon collision and consequently the resonance-fluorescence is diminished, "quenched" [cf. 26]. It appears that molecules have in general a much greater quenching effect than noble gas atoms. In the case of N_2 or CO, which are hard to dissociate, the energy originally contained in the excited metal atom is undoubtedly transferred in the quenching collision to one of the *internal* degrees of freedom of the molecule. Inversely, we should now expect that molecules are much more effective in exciting metal atoms than are noble gas atoms, and that in this excitation (part of) the internal molecular energy is transferred to the excited atom.

In particular, the molecular *vibrational* energy should be readily transferred since this transfer is not impeded by the conservation laws of linear or angular momentum. Moreover, these levels are usually rather closely spaced, so that one of these levels will be fairly close to the electronic level of the atom to be excited (quasi-resonance). The two N_2-vibrational levels that approach best the lowest excited Na level, have energy discrepancies of only +0.15 and -0.11 eV.

b. *Excitation by absorption of radiation.* Of course, when excited metal atoms can be de-activated by emission of a photon, then atoms in the lower state can also be excited by absorption of a photon. This is the very basis of the well-known self-absorption of resonance radiation. In the usual flames absorption of radiation is not the main process in maintaining the population of the excited level. This may again be deduced from Figure 4 which has already been shown in discussing excitation by electrons. In fact, the line-reversal temperature, which is a direct indication of the relative population of the excited level, remains unchanged when the metal concentration, and hence the radiation density, is reduced to low values.

It should be noted that when metal vapor is irradiated by a light-source with continuous spectrum, only those frequencies which correspond to possible transitions of the atom will be effective in exciting it.

c. *Excitation caused by chemical reactions.* A third possibility of exciting atoms is conversion of chemical energy into electronic excitation energy. Of course, all energy available in combustion flames ultimately stems from chemical energy released in the reaction zone. Here we consider only those processes in which the excitation is accompanied by an exothermic chemical reaction in which chemical energy is directly or indirectly transferred to the excited atom. For simplification we distinguish between "one-step" and "two-step processes":

I. *One-step process*

a. $M + A + B \rightarrow M^* + AB$; $(K + H + H \rightarrow K^* + H_2)$.

b. $M + AB + CD \rightarrow M^* + AC + BD$;

$(Sn + CH + OH \rightarrow Sn^* + H_2 + CO)$.

c. $MA + B \rightarrow M^* + AB$; $(SnO + C \rightarrow Sn^* + CO)$.

II. *Two-step process*

$$\text{a.}\left\{\begin{array}{l} F + A + B \rightarrow F^* + AB \\ F^* + M \rightarrow F + M^* \end{array}\right. \left(\begin{array}{l} N_2 + H + H \rightarrow N_2^* + H_2 \\ N_2^* + Na \rightarrow N_2 + N_a^* \end{array}\right)$$

$$\text{b.}\left\{\begin{array}{l} F + AB + CD \rightarrow F^* + AC + BD \\ F^* + M \rightarrow F + M^* \end{array}\right. \left(\begin{array}{l} N_2 + CH + O \rightarrow N_2^* + CO + H \\ N_2^* + Na \rightarrow N_2 + Na^* \end{array}\right)$$

$$\text{c.}\left\{\begin{array}{l} AB + CD \rightarrow AC^* + BD \\ AC^* + M \rightarrow AC + M^* \end{array}\right. \left(\begin{array}{l} CH + O_2 \rightarrow CO + OH^* \\ OH^* + M \rightarrow OH + M^* \end{array}\right)$$

Here M denotes a metal atom; A, B, C, D and F denote a flame molecule or radical. The classification suggested here is only a practical one. We do not want to go into the theoretical details of the chemical reaction itself. A chemical reaction listed here as a one-step process could, in fact, involve more intermediate steps in which short-lived, unstable compounds are formed.

The examples given could be supplemented by numerous others of even more complicated nature; they may also involve ionic species such as H_3O^+.

Reaction Ia. is a typical recombination reaction, which is in general exothermic. In the other reactions energy is set free by exchange of molecular fragments. In most reactions the metal atom is chemically not affected; it serves only as a stabilizing collision partner which carries away part of the energy released. In reactions of Type Ic., however, the excited metal atom emerges as a direct reaction product [cf. 15, 18]. This reaction may be important in those cases where the metal is mainly present as an oxide in the flame. In the two-step process IIa. and b. the chemical energy is transferred to the metal atom through an intermediate flame molecule (F) which acts as a stabilizing collision partner [cf. 3, 11]. In the two-step process IIc. an excited flame molecule is formed by a chemical reaction [cf. 11]; it gives up its energy to the atom in the following collision process.

Here we shall only make a few general remarks. Chemiluminescence as such will be dealt with briefly in the next Section.

1. A first condition for the above reactions is that sufficient energy is set free to excite (and in case Ic. also to dissociate) the metal. A possible negative or positive discrepancy between excitation energy and available energy may be balanced preferably by simultaneous vibrational transitions of the molecules involved. Conversion of translational energy seems to be less probable to balance the energy budget.

2. There is, of course, also the law of conservation of linear momentum that should be obeyed in any chemical reaction. This conservation law might be of some interest, if the excess energy that is left after excitation of the metal atom, is converted mainly into translational energy of the reaction products. In the case of binary reactions resulting in an excited metal atom (such as Ic) the conservation laws of energy and linear momentum determine which fraction of the excess energy (Q) is imparted to each of the reaction products including the excited atom. The excited metal atom will accordingly fly away with an extra velocity and the spectral line emitted subsequently will have an extra Doppler broadening. Of course, in full thermodynamic equilibrium, where also the binary reaction under discussion is equilibrated, the Doppler broadening of the spectral line emitted in total by the flame must again equal its equilibrium value and is not affected by such processes. But if there is no equilibrium and if we are dealing with chemiluminescence radiation following reactions of type Ic., it can be shown that the Doppler width of the chemiluminescent line exceeds its thermal equilibrium value by a factor

$$\left(1 + \frac{\delta}{1+\delta} \cdot \frac{Q}{Q_0}\right)^{1/2}$$

(cf. Appendix). Here δ = mass ratio of the molecular reaction product (e.g., CO) and the excited metal atom, and $Q_0 = 3/2\ k \cdot T$ = equipartition value of the mean translational energy.

3. There is also a conservation law for the spin angular momentum that should be obeyed in chemical reactions. This law, better known as "Wigner's spin-conservation rule," states that in molecular collisions the multiplicity of the system as a whole should be the same before and after the collision (or reaction) has taken place. In other words: a reaction which is energetically allowed will preferentially proceed in such way that the spin vector sum of the reactants equals that of the products [cf. 20]. It is not a quite rigorous rule, however.

4. It might be interesting to compare a priori the probability of one-step process Ia. or b. with that of two-step process IIa. or b. The final outcome of both processes, in which the metal atom M and the intermediate flame molecule F, respectively, act as a stabilizing collision partner, is the same. The second process, however, requires *two* subsequent collisions and might seem therefore to be less probable a priori.

Let us suppose, for lack of more specific information, that the probability of reaction Ia. and that of the first reaction of IIa. are in the proportion of the ratio, x, of the metal concentration to the concentration of F. We suppose that F is the major constituent of the flame gases and we put its concentration equal to unity. We also assume that the probability of molecule F to collide with another molecule is 1/x times as large as the probability that it collides with a metal atom. If now flame molecule F would lose its excitation energy acquired in the chemical reaction upon the first collision with another flame molecule, then the frequency of process IIa. would equal $1/x \cdot x \cdot \eta = \eta$ times that of the first process. Here η is the yield factor describing the probability that an excited F molecule actually excites the metal atom upon colliding with it. η may be of the order unity for the sodium D-doublet in nitrogen (cf. Section 5). However, when an excited F molecule is able to maintain its excitation energy on the average during n successive collisions with other molecules, the relative frequency of the two-step process may be raised by the same factor, so that it will now amount to: $n \cdot \eta$, which may exceed unity. In the case that F is vibrationally excited, the "persistence factor" n might be considerable. This may be concluded from what has been said already about the long relaxation time of the equilibration of the vibrational energies (cf. Section 3). So under suitable circumstances the two-step process IIa. may be definitely more probable than the direct excitation process Ia., since the intermediate flame molecule may function as a depository of energy for some time.

SECTION 5. NON-THERMAL RADIATION OF METAL SPECTRA

Our insight into the deviations from flame equilibrium and into the excitation mechanisms now permits us to investigate more closely how these deviations result in non-thermal radiation of metal lines. We shall be mainly concerned with three kinds of non-thermal metal emission:

(i) infra-thermal emission caused by radiative disequilibrium,
(ii) supra-thermal fluorescent radiation,
(iii) supra-thermal chemiluminescent radiation.

(i) *Infra-thermal metal emission caused by radiative disequilibrium* occurs when the population of the excited level is below the equilibrium population owing to a deficiency of radiative excitation. It has been argued in Section 2 that a deficiency of radiative excitation (i.e., excitation by absorption of photons from the surrounding radiation field) exists when the radiation density in the flame is lower than that of a black-body at flame temperature. We shall consider here more quantitatively the deviation from thermal radiation to be expected on account of this effect.

Let us suppose we are working under conditions such that the radiation density is, virtually, zero (low metal concentration) and that excitation occurs mainly through collisions of the first kind, with rate constant k_1. The number of excitations per second and per cm^3 thus equals $N \cdot k_1$, where N is the number of metal atoms in the ground-state per cm^3. We have the balance equation:

$$Nk_1 = N^* (k_{-1} + A). \tag{5.1}$$

Here N^* is the number of excited atoms per cubic cm and k_{-1} and A are the rate constants for de-activation by collisions of the second kind and by photon emission, respectively. In the case that photon emission is a very improbable process ($A \ll k_{-1}$), N^* approaches its equilibrium value $(N^*)_{eq.}$ determined by

$$Nk_1 = (N^*)_{eq.}\, k_{-1}. \tag{5.2}$$

In the general case we have, however, from (5.1) and (5.2)

$$\frac{N^*}{(N^*)_{eq.}} = 1 - p \quad \text{with } p \equiv \frac{A}{k_{-1} + A} \tag{5.3}$$

which shows that the deviation from thermal metal emission is governed by the ratio p. When the metal concentration, and hence the radiation density in the flame, is increased, the deviation will be smaller (cf. Section 2).

The value of p can be measured in actual flames by means of resonance fluorescence [cf. 1]. The flame containing, e.g., sodium vapor is irradiated by a sodium discharge lamp (see Figure 5). Part of the incident light-beam is absorbed in the flame in raising metal atoms from the ground state to the first excited state. The excited atoms have a relative probability = p of losing their excitation energy by re-emitting a photon. We may therefore call p the yield factor of resonance fluorescence. This yield factor can be determined by measuring the ratio of the total flux of the fluorescent radiation to the primary radiation flux that is absorbed in the flame. In our experiment the fluorescent radiation could be distinguished from the strong, constant sodium-radiation that was thermally excited in the flame, by using an a.c. measuring device with periodic light-chopper placed *between* lamp and flame (see Figure 5). Disturbing effects owing to self-absorption or scattering of radiation could be easily allowed for. Table 1 lists the yield factors as measured by Mr. Hooymayers at our laboratory for various flames at atmospheric pressure.

It is clearly seen that replacing the molecular gas by a noble gas as diluent considerably enhances the yield factor. This confirms what has been said in Section 4 about the efficiency of noble gas atoms as compared with molecules in de-activating (and exciting) metal atoms. From this Table the quenching cross sections for Na of the major molecular constituents in

Table 1

Yield Factor, p, of Resonance Fluorescence for Na-D Doublet

Supply Gases	Composition of Flame Gases (in %)	Flame Temperature	p-Factor (in %)
H_2, O_2, CO_2	48 H_2O, 51 CO_2, ...	2030°K	2.5 ± 0.1
H_2, O_2, N_2	38 H_2O, 61 N_2, ...	2100	5.8 ± 0.2
H_2, O_2, Ar	33 H_2O, 66 Ar, ...	2100	26 ± 1
C_3H_8, air	--	2100	3.6 ± 0.2
C_3H_8, O_2, Ar	--	2000	10 ± 0.5
C_3H_8, O_2, Ar	--	2100*	10 ± 0.5
C_3H_8, O_2, CO_2	--	2000	1.7 ± 0.1

*Temperature raised by electrical heating of burner.

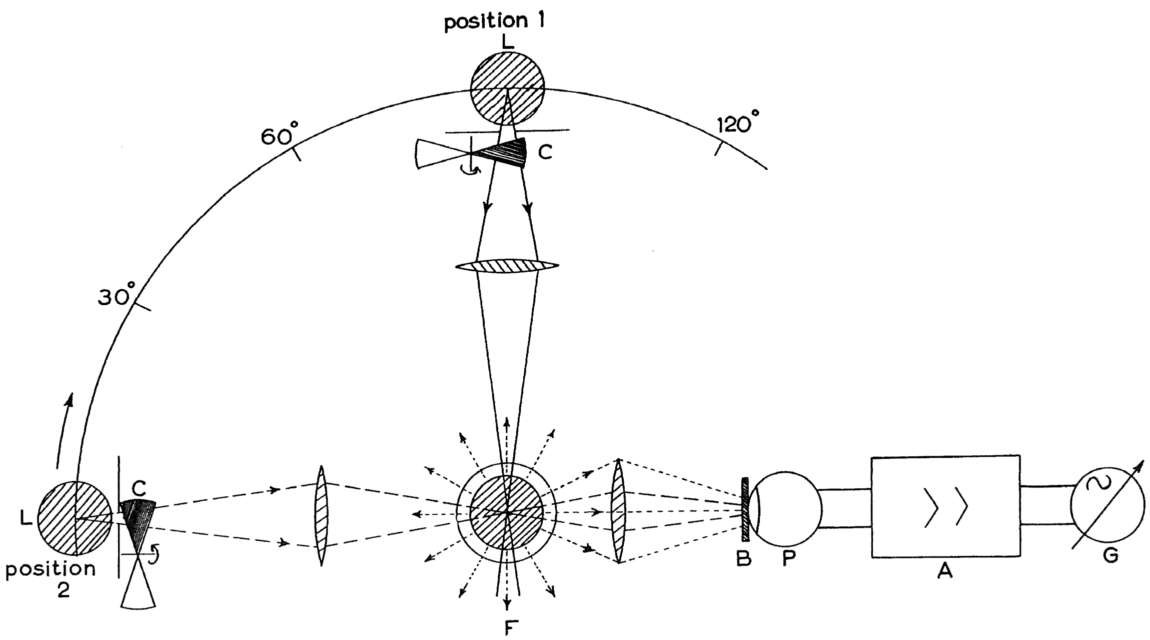

Figure 5. Experimental arrangement for measuring the yield factor of resonance fluorescence. L = Na-discharge lamp; C = periodic light-chopper; F = shielded flame coloured by Na-vapour; B = filter; P = phototube; A = a.c. amplifier; G = synchronous meter. The intensity of the fluorescence radiation is measured with L in position 1. The primary radiation flux absorbed in the flame is measured with L in position 2.

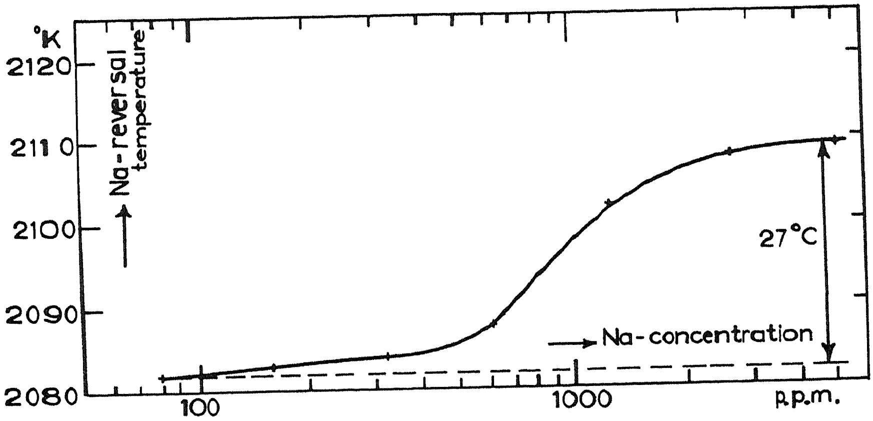

Figure 6. Na-reversal temperature of a shielded, pre-mixed hydrogen-oxygen-argon flame as a function of the Na-concentration in the sprayed solution.

the flame gases can be derived, if one supposes, approximately, that argon has practically no quenching effect. For N_2, CO_2 and H_2O one finds the following quenching cross sections for Na: $\pi\sigma^2 = 20 \times 10^{-16}$, 70×10^{-16} and 7×10^{-16} cm^2, respectively. The values for N_2 and CO_2 appear to exceed noticeably the gas-kinetic cross section, so the exchange of (excitation) energy between sodium atoms and these molecules is an easy process.

It follows that in usual flames with mainly molecular constituents the deviation from thermal radiation, at least for sodium, will be negligible [cf. form. (5.3)]. However, in the hydrogen-argon flame this deviation may be as large as 26 percent, which is equivalent to a decrease in "excitation temperature'' of 41 °C. This has been confirmed by a photoelectric measurement of the Na-reversal temperature in a shielded, pre-mixed H_2 - O_2 - Ar flame as function of Na concentration sprayed into the flame (see Figure 6). The reversal temperature measured with low Na concentration appeared to be 27 °C lower than that with high concentration. It should be noted that at high concentrations the radiation intensity approaches the black-body value closely in the interior part of the flame. At the very flame surface, however, it will never exceed half the black-body value (cf. Section 2).

(ii) *Supra-thermal fluorescent radiation* of metal atoms may be generated when the flame containing metal vapor is irradiated by a strong light source emitting the metal spectrum (cf. above). A hollow-cathode discharge lamp containing the metal wanted, as used in absorption flame photometry, would be suitable for that purpose. The metal atoms in the flame will partly absorb the resonance lines of the incident radiation, and a fraction, p, of the absorbed photons will be re-emitted, if we disregard self-absorption. The fluorescent light is specific for the element tested. Spectral interference from background radiation or neighbouring metal lines can be eliminated by using an a.c. method (cf. above).

A few attempts have been made to try this method. Robinson [cf. 31] found a moderate effect with Mg 2852 Å only, and not with Na or Ni. In our experiment described above we did find fluorescent radiation from Na with the aid of an a.c. measuring device. It should be realized that in our flame with argon gas the fluorescent radiation amounted to but 0.6 percent of the thermal Na radiation. However, with metal lines from higher excitation levels better results should be expected.

For a given flame and metal line the flux, W_f, of the fluorescent radiation received by the detector, at low metal concentration (no self-absorption), is given by

$$W_f = \text{constant} \cdot NBI_p \cdot \Omega_p \cdot (\Omega_f/4\pi) \cdot p. \qquad (5.4)$$

Here N is again the number of metal atoms per unit volume in the flame; $(BI_p\ \Omega_p)$ is the probability per sec that a metal atom in the ground state, exposed to primary radiation with intensity I_p incident under solid angle Ω_p, will absorb a photon; Ω_f is the solid angle under which the flame "sees" the detector.

Since the fluorescence radiation should be observed in a direction outside the solid angle occupied by the incident primary radiation, optimum conditions are obtained when $\Omega_p = \Omega_f = 2\pi$ sterad. It may be interesting now to compare the sensitivity of the fluorescence method and the usual flame absorption method, which have so many features in common. Therefore, we consider the flux, W_a, of the radiation that is absorbed by the metal vapor in the flame (at low metal concentration),

$$W_a = \text{constant} \cdot NBI_p\,\Omega_p \qquad (5.5)$$

with the same constant as in Equation (5.4). We assume that all transmitted radiation is received by the detector. Here optimum conditions occur when $\Omega_p = 2\pi$. The sensitivity of both methods may be compared by considering the ratio $(W_f/W_a)_{opt.}$ under optimum conditions. From Equations (5.4) and (5.5) it follows that $(W_f/W_a)_{opt.} = 1/2\ p$, which equals 0.13 for the Na doublet in the hydrogen-argon flame considered above. It might be interesting to investigate the value of 1/2 p for other metal lines in flames with a noble gas as diluent.

A characteristic difference between the two methods is that with the fluorescence method the detector receives only (non-modulated) weak background radiation from the flame when no metal is present. With the other method, however, the detector then receives the full (modulated) radiation from the hollow-cathode lamp, which should be compensated. This difference may be significant when the detection limit is determined by fluctuations in the compensating device, or by shot noise in the (strong) lamp radiation.

(iii) *Supra-thermal chemiluminescent radiation* of metal atoms occurs when the rate of excitation by chemical reactions *exceeds* the rate of de-activation by the reverse reaction. It should be realized that chemical excitation as such does not necessarily involve supra-thermal chemiluminescence; it may occur only if the chemical reaction is not equilibrated. This condition will be realized when the concentration of the reactants of the excitation reaction exceeds the thermodynamic equilibrium concentration. Since most of the reactants listed in Section 4 are more or less unstable, short-lived radicals, it may be expected that chemiluminescence will be found mainly in the reaction zone, where these radicals are formed in excess, or at a short distance beyond this zone. We shall discuss here briefly only two typical examples of chemiluminescent reactions.

Padley and Sugden[cf. 29] found chemiluminescent radiation at a short distance above the reaction zone with Na, Tl, Fe, etc., in cool hydrogen-air flames, which they explained by reactions of the type (cf. Section 4)

$$H + H + Na \rightarrow H_2 + Na^*.$$

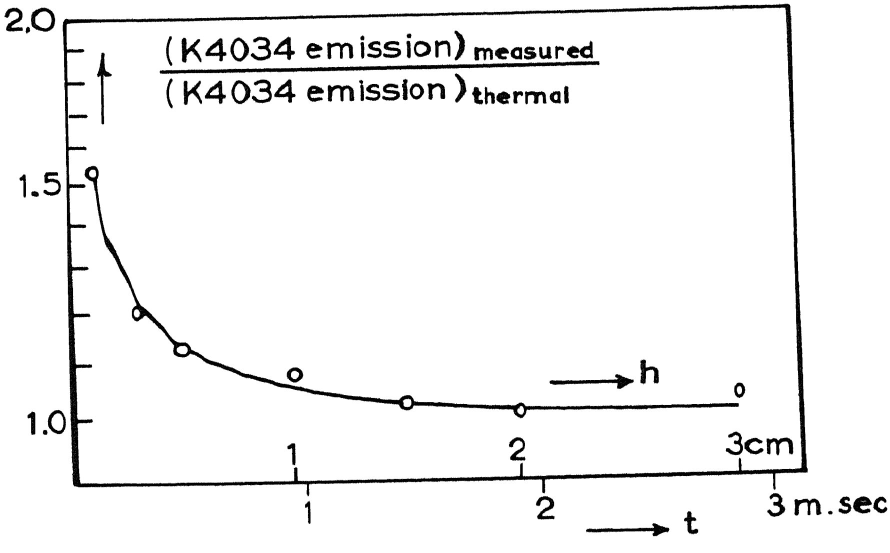

Figure 7. Supra-thermal emission of blue K-doublet in air-acetylene flame is shown as a function of height, h, and time, t.

Hydrogen radicals were found, indeed, in excess above the reaction zone, whereas hydrogen molecules are present, virtually, in equilibrium concentration (cf. Section 3). This excitation reaction has been known for long time and energy surfaces have even been constructed for the H - H - Na complex in its various excitation states [cf. 21]. The chemiluminescent radiation was more pronounced with elements having higher excitation levels. This is clearly due to the masking effect caused by thermal radiation, which will be weaker for elements with higher excitation levels (and in cooler flames). Mr. Zeegers of our laboratory has found similar chemiluminescent radiation also in the hotter acetylene-air flame with the blue K doublet at 4040 Å. In Figure 7 the suprathermal emission of this K doublet is plotted as a function of distance from the reaction zone.

In the explanation of these chemiluminescence effects we might propose the two-step excitation process

$$\left\{\begin{array}{l} H + H + N_2 \rightarrow H_2 + N_2^* \\ N_2^* + Na \rightarrow N_2 + Na^* \end{array}\right.$$

as another possibility besides the one-step process already mentioned. The a priori probabilities of both processes have been compared in Section 4.

Recently Sugden [cf. 35] reported that chemiluminescent Pb emission may also occur when one of the H radicals in the excitation reaction is replaced by a halogen atom, which leads to the formation of halogen acids.

A more powerful and promising method of enhancing the metal emission by making use of the chemiluminescence effect, has recently attracted considerable attention [cf. 9]. It has appeared that adding hydrocarbon compounds to a hydrogen-air flame considerably raises certain u.v. metal lines in the reaction zone. The hydrocarbon compound may be added either by spraying some organic solvent or by additionally supplying acetylene gas. The effect found is restricted to the reaction zone, in distinction from the effects described above. As this topic will be dealt with extensively by more competent authors in the following papers [cf. 10, 14, 18], I shall restrict the discussion here to only a few remarks.

1. Whenever a reaction is proposed to explain these chemiluminescence effects, it should be determined that the excitation rate does, indeed, exceed the de-activation rate of the reverse reaction.

2. Chemiluminescent emission may be enhanced when we replace, e.g., nitrogen by a noble gas as diluent, since noble gases have a smaller quenching effect than molecular gases [cf. 18]. However, if the chemiluminescent reaction proceeds by a two-step process, involving nitrogen as the intermediate molecule, this replacement might not always be advantageous.

3. Let us suppose that the remaining part of the chemical energy that is not consumed in the metal excitation is converted into translational energy of the reaction products including the excited metal atom. The chemiluminescent spectral line will then have an extra Doppler broadening, as was shown in Section 4. This may affect the shape of the curve of growth (working curve), which depends on the Doppler width if self-absorption occurs. It has been suggested by Sternberg and Gilbert [cf. 15, 18] that the chemiluminescent reaction could be of the type $SnO + C \rightarrow Sn^* + CO$. Application of the formula given in Section 4 yields in that case the following results for the ratio of the Doppler width of the chemiluminescent line to the Doppler width in thermal equilibrium: Sn (2863 Å) : 1.3 x; Bi (3068 Å) : 1.5 x; Sb (2311 Å) : 1.5 x; Cr (2366 Å) : 1.7 x. The calculated values suggest that one should be careful in interpreting the working curve of chemiluminescent resonance lines. Of course, the derived results hold only if the excited metal atom emits a photon before colliding with other molecules.

4. If the chemiluminescent reaction proceeded as proposed above sub 3, it might give emission flame photometry an advantage over absorption flame photometry in the detection of metals that are present in the flame only as oxides.

I may conclude therefore, more generally, by expressing the hope that the exploration of the possibilities of the various excitation mechanisms in the flame will support emission flame photometry in its rivalry with absorption flame photometry. It is not that we envy the latter method its undeniable successes, but honest competition between these methods will yield maximum profit for the analyst.

APPENDIX: CALCULATION OF DOPPLER-WIDTH OF CHEMILUMINESCENT SPECTRAL LINES

Assume there are two reaction products, an excited metal atom with mass = m_1, and a flame molecule with mass = m_2. In the coordinate system of the center of gravity they have velocities v_1' and v_2' respectively. We have from the conservation laws of linear momentum and energy

$$m_1 v_1' = m_2 v_2' \text{ and } \frac{1}{2} m_1 v_1'^2 + \frac{1}{2} m_2 v_2'^2 = Q + q_o$$

with Q = energy released by the reaction and available for translational motion; q_o = total translational energy of the reactants (before the reaction) considered in the coordinate system of the center of gravity. Combining both equations one finds

$$\frac{1}{2}\, m_1\, v_1'^2 = (Q + q_o)\ \delta/(1 + \delta) \quad \text{with} \quad \delta \equiv m_2/m_1 \ .$$

Or, after averaging over a large number of similar reactions

$$<\frac{1}{2}\, m_1 v_1'^2> = (Q + Q_o)\ \delta/(1 + \delta)$$

with $Q_o = <q_o> = 3/2\ kT$, according to the equipartition law. Considering now the velocity, v_1, of mass m_1 in a coordinate system at rest, we have

$$<v_1^2> = <v_1'^2> + <v_c^2>$$

with v_c = velocity of center of gravity.

It follows that

$$<\frac{1}{2}\, m_1\, v_1^2> = <\frac{1}{2}\, m_1\, v_1'^2> + <\frac{1}{2}\, m_1\, v_c^2> = (Q + Q_o)\ \delta/(1 + \delta) +$$

$$+\ Q_o/(1 + \delta) = Q_o + Q \cdot \delta/(1 + \delta)\ ,$$

since $<1/2\ (m_1 + m_2)v_c^2> = Q_o$, again according to the equipartition law.

The Doppler width of the emitted spectral line is proportional to $(<v_1^2>)^{1/2}$. Consequently the ratio of the Doppler width of the chemiluminescent spectral line to the Doppler width of the same line under thermal equilibrium conditions is equal to

$$\left(1 + \frac{Q}{Q_o} \cdot \frac{\delta}{1 + \delta}\right)^{1/2} ,$$

since in thermal equilibrium $<1/2\ m_1 v_1^2> = Q_o$.

SUMMARY

A discussion is given of the processes that lead to excitation of metal atoms in conventional "chemical" flames. First the case of thermodynamic equilibrium is considered, and the influence of flame temperature on the excitation of metal spectra is pointed out. The concept of "thermal radiation" is critically examined. Possible deviations from flame equilibrium caused

by relaxation effects in the equipartition of energy and by slow recombination of free radicals are treated next. This discussion is followed by an exposition of the specific mechanisms through which metal atoms may be excited and de-activated respectively. Finally three types of non-thermal radiation of metal spectra, viz., infra-thermal emission owing to radiative disequilibrium, supra-thermal fluorescent radiation and supra-thermal chemiluminescent radiation, are considered. In particular, attention is paid to the applicability of the fluorescent method in flame photometry.

REFERENCES

1. Boers, A. L., Alkemade, C. Th. J., and Smit, J. A., Physica, 22, 358 (1956).
2. Broida, H. P., and Carrington, T., J. Chem. Phys., 23, 2202 (1955).
3. Broida, H. P., and Schuler, K. E., J. Chem. Phys., 27, 933 (1957).
4. Broida, H. P., and Schuler, K. E., Rev. Inst. Franc. Pétrole et Ann. Combustibles Liquides, 13, 620 (1958).
5. Buriel-Marti, F., and Ramírez-Muñoz, J., "Flame Photometry," Elsevier, New York, 1957.
6. Calcote, H. F., 8th Symposium (International) on Combustion, Baltimore, 1960.
7. Cottrell, T. L., and McCoubrey, J. C., "Molecular Energy Transfer in Gases," Butterworths, London, 1961.
8. Dean, J. A., "Flame Photometry," McGraw-Hill, New York, 1960.
9. Dean, J. A., Record of Chemical Progress, 22, 179 (1961).
10. Fassel, V. A., Curry, R. H., Myers, R. B., and Kniseley, R. N., Intern. Conference on Spectroscopy, 1962.
11. Gaydon, A. G. and Wolfhard, H. G., "Flames," Chapman and Hall, London, 1960.
12. Gaydon, A. G., "The Spectroscopy of Flames," Chapman and Hall, London, 1957.
13. Gaydon, A. G., and Hurle, I. R., 8th Symposium (International) on Combustion, Baltimore, 1960.
14. Gibson, J. H., Grossman, W., and Cooke, W. D., Intern. Conference on Spectroscopy, 1962.
15. Gilbert, P. T., Eastern Analytical Symposium, New York, 1960.
16. Gilbert, P. T., Symposium on Spectroscopy, Spec. Techn. Publ. No. 269, Am. Soc. Testing Materials, Philadelphia, 1960.

17. Gilbert, P. T., 13th Pittsburgh Conference, 1962.
18. Gilbert, P. T., Intern. Conference on Spectroscopy, 1962.
19. Herrmann, R., and Alkemade, C. Th. J., "Flammenphotometrie," Springer-Verlag, Berlin, 1960.
20. Laidler, K. J., "The Chemical Kinetics of Excited States," Clarendon Press, Oxford, 1955.
21. Magee, J. L., and Ri, T., J. Chem. Phys., 9, 638 (1941).
22. Margoshes, M., Symposium on Spectroscopic Excitation, Special Techn. Publ. No. 259, Am. Soc. Testing Materials, Philadelphia, 1959.
23. Mavrodineanu, R., and Boiteux, H., "L'analyse spectrale quantitative par la flamme," Masson & Cie, Paris, 1954.
24. Mavrodineanu, R., Colloquium Spectroscopicum Intern. VIII, Luzern, 1959.
25. Mavrodineanu, R., Spectrochim. Acta, 17, 1016 (1961).
26. Mitchell, A. C. G., and Zemansky, M. W., "Resonance Radiation and Excited Atoms," University Press, Cambridge, 1961.
27. Nikitin, E. E., 8th Symposium (International) on Combustion, Baltimore, 1960.
28. Padley, P. J., and Sugden, T. M., Proc. Roy. Soc. (London), A 248, 248 (1958).
29. Padley, P. J. and Sugden, T. M., 7th Symposium (International) on Combustion, London-Oxford, 1958.
30. Padley, P. J. and Sugden, T. M., 8th Symposium (International) on Combustion, Baltimore, 1960.
31. Robinson, J. W., Anal. Chim. Acta, 24, 254 (1961).
32. Schuhknecht, W., "Die Flammenspektralanalyse," F. Enke, Stuttgart, 1961.
33. Schuler, K., 7th Symposium (International) on Combustion, London-Oxford, 1958.
34. Snelleman, W., and Smit, J. A., Physica 21, 946 (1955).
35. Sugden, T. M., Summer School, Cambridge, 1961.
36. Unsöld, A., "Physik der Sternatmosphären," Springer-Verlag, Berlin, 1955.
37. Willey, E. J. B., "Collisions of the Second Kind," London, 1937.
38. Windsor, M. W., 7th Symposium (International) on Combustion, London-Oxford, 1958.

CHEMILUMINISCENT FLAME SPECTROPHOTOMETRY

Paul T. Gilbert, Jr.
Beckman Instruments, Inc.
Fullerton, California, U.S.A.

INTRODUCTION

The present study commenced with the accidental observation that tin in isopropanol, sprayed into an air-hydrogen atomizer-burner flame, emits a rich line spectrum of surprising intensity, extending at least to 2100 A. Some of the lines are 1000 times as intense as they would be if they were excited thermally and if the tin were present entirely as atomic vapor; but if the tin and its oxide, SnO, were in chemical equilibrium, only 0.01% of the SnO would be dissociated. The anomaly thus runs to 7 orders of magnitude. Clearly it is a very helpful anomaly from the viewpoint of the spectrochemist.

Several other elements behave similarly. Only a start has been made in exploring applications of the phenomenon. It begins to look as if chemiluminescence and the associated phenomenon of dissociation of stable oxides in the incandescent acetylene flame will make possible the determination of nearly all the chemical elements by flame spectrophotometry with high specificity and good sensitivity. The field now offers opportunity for a great range of spectroanalytical development.

Earlier Work

Observations of probably chemiluminescent emission in the reaction zones of various flames have been recorded by Lundegårdh for As, Sb, Bi, Sn, Cd, Au, and Pt [52,53], Alekseeva and Mandel'shtam for As, Bi, Sn, and Cd [1,2], Gaydon and Wolfhard for Fe [33-35; 38, p. 233] and Pb [29; 38, Plate 17], Broida for Hg [8], Broida and Shuler for Fe [9,10], Egerton and Rudrakanchana for Zn, Cd, and Hg [23], Mavrodineanu for Mg, Zn, Sn, Mo, Fe, and Cr [54-56], Padley and Sugden for Na [59,60], King for

Fe [49], and Bugrim et al. for Mg [14]. Gaydon observed it also in flames of organic compounds supported by free atoms or radicals [31,36,37], and he discussed the phenomenon in his book [32, pp. 139, 200].

In 1952 I examined the emission of Zn, Cd, Hg, and Bi in the inner cone of an oxyacetylene flame from an atomizer-burner. Only Hg 2537 showed a useful enhancement, while Bi 3068 appeared in absorption against the OH bands [41-43,47].

The only analytical application of chemiluminescent flame emission reported up to the start of the present work is that of Honma and Smith [48], who determined nitrogen by the CN emission from the inner cone of an air-gas flame burning in a Smithells flame separator.

The related phenomenon of enhancement in a fuel-rich, highly reducing flame was first put to use by Knutson for Mg [50]. Robinson [62] noticed a similar effect with Fe in the oxycyanogen flame. In absorption flame photometry the corresponding effect was first observed by Allan for Mg [4]. It was reported by David for Mo [19,20], Gatehouse and Willis for Mo and Sn [28], and Allan for Mo, Sn, Cr, and Ru [5].

Current Work

Buell's early data on Mo, N, and Zn were included in our tables of flame spectra [42,43,47]. Working chiefly with naphtha solutions and oxyhydrogen, he has studied chemiluminescence of Mg, Ca, Sr, Ba, Ti, V, Cr, Mn, Fe, Co, Ni, Cu, Ag, Cd, B, Al, Si, Sn, Pb, and P. A few of these data appear in his recent paper [12]; the bulk of his work on chemiluminescence [13] may be published soon. The thesis by Carnes [16] reports useful chemiluminescence of Zn, Cd, Hg, As, Sb, Bi, Sn, and Pt in hexone solution in the inner cone of oxyacetylene. The work is being published by Dean and Carnes [17,21]. The paper by Gibson, Grossman, and Cooke [40], an extension of earlier work by Gibson and Cooke [39], is a study of excitation in atomizer-burner flames, confirming the chemiluminescence of tin.

The first practical application of the present work has been published by Schmidt [63]. He determined tin in plastic stabilizers, using toluene-butanol solutions and air-hydrogen. The line at 2706 Å gives a straight working curve, with negligible background and no interferences.

Fassel, Curry, Myers, and Kniseley [25] report extraordinary enhancements of the line spectra of Ti, Th, V, Nb, Ta, Mo, W, U, Re, and the rare earths in the fuel-rich oxyacetylene flame with ethanol as solvent. The rare-earth data are being published by Fassel, Curry and Kniseley [24]. According to Curry [18], the thesis of R. B. Myers will report the flame spectra of the other elements, including Ir. It is curious that the enhancement in incandescent flames has been discovered independently at least 5 times—by Knutson for Mg [50], Allan for Mg [4], David for Mo [19], Curry for Lu [18], and the writer for Si.

APPARATUS

The apparatus included a Beckman DU spectrophotometer with flame attachment, uncoated mirror for the burner housing (the standard mirror is now coated with hard magnesium fluoride and is usable throughout the entire wavelength range), 1P28 photomultiplier, electronic power supply (Cat. No. 23700), wavelength drive, energy recording attachment, and Bristol 10-mv., 0.4-sec. strip-chart recorder. A special gas handling system provided complete flexibility in supplying gas mixtures to the atomizer-burner. For most of the observations with air-hydrogen a standard-bore hydrogen atomizer-burner (Cat. No. 4020) was used; other burners with a wide range of dimensions were also tested.

Burner Sheath

For producing some of the spectra, the burner sheath recently developed [6,44] was used. With the air-hydrogen flame, to which it supplied auxiliary air, the principal function of the sheath was to stabilize the flame when high concentrations of alcohol were used. With the other flames the sheath supplied the same oxidant mixture as was fed to the atomizer. Sheathed oxyacetylene proved to be extraordinarily steady. Even the fuel-rich flame, which is less steady than the normal oxyacetylene flame, showed peak-to-peak flicker with the sheath as low as 0.3% at a time constant below 0.2 sec. A 4020 burner with narrow fuel port (0.25 mm.) is required for best performance with sheathed oxyacetylene.

Sample Pump

The burner housing was equipped with a special gas-piston sample pump [41, p. 88]. This pump permits control of sample flow independently of atomizer pressure. For most of the work, however, the sample was allowed to spray without constraint, since trials with the pump showed that the standard burner provided a nearly optimal flow rate without assistance.

The Flame

The reaction zone of the flame from an atomizer-burner is rather diffuse. In normal oxyacetylene it is fairly sharply localized just above the burner tip, but in air-hydrogen it extends over a height of 2 cm. or more. Since the gases are not premixed, they can react only as they diffuse into each other. Emerging at transonic speeds and disrupting the liquid as it goes, the atomizer gas generates extreme turbulence and at the same time entrains copious amounts of the ambient air. The entrained air penetrates to the core of the flame about 2 cm. above the burner, unless the sheath is present. Consequently, the chemiluminescence, which normally occurs only in the thin reaction zone of a laminar, premixed flame, is spread over a large region of the air-hydrogen flame from an atomizer-burner. In the presence of a carbon-hydrogen compound the reaction zone is made visible by the light blue color due to CH and C_2 bands. The zone gradually shrinks as oxygen is added to the air.

The best air pressure was usually about 20 p.s.i., and the hydrogen flow was optimized for each element.

Entrance Optics

The manner of viewing the flame is governed by the diagonal slit mirror of the spectrophotometer and concave mirror of the burner housing. If the entrance beam is made to bypass the flame [6], so that the spectrophotometer views the flame only via the concave mirror, which selects an area about 6 mm. high and 2 mm. wide, slightly higher ratios of net line emission to background can be achieved. This is advantageous with rich oxyacetylene, since its great brightness permits use of the limiting resolution of the monochromator. With air-hydrogen, however, the wider slit required for equal shot-noise contribution outweighs the gain in line-to-background ratio realized with the bypassed beam.

THE CHEMILUMINESCENT SPECTRA

Air-Hydrogen

The chemiluminescent spectra observed in aqueous-isopropanol solutions in the air-hydrogen flame are listed in Tables 1 and 2. The relative intensities in Table 1 represent the net line emission above background, and are so defined that the intensity equals 1 when 1 mg./l. of element gives a signal equal to that from a continuum of 4×10^{-13} w./cm^2 sr.mμ (sr. = steradian) at 450 mμ, as seen by the DU spectrophotometer with a spectral slit width equivalent to 0.03 mm. (which is essentially the limiting resolution of the instrument) for both line and continuum. The band intensities in Table 2 are on an arbitrary scale and are intercomparable for a slit of 0.14 mm., but should not be compared with the line intensities of Table 1.

Table 1

Relative Intensities of Lines in Chemiluminescent Spectra in Air-Hydrogen with Alcohol

CHROMIUM

2364.7 2365.9 2366.8	2

IRON

2166.8	1
2178.1	1
2186.5	1
2191.8	0.4
2200.4	1
2292.5	1
2297.8	3
2299.2	1
2373.6	1
2457.6	2
2462.6	8
2472.9	11
2479.8	8
2483.3	60
2488.1	40
2490.6	40
2496.5	1
2501.1	5
2510.8	9
2518.1	9
2522.8	35
2524.3	5
2527.4	20
2529.1	8
2535.6	5
2541.0	7
2546.0	6
2549.6	6
2584.5	4
2719.0	35
2720.9	20
2723.6	7
2733.6	7
2737.3	7
2742.4	12
2750.1	7
2756.3	3
2767.5	4
2788.1	12
2953.9	10
2966.9	35
2973.2	20
2981.4	15
2983.6	25
2994.4	20
3001.0	60

NICKEL

2290.0	9
2300.8	3
2311.0	35
2312.3	25
2314.0	27
2317.2	15
2320.0	45
2321.4	25
2325.8	20
2330.0	8
2337.5	6
2345.5	15
2360.6	1
2362.1	1
2401.8	1
2419.3	1
2992.6	12

COPPER

2492.1	20

GERMANIUM

2498.0	0.5
2592.5	7
2651.2 2651.6	30
2691.3	7
2709.6	15
2754.6	15
3039.1	10
3269.5	5

TIN

2113.9	0.5
2148.7	0.5
2151.4	0.5
2194.5	2
2199.3	5
2209.7	6
2231.7	0.5
2246.1	35
2268.9	20
2286.7	4
2317.2	4
2334.8	20
2354.8	100
2380.7	2
2408.2	1
2421.7	15
2429.5	120
2483.4	13
2495.7	4
2546.6	70
2571.6	10
2594.4	5
2661.2	25
2706.5	350
2779.8	8
2840.0	1000
2850.6	25
2863.3	500
3009.1	350
3034.1	800
3175.0	1200
3262.3	750
3330.6	100
3801.0	200
4524.7	40

LEAD

2170.0	4
2203.5(a)	0.01
2237.4	0.3
2246.9	2
2332.4	0.2
2388.8	0.1
2393.8	4
2399.6	0.05
2401.9	3
2411.7	0.6
2443.8	1.7
2446.2	3
2476.4	9
2577.3	7
2613.7 2614.2	80

Table 1—Continued

LEAD—Cont.	
2663.2	25
2802.0	90
2823.2	10
2833.1	35
2873.3	20
3572.7	25
3639.6	110
3683.5	250
3739.9	25
4057.8	350

(a)Due to Pb II.

ARSENIC	
2288.1	17
2349.8	30
2381.2	2.5
2437.2	see AsO
2456.5	6
2492.9	6
2780.2	5

ANTIMONY	
2068.4	8
2127.5	1
2139.8	2
2145.0	1.5
2175.9	80
2179.3	6
2208.5	2
2220.8	2
2224.9	2
2311.5	200
2445.5	8
2528.5	180
2598.1	280
2769.9	40

BISMUTH	
2061.7	0.8
2110.3	0.6
2228.3	17
2230.6	30
2276.6	7
2400.9	0.6
2524.5	0.8
2627.9	(8)(a)
2898.0	(35)(a)
3067.7	400 (a)

(a)On OH bands.

TELLURIUM	
2383.2	(5)
2385.8	(7)

Table 2

Relative Intensities of Bands in Chemiluminescent Spectra in Air-Hydrogen with Alcohol

NITROGEN	
2149.1	0.5
2154.9	0.4
2239.4	0.3
2245.4	0.3
2262.8	1.5
2269.4	0.9
2363.3	3.0
2370.2	1.5
2440.0	1.0
2447.0	1.2
2471.1	3.0
2478.7	1.5
2550.0	1.2
2559.0	1.2
2587.5	2.0
2595.7	1.2
2671.4[a]	0.8
2680.0[a]	0.6
2713.2[a]	1.0
2722.2[a]	0.5

PHOSPHORUS	
2288.2	4
2294.9	8
2301.7	8
2306.9	8
2313.7	4
2320.6	4
2367.3	30
2375.2	50
2379.9	40
2383.5	50
2387.9	35
2396.3	30
2454.6	70
2464.2	140
2477.9	100
2518.7	50
2529.4	70
2540.4	80
2555.0	50
2595.7	35

ARSENIC	
2438	10[b]
2504	20
2570	20

[a] Intensities for these last four bands are estimated from earlier data on the oxycyanogen flame.

[b] Probably with some contribution from the As line 2437.2. These bands are double, the heads spaced about 1.2 Å apart.

Rich Oxyacetylene

The fuel-rich, incandescent oxyacetylene flame obtained with a sheathed atomizer-burner is of dazzling brilliance. This flame excites certain spectra that are absent from the normal (blue) flame. These spectra, which are emitted from an extended area of the flame, are due largely to dissociation of stable gaseous monoxides, but chemiluminescence may be present as well. The very intense background is strongest in the visible, dropping off rapidly through the ultraviolet. Table 3 lists the spectra observed in this flame, on the same intensity scale as in Table 1.

Table 3

Relative Intensities in Sheathed, Rich Oxyacetylene

BERYLLIUM

λ	Water	Methanol
2348.6	11,000	55,000
2494.7	90	
2650.6	290	
3321.3	300	

VANADIUM

λ	Water	Methanol (50%)
3183.4 3184.0 3185.4	4000	7500

RHENIUM

λ	Water	Methanol (50%)
3451.8	170	500
3460.5	600	1900
3464.7	320	1000

CADMIUM

λ	Water
2288.0	4000

MERCURY

λ	Water
2536.5	250

SILICON (Si I Lines)

λ	Water	Methanol
2506.9	60	300
2514.3	40	200
2516.1	160	800
2519.2	35	170
2524.1	50	250
2528.5	60	300

SILICON (SiO Bands)

λ	80% Methanol
2344.3	11
2413.8	14
2481.9	6
2486.8	15

TIN

λ	Water	Methanol
2246.1		500
2268.9		500
2354.8	700	1200
2429.5		1900
2546.6		1000
2706.5		3700

Other Flames

Tin was studied in air-hydrogen with various additives, and lead was observed in oxyhydrogen with gasoline. Both metals were observed in the inner cone of a premixed air-methanol flame produced by a burner built by Edmund Buzza of Beckman Instruments. In all of these flames the relative intensities within each spectrum were the same as in Table 1. The air-oxygen-hydrogen-acetylene flame (in the regular atomizer-burner) excited nitrogen (NO) well; it also excited silicon but not nearly as well as the rich oxyacetylene flame. The air-oxyacetylene flame proved best for sulfur; the data for the CS bands, including vibrational transitions, are given in Table 4, with the same intensity scale as in Table 1.

THE INDIVIDUAL ELEMENTS

Flame spectrograms of Be, Fe, Ni, Si, Ge, Sn, Pb, N, P, As, Sb, Bi, and S, obtained in this work, are to be published in the atlas accompanying the translation of Herrmann and Alkemade's book [47], and spectrograms of Sn and P appear in [44]. A few are selected for illustration here (Figures 1, 2, 3). Supplementary information on the elements is given below.

Beryllium

Although the resonance line 2349 Å. is quite sensitive in rich oxyacetylene, it has the drawback of strong self-absorption

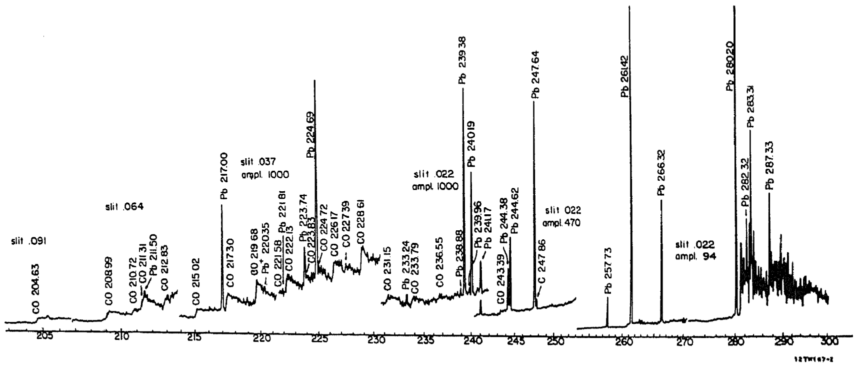

Figure 1. Spectrogram of lead, 1100 mg/l in gasoline, in sheathed oxyhydrogen flame. Slit widths and relative amplifications shown on sections of curve. In this and Figures 2 and 3, the wavelength scale represents zero intensity. Wavelengths in mμ.

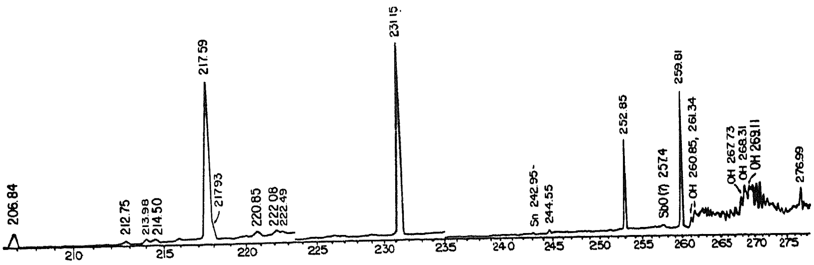

Figure 2. Antimony, 600 mg/l in 40% isopropanol, in air-hydrogen. Slits 0.26 mm. (left), 0.14 mm. (center), 0.08 mm. (right).

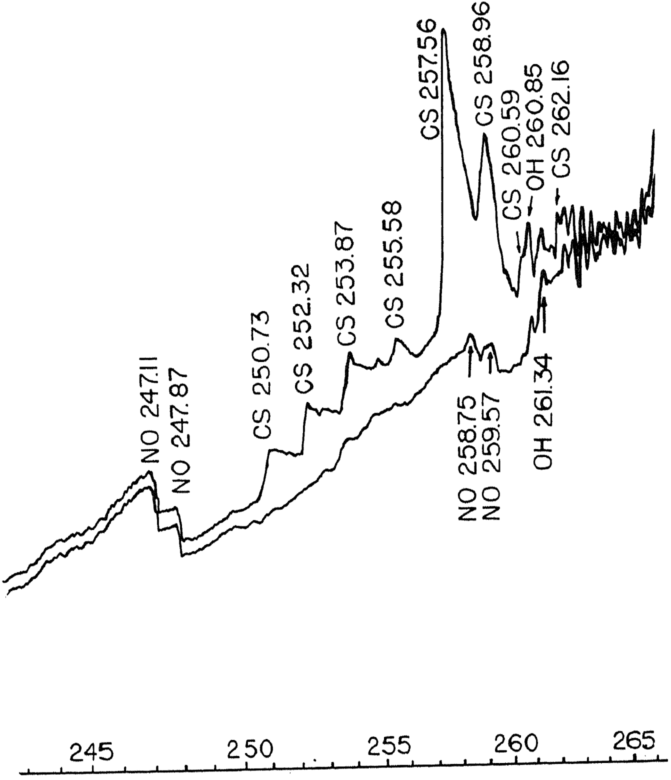

Figure 3. Sulfur, 5000 mg/l in 50% methanol, present as sulfuric acid, in sheathed air-oxygen-acetylene flame. Slit 0.05 mm. Blank spectrogram superposed.

curvature (Figure 4). Addition of either hydrogen or air to the optimized flame weakens the line. It is undetectable in normal oxyacetylene and cooler flames, although it is strong in oxy-cyanogen [41]. Methanol enhances the line, up to a factor of

Table 4

Spectrum of Sulfur (CS Bands from Sulfuric Acid) in Air-Oxygen-Acetylene Flame

λ	v', v''	Water	Methanol
2507.3	1, 0	0.7	1.6
2511.2	6, 4	0.6	1.3
2523.2	2, 1	0.9	2.0
2530.0	7, 5	0.8	1.7
2538.7	3, 2	0.9	2.1
2549.5[a]	8, 6	0.7	1.4
2555.8	4, 3	0.8	1.7
2572.7	5, 4	0.7	1.3
2575.6	0, 0	3.5	8.5
2589.6	1, 1	2.3	5.5
2605.9	2, 2	1.1	
2621.6	3, 3	0.7	
2662.6	0, 1	0.7	
2677.0	1, 2	0.9	
2693.2	2, 3	0.9	

[a] Wavelength measured from DU spectrogram.

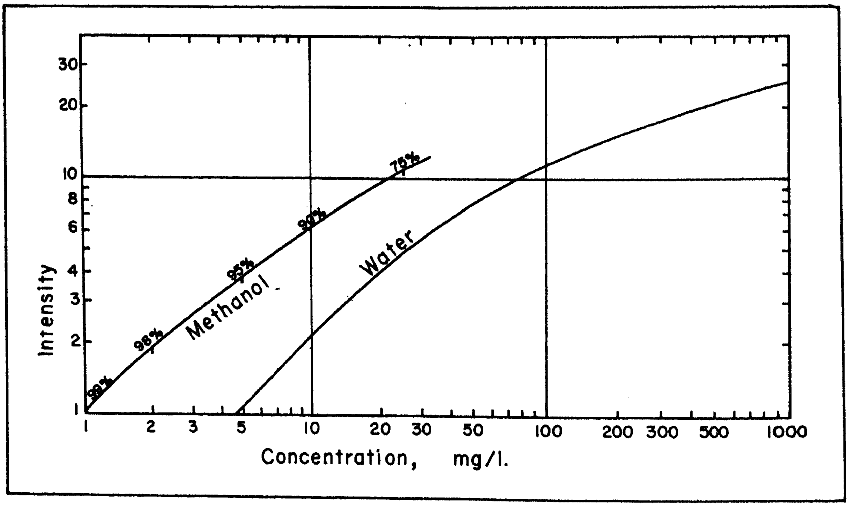

Figure 4. Working curves for beryllium at 2349 Å in the sheathed, incandescent oxyacetylene flame, in water and methanol-water solvents; concentration of methanol varies along curve as shown.

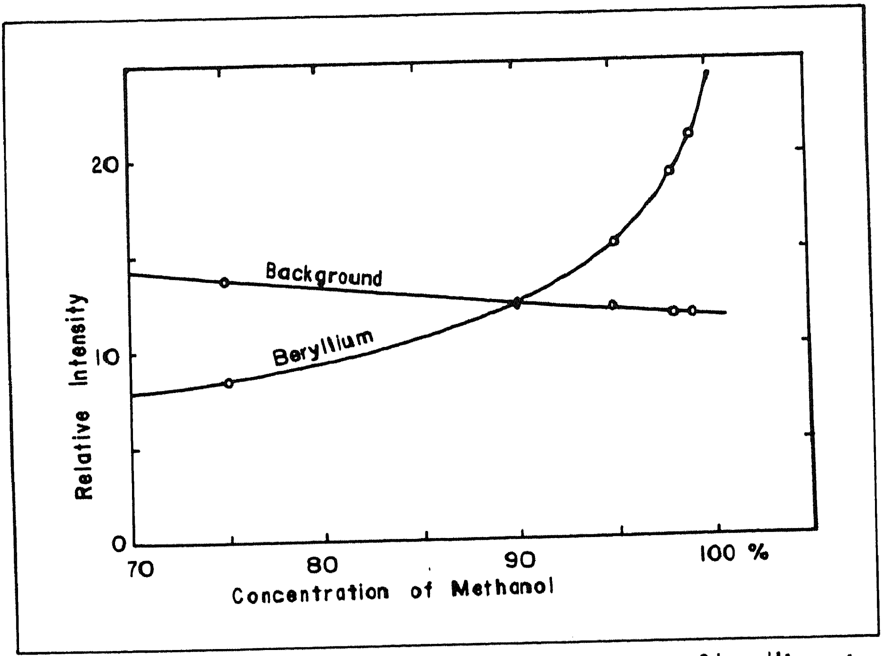

Figure 5. Effect of methanol concentration on emission of beryllium at 2349 Å and on background in sheathed, incandescent oxyacetylene.

about 4 (Figure 5). In a detection limit test for beryllium in methanol (cf. Table 6), the standard error of the mean was 0.024 mg./l.

Vanadium

Since the dissociation energy of VO is 6.4 e.v. [7], only oxy-cyanogen is hot enough to yield a vanadium line spectrum by thermal dissociation [41]. However, air-hydrogen with alcoholic vanadium emits a weak line spectrum (3703.6, 3704.7, 3855.8, 3864.9, 4111.8, 4379.2, 4408.5 Å.). The lines are of low excitation energy and not necessarily chemiluminescent, but they show that some atomic V vapor is generated in the reaction zone. The strong continuum suggests that the vanadium is present largely as condensed-phase oxide aerosol and that the chief impediment to better emission in air-hydrogen is the involatility of the lower oxides of vanadium. Rich oxyacetylene provides fairly complete vaporization, but the strongest emission (the multiplet at 3184 Å.) lies in a region of intense background continuum and strong OH emission; the background could be attenuated with higher spectroscopic resolution. Methanol (50%) doubles the intensity. Hydrogen weakens the 3184 Å. line, and it disappears if the acetylene flow is reduced.

Table 5

Detection Limits for Best Lines and Bands in Chemiluminescent Flames, and Comparisons with Other Flames, for DU with 1P28

Element	Wavelength	Character	Flame, Solvent, and Detection Limit (mg./l.)			
Antimony	2175.9	p	AH,P 0.6			
	2311.5	p	0.4	AH 150		
	2528.5	a	1.2	1000		
	2598.1	f	1.4	400		
Arsenic	2288.1	a	AH,P 4			
	2349.8	a	2.5			
	2492.9	a	AH,P$_{50}$ 15			
	2504	dv	15			
Beryllium	2348.6	p	OAz,M 0.1	OAz 0.4		
Bismuth	2230	dpf	AH,P 1.5			
	2276.6	f	30			
	3067.7	p	AH,P$_{85}$ 50	AH 50	OH 600	OAi 1000$^{(a)}$
	4722.6	a	(b)	20	40	OA 200
Cadmium	2288.0	p	AH,P 0.3	OAz 0.8	AH 50	OH,P$_{50}$ 0.6
	3261.1	f	1.8	OH 5	0.5	OH,Ac 2$^{(f)}$
Chromium	2366	tp	AH,P$_{75}$ 40			
Copper	2492.1	p	AH,P$_{75}$ 7			
Germanium	2592.5	p	AH,P 14	OAi,P$_{50}$ 400	OH,P$_{50}$ 400	
	2651.4	dp	5	200	300	OH 1000
	2709.6	p	25	500		
	2754.6	p	13	OAi 1300		
Iron	2483.3	p	AH,P$_{75}$ 3			
	2488.1	p	4			
	2490.6	p	4			
	2522.8	p	5			
Lead	2170.0	p	AH,P 7	OHi,G 5		
	2476.4	a	AH,M 9	4		
	2614	da	2.5	0.9		
	2663.2	a	10	3		
	2802.0	a	2.5	1.1		
	2833.1	p	10	OH 25	OA,G 2.5	
	3639.6	a	AH,P 12	2	AH 7	OH,G 1.5
	3683.5	a	5	1	3	0.7
	4057.8	a	4	1	3	0.7

Table 5—Continued

Element	Wavelength	Character	Flame, Solvent, and Detection Limit (mg./l.)				
Mercury	2536.5	f	AH,P 4	OAi 8	OAz 40	AH 6	OH,Ac 6
Molybdenum	3798.3	p	OHi,N 1(c)	OA,H$_{50}$Ac$_{20}$P$_{20}$ 0.5			
	3864.1	p	1	0.5			
	3903.0	p	2	0.5			
Nickel	2290.0	p	AH,P$_{75}$ 8				
	2311.0	p	2.5				
	2312.3	p	3.5				
	2314.0	p	3				
	2317.2	p	7				
	2320.0	p	2				
	2321.4	p	4				
	2325.8	p	4				
	2345.5	p	6				
Nitrogen	2149	dv	AH,P 25				
	2263	dv	25	AOHA 25			
	2363	dv	20	14			
	2471	dv	50	40			
	3851 3855	v	OHi,N 60(c)				
Phosphorus	2375	dvb	AH,P 1.3	AH 25			
	2383	dvb	1.2	25			
	2396	dv	2.2	45			
	2464	dv	1.0	20	AHA 8		
	2478	dv	1.3	25	10		
	2529	dvb	2.5	50			
	2540	dv	4	80			
Rhenium	3460.5	p	OAz,M$_{50}$ 120	OAz 300			
Silicon	2344	r	AOHA 300				
	2487	r	1000	OAz,M$_{80}$ 55			
	2506.9	p	1100	OAz,M 20	OAz 60		
	2516.1	p	400	7	20		
	2524.1	p	1500	22	70		
	2528.5	p	1300	20	70		
Sulfur	2576	r	AOA,M 25	AOA 70	AOHA 500		
	2590	r	40	110	700		
Tellurium	2383.2 2385.8	a	AH,P 10	AH 1000			

Table 5—Continued

Element	Wavelength	Character	Flame, Solvent, and Detection Limit (mg./l.)				
Tin	2246.1	p	AH,P 1.3	OAz,M$_{80}$ 7	OHi,P 17		
	2354.8	p	AH,M 0.5	4	7	OAz 8	
	2429.5(g)	a	0.5	4	7	7	
	2706.5	p	0.6	OAi 6(d)	AH 120	OH 800	OAz,M 6
	2840.0	a	0.8	50	120	(700)	
	2863.3	p	1.0	60	90	600	
	3009.1	p	1.2	30	50	250	
	3034.1	p	0.6	25	25	200	OHi,N 1(c)
	3175.0	a	AH,P 1.5	80	80		
	3262.3	a	1	25	25(e)		
	3330.6	f	6	25			
	3801.0	f	3.5	30	4(e)		
Vanadium	3184	tp	OAz,M$_{50}$ 25	OAz 40			
Zinc	2138.6	p	AH,P$_{50}$ 60	AH 250	OH 160	OH,Ac 10(f)	
	4810.5	a	OHi,N 16(c)				

Abbreviations: AH = air-hydrogen, OH = oxyhydrogen, OA = oxyacetylene, AHA = air-hydrogen-acetylene, AOA = air-oxyacetylene, AOHA = air-oxygen-hydrogen-acetylene, OHA = oxyhydrogen-acetylene.

Ac = acetone, G = gasoline, H = hexone, M = methanol, N = naphtha, P = isopropanol; if solvent is not named, it is water.

Subscript numbers denote percentage concentration of solvent.

a = arc line (not resonance), b = band, d = double, f = intercombination line, i = inner cone, p = resonance line, r = head of band degraded toward longer wavelength, t = triplet, v = head of band degraded toward shorter wavelength, z = fuel-rich, sheathed.

Notes:
(a) Appears in absorption against a brighter OH band.
(b) Obscured by C_2 band.
(c) Data from B. E. Buell.
(d) Estimated from spectrogram in [56].
(e) Line superposed on SnO band.
(f) Observation by H. Watanabe, Beckman Instruments, Inc.
(g) Additional data: AHA 1.5; OHA 1.7.

Molybdenum

Although it yields only a continuum in conventional flames, molybdenum emits its resonance spectrum in oxycyanogen [41], in the reaction zone of air-acetylene [56], and in oxyhydrogen with naphtha [11,43]. Acetone and an acetone-hexone-isopropanol mixture were found inferior to naphtha in eliciting the Mo spectrum in oxyhydrogen; it occurred low in the flame. Oxyacetylene was better; with isopropanol the Mo was excited in the reaction zone, but with the acetone-hexone-isopropanol mixture in the

Table 6

Detection Limit Tests. (Flame and Solvent Indicated as in Table 5)

Element	Wave-length Å.	Concen-tration mg./l.	Slit mm.	Standard Error mg./l.	Defined Det. Lim. mg./l.	Remarks
Cadmium (AH,P)	2288	1.0	0.6	0.16	0.3	
		1.0	1.0	0.06	0.25	
		1.0	1.0	0.16	0.32	With sheath
		1.0	1.0	0.15	0.42	More sheath air
		0.5	1.0	0.07	0.55	50% isopropanol; sheath
		0.5	1.0	0.19	0.43	Same, more hydrogen
Bismuth (AH,P)	2230	5.0	1.1	0.6	2	No sheath
		5.0	1.1	0.3	2.5	4030 burner
Phosphorus (AH,P)	2464	16	0.5	0.9	1.0	No sheath
		16	0.5	1.3	1.3	Less air
		16	0.5	1.9	1.9	Higher background
Lead (AH,P)	2170	50	1.3	6	9	No sheath
	2614	50	0.23	1.2	7	Steadier flame
	2802	50	0.14	5	14	
	4058	50	0.08	1.7	8	
Beryllium (OAz,M)	2349	1.0	0.02	0.06	0.08	Recorder used
Vanadium (OAz)	3184	200	0.02	19	50	Recorder used
Silicon (OAz,M)	2516	190	0.04	7	4.5	Recorder used
Sulfur (AOA,M)	2576	100	0.05	10	24	Recorder used

upper part of a large, rich (not incandescent) flame, excitation was sufficient for a detection limit of 0.5 mg./l.

Rhenium

No flame spectrum could be detected for rhenium in water or isopropanol in the conventional flames, including sheathed (blue) oxyacetylene. However, the strongest resonance lines appear in incandescent oxyacetylene (Table 3); the resonance line

2275 Å. was also detected. Methanol (50%) enhanced the rhenium threefold. At best, emission was surprisingly weak; Fassel [25] reported much better sensitivity for rhenium in rich oxyacetylene.

Iron Group

Detection limits for Fe and Ni lines in the chemiluminescent air-hydrogen flame with alcohol (Table 5) do not rival those of the strong near-ultraviolet lines; but, lying in a region of little spectral interference and probably no background interference, where the dispersion of a quartz monochromator is high, the chemiluminescent lines should prove more convenient for the analysis of mixtures. Fe 2483 and Ni 2320 are most sensitive; cobalt would doubtless emit a similar spectrum (cf. 41, p. 120), with 2407 Å. as the most sensitive line.

Rhodium

Although rhodium emits an excellent spectrum in conventional flames [41,42], there was no evidence of chemiluminescence in air-hydrogen with alcohol.

Zinc

Although a chemiluminescent spectrum has been observed in air-acetylene [56], oxyhydrogen-naphtha [11], and flames containing zinc dimethyl [23], no marked chemiluminescence was found in air-hydrogen with isopropanol. However, weak lines at 2684 and 2712 Å., with the very high excitation potential of 8.6 e.v., show that a chemiluminescent reaction is certainly occurring in this flame. The 4810 Å. line, observed by Buell (Table 5), should have the advantage over 2139 Å. of enjoying a straight working curve.

Cadmium

The resonance line 2288 Å. is very favorably excited in air-hydrogen with alcohol, and it exhibits chemiluminescence in incandescent oxyacetylene. The high curvature of the working curve is a drawback from which Cd 3261 is free. The latter, like its homologs Zn 3076 and Hg 2537, all of them intercombination lines, is highly anomalous, being abnormally strong in the cooler flames in aqueous solution. Its intensity in air-hydrogen is 300 times the expected equilibrium intensity, and in this flame it is not enhanced at all by addition of alcohol—a unique phenomenon.

Mercury

In the reaction zone of normal oxyacetylene with water, Hg 2537 is 10 times as bright as in the mantle. Air-hydrogen with alcohol gives better sensitivity (Table 5), but the reaction zone of oxyacetylene with hexone is better still [16], offering a detection limit of 2 mg./l. The line shows some chemiluminescence in incandescent oxyacetylene.

Boron

Despite positive results reported by Buell for oxyhydrogen-naphtha [11,12] and by Robinson for oxycyanogen [62], I failed to detect B 2497 in rich oxyacetylene or in oxycyanogen. The high dissociation energy (8.0 e.v.) of BO prevents B vapor from forming in normal flames.

Carbon

The highly characteristic bands of C_2 and CH in the reaction zone and the line C 2479 in hotter flames could serve for the determination of carbon in solution. In a hydrogen flame, about 0.01% of an alcohol can be detected by the bands.

Silicon

No spectrum in air-hydrogen with isopropanol was found for silicon at 2500 mg./l. (dissolved in hydrofluoric acid). However, sheathed air-oxygen-hydrogen-acetylene emits the resonance lines of Si and a weak SiO spectrum. The Si lines brighten as air and hydrogen flow are reduced and acetylene flow raised; the best flame is incandescent oxyacetylene. Methanol produces a 5-fold enhancement.

Germanium

The dioxide in hydrofluoric acid yields the line spectrum of Ge in air-hydrogen with alcohol. The spectrum is much weaker in oxyhydrogen and oxyacetylene with or without alcohol, and undetectable in air-hydrogen without alcohol.

Tin

This metal yields a beautiful spectrum in air-hydrogen with alcohol. Buell [13] has detected lines as far down as 2067 Å. Conventional flames emit a weak band spectrum of SnO with still weaker Sn lines [41,43], and, especially in air-hydrogen with aqueous solutions, a diffuse band at 4850 Å. of unknown origin. This latter flame, moreover, shows anomalously high dissociation of SnO. Only a little alcohol is needed to bring out the chemiluminescence: 3.6% isopropanol produces a strong effect; the intensities are doubled at 11% and become a third again as strong at 20%; with higher alcohol concentrations the gains in intensity are proportionally smaller. In alcohol, the spectrum is weaker in oxyhydrogen than in air-hydrogen, but Buell [11,13] finds the contrary to be true in naphtha. The spectrum in the reaction zone of a premixed, laminar air-methanol flame is like that of the atomizer-burner flames and in sharp contrast with that in the mantle of the air-methanol flame, where only the SnO bands and a few very weak Sn lines appear. The behavior of tin in air-hydrogen with various additives will be discussed later. Whereas normal oxyacetylene emits only a weak, thermal Sn spectrum, incandescent oxyacetylene produces marked chemiluminescence (Table 3). Methanol gives a merely normal enhancement in this flame, doubling the intensity.

It should be pointed out that the standard wavelength tables in current use wrongly classify the Sn lines 2209.7, 2246.0, and 2483.4 Å. These lines belong to the neutral atom, not the ion. The same is true of 2151.43 ($5p^2\ ^3P_2 - 5d\ ^1F^\circ_3$), as pointed out by Dr. Marvin Margoshes of the Bureau of Standards; I had earlier identified it as 2151.48 of Sn^+ ($5p\ ^2P^\circ_{1/2} - 5p^2\ ^4P_{1/2}$). The new tables by Meggers, Corliss and Scribner [57] give correct classifications and excitation energies. Thus, no definite ion lines of tin have been identified in flames.

Lead

In gasoline the chemiluminescent lead spectrum is 50 times as bright in oxyhydrogen (Figure 1) as in air-hydrogen, unlike tin in alcohol. (Note the "fourth positive" CO bands in Figure 1.) In the laminar air-methanol flame the chemiluminescent lead spectrum is about as sensitive as in air-hydrogen-alcohol, whereas with tin the latter flame is better. The lead lines have about the same relative intensities in all the flames. Despite the widespread use of the atomizer-burner for the determination of lead in gasoline, the chemiluminescent spectrum, occurring only in the lower part of the flame, does not seem to have been noticed before by flame photometrists. The lines 2614 and 2802 Å. in gasoline are about as sensitive as the normal lines and might have advantages for analysis. The different behavior of the normal lines 3640 and 3684 Å. (which are little enhanced by alcohol) and the nearby chemiluminescent lines 3573 and 3740 Å. (which are invisible without alcohol) was noticed earlier by Gaydon [32, Plate 6]. The weak ion line 2203.5 Å. visible in Figure 1 and corroborated by repeated scans, has been confirmed by Buell [11].

Nitrogen

The CN bands 3851-3883 Å. have been used for analysis [11, 12,48], but the NO gamma bands offer better sensitivity in air-hydrogen with alcohol or air-oxygen-hydrogen-acetylene with aqueous solutions. In the latter flame 29% oxygen in the oxidant mixture provided the best sensitivity for either nitric acid or ammonia, but the NO intensity was only half as great with ammonia. However, adjustment was much less critical with ammonia, and at 28% oxygen ammonia gave the stronger NO emission (threefold). Thus an adjustment could be found at which nitric acid and ammonia would give equal nitrogen readings, but nothing is known of the behavior of other nitrogen compounds. The N_2 present in this flame yields no NO bands, although the somewhat hotter air-oxygen-acetylene flame shows the NO bands distinctly with a methanol blank (Figure 3), more weakly with water. We thus have a flame that ignores elemental nitrogen but can determine combined nitrogen in water with a sensitivity of about 0.002%.

Phosphorus

Phosphoric acid in alcohol gives rise to the analogous gamma system of PO. The 2464 Å. head is particularly strong and sharp. The PO spectrum is much stronger than the NO spectrum, and can be detected also in the absence of alcohol. With aqueous solutions, air-hydrogen-acetylene is better than air-hydrogen. Addition of oxygen merely raises the background without much affecting the PO intensity.

Arsenic

The air-hydrogen-alcohol spectrum of As is about as intense as that of Ge. Arsenic lines are not detectable at ordinary concentrations in normal flames, even oxycyanogen, although Lundegårdh [52,53] and Carnes [16] have reported them in the reaction zone of acetylene flames. Carnes could detect 2 mg./l. in hexone. The "B" system of AsO is also fairly intense in air-hydrogen-alcohol; the "A" system, with strongest heads at 3278 Å., could not be detected, although it is known to occur in flames and was seen faintly in oxyhydrogen by Hartley in 1894 [46].

Antimony

The Sb spectrum in air-hydrogen-alcohol is quite intense (Figure 2). In water solution the lines are about .001 as intense as in alcohol; they are hardly detectable in oxyhydrogen and very weak in oxycyanogen. A band spectrum was also observed, with peaks at 2565 and 2574 Å., best developed in water solution and apparently not chemiluminescent with alcohol. This was subsequently identified, through Shimauchi's work [64], as due to SbO.

Bismuth

The strong resonance line Bi 3068 unfortunately coincides with an OH band head, and so Bi 2231 is more sensitive in air-hydrogen-alcohol. The normal flame spectrum of bismuth [41,47] is quite different from the chemiluminescent spectrum.

Sulfur

A sulfuric acid solution emits the spectrum of CS in air-oxygen-hydrogen-acetylene, and with 10 times greater sensitivity in incandescent air-oxygen-acetylene (Figure 3); there is an optimal air-oxygen mixture. The SO and S_2 bands were sought but not found, although S_2 bands are said to be very persistent in hydrogen flames [32]. When methanol is added to the solution, the background first rises and then drops to less than that with water, while the CS intensity rises steadily (Figure 6). A reproducibility run showed a standard error of the mean of 4 mg./l. of S in methanol (cf. Table 6).

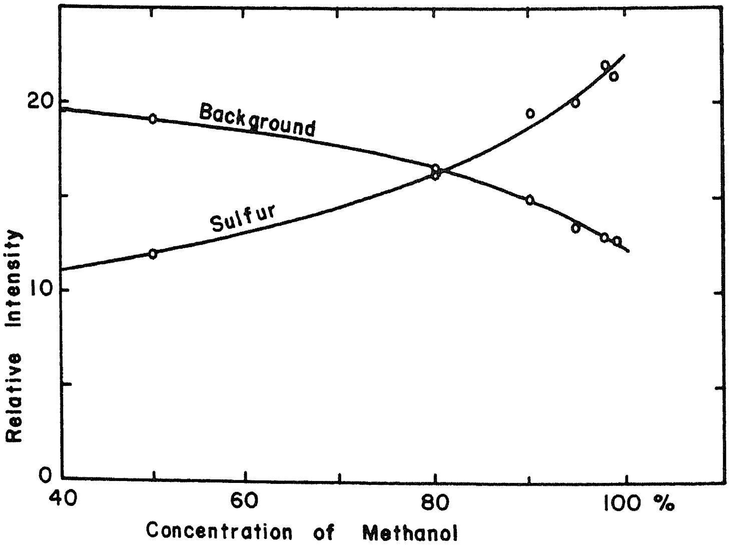

Figure 6. Effect of methanol concentration on emission of sulfur (CS 2576 Å) and on background in air-oxygen-acetylene flame.

Selenium

This element was not studied, but on the basis of dissociation energies one might expect bands of CSe in incandescent flames and of SeO in air-hydrogen (cf. 32, p. 225). The detailed description of the band spectrum in oxyhydrogen given by Hartley [46] does not agree at all with recent data on Se_2 or SeO. Se lines might appear in chemiluminescent flames: 1960 and 2040 Å. should be about equally strong [57]. Allan [5] observed Se 2040 in absorption in air-acetylene, with a detection sensitivity of 5 p.p.m.

Tellurium

An alcoholic solution emits the line spectrum of Te in air-hydrogen, the 2383-2386 Å. lines being strongest. Detailed data were not obtained. In water solution the lines are very much weaker in air-hydrogen and invisible in oxyacetylene; but they should be expected in air-hydrogen-acetylene. The normal flame spectrum is that of TeO, first described by Hartley [46], and best seen in air-hydrogen with water (47, English edition).

ANALYTICAL DATA

Specificity

The chemiluminescent flames used with a quartz monochromator are better than most flames with respect to specificity. The lines lie mostly in the deep ultraviolet, where they are easily separated. The bands of PO and CS are narrow and distinctive, and are nearly as useful as lines for analysis. The NO bands, though more gently shaded, have sharp heads. On the whole, spectral overlap will be infrequent, and the slits can nearly always be kept narrow enough to separate lines spaced by no less than 2 or 3 Å.

Sensitivity

Table 5 lists detection limits for the stronger or more characteristic chemiluminescent emissions (together with a few normal lines) of the 22 elements studied, both in the flames in which the chemiluminescence or exceptional dissociation occurs and, where known [43], in selected normal flames for comparison.

Recalling the definition of intensity (I) used in Tables 1, 3, and 4, we define the detection limit L (as given in Table 5) equal to $190(W + \Delta W)/IW^2$, where W is the slit width at which the blank or background signal has shot noise at the anode of the photomultiplier equal to 0.7% peak-to-peak at a time constant of 1 second, and ΔW, the equivalent limiting resolution, is about 0.03 mm. in the DU monochromator except at the shorter wavelengths, where it rises somewhat. The flame and mirror are assumed optimized for each element. The data of Table 5 apply, of course, only to the DU with 1P28 photomultiplier, although suitable factors can adapt them to other instruments [45]. No adequate treatment of the definition of detection limits in emission spectrochemical analysis has yet been published; a partial treatment for flames will be found in reference 43 (3rd edition). The above-defined L approximately equals the concentration of element in mg./l. giving a net signal equal to total noise (flame plus shot) at the slit width minimizing this concentration.

There are many aspects of this definition of L that call for discussion, but we confine ourselves here to examination of an experimental test of its adequacy. Table 6 shows such a test. It is particularly severe in that the chemiluminescent flames tend to flicker more than other flames. The standard error of a single net reading (difference between sample and blank) is given in terms of equivalent concentration, and compared with the "defined" detection limit, L, calculated as above for each individual case. Note that, for lines, the optimal slit width is less than W and is not at all critical; the slit widths of Table 6 are not far from optimal.

We find from Table 6 that the mean ratio (logarithmically averaged) of L to standard error is 2.4. Hence, on the average, a *single* pair of readings (on sample and blank) at a concentration of analyte equal to L will give a positive result 99% of the time, while 3 or 4 pairs of readings, as commonly obtained in flame photometry, will place the certainty of detection beyond reasonable doubt.

Precision

The flicker of the unsteadiest flames (air-hydrogen with nearly pure alcohol) averaged 5% peak-to-peak with a time constant of 0.2 sec. and a little over 2% at 1 sec. Flicker was somewhat less in air-hydrogen with lower concentrations of alcohol and in the mixed flames. Since a really good sheath was not built until toward the end of the investigation, most of the data are afflicted with imprecision that is now avoidable. Coefficients of variation of the readings on samples and blanks that provided the data of Table 6 were 0.4% under good conditions, 0.8% typically, and over 1.5% at worst. (In a sheathed oxyacetylene flame it can be held to 0.1-0.2%.) However, since much of the standard error in a set of replicate readings is due to drift, not flicker, if sample and blank are read alternately the drift is largely self-compensating and analytical precision benefits. Further, when a flame is unsteady, the slit width can be made much narrower than *W* before shot noise becomes comparable with flame noise, and the resulting gain in line-to-background ratio has the consequence that precision at low concentrations does not deteriorate as rapidly as flame stability. Hence the standard errors in Table 6 are a good deal smaller than would be predicted from the above coefficients of variation on single solutions.

Table 7 shows a test of analytical precision for tin. The gas flow rates and often the mirror were changed after every set of three readings ("unknown", standard, and blank). There were 17 determinations. These excessively variegated conditions would not occur in ordinary analysis.

Table 7

Precision with a Chemiluminescent Line

Tin at 2430 Å. in O -Ar-H -Hydrocarbon Flame

Sample at 100 p.p.m. Compared with Standard at 500 p.p.m.

Hydrocarbon	Concentration Found p.p.m.	Standard Error of Single Measurement p.p.m.
Acetylene	100.8	0.8
Propylene	100.8	1.4
Propane	99.8	1.4
Average	100.4	1.2; $\sigma_m = 0.3$

Linearity

Table 8 summarizes various indirectly obtained data on working curves for the air-hydrogen flame with isopropanol solutions, and Table 9 for the acetylene flames. The "logarithmic slope" is *b* in the equation $I = aC^b$, expressing net intensity *I* as a function of concentration *C*; *a* and *b* usually remain constant over wide ranges of *C*. In a homogeneous flame, the curve should be linear ($b = 1$) below and, owing to self-absorption, parabolic ($b = 1/2$) above a certain rather narrow range of *C*, the "knee" of the curve. The location of the knee is determined by the oscillator strength and collision cross section, as well as the population of the lower state and other things, and provides food for valuable theoretical study. When the curvature exceeds parabolic, as with Be 2349, this is probably due to self-reversal by cooler metal vapor in the periphery of the flame.

Table 8

Working Curves in Air-Hydrogen-Isopropanol

Element	Wavelength	Logarithmic Slope	Concentration Range, mg./l.
Cadmium	2288	Probably 1.0	below 3
		0.5	5 - 500
	3261	1.0 - 0.8	5 - 500
Mercury	2537	1.0	40 - 1000
Germanium	2592	1.0	50 - 200
		ca 0.6	200 - 1000
	2651	1.0	50 - 200
		0.7 (?)	200 - 1000
	2691	ca 0.7	200 - 1000
	2710	Probably 1.0	200 - 1000
	2755	Probably 1.0	200 - 1000
Tin	2246	1.00	10 - 200
		ca 0.9	200 - 2000
	2269	1.00	10 - 200
		1.0 - 0.9	200 - 2000
	2335	1.00	25 - 2000
	2355	1.00	10 - 200
		ca 0.96	200 - 2000
	2422	1.00	10 - 200
		0.9 - 0.8	200 - 2000
	2430	1.00	10 - 2000
	2483	1.00 ± .02	100 - 2000
	2547	1.05 - 1.10	25 - 2000
	2706	1.06	10 - 2000
	2706[a]	0.97	100 - 2000
	2840	1.00	100 - 2000
	2863	1.00	100 - 2000
	3009	1.00 ± .02	100 - 2000
	3034	1.00 ± .02	100 - 2000
	3262	1.00	100 - 2000
	3331	1.0	100 - 2000
	3801	1.1	100 - 2000
	4525	1.05 ± .05	100 - 2000
Lead	2170	ca 1	50 - 200
		ca 0.5	200 - 500
	2394	ca 0.7	200 - 500
	2476	ca 0.9	200 - 500
	2614	1.00 - 0.95	50 - 500
	2663	1.00 - 0.95	50 - 500
	2802	ca 0.8	200 - 500
Nitrogen	all bands	ca 1.0	up to 10,000

Table 8—Continued

Element	Wavelength	Logarithmic Slope	Concentration Range, mg./l.
Phosphorus	all bands	Probably 1.0 - 0.9	15 - 800
Arsenic	2288	1.0	20 - 200
	2350	1.0 - 0.9	20 - 500
Antimony	2176	ca 1.0	10 - 25
		ca 0.7	25 - 100
	2311	0.8	10 - 100
	2528	1.0 ± .1	10 - 100
	2598	1.0 ± .1	10 - 100
Bismuth	2230	1.0	below 50
		0.7	50 - 200
		0.5	200 - 1000
	2277	1.0	100 - 1000

[a] The tin lines preceding this are referred to 2430; those following, to the best near-ultraviolet lines. The apparent rise of logarithmic slope with wavelength is an artifact due to the manner of estimating the slopes and the higher component of thermal excitation in the longer-wavelength lines.

Interferences

Chemical interference was studied briefly only with tin (Table 10), owing to the need of additives to keep it from precipitating on aging. It was noted that the decanted supernatant from an aged solution originally containing 50 p.p.m. of tin showed less than 1 p.p.m., but if the mixture was stirred, the apparent concentration was 40-45 p.p.m. Thus the tin does not have to be in solution to be excited in the flame. Most of the tests of Table 10 were with aqueous solutions in air-hydrogen-acetylene; but hydrofluoric acid was tested also with an alcoholic solution in air-hydrogen, in which it gave the same interference.

Data on mutual interferences of As, Sb, Bi, Sn, and Zn in the inner cone of oxyacetylene with hexone are given by Carnes[16].

SOLVENT, FUEL, AND OXIDANT

Effect of Solvent

Solutions of tin in 20 and 60% acetone gave spectra in air-hydrogen showing the same relative line intensities as in isopropanol, but 0.75 as intense (at the same solvent concentrations). Methanol gave the same absolute line intensities but 0.4 as intense

Table 9

Working Curves in Chemiluminescent Acetylene Flames

Element	Flame, Solvent	Wavelength	Logarithmic Slope	Concentration Range, mg./l.
Beryllium	OAz	2349	1.0 0.8 0.65 0.5 0.3	below 5-10 at 25 at 50 at 100 at 1000
Vanadium	OAz	3184	0.95	200 - 2000
Silicon	OAz, M	all lines	Probably 1.0	200 - 1000
Sulfur	AOA, M	all bands	1.0	100 - 5000

Table 10

Interferences with Tin
Sn 50-500 p.p.m. at 2430 Å

Interferent	Concentration	Effect
HNO_3	0.5%	0%
H_2O_2	several %	0
$H_2O_2 + HNO_3$	several % each	0
I_2	excess	0
I_2, heated	excess	0
HCl	2%	0
HCl + HF	1% each	0
$+ I_2$	excess	
Sterox	50 p.p.m.	0
EDTA	saturated	0
HF	2-4%	-4
HF	2.5%	-3
$+ I_2$	excess	

a background as isopropanol. Tin emission was 8% higher in 100% methanol than in 90%. With lead in air-hydrogen, gasoline and isopropanol gave practically identical spectra, while methanol yielded somewhat better detection limits, as with tin. Carbon tetrachloride and methyl chloroform, mixed with isopropanol, had little effect on tin in air-hydrogen, but they somewhat raised the background.

In oxyhydrogen, lead in gasoline gave a much more intense spectrum (in the reaction zone) than in air-hydrogen, whereas tin in isopropanol (and in *n*-butanol [63]) gave a weaker spectrum and (owing to the much higher background) much poorer detection sensitivity than in air-hydrogen. Similarly, Buell [11] found that chemiluminescent spectra in oxyhydrogen are weaker in naphtha-isopropanol than in naphtha and may be absent in acetone. Thus hydrocarbons seem superior in oxyhydrogen but not necessarily in air-hydrogen.

Effect of Oxidant Mixture with Alcoholic Solutions

J. C. Sternberg of Beckman Instruments had suggested that the nitrogen of the air might be tending to quench the chemiluminescence by collision deactivation of the excited atoms, and that replacement of the nitrogen by a noble gas might enhance the chemiluminescent emission. Argon did in fact improve the sensitivity for tin in isopropanol, although without the sheath the flame still contained nitrogen entrained from the ambient air. The atomizer was operated on mixtures ranging from pure argon to pure oxygen, while hydrogen was supplied to the fuel port as usual. The results are shown in Figure 7. The "sensitivity" of Figures 7-11 is the ratio of net reading on Sn 2430 at 100 mg./l. to the square root of the blank reading with slit 0.14 mm; it is nearly proportional to $1/L$ and is convenient for comparison. The peak sensitivity obtained with air-oxygen mixtures (Figure 8) is only about 0.7 of that available with argon.

Germanium in isopropanol was tried in air-hydrogen with oxygen supplied through a sheath. The oxygen brightened the Ge lines somewhat but raised the background more rapidly.

Chemiluminescence with Aqueous Solutions and Gaseous Additives

In view of the remarkable effect of alcohol in the air-hydrogen flame, Sternberg suggested that any carbon-hydrogen compound in the flame might elicit the chemiluminescence. It would obviously be convenient to have a flame capable of giving the chemiluminescent spectra with aqueous solutions. A trial showed that natural gas, propane, propylene, and acetylene added to air-hydrogen all excited the tin spectrum very well. Although the

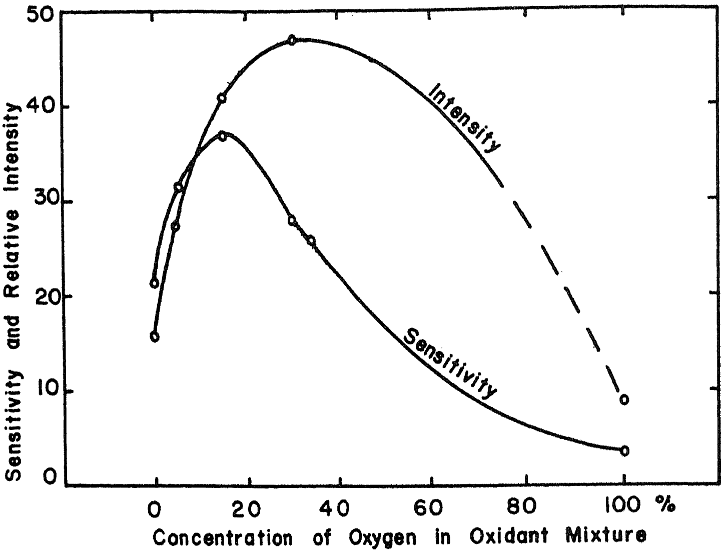

Figure 7. Effect of oxygen concentration on the spectrophotometric detection sensitivity and on emission intensity of tin at 2430 Å in 98% isopropanol in the argon-oxygen-hydrogen flame. In this and the next three figures each sensitivity value is separately maximized with respect to hydrogen flow and mirror focus.

gaseous additives gave less intensity than liquid additives, the line intensity ratios for tin were identical in acetylene and isopropanol.

Cyanogen added to air-hydrogen produced an emission of Sn 2430 (in water solution) equal to only about 3% of that produced by isopropanol. The cyanogen gave rise to strong CN bands (violet system) and greatly raised the background in the deep ultraviolet (much more than other fuels or solvents). Carbon monoxide brought out no emission of tin at all. Neither cyanogen nor carbon monoxide appreciably affected the intensity of Sn 2430 obtained with isopropanol; they both raised the background—carbon monoxide somewhat, cyanogen greatly.

A search was made for a combination of gases that would provide optimal detection sensitivity for tin in aqueous solution. The best combinations attained 40-50% (or 60% with a wetting agent) of the sensitivity with isopropanol and 30% of the sensitivity with methanol; see the data for Sn 2430 in Table 5. Many variables are involved in such a search. Some of these are discussed below.

The sheath was operated with various mixtures (always the same as that supplied to the atomizer), including air-oxygen, argon-oxygen, and air-propane. In no case did it affect the emission except to stabilize it somewhat. The sample pump, likewise, conferred little advantage under any of a variety of conditions, since sample flow rate was not at all critical and was already nearly optimal under unimpeded suction. Optimal dimensions for the atomizer-burner were: capillary bore 0.35 mm., atomizer port 0.08 mm. wide, fuel port 0.25 mm. wide. Atomizer pressures of 20-25 p.s.i. were best. An extended trial of a burner with an atomizer port of 0.025 mm. run at 30-50 p.s.i. with various argon- or air-oxygen-hydrogen-acetylene mixtures revealed no advantage of high-pressure atomization. Adjustment of the concave mirror became more critical with higher oxygen content.

The order of mixing or feeding the gases had little effect on the emission. In every comparison, the results were slightly better when the fuel mixture was supplied to the fuel port and the oxidant mixture to the atomizer, instead of, e.g., air-propane for atomizing and hydrogen for the fuel port. Note, however, that in the sheathed oxyacetylene flame the interchange of oxygen and acetylene provides higher sensitivity and suppresses incrustation of the atomizer [6,44].

In a comparison of hydrocarbons as additives for the air-hydrogen flame, natural gas, propane, and acetylene yielded closely similar sensitivities for tin, acetylene being 5-10% better than the others. Propane, propylene, and acetylene as additives for the argon-oxygen-hydrogen flame gave nearly identical sensitivities (Figure 9), but acetylene gave somewhat higher absolute intensity of tin and background.

Acetylene as Additive

In view of these results, acetylene was singled out for further experiments. First of all, it should be noted that in hydrogen-hydrocarbon flames in a normal burner with aqueous solutions, the sensitivities for tin are more nearly alike for argon-oxygen and air-oxygen atomizing mixtures than they are in hydrogen flames with alcoholic solutions, where argon-oxygen (Figure 7) has an advantage over air-oxygen (Figure 8).

With the high-pressure atomizer mentioned above, the tin sensitivity was highest with pure oxygen, hydrogen so low that the flame tended to blow out, and acetylene high enough to make the flame incandescent. Flow rates of both hydrogen and acetylene had to be adjusted within 10% for best results. Owing to the high intensity of both tin and background emission, this flame permitted use of very narrow slits while offering a detection limit of 2 p.p.m. tin in aqueous solution. Figure 10 shows the effect of oxygen on sensitivity, and Figure 11 shows the effect of the fuel flow rates. With constant atomizer pressure (30 p.s.i.), about 400 readings were taken with different oxygen, hydrogen,

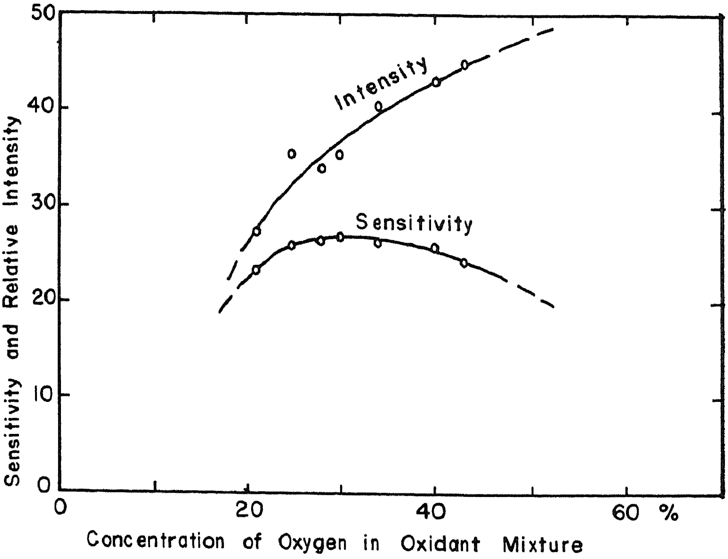

Figure 8. Effect of oxygen concentration on the sensitivity and intensity of tin at 2430 Å in 90% isopropanol in the air-oxygen-hydrogen flame.

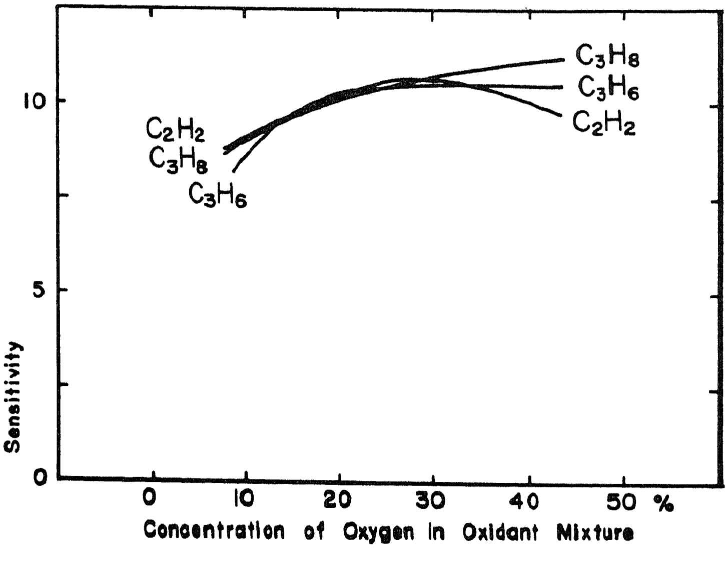

Figure 9. Effect of oxygen concentration on the sensitivity of tin at 2430 Å in aqueous solution in argon-oxygen-hydrogen-hydrocarbon flames.

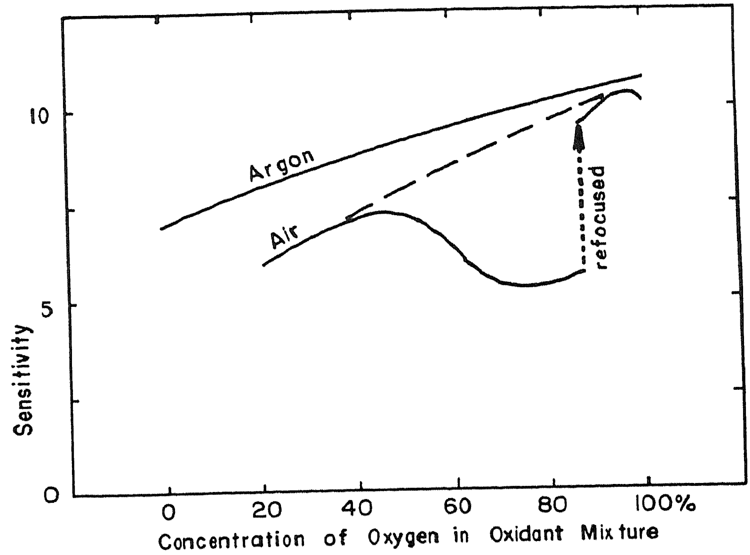

Figure 10. Effect of oxygen concentration on the sensitivity of tin at 2430 Å in aqueous solution in air- and argon-oxygen-hydrogen-acetylene flames with a high-pressure atomizer-burner. On the air curve, mirror focus drifted from optimal until reoptimized at 87% oxygen.

and acetylene pressures, with air or argon as diluent. For each oxygen value, a contour map was drawn showing sensitivity as a function of hydrogen and acetylene pressures. Four of these maps appear in Figure 11. The curves of Figure 10 are loci of the hilltops of the contour maps.

These results are peculiar to the burner. The standard No. 4020 burner can provide slightly better detection sensitivity (1.5 p.p.m.) for tin in aqueous solution in a blue flame of air-oxygen-hydrogen-acetylene, although with lower intensity and therefore lower available resolution at a given concentration. In the blue flames the acetylene pressure is less critical; as acetylene is added, the chemiluminescent emission suddenly comes into view, rising up on to a gently sloping plateau. More acetylene raises the background and lowers the sensitivity. It is curious that in the white flames the background intensity may show a minimum following a maximum, as acetylene is added.

With the help of the sheath, it is possible to shift gradually to pure oxyacetylene without losing the chemiluminescent Sn lines. The flame must be kept incandescent or the lines vanish. Although Sn 2430 is about 20 times as intense in sheathed oxyacetylene (Table 3) as in air-hydrogen-acetylene, the much higher

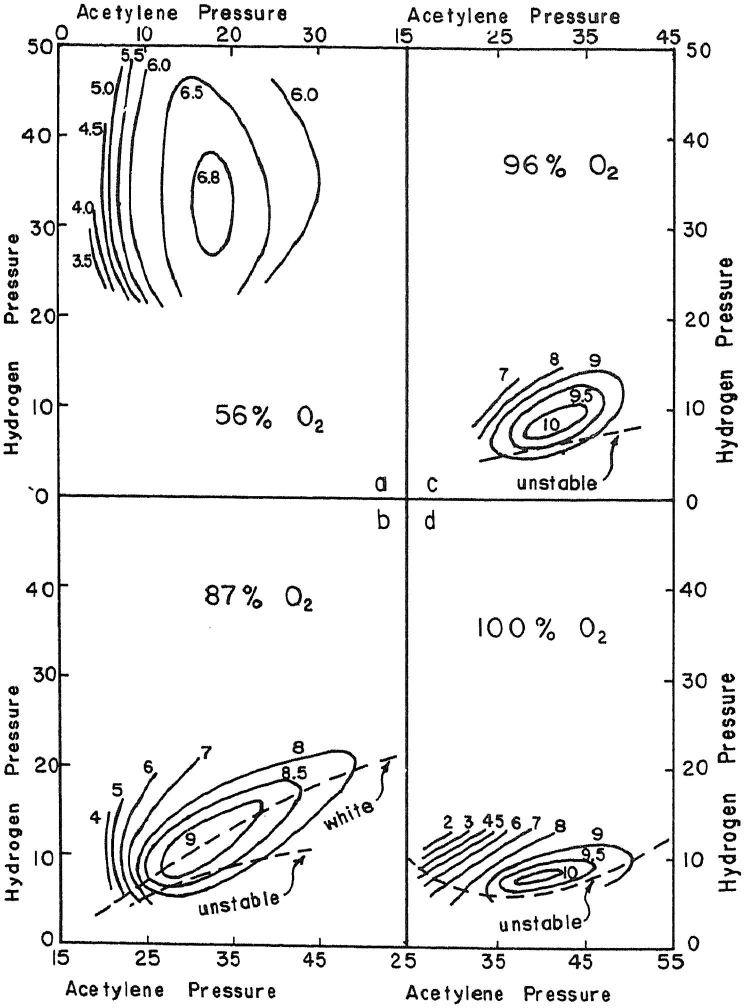

Figure 11. Sensitivity of tin at 2430 Å in air-oxygen-hydrogen-acetylene flames at four different concentrations of oxygen in the oxidant mixture, as function of hydrogen and acetylene pressures (in inches of water) in the high-pressure atomizer-burner. Contour values are sensitivities. Boundaries of regions of instability and incandescence are shown.

background of oxyacetylene limits the sensitivity to about 7 p.p.m. in aqueous solution.

In the light of earlier remarks on Si, Ge, N, P, and S, it is clear that no generalizations for other elements based on this work with tin would be safe.

Liquid Additives with Hydrogen-Hydrocarbon Flames

Attempts were made to improve sensitivity by combined use of alcohol and gaseous hydrocarbon. The hydrocarbon did not further enhance the emission already produced by the alcohol, while it did somewhat raise the background. Possibly hydrocarbon might help at low concentrations of alcohol. If the flame excites a chemiluminescent spectrum with aqueous solutions, alcohol produces only a normal, moderate enhancement, typically threefold.

Since water is not as finely atomized nor as quickly evaporated in an atomizer-burner flame as are most nonaqueous solvents, it was thought that sensitivity might be enhanced by a wetting agent. In fact, addition of Tergitol Nonionic TMN brightened Sn 2430 by 24%, giving the best detection limit (about 1 p.p.m.) observed in any experiment with aqueous solutions; this was in a hydrogen-propane flame with argon-oxygen (66%-34%) for atomizing.

MECHANISM OF CHEMILUMINESCENCE

Work on interpreting the phenomena described above is still in progress, and so only a preliminary report can be given. Basic considerations have been presented by Alkemade [3]. The special chemiluminescences observed by Egerton [23], Padley and Sugden [59], and Bugrim [14] appear to be quite different from those described here, and are apparently due in each case to reactions involving hydrogen atoms.

The phenomena of interest for analytical flame spectrophotometry include chemiluminescence of line and band spectra, chemiionization (these two occurring only in the reaction zone of carbon-containing flames), and enhancement of atomic spectra in incandescent flames. Two other useful but unexplained anomalies are the excessive populations of the ground-state of tin and of cadmium in the lowest $^3P_1$ state in air-hydrogen without organic additives. The degree of dissociation of SnO in air-hydrogen (with aqueous solution) should be 0.0001 if the dissociation energy is 5.7 e.v., whereas the line intensities indicate a dissociation of about 0.2. In oxyhydrogen, however, the tin behaves more nearly as expected. Cooke [40] confirms this by absorption measurements. In this respect tin seems to be unique among the many elements studied in flames. The case of Cd 3261 was mentioned earlier, and even in oxyhydrogen it is 20 times too strong. The homologous Hg 2537 is about 60 times too strong in air-hydrogen.

Quantitative Approach

Recalling the definitions of I and L, we can write for radiative equilibrium

$$I = \frac{c\,d\,Q\,f\,g}{\lambda^3 A}\,10^{-5040\,E/T}\quad, \tag{1}$$

where c is a constant depending on the flame and solvent, d is the degree of dissociation or ratio of atomic vapor to total analyte concentration, f is the oscillator strength, g is the statistical weight of the lower state, E is the excitation energy of the line, T is the absolute temperature, λ is the wavelength, A is the atomic weight of the analyte, and Q, a characteristic of the monochromator, equals PST, a function of wavelength, P being the absolute photocathode sensitivity, S the luminosity of the monochromator per unit slit width, and T the transmittance.

The constant c can be found for each flame from the L or I values for many lines of many elements; several thousand of these are on hand. An assumed value of c is first taken; T is then calculated for many values of E, and if a trend is apparent, c and T can be adjusted by least squares to remove the trend. The chief stumbling block is the lack of adequate data for f, but this will be largely removed by the appearance of Monographs 50 and 53 of the Bureau of Standards, now in press.* Pending availability of these Monographs, I estimated fg values, when they were not elsewhere available, from the intensities, J, given by Meggers, Corliss and Scribner [57], by the equation

$$fg = 7 \times 10^{-16}\, J\, \lambda^3\, 10^E\ , \tag{2}$$

with λ in μ and E in e.v. The coefficient was estimated from many literature values of f, but uncertainties often amount to a factor of 2 or more.

This approach has yielded preliminary temperatures for the air-hydrogen, oxyhydrogen, and oxyacetylene flames, with water spraying, as produced by the Beckman atomizer-burner: 2240, 2610, and 2740°K, respectively. The evidence also suggests the following pressures of atomic oxygen in these flames when optimized for a typical element: 0.0003, 0.0035, and 0.007 atm., respectively; the first two represent essentially stoichiometric flames (allowing for entrainment of ambient air), while the last corresponds to a slightly lean oxyacetylene flame, and is likely to vary more than the other two. With these data and with the known or estimated internuclear distances, vibrational constants, and statistical weights, dissociation energies of the gaseous monoxides can be calculated from the line intensities [30, p. 144]. Some preliminary values are listed in Table 11; these are subject to revision when better f-values become available.

---

*The latter has appeared: Corliss, C. H., Bozman, W. R., "Experimental Transition Probabilities for Spectral Lines of Seventy Elements," Natl. Bur. Standards Monograph 53, Washington, D. C., 1962.

Table 11

Dissociation Energies of Gaseous Monoxides

Calculated from Line Intensities in Air-Hydrogen,
Oxyhydrogen, and Oxyacetylene Flames
with Aqueous Solutions

CaO	4.4 e.v.	BeO	> 5.5 e.v.
SrO	4.6	AlO	5.4
BaO	5.3	SbO	3.7
CrO	4.3	BiO	< 3.8

Enhancement in Incandescent Flames

As already suggested by Fassel [25], the extraordinary enhancements of the spectra of elements with stable gaseous oxides in incandescent oxyacetylene are due to dissociation of the oxides in the strongly reducing environment. Taking Fassel's estimate of the temperature of incandescent oxyacetylene with ethanol spraying (2900°K) and my estimate for normal oxyacetylene with water (2740°), and allowing for the sheath, a reasonable guess is 2700° for the sheathed incandescent oxyacetylene flame. If solid carbon is present, the pressure of atomic carbon should be 2×10^{-6} atm. [32]. If the equilibrium constant of the reaction $CO = C + O$ is 1.6×10^{-14} [32], with 40% CO in the flame the pressure of atomic oxygen should be 3×10^{-9} atm., and this changes little with temperature. We then conclude that any oxide MO with a dissociation energy D not greater than 8.0-8.5 e.v. (depending on the other properties of M and MO) will be extensively dissociated at this pressure of O. With the higher temperatures attained with ethanol solution, higher values of D can be tolerated. Since very few elements have D(MO) as high as 8.5 e.v., all or nearly all elements should yield useful concentrations of atomic vapor in incandescent oxyacetylene. Even thorium, with D(ThO) = 8.6 e.v., was reported by Fassel to emit a weak line spectrum in this flame.

Next, from the data of Table 3 the apparent temperature can be found by equation (1) for each element (in water solution) by assuming complete conversion of analyte to atomic vapor ($d = 1$) and taking c the same as in ordinary oxyacetylene. Table 12 lists these temperatures. The high-energy Be lines doubtless give too high a T, since equation (2) implies impossibly large f-values, Corliss's normalizing function not having been available. Nevertheless, Be 2349, and also Cd 2288, Hg 2357, and the Sn lines, look definitely chemiluminescent, since the flame can hardly be so hot. For the Sn lines, T rises at shorter wavelengths; this effect is mentioned again below. As for V, the low

Table 12

Apparent Excitation Temperatures in Sheathed Incandescent Oxyacetylene

Calculated from Line Intensities for Aqueous Solutions, Assuming Complete Dissociation

Be	3000°K	Hg	3200°K
V	2500	Si	2500
Re	2100	Sn	2900–3400
Cd	3300		

T may be due to poor f-values or to incomplete vaporization of lower oxides of vanadium; if $T = 2700°$, d would have to be 0.15, but gaseous VO should be fully dissociated. The Re intensities (observed at 2000 p.p.m. Re) imply a concentration of 2×10^{-7} atm. of Re in the flame, and it happens that the vapor pressure of Re at 2700° is 3×10^{-7} atm. The weakness of the Re lines may thus be due to saturation; a test would be very easy. As for Si, if $D(\text{SiO}) = 8.0$ e.v. [51], d should be 0.1 at 2700° in this flame. Taking $T = 2700$, the intensities of the six Si lines imply $d = 0.17$, 0.11, 0.21, 0.13, 0.09, and 0.14, respectively, with f found by equation (2). This agreement suggests that silicon enjoys approximate radiative and thermodynamic equilibrium in incandescent oxyacetylene.

The apparent chemiluminescence in this flame might be explained by a reaction first proposed by Sternberg:

$$\text{C} + \text{MO} = \text{CO} + \text{M}^*; \quad \Delta\text{H}° = -11.1 + D(\text{MO}) + E(\text{M}^*) \text{ e.v.,} \qquad (3)$$

E being excitation energy. The concentration of C is high enough to make this reaction likely. Energy is sufficient to yield the upper state of Be 2349 but not of the higher-energy Be lines, and better f-values may corroborate the selective chemiluminescence of Be 2349. Spin conservation contraindicates the reaction for Be 2349, but the rule is known to fail rather easily, even for light elements. Further, Sternberg's reaction is inadequate by nearly 2 e.v. to excite the Si lines, in conformity with their apparent radiative equilibrium. The reaction should, however, give chemiluminescence with Cd, Hg, V, and Sn.

These hypotheses can be subjected to extensive testing when the complete data of Fassel, Curry, Myers, and Kniseley become available.

Mechanisms in Blue Flames

One approach is to correlate the populations of the excited states with excitation energy. From equations (1) and (2), we can write for the population of an excited state as calculated from the observed intensity,

$$C = IA\,10^{-E}/c'Q\,J\,, \tag{4}$$

c' being constant for each flame and solvent. If a Boltzmann distribution can be assumed, C should be proportional to $10^{-5040\,E/T}$. Hence a plot of log C vs. E should give a line whose slope yields T. Utilizing all the Sn lines of Table 1, we do in fact find a consistent T of about 3000°K, but only if the lines are selected from suitable ranges of λ. Taking $T = 3000$, log $C + 1.7\,E$ ought to be constant, aside from expected scatter. Oddly, this function shows a dependence on λ (not on E), in that it rises abruptly below 2500 A., increasing by log 50 between 2500 and 2100 A. If equation (1) is applicable, it implies $d = 0.02$ above 2500 A., but $d = 1$ at 2100 A. This behavior may be due entirely to instrumental miscalibration both in the copper arc of Meggers, Corliss, and Scribner, and in my DU spectrophotometer. Admittedly, intensities in the deeper ultraviolet are hard to determine absolutely, but a factor of 50 seems out of line. The same effect, whatever its cause, may be at work in the incandescent oxyacetylene flame, where the shorter-wavelength tin lines show the higher T, regardless of E. The intensity data on other elements have not yet been evaluated.

Approaching the problem now from the point of view of reaction mechanisms, we can, thanks to recent basic work by various investigators, formulate a simple hypothesis that appears to account for all observations accumulated to date, although it does not yet explain the relative line intensities quantitatively. Fenimore and Jones [26] find that the carbon monoxide in methane flames is formed chiefly from O (and not from O_2, OH, or H_2O). The O can react with CH_3 or other radicals; there are a great many possible reactions [15,27,58,65].

Next, the most abundant positive ion present in the reaction zone of chemiluminescent flames is now known to be H_3O^+ [15, 22,58,66], accounting typically for 90% of the ions. (The negative ions are practically all electrons.) The H_3O^+ can originate in the following way, starting with CH as a typical radical [15,27,65]:

$$CH + O = CHO^+ + e^-; \quad \Delta H^\circ = 0 \text{ kcal./mole} \tag{5}$$

or

$$CH^* + O = CHO^+ + e^-; \quad \Delta H^\circ = -66 \text{ to } -91 \text{ kcal./mole } (-2.9 \text{ to } -3.9 \text{ e.v.}) \tag{6}$$

$$CHO^+ + H_2O = H_3O^+ + CO; \quad \Delta H^\circ = +23 \text{ kcal./mole } (+1.0 \text{ e.v.}). \tag{7}$$

The excited CH* can be in a $^2\Delta$, $^2\Sigma^-$, or $^2\Sigma^+$ state (2.9, 3.2, or 3.9 e.v.) in which it emits the familiar 4315, 3889, or 3145 Å bands, respectively. Although this route is simple and probable, Mukherjee et al. [58] are inclined to discount the importance of CHO^+ as primary ion, favoring $COOH^+$, which is a better proton donor. Van Tiggelen [66] reported $COOH^+$ only in air-acetylene with chlorine compounds.

In any case, the H_3O^+ carries indirectly the energy of formation of CO from CH, since the difference of their dissociation energies is 7.7 e.v., while the sum of reactions (5) and (7) is endothermic to the extent of 1.0 e.v. (Calcote [15] gives +41 kcal./mole for reaction (5) and Fueno et al. [27] give +39 kcal./mole, but these are based on older values of the heat of sublimation of graphite; Sternberg [65] prefers 0 kcal./mole for reaction (5).) The over-all reaction is then

$$CH + O + H_2O = H_3O^+ + CO + e^-;\quad \Delta H^\circ = +23 \text{ kcal./mole } (+1.0 \text{ e.v.}). \tag{8}$$

Subtracting the dissociation energy difference of CO and CH, we get

$$H_3O^+ + e^- = H_2O + H;\quad \Delta H^\circ = -201 \text{ kcal./mole } (-8.7 \text{ e.v.}). \tag{9}$$

The hydronium ion is thus highly unstable with respect to dissociative recombination, but the excessive energy cannot be readily liberated without the help of a third body to carry it off in some form other than translation.

Chemiionization

The hydronium ion might produce ions of the analyte by any of the following reactions:

$$H_3O^+ + M = M^+ + H_2O + H;\quad \Delta H^\circ = -8.7 + I(M) \text{ e.v.} \tag{10}$$

$$H_3O^+ + MO = M^+ + H_2O + OH;\quad \Delta H^\circ = -13.1 + I(M) + D(MO) \text{ e.v.} \tag{11}$$

$$H_3O^+ + MOH = M^+ + 2H_2O;\quad \Delta H^\circ = -13.8 + I(M) + D(MOH) \text{ e.v.} \tag{12}$$

$$H_3O^+ + MO = MOH^+ + H_2O;\quad \Delta H^\circ = -13.1 - D(MOH) + D(MO) + I(MOH) \text{ e.v.} \tag{13}$$

Here *I* means ionization potential.

Reaction (10) accounts for the chemiionization of sodium, according to Padley and Sugden [61], but it is at variance with some of the observations on the presence or absence of certain ions in the oxyhydrogen flame with naphtha, vis., those of Ti, Co, and Cd. Reaction (11), however, shows the proper energy relations for all observed cases, and seems to be the most likely cause of the chemiionization of analyte introduced into the flame. Table 13 shows a test of reaction (11), taken from the work of Buell [11], for ion lines in the oxyhydrogen-naphtha flame of all elements having ion lines that ought to be visible if present. Pending acquisition of Brewer's table of D(MO) [7], some of the data remain dubious. Chromium demands further scrutiny, and the case of cobalt seems odd. If D(CoO) is high enough (5.2 e.v.) to prevent ionization, then the Co spectrum should be much weaker than those of Fe and Ni in conventional flames, but this is not true.*

Reaction (12) can certainly also account for ionization, but data on D(MOH) are very scanty, and probably only a few elements have sufficiently stable gaseous hydroxides to enter significantly into this reaction. No data are available for testing reaction (13),

Table 13

Ionization in the Oxyhydrogen-Naphtha Flame

Observations by Buell [11]

	Ion Lines Seen	H° of Reaction (11)
Be	No	-1.6 e.v.
Mg	Yes[a]	1.2
Ti	No	-0.6
V	Yes	0.0
Cr	Yes?[b]	2.1
Mn	Yes	1.4
Fe	Yes	0.9
Co	No[c]	?
Ni	Yes	1.1
Zn	No	-0.3
Cd	Yes	0.3
Pb	Yes	1.6

Notes: a—Ionization exceeds thermal. b—Buell reports Cr II 2853.2 (E = 8.1 e.v.), but it is probably Mg 2852.1; Cr II 2766.5 should appear in Buell's spectrogram but does not. c—Buell's Co II 3621.2 is probably Co I 3620.4 [57], with Ni 3619.4.

---

*Later data kindly supplied by Brewer on dissociation energies and by Buell on ion lines of Cr and Co remove these discrepancies but, in turn, suggest that zinc may possibly be ionized, despite its very high *I*.

but it seems like a probable source of such ions MOH^+ as are known to exist.

Chemiluminescence

Of the various reactions that might be written to account for electronic excitation in the reaction zone, the following are simple and probable:

$$H_3O^+ + MO + e^- = M^* + H_2O + OH; \quad \Delta H^\circ = -13.1 + D(MO) + E(M) \text{ e.v.} \tag{14}$$

$$H_3O^+ + M + e^- = M^* + H_2O + OH; \quad \Delta H^\circ = -8.7 + E(M) \text{ e.v.} \tag{15}$$

At this writing, reaction (14) best fits the observations. It is exothermic or thermoneutral for the most highly excited observed line of each of the 28 elements thus far known to chemiluminesce in atomizer-burner flames. As an example, in the case of zinc, although the spectrum of ZnO has not been observed in flames except under very special conditions by Egerton [23], the occurrence of Zn 2515.8 ($E = 9.00$ e.v.) in oxyhydrogen-naphtha [11] points to the intermediation of ZnO according to reaction (14). At the same time, the high D of TiO, VO, SiO, and GeO limits ΔH° of reaction (14); and, conformably, the chemiluminescent spectra of these elements show lower maximal E than do those of neighboring elements with higher ΔH°.

The concentration of H_3O^+ in the reaction zone is about 10^{-6} atm. [66], so that a molecule of MO will strike a H_3O^+ once per millisecond. Since they may pass through the reaction zone in 10^{-4} sec., most of the MO molecules will never strike a H_3O^+. This is not in conflict with the tentative value $d = 0.02$ found above for Sn in air-hydrogen-alcohol, or with the fact that the thermally excited spectrum of MO (e.g., SbO, SnO) is little affected by the chemiluminescence of M, except in cases (NO, PO) where excited atoms are not observed. It is conceivable that high concentrations of analyte could deplete the H_3O^+ and thereby cause departures from linearity of the working curve. Such an effect has not yet been observed, at least up to 3000 mg./l. of tin [63].

Comparison of Agents Causing Chemiluminescence

It seems inescapable that the energy of chemiluminescent excitation in these carbon-containing flames, regardless of the exact route, is derived from the difference between the dissociation energy of CO and the carbon bond energy of the carbon compound introduced into the flame. Similarly, Van Tiggelen [66] concludes that the chemiionization in these flames results from the formation of the double C=O bond, and that if the carbon is thus bonded at the start, no ionization occurs.

Consider the following sequence of dissociation energies: CCl 3.4, CH 3.5, CF 4.6, CN 7.6, CS 7.9, CO 11.1 e.v. Additives in which the carbon is bonded primarily to Cl, H, F, N, S, or O elicit chemiluminescence and ionization decreasing in that order. C-Cl compounds (e.g., CCl_4) produce strong ionization and seem about as effective as C-H compounds in producing chemiluminescence. Nothing is known of CF_4. C_2N_2 produces little and CS_2 little or no ionization or luminescence [32,49,65,66] ($D(CO) - D(CN) = 3.5$ e.v.; $D(CO) - D(CS) = 3.2$ e.v.). CO causes none at all, and neither does HCHO [38,66]; C_3O_2 and HCOOH give no ionization [66] (they have not been tested for chemiluminescence).

A close correlation exists between chemiionization and chemiluminescence also among the C-H compounds. The efficacy of a compound for producing ionization in the hydrogen flame detector for gas chromatography can be described in terms of the effective carbon number contribution to the current, as shown by Sternberg, Gallaway and Jones [65]. This number is 1.3 for acetylenic carbon, 1.0 for paraffinic and olefinic carbon, 0.0 for carbonyl carbon, -0.6 for the oxygen in a primary alcohol, -0.75 for the oxygen in a secondary alcohol, and -0.12 for (multiple) chlorine on an aliphatic carbon. This agrees with the observations that acetylene produces a little stronger chemiluminescence than propane, propylene, or natural gas, while these three are very much alike; that gasoline and naphtha are better than alcohol (in which the oxygen atom competes for one of the carbon atoms); that alcohols are a little better than acetone (in which the carbonyl is useless); and that carbon tetrachloride and methyl chloroform are similar to isopropanol. The different viscosities of these liquids evidently do not affect the comparisons very much.

The observed parallelism between the chemiluminescence and the intensity of the CH bands, both locally in a given flame and among flames with different additives, follows from reactions (5) and (6). On the other hand, since C_2 is not directly involved in this sequence of chemiluminescent reactions, its emission does not show as close a relation. To be sure, it cannot be argued that CH, CHO^+, and H_3O^+ are the principal agents for nonhydrogenous additives such as cyanogen. One or more of the many other reactions proposed by various authors [15,27,58,65] may then take over.

ACKNOWLEDGMENT

I am greatly indebted to Dr. James C. Sternberg for his discussions of theory and excitation mechanisms, and for his calling my attention to the recent work on flame ionization. It was at his suggestion that the experiments with argon, with the hydrocarbon additives, and with the chlorinated solvents were carried out.

I am grateful also to Mr. Bruce E. Buell, who has kept me posted on his work in chemiluminescence since early 1960. His data, supplied in advance of publication, have been indispensable in my attempts to explain the phenomenon.

REFERENCES

1. Alekseeva, V. G., Mandel'shtam, S. L., Zhur. Exptl. i. Teoret. Fiz. 17, 759 (1947).
2. Alekseeva, V. G., Mandel'shtam, S. L., Zhur. Tekh. Fiz. 17, 765 (1947).
3. Alkemade, C. T. J., "Excitation and related phenomena in flames," International Conference on Spectroscopy, Washington, D. C., June 1962. See paper in this volume.
4. Allan, J. E., Analyst 83, 466 (1958).
5. Allan, J. E., Spectrochim. Acta 18, 259 (1962).
6. Beckman Instruments, Inc., Fullerton, Calif., "Sheathed atomizer-burner," Bulletin 3063, March 1962.
7. Brewer, L., U. S. Atomic Energy Commission, UCRL-8356 (1958).
8. Broida, H. P., J. Chem. Phys. 19, 1383 (1951).
9. Broida, H. P., Shuler, K. E., J. Chem. Phys. 27, 933 (1957).
10. Broida, H. P., Shuler, K. E., Rev. inst. franç. pétrole et Ann. combustibles liquides 13, 620 (1958).
11. Buell, B. E., Union Oil Co., Brea, Calif., private communications, 1960-62.
12. Buell, B. E., Anal. Chem. 34, 635 (1962).
13. Buell, B. E., "Limited area flame spectrometry. II. Chemiluminescence," Mid-America Spectroscopy Symposium, Chicago, May 1962.
14. Bugrim, E. D., Lyutyi, A. I., Rossikhin, V. S., Optika i Spektroskopiya 10, 801 (1961).
15. Calcote, H. F., "Eighth Symposium (International) on Combustion," p. 184, Williams and Wilkins, Baltimore, 1962.
16. Carnes, W. J., Ph.D. Thesis, University of Tennessee, Dec. 1961.
17. Carnes, W. J., Dean, J. A., Analyst, in press.

18. Curry, R. H., Iowa State University, private communications, 1960-1961.
19. David, D. J., *Nature 187*, 1109 (1960).
20. David, D. J., *Analyst 86*, 730 (1961).
21. Dean, J. A., Carnes, W. J., *Analyst*, in press.
22. De Jaegere, S., Deckers, J., Van Tiggelen, A., "Eighth Symposium (International) on Combustion," p. 155, Williams and Wilkins, Baltimore, 1962.
23. Egerton, A., Rudrakanchana, S., *Proc. Roy. Soc.* (London) *A225*, 427 (1954).
24. Fassel, V. A., Curry, R. H., Kniseley, R. N., *Spectrochim. Acta*, *18*, 1127 (1962).
25. Fassel, V. A., Curry, R. H., Myers, R. B., Kniseley, R. N., "Excitation of line spectra in fuel-rich oxyacetylene flames," International Conference on Spectroscopy, Washington, D. C., June 1962.
26. Fenimore, C. P., Jones, G. W., *J. Phys. Chem.* *65*, 1532 (1961).
27. Fueno, T., Mukherjee, N. R., Ree, T., Eyring, H., "Eighth Symposium (International) on Combustion," p. 222, Williams and Wilkins, Baltimore, 1962.
28. Gatehouse, B. M., Willis, J. B., *Spectrochim. Acta 17*, 710 (1961).
29. Gaydon, A. G., *Nature 165*, 170 (1950).
30. Gaydon, A. G., "Dissociation Energies," 2nd ed., Chapman and Hall, London, 1953.
31. Gaydon, A. G., "Energy Transfer in Hot Gases," p. 1, Natl. Bur. Standards *Circ*. *523*, Washington, D. C., 1954.
32. Gaydon, A. G., "The Spectroscopy of Flames," Wiley, New York, 1957.
33. Gaydon, A. G., Wolfhard, H. G., *Proc. Roy. Soc.* (London) *A194*, 169 (1948).
34. Gaydon, A. G., Wolfhard, H. G., *Proc. Phys. Soc.* (London) *63A*, 778 (1950).
35. Gaydon, A. G., Wolfhard, H. G., *Proc. Roy. Soc.* (London) *A205*, 118 (1951).
36. Gaydon, A. G., Wolfhard, H. G., *Proc. Phys. Soc.* (London) *65A*, 19 (1952).
37. Gaydon, A. G., Wolfhard, H. G., *Proc. Roy. Soc.* (London) *A213*, 366 (1952).
38. Gaydon, A. G., Wolfhard, H. G., "Flames, Their Structure, Radiation and Temperature," Chapman and Hall, London, 1953; 2nd edition, Macmillan, New York, 1960.
39. Gibson, J. H., Cooke, W. D., "Factors affecting excitation in flame spectroscopy," Pittsburgh Conference on Anal. Chem. and Appl. Spectroscopy, March 1961.

40. Gibson, J. H., Grossman, W. E. L., Cooke, W. D., "Excitation processes in flame spectroscopy," International Conference on Spectroscopy, Washington, D. C., June 1962.
41. Gilbert, P. T., Jr., "Symposium on Spectroscopy," p. 73, *Am. Soc. Testing Materials, Spec. Tech. Publ. No. 269*, 1960.
42. Gilbert, P. T., Jr., "Encyclopedia of Spectroscopy," p. 346, G. L. Clark, ed., Reinhold, New York, 1960.
43. Gilbert, P. T., Jr., Beckman Instruments, Inc., Fullerton, Calif., Bull. 753A (2nd ed.), 1961; Bull. 753B (3rd ed.), in press.
44. Gilbert, P. T., Jr., *Analyzer* (Beckman Instruments, Inc.) 2, No. 4, p. 3 (Oct. 1961).
45. Gilbert, P. T., Jr., Table 6-41, "Handbook of Analytical Chemistry," L. Meites, ed., McGraw-Hill, 1962 (in press).
46. Hartley, W. N., *Trans. Roy. Soc.* A185, 161 (1894).
47. Herrmann, R., Alkemade, C. T. J., "Flammenphotometrie," 2nd ed., Springer, Berlin, 1960; "Chemical Analysis by Flame Photometry," Wiley, New York, in press.
48. Honma, M., Smith, C. L., *Anal. Chem.* 26, 458 (1954).
49. King, I. R., *J. Chem. Phys.* 31, 855 (1959).
50. Knutson, K. E., *Analyst* 82, 241 (1957).
51. Lippincott, E. R., Steele, D., Caldwell, P., *J. Chem. Phys.* 35, 123 (1961).
52. Lundegårdh, H., *Lantbruks-Högskol. Ann.* 3, 49 (1936).
53. Lundegårdh, H., *Metallwirtschaft* 17, 1222 (1938).
54. Mavrodineanu, R., *Proceedings*, VIII. Colloquium Spectroscopicum Internationale, p. 15, Sauerländer, Aarau (Switzerland), 1960.
55. Mavrodineanu, R., *Spectrochim. Acta* 17, 1016 (1961).
56. Mavrodineanu, R., Boiteux, H., "L'analyse spectrale quantitative par la flamme," Masson, Paris, 1954.
57. Meggers, W. F., Corliss, C. H., Scribner, B. F., "Tables of Spectral-Line Intensities," Natl. Bur. Standards Monograph 32, Washington, D. C., 1961.
58. Mukherjee, N. R., Fueno, T., Eyring, H., Ree, T., "Eighth Symposium (International) on Combustion," p. 1, Williams and Wilkins, Baltimore, 1962.
59. Padley, P. J., Sugden, T. M., *Proc. Roy. Soc.* (London) A248, 248 (1958).
60. Padley, P. J., Sugden, T. M., "Seventh Symposium (International) on Combustion," p. 235, Butterworths, London, 1959.
61. Padley, P. J., Sugden, T. M., "Eighth Symposium (International) on Combustion," p. 164, Williams and Wilkins, Baltimore, 1962.
62. Robinson, J. W., *Anal. Chem.* 33, 1226 (1961).
63. Schmidt, W., *Beckman Report* (Beckman Instruments, G.m.b.H., Munich), No. 4, p. 6 (1961).

64. Shimauchi, M., Science of Light 9, 109 (1960).
65. Sternberg, J. C., Gallaway, W. S., Jones, D. T. L., "1961 International Symposium on Gas Chromatography," ISA Proc. 3, 159-184 (1961).
66. Van Tiggelen, A., Bertrand, J. N., Philippaerts, H., "Experimental investigations of ionization processes in flames," ASTIA document No. AD-258,050 (1961).

EXTREME ULTRAVIOLET SPECTROSCOPY

B. Vodar
Laboratoire des Hautes Pressions
CNRS, Bellevue (S. & O.) France

The vacuum ultraviolet spectrum extends from the beginning of the absorption of oxygen near 2000 A (5×10^4 cm^{-1} or about 6 eV) down to the wavelength region where crystal diffraction X-ray techniques are easily applicable, that is about 10 A (10^7 cm^{-1} or about 1200 eV).

This spectral range is characterized by the practical necessity of placing the whole apparatus in vacuum, because not only oxygen but all other gases including rare gases exhibit strong absorption regions; it is also characterized by the lack of transparent materials (in bulk thickness at least). The lowest transmission limits are those of calcium fluoride (1250 A) end of the Schumann region) and lithium fluoride (1050 A). Therefore reflection concave gratings are the essential dispersing instruments; under normal incidence reflecting power becomes so low at shorter wavelengths that the useful range ends at about 500 A (limit of the Lyman region); for shorter wavelengths grazing incidence is generally used together with more powerful sources (Millikan region).

Progress in the spectroscopy of the vacuum ultraviolet, which was rather neglected for a long time, was important in the past ten or fifteen years due mainly to three factors:

—Geophysical and astrophysical interest connected with the extension of the solar spectrum first below the absorption limit of ozone (2900 A), later below the limit of oxygen (1850 A), and finally down to the X-ray range (20 A); in particular the photochemistry of the upper atmosphere is produced by the energetic vacuum ultraviolet photons and more information on molecular spectra and photoionization yields is required.

—High temperature plasma research is directly related to the study of the short wavelength part of the optical spectrum, where the energies lie, expressed in degrees Kelvin, between about 5.10^4 °K and 10^7 °K; in that respect much new information is obtained from the vacuum ultraviolet emission spectrum of astronomical sources like the sun.

—The vacuum ultraviolet constitutes a wide, until recently almost unexplored, region for absorption and emission spectrochemical analysis: some recent developments like the analysis of metalloids by emission spectroscopy have led recently to some industrial applications.

Finally, the development of modern vacuum technology helped greatly in the design of improved laboratory instrumentation for far ultraviolet spectroscopy.

We will not attempt to present even briefly a consistent review of the subject, as a very important part of recent progress has been made in the USA, in particular for geophysical applications, and are described in the paper presented by Dr. Chubb. In the oral presentation we described essentially the subjects which were studied at Bellevue with some references to the work of others, when connected to the discussed topics. In the present paper we will restrict ourselves to a brief description on the contribution from Bellevue which was never so far published in the American literature.

A general survey of the present status of far ultraviolet spectroscopy is constituted by the whole set of papers contained in the "Proceedings of the First International Conference on Vacuum Ultraviolet Radiation Physics" organized last April by Dr. G. L. Weissler at the University of Southern California, and which will be published in full shortly in the J. Quant. Spectroscopy. Classical references on vacuum U. V. spectroscopy may be found in [1] and [62], in which is mentioned a review paper by E.C.Y. Inn.

Our activity in the spectroscopy of the vacuum ultraviolet started just after the war and was associated with the following names: J. Romand, Mme. Damany-Astoin, Schwetzoff, Mme. Johannin-Gilles, Mme. Granier, Mme. Robin-Solomon, Mme. Robin-Kandare, Melle. Balloffet, Roncin, Schwob, Chandrase-Kharan, Chameroy and Lotte. Some indications will be given on the work done at and/or in association with the C.E.A. (French Atomic Energy Commission) at Saclay (Julliot) and at Fontenay aux Roses (Hubert and Breton); work done in association with the I.R.S.I.D. (Research Institute for the Steel Industry) at St. Germain will be presented (Berneron).

Several subjects will be successively discussed; it is pointed out that, as none of the subjects was covered as extensively as it was desired at our laboratory, only a brief description of each of them will be adequate.*

---

*More details on older work are given in [62].

EXPERIMENTAL METHODS

Light Sources

Ordinary sustained gas discharges of the hydrogen lamp type were used essentially down to about 1000 A; a windowless high intensity lamp was designed [2, 3], whose main features include water cooled electrodes, and in which the slit is not used as an electrode.

More original sources were developed for the shorter wavelengths region. These sources are high vacuum sparks of various novel designs. They are to be described in the paper presented by J. Romand [4], and, as already said above, only brief remarks on these sources will be made here. Our work started in 1950 when we found [5, 6, 7] that a spark can be operated satisfactorily under a high vacuum provided that the discharge is propagated by surface ionization on a suitable insulator or semiconductor ("vacuum sliding spark"). The next step [8, 9] was to use this vacuum sliding spark for triggering the breakdown of another vacuum gap ("three electrode triggered vacuum spark"). Both of these sparks are reproducible and relatively stable pulsed sources (see Figure 1), producing high ionization

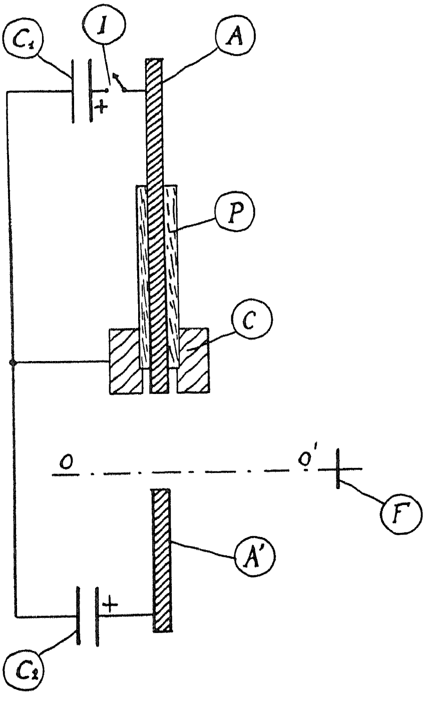

Figure 1

degree spectra like, for example, the O_{VI} spectrum; when used with heavy metal electrodes they emit a many line spectrum down to the limit of our grazing incidence spectrograph (about 100 A). Such many line spectra (emitted by uranium for example) were used as a background for studying continuous photoionization absorption spectra of gases in the extreme ultraviolet, and for studying absorption spectra of some solids. In emission these sparks had been applied to analytical spectrochemistry (detection of metalloids).

Recently a modification of the three electrode triggered vacuum spark permitted obtaining an intense continuous spectrum [10, 11] extending from the visible down to the limit of our direct observations (80 A) and even possibly down to the soft X-ray range. It is hoped that this source can help the development of higher resolution spectroscopy in the whole range of the vacuum ultraviolet (see Figure 2).

In Figure 3 is reproduced a microphotometric recording of the absorption spectrum of nitrogen (upper curve) taken with this source; the lower curve corresponds to the spectrum of the source, which appears as a clean continuum, practically without emission or absorption lines. More detailed information on the development of vacuum sparks at Bellevue can be found in [4] and in the paper presented at this Conference by J. Romand, Melle. G. Balloffett and B. Vodar.

Photographic Spectrophotometry

Both photographic and photoelectric spectrophotometric methods were used. For photographic spectrophotometry the calibration of the sensitive emulsion was checked by wire screens [12, 13], in the case of a grazing incidence spectrograph, where the angular aperture of the beam is small, the screen used was a fine mesh electron microscope wire screen placed near and behind the slit [7].

Elimination of Spectra of Different Diffraction Orders

In the case of a many line spectrum (as produced for example by a vacuum sliding or triggered spark) and a grazing incidence spectrograph the identification of lines is difficult. Prism predispersion, as used for instance by Herzberg, is not applicable in the shorter wavelength range below the limit of lithium fluoride transmission. Therefore we proposed [14] and used a simple method which helped us considerably, i.e., the use of the so-called "external" total reflection on a mirror; wavelengths shorter than those corresponding to the cut-off limit are much less intensely reflected in the case of our tests

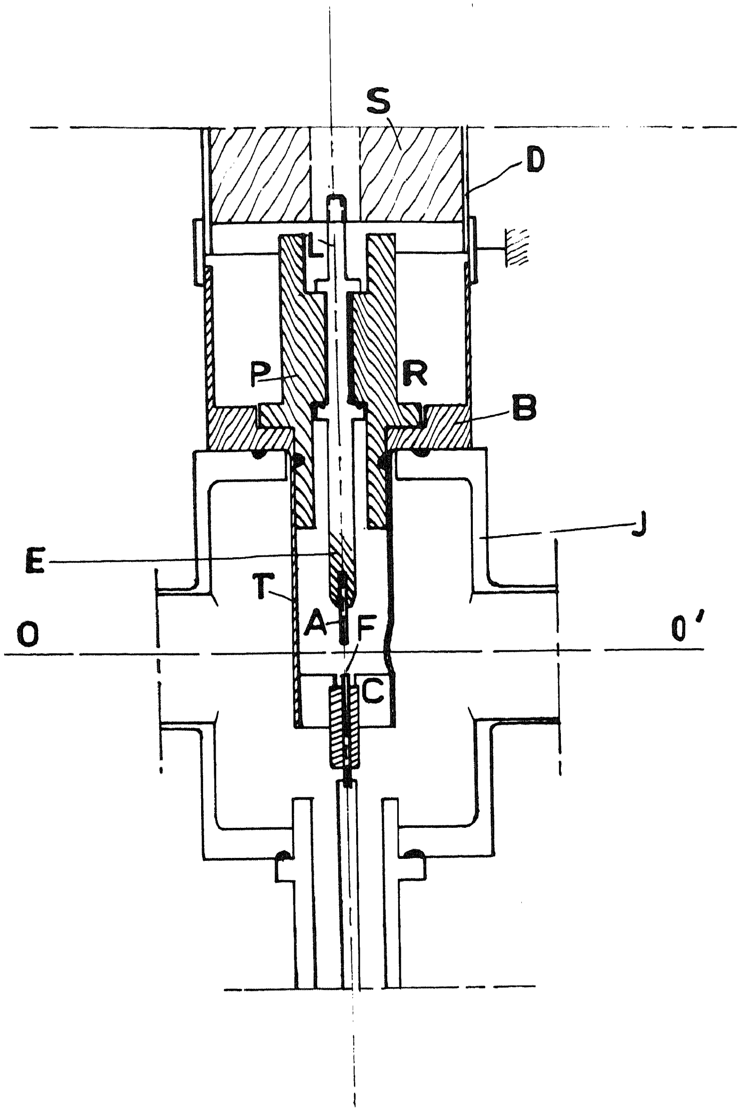

Figure 2

on a grazing incidence spectrograph having intense second and fourth order spectra; we were able to reduce greatly the intensity of the second order and to eliminate completely the fourth order by the use of one single reflection, thus making the identification of the first order spectrum much easier over the studied range extending from 600 to 800 A. This method or its various possible extensions can also be helpful in the case of a continuous

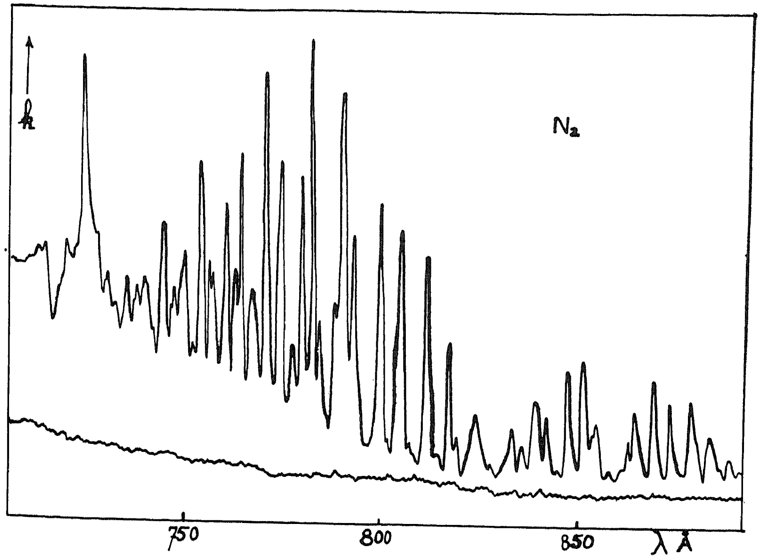

Figure 3

spectrum, where overlapping is a very serious problem. Grating predispersers [15], as used by others, are certainly very interesting, but obviously do not solve simply and entirely the problem, as the grating relation applies equally to all gratings, and therefore the elimination which may be observed relies only on a special distribution of intensities in the different orders. It seems for that reason that "total reflection filtering" might be a useful simple method.

Silicon Monoxide Films as Windows or Transparent Substrates

Thin organic films, such as collodion films, are transparent but not thermally stable; therefore we looked for thermally more resistant films, and studied films made of evaporated silicon monoxide [16] which are transparent down to about 120 A and can withstand a pressure difference of a few mm of mercury. They may be used as substrates for evaporated solid materials or as windows for absorption cells.

Photoelectric Receivers

Until recently mostly ordinary commercial photomultipliers were used, in combination with the fluorescent screen method (sodium salicylate) [3], in which the screen placed in vacuum converts the vacuum ultraviolet light to visible or near ultraviolet light that reaches the photomultiplier through a glass or quartz window. Recently, Julliot and co-workers at C.E.A. (Saclay) have studied some organic phosphors and found that vacuum evaporated terphenyl was 50% superior to the conventional sodium salicylate layers [18]. It may be recalled here that, at an earlier stage, thin bubble quartz ("Homosil") window magnetic photomultipliers were built and tested [19, 20]; whereas their range was limited by the transmission limit of the window (1450 A), they seem to have been the first photomultipliers directly sensitive in the near Schumann region; their signal-to-noise (or rather background) ratio was better than in the fluorescence method. Because of this latter result, and mainly because of the detailed data published in the USA on windowless photomultipliers, more recently electrostatic photomultipliers of this type were developed by Julliot and coworkers at the C.E.A. (Saclay) and they have been tested partially in collaboration with us [18]. A description of these photomultipliers was included in the program of this Conference. They are composed of a wide venetian blind photocathode followed by an electron condensing system, a number of electrostatic copper-beryllium dynodes, and a collecting anode, a few different metals were tested as materials for the photocathodes.

Figure 4 shows the sensitivity of a windowless photomultiplier of this type (with a gold cathode and oxidized Cu Be cathode) with respect to the fluorescent method (with terphenyl combined with a commercial photomultiplier from "Radio-technique"); in addition the response of a Bendix windowless photomultiplier with a stainless steel cathode has been incorporated in this figure; it is clear that the direct reading photomultiplier is superior in regard to the signal-to-background ratio.

Such windowless photomultipliers are utilized in a multichannel direct reading analytical normal incidence concave grating vacuum spectrometer; they have been applied also to multichannel time-resolved spectroscopy with the same spectrometer; for both of these applications the photomultipliers are mounted as shown in Figure 5 behind a number of exit slits of the spectrometer.

EMISSION ATOMIC SPECTROSCOPY (ANALYTICAL APPLICATIONS AND PLASMA PHYSICS)

Both of these applications are based on an extension of the well known Meggers rule which was proposed [25, 22, 21] and verified experimentally, and according to which the most intense line of an element corresponds to an s-p transition either of a neutral atom or of the ion having only one electron left on the outer shell (hydrogen-like ion, for example O_{VI}). According to the Balmer formula, these spectra for most of the elements

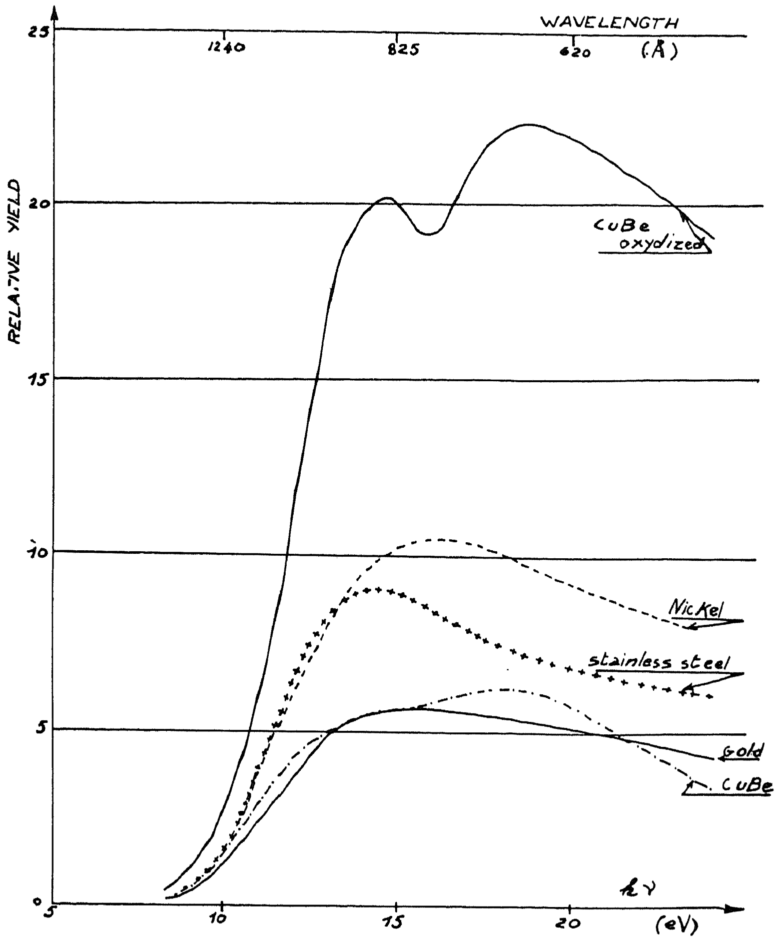

Figure 4

correspond to high energy transitions lying in the vacuum ultraviolet. The lines of some nonmetallic elements which correspond to such transitions are listed on Table 1; it was verified experimentally that these lines are indeed the most sensitive and the most intense lines of these elements [22].

It is well known that emission spectrochemical analysis of solids was generally limited, in the usual spectral ranges, to metallic elements. By extending the spectral range to the long wavelength part of the Schumann region (down to 1600 or 1500 A) with a usual spark in argon gas, and a window between the source and the vacuum spectrograph, it was possible to reach more intense lines of neutral atoms of C, S and P and to analyze these elements. This procedure is used presently, as it is well known, in a number of commercial instruments. On the other hand, by

Table 1

Wavelengths of Sensitive Lines

Element	Carbon	Nitrogen	Oxygen	Fluorine
Degree of ionization	IV	V	VI	VII
$2s^2\,S_{1/2} - 2p\,^2P_{3/2}$	1548.195	1238.800	1031.912	883
$2s^2\,S_{1/2} - 2p\,^2P_{1/2}$	1550.768	1242.778	1037.613	891
Degree of ionization	III	IV	V	VI
$2s^2\,{}^1S_0 - 2sp\,{}^1P_1^0$	977.026	765.140	629.732	535.204

Element	Silicon	Phosphorus	Sulfur	Chlorine
Degree of ionization	IV	V	VI	VII
$3s^2\,S_{1/2} - 3p\,^2P_{3/2}$	1393.73	1117.979	933.382	800.698
$3s^2\,S_{1/2} - 3p\,^2P_{1/2}$	1402.73	1128.006	944.517	813.002
Degree of ionization	III	IV	V	VI
$3s^2\,{}^1S_0 - 3sp\,{}^1P_1^0$	1206.52	950.669	786.476	--

Element	Germanium	Arsenic	Selenium	Bromine
Degree of ionization	IV	V	VI	VII
$4s^2\,S_{1/2} - 4p^2\,P_{3/2}$	1188.99	967.69	844.15	736.09
$4s^2\,S_{1/2} - 4p^2\,P_{1/2}$	1229.81	1029.50	886.82	779.58
Degree of ionization	III	IV	V	VI
$4s^2\,{}^1S_0 - 4sp\,{}^1P_1^0$	1088.46	892.68	759.11	661.05

Element	Tin	Antimony	Tellurium	Iodine
Degree of ionization	IV	V	VI	VII
$5s^2\,S_{1/2} - 5p^2\,P_{3/2}$	1314.45	1104.32	951.01	?
$5s^2\,S_{1/2} - 5p^2\,P_{1/2}$	1437.63	1226.00	1071.40	
Degree of ionization	III	IV	V	VI
$5s^2\,{}^1S_0 - 5sp\,{}^1P_1^0$	1251.43	1042.21	895.20	--

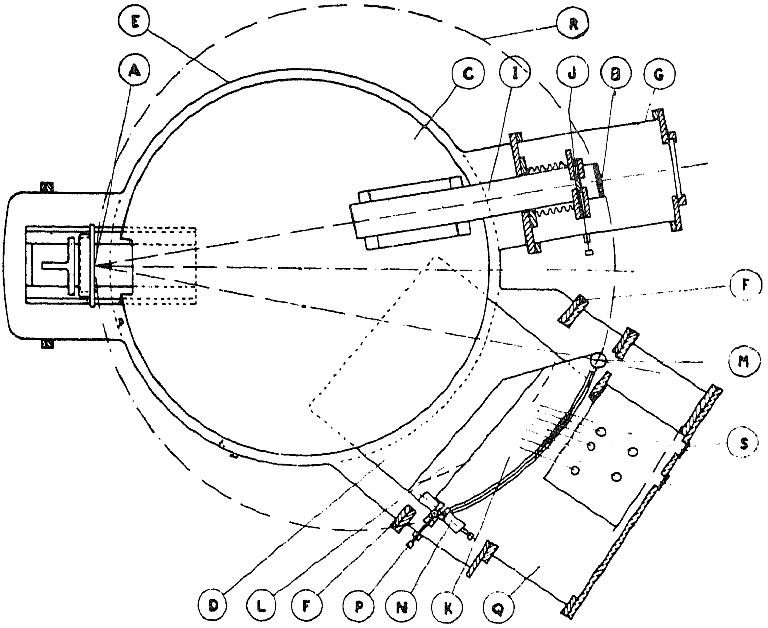

Figure 5

using a sliding or triggered vacuum spark, the excitation energy is higher and no window is required; therefore there is no limitation towards the short wavelengths and, as may be seen in Table 1, not only the analysis of C, S, and P [23], but also the analysis of gases like N and O is possible [24]; for example Figure 6 shows the results obtained for nitrogen in steel samples by direct reading photoelectric photometry; quantitative analysis of N and O in steels and titanium [24] can be made down to 100 ppm (0.01%) or even lower concentrations (on Figure 6 the lowest point corresponds to 5 ppm); Figure 4 shows also that the windowless photomultipliers (upper curve) give better results because they are less sensitive to stray light. Similar but less detailed data have been obtained for the analysis of various metalloids including halogens [26, 22] in some oxides as well as in some semiconductors (oxygen in cadmium sulfide single crystals). It may be added here that high ionization lines of the rare gases (neon V_{III}) were obtained in Israël by Frankel and coworkers [27] with the triggered vacuum spark using a gas saturated anode.

Time-resolved spectroscopy with simultaneous recording of the intensity versus time of several vacuum ultraviolet lines [28] was developed at the C.E.A. (Atomic Energy Establishment) at Fontenay aux Roses in collaboration with our group. The one meter direct reading normal incidence grating spectrometer

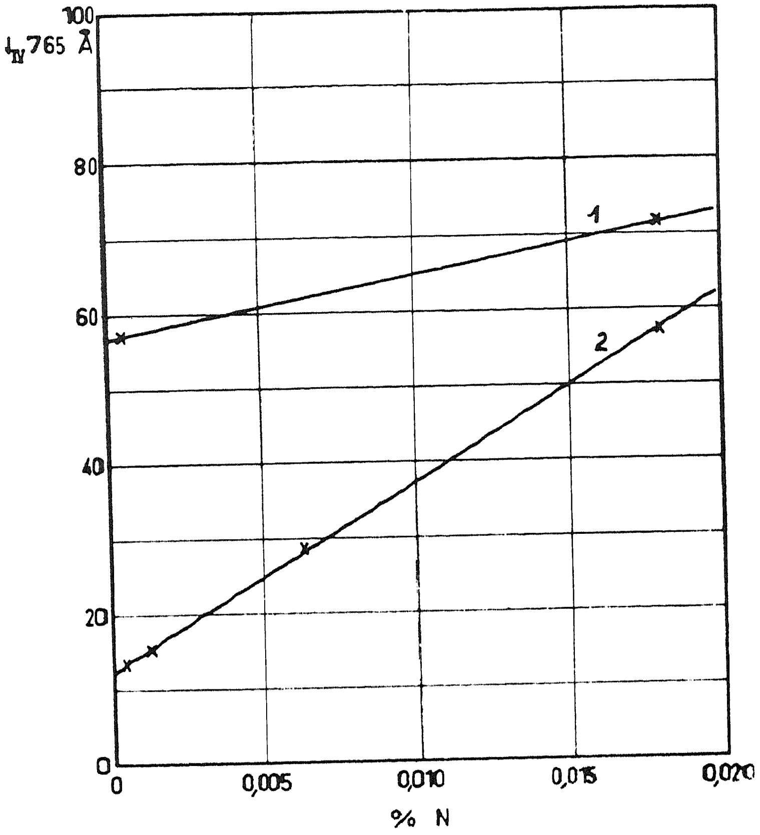

Figure 6

(see Figure 5) was used, mainly, so far, for detecting impurities in high temperature plasmas, like the one produced in the toroidal apparatus called TA 2000. An example of the detection of nitrogen is given in Figure 7 for lines of various ionization degree (from N_{II} to N_V); when nitrogen is injected from the walls into the discharge by an arcing process, the behaviour is erratic in intensity and in time; when nitrogen is added purposely, one notes that then the lines appear earlier and their behaviour is more reproducible; it may be noted also that higher ionization lines are consistently delayed with respect to the lower ionization lines. This seems to be in agreement with a purely electronic excitation process of the plasma. This delay is shown more clearly in the case of several lines of oxygen ranging (from O_{II} to O_{VI} (Figure 8)).

The grazing incidence spectrograph was also used for detecting impurities in the same TA 2000 plasma. Over the spectral range of this apparatus it was possible to detect not only O

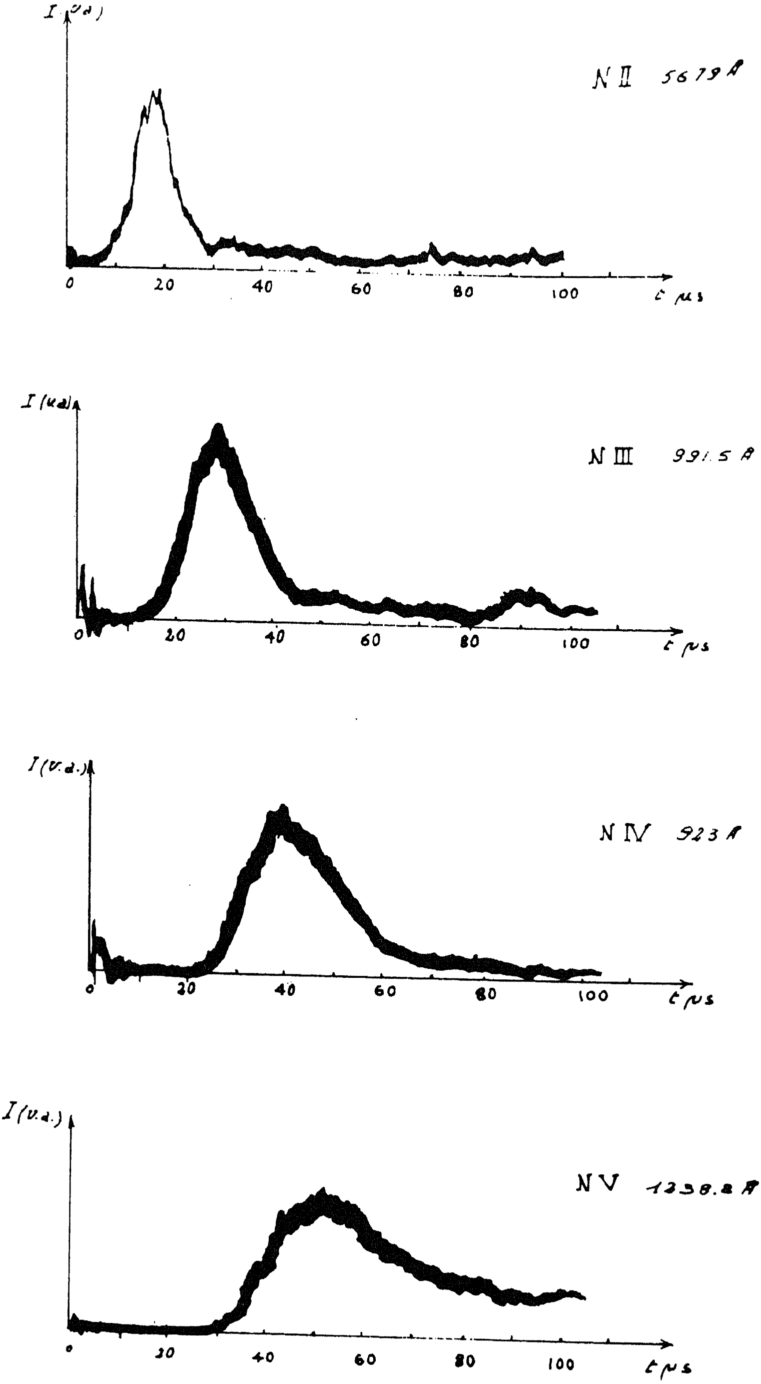
I (u.a.)
N II 5679 Å
0
20
40
60
80
100
t μs
I (u.a.)
N III 991.5 Å
0
20
40
60
80
100
t μs
I (u.a.)
N IV 923 Å
0
20
40
60
80
100
t μs
I (u.a.)
N V 1238.8 Å
0
20
40
60
80
100
t μs

Figure 7

but also Si, in the case when a silica probe (for field measurements) was present in the discharge; the shortest wavelength line detected was a SiX line at 51 A.

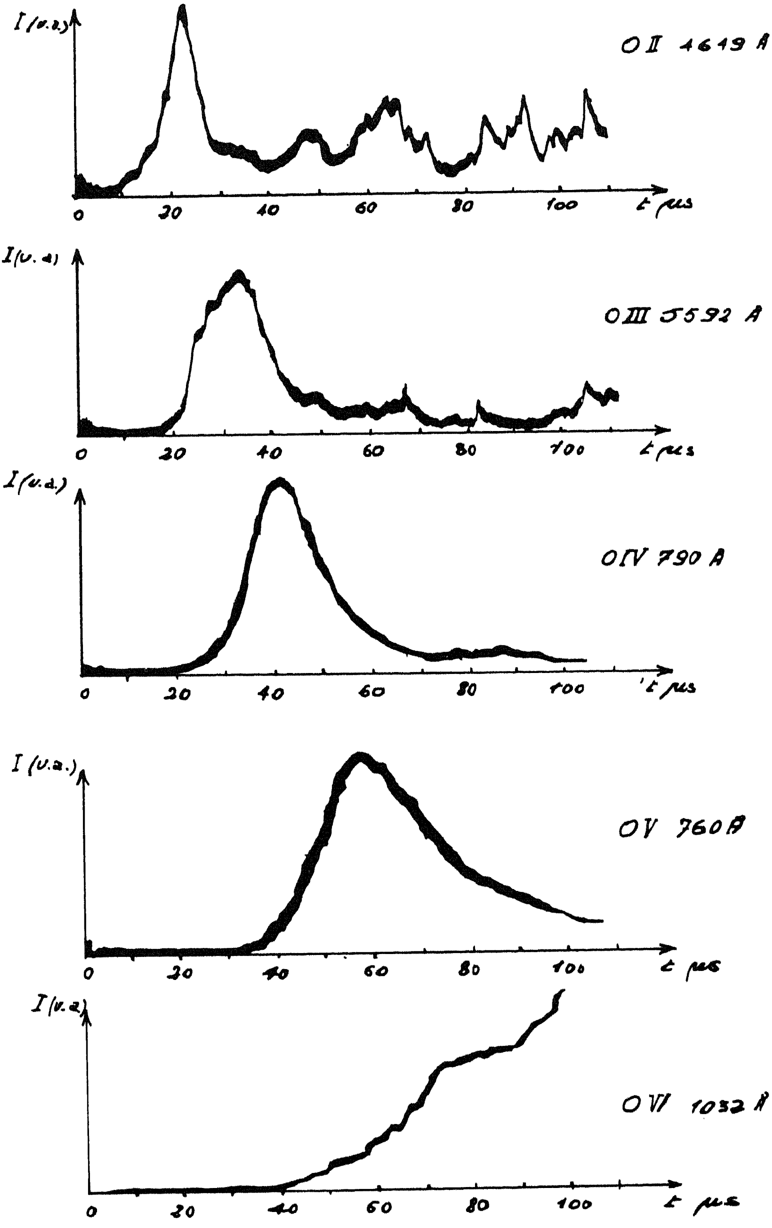

Figure 8

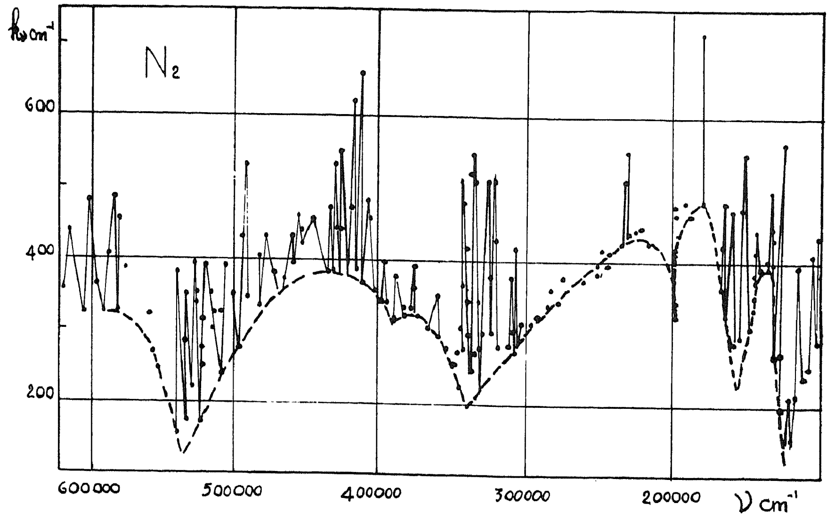

Figure 9

CONTINUOUS ABSORPTION OF GASES IN THE EXTREME ULTRAVIOLET

These investigations were exclusively performed by photographic spectrophotometry with a grazing incidence spectrograph and as a source the sliding vacuum spark or the triggered vacuum spark. The gases to be studied were directly introduced into the body of the spectrograph, and the pressure was measured with diaphragm manometer of high sensitivity and accuracy. The spectral range of these measurements extended from 1000 to about 100 A. Therefore our work in this field simply extends to shorter wavelengths the numerous results obtained by others, namely by American scientists and in particular by Weissler and coworkers.

The following gases have been studied [1, 29]: N_2, NO, N_2O, H_2O, D_2O, CO_2 and CH_3OH; oxygen is being presently investigated.

As many of these results are old and have been published in full, we will only give here three examples.

The spectrum of nitrogen [30, 29], as obtained from our measurements, is reproduced in Figure 9. As the background used for obtaining these data is a many line spectrum, the absorption coefficient is measured for each line; therefore no structure of the spectrum can be resolved, and the only meaningful points are the lower ones, which should correspond to the continuous photoionization absorption. From the curve corresponding to these points are deduced the photoionization discontinuities and the photoionization potentials. At the time of this publication [30] the following assignments were given (some of them tentatively only) to the observed potentials.

127,000 cm^{-1} (15.6 eV) first potential of N_2 (see Weissler)
152,000 cm^{-1} (18.9 eV) second potential of N_2 (see Weissler)
197,000 cm^{-1} (24.5 eV) N^+ (4S) + N (3P)
or N_2^+ $(C^2\Sigma^+)$
340,000 cm^{-1} (42 eV) N (2P) + N^+(3P)
or N_2 ++ ?
} Ionization with or without'dissociation

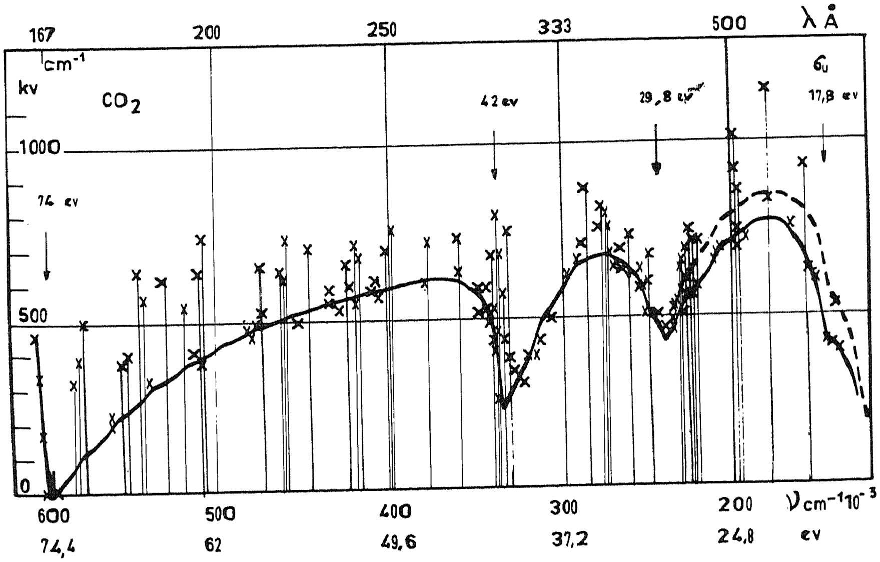

Figure 10

390,000 cm^{-1} (48.5 eV) N_2^{++} ?
530,000 cm^{-1} (66 eV) N^{++} ?
} Double ionization
for N(2P) + N^{++} (4P)

The absorption spectrum of CO_2 [31] is given in Figure 10 between 1000 and 160 A and compared with the data of Sun and Weissler [32], with which there is good agreement in the common range.

The corresponding ionization potentials are:

144,000 cm^{-1} (17.8 eV) 2nd I.P. (the first one being at 13.7 eV, outside the range of our measurements)

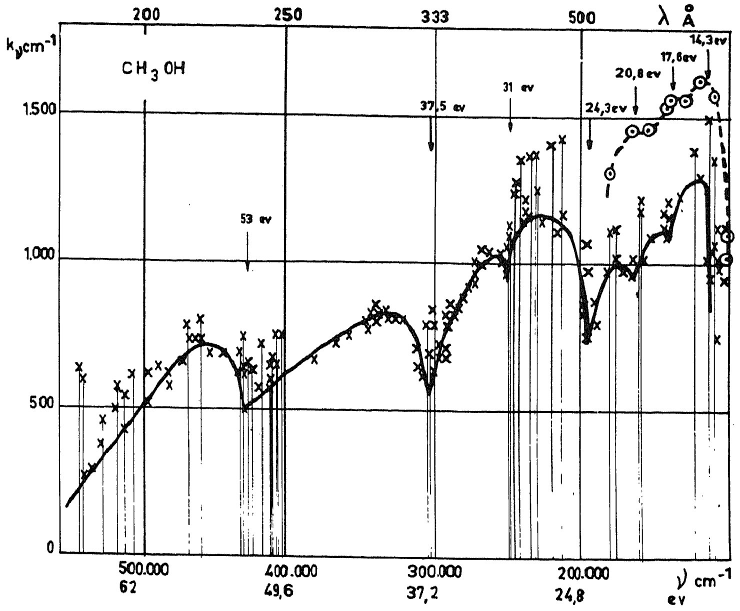

Figure 11

240,000 cm^{-1}	(29.8 eV)	$C^+ (2P) + 2O (4S)$ or more likely $CO^+ (B^2+) + O (D)$, similar to the process found for N_2O
340,000 cm^{-1}	(42 eV)	$C + O^+ + O$ (?)
600,000 cm^{-1}	(74 eV)	certainly a double ionization process

Figure 11 gives similar results for CH_3OH [33] between 600 and 160 A, and their comparison with the Ogawa and Cook [34] data. The following tentative assignments were made for the ionization potentials:

14.3 eV	Ionization of the y' orbital of the O-C bond Calculated value according to Mulliken: 16 eV)
17.6 eV	z'orbital of OH (calculated by Mulliken: 17.5 eV)
20.8 eV	s orbital of CH_3 (calculated by Mulliken: 22 eV)
24.3 eV	$CH_2OH^+ + H(2P)$ or $CH_3^+ + O(^1S) + H(^2S)$ or $COH^+ + H_2 + H(2P)$
31 eV	2S electron in O_2 (Mulliken: 32 eV)

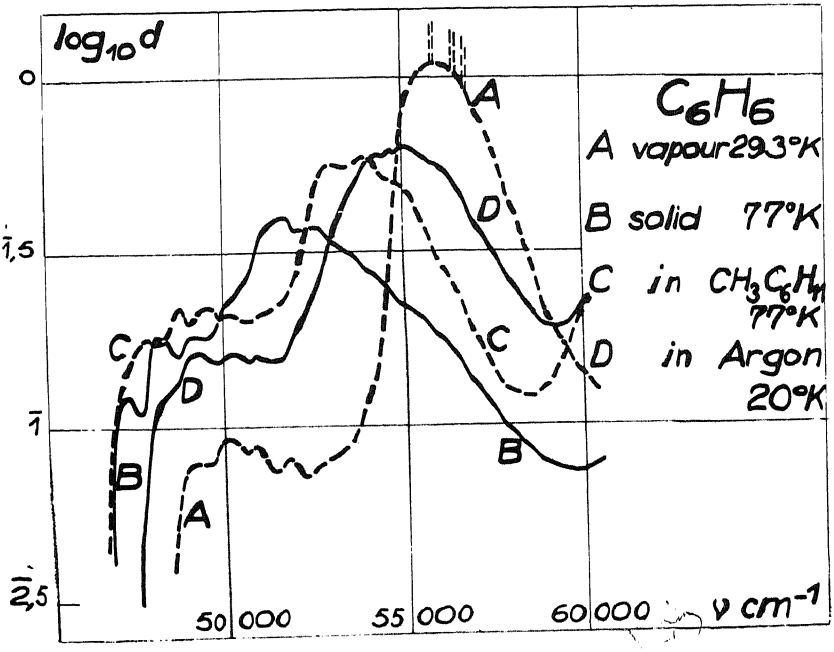

Figure 12

37.5 eV	double ionization
53 eV	double ionization

It may be remarked that the theoretical values [35] are generally in fair agreement with the experimental ones, but that they are somewhat higher, probably because environmental effects were neglected in these calculations.

ABSORPTION SPECTRA OF CONDENSED GASES AND VAPORS

Several years ago an optical cryostat, similar to the one used by Thomas at Göttingen, was built [36] and some data were obtained on the absorption spectra of solid O_2 [37], N_2O, NO [38] and C_6H_6 down to liquid hydrogen temperatures in the Schumann region.

Formation of NO by photo dissociation of solid N_2O was detected [40]; this result, which may be regarded as the formation of frozen species in a solid matrix, is being reinvestigated presently by the method of condensation on a cold window, as developed by Broida and by Pimentel.

Studies on the spectra of solids are of particular interest for us, as they can be connected with the general problems of pressure broadening, shifts and induced absorption, which are being studied in compressed gases up to densities reaching the density of the solid phase.

Because of the complexity of the interpretation of such phenomena in dense media, we can only give here a few examples and conclusions of a qualitative nature.

For NO and O_2 there is a very likely association in the solid state. At least the spectra are completely different from those of the free molecules, and shift to longer wavelengths ("red" shift).

In the case of benzene [41] the results are rather complex, as shown on Figure 12. This figure corresponds to the "forbidden" transition $^1A\ 1g \rightarrow {}^1B_{1u}$ at 2100 Å in the vapor, and to the allowed transition $^1A_{1g} \rightarrow {}^1E_{1u}$ at 1850 Å in the vapor; curve A refers to the vapor; curve B to the pure solid at 77°K, and curve C to benzene frozen in methylcyclohexane at 77°K. One observes a red shift from the vapor to the solid phases. Other conclusions are given in the original papers [41, 42].

The opposite shift, a blue shift, was found in the case of ICH_3 and similar bromine and chlorine compounds [43, 42]. This is probably at least partly due to the polarity of the hydrogen halide molecules in the ground state; as a matter of fact, if, in the excited state the polarity is suppressed or reduced, the net effect of the polar interactions is to shift the spectrum to higher energies ("blue" shift).

The question of what happens to the Rydberg lines in dense states is not definitely answered by our results; these lines are completely absent at 77°K but at 20°K it seems that some structure comes out. It may be assumed provisionally that the Rydberg lines merge in a continuum, but further work at lower temperature and in rare gas matrices appears necessary, and is now in progress. (A study of atomic species trapped in condensed matrices was started to complete the investigations carried on by McCarty and Robinson [45] and Dressler and Schnepp [30].) Figure 13 exhibits the results on the 2nd resonance line of mercury trapped in isopentane and argon at 20°K [44]. The line is broadened to a band. It may be remarked here that in the gas phase a broadening and an "induction" of satellites were observed [46]. The band in the solid seems to correspond to one of these satellites. These satellites are not well understood [47, 48, 49] but they are evidently due to close range interactions; the data obtained in the solid phase, where the bands are sharper, may contribute to a better understanding of satellites. It should be noted also that in the isopentane matrix a structure of the band is observed, which may be due to a coupling of the electronic transition in mercury with the frequency of one of the vibration modes in isopentane. Results similar to

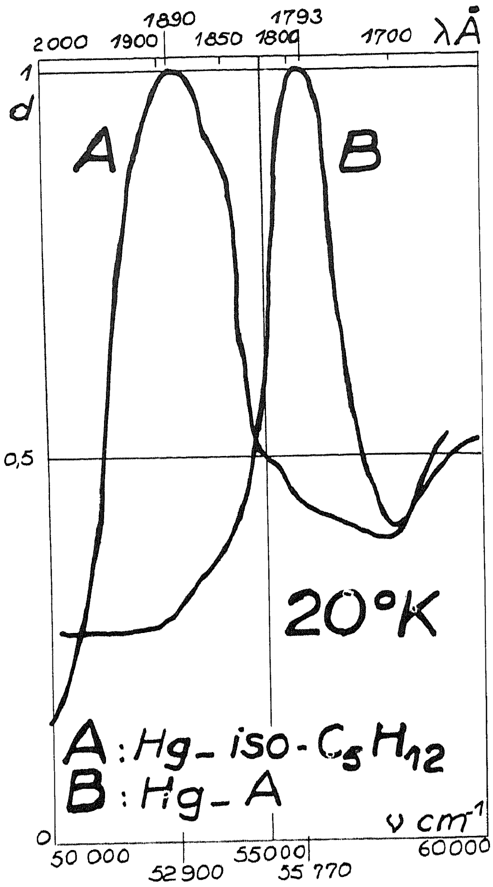

Figure 13

these obtained with frozen atomic species might possibly be obtained with sharp electronic transitions in molecules, which are quite frequent in the vacuum ultraviolet (lone electron spectra).

As a conclusion to this section one must mention the interesting results obtained more recently by other workers, and which were presented at this Conference by Dressler [50]. In particular one should note that a fine structure was detected, for example in the case of oxygen; this new and important observation was possible because rare gas matrices (and not pure solid oxygen) were used and because the temperature was lower.

REFLECTION AND ABSORPTION OF SOLIDS

Reflection and absorption spectra of a few solids, in bulk state and in evaporated layers, were studied in various spectral regions, varying from the visible to about 100 A.

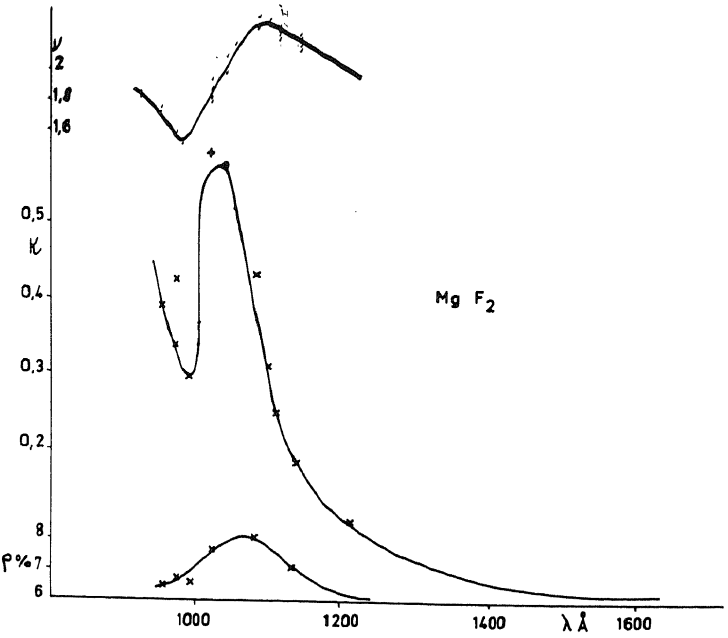

Figure 14

(1) Reflecting powers of some solids were studied between 3000 A and 1000 A several years ago by Mme. Robin Solomon [51, 52], by a method involving two measurements made at two different angles of incidence [51], with photoelectric receivers and a 1 meter normal incidence monochromator.

(2) More recently some work was carried, with the same equipment, for determining the optical constants of evaporated MgF_2. The method used [53, 54] is the following: one evaporates a wedge of MgF_2 onto a certain substrate (glass for example); the thickness (y) versus length (x) of this wedge is measured by usual interference methods, the wedge is mounted behind the exit slit of the monochromator and the reflective power near normal incidence is measured as a function of the displacement. Assuming that the absorption of the MgF_2 layer is not large and taking into account only two interfering reflected beams, from the reflected intensity curve versus the thickness (y), one can obtain graphically the refractive index ν, the extinction index κ and the reflective power ρ (Figure 14). This method is independent of the optical constants of the substrate; this point is, in our opinion, important because the optical properties of a surface are, in the vacuum ultraviolet region, very sensitive to many factors. As it can be seen in Figure 14, the extinction index is much larger, outside of the high absorption region, than

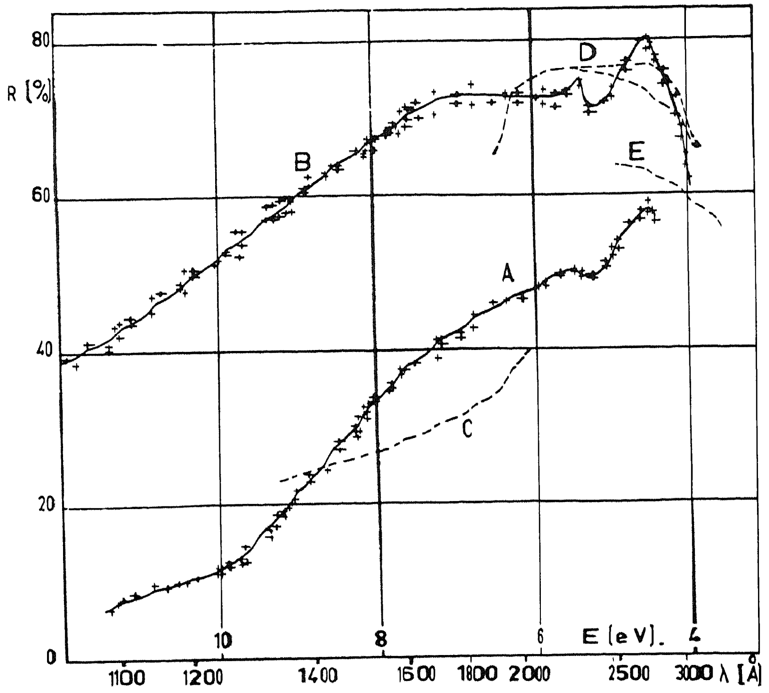

Figure 15

for the bulk single crystal. Whether this is due to some possible impurities introduced during evaporation or to structural properties (possibly scattering) of the evaporated layers is not yet established. On the other hand, a variation of each constant as a function of the thickness of the layer (different positions of the wedge) was found; the method is particularly convenient for studying such thickness effects.

(3) Mme. Robin-Kandare performed a systematic study of some semiconductors Ge, Si, Se, Te [55, 56]. Reflection and absorption spectra of evaporated layers and in certain cases of bulk single crystals were obtained. The spectral range which was covered extends from the visible down to 100 Å (but reflectance measurements were not made below 1000 Å).

We will here briefly mention some of the results obtained from these investigations.

High reflectance was found for silicon, confirming the remark which was already made by Lyman in his book [57]. The importance of the surface structure (and probably of the oxide layer) is demonstrated on Figure 15: curve (A) corresponds to an optically polished silicon single crystal; whereas curve (B) was obtained with an etched and subsequently lightly polished surface. This result seems to have a general meaning: the reflective power is high only if the "amorphous" surface layer is not too thick. For bulk materials etching improves the reflective power (as shown on Figure 15) while for evaporated layers an adequate heat treatment prior to exposure to the atmosphere produces a well developed crystalline structure; and the reflective power of this crystalline layer may be also quite good. Exposure to the atmosphere before heat treatment prevents the crystallization of the layer, as was shown by reflected electron diffraction patterns; under these conditions the reflectance remains poor.

Evaporated germanium was found to be also a reasonably good reflector, and as it is easier to evaporate and less

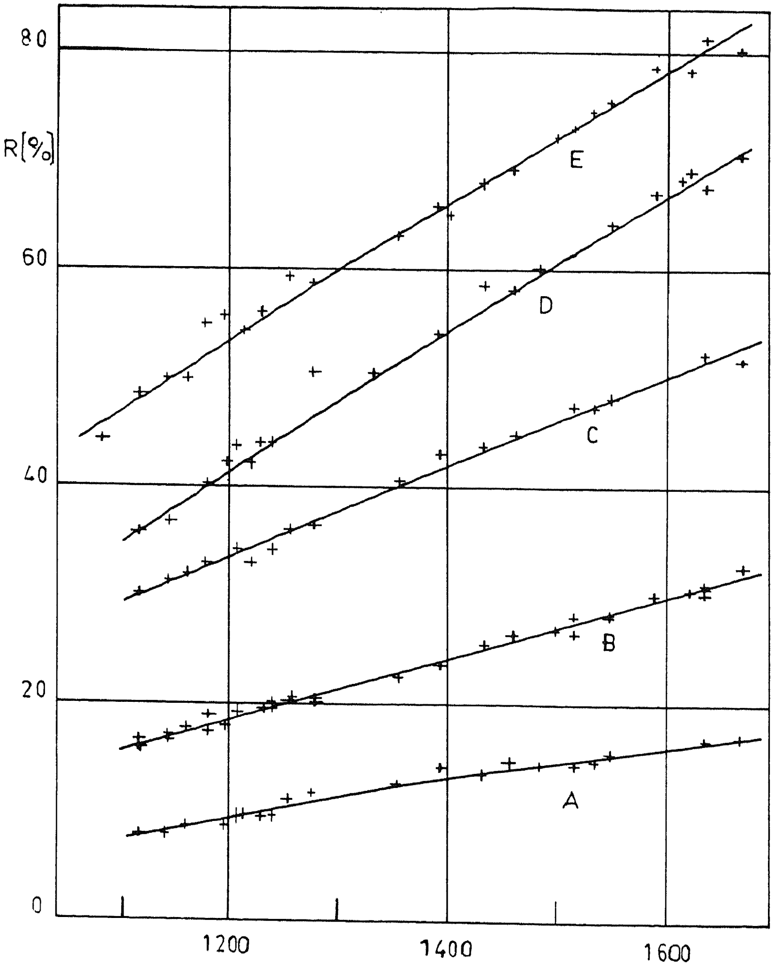

Figure 16

sensitive to aging in air, it was used practically in optical parts. Evaporation conditions were shown to affect tremendously the reflectance of germanium layers; in particular, when evaporating from tantalum heaters, reflectance of germanium depends on the temperature of the heater; very high reflectances can be obtained for high temperature (faster) evaporations, Figure 16, but they are rapidly, because, possibly, of contamination by tantalum. For germanium films prepared by electron bombardment heating, the reflectance is not so high as the reflectance of the interference films described by Hass and Tousey [58] but it exhibits a reasonable value over a large spectral range. We used successfully germanium coating of Bausch and Lomb replica gratings, after their aluminium layer was stripped off.

In absorption generally only amorphous layers were studied. The substrate was a thin film of plastic ("parlodiun") and therefore no heat treatment was possible. Selenium, according to Givens [59], can be crystallized at moderate temperatures by evaporation onto a very thin tellurium layer; therefore selenium was studied in absorption both in "amorphous" and in crystalline states (except for the thinnest layers, which do not crystallize).

Vacuum ultraviolet spectra, and particularly absorption spectra which are more characteristic, give wealthy and detailed information on the electronic band structure of semiconductors. As an example, Figure 17, which exhibits the absorption spectrum of an "amorphous" layer of selenium between

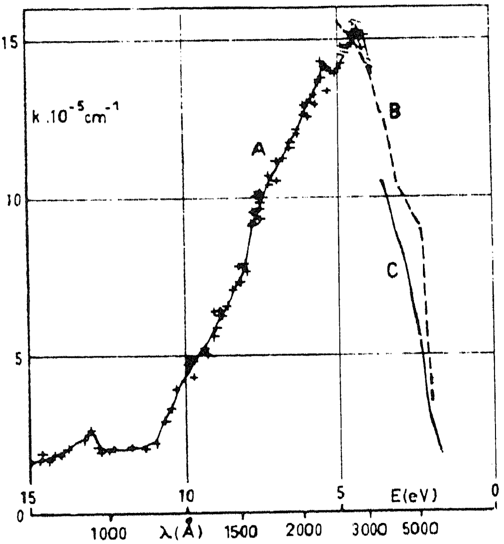

Figure 17

2500 and 500 A, shows 3 maxima. According to the theoretical considerations developed by Reitz [61] the 4p state is split into three bands, p_1, p_2, p_3 in the hexagonal lattice of selenium (helicoidal molecular chains along the c axis, with a bond angle of 105°). The lower bands p_1 and p_2 (together with the s band) form the valence band; the upper p band p_3 (together with the d band) forms the conduction band. From longer to shorter wavelengths the observed peaks should correspond to the following transitions: $p_2 \rightarrow p_3$ (near 2500 Å); $p_2 \rightarrow d$ (weak maximum near the preceding one, due to the onset of transitions to the d band, which overlaps the p_3 band); $p_1 \rightarrow p_3$ (strong maximum near 1500 A); in addition there is possibly a fourth maximum near 750 Å which was not ascertained experimentally because the number of experimental points in this region was not large enough (the background, as usual in this range, was a line spectrum produced by a sliding vacuum spark); the corresponding transition could be a $p_1 \rightarrow d$ transition.

The absorption spectrum of an "amorphous" layer of selenium in the shorter wavelength region corresponding to "internal transitions" is reproduced on Figure 18 together with the earlier data of Givens [60] with which there is a fair agreement in the common spectral range. The large number of experimental points (obtained with a many line source) made it possible to obtain some relatively fine details which could not be detected otherwise (except by using a continuous spectrum source). There are two main absorption regions, one near 28-30 eV and another near 55-57 eV. The latter corresponds to a transition from a $M_{4,5}$ (d) band to the conduction band; this maximum exhibits a substructure (at least a splitting in two components), which confirms the fact that the M band is double. The first maximum near 28-30 eV corresponds to a N_1 (45° conduction band) transition; as the N_1 (4S) band is simple, whereas the experimental

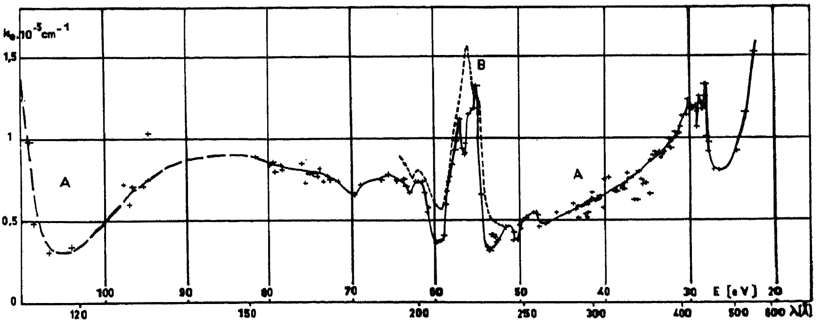

Figure 18

curve exhibits a substructure (at least a double peak) it should be concluded that the conduction band is complex.

A similar absorption spectrum is observed (Figure 19), when crystalline hexagonal selenium is studied, except that there is a fine structure of the background, which is the structure well known in the X-ray range under the name of the Kronig structure, due to the selection rules on the momentum of the photoelectron (if the momentum reaches the surface of the Brillouin zone, the Bragg relation for the associated wave is satisfied and the corresponding transition is forbidden, which means that the absorption should exhibit a number of minima). Vacuum ultraviolet is interesting for studying such a structure, because of the high resolution in energy units as compared to the one available in the X-ray spectrum. The point which we would like to stress here is simply how sensitive are the Kronig bands (and also the shapes of the main transitions) with respect to the crystalline structure of the solid; this is obvious from the observations of Figures 16 and 17. Therefore, the "internal transitions" spectrum may be, together with the study of reflective powers, a powerful means for studying the imperfections of solids in thin layers and, more generally, the surface physics of solids.

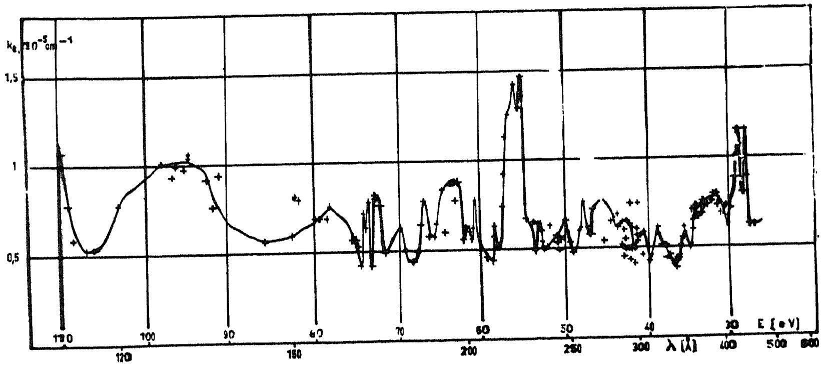

Figure 19

INSTRUMENTATION

The following spectroscopic instruments for the far ultraviolet have been designed at Bellevue and are manufactured industrially in France:

(1) A normal incidence 1-meter grating spectrograph equipped with a vacuum spark chamber, for the spectro-chemical analysis of metalloids and gases in metals, especially in steel [63, 64, 23]. A photoelectric attachment with several exit slits

and photomultipliers (with and without window) is associated, the whole assembly being a direct reading apparatus (see Figure 5).

(2) A grazing incidence (85°) 3-meters grating spectrograph, for the general purpose of emission and absorption work in the extreme ultraviolet [65]. This apparatus is divided into three sections, each separated from the other by vacuum valves. The principal section contains the grating. Another one contains the photographic film-holder and the isolation from the grating section allows changing the film without letting air enter into the principal section. The motion of the film holder and the width adjustment of a slit limiting the height of the spectrum on the film, are controlled externally. The combined use of two shutters allows one to insert the film holder or to withdraw it from the instrument in a lighted room. Lines down to about 60 A have been recorded with this apparatus from hot plasma discharges as mentioned above.

(3) A normal incidence 1-meter grating monochromator. In this apparatus [67] the grating (see Figure 20) is fixed at a right angle to one end of an arm OA which is connected to a second arm OB, the B end of which is attached at a fixed point. The grating is located on a carriage moving along the direction XX' passing through B. The two slits are near B and separated from each other by 20 cm. It can be shown that the distance OH is related to λ by a linear relation. Thus by varying OH with a screw, one gets a linear scale. The wavelength range of this

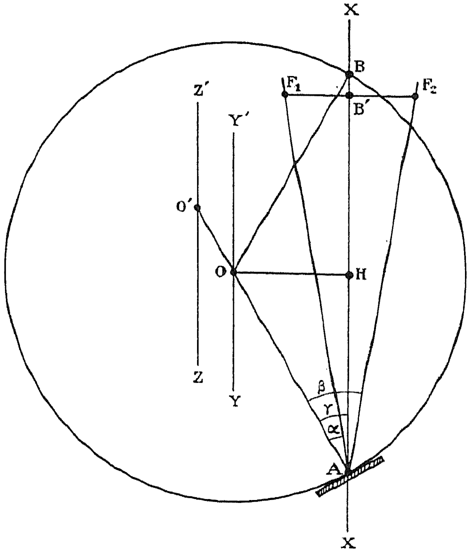

Figure 20

apparatus extends from 0 to 3000 Å (with a 1200 lines/mm grating); the resolution, the linearity of the scale and the reproducibility are better than 0.5 A.

(4) A grazing incidence (82°) 3-meters grating monochromator. In this apparatus [68, 69] (Figure 21) the scanning of the spectrum is accomplished in the following way:

a. the angle of incidence α is constant,
b. the distance ER is constant,
c. the grating moves along the line XX'.

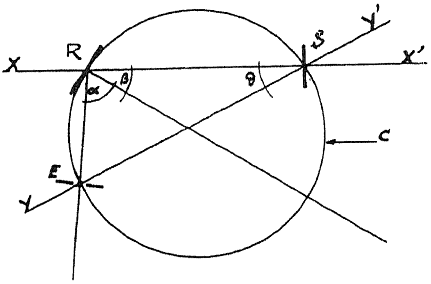

Figure 21

The Rowland circle C must (in principle) always pass through S, and E must also remain on the circle.

Since ER has a constant length, one sees that the angle θ is constant, that is, that the entrance slit moves along the fixed line ES making on angle θ with XX' and passing through the exit slit S. The assembly is supported by a bench lying along XX'. This bench holds two rails along XX' and a third upon which the entrance slit moves. The grating is in a housing which is held by a carriage. This housing slides along XX' without turning; it is the grating which turns in the housing.

The exit slit is fixed and its connection to the grating housing is made by telescopic tubes. The entrance slit E is solidly attached to a rigid arm, which can turn about the grating housing, by two sets of needle bearings. Because of this connection the incident light always passes through the center of the housing. The grating is mounted on a support attached to an axis, the connection being made by an external arm whose end is solidly attached to the entrance slit arm.

With a 600 lines/mm grating the dispersion is about 1 mm/A near 100 A and 0.45 mm/A near 1000 A as a function of the displacement of the grating carriage along XX'. The signal-to-stray light ratio varies from 10 to 30 for intense lines of vacuum spark spectra, reaches 140 in the case of the 303.8 A helium line and is better than 500 for the 584.3 A helium line. The detector was a windowless photomultiplier, equipped with a gold cathode.

REFERENCES

1. J. Romand and B. Vodar, Spectrochimica Acta, 1956, 8, 229 - 248.
2. Robin, Mlle S., Robin, S., and Vodar, B., J. Phys. Rad. 1952, 13, 671.
3. Robin, Mlle. S., Rev. d'Opt. 1954, 33, 193.
4. J. Romand, Conference on "Physics on Vacuum Ultraviolet Radiations" 1962, USC, Los Angeles, U.S.A.
5. Vodar, B. and Astoin, Mlle. N., Nature, 1950, 166, 1029.
6. Astoin, Mlle. N. C. R., Acad. Sc. 1952, 234, 2050.
7. Astoin, Mlle. N. and Vodar, B., J. Phys. Rad. 1953, 14, 494.
8. Romand, J. and Vodar, B., J. Phys. Rad. 1958, 19, 732.
9. Romand, J., Balloffet, Mlle. G., Vodar, B., Spectrochimica Acta, 1958, 13, 150.
10. Balloffet, Mlle. G., Romand, J. and Vodar, B., C. R. Acad. Sc. 1961, 252, 4139.
11. Balloffet, Mlle. G., Romand, J. and Kieffer, J., Spectrochimica Acta (in press).
12. Romand, J., Ann. Phys. Paris, 1949, 4, 529.
13. Johannin-Gilles, Mme. A., J. Rech, CNRS 1955, No. 31, 205.
14. Astoin, Mlle. N., Romand, J. and Vodar, B., J. Phys. Rad. 1955, 16, 491.
15. Douglas, M. E. and Herzberg, G., J. Opt. Soc. Am. 1957, 47, 625.
16. Astoin, Mlle. N. and Vodar, B., J. Phys. Rad. 1953, 14, 424.
17. Robin, Mlle. S. and Vodar, B., J. Phys. Rad. 1951, 12, 634.
18. Brunet, M., Julliot, C. and Vasseur, J. (Paper to be presented at the "Colloquium Spectroscopicum Internationale" University of Maryland, June 1962.
19. Schwetzoff, V., Robin, Mlle. S., and Vodar, B., C. R. Acad. Sc. 1952, 234, 426.
20. Schwetzoff, V., Rev. Gen. Elect. 1954, 63, 71.
21. B. Vodar, Spectroscopie d'émission dans l'ultraviolet lointain, published by GAMS - Paris.
22. Balloffet, Mlle. G., Acad. Phys. Paris, 1960, 5, 1243 (Dissertation).
23. Romand, J., Bachet, C. and Berneron, R., Rev. Metallurgie 1961, 58 (7), 481.
24. Romand, J., Balloffet, Mlle. G., Vodar, B., Spectrochimica Acta, 1959, 15, 454.
25. Balloffet, Mlle. G. and Romand, J., C. R. Acad. Sc. 1956, 242, 1964.
26. Balloffet, Mlle. G., Romand, J. and Vodar, B., J. Phys. Rad. 1959, 20, 510.
27. Franckel, private communication.

28. Schwob, J. L., and Balloffet, Mlle. G., J. Phys. Rad. 1961, 22, 389.
29. Astoin, Mlle. N., J. Red. CNRS, 1957, 38, 1.
30. Astoin, Mlle. N. and Granier, Mme. J., C. R. Acad. Sc. 1957, 244, 1350.
31. Damany-Astoin, Mme. N., Sanson, Mlle. S., and Bonnelle Mlle. M. C., C. R. Acad. Sc. 1960, 250, 1824.
32. Sun, M. and Weissler, G. L., J. Chem. Phys. 1955, 23, 1625.
33. Sanson, Mlle. L. and Damany-Astoin, Mme. N., C. R. Acad. Sc. 1960, 250, 4138.
34. Ogawa, M. and Cook, G. R., J. Chem. Phys. 1958, 28, 747.
35. Mulliken, R., J. Chem. Phys. 1935, 3 - 506.
36. Romand, J. and Vodar, B., C. R. Acad. Sc. 1951, 233, 930.
37. Granier-Mayence, Mme. J., and Romand, J., J. Phys. Rad. 1954, 15, 62.
38. Granier-Mayence, Mme. J. and Romand, J., C. R. Acad. Sc. 1953, 236, 1148.
39. Schnepp, O. and Dressler, K., J. Chem. Phys. 1960, 32, 1682.
40. Romand, J. and Granier-Mayence, Mme. J., C. R. Acad. Sc. 1952, 235, 1023.
41. Granier, Mme. J., Damany-Astoin, Mme. N., Cordier, Mme. M., C. R. Acad. Sc. 1960, 251, 2672.
42. Roncin, J. Y., Chen, S. Y., Granier, Mme. J. and Damany-Astoin, Mme. N., Spectrochimica Acta, 1962, 18, 907.
43. Astoin, Mme. N., Granier, Mme. J. and Cordier Mlle. M., J. Phys. Rad. 1958, 19, 506.
44. Roncin, J. Y., Damany-Astoin, Mme. N., C. R. Acad. Sc. 1961, 253, 835.
45. McCarty, M. and Robinson, G. W., J. Chem. Phys. 1959, 56, 723.
46. Robin, S. and Robin, Mme. S., Rev. d'Opt. 1957, 37 (4) 161.
47. Vodar, B., Proc. Roy. Soc. 1960, 255 (2), 44.
48. Vodar, B., Proceedings of the 7th IUPAC Conference, Munich, 1957, Ed. Batterworth; London, 1960.
49. Robin, J., Bergeon, R., Galatry, L., and Vodar, B., Disc. Faraday Soc. 1956, 22, 30.
50. Dressler, K., Conference on ''Vacuum Ultraviolet'' Radiation Physics 1962 USG, Los Angeles, U.S.A.
51. Robin, Mme. S. and Vodar, B., J. Phys. Rad. 1952, 13, 492.
52. Robin, Mme. S., Rev. D'Optique 1954, 33, 377.
53. Fabre, Mlle. D. and Romand, J., J. Phys. Rad. 1961, 22, 324.
54. Fabre, Mlle. D., Romand, J. and Vodar, B., Opt. Acta, 1962, 9 (1), 73.
55. Robin-Kandare, Mme. S., J. Rech. CNRS, 1959, 49, 311.
56. Robin-Kandare, Mme. S., J. Phys. Rad. 1960, 21, 31.

57. Lyman, Th., The Spectroscopy of the Extreme Ultraviolet Longmans (Green & C), London, 1928.
58. Hass, G. and Tousey, R., J. Opt./Soc. Am., 1959, 49, 593.
59. Givens, M. P., Rev. Sc. Inst. 1956, 25, 1130.
60. Givens, M. P., Koester, C. J. and Goffe, W. L., Phys. Rev. 1955, 100, 1112.
61. Reitz, J. R., Phys. Rev. 1957, 105, 1233.
62. Vodar, B. and J. Romand, Mikrochimica Acta, 1955, n° 2-3, 429-445.
63. J. Romand and B. Vodar, Rev. d'Optique 37, 329 (1958).
64. J. Romand and B. Vodar, Rev. Sci. Instr. 29, 732 (1958).
65. Technical Brochure of the "Sté Jobin & Yvon."
66. J. Romand and B. Vodar, Rev. d'Optique 39, 167 (1960).
67. Technical Brochure of the "Ets Beaudouin."
68. M. Salle and B. Vodar, C. R. Acad. Sci. Paris 230, 380 (1950).
69. J. Romand and B. Vodar, Optica Acta, 1962 (to be publ. in October).

A PULSED LIGHT SOURCE FOR THE EXTREME ULTRAVIOLET*

W. R. Hunter
U. S. Naval Research Laboratory
Washington 25, D. C., U.S.A.

INTRODUCTION

For a number of years an investigation of the optical properties of materials in the extreme ultraviolet has been underway at the U. S. Naval Research Laboratory (NRL) with a twofold purpose; to measure the optical constants of materials, and to obtain more efficient reflectors. Various materials have been investigated [1-5] but only at wavelengths longer than 900 Å, at Ne I, 736 Å, and at He I, 584 Å; radiations produced readily in a d.c. glow discharge. The light source to be described is the result of an effort to provide radiation at many wavelengths shortward of 900 Å with sufficient intensity for making reflectance and transmittance measurements using photoelectric detection, and with good stability during the time required for a measurement, which is usually two to three minutes.

A one-meter normal incidence monochromator with a 600 line/mm grating was used with a nominal resolution of 1.6 Å. The detectors employed were a 1P21 multiplier phototube, sensitized for the extreme ultraviolet by spraying a concentrated solution of sodium salycilate in methyl alcohol over its envelope, or a magnetically focussed continuous strip multiplier with a tungsten cathode, developed by the Bendix Corporation.

The spectral response curves of both detectors are shown in Figure 1 where the ordinate represents the current output in amperes for an irradiance value of 1 erg/cm^2/sec. The curve for the 1P21 + sodium salycilate was calculated assuming a

---

*This research was supported in part by the National Aeronautics and Space Administration Contract No. R-21.

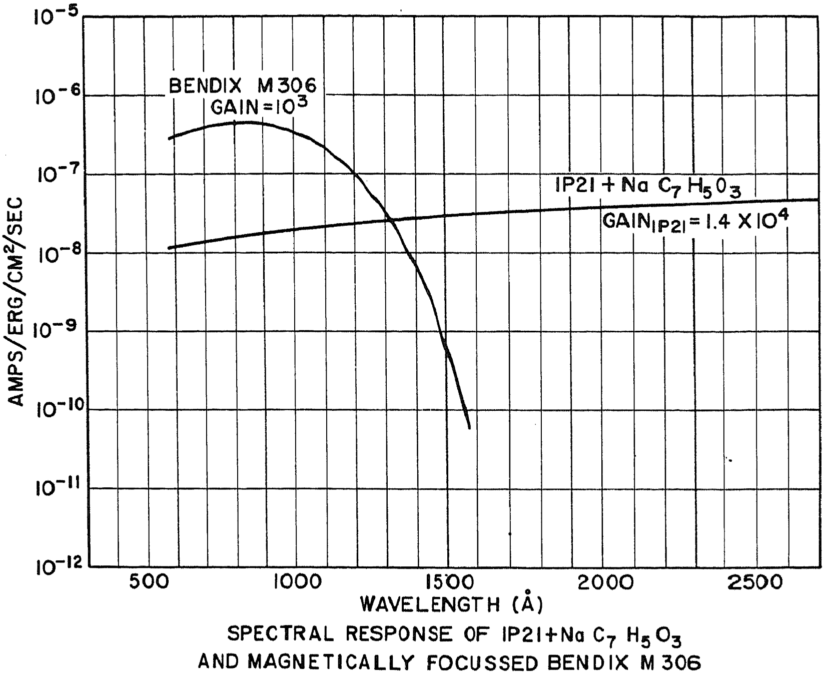

Figure 1. The spectral response of an extreme ultraviolet sensitized 1P21, and of a Bendix magnetically focussed multiplier, M306.

constant quantum efficiency for sodium salycilate from 584 to 2500 Å [6,7] and was calibrated absolutely, at 1216 Å, with an accuracy of ±15% using a nitric oxide ion chamber [8,9]. This detector was then used to calibrate the magnetically focussed multiplier.

For wavelengths longer than 1600 Å, the response of the magnetically focussed multiplier is essentially zero. Thus it is very useful at the short wavelengths where, as the zero order image is approached, the intensity of the scattered visible and near ultraviolet radiations may be quite large. It has the additional advantage that the noise and dark current are low enough to permit measurement of currents as low as 10^{-14} amperes, whereas with the 1P21, this lower limit is about 10^{-11} amperes.

Figure 2 shows the spectral emissions and detector output currents obtained from the NRL instrument with d.c. glow discharge excitation using a discharge current of 0.25 amperes, a sensitized 1P21 for a detector and gas pressures of 350 μ for hydrogen and 1 mm for He and Ne. The constant power curve represents the multiplier phototube output current that would be measured with an irradiance value of 10 ergs/cm^2/sec at the exit slit, of dimensions 0.01×0.4 cm, and a 1P21 gain of 1.4×10^4.

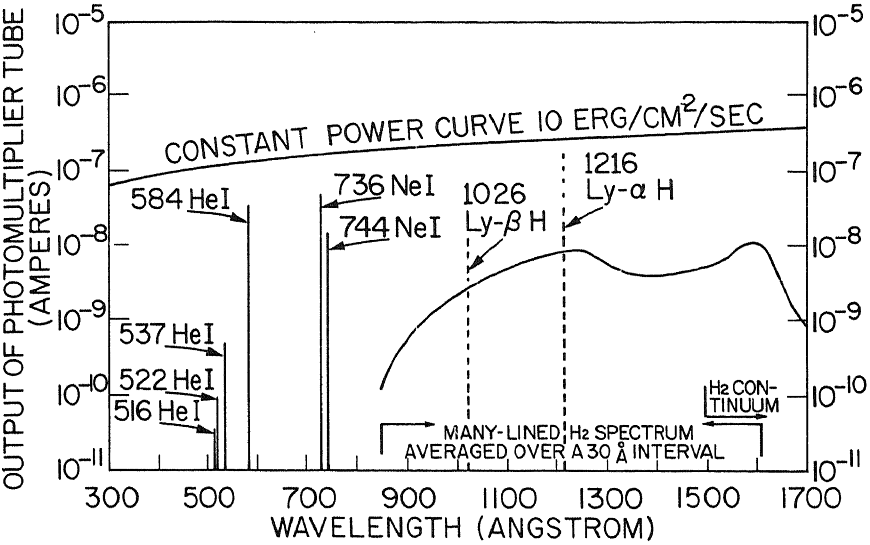

EXTREME ULTRAVIOLET RADIATION OBTAINED
BY GLOW DISCHARGE EXCITATION

Figure 2. The extreme ultraviolet radiation produced by d.c. glow discharge excitation. A sensitized 1P21 was used for the detector with a gain of 1.4×10^4.

Unfortunately, there are very few useful emissions from this type of discharge below 900 Å. Other types of discharge, such as RF excited, or hollow cathode discharges, have been found to produce no emissions in this range other than those produced in the d.c. discharge. The helium continuum that extends from approximately 600 Å to 900 Å would fill part of the region, but it is very difficult to obtain using d.c. excitation and the intensity is too low for reflectance and transmittance measurements. D.C. discharges using thermally heated cathodes have been described [10] but were not considered useful, because the intensities were at least two orders of magnitude below those shown in Figure 1. Weissler and associates at the University of Southern California have developed a condensed discharge type of light source [11] in which the capacitor is periodically discharged through a gas at low pressure by means of a rotating spark gap. They obtained lines to wavelengths as short as 450 Å with sufficient intensity for the reflectance and transmittance measurements they have reported [12].

A similar light source, constructed at NRL, was found to be unstable, with intensity fluctuations of a factor of two to three during periods of a few seconds. The reasons for this instability were not known but were thought to be partly due to the rotating

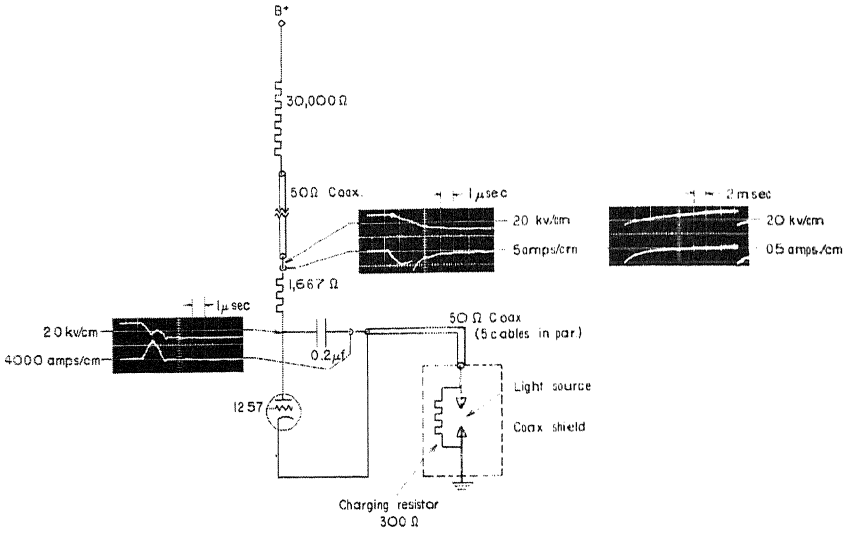

Figure 3. The pulsed light source switching circuit using a 1257 hydrogen thyratron as the switch. Voltages and currents measured at the indicated points of the circuit are shown in the oscillograms where positive voltages are above the base lines and electron flow toward the power supply is below the base lines. Large divisions on the oscillograms, such as those indicated by the time scales, are in cm.

gap. The source to be described is fundamentally the same type as the Weissler source, but was modified to improve the stability and convenience. There were two principle changes; the use of a 1257 hydrogen thyratron for the switch instead of the rotating gap, and a redesign of the lamp configuration.

THE PULSED LIGHT SOURCE

The circuit developed for switching the pulsed light source is shown in Figure 3 together with some oscillograms showing voltages and currents. Triggering pulses were obtained by differentiating the output of a square wave generator, and amplifying the pulses until they had sufficient amplitude to trigger the 1257, thus discharging the 0.2 μfd capacitor through the light source. It is this discharge that produces the spectra of multiply ionized atoms together with the first spectrum. The discharge current, of approximately 4000 amperes peak value, is shown in the lower left oscillogram and was measured using a pulse transformer. It was not an oscillatory discharge because of the rectifying action of the thyratron, although a comparatively small current reversal of about 300 amperes occurred before the thyratron cut off. The form of the discharge current was approximately sinusoidal with a half-period of 1.5 μsec. An inductance of 1.1 μH was required to resonate with 0.2 μfd at this frequency and was distributed in the circuit as follows: 0.5 μH measured in the capacitor, 0.15 μH calculated for the coaxial cables, and 0.04 μH calculated for the discharge considering it to be a conductor of 6 mm diameter and 10 cm long. This left 0.41 μH inductance due to the 1257 and associated leads. The oscillogram at the extreme right shows the voltage-current relationship during charging of the capacitor. Since the capacitor became charged to about 8 kv in the opposite polarity during the discharge, the voltage across the limiting resistor of 31.7 k Ω was close to 20 kv at the beginning of charging. This caused the average charging current to be about 40% higher than calculated from the supply voltage and limiting resistor. In the oscillogram, the charging current trace crosses the base line because it was measured with a transformer and has no d.c. component.

The center oscillogram shows the voltage and current at the same point but on a much faster time scale. A current of 5 amperes peak value flowed during the first 1-1/2 μsec after the discharge was initiated and was attributed to the charging of the capacitor that is the twenty feet of 50 Ω coaxial cable between the 1.6 k Ω resistor and the 30 k Ω resistor. No explanation could be found for the sudden small increase in current which coincided with the termination of the discharge.

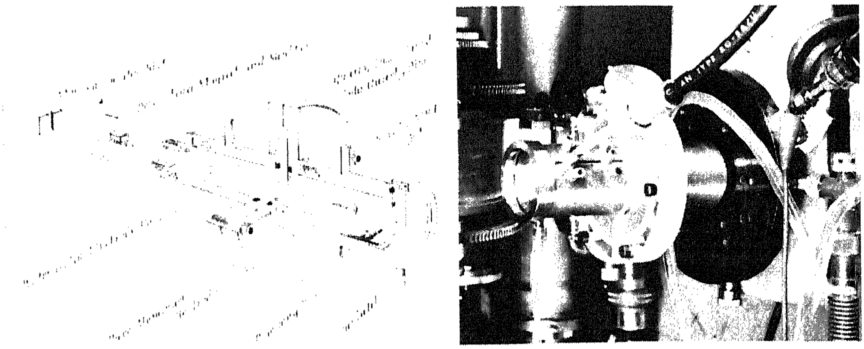

Figure 4. The lamp. To the right is a photograph of the lamp with the coaxial shield removed showing the manner of making electrical connections, and to the left is a cut-a-way drawing.

Charging of the capacitor can be accomplished in either of two modes; through the resistor shown in parallel to the light source, or without this resistor. In the latter case, the capacitor was charged through the light source and, in the process, a glow discharge was produced giving rise to emission lines from neutral atoms. When the resistor was used, the capacitor was charged through it and this glow discharge did not occur; therefore the intensity of the first spectra was decreased. Operations were usually carried on without this charging resistor since the presence of these first spectrum lines was desirable.

Repetition rates are controllable and can be as low as desired or as fast as deionization time of the thyratron will allow provided that the capabilities of the power supply are not exceeded.

The lamp configuration, shown in Figure 4, was designed to fulfill two conditions; first, to be suitable for either d.c. or pulsed discharge excitation and second, in the event of breakage in the capillary, to prevent any sudden influx of water or air into the vacuum system. To the right is a photograph of the lamp with its coaxial shield removed, showing the method of making electrical connections, and to the left is a cut-a-way drawing of the lamp.

A quartz capillary with the desired inside diameter, 10 cm long and with a wall thickness of at least 1 mm, was fused into the center of a quartz disc. Water-cooled electrode holders containing removable pure aluminum electrodes were clamped to either side of the disc by means of insulating clamping plates. Since this configuration did not permit cooling of the capillary, it was essential to use material that could withstand the discharge conditions and quartz was satisfactory in this respect. Earlier experiments with Pyrex showed it to be unsatisfactory for even the relatively cool operation encountered in the d.c. glow discharge. Gas was fed into the cathode through a six-foot length of tygon tubing. When shorter lengths of tygon were used, the discharge occasionally occurred in the tubing rather than the capillary. Successful operation was also possible with gas introduction directly at the anode which was at ground potential. Under these conditions, however, gas pressures four to five times higher were necessary to make the discharge operate. Therefore this method of introducing the gas was abandoned. Cooling water was run to the electrode holders through 25-foot lengths of tygon tubing which were long enough to isolate the electrodes from the grounded water supply. A Pyrex window was used on the end of the cathode, where the heating was not as intense, for viewing the discharge and to permit alignment of the various monochromator attachments without the necessity of removing the light source.

Most of the emissions produced by condensed discharge excitation in this lamp were stable to within ±3% over periods of about 3 minutes, with drifts about twice greater during 15- to 20-minute periods. When used for d.c. operation the drifts are only one or two percent over periods of an hour. Eventually instability does occur, but it has always been cured by cleaning the surfaces of the pure aluminum electrodes.

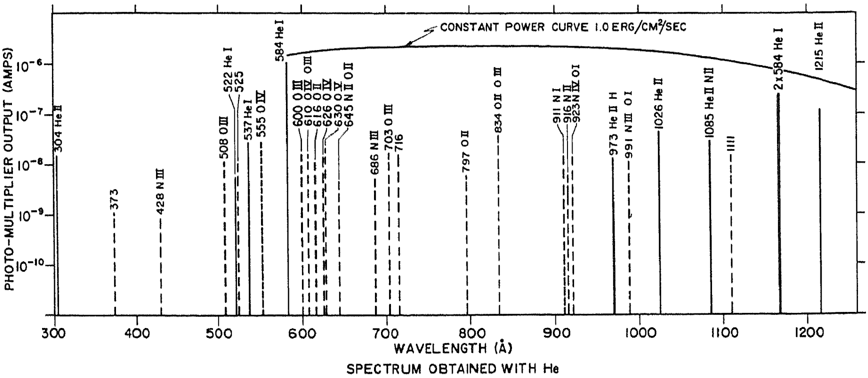

Figure 5. The spectrum produced by the pulsed light source using helium. Detector: Magnetically focussed multiplier; gain 5 x 10^3.

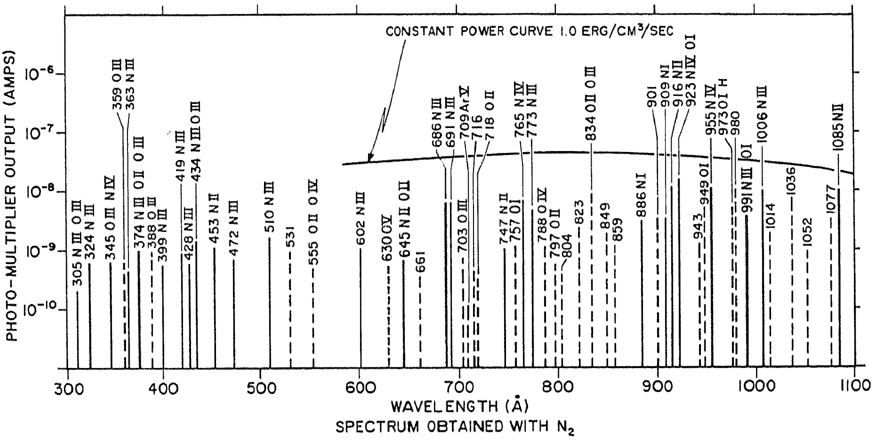

Figure 6. The spectrum produced by the pulsed light source using nitrogen. Detector: Magnetically focussed multiplier; gain 10^2.

A magnet was placed between the lamp and the entrance slit to deflect away charged particles that were likely to coat the grating and cause a loss in intensity. Judging from the deposits found around the magnet, it served its purpose fairly well and grating contamination has been retarded.

SPECTRA

Diagrams of the spectra obtained with the pulsed light source are presented in Figures 5, 6, 7, and 8; all prepared from recordings made with the magnetically focussed multiplier with tungsten cathode. The discharge conditions were: pressure in the anode chamber 1 mm, supply voltage 12-1/2 kv, capillary diameter 6 mm, and a repetition rate of 60 discharges per second. Most of the lines have been identified with the aid of the lists of Boyce and Robinson [13] and of Moore [14]. Those lines arising from the gas deliberately introduced into the light source are shown as solid lines and the impurity lines are shown broken. Although the diagrams extend only to 300 Å, a few lines to shorter wavelengths were observed in some cases but with intensities too low to be useful. The effective long wavelength limit, when using the tungsten photocathode, was about 1300 Å, however the spectra are shown only over the wavelength ranges where they are useful.

The ordinates give the time-averaged detector output current on a logarithmic scale. A constant power curve, the spectral response curve of the detector, shown for wavelengths longer than 584 Å, makes it possible to derive time-averaged intensities.

The spectrum produced by the pulsed light source using helium, shown in Figure 5, included the second, third, and fourth members of the Balmer series of He II at 1215 Å, 1085 Å and 1026 Å. The first member at 1640 Å could be seen using a sensitized 1P21 and is not shown on the diagram. All three may be

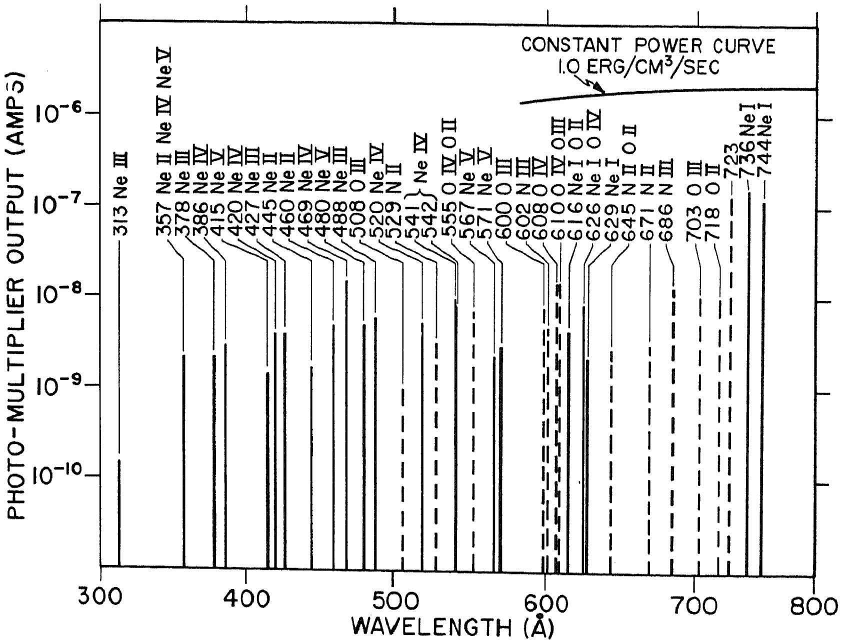

SPECTRUM OBTAINED WITH Ne

Figure 7. The spectrum produced by the pulsed light source using neon. Detector: Magnetically focussed multiplier; gain 5 x 10^3.

blended to some extent, λλ 1215 and 1026 with hydrogen impurities and λ 1085 with N II. The He II, 304 Å line was also present with good intensity.

Several members of the principal series of He I were also present, with the resonance line at 584 Å the most intense line present. Most of the other lines were due to oxygen and nitrogen and were present regardless of the gas used.

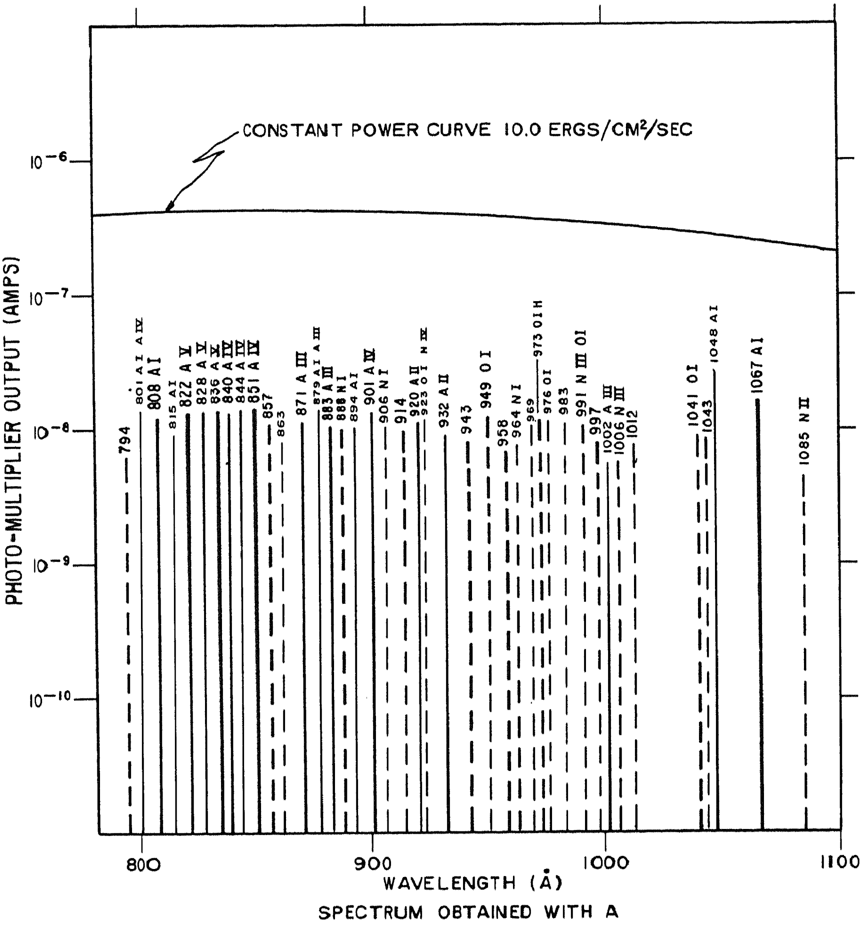

Figure 8. The spectrum produced by the pulsed light source using argon. Detector: Magnetically focussed multiplier; gain 10^3.

The spectrum obtained using nitrogen is shown in Figure 6. The resonance lines N II, 1085 Å; N III, 991 Å and N IV, 765 Å were present, together with many other lines of these ions and the impurity, oxygen. From 900 to 700 Å, the density of lines was greater than with helium. Toward shorter wavelengths, the lines occurred further apart and were less intense. Wavelengths as short as 305 Å were observed but with intensities roughly 1/50 that of the 304 Å line of He II.

Neon, shown in Figure 7, is the most suitable for the region 700-300 Å, with lines present from Ne I to Ne V. Intensities were low near 300 Å and increased toward longer wavelengths with the Ne I, 736 Å and 744 Å lines quite intense. To longer wavelengths, not shown in the figure, were many other lines including the Lyman-α and Lyman-β of hydrogen, present as an

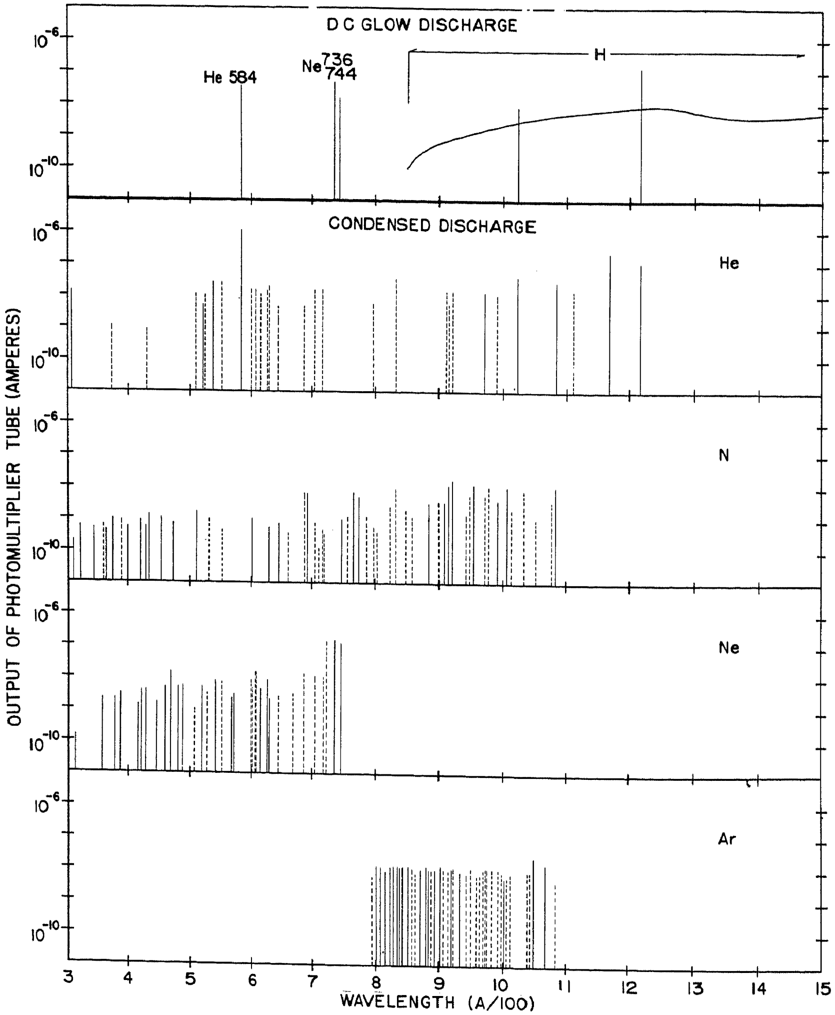

Figure 9. A summary of the spectra obtained using different gases in the pulsed lightsource. The spectra produced by d.c. glow discharge excitation measured with a sensitized 1P21 is shown for comparison.

impurity although the neon was graded, "spectroscopic pure."

Figure 8 shows the results obtained using argon. Many lines were observed between 800 and 1000 Å but practically no argon or impurity lines were seen below 800 Å. Argon filled this region even better than nitrogen and provided a transition from the many-lined hydrogen spectrum down to 800 Å.

Figure 9 summarizes the spectra. The top row shows the emissions that were obtained from the NRL instrument using d.c. glow discharge excitation. The next four rows show the spectra obtained using different gases in the pulsed light source. Thus, most of the spectral region from 900 to 300 Å can be filled by the proper choice of gas. Hydrogen, of course, can be used in the pulsed discharge, but offers no advantages; below 850 Å there were only the impurity lines that were present with the other gases, and above 850 Å the many-lined spectrum was excited

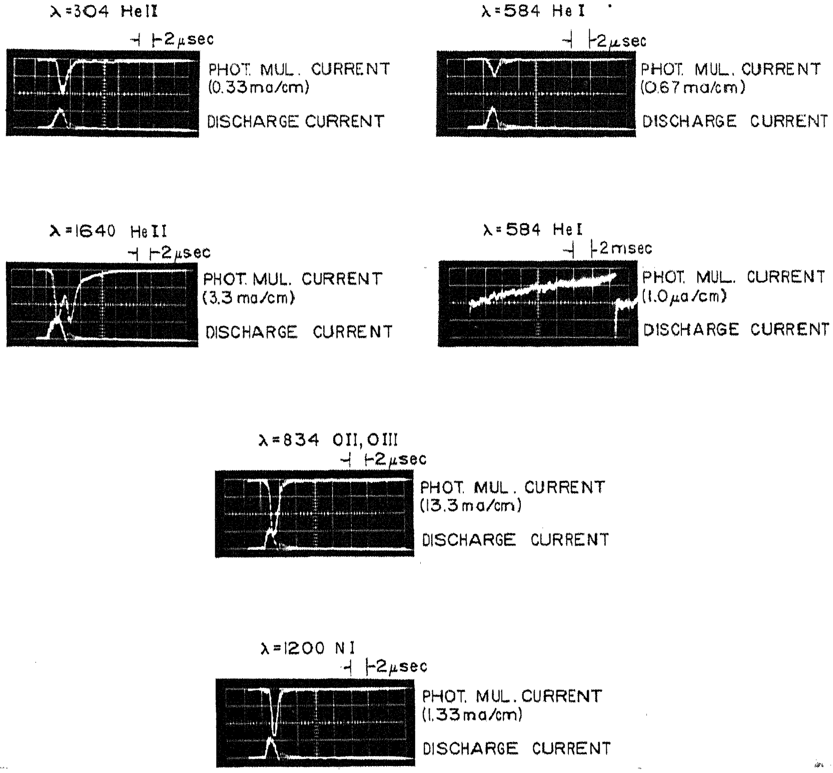

Figure 10. The intensity vs time for some strong lines produced by the pulsed light source using helium. A sensitized 1P21 was used for the detector with a gain of ~ 10^6. Large divisions on the oscillograms, such as those indicated by the time scales, are in cm.

more conveniently in the d.c. glow discharge and with the same intensity.

TIME HISTORY OF THE STRONGEST LINES

A study was made of the instantaneous intensity in certain of the strongest lines in order to obtain further insight into the mechanism of the discharge, and also to determine the peak intensity. The light curve was measured with a sensitized 1P21 with a gain of approximately 10^6 and analyzed oscillographically.

Figure 10 shows the detector output current vs time using helium in the pulsed light source and with a capillary diameter of 4 mm. To the left are shown the 1640 Å and 304 Å lines of He II. The peak intensities coincided approximately with the discharge current peak. At 1640 Å, a second intensity peak occurred about 1-1/2 μsec after the first. It is not certain that this double peak is characteristic of helium because it was not observed for any other helium line. However, the higher members of the series were blended with lines of other atoms and this may have prevented detection of a double peak. Using higher sensitivity than shown here, the 304 Å line showed some evidence of a second peak; higher members of this series were not intense enough to analyze.

The 584 Å line of He I, shown to the upper right, had its peak intensity coinciding with the discharge current; this was followed by a very broad second peak, too faint to be seen in this trace, some 8 to 10 μsec later. This pattern is characteristic of all neutral resonance lines observed, although the relative intensity of the peaks differed depending on the gas. When the 584 Å line was observed on a slow time scale, shown at the lower right, emission was observed during the time between discharges and was due to the glow discharge caused by the charging current. When the charging resistor was used, the glow discharge did not occur and only the first sharp and second broad peaks were seen. The average detector output current due to these two peaks was small compared to that due to the glow discharge, thus use of the charging resistor reduced the average signal; in the case of the 584 Å line by a factor of about 30.

The two traces shown at the bottom of Figure 10 are of impurity lines; 834 Å arising from O II and O III, and 1200 Å from N I. In both cases the peak intensity did not coincide with the peak discharge current but occurred about 1/2 μsec later.

At first, there was some doubt about the linearity of the detector at large peak currents, since earlier measurements[15] on 1P21 multiplier phototubes had shown that saturation effects were likely to occur for peak currents in excess of 10 mA. For example, the O II, O III, 834 Å emission lines are very intense,

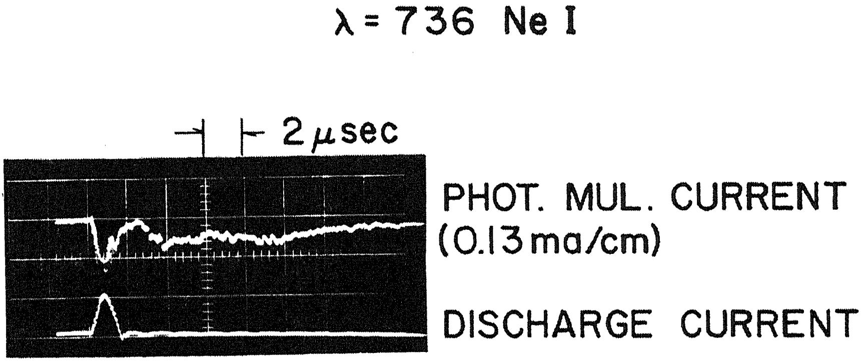

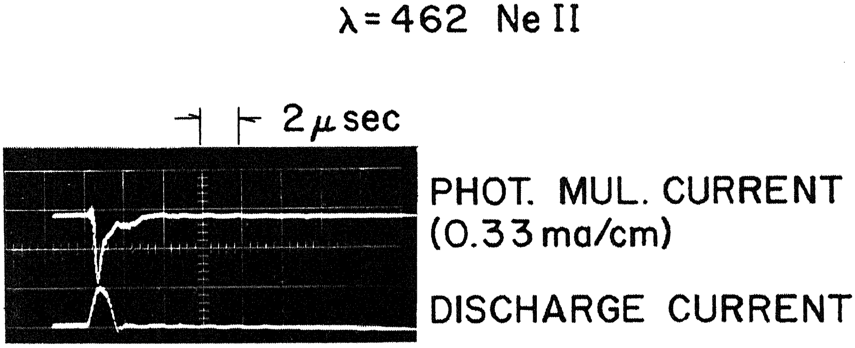

Figure 11. Two neon lines observed using neon in the pulsed light source. A sensitized 1P21 was used for the detector with a gain of ~ 10^6. Large divisions on the oscillograms, such as those indicated by the time scales, are in cm.

giving rise to a peak current from the detector in excess of 40 mA. However, reflectance measurements on ZnS gave a reflectance of 18% at this wavelength which was in agreement with reflectance measurements [3] using d.c. glow discharge excitation where detector currents were of the order of 10^{-8} amperes. Evidently this particular 1P21 was not saturating with peak currents of up to 40 mA.

Intensity vs time oscillograms for two Ne lines, obtained with a 6 mm diameter capillary, are shown in Figure 11. As with the 584 Å line of He I, the 736 Å resonance line had a second broad intensity peak about 8 to 10 μsec after the first sharp peak and radiation was emitted during the entire charging time when the charging resistor was not used. The same held true for the 744 Å resonance line. By contrast, the 462 Å line, which is a principal line of Ne II, had no broad delayed second intensity peak and no emission occurred during the charging cycle. Its intensity vs time trace resembles that of the 1640 Å line of He II in that a faint second intensity peak can be seen about 2 μsec after the first. Changing the capillary diameter from 6 to 4 mm decreased the time between the first and second sharp peaks in both helium and neon, and increased the intensity of the second sharp peak.

Except for those lines with wavelengths shorter than 584 Å, the absolute peak intensities can be calculated by multiplying the absolute sensitivity of the sensitized 1P21, shown in Figure 1, by a factor accounting for the increased gain and dividing the new absolute sensitivity into the peak current. For example, at λ 834, Figure 1 gives a sensitivity of 1.7×10^{-8} amps/erg/cm^2/sec. This times the gain ratio of 71.5 gives a new sensitivity of 1.2×10^{-6} amps/erg/cm^2/sec. Dividing this into the peak current of 40 mA gives an intensity of 3.3×10^4 ergs/cm^2/sec. A similar calculation for λ 1640 gives an intensity of 4.4×10^3 ergs/cm^2/sec for either peak.

ACKNOWLEDGMENT

The author would like to acknowledge the help he received from T. Godlove, and from A. C. Kolb and his associates, in particular R. C. Elton.

REFERENCES

1. G. Hass, W. R. Hunter, and R. Tousey, J. Opt. Soc. Am. 46, 1009, (1956).
2. G. Hass, W. R. Hunter, and R. Tousey, J. Opt. Soc. Am. 47, 1070, (1957).
3. J. T. Cox, J. E. Waylonis, and W. R. Hunter, J. Opt. Soc. Am. 49, 807, (1959).
4. G. Hass and R. Tousey, J. Opt. Soc. Am. 49, 593, (1959).
5. D. W. Angel, W. R. Hunter, R. Tousey, and G. Hass, J. Opt. Soc. Am. 51, 913, (1961).
6. F. S. Johnson, K. Watanabe, and R. Tousey, J. Opt. Soc. Am. 41, 702, (1951).
7. K. Watanabe and C. Y. Inn, J. Opt. Soc. Am. 43, 32, (1953).
8. E. T. Byram, T. A. Chubb, H. Friedman, J. E. Kupperian, Jr. and R. W. Kreplin, Astrophys. J. 128, No. 3, 738, (1958).
9. T. A. Chubb, H. Friedman, and R. W. Kreplin, Mémoires Soc. R. Sc. Liège, cinquième série, 4, 216, (1961).
10. P. Hartman, J. Opt. Soc. Am. 51, 113, (1961).
11. G. L. Weissler - Private communication.

12. W. P. Walker, O. P. Rustgi, and G. L. Weissler, J. Opt. Soc. Am. 49, 471, (1959).
13. J. C. Boyce and H. A. Robinson, J. Opt. Soc. Am. 26, 133, (1936).
14. Charlotte E. Moore, An Ultraviolet Multiplet Table, Nat. Bur. Stand. Circular 488, (1950).
15. R. W. Engstrom, J. Opt. Soc. Am. 37, 420, (1947).

SUR QUELQUES METHODES DE SPECTROMETRIE X

J. Philibert
Département Physique
Institut de Recherches de la Sidérurgie
Saint-Germain-en-Laye (S. et O.), France

INTRODUCTION

Les bases physiques de la spectrométrie de Rayons X remontent à environ un demi-siècle. Les études célèbres de MOSELEY ont été publiées en 1913 et 1914.

Une étape importante en spectrométrie X a été marquée par la publication du livre de Von HEVESY en 1932, mais ce n'est qu'après la seconde guerre mondiale que la spectrométrie X est vraiment entrée dans les laboratoires en tant que méthode d'analyse élémentaire de routine, au même titre que la spectroscopie lumineuse par exemple.

Ce développement tardif peut s'expliquer par des raisons de commodité et de précision, que seul a permis l'abandon de la plaque photographique, et de son corollaire la photométrie, au profit de nouveaux détecteurs de rayonnement: les compteurs de photons.

Quand on parle spectrométrie X, on pense le plus souvent à la fluorescence X, méthode maintenant si largement répandue dans les laboratoires, grâce à de très nombreux modèles d'appareils commerciaux, et utilisée tant pour la recherche proprement dite que pour le contrôle de production. Cependant d'autres méthodes d'analyse élémentaire sont fondées sur la spectrométrie X, au premier rang desquelles il convient de citer la "Microanalyse à Sonde Electronique" dont la première réalisation est due à CASTAING et GUINIER dès 1948.

Je voudrais, dans cet exposé, souligner d'une part *la diversité des méthodes* d'analyse fondées sur la spectrométrie X, et d'autre part insister plus particulièrement sur *les conditions théoriques de l'analyse quantitative*. Je passerai donc en revue les divers types de spectrométrie et les divers modes d'excitation du spectre X, en insistant plus particulièrement sur la méthode démission directe plutôt que sur la fluorescence, et en empruntant la plupart des exemples à la microanalyse. Enfin la discussion des relations quantitatives émission X — concentration sera limitée à la microanalyse, des conditions physiques plus simples ayant permis de développer complètement la théorie de l'émission.

I - METHODE DE SPECTROMETRIE X

Tout comme en spectrométrie lumineuse, on doit distinguer ici entre spectrométrie d'émission et spectrométrie d'absorption.

A - SPECTROMETRIE D'EMISSION

1. Lois Fondamentales

Les spectres émis par un élément pur sont constitués d'un petit nombre de raies groupées en séries caractéristiques: K, L, M de complexité croissante. La fréquence d'une raie donnée varie simplement avec le numéro atomique de l'émetteur, comme l'a montré MOSELEY (1913, 1914).

$$\sqrt{\nu} = A\,(Z - B).$$

Le domaine de longueur d'onde commode pour l'analyse est tel que l'on ne travaille guère qu'avec les séries K ou L (très rarement M) des divers éléments. Ceci correspond à des énergies comprises entre 1 keV et quelques dizaines de keV. D'où plusieurs avantages:

a. Conditions d'excitation du spectre faciles avec les sources usuelles.

b. Simplicité des spectres (la série K n'a que trois raies intenses), d'où rareté des *superpositions* de raies d'éléments différents. Ce risque de superposition devient plus grand avec la série L, et a fortiori la série M, et il est encore accru par les possibilités de réflexion d'ordre multiple par le cristal analyseur. Un exemple célèbre de telles superpositions est celui de l'analyse de faibles concentrations de hafnium dans le zirconium. On a:

$$K\alpha_1\,Zr = 0{,}7843\ kX$$

$$L\alpha_1\,Hf = 1{,}566\ kX.$$

La différence de longueur d'onde apparente entre $L\alpha_1$ Hf et le second ordre de $K\alpha_1$ Zr n'est que de 0,0025 kX. Ceci correspond à une différence d'angle de Bragg de 1 1/2' avec un cristal de quartz $(10\bar{1}1)$, de l'avec un cristal de LiF. D'où la nécessité de spectromètres à haute résolution pour certaines études.

c. Les raies utilisées sont dues à des transitions entre les niveaux électroniques les plus proches du noyau, et donc insensibles à l'état de liaison chimique où sont engagés les atomes. Mais pour les éléments de plus en plus légers ($Z < 10$), les raies K s'élargiront progressivement en bandes, occupant une certaine largeur spectrale.

Nous n'insisterons pas ici sur l'application de l'analyse des bandes des séries molles pour l'étude de la structure électronique des solides.

2. Spectromètres

Il y a deux types de spectromètres, qui d'ailleurs peuvent être combinés, le spectromètre à cristal et le spectromètre à discrimination électronique.

1) *Spectromètre à cristal.* Un cristal est utilisé comme monochromateur par application de la loi de Bragg. Le meilleur rendement est obtenu avec *les spectromètres à cristal courbe,* grâce à l'effet de focalisation du rayonnement divergent qui tombe sur le cristal. Le rayon de courbure du cristal doit être égal à 2 R, si R est le rayon du cercle de focalisation qui passe par la fente d'entrée, le cristal et la fente de sortie où l'on place le récepteur (Figure 1).

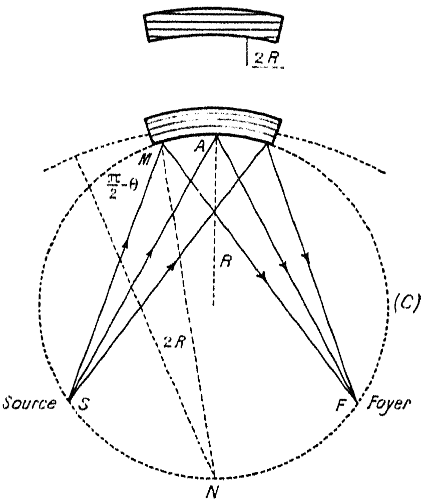

Figure 1. Spectromètre à cristal courbe, type Johansson, d'après Guinier.

Un gain de rendement est obtenu si les conditions de focalisation sont réalisées plus rigoureusement en utilisant un cristal dont la surface épouse exactement le cercle de focalisation. On utilise pour cela un cristal taillé avec une courbure 1/2 R. Placé dans une presse de courbure 1/R, les plans réticulaires prennent la courbure:

$$1/R - 1/2\,R = 1/2\,R$$

tandis que la surface a bien la courbure 1/R: la condition de focalisation est alors assurée exactement sur toute la surface du cristal.

Un autre artifice utile est *l'angle de taille*. Si les plans réticulaires utilisés font un angle faible α avec la surface du cristal, on voit facilement que les angles au centre (Figure 2) ne sont plus égaux, mais présentent une différence égale à 4 α: cette dissymétrie permet, pour une distance minimale fente d'entrée - monochromateur (limitation géométrique due à l'encombrement de la source; au contraire le récepteur peut être approché au voisinage immédiat du cristal) d'étendre le domaine du spectromètre. Un tel montage est utilisé avec un cristal de quartz, sur la microsonde française.

Monochromateur. La loi de Bragg montre que l'on doit avoir $\lambda \leq 2$ d. Cependant, une autre limite d'un monochromateur est son *pouvoir dispersif*

$$\frac{d\theta}{d\lambda} = \frac{n}{2\,d \cos\theta}$$

qui décroît si d croît, mais croît avec θ.

Le choix de la taille du cristal (c'est-à-dire de la famille des plans réticulaires utilisés pour réfléchir le rayonnement) et de la nature de ce cristal est conditionné non seulement par la valeur optimale du paramètre d, mais encore par le *pouvoir réflecteur* du cristal pour la réflexion utilisée.

Les cristaux les plus fréquemment utilisés sont, aux longueurs d'onde moyennes et courtes ($\lambda < 4$ Å), le quartz

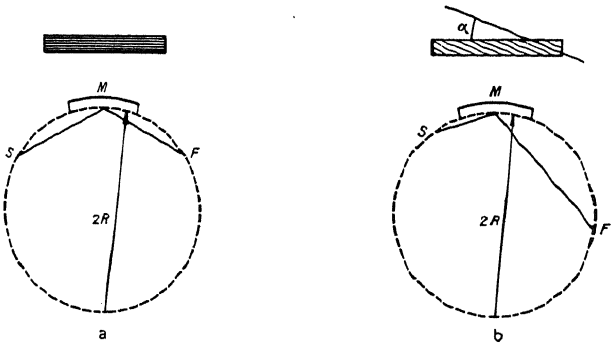

a) $\alpha = 0$ monochromateur symétrique.
b) $\alpha \neq 0$ monochromateur dissymétrique.

Figure 2. Spectromètre à cristal courbé et angle de taille, d'après Guinier.

(plusieurs tailles) et le fluorure de lithium, aux longueurs d'onde longues le mica, le gypse, l'EDDT ou l'ADP. Le tableau I rassemble les caractéristiques d'un certain nombre de monochromateurs.

Tableau 1

Caractéristiques de Quelques Monochromateurs
Utilises en Réflexion

Cristal	Plan Réflecteur	d (k X)
CaF_2	(220)	1,93
LiF	(200)	2,01
CaF_2	(111)	3,15
Quartz	$(10\bar{1}1)$	3,34
Quartz	$(10\bar{1}0)$	4,25
EDDT*	(020)	4,39
ADP†	(200)	5,31
Gypse	(020)	7,55
Mica	(002)	9,94

*Ethylène diamine d-tartrate.
†Ammonium diphosphate.

Récepteurs. C'est un compteur Geiger, un compteur proportionnel ou un scintillateur. L'avantage du premier est de délivrer des impulsions de forte amplitude, d'où un ensemble de comptage électronique simple. Son gros défaut est son temps mort élevé ($> 100\ \mu s$) qui ne permet pas les taux de comptage élevés. Le compteur proportionnel et le scintillateur, outre leur temps mort faible, ont l'avantage de permettre une discrimination électronique des impulsions (cf. paragraphe suivant). Le scintillateur offre aux courtes longueurs d'onde (0,5 - 1,5 kX) l'avantage de son rendement quantique pratiquement égal à 1.

La Figure 3 montre à titre d'exemple la finesse des raies obtenues avec le spectromètre à cristal de quartz de la microsonde de Castaing. La distance angulaire des raies du doublet K α_1 α_2 du cuivre n'est que de 3,8 kX ($\Delta\theta \approx 2$ minutes). La Figure 4 montre le spectre L du Xénon enregistré pour la première fois par KIRIANENKO et al (1961) avec un spectromètre à quartz courbé.

2) *Spectrométrie par discrimination électronique.* Les impulsions délivrées par un compteur proportionnel ou un

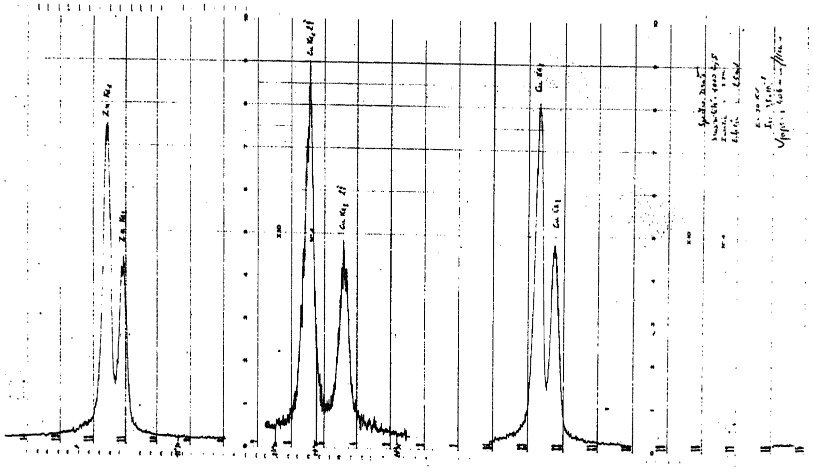

Figure 3. Enregistrement du doublet K α_1 α_2 du zinc (à gauche) et du cuivre (à droite, réflexions du 1er et au centre du 2ème ordre) obtenu avec le spectromètre à cristal de quartz courbé (R = 50 cm, plan (10$\bar{1}$1) de la microsonde de Castaing.

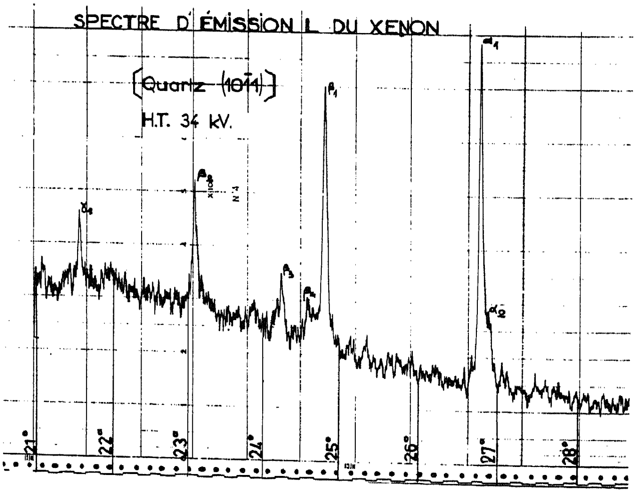

Figure 4. Enregistrement du spectre L du Xénon réalisé pour la première fois par Kirianenko et al (1961). L'objet est constitué d'argent pur chargé de Xénon par décharge basse tension.

scintillateur ont une hauteur proportionnelle à l'énergie des photons incidents. Une méthode spectrométrique consiste donc à ne compter que des impulsions d'amplitude comprise entre deux niveaux choisis au moyen d'un discriminateur.

Malheureusement les impulsions ont des amplitudes distribuées statistiquement autour de leur amplitude moyenne (Figure 5). On définit la largeur de cette distribution par son écart type, évalué en valeur relative $\sigma_p/\overline{P}$:* il varie comme. $E^{-1/2}$, si E est l'énergie des photons incidents (Figure 6). Deux distributions ne pourront être distinguées que si leur écart est suffisant (disons $> 2\,\sigma_p$). Cette condition interdit la distinction des raies K α de deux éléments consécutifs dans la classification périodique, et les distributions ne seront distinctes qu'à condition que:

$$\Delta Z > 3$$

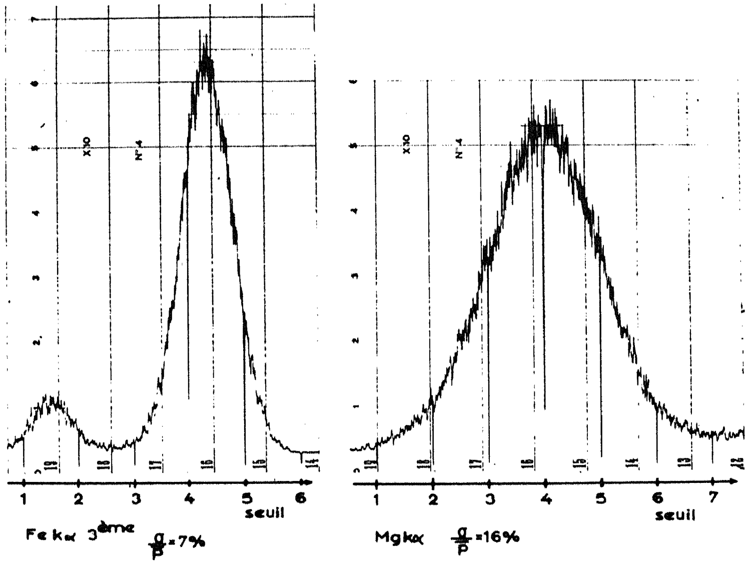

Figure 5. Courbe de distribution des amplitudes d'impulsions délivrées par un compteur proportionnel à flux (mélange gazeux Argon + 10% méthane). A droite émission K du magnésium, à gauche émission K du fer avec le "pic de fuite" dû à l'excitation par fluorescence de l'argon du compteur. Abcisses en unités arbitraires.

---

* - $\overline{P}$ désigne l'amplitude moyenne des impulsions.

si ΔZ désigne la différence des numéros atomiques des 2 éléments considérés.

La Figure 7 montre la forme des impulsions enregistrées avec un oscillographe dans le cas d'un échantillon composé d'un mélange de SiO_2 + CaO + FeO. On voit nettement les trois groupes d'impulsions correspondant, de bas en haut, aux émissions K de Si, Ca et Fe. Un spectromètre à cristal n'est donc pas nécessaire pour l'analyse de ces mélanges.

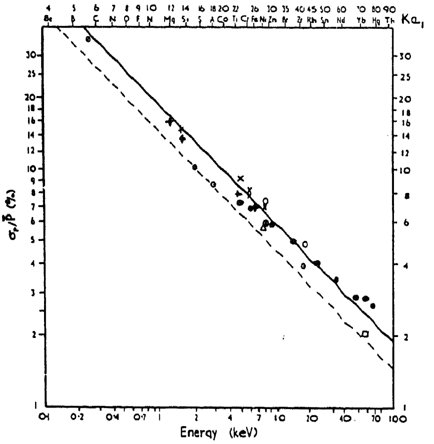

Relative standard deviation of pulse height distribution with energy

—— theoretical (Snyder, Frisch, Fano).
- - - empirical [equation (8)].
× Mulvey and Campbell.
● Bisi and Zappa.
○ Hanna, Kirkwood and Pontecorvo.
△ Arndt, Coates and Riley.
◌ Curran, Cockroft and Angus.
⊗ Lang.
□ West and Bradley.
+ IRSID

Figure 6. Variation de la résolution $\sigma_p/\bar{P}$ d'un compteur proportionnel en fonction de l'énergie E des photons incidents. σ_p désigne l'écart type de la distribution des amplitudes des impulsions délivrées par le compteur et $\bar{P}$ leur amplitude moyenne. D'après Mulvey et Campbell (1958).

On a cherché à surmonter la limitation $\Delta Z > 3$ par une analyse de la courbe de distribution des amplitudes d'impulsions résultant de la superposition de plusieurs courbes de niveau moyen $\bar{P}$ différent et de hauteur différente correspondant aux émissions de chaque élément constitutif (Figure 8). Cette analyse est simple dans le cas où l'on doit résoudre les émissions de 2 ou 3 éléments seulement, ainsi que l'a montré en particulier DOLBY (1960).

Considérons en effet (Figure 9) les courbes des distributions d'amplitude d'impulsions relatives à plusieurs éléments de hauteurs A, B, C . . . proportionnelles aux concentrations C_A, C_B, C_C à déterminer. La réponse donnée par le compteur se présentera sous forme d'une courbe de distribution somme des courbes de distribution élémentaires. Dans le cas de trois composantes, on peut mesurer les ordonnées M_1, M_2, M_3 correspondant à 3 niveaux, ou plutôt à 3 bandes étroites: dV_1, dV_2, dV_3. L'on aura:

$$\left(\begin{array}{l} M_1 = K_{11}A + K_{12}B + K_{13}C \\ M_2 = K_{21}A + K_{22}B + K_{23}C \\ M_3 = K_{31}A + K_{32}B + K_{33}C \end{array}\right. \quad \text{d'où} \quad \left(\begin{array}{l} A = k_{11}M_1 + k_{12}M_2 + k_{13}M_3 \\ B = k_{21}M_1 + k_{22}M_2 + k_{23}M_3 \\ C = k_{31}M_1 + k_{32}M_2 + k_{33}M_3 \end{array}\right.$$

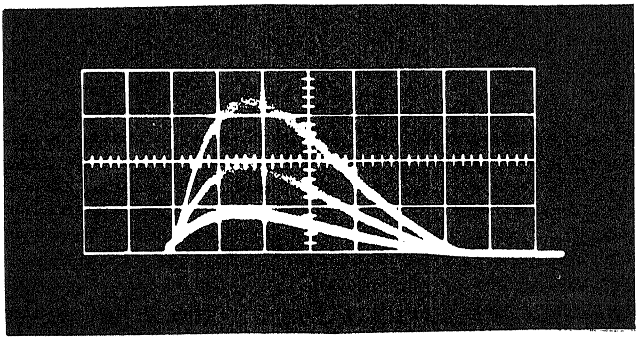

Figure 7. Enregistrement oscillographique des impulsions délivrées par un compteur proportionnel à flux détectant les raies K de fluorescence émises par un mélange de poudre comprimée 20% Fe_2O_3 + 60% SiO_2 + 20% $CaCO_3$. De haut en bas, impulsions correspondant à Si, Ca, Fe. cf. Fig. 16. D'après Le Traon et Seibel (1962).

d'où les valeurs de A B C par inversion de la matrice K.

Si les courbes de distribution étaient exactement gaussiennes, les 9 coefficients k_{ij} seraient calculables à partir des écarts types des distributions d'impulsions et des différences entre leur niveau moyen $\bar{P}$. En pratique, on les déterminera expérimentalement en mesurant M_1, M_2, M_3 successivement sur trois témoins constitués des trois éléments purs. Les trois équations donnant A, B, C et donc les concentrations des trois éléments peuvent être résolues au moyen d'un calculateur simple à 3 canaux, si les trois niveaux M sont mesurés et amplifiés simultanément. Deux difficultés doivent être signalées: d'une part la présence d'un fond continu d'intensité variable avec l'énergie et qu'il faut soustraire des mesures M_1, M_2, M_3, et, d'autre part, l'existence des "pics de fuite"; c'est ainsi que le pic de fuite dû à la fluorescence de l'argon du compteur sous l'effet du rayonnement du fer (visible sur la Figure 5) se superpose au pic normal du calcium.

Un avantage de la discrimination d'amplitude montée à la suite d'un spectromètre à cristal est d'éviter les erreurs dues à la superposition à la raie analysée, d'une réflexion d'ordre multiple d'une autre radiation. Ceci est particulièrement fréquent dans le cas des grandes longueurs d'onde.

B - SPECTROMETRIE D'ABSORPTION

Le coefficient d'absorption d'une raie donnée variant à peu près comme Z^3, les différences de composition seront facilement décelées en mesurant l'intensité du rayonnement transmis:

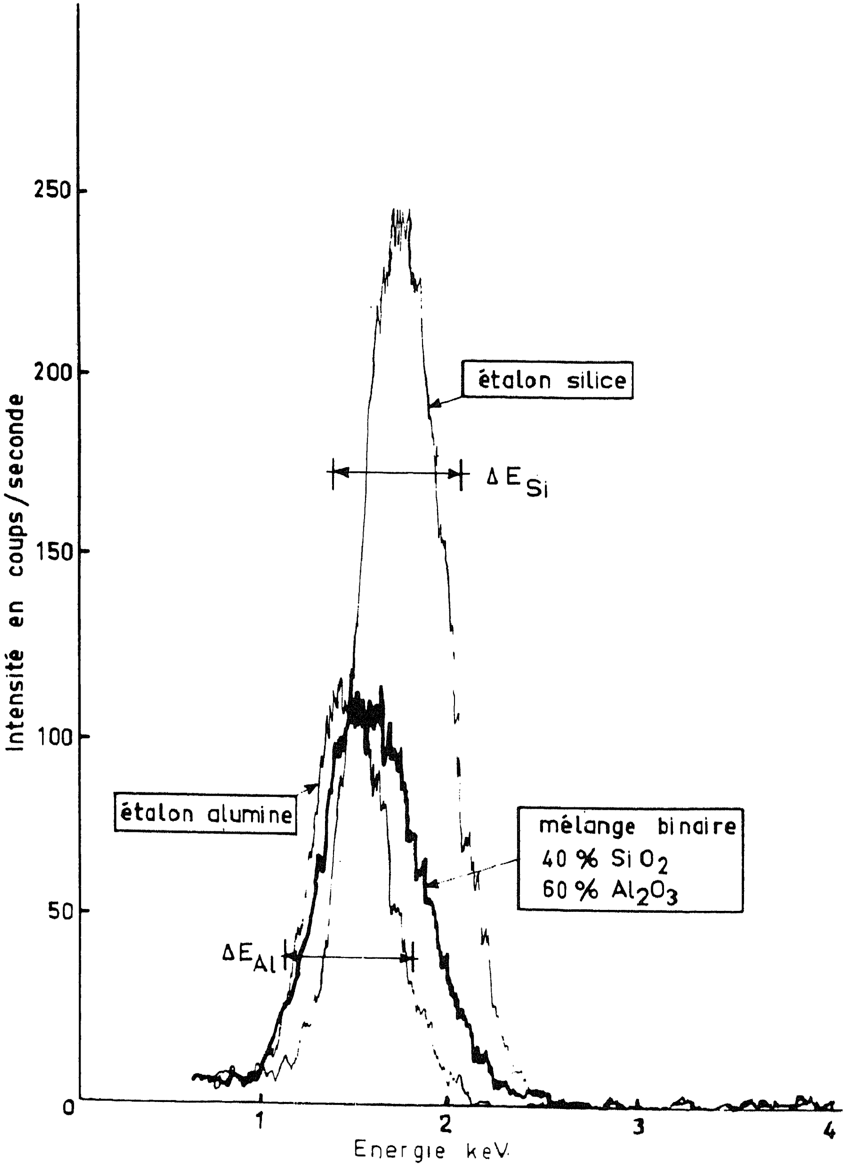

Figure 8. Courbes de distribution des impulsions d'un compteur proportionnel à flux, données par les étalons de silice et alumine pure et par un mélange Al_2O_3 + SiO_2. D'après Le Traon et Seibel (1962).

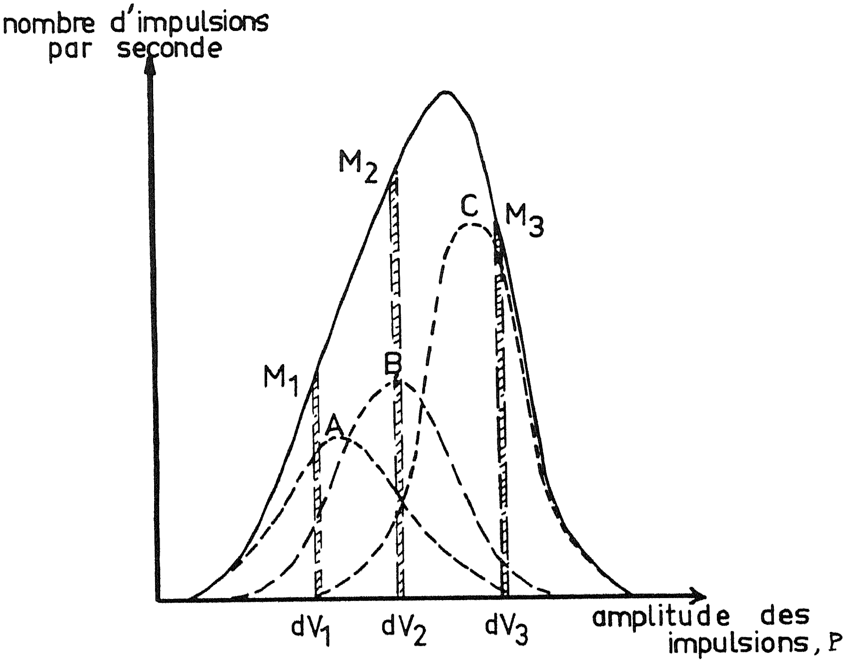

Figure 9. Courbe de distribution des amplitudes P d'impulsions délivrées par un compteur proportionnel dans le cas de l'émission de trois éléments et analyse en courbes élémentaires A B C.

c'est la base de la radiographie et de la microradiographie, qualitative ou quantitative.

Une autre loi d'absorption fondamentale est la variation du coefficient d'absorption avec la longueur d'onde: cette variation en λ^3 n'est pas continue mais présente des sauts caractéristiques correspondant aux niveaux K, L_I, L_{II} . . . de l'atome. Ceux-ci sont utilisés pour accroître la sensibilité et la résolution de la radiographie. Les applications à l'analyse macroscopique ou microscopique peuvent être très intéressantes, surtout si on la combine avec une méthode spectrométrique pour mesurer les intensités transmises à différentes longueurs d'onde; bien que l'analyse quantitative ne soit guère possible pour des échantillons renfermant plus de 2 éléments.

Cette méthode est applicable à l'analyse microscopique. Une source ponctuelle de rayons X est constituée en bombardant une anticathode mince par une sonde électronique. Si la distance source-objet est n fois plus petite que la distance objet-plaque photographique, on a sur celle-ci une microradiographie à grossissement n. Remplaçons—la plaque par un diaphragme de diamètre d. Celui-ci correspond à une région de l'échantillon de diamètre d/n. Un spectromètre à cristal ou à discrimination permet de doser le rayonnement de longueur d'onde λ. On mesure alors les intensités transmises I_1 et I_2 aux longueurs d'onde λ_1 et λ_2. En désignant par $(\mu/\rho)_i^X$ le coefficient d'absorption massique de λ_i par X, et par m_A et m_B les masses par unité de surface de deux éléments A et B dans l'échantillon on a évidemment:

$$\log \frac{I_1}{I_2} = m_A \left[\left(\frac{\mu}{\rho}\right)_1^A - \left(\frac{\mu}{\rho}\right)_2^A \right] + m_B \left[\left(\frac{\mu}{\rho}\right)_1^B - \left(\frac{\mu}{\rho}\right)_2^B \right] .$$

Si les longueurs d'onde λ_1 et λ_2 ont été choisies de part et d'autre de la discontinuité d'absorption de A et aussi rapprochés que possible, le second terme de l'équation ci-dessus est négligeable devant le premier et l'on peut doser directement A (Figure 10). Remarquons que dans ce cas B peut désigner aussi bien un second élément que la matrice complexe dans laquelle est dissout A.

Cette méthode de microanalyse par absorption est utile en particulier pour des objets qui supportent mal le bombardement électronique (objets biologiques ou minéralogiques, LONG 1958, Figure 11).

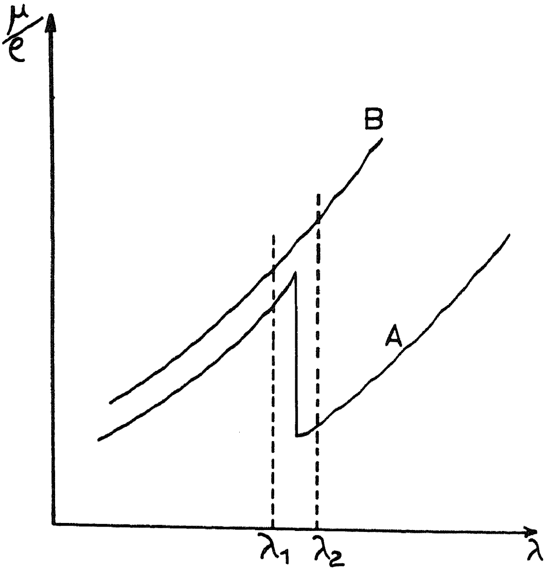

Figure 10. Principe de l'analyse par spectrométrie d'absorption: variation du coefficient d'absorption avec la longueur d'onde de l'élément A et de la matrice B où il est dissous.

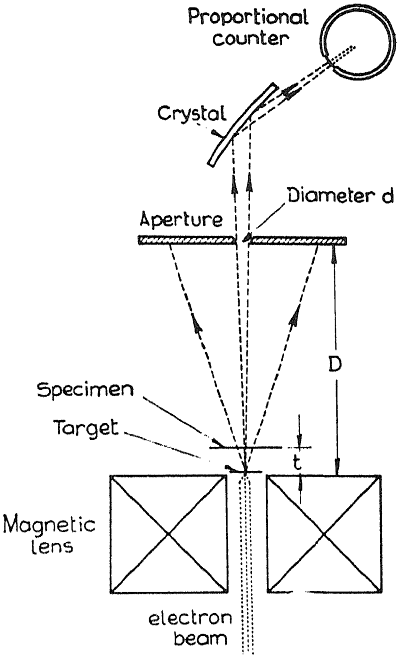

Figure 11. Schéma d'un appareil de microanalyse par absorption d'après P. Duncumb (1959).

Signalons juste en passant une autre application importante: l'étude fine des discontinuités d'absorption en relation avec la structure électronique et l'état physico-chimique de l'atome absorbant.

C - DOMAINE DE LA SPECTROMETRIE DE RAYONS X

Les caractéristiques des spectromètres limitent le domaine des longueurs d'onde utiles et donc la nature des éléments chimiques qui peuvent être analysés. Le spectromètre doit posséder un cristal (éventuellement) de bon paramètre et bon pouvoir réflecteur, un récepteur de rendement suffisant. Il doit de plus éviter l'absorption du rayonnement tant par l'air que par fenêtres intermédiaires. Cette dernière condition nécessite des spectromètres fonctionnant sous vide pour les longueurs d'onde supérieures à 2 Å et l'utilisation de fenêtres en matériaux très peu absorbants: béryllium très mince (< 80 μ) ou matière plastique (Mylar, 0,5 mg/cm^2). Le scintillateur est donc exclu aux grandes λ, à moins de supprimer sa fenêtre et de le faire travailler dans le vide même du spectromètre. Le compteur Geiger ou le compteur proportionnel sont pratiquement les seuls utilisés. L'emploi de fenêtre très mince ne permet malheureusement plus de fabriquer un compteur scellé, si bien que le gaz de remplissage doit circuler en permanence dans le compteur.

Ces progrès ont permis depuis peu d'années de faire passer la limite inférieure des éléments analysables de $Z \approx 18$ à $Z = 11$. De nouveaux progrès ont été réalisés en vue d'abaisser cette limite en utilisant des compteurs à flux à fenêtre très mince. L'emploi de réseau optique sous incidence rasante (conditions de réflexion totale des rayons X) ne donnant pas des raies intenses, ni une grande dispersion, on s'est orienté vers la spectrométrie par discrimination en utilisant des compteurs proportionnels. Les rayonnements des éléments très légers ont pu être ainsi décelés (DOLBY, 1960, DUNCUMB, 1961, MULVEY, 1960) et la limite de détection abaissée au rayonnement du Be vers 110 Å! (HOLLIDAY, 1960, CAMPBELL, 1962).

Les difficultés pour l'analyse de ces éléments doivent cependant être notées: les coefficients d'absorption de ces radiations sont très élevés, si bien que le rayonnement reçu n'est émis que par une mince couche à la surface de l'échantillon.* On peut alors se demander si les mesures seront bien caractéristiques de l'échantillon, du fait des perturbations mécaniques et chimiques possibles de la surface. Dans le cas de l'émission directe (cf. plus bas) il faut absolument éviter la contamination de l'échantillon, surtout pour l'analyse du carbone.

Une autre difficulté réside dans la forte probabilité de superposition à la raie analysée, la raie K α C émise par un carbure par exemple, de raies de série M (très nombreuses) d'éléments lourds contenus dans ce carbure, d'autant plus que ces raies sont larges et que la résolution du compteur proportionnel n'est pas très bonne pour les faibles énergies (cf. ci-dessus).

II - PRODUCTION DU SPECTRE X

A - METHODES D'EXCITATION

Il existe deux méthodes pour exciter l'émission X d'un échantillon:

---

*Le coefficient d'absorption de la raie K α Al dans le fer par exemple est égal à 2.800, ce qui correspond à une transmission de 30% par une lame de fer de 1/2 μ. Pour les raies de C, N ou O ces coefficients seront encore plus éléves. Dans l'air par exemple, on a pour les raies K α du Fe, Al et C, des coefficients d'absorption égaux respectivement à 19, 1.200 et 5.100. Le coefficient d'absorption de la raie Kα C dans l'aluminum est égal à 25000.

a. Par bombardement électronique: c'est *l'émission directe*.

b. Par irradiation par un rayonnement X primaire: c'est *l'émission de fluorescence*.

Ces deux modes d'excitation conduisent à des rayonnements de caractéristiques différentes:

1) *Intensité*. A puissance dépensée égale, l'émission directe fournit des raies 100 à 1000 fois plus intenses que la fluorescence. Cette différence vient en grande partie d'effets purement géométriques. Dans les appareils de fluorescence actuels, seule une faible fraction du rayonnement X produit dans le tube est utilisé pour irradier l'objet. Il serait intéressant d'améliorer sur ce point les appareils de fluorescence X. Le meilleur rendement est obtenu dans la sonde de CASTAING, où la limitation provient uniquement de la fraction de rayonnement reçu dans le spectromètre. L'expérience et le calcul montrent que l'intensité de la raie K α_1 Zn reçue dans le spectromètre est égale à (HENOC, 1962):

$$1{,}7.10^{-3} \text{ photon/électron, sous } 30 \text{ kV.}$$

2) *Rapport raie/bruit de fond*. Les impulsions arrivant au système de comptage suivant une loi de distribution aléatoire, la précision de la mesure est limitée par la largeur de cette distribution. La mesure de la hauteur de la raie et du bruit de fond B.F. sont caractérisés par des écarts types σ_R et σ_{BF}, de sorte que la différence (hauteur de raie - B.F.) est affectée d'un écart type

$$\sigma = \sqrt{\sigma_R^2 + \sigma_{BF}^2} .$$

Or l'émission directe provoque un bruit de fond important, du à l'émission d'un spectre continu superposé au spectre de raies.

L'intensité totale du spectre continu est proportionnelle à $Z E_o^2$ si E_o désigne l'énergie des électrons incidents. La fraction de l'énergie incidente convertie en rayonnement continu est donc proportionnelle à $Z E_o$. Pour une anticathode de cuivre, à 50 kV, cette fraction est d'environ 10^{-3}. Dans un domaine de fréquence $d\nu$, l'intensité du spectre continu est proportionnelle à

$$dJ = Z(\nu_o - \nu)\, d\nu$$

si $\nu_o = E_o/h$.

L'intensité d'une raie varie avec E_o suivant une loi différente. Dans la série K, celle-ci est proportionnelle à $(E_o - E_k)^{1,65}$. Le rapport raie/spectre continu émis dans une bande de fréquence étroite dν autour de la raie augmente donc continûment avec E_0 sans présenter de maximum (c'est ce rapport qui est intéressant en spectrométrie, plutôt que le rapport raie/intensité totale émise dans le spectre continu (cf. COSSLETT, 1960).

En fluorescence, le fond continu consiste uniquement dans les radiations diffusées soit élastiquement, soit inélastiquement (par effet Compton). Cette diffusion ne devient importante que pour les objets de faible numéro atomique. C'est un spectre continu lorsque le rayonnement primaire est constitué luimême d'un spectre continu. Si bien que dans le cas de l'analyse de traces d'éléments "lourds" dans une matrice "légère", l'émission directe peut être à ce point de vue plus advantageuse que la fluorescence.

Avec la microsonde de CASTAING, en utilisant un cristal de quartz $(10\bar{1}1)$ courbé, nous avons obtenu pour la raie Cu K α_1 un rapport raie/bruit de fond d'environ 750 avec un compteur Geiger, et 1500 avec un compteur proportionnel et discrimination des impulsions. Un tel rapport permet d'atteindre une sensibilité élevée pour l'analyse d'éléments en faible concentration.

3) *Finesse des raies.* La plus grande intensité obtenue à l'heure actuelle par émission directe permet d'utiliser le spectromètre avec des fentes très fines, d'où de meilleures conditions de focalisation dans le spectromètre et des raies plus fines. Ceci permet de séparer les raies voisines dans le spectre, alors que ce n'est pas possible par fluorescence. Nous citerons deux exemples. L'analyse des traces de tantale dans le niobium a été effectuée par CROUTZEILLES (1962) sur un appareil qui permet de travailler en fluorescence ou en émission directe: l'objet est alors placé dans une encoche pratiquée sur l'anticathode du tube. Ce n'est que grâce à la meilleure focalisation possible en émission directe que la raie L α Ta a pu être bien séparée de la réflexion du second ordre de K α Nb. L'émission de cette raie peut d'ailleurs être supprimée en abaissant le potentiel du tube, ce qui n'est pas possible en fluorescence.

La microsonde offre un exemple où la source étant ponctuelle, les conditions optimales de focalisation peuvent être réalisées. La finesse des raies obtenues nous a permis le dosage précis du vanadium et du chrome dans un alliage de titane au vanadium-chrome, bien que la raie K α_1 V ne soit qu'à 7 uX de K β Ti et K α Cr à 5 uX de K β V, ce qui avec un quartz $(10\bar{1}1)$ correspond à des différences d'angle de Bragg de 4 1/2 et 3 minutes respectivement (Figure 12).

4) *Taux d'excitation.* Nous avons ci-dessus signalé un avantage de l'émission directe: le taux d'excitation peut être ajusté de façon à n'obtenir que les raies de certains éléments à l'exclusion d'autres.

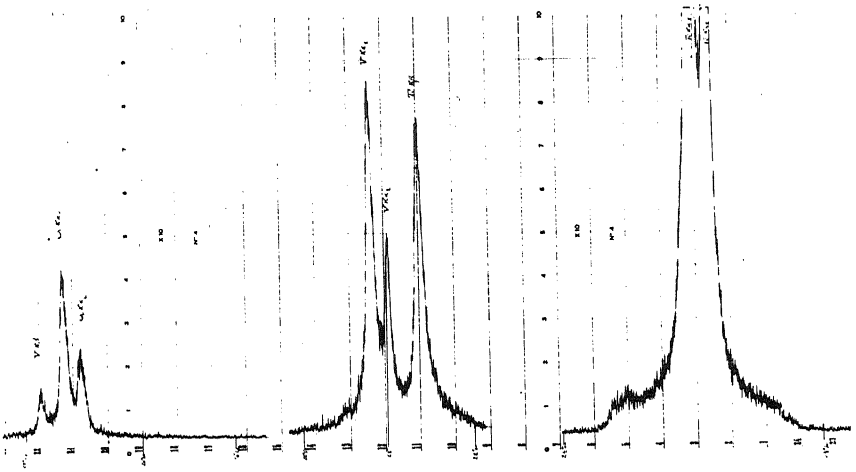

Figure 12. Enregistrement du spectre K d'un alliage à base de titane, contenant du vanadium et du chrome. Spectromètre à cristal de quartz $(10\bar{1}1)$ courbé de la microsonde de Castaing. De gauche à droite, raies $VK\beta$, $CrK\alpha_1\ \alpha_2$, $VK\alpha_1\ \alpha_2$, $TiK\beta$, $TiK\alpha_1\ \alpha_2$.

B - EXCITATION PAR DES SOURCES RADIOACTIVES

L'utilisation de sources radioactives permet de résoudre de manière simple et élégante le problème de l'excitation. D'une part les sources sont peu encombrantes, d'où une simplification considérable de l'appareillage, et une économie. D'autre part, l'intensité est absolument stable, si la période radioactive est assez longue, d'où suppression du problème de la stabilité du générateur, qui se pose de façon souvent aigue dans les laboratoires d'usines.

Le tableau 2, d'après MARTINELLI et SEIBEL (1961), rassemble les principaux types de sources actuellement utilisables en distinguant:

a. Les émetteurs de rayonnement β.

b. Les émetteurs de rayonnement X. Le rayonnement X peut être produit par une cible intermédiaire ou dans la source elle-même: on obtient alors un spectre continu (freinage des électrons) et un spectre de raies. Les excellentes conditions géométriques de freinage dans la source elle-même fournissent un rayonnement X avec un rendement optimal. Enfin on dispose de sources monochromatiques, le rayonnement X étant produit par capture K.

Cependant, un défaut de ces sources réside dans leur intensité relativement faible par rapport aux sources classiques. Le rayonnement X émis n'est pas assez intense pour être analysé avec un spectromètre à cristal. C'est là une petite

Tableau 2

Sources Radioactives Utilisables en Spectrométrie X
D'Après Martinelli et Seibel, 1961

Sources radio-actives	Emission directe		Electrons (β)	Emetteur β (< 4 Curies) 90_{Sr}: $E_{max} = 0{,}61$ et 2,18 Mev; T = 20 ans 85_{Kr}: $E_{max} = 0{,}67$ Mev; γ 0,7% 0,52 Mev; T = 10,6 ans 147_{Pm}: $E_{max} = 0{,}223$ Mev; T = 2,3 ans
	Fluorescence X	Source β et cible intermédiaire	Rayons X	Emetteur β (< 4 Curies) 90_{Sr}, 85_{Kr}, 147_{Pm}
		Source de rayonnement X de freinage		Emetteur β 147_{Pm} (~200 Curies) 63_{Ni}: $E_{max} = 0{,}067$ MeV T = 125 ans 3_{H}: $E_{max} = 0{,}018$ MeV T = 12,3 ans (< 20 Curies)
		Source de rayonnement X ou γ		Emetteur X par capture K (< 100 μC) 55_{Fe}: 5,9 kev; T = 2,94 ans 109_{Cd}: 22 kev; T = 470 j. 181_{W}: 56,9 kev; T = 145 j. Emetteur γ-X (freinage) 241_{Am}: 60 kev; X divers; T = 470 ans

complication pour l'analyse d'éléments de numéro atomique proche (cf. ci-dessus).

Les conditions géométriques de l'ensemble source + échantillon + compteur peuvent être très variées. Quelques schémas, d'après G. SEIBEL, sont donnés sur la Figure 13 à titre d'exemple. On note dans le cas de l'excitation β la présence d'un aimant permanent pour dévier les électrons rétrodiffusés en dehors de la fenêtre du compteur. On pourrait aussi utiliser un filtre (en plexiglass par exemple), si l'énergie des rayons X à analyser est assez élevée.

Ces méthodes ont conduit récemment en France à des applications à l'analyse de routine d'un très grand intérêt. Citons un appareil automatique d'analyse des carottes de sondage des minerais de fer. La source est constituée de tritium (émetteur β de 18 kV, 25 curies) absorbé dans des dépôts minces de titane ou de zirconium. La raie K α du titane est très intense dans le premier type de source et excite très bien le rayonnement du calcium. Une telle source évidée en son centre irradie une aire de 12 x 20 mm^2 environ. Les impulsions sont reçues par un compteur proportionnel scellé (cf. Figure 13) et comptées après discrimination. Cet ensemble défile à vitesse constante le long de la carotte et l'on enregistre simultanément les concentrations de fer et de calcium (Figure 14).

DISPOSITIF DE MESURE

Prométhéum^{147}

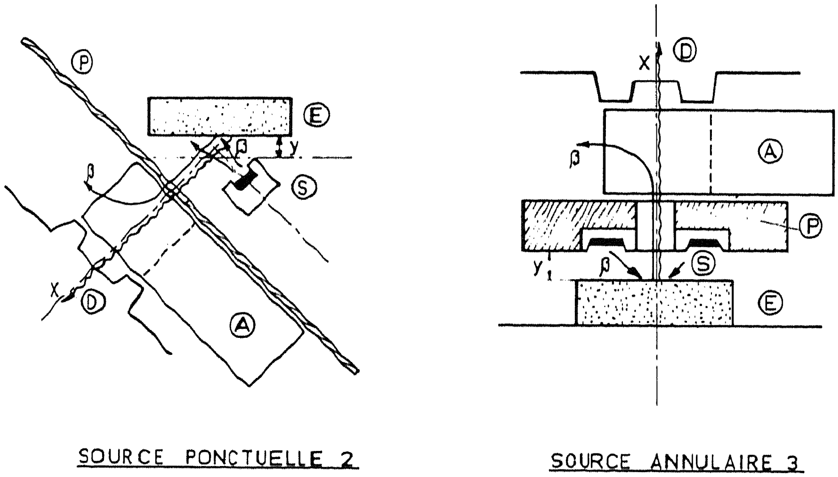

SOURCE PONCTUELLE 2 SOURCE ANNULAIRE 3

Figure 13-A. Schémas des dispositifs de l'ensemble source radioactive S+ récepteur R+ échantillon E. Excitation par des rayons β émis par une source ponctuelle ou une source annulaire. A, aimant permanent. D'après SEIBEL (1960-1961).

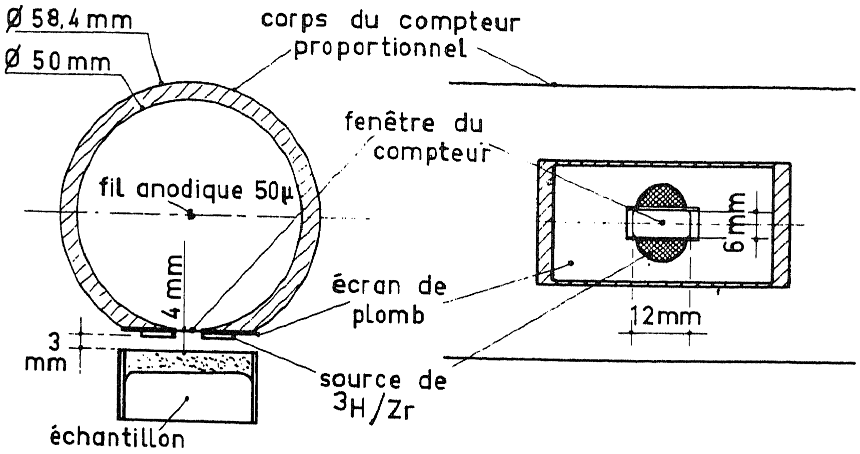

Figure 13-B. Schéma du dispositif de l'ensemble source radioactive + récepteur + échantillon. Exemples d'excitation par les rayons X émis par une source annulaire. D'après Seibel (1960-1961).

Des sources de tritium absorbé sur zirconium (spectre donné par la Figure 15) permettent d'analyser le silicium, le calcium et le fer dans des minerais de fer. Les pastilles sont préparées comme en fluorescence, et introduites dans une enceinte sous vide. Un compteur proportionnel à flux permet de discriminer les rayonnements des trois éléments à analyser, comme le montre la Figure 16. C'est la raie L du zirconium (à 2 KeV, cf. Figure 15) qui excite convenablement le spectre K du silicium; le rayonnement de Ca et Fe est excité par le spectre continu.

Plusieurs autres applications de ce type de source sont actuellement à l'étude.

C - MICROSONDE DE CASTAING

1. Caractéristiques Générales

L'application la plus importante à ce jour de l'émission directe est l'utilisation de sondes électroniques pour effectuer l'analyse élémentaire à l'échelle microscopique. Les tout premiers résultats ouvrant la voie à cette méthode furent présentés par CASTAING et GUINIER en 1949. Dans son travail publié en 1951, CASTAING montrait non seulement la réalisation du premier appareil expérimental et quelques applications métallurgiques, mais encore édifiait la théorie de l'analyse quantitative en précisant la forme de la relation émission-concentration et exposant une méthode de calcul de correction des résultats.

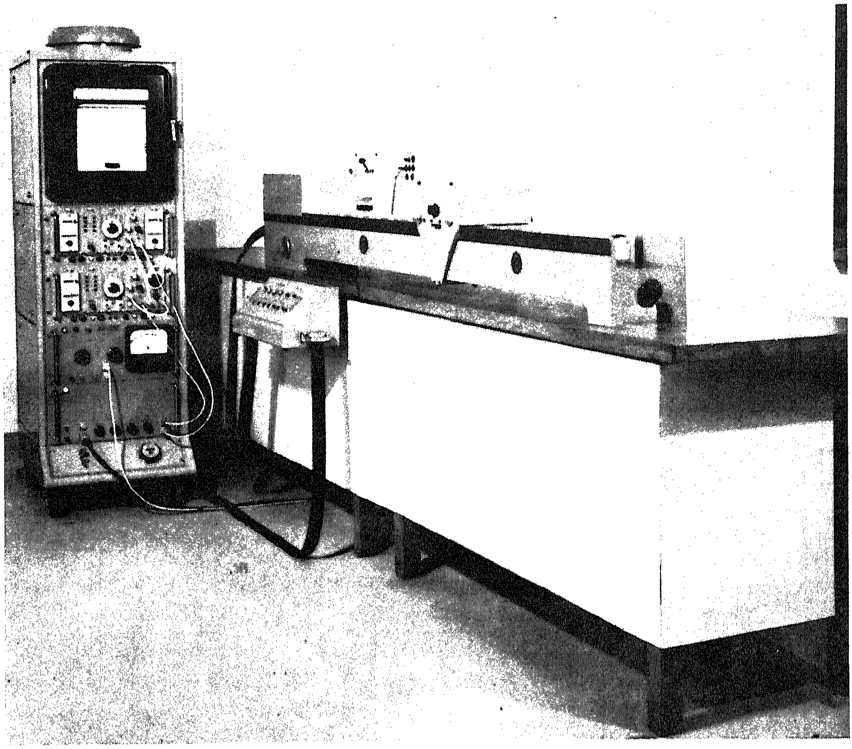

Figure 14. Photographie de l'appareil de dosage automatique du fer et du calcium dans les carottes de minerai de fer. D'après Seibel (1961).

Par la suite, il devait construire un appareil d'un modèle perfectionné, le Microanalyseur à Sonde Electronique, bien connu souvent sous le nom de Microsonde. Cet appareil présenté en 1955 à l'Exposition de la Société Française de Physique à Paris a ensuite été construit commercialement par une société française (Figures 17 et 18).

BOROVSKI en URSS travaillant dans la même voie publia peu après CASTAING une description d'un appareil de principe similaire (1953). Puis à la suite de ces travaux de nombreux expérimentateurs, en Grande Bretagne et aux USA en particulier, construisent des appareils de conceptions et caractéristiques variées.

Parmi tous ces travaux, il faut citer surtout la méthode de balayage, dont les premiers résultats furent publiés en 1956 par DUNCUMB et COSSLETT. Comme on le sait, cette méthode permet d'obtenir sur l'écran d'un oscillographe des images de la répartition de tel ou tel élément chimique présent dans

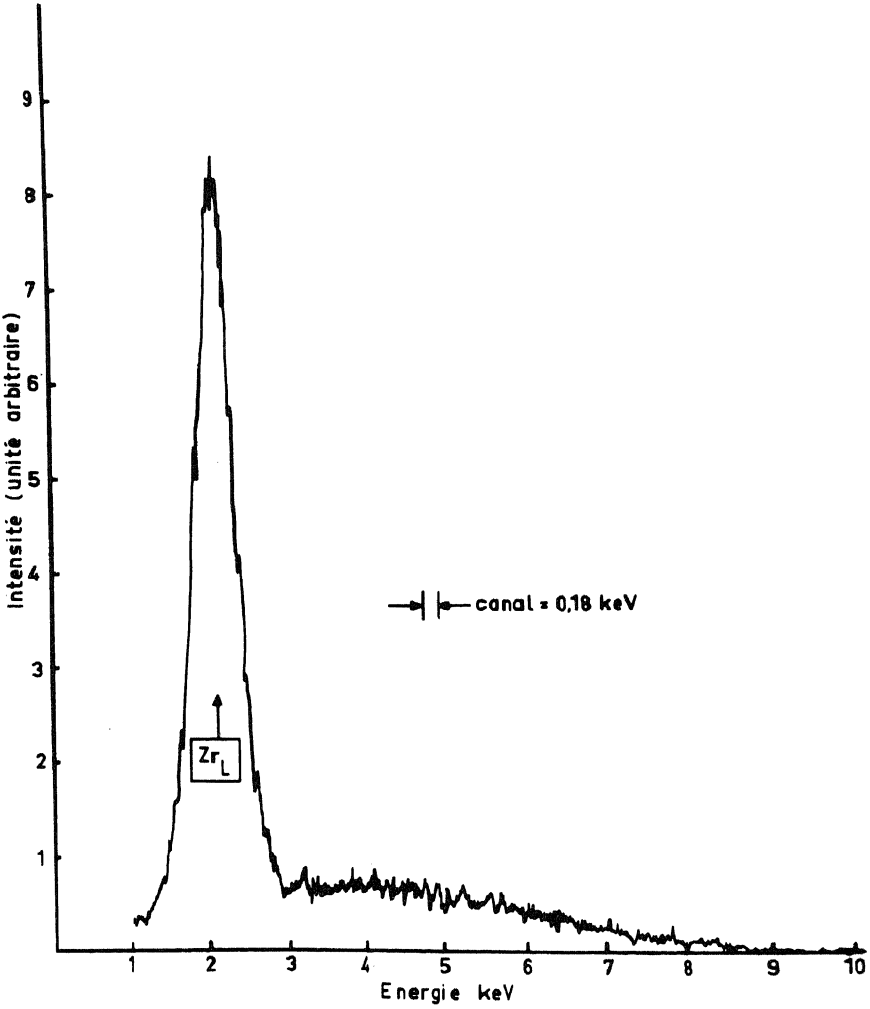

Figure 15. Spectre d'une source de tritium absorbé dans du zirconium. D'après Seibel et Le Traon (1962).

l'échantillon. Cette méthode a l'avantage de fournir une image qualitative très représentative et d'interprétation généralement aiseé. Ce sujet ayant été traité par le Professeur COSSLETT, nous ne ferons ici que donner à titre d'exemple une série d'images obtenues à l'aide de l'appareil français (Figures 19 et 20).

Par la suite, des discussions se sont poursuivies sur les diverses caractéristiques que devaient présenter un microanalyseur et en particulier sur la priorité à donner au balayage par rapport à l'analyse point par point, et sur le mode d'observation de l'échantillon.

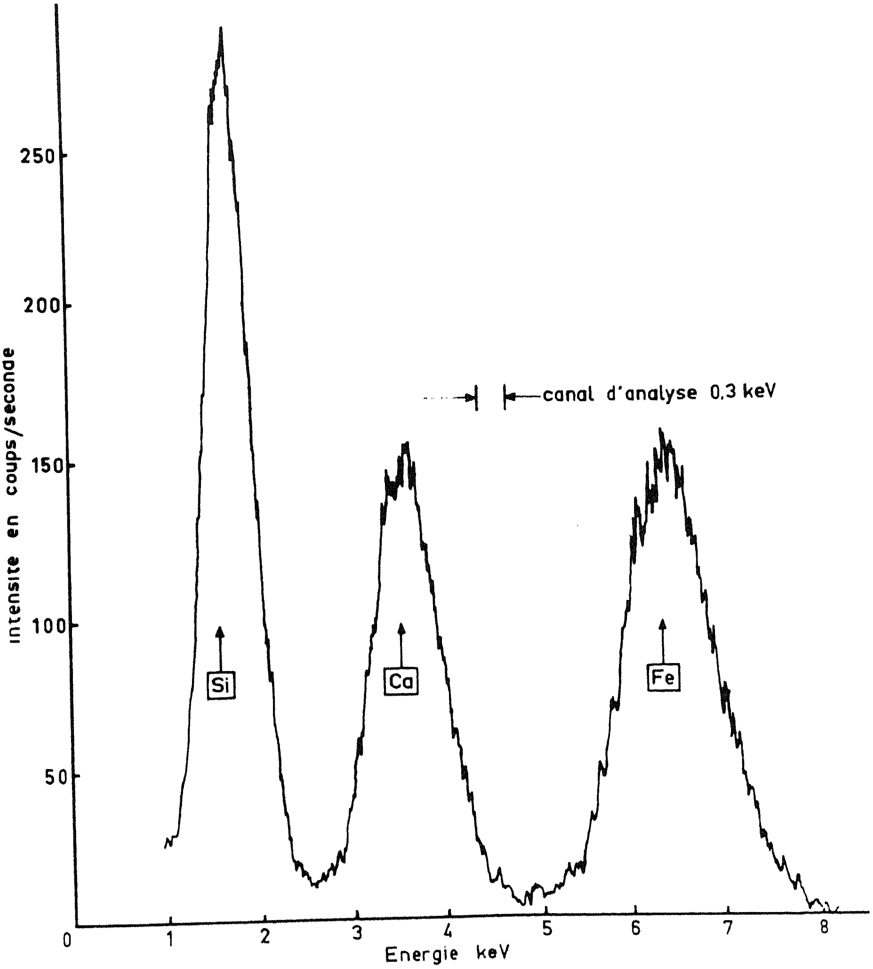

Figure 16. Courbes de distribution des impulsions données par un compteur proportionnel à flux, recevant les rayonnements K émis par un mélange 20% Fe_2O_3 + 60% SiO_2 + 20% $CaCO_3$ (vide: 4 mm de mercure). D'après Seibel et Le Traon (1962).

A vrai dire tout dépend de la qualité de l'information que l'on désire obtenir et du temps que l'on accepte de consacrer pour obtenir ces résultats. Dans les conditions actuelles, il nous semble que l'appareil idéal devrait posséder les caractéristiques suivantes:

a. Observation microscopique (par réflexion ou par transmission) simultanée à l'analyse. Il ne nous parait pas en effet que l'image électronique soit suffisante pour choisir

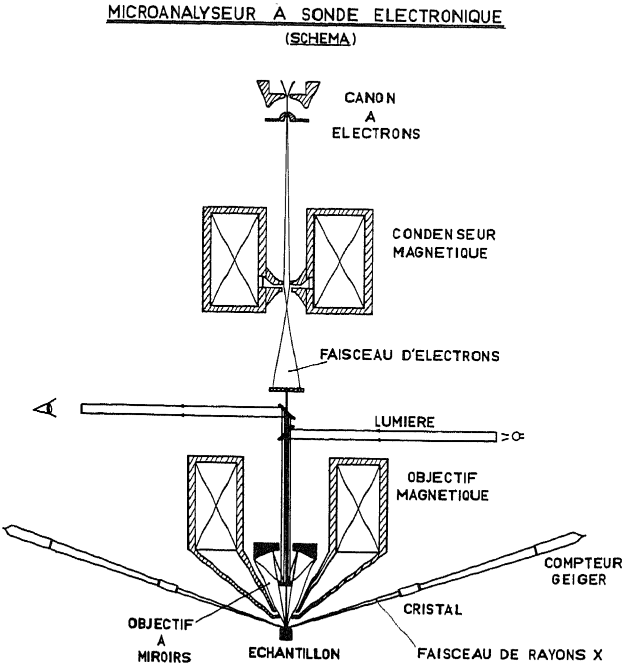

Figure 17. Schéma de principe de la microsonde de Castaing. D'après Castaing (1955).

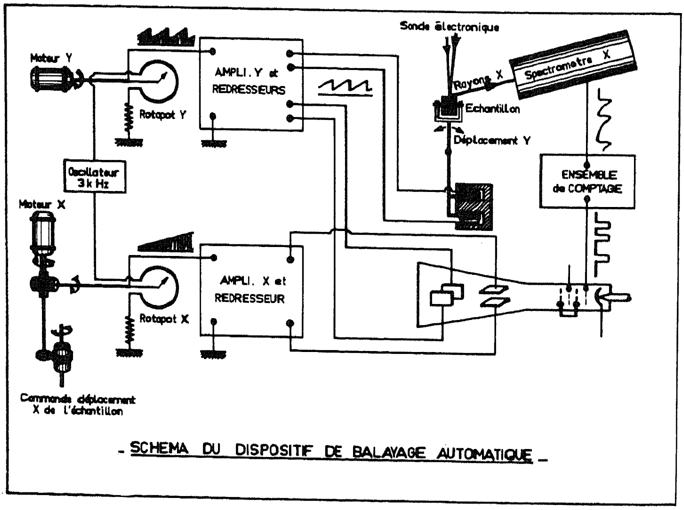

Figure 18. Schéma de principe du dispositif de balayage automatique de la microsonde française.

ALLIAGE Be-Al (10%)

Recuit 100 heures, 700°C.

Balayage 300 μ x 300μ - 450 lignes.

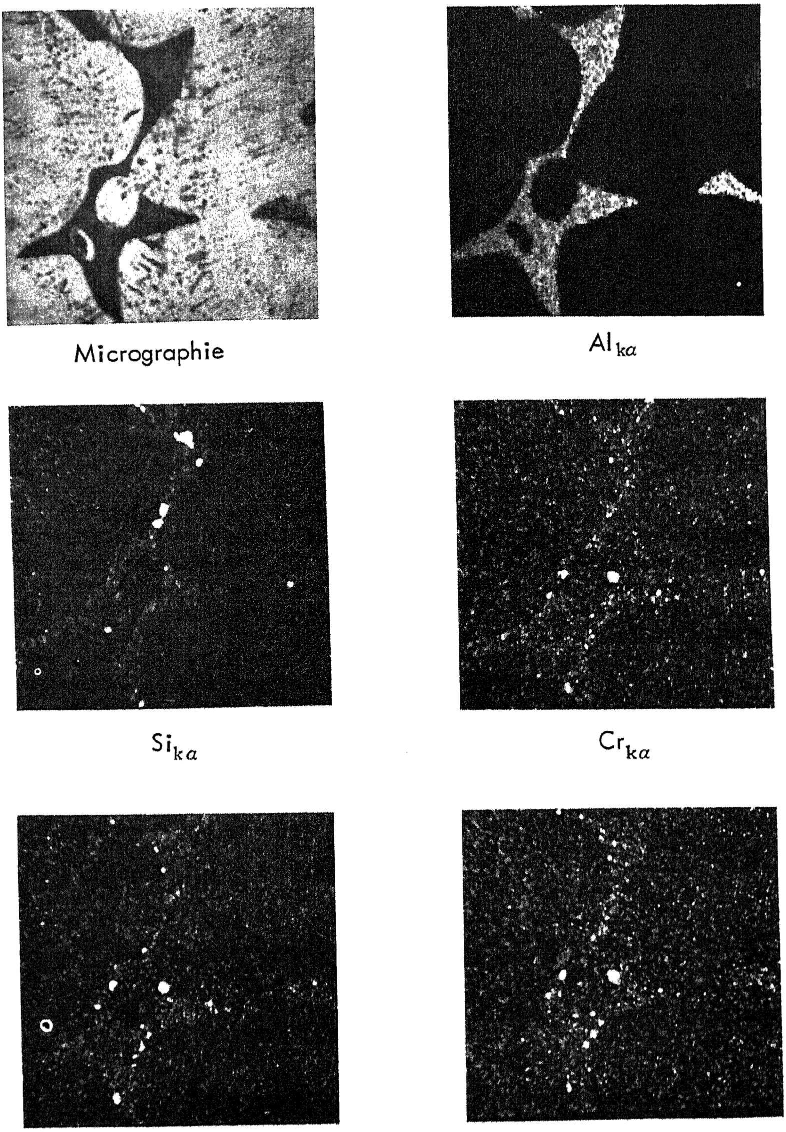

Micrographie

Al$_{k\alpha}$

Si$_{k\alpha}$

Cr$_{k\alpha}$

Mn$_{k\alpha}$

Fe$_{k\alpha}$

Figure 19

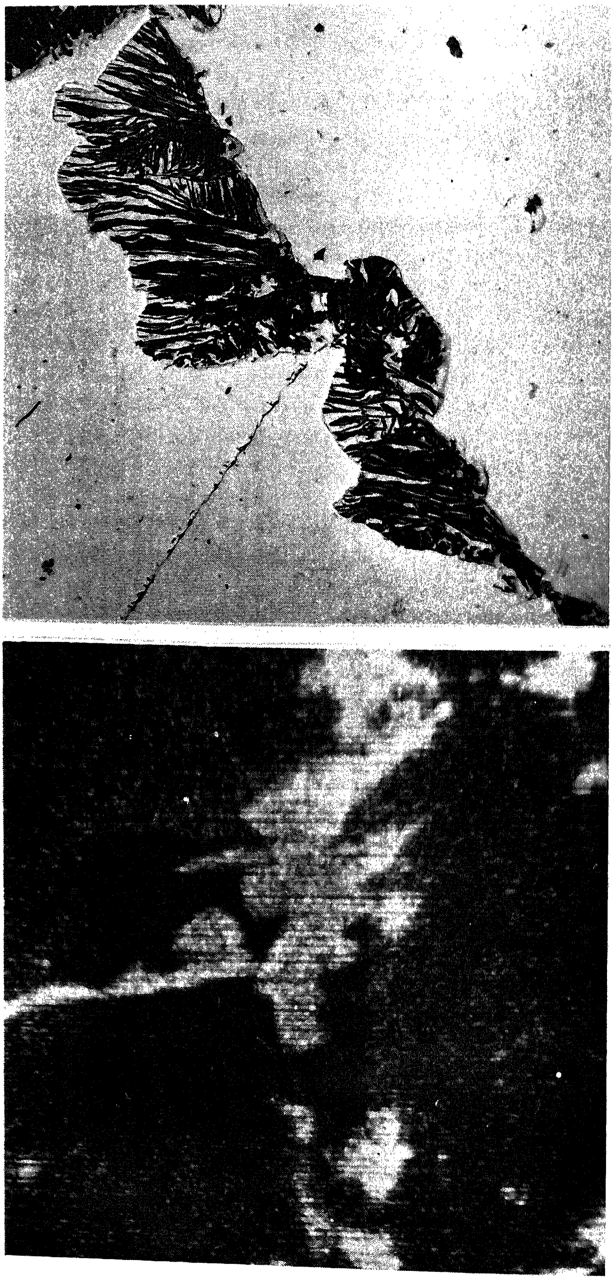

Figure 20. Images obtenues par balayage sur une réplique avec extraction. Acier inoxydable au Cr-Mn-N. Précipités de Cr_2N extraits sur film de carbone après un revenu de 24 h à 650°C. Comparaison de la micrographie électronique (X 6000) et du balayage avec la raie K α Cr (100 μ x 100 μ, 300 lignes) effectués sur la même réplique.

correctement les points à analyser. Le microanalyseur doit se présenter, aux yeux du métallographe ou du minéralogiste, comme un outil qui apporte un supplément d'information à l'observation microscopique, la faisant passer du stade qualitatif au stade quantitatif. Il importe donc de lui offrir les conditions d'observations habituelles de l'échantillon qu'il a préalablement observé au microscope. Ce microscope permet en outre de placer la surface de l'échantillon et des témoins dans le plan de focalisation de la sonde, ainsi que sur le cercle de focalisation du spectromètre.

b. Plusieurs spectromètres à focalisation à *haute* résolution, pour des conditions optimales d'analyse quantitative point par point. Ces spectromètres permettent non seulement la séparation de raies voisines (cf. Figure 3 et 12), mais encore donnent un rapport raie/bruit de fond élevé-condition nécessaire pour une sensibilité élevée (en particulier dans le cas d'éléments en faible concentration). Ces spectromètres seraient équipés des monochromateurs convenables pour couvrir de facon commode l'étendue de longueurs d'onde analysables et permettre l'analyse simultanée de deux (ou plus) éléments.

c. Un système de balayage, sur des aires allant de 50 à 500 μ de côté. Ce système devrait permettre d'obtenir des images dans un temps court, mais pouvoir de plus travailler à vitesse très lente pour obtenir en des temps beaucoup plus longs des images de haute résolution.

d. Un équipement pour l'analyse des éléments très légers ($Z \leq 10$); vu les progrès incessants dans ce domaine, il est peut-être prématuré d'en préciser les conditions optimales.

Il nous semble de plus que pour l'utilisation minéralogique courante un appareil de conception spéciale et adaptée aux besoins des minéralogistes serait souhaitable. Des travaux remarquable ont été effectués dans ce domaine par J. LONG en Grande Bretagne.

2. Pouvoir Séparateur

Les possibilités de la microsonde découlent immédiatement des caractéristiques de la spectrométrie X que nous avons résumées au début de cet exposé. Il nous reste encore à préciser le pouvoir de résolution, c'est-à-dire à déterminer les dimensions du plus petit volume analysable. Ces dimensions dans le cas d'un échantillon massif ont été discutées par divers auteurs. On sait qu'il serait illusoire de réduire le diamètre de la sonde au-delà d'une certaine valeur par suite de la diffusion des électrons dans la matière d'une part, et d'autre part de l'émission de rayons X de fluorescence dans une région plus grande que le volume où les électrons ont provoqué des ionisations. La trajectoire utile de l'électron, c'est-à-dire la portion de sa trajectoire où son énergie est supérieure à l'énergie d'ionisation, a une longueur z_m déterminée par la loi de décélération. Par suite de la diffusion des électrons dans toutes les directions, le diamètre de la région analysée sera égal à $\delta_s + z_m$, si δ_s est le diamètre de la sonde. Il serait donc vain de réduire celui-ci au-dessous de 1μ si $z_m = 2\mu$ par exemple.

En fait le problème est de trouver les conditions optimales pour un diamètre $\delta_s + z_m$ minimum, mais une intensité X émise suffisante pour la précision exigée. Ce compromis a été étudié par WITTRY (1958) d'où il résulte que le diamètre de la région analysée est minimum, si le taux d'excitation E_o/E_k est compris entre 1,9 et 1,6 suivant que l'on tient compte ou non du spectre continu, c'est-à-dire que la concentration est faible ou forte.

Une évaluation un peu différente a été faite par DUNCUMB (1960). Avec un compteur proportionnel, on pourrait obtenir avec une intensité de 10^4 cps une résolution de $0{,}1\mu$ si le potentiel d'accélération est de 3 à 5 kV. On ne pourrait donc utiliser des raies K qu'avec des éléments légers, dans les autres cas ce sont les raies L ou M qui devraient être choisies.

En conclusion, nous rappellerons l'exemple donné par CASTAING (1961). Soit à analyser de faibles concentrations de cuivre dans un alliage à base d'aluminium. Pour avoir une émission K α (Cu) de 500 cps, les conditions optimales seraient $V = 12{,}2$ kV, $\delta_s + z_m = 1{,}7\mu$. A 30 kV, le diamètre de la région analysée atteindrait 7μ.

3. Analyse de Très Petits Objets

Il est cependant possible d'analyser de très petits objets, par exemple dans un alliage, des précipités de dimension inférieure ou très inférieure au micron. L'objet est alors soit une lame mince, soit, une réplique avec extraction, préparée suivant une technique bien connue en microscopie électronique. Dans ces dernières conditions les effets de matrice sont supprimés. C'est là un avantage important car très souvent le même élément se recontre, en concentrations différentes, dans la matrice et dans les précipités. Enfin il n'est pas de limite de taille pour ces précipités, car l'extraction peut comporter un nombre aussi grand qu'on le désire de particules, de sorte que l'intensité X émise soit suffisante pour l'analyse. La principale limite réside dans la préparation de l'objet: il s'agit de trouver le réactif qui dissolve sélectivement la matrice. (HENRY, PLATEAU et PHILIBERT, 1958, 1961.)

Une analyse quantitative de tels objets est possible; comme on ne connaît pas leur épaisseur ni leur taille, seule a une signification le rapport des concentrations des éléments pris deux à deux. Enfin, des examens par balayage peuvent préciser la répartition des éléments chimiques entre divers types de précipités et donc permettre de distinguer ces types. La Figure 20 montre, à titre d'exemple, et par comparaison avec une micrographie électronique, que l'image des précipités obtenue par cette méthode est bien fidèle.

4. Domaines d'application

Dès ses premiers travaux, CASTAING avait montré des applications de sa méthode à divers objets métallurgiques. Par la suite nous avons eu l'occasion de décrire un assez grand nombre d'applications effectuées en France, en particulier au congrès de 1957 de l'AIME (CASTAING, PHILIBERT et CRUSSARD).

Il n'est pas dans notre but de décrire ces applications. Le nombre croissant de publications et d'appareils en service montrent combien le microanalyseur à sonde électronique devient un outil indispensable au métallurgiste et au minéralogiste (J. PHILIBERT, H. BIZOUARD, 1959; J. PHILIBERT, 1962). Des applications à des objets biologiques ont même été signalées depuis quelque temps par BOYDE, SWITSUR, PEARNHEAD (1961) et MELLORS et CARROL (1961).

III - CONDITIONS DE l'ANALYSE QUANTITATIVE

A - POSITION DU PROBLEME

La relation entre l'intensité émise par un élément A et la concentration de cet élément est à la base de l'analyse quantitative. Malheureusement elle ne peut être établie que dans des cas simples (rayonnement excitateur monochromatique par exemple). Cependant les relations obtenues ainsi peuvent être utiles pour déterminer les conditions optimales à remplir dans des cas moins simples.

Considérons un échantillon complexe (où l'élément A de concentration C_A est dissous dans une matrice M) irradié par un rayonnement X monochromatique λ, émettant un rayonnement λ' que l'on analyse. Si l'angle d'incidence et l'angle d'émission sont égaux, il est facile de voir (GUINIER, 1961) que le rapport des intensités de la raie λ' émises par l'échantillon I_A et par un témoin A pur I_A° est égal à:

$$\frac{I_A}{I_A^\circ} = \frac{C_A}{K + (1 - K)\, C_A} \qquad (1)$$

avec

$$K = \frac{(\mu/\rho)^M_\lambda + (\mu/\rho)^M_{\lambda'}}{(\mu/\rho)^A_\lambda + (\mu/\rho)^A_{\lambda'}} \qquad (2)$$

en désignant par $(\mu/\rho)_\lambda^X$ le coefficient d'absorption de X pour la longueur d'onde λ. Il n'y aura proportionnalité entre l'intensité émise et la concentration que si K = 1, c'est-à-dire si les coefficients d'absorption de A et M sont égaux. Sinon on obtient des courbes hyperboliques (Figure 21) qui montrent que la sensibilité varie considérablement suivant la concentration, puisque:

$$\frac{d\,(I_A/I_A^\circ)}{dC_A} = \frac{1}{K} \quad \text{pour } C_A = 0 \tag{3}$$

$$\frac{d\,(I_A/I_A^\circ)}{dC_A} = K \quad \text{pour } C_A = 1. \tag{4}$$

En particulier si K est très petit (élément A dissous dans une matrice de bas numéro atomique), l'intensité varie d'abord très rapidement avec C_A puis reste ensuite à peu près constante: l'analyse n'est possible qu'aux faibles concentrations.

Lorsque le rayonnement excitateur est formé d'électrons, le coefficient d'absorption du rayonnement X est en première

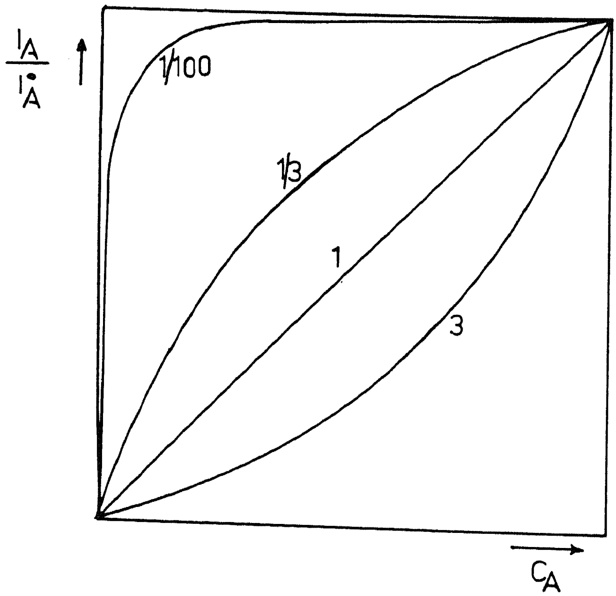

Figure 21. Relation intensité émise I_A/I_A°-concentration de l'élément A. Le nombre indiqué près de chaque courbe est le paramètre K de la relation (1) ou α de la relation (17).

approximation négligeable devant celui des électrons et, comme de plus celui-ci est à peu près indépendant du numéro atomique,

$$K \approx (\mu/\rho)^M_\lambda/(\mu/\rho)^A_\lambda \approx 1 . \tag{5}$$

Il y a proportionnalité émission-concentration. C'est en particulier le cas de la microanalyse à sonde électronique, que nous voudrions discuter de manière plus détaillée, car les diverses approximations et les interactions des éléments constitutifs ont été étudiées théoriquement par CASTAING (1951, 1955 et 1960).

B - MICROANALYSE A SONDE ELECTRONIQUE

1. Relation Emission-Concentration

Considérons un faisceau d'électrons bombardant sous incidence normale une anticathode de densité ρ, contenant l'élément A de masse atomique A en concentration massique C_A, et étudions l'émission d'une raie, K α par exemple, caractéristique de l'élément A. Suivons un électron le long de sa trajectoire: sur un élément de parcours dx le nombre d'ionisation dn_K sera proportionnel au nombre d'électrons K (A) par unité de volume et à la section efficace d'ionisation K des atomes A. La première quantité est proportionnelle à $\rho C_A/A$, nombre d'atomes A par unité de volume. La seconde peut s'écrire sous la forme d'une fonction de l'énergie E de l'électron et des caractéristiques de l'atome A: ψ_A (E). De sorte que le nombre d'ionisation peut s'écrire:

$$dn_K = \rho \frac{C_A}{A} \psi_A(E)\, dx = \frac{C_A}{A} \psi_A(E)\, d(\rho x) \tag{6}$$

ou

$$dn_K = \frac{C_A}{A} \frac{\psi_A(E)}{dE/d(\rho x)} dE \tag{7}$$

en faisant apparaître la loi de décélération des électrons $dE/d(\rho x)$. Le nombre total d'ionisation K par électron incident s'obtiendra en intégrant l'expression précédente entre E_o, énergie initiale de l'électron, et E_K:

$$n_K = \frac{C_A}{A} \int_{E_o}^{E_K} \frac{\psi_A(E)}{dE/d(\rho x)} dE . \tag{8}$$

Une première approximation consiste à admettre pour loi de décélération une loi universelle indépendante de la nature des éléments constituant l'anticathode

$$dE/d(\rho x) = \varphi(E) \tag{9}$$

de sorte que l'expression (8) peut s'écrire

$$n_K = \frac{C_A}{A} \int_{E_o}^{E_K} f_A(E)\, dE \tag{10}$$

la fonction $f_A(E)$ ne dépendant que des caractéristiques de l'élément A. Cette fonction sera donc la même pour l'échantillon et le témoin constitué de A pur. Pour celui-ci, on aura:

$$n_K^{\circ} = \frac{1}{A} \int_{E_o}^{E_K} f_A(E)\, dE\,. \tag{11}$$

Le rapport des intensités de la raie considérée émises par l'échantillon I_A et le témoin I_A° est égal au rapport n_K/n_K°; d'où:

$$\frac{I_A}{I_A^{\circ}} = C_A\,. \tag{12}$$

Il y a *proportionnalité vraie émission-concentration:* c'est la première approximation.

En réalité la loi de décélération est un peu plus complexe que ne le suppose la relation (9): elle est fonction des caractéristiques de tous les élément présents dans l'anticathode. Citons à titre d'exemple la loi de décélération de BETHE, qui pour un élément pur s'écrit:

$$\frac{dE}{d(\rho x)} = -2\pi N e^4 \,\frac{Z}{A}\, \frac{\log(2E/J)}{E} \tag{13}$$

où J désigne un potentiel moyen d'ionisation des atomes A de numéro atomique Z et N le nombre d'Avogadro.

Nous écrirons la relation (13) sous la forme

$$\frac{dE}{d(\rho x)} = S_A\, \varphi(E) \tag{13'}$$

et pour une anticathode complexe

$$\frac{dE}{d(\rho x)} = S_{\text{alliage}}\, \varphi(E) \qquad (14)$$

d'où

$$n_K = \frac{C_A/A}{S_{\text{alliage}}} \int_{E_o}^{E_K} f_A(E)\, dE \qquad (15)$$

et, pour le témoin:

$$n_K^{\circ} = \frac{1/A}{S_A} \int_{E_o}^{E_K} f_A(E)\, dE \qquad (16)$$

d'où

$$\frac{I_A}{I_A^{\circ}} = \frac{\alpha_A C_A}{\Sigma \alpha_i\, c_i} \quad \text{avec} \begin{cases} S_{\text{alliage}} = \Sigma S_i\, c_i \\ \alpha_i = S_i \end{cases} . \qquad (17)$$

C'est la *seconde approximation* qui prévoit un écart par rapport à la loi de proportionnalité vraie de la première approximation. Considérons par exemple un alliage binaire AB:

$$\frac{I_A}{I_A^{\circ}} = \frac{\alpha_A C_A}{\alpha_A C_A + \alpha_B C_B} = \frac{C_A}{C_A + \alpha(1 - C_A)} = \frac{C_A}{C_A(1-\alpha) + \alpha} \qquad (18)$$

avec $\alpha = \alpha_B/\alpha_A$.

On voit (Figure 21) que si $\alpha_B/\alpha_A > 1$, la concentration mesurée est inférieure à la concentration vraie et inversement.

Notons bien que la démonstration précédente n'est valable que si toute la trajectoire utile de l'électron, c'est-à-dire la portion de trajectoire le long de laquelle l'énergie de l'électron est comprise entre E_o et E_K, est entièrement située à l'intérieur de l'anticathode. Ceci n'est pas le cas général du fait de la rétrodiffusion des électrons. L'intensité mesurée I_A est inférieure à celle qu'on mesurerait s'il n'y avait pas de rétrodiffusion des électrons, soit $\overline{I_A}$. Posons

$$I_A^{\circ} = \overline{I_A^{\circ}}/\lambda_A \qquad (19)$$

le coefficient λ_A étant supérieur à l'unité. On aura donc:

$$\frac{I_A}{I_A^\circ} = \frac{\overline{I_A}}{I_A^\circ}\,\frac{\lambda_A}{\lambda_{\text{alliage}}} = \frac{n_K}{n_K^\circ}\,\frac{\lambda_A}{\lambda_{\text{alliage}}} \tag{20}$$

en supposant que $(S\lambda)$ alliage peut s'exprimer sous la forme $\Sigma S_i \lambda_i c_i$, la relation (17) demeure valide mais avec

$$\alpha_i = S_i \lambda_i . \tag{21}$$

Les paramètres S_i sont fonction décroissante du numéro atomique Z*. Au contraire les paramètres λ_i sont fonction croissante de Z, puisque la fraction d'électrons rétrodiffusés augmente avec Z.

Par conséquent, dans le cas *d'échantillons composés d'éléments de numéros atomiques voisins, la première approximation est valide.* Ce n'est que lorsque les éléments constitutifs ont des Z trop différents, que la seconde approximation, et donc le problème de déterminer les coefficients α, doivent être envisagés.

Nous avons déjà noté que si le taux d'excitation est voisin de l'unité ($E_0 \approx E_K$), l'effet de rétrodiffusion est négligeable, car l'électron perd toute son énergie utile dans l'échantillon et quand il est rétrodiffusé son énergie est inférieure à E_K. La seconde approximation doit être alors vérifiée avec $\alpha = S$. Dans ces conditions de faible excitation, les coefficients α seront très différents pour les divers éléments et la relation émission-concentration sera très éloignée d'une relation linéaire.

Mais, comme l'a fait remarquer CASTAING, c'est probablement le seul cas où l'on peut attacher des coefficients α à chaque élément. En effet, si l'on élève le taux d'excitation, la rétrodiffusion n'est plus négligeable, mais devient de plus en plus importante au fur et à mesure que E_0/E_K croît. Il peut même se produire une compensation entre les effets de rétrodiffusion et de décélération, telle que pour un certain taux d'excitation

$$\alpha = S\lambda \approx 1$$

si bien que la première approximation se vérifie.

---

*cf. la relation (13) ci-dessus par exemple; deux effets s'ajoutent: le nombre d'électrons par unité de masse Z/A décroît quand Z croît; d'autre part le potentiel moyen d'ionisation augmente avec Z, les électrons devenant en moyenne plus fortement liés au noyau.

Pour un taux d'excitation quelconque, il n'est pas possible en toute rigueur d'affecter un coefficient α à chaque élément. Considérons par exemple un alliage binaire AB. Par comparaison des concentrations vraies et mesurées de l'élément A, on peut calculer un rapport de coefficients α_A/α_B. Les mêmes mesures avec B donnent de même α_B/α_A. Mais puisque pour une même tension les taux d'excitation de A et B seront différents, on n'observera pas que α_A/α_B est l'inverse de α_B/α_A.

Cependant POOLE et THOMAS (1962) ont essayé d'établir une table des coefficients $\alpha = S\lambda$ caractéristiques de chaque élément. Pour cela ils ont pris les valeurs de S calculées par NELMS et ajusté les valeurs de λ d'après un certain nombre d'alliages pris comme étalons. Si cette méthode n'est pas absolument rigoureuse, elle représente néanmoins une tentative intéressante, valable pour des taux d'excitation ni trop faibles ($\alpha \to S$), ni trop forts ($\alpha \to \lambda$). Elle donne des résultats satisfaisants pour les alliages binaires étudiés, où les différences de numéro atomique peuvent être très élevées. Un cas important est celui des alliages d'uranium. Cependant il serait intéressant de mesurer expérimentalement S en travaillant à de très bas taux d'excitation, et ensuite d'utiliser une famille de courbes $\lambda(Z)$, λ croissant avec le taux d'excitation E_o/E_K. Cette méthode permettrait peut être d'analyser les alliages ternaires les plus complexes où il ne peut plus être question d'ajuster les paramètres avec des alliages étalons, leur nombre devenant trop élevé.

Remarque. Considérons un élément léger A dissous dans une matrice de Z élevé, en faible concentrations C_A. Pour les faibles taux d'excitation on aura $\alpha_A/\alpha_B \approx S_A/S_B > 1$ et la concentration mesurée sera supérieure à la concentration vraie; si pour de forts taux d'excitation, l'effet de rétrodiffusion l'emporte on aura $\alpha_A/\alpha_B < 1$ et la concentration mesurée sera inférieure à la concentration vraie. On balaye le faisceau de courbes de la Figure 21. Il peut alors se trouver un taux d'excitation tel que la proportionnalité émission-concentration soit vérifiée.

2. Corrections d'absorption et de fluorescence

Le problème de l'analyse quantitative n'est cependant pas limité à la validité de la première ou de la seconde approximation, c'est-à-dire aux effets primaires que sont les lois de décélération et de diffusion des électrons dans l'objet. Dans le cas où l'alliage est formé d'éléments de numéros atomiques voisins, et où la première approximation est valide, on observe encore des écarts à la proportionnalité émission-concentration. Ces écarts sont dûs à des effets que nous qualifierons de secondaires, car ils agissent non pas comme les précédents sur les électrons incidents, mais sur les rayons X émis.

a. Le rayonnement émis par les atomes A de l'échantillon subit des réabsorptions à l'intérieur de l'échantillon lui-même.

b. Les atomes A émettent un spectre X de raies par suite des ionisations provoquées non seulement par les électrons excitateurs, mais encore par certaines raies caractéristiques émises par les autres éléments présents ou par le spectre continu.

Trois corrections à appliquer aux rapports d'intensités de raies mesurées doivent donc être envisagées: *absorption, fluorescence* par des raies caractéristiques, *fluorescence* par le spectre continu.

L'importance de ces effets sont différents pour l'échantillon et le témoin pur (le second effet est évidemment nul pour le témoin). Elle dépend en particulier des valeurs des coefficients d'absorption des divers éléments présents pour les diverses longueurs d'onde émises. Un examen de ces coefficients d'absorption indique l'existence des effets d'absorption et de fluorescence par raies caractéristiques. L'importance de la fluorescence par le spectre continu est plus difficile à évaluer.

a) *Correction d'absorption*

Etudions l'émission X non plus en suivant un électron le long de sa trajectoire, mais en considérant l'effet global d'absorption et de diffusion des électrons en fonction de la profondeur z dans l'échantillon.

Soit une couche de matière parallèle à la surface de l'échantillon d'épaisseur $d(\rho z)$, située à la profondeur ρz. L'intensité de la raie $K\alpha$ (A) émise par cette couche peut s'écrire

$$dI_A = C_A \varphi_1(\rho z)\, d(\rho z). \qquad (22)$$

La fonction $\varphi_1(\rho z)$ est le produit de trois fonctions.

La première exprime la fraction du nombre initial d'électrons qui atteignent la couche considérée. Elle est donnée en première approximation par la loi de LENARD: $\exp(-\sigma\rho z)$. La seconde fonction exprime le "rendement" de la couche $d(\rho z)$: celle-ci n'est pas traversée orthogonalement par les électrons, car par suite de leur diffusion, ceux-ci la traversent sous des angles d'incidence variés et aussi bien de haut en bas que de bas en haut; le parcours moyen d'un électron dans une couche sera non pas $d(\rho z)$ mais $R(\rho z)\, d(\rho z)$. La troisième fonction est la fonction d'ionisation des atomes A sur le niveau K considéré. Elle peut se calculer, connaissant la section efficace d'ionisation. Elle peut être considérée comme approximativement constante tant que $E > 1{,}5\ E_K$.

L'émission dans le témoin peut s'écrire de la même façon:

$$dI_A^\circ = \varphi_A(\rho z)\; d(\rho z). \tag{23}$$

Intégrons de 0 à l'infini pour avoir les émissions totales et faisons le rapport des deux expressions obtenues; il vient:

$$\frac{I_A}{I_A^\circ} = C_A \; \frac{\int_0^\infty \varphi_1(\rho z)\; d(\rho z)}{\int_0^\infty \varphi_A(\rho z)\; d(\rho z)}\,. \tag{24}$$

Il n'y aura proportionnalité émission-concentration que si les deux intégrales sont égales. On retrouve ainsi les deux approximations.

Nous allons maintenant tenir compte de l'absorption du rayonnement émis au sein de l'objet lui-même. Soit $(\mu/\rho)^{AB}$ et $(\mu/\rho)^A$ les coefficients d'absorption massique de la raie analysée dans l'échantillon et le témoin:

$$(\mu/\rho)^{AB} = \Sigma\,(\mu/\rho)^i\, c_i\,. \tag{25}$$

Soit θ l'angle d'émission du rayonnement mesuré (déterminé par la construction du spectromètre).

On recueillera (Figure 22) l'intensité dI'_A telle que

$$dI'_A = dI_A \exp\left[-\left(\frac{\mu}{\rho}\right)\frac{\rho z}{\sin\theta}\right]. \tag{26}$$

Pour alléger la notation, nous appelerons χ^{AB} le quotient

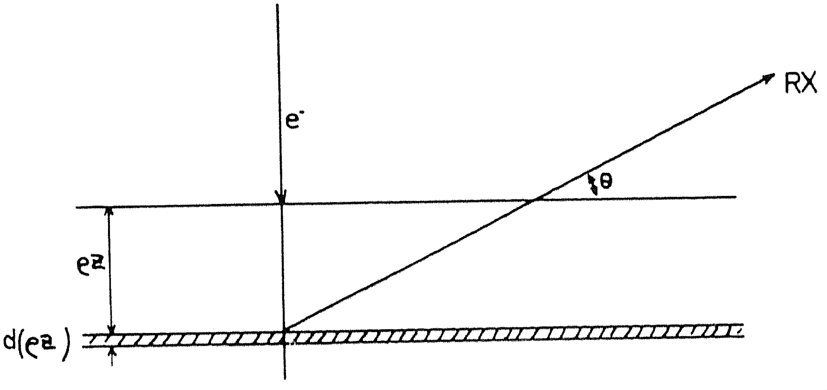

Figure 22. Schéma pour le calcul de l'intensité émise par la couche d (ρz).

$$\chi^{AB} = \left(\frac{\mu}{\rho}\right)^{AB} \Big/ \sin\theta \tag{27}$$

de sorte que:

$$I'_A = C_A \int_0^\infty \varphi_1(\rho z) \exp\left[-\chi^{AB} \rho z\right] d(\rho z) \tag{28}$$

$$= C_A F_1(\chi^{AB}) \tag{29}$$

en désignant par $F_1(\chi)$ la transformée de LAPLACE de la fonction $\varphi_1(\rho z)$.

Une relation analogue est obtenue pour le témoin

$$I'^{o}_A = \int_0^\infty \varphi_A(\rho z) \exp\left[-\chi^{A} \rho z\right] d(\rho z) \tag{30}$$

$$= F_A(\chi^A) \tag{31}$$

d'où finalement:

$$\frac{I'_A}{I'^{o}_A} = C_A \frac{F_1(\chi^{AB})}{F_A(\chi^A)} . \tag{32}$$

La concentration vraie s'obtient en multipliant le rapport des intensités mesurées par $F_A(\chi^A)/F_1(\chi^{AB})$. La variable χ dépend de la composition de l'alliage, mais le calcul de la correction exigera la connaissance des fonctions $F(\chi)$.

On voit en particulier que l'intensité vraie I_A et l'intensité mesurée I'_A sont reliées par:

$$I_A = I'_A F(0)/F(\chi) = I'_A/f(\chi). \tag{33}$$

Les courbes $f(\chi)$ ont été établies expérimentalement par CASTAING et par CASTAING et DESCAMPS soit en faisant varier l'angle d'émergence θ, soit en calculant la transformée de LAPLACE de la fonction $\varphi(\rho z)$ établie expérimentalement.

Il est facile de voir que la fonction $F(\chi)$, comme la fonction $\varphi(\rho z)$ n'est pas une fonction universelle. Elle dépend de deux paramètres: la tension d'accélération des électrons, qui détermine en particulier le coefficient de LENARD σ, et les caractéristiques atomiques des éléments constitutifs de l'antacathode qui conditionnent particulièrement la diffusion des électrons, et à un moindre degré leur pénétration.

Aussi faudrait-il disposer d'une double famille de courbes, les paramètres étant d'une part la tension d'accélération, d'autre part la nature des éléments chimiques (caractérisés par exemple par leur numéro atomique).

Le nombre de courbes expérimentales demeurant restreint, il paraît intéressant de représenter analytiquement la fonction F(χ), afin de pouvoir calculer la correction d'absorption sans l'aide de courbes expérimentales. Diverses tentatives ont été faites en ce sens. Nous donnerons ici l'expression que nous avons proposée (PHILIBERT, 1961). Nous avons exprimé analytiquement la fonction $\varphi(\rho z)$ en supposant que le coefficient σ ne dépend que de la tension d'accélération et que la diffusion des électrons ne dépend que de la nature des éléments chimiques. Calculant la transformée de cette fonction, on trouve une expression un peu lourde, dont une formule simplifiée, plus commode pour le calcul, s'écrit:

$$\frac{1}{F(\chi)} = \left(1 + \frac{\chi}{\sigma}\right)\left[1 + h\left(1 + \frac{\chi}{\sigma}\right)\right]. \qquad (34)$$

-σ est un coefficient fonction de la tension, dont une table a été établie. Voici quelques valeurs $\sigma = 1820$ à 30 kV, 2550 à 25 kV, 3725 à 20 kV, 5900 à 15 kV, 9600 à 10 kV.

-$h = 1{,}2\ (A/Z^2)$; dans un alliage, h est calculé en considérant la valeur moyenne de A et Z.

Les paramètres σ et h ont éte ajustés pour représenter correctement les courbes f(χ) établies par CASTAING et DESCAMPS sur Al, Cu, Au. Comme l'expression (34) n'est qu'approchée, ceci fait perdre un peu de leur signification physique à σ et h. Mais nous croyons qu'il est important d'avoir une expression analytique commode pour le calcul numérique, même au prix de cette simplification.

Remarquons que, bien que la fonction F(χ) dépende du numéro atomique, elle ne groupe pas l'effet d'absorption et la seconde approximation. Il aurait fallu pour cela conserver la relation non simplifiée et de plus tenir compte de la variation du paramètre σ avec Z.

La relation (34) peut être utilisée de la façon suivante. On se donne a priori deux compositions possibles de l'alliage étudié. On calcule alors χ puis F(χ) pour cet alliage et le témoin. La relation (32) donne alors les rapports d'intensité correspondants. Par comparaison avec les intensités mesurées, on en déduit par simple interpolation la valeur vraie de la concentration (à la première approximation).

b) Correction de fluorescence

La correction de fluorescence peut être importante dans le cas où l'élément A présente une forte absorption pour une raie intense émise par B. L'intensité de la raie émise par A est alors renforcée par fluorescence. Le calcul de correction demande d'évaluer le rapport

$$I_f^A / I^A$$

rapport de l'intensité émise par A dans la raie analysée par fluorescence et par émission directe. L'intensité mesurée effectivement serait $I^A + I_f^A$, s'il n'y avait pas d'effet d'absorption. La correction de fluorescence doit donc être calculée en premier lieu.

Le rapport I_f^A/I^A a été calculé par CASTAING et par WITTRY moyennant différentes hypothèses. A titre d'exemple, citons le cas d'alliages binaires Fe-Cr* ou ternaires Fe-Ni-Cr, où la formule de CASTAING nous a permis de calculer des valeurs de la concentration en Cr en très bon accord avec les valeurs expérimentales comme le montre le tableau ci-dessous, qui permet d'apprécier l'importance de cette correction dans un cas où elle est très forte.

Alliage	Analyse Chimique		Microanalyse Cr %		$\frac{\Delta C}{C}$
	Ni %	Cr %	Mesuré	Corrigé	
A	35,95	10,32	12,45	10,6	+3%
B	35,9	10,34	10,34	10,4	-0,6%
C	35,7	4,66	4,66	4,55	-2,5%
D	35,8	7,46	7,46	7,9	+5,4%
E	40,5	10,30	10,3	10,1	-2%

La fluorescence par le spectre continu est plus difficile à évaluer, car elle dépend d'un plus grand nombre de facteurs. Son importance a été mesurée expérimentalement par CASTAING et DESCAMPS (1955) pour des anticathodes de Zn, W, Bi. Récemment HENOC (1962) a donné une formule qui permet de calculer I_f^A, intensité d'une raie donnée émise par fluorescence sous l'effet du spectre continu dans le cas d'anticathodes simples ou complexes. Le rapport I_f^A/I^A ainsi calculé a été comparé aux valeurs expérimentales. L'accord est satisfaisant et les résultats montrent que l'importance de cet effet est assez faible et varie peu avec le numéro atomique, comme le montre le tableau ci-dessous (valeurs calculées pour une tension de 30 kV).

---

*Le coefficient d'absorption de la raie K α (Fe) dans le chrome est particulièrement élevé: 450.

Anticathode	Zn	W	Au	Bi
I_f^A/I^A (calculé)	0,032	0,023	0,029	0,035
Raie	$K\alpha_1$	$L\alpha_1$	$L\alpha_1$	$L\alpha_1$

L'évaluation de cet effet est particulièrement complexe pour les raies L du fait des trois niveaux L_I, L_{II}, L_{III}, les paramètres nécessaires n'étant pas toujours bien connus entre les discontinuités d'absorption correspondantes.

En résumé les divers calculs de correction tels qu'ils sont pratiqués actuellement donnent des résultats satisfaisants, tant que les numéros atomiques des éléments constitutifs ne sont pas trop différents. Sinon l'importance de la seconde approximation nécessite de nouvelles recherches. Ces travaux devront en particulier s'attacher à préciser l'influence du taux d'excitation, qui en général est choisi à une valeur commode, qui dépend de l'appareil utilisé, de la sensibilité et du pouvoir séparateur que l'on vise, mais qui n'est pas forcément la valeur optimale pour une bonne évaluation des coefficients α de la seconde approximation.

CONCLUSIONS

La spectrométrie de rayons X grâce à ses principes simples a donc été exploitée suivant des voies très différentes, mais avec des techniques de mesures voisines, particulièrement en ce qui concerne les détecteurs et l'électronique qui doit les accompagner. Deux techniques se sont surtout développées à ce jour: l'analyse macroscopique par fluorescence, et la microanalyse à sonde électronique. Les progrès récents ont concerné des perfectionnements de ces deux méthodes (en particulier extension de l'analyse aux éléments légers, puis très légers) plutôt que le développement d'autres méthodes déjà connues (émission directe ou microabsorption et microfluorescence en particulier). Cependant l'utilisation de sources radioactives peut un jour apparaître comme un concurrent sérieux des appareils de fluorescence, car de nombreux laboratoires ont besoin d'un appareil particulier répondant à un besoin précis, plutôt que d'un appareil très puissant, aux multiples applications et aussi au prix de revient élevé. Il est possible enfin que le domaine de la microanalyse à sonde électronique soit étendu à une échelle plus fine. L'utilisation de lames minces, qui évite la diffusion des électrons, peut conduire à des pouvoirs de résolution élevés qui nécessitent l'observation de l'objet dans l'appareil lui-même par microscopie électronique. Des projets dans cette voie sont déjà en cours de réalisation.

BIBLIOGRAPHIE

A. BOYDE, V. R. SWITSUR, R. W. PEARNHEAD (1961). J. Ultrastructure Research, 5, 201.
I. B. BOROVSKI (1953). Problèmes de métallurgie (70è anniversaire de l'Académicien O. P. BARDIN); Acad. Sci. URSS.
A. J. CAMPBELL, R. GIBBONS (1962). Nature, 199, 76.
R. CASTAING, A. GUINIER (1949). Proceedings of the Conference on Electron Microscopy. Delft (juillet), p. 60.
R. CASTAING (1951). Thèse, Paris. ONERA, Publication no. 55.
R. CASTAING, J. DESCAMPS (1955). J. Physique Radium, 16, 304.
R. CASTAING, J. DESCAMPS (1958). Recherche Aéronautique, 63, 41.
R. CASTAING, J. PHILIBERT et C. CRUSSARD (1957). Trans. AIME, 209, J. of Metals, avril, 9, 389.
R. CASTAING (1960). Advances in Electronics, 13, 317.
V. E. COSSLETT, P. DUNCUMB (1956). Nature, 177, 1172.
V. E. COSSLETT (1960). X-ray Microscopy and Microanalysis. Elsevier Publishing, p. 346.
M. CROUTZEILLES (1962). Communication privée.
P. DUNCUMB (1959). Brit. J. Applied Physics, 10, 420.
P. DUNCUMB (1960). X-ray Microscopy and Microanalysis. Elsevier Publishing, p. 365.
P. DUNCUMB (1961). Revue Universelle des Mines, 17, 240.
R. M. DOLBY (1959). Proc. Phys. Soc. (London), 73, 81.
A. GUINIER (1961). Revue Universelle des Mines, 17, 143.
J. E. HOLLIDAY (1960). Rev. Scient. Instr., 31, 891.
J. HENOC (1962). Rapport CNET, Paris.
G. HENRY, J. PLATEAU et J. PHILIBERT. 1958, C. R. Acad. Sci., 246, 2753.
A. KIRIANENKO et al. 1961, C. R. Acad. Sci., 252, 876.
J. LONG (1958). J. Scientific Instruments, 35, 323.
R. MELLORS, K. CARROL (1961). Nature, 192, 1090.
T. MULVEY (1960). X-ray Microscopy and Microanalysis. Elsevier Publishing, p. 372.

J. PHILIBERT, G. HENRY, M. ROBERT et J. PLATEAU (1961). C. R. Acad. Sci., 252, 1320.

J. PHILIBERT (1961). Rapport intérieur IRSID.

J. PHILIBERT, Mme H. BIZOUARD (1959). Mém. Scient. Rev. Métallurgie, 56, 187.

J. PHILIBERT (1962). J. Inst. Metals, 90, 241.

D. M. POOLE, P. M. THOMAS (1962). J. Inst. Metals, 90, 228.

G. SEIBEL, Y. LE TRAON, P. MARTINELLI (1961). Revue Universelle des Mines, 17, 260.

G. SEIBEL (1962). Communication privée.

D. WITTRY (1958). J. Appl. Physics, 29, 1543.

D. WITTRY (1957). Thèse, Cal. Inst. Techn., Pasadena.

G. VON HEVESY (1932). Chemical Analysis by X-rays and its applications, New York.

X-RAY EMISSION SPECTRA AND CHEMICAL BOND

A. Faessler
I. Physical Institute, University of Munich
Munich, Germany

I. INTRODUCTION

X-ray spectroscopy has contributed a great deal to our knowledge of the inner electron shells of the atom. It is now well known that it may also provide valuable information about valence electron states. In recent years it was recognized that the study of X-ray spectra is of special interest for the elucidation of the electronic structure of crystals and for the investigation of the bond character in molecules and solids.

II. X-RAY SPECTRA OF BOUND ATOMS

In studying valence electron states by means of X-ray spectroscopy we have a direct and a more indirect way of approach to the problem in question. To make this clear, let us consider an element of the third period of the periodic table, e.g., 14 silicon, 15 phosphorus, or 16 sulphur. The atoms of these elements have a complete K- and L-shell; the electrons of the M-shell are the valence electrons. If the element in question is bound in a solid then the valence electron states form a broad energy band, part of which is occupied by electrons.

Now the following electron transitions are possible (Figure 1): From L to K, from M to K and from M to L, giving rise to the emission of Kα-, Kβ-, and L-radiation respectively; the transitions from K and L to M correspond to the K-absorption and L-absorption spectrum.

The whole of this spectrum, emission and absorption, shows effects of the physical and chemical state of the emitting or absorbing atom. This is not surprising for transitions which begin or end in a valence electron level: with a solid substance we observe more or less broad emission bands corresponding to

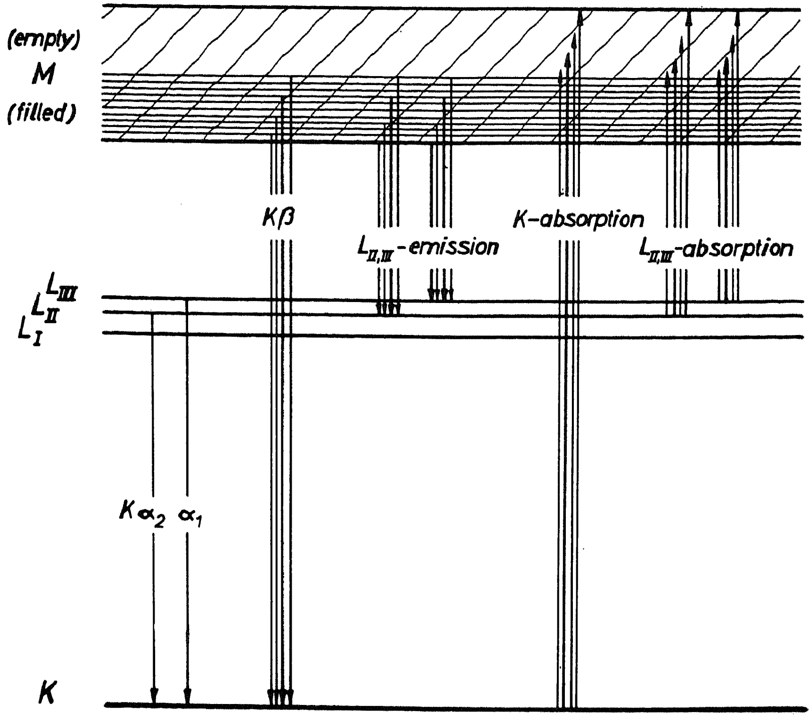

Figure 1. Simplified level system showing possible transitions for atoms like 14 Si, 15 P, 16 S.

the energy bands of the crystal and generally varying in wavelength and structure from substance to substance. This is true for the Kβ-spectrum as well as for the L-spectrum. Taking silicon as an example, we find the Kβ-band near 6.7 Å or 1840 eV, the L-emission band in the soft X-ray region at 120-160 Å or 80-100 eV.—the absorption spectrum in the K-series shows edges with a more or less pronounced structure, in the L-series we find broad absorption bands, both different for different substances.

It is remarkable that not only the spectra resulting from valence electron transitions but also the Kα-lines, arising from transitions between the two inner levels, are influenced by the physical and chemical state of the atom. In this case the dominating feature is a change in wavelength rather than a pronounced structural change, both lines being shifted by the same amount so that always the well known characteristic doublet appears, the wavelengths of which are easily measured with high precision.

III. ELECTRONIC STRUCTURE AND BOND TYPE STUDIES BY X-RAY SPECTROSCOPY

What can we hope to find in studying these effects more closely? The answer is again clear in the case of the direct valence electron bands. We may expect them to give us a picture of the energy band system, the emission bands representing the occupied part, the absorption band representing the empty part of the band system. Work in the soft X-ray range—for several reasons long wavelength X-rays give the most detailed information—has indeed confirmed the principal concepts of the energy band model.

However, clear results have been obtained only with the elementary crystals of light elements. The study of compounds and elements of higher atomic number has so far not been very successful. The reasons shall not be discussed here in detail, it may only be mentioned that there are considerable experimental difficulties to obtain reliable results in this spectral range. We shall come back to the question of the direct valence electron transitions later.

As to the influence of the chemical bond on the Kα-lines, it is clear that the shift of these lines is a second order effect resulting from the change in the screening of the K- and L-electrons if a change occurs in the valence electron shell. Obviously this effect offers the possibility to study the contribution of the different electron shells to the polarization of the atom. But this is a question which shall not be discussed here.

There are other applications of the line shifts. In a systematic investigation [1] of the wavelengths of the sulphur Kα-lines for a large number of different compounds using fluorescence excitation we found surprisingly simple rules for the shifts of the Kα-doublet, indicating that it is the charge of the atom which determines the position of the lines. Thus by precise wavelength measurements of the Kα-lines valuable information can be gained concerning the bond type in a great variety of compounds, metallic phases, semiconductors and insulators. This will be shown in some detail in the following parts.

IV. THE SHIFT OF THE SULPHUR Kα-DOUBLET

In the first place the wavelengths of the Kα-lines are determined by the oxidation number of the emitting atom (table 1). Relative to the free element the shift is toward longer wavelengths, if the charge of the atom is negative as in sulphides; the shift is toward shorter wavelengths, if the charge is positive. The higher the oxidation number, the shorter are the wavelengths.

Table 1

Mean Wavelengths and Shifts of S $K\alpha_{1,2}$ for the Different Oxidation States of Sulphur

Oxidation State	λ (XU)		Mean Shift	
	$K\alpha_1$	$K\alpha_2$	$\Delta\lambda$(XU)	ΔE (eV)
S^{6+}	5358.08	5360.89	-2.76	+1.19
S^{4+}	58.63	61.47	-2.20	+0.95
S^{2+}	60.13	62.93	-0.72	+0.31
S^{o}	60.83	63.66	-	-
S^{2-}	61.15	63.99	+0.33	-0.14

In different compounds of the same oxidation number one does not always find the same wavelengths. In more covalent molecules and complexes the exact position of the lines is dependent upon the electronegativity of the next neighbours of the emitting atom. An example of this is given in Figure 2, showing the series sulphite, thiosulphate, sulphate, fluorsulphonate. The lines indicated in Figure 2 refer to the central sulphur atom which in the case of sulphite is surrounded by three oxygen atoms, in the case of the other compounds again by three oxygen atoms and a fourth neighbour, the electronegativity of which is increasing in the order given above (sulphur 2.5; oxygen 3.5; fluorine 4.0). Thus the central atom becomes more and more positive in the same order, and again we find that the higher the charge of the emitting atom the shorter are the wavelengths.

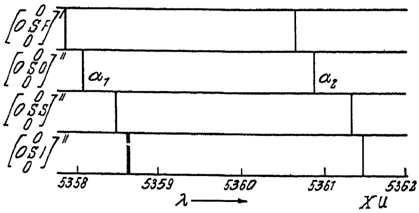

Figure 2. Position of the S Kα-doublet in the series sulphite, thiosulphate, sulphate and fluorsulphate.

Corresponding results have been obtained for the elements phosphorus and silicon. Though the measurements for these two elements have not been as extensive as for sulphur, it seems that the same rules are valid for all three elements. They may be summarized in the following way:

Relative to the lines of the free element the lines of the atom in a compound are shifted toward shorter wavelengths or higher energies, if the atom has a positive charge, toward longer wavelengths or lower energies, if it has a negative charge in the compound. The special position of the lines is determined by the oxidation state of the emitting atom and by the electronegativity of its neighbours, i.e., by the actual charge of the atom.

V. EXPERIMENTAL

If one wishes to study a greater variety of compounds, investigations of the kind described above require of course pure fluorescence excitation, which has been applied to this kind of work for the first time by the author [2]. Moreover high resolving power of the spectroscopic apparatus is necessary. It is true that in the case of sulphur the maximum shift is about 3 XU or 1.3 eV (between S^{6+} and S^{2-}), a surprisingly large shift, considering the fact that the bond energies themselves are not higher than a few electron volts. However, for the study of finer details of chemical bonds it is desirable to cover shifts down to about 0.1 XU. This means that commercial units for X-ray fluorescence analysis cannot be used, their resolving power being much too small. Larger Bragg spectrographs or better curved crystal spectrographs together with special secondary X-ray tubes satisfy the conditions of high luminosity and high resolving power.

VI. STUDIES OF SULPHUR COMPOUNDS USING THE SHIFT OF THE Kα-DOUBLET

Molecules and Complex Ions

There are several sulphur compounds containing sulphur atoms in two different oxidation states, a well known example being the above mentioned thiosulphate. With regard to the results described in Part IV one would expect to find in such cases two doublets corresponding to the two kinds of sulphur atoms. This has indeed been found in the case of thiosulphate.

With this substance three lines are obtained, one with $\lambda =$ 5358.49 XU, the $K\alpha_2$-line of the central S-atom, a second one with $\lambda = 5361.35$ XU, the $K\alpha_2$-line of the central S-atom, superimposed by the $K\alpha_1$-line of the S-atom of low oxidation number, and a third one with $\lambda = 5363.95$ XU, the $K\alpha_2$-line of the latter S-atom (compare table 1 and Part IV). Thus the result demonstrates in a very direct way that the chemical formula according to the classical valence theory is correct.

Another group of compounds with sulphur atoms of different oxidation states are the polythionates. All polythionates KO_3S-S_n-SO_3K ($n = 1,2,3,4$) give three lines, resulting as in the case of thiosulphate from the superposition of two doublets shifted one against the other for about the distance of the two components. The intensities of the three lines vary from polythionate to polythionate, as is to be expected an account of the ratio of the two kinds of S-atoms. With dithionate KO_3S-SO_3K one observes a normal doublet, the two S-atoms being equivalent.

On the basis of these results it seemed worthwhile to study a problem concerning the electronic structure of the molecule N_4S_4, nitrogentetrasulphide. This molecule forms an eight-ring system with S- and N-atoms alternating. Writing out the formula according to the classical valence theory places different charges on the sulphur atoms, say 2 + and 4 +. According to this one would expect two doublets as in the above mentioned cases. What is actually observed, however, is one normal doublet, the wavelengths of the two lines being 5359.83 XU for $K\alpha_1$ and 5362.85 XU for $K\alpha_2$, thus indicating sulphur of an oxidation state of about 3+ (see table 1). This means that the electron distribution in the molecule N_4S_4 is equalized by mesomerism.

In $S_4(NH)_4$ the S-atoms are also positive but less than in N_4S_4. The wavelengths 5360.11/5363.25 XU correspond to S^{2+}, in agreement with the chemical formula. For polynitrogensulphide $(SN)_x$ again only one doublet is found with wavelengths 5360.57/5363.62 XU which means that all S-atoms have the same rather small positive charge, in agreement with the physical and chemical properties of the substance [3].

Solid State Problems

A problem much discussed in recent years is the bond type in zincblende, ZnS. Formerly looked at as a purely ionic crystal, it is now mostly considered to be a covalent crystal because of its tetrahedral structure suggesting a covalent bond of sp^3-character. A certain ionic character is admitted, the values of the effective charge per ion as given by different authors varying widely.

In studying this question we made careful measurements of the wavelengths of S $K\alpha$ in numerous metal sulphides of different bond character, including natural and synthetic zincblende [4]. The surprising result was that the wavelength of S $K\alpha$ for all metal sulphides is the same within very narrow limits, probably within the limits of error. The value for S^{2-} given in table 1 is the mean value as found from the investigation of 18 metal sulphides. From all we know about the shifts of $K\alpha$ we have to conclude that all metal sulphides have the same S-ion and hence one cannot speak of a covalent bond between Zn and S in zincblende.

It must be emphasized here that the method is sensitive enough to differentiate between different bond types of sulphur of low oxidation number. This is demonstrated in Figure 3, showing the lines for metal sulphides, which have the extreme position on the long wavelength side, for organic sulphides (λ = 5360.98/5363/78 XU) with clearly less negative sulphur, elementary sulphur with atoms of charge zero and finally sulphur with positive charge (in thiopiperidine, where sulphur is bound to nitrogen, the electronegativity of which is higher making sulphur positive), giving lines with wavelengths shorter than those of the element.

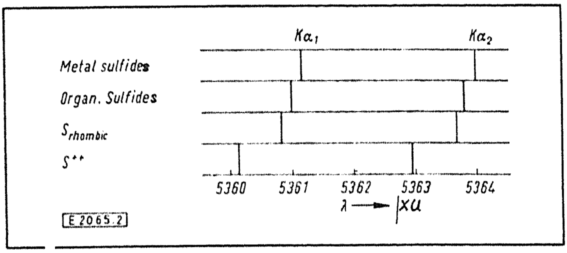

Figure 3. Position of the S Kα-doublet in metal sulphides, organic sulphides, elementary sulphur and thiopiperidine (S^{2+}).

The extreme covalent bond in ZnS would mean charge 2+ for sulphur, a bond with 50% ionic character would mean about charge zero. Hence the S Kα-doublet of ZnS should be found somewhere between the doublets of S^{2+} and sulphur in the elementary form or perhaps in organic sulphides. This, however, is not the case. The doublet for ZnS has the wavelengths 5361.23/5364.13 XU, well within the range of the other metal sulphides, the mean value of S Kα for all metal sulphides being 5361.15/5363.99 XU. So the assumption of a covalent bond in zincblende is not in agreement with these results and can hardly be maintained.

VII. STUDIES OF PHOSPHORUS COMPOUNDS USING THE P Kα-DOUBLET

Investigations on these lines using the P Kα-doublet have recently been carried out with phosphides [5], some of which having zincblende structure are well known semiconductors of the group of the A^{III} B^{V}-compounds (table 2). The P Kα-doublet of the phosphides is shifted toward longer wavelengths relative to the doublet of the element, corresponding to the negative charge of the P-atom. However, the shifts are quite different for different phosphides, indicating charges on the P-atoms which are dependent upon the nature of the A^{III} -element and vary from

Table 2

Mean Wavelengths and Shifts of P K $\alpha_{1,2}$ for Different Compounds of Phosphorus

Substance	λ (XU)		Mean Shift	
	$K\alpha_1$	$K\alpha_2$	Δλ (XU)	Δ E (eV)
P red	6144.0	6146.7	-	-
$Ca(PH_2O_2)$	42.9	45.4	-1.20	+0.40
P_2O_5	41.4	44.0	-2.45	+0.81
Mg_3P_2	44.4	47.2	+0.45	-0.15
Ca_3P_2	44.1	46.8	+0.10	-0.03
BP	44.6	47.4	+0.65	-0.17
AlP (I)	44.5	47.5	+0.65	-0.17
GaP	44.7	47.3	+0.65	-0.17
InP	44.3	47.3	+0.45	-0.15

substance to substance. Here we are justified to speak of a mixed bond type between the extremes of purely ionic and purely covalent bond. So the picture of the tetrahedral A^{III} B^{V}-compounds as being practically covalent crystals cannot be maintained either. The ionic character appears to be quite pronounced as may be concluded from the amount of the shift. It is noteworthy, however, that the ionic character as indicated by the shifts is not as it should be according to the electronegativities of B, Al, Ga and In. GaP should be less ionic than AlP; BP should be nearly covalent. Finally it may be remarked that there are other observations supporting the general result that the semiconducting A^{III} B^{V}-compounds are more ionic than has been assumed so far [6].

VIII. ISOELECTRONIC COMPOUNDS WITH SEMICONDUCTOR PROPERTIES

Another semiconducting compound of the same structure is carborundum, SiC. This substance has always been considered as a covalent solid, having about 10% ionic character according to the electronegativities of Si (1.8) and C (2.5). As will be shown in the Part IX, wavelength measurements of Si Kα are in good agreement with this assumption. Carborundum is isoelectronic with the above-mentioned phosphides and with zincblende. The results of the X-ray spectroscopic study of these isoelectronic series of compounds with semiconductor properties can be summarized like this: The A^{IV} B^{IV}-compound SiC is a covalent solid, its ionic character being small, in agreement with the electronegativities of Si and C. The A^{III} B^{V}-compounds show mixed bond type, the ionic character being considerable and not in agreement with the electronegativities of the elements concerned. For zincblende representing the A^{II} B^{VI}-compounds no indication was found for covalent bonds between Zn and S. Direct measurements with tetrahedral A^{I} B^{VI} -compounds have not been made so far, but there are other observations showing that it is very unlikely that covalent bonds exist between metal and negative ion, just as in the case of the A^{II} B^{VI}-compounds.

IX. THE K-SPECTRUM OF SILICON

In a recent investigation of the K-spectrum of silicon we studied not only the $K\alpha$-lines but also the $K\beta$-band and the K-absorption spectrum in numerous compounds [7,8]. This work still being in progress, only a few of the results shall be reported here.

There are a few older measurements [9] with the fluorescence method (table 3) which are in full agreement with our new values. The wavelengths given in table 3 for Si, SiO_2 and SiC make it immediately clear that SiC is not a ionic crystal as has concluded from infrared determinations of the effective charge [10]. It is generally accepted that the bond in SiO_2 has 50% covalent and 50% ionic character. Since the Si-doublet of SiC is shifted much less to the short wavelength side than that of SiO_2, it is safe to say that SiC is a more or less covalent crystal, Si having a small

Table 3

Wavelengths and Shifts of Si $K\alpha_{1,2}$ for Different Compounds of Silicon

Substance	λ (XU)		Mean Shift	
	$K\alpha_1$	$K\alpha_2$	$\Delta\lambda$ (XU)	ΔE (eV)
Si	7110.94	7113.58	-	-
Na_2SiF_6	07.37	09.99	-3.58	+0.87
SiO_2	08.43	11.16	-2.47	+0.59
SiS_2	08.49	11.56	-2.04	+0.50
Si_3N_4	08.96	11.58	-1.99	+0.49
SiC	10.07	12.67	-0.89	+0.22
Mg_2Si	11.52	14.26	+0.63	-0.15

positive charge as it should be according to the electronegativities of Si and C. The structure of the Si K-band of SiC is further direct evidence for the covalent character of the bond.

Small shifts, hardly beyond the limits of error, have also been found for several silicon-metal compounds, which means that they are metallic phases rather than compounds. This direct approach to the problem of the bond character in such systems has been very helpful to the chemists.

The Suboxides of Silicon

In the course of these investigations we could identify the lower oxides of silicon. Hitherto only one solid oxide of silicon, SiO_2, has been known. The technical product SiO is not a pure chemical compound, as is well known. However, it is not a mixture of Si and SiO_2 as is often assumed. We checked this by making an artificial mixture of Si and SiO_2, in the ratio 1 atom Si to 1 molecule SiO_2. The Kα-spectrum of this mixture shows three sharp lines, the superposition of the doublet of Si and that of SiO_2 (table 3). The technical SiO gives a broad blackening showing that its composition is more complicated, the product probably containing lower oxides in addition to Si and SiO_2.

The first suboxide of silicon which we could identify was Si_2O_3. It was obtained by E. Cremer, Th. Kraus and E. Ritter [11] in the form of thin layers produced by evaporation of technical SiO with a certain O_2 partial pressure in the high vacuum apparatus. For layers with the composition of 1 atom Si to 1.5 atoms O optical extinction measurements seemed to indicate the existence of Si_2O_3. This could be proved by taking the Kα-spectrum of the substance [12]. It showed a proper doublet with wavelengths longer than those of SiO_2 (table 4). In SiO_2 each atom is surrounded by 4 O-atoms, in Si_2O_3 the arrangement is most likely such that each Si-atom is surrounded by three O-atoms and one Si-atom. Because of the electronegativity of Si being smaller

Table 4

Wavelengths and Shifts of Si $K\alpha_{1,2}$ for Silicon Oxides

Substance	λ (XU)		Mean Shift	
	$K\alpha_1$	$K\alpha_2$	Δλ(XU)	ΔE(eV)
Si	7111.16	7113.77	-	-
"Si_2O"	09.32	12.00	1.81	0.44
Si_2O_3	08.89	11.55	2.25	0.55
SiO_2	08.69	11.36	2.44	0.60

than that of O the charge of the Si-atom in Si_2O_3 should then be lower than in SiO_2. A smaller charge means a longer wavelength, which is actually found.

E. Wiberg and W. Simmler [13] have announced this oxide several years ago, but they were not able then to identify it since it was amorphous. It could now be proved that their substance actually was also Si_2O_3.

The suboxide Si_2O could not be obtained, but there has been obtained a compound of the same oxidation state + 1, $Si_2O \cdot R_2O = SiOR$ ($R = C_2H_5$) [14]. Here each Si-atom is surrounded by 3 Si-atoms and 1 O-atom. Consequently the Si Kα-doublet has still longer wavelengths (table 4).

Attempts to prepare and identify pure solid SiO have also been successful, but the experiments are still in progress.

The Kβ-Spectrum of Silicon

As mentioned above we have also studied the Si Kβ-band of the substances under investigation, using fluorescence excitation as in the case of Kα. For Si, SiO_2 and SiC the whole X-ray spectrum, including all emission and absorption bands of all three elements, is now known [7]. The consistency of the results is evident. As an example, Figure 4 shows the Si Kβ-band of SiC together with the C K-band of SiC and for comparison the C K-band of diamond. It will be seen that the three curves are very much of the same character, the first two curves representing the same energy band as projected to the K-level of Si and C respectively, the third one representing the energy band of a covalent crystal of similar electronic structure.

Quite different from these curves is the curve representing the Kβ-emission of quartz, a crystal of a distinctly different electronic structure. The band is narrower in this case and with a tendency to the shape of a line which seems to be a general feature of crystals with a more ionic bond character.

These results are of interest because there has been some discussion [15,16] that the form of the bands might be changed by exciton and other special excitation states in such a way that it might be practically impossible to reveal the proper structure of the energy bands.

Our results do not justify this scepticism, and there are other arguments against this view. We found, e.g., that by variation of the excitation—as long as chemical effects are excluded—the shape of the bands is not changed, which is unlikely if exciton states are involved.

It is true that the long wavelength ends of the bands are broadened by an effect not yet quite understood. But the short wavelength ends and edges of the bands are certainly often

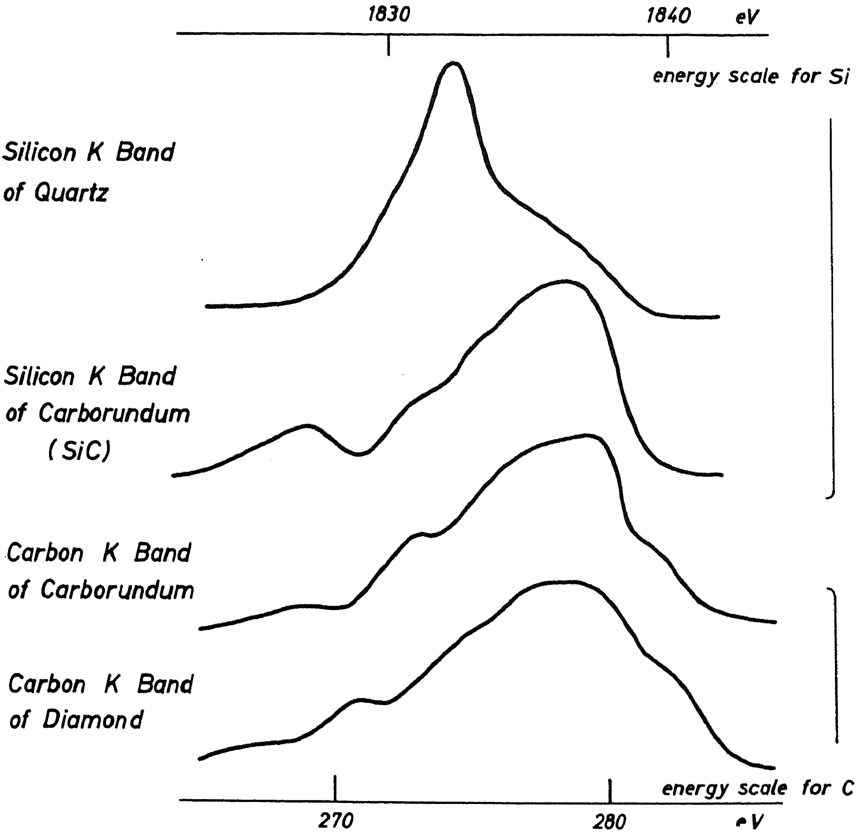

Figure 4. K-emission bands of diamond, carborundum and quartz.

undisturbed, as in the case of Si, SiO_2 and SiC, where the energy difference between the short wavelength ends of the K- and L-emission bands is equal to the energy of Kα within the precision of the method.

As far as experimental results could be compared with results of theoretical calculations, they were never in contradiction, at least with regard to the fundamental features. One should also remember the consistency of H. W. B. Skinner's work [17,18,19]. In order to get the complete picture of the energy band system of a crystal it will of course be necessary to study all emission bands of the atom in question because of the complementary character of the transition probabilities.

The author is indebted to Dr. B. Kern and Dipl.-Phys. M. Ficker for discussion and help in preparing this paper.

1. A. Faessler and M. Goehring, Naturwiss. 39, 169 (1952).
2. A. Faessler, Z. Physik 72, 734 (1931).
3. M. Goehring and D. Vogt, Z. anorg. Chem. 285, 181 (1956).
4. A. Faessler and M. Goehring, Z. Physik 142, 558 (1952).
5. A. Faessler and M. Ficker, Physik. Verh. 10, 129 (1959).
6. O. G. Folberth, Z. f. Naturforschung 13 a, 856 (1958).
   15 a, 425 (1960).
7. B. Kern, Z. Physik 159, 178 (1960).
8. H. Krämer, Diss. München (1960).
9. N. G. Johnson, Diss. Lund (1939).
10. W. G. Spitzer, D. A. Kleinman and C. J. Frosch, Phys. Rev. 113, 133 (1959).
11. E. Cremer, Th. Kraus and E. Ritter, Z. Elektrochemie 62, 939 (1958).
12. E. Cremer, A. Faessler and H. Krämer, Naturwiss. 46, 377 (1959).
13. E. Wiberg and W. Simmler, Z. anorg. allgem. Chem. 283, 401 (1956).
14. A. Faessler and H. Krämer, Ann. Physik 4, 263 (1959).
15. J. Friedel, Phil. Mag 43, 153, 1115 (1952).
16. L. G. Parratt, Rev. Mod. Phys. 31, 616 (1959).
17. H. W. B. Skinner, Rep. on Progress in Physics, 5, 257 (1939).
18. H. W. B. Skinner, Phil. Trans. Roy. Soc. London (A), 239, 95 (1940).
19. H. M. O'Bryan and H. W. B. Skinner, Proc. Roy. Soc. London (A) 176, 229 (1940).

SPECTROSCOPIE X D'ELEMENTS RADIOACTIFS

Y. Cauchois
Laboratoire de Chimie Physique de la Faculté des
Sciences de Paris, France

L'extension des études de spectroscopie X aux éléments encore peu ou pas étudiés, parmi lesquels se trouvent surtout des radioéléments, présente évidemment un interêt de principe. Mais elle pourrait paraître de peu d'importance eu égard au grand nombre d'éléments déjà bien étudiés et aux régularités de modification des spectres avec le numéro atomique. Cependant les prévisions de fréquences par interpolations et extrapolations basées sur la loi de Moseley, ou par l'application de relations théoriques, ne suffiraient qu'aux précisions exigées pour certains objectifs, comme l'analyse élémentaire; elles ne sauraient remplacer l'examen direct des spectres sur lesquels doivent être effectuées par exemple, outre les mesures precises de longueurs d'onde, les déterminations de largeurs et de formes ou d'intensités.

On sait que la spectroscopie X reste l'une des méthodes les plus directes et précises de l'indispensable détermination des niveaux d'énergie des atomes. On sait aussi que des informations intéressantes ont déjà pu être déduites de déterminations précises des fréquences de doublets pour les termes correctifs aux expressions de Sommerfeld provenant, en particulier, d'effets nucléaires. De telles études nécessitent des analyses spectrales rigoureuses pour chaque atome.

Dans un autre ordre d'idées, la spectroscopie X de précision, portant d'ailleurs sur des intensités d'émissions généralement faibles ou sur des variations petites de coefficients d'absorption, peut apporter des données très directes sur les configurations électroniques et les niveaux d'énergie des atomes libres ou liés et sur les propriétés électroniques des solides.

Des recoupements peuvent être faits avec d'autres méthodes relevant entre autres de l'optique, de la physique nucléaire ou de la physique du solide. Mais la précision et la diversité croissantes de leurs moyens expérimentaux et théoriques ne semblent pas exclure les déterminations plus classiques du domaine de la spectroscopie X.

Nous ne parlerons pas ici de l'identification ni de la dosimètrie d'éléments plus ou moins fortement actifs qui posent des problèmes techniques spéciaux; mais seulement de mesures relatives aux spectres peu ou pas connus d'éléments actifs et nous nous limiterons à quelques exemples.

Afin d'étudier des éléments actifs, des modes opératoires appropriés sont nécessaires soit pour protéger l'expérimentateur, soit pour protéger le détecteur qui doit assurer l'enregistrement du spectre. Nous avons démontré depuis longtemps dans notre Laboratoire qu'il était possible d'observer (dans de très bonnes conditions par rapport aux éléments inactifs) les spectres d'éléments fortement actifs en rayonnement α et γ comme le radium [1] ou en rayonnement α comme le polonium [2]. L'observation est basée sur l'emploi de spectrographes à focalisation, donc de grande luminosité et de grand contraste, c'est-à-dire de pouvoir de résolution aussi élevé que possible pour une dispersion convenablement choisie, permettant l'usage de quantités petites de radioéléments. Pour les émissions, l'excitation cathodique avait été employée dans des tubes à rayons X démontables de modèles normaux. Ainsi, les spectres L d'émission et d'absorption du radium avaient été analysés complètement à l'aide de la réflexion $(13\bar{4}0)$ d'une lame de quartz avec quelques centièmes de milligrammes de chlorure. Quant à notre travail sur le spectre L du polonium, à l'exception d'un résumé de ses premiers résultats [2], il ne fut publié que dans une revue peu accessible [3] Je crois donc utile d'y revenir (*).

L'analyse spectrale était faite avec un spectrographe à cristal courbé utilisant en transmission les plans (100) et $(\bar{2}01)$ du mica; la dispersion était d'environ 12 uX par mm. Le polonium 210 extrait du radium D était déposé électrochimiquement à l'état métallique sur une anticathode en nickel, à partir d'une solution chlorhydrique, après les purifications habituelles. La surface du dépôt était étroitement limitée à celle du foyer du tube à rayons X. La quantité déposée correspondait au plus à environ 10000 ues soit à environ $2,5.10^{-6}$ g. L'émission $L\alpha_1$ apparaissait déjà avec 40 ues, soit environ 10^{-9} g seulement.

Les Figures 1 et 2 ci-contre présentent des exemples d'émissions observées. Le tableau 1 rappelle les prévisions d'après [4], les résultats de nos mesures (1938-1940), ainsi que les valeurs actuellement prévisibles à partir de nos tables de niveaux d'énergie (1952-1955) [5].

---

*L'un de nos clichés fut reproduit dans la 3ème édition du livre de Jean PERRIN "les Atomes" (1939).

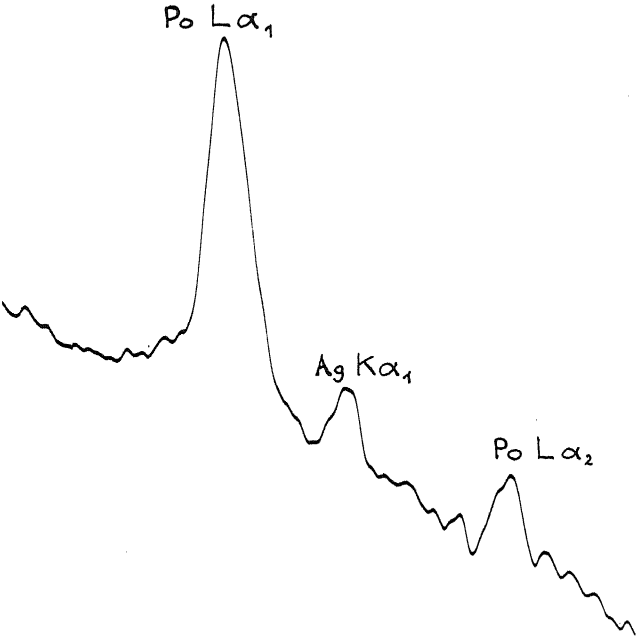

Figure 1.

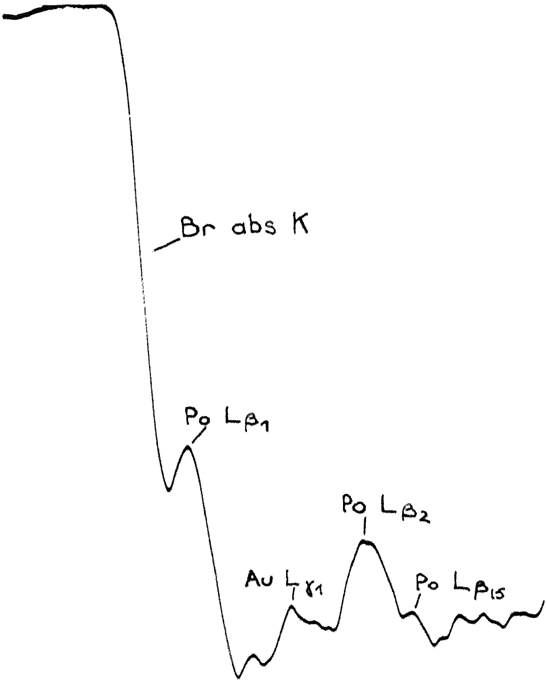

Figure 2.

Tableau 1

Spectre d'Emission L du Polonium

Emissions	λ uX calculée (1938)	λ uX mesurée (1938-40) N.B.	ν /R expérimentale	ν/R calculée (1952)
$L_I M_{II} \beta_4$	945,26	945,54	963,76	963,51
$M_{III} \beta_3$	906,93	907,22	1 004,46	1 004,02
$N_{III} \gamma_3$	762,49	762,88	1 194,51	1 194,03
$L_{II} M_{IV} \beta_1$	919,76	920,33	990,15	990,08
$N_{IV} \gamma_1$	785,52	785,90	1 159,52	1 159,45
$O_{IV} \gamma_6$	763,06	voir N. B.	--	1 193,62
$L_{III} M_{IV} \alpha_2$	1 123,10	1 123,29	811,25	811,40
$M_V \alpha_1$	1 111,59	1 111,52	819,84	819,80
$N_I \beta_6$	964,90	965,20	944,12	944,43
$N_{IV} \beta_{15}$	929,20	929,29	980,61	980,77
$N_V \beta_2$	927,31	927,43	982,57	982,63
satellite: β_2^{II}	--	922,42	987,91	--

N. B. η masquée par W$\gamma_4 \gamma_4'$; ℓ en dehors des spectres enregistrés; la mesure de γ_6 est gênée par γ_3. L'erreur expérimentale affecte une ou deux décimales selon l'intensité.

En 1957 parut une étude américaine effectuée avec 2 milligrammes de polonium déposés sur une anticathode de cuivre en tube scellé [6]. Elle précisait la mesure de 4 raies: Kα_1, α_2, β_1, β_2 (mais non β_3), à l'aide d'un spectrographe par transmission et avait permis d'observer 10 raies L à l'aide d'un spectrographe de Bragg. Les mesures de ces dernières sont basées sur des longueurs d'onde de référence dont certaines valeurs, indiquées dans le mémoire cité, diffèrent beaucoup de celles admises [4]. Il n'est donc pas surprenant qu'un désaccord apparaisse avec les nombres du tableau 1 que nous croyons plus corrects.

Les exigences actuelles de sécurité ne permettraient sans doute plus d'effectuer de telles manipulations dans un Laboratoire ordinaire.

Pour l'analyse spectrale X des transuraniens, nous avons mis au point des modes opératoires plus satisfaisants quant à la sécurité. Nous nous sommes assurés, de plus, la possibilité de contrôler la nature des échantillons étudiés à l'aide d'analyses à priori et à postériori par diffraction X et diffraction électronique.

Les travaux qui vont être résumés ici sont dus à un groupe de Chercheurs, Ingénieurs et Collaborateurs Techniques du Laboratoire que je tiens à associer à cette publication et au premier rang desquels doivent être cités: I. MANESCU, C. BONNELLE et L. de BERSUDER.

La quantité de produit actif est toujours réduite au strict minimum compatible avec les caractéristiques du spectrographe. Les échantillons actifs sont emprisonnés sous des couches protectrices inactives qui en évitent la dispersion et assurent que l'état physicochimique reste inaltéré, couches quasi transparentes pour le rayonnement à l'étude. Si l'émission propre corpusculaire ou ondulatoire de l'échantillon actif restait dangereuse ou gênante, il faudrait s'en affranchir soit par des champs convenables, soit par réflexion préalable du rayonnement X sur un cristal auxiliaire ou un miroir adjoint au spectrographe. Les études spectroscopiques effectuées avec le plutonium n'ont pas exigé de telles précautions. Par spectroscopie dans l'air, nous avons étudié successivement le spectre L d'absorption du plutonium à l'état d'oxyde avec un écran autonome de 10 mg de PuO_2 et le spectre L d'émission excité par fluorescence, en utilisant comme radiateur secondaire l'échantillon précédent [7,8,9]; puis le spectre L d'absorption du métal avec des écrans autonomes [10] de pureté contrôlée préparés par évaporation thermique à l'aide d'une technique spécialement élaborée par L. de BERSUDER, tout d'abord pour l'uranium [11] et transposée au plutonium. Toutes nos études ont porté sur l'isotope 239.

Les différents écrans ont été préparés dans les Laboratoires spécialisés du Commissariat à l'Energie Atomique. Mais toutes les manipulations ultérieures ont été effectuées dans nos Laboratoires. Des contrôles fréquents au scintillateur α et des prélèvements d'air ont permis de s'assurer qu'aucune fuite de plutonium ne se produisait pendant ces opérations, échelonnées sur plusieurs mois de travail effectif au cours de plusieurs années. L'enregistrement des spectres a jusqu'à présent été fait exclusivement par photographie, à l'aide d'un spectrographe à focalisation par transmission, utilisant généralement des micas courbés cylindriquement sous 40 cm de diamètre travaillant dans l'air, analogue à celui utilisé pour le polonium et le radium (Figure 3). Nous présentons ci-contre des exemples de spectres obtenus Figures 4, 5, 6, 7 et 8 et dans les tableaux 2 et 3 les résultats de nos mesures.

Pendant que se poursuivait notre étude, un travail effectué dans des conditions analogues avec 200 milligrammes d'oxyde apportait la mesure de 8 raies d'émission [12]; les valeurs

Spectrographe à rayons X **utilisant des lames cristallines courbées, par transmission. (Schéma du principe de la construction).**

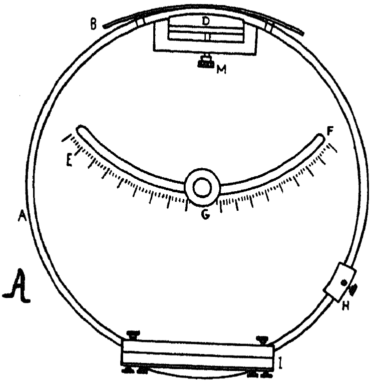

A: Projection horizontale

B—Ecran de Pb. D—Porte cristal amovible. G—Graduation indiquant la position du spectrographe. H—Viseur à pointe pour les réglages. I—Châssis photographique mobile.

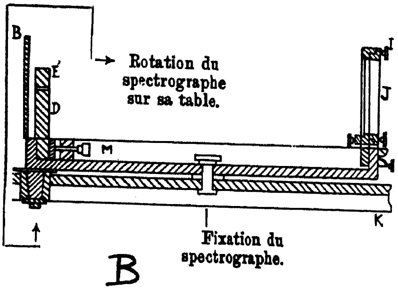
B
E
D
Rotation du spectrographe sur sa table.
M
I
J
K
Fixation du spectrographe.
B

B: Coupe verticale

B—Pb. D—Porte cristal. E—lame cristalline. I—Châssis photographique mobile amovible. J—Plaque photo. K—Table portant l'appareil.

Figure 3.

exprimées en longueurs d'onde dans notre normalisation sont données colonne 2 tableau 3. Un certain nombre de raies d'émission ont été remesurées par J. du MOND et ses collaborateurs au spectromètre à deux cristaux [13] [14]. Il faut souligner que la quantité de plutonium utilisée atteignait la valeur considérable de 5 g 86. Il est vrai que 50 milligrammes d'oxydes de différents transuraniens ont suffi à ces auteurs pour mesurer les raies L les plus fortes et pour observer l'absorption L_{III}, mais non L_{II} ni L_I; ce dans des conditions qu'ils donnent comme peu satisfaisantes. Dans le tableau 3 colonne 4, nous avons indiqué leurs valeurs rapportées à la même normalisation que la nôtre (*).

---

*Les conventions adoptées par Du MOND pour l'unité X reviennent à prendre pour la longueur d'onde de $MoK\alpha_1$ 707,848 uX alors que nous conservons comme dans la référence [4], la valeur de Siegbahn 707,831.

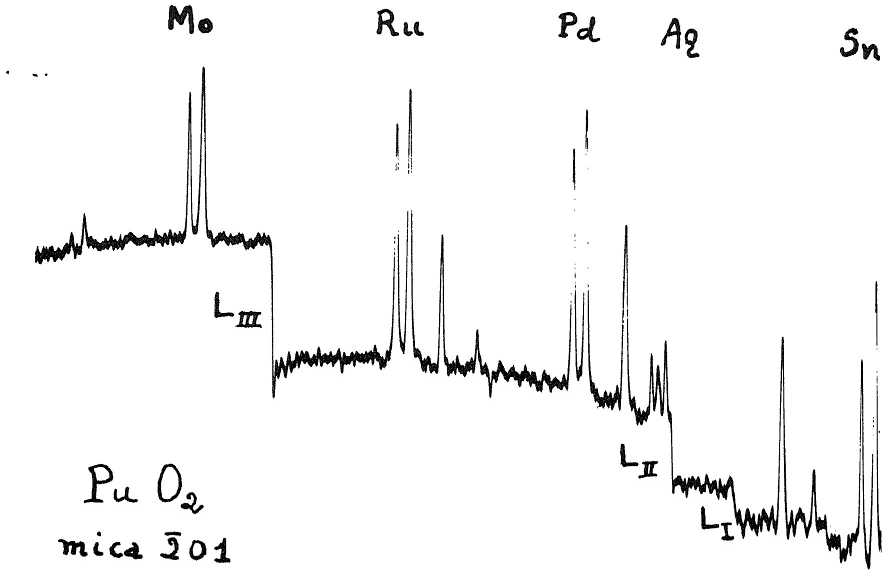

Figure 4. PuO_2, mica $\bar{2}01$.

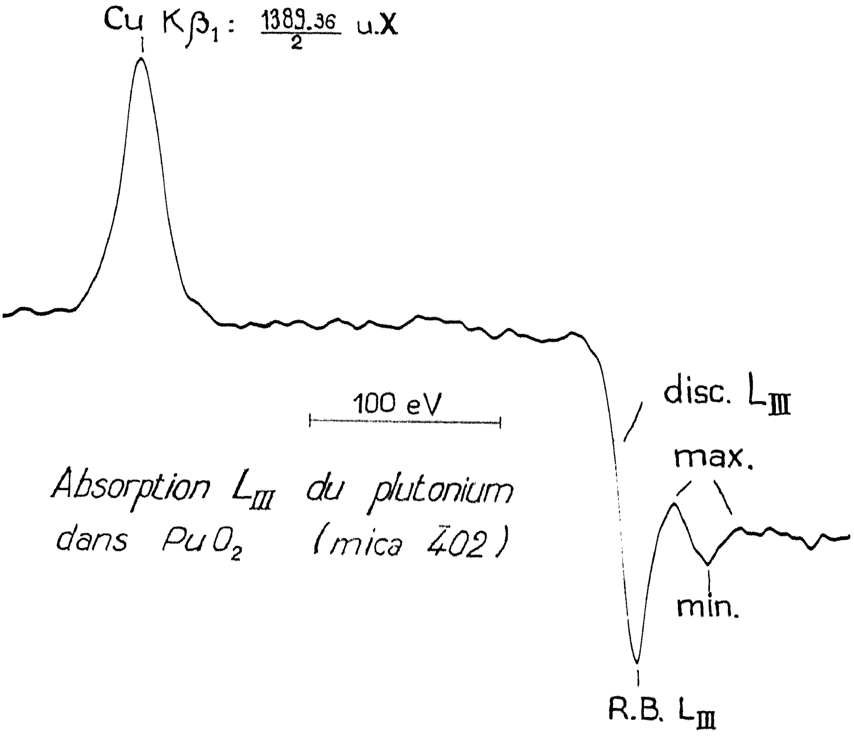

Figure 5. Absorption L_{III} du plutonium dans PuO_2, mica ($\bar{4}02$).

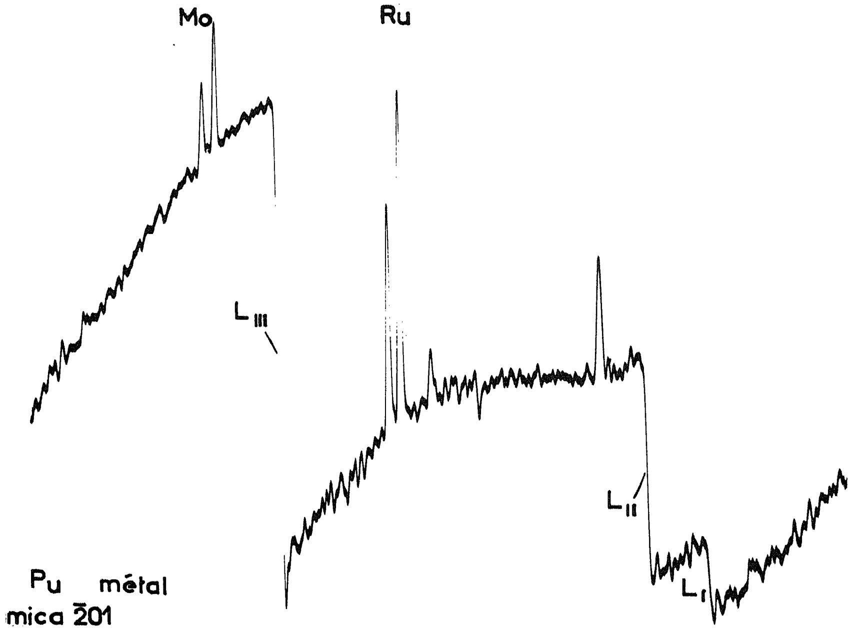

Figure 6. Pu métal, mica (2̄01).

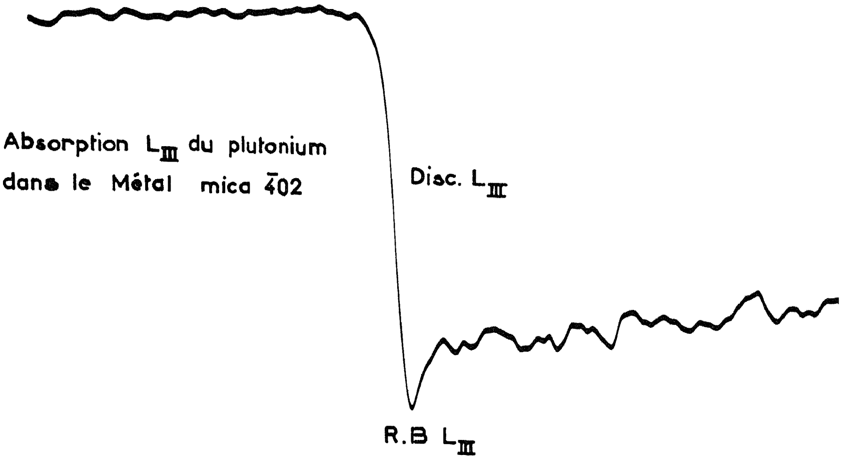

Figure 7. Absorption L_{III} du plutonium dans le métal, mica (4̄02).

On voit que l'accord est très bon. La décroissance radioactive de 96 Cm^{242} conduisant par émission α à 94 Pu^{238} entraîne l'émission spontanée du rayonnement X caractéristique du plutonium. Cette émission a été analysée en particulier à Berkeley [15] avec un spectromètre à cristal courbé. Les résultats, corrigés pour certaines erreurs et ramenés aussi à notre normalisation, figurent colonne 1 tableau 3.

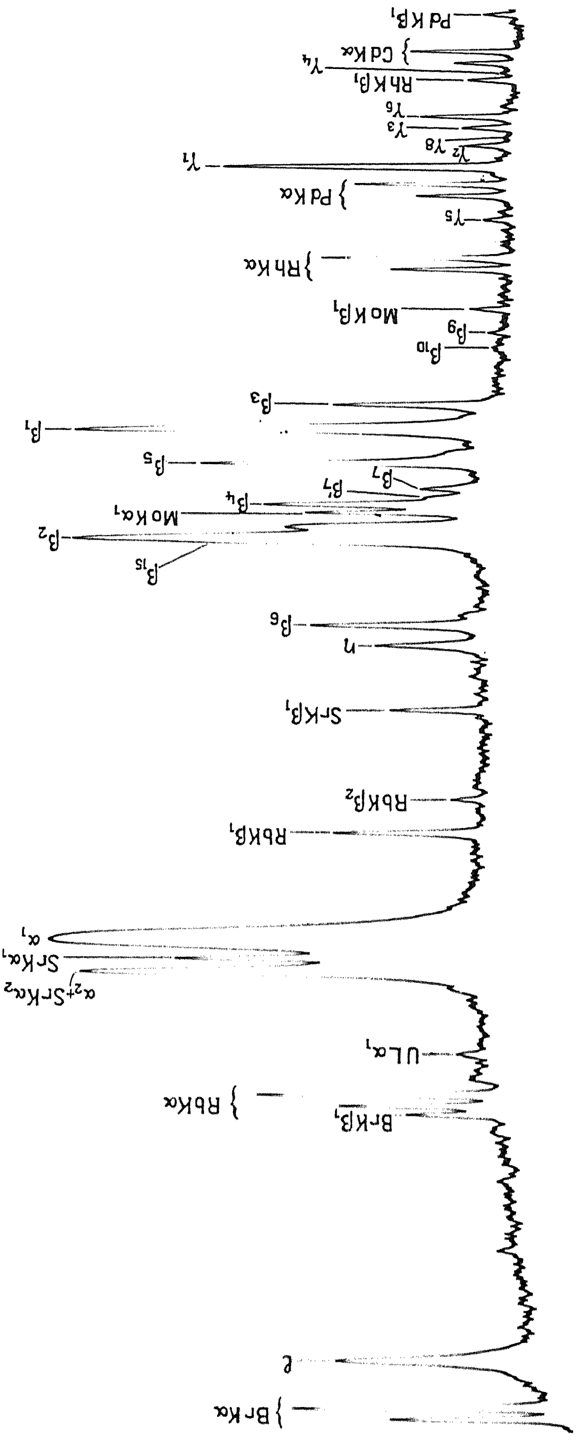

Figure 8. Spectre L d'émission de PuO_2.

Tableau 2

Spectre d'Absorption L du Plutonium‡

			$Pu_{\text{métal}}$	PuO_2
L_{III}	disc.	λuX	685,34	685,25
		ν/R	1 329,66	1 329,83
		eV	18 050	18 052
	R.B.	λuX	684,9	684,8
		ν/R	1 330,5	1 330,7
		eV	18 062	18 064
L_{II}	disc.	λuX	555,74	555,95
		ν/R	1 639,74	1 639,12
		eV	22 259	22 251
	min	λuX	555,3	555,3
		ν/R	1 641,0	1 641,0
		eV	22 277	22 277
L_I	disc.	λuX	535,5	535,4
		ν/R	1 701,7	1 702,0
		eV	23 101	23 105

‡L'erreur affecte les derniers chiffres.

Le tableau 4, colonnes 1 et 2, donne les valeurs des niveaux du plutonium calculés (en ν/R et en eV*) à partir de nos valeurs pour la discontinuité L_{III} du métal et de toutes nos mesures sur le spectre L. Dans les colonnes 3 et 4 sont indiqués les calculs des niveaux obtenus par extrapolation à l'aide d'une méthode des moindres carrés, à partir des valeurs données dans la référence [5] et de quelques nouvelles valeurs expérimentales.

Je ne rapporte ici que les résultats propres à des éléments très actifs qui présentent un danger pour l'expérimentateur, puisque l'on estime par exemple à peut-être $0,1.10^{-6}$ g la dose toxique de plutonium et que l'on tient le polonium pour plus nocif encore. Mais notre Laboratoire a mis au point ou utilisé les méthodes indiquées, pour d'autres éléments lourds, comme le thorium et l'uranium. Les études portent actuellement aussi sur la détermination des coefficients d'absortion. Nous avons établi

---

*Les facteurs de conversion, à partir de la valeur "Siegbahn" pour l'uX sont indiquées dans [4] et [5].

Tableau 3

Spectre d'Emission L du Plutonium (λ en uX).

Emissions		Valeurs Expérimentales				Prévisions
		G. W. Barton, H. P. Robinson, J. Perlman 1951	G. Rogosa, W. E. Peed 1956	Y. Cauchois, I. Manescu 1954 - 1956	J. W. M. Du Mond, J. Merrill 1958 - 1960	d'après Réf. [5]
L_I	$M_{II}\ \beta_4$		704,9	704,74	704,739	704,95
	$M_{III}\beta_3$		667,5	667,33	667,315	667,54
	$M_{IV}\beta_{10}$			646,$_{65}$		646,90
	$M_V\beta_9$			640,1$_2$		640,44
	$N_{II}\gamma_2$			569,52	569,496	569,74
	$N_{III}\gamma_3$			562,80	562,833	563,00
	$O_{II}\gamma_4'$			542,$_{15}$		542,20
	$O_{III}\gamma_4$			540,$_{50}$		540,65
L_{II}	$M_I\eta$			757,49		757,82
	$M_{IV}\beta_1$	676	676,5	676,32	676,304	676,55
	$N_I\gamma_5$			597,55		597,60
	$N_{IV}\gamma_1$	578	577,9	577,71	577,683	577,93
	$O_I\gamma_8$			564,$_{52}$		564,93
	$O_{IV}\gamma_6$	558		558,63	558,566	558,40

Tableau 3—Continued

Emissions	Valeurs Expérimentales				Previsions
	G. W. Barton, H. P. Robinson, J. Perlman 1951	G. Rogosa, W. E. Peed 1956	Y. Cauchois, I. Manescu 1954 - 1956	J. W. M. Du Mond, J. Merrill 1958 - 1960	d'après Réf. [5]
$L_{III}\ M_I\ \ell$			1 020,46		1 020,37
$M_{IV}\ \alpha_2$	876,6	878,5	878,43	878,458	878,31
$M_V\ \alpha_1$	866,3	866,5	866,53	866,470	866,42
$N_I\ \beta_6$			750,00	749,918	749,73
$N_{IV}\ \beta_{15}$			719,02		719,02
$N_V\ \beta_2$	717	717,2	717,00	717,016	717,09
$N_{VI,\ VII}\ \beta'_7$			$701,_{65}$		700,98
$O_I\ \beta_7$			$698,7_1$		699,01
$O_{IV,V}\ \beta_5$	692	689,4	689,25	689,247	689,04

Tableau 4

Niveaux d'energie du Plutonium

	A partir de nos mesures		Calculés à partir de réf. [5]	
	ν/R	e V*	ν/R	e V
K			8 968,6$_6$	121 750
L_I	1 701,6$_2$	23 099	1 701,4$_8$	23 098
L_{II}	1 639,6$_8$	22 259	1 639,7$_6$	22 260
L_{III}	1 329,6$_6$	18 050	1 330,3$_5$	18 060
M_I	436,6$_6$	5 928	437,2$_7$	5 936
M_{II}	408,5$_6$	5 546	408,8$_1$	5 550
M_{III}	336,0$_7$	4 562	336,3$_6$	4 566
M_{IV}	292,2$_8$	3 968	292,8$_2$	3 975
M_V	278,0$_3$	3 774	278,5$_9$	3 782
N_I	114,6$_5$	1 556	114,8$_8$	1 559
N_{II}	101,5$_5$	1 379	102,0$_3$	1 385
N_{III}	82,4$_5$	1 119	82,8$_8$	1 125
N_{IV}	62,2$_9$	846	62,9$_8$	855
N_V	58,7$_1$	797	59,5$_7$	809
$N_{VI,VII}$	30,9$_1$	420	30,3$_6$	412
O_I	25,4$_4$	345	26,6$_9$	362
O_{II}	20,7$_8$	282	20,8$_0$	282
O_{III}	15,6$_4$	212	15,9$_8$	217
$O_{IV,\ V}$	7,5$_4$	102	7,8$_2$	106

*L'incertitude sur les déterminations expérimentales de longueurs d'onde entraîne une erreur qui affecte le chiffre des eV pour les niveaux calculés.

une méthode photométrique qui fournit une suite continue de valeurs de ces coefficients en fonction de la longueur d'onde. Les valeurs obtenues pour l'uranium, par exemple pour les longueurs d'onde du doublet K α du molybdène, sont compatibles avec celles connues [16].

La spectroscopie des radioéléments dans la région des rayons X mous présente des difficultés supplémentaires par rapport à celle du domaine accessible à l'air. Mais elle apporte des informations complémentaires et parfois plus intéressantes par la meilleure résolution en énergie, particulièrement quant aux propriétés physiques et chimiques des solides.

Dans une étude entreprise avec l'aide du Commissariat à l'Energie Atomique, nous nous sommes proposés, entre autres, d'étudier les spectres M des transuraniens. Nous avons, en fait, réalisé un montage comprenant un spectrographe à cristal courbé utilisé par réflexion sous atmosphère d'hélium, qui permet l'analyse de longueurs d'onde comprises entre environ 1,8 Å et 4,5 Å. Ce montage (Figure 9) est donc susceptible de fournir les spectres K des éléments 17 Cl à 25 Mn, L de 59 Pr à 44 Ru, M de 96 Cm à 84 Po, inclusivement. Il comporte une enceinte spectrographique sous hélium, un châssis photographique attaché à cette enceinte, mais placé dans l'air, et un tube à rayons X, sur pompes, indépendant du spectrographe. Le tube est aisément mis en place avec une précision suffisante par rapport au spectrographe, grâce à des guidages mécaniques. Son foyer se trouve en général placé à 105 mm du cristal dont le rayon de courbure est de 250 mm. Sortant de sa fenêtre en béryllium de 40 μ d'épaisseur, le rayonnement franchit une très petite lame d'air et entre dans l'enceinte spectrographique par une large fenêtre obturée soit par du Mylar "aluminé" de 6 μ d'épaisseur, soit par du béryllium.

Grace à la réalisation d'une enceinte spectrographique close, étanche à l'air ambiant, mais baignée d'hélium à une pression très légèrement inférieure à l'atmosphère extérieure, on évite toute contamination extérieure à partir d'éventuelles contaminations

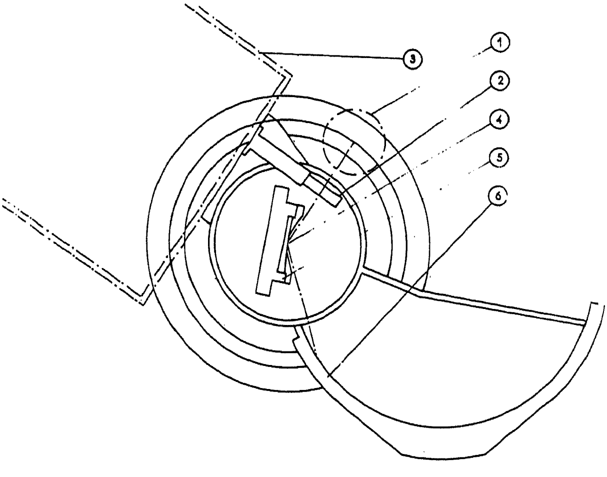

Figure 9.

(1) tube à rayons X
(2) porte-échantillon
(3) boîte à gants
(4) cristal
(5) glissière
(6) châssis photographique

de son intérieur. Il est possible d'y introduire et maintenir des échantillons actifs autonomes autoprotégés, comparables à ceux utilisés pour la spectroscopie dans l'air, quoique dans leur ensemble beaucoup plus minces et fragiles, ce qui serait pratiquement très difficile si l'enceinte était vidée. Les échantillons actifs destinés à l'absorption ou à l'émission secondaire du rayonnement X caractéristique peuvent être introduits à l'intérieur de l'enceinte spectrographique par l'intermédiaire d'une petite boîte à gants fixée sur l'un de ses côtés, baignée par la même atmosphère d'hélium. En fait, les échantillons introduits n'ont jusqu'à présent apporté aucune contamination décelable dans l'enceinte spectrographique. L'altération chimique a été totalement évitée par leur maintien sous hélium, assuré déjà pendant toutes les manipulations grâce à un petit sac de polythène.

Trois porte-cristaux sont montés sur une glissière de précision; dans chacun est courbée une lame cristalline de nature et d'orientation choisies; un dispositif de commande extérieur permet d'amener l'un ou l'autre en position de travail. Il est ainsi possible d'analyser, dans des conditions variées, tout le large domaine de longueur d'onde indiqué, sans ouvrir l'enceinte.

Du côté du porte-film, l'enceinte spectrographique est obturée par une paroi en Mylar de 6 μ d'épaisseur. L'émulsion du film photographique se trouve amenée soigneusement en coïncidence avec le cylindre de focalisation de 125 mm, grâce à une pièce dont l'usinage et la mise en place ont dû être réalisés avec une grande précision, par rapport aux porte-cristaux. Les cristaux doivent avoir une grande perfection et une courbure rigoureuse. Toutes ces exigences sont absolument essentielles pour l'obtention de spectres à haute résolution, de contraste optimum, mesurables avec précision.

Grâce à un obturateur, la mise en place du porte-film sur l'enceinte spectrographique à hélium s'effectue facilement au jour; l'enceinte munie du porte-film est parfaitement étanche à la lumière.

Le spectrographe peut tourner autour d'un axe passant par la génératrice médiane des cristaux, le tube restant fixe, de telle sorte que l'angle de Bragg varie de 25 à 80°. Ce réglage ne demande pas une haute précision. Le domaine d'angle accesible, la nature des cristaux et des systèmes réflecteurs utilisables, ainsi que l'absorption du rayonnement par les milieux traversés (essentiellement les fenêtres) justifient la gamme des longueurs d'onde indiquées: environ 1,8 à 4,5 Å. A l'intérieur du spectrographe, des caches doivent limiter convenablement les faisceaux pour éviter tout rayonnement direct ou parasite dans la région du spectre; ils doivent être commandés de l'extérieur.

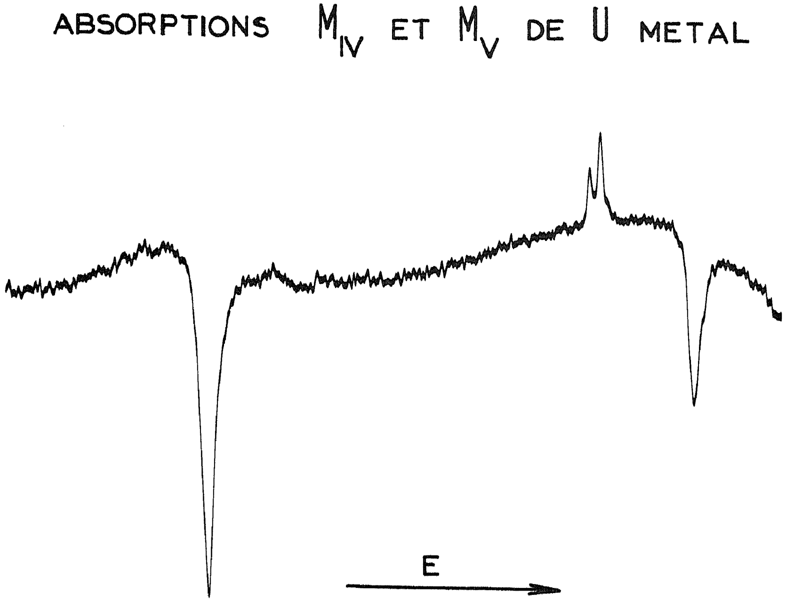

Figure 10.

Le montage a été mis à l'épreuve dans notre Laboratoire pour une étude précise du spectre d'absorption M de l'uranium. On a pu observer les 5 discontinuités d'absorption M du métal avec des écrans "autonomes" de pureté controlée protegés de l'oxydation (*). Figure 10 et 11.

L'étude a confirmé nos travaux antérieurs sur le spectre L complétés par nos nouvelles observations—non publiées—sur des absorbants constitués d'empilements d'écrans, analogues à ceux utilisés pour le spectre M. Les maxima d'absorption voisins des discontinuités L_{III} et L_{II} (2p), M_{III} et M_{II} (3p) et les très fortes absorptions M_{V} et M_{IV} (3d) sont conformes à la présence d'états d ef f au voisinage de la limite de Fermi dans ce métal.

Le montage a été transporté dans le Département du Plutonium du Commissariat à l'Energie Atomique, au voisinage de dispositifs d'évaporation sous vide et de diffraction électronique, réalisés là par L. de BERSUDER pour la préparation et le contrôle des écrans. (*)

De l'étude en cours sur les spectres M du plutonium (*) sont extraits les documents présentés ici pour les absorptions M_{V} M_{IV}, et M_{III} du métal, Figures 12 et 13.

Voici à titre d'exemples quelques indications sur les conditions d'expérience:

---

*à paraître

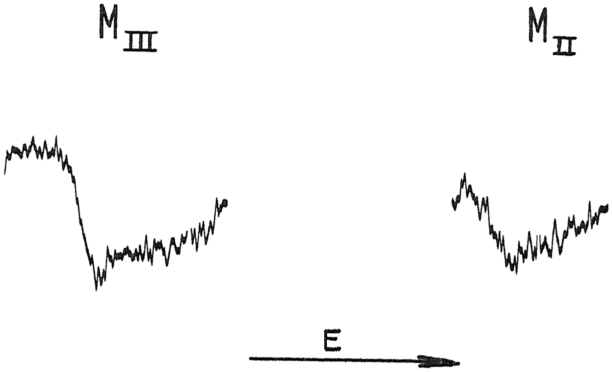

ABSORPTIONS M DE U METAL

Figure 11.

- M_V et M_{IV} : cristal analyseur de quartz, réflexion $(11\bar{2}0)$, dispersion environ 15 uX/mm, soit 18 eV/mm sur le cliché photographique; quantité de plutonium variable de 0,3 à 1 mg/cm^2 suivant les cas; rayonnement du tungstène excité à 7 kV; durée d'exposition sur film Kodak "Diffrax" de 1 à 4 h pour 15 mA.

- M_{III} : quartz (0001) donnant 9 uX, soit 16 eV/mm; 1,5 à 2 mg/cm^2 de plutonium; durée d'exposition jusqu'à 20 h. Ref.: raies K de Cu, Ni, Co, Ti.

Le rôle de l'épaisseur sur l'aspect du spectre est tres important, surtout pour M_{IV} et M_V; on peut le comprendre en considérant la réponse de l'émulsion photographique et les variations rapides considérables du coefficient d'absorption au voisinage de la discontinuité relativement au saut d'absorption correspondant. Les dépouillements corrects en fréquence comme en intensité, nécessitent donc une longue analyse photomètrique.

Les premières mesures ont donné les résultats du Tableau 5 ci-contre que nous donnons sous toutes réserves.

Cette étude de radioéléments est en cours d'extension à l'américium.

Pour terminer, rappelons que nos montages spectrographiques (Figures 3 et 14) nous ont permis d'obtenir dès 1934 les premiers spectres d'émissions spontanées de radioéléments [17]; ainsi la Figure 15 montre les émissions L du RaC formé dans la décroissance du radon.

Les recherches exposées dans cet article et tout particulièrement celles relatives au plutonium, n'auraient pu se poursuivre

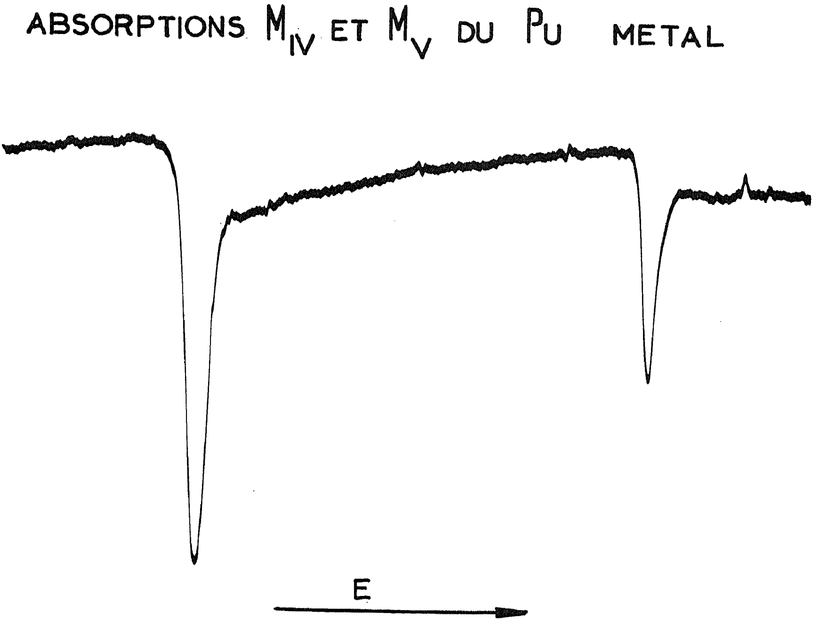

Figure 12.

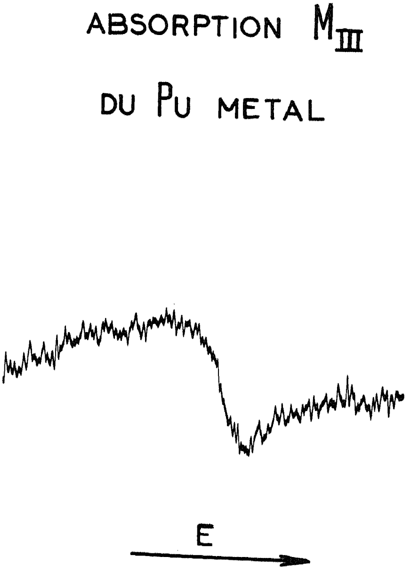

Figure 13.

Tableau 5

Spectre d'Absorption M du Plutonium Métallique

Premières déterminations

	λ uX	ν/R	eV
M_V	3 278,$_2$	277,9$_8$	3 773,$_6$
M_{IV}	3 117,$_8$	292,2$_8$	3 967,$_7$
M_{III}	2 710	336,$_3$	4 565

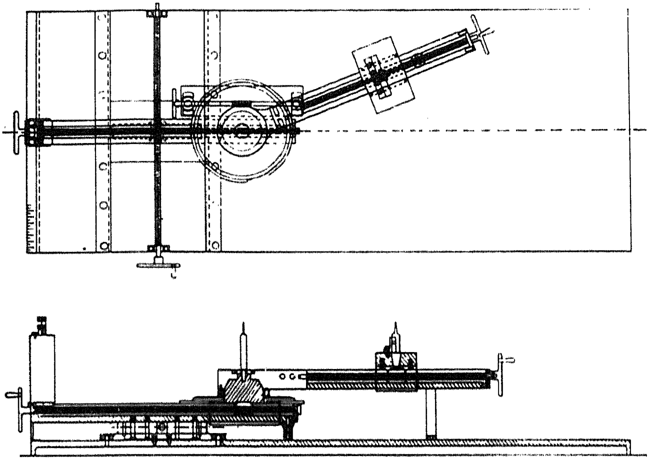

Figure 14.

sans l'aide que nous apporte le Commissariat à l'Energie Atomique. J'adresse mes très vifs remerciements à Monsieur le Haut Commissaire Francis PERRIN, à Monsieur E. GRISON Chef du Département du plutonium et à Messieurs P. REGNAUT et F. SEBILLEAU, pour toute leur contribution à ce programme d'étude.

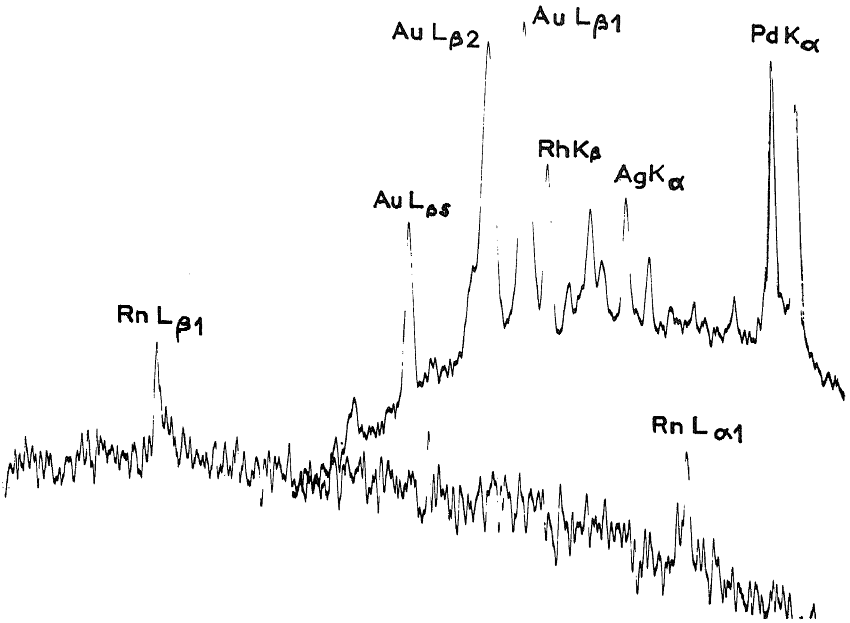

Figure 15.

REFERENCES

1. H. Hulubei, J. Phys. Rad. VIII, 260, 1937.
2. H. Hulubei, Y. Cauchois, S. Cotelle, C. R. 207, 1204, 1938.
3. H. Hulubei, Y. Cauchois, Disq. Math. Phys. 1, 141, 1940.
4. Y. Cauchois, H. Hulubei, Tables de constantes et données numériques - Longueurs d'onde des émissions X et des discontinuités d'absorption X - Paris 1947.
5. Y. Cauchois, J. Phys. Rad. 13, 113, 1952; 16, 253, 1955.
6. W. F. Peed, L. E. Burkhart, R. A. Staniforth and L. G. Fauble, Phys. Rev. 105, 588, 1957.
7. Y. Cauchois, I. Manescu, L. Le Berquier, C. R. 239, 1780, 1954.
8. Y. Cauchois, J. Phys. Rad. 16, 81 S, 1955.
9. Y. Cauchois, I. Manescu, C. R. 242, 1433, 1956.
10. Y. Cauchois, I. Manescu, L. de Bersuder, C. R. 253, 1042, 1961.
11. L. de Bersuder, Rapport C.E.A. n° 1792.
12. G. L. Rogosa, W. F. Peed, Phys. Rev. 101, 591, 1956.
13. J. J. Merrill, J. W. M. du Mond, Phys. Rev. 110, 79, 1958.
14. J. J. Merrill, J. W. M. du Mond, Ann. Phys. 14, 166, 1961.
15. G. W. Barton, H. P. Robinson, I. Perlman, Phys. Rev. 81, 208, 1951.
16. R. B. Roof, Phys. Rev. 113, 820, 1959.
17. H. Hulubei, Y. Cauchois, C. R. 199, 857, 1934; 209, 39, 1939.

X-RAY EMISSION SPECTROGRAPHY AT LONG WAVELENGTHS

P. D. Zemany
General Electric Company
Schenectady, New York, U.S.A.

X-ray emission spectrography became one of the tools of analytical chemistry about ten years ago, that is in 1952, when the first commercially produced instruments became readily available. This paper will review the development of practical applications of this analytical tool in the long wavelength or light element field since that time from the viewpoint of an analytical chemist. Also it will try to point out the problems that will have to be solved to extend the method to still lighter elements and comment on the various approaches that have been made.

It was found, by 1953, that the new tool was useful for the analysis of titanium, atomic number 22, with a K_α at 2.75 Å, and all the heavier elements. The things that hindered the extension of the method to the determination of the elements lighter than titanium were excessive absorption in the x-ray path, a lack of suitable detectors and crystals, and insufficient excitation of the longer wavelengths. Now, 10 years later it has become practical to analyze for sodium, atomic number 11, with a K_α line at 11.9 Å. The hindrances to analyzing for still lighter elements are still the same, excessive absorption, lack of good detectors and crystals, and insufficient excitation of the long wavelengths.

By extrapolation, one might hope that in 1972, when these problems are solved, and hydrogen yields to analysis, x-ray emission will be able to determine all the elements in a sample of material.

The frontier is now at sodium. If some analytical chemists are pioneers in the region beyond, then the physicists are the Indians. They had worked out methods and instruments useful at the long wavelengths involved many years ago, but the methods they used are not yet practical for the analytical chemists, who require from an analytical procedure that it give reliable information on composition in a relatively short time, at a price the customer is willing to pay. This last requirement is the one that really counts.

X-ray emission spectrography is simple in principle. There are just two steps, other than obtaining a suitable sample. First, one measures the intensity of a characteristic line, and second, computes the amount of the element. The difficulties mentioned were instrumental difficulties that result in an unsatisfactory estimate of line intensity, but that is only half the story, because as the wavelength increases, the second step from line intensity to analytical result also becomes more difficult.

This step involves determining the background correction, very complex absorption and enhancement effects, interfering lines, chemical effects and a few more things. Also there are problems of sampling, which includes the effects of heterogeneity and surface structure.

Figure 1 shows the elements concerned. Titanium and heavier elements could be determined, or at least a useful signal obtained in 1952. The group from scandium to sodium has been added to the list of elements that can be analyzed in the intervening years. The heaviest element that could then be determined by its K spectrum was about barium, atomic number 56. The heavier elements were determined by use of the L spectrum. With only eleven elements added to the seventy that could be determined in 1953, it doesn't seem that much has been added, but if the wavelengths involved are plotted, as in Figure 2, it will be seen how far the spectrum has been extended and how much further there is to go. Not shown in the figure are the L, M, or N spectra of the heavier elements. These spectra are very complex, and have been studied for only a very few elements.

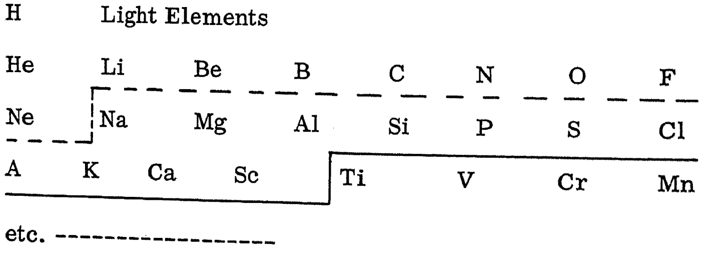

Figure 1. The solid line of demarcation separates the heavy elements (below), that could be determined on the earliest spectrographs from the light elements (above). The elements above the dotted line have not yet been determined by conventional x-ray emission spectrographs.

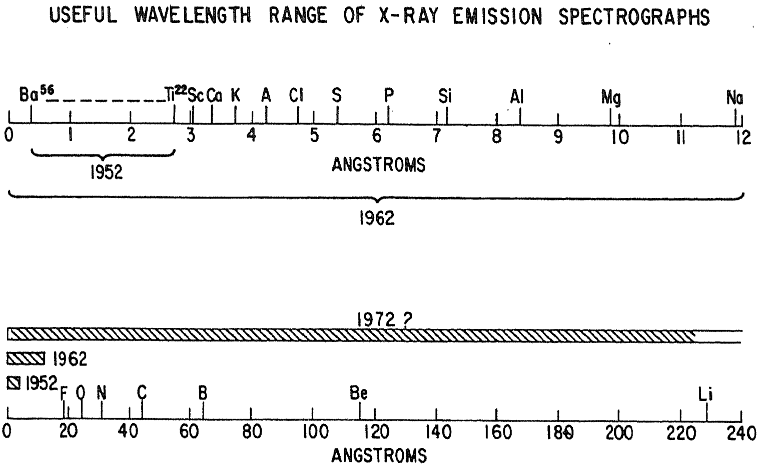

Figure 2. The upper half of the figure shows the wavelengths of K_α lines of elements that can now be determined. The lower half (on a different wavelength scale), shows K_α lines of elements beyond the capabilities of present day x-ray emission spectrographs.

The steps that have been taken in going beyond titanium involve three different developments in instrumentation, a helium, hydrogen, or vacuum path, in place of air, crystals with a longer spacing, and new counters with thinner windows. The helium or vacuum path reduces the absorption in the x-ray path between tube and counter. The extent of the improvement is shown in Figure 3, which shows the expected performance of a spectrograph filled with air, or with helium, or when evacuated with a mechanical pump, when air is the residual gas. The lower trace in the figure plots the absorption of the three atmospheres at the longer wavelengths, that is for the elements yet to be done. The absorption by 100 microns of air pressure would not present any major difficulties for the analysis of boron. Even for lithium this is no problem, since it would be simple to provide faster pumping, and reduce the pressure to the point where there would be negligible absorption.

There are two other absorbers to be considered: They are the windows on the x-ray tube and the counter tube. Various window materials are used on counter tubes but the most common are the metals beryllium and aluminum or an organic polymer film. Figure 4 shows calculated transmissions for these windows. Beyond 20 Å there are few good measurements of absorption coefficients, so the estimates there are apt to be far from exact. The nitrocellulose curve shown is an experimental one, but the thickness was not reported. Beryllium can be rolled as thin as one mil, but such a window is either porous or expensive at

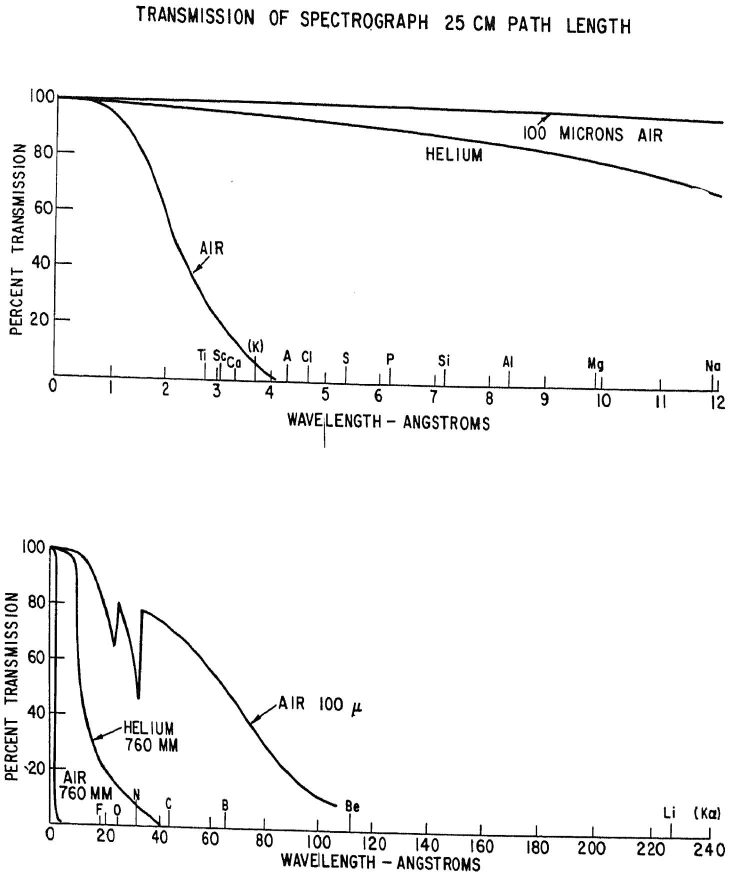

Figure 3. Calculated transmission of various atmospheres in an x-ray emission spectrograph. A mechanical pump should easily maintain a pressure of 100 microns if the system is free of leaks, and a lower pressure could be gotten if a cold trap is added.

present for larger areas. Aluminum can be easily made 1/10 mil or thinner. Several plastics have been used for windows, the most popular being 1/4 mil Mylar and more recently 1/10 mil Mylar. Thinner films can be cast with the limit set by the strength required in the film, which in turn is determined by the pressure differential and means of support. A Formvar film less than a micron thick can be used in a helium filled spectrograph on a gas flow counter tube with an area of 2 or 3 cm . Thinner films down to a few hundred angstroms can be made, but they are very fragile. These thin polymer films, even if free from holes allow the rapid diffusion of gas. As a result a more rapid flow of helium through the spectrograph, or faster pumping in a

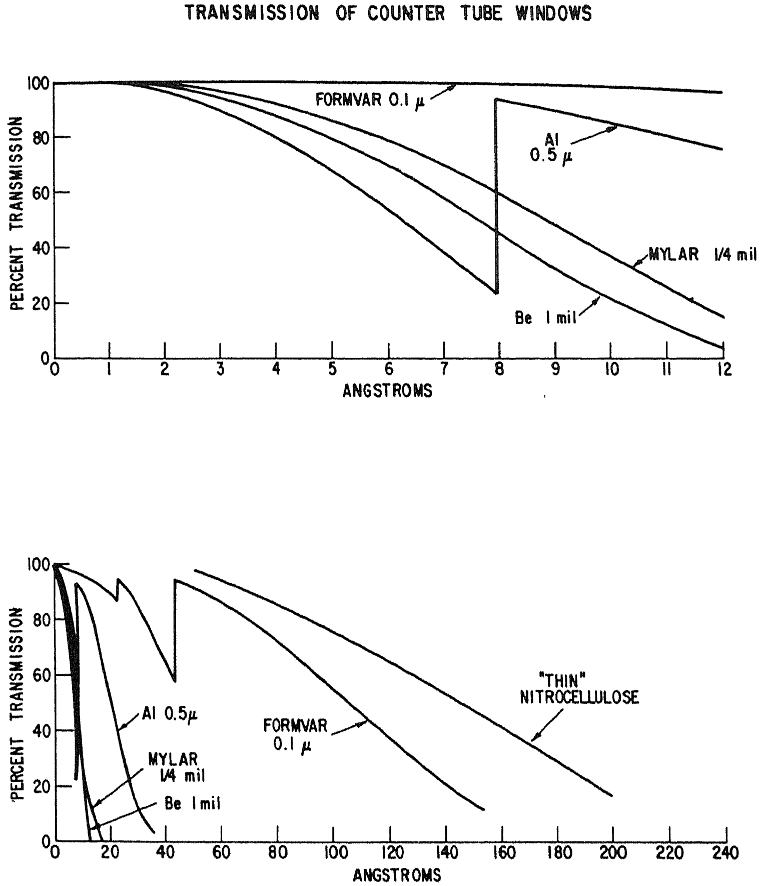

Figure 4. Transmission of various windows of practical thickness. Nitrocellulose measured transmission, others calculated.

vacuum spectrograph may be needed. The 100 microns residual gas in spectrographs evacuated with mechanical pumps is likely to be greatly enriched in argon.

The calculations represented in Figures 3 and 4 demonstrate that absorption in the x-ray path, with equipment now available, should not limit the determination of the elements through carbon, but might interfere with still lighter elements to some extent.

No special detectors have been developed specifically for the long wavelengths. The proportional counters that have proved so useful were first used in the short wavelength region. The two characteristics that make proportional counters the present best choice for the long wavelength region are the fact that they are easily fitted with thin windows and that pulse height selection can be used with them to reject higher order radiation.

The second problem, that of crystals, has also been partly solved. In 1952 NaCl and LiF were the two crystals in use for reflection and mica for transmission. The reflecting crystals now in use, and some others are shown in Figure 5 along with their wavelength limits.

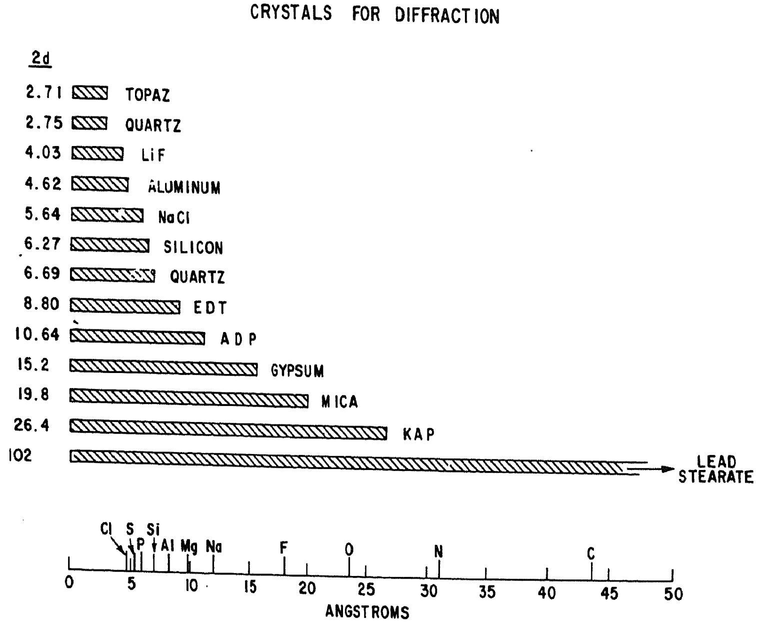

Figure 5. Useful wavelength range for several crystals.

Only the last 6 are of interest in the long wavelength region. Some 5 or 6 years ago EDT and a bit later ADP came into use and made possible the determination of Al and Mg. Gypsum is useful for sodium and within the past year potassium acid phthalate (KAP) became available. KAP should be able to diffract oxygen K_α. The last crystal listed, lead stearate, is a soap which can be built up in layers by the Langmuir-Blodgett technique on a suitable flat surface. With such a crystal, it has been reported that carbon K_α has been detected, but not in a conventional spectrograph for analytical work.

If a soap film like this or other similar materials prove satisfactory for practical use, then the crystal problem will be solved at least through carbon.

The remaining instrumental difficulty to be considered is that of insufficient excitation and it is the one on which little practical progress has been made. Improvements could be made in the geometry of the spectrographs to give a larger effective aperture, but the basic difficulty is in the x-ray source.

It is hardly a coincidence that the Machlett AEG series of tubes become available just a year before x-ray emission apparatus became available. The tungsten target version of this tube and others like it have long been the type most commonly used; however they have some shortcomings when used for the excitation of the lighter elements.

Figure 6 shows the spectrum of this tube, as scattered by polystyrene, along with the spectrum of a chromium target tube of similar design.

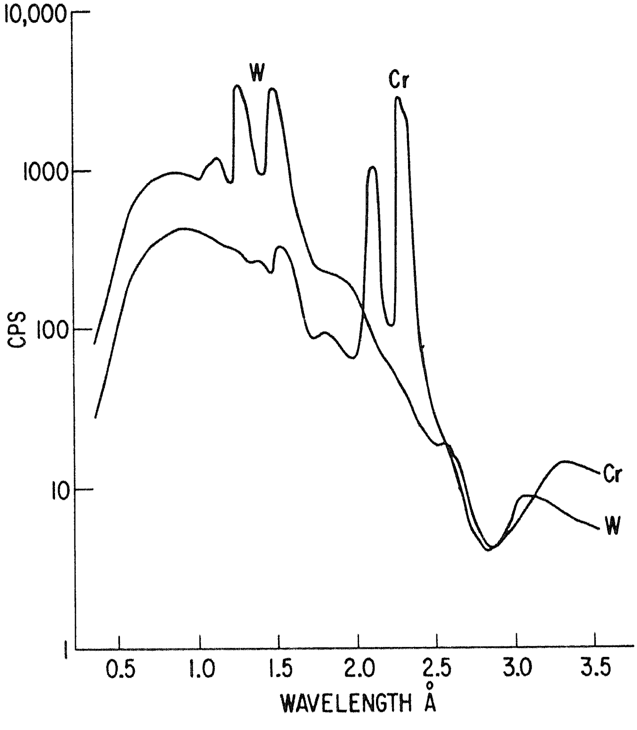

Figure 6. Intensity in cps on log scale of radiation scattered from lucite block with Machlett AEG50S tungsten target tube, 40 mil (nominal) Be window, and a similar tube with Cr target, 10 mil Be window.

A brief calculation will be used to compare how effectively the tungsten target tube will excite the elements iron and silicon. The effective wavelength of the tungsten target tube is about 1.48 Å. At this wavelength, iron has an absorption coefficient near 300, while that for silicon is only 1/6 as much. On the other hand, the critical thickness of silicon, for its own characteristic radiation is about 1/4 that of iron for its K lines, and since the exciting radiation is so much shorter in wavelength, this critical thickness is the one that has to be used. Combining these two factors, the silicon absorbs 1/24 as many quanta that will possibly emit as does iron. This factor must be multiplied by the ratio of fluorescence yields, which is about 1/4; so one might expect a factor of 96 or 100 in the relative count rates of iron and silicon. Actually a spectrograph that gives 500,000 cps for iron gives about 5000 cps for silicon.

Next compare the efficiency of the tungsten and chromium target tubes for exciting silicon. At the chromium tube's effective wavelength, silicon has an absorption coefficient about 5 times greater than it does for radiation from the tungsten target tube, but the integrated intensity in counts per second of the Cr tube is only half that of the tungsten tube, which leaves a net gain of intensity of 2.5. The actual gain observed was a factor of 3.

Table 1 shows a comparison of count rates from the two tubes, under similar conditions, demonstrating the desirability of having the excitation wavelength close to the absorption edge. If one could use the same number of quanta of monochromatic radiation at the optimum wavelengths the intensity, in cps, from a light element such as oxygen would be less than that of a heavier element such as iron by about the ratio of their fluorescence yields. This is a factor of only 5 or 10. On an equal power input basis at optimum wavelengths, the oxygen K_α radiation count rate might be equal to or greater than the count rate for iron since several times as many quanta will be available.

There is a second important difference in the construction of the two tubes that were compared in Figure 6. The beryllium window on the Cr tube is 10 mils thick; that on the tungsten tube

Table 1

Count Rates for Light Elements
XRD-5 — Helium — Gypsum Crystal
Gas Flow Counter — 1/4 mil Mylar Window

Element	% in Sample	$K_\alpha\lambda$, Å	C.P.S.	
			W Tube	Cr Tube
Si	29.6	7.13	347	1052
Al	100	8.34	---	3201
Mg	19.2	9.89	15	47
Na	39.3	11.9	6	18

is 40 mils thick. At present 10 mils is about as thin a vacuum tight window as can be built in regular production, strong enough to withstand an atmosphere of air and ordinary handling which a sealed off tube must do, even if it is operated with a vacuum spectrometer. Of course tubes with thinner windows have been built on an experimental basis, but they are not readily available.

While chromium and 10 mils of Be is a step in the right direction, it would be desirable to go further. 10 mils of Be absorbs half of the chromium radiation. The molybdenum L spectrum is another possibility for long wavelength excitation. It peaks about 5.4 Å. 10 mils of Be would absorb 90% of this radiation. Obviously, a thinner window is required to make much progress in the direction of longer wavelength x-ray sources with sealed off tubes. As techniques for making windows improve, it is not unreasonable to expect the development of a one half mil window that would transmit out to the region of 10 Å. Used with an appropriate target, such a tube would be quite useful for the elements sodium to carbon, which are now excited with extremely low efficiency.

Various targets have been suggested for a long wavelength x-ray source. These can be classified as K or L characteristic line, or white radiation emitters. Relatively few comparisons have as yet been made, but they do indicate that the band of white radiation from the best—that is the heaviest—target is not as intense as a characteristic line from a suitable source of line radiation. A tungsten target with a 10 mil Be window was made and compared to the chromium tube and the standard tungsten tube. The additional white radiation transmitted by this thin window made practically no difference in the excitation of the light elements showing that the intensity of the added long wavelength white radiation was quite low. The comparison that was made of tungsten L from the standard tube and chromium K radiation, even though not at the same wavelength, would seem to indicate that K radiation is more suitable than L; but as yet there is insufficient experience to prove what source will be best. There are many more possible sources of long wavelength L radiation, and generally, they can be operated at higher power than the K emitters.

So far, I have avoided mentioning windowless x-ray tubes, direct electron excitation, windowless counters, gratings and high vacuum operation of the entire spectrometer. All these things have been done successfully but not routinely; also they involve drastic change and would be difficult to adopt as accessories on presently available equipment; they may be cumbersome to use, and they impose drastic restrictions on the sample. Back in 1952, when there was discussion of extending the useful range to elements lighter than titanium, these modifications, already used successfully by the physicists were suggested but as things turned out, the equipment and methods of practical analysis for the elements Ti to Na were accomplished in the same way and on modifications of the same apparatus as that first developed. It may eventually prove necessary to use these drastic modifications to determine the lighter elements but until that point is reached, it is worth exploring the possibility of modification of existing equipment.

The usual window on gas flow counter tube is 1/4 mil Mylar. A thin Formvar film was used to replace the Mylar on a gas flow counter tube. The counting rates for some samples are shown in Table 2.

Table 2

Count Rates for Light Elements — Cr Target Tube
XRD-5 — Helium — SPG-4 Counter

Element	% in Sample	λ, Å	C.P.S.		
			1/4 mil Mylar	Formvar	
SiK$_\alpha$	29.6	7.13	1052	2,338	Gypsum
AlK$_\alpha$	100	8.34	3201	11,483	
MgK$_\alpha$	19.2	9.89	47	306	
NaK$_\alpha$	39.3	11.9	18	290	
CuL$_\alpha$	100	13.4	--	206	
NiL$_\alpha$	100	14.6	--	57	
FeL$_\alpha$	100	17.6	--	5	KAP
F K$_\alpha$	74	18.0	--	40	

Forty counts per second from fluorine in lithium fluoride is hardly enough as a basis for practical analysis, but at least fluorine can be detected. One could get a gain of a factor of about 4 on fluorine by using a vacuum x-ray path instead of helium. The count rate then might be enough for some kinds of analyses, but the big gain will come with a long wave length x-ray tube.

Some interesting comparison of the data in Table 2 can be made. In the series from Si to Na, the Formvar window transmits twice as much of the Si radiation and 15 times more Na radiation as does the Mylar. Obviously, 1/4 mil Mylar is too thick for use with wavelengths much beyond silicon. In the series copper to iron, there is a factor of 40 difference in intensities. This is due to several factors, such as the increased absorption by helium, the smaller critical thickness of iron, window absorption and a less efficient crystal.

Some measurements were made of the intensity of the CuL$_{\alpha}$ line at 13.4 Å from copper, cuprous oxide and cupric oxide. The relative intensities were 100:59:21. If the K radiations of the same materials are compared, cupric oxide gives over 95% of the intensity of metallic copper. The reason for the large difference in the long wavelength region is due chiefly to the absorption by oxygen which has an absorption coefficient of 5400, almost 4 times that of copper. When the copper was lightly oxidized, by passing a flame over the surface, the intensity of CuL$_{\alpha}$ dropped to 55% of the original. These experiments suggest two things. First, this may be the basis for an indirect method of determining oxygen, and second, it may be possible to measure the thickness of oxide--or nitride films, by making use of the extremely high absorption coefficient of oxygen and nitrogen in this wavelength region. In a series of experiments on silicones it was found that the intensity of silicon K$_{\alpha}$ at a given silicon concentration is a function of the ratio of carbon to oxygen, being lower for those materials that had a higher oxygen content, since oxygen has a higher absorption coefficient than carbon. Although direct determination of oxygen and carbon is still not possible, these examples suggest that there may be an indirect approach.

Sodium, from sodium chloride, gave a count rate high enough to be useful. Figure 7 shows count rates observed for Na in mixtures of NaCl and KCl. This is an idealized situation and the results are better than one might expect in trying to determine sodium in a complex mineral. In this long wavelength region interelement effects are quite important and sometimes unusual. Absorption coefficients, fluorescence yields and other basic data needed for calculations are apt to be inaccurate, or not available at all; so empirical calibrations have to be used.

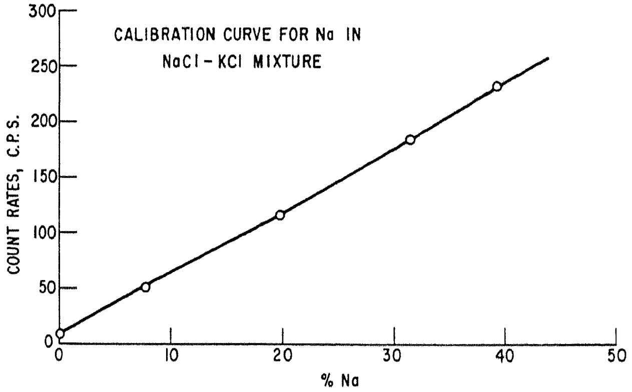

Figure 7. Count rates observed for NaK$_{\alpha}$ for mixtures of NaCl-KCl.

The various indirect analyses that have been suggested, that is copper oxide film, the carbon-oxygen ratio in silicones and so forth are not yet practical methods of analysis, and probably will not be until a great deal more is learned of the interelement effect. But these examples do point out that in some cases it may be possible to put these effects to use, instead of being an added complication to the analysis. In the shorter wavelength region, the measurement of film thickness by determining the count rate of the substrate is an example of an indirect determination but these methods are quite likely to become more important in determinations involving the lighter elements. There are two reasons for this, first, the effects are much larger and second, the longer wavelength may be inaccessible. At present this indirect method is very speculative; its something to try if everything else fails.

It also should be pointed out that beyond about 10 or 12 Å absorption coefficients are generally in the thousands. In the short wavelength region, below titanium, most absorption coefficients have values in the tens or hundred. Also, in the long wavelength region, the light elements may have absorption coefficients that are higher than those for the heavy elements. At 15 or 20 Å the absorption coefficient of oxygen is comparable in magnitude to that of uranium. Even at a wavelength as short as 6 Å aluminum has an absorption coefficient that is greater than that for lead. The very high absorption coefficients that all elements have in the long wavelength region results in extremely small values for the critical thicknesses. It may be as small as 100 Å. This fact will impose very severe requirements on the surface condition of samples for analysis, because in general, any irregularity of geometry or composition (roughness, absorbed surface layers, heterogeneity) will affect the measured intensity of fluorescent radiation when the dimensions of the irregularity exceeds a few percent of the critical thickness.

At present reliable analytical results have been gotten on the light elements up to magnesium. These are now all routine determinations being paid for by a customer. To mention a few; silicon in iron in the hundredth percent range, silicon, aluminum and magnesium in cements, chlorine in polymers at concentrations near the parts per million range.

There is no point in describing the details of these analysis here, but it should be pointed out that they have several common features. First, sampling and the preparation of a suitable surface are quite important. In the case of cements, the best results can only be obtained when a homogeneous glass is made of the sample by dilution in a suitable flux. Second the count rates are low. With silicon in iron a few counts per second are significant. Ten years ago a count rate that low could not be used. Learning how to use the low count rates has been another step that has made these long wavelength analyses possible. Third, there are apt to be interfering lines. Those due to higher order reflections can be avoided by pulse height selection.

Another complication that is barely detectable for elements heavier than sodium may well become the most significant above. It is the effect of chemical state. In the case of sulfur K_α and manganese K_β there were observed slight shifts in wavelength, peak shape, and intensity with valence state. It probably occurs with other elements, but has not been troublesome in analyses except in the case of sulfur where one must choose compounds with sulfur in the same valence state for calibration as is the sulfur in the unknowns. Above sodium the chemical effects become quite significant and may possibly be more significant than any other. If this occurs the simple relationship between line intensity and composition, that is the basis for x-ray emission spectrography, will lose its importance, and direct determinations of the elements will not be the primary object of the analysis. Instead, other information, equally important may be deduced from the shape and wavelength of the band. If this occurs the resolution of spectrographs will have to be high, which is not the case at present. Now, the wavelength of an emission line is only an index point to identify the element, and the intensity is the important measurement. Resolution needs to be sufficient to separate lines of adjacent elements, and there is little advantage, in having it any higher. However, if resolution should become important, because of the increased significance of the chemical state of samples, new instrumentation may be required to give that resolution. Also, although it appears that modification of present equipment for x-ray emission may get to carbon K_α, that is 40-50 Å, it may not get much further without drastic changes.

One cannot predict what new instrumentation will prove successful for the analytical chemists. The fact that the photographic recording, vacuum spectrographs with gratings have not been adopted for general analytical use may be sufficient proof that they are not suited for this application.

Various things have been proposed to extend the wavelength range to extremely long wavelengths. Three functions will be considered, excitation, separation of wavelengths, and detection.

First, there is required some way to cause the sample to emit x-rays. Up to now, x-rays from a sealed off tube have been in use to bombard the sample, but the difficulties of that approach have already been described. There are several alternatives. One is to use a windowless x-ray tube and high vacuum in the spectrograph. Some light element-perhaps Mg or Al would be the tube target. This seems straightforward enough, but relatively little is known about the intensity of the long wavelength x-rays that can be obtained, compared to those at shorter wavelengths. Theoretical predictions are rather unfavorable, but some recent measurements on the light elements give count rates several times greater than the prediction, another possibility is direct excitation of the sample by electron bombardment. This will increase the intensity considerably, a factor of 100 due to the improved geometry of the system, another factor of 10, due to fluorescence yield, and another factor of unknown magnitude due to the critical thickness of the sample. However most samples cannot be bombarded with as much power input as can be used with a properly designed x-ray tube target. Direct excitation will bring with it the problem of surface contamination or change, particularly with regard to the elements of greatest interest, carbon and oxygen. Unless an extremely high vacuum can be maintained, carbon from the residual gases in the system will be deposited in layers thick enough to effect any attempt to measure the light elements like C, N or O and lighter. Also in high vacuum, oxides or nitrides might be altered in their surface layers. It remains to be seen how serious this problem will be. The relatively high intensities for elements like magnesium or aluminum observed in the electron beam microprobe indicate that there will probably be adequate excitation of x-rays produced by direct electron bombardment. The microprobe experience also shows that a high background of white radiation is to be expected. These complications may, to a large extent, offset the gain in intensity.

So much for the difficulties and uncertainties of sample excitation. The next problem is that of separating the various spectral lines. This might be done by energy selection in the detector, that is pulse height selection, by diffraction from a crystal or from a grating at grazing incidence. Another possibility is the use of selective filters. The K absorption jump of the lighter elements, like carbon, is quite high, so, a carbon film would attenuate oxygen or nitrogen characteristic radiation and transmit the carbon line far more effectively than the filters that have sometimes been used at shorter wavelengths. Diffraction from a crystal, such as a heavy metal soap would, if practical, result in a simpler optical system than the use of a grating; however, these long wavelength crystals will have to be developed and tested further. Diffraction from a grating requires greater mechanical precision in the optics than is needed with a crystal but this is not a limiting factor.

The possibility of energy resolution in the detector leads to the next component, that is detectors. This possibility is particularly attractive, because it has a potentially higher efficiency, by 2 or 3 orders of magnitude, than does diffraction from a crystal, which is especially desirable when few quanta are produced, and there is a bonus in that the complicated optics required for diffraction are eliminated. Of course, if high resolution is required as has been suggested, then only diffraction will give adequate resolution.

The detector that has had the most use is this long wavelength region is the photographic plate. It is particularly good for wavelength measurements and band shapes, but is not well suited for reliable intensity measurements or for producing rapid results. Nor is it very well adapted for use as a practical energy discriminator, despite the use of nuclear emulsions for that purpose in the high energy range.

The next detector to consider is the scintillation counter. In the long wavelength region sodium salicylate has been used as the energy converter in preference to activated sodium iodide. In this wavelength region the noise from the multiplier is quite high and pulse counting can be done only in the presence of a very high background count rate. The energy resolution falls off rapidly with increase in wavelength, and while the phosphor-photomultiplier combination may be useful as a rate meter, or simply as a current amplifier, it is difficult to operate as a counter in the conventional manner. It is not likely that it will be able to discriminate between elements directly. Another way the photomultiplier could be used is to dispense with the "photo" part and use it as a secondary electron multiplier. The simplest arrangement is to remove the glass envelope with the photoelectron emitter, and to seal the dynode structure into the spectrometer. Now x-rays will produce secondary electrons on striking the first dynode which can be multiplied to give a useful pulse by the rest of the dynodes. This arrangement eliminates the photo emitter, which is the source of most of the noise in the conventional system. However, since usually only one secondary electron is produced by the x-ray quantum, energy resolution is not feasible. Recently there became available a more efficient multiplier using magnetic focusing of the secondary electrons along a high resistance or semiconductor plate. It is said to be useful in this region of the spectrum and may have some features that make it superior to the usual type.

Proportional or Geiger counters have been used in this region, but they require some sort of window if the rest of the spectrometer is at high vacuum. The difficulties associated with a thin window were mentioned earlier. With the proportional counter pulse height selection is possible, however a carbon K_α quantum will produce about 9 ion pairs, with a spread, under very best conditions, corresponding to a standard deviation of 4 or 5. Nitrogen will give 13 ion pairs and a spread of 6, so resolution of adjacent elements is only partial. Filters might be quite useful here.

Other types of detectors still in the stage of arguments over feasibility, are the film semiconductor or other solid state devices. One attractive characteristic of these solid state devices is that it requires something like 3 volts or less to produce an electron, as compared to 30 for an ion pair in a proportional counter. A carbon K_α quantum would produce 90 conduction band electrons. It this large number could be utilized as effectively as they are in the proportional counter resolution of adjacent elements could be readily accomplished. Unfortunately, this detector is hardly past the idea stage as yet at least for long wavelengths. One difficulty that will be encountered with any of the direct viewing systems is the spurious counts that may be obtained due to secondary emission caused by ion or electron bombardment of the dynodes. This can be avoided by electrostatic or magnetic deflection of the charged particles, or by pulse height selection.

I have tried to indicate that the extension of x-ray emission to the lighter elements requires some means of getting a useful signal from these light elements. It appears that the requirement here can be met by a long wavelength x-ray tube, or electronic excitation. A second requirement before analysis in this region can be done is to be able to interpret the measurements. The data that are obtained have to be related to the composition of the sample to give a useful result. This may prove more difficult than getting the necessary signals. There is a very serious lack of basic data such as a listing of all the x-ray lines, absorption coefficients, fluorescence yields and so forth in the long wavelength region.

In the region beyond about 20 A new phenomena become significant, these are phenomena associated with the valence or conduction electrons and molecular structure. As yet they have not been exploited very much either by those interested in long wavelength x-rays, or by those working in the same wavelength region, but approaching it from the ultraviolet. This may prove to be a very fruitful field and lead to much new knowledge about the properties of matter.

SCANNING TECHNIQUES IN ELECTRON PROBE MICROANALYSIS, WITH SOME APPLICATIONS IN MINERALOGY AND BIOLOGY

V. E. Cosslett
Cavendish Laboratory
University of Cambridge, England

Editors' Note: Dr. Cosslett was invited to present this paper at the Xth Colloquium Spectroscopicum Internationale; however, last-minute circumstances prevented his attendance. Even though the paper was not actually presented at the Colloquium, it is included in these Proceedings because of its general interest and because it complements related papers which are also included.

INTRODUCTION

The X-ray microspectrometer of Castaing [1], now known as the electron probe microanalyser, was designed for point by point analysis. The electron spot was focused to a given point on the lens axis and the sample was mechanically shifted to bring different parts of its surface to this point. A great deal of quantitative analysis has been done with this system, especially in metallurgy, as described by Philibert elsewhere in this Conference [2]. However, the procedure is slow and not readily adaptable for survey work or semi-quantitative operation. There are many problems in which less than the highest degree of analytical precision is adequate and speed of answer is important. For this reason, and also to avoid the inconvenience of building a high-powered optical viewing system into a strong electron lens, we decided in 1953 to investigate the practicability of combining television technique with microspectrometry. By building deflection coils into the final magnetic electron lens (which we preferred to the electrostatic system of Castaing), we were able to scan the sample surface continuously and build up an image of it on a cathode-ray tube screen either from the back-scattered electrons or from the characteristic X-ray emission of any selected element [3]. This scanning microanalyser has proved to be extraordinarily successful in a wide range of analytical problems, from qualitative to high precision operation. Some of the metallurgical applications have been described in a recent Symposium of the Institute of Metals in London [4] and some biological and medical applications in a Symposium of the New York Academy of Sciences [5]. The present survey, therefore, will be confined to a few typical examples, particularly from mineralogy and biology; Dr. Philibert will have more to say about the metallurgical uses.

It is as well at the outset to dispel some current misconceptions about the respective roles of the scanning and static probe instruments. It is sometimes suggested that the one is mainly for survey and the other for high precision work. There is nothing inherent in the design of either to limit it to one role or the other. Rather they should be seen as emphasising different, but complementary, features which should be (and now are being) brought together in a single all-purpose instrument. The flying spot of the scanning microanalyser can be brought to a stop over any desired point of the sample so that it becomes a static-probe system, or, more usefully, a line scan can be generated. A fully-focusing spectrometer is then needed for highest precision, in place of the semi-focusing type which is adequate for full-field scanning operation. Vice versa, the static probe model can easily be fitted with a scanning system and arrangements made to defocus its high precision spectrometer, when a problem calls for lower accuracy and quicker results. Experience seems to be confirming our original view that what most users want is a versatile instrument, since microanalytical problems vary greatly in nature. In effect, the scanning version comprehends and supersedes the static probe model. If any proof were required it is to be found in the general trend now to convert static probe microanalysers into scanning systems, and for the scanning instruments in turn to borrow the best features of the static type.

DESIGN AND OPERATING FEATURES

The general principles of the scanning microanalyser are shown schematically in Figure 1. A fine electron probe is formed by successive demagnification in two electron lenses and is scanned across the sample in a regular raster by deflection coils, or sometimes with electrostatic deflecting plates. The impact of the probe on the sample produces both X-ray emission and back-scattering of electrons. Since an appreciable fraction of the beam is back-scattered (10%-50%, increasing with atomic

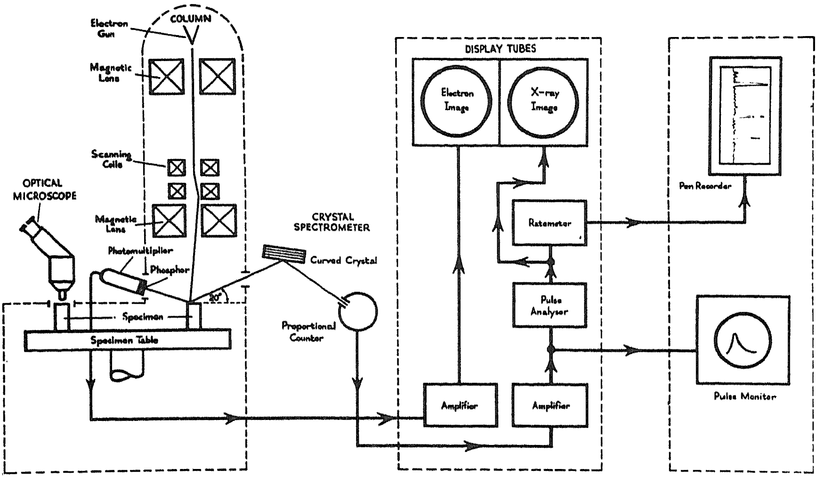

Figure 1. Schematic diagram of scanning electron probe microanalyser.

number), and the efficiency of X-ray production is low (at most 10^{-3}, and increasing with atomic number and voltage), the electron signal is always very much stronger than the X-ray signal. The former is collected with a scintillation counter and the latter with a proportional counter, a crystal spectrometer being interposed for wavelength selection. The signals are amplified and fed to display tubes scanning in synchronism with the probe scan, so that images are formed in which brightness varies with local intensity of electron scattering or X-ray emission respectively. The electron image is determined by differences in both atomic number and surface slope over the sample. Since the area scanned may be as much as 0.5 x 0.5 mm., the electron image allows the operator to recognize features of the specimen seen in the optical microscope, which can now be separated from the electron lens system (as shown), the sample being rotated or translated from the one position to the other. It is desirable to retain an optical microscope on the microanalyser, since the process of analysis is usually complementary to other techniques of examination.

The X-ray image may be formed by the total emission, by the selection of a particular K- or L-line with the spectrometer, or by selecting a broader band of wavelengths with the proportional counter and pulse-height analyser. Owing to the weakness of the signal, a long-persistence tube is used and a slow speed of scan, such as 1 frame of 300 lines in 2 sec. A camera is provided for photographing the image, and exposure time may vary from 2 to 20 min. depending on the image quality. As seen by the eye it is usually very grainy, but the photograph integrates the statistical fluctuations; exposure time will depend on the amount of "noise" that can be tolerated. If a true storage tube, of infinite persistence, is available it can take the place of the camera [6]; alternatively, a Polaroid-Land camera is a useful aid, especially when the X-ray signal is so weak that the eye has difficulty in appreciating element distribution in the displayed image.

In forming the image, the magnification is under direct control, being the ratio of the widths of scan on the display tube and on the actual sample respectively. Normally the former is kept constant and the latter varied, but both may be reduced together to allow examination of a particular area with less statistical graininess in the image. The contrast is also variable by electronic controls, according to the degree of contrast in the sample. This control is more conveniently exercised when the X-ray image is formed not as shown in Figure 1, but by means of the integrated output from the ratemeter. It is then possible to suppress background noise and show only those parts of the sample which contain more than a set amount of a particular element. This system has recently been put to use by Melford [7] in metallurgical analysis, and an example is shown in Figure 5.

The X-ray image, when formed from a selected wavelength, shows the distribution over the sample of any element present. For many purposes, such as impurity identification, this knowledge is sufficient. If an accurate analysis is desired at a particular point, the scan is stopped and the probe positioned over that point in the sample by reference to the after-glow image. The spectrometer is then run through the appropriate wavelength range whilst the X-ray signal is routed through the ratemeter to a pen-recorder. Alternatively, the variation in concentration of a single element along a line can be plotted by forming a line scan with the deflection system and keeping the spectrometer at a fixed angle. In this case it is necessary for the line scan to be at right angles to the X-ray path from sample to spectrometer, to ensure uniform accuracy of analysis, and so the sample holder should be provided with a rotation as well as two normal translations.

From the analytical, as distinct from the electron-optical, aspect the spectrometer is the key point of the whole instrument. Ideally one needs a semi-focusing type for rapid survey and semi-quantitative operation, and a fully-focusing type, with high resolving power but consequently lower collection efficiency, when high analytical precision is demanded. In our original scanning microanalyser, in that of Duncumb and Melford [8] and in the Cambridge "Microscan" model, a semi-focusing spectrometer only was fitted (Figure 2). The essential difference from the fully-focusing type is that the axis of the crystal is fixed and the counter moves round it, instead of both moving round the Rowland circle. There is a gain in simplicity and compactness, important in a vacuum system, and also in collection efficiency. The resolving power is about 10' in Bragg angle, which is adequate for very many problems, giving a peak to background ratio of 250 to 1 and a detection limit of 0.01% in favourable cases. A specially curved crystal can be inserted when a higher resolution is demanded, but clearly an all-purpose instrument ought to have both a fully-focusing spectrometer and a semi-focusing spectrometer built in.

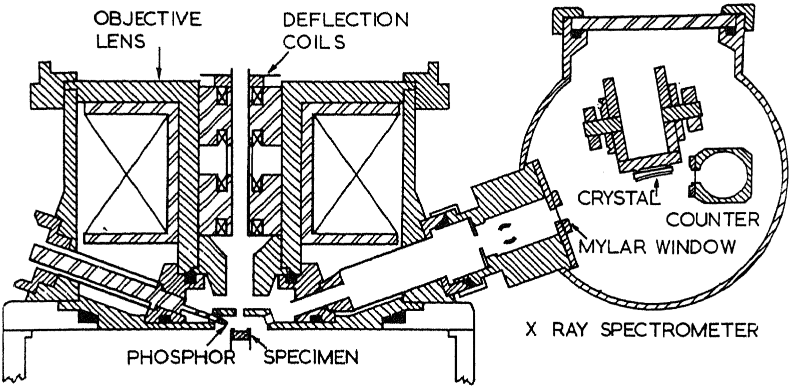

Figure 2. Cross-section of final electron lens and X-ray spectrometer of the scanning electron probe microanalyser [8].

In the scanning instrument it is usual to provide 3 or 4 crystals, interchangeable under vacuum, to cover the X-ray spectrum from 10° to 60° Bragg angle. In this way elements in the periodic table from magnesium to uranium can be analysed, by their K-lines up to molybdenum and for higher elements by the L-lines. The K-lines of the elements below magnesium are of such long wavelength that special methods are needed for their detection, either with a ruled grating or by a proportional counter and pulse analyser system, as described below. With the latter system, Dolby [9] has now been able to analyse for carbon and beryllium at moderate accuracy.

The electron optical problems of the microanalyser need not be discussed here. They have been investigated in some detail by Duncumb [10] and by Wittry [11]. There is no difficulty in the way of making probes as small as 100 A; the practical limitation is on the current that can be focused into them. At present the minimum useful working spot size is about 0.3-0.5 μ; smaller spots generate insufficient X-rays to give a visible scanning image or to allow analysis, except with unacceptably long counting times. The volume analysed can thus be as small as 10^{-13} cc, the ultimate detection limit being about 10^{-15} gr. The visual resolution attainable is shown in Figure 3. Duncumb and others are experimenting with probes of 0.1 μ and less in the hope of improving practical resolution. Improvements in astigmatism correction, in electron gun output and in X-ray collection efficiency are all desirable. The spreading of the probe in the sample, by electron scattering, is also a limitation, and in consequence the beam voltage has to be reduced in parallel with probe diameter. It may prove that a better spatial resolving power will only be useful on extraction replicas or on thin sections of a sample. In this direction it is interesting to explore the possibilities of combining microanalysis with electron microscopy in a single instrument.

The design of the scanning microanalyser has been discussed by Duncumb and Melford [8] and Duncumb [12]. A photograph of the Cambridge Microscan instrument is shown in Figure 4; the AEI microanalyser [13] has now also been fitted with a scanning system, as have several other American and Japanese models. Wider surveys of microanalyser principles and applications have been published by Castaing [14] and Cosslett [15].

METALLURGICAL APPLICATIONS

It is in metallurgy that the microanalyser has found its most immediate and extensive applicability. There is a growing literature both on particular applications [7,16,17,18] and on the corrections necessary for high analytical accuracy [19,20]. This part of the subject is dealt with by Philibert [2] and others in this Conference, but it may be of interest to mention here some of the types of problem in which the scanning facility is of special value.

The identification of inclusions, known to be present from optical metallography, is a constantly recurring problem. They are frequently non-metallic and it is usually enough to show that sulphide, silicate or oxide (for example) is present and, if possible, the nature and proportion of the metallic constituents. Melford [7] has given an example of how it was possible with the microanalyser to differentiate two types of globular silicate inclusion in a continuously cast steel. The images formed from the relevant K-lines served to prove that whilst both were manganese silicate with a precipitate of silica, one of them contained much more calcium than the other. This work promises to contribute to a solution of the problem of steel cleanliness by continuous monitoring. The scanning microanalyser could, without great extra complication, be adapted for automatic inclusion counting and identification, going a stage beyond the optical flying spot particle sizers already available.

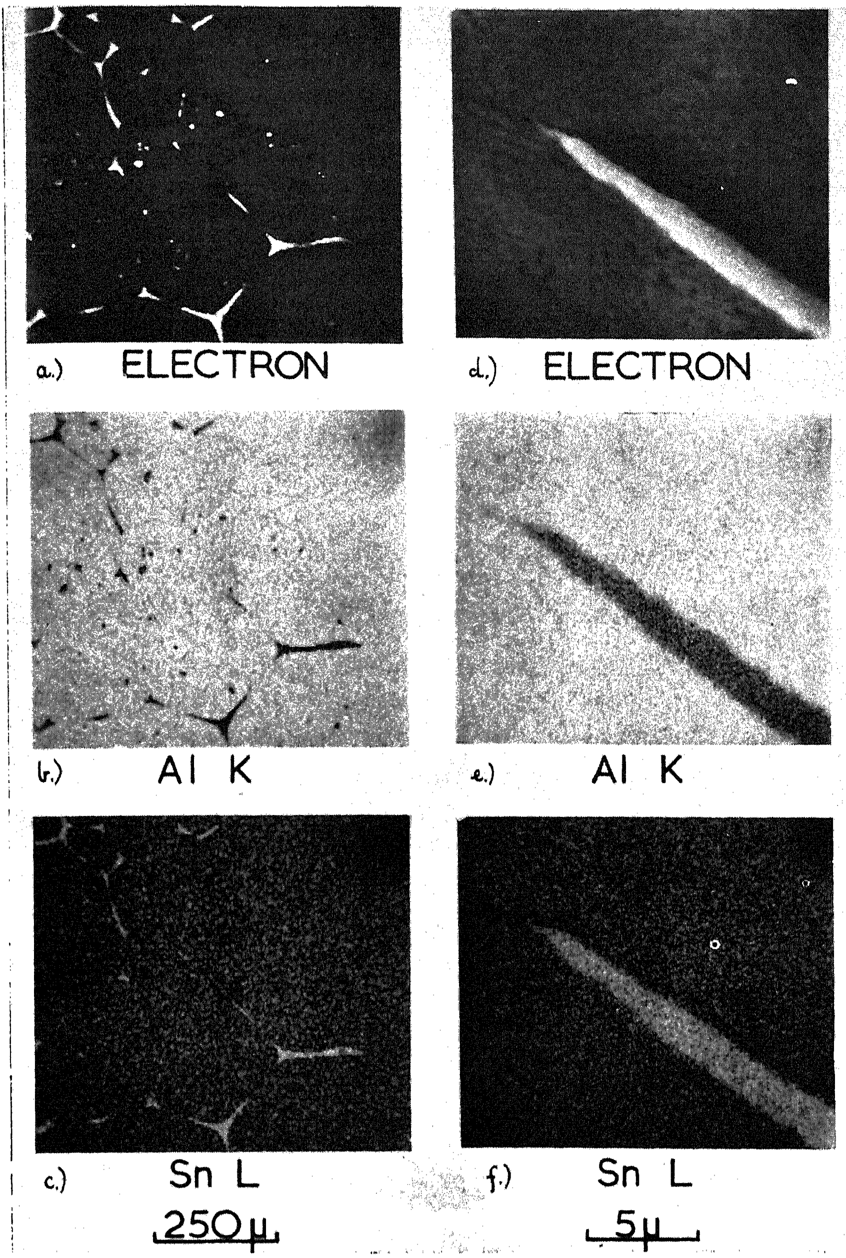

Figure 3. Scanning microanalyser micrographs of an aluminium—6% tin alloy. (a) and (d) electron images; (b) and (e) X-ray images formed from Al-Kα radiation; (c) and (f) X-ray images formed from Sn - L radiation. Magnification of (a), (b) and (c), x 80; of (d), (e) and (f), x 3,500. (P. Duncumb, X-ray Microscopy and X-ray Microanalysis (Elsevier, Amsterdam), p. 365, Figure 3).

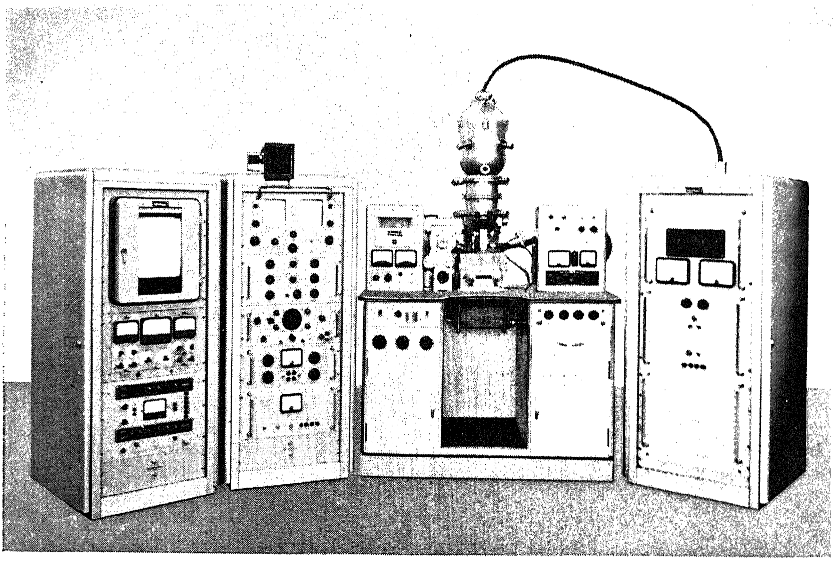

Figure 4. The "Microscan" electron probe microanalyser; high voltage and electron lens supplies at the right of the instrument, display tubes, counting racks and pen-recorder at the left. (Courtesy of Cambridge Instrument Co. Ltd.).

The silicon X-ray image of these precipitate particles seemed to show variations in brightness over a single particle, indicating that it might be complex. Some confirmation of this was obtained by reducing the operating voltage from 29 kV to 9 kV, thus reducing both the absorption effect and the background of "white" X-rays; it was then clear that the intensity of silicon radiation was greater from parts of the periphery than from the centre. To improve this type of detection sensitivity, Melford then devised an electronic means of "expanding" the X-ray image contrast so as to make small changes in characteristic emission more readily visible. The output of the ratemeter was used to form the image instead of that from the pulse analyser, i.e., an integrated signal in place of a train of pulses. A slow speed of scan (1 line in 20 sec.) and a reduced time constant is essential for improving statistical accuracy. By appropriate setting of the brightness controls of the display tube, only those parts of the sample giving more than a given threshold count-rate are imaged. The same principle was applied to the image formed by back-scattered electrons. It was clear from both the silicon K-line and electron images that there were silica-rich particulate inclusions within the precipitate itself, and these were inferred to be silica.

The scanning facility also lends itself to investigation of suspected grain-boundary enrichment and depletion, where a relatively wide field of the sample must be examined. Melford [7] gives also an example of this type, in which the distribution of residual copper and nickel in a mild steel was studied. The improvement in visibility afforded by using the ratemeter output is demonstrated in Figure 5, where the expanded contrast images are compared with the normal X-ray images. A further extension of this technique, utilising both ratemeter and pulse analyser, would allow iso-concentration contours of an element in the sample to be plotted directly.

This type of application can be extended to a variety of problems in which the proportion of an element varies over the surface of the sample, including diffusion gradients. Distribution in depth, within the range of the fastest electrons available, can also be studied by observing the variation in X-ray signal from a given element as the electron beam voltage is reduced down to the excitation value. The stratification of surface layers is open to investigation by this technique; Wood and Melford [21] studied the change in iron and chromium content through a 2000 A thick film of oxide on an iron-14.6% chromium alloy. Due regard must be paid in all such work to the important corrections for absorption loss and fluorescent contribution.

Existing microanalysers can deal satisfactorily with elements from uranium down to magnesium, as illustrated in Figure 6. The analysis of the lighter elements is of great importance and a practicable solution is in sight. Although the scanning technique is not essential to it, speed of working is now limited to such a degree that a point by point survey could hardly be contemplated. The reason is that both the output of characteristic X-rays and the efficiency of their detection fall rapidly with atomic number. Physically this is connected with the long wavelength of the K-lines (44A for carbon): even if a crystal of large enough spacing were available for selecting it, the gathering power of a spectrometer is much too small. A ruled grating might in principle be designed with large gathering power, but we have put our faith in an electronic system of wavelength discrimination [22]. It uses a proportional counter as detector, placed close to the sample to collect enough X-rays, and an electrical network (essentially a simple computer) to unscramble the composite signal received when the sample contains several elements which are close neighbours in the periodic table. With this apparatus Dolby [23] has been able to make a semi-quantitative analysis of an oxidised beryllium specimen (Figure 7). So far it is operating at comparatively low magnification and an

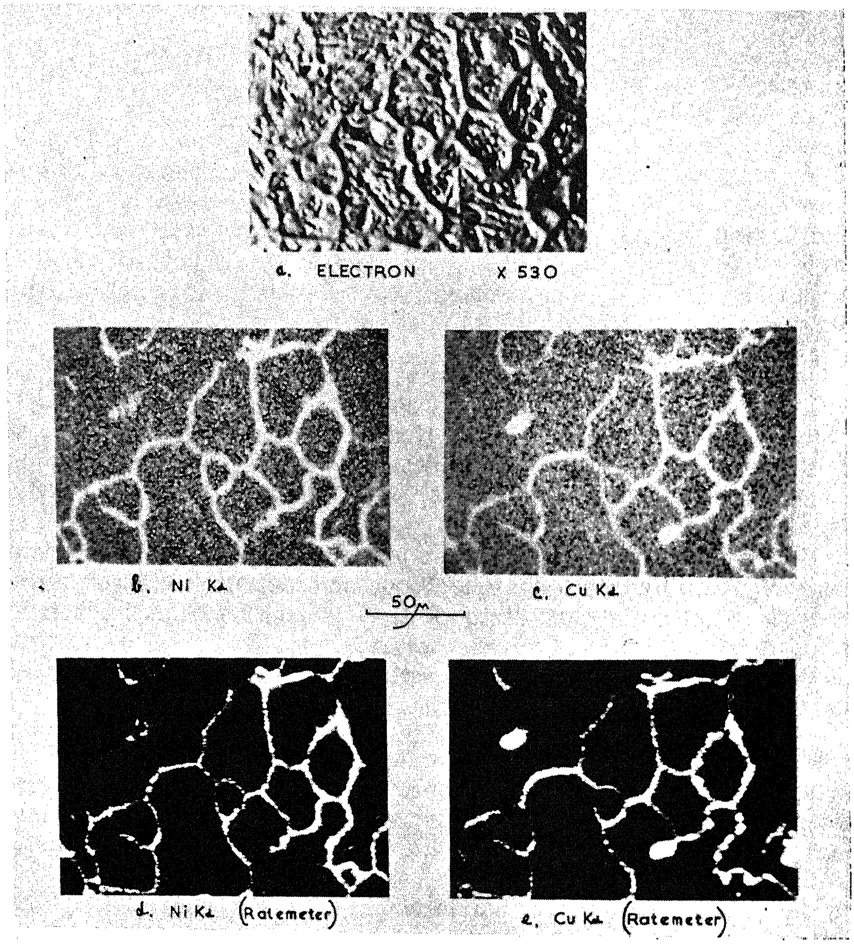

Figure 5. Enrichment in residual elements at grain boundaries near the surface of a mild-steel specimen quenched from 870°C. Scanning microanalyser images obtained with and without "expanded contrast" as given by ratemeter output. (a) Electron, magnification x 530; (b) NiKα (normal), (c) CuKα (normal), (d) NiKα (ratemeter), (e) CuKα (ratemeter), magnifications x 320. (D. A. Melford, J. Inst. Metals, 90, 217, 1961-62, Figure 4.)

analytical accuracy of a few per cent. The accuracy can be appreciably improved by leaving the probe on a selected point long enough to collect the necessary number of counts for statistical significance. The value of the scanning facility lies in selecting the points for analysis from the displayed image. The most important and the most difficult problem is to obtain high accuracy in the analysis of carbon, where deposition of contamination on the sample during analysis confuses the result. If this can be

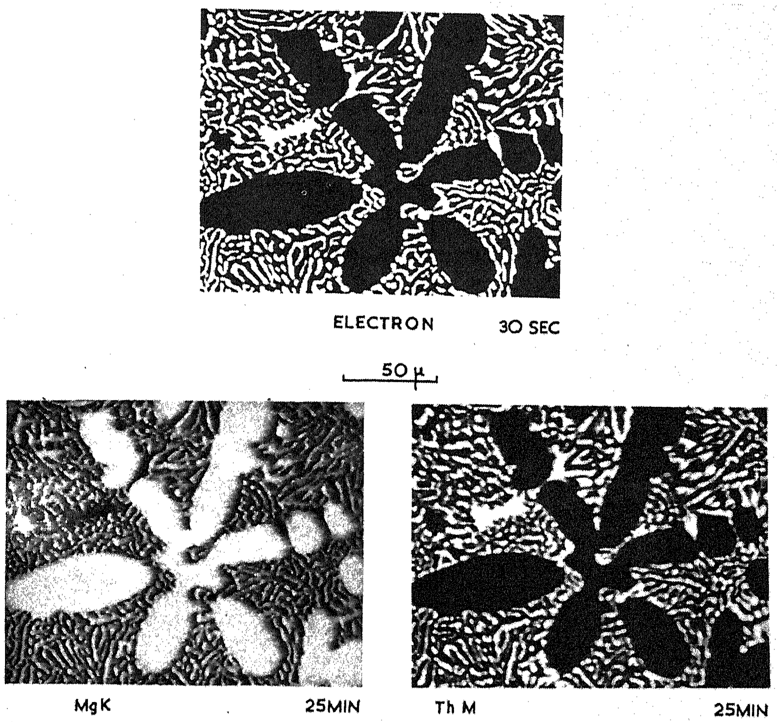

Figure 6. Scanning microanalyser micrographs of a magnesium—37% thorium alloy, obtained by the "expanded contrast" method. Magnification x 300. (P. Duncumb, unpublished.)

satisfactorily solved, the microanalyser should be applicable in many aspects of ferrous metallurgy.

MINERALOGICAL APPLICATIONS

There is a similarly wide range of problems for the microanalyser in mineralogy and petrology, as pointed out by Agrell and Long [24]. The requirements in instrument design are rather different from those in metallurgical applications, if only because the mineralogist is used to preparing his samples as transparent sections mounted for light optical observation. Agrell and Long discuss these special needs and describe the microanalyser built by Long [25] to meet them. It provides for examination of the sample in polarised light whilst it is in the electron beam (Figure 8). There is enough visible emission from most minerals for the region analysed to be directly seen.

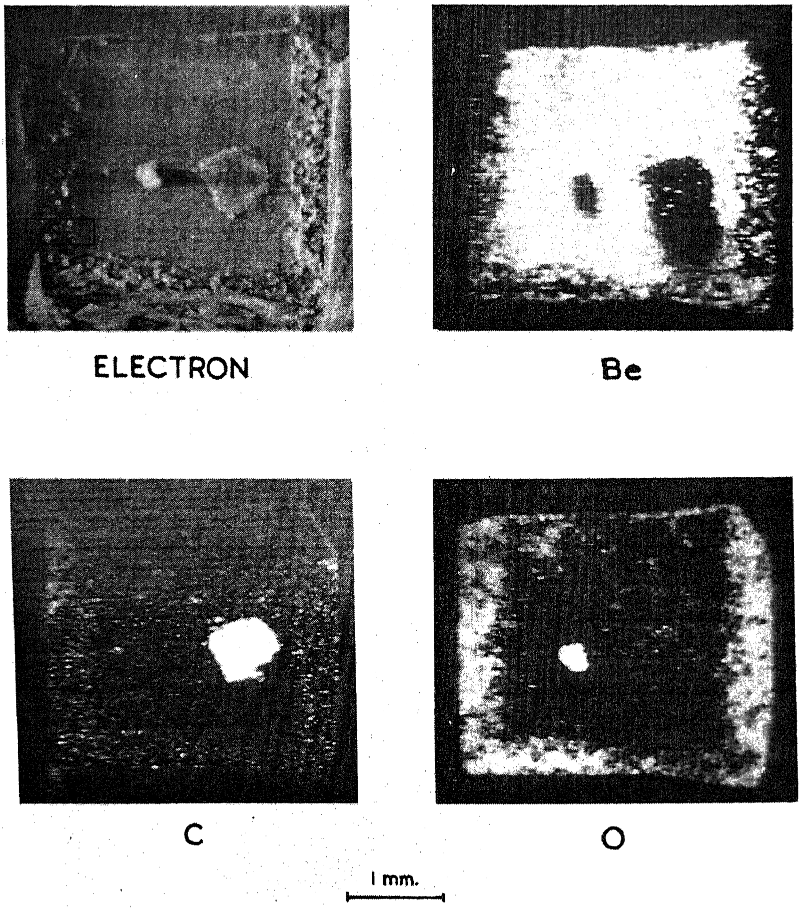

Figure 7. Oxidised beryllium sample, imaged in the scanning microanalyser with back-scattered electrons and with the X-ray Kα lines of beryllium, carbon and oxygen. The two spots in the centre of the field are lithium hydroxide (left) and graphite (right), used as oxygen and carbon standards respectively. Magnification x 16. (R. M. Dolby, unpublished.)

The types of mineralogical specimens particularly suited for investigation with the microanalyser are listed by Agrell and Long. In addition to those mentioned above under metallurgical applications, they include the examination of composition zoning

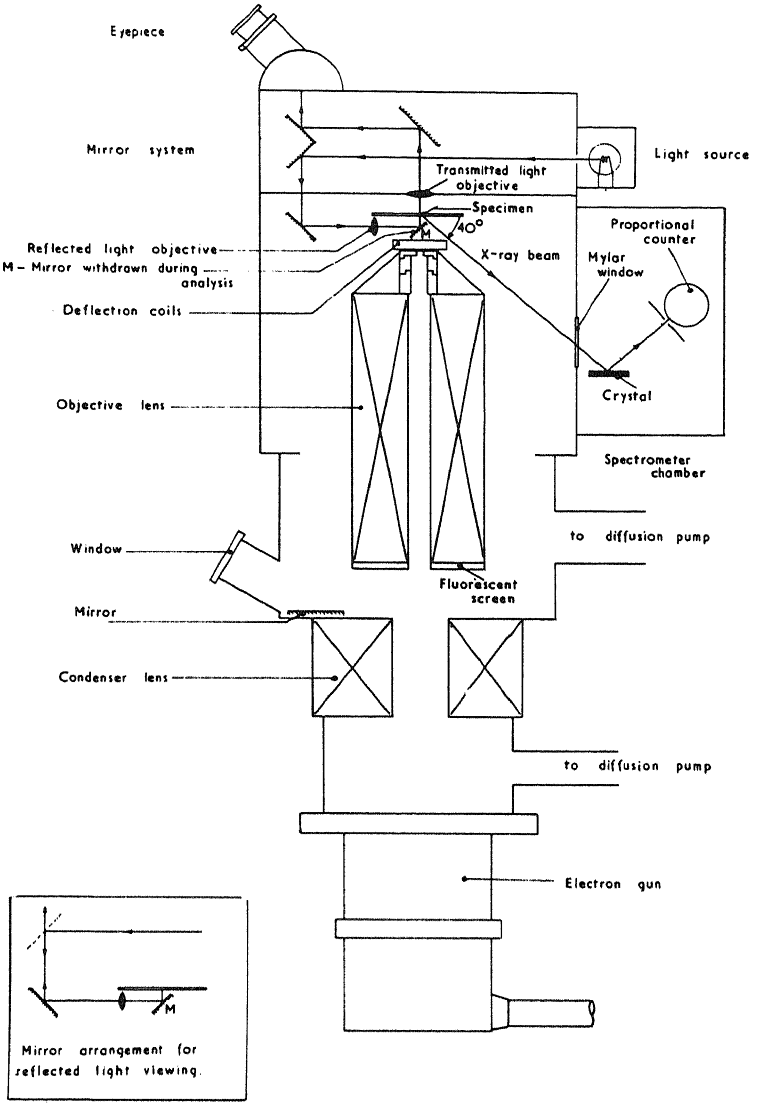

Figure 8. Schematic cross-section of scanning microanalyser for mineralogical applications. (J. V. P. Long, unpublished.)

and of scarce minerals available in very small amount. Opaque minerals can also be investigated, where the normal mineralogical techniques fail. Agrell and Long detail three investigations they had made: the determination of phases in exsolution intergrowths in an inverted pigeonite, the analysis of a complex metasomatised lithomarge containing spinels, and the variation of

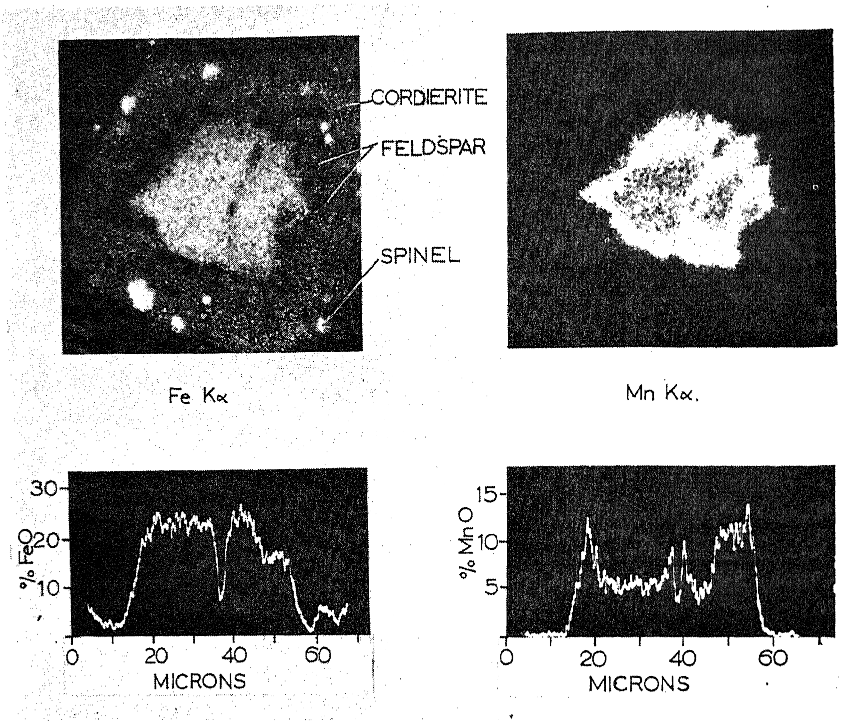

Figure 9. Scanning images and composition traces showing partial decomposition of a garnet into cordierite and feldspar; note enrichment of manganese at outside edges and at crack. Magnification x 700. (G. A. Chinner and J. V. P. Long, to be published.)

nickel content in the kamacite and taenite phases of meteorites. The last-named problem has also been tackled by other workers with the aid of the static probe microanalyser [26].

As a further illustration, Figure 9 shows the distribution of iron and manganese in a garnet. The evidence from the microanalyser served to confirm a hypothesis that the garnet had undergone a local reaction with biotite in the rock, giving a mixture of cordierite and feldspar [27]. More recently Long has turned his attention to determining the H_2O content of hydrated minerals by following in the microanalyser the change in the proportion of metallic element under the heating effect of the electron beam. Figure 10 shows the result of some test experiments with gypsum. The dehydration process is started by suddenly reducing the area of scan on the sample, thus raising the local temperature. Chemical decomposition can be followed in the same way, the evolution of carbon dioxide from a carbonate, for instance.

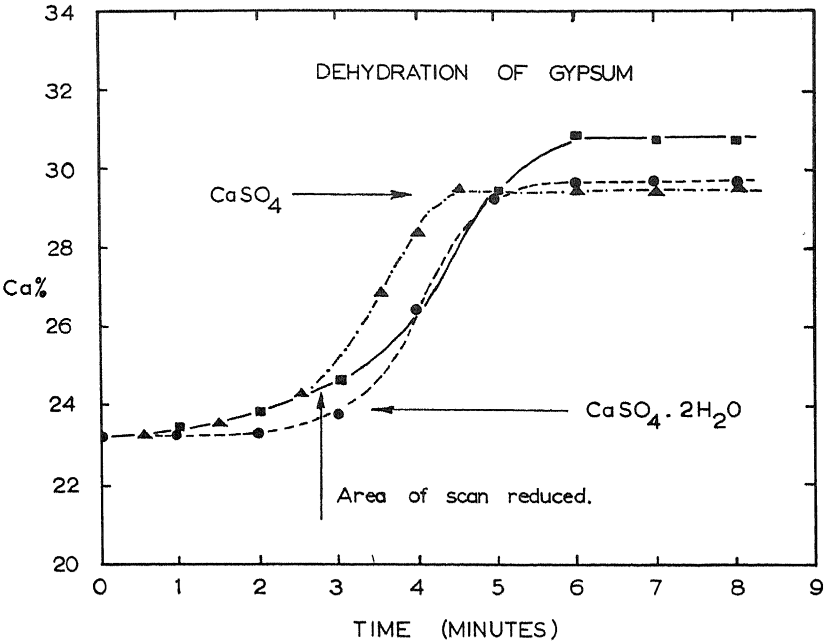

Figure 10. Dehydration of gypsum, as followed by change in proportion of calcium during irradiation by electron beam; intensity was increased at point indicated by reducing area of scan. (J. V. P. Long, unpublished.)

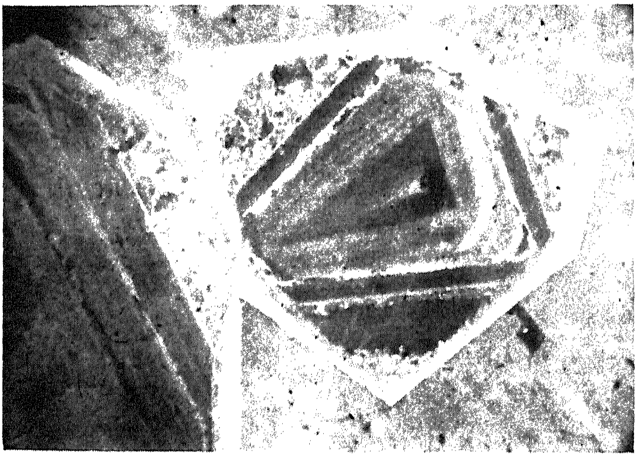

Figure 11. Half-tone reproduction of colour picture of luminescence produced in a zoned calcite mineral by electron irradiation; no zoning is seen in transmitted polarised light. (J. V. P. Long, unpublished.)

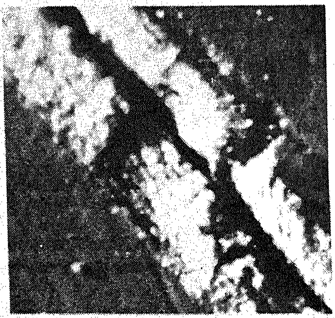

Electron image

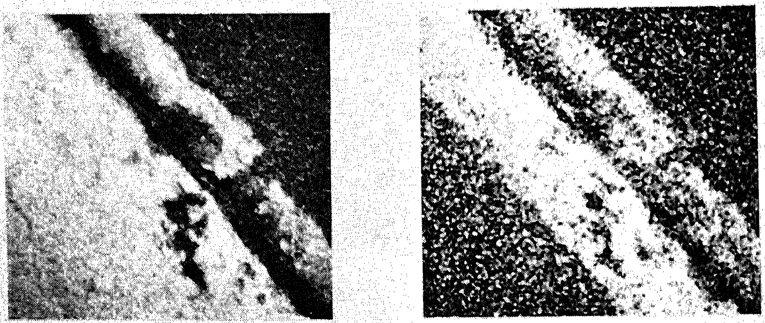

Sulphur

Arsenic

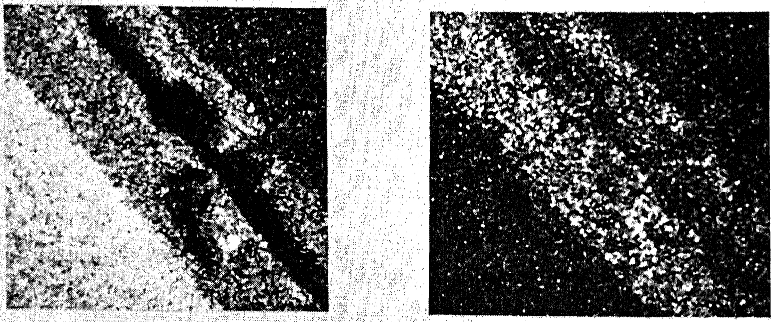

Calcium

Iron

Figure 12. Electron and X-ray $K\alpha$-line images of a section through a painting of "The Holy Family" by Titian, in the National Gallery, London, revealing over-painting. Magnification x 140. (V. R. Switsur and Miss J. Plesters, unpublished.)

In mineralogical samples the visible emission excited by the electron beam provides a source of additional information. As shown by Figure 11, which in the original is coloured deep red in shades of varying intensity, details of zoning are immediately apparent. Very different visible images are given by minerals differing very little in chemical composition, and it is known that trace elements have a great effect on the wavelengths emitted. We are currently investigating the possibilities offered for microanalysis by these effects, with a special type of scanning system.

ARCHAEOLOGICAL APPLICATIONS

An obvious extension of the metallurgical and mineralogical uses of the microanalyser is to the evaluation of objects of archaeological interest. One of the first samples we examined was a piece of whet-stone from an ancient site, the question being whether it had been used to sharpen bronze or iron tools. In this case no positive evidence was obtained, metallic elements not being found except for small traces of titanium. Since then we have examined a variety of samples of ancient and medieval origin. Problems arise of even later date, for instance as to the overpainting of a masterpiece in oils or the date of a ceiling in an historical building, deducible from the type of plaster used. A section from a painting by Titian in the National Gallery, London, is shown in Figure 12. The iron content derives from the varnish and the arsenic from the orpiment used in green paint; the substrate gesso is mainly gypsum. It is evident that the original was overpainted at some later date.

A scanning microanalyser, largely based on the AEI model, has now been built by Dr. E. T. Hall at the Laboratory for Art and Archaeology at Oxford University for this type of application [28]. It has already been used for plotting the variation in silver content through a coin, in connection with studies of the debasement of coinage in Roman times.

BIOLOGICAL AND MEDICAL APPLICATIONS

The scope of the microanalyser in biology and medicine is less obvious than in the areas discussed above. We are currently engaged in exploring the possibilities, with the aid of a grant from the Medical Research Council of London. A preliminary survey was presented to the New York Academy of Sciences recently [5] and therefore only an outline will be given here. A number of other authors have also published preliminary results, some at the International Conference on Spectroscopy [29,30].

The most straight-forward application is the identification of foreign bodies, usually metallic in nature, in tissues. Our initial interest in the electron probe microanalyser was stimulated in part by a request from a pneumokoniosis laboratory to distinguish silica from other particles in a lung section, which electron microscopy failed to do. In collaboration with specialist laboratories, we have examined tissues from patients and experimental animals afflicted with a number of industrial diseases. Figure 13 illustrates the identification of tin in a case of stannosis [31]. The investigation can be taken further back, to the examination of air-borne dusts from industrial areas. Figure 14 shows how a particle was identified as brass in one such study. Dusts from other sources can also be usefully examined. We have looked at particles from dust storms in Nigeria, in the hope of tracing their origin, and from high in the atmosphere, prospectively connected with nuclear explosions.

A further set of problems is concerned with metallic objects deliberately introduced into the body, such as a stainless steel implant in a hip or knee joint. In the course of time corrosion occurs and it becomes important to trace the diffusion of the products. We have looked at such samples from the National Orthopaedic Hospital, London, and the distribution of iron, nickel and chromium in a particular case was reproduced in the article quoted [5].

A wide range of applications arises in regard to hard tissues, where the distribution of calcium and occasionally of other elements is in question. Microradiography has been used to some extent in these investigations, but the microanalyser gives results very much more readily, especially when a semi-quantitative answer is adequate, as is often the case. The variation of calcium content with age, with nutrition and with site in a single type of animal is a whole research programme in itself. Figure 15 shows the very different degree of mineralisation which is found in chick bone of differing origin. Similar problems arise in teeth, where the onset of disease offers a fruitful study. In conjunction with the London Hospital Dental Department we are examining a variety of human teeth of normal and pathological type. We have also shown the cause of the red colouration of the teeth of rats and some other animals to be due to an iron content which can be as high as 7% in the front layer of the enamel [32]. Figure 16 shows the images obtained from a section of a squirrel's tooth.

In these examples the inorganic content in the tissue is high enough to be readily measured. A different set of problems arises in connection with the metallic elements normally present

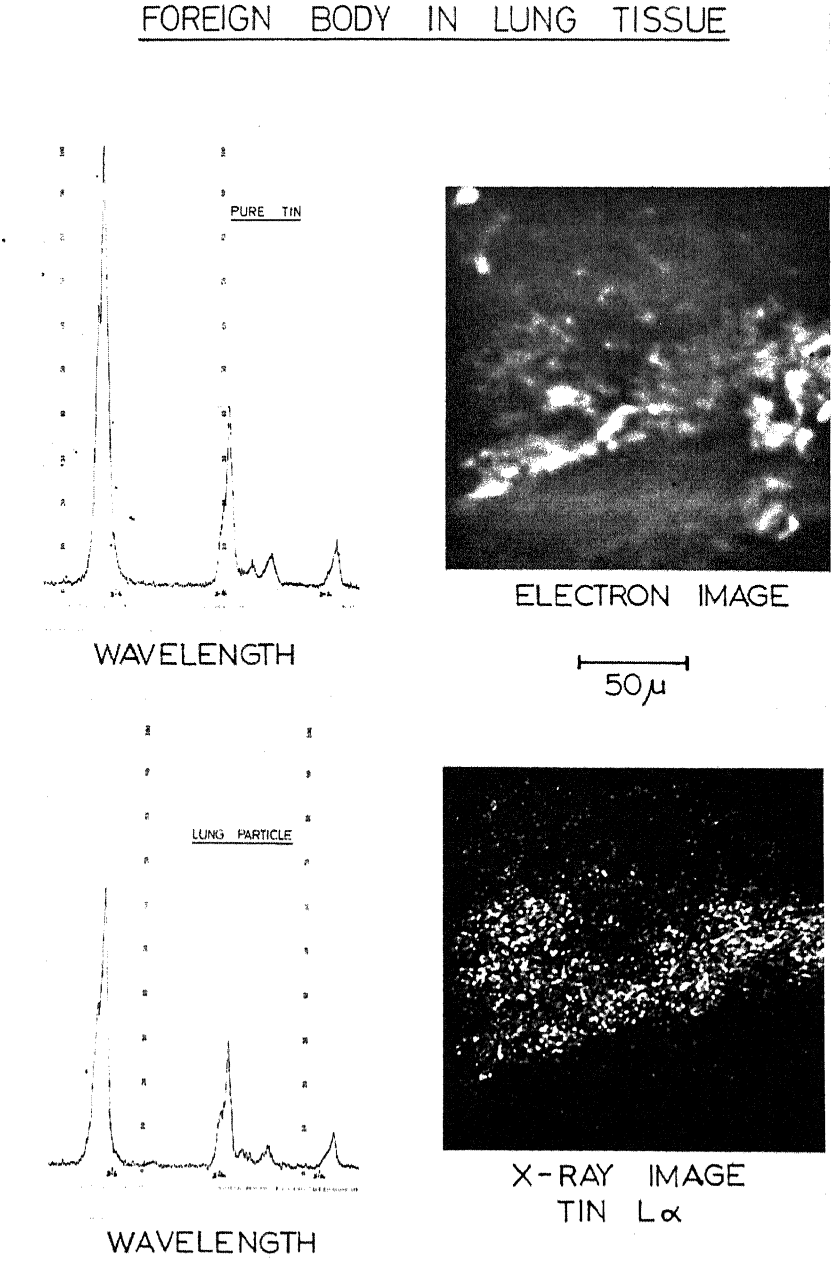

Figure 13. Detection of tin in section of miner's lung. Magnification x 350. (A. J. Robertson and V. R. Switsur, unpublished.)

in certain tissues of the body. They rarely occur in a concentration approaching 1% and more usually in parts per ten thousand or less, as trace elements. With its present detection sensitivity

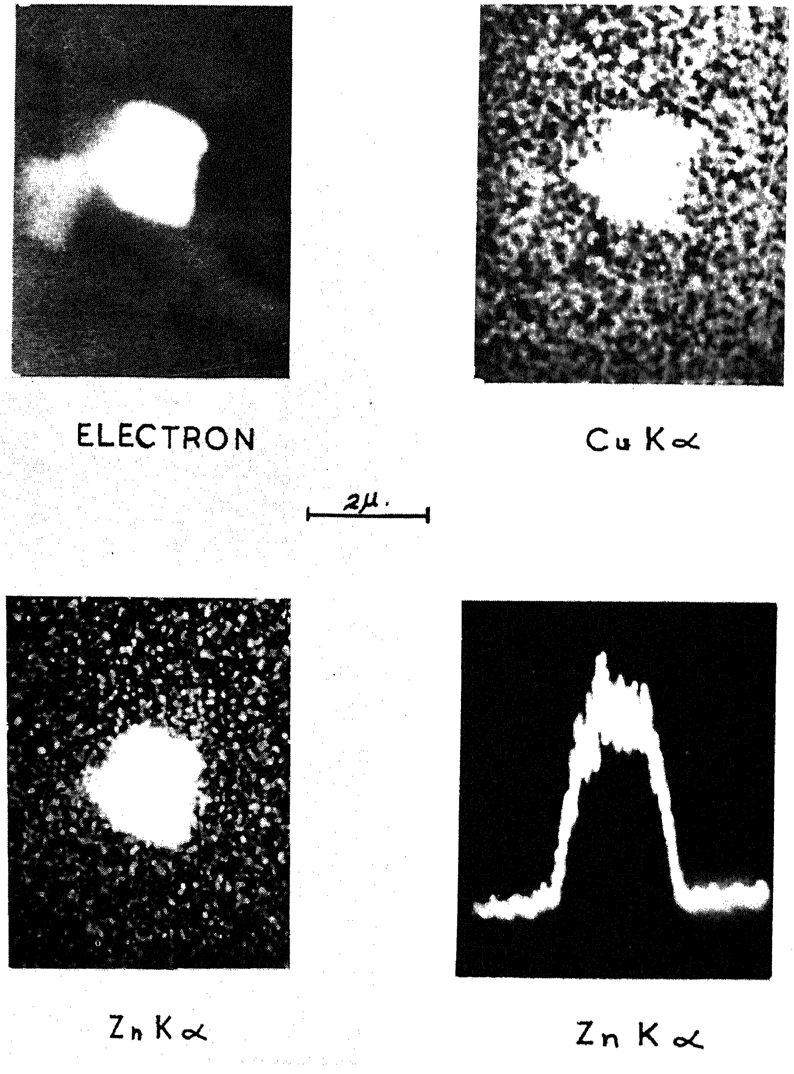

Figure 14. Electron and X-ray images of particle of atmospheric dust, identifying it as brass. Magnification x 950. (V. R. Switsur; Courtesy of New York Academy of Sciences: Figure 4 in Cosslett, Annals N. Y. Acad. Sci. 97, 464, 1962.)

few of them seem to be accesible to the microanalyser. Iron in the liver [33] and zinc in the prostate [34], and perhaps in the skin, come within its range. There is scope here for investigating the possibility of "amplification" of naturally occurring metallic compounds by feeding metal-rich diets or by injections,

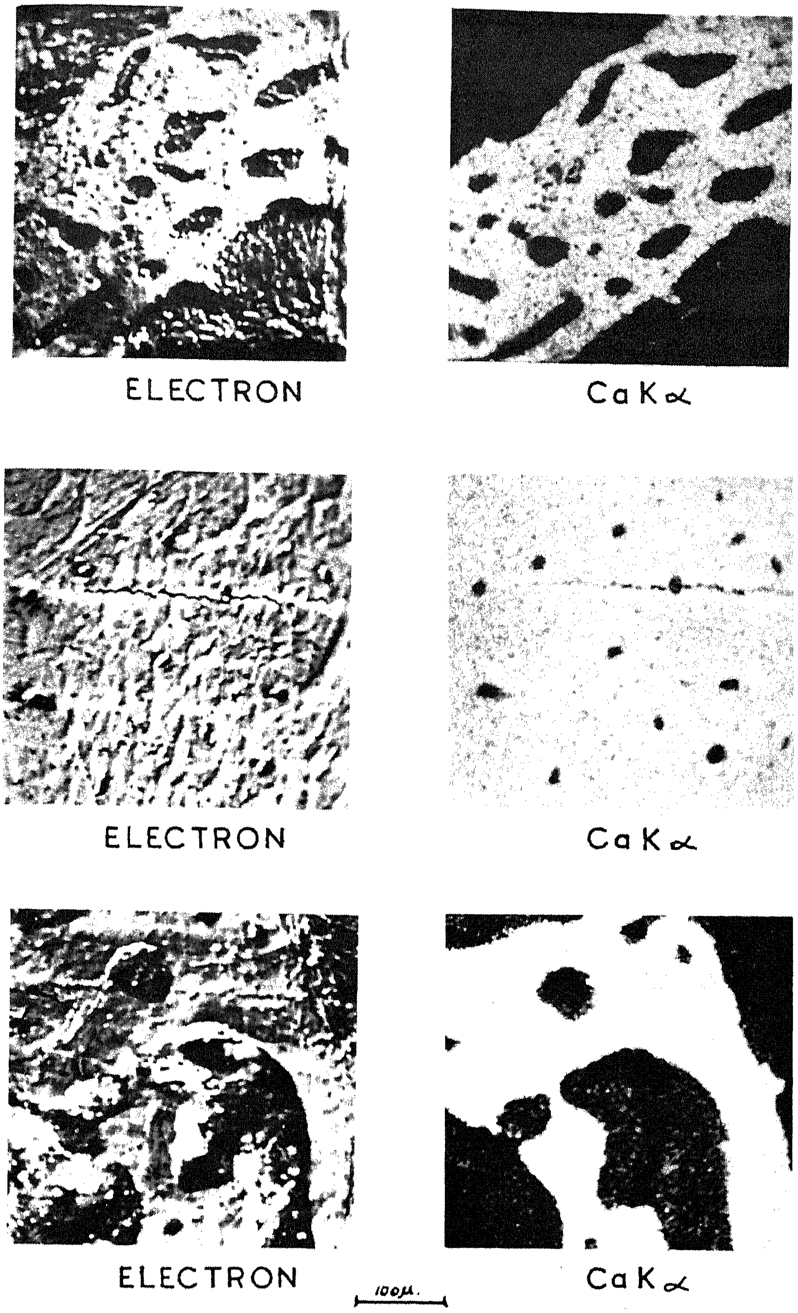

Figure 15. Effect of nutrition on calcium distribution in phalange of chicken. Centre pair of images from undernourished bird; top pair from normal bird of same weight; lower pair from normal bird of same age. Magnification x 140. (R. A. McCance and V. R. Switsur, unpublished.)

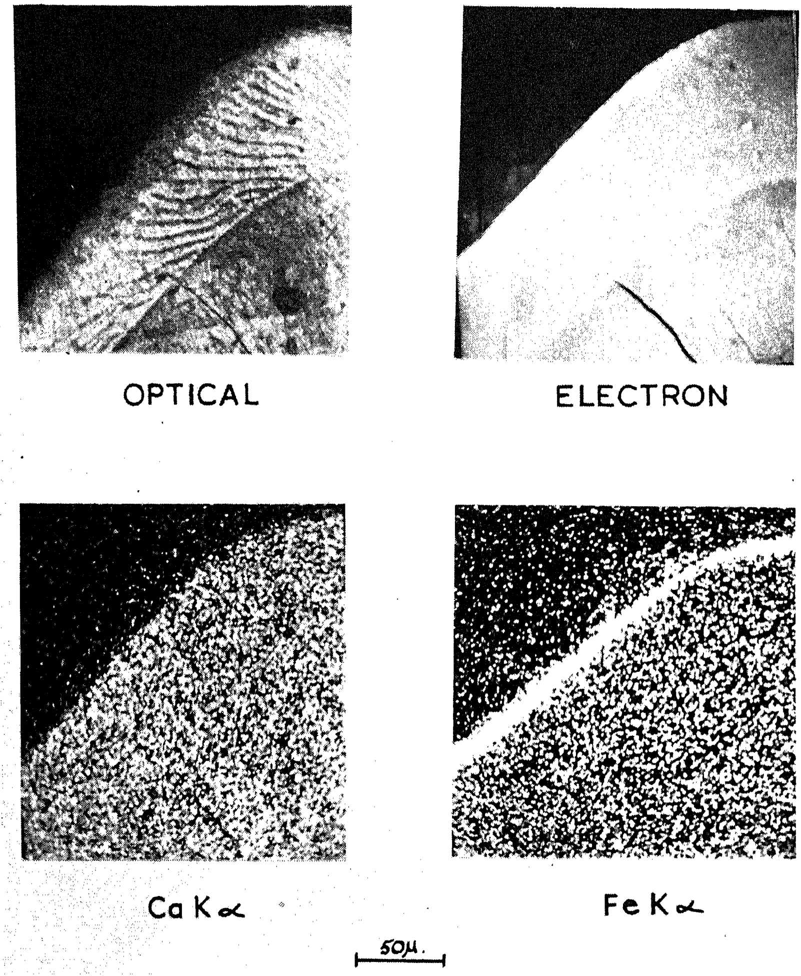

Figure 16. Micrographs of section of squirrel tooth (incisor), showing iron-rich layer at surface of enamel. Magnification x 280. (A. Boyde, V. R. Switsur and R. W. Fearnhead, unpublished.)

or other means of adding to the deposits. Obviously close control is necessary, perhaps by electron microscopy, to make sure that the added material does in fact come down at the natural sites. A particular instance of this type of application is the identification of the products of reactions used to detect the sites of specific enzyme activity in cells, e. g., phosphatase. The advantages of using the microanalyser for this purpose, instead of microradiography, have been demonstrated by Hale [35]. If the

X-ray emission method can be proved to be quantitatively reliable, a wide field of use for the microanalyser will be opened up in cytochemistry.

It should be emphasised that even more care is needed with biological samples, in converting microanalyser counts into quantitative proportions, than in metallurgical applications. In addition to the usual corrections, account must be taken of possible variations in density and so in electron penetration. Boyde and Switsur have discussed some of the pitfalls in biological microanalysis [36]. In addition the beam may partly decompose the specimen or chemically change it. It seems desirable to analyse simultaneously for all the elements of interest, which would demand an instrument with two or three independent recording channels. The design of a microanalyser for biological applications has been discussed by Switsur and Boyde also [37].

The ultimate problem before us is that of organic microanalysis. Will it be possible, with acceptable accuracy, to determine the carbon, nitrogen and oxygen content in different parts of a tissue·section? As mentioned above, the analysis of these elements is now practicable in inorganic samples, with relatively crude accuracy. With biological material we have to face the possible effect of the beam on the specimen as well as the deposition of carbonaceous contamination. At the moment it seems unlikely that these problems will be quickly solved to the extent needed to give the cytochemist the detailed information he is seeking. However, there may be a better prospect of obtaining more limited data, such as the sulphur content or the nitrogen-phosphorus ratio in different parts of a sample or from the same region of comparable specimens.

CONCLUSION

The electron probe microanalyser is not much more than ten years old, the scanning version only five, and commercial models have just recently become available. It is early days to attempt an assessment of the range of usefulness of this new technique. But the general field of applicability follows from the physical principles involved; whilst it cannot approach the detection sensitivity of some other methods of microanalysis, it gives a higher degree of localisation than any other. Its primary advantage being thus dependent on knowing what part of the sample is analysed, the scanning system is likely to become an essential part of the instrument because it gives a visible image. Many uses can be foreseen in metallurgical and mineralogical research, and at least some routine applications in practical metallurgy. The biological and medical applications are less easy to define, partly because quantitative microscopy is a new idea in these areas and partly because of formidable experimental difficulties due to the nature of the sample. It may well be that the historical development of electron probe microanalysis will reverse that of electron microscopy, in which the biological applications for many years far outran the metallurgical.

REFERENCES

1. Castaing, R., Thesis. University of Paris, 1951.
2. Philibert, J., Proc., 10th Coll., Spectroscopicum, Spartan Books, 1962.
3. Cosslett, V. E. and Duncumb, P., Nature, 177, 1172, 1956; X-ray Microscopy and Microradiography (Academic Press, New York), 1957, pp. 374 and 617.
4. See J. Inst. Metals, January, February and March, 1962.
5. Cosslett, V. E., Annals N. Y. Acad. Sci., 97, 464, 1962.
6. Ranzetta, G. V. T. and Scott, V. D., J. Sci. Instrum., 39, 50, 1962.
7. Melford, D. A., J. Inst. Metals, 90, 217, 1961-62.
8. Duncumb, P. and Melford, D. A., X-ray Microscopy and X-ray Microanalysis (Elsevier, Amsterdam), 1960, p. 358.
9. Dolby, R. M., Thesis, University of Cambridge, 1962.
10. Duncumb, P., Thesis, University of Cambridge, 1957; Brit. J. Appl Phys., 10, 420, 1959.
11. Wittry, D. B., Thesis, California Inst. Technology, 1957; J. Appl. Phys., 29, 1543, 1958.
12. Duncumb, P., Brit. J. Appl. Phys. 11, 169, 1960; J. Inst. Metals, 90, 154, 1961-62.
13. Page, R.S. and Openshaw, I.K., X-ray Microscopy and X-ray Microanalysis (Elsevier, Amsterdam), 1960, p. 385.
14. Castaing, R., Advances in Electronics and Electron Physics, 13, 317, 1960.
15. Cosslett, V. E., Metallurgical Reviews, 5, 225, 1960.
16. Philibert, J. and Beaulieu, C. de., Rév. Mét., 56, 171, 1959.
17. Melford, D. A. and Duncumb, P., Metallurgia, 61, 205, 1960.
18. Birks, L.S. and Seebold, R. E., J. Nuclear Materials, 3, 249, 1961.
19. Philibert, J. and Bizouard, H., X-ray Microscopy and X-ray Microanalysis (Elsevier, Amsterdam), 1960, p. 416.
    Philibert, J., J. Inst. Metals, 90, 241, 1961-62.
20. Poole, D. M. and Thomas, P. M., J. Inst. Metals, 90, 228, 1961-62.
21. Wood, G. C. and Melford, D. A., J. Iron and Steel Inst., 198, 142, 1961.

22. Dolby, R. M., Proc. Phys. Soc., 73, 81, 1959.
Dolby, R. M. and Cosslett, V. E., X-ray Microscopy and X-ray Microanalysis (Elsevier, Amsterdam), 1960, p. 351.
23. Dolby, R. M., X-ray Optics and X-ray Microscopy (Academic Press, New York), in publication.
24. Agrell, S. O. and Long, J. V. P., X-ray Microscopy and X-ray Microanalysis (Elsevier, Amsterdam), 1960, p. 391.
25. Long, J. V. P., Thesis, University of Cambridge, 1958.
26. Austin, A. E., Richard, N. A. and Schwartz, C. M., X-ray Microscopy and X-ray Microanalysis (Elsevier, Amsterdam), 1960, p. 401.
Maringer, R. E., Richard, N. A. and Austin, A. E., Trans. AIME, 215, 56, 1959.
27. Chinner, G. A., J. Petrology (in the press).
28. Aitken, M. J., Physics and Archaeology (Interscience, New York and London), 1961.
29. Mellors, R. C. and Carroll, K. G., Nature, 192, 1090, 1961.
30. Tousimis, A. J., This volume, p. ...
31. Robertson, A. J., Rivers, D., Nagelschmidt, G., and Duncumb, P., Lancet, May 20, 1961, p. 1089.
32. Boyde, A., Switsur, V. R. and Fearnhead, R. W., J. Ultrastructure Res., 5, 201, 1961.
33. Lever, J. D. and Duncumb, P., Electron Microscopy in Anatomy (Arnold, London) 1961, p. 278.
34. Mackenzie, A. R., Hall, T. and Whitmore, W. F., Nature, 193, 72, 1962.
35. Hale, A. J., J. Biochem. (in publication).
36. Boyde, A. and Switsur, V. R., X-ray Optics and X-ray Microscopy (Academic Press, New York), in publication.
37. Switsur, V. R. and Boyde, A., X-ray Optics and X-ray Microscopy (Academic Press, New York), in publication.

QUANTITATIVE ELECTRON MICROPROBE ANALYSIS OF RADIOACTIVE AND IRRADIATED MATERIALS

R. Theisen and J. P. Lecoq
Euratom
Ispra, Italy

It is necessary to evaluate the analytical possibilities of an electron microprobe in the presence of samples containing alpha or gamma emitters.

MICROANALYSIS OF ALPHA EMITTING SAMPLES

Quantitative microanalysis of alpha emitters equipped with fully focalized spectrometers may raise the following difficulties, if the method described recently by D. Scott and G. Ranzetta [4] is used. (Formvar coating of samples and standards.)

a. Under the impact of the electrons, the Formvar layer becomes electrically charged. This deformation of the electric field brings about a deviation in the electron beam. The shift in the point of impact of the electrons in relation to the analyzer crystal and the X-ray detector varies as a function of the accelerating voltage of the electron beam and of the thickness of the protective layer. This defocalization can cause a drop in the X-ray intensity of over 10% and is variable between different points of the sample.

b. Since Formvar is a heat insulator, the heat evacuation may prove to be inadequate. Puncturing of the film must be avoided to prevent contamination of the apparatus. The crater thus formed could cause a new deformation of the electric field.

c. Unequal electron absorption in the Formvar film of unequal thickness. In order to reduce these effects, which could partially explain the unexpected results described by Scott, we suggest an alternative solution.

The sample and the controls are simultaneously encased in a conducting mount (Struers Mounting Resin II). They can then be handled without risk, polished in the glove-box, lightly etched by means of ionic bombardment and then immediately metallized by vacuum evaporation in order to avoid all surface oxidation and subsequent contamination of the apparatus. The encased sample together with the controls (standard 1 inch metallographic mount) can be easily inserted in the special specimen holder described below (Figure 1).

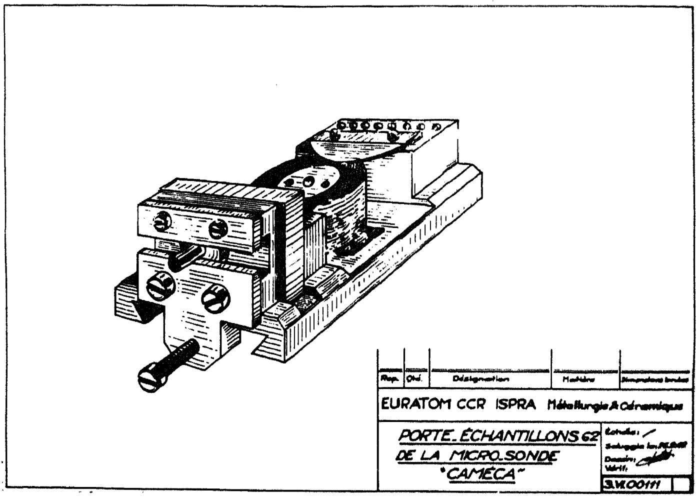

Figure 1

POSSIBILITIES FOR QUANTITATIVE ANALYSIS OF IRRADIATED SAMPLES

General Remarks

For the preliminary tests on gamma emitters, we used a natural uranium pellet irradiated for 24 hours at a thermal flux of 10^{13} n/cm^3 sec. in the Avogadro I reactor. The analyses were carried out with the aid of a Castaing [6] microprobe manufactured by the Cameca Company. The spectrometer for heavy microprobe elements is supplied with a quartz crystal working by reflection on the $10\bar{1}1$ plane and a Geiger-Müller counter. This spectrometer involves the following drawbacks with regard to the analysis of irradiated uranium and its alloys.

a. For the line $L\alpha_1$ of uranium, the point of impact of the electrons on the radioactive samples, the insertion window of the spectrometer and the Geiger-Müller counter are aligned. As a result, in addition to the characteristic radiation reflected by the analyzer crystal, the counter also registers the gamma radiation emitted by the sample.

b. The Geiger-Müller counter is unable to discriminate sufficiently between energy spectra.

Since the Geiger-Müller counter provides a considerable continuous background due to radioactivity, more conclusive tests were carried out with the Cameca gas circulation proportional counter and the Philips 18511 sealed proportional counter.

The new specimen-holding device (Fig. 1) contains a wide slot in which the sample, the standards, the metallographic and the lead mounting are inserted by means of remote-control handling equipment.

The whole mount is then placed against the upper plates by means of an elastic strip. The surface of the samples and the standards are therefore within the focal plane. At the front of the specimen-holder there is a radiobiological screen designed to protect the operator from surface radiation. An increase in the permitted activity may be obtained by incorporating an additional lens in the ocular tube of the metallographic microscope. The length of the ocular tube is therefore increased by 30 cm and the eye of the observer is located at a distance of 50 cm. At the same time, the magnification of the microscope is stepped up from 350 × to about 450 × (Figure 2).

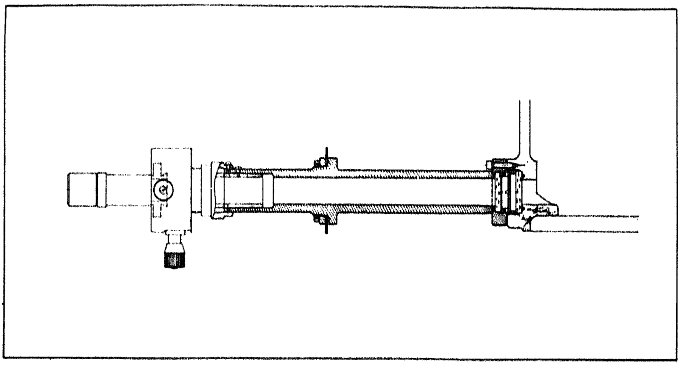

Figure 2

Experimental Results

A lead collimater approximately 2 cm thick, partially covered the X-ray exit window. The results are given in Tables 1 and 2.

DISCUSSION

It therefore seems possible to carry out analyses using a short interreticular distance crystal ($13\bar{4}0$ or $11\bar{2}0$ quartz or

Table 1

Quartz used:	$13\bar{4}0$ $2d = 2.35$ Å
Bragg angle for $UL\alpha_1$:	22° 45'
Probe intensity:	1.2×10^{-6} A
Ray intensity on $UL\alpha_1$:	200 c/s
Background due to radioactivity and counter:	6 c/s
Increase in background without lead shielding:	30%
Cameca proportional counter (gas circulation)	

Table 2

Quartz used:	$10\bar{1}1$ $2d = 6.686$ Å
Angle of cut:	3°
Bragg angle:	$UL\alpha_1$: 7° 49'
Probe intensity:	1.2×10^{-6} A
X-Ray intensity on $UL\alpha_1$:	11206 c/s
Background due to radioactivity and counter:	312 c/s
Philips 18511 proportional counter (sealed)	

LIF), a proportional counter followed by a preamplifier and a linear amplifier with pulse height selector, and judiciously placed lead screens.

Several modifications have been developed in order to step up the peak to background ratio.

The use of an orientable quartz press can effectively counteract grinding imperfections and the aging of the crystal and facilitate the adjustment of the spectrometer [7]. The preamplifier, which consists of a cathodyne-mounted triode, is to be replaced by a more satisfactory system providing a higher gain (10 X).

The background, due to radioactivity, can be decreased even more by adding to the exit window of the spectrometer a channel through which only the X-rays pass in the direction corresponding to the line being analyzed. The angle of aperture of this channel can be easily determined with the aid of the diagram of the modified spectrometer (Figure 3).

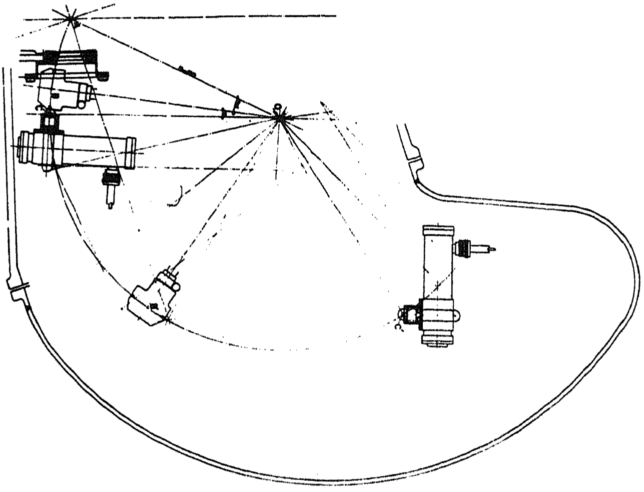

Figure 3

PROTECTION

In addition to purely technical questions connected with the correct functioning of the Castaing microanalyzer in the presence of an intense source of gamma radiation, there is also the problem of the radiobiological protection of the operator. On the basis of a number of simple hypotheses, we have endeavoured to calculate the maximum weight of irradiated uranium which can be safely examined in the normal microanalyzer or with the aid of an additional protection device.

Basic Hypothesis

1. The sample is assumed to be irradiated to saturation, i.e., that the duration of irradiation is equal to at least five times the half-life of gamma-emitter fission products or their parents or daughters, that is, in the case of uranium, about three months.
2. The tolerance dose permitted for the operator is 0.1 rem/week, Euratom protection standard [8].

If the Microanalizer is Used Without Auxiliary Protection

The natural protection of the apparatus is reduced to about 3 cm of brass, or the equivalent of 1 cm of lead for 1 MeV radiation.

For natural uranium irradiated to saturation at 1 W/g, the following table gives us the weight of natural uranium which can be examined as a function of the cooling time of the sample:

Cooling time in days	0	2	5	10	20	50	90
Weight in mg. of natural U irradiated to saturation at 1 W/g	0.5	2	2.7	3.2	4.7	8.3	13.5

Microanalyzer with Auxiliary Protection

The use of the special specimen holder (Figure 1) — additional protection equivalent to 2 cm of lead—permits a gain of a factor four for the allowed mass of uranium.

In event of use being made also of the elongated ocular tube (Figure 3), the permissible weights will be multiplied further by 2.8.

Without aid of any complex device, we can examine samples which are ten times larger than those in the standard apparatus and forty times larger, if we confine ourselves to 10 hours of controlled work per week.

Cooling time in days	0	2	5	10	20	50	90
Weight in mg of natural uranium irradiated to saturation at 1 W/g	22	90	124	145	213	370	580

CONCLUSION

The problem of the analysis of alpha-emitting samples can be solved by a relatively simple method, even with an apparatus equipped with fully focalized spectrometers. It is sufficient to encase the sample and the standards simultaneously in a conducting mount, with the fugitive activity stopped by a metal film deposited by vacuum evaporation.

The analysis of irradiated samples, which is a more delicate matter, requires slight modification of the commercial instrument, involving in particular the use of a proportional counter equipped with a pulse height selector, the use of a special specimen holder and judiciously placed lead screens, an orientable crystal press and short interreticular distance analyzing crystals ($13\bar{4}0$ or $11\bar{2}0$ quartz or LIF).

REFERENCES

1. R. Castaing. ONERA, Publ. No. 55 (1952).
2. R. Castaing. Advances in Electronics and Electron Physics, 8, 318-86 (1960).
3. V. D. Scott. J. Nucl. Mat., 3, 284 (1961).
4. V. D. Scott and G. V. T. Ranzetta. J. Inst. Met., 6, 160 (1962).
5. P. Duncumb. J. Inst. Met:, 6, 152 (1962).
6. R. Castaing and Descamps. Recherche Aéronatique, No. 68 (1958).
7. H. Elion, R. Ogilvie and L. Shapiro. XIX Pittsburgh Diffraction Conference (1961).
8. Journal Officiel European Communities, No. 11 (1959).

HIGH PRECISION MICROPROBE ANALYSIS BY THIN METALLIC FILM CALIBRATION

R. Theisen and J. Lemaître
EURATOM, CCR
Ispra, Italy

INTRODUCTION

With the increasing availability of electron microprobes, the theory of quantitive microanalysis has been the object of new investigations.

Starting from the calculations published by R. Castaing in his thesis [1], it has been attempted to establish experimental and theoretical correction formulae for local microprobe analysis.

The effects of diffuse penetration of electrons and mass absorption of X-rays in the anticathodes [2-7], the effects of fluorescence excited by characteristic radiations [8-10] and of enhancement by the continuous spectrum [11] have been evaluated.

Measured X-ray intensities and calculated values of binary alloys are in reasonable agreement except:

a. At low concentration,
b. for great atomic mass difference of components combined with secondary fluorescence emission,
c. for analysis of inclusions (direct emission and fluorescence enhancement of matrix).

For high precision analysis of these alloys (no limitation in number of components) in the absence of calibration standards homogeneous on a $1/\mu$ scale, the use of thin films, 0.01 to $0.1/\mu$, obtained by ultramicrotomy permit high resolution analysis with negligible absorption and fluorescence corrections.

THEORY

Suppose, an electron beam of intensity I_o impinges perpendicularly on a metallic film of thickness z cm. The intensity of the characteristic radiation I_t collected from a constant area at an emergent direction θ will be [6]:

$$I_t = K \frac{M_t}{A_t} I_o \int_{z=o}^{z} e^{-\alpha\rho z} e^{-(\mu/\rho)\csc\theta} \, dz, \qquad (1)$$

where

K = constant depending on the voltage ratio V/V_k,

M_t/A_t = number of atoms T per unit volume,

$\alpha = K/V^2$ (V being the accelerating voltage),

$\rho = \Sigma M_i$ = density,

M_t = mass of element T per volume unit,

A_t = atomic weight of element T,

μ/ρ = mass absorption for characteristic radiation in analysed alloy.

A considerable simplification is obtained when z and α become so small that the exponential term approaches unity. The physical significance of this simplification is that absorption effects are negligible.

By using sufficiently thin samples (0.01 μ) and a highly accelerated electron beam (35 KV and more if possible), it is possible to assume a direct proportionality between the characteristic X-ray emission and the masses per unit area of the analysed elements.

$$\frac{I_A}{I_{(A)}} = M_A \, . \qquad (2)$$

$I_A/I_{(A)}$ is the ratio of X-ray intensities emitted respectively in the K α (A) line, under the same experimental conditions by the pure element A and the analysed alloy. Similarly

$$\frac{I_B}{I_{(B)}} = M_B \, , \qquad (2')$$

$$\frac{I_C}{I_{(C)}} = M_C \, . \qquad (2'')$$

Considering

$$\rho = \Sigma M_i = M_A + M_B + M_C , \tag{3}$$

$$C_A = \frac{M_A}{\Sigma M_i} = \frac{M_A}{M_A + M_B + M_C + \ldots\ldots} , \tag{4}$$

$$C_B = \frac{M_B}{\Sigma M_i} . \tag{4'}$$

Using equation (4) the chemical composition of a sample is obtained by the determination of the superficial masses of all the elements being present in the sample.

EXPERIMENTAL PROCEDURE

The thin films 0.01μ thick (samples and pure elements) should be of identical thickness, condition which can be most easily fulfilled by the automatic advance of an ultramicrotome after Fernandez Moran [12], followed by an interferometric thickness control of the films.

Films of about 2500μ^2 were collected on standard electron microscope grids and inserted into a special probe holder (Figure 1).

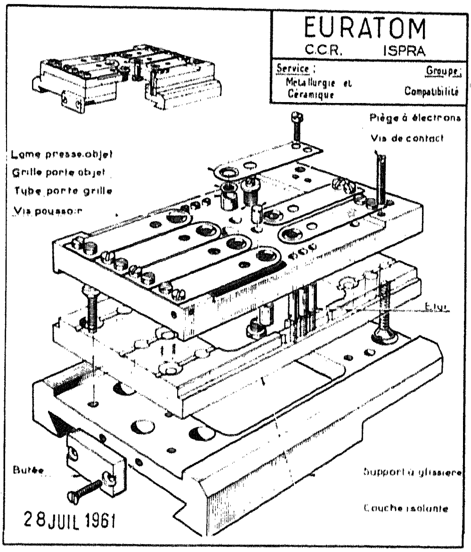

Figure 1. Special sample holder for French Microanalyser.

The highest available accelerating voltage (35 KV) of a CAMECA Microanalyser was used in order to avoid a notable deceleration of electrons in the anticathodes, to diminish the absorption effect of superficial oxide or contamination layers, as well as to increase the peak-to-background ratio of the analysed radiation.

APPLICATIONS

Quantitive microanalysis of small inclusion is a very difficult task because it is impossible to predict the direct emission and fluorescent contribution of the matrix. The thin film technique resolves this problem as it is possible to localize the inclusion on both surfaces of the thin sample. This method permitted the identification of 3 phases of an iron rich inclusion of SAP (sintered aluminum powder) (Figure 2). Several applications are listed in Table 1.

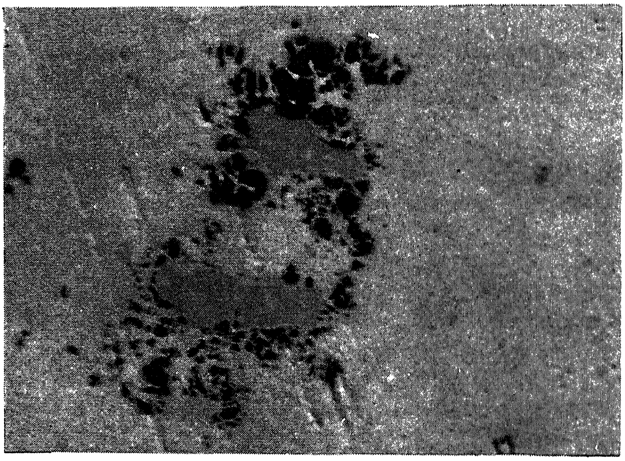

Figure 2. Iron rich inclusion in SAP 980. Electron image X700.

In microanalysis of infinitely thick samples, the diffuse penetration of electrons limits the resolution power of the method to about 0.5μ [13].

A considerable improvement of the volume resolution can be obtained by the thin film technique, as this limitation is no longer valid.

For additional information the use of the special sample holder transforms the French Microanalyser into a projection X-ray microscope with a typical Cosslet-Nixon [14] X-ray microfocus (Figure 3).

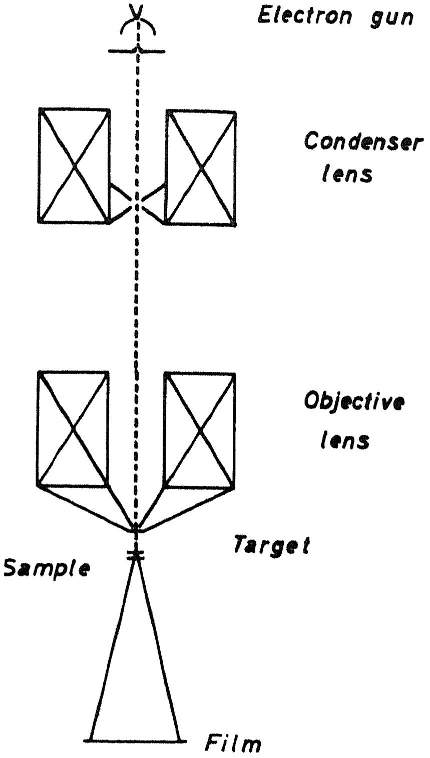

Figure 3. Projection Microradiography.

Table 1

Results of Chemical Analyses and Microanalyses

Alloy	Chemical Analyses	Microanalyses	$\frac{\Delta c}{c}$
	Al W% Theoretical Concentration	Experimental	
UAl_3	25.37	25.12	-0.99%
Sol × Sol × Al-Ni	5.0	4.99	-0.02%
SAP Inclusion $FeAl_3$	59.1	59.63	+1.06%
SAP Inclusion $FeO \times Al_2O_3$	31.0	31.58	+1.88%

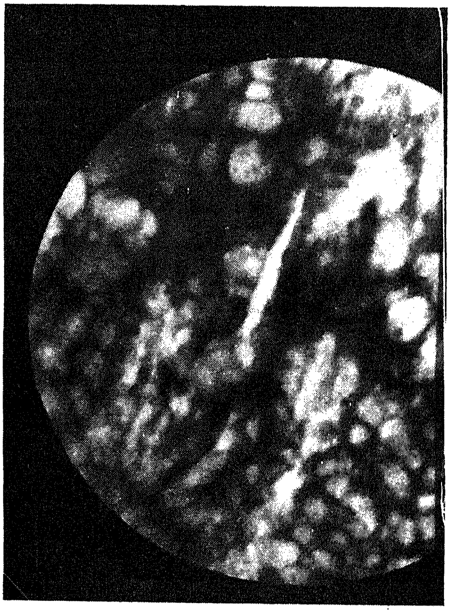

Figure 4. X-ray projection micrography of U Ni Al diffusion X250 layer; U Ni Al = dark zone; Ni_2Al_3 = bright grey dentrites.

In U-Ni-Al nuclear fuel elements, treated at 450°C, the formation of a ternary diffusion layer of approximate composition U Ni_7Al_{13} has been identified by microprobe analysis [15].

At heat treatments above 650°C this layer decomposes into two different phases. The composition of these phases were determined by microprobe analysis.

$$U\,Ni_7Al_{13} \rightarrow U\,Ni\,Al_4 + 3\,Ni_2Al_3\,.$$

A film 1 μ thick of Cu was chosen as X-ray source. The selective absorption of Cu radiation by a 15 μ thick sample produces the X-ray micrograph shown in Figure 4.

Furthermore, the special sample holder may be used for studies on electron transmission and backscattering by thin films as well as for electron diffraction purposes.

CONCLUSIONS

High resolution and precision microanalysis may be achieved by the proposed use of the thin film technique.

General use of this method is limited by the delicate and time consuming preparation of samples and standards.

Application includes microanalysis of small inclusions and setting up of calibration curves for complex alloys. Furthermore, projection X-ray metallography combined with electron probe microanalysis may lead to valuable information in physical metallurgy.

REFERENCES

1. Castaing, R. Publ. ONERA No. 55 (1952).
2. Birks, L. S. J. Appl. Phys. 31, 1297 (1960).
3. Ilhyine, Borowski. Izvest Akad. Nauk TXXV No. 8 (1961).
4. Philibert, J. J. Inst. Metals 90, 241-252 (1962).
5. Poole and Thomas. J. Inst. Metals 90, (1962).
6. Theisen, R. EUR-I-1 Metallurgy and Ceramic (1961).
7. Tong: Unpublished work (1960).
8. Birks, L. S. J. Appl. Phys. 32, 387 (1961).
9. Castaing, R. Publ. ONERA No. 55 (1952).
10. Wittry, D. B. Thesis, Calif. Inst. Techn. (1957).
11. Hénoc, J. Unpublished work (1962).
12. Moran, F. H. Mikroskopie 12, 81-88 (1957).
13. Wittry, D. B. J. Appl. Physics 29, 11 (1958).
14. Cosslet, N. X-Ray Microscopy, Cambridge University Press (1960).
15. Brossa, F.; Huet, J. J.; Theisen, R; Tytgat, D.: EUR 17.F (1962).

SPECTROSCOPIC STUDIES WITH THE RUBY OPTICAL MASER

B. P. Stoicheff
Division of Pure Physics
National Research Council
Ottawa, Canada

INTRODUCTION

A radically new light source—the optical maser—has recently become available for spectroscopic studies. The emission from such a light source is characterized by its high intensity of coherent and extremely monochromatic light in a narrow beam. Some of these properties are obviously highly desirable in special fields of spectroscopic research and it seems worthwhile to investigate the potentialities of masers in such studies.

It is the purpose of this paper to review briefly the present achievements in the development of maser sources and in particular to describe the pertinent optical characteristics of the ruby maser and to discuss its possible use in spectroscopy along with some preliminary results that have already been obtained.

SURVEY OF AVAILABLE MASERS

The feasibility of producing light sources which radiate by stimulated emission in the infrared and optical regions was discussed by Schawlow and Townes [1] in 1958. The first successful demonstration of an optical maser was made by Maiman [2] in 1960. He used a ruby crystal (0.05% Cr^{3+} in Al_2O_3) excited by a xenon flash lamp and obtained a pulse of maser emission at 6940 Å lasting for about 0.5 millisec. A continuously operating maser making use of a gaseous discharge of He + Ne was developed by Javan, Bennett and Herriott [3] in 1961. Since then, many other solid state masers have been operated with pulsed emission, and masers of ruby, Nd^{3+} in $CaWO_4$, U^{3+} in CaF_2 and Dy^{2+} in CaF_2 have been successfully operated with continuous emission. Recently several new gas masers using Cs, Ar+O_2 and Ne+O_2 have been operated continuously. A list of the available maser materials and the approximate wavelengths of their emission is given in Table 1. Already maser emission has been observed at about 30 different wavelengths in the region of 7000 Å, 11000 Å and 2.5 μ.

Of course, the gas masers approach the theoretical expectations more closely than do the solid state masers, but even so all of these sources exhibit most remarkable properties. Some

Table 1

Presently Available Optical Masers[a]

Source Material	Wavelength of Emission
Ne - He	11,180, 11,530,[b] 11,600 11,990, 12,070 Å
Cs	7.18 μ
Ne-O_2, Ar-O	8446 Å
0.05% Cr^{3+} in Al_2O_3	6943 Å
0.5% Cr^{3+} in Al_2O_3	7009, 6943, 7041 Å
U^{3+} in CaF_2	2.613 μ
U^{3+} in BaF_2	2.556 μ
U^{3+} in SrF_2	2.407 μ
Sm^{2+} in CaF_2	7082 Å
Nd^{3+} in $CaWO_4$, $SrMoO_4$, $CaMoO_4$, $PbMoO_4$	10,580, 10,650 Å
Nd^{3+} in CaF_2	10,460 Å
Nd^{3+} in barium crown-base glass	10,600 Å
Pr^{3+} in $CaWO_4$	10,470
Ho^{3+} in $CaWO_4$	2.046, 2.059 μ
Tm^{3+} in $CaWO_4$	1.911 μ
Tm^{2+} in CaF_2	11,600, 11,890 Å
Dy^{2+} in CaF_2	2.36 μ
Er^{3+} in $CaWO_4$	1.612 μ

[a] This survey includes masers reported in publications up to July 1, 1962.

[b] Wavelength of the most intense emission in the He-Ne maser.

typical observations of their emission characteristics may be of interest. In the He-Ne maser with emission at 1.15μ, the frequency width [4] is better than 2 cps (at 2.6×10^{14} cps), although due to thermal and mechanical instabilities the frequency drift is of the order of 2 parts in 10^9 for periods of about 100 sec. In the ruby maser, frequency widths as narrow as 2 to 10 Mc/sec (that is about 10^{-4} cm^{-1}) have been measured [5,6], but as shown below, during one complete pulse thermal effects lead to a line width of the order of 0.01 to 0.2 cm^{-1}, depending on the temperature, power output and quality of the ruby. The Nd^{3+}-glass maser [7] has a width of approximately 1 cm^{-1} at threshold and about 100 cm^{-1} at high power levels. The power output of the continuously emitting gas and crystal masers is in the range of 1 to 300 milliwatts. On the other hand the power output of the pulsed masers such as ruby and Nd^{3+}-glass is of the order of kilowatts: they emit radiation in the energy range of 0.1 to 1 joule in a millisecond or less and energies as high as 50 to 100 joules have already been obtained. "Giant pulses" of short duration ($\sim 10^{-8}$ sec) and extremely high intensity (~10 megawatt) have been produced with the ruby maser by suddenly changing the regenerative power of the resonant cavity [8] (by varying the effective reflectivity of the end faces of the ruby rod).

At the present time, the pulsed ruby maser (~0.05% Cr^{3+}) appears to be one of the more promising of the available masers as a spectroscopic source. As already mentioned its emission is in the region of 6940 Å and is the shortest wavelength yet attained with masers. Photographic emulsions and photodetectors are still fairly sensitive to this radiation (although their sensitivity is higher at even shorter wavelengths). The reported line width of the ruby emission is relatively narrow in comparison with ordinary sources. High energy emission (~1 to 10 joules) is readily achieved. Moreover, the emission occurs in a highly directional beam confined to an angle less than 30 minutes. In addition, the radiation is linearly polarized or nonpolarized depending on whether the optic axis of the crystal is perpendicular or parallel, respectively, to the ruby rod axis. Finally, high quality ruby crystals are readily available and complete units including flash lamps and power supplies are now produced commercially.

The many favourable qualities of the ruby maser prompted the present investigation to assess the usefulness of this extraordinary light source for spectroscopic studies. For this purpose it was desirable to begin with a detailed study of the wavelength and line width characteristics of the emission.

RUBY MASER APPARATUS

A schematic diagram of one of the ruby masers used in this investigation is shown in Figure 1. The ruby used was of 0.05% Cr^{3+} concentration and was cut in a square rod 6.0 cm long with sides of 0.4 cm. The ends were polished flat to 1/5 of a fringe and parallel to better than 10 sec: both ends were silvered, the front end having a transmission of about 5 per cent. The ruby was held in a glass tube to facilitate cooling (by streaming cold N_2 vapor) and to maintain the ruby at a predetermined temperature before each firing of the flash lamp. Temperature control to about 0.01 degree was easily obtained over the range 20°C to -120°C by evaporating liquid N_2 at a constant rate by means of a heater immersed in the liquid N_2. The flow rate of the N_2 vapor, and therefore the temperature of the ruby was varied by changing the voltage applied to the heater terminals. Temperature readings were obtained with a copper-constantan thermocouple in contact with the ruby. As shown, the Xe flash lamp has four linear sections which form a symmetrical parallel array close to and surrounding the ruby rod. The efficiency of this arrangement was almost doubled by enclosing the lamp in a cylindrical reflector coated with MgO. The input power required for maser emission was approximately 700 joules.

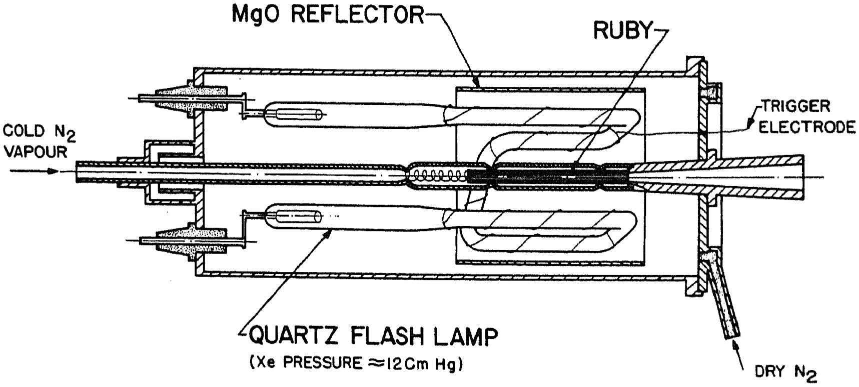

Figure 1. A typical ruby optical maser. This schematic diagram shows the ruby rod, xenon flash lamp, MgO-coated reflector and housing.

For work at 77°K, the same ruby was kept immersed in liquid N_2 in a special dewar [6]. The ruby, with a similar arrangement of flash lamp and reflector as in Figure 1, was kept in a vertical position in this apparatus. Threshold for maser emission was about 400 joules. The output energy of the emission from these masers when the electrical energy to the flash lamp was double the threshold value is estimated to be in the range of 0.1 to 1 joule.

WAVELENGTH AND LINE WIDTH OF MASER EMISSION

When the flash lamp is fired at an energy below threshold for maser emission, the well-known ruby fluorescence in the broad R_1 and R_2 lines is obtained. Above threshold, the emission is in a very intense and sharp line at the wavelength of the peak of the R_1 line. The spectra of the fluorescence and maser emission (for the ruby at -70°C) are compared in Figure 2. The peak intensity of the maser line is greater than 5000 times that of the broad fluorescence line and its spectral width is only about 1/20 of the fluorescence line.

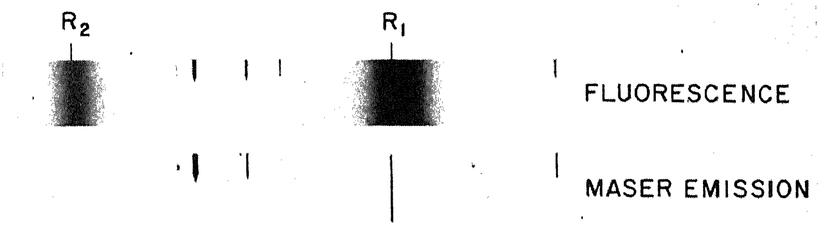

Figure 2. Spectra of the spontaneous and induced emission of ruby at -70°C. The fluorescence spectrum was obtained with 6 flashes of the lamp fired just below threshold. The maser emission was obtained with one flash a few percent above threshold and with neutral density filters to reduce the beam intensity by 1,000 before entering the spectrograph. Both spectra were photographed in the first order of a 35 ft. grating spectrograph with a slit width of 30 μ and a reciprocal linear dispersion of 0.6 Å/mm.

It has already been shown [9] that the wavelength of the ruby maser emission is strongly temperature dependent (and as expected the change in wavelength follows closely the thermal shift of the R_1 line in fluorescence and absorption). This dependence on temperature is illustrated in Figure 3 and in the graph of Figure 4 for the ruby used in the present study. The total wavelength shift is about -10 Å from 30°C to -196°C. In the temperature range of 30°C to -100°C the shift is almost linear and approximately -0.05 Å/degree, but its rate of change is considerably less below about -190°C. These observations are in general agreement with the earlier results of Abella and Cummins [9].

This temperature dependence of the wavelength is an important characteristic of the ruby maser emission. One practical advantage of this dependence is that it provides a method of "tuning" the wavelength by ~10 Å (or the frequency by ~20 cm^{-1}).

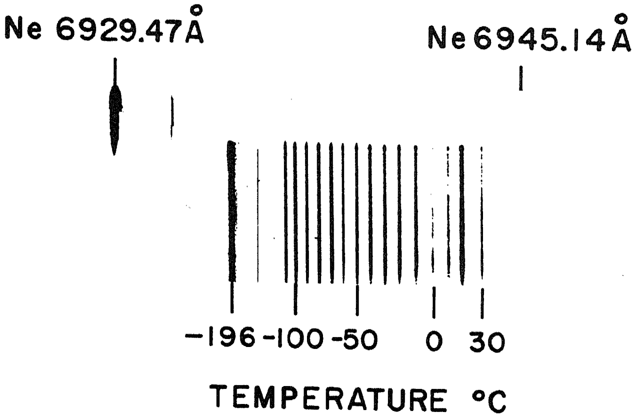

Figure 3. The variation of wavelength of the ruby maser emission with temperature in the range 30°C to −196°C. Each spectral line was produced by a single flash of the maser with input power close to threshold and the ruby at the designated temperature immediately before the flash. The spectra were photographed in the second order of a 21 ft. grating spectrograph with a slit of 50μ and a reciprocal linear dispersion of 1.25 Å/mm.

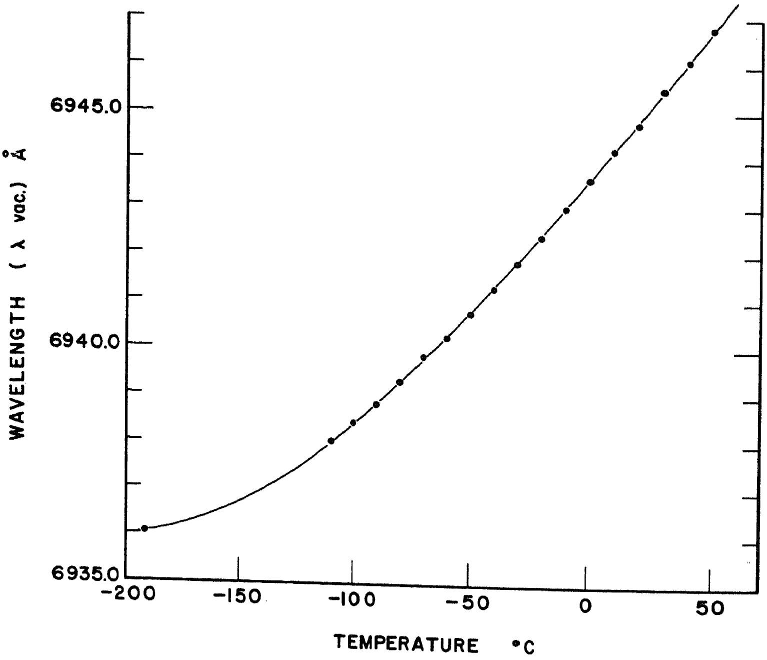

Figure 4. A graph of the wavelength variation of the ruby maser emission with temperature.

However, it is evident, that, in order to obtain a predetermined wavelength, or a constant wavelength, fairly accurate temperature control of the ruby is necessary. For a constant wavelength, especially in applications where many repetitive flashes are necessary, optimum control is obtained at a temperature below about -190°C: as shown, this is most readily achieved by immersing the ruby in liquid N_2 (-196°C).

The dependence of the line width on temperature is illustrated by the interferograms of Figure 5. At -60°C (Figure 5a) the emission at threshold is in a group of four sharp lines (3 strong components and one weak) separated by approximately 0.05 cm^{-1} . At lower resolution the group forms a line of width about 0.2 cm^{-1} . Similar groups of several components were observed at various temperatures down to about -100°C. On the other hand, with the ruby immersed in liquid N_2 only a single sharp line is observed at threshold, with a width of between 0.01 to 0.02 cm^{-1} .

These results are understood with the aid of the schematic diagram of Figure 6. Here it is seen that at least three (and possibly four) cavity modes with a separation of 0.05 cm^{-1} , are contained in the intensity peak of the broad fluorescence line at -60°C. Only one mode is near the peak of the stronger ($m = \pm 3/2$) component of the sharp fluorescence doublet at -196°C. Admittedly, this favourable circumstance of obtaining a single line at -196°C is fortuitous since the frequencies of the cavity modes

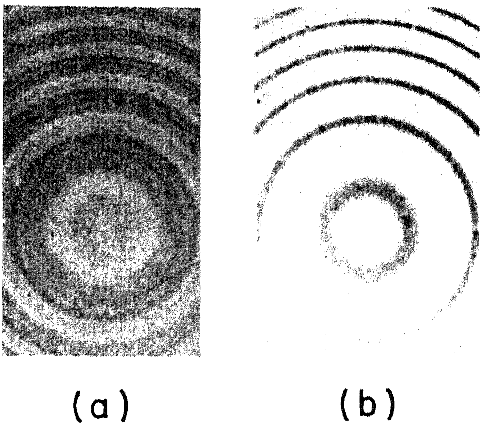

Figure 5. Interferograms of ruby maser emission taken with a plane Fabry-Perot etalon having a spacing of 25 mm and inter-order separation of 0.2cm^{-1} (a) emission in several axial modes (separated by 0.05 cm^{-1}) with ruby at -60°C. (b) emission in a single axial mode, at threshold, with ruby immersed in liquid N_2(-196°C).

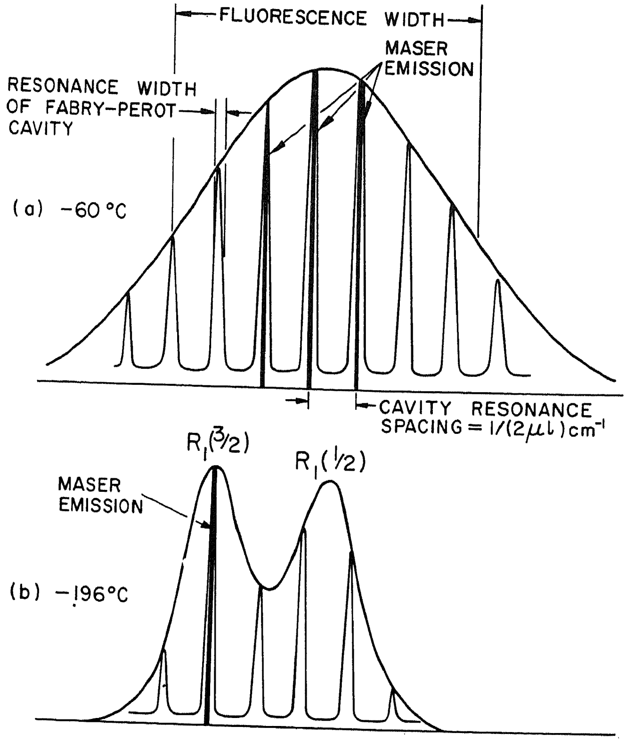

Figure 6. Line width characteristics of ruby fluorescence, Fabry-Perot cavity resonances and maser emission (schematic), with (a) ruby at -60°C and (b) ruby immersed in liquid N_2 (-196°C).

are dependent on the optical path within the ruby. Nevertheless, for a high quality ruby at -196°C at most two sharp lines are obtained corresponding to the two components of the fluorescence doublet with a separation of 0.37 cm^{-1} . With the present ruby, the additional component appears a few per cent above threshold. Only at very high powers (more than double threshold) are other axial modes observed.

The spectral characteristics of the ruby emission at -196°C and at -60°C (taken to be representative of the emission at higher temperatures) are compared in Figure 7 by means of the interferograms observed with consecutive flashes of the ruby maser at these temperatures. Here it is shown that the reproducibility of wavelengths and line width is good at the lower temperature and considerably better than at the higher temperature. In fact it is seen that at -196°C, the wavelength is reproducible to within the line width of about 0.01 Å (that is 0.02 cm^{-1}). Therefore, for many applications in high resolution spectroscopy it is desirable to work with the ruby at -196°C. The advantages just discussed may well outweigh the inconvenience of keeping the

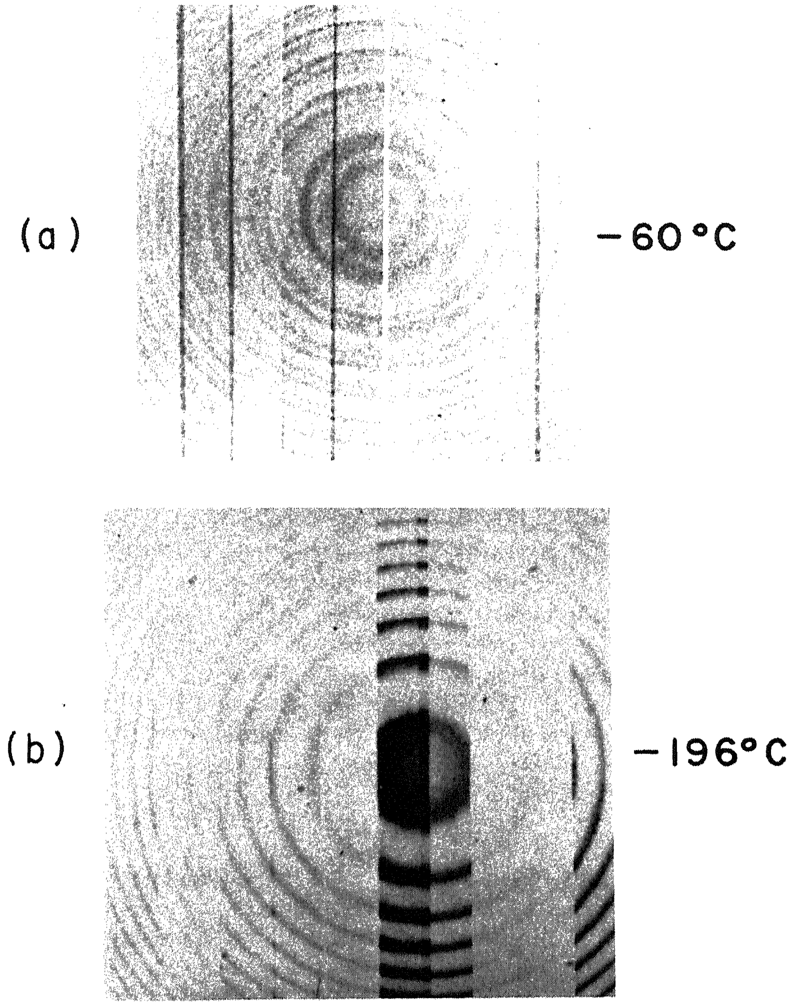

Figure 7. Interferograms to show the reproducibility of the wavelength and line width of maser emission with (a) ruby at −60°C and (b) ruby immersed in liquid N_2(−196°C). Each vertical strip arises from a single pulse of maser emission, the time between pulses being 30 sec and 15 sec for (a) and (b) respectively. The Fabry–Perot etalon has a spacing of 25 mm.

ruby immersed in liquid N_2. Further, it may be noted that the thermal conductivity of ruby is high and is near its maximum value at -196°C so that the time for thermal recovery is near a minimum at this temperature resulting in a faster firing rate of the maser.

SPECTROSCOPIC APPLICATIONS

The potential applications of the ruby optical maser, and of optical masers in general, may conveniently be discussed under two headings. Under the one, "conventional spectroscopy," would be included such fields as for example, fluorescence, Raman effect [10], Brillouin scattering and light scattering in general, that is fields of research in which the particular wavelength of the maser or its high light intensity or its narrow line width might result in considerable improvements over the established techniques using conventional light sources. Under the other, and perhaps more exciting class of "new experiments", would be included all those which are impossible to perform with sources based on spontaneous emission of radiation, that is with sources which do not possess the high intensity and/or coherence of the maser emission. Here would be included for example, the simultaneous absorption of two (or more) photons [11], the generation of optical harmonics [12], the mixing of optical frequencies [5,13], and the production of high temperature flames. Many other new applications are expected in the near future.

As indicated by the above references to the published literature on masers and their applications, many results of interest in spectroscopy have already been reported. A few applications of the ruby maser to spectroscopic investigations have been attempted at the N.R.C. Laboratories (Ottawa) and these will be briefly discussed here along with preliminary results obtained.

Fluorescence

The ruby maser line at λ 6940 Å may be a very useful addition to the large list of atomic lines already available for fluorescence studies. Although, of course, its usefulness will be limited to substances absorbing this wavelength, its high intensity may find special uses in exciting the fluorescence spectra of crystals (as shown below) and of gases. Also, it will be remembered that the ruby emission has the advantage of being tunable over a wavelength region of about 10 Å (Section D). This feature could be useful in some special studies of resonance fluorescence (for example, of NO_2) where the wavelength of the exciting line can be made coincident with various absorption lines in turn, thereby producing fluorescence in only a few labelled lines.

Some examples of fluorescence spectra of crystals excited by the ruby maser line are shown in Figure 8. In these experiments, carried out in collaboration with Dr. Shobha Singh, the usual simple experimental arrangement was used: the maser beam was focussed to illuminate the whole volume of the crystal (at room temperature) and the fluorescence emission at right

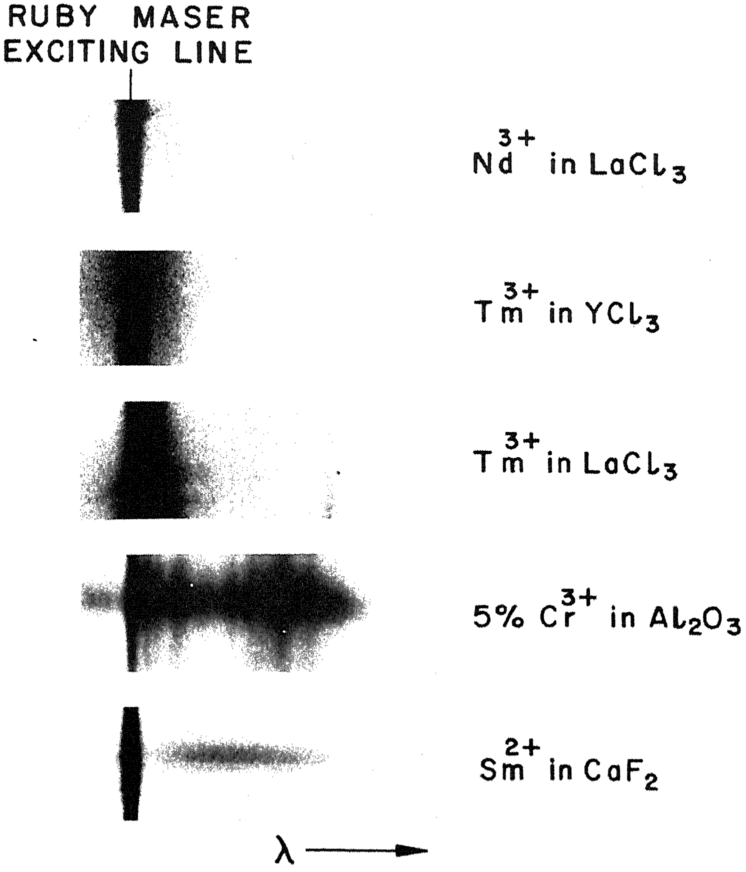

Figure 8. Fluorescence spectra of several crystals excited with ruby maser emission.

angles to the incident beam was photographed with a small Hilger spectrograph on sensitized I-N plates. Only 1 to 3 flashes of the maser were used. It is seen that fairly intense fluorescence lines and bands are recorded in effective exposure times of a few milliseconds.

The appearance of the broad fluorescence bands in crystals of Sm^{2+} in CaF_2 and of dark ruby is in agreement with earlier fluorescence data on these crystals. The origin of the relatively sharp fluorescence lines at 7030 Å and 8000 Å due to Tm^{3+} in $LaCl_3$ and Tm^{3+} in YCl_3 is shown by the energy level diagram in Figure 9 (based on unpublished results of Dr. Shobha Singh). The origin of the two lines at 7800 Å and 8800 Å in Nd^{3+} in LaC_3 is also shown in Figure 9 (after Carlson and Dieke [14]): they

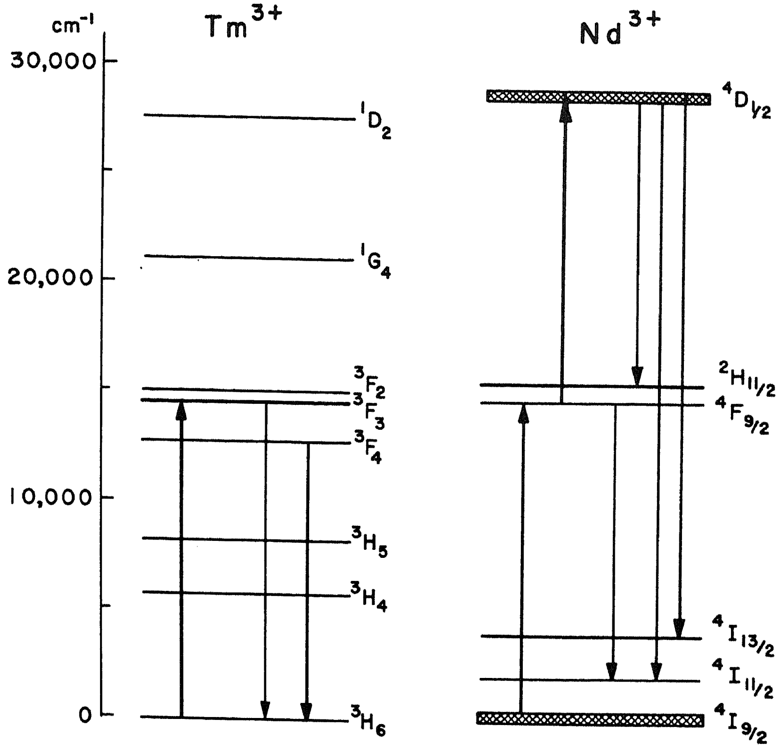

Figure 9. Energy level diagram of Tm^{3+} and Nd^{3+} in $LaCl_3$ showing some of the transitions giving rise to the observed fluorescence (Figure 8).

arise from the transitions $^4F_{9/2} \rightarrow {}^4I_{11/2}$ and $^4D_{1/2} \rightarrow {}^2H_{11/2}$ respectively. It is especially interesting to note that excitation to the $^4D_{1/2}$ state is only possible by stepwise excitation with two photons of ruby maser emission via the intermediate state $^4F_{9/2}$ as shown in the energy level diagram for Nd^{3+}. Confirmation of this two photon excitation to the $^4D_{1/2}$ state was obtained by the subsequent observation of two additional relatively intense emission lines at shorter wavelengths, namely at 3850 and 4150 Å, which are identified as transitions from a common $^4D_{1/2}$ upper state to $^4I_{11/2}$ and $^4I_{13/2}$ lower states, respectively.

Further fluorescence experiments with these and other crystals are now in progress.

Raman Effect

The high intensity and narrow line width of the ruby maser emission make this an obvious source for the excitation of Raman spectra. A comparison of the pertinent spectral characteristics of the maser emission and of the Hg 4358 emitted by a typical "Toronto-type" mercury lamp commonly used in Raman spectroscopy, may be of interest. The line widths are comparable (~0.2 cm^{-1}), although, with the ruby at -196°C the maser line is narrower and therefore would be superior for high resolution studies. The power output in the 4358 Å line is between 1 to 10 watts and is comparable to the average power output of the ruby maser if it is flashed once a second. The maser may have an advantage in special applications (e.g., with crystals) because its output is in a collimated beam whereas the emission of the lamp is in 4π steradians and must be efficiently collected. Also, as mentioned in Section B, the ruby emission may be polarized. However, since the maser line is at λ 6940 Å there is a loss of a factor of about 6 compared to λ 4358, arising from the λ^{-4} law for scattered light intensity. Moreover, sensitized I-N emulsions must be used for photographing the maser line (and the Raman spectrum) and their sensitivity is down by a factor of 5 to 10 from the I-O emulsions used with the λ 4358 line. A similar loss in sensitivity is obtained with photomultiplier detectors. For the study of vibrational Raman bands with $\Delta\nu > 2000\ cm^{-1}$ which would lie at $\lambda > 7800\ cm^{-1}$, even a greater loss in sensitivity will be suffered. Thus, it seems a reasonable estimate that about 50 maser flashes would be required to produce a Raman spectrum of about the same intensity as that obtainable with conventional apparatus in an exposure time of one second. It may also be mentioned that, while 50 flashes of the maser would correspond to an effective exposure time of 50 millisec, the usual repetition rate of firing one flash every 30 sec. would lead to a total time of about 25 min.

The use of the ruby maser to excite the Raman spectra of liquid C_6H_6 and CCl_4 has been successfully demonstrated by Porto and Wood [10] who obtained fairly complete spectra with 50 to 100 flashes of the maser. In their experiments, the maser beam was diffusely reflected many times through the sample by a coating of white $BaSO_4$ deposited on the surface of the cell and the scattered light was observed with a high aperture spectrograph.

A different type of Raman cell, based on total internal reflection of scattered light, was used in the present experiment. As shown in Figure 10, the maser beam enters a small window and is reflected many times (by the silvered mirrors which form the cell walls) through the liquid sample until it reaches the light trap at the rear end of the cell. The scattered light is internally reflected until it finally emerges at the small front window and is focussed into the spectrograph. A rather weak spectrum of liquid CS_2 obtained with 20 maser flashes is shown in Figure 11.

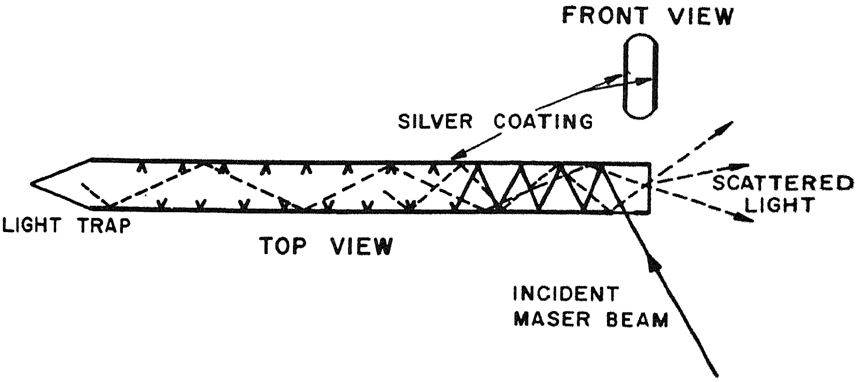

Figure 10. A "lightguide" Raman cell for liquids.

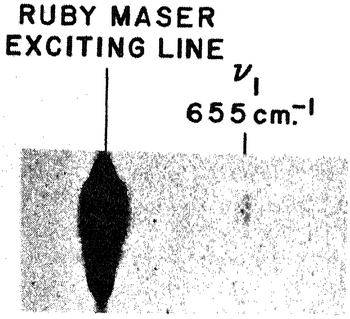

Figure 11. A weak Raman spectrum of liquid CS_2. The effective exposure time is 20 millisec: twenty maser pulses, each lasting about 1 millisec, were fired at 30 sec intervals. A small Hilger spectrograph and Kodak sensitized IN plates were used.

While these preliminary results are by no means as good as Raman spectra obtained with conventional apparatus, they do indicate that with further developments the optical maser may be an important excitation source for the Raman spectra of coloured liquids and solids, of small crystalline samples and of gases, especially for studies at high resolution. In this connection, the development of detectors making use of optical mixing techniques [15] to detect beats between the frequencies of the incident and scattered radiations will open exciting new possibilities for Raman and Brillouin spectroscopy as suggested by Townes [16].

High Temperature Flame Spectroscopy

The high intensity, coherence, monochromaticity and directionality, in short, all of the properties of the ruby maser discussed in Section B, combine to make possible the attainment of very high temperatures when the maser beam is focussed on substances which absorb this wavelength. Theoretically, it should be possible to focus this beam to an area having the dimensions of the maser wavelength. In practice, it is easily possible to focus the beam to an area of the order of 0.1 mm^2 and thus to obtain extremely high energy densities, of the order of kilojoules/cm^2 for the duration of the maser flash ($\sim 10^{-3}$ sec). In this way, it should be possible to obtain temperatures of about 10,000°K with microsamples of absorbing materials.

When the ruby maser beam is focussed on a carbon surface in air, a blue jet-like flame is observed. The flame and hot particles produced with a boron carbon powder in air and in vacuum are shown in Figure 12. Spectra of the carbon and boron flames in air are shown in Figure 13 with the main features

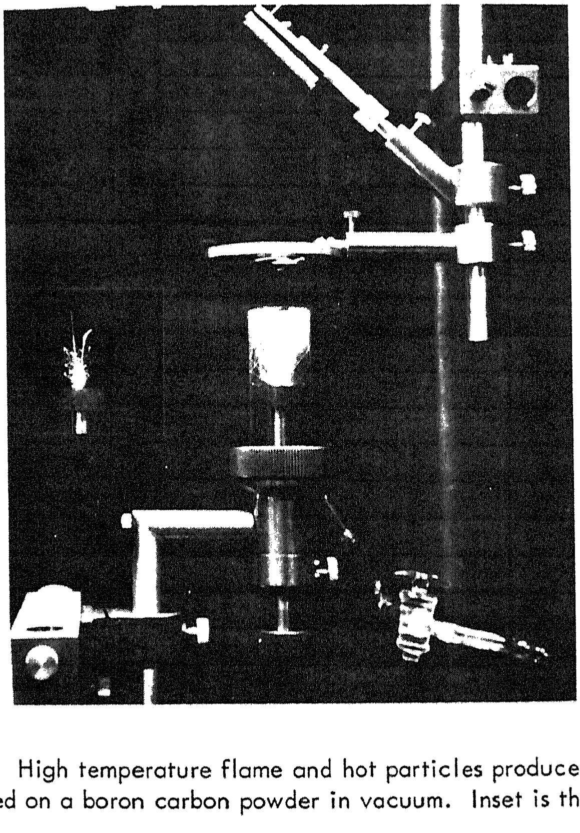

Figure 12. High temperature flame and hot particles produced by a maser beam focussed on a boron carbon powder in vacuum. Inset is the flame in air.

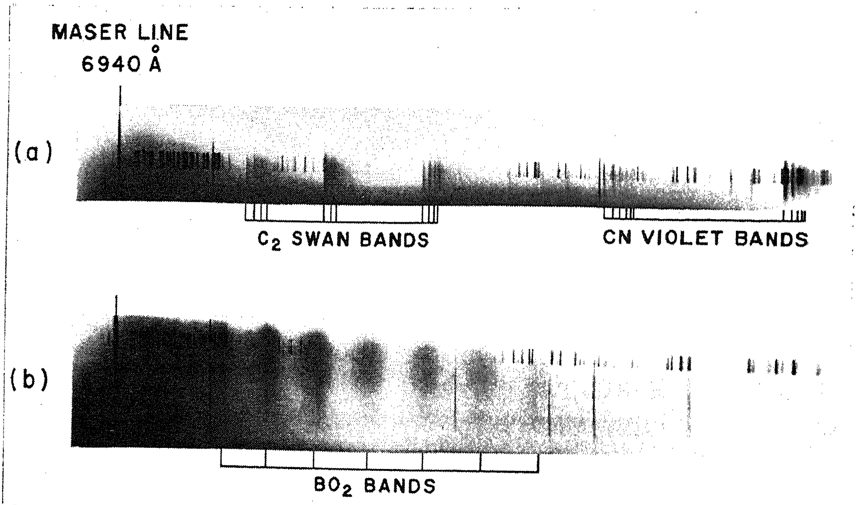

Figure 13. Flame spectra in air produced by a maser beam focussed on (a) a carbon surface, and (b) on boron powder. Two maser pulses were used to obtain each of the spectra on Kodak IF plates with a small Hilger spectrograph.

identified as molecular bands of C_2, CN and the "fluctuation bands" of BO_2. Many atomic lines of various impurities are observed as well as strong continua in some regions of the spectrum.

Experiments with flames produced in this way may be useful in investigations of the spectra of ions, free radicals and various molecules. Time-resolved spectroscopy would be helpful in kinetic studies in these explosive flames and it would be useful to determine the vibrational and rotational temperatures of molecular species excited in this way. Both emission and absorption spectra of the flames can be obtained and the region of observation can easily be extended to the vacuum ultraviolet region. This technique of obtaining high temperatures may also be a useful source of atomic and molecular species for investigation by mass spectrometry.

In conclusion, it may be mentioned that while only a few of the potential spectroscopic applications of the ruby maser have been discussed here, clearly many spectroscopic applications are anticipated and new developments will be awaited with great interest.

ACKNOWLEDGEMENTS

I am indebted to Mr. E. Pfitzer for valuable technical assistance during the course of the investigations reported here: to

Dr. S. Singh for collaboration in obtaining the fluorescence spectra and to Mr. D. R. Taylor and Mr. R. K. Carnegie for assistance in photographing spectra of the maser emission and of the high temperature flames.

REFERENCES

1. A. L. Schawlow and C. H. Townes, Phys. Rev. 112, 1940 (1958).
2. T. H. Maiman, Nature 187, 493 (1960); T. H. Maiman, R. H. Hoskins, I. J. D'Haenens, C. K. Asawa and V. Evtuhov, Phys. Rev. 123, 1151 (1961); R. J. Collins, D. F. Nelson, A. L. Schawlow, W. Bond, C. G. B. Garrett and W. Kaiser, Phys. Rev. Letters 5, 303 (1960).
3. A. Javan, W. R. Bennett and D. R. Herriott, Phys. Rev. Letters 6, 106 (1961).
4. A. Javan, E. A. Ballik and W. L. Bond, J. Opt. Soc. Amer. 52, 96 (1962).
5. B. J. McMurtry and A. E. Siegman, Appl. Optics 1, 51 (1962).
6. G. R. Hanes and B. P. Stoicheff, J. Opt. Soc. Amer. 52, 595 (TD15) (1962): Nature 195, 587 (1962): to be published.
7. E. Snitzer, Phys. Rev. Letters, 7, 444 (1962).
8. F. J. McClung and R. W. Hellwarth, J. Appl. Phys. 33, 828 (1962).
9. I. D. Abella and H. Z. Cummins, J. Appl. Phys. 32, 1177 (1961).
10. S. P. S. Porto and D. L. Wood, J. Opt. Soc. Amer. 52, 251 (1962).
11. W. Kaiser and C. G. B. Garrett, Phys. Rev. Letters 7, 229 (1961); D. A. Kleinman, Phys. Rev. 125, 87 (1962); R. Braunstein, Phys. Rev. 125, 475 (1962).
12. P. A. Franken, A. E. Hill, C. W. Peters and G. Weinreich, Phys. Rev. Letters 7, 118 (1961); P. D. Maker, R. W. Terhune, M. Nisenoff and C. M. Savage, Phys. Rev. Letters 8, 21 (1962); J. A. Giordmaine, Phys. Rev. Letters 8, 19 (1962); R. W. Terhune, P. D. Maker and C. M. Savage, Phys. Rev. Letters 8, 404 (1962).
13. M. Bass, P. A. Franken, A. E. Hill, C. W. Peters and G. Weinreich, Phys. Rev. Letters 8, 18 (1962).
14. E. H. Carlson and G. H. Dieke, J. Chem. Phys. 34, 1602 (1961).
15. A. T. Forrester, J. Opt. Soc. Amer. 51, 253 (1961).
16. C. H. Townes, in Advances in Quantum Electronics (J. R. Singer ed.) Columbia University Press, N. Y., p. 3, 1961.

THE RUBY OPTICAL MASER AS A RAMAN SOURCE

S. P. S. Porto
Bell Telephone Laboratories, Incorporated
Murray Hill, New Jersey, U. S. A.

The use of the ruby optical maser as a Raman source has been recently described by Porto and Wood [1].

Figure 1 gives the experimental arrangement used in their work. The exciting lamp is a GE FT524 or a 4H4-T Kemlite flash lamp, operated by a 4000 V, 400 μfarad power supply. The ruby rod, R, of 0.05% nominal Cr concentration, is about 5 cm long, 6 mm diameter, flat to 1/5 fringe and parallel to better than 30 sec of arc. The ruby rod was silvered opaque at one end and with 25% reflectance at the other. More recent determinations of the total output of maser light against the reflectance of the light by coated side of the ruby, made for a number of different crystals, show however, that at 77°K a reflectance of 50 to 60% at the light coated side of the ruby gives the maximum maser output. The ruby was kept near 77°K by blowing dry nitrogen through a coil immersed in liquid N_2 and through the tube T in Figure 1; this tube surrounds the ruby and has a few openings that help cool the lamp. The liquid sample was contained in a cylindrical cell coated with reflecting $BaSO_4$ (reflectance of ~98.5%). Light scattered out of the cell was focused on the entrance slit of a high aperture spectrograph built after the design of Bass and Kessler [2]. The spectrum was recorded on a non-sensitized 1N Kodak film, and to obtain the Raman spectrum, exposures consisting of from 16 to 100 flashes were used.

Some of the problems encountered in the successful operation of the ruby optical maser as a Raman source and their solutions are: (a) the wavelength of the ruby optical maser varies as a function of temperature, as shown in Figure 2. Since many flashes had to be integrated into one picture, constancy of the wavelength was important, and this was achieved by operation at, or close to, liquid N_2 temperature. (b) Besides the usually described parallel maser light coming from the ruby, a large number of weak lines

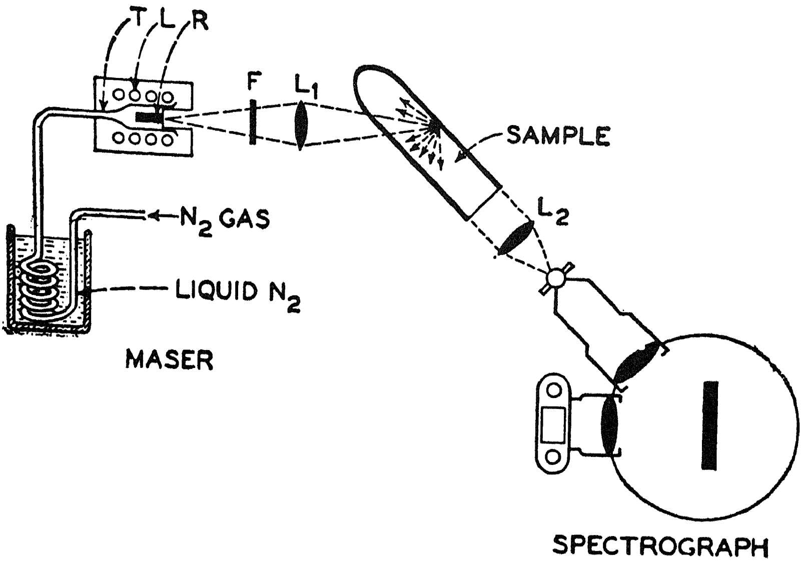

Figure 1. Experimental arrangement.

are observed with intensities comparable to those of the Raman lines, as shown in Figure 3. In the figure, E is the maser line, R is an unfortunate reflection, G is a grating ghost and Xe are Xe flash lamp lines. To avoid this problem the Raman tube should be placed at least 150 cm away from the ruby maser and a number of diaphragms interspaced between the two; since the maser beam is parallel and the weaker incoherent lines fall off as $1/R^2$ a successful filtering is thus accomplished. (c) A fairly large number of flashes is needed to obtain a Raman spectrum. In Porto and Wood's experiments the energy output of the maser was estimated to be less than 0.5 joules, and thus the Raman spectra in their experiments were obtained with less than 50 joules. At present, however, there are commercial units that have energy outputs of 30 to 70 joules, so, good Raman spectra should be obtainable with a single flash. (d) A further problem appears when one thinks of using the optical maser source to obtain high resolution Raman spectra. Some applications here would be the observation of rotational spectra in gases or of Brilloium bands in solids. When the maser is pumped well above threshold, many modes of oscillations are excited, with frequencies extending throughout the emission line utilized. In the case of vibrational Raman effect and other relatively low resolution work, this is not as important however, since at 77°K ruby maser lines about 0.1 or 0.2 cm^{-1} wide can be obtained even well above threshold.

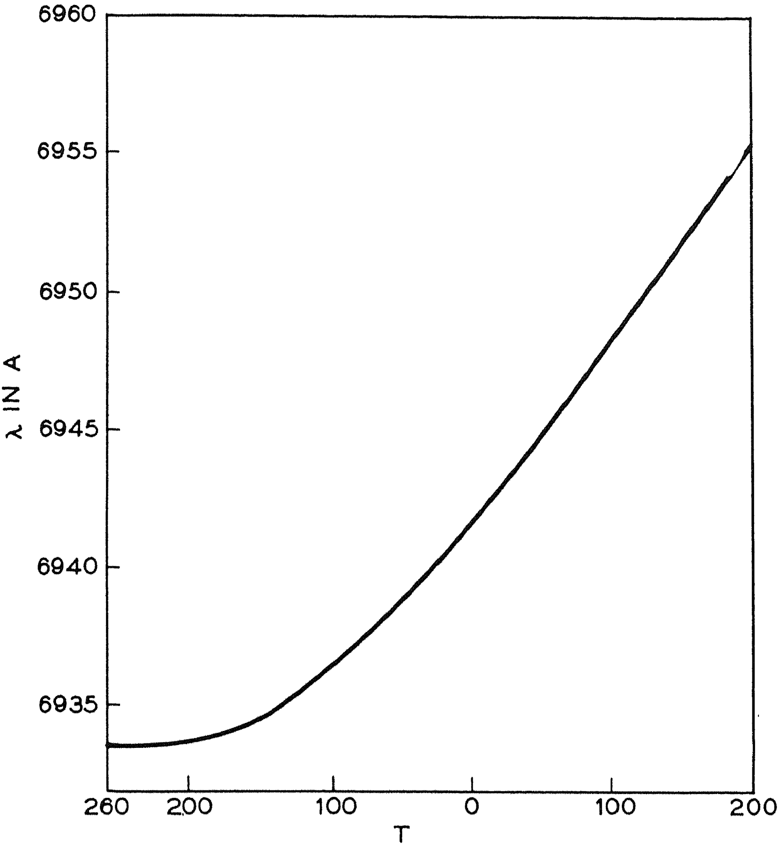

Figure 2. Variation of the ruby maser wavelength as function of the ruby temperature.

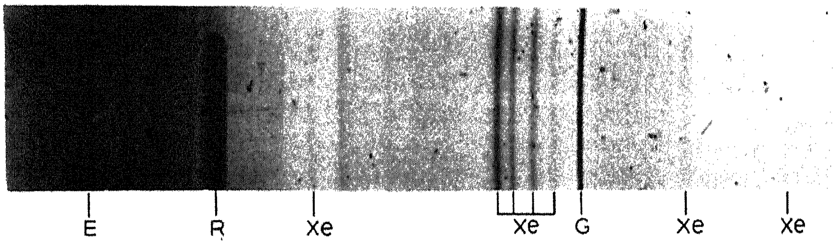

Figure 3. Output spectrum of a ruby maser showing the unwanted radiation and some Xe lines due to the flash lamp.

Figure 4 shows Raman spectra of C_6H_6 and CCl_4 as obtained by Porto and Wood. The CCl_4 spectrum shows essentially all the lines expected while in the C_6H_6 spectrum the 3050 cm^{-1} band is

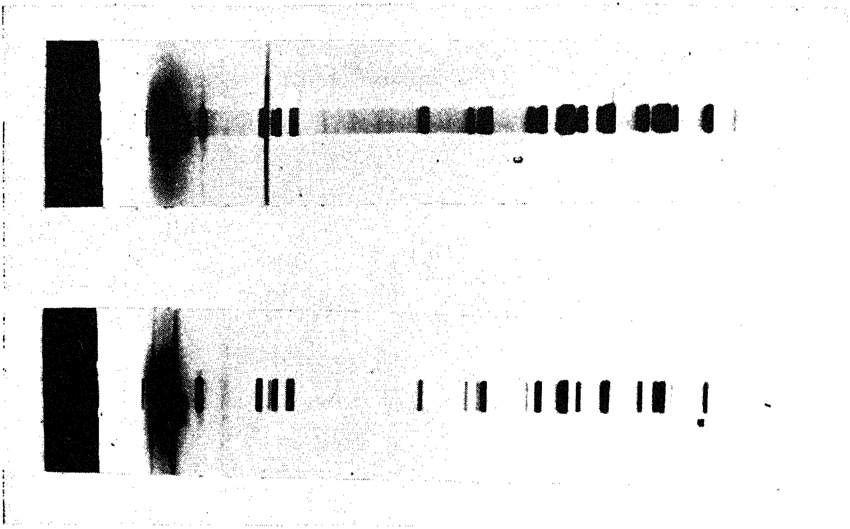

Figure 4. (a) Raman effect of C_6H_6 with a comparison Ne spectrum.
(b) Raman effect of CCl_4 with a comparison Ne spectrum.

missing. This is due to the sharp decrease in sensitivity of the film about 8800A. In both pictures the maser frequency has been absorbed by a small mask on the photographic plate.

REFERENCES

1. S. P. S. Porto and D. L. Wood, J. Opt. Soc. Am. 52, 251, 1962.
2. A. M. Bass and R. G. Kessler, J. Opt. Soc. Am. 49, 1223, 1959.

THE EMISSION MODE PATTERNS OF RUBY LASERS

E. S. Dayhoff
U. S. Naval Ordnance Laboratory,
White Oak, Silver Spring, Maryland, U.S.A.

INTRODUCTION

Rubies used as lasers in the conventional way usually exhibit a spiking phenomenon. The electromagnetic oscillations relax in a period of about a microsecond and recur in a random time sequence until the pumping is ended. In order to observe directly the nature of the modes of oscillation during these short time intervals we employed high-speed photography techniques [1]. The nature of these modes has implications for laser spectroscopy since presumably each fundamental mode will have both a distinct frequency and a distinct transverse pattern in the photographs.

In Figure 1 we show a cylindrical ruby crystal with an internal cylindrical section forming an active "filament." A standing wave in the z-direction is shown schematically and also a schematic transverse mode pattern of emitting patches on the upper face. A change of one in the number of standing half-waves in the z-direction produces a change of frequency as illustrated on the frequency plot. Changes in the transverse mode distribution cause a relatively smaller change in mode frequency. It would appear that for typical crystals approximately 10 to 100 longitudinal modes will fall within the amplification band of the ruby, and a very large number of transverse mode patterns should be possible. These may occur in simultaneous or sequential combinations associated with a multiplicity of emitted frequencies. Many kinds of perturbing influences arising from imperfections in the crystal may be present making it difficult to predict such things as the transverse mode patterns. We wish to study what these are by observational means.

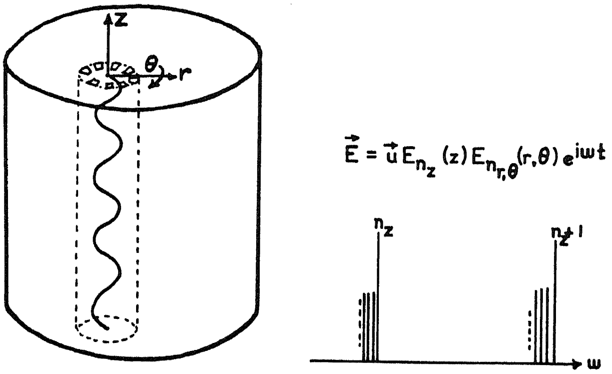
z
θ
r
$\vec{E} = \vec{u} E_{n_z}(z) E_{n_{r,\theta}}(r,\theta) e^{i\omega t}$
n_z
n_z+1
ω

Figure 1. Fabry-Perot laser crystal with active region or "filament" supporting a standing wave mode, together with a plot of mode frequencies.

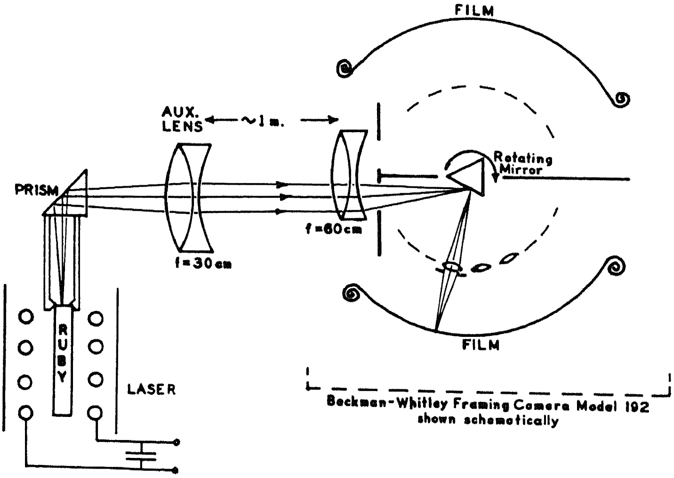

Figure 2. Arrangement of experimental apparatus. Sometimes a Wollaston prism was used also near the output end of the laser.

APPARATUS

In Figure 2 we see the general arrangement of our camera and laser. The camera is a Beckman-Whitley Model 192 [2]. Shuttering is accomplished by means of a turbine driven triangular mirror and a stationary film. Frames are ordinarily taken at a standard rate of 500,000 per second or one every two microseconds for a total of 82 frames. Each frame is exposed for about 2/3 microsecond. The camera is actually dual, each half taking one-half of the frames through its own entrance pupil. This factor complicates the aiming of the laser and often results in shading of the pictures. The camera cannot be synchronized with the laser output spikes so some frames are expected to be blank. No auxiliary shutter was used to cut off the light after one revolution of the mirror so we depended upon the termination of the laser pulse train to avoid doubly exposing the film. The laser is pumped by means of a spiral flash tube with MgO reflector in order to provide as uniform a pumping light distribution as possible. All of the crystals we will show are of 0.04 to 0.05% Cr ruby 1/4 inch in diameter and 2 inches long and Fabry-Perot geometry unless otherwise stated.

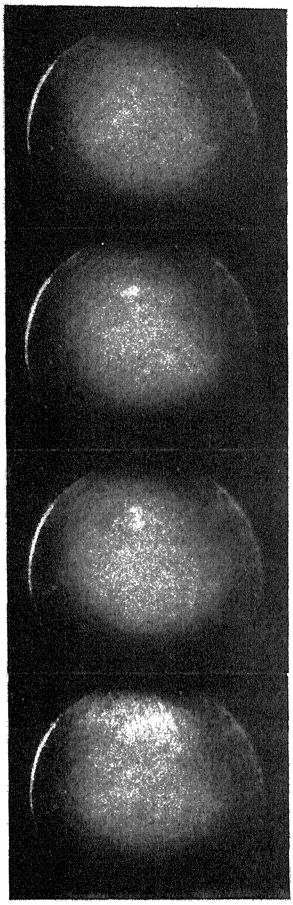

Figure 3. Four successive frames of near field pattern of lasing ruby T 1. Camera focussed on end of crystal. Time advances downward. The bright crescent is caused by a leakage of pumping light. Pump power near threshold. Standard framing rate of 500,000 per second.

OBSERVATIONS

Fabry-Perot Crystals

In Figure 3 we see the end of a ruby which was cut with an angle of 90° between the crystalline axis and the rod axis. It had multiple layer dielectric coatings of high reflectivity on both ends. One part appeared to be more active than the rest and produced a number of fan-like patterns of high symmetry. The rest of the face produced a large number of randomly scattered small spots which flash on and off with the active spot. In this firm strip, the laser output from a substantial part of the crystal face was cut off by aperture shadowing.

In Figure 4 we see another crystal from the same source and having the same orientation. This crystal had a substantially lower threshold than the first. Its most active region seemed to prefer to form more of a straight line array of spots rather than an arc or fan arrangement. It also produced many small random spots simultaneously with the main pattern. At higher pump powers there was a tendency for the random spot pattern to

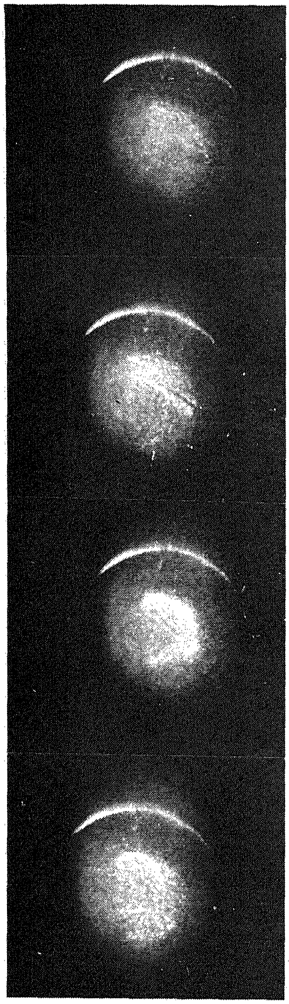

Figure 4. Four successive frames of near field pattern of ruby T 2. Conditions same as for figure 3; pump power is 1.09 times threshold.

aggregate into long bars with a somewhat defocussed appearance to which we have applied the descriptive word "cloudy." This kind of pattern is apparently not accompanied by the geometrical type and may represent a sort of merger of the two.

Figure 5 shows a ruby with the crystalline axis cut parallel to the rod axis and the cylindrical surface left rough ground rather than polished. This particular crystal was studied by Atwood, Adams, Dueker and Gratz [3] and found to have a high anisotropic light scattering power. In these pictures we have used a Wollaston prism to produce separate images for the two polarizations. The active region is in the center of the crystal. It seems to be rather small and produces fairly distinctive geometrical patterns which are often different in detail for the two polarizations. Thus each polarization has its own characteristic mode going at the same time and in the same region of the crystal. In addition, we see in many frames streamers of light with interference bands which lead away from the central region toward the sides, but only in certain directions. The anisotropic distribution seems to suggest that these streamers are associated with the scattering processes within the crystal and are most prominent when the central mode seems strongest.

In Figure 6 we see another crystal having exceptionally low optical scattering power according to Atwood et al [3]. Other properties are the same as for Figure 5. The mode distribution is entirely different, however, having principally a large centrally located region comprising about 2/3 the area of the crystal, broken up into fairly large patches arranged in somewhat irregular whirls and patterns with a rather uniform light intensity. Around this large region there appears to be relatively little light. Conspicuously absent are the streaks leading toward the edge as

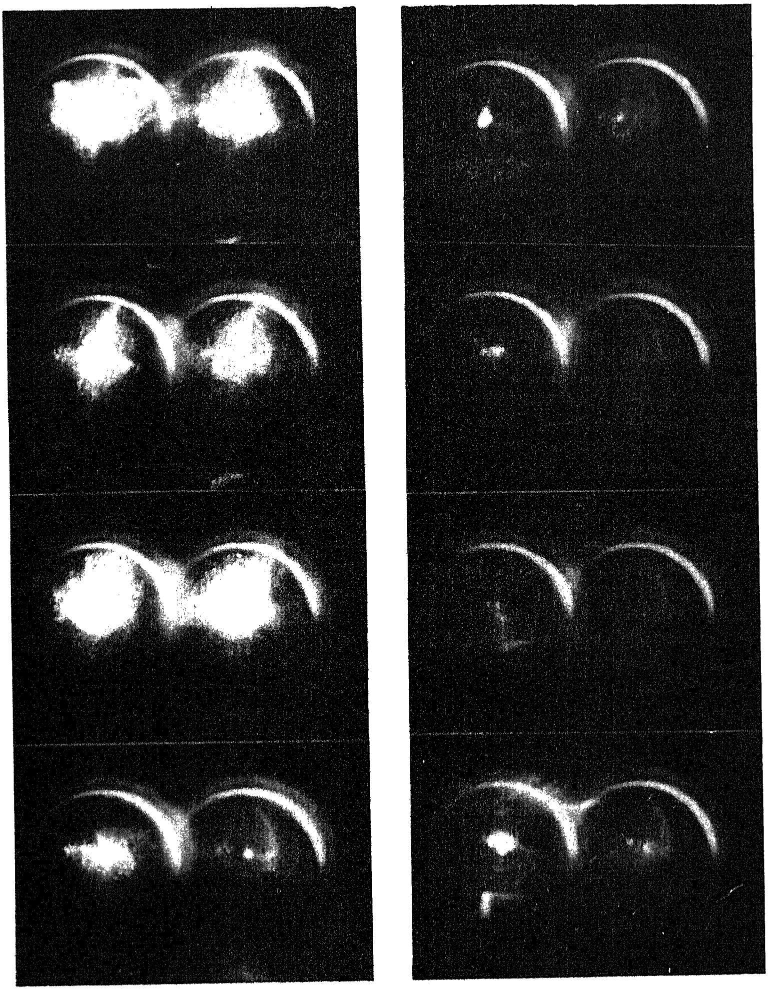

Figure 5. Eight successive frames of near field pattern of ruby PE 200. Pumping energy was 1.13 times threshold. Standard framing rate.

with the last crystal. There are differences in patterns for the two polarizations. This crystal had almost the same threshold as the one of Figure 5.

In Figure 7 we see some far field patterns produced by a ruby with high scattering power. To obtain these photographs the camera is focussed at infinity so the pattern appearing on the film is the angular spectrum of rays from the crystal. Due to aiming errors we do not see the center of the pattern. This crystal produces many small randomly distributed spots which extend to rather large angles, as far as several degrees from the beam center. We also notice that a certain clumping of these

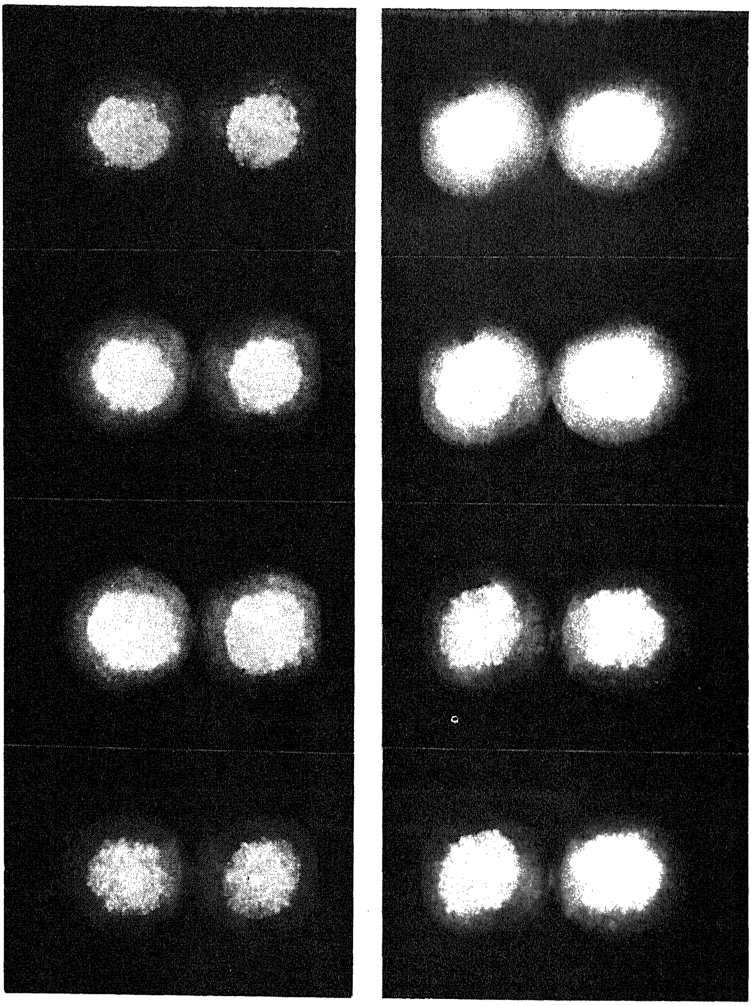

Figure 6. Eight successive frames of near field pattern of ruby PE 189. Pumping energy was 1.13 times threshold. Standard framing rate.

spots into rings occurs which appear to be the diffraction rings corresponding to the edge of the crystal face which acts as an aperture for the light emitted from the crystal.* Since it seems evident that the small random spots in the diffraction pattern correspond to the small random spots in the source, the presence of the diffraction ring modulation in the far field patterns is evidence that there is a considerable coherence to the light coming from the small random spots on the ruby face. The crystal of Figure 7(b) appears to have less internal scattering than the one of Figure 7(a).

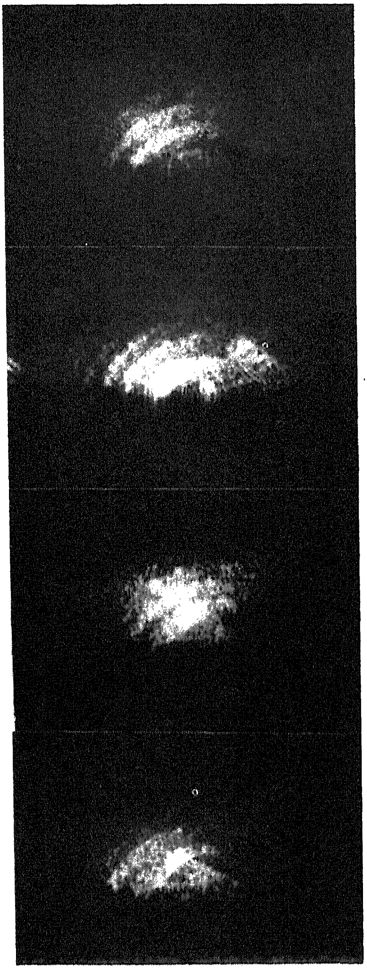

7a

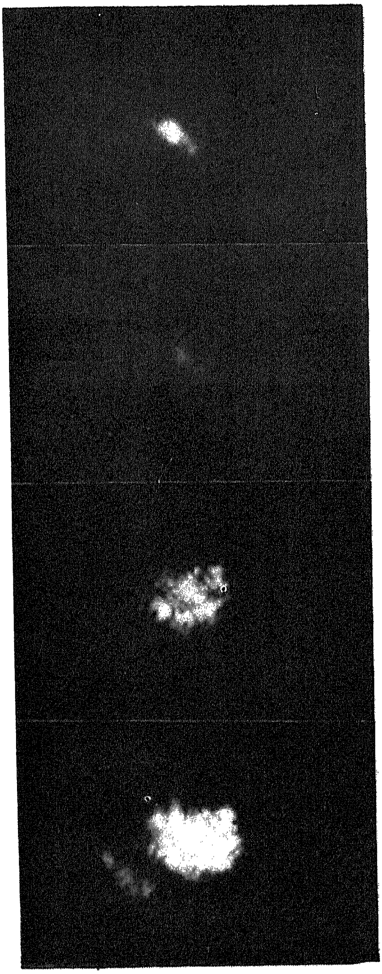

7b

Figure 7a. Four successive frames of far field pattern of ruby PE 196, a ruby of fairly high scattering power, producing near field patterns of a character similar to Figure 5. Pumping energy was 1.47 times threshold. Aperture vignetting effects are very severe in this figure, resulting in center and upper half of pattern being lost but ring structure is quite visible. Standard framing rate.

Figure 7b. Four successive frames of far field pattern of ruby PE 199, a ruby of moderately low scattering power. Pumping energy was 1.03 times threshold. Relatively simple patterns of small angular spread are typical of near threshold operation even with crystals of high scattering power. Vignetting effects in these frames are relatively unimportant. Standard framing rate.

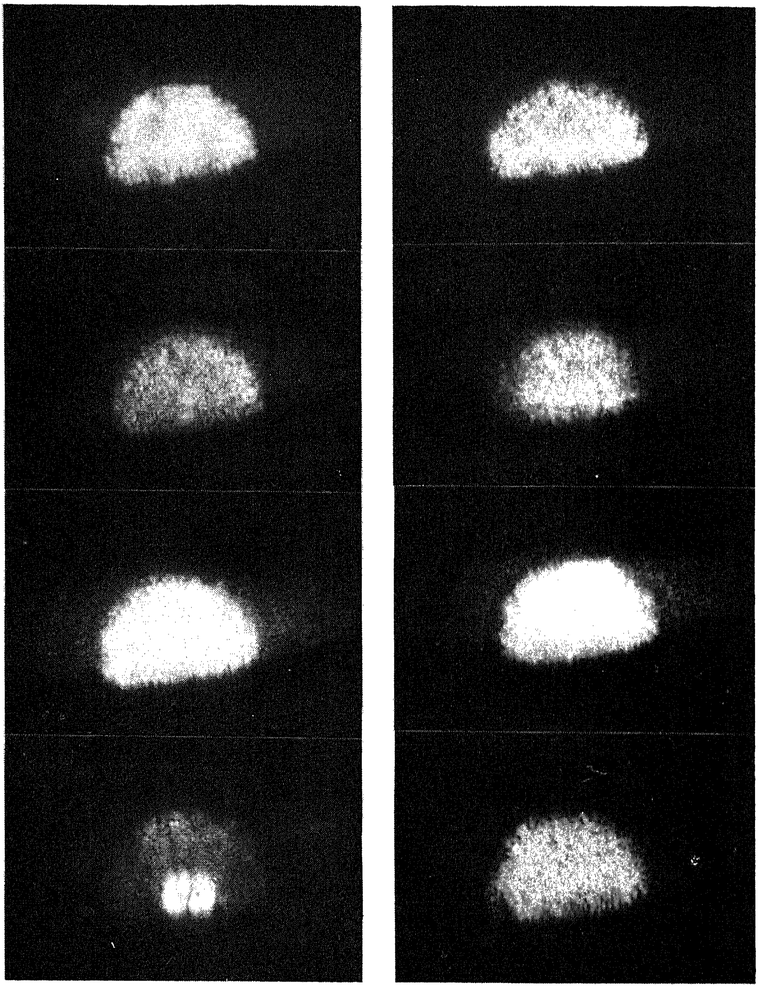

Figure 8. Eight successive far field frames of ruby PE 189. Pumping energy was 1.13 times threshold. Vignetting effects result in loss of lower part of image and also a portion near the top. Standard framing rate.

In Figure 8 we see some far field patterns produced by the crystal of Figure 6 having very low optical scattering. We see that the higher angle random spot patterns with ring modulation are weak. The cone which contains strong light is fairly uniformly illuminated and shows a fine grained pattern of fairly random spots. A geometrical pattern is occasionally superimposed, which must be the Fraunhofer diffraction pattern of a geometrical source mode. Although this crystal is said to be one having relatively low optical scattering, it is evident that its laser output is still strongly affected by scattering. It does, however,

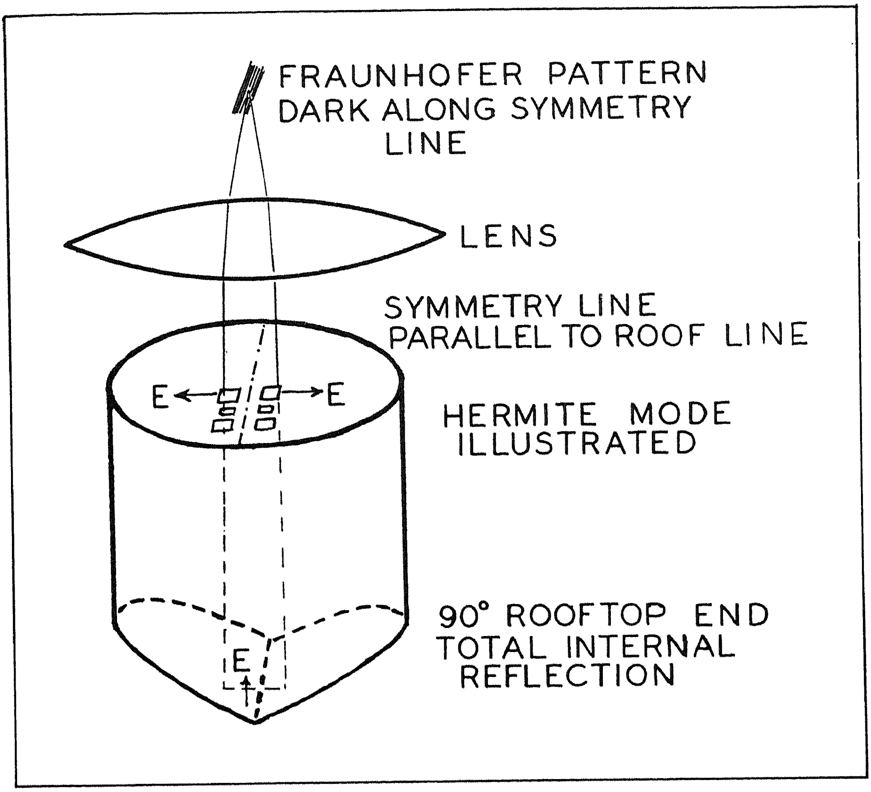

Figure 9. Geometry of "rooftop" total internal reflection crystal designated PE 141. The flat end has a high reflectivity dielectric coating.

come closer to operating as a single unit than the other crystals studied.

Rooftop Crystal

This crystal (Figure 9) has been cut with a 60° angle between its crystalline axis and the rod axis and consequently emits polarized light. One end is flat with dielectric reflective coating and the other was cut with a 90° dihedral angle like a rooftop so it is effectively 100% reflective. Note the phase reversal of the electric field component of the ray shown. Figure 10 shows the source patterns which were observed from this crystal. Some obvious features are as follows: There is a line of symmetry for most of the patterns. This line is the projection of the dihedral angle line. An active area lies on this line in this crystal. The patterns produced in this active area are always symmetrical about the line of symmetry and are always dark right on the line.

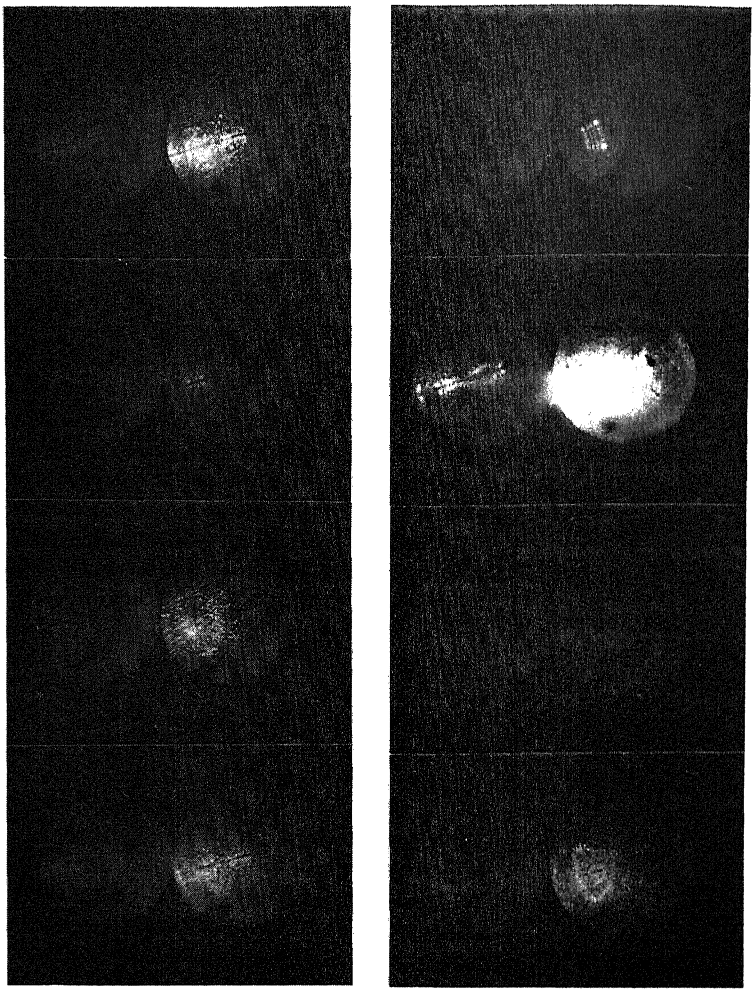

Figure 10. Eight successive near field patterns produced by ruby PE 141. The Wollaston prism was used in these views, but its axes were not perfectly aligned with the polarization axis, allowing a weak image to form on the left-hand side. Pumping energy was 1.71 times threshold. Standard framing rate.

They sometimes resemble checkerboards that may be somewhat distorted. A very strong difference in character exists between the patterns in the active region and the rest of the crystal where the light is emitted in the form of very many small spots in a quite random array. The small spot patterns show little if any symmetry. In a small percentage of the time a geometrical pattern will be seen in the region normally occupied by the small spots.

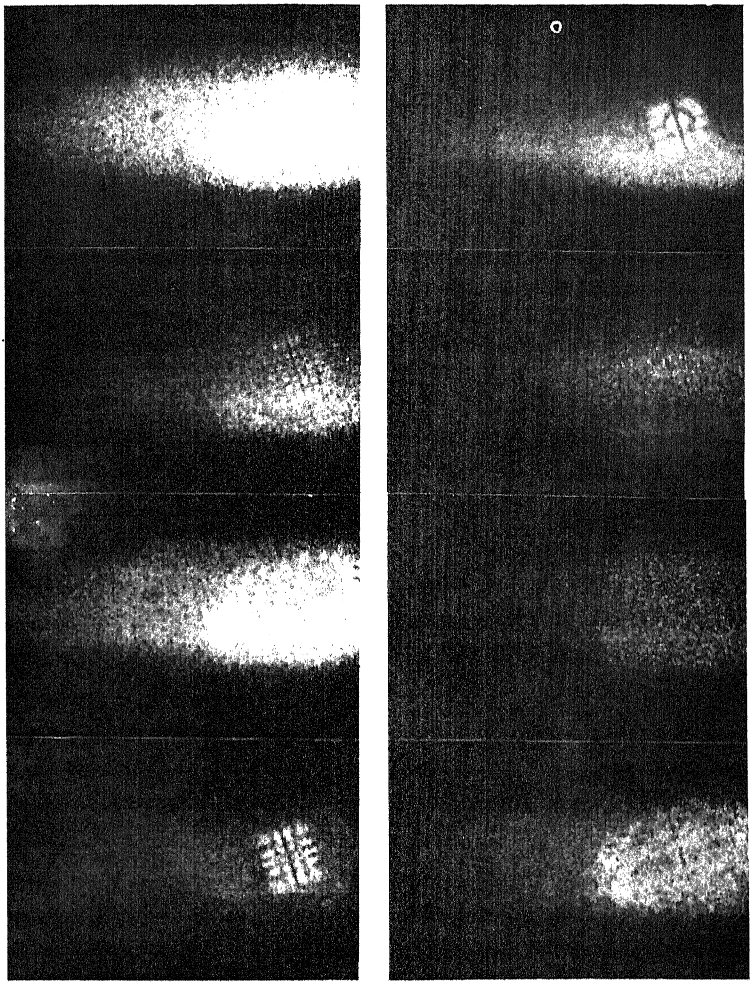

Figure 11. Eight successive views of the far field pattern of ruby PE 141. Pumping energy was 2.11 times threshold. Vignetting effects cause loss of the upper and lower parts of the image while aiming errors caused the center of the pattern to be near the right-hand edge of the picture. Standard framing rate.

Far field pictures of the same crystal (Figure 11) show that the far field pattern also breaks into an outer part with random spot structure obviously correlated with the random spot source pattern and an inner part evidently related to the primary mode patterns in the active area. The primary mode diffraction pattern always has a line of symmetry and the symmetry line always shows as a narrow dark line. From this we conclude that the source distribution producing this is highly coherent and has opposite phase on the two sides of the symmetry line. The black symmetry line usually does not extend far into the random spot region, if at all, showing that their mechanism of production is basically different.

INTERPRETATION

In Figure 12 we illustrate in a schematic way the sorts of common crystal defects that are significant. On the left is a typified end view of a crystal in which the optical path between ends varies from point-to-point. Such variations may occur because the ends are not ground truly flat and parallel or because the index of refraction of the crystal contains irregular gradients on a scale comparable to the crystal dimensions. On the right-hand side we illustrate striae, that is, thin threadlike regions crossing the crystal at various places having a refractive index gradient able to cause a small angle deflection of rays intersecting the stria. Such striae are quite numerous in ordinary rubies, perhaps thousands per square centimeter, may form families by having preferred directions in the crystal, and may tend to lie one on top of the other when viewed along the rod axis in certain regions.

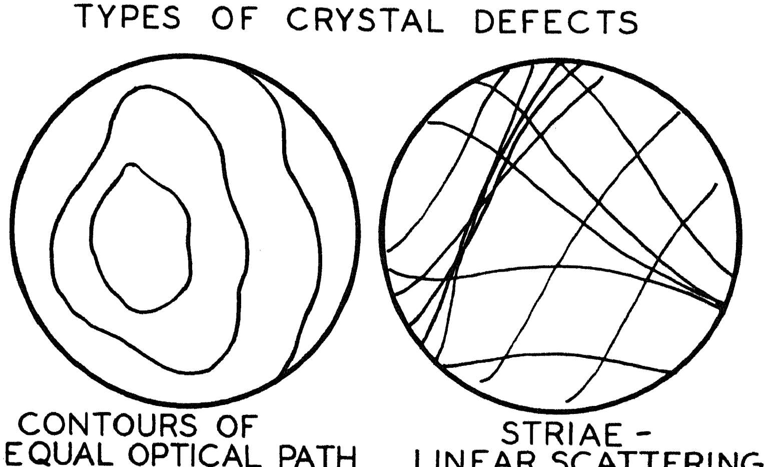
TYPES OF CRYSTAL DEFECTS
CONTOURS OF EQUAL OPTICAL PATH BETWEEN ENDS
STRIAE - LINEAR SCATTERING REGIONS

Figure 12. Illustration of two significant classes of laser crystal defects.

In Figure 13 we illustrate the effect that one would expect this structure to have on the laser oscillation. The small angle scattering centers are represented here by small prisms scattered through the crystal. A region which for some reason is

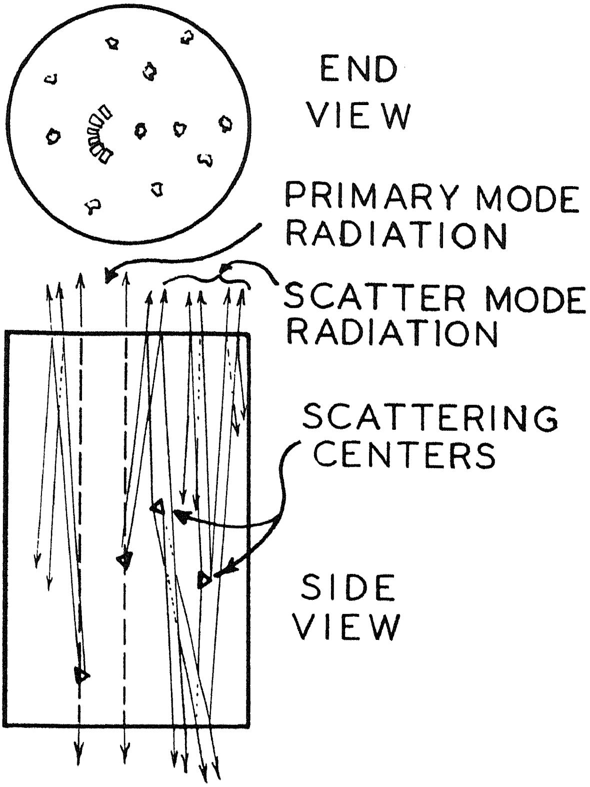

Figure 13. Cylindrical laser rod showing manner in which an active "filament" may excite surrounding parts of crystal via scattered rays.

more active than the rest has begun oscillating in a characteristic mode. The nature of this mode is controlled by geometry and large-scale gradients in the crystal; also some dynamic induced factors may enter. Having started into a primary oscillation mode, some scattering centers intersecting this mode will deflect some rays of light into the surrounding parts of the crystal. Only a very small angle of deflection is involved in each scattering, but as the ray progresses through the crystal, being amplified as it goes, it intersects more scattering centers and is both split and deflected. A large number of such splits and deflections can occur, so the angle which the emitted light rays make with the crystal axis can be much greater than the angle of a single scattering event. In general these scattered beams will not close back on themselves, although occasionally a secondary self regenerative mode may form in the crystal driven by the primary mode.

In Figure 14 we show the way in which the source pattern is related to the far field pattern. The primary mode produces a Fraunhofer pattern by itself. In addition, the scattered beams being small in cross section illuminate a fairly large area of the focal plane and, having an essential phase coherence with each other, produce interference bands in the focal plane. In the Figure 14, two such source areas Q_1 and Q_2 are pictured as illuminating an area around P. Since there are so many randomly placed source spots, the interference bands produced by the various pairs of source points will be randomly superimposed and the net result is that the illumination in the focal plane is itself broken into irregular small spots. The small size of these, that is the small angular spread they represent, is an indication that there is a considerable degree of phase coherence among

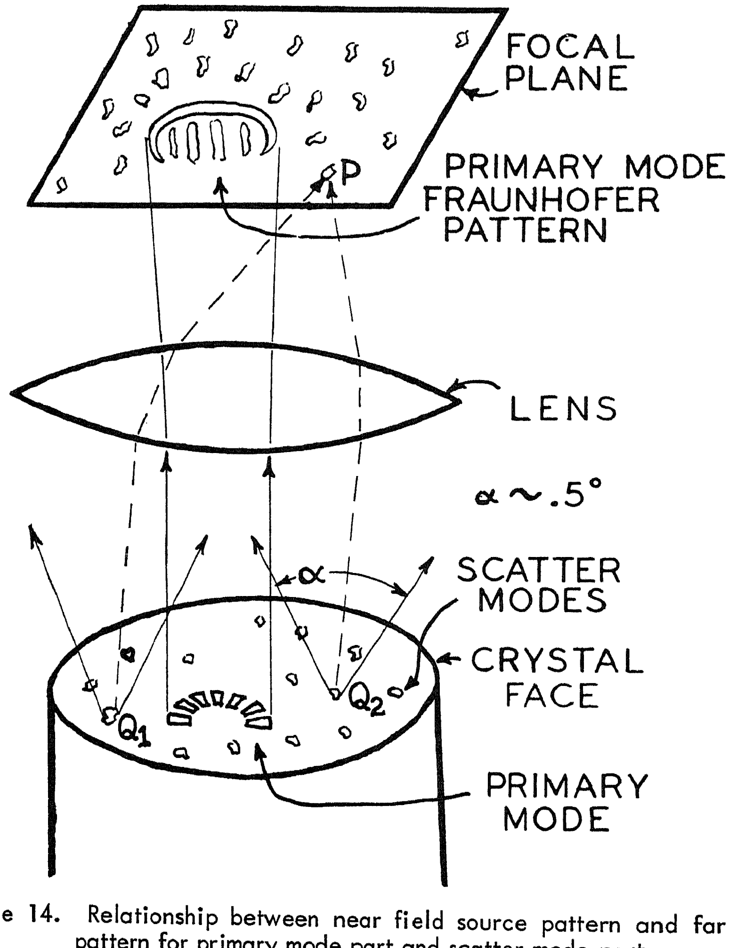

Figure 14. Relationship between near field source pattern and far field pattern for primary mode part and scatter mode part.

source spots that are separated by relatively large distances. Thus, we seem to have evidence of a sort of incomplete coherence where the crystal radiates a wave front of perhaps highly irregular shape but nevertheless a shape which changes but little over many cycles of oscillation.

CONCLUSIONS

From the processes and data described above, one expects the following significant characteristics:

1. In each light spike of about a microsecond duration, the entire crystal generally becomes emissive with a pattern of small spots, excepting when near threshold excitation is used.
2. The pattern appearing on the crystal face often consists of an identifiable primary mode part and a scatter part.
3. The divergence of the beam is considerably greater than the diffraction pattern which any recognizable primary pattern structure would suggest and is greater than would result from single event scattering in the crystal.
4. Although the scattered beams emerge from the crystal at quasi-random places, a phase relation exists between their phase on emergence and the phase of the primary mode; therefore the far field pattern resulting from them shows some effects of coherence over a scale comparable to the dimensions of the crystal face.
5. Successive light spikes of the crystal show considerable change in primary patterns and even greater changes in scattered beam patterns; coherence experiments done with light from many spikes are therefore expected to indicate a lesser apparent transverse coherence range than single flashes would provide.
6. There is a considerable difference from one specimen to another due to the many ways in which the striae can be oriented and stacked.

In addition, it is predicted from our model that only frequencies present in the primary mode will be present in the scattered beams.

We believe that these results are typical of ordinary ruby crystals, that is those having highly reflective end coatings, Fabry-Perot geometry and operated at room temperature with spiral tube pumping. (We have recently photographed a grossly different crystal, however. It had no reflective coating on one end, operated at liquid nitrogen temperature, and had very high output power. It was found to operate continuously without spiking and its source pattern was simply a fuzzy disk.)

SUMMARY AND ACKNOWLEDGEMENTS

In summary, we have shown the nature of the laser oscillations in a common form of ruby laser on a variety of crystal specimens by means of high-speed photography and have described an interpretation in terms of crystal imperfections.

The author wishes to express thanks to J. G. Atwood of the Perkin Elmer Corporation, to S. Kass of the Raytheon Company, and to P. Leavy, formerly of the Trident Corporation, for useful discussions and the loan of several interesting crystals. The photographs were made by B. V. Kessler of the U. S. Naval Ordnance Laboratory.

REFERENCES

1. E. S. Dayhoff, Proc. IRE 50, 1684 (1962).
2. M. C. Kurtz, J. of the SMPTE 68, 16 (1959).
3. J. G. Atwood, N. I. Adams, G. W. Dueker, W. Gratz, Optical Society of America, Washington, D. C., March 1962, paper TD-17.

---

*Note added in proof: The part of this statement about the rings being related to the edge of the crystal face is incorrect.

RECENT DEVELOPMENTS IN INFRARED REFLECTION SPECTROSCOPY ATTENUATED TOTAL REFLECTION

J. Fahrenfort
Koninklijke/Shell-Laboratorium
Amsterdam, Netherlands
(Shell Internationale Research Maatschappij N.V.)

SUMMARY

A survey is given of the reflection method in general and of the methods for determining the optical constants from reflection spectra.

The possibility of increasing sensitivity by the use of attenuated total reflection is demonstrated and the experimental technique is described, including double-beam operation and multiple reflection. Application of this technique for routine and for fundamental analysis is indicated. For the latter, a method based on experiments at two angles of incidence is preferred over application of the Kramers-Kronig relations. From an error analysis, the experimental two-angle procedure giving highest accuracy is derived.

INTRODUCTION

We know from everyday experience that a beam of electro magnetic radiation falling onto a flat surface of a dense medium splits into a reflected and a refracted beam.

The intensity of the two waves, as well as other features such as amplitude and phase, are determined by the specific optical properties of the medium. Information on these optical properties is thus carried by both waves, and for studying the material we can make use either of the reflected, or of the refracted (transmitted) wave.

The general preference in infrared spectroscopy for the transmission technique has primarily been due to two circumstances. One is the complexity of the relations between molecular properties and the intensity of reflected light; the other is the lack of detail and intensity in the reflection spectra of many materials, including practically all organic compounds.

By the recent development of a comparatively simple computing method the first of these factors has lost much of its importance, while that of the second factor is greatly reduced by the introduction of a special reflection technique giving detailed information on organic compounds as well. Thus the scope of infrared reflection spectroscopy now overlaps that of transmission to a considerable extent and the choice between the two independent techniques will largely depend on special features of the problem to be investigated.

The reflection technique has definite advantages in giving results essentially independent on sample thickness, and in making use of only one single characteristic phenomenon. In transmission on the other hand, always a superposition is measured of absorption and reflection, while sample thickness plays an essential role. Therefore reflection experiments are often to be preferred in any of the following cases:

1. the sample is strongly absorbing;
2. the sample resists preparation in a thin layer;
3. the sample is characteristic only in a thick layer;
4. the sample is only available fixed on a non-transparent support.

Reflection spectra can be used for quantitative purposes just as in transmission, either by calibration or by calculation. Before we turn to these possibilities, however, we will first review the theoretical relations between characteristic reflection and molecular constants.

THE RELATION BETWEEN REFLECTION AND ABSORPTION

By a combination of the formulae of Fresnel and of Snellius, which follow directly from electro-magnetic theory, expressions can be found for the reflecting power of a flat surface of a medium of refractive index n', illuminated by a parallel beam of unit intensity at an angle of incidence θ.

For a beam, polarized perpendicularly to the plane of incidence, we find for the reflecting power, R_s:

$$R_s = \left| \frac{1 - N_s}{1 + N_s} \right|^2, \tag{1}$$

where:

$$N_s = \frac{\left(n'^2 - \sin^2 \theta\right)^{1/2}}{\cos \theta} \tag{1a}$$

For a beam polarized in the plane of incidence we have

$$R_p = R_s \left| \frac{1 - N_p}{1 + N_p} \right|^2 , \tag{2}$$

where:

$$N_p = \frac{(n'^2 - \sin^2 \theta)^{1/2}}{\sin \theta \tan \theta} . \tag{2a}$$

For a beam of normal incidence at the surface these equations reduce to

$$R = \left| \frac{1 - n'}{1 + n'} \right|^2 . \tag{3}$$

The refractive index n' is in general a complex number and can be written as

$$n' = n - in\kappa . \tag{4}$$

The real part n has the meaning of the ratio between the velocity of light in the two media adjacent to the reflecting interface. The imaginary part $n\kappa$, being the product of the two optical constants, is related to the damping of the amplitude of the light wave in the second medium, and is connected to the absorption coefficient α of Lamberts law by

$$\alpha = \frac{4\pi n \kappa}{\lambda} . \tag{5}$$

Therefore the determination of the optical constants n and κ from reflection is equivalent to the determination of α from transmission.

The relation between the complex refractive index and the properties of the oscillators in the medium is given by dispersion theory.

In a harmonic approximation, n' may be expressed by the dispersion formula

$$n'^2 = n_o^2 + \frac{\rho_j}{\nu_j^2 - \nu^2 + i\gamma\nu} , \tag{6}$$

where ν_j is the resonant frequency of the j^{th} type of oscillator in the medium, n_o is the refractive index in the region of the j^{th} band due to all other absorption bands, γ is the damping constant related to the relaxation time of the j th vibration and ρ_j is the effective oscillator strength. For an isotropic medium ρ_j is related to the matrix element $|R_j|$ of the dipole moment of the j th transition by

$$\rho_j = \left(\frac{n_o^2 + 2}{3}\right)^2 \frac{8}{3} \frac{N \pi \nu_j}{h} \left| R_j \right|^2 , \tag{7}$$

N being the number of oscillators per cm³. Splitting Eq. (6) into its components, and multiplying the imaginary part with ν, we obtain:

$$2n^2 \kappa \nu = \frac{\rho_j \gamma \nu^2}{\left(\nu_j^2 - \nu^2\right)^2 + \gamma^2 \nu^2} . \tag{8}$$

The resonant frequency ν_j is found at the maximum value of (8), γ is given by the half-width of the curve and ρ_j is found either by

$$\rho_j = \gamma (2n^2 \kappa \nu)_{max} \tag{9}$$

or by integrating the curve. For an isolated band we have

$$\int_0^\infty 2n^2 \kappa \nu d\nu = \frac{\pi}{2} \rho_j , \tag{10}$$

but also, if we assume that n varies so little over the band that it may be brought outside the integral [1]:

$$\int_0^\infty 2n^2 \kappa \nu d\nu = \frac{1}{2\pi} \int_0^\infty n \alpha d\nu = \frac{1}{2\pi} \bar{n} A_i , \tag{11}$$

A_i being the integrated absorption coefficient, and $\bar{n}$ representing the mean refractive index. From (10) and (11) it is seen that a determination of ρ_j is equivalent to a determination of the integrated absorption, and that it can be made from the knowledge of the optical constants through the band. For dense media the reflection method leads more directly to the transition moment $|R_j|$ as n_o and $\bar{n}$ are immediately available.

THE METHODS FOR DETERMINING n AND κ FROM REFLECTION SPECTRA

The derivation of fundamental data from reflection spectra proceeds via the optical constants.

With two constants to be determined, in any case two independent equations involving them must be available. For the two cases of experiments carried out with oblique - or with normal incidence these equations are obtained in different ways.

Oblique Incidence

As reflecting power is given by (1) or (2), we have $R_s = f(n, \kappa, \theta)$ and $R_p = f'(n, \kappa, \theta)$. Therefore we can obtain the two equations needed from either of the following experimental data:

(a) R_s measured at two angles θ_1 and θ_2;
(b) R_p measured at two angles θ_1 and θ_2;
(c) R_s and R_p measured separately at one angle;
(d) R_p/R_s measured at two angles θ_1 and θ_2.

In judging the relative merits of these four methods, we have to consider that for conventional reflection experiments in (a) and (b) the specimen must be accurately replaced by a standard mirror. Method (c) requires in addition a turning of the polarizer, which may introduce an error, if it shifts the beam laterally. The same holds a fortiori for method (d), because there the common reference mirror is omitted, so that polarization effects in the monochromator must also be corrected for. Fore optics suitable for the above-mentioned methods were described by Simon [2] for vertical, and by Fahrenfort [3] for horizontal samples. An accessory for reflection measurements with double-beam spectrometers will be described in section 5B.

For the solution of the optical constants from the two reflectivity data obtained at one frequency, graphical methods were given by Simon [2] for the methods (a), (b) and (c) and by Avery [4] for method (d). These procedures involve precalculated families of curves giving the reflecting power for a large number of n and κ values at a pair of fixed angles of incidence.

For the reflecting power obtained from experiment at each of these angles, a series of possible n-κ combinations is read from the two graphs. These combinations determine two curves in the n-κ plane. The intersection of the curves yields a pair of constants which holds for both experiments and hence is the unique combination. Simon's curves are given in Fig. 1. They give a clear survey of the dependence of reflecting power on n and κ, and can therefore be used as a lead in choosing from the above methods the one best suited for a certain problem.

The graphical procedure is both tiring and tiresome. Therefore a direct calculation of n and κ from experimental data with the help of an electric calculator capable of taking square roots, or better still with an electronic computer is more attractive if many data are to be handled.

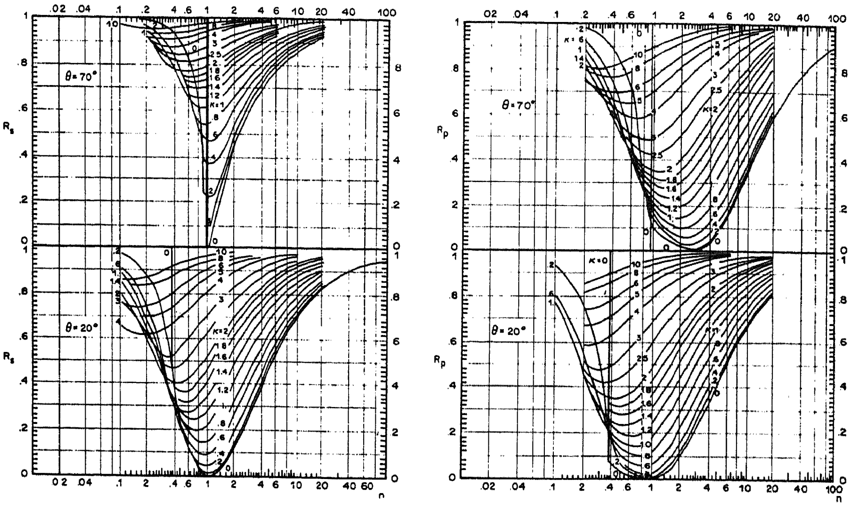

Figure 1. Relation between reflecting power and optical constants for parallel and perpendicularly polarized light.

A calculating procedure for method (c) has recently been published by Heilmann [5], and for method (a) also adaptable to (d) by Fahrenfort and Visser [6]. We will give these procedures for the sake of compactness without proof.

From the experimental data of method (c) we can make up:

$$V = \frac{R_s - R_p}{R_s + R_p} \quad \text{and} \quad X = V\frac{1 + R_s}{1 - R_s}.$$

We calculate:

$$Y = \frac{\tan^2\theta\,(X-1)}{\tan^2\theta - X}; \qquad \sqrt{Z} = \frac{\tan^2\theta - 1}{(2\cos\theta)^{1/2}}\;\frac{V}{\tan^2\theta - X},$$

and with

$$n^2(1-\kappa^2) = Z - Y,$$

and

$$n^2(1+\kappa^2) = (2Z\sin^2\theta + Y^2)^{1/2},$$

we can easily calculate n and κ explicitly.

From the experimental data obtained from method (a) we can find the expressions:

$$A_1 = \left(\frac{1 - R_1}{R_1}\right)^4 ; \qquad B_1 = (1+R_1)^2 \cos^4 \theta_1 ;$$

$$C_1 = (1 - R_1)^2 \cos^2 \theta_1 ; \quad D_1 = R_1 \cos^4 \theta_1 ,$$

and similarly A_2, B_2, C_2 and D_2 from the experimental data at θ_2.

We calculate

$$P = \frac{A_1 D_2 - A_2 D_1}{C_1 D_2 - C_2 D_1} ; \quad Q = \frac{B_1 D_2 - B_2 D_1}{C_1 D_2 - C_2 D_1} ;$$

$$X = \frac{1}{4}\left(A_1 - C_1 P + \frac{1}{4} D_1 P^2 \ ;\right)$$

$$Y = 4\left(-B_1 + C_1 Q - \frac{1}{2} D_1 QP\right);$$

$$Z = 16 D_1 Q^2 .$$

From these parameters we calculate

$$M = \frac{-Y - (Y^2 - 4XZ)^{1/2}}{2X} ,$$

and we find the optical constants from

$$U = 1 - n^2 + n^2 \kappa^2 = -\frac{PM}{16} + Q ;$$

$$W = 2n^2 \kappa = (M - U^2)^{1/2}$$

Normal Incidence

The simplicity of the experiment and of the relation (3) between n' and intensity, has led many workers to use normal incidence, even though experimentally normality can only be approximated.

At normal incidence the θ dependence and the difference between R_p and R_s are meaningless and hence can no longer be used for obtaining the equations necessary for the determination of n and κ. Therefore one is obliged to bring other relations than are given by electromagnetic theory into play.

One possibility is to assume the validity of the dispersion formula (6). Then, by successive trial and adjustment of the constants appearing in this formula one can find the optical constants that give the best fit with the experimental reflection spectrum. Though this method requires elaborate calculations, it has been applied by several authors [7].

Another possibility is to make use of the fundamental relation which exists between the amplitude $|r| = \sqrt{R}$ of the reflected wave and its phase shift φ. If the intensity is known over the complete spectrum or, in good approximation, so far into the wings of a band that the reflection spectrum has zero slope, the phase shift may be calculated at a frequency ν_c by means of the Kramers-Kronig relation

$$\varphi_c = \frac{2\nu_c}{\pi} \int_0^\infty \frac{\ln|r| - \ln|r|_c}{\nu^2 - \nu_c^2}\, d\nu . \tag{12}$$

This relation can be shown to be the logical equivalent of strict causality, i.e., the condition that no reflected signal can appear before the incident signal has reached the surface, and hence the relation is quite general [8]. The first application to reflection spectroscopy was given by Robinson and Price [9].

For computational purposes Eq. (12) can be written in a more suitable form:

$$\varphi_c = \frac{1}{\pi} \int_0^\infty \frac{d \ln|r|}{d\nu} \ln \left| \frac{\nu + \nu_c}{\nu - \nu_c} \right| d\nu , \tag{13}$$

which shows that the phase shift at frequency ν_c depends on the slope of the amplitude $|r|$ over the whole spectrum although the slope at frequency ν_c makes a large contribution due to the weight factor $\ln|\nu + \nu_c/\nu - \nu_c|$. The integration has the effect of smearing out an experimental error at one particular frequency over the whole spectrum. Unfortunately this means that the lower accuracy of measurement in the wings of the bands weighs heavily also on the accuracy of the calculated phase shift in the centre of the band.

Once the complex amplitude $|r|e^{i\varphi}$ is known completely from the calculation, the optical constants follow from a transformation of the equation

$$|r|e^{i\varphi} = \frac{1 - n'}{1 + n'}$$

into

$$n' = \frac{1 - |r|e^{i\varphi}}{1 + |r|e^{i\varphi}}, \tag{14}$$

and splitting the latter into its real and imaginary components.

Although measurement at normal incidence has certain experimental advantages, the analysis of the spectra is very complicated, while the possibilities of checking on deviations from theory are substantially smaller than in the case of oblique incidence, where analysis is based on electromagnetic theory only.

THE SENSITIVITY OF REFLECTION TO VARIATIONS IN n AND κ

The failure of reflection spectra to show bands at the frequencies of all but the strongest transitions clearly appears from Figure 1. In the region around $n = 1.5$, which is a normal value of the refractive index of organic compounds we see that there is little difference between the curves for $\kappa = 0$ and $\kappa = 0.2$, although the level at $\theta = 70°$ is different from that at $\theta = 20°$. This means that any change of κ within this region will hardly be recorded in a reflection spectrum.

A κ value of 0.2, however, already stands for a strong absorption, corresponding to a transmission of only 0.07% if measured in a cell of 0.01 mm length at a wave length of 5μ and if $n = 1.5$.

ATTENUATED TOTAL REFLECTION

General

A closer inspection of Figure 1, however, shows that in reflection also a much greater sensitivity to variations of κ in the 0-0.2 region is possible. This is found for values of n lying below unity, in the region where for non-absorbing substances ($\kappa = 0$) the incident beam is totally reflected. For $\theta = 70°$ this region begins at $n = 0.94$ and for $\theta = 20°$ at $n = 0.34$.

Furthermore it is seen that in these regions the intensity of reflection falls with growing κ contrary to its usual behaviour.

If the phenomenon of total reflection is examined more closely with the help of electromagnetic theory, one finds that the macroscopic observation of zero energy transfer from the first to the second medium is due only to the effect of averaging over time and area. A microscopic analysis shows, at any time, an alternation of places where energy penetrates into the second medium and places where the energy stream is in the opposite direction.

From the study of Schaefer and Gross [10], one may even conclude that the energy stream follows a curved path from the entrance to the exit area, such that the light waves are actually traveling over some distance through the second, optically less dense medium.

By virtue of this image one might expect the reflected beam not to spring from exactly the same surface element as is illuminated by the incident beam. Goos and Hänchen [11] succeeded in demonstrating this effect by comparing the total internal reflection with a metallic reflection. Shortly afterwards Artmann [12] derived theoretically an expression for the displacement D of a narrow beam on total reflection:

$$D = \frac{\lambda}{\pi} \frac{\sin \theta}{\left(\sin^2 \theta - \sin^2 \theta_{\text{crit}}\right)^{1/2}} \cdot \qquad (15)$$

Thus the light wave has an opportunity to interact with the molecules of the second medium over comparatively long distances. If these molecules are capable of dissipating energy from the radiation field, only part of the energy will return to the first medium

Although Artmann's formula has only approximate value for reflection at an absorbing medium, it shows nevertheless that the light path increases according as θ is closer to θ_{crit}, and grows with growing θ and hence with θ_{crit}. In well-chosen circumstances the light path may become as long as several wave lengths.

Experimental

Experimentally this situation of higher sensitivity can always be created if the specimen is brought into optical contact with a transparent medium, having a refractive index which is superior to the index of the specimen. In that case the relative refractive index at the reflecting interface will be smaller than unity, and there will be a critical angle where "total" reflection sets in.

If a spectrum is made of the reflected radiation, the regions where $\kappa > 0$ will appear as attenuation bands, very much like the absorption bands in a transmission spectrum. Such spectra are called Attenuated Total Reflection (ATR) spectra [3]. A typical example of the sensitivity gain is given in Figure 2, showing the conventional and the ATR reflection spectra of an epoxy resin.

As the refractive index grows towards longer wave lengths with the passage of each band and fluctuates in each band owing to the anomalous dispersion effect, it is desirable to set the angle θ somewhat larger than the critical angle corresponding with the highest n value reached in the spectrum.

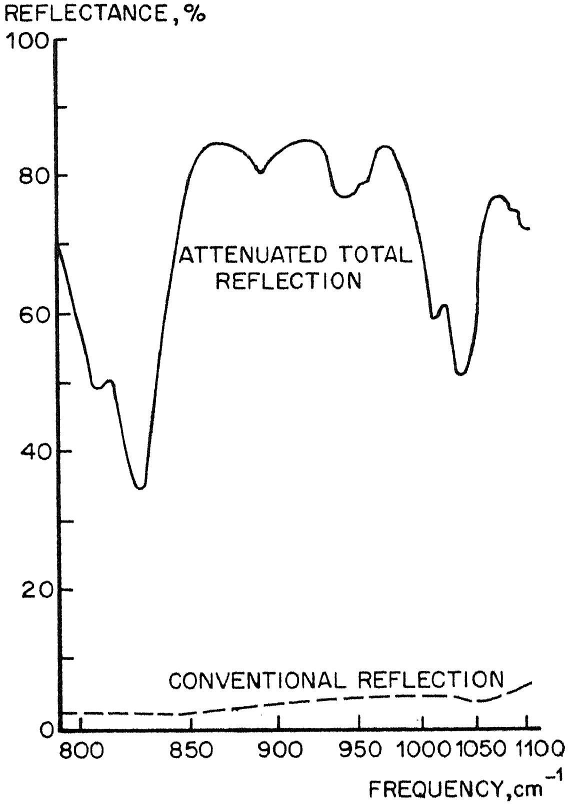

Figure 2. Comparison between conventional and ATR spectrum of an epoxy resin.

In practice, the high-index crystal, for which AgCl, KRS_5, Ge and similar materials can be used, has the shape of a hemicylinder. The sample is in contact with the face containing the cylinder axis, and the cylindrical surface acts as entrance and exit window. This gives us not only the possibility to change θ without directional changes of the incident or reflected beams, but it can also serve as a means to obtain a parallel beam, as shown in Figure 3. The mounting of such a crystal for solid samples is shown in Figure 4. The specimen is pushed against the bottom of the hemicylinder by means of a threaded plug.

For the cases of low band intensity, a single reflection may be insufficient to yield enough detail in the spectra, even if a cylinder material of comparatively low index (and hence giving large critical angles) such as CsBr is used. Then, multiple reflection crystals can be used, of the type shown in Figure 5. Such crystals still allow a fair range of angle settings. Dimensions

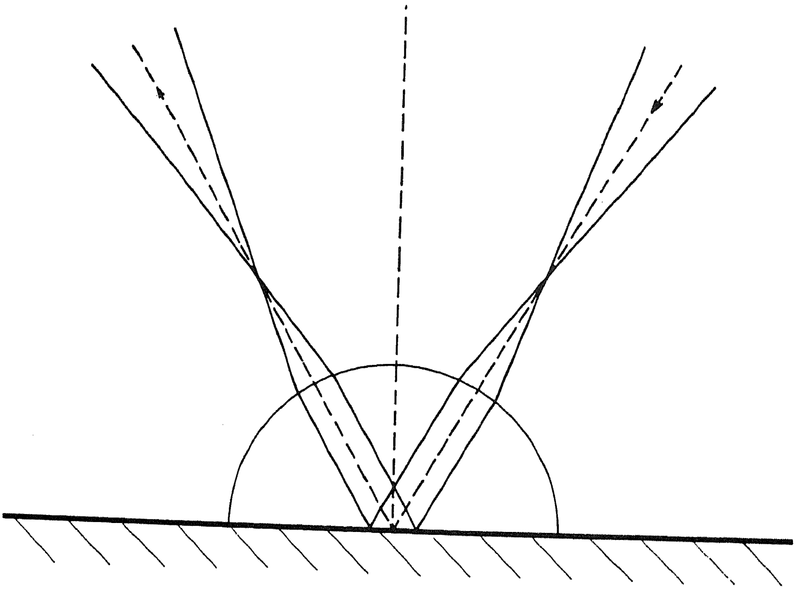

Figure 3. Arrangement for parallel incidence on the interface.

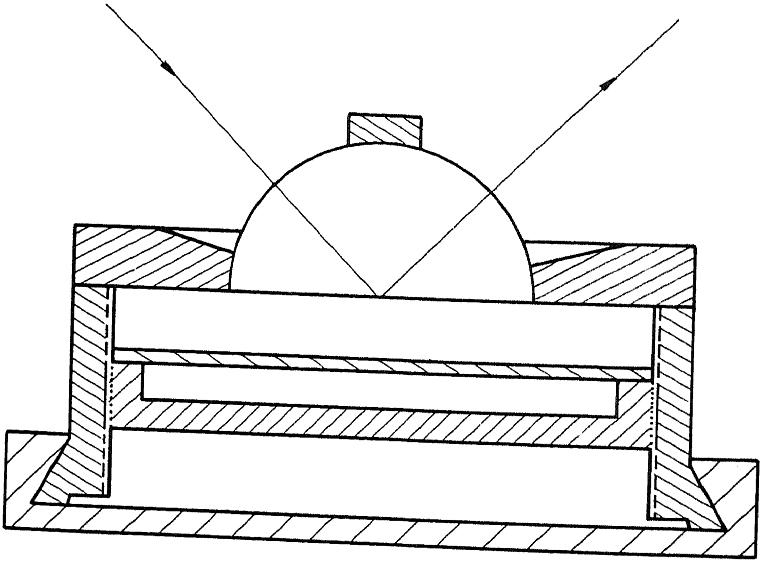

Figure 4. Hemicylinder mounted in a cell for solid samples.

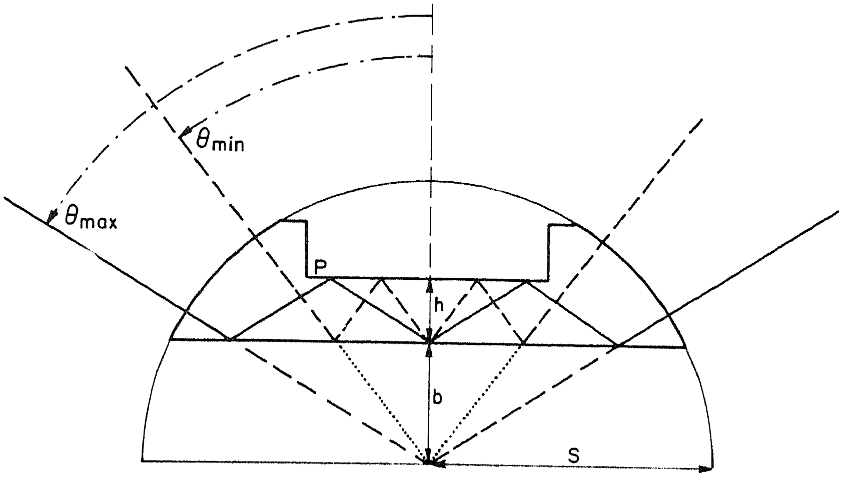

Figure 5. Five-reflection crystal showing the symmetrical light path.

of these crystals must be such that the light path is symmetrical with respect to the plane of symmetry containing the cylinder axis [6]. Figure 6 shows a one-reflection type cell in position in the reflectometer, which was designed for use in double beam spectrometers [6]. Angles of incidence can be set between 30 and 63° with an accuracy of 3 arc minutes. On setting θ, the reflected beam remains focussed on the slit of the spectrometer. The light path is given in Figure 7.

Application

When applying this reflection technique, one has the choice between two general approaches, just as in transmission. One can either record the spectra and use them as such for qualitative, and with calibration curves for quantitative analysis, or one can run the experiments according to a specific system, in order to fulfill the demands for accurate determination of the optical constants.

(a) The use of the spectra as such

For many practical problems the spectra as such will suffice. No care has to be taken to ensure parallel incidence, or polarization of the incident beam.

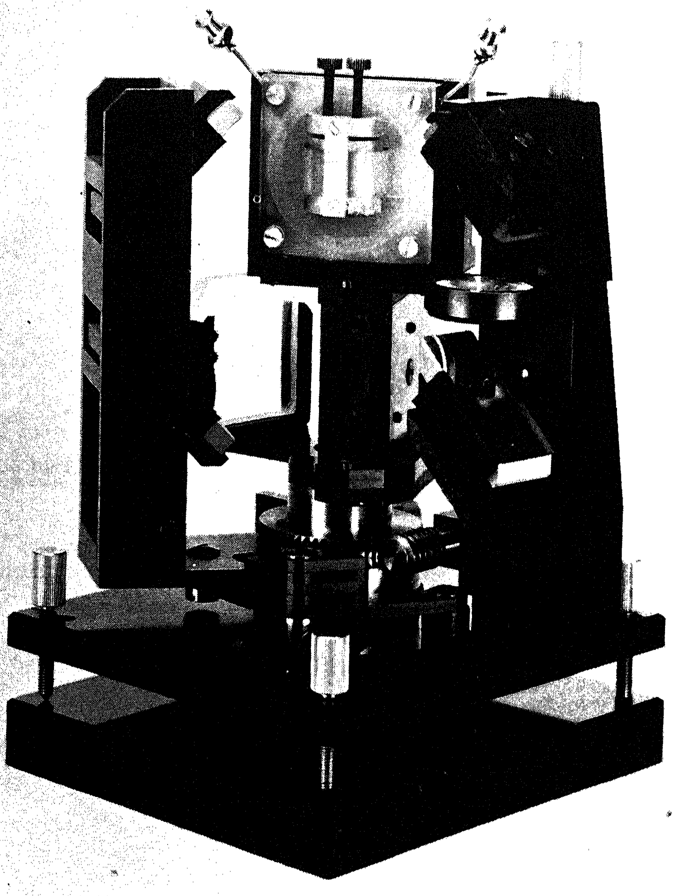

Figure 6. Reflection accessory for use in double-beam spectrometers.

For quantitative analysis the band intensity should be calibrated, and it is interesting to see that, although Beer's law is not valid for reflection spectra, it may still be a fair approximation.

In Figure 8 spectra are reproduced of solutions of decene-1 in nujol at various concentrations. Taking the reflecting power of the pure solvent as a substitute for I_o, a formal application of Beer's law in the band maxima yielded the calibration curves of Figure 9. Deviation from linearity is not worse than normally found for transmission spectra.

In the field of solids, most polymers and elastomers can easily be brought into optical contact with the high-index crystal by exerting a slight pressure (Figure 10).

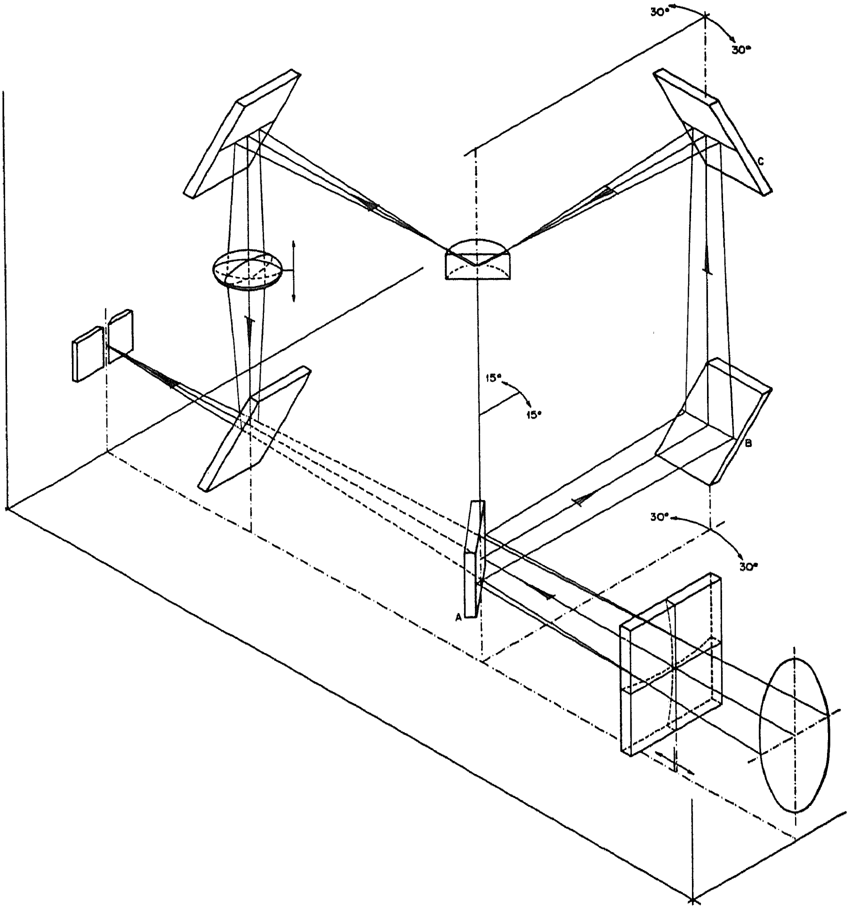

Figure 7. Light path in the reflection accessory.

Even of powdered materials spectra may be obtained, though contact of course cannot be complete and the reflection of the "free" interface sets a limit to the modulation depth of the bands.

It is noteworthy that even in the absorption regions the attenuation of ATR spectra never reaches the stage of a complete blackout. This may be used advantageously for the recording of spectra of solutes in absorbing solvents such as water, as compensation in a double-beam system is easily achieved.

An accessory for ATR studies offering the possibility of angle adjustment is now available commercially.* This is well suited for this type of practical studies and can easily be installed in common spectrometers.

---

*Connecticut Instrument Corporation, Wilton, Conn.

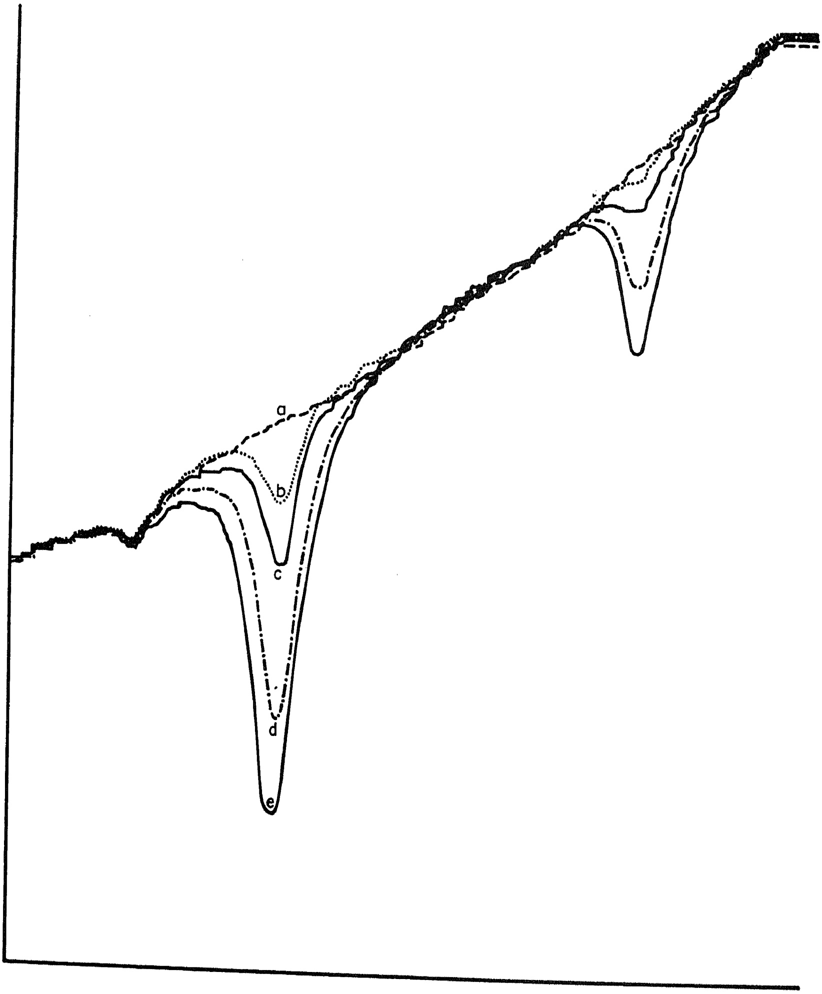

Figure 8. Attenuated total reflection of solutions of decene-1 in nujol. Concentrations: in spectrum a: 0%, b: 10%, c: 20%, d: 50% and e: 100% decene-1.

For materials of great hardness, it will sometimes become difficult to obtain optical contact over a sufficiently large area, though in contacting small areas no difficulties arise. In these cases a micro method should be useful; a possible system is shown in Figure 11. The hemicylinder has been replaced by hemisphere, which is illuminated by a strongly convergent beam from a large elliptical or spherical mirror. The action of the hemisphere is to reduce the dimensions of the image on the reflecting surface. An illuminated area as small as 2 × 0.5 mm is easily obtained. No difficulty is encountered in reproducing by

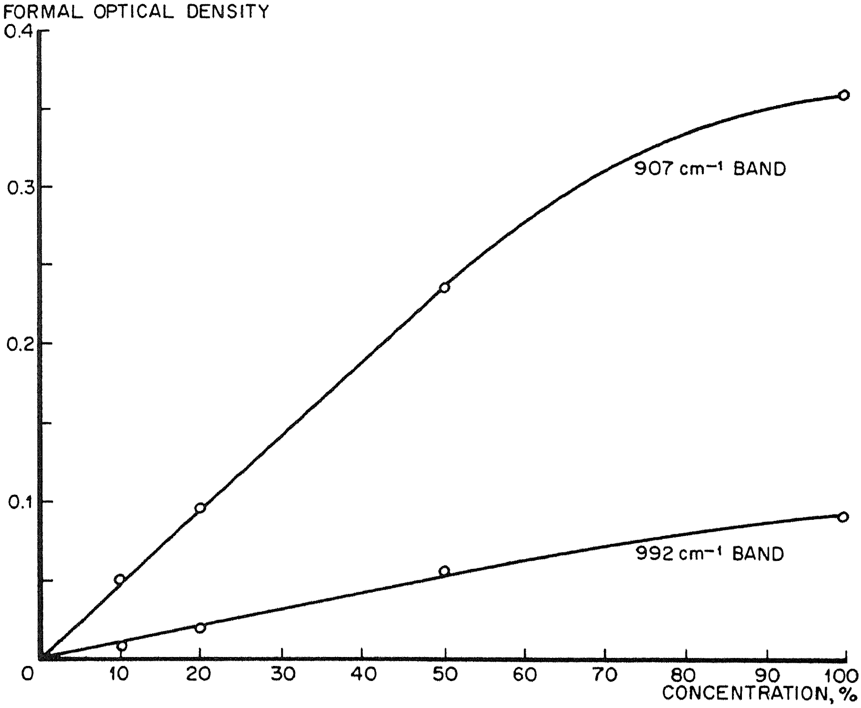

Figure 9. Relation between formal "optical density" and concentration for two bands of decene-1 in nujol.

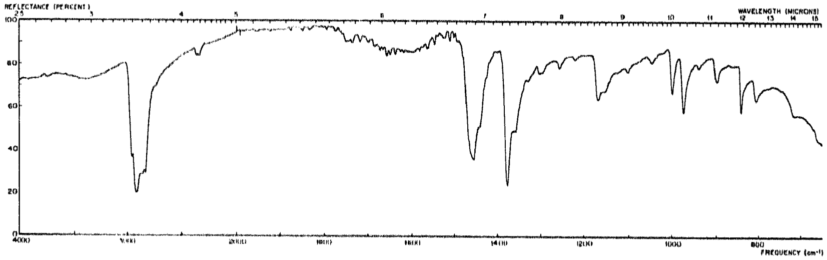

Figure 10. ATR spectrum of an ethylene-propylene copolymer.

a second mirror an image of good optical quality for focussing on the spectrometer slit. As a wide range of angles of incidence is present in the incident beam, no angle adjustment should be required.

(b) Determination of optical constants

Measurements for determining the optical constants have to be carried out with parallel incidence, which necessitates a

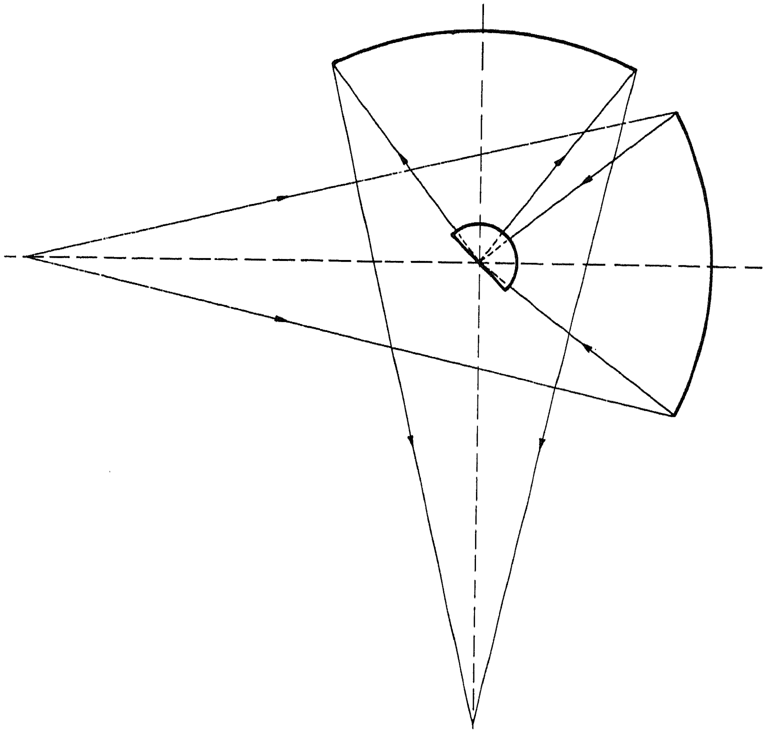

Figure 11. Possible arrangement for an ATR micromethod.

sufficiently large area of good optical contact. This means that the surface of hard materials has to be carefully prepared. For liquids there is no difficulty, of course, and a few examples of complete analysis are now available. These were also compared with the implications of dispersion theory and the Kramers-Kronig relations.

In Figure 12 the κ and n values in a few bands of acetone, toluene and benzene are given; they were calculated with the computing system for method (a) (Oblique Incidence) from spectra recorded for highest accuracy as treated in the next section.

Values for the integrated absorption obtained from the oscillator strengths by a combination of Eqs. (10) and (11) are given in Table 1, together with the fundamental constants.

In Table 1 the A_i values have not been corrected for finite slit width, being 3.2 cm^{-1} at 1035 cm^{-1} and 3.5 cm^{-1} at 1300 cm^{-1}. For benzene and acetone a comparison is given in Figure 13 between the curves of $2n^2\kappa\nu$ as obtained directly from the optical constants, and indirectly by calculation via Eq. (8) with the constants from Table 1. It is seen that agreement is better

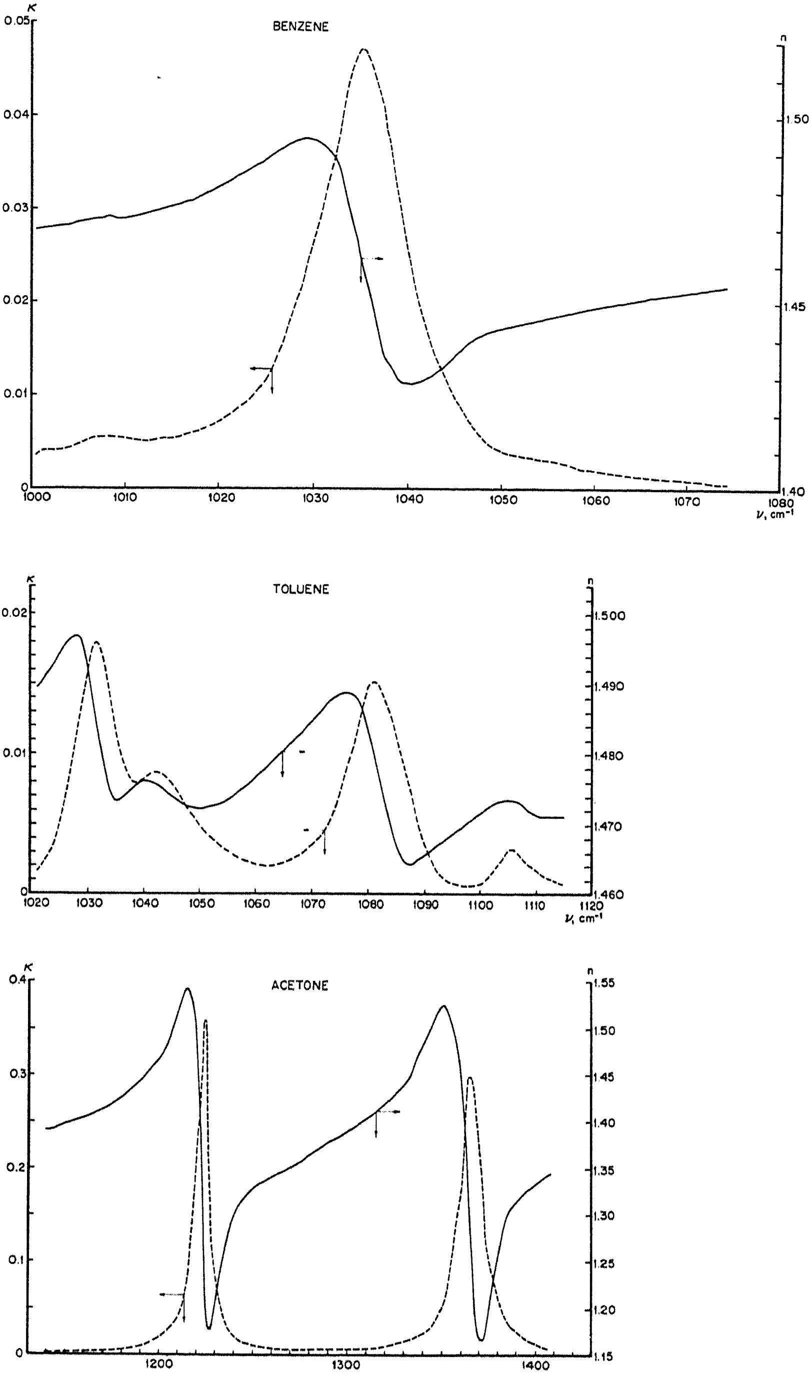

Figure 12. Optical constants in a few bands of benzene, toluene and acetone.

Table 1

Fundamental Constants for Absorption Bands

	Benzene	Acetone	
ν_o, cm^{-1}	1035.2	1222.0	1364.5
γ, cm^{-1}	10.2	10.0	16.8
ρ, cm^{-2}	2131.8	12850	21470
$\bar{n}$	1.462	1.383	1.361
A_i, cm/mmole	1.275×10^3	6.7×10^3	11.4×10^3

for acetone than for benzene, where low-frequency side bands have a disturbing effect.

For benzene the phase shift φ on reflection at θ_1 is given in terms of the constants defined in Section 3A by [6]:

$$\varphi = \text{arc sin} \frac{4W}{(1 - R_1)\, M} D_1^{\,1/2}, \tag{16}$$

and hence can be calculated from the optical constants and the reflection spectrum. For $\theta = 46.5°$ the spectrum is reproduced as the drawn line in Figure 14a. The phase shift is given in Figure 14b, curve I.

By the application of the Kramers-Kronig relation [13], this shift was also calculated from the same experimental data (Figure 14b, curve II). Although the shape of curve II is approximately correct, there is a large difference in level between the curves I and II. On omitting the region indicated by 0 in Figure 14a, and recalculating, a phase shift was obtained (curve III), lying on a still higher level than II, indicating that the difference between II and I is due to the measurements not having been pushed forward far enough into the wings of the reflection band. A reasonable extrapolation of the experimental spectrum is indicated by the dotted line in Figure 14a. The recalculated phase shift based upon this extended spectrum yielded the curve IV in Figure 14b, in better if not full agreement with the phase shift calculated from the optical constants.

Evidently the phase shift as calculated by the Kramers-Kronig relations is very sensitive to the reflection characteristic in the band wings, which makes it rather unreliable, as experimental data in the far wings of a band usually are inaccurate.

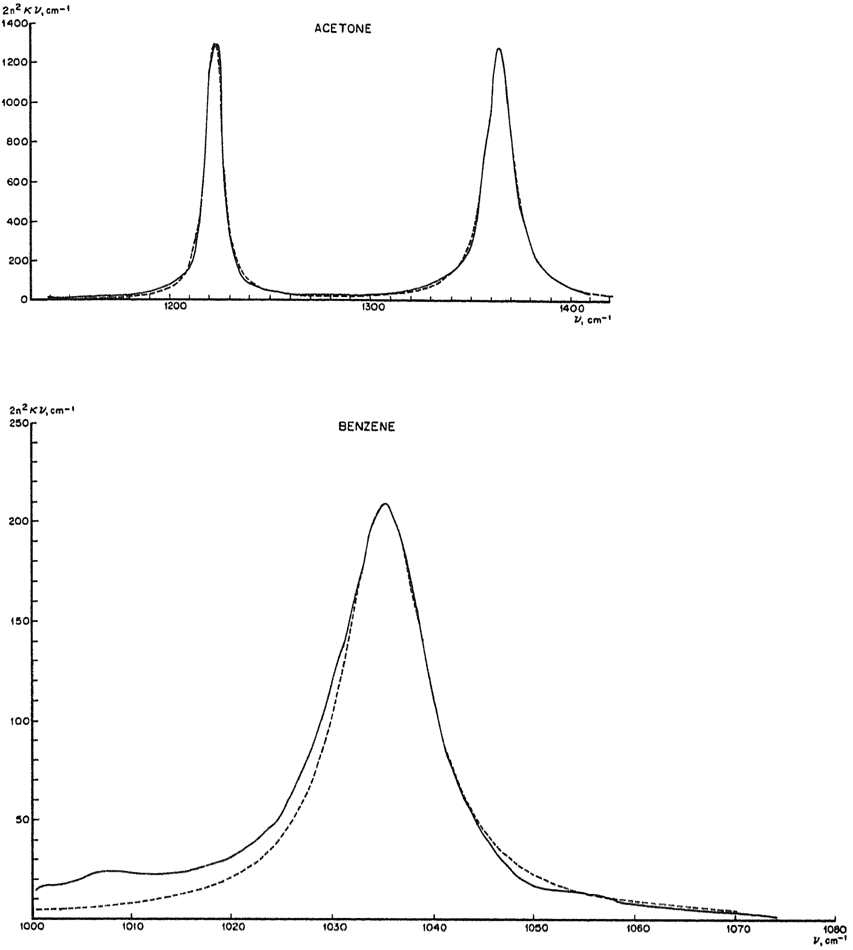

Figure 13. Curves of $2n^2\kappa\nu$ for benzene and acetone: ——— calculated from experiment; ------ calculated with dispersion formula.

Applications of the computing method (Oblique Incidence), giving results for any arbitrary frequency without the need for data at other frequencies should therefore be preferred. This type of computation has the additional advantage of being at least ten times as fast as the Kramers-Kronig calculation.

Accuracy of the Method

The swift operation of the calculating system allowed us to assess the errors introduced by the inevitable inaccuracy of the experiments.

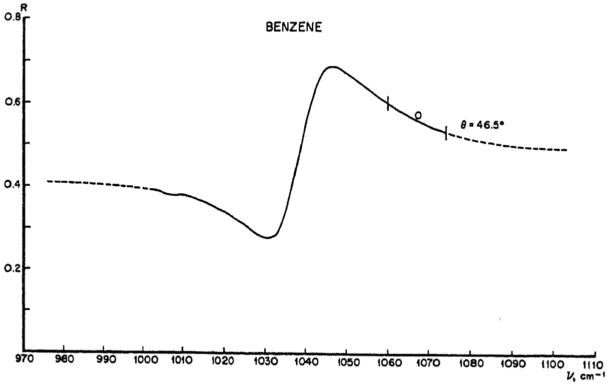

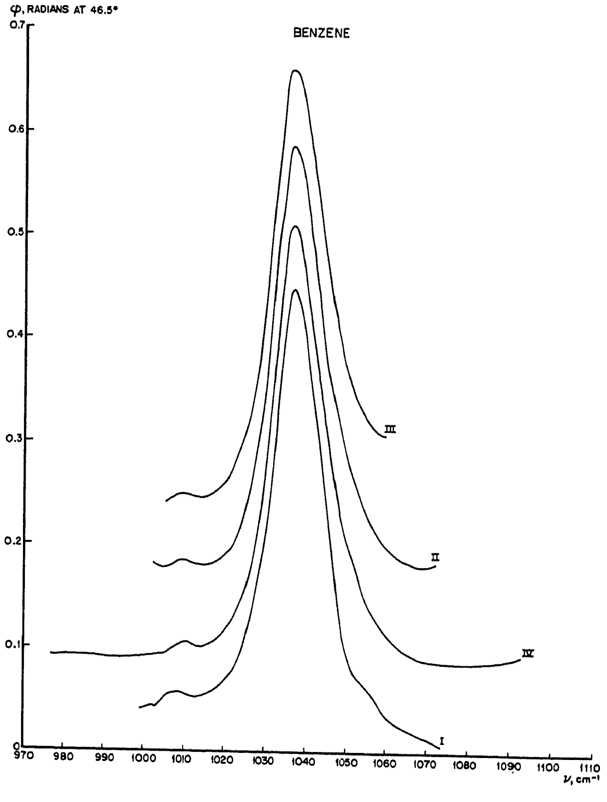

Figure 14a. ———— ATR spectrum of 1035 cm^{-1} band of benzene; ------ extrapolation of the spectrum.

Figure 14b. Calculated phase shifts at $\theta = 46.5°$: I. phase shift calculated by Eq. (16); II. phase shift calculated from Kramers-Kronig relation; III. Kramers-Kronig calculation after omission of region 0 in Figure 14a; IV. Kramers-Kronig calculation after extrapolating according to Figure 14a.

The two reflection coefficients calculated for a hypothetical two-angle experiment were varied with ±0.005 from the true values. The errors were calculated for a number of κ levels at different values of θ_1 and θ_2 such that θ_1 was taken at increasing distance on either side of the critical angle. At each of these θ_1 values, a number of intervals $\Delta\theta = \theta_2 - \theta_1$ was considered. The outcome of this test is illustrated by Figure 15, which gives the results for $\Delta\theta = 5°$ and $10°$. The κ range was chosen from $\kappa = 0.1$ to $\kappa = 0.002$ and θ_1 ranged from 35° to 47°, the critical angle being 44° 26' in all cases, corresponding to a refractive index $n = 0.7000$.

It is seen that the most accurate κ is obtained if the two angles θ_1 and θ_2 are on opposite sides of θ_{crit}. The best results are obtained for the range $0.02 < \kappa < 0.1$ at $\Delta\theta = 10°$. Then the relative error is limited to some ±5% for the experimental error given above over a fairly wide range of θ_1 values.

The error curves for the refractive index are given in Figure 15b. Here the error is largest for high κ where it varies between 0.4% and 0.6%. Otherwise the error is well below this value and becomes as low as 0.04% for $\kappa = 0.002$ and θ_1 near θ_{crit}.

On the basis of these error analyses, a general procedure for the best way of recording ATR spectra for calculating purposes can be given:

The angle of incidence is first changed, until the reflected energy starts to rise steeply. The angle is then adjusted until

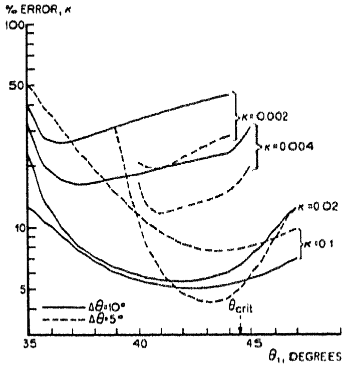

FIGURE 15a

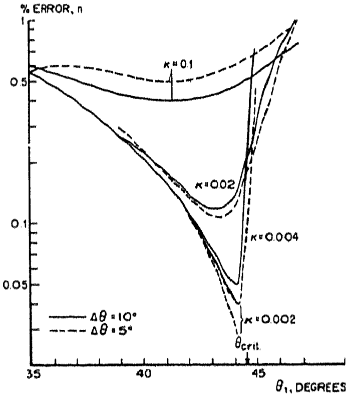

FIGURE 15b

Figure 15a. Relative error in κ due to an error ±0.005 in reflectivity, given as function of θ_1.

Figure 15b. Relative error in n due to an error ±0.005 in reflectivity, given as function of θ_1.

the highest reflecting power on scanning the band manually reaches some 70-80%. In this way, θ_1 is near θ_{crit} for the lowest value of n encountered, and in consequence it is now up to a few degrees on the lower side of θ_{crit} for the remainder of the band.

We have seen that this is the value yielding highest precision when combined with a second angle, some 5-10° higher.

CONCLUSIONS

The development of infrared reflection techniques for other than strongly absorbing substances offers many possibilities to extend the field of application of infrared analysis.

Although the experimental methods are still in development one can already obtain, with simple means, spectra of materials that used to the inaccessible or could only be studied with considerable effort. If wanted, the specific optical characteristics can be obtained as well, by application of comparatively simple computing methods.

REFERENCES

1. P. M. Schatz, J. Chem. Phys. 32 (1960) 894. E. E. Ferguson and R. E. Kagarise, J. Chem. Phys. 31 (1959) 236.
2. I. Simon, J. Opt. Soc. Am. 41 (1951) 336.
3. J. Fahrenfort, Spectrochim. Acta 17 (1961) 698.
4. D. G. Avery, Proc. Phys. Soc. (London) B65 (1952) 425.
5. G. Heilmann, Z.f. Naturforsch. 16^a (1961) 714.
6. J. Fahrenfort and W. M. Visser, Spectrochim. Acta, 18 (1962) 1103.
7. J. A. A. Ketelaar, C. Haas and J. Fahrenfort, Physica XX (1954) 1259. C. Haas, Diss., Amsterdam, 1956. W. G. Spitzer and D. H. Kleinman, Phys. Rev. 121 (1961) 1324. Spitzer, Kleinman et al., 113 (1959) 127, 133; 118 (1960) 110, J. Phys. Chem. Solids 11 (1959) 190.
8. J. S. Toll, Phys. Rev. 104 (1956) 1760. N. G. van Kampen, ibid. 89 (1953) 1072. H. W. Bode, Network Analysis and Feedback Amplifier Design, van Nostrand, New York, 1945.
9. T. S. Robinson, Proc. Phys. Soc. (London) B65 (1952) 910. T. S. Robinson and W. C. Price, ibid. B66 (1953) 969.
10. C. Schaefer and G. Gross, Ann. Physik 4.F.32 (1910) 648.
11. F. Goos and H. Hänchen, Ann. Physik 1 (1947) 333.
12. K. Artmann, Ann. Physik 2 (1948) 87.

COMPARATIVE STUDIES OF INFRARED AND RAMAN GROUP FREQUENCIES AND THEIR APPLICATIONS*

R. N. Jones, P. J. Krueger(a),† K. Noack(b),† J. J. Elliott(c),† R. A. Ripley(d),† G. A. A. Nonnenmacher(e)† and J. B. DiGiorgio‡

INTRODUCTION

Between 1930 and 1940 several hundred papers were published on the Raman spectra of organic compounds. In particular Professor Kohlrausch and his colleagues at Graz established numerous correlations between molecular structure and Raman band positions in complex organic compounds where vibrational analysis in terms of normal co-ordinates was impracticable. Their work played a leading part in establishing the characteristic group vibration frequencies that were later taken over by analytical infrared spectroscopists and, as such, contribute predominantly to the livelihood of many in the audience here this afternoon.

As you all know, great advances took place in the technique of infrared spectrometry in the early 1940's, and those chemical spectroscopists who were primarily concerned with the structural analysis of complex organic compounds lost interest in Raman spectroscopy. This shift of interest to the infrared was not, of course, complete. To cite a specific example, notable work on the Raman spectra of aqueous solutions of peptides and amino acids has come from the laboratory of Prof. J. T. Edsall at Harvard University [1]. The Raman spectra of alicyclic and aliphatic hydrocarbons and their unsaturated derivatives have also continued to receive attention, particularly from laboratories in the United States and the Soviet Union. By and large, however, Raman spectroscopy, in latter years, has been abandoned to the small molecule people.

---

*Published as Contribution No. 6925 from the Laboratories of the National Research Council of Canada. Lecture delivered by R. N. Jones.

†National Research Council of Canada Postdoctorate Fellow. (a) 1958-1959; (b) 1958-1960; (c) 1959-1961; (d) 1960-1962; (e) 1961.

‡United States National Institutes of Health Postdoctorate Fellow.

From the utilitarian point of view, this was a natural course of events. The infrared spectrum is, today, much easier to measure than the Raman spectrum, and a much smaller quantity of sample suffices. Until recently a gram or more of material was customarily required for a Raman spectrum. Furthermore, it is essential that the compound be non-fluorescent in the exciting radiation, and it must also be scrupulously free from fluorescing impurities. Additional complications arise if the compound is colored.

It is obvious, therefore that Raman spectrometry has little to offer the chemist where similar information is obtainable from the infrared spectrum. Spectroscopists know, however, that Raman and infrared spectra depend on different electrical characteristics of the molecular vibration, and therefore provide different information about the molecular structure. Our present knowledge of the structure of molecules in the electronic ground state could never have been obtained by the use of either the infrared or the Raman spectra alone, and the structural information from the two types of vibration spectra complement rather than duplicate one another. If the technical difficulties of obtaining Raman spectra from small samples could be overcome, our knowledge of group frequency vibrations would be greatly enriched, and it is reasonable to anticipate that for complex molecules, as for simpler molecules, comparison of the two types of vibration spectra should yield more detailed information about the molecular structure than organic chemists currently derive from the infrared spectrum alone.

During the past three years we have been investigating the potentialities of semi-micro Raman spectrophotometry using a Cary Model 81 Raman spectrophotometer; the greater part of the work has been carried out with a capillary sample system that has a volume of approximately 200 microliters. This afternoon I want to summarize our experiences and review both the possibilities and the limitations of the technique as we have developed it. In our investigations we have kept in mind the routine methods used by chemists to obtain infrared spectra of complex organic compounds in the liquid state and in solution, and we have endeavored to develop our Raman technique so that the spectra are obtained under conditions that conform as closely as possible with those commonly used in the infrared.

In Figure 1 is shown a cross-section through the cell compartment and the source unit. A horizontal Toronto type mercury

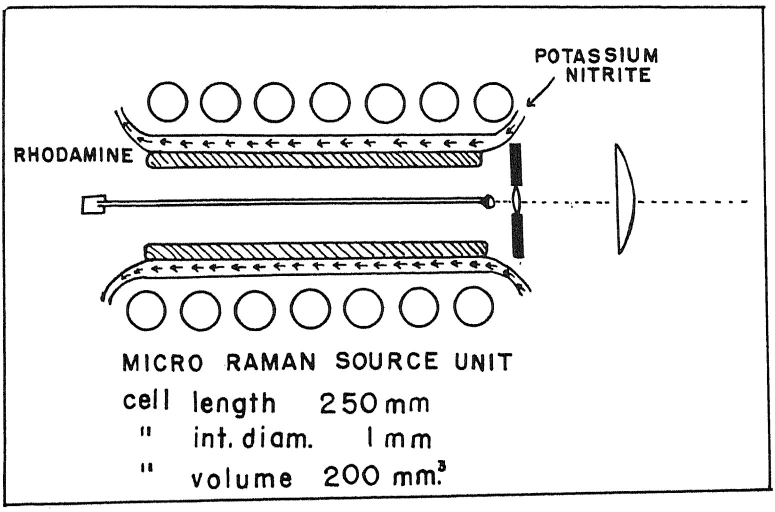

Figure 1

arc is used with water cooled electrodes. The helix is constructed of Corning 1720 glass and the 4358 Å mercury line is isolated by a double walled Pyrex glass filter jacket. Aqueous potassium nitrite solution is circulated by means of stainless steel and Teflon tubing through the outer compartment of the filter jacket, while a static aqueous solution of Rhodamine (5DGN extra) is used in the inner annular space. This is a modification of the source unit provided by the manufacturers which employs a Pyrex glass helix and a filter system of two organic materials circulating in a common solvent through a single annular jacket. The sample cell lies on the axis of the cylindrical source system and consists of a Pyrex glass capillary tube of the dimensions shown. The closed end of the tube rests against a wide angle collecting lens with emersion contact provided by a drop of glycerol.

The total capacity of the cell is about 200 mg. though, as will be described later, we commonly add carbon tetrachloride or some other miscible organic liquid as an internal intensity standard. When measuring the spectra of organic liquids the optimum quantity in the tube is about 150 mg. The Raman bands are normally scanned at a rate of 15 cm.$^{-1}$ per minute, and a complete scan from 150 to 4000 cm.$^{-1}$ therefore requires between 4 and 5 hours. In practice we can scan more rapidly through regions that contain no bands and a complete run takes about 3 hours. When measuring the spectra of liquid samples under these conditions we use a cylindrical transverse Polaroid polarizer between the filter jacket and the sample tube to eliminate the undesirable effects of oblique radiation. For more dilute solutions, where the energy limitations are severe, the polarizer is dispensed with in survey spectra, though it is practicable to use polarizers to measure the depolarization ratios of the stronger bands.

DEVELOPMENT OF AN INTENSITY SCALE

A good deal of our time and effort has been taken up with the establishment of an intensity scale that will permit semi-quantitative comparison of Raman spectra measured under different experimental conditions. There is at present considerable interest in the absolute measurement of Raman band intensities and an extensive literature is accumulating on this subject. Most of this work is motivated by a desire to obtain an absolute measurement of the Raman intensity, free of instrumental variables, in a form that will ultimately permit theoretical and experimental study of the relationship between the Raman band and the intrinsic properties of the associated normal vibration. We shall not review this here, but those interested will find access to it through the publications of Bernstein [2], Michel [3], Rea [4], Tunnicliff [5] and the recent monograph of Brandmüller and Moser [6].

Our studies of Raman band intensities have had a more limited objective as we are not, for the present, attempting to attach

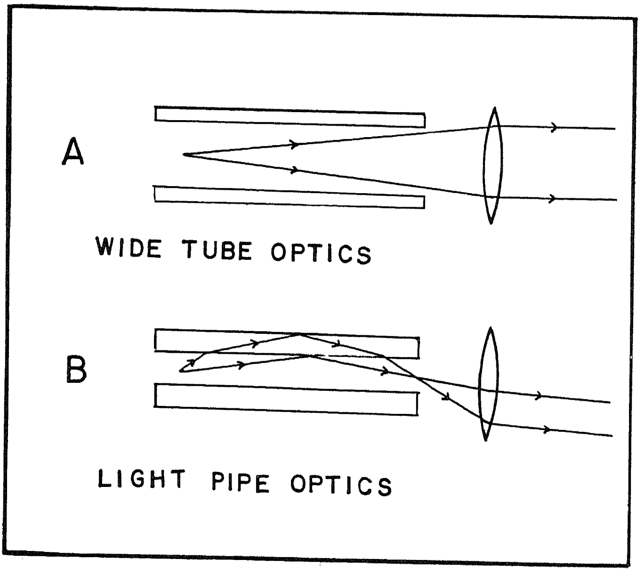

Figure 2

diagnostic significance to difference in absolute band intensities. We are satisfied if we can reduce the raw data to an approximately common ordinate scale and are not particularly concerned if it should later be shown that systematic errors occur. When all is said and done, this has been the status of a fair proportion of the infrared data recorded on small prism spectrometers over the past twenty years, and such measurements have still yielded much useful information.

As the Raman effect is an emission process, we are dealing with an absolute light intensity measurement, not a ratio, and it is expedient to express the measured intensity as a ratio of that of a standard band. For this purpose the band at 459 cm.$^{-1}$ in the spectrum of carbon tetrachloride is commonly used. We have followed this practice, though with some misgiving, since the band is highly polarized and of asymmetric shape. A more symmetric depolarized band would be preferable as an intensity standard. The principle factors known to influence the measured band intensity are summarized in Table 1, which is based on the treatment of Raman band intensities by Bernstein and Allen [7].* It is the third term of the expression, involving the refractive index of the sample, that has given us the main concern, and this is the only element of this expression with which we need to deal this afternoon. Most investigations of refractive index effects on Raman band intensities are based on optical systems in which a large sample volume is employed, so that none of the radiation generated near the walls of the sample tube enters the spectrometer, and the instrument "sees" only a cone of rays coming from the central part of the cell. (Figure 2A.) In the micro sample tube, multiple internal reflection takes place, both at the liquid/glass intersurface and at the glass/air intersurface of the cell (Figure 2B). As a result of this we are dealing with light-pipe optics, and the Raman intensity recorded by the spectrophotometer becomes highly sensitive to the efficiency of the capillary tube as a light-pipe. This, in turn, depends on the refractive index of the liquid in the cell.

A detailed analysis of this problem has recently been carried out by D. D. Tunnicliff and A. C. Jones [5] at the Shell Development Company at Emeryville. They have used a wider tube of 6 mm. internal diameter, and their results and conclusions are

---

*Bernstein and Allen included an additional term in their original expression to take care of reflection losses at the air/glass intersurface of the sample cell. An analytical treatment by Rea [4] has subsequently indicated that, under the conditions of his analysis, this factor has no effect, a conclusion with which Bernstein now concurs [8]. In Table 1

Table 1

Raman Intensity (Bernstein and Allen)

$$S = \frac{I}{I_{459}^{CCl_4}} \quad \frac{1+\rho_{459}}{1+\rho} \quad \frac{n^2}{n^2_{CCl_4}} \quad \frac{\sigma}{\sigma_{459}} \quad \frac{M}{d}\left(\frac{d}{M}\right)_{CCl_4}$$

$$\times \frac{\Delta\nu}{459}\left(\frac{\nu - 459}{\nu - \Delta\nu}\right)^4 \quad \frac{1 - \exp(-1.44\Delta\nu/T)}{1 - \exp(-1.44 \times 459/T)}$$

— — — — — — — — — — — — —

$$S = \frac{I}{I_{459}^{CCl_4}} \text{ (Depolarization) (Refractive Index)}$$

(Photo. Sensitivity)

(Conc.) (Raman Shift) (Temperature)

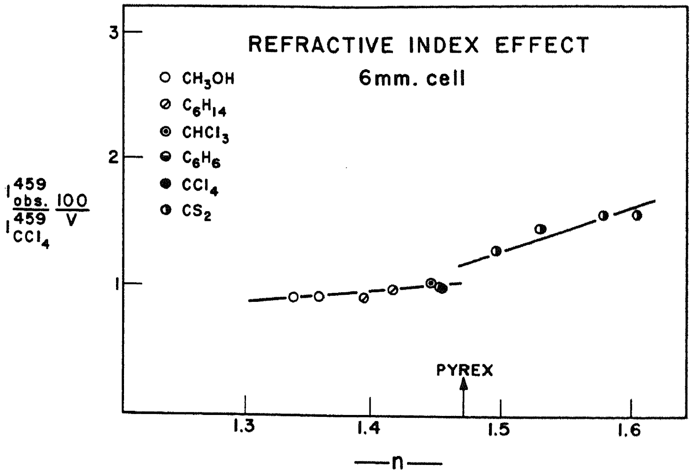

Figure 3

in good accord with ours, provided allowance is made for the fact that the wall effects are much intensified when the internal cell diameter is reduced from 6 mm. to 1 mm. These effects are illustrated in Figures 3 and 4 which show the influence of the refractive index of the medium on the peak height of the 459 cm.$^{-1}$ band of carbon tetrachloride in solutions of varying refractive index. The intensities were in all cases corrected for the volume dilution. You will observe that for both the wider and the narrower tube a distinct break occurs in the slope of the line at a

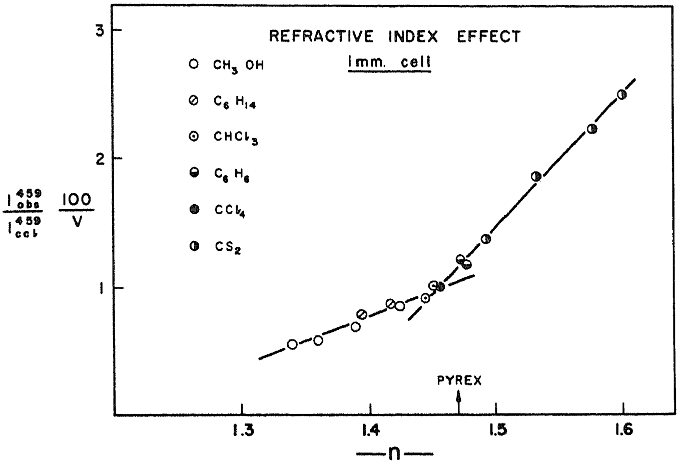

Figure 4

point falling near to the refractive index of the Pyrex glass used. Above this point total internal reflection at the liquid/glass intersurface can occur to increase the light-pipe efficiency. For the cell of 6 mm. internal diameter the overall intensity increases from 0.9 to 1.6, and for the 1 mm. cell from 0.5 to 2.5, taking that of liquid carbon tetrachloride as unity. The observed values were all obtained for a selected cell of each size; they vary appreciably from one cell to another, particularly for the narrower cells.

To minimize the complications introduced by this refractive index effect we add a known quantity of carbon tetrachloride to the liquid sample, where miscibility permits, and use the 459 cm.$^{-1}$ band as an internal intensity standard. In this way it is insured that the carbon tetrachloride band is measured under the same conditions of refractive index as the sample. In adopting this practice it is tacitly assumed that the intrinsic intensity of the Raman band of carbon tetrachloride is insensitive to the surrounding medium. This is unlikely to be true, and recent measurements by Bernstein[8] suggest that the variation could amount to 30% or more as between polar and non-polar solvents. In the survey work with which we are primarily concerned we shall not normally be dealing with liquid systems of extremely different polar character, and these systematic errors are therefore unlikely to reach this magnitude. Bearing these considerations in mind we have employed the simplified intensity expression shown in Table 2 where corrections are applied only for the dilution with the reference standard and for the spectrophotometric response of the spectrophotometer, which is checked periodically against a standard intensity source.

Table 2

SIMPLIFIED INTENSITY FORMULAE

(CCl_4 internal standard)

PEAK HEIGHT

$$K_A^{\nu} = \frac{I_A^{\nu}}{I_{CCl_4}^{459}} \times \frac{N_{CCl_4}}{N_A} \times \frac{\sigma_{\nu}}{\sigma_{459}} \times 100$$

I = PEAK HEIGHT

N = MOLE FRACTION

σ = SPECTRAL SENSITIVITY

BAND AREA

$$L_A^{\nu_{max}} = K_A^{\nu_{max}} \times \frac{\Delta\nu_{1/2}(A)}{\Delta\nu_{1/2}(CCl_4)}$$

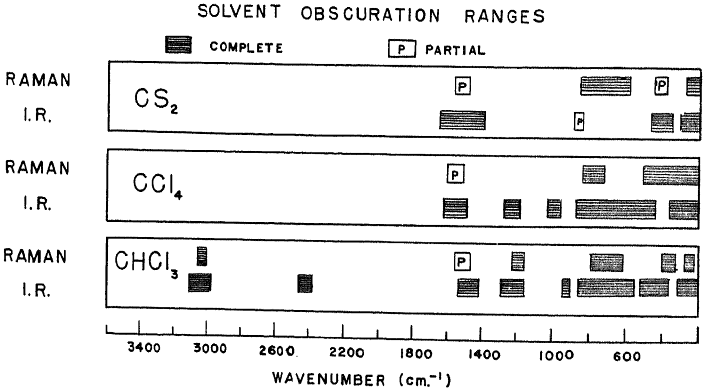

Figure 5

The Raman spectra of substances that are solid at room temperature are best measured in solution, and since our object is to compare Raman spectra with infrared spectra it is desirable to use the same solvents as are normally employed in infrared spectrometry. The Raman obscuration regions of the common infrared solvents are shown in Figure 5 together with the corresponding obscuration ranges for the infrared at 1 mm. path length. Above 850 cm.$^{-1}$ carbon disulfide, carbon tetrachloride and chloroform all obscure less seriously in the Raman than in the infrared technique, and this is particularly important for the range 1650-1500 cm.$^{-1}$ where the C = C stretching bands occur. Raman obscuration below 850 cm.$^{-1}$ tends to be more severe though a very useful partial window is present in carbon disulfide between 600 and 300 cm.$^{-1}$. In the selection of a solvent for Raman measurements the importance attached to high refractive index increases the preference for carbon disulfide. The most dramatic difference between infrared and Raman solvent obscuration exists for aqueous solutions; Raman spectra measured in water are free from significant obscuration below 3200 cm.$^{-1}$ and it is unfortunate that the low refractive index of water limits the advantage that can be taken of this.

Most of our spectra have been measured in carbon disulfide, chloroform or carbon tetrachloride, in that order of decreasing preference, and selected bands in the spectra of carbon disulfide and chloroform have been chosen as secondary intensity standards. Conversion factors have been determined relating these to the carbon tetrachloride 459 cm.$^{-1}$ primary standard, both for peak height and total area measurements, under the different conditions of illumination that we normally employ. These figures are listed in Table 3. They permit the transfer of intensity data between measurements in different solvents, subject to the assumption that the absolute intensity of the standard bands do not vary with the medium.

REPRESENTATIVE EXPERIMENTAL DATA

Having disposed of these introductory considerations, we may now take a look at some actual spectra. In Figure 6 is shown a typical spectral chart record obtained from 50 mg. of a

Table 3

Peak Height Conversion Ratios for Secondary Raman Standards

	6 mm. Tube (I.D.)	1 mm. Tube (I.D.)
Carbon Disulfide 656 cm.$^{-1}$		
(No polarizer)	2.53 ± 0.01	2.48 ± 0.02
(⊥ polarizer)	2.29 ± 0.05	2.28 ± 0.07
Chloroform 366 cm.$^{-1}$		
(No polarizer)	0.67 ± 0.01	0.68 ± 0.02
(⊥ polarizer)	0.63 ± 0.01	0.63 ± 0.01
Chloroform 668 cm.$^{-1}$		
(No polarizer)	0.77 ± 0.02	0.77 ± 0.02
(⊥ polarizer)	0.77 ± 0.03	0.77 ± 0.03

The primary standard is the 459 cm.$^{-1}$ band of carbon tetrachloride.

ketosteroid in carbon disulfide solution. This can be considered representative of the quality of numerous steroid Raman spectra we have obtained under conditions of favorable solubility and low background fluorescence. In Figure 7 we see the spectrum of a slightly higher concentration of the same ketosteroid in chloroform solution, measured under the same instrumental conditions. This illustrates the profound effect of the refractive index when using capillary sample tubes. The arrows designate the known band positions, but the signal to noise ratio is too low to yield reliable band measurements unless the spectrum is rescanned several times. The spectrum in Figure 8 is that of a different steroid with 140 mg. in the cell in chloroform solution; it shows that, where the solubility is sufficiently high, the acceptable signal to noise ratio can be reestablished by raising the sample concentration.

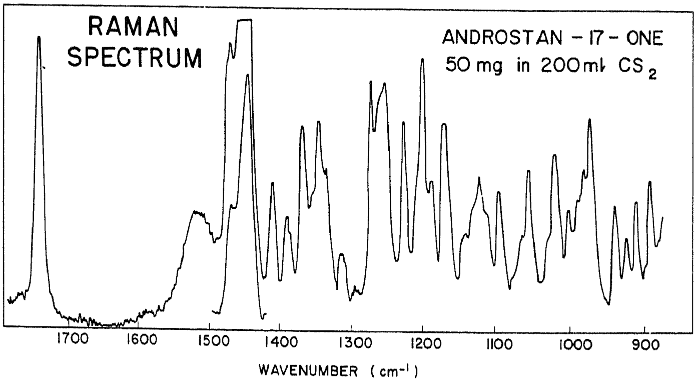

Figure 6

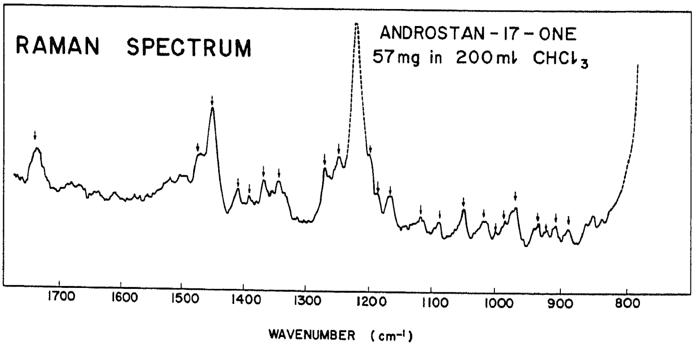

Figure 7

Figure 9 shows the spectrum of a concentrated aqueous solution of a sugar derivative. Here the raw data have been corrected

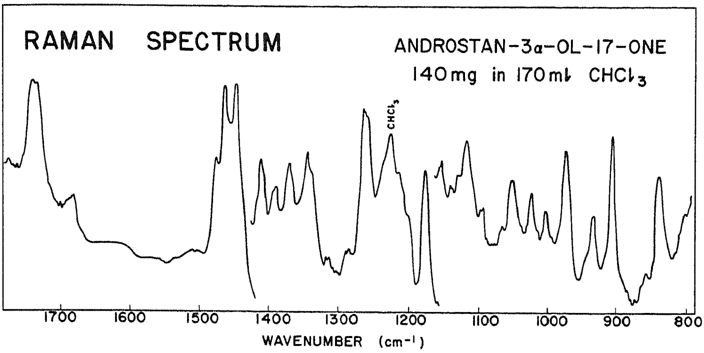

Figure 8

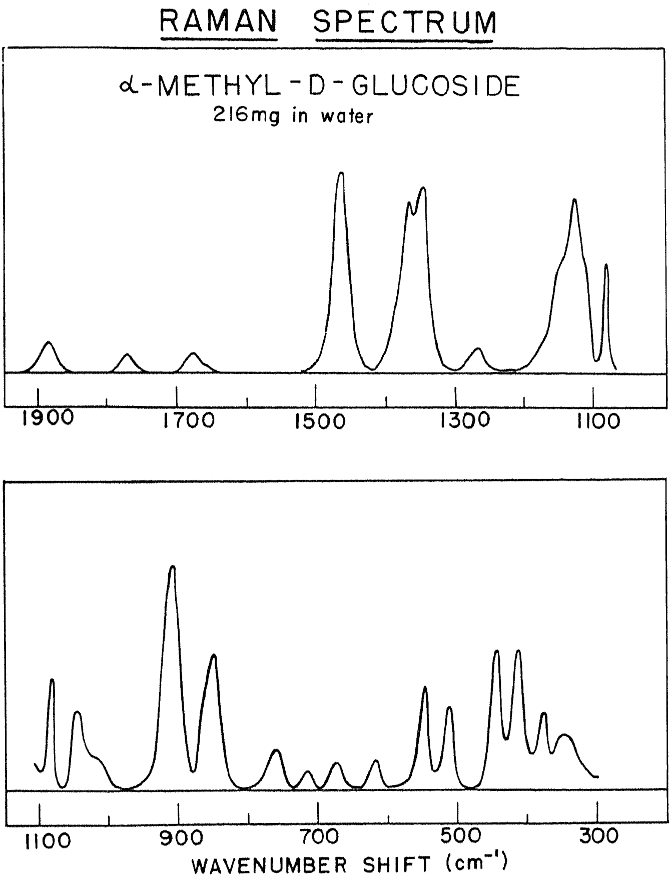

Figure 9

for background slope by drawing tangential baselines to the individual bands. This illustrates the vibrational band structure that can be obtained under favorable circumstances for compounds that have high solubility in water. It is particularly interesting to observe the prominent and well resolved structure between 900 and 300 cm.$^{-1}$.

In order to compare Raman and infrared spectra we replot both curves on adjacent charts using ordinate scales that are chosen to emphasize the band intensity differences. The spectra shown in Figure 10 are representative of such comparative sets of steroid Raman and infrared spectra we have obtained recently.*

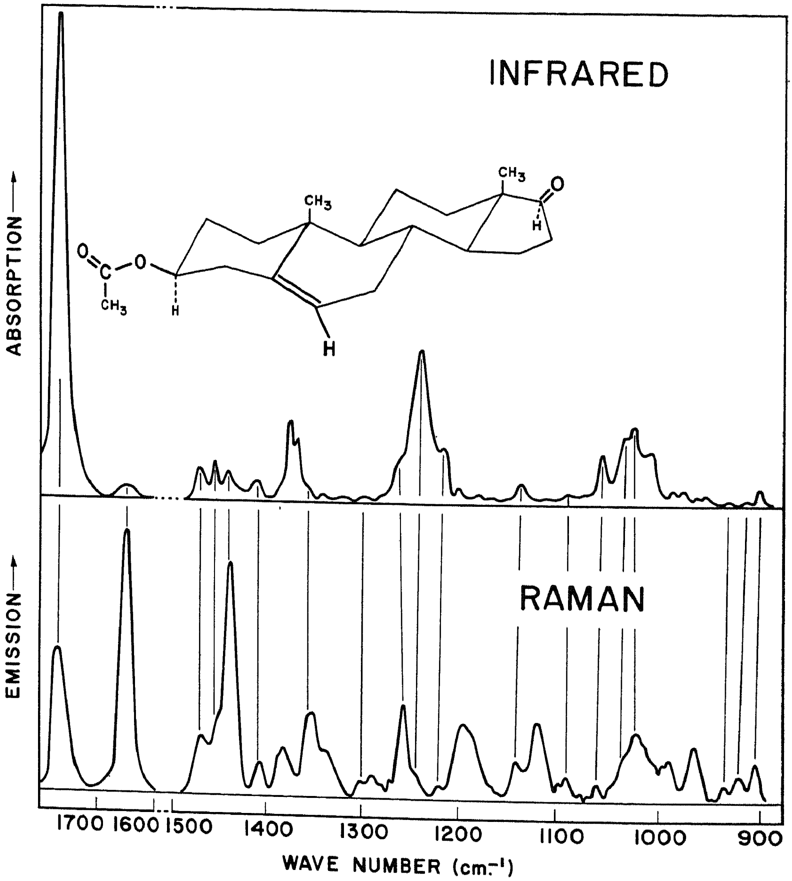

Figure 10

---

*Although the positions of Raman bands should correctly be reported as wavenumber displacements (Δν), it is expedient to overlook this nicety, particularly when detailed comparisons with infrared spectra are being made.

Most notable is the prominent difference in the relative intensities of the C = O and C = C stretching bands; the carbonyl band in Figure 10 is a superimposed doublet from the acetate and the cyclopentano-ketone groups. Since the olefinic C = C stretching bands are relatively so intense, they can be observed at lower concentrations as is shown for the 10 mg. steroid sample in Figure 11.

In the infrared spectrum in Figure 10 the three groups of strong bands near 1360 cm.$^{-1}$, 1240 cm.$^{-1}$ and 1020 cm.$^{-1}$ are all associated with the acetate group, and in the infrared spectra of steroid acetates there is little structure in this "fingerprint" region that can be directly associated with the four ring steroid skeletal system. In the Raman spectrum these acetate bands are weak or absent, but the spectrum as a whole is richer in bands than the infrared spectrum and the greater part of this structure is associated with the carbocyclic skeleton and its attached

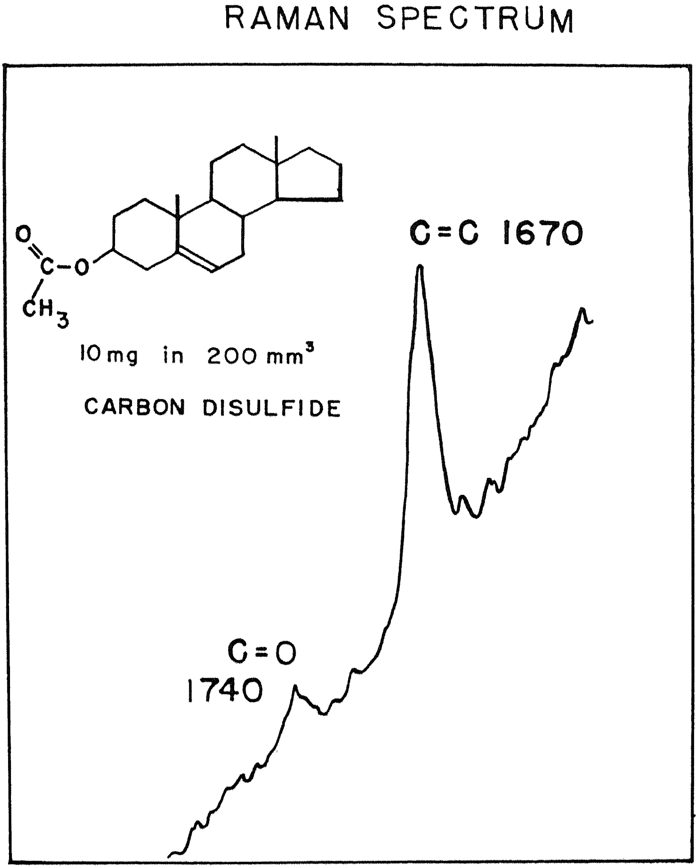

Figure 11

hydrogen atoms. It is indeed a general observation that for aliphatic and alicyclic molecules that contain functional substituents and hetero-atoms, the infrared spectrum below 1350 cm.$^{-1}$ is dominated by strong bands associated with the hetero-atom and its vicinal structure, whereas the Raman spectrum tends to reflect the structure of the carbon skeletal system. This is illustrated also by comparative studies we have recently made of the infrared and Raman spectra of aliphatic methyl esters.

In these investigations methyl laurate was selected as a representative straight chain methyl ester and the derivatives listed in Table 4 were prepared [9]. From a comparative analysis of the infrared spectra of these compounds [10] it was possible to associate all of the bands with specific units of the molecular structure as shown in Figure 12A. The Raman spectra of these compounds show only small differences from one another. The ester group is characterized only by the weak C = O stretching band and the Raman emission in all cases comes predominantly from the chain of nine methylene groups as is indicated by the band identifications in Figure 12B.

Table 4

Methyl Laurate Derivatives

$CH_3 — (CH_2)_9 — CH_2 — CO — OCH_3$
$CD_3 — (CH_2)_9 — CH_2 — CO — OCH_3$
$CH_3 — (CH_2)_9 — CH_2 — CO — OCD_3$
$CD_3 — (CH_2)_9 — CH_2 — CO — OCD_3$

$CH_3 — (CH_2)_9 — CD_2 — CO — OCH_3$
$CD_3 — (CH_2)_9 — CD_2 — CO — OCH_3$
$CH_3 — (CH_2)_9 — CD_2 — CO — OCD_3$
$CD_3 — (CH_2)_9 — CD_2 — CO — OCD_3$

$CH_3 — (CH_2)_{10} — CH_3$
$CD_3 — (CH_2)_{10} — CH_3$
$CD_3 — (CH_2)_{10} — CD_3$

$CCl_3 — (CH_2)_9 — CH_2 — CO — OCH_3$
$CH_3 — (CH_2)_9 — CCl_2 — CO — OCH_3$
$[CH_3 — (CH_2)_9 — CH_2 — CO — OCCl_3]$

The Raman spectra of two other lipids are shown in Figures 13 and 14. In comparing these with the infrared spectra it is interesting to observe the absence from the Raman spectrum of

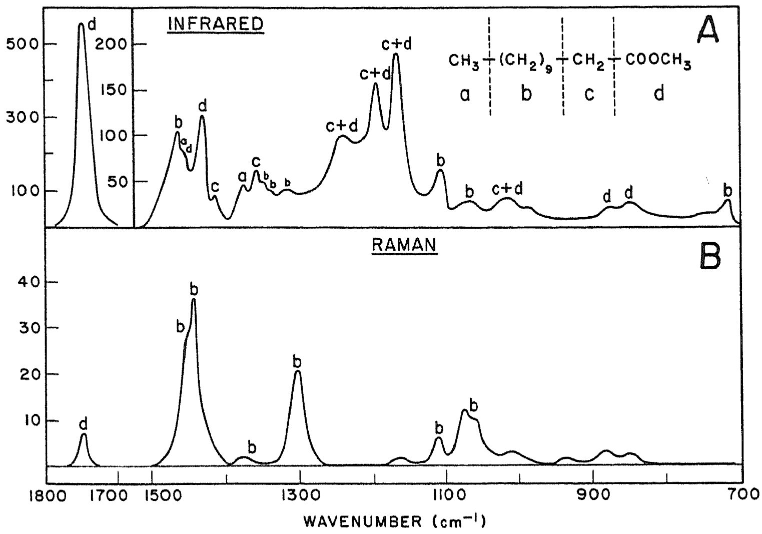

Figure 12

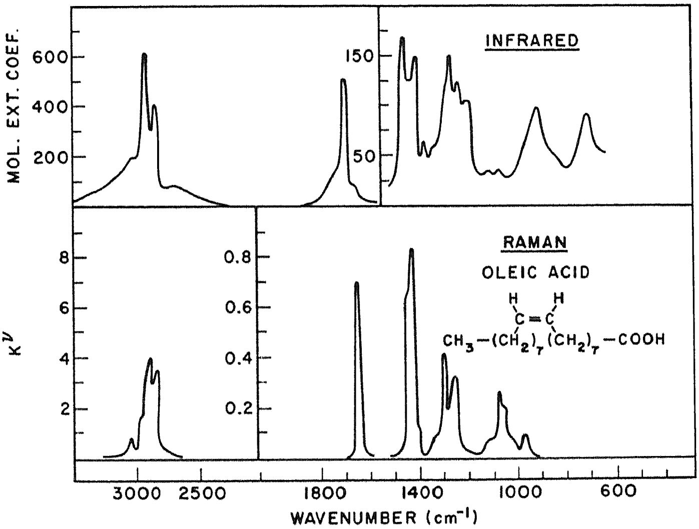

Figure 13

the broad band between 3100 and 2800 cm.$^{-1}$ associated with the hydrogen bonded carboxylic acid dimer group. Because of this, the olefinic C - H stretching band of oleic acid near 3020 cm.$^{-1}$ is seen much more prominently in the Raman than in the infrared spectrum. The displacement of the C = O stretching band of the carboxylic acid dimer from 1707 cm.$^{-1}$ in the infrared spectrum to 1656 cm.$^{-1}$ in the Raman spectrum is well known and was

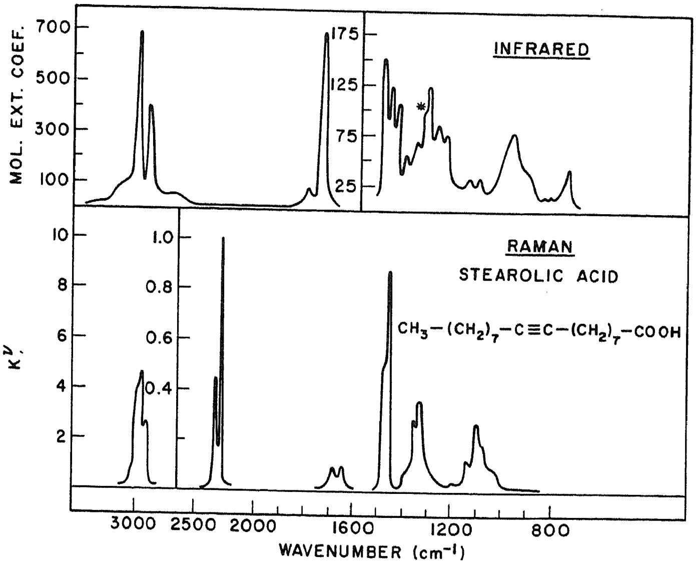

Figure 14

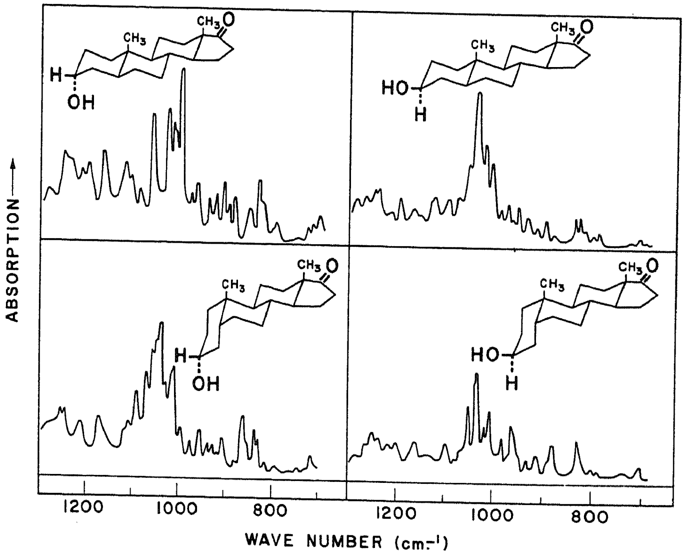

Figure 15

recorded several years ago by Davies and Sutherland [11]. Generally however C = O stretching frequencies of esters and ketones do not differ significantly in Raman and infrared spectra if allowance is made for solvent effects. The prominence of the C ≡ C stretching band (a doublet) in the Raman spectrum of stearolic acid is notable, particularly when it is considered that we were unable to detect this in the infrared spectrum at path lengths up to 2 mm. of the liquid acid. This will not surprise molecular spectroscopists but it is significant from the point of view of organic structural analysis. The only indication of the presence of the acetylenic linkage to be observed in the infrared spectrum of stearolic acid is the weak band (*) at 1335 cm.$^{-1}$ which Mannion and Wang have shown to be associated with a methylene wagging vibration in the $-CH_2-C \equiv C-$ linkage [12]. The intense Raman band associated with the $- C \equiv C -$ group therefore has considerable diagnostic value and was used for this purpose by Pfau, Pictet, Plattner and Süss as long ago as 1935 [13].

THE RAMAN AND INFRARED SPECTRA OF STEROIDS BETWEEN 1350 AND 650 CM.$^{-1}$

Before concluding I would like to deal in more detail with some comparative observations we have been making recently on the Raman and infrared spectra of steroids in the "fingerprint region." Substitution can occur at all positions in the steroid molecule, but we are concerned today only with substitution in one or both of the two end rings. The four infrared spectra shown in Figure 15 have been used before to illustrate the specificity of these spectra and these compounds differ only in the stereochemistry at one ring junction and the attachment of the hydroxyl group. Attempts to relate the bands in these spectra to known group frequency vibrations in simpler molecules have been singularly unsuccessful except for the most prominent band associated with the alcohol group [14-16].

By a purely empirical comparison of the spectra of numerous steroids it is possible to identify the greater part of this infrared band structure with sets of bands associated with the presence of a particular functional group in a terminal ring of specified stereochemistry [17-19]. We have assumed that these bands involve normal modes of vibration in which the hetero-atom of the functional group and the skeletal structure in its immediate environment participate predominently. These bands can be represented by diagrams which we call zone patterns [20,21] and by a linear combination of the zone patterns for different terminal ring systems, the infrared spectra of steroids substituted in both terminal rings can be simulated in good approximation, as is shown in Figures 16-18.

This behavior can be rationalized in terms of the band intensities. Throughout the 1350-650 cm.$^{-1}$ range the infrared absorption intensity of steroid hydrocarbons is much weaker than that of the oxygenated derivatives (Figure 19). In the alicyclic steroid hydrocarbon the charge distribution is fairly even over

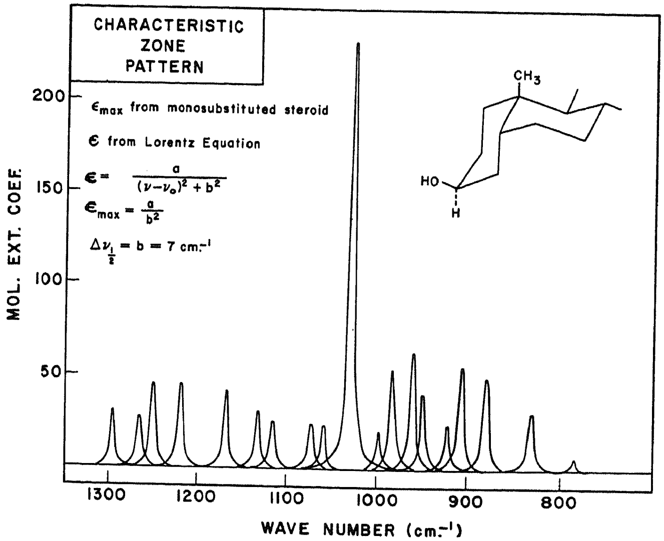

Figure 16

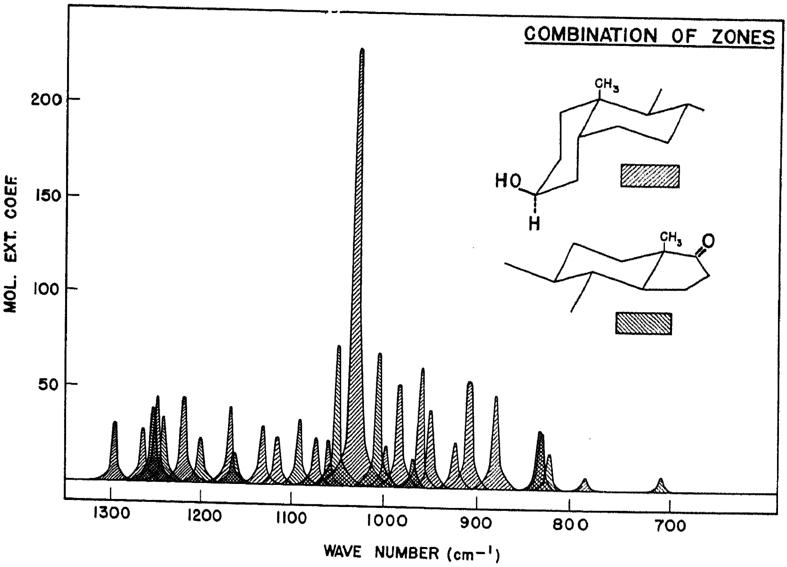

Figure 17

all the hydrogen and carbon atoms so that the dipole moment changes associated with the normal vibrations of such systems will tend to remain small. The introduction of oxygen atoms in C = O, C - O - H or C - O - C linkages will induce larger charge displacements on these bonds and on the neighboring C - C and

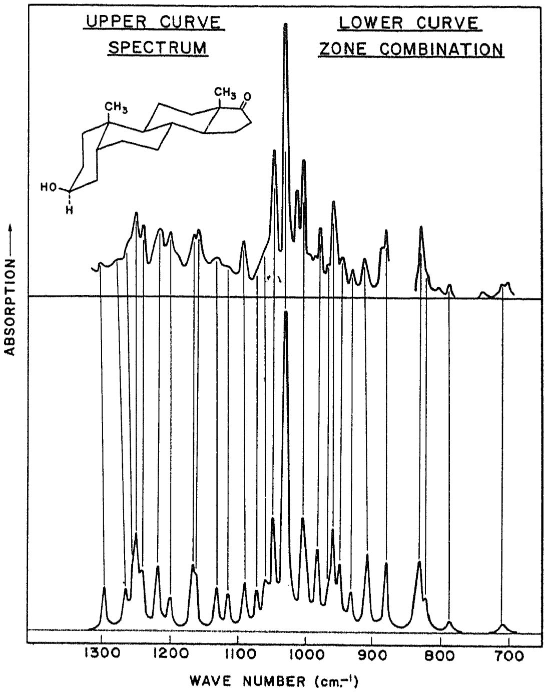

Figure 18

C - H bonds and the normal vibrations that predominantly involve motions of the atoms in this part of the molecule will intensify.

We are now beginning to accumulate a sufficient number of steroid Raman spectra to make similar comparisons, and it is not surprising to find that the emerging patterns of structure-spectra correlations differ radically from those seen in the infrared spectra. In Figure 20 the Raman spectrum of a steroid hydrocarbon is compared with corresponding spectra for a steroid alcohol and ketone, all measured in carbon disulfide solution. Here there is no pronounced enhancement of the overall band intensity on introduction of the functional group, such as we see for the infrared spectra in Figure 19. In Figure 21 Raman spectra are shown for several steroids of the 5β stereochemical series. It is not difficult to recognize a set of six bands that appear to be common to all the spectra. These we can tentatively associate with skeletal vibrations that predominantly involve the central part of the cyclic system and are therefore relatively undisturbed by substitution in the terminal rings. An analogous, but significantly different, set of bands can be discerned in the Raman spectra of the 5α-steroids which differ in the sterochemistry at the junction of the left hand ring.

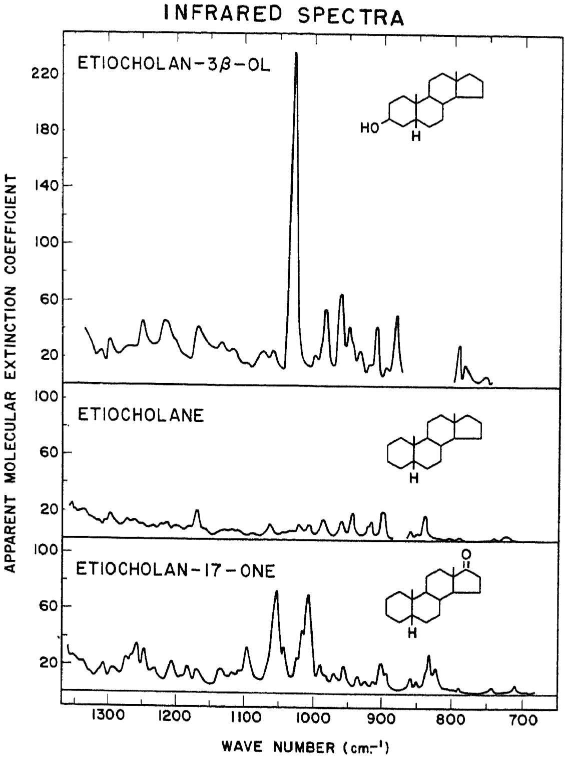

Figure 19

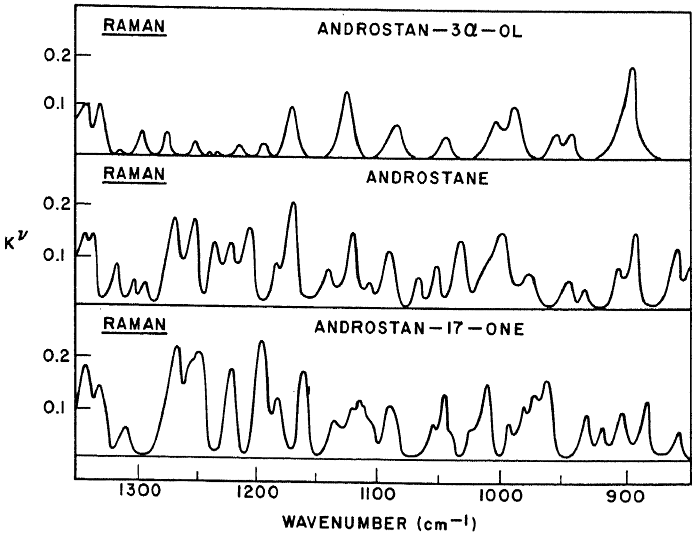

Figure 20

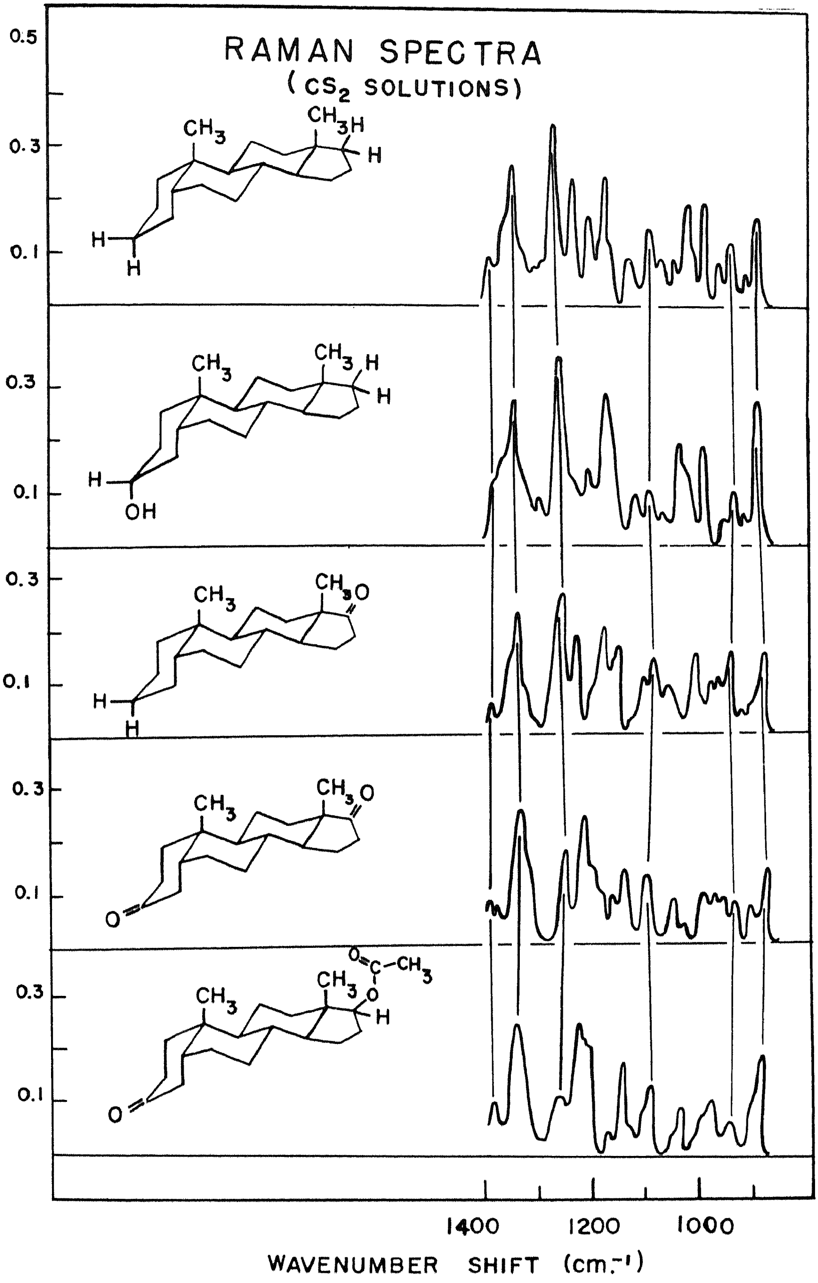
RAMAN SPECTRA
(CS_2 SOLUTIONS)
0.5
0.3
0.1
0.3
0.1
0.3
0.1
0.3
0.1
0.3
0.1
CH_3
CH_3
H
H
OH
O
O=C–CH_3
1400
1200
1000
WAVENUMBER SHIFT (cm.$^{-1}$)

Figure 21

Our next step in this analysis is to re-examine the infrared spectra in regard to the information gained from the Raman spectra. Figure 22 is the infrared spectrum of a 17-ketosteroid of the 5α-series. The bands identified with the functional group are indicated by the lines drawn down from the top of the figure while the lines drawn up from the bottom indicate the positions of the Raman bands. It will be seen that while there are several coincidences, a good number of the prominent Raman bands correspond with weak infrared bands that are not specific to the functional group structure.

In our attempts to characterize bands in steroid infrared spectra we have also made use of selective deuteration, and this has been particularly effective when applied to ketones, where the hydrogen atoms on vicinal methylene groups are replaced by deuterium on enolization [22,23].

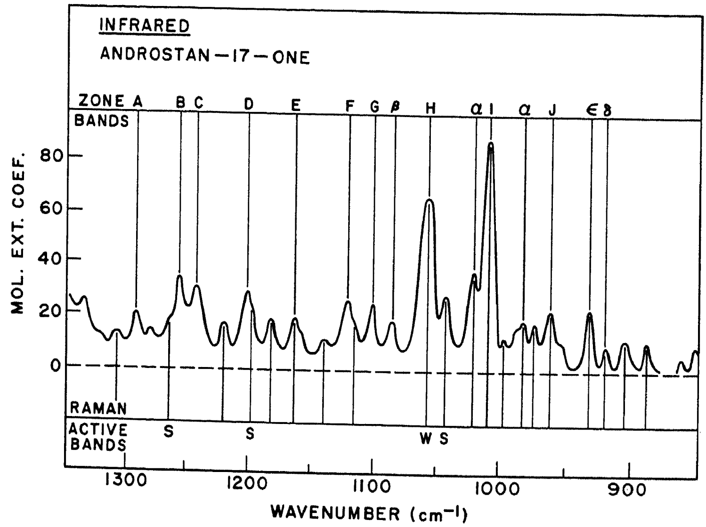

Figure 22

In Figure 23 we have summarized the total information we have acquired about the infrared spectrum of a representative steroid, etiocholan-3, 17-dione, by a combination of deuterium substitution, functional group zone analysis and Raman spectrometry. It will be seen that most of the bands can be associated by one or other of these methods with specific units of the molecular structure, and that where the evidence from two methods overlap it is consistent. In the lowest panel of Figure 23 the uncharacterized residual absorption is indicated. With one exception, this consists only of weak bands and inflections. Notable however is the prominent band at 1017 cm.$^{-1}$. We chose etiocholan-3, 17-dione for this illustration since prominent bands of

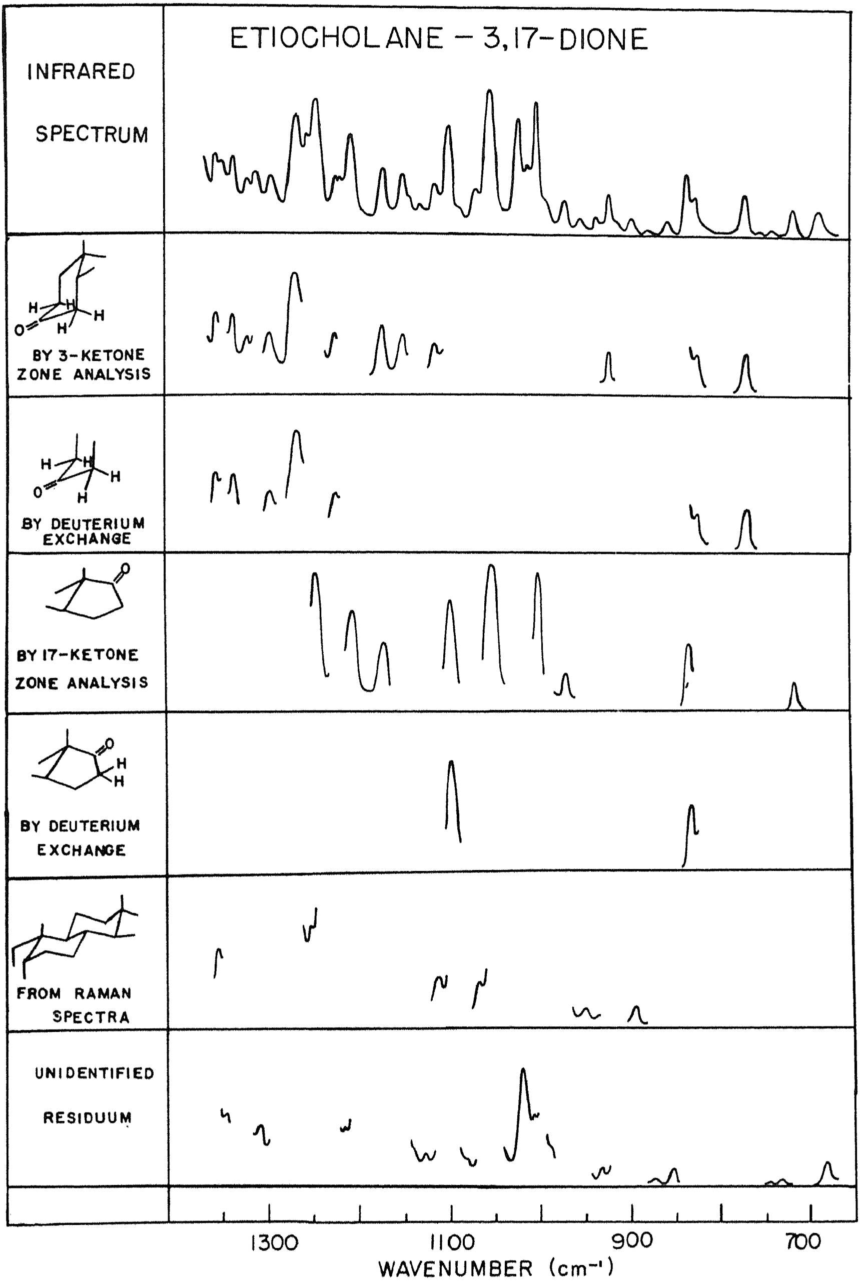
ETIOCHOLANE – 3,17–DIONE
INFRARED SPECTRUM
H
H
H
H
O
BY 3–KETONE ZONE ANALYSIS
H
H
H
H
O
BY DEUTERIUM EXCHANGE
O
BY 17–KETONE ZONE ANALYSIS
O
H
H
BY DEUTERIUM EXCHANGE
FROM RAMAN SPECTRA
UNIDENTIFIED RESIDUUM
1300
1100
900
700
WAVENUMBER (cm⁻¹)

Figure 23

this kind are unusual and it does indicate that functional groups at remote positions can induce strong perturbations of the molecular vibrations of steroid molecules, though our general conclusion is that this effect is much less extensive than one might anticipate. The recognition of strong anomalous infrared bands such as this 1017 cm.$^{-1}$ band of etiocholan-3, 17-dione may have some bearing on the problem of the "long range" chemical effects that have been investigated extensively by Prof. Barton and his collaborators [24] and attributed by them to the transmission of conformational strain through the ring system. These spectroscopic observations suggest a new way for the systematic investigation of the physical basis of such long range chemical effects.

I should emphasize that, in the present state of our knowledge, we do not feel there is justification for making vibrational assignments to any of these bands. If we can successfully pull apart the infrared and Raman spectra of some of these complex molecules in this fashion, we are satisfied, for the time being, to accept this as an end in itself. We are working only by guess and intuition. We have no real way of telling if bands at similar positions, with comparable intensities in the spectra of a series of related compounds are, in fact, associated with related normal modes of vibration. If our guesses prove correct three times out of four, I would consider that an acceptable batting average. Only if the patterns prove to hold consistently over a continuously increasing body of data can we feel confident of their physical significance and justifiably press the analysis further.

CONCLUSION

This seems to have brought us a long way from our original concern with the measurement of Raman spectra. In the present state of that art, I think the most profitable use the organic chemist can make of Raman spectrometry is to learn more about the behavior of the infrared group frequency vibrations. For this purpose he can select compounds that are in good supply and purify them rigidly. In the immediate future this is likely to be more profitable than the direct application of Raman spectrometry to the analysis of naturally occurring organic compounds and their degradation products. The more interesting new compounds obtained from natural sources are rarely available in sufficiently large quantities for Raman spectrometry, even using these improved semi-micro methods. Because of the problems presented by fluorescing impurities, solubility limitations, and refractive index restrictions, the measurement of each Raman spectrum poses a miniature research problem of its own. We have not yet found a general method of preparing steroid samples for Raman spectrometry. Some compounds respond to vacuum sublimation, others to multiple recrystallization from a suitable solvent, while still others must be converted to a derivative and reconverted back after purification. We find many recalcitrant compounds that fail to respond to any kind of purification treatment we have so far managed to devise.

In spite of these difficulties, I am confident that the technical problems limiting the routine use of Raman spectrometry as a tool in organic structural analysis can be overcome if there is sufficient incentive to do so. The fluorescence problem could be greatly alleviated by using exciting radiation of longer wavelength. Dr. Lippincott, here at the University of Maryland, Dr. Stammreich, and others are already working with conventional emission sources of red radiation, while ruby and neodymium masers hold promise of a technical break-through in long wavelength Raman sources. More accurate intensity measurements and further reduction in the minimum sample size will be difficult to achieve as long as the capillary light-pipe source optics are employed. The total volume of the present capillary liquid cell is equivalent to that of a cube of 6 mm. face. If a means could be developed of generating the same total flux of Raman radiation in a cell of this geometry, multiple reflection from the lateral cell walls might be avoided, and with it, the critical intensity dependence on the refractive index of the medium.

While awaiting these developments we believe there are many interesting things to be learned about the Raman spectra of complex molecules that can be tackled with the facilities at present available, and we look forward to having a lot of fun while doing it.

REFERENCES

1. D. Garfinkel and J. T. Edsall, J. Am. Chem. Soc., 80, 3818 (1958) and earlier publications.
2. H. J. Bernstein, Pure and Applied Chemistry 4, 23 (1961).
3. G. Michel and R. Gueibe, Bull. Soc. Chim. Belges, 70, 323 (1961).
4. D. G. Rea, J. Opt. Soc. Amer., 49, 90 (1959).
5. D. D. Tunnicliff and A. C. Jones, Spectrochim. Acta, 18, 569, 579 (1962).
6. J. Brandmüller and H. Moser, Einführung in die Ramanspektroskopie. Dietrich Steinkopff Verlag. Darmstadt 1962. pp. 235-280.
7. H. J. Bernstein and G. Allen, J. Opt. Soc. Amer., 45, 237 (1955).
8. H. J. Bernstein. Personal communication.
9. M. E. Isabelle and L. C. Leitch, Can. J. Chem., 36, 440 (1958).
10. R. N. Jones, Can. J. Chem., 36, 301 (1962).

11. M. M. Davies and G. B. B. M. Sutherland, *J. Chem. Phys.*, *6*, 755 (1938).
12. J. J. Mannion and T. S. Wang, *Spectrochim. Acta*, *17*, 990 (1961).
13. A. St. Pfau, J. Pictet, P. Plattner, and B. Susz, *Helv. Chim. Acta*, *18*, 935 (1935).
14. A. R. H. Cole, R. N. Jones, and K. Dobriner, *J. Am. Chem. Soc.*, *74*, 5571 (1952).
15. W. G. Dauben, E. Hoerger and N. K. Freeman, *J. Am. Chem. Soc.*, *74*, 5206 (1952).
16. H. Rosenkrantz, A. T. Milhorat and M. Farber, *J. Biol. Chem.*, *195*, 509 (1952).
17. R. N. Jones, F. Herling and E. R. Katzenellenbogen, *J. Am. Chem. Soc.*, *77*, 651 (1955).
18. R. N. Jones and F. Herling, *J. Am. Chem. Soc.*, *78*, 1152 (1956).
19. R. N. Jones and G. Roberts, *J. Am. Chem. Soc.*, *80*, 6121 (1958).
20. R. N. Jones, *Trans. Roy. Soc. Canada*, *52*, (III), 9 (1958).
21. R. N. Jones, *Selected Scientific Papers from the Istituto Superiore di Sanitá*, *2*, 514 (1959).
22. B. Nolin and R. N. Jones, *Can. J. Chem.*, *30*, 727 (1952).
23. R. N. Jones, B. Nolin and G. Roberts, *J. Am. Chem. Soc.*, *77*, 6331 (1955).
24. D. H. R. Barton, F. McCapra, P. J. May and F. Thudium, *J. Chem. Soc.*, 1297 (1960).

THE ORIGINS OF GROUP FREQUENCY SHIFTS. PART II THE INFLUENCE OF INDUCTIVE EFFECTS AND OF NON-BONDED INTERACTIONS ON INFRARED GROUP FREQUENCIES

L. J. Bellamy
Ministry of Aviation, E.R.D.E.
Waltham Abbey, Essex, England

INTRODUCTION

A good deal of progress has been made in the past few years in our understanding of group frequencies. Studies have of course been limited to those vibrations which are least sensitive to mass or coupling effects, but this is not a serious limitation as these are the most reliable and widely used correlations. The behaviour of such group frequencies with changes in the substituents have been explained in terms of the impact of inductive and resonance effects, together in a few cases with "field effects" between non-bonded atoms. The evidence for this rests upon the large number of successful correlations which have been found between the changes in frequency and the changes in some other physical property which are known to depend upon these same factors. Thus group frequency shifts have been related to changes in Hammett σ [1-19] and Taft σ^* [20-23] values, to ionisation potentials [24, 25], to electronegativities [20, 26-29], to half wave potentials [30-31], to redox potentials [32-34], to the exaltations of molecular refraction [20] and other similar properties.

While the results appear to afford a generally satisfactory picture of the behaviour of these group frequencies, a detailed study, particularly in relation to the impact of inductive effects, is more disquieting. It is to be expected that inductive effects operating along the bonds will depend only upon the relative electron attracting properties of the substituents. A constant and reproducible order of effectiveness of the various substituents should therefore be found in all instances. This is very far from the case. Some group frequencies such as νOH in CH_2RCOOH [20], νNO_2 as in RCH_2NO_2 [23] and νSiH in SiR_3H [22] follow Taft σ^* values (F > Cl > Br > CCl_3 > OR > CH_3), but others such as νP = O [27] and νS = O [28] are reported to follow an order more nearly related to the electronegativities (F > OR > NR_2 = Cl > Br > CH_3). The sym. deformation frequencies of CH_3X compounds follow yet another order (F > OR > NR_2 > CH_3 > Cl > Br), which is the same as that of the XH vibrations themselves [35, 36]. The contrast between the methyl and silyl series is particularly striking as both have the same hybridisation and the same valence state. Finally, the frequencies of the CH_2 deformation of vinyl and vinylidene compounds [37] follows the remarkable order CF_3 > SiR_2 > CH_2Cl > CH_2OR > CH_3 > Br > Cl > F > OR.

In multiple bond systems the confusion is even worse. Carbonyl frequencies have been correlated with electronegativities [26], with Taft σ^* values [21] and with ionisation potentials [25] despite the internal differences of these separate measures of the inductive effect. Moreover, Overend and Scherer [38] have shown that a significant part of the frequency shifts must be attributed to the effects of mass and of non-bonded interactions. The differences in νCO in COF_2 and $COCl_2$ for example are stated to arise wholly in this way.

A detailed study of the various correlations between frequencies and physical properties shows that the majority of them at least are experimentally sound. The question therefore arises, why does the "inductive effect" of a given group, in relation to that of another vary so widely in different situations? This is of course a problem of general chemistry, but it is of particular importance to the spectroscopist if he is ever to achieve a proper understanding of the behaviour of group frequencies. A review of the existing data (details below) indicates that (a) correlations between frequency shifts and physical properties appear to work best when the comparison involves some experimental measurement of the bond polarity (i.e., proton acceptance, ionisation potential reactivity, etc.). Correlations with generalised functions such as electronegativity are less sound. (b) The substituent groups do show a uniform order of effectiveness (that of Taft σ^* values) provided the study is limited to groups well removed from the vibrating group under examination. The alteration of a substituent directly attached to either of the vibrating atoms usually changes this order. This last observation is particularly suggestive when it is recalled that the Taft σ^* values are themselves determined only as groups well removed from the COOR group which undergoes hydrolysis. These observations therefore lead to the idea that the Taft σ^*

order represents the true incidence of inductive effects operating along the bonds, and that deviations occur due to non-bonded interactions when the substituent is brought nearer in space to the vibrating group. Unfortunately the only measure we have at present of such interactions is through normal coordinate calculations using the Urey-Bradley Force Field. This has well recognised limitations, not the least of which is the failure to discriminate between the different repulsive effects which will arise between bonding and non-bonding electrons. Nevertheless whatever its deficiencies in yielding absolute values for the magnitude of non-bonded interaction, it is at least likely to provide relative values which have some validity. The non-bonded interactions assessed in this way are assumed to originate in van der Waals forces. However the fact that the values so obtained frequently relate to the electronegativities of the atoms concerned suggests that coulombic forces are also involved. In the following review the incidence of inductive effects upon group frequencies is considered in the light of the results of Urey-Bradley calculations to see how far this concept is able to rationalise the otherwise chaotic data.

GROUP FREQUENCIES INVOLVING MOTIONS OF HYDROGEN ATOMS

XH Stretching Frequencies

These will be considered briefly as they have some relevance to the discussion of CH_3X frequencies which follows. It has been suggested that the force constants k_{HX} depend only upon the polarity of X and that they might therefore be used to provide an electronegativity scale [24]. However while the force constants for the radicles do appear to be related to Pauling electronegativities, the corresponding relationships for the normal valence states are more limited. It can be shown that linear relationships exist between k and E (Electronegativity) within any one row or any one period of the periodic table but there is no overall relationship [39].

E will be the major factor in determining k because it is a function of the radius and polarity of X, and k will primarily depend upon the bond length and on the polarity (which influences the bond strength by causing changes in the electron distribution). This is very well illustrated in the simple plot in Figure 1 in which k_{HX} is plotted against N, the residual nuclear charge, the k values being taken from the useful compilation of Cottrell [42]. Within the first row of the periodic system a good straight line results which passes as it should, through the origin (k_{HeH} = O).

Within this row the covalent radius changes only slowly compared with the changes in N. However a new line of different slope is produced by the second row of the table as major change in the bond length is now involved.

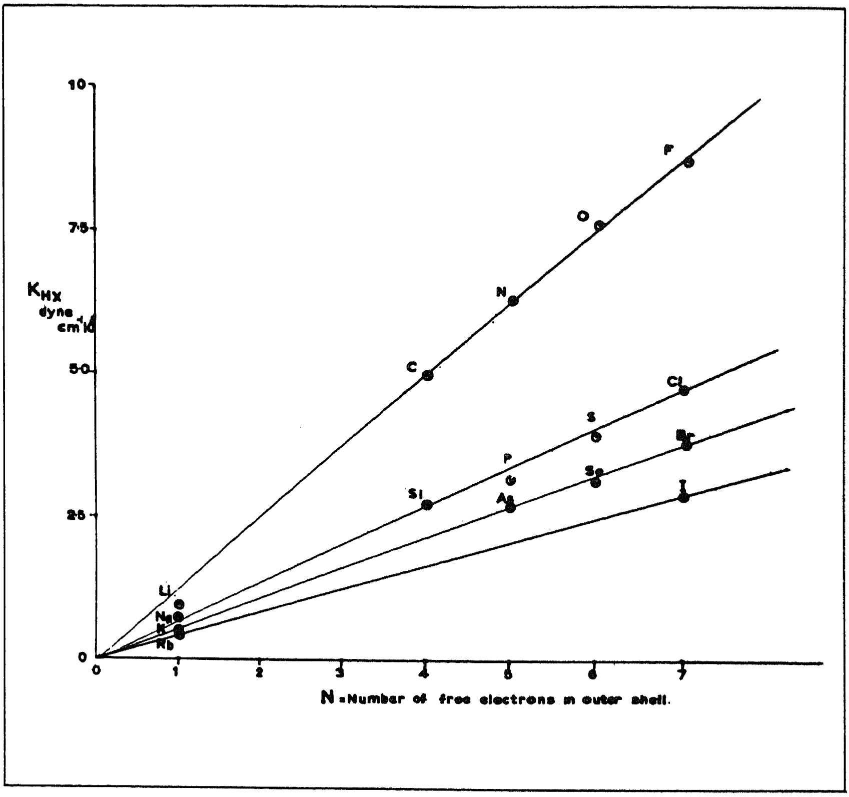

Figure 1

The frequency is therefore determined by two variables—the polarity and the radius—neither of which is wholly independent of the other. The polarity (E) is a function of the effective nuclear charge of X and of the distance away (r) that this is from the H atom. However, when, as here, the X atom is part of the vibrating bond the radius plays a direct part in determining the frequency as it fixes the approximate bond length. This in turn is somewhat modified by the effect of the polarity.

The result is that *k* is not a simple function of the polarity E but is related to it, as mentioned above only within any one row or any one column of the periodic table. In the simplest terms, the C-H stretching frequency is higher than HCl because the bond is shorter, even though the latter is more polar.

CH_3X *Sym* Deformation Frequencies

These frequencies have been studied by several workers. Sheppard [35] has shown that like *k* HX they show relationships with E which are valid within any one row or period of the periodic system, and Wilmshurst [29, 40] has developed a series of group electronegativities based on these values. These however do not seem to be well related to other measures of the inductive effect, the CH_2Cl group for example having a higher electronegativity than chlorine itself. A similar difficulty arises if one attempts to extend the electronegativity relationships suggested by King and Crawford [60]. A direct relation has also been described between HX and the frequencies of each of the five CH_3 modes of the CH_3X series [36]. This relation is particularly good for the δCH_3 symmetrical mode which shows the largest shifts but is less effective for νCH which is less sensitive to changes in X and in which the frequencies sometimes follow a different order. The relation between k_{HX} and δCH_3X has been extended and is shown in Figure 2. The values for k are taken from [42] and of δCH_3X from [35]. The curvature found is to be expected from a plot of force constants against frequencies.

The relationship is a good one and shows that like k_{HX}, these frequencies must depend upon the polarity of X, its distance from the CH_3 group and upon angle effects due to alterations in the valence state. It also indicates that the δCH_3 vibration is relatively free from mass effects which would otherwise invalidate this relation. This is also implied by the findings of King and Crawford [60]. The dependence of the CH_3 deformation frequency on the C-X bond length is surprising, as X does not now form part of the vibrating group and inductive effects operating through the bonds would therefore be expected to relate only to the polarity of X at its normal covalent distance (i.e., to the electronegativity). The fact that there is such a dependence is nevertheless very clear from Figure 3 in which δCH_3X is plotted against the value of ν C-X given in [53]. The C-X radius changes little along any one row of the periodic table and the frequencies rise with the effective nuclear charge. A change of radius following a change of row however leads to substantial alteration in δCH_3.

Although the C-X distance is unlikely to be an important factor in inductive effects relayed along the bond it will influence the magnitude of non-bonded interactions between the hydrogen and X atoms particularly in the deformation mode when all three hydrogen atoms move simultaneously towards X. Overend and Scherer [41] have attempted to calculate the magnitude of these interactions using the Urey-Bradley Force Field.

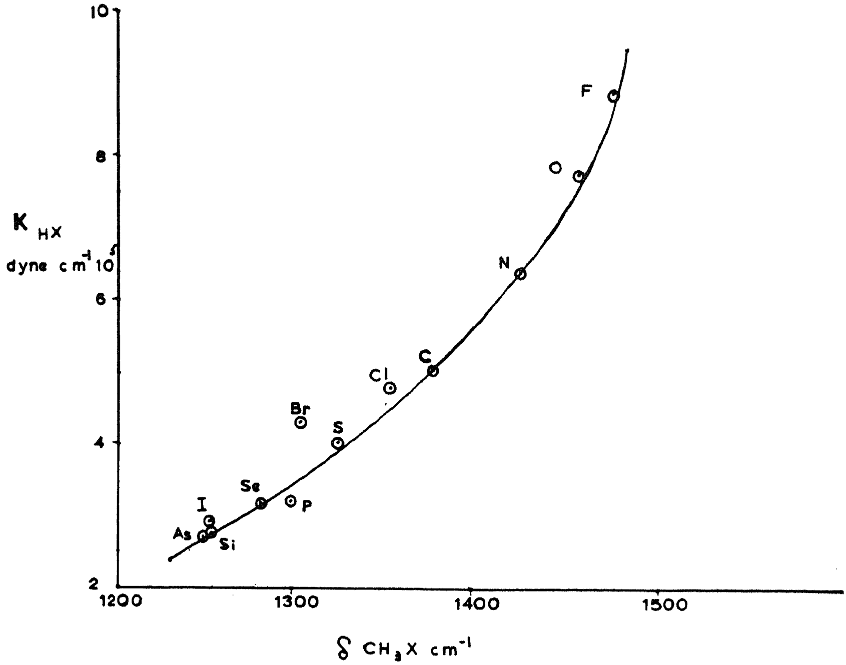

Figure 2

On passing from methyl fluoride to methyl iodide, the CH force constant changes from 4.372 md/A to 4.851 md/A, but the non-bonded interaction constants F_{HX} change from 1.118 md/A to 0.393 md/A.

Whatever the absolute validity of these values they do show that the non-bonded interactions in this series are considerable. It is therefore reasonable to suggest that the δCH_3X frequencies depend upon a combination of inductive effects and of non-bonded interactions. If this is so, the parallel behaviour with HX frequencies shown in Figure 2 follows at once, as these also depend upon the radius and charge of X and upon the valency state. More important, it explains also the marked differences in behaviour of the methyl and silyl group frequencies. Parallel calculations by Overend and Scherer [54] show that the non-bonded interactions are smaller in the silyl halides, as is to be expected from the large size of the silicon atoms. These frequencies should therefore be mainly dependent upon inductive effects operating along the bonds. The observation that $SiHR_3$ stretching frequencies follow good Taft σ^* relationship [22] whereas the

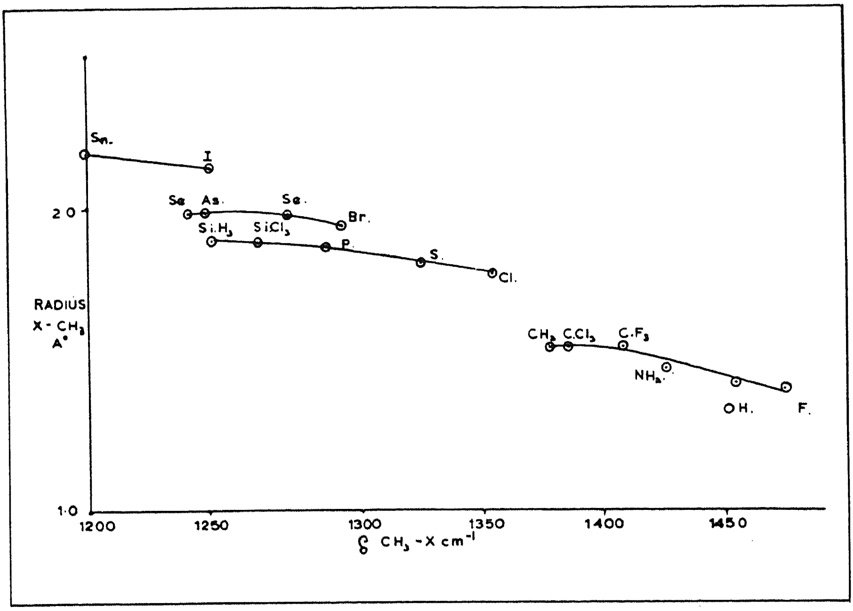

Figure 3

corresponding CH stretching frequencies behave erratically is therefore understandable on this basis. Similarly the relationship found by Hyde et al. [59] between νSiH and the log of the equilibrium constant for the hydrolysis of the corresponding chlorosilanes is to be expected if both are controlled only by normal inductive effects. Some minor support for the importance of non-bonded interactions on CH_3X deformation frequencies is also given by our observation that an excellent straight line relationship exists between Overend and Scherer's F_{HX} for CH_3X systems and the corresponding HX force constants (Fig 4).

The Vinyl and Vinylidene CH_2 Wagging Mode

This band appears in olefines as a very characteristic strong absorption near 900 cm⁻¹ and has been studied by several workers. Some years ago it was shown that the frequency followed a reasonably good relation with E for simple substituents [20], although a more recent assignment for the vinyl ethers would now throw oxygen out of line. However, as noted above, groups such as CH_2Cl alter the frequency in the opposite direction to halogen substitution, and no simple correlation with E can be obtained. Potts and Nyquist [37] have published extensive data on this frequency, and have attempted to relate it to the resonance characteristics of the R groups through relations

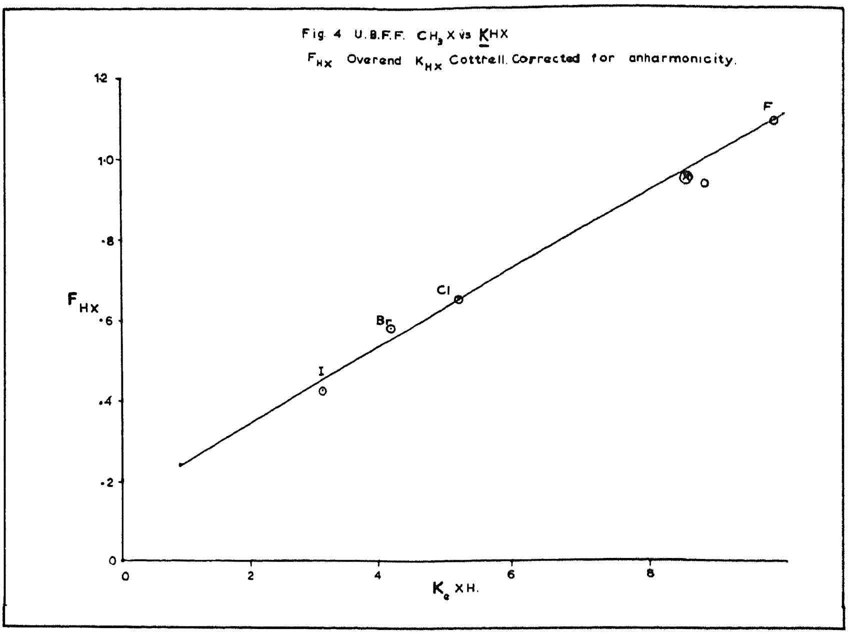

Figure 4

with either the percentage of meta isomer produced on the nitration of C_6H_5R or with a complex function involving the difference between Hammett para σ values and Roberts and Morelands σ' factor. However neither of these correlations is wholly convincing.

It seems inherently improbable that resonance effects will affect this frequency if only because the fully conjugated systems 1:3 butadiene and styrene show the same frequency as propylene, and resonance interactions through lone pair orbitals are likely to have smaller effects than a full double bond. Similarly, active groups in the meta or para positions of styrene have only very small effects on this frequency. Equally however the data suggests that direct inductive effects operating through the change of hybridisation of the carbon atom carrying the substituent are not likely to have much effect either. This can be seen from a comparison of the δCH_2 frequencies of exocyclic methylene groups attached to rings of various sizes. Here, there are substantial changes in the hybridisation of the ring carbon atom with alterations in the bond angles. Despite this, the δCH_2 frequencies show little change. This is illustrated by the following values taken from cards in the D.M.S. series. Camphene 885 cm^{-1}, pinene 884 cm^{-1}, 1:2 dimethylene cyclopentane 881 cm^{-1}, 1:3 dimethylene cyclobutane 880 cm^{-1}, 1:2 dimethylene cyclobutane 887 cm^{-1}, methylene cyclopropane 892

cm^{-1}. These are to be compared with the range 885-890 cm^{-1} given by Potts and Nyquist for alkyl substituted vinylidene compounds. The differences are small and may well be due to the fact that the measurements were made in various laboratories.

It therefore seems possible that this is an exceptional group frequency which is primarily controlled by non-bonded interactions between the R group and the carbon atom of the CH_2. The interactions with the hydrogen atoms are likely to be small with simple substituents, as the distances are greater, and the F values will fall off in exponential fashion following at least a sixth power law. In order to test this suggestion it is necessary to have some measure of the non-bonded interaction forces which can be related to the frequencies. Unfortunately in many atom systems such as the vinylidene compounds, Urey-Bradley Force Field treatment yield poor values for the non-bonded F_{RC} interactions and the few examples which are available show considerable dispersions. However the same considerations do not apply to the four atom systems $R_1R_2C{=}O$, for which a number of refined F_{RO} values are available [38]. The geometry of the carbonyl and vinylidene systems is so very similar that it is reasonable to suppose that the various R substituents will show the same relative order of non-bonded interaction with the carbon atom, even though there will be differences in their absolute magnitudes in the two cases.

We have therefore compared the variation in δCH_2 with the sum of the F_{RO} values for the same substituents in the carbonyl series. The result is shown in Figure 5 and is surprisingly good. The failure to pass through the points corresponding to R=H (ethylene) or $R{=}SiH_3$ (F=O) is to be expected from the fact that F_{RO} values are used and not F_{RC}. However the close similarity of the frequencies of ethylene and of the SiH_3R_3 substituted compound fits in well with this picture as the non-bonded interaction can be assumed to be very small in both cases, due to the small charge in the hydrogen atom and to the large radius of silicon. This therefore, rather than the reduced electronegativity of silicon is responsible for the raised frequency over the value for alkenes.

Figure 5 offers also interesting possibilities for use in normal coordinate treatments. It does show that whatever their absolute validity, the F values of Overend and Scherer for the carbonyl series have a real internal consistency. If the programming of the computer could be arranged to select values showing the same order of internal consistency in the vinylidene series, it might be possible to reduce some of the errors which arise from the multiplicity of interaction terms.

While the figure suggests that non-bonded interactions are indeed responsible for the greater part at least of the frequency

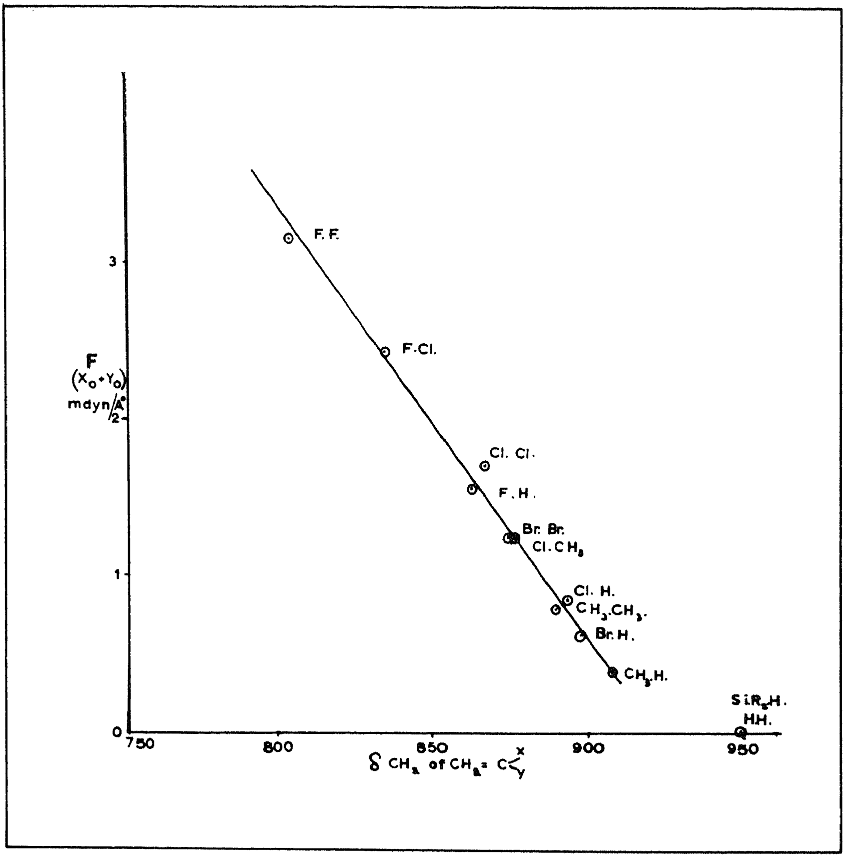

Figure 5

shifts, it does not immediately explain the low frequencies shown by oxygenated substituents or the high frequencies shown by CH_2Cl groups. In the absence of F values, it is not possible to decide the origin of these effects with any certainty. However it seems likely that in the case of oxygen, resonance effects are indirectly responsible. While these are unlikely to affect the frequency through delocalisation effects they will lead to an increase in the effective charge on the oxygen atom which could result in an F_{OC} value greater than that of fluorine. This is supported by the fact that when the resonance is reduced by the presence of a carbonyl group, as in vinyl esters (*vide* their high carbonyl frequencies) the δCH_2 frequencies fall to a value which is consistent with the electronegativity of oxygen, and which is intermediate between the values for fluorine and chlorine substituents.

In the case of substituents such as CF_3 or CCl_3 it is clear that one halogen atom now comes nearer in space to a hydrogen atom of the $=CH_2$ group than it does to the corresponding carbon. The interaction will therefore be dominant and as the effect of this will be to close down the HCH angle—as in the case of the methyl halides, it is possible to see why it is that these electronegative substituents actually lead to a frequency rise. The case of substituents such as CH_2Cl are complicated by the possibility of rotational isomerism and must await further study. If however it should prove that the stable isomer is one in which the chlorine atom is brought close to the $=CH_2$ group—i.e., if they are similar to the corresponding carbonyl compounds [43-45]—then the interpretation of the frequency rise again becomes possible. In this connection it is interesting to note that a difference of some 14 cm^{-1} is found between the equatorial and axial isomers of substituted methylene cyclohexanes with OR groups in the 2 position [55]. These differences could only arise from differences in non-bonded interactions of the same type. However this possibility (which would allow a complete explanation of the remarkable order in which substituents influence this group frequency) must await further experimental evaluation.

Hydrogenic Frequencies following Hammett σ and Taft σ^* Relationships

The CH deformation frequencies discussed above represent extreme cases in which non-bonded interaction effects are particularly important. In compounds in which the polar substituent is well removed from the vibrating group, the opposite will be true and only inductive forces will be effective. This is clearly so in the many aromatic systems in which relationships have been demonstrated between group frequencies [1-19] or intensities [10, 13, 16, 46-48] and the Hammett values of meta and para substituents. Here the frequencies reflect accurately the polarity change resulting from the resonance and inductive effects of the substituents and a statistical study of the extensive data available would probably yield σ values of greater reliability than those derived originally from kinetic data. In the aliphatic series, this is true also for those frequencies which follow a relationship with Taft σ^* values [20-33, 49]. Although Taft values are quoted [50] for the effects of directly attached substituents, these are obtained by the use of a scaling factor and the basic measurements are made with R substituents at the α or β carbon atom attached to the COOR group. (The value for a fluorine substituent is for example derived from studies on CH_2FCOOR, and the acid FCOOH does not exist.) Nonbonded interactions are therefore likely to be minimised in this series.

The observed relationship between Taft σ^* values in acids and the νOH monomeric frequencies in solution [20] therefore arise because the reaction rates and the frequencies are both controlled by genuine inductive forces. The differences noted earlier in the behaviour of CH_3X and $SiHX_3$ frequencies are also understandable on this basis.

GROUP FREQUENCIES INVOLVING MULTIPLE BONDS

The Carbonyl Group

This frequency is of course influenced by resonance effects as well as by induction. However even when the former is absent we have the conflicting relationships already referred to. A detailed study of the relationships between νC=O and electronegativity [26], or Taft σ^* values [21], shows that both are based on a limited range of compounds and that neither is valid when this range is extended. The former for example is based only on halogen substituents and assigns effective electronegativities to groups such as CH_2Cl which we now know to influence the frequency primarily through "field effects." The Taft relationship fails in other cases as Thompson [15] has pointed out and for example, predicts a value for νC=O in acetone in the vapour phase, of 1690 cm^{-1}. On the other hand there are a number of relationships between νC=O and various measures of the polarity of the carbonyl bond which are clearly experimentally valid. These include the numerous Hammett σ type relationships and those with such properties as the ionisation potential of the carbonyl group and with its polarity as measured by solvent shift studies [25]. These findings must be reconciled with those of Overend [38], that inductive and resonance effects alone are not sufficient to account for the observed frequency changes.

The chemist has always assumed that the polarity changes in the carbonyl group, which are measured by these various physical properties are produced by effects operating along the bonds. If it is now accepted that they arise from a combination of inductive forces and of non-bonded interactions, the parallelism of the physical properties with the observed frequencies follows immediately and the discrepancy between these relationships and Overend and Scherer's findings [38] largely vanishes.

The field effects described earlier between carbonyl groups and halogen [45, 56] or oxygen [57] atoms on the α carbon atom can now be seen to be just another example of the impact of non-bonded interactions, and the fact that they are operative only in conformations in which the polar group is near in space to the carbonyl oxygen, is clear evidence that this is so. Once it is accepted that the chlorine atom in chloroacetone can give rise to a frequency shift of 25 cm^{-1} due to non-bonded interactions, it is clear that similar effects must operate in say phosgene in which the chlorine-oxygen distances are slightly less.

Table 1 summarises some typical CO and SO frequencies for compounds with the same substituents. It will be seen that whereas the SO frequencies behave in a reasonably stepwise fashion with the introduction of chlorine or oxygen atoms, the CO frequencies do not. Thus on going from acetyl chloride to phosgene, νCO is raised only 6 cm^{-1} whereas on going from acetone to acetyl chloride the rise is about 80 cm^{-1}. Similarly on going from acetyl chloride to the chloro formate the frequency actually falls, whereas in the sulphoxide series it rises in the way one would expect. These differences would now be explained in terms of the fact that the carbon atom is small so that the X...O and X...X distances will be short and non-bonded interactions will occur, whereas the sulphur atom is large and these effects will be minimised.

Table 1

Substituents	ν CO	ν SO
$CH_3 \times CH_3$	1740 cm^{-1}	1050 cm^{-1}
$CH_3 \times Cl$	1821	1150
$Cl \times Cl$	1827	1231
$CH_3 \times OR$	1750	1130
$Cl \times OR$	1780	1213

This interpretation involves the assumption that interactions between X...X atoms as well as between X...O will play a part in the frequency shift, and there is evidence that this is so from the study of the rotational isomers of chlorinated acetyl chlorides reported by Bellamy and Williams [58]. Thus chloroacetyl chloride shows two carbonyl frequencies. That due to the form in which the chlorine is cis with respect to the carbonyl group is 14 cm^{-1} higher than in acetyl chloride. That due to the gauche form is however not the same as in acetyl chloride (as is the case with gauche chloroacetone) but is 23 cm^{-1} lower. This effect follows through the rest of the series. Dichloroacetyl chloride shows one band at the same point as acetyl chloride (one is chloride and one gauche) and one at 1790 cm^{-1}, which is 31 cm^{-1} less; this must be due to the gauche/gauche configuration. Finally in trichloro acetyl chloride the frequency of 186 cm^{-1} is distinctly lower than that of the parent molecule.

These results do suggest very strongly that there are interactions between the chlorine atoms when they are sufficiently near to each other and that these interactions alter the polarity of the substituents, and so the frequencies.

A second possibility is to investigate any polarity changes produced by field effects through solvent studies. Table 2 lists a number of compounds in which interactions through field effects have been demonstrated. We have measured the NH stretching frequency of pyrrole when dissolved in small amounts in each of these compounds. The results are shown in Table 2, along with the carbonyl frequencies in carbon tetrachloride alone. It will be seen that in all these cases in which a frequency rise occurs in νCO due to a field effect the corresponding polarity is diminished and νN-H rises to a higher value than was found in the unchlorinated compound. This series therefore provides evidence that non-bonded interactions do produce real changes in polarity.

Table 2

	ν CO × (CCl_4)	ν NH Pyrrole
$CH_3COOC_2H_5$	1745	3404
$CCl_3COOC_2H_5$	1773	3450
$CF_3COOC_2H_5$	1791	3460
$CH_2CH_2Br \times COOC_2H_5$	1747	3419
$C_2H_5COOC_2H_5$	1743	3401
CCl_3CHO	1771	3444
CH_3CHO	1734	3419
C_6H_5COCl	1781	3460
$O \times Cl \times C_6H_4COCl$	1794	3462

The suggestion that such interactions occur more commonly than has been previously supposed and that, in particular they occur between two atoms each bonded to the same carbonyl group, is therefore not unreasonable. This concept then allows us to understand the differences in the behaviour of νCO and νSO, and to reconcile the findings of Overend and Scherer with the observed fact that carbonyl frequency shifts do relate well to physical properties which measure the polarity of the carbonyl bond.

The as × NO_2 Stretching Vibration

It has recently been shown that $-C(R)_2NO_2$ compounds afford *as*NO_2 stretching frequencies which are directly related to the Taft σ^* values [23] of the R substituents. The experimental data is considerable and there is no reason to question its validity. However any attempt to extend this relation to the more general series RNO_2 is found to fail. Thus the effect of a single chlorine atom directly attached to the nitro group is very much greater than that of the CCl_3 group although the Taft values would indicate only a small further rise. These results are in line with the general concepts outlined above. When attached to a carbon atom the polar substituents influence the frequency primarily by inductive effects, as the R...O distances are large and the non-bonded interactions will be small. However when the substituents are directly attached to the nitrogen atom, non-bonded effects are also brought into play and the relation with the Taft values loses its validity.

$\nu P = O$, νSO_2, etc.

The phosphoryl frequencies have been shown to follow a generalised relationship with the electronegativities of the substituents [27], but the value for OR substituents for example needs to be lowered below the Pauling value to bring the results into line. The $as \times SO_2$ and the $\nu S = O$ frequencies behave similarly [28, 51, 52] and although the frequencies follow the same general trends they cannot be related directly either to each other or to the P = O frequency.

It seems likely that in view of the relatively large size of the phosphorus and sulphur atoms, the frequencies will be controlled largely by true inductive effects. The observation that in both cases OR substituents are less effective than chlorine substituents in raising the frequencies is in line with this and suggests that the true order of effectiveness of substituents is that of Taft σ^* ($OR < Cl$) rather than the closely related but not identical electronegativity scale. However, the possibility of an effect due to non-bonded interactions cannot be wholly excluded and will depend upon the geometrical arrangement. Thus, while in phosphates the O...O interactions are likely to be small it is nevertheless possible that there will be an interaction between the phosphoryl oxygen and the substituent on the other side of the oxygen atom provided the OR group has a cis conformation. The observation that triphenyl phosphate shows rotational isomerism and exhibits two P = O frequencies is in line with this possibility.

These frequencies will therefore generally follow Taft σ^* values but will show deviations from this in special cases.

CONCLUSIONS

It is suggested that the "inductive" effect of a polar group upon a given linkage should now be regarded as a composite of true induction effects working along the bonds and of non-bonded interactions working across intramolecular space. As both of these alter the polarity of the linkage, and so its vibrational frequency, this does not in any way invalidate the many valuable correlations which relate frequency shifts to changes in physical properties brought about by "induction" effects.

This picture does however enable us to see why it is that substituents show such wide differences in their "inductive" effects in different environments. When the substituent is so far removed from the vibrating group that the non-bonded interactions are eliminated, a common order of effectiveness (that of Taft σ^* values) is found, as the frequencies then depend upon the true inductive effects. In situations in which the non-bonded interactions predominate, a second order of effectiveness will be found which is more closely related to the Pauling electronegativities. In most cases however the frequency will depend upon both effects and the substituents will behave in a way that is unique to that particular system and which depends in part upon the molecular geometry and steric form.

These suggestions are admittedly speculative but they do have the merit of bringing some measure of unity to a mass of experimental data which is otherwise wholly confusing and contradictory. They are put forward at this stage in the hope that they will stimulate further work on these problems which are of real importance to organic chemists who use group frequencies. It might be also that some advances could be made by using the deviations from Taft σ^* relationships as a direct relative measure of the non-bonding interactions themselves, the results being fed back into Urey-Bradley type calculations to see how far some refinement of these could be achieved.

REFERENCES

1. Flett, N. St. C., Trans. Faraday Soc., 1948, 44, 767.
2. Davison, J., J. Chem. Soc., 1951, 2456.
3. Ingraham, L. L., Corse, J., Bailey, G. F. and Stitt, F., J. Amer. Chem. Soc., 1952, 74, 2297.
4. Scrocco and Liberti, Ricvca Sci., 1954, 24, 1684.
5. Fuson, N., Josen, M. L. and Shelton, J. Amer. Soc., 1954, 76, 2526.
6. Bellamy, L. J., J. Chem. Soc., 1955, 2818.
7. Kellie, A. E., O'Sullivan, D. G., and Sadler, R. W., ibid., 1956, 3809.
8. Kross, R. D. and Fassel, V. A., J. Amer. Chem. Soc., 1956, 78, 4225.

9. Thompson, H. W. and Steel, C., Trans. Faraday Soc., 1956, 52, 1451.
10. Krueger, P. J. and Thompson, H. W., Proc. Roy. Soc. A., 1957, 243, 143.
11. O'Sullivan, D. C., and Sadler, P. W., J. Chem. Soc., 1956, 2202; 1957, 2916.
12. Shindo, H., Chem. and Pharm. Bull (Japan) 1957, 5, 472; 1958, 6, 117; 1959, 7, 791; 1960, 8, 33.
13. Stone, P. J. and Thompson, H. W., Spectrochim. Acta., 1957, 10, 17.
14. Thompson, H. W., Needham, R. W. and Jameson, D., ibid., 1957, 9, 208.
15. Caldow, G. L. and Thompson, H. W., ibid., 1958, 13, 212.
16. Thompson, H. W. and Jameson, D. A., ibid., 236.
17. Holt, S. J., Kellie, A. E., O'Sullivan, D. C. and Sadler, P. W., J. Chem. Soc., 1958, 1217.
18. Baker, A. W., J. Phys. Chem., 1958, 62, 744.
19. Baker, A. W. and Shulgin, A. T., J. Amer. Chem. Soc., 1959, 81, 1523.
20. Bellamy, L. J., J. Chem. Soc., 1955, 4221.
21. O'Sullivan, D. C. and Sadler, F. W., J. Chem. Soc., 1957, 4144.
22. Thompson, H. W., Spectrochim. Acta, 1960, 16, 238.
23. Lunn, W. H., ibid., 1088.
24. Walsh, A. D., Proc. Roy. Soc., 1951, A207, 13.
25. Cook, D., J. Amer. Chem. Soc., 1958, 80, 49.
26. Kagarise, R. E., ibid., 1955, 77, 1377.
27. Bell, J. V., Heisler, J., Tannenbaum, H. and Goldenson, J., ibid., 1954, 76, 5185.
28. Daasch, L. W., Spectrochim. Acta, 1958, 13, 257.
29. Wilmshurst, J. K., Can. J. Chem., 1957, 35, 937.
30. Brockman, R. W. and Pearson, D. C., J. Brit. Chem. Soc., 1952, 74, 4128.
31. Josien, M. L., Fuson, N. and Pearson, D. C., Compt. Rendn., 1952, 235, 1206.
32. Josien, M. L. and Fuson, N., Bull. Soc. Chim. France, 1952, 19, 389.
33. Idem, Compt. Rendn., 1952, 234, 1680.
34. Josien, M. L., Fuson, N., Lebus, J. M. and Gregory, T. H., J. Chem. Phys., 1953, 21, 331.
35. Sheppard, N., Trans. Faraday Soc., 1955, 51, 1465.
36. Bellamy, L. J. and Williams, R. L., J. Chem. Soc., 1956, 2753.
37. Potts, W. J. and Nyquist, R. A., Spectrochim. Acta, 1959, 15, 679.
38. Overend, J., and Scherer, J. R., ibid., 1960, 16, 773.

39. Bellamy, L. J., The Infrared Spectra of Complex Molecules, 2nd Ed. 1958, Methuen, London, and J. Wiley, New York, p. 389.
40. Wilmshurst, J. K., J. Chem. Phys., 1957, 26, 426.
41. Overend, J. and Scherer, J. R., J. Chem. Phys., 1960, 33, 446.
42. Cottrell, T. L., The Strengths of Chemical Bonds, Butterworths, London, 2nd Ed. 1958, p. 270.
43. Mizushima, S. I., Shimanouchi, T., Miyazawa, T., Ichishima, I., Kuratani, K., Nakagawa, I. and Shido, N., J. Chem. Phys., 1953, 21, 815.
44. Nakagawa, I., Ichishima, I., Kuratani, K., Miyazawa, T., Shimanouchi, T. and Mizushima, S. I., ibid., 1952, 20, 1720.
45. Bellamy, L. J. and Williams, R. L., J. Chem. Soc., 1957, 4294.
46. Brown, T. L., Chem. Review, 1958, 58, 581.
47. Idem., J. Phys. Chem., 1957, 61, 820.
48. Moccia, R. and Thompson, H. W., Proc. Roy. Soc., Ser. A., 1957, 243, 154.
49. Brown, T. L., J. Amer. Chem. Soc., 1958, 80, 6489.
50. Taft, R., in "Steric Effects in Organic Chemistry," Ed. Newman, M. S., Wiley, New York, 1956, p. 556.
51. Bellamy, L. J., in "The Organic Chemistry of Sulphur Compounds," Ed. Kharasch, N., Pergamon Press, in press.
52. Robinson, E. A., Can. J. Chem., 1961, 39, 247.
53. Chemical Society Special Publication No. 11. Tables of Interatomic Distances. The Chemical Soc., London, 1958.
54. Overend, J. and Scherer, J. R., J. Chem. Phys., 1961, 34, 574.
55. Cross, B. and Whitham, G. H., J. Chem. Soc., 1961, 1650.
56. Jones, R. N. and Spinner, E., Can. J. Chem., 1958, 36, 1020.
57. House, H. O. and Blaker, J. W., J. Amer. Chem. Soc., 1958, 80, 6389.
58. Oki, M. and Hirota, M., Spectrochim. Acta., 1961, 17, 583.
59. Hyde, J. F., Brown, P. L. and Smith, A. L., J. Amer. Chem. Soc., 1960, 82, 5854.
60. King, W. T., and Crawford, B. L., J. Mol. Spectroscopy, 1960, 5, 421; 1962, 8, 58.

SUBSTITUENT EFFECTS ON THE INFRARED AND ELECTRONIC ABSORPTION SPECTRA OF ORGANIC MOLECULES*

C. N. R. Rao,† *R. Venkataraghavan, K. R. Bhaskar*
and A. Balasubramanian
Department of Inorganic and Physical Chemistry
Indian Institute of Science
Bangalore-12, India

Effects of substituents on the spectra and reactivity of organic molecules has been a subject of extensive investigation for the past few years. Several quantitative and semi-quantitative correlations of the spectra of organic molecules with structural parameters have been reported in the literature. In this article we shall only concern ourselves with the correlations of the electrical effects of substituents in related series of organic molecules. The term "electrical effect" includes the inductive, mesomeric and field effects. All of these influence the electron density or bond order. The most successful and useful empirical correlations of the spectra of organic molecules are those with the *substituent constants*.

The substituent constants, σ, were first evaluated by Hammett [1] who observed that a particular group in *p*- or *m*-position in a benzene ring exerts a constant effect on the reactivity of the compound, depending on its inductive and resonance contributions. The substituent constant of a group measures its ability to change the electron density at the reaction center. The substituent constants have been employed to correlate the kinetic

---

*Contains material from the Ph.D. theses of R. Venkataraghavan, K. R. Bhaskar and A. Balasubramanian to be submitted to the Indian Institute of Science.
Joint contribution from the Department of Organic Chemistry and the Department of Inorganic and Physical Chemistry, Indian Institute of Science, Bangalore.

†To whom all the correspondence should be addressed.

and equilibrium data in related series of organic molecules [2]. A set of reliable values of Hammett σ constants has been compiled recently by McDaniel and Brown [3] based on the thermodynamic dissociation constants of benzoic acids. In recent years several other substituent constants have been proposed for use in different types of systems: σ^+ in electrophilic reactions of benzenoid derivatives [4,5], σ^* in aliphatic systems [6] and σ^- for electron-withdrawing groups in substituted anilines and phenols [2]. The σ^* constants mainly represent inductive effects of substituents in aliphatic systems. The substituent constants σ, σ^+, and σ^- include both induction and resonance terms and are applicable in benzonoid systems. The inductive term remains the same in these three constants and only the resonance parameter varies. The σ, σ^+ and σ^- constants can be separated into inductive and resonance parameters of groups [6]. Thus, the Hammett σ value is equal to $\sigma_I + \sigma_R$. The various substituent constants have been recently reviewed by Rao [7]. Although the various substituent constants were devised to correlate the structure of organic molecules with their chemical reactivity, many physical properties of the molecules may also be correlated with these constants. Such empirical or semi-empirical relations give a better insight into the structure and behaviour of organic molecules particularly when the chemist cannot yet disentangle the various structural factors into finer and more fundamental contributions.

CORRELATIONS OF SUBSTITUENT EFFECTS ON THE INFRARED SPECTRA OF ORGANIC MOLECULES

Considerable interest has been exhibited in recent years in correlating the infrared group frequencies and band intensities of related groups of organic molecules with substituent constants [8-13] and both the group frequency and band intensity have been found to give linear relations (Figures 1 and 2). While the frequency is mainly determined by the bond force constants, the intensity is controlled by dipole derivatives with respect to bond length, $(\delta\mu/\delta r_{ij})$. Change of substituent group may affect the force constants, static dipole moments, or $(\delta\mu/\delta r_{ij})$, through inductive or (and) resonance effects. It is interesting to note that the dipole moments of substituted benzene derivatives linearly correlate with the substituent constants [14,15]. Substituent groups generally affect both the frequency and the intensity, though not always in the same direction. Sometimes, the frequency shift is very small and the change in band intensity is large or *vice versa*. It is therefore important to correlate the frequencies and intensities of groups with substituent constants to understand the mechanism(s) involved. Although there have

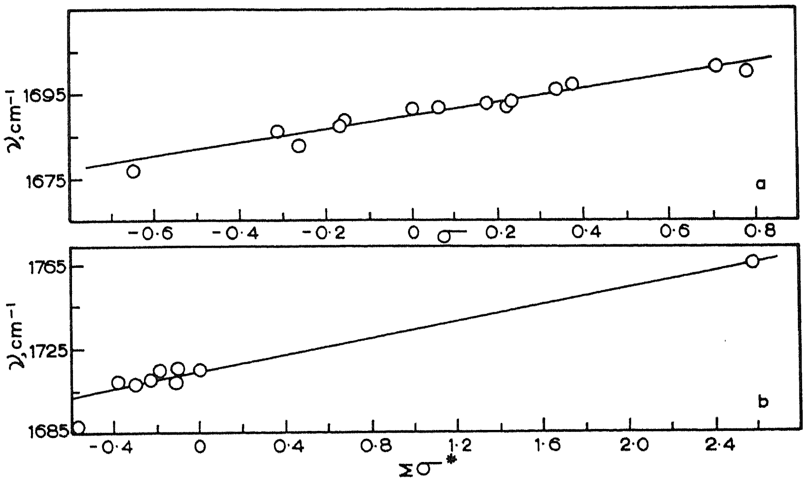

Figure 1. Correlations of infrared group frequencies with substituent constants: a, C=O stretching in acetophenones with Hammett σ values; b, C=O stretching in aliphatic ketones with Taft σ^* values.

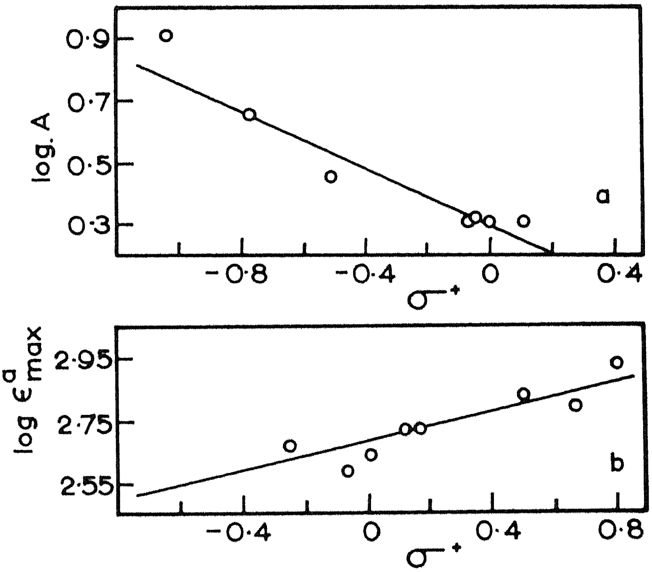

Figure 2. Correlations of integrated band intensities of benzonitriles (a); and apparent molecular extinction coefficients of anisoles (b) with the σ^+ substituent constants.

been several reports of such correlations with substituent constants in the literature, there has been no systematic evaluation of these correlations. A statistical evaluation [2] of these correlations of group frequencies and band intensities of aliphatic and benzene derivatives has been carried out by Rao and

Venkataraghavan [16] in order to test the validity and utility of the correlations. Such an evaluation is justified by the high precision and accuracy of the recent infrared data on related groups of organic molecules used in these correlations. The results of the least square treatment have been given in terms of the correlation coefficient, r, standard deviation, s, and the number of points employed, n.

Infrared Group Frequencies

A linear relation of the infrared group frequencies in *meta-* and *para-*disubstituted benzene derivatives with the Hammett σ constants [1] has been suggested by several workers [8-13]. The relation may be expressed by a Hammett-type equation,

$$\nu = \nu_o + \rho\sigma$$

where ν is the observed group frequency in the *meta-* or *para-*disubstituted benzene, ν_o is the group frequency in the monosubstituted derivative, and σ and ρ have their usual significance (Figure 1). Thompson *et al.* [8] have expressed doubt about the roughly linear plots of ν against σ having much significance and have considered the possibility of plotting ν^2 *versus* σ. A linear relationship of the group frequencies in *meta-* and *para-*substituted benzene derivatives has also been proposed [17] with the electrophilic substituent constants σ^+[4,5]

$$\nu = \nu_0^+ + \rho^+ \sigma^+$$

The results of the statistical treatment of the correlation of the infrared group frequencies of 18 sets of *meta-* and *para-*substituted benzene derivatives with the σ and σ^+ constants gave an average standard deviation of 3.3 cm^{-1} with both the constants, while the correlation coefficients are 0.938 and 0.924 respectively. It may be concluded that both the substituent constants correlate the frequencies equally well. This is not completely unexpected, because the vibrational frequencies being associated with mechanical properties of bonds, may not show any preference between σ and σ^+ constants. In Table 1, some of the results of the statistical evaluation with σ constants have been summarized.

A linear relationship of the infrared frequencies in aliphatic derivatives with the σ^* constants of Taft [6] has been proposed (Figure 1).

$$\nu = \nu_0^* + \rho^* \sigma^*$$

The results of the statistical evaluation of the correlation of the available data with the σ^* constants have been summarized in Table 2. The average standard deviation is rather high (14.1 cm^{-1}) compared to the value of 3 cm^{-1} in the case of benzene derivatives.

Table 1

Correlation of Infrared Group Frequencies in *p*- and *m*-Substituted Benzene Derivatives with σ Constants

Series	Solvent	Frequency	ν_0 (cm^{-1})	ρ	s	r	n
Phenols[25]*	CCl_4	ν_{OH}	3610	-13.4	5.3	0.958	15
Benzoic acids[26]	CCl_4	ν_{OH}	3553	-10.1	3.4	0.793	6
Acetophenones[27]	CCl_4	$\nu_{C=O}$	1690	15.9	1.6	0.975	14
Benzoic acids[26]	CCl_4	$\nu_{C=O\,(monomer)}$	1742	12.9	1.5	0.962	6
Benzoic acids[26]	CCl_4	$\nu_{C=O\,(dimer)}$	1695	14.2	3.1	0.994	6
Ethylbenzoates[8]	CCl_4	$\nu_{C=O}$	1717	14.9	2.9	0.959	6
Anilines[28]*	CCl_4	$\nu_{NH\,(asym)}$	3476	30.5	3.8	0.979	16
Anisoles[18]	CCl_4	ν_{C-O-C}	1243	14.6	5.1	0.868	10
Nitrobenzenes[29]	$CHBr_3$	$\nu_{NO_2\,(asym)}$	1523	30.5	3.6	0.961	9
Benzonitriles[30]	CCl_4	$\nu_{C\equiv N}$	2230	7.4	1.4	0.965	9

*In these systems σ^- values ("dual" values) were used for some of the electron-withdrawing groups.

Infrared Band Intensities

Several possible correlations of infrared band intensities in *meta-* and *para-*substituted benzene derivatives with σ and σ^+ constants have been suggested [8,9,13,17]. The best correlation is probably between the logarithm of the vibrational band intensities log A and the substituent constants. Thompson and coworkers [8,12] have correlated log A with Hammett σ constants:

$$\log A = \log A_0 + \rho\sigma$$

A similar linear relation has been suggested with the σ^+ constants [13,17].

$$\log A = \log \overset{+}{A}_0 + \rho^+\sigma^+$$

A statistical evaluation of the correlations of log A with σ and σ^+ constants seems to indicate that σ^+constants are probably better suited for the correlations (Figure 2). In some cases like benzonitriles and anilines, the correlations with σ^+ constants are far superior. Such a preference to σ^+ constants is understandable, since band intensities are related to electrical properties of bonds. Excellent linear correlations have also been found between the logarithms of molar extinction coefficients, log ϵ, and σ^+ constants in the case of C-O-C stretching vibrations of anisoles [18] and NH stretching over-tones of anilines [19] (Figure 2). In Table 3 are given the results of the statistical evaluation of log A_ σ^+ relation for a few benzene derivatives.

On the basis of a molecular orbital model of infrared band intensities Brown [20] has recently suggested that the substituent constants should be linearly related to the square roots of the infrared absorption intensities in substituted benzene derivatives. A statistical evaluation of the linear relations of $A^{1/2}$ with σ and σ^+ constants shows that the $A^{1/2}$ - σ^+ correlations are as good as the log A_ σ^+ correlations. The average standard deviation and correlation coefficient of $A^{1/2}$ - σ^+ correlations for six series of benzene derivatives are found to be 0.081 and 0.957 respectively.

The infrared band intensities in aliphatic derivatives may be correlated with σ^* constants:

$$\log A = \log A_0^* + \rho^*\sigma^*$$

The average standard deviation and correlation coefficients are found to be 0.066 and 0.755 respectively and are therefore not very satisfactory.

Table 2

Correlation of Infrared Group Frequencies in Aliphatic Derivatives with Taft σ^* Constants

Series	Solvent	Frequency	ν_o^*	ρ^*	s	r	n
Simple aliphatic ketones[31]	CCl_4	$\nu_{C=O}$	1714	19.6	9.9	0.906	9
Heteroatom conjugated ketones[32]	Condensed phase	$\nu_{C=O}$	1654	53.8	17.3	0.954	6
Amides[33]	$CHCl_3$	$\nu_{C=O}$	1685	19.9	12.1	0.901	7
Acids[34]	CCl_4	$\nu_{C=O}$	3530	-9.4	0.5	0.995	11
Nitrocompounds[35,36]	CCl_4	ν_{NO_2} (asym)	1557	25.1	5.7	0.989	7
Simple and β-substituted nitriles[37]	$CHCl_3$	$\nu_{C\equiv N}$	2253	14.7	38.8	0.889	8

Table 3

Correlation of Infrared Band Intensities in *m*- and *p*-Substituted Benzene Derivatives with σ^+ Constants

Series	Solvent	Frequency	log A_o^+	ρ^+	s	r	n
Benzaldehydes[8]	CCl_4	$\nu_{C=O}$	1.040	-0.067	-0.068	0.986	5
Ethylbenzoates[8]	CCl_4	$\nu_{C=O}$	1.205	-0.055	-0.062	0.955	6
Acetanilides[12]	CCl_4	$\nu_{C=O}$	1.173	-0.099	0.020	0.969	8
Phenols[25]*	CCl_4	ν_{O-H}	0.813	0.106	0.040	0.875	14
Anilines[28]*	CCl_4	$\nu_{N-H\,(asym)}$	1.217	0.130	0.044	0.923	16
Anilines[28]*	CCl_4	$\nu_{N-H\,(sym)}$	1.264	0.273	0.083	0.938	16
Benzonitriles[38]	CCl_4	$\nu_{C\equiv N}$	0.299	-0.461	0.033	0.982	7

*In these systems σ^- values ("dual" values) were used for some of the electron-withdrawing groups.

Generalizations

In the correlations of band intensities, there is a systematic variation of the sign of ρ with the nature of the bond involved. A negative slope of the log A_- σ, log A_- σ^+ or log A_- σ^* plot is always found when the bond or the group involved is electron-withdrawing in nature as in carbonyl derivatives and nitriles. A positive slope is found when the bond or group involved is electron-donating in character. The magnitude of ρ seems to vary in proportion to the extent to which the groups can withdraw or donate electrons. The slope of the log A- σ or log A- σ^+ plot decreases with the increasing electron-withdrawing power of the group. These generalizations may be clearly seen from Table 4. The greater sensitivity of the NH_2 symmetric stretching band intensity to substituent effects compared to the asymmetric band intensity may be explained on the basis of hydridization changes at the nitrogen atom during the vibrations [21].

Table 4

Generalizations Regarding the Correlation of Infrared Spectra of Organic Molecules with Substituent Constants

Series	Frequency	Group	*Para*-σ of the Group	log A-σ ρ	log A-σ^+ ρ^+
Anilines[28]	$\nu_{NH(asym)}$	$-NH_2$	-0.66	0.166	0.130
Anilines[28]	$\nu_{NH(sym)}$	$-NH_2$	-0.66	0.355	0.273
Phenols[25]	ν_{OH}	-OH	-0.37	0.137	0.106
Ethylbenzoates[8]	$\nu_{C=O}$	$-COOC_2H_5$	0.45	-0.08	-0.055
Nitriles[30]	$\nu_{C\equiv N}$	-CN	0.66	-0.26	-0.509

This relation of the sign of ρ in the log A- σ, log A- σ^+ or log A- σ^* plot to the electrical property of the bond or group is found because the band intensity is itself dependent on $(\delta\mu/\delta r_{ij})$. Substituents favouring the dipole of a bond always increase its band intensity. Thus, the OH band intensity in phenols increases with the electron-withdrawing ability of the group in the *para*- or *meta*-position (positive slope) while the C≡N band intensity in benzonitriles increases with the increasing electron-donating ability of the *para*- or *meta*-substituent (negative slope). This type of generalization is extremely useful in identifying the prominent resonance forms in aromatic systems. For example, the most prominent resonance structures in phenols and anisoles should be similar since the slopes of the log A- σ plots are positive in both cases [18]. The most prominent resonance structure of the organic isothiocyanates has been proposed to be I, II or III.

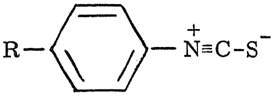

I

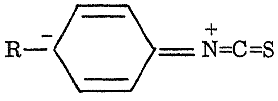

II

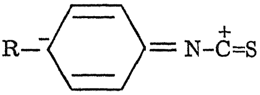

III

This proposal may now be supported by the band intensity measurements of Caldow and Thompson [22] in *para*- and *meta*-substituted phenyl isothiocyanates. The -NCS band intensity increases with the electron-withdrawing power of the substituents. Based on the reactivity of substituted phenyl isothiocyanates it has been shown that III is probably the most prominent resonance structure. The rate of addition of alcohols to the isothiocyanates increases with increasing electron-withdrawing power of the *para*-substituent, R, similar to the infrared band intensities [23].

In the correlation of group frequencies with substituent constants there appears to be no definite relation between the sign and magnitude of ρ and the nature of the bond or group involved in the vibration. However, a closer examination reveals that in the case of simple bonds such as OH, CO and CN, that the direction of the ν - σ correlation is always opposite to that of the intensity correlation (Table 5). The opposite signs of the slopes can be understood in terms of the prominent resonance forms in these cases. Thus, electron-withdrawing substituents which enhance the intensity of the OH band in phenols should necessarily render the OH bond weaker and therefore lower the OH frequency. In the case of benzonitriles, electron-donating substituents, that favor nitrile band intensity lower the bond order and hence the frequency.

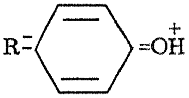

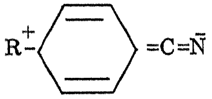

An obvious application of these different linear relations would be in the estimation of substituent constants of groups. The frequency correlation would be more useful for this purpose

Table 5

Relation Between the Frequency and Intensity Correlations

Series	Frequency	$\nu - \sigma$ ρ	log A - σ ρ
Phenols	OH	-13.4	0.137
Ethylbenzoates	C=O	14.9	-0.080
Benzonitriles	C≡N	7.4	-0.787

because frequencies can be measured very easily with high precision and accuracy. The measurement of band intensities is rather tedious. One could, however, make use of extinction coefficient data to a certain extent. If one were to employ the frequency correlations for estimating the substituent constant for a group, one has to determine the characteristic frequency of a functional group in the unsubstituted and substituted derivatives and then calculate the substituent constant by making use of the ρ values given in the tables (employing the same solvent). One should choose a functional group which has the most structure-sensitive frequency. Carbonyl stretching vibration is probably best for the purpose. In the case of dicarbonyl compounds where at least one carbonyl group is associated with a benzene ring, assignments have been made on the basis of $\nu - \sigma$ correlations [24].

C=S STRETCHING FREQUENCY AND THE "-N-C=S BANDS"

Frequencies ranging from 850 to 1550 cm^{-1} have been attributed to the C=S stretching frequency in the literature and there seems to be no adequate correlation of the literature data [39]. A careful examination of the data reveals that the assignments of very high or low frequencies are always in the nitrogen-containing thiocarbonyl compounds. It therefore becomes necessary to distinguish two groups of thiocarbonyl derivatives: the first group, where the thiocarbonyl group is linked to atoms such as carbon, sulfur, oxygen and chlorine and the second group where the thiocarbonyl group is linked to one or two nitrogen atoms. An unambiguous assignment of the C=S stretching frequency seems to be possible only when the C=S group is attached to atoms other than nitrogen.

A correlation of the infrared spectra of thiocarbonyl derivatives based on the literature data has been carried out by Rao and Venkataraghavan [40]. Assignments have also been made in some new systems. The C=S stretching frequency in thiofenchone has been found around 1180 cm^{-1} which is in fair agreement with the value calculated for thioformaldehyde [41]. In the case of thiocarbonyl derivatives where the C=S group is linked to elements other than nitrogen, the stretching frequency is generally found in the region 1025-1225 cm^{-1}. No simple correlation of the C=S stretching frequency with electro-negativities of the atoms directly linked to the group is apparent. In substituted phenyl thiocarbonyl derivatives [42,43] the C=S stretching frequency does not show any simple relationship with the Hammett σ or σ^+ constants [16]. The thiocarbonyl group is not at all similar to the carbonyl group with regard to bond polarity and electrical effects of substituents [44]. The insensitivity of the thiocarbonyl stretching frequency to electrical effects is further confirmed by the fact that the calculated frequency of 1120 ± 40 cm^{-1} for thioformaldehyde is not very different from the observed frequency of 1140 cm^{-1} for thiophosgene [41] and 1180 cm^{-1} for thiofenchone. Strong vibrational coupling is operative in the case of the nitrogen containing thiocarbonyl derivatives and three bands seem to consistently appear in the regions 1395-1570 cm^{-1}, 1260-1420 cm^{-1} and 940-1140 cm^{-1} due to mixed vibrations. These bands which may be tentatively designated as the "$-\underset{|}{N}-C=S$ I, II and III bands" could be useful in qualitative analysis. The vibrational coupling effects evidenced in these nitrogen derivatives are similar to those found in amides [45].

SUBSTITUENT EFFECTS AND FERMI RESONANCE

Deuteration technique may be successfully employed to establish Fermi resonance between two vibrations if at least one of them involves the motion of a hydrogen. Typical cases where the deuteration technique has been employed are in cyclopentanone and in the 3090 cm^{-1} band of secondary amides [47, 48]. The study of Fermi resonance by this technique is possible since deuteration shifts the hydrogenic vibration due to mass effects.

Recently, the anomalous splittings of the carbonyl bands of benzoyl chloride have been studied by Rao and Venkataraghaven [49] and the effects have been attributed to Fermi resonance. In this study the electronegativity of the substituents has been varied in order to alter the magnitude of the vibrational interaction between the C=O stretching and the Ph-C stretching overtone. Electron-withdrawing groups decrease the magnitude of this interaction considerably and in the case of 3,5-dinitrobenzoyl chloride only a single carbonyl band is observed. The relevant bands of a few substituted benzoyl chlorides are shown in Figure 3.

Examination of the spectra of dialkyl dixanthogens has shown that the splittings of the C-O and C=S stretching bands vary with the alkyl group. The combination band of C-S and S-S stretching frequencies seems to interact with the C-O stretching. The dependence of the splittings of the C-O and C=S bands on alkyl substitution is in opposite directions. This is probably because the substituents which increase the C-S bond order will decrease the S-S bond order. It is also possible that substituents may affect the C-O frequency differently compared to the C=S frequency.

The splitting of the asymmetric stretching band of the azido group in substituted phenyl azides seems to depend on substitution. The splitting appears to be due to the Fermi resonance between the asymmetric stretching frequency of the azido group

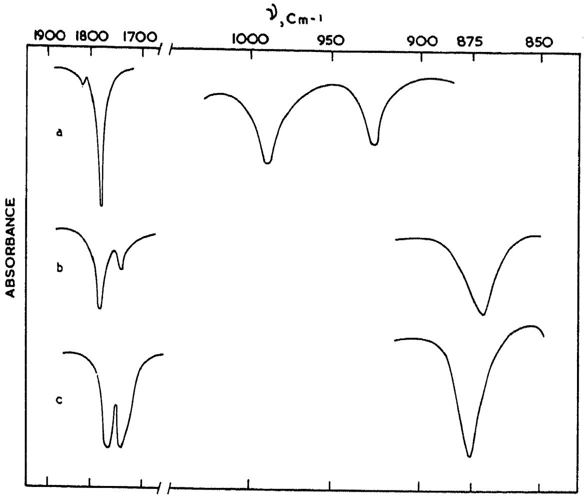

Figure 3. Infrared spectra of benzoyl chlorides in the carbonyl stretching and in the 1000-850 cm^{-1} region.
(a) 3,5-dinitro benzoyl chloride
(b) benzoyl chloride
(c) 4-methoxy benzoyl chloride

and the overtone of one of the skeletal frequencies of the benzene ring. Similar effects seem to be present in substituted phenyl carbodiimides. These systems are presently being investigated in detail.

CORRELATIONS OF SUBSTITUENT EFFECTS ON THE ELECTRONIC ABSORPTION SPECTRA OF ORGANIC MOLECULES

Several empirical correlations of the effect of substituents on the electronic absorption spectra of organic molecules have been reported in the literature [50]. In all such correlations, the effect of a substituent on the absorption of a chromophore is generally expressed in terms of the wavelength-shift (bathochromic or hypsochromic). Particular mention must be made of the correlations of Woodward [51] for dienes and $\alpha\beta$-unsaturated ketones. Although several theoretical calculations have been carried out on the electronic absorption spectra of organic molecules, there have not been any quantitative relations between the absorption maxima and the properties of substituents, in related series of organic molecules. In this article, correlations of the electronic absorption spectra of related series of organic molecules with the substituent constants will be discussed. Although such correlations may not be as satisfactory as in the case of infrared spectra, it is possible to obtain interesting information regarding the mechanism of absorption and the nature of interaction of substituent groups. We have subjected various correlations of the ultraviolet absorption maxima with the substituent constants to the least square treatment. Such a statistical evaluation is justified by the reliability and precision of the data employed.

Benzenoid Derivatives

The effect of substitution on benzenoid absorption has been treated by the use of quantum mechanics by Sklar [52] and Matsen and coworkers [53]. Platt [54] has deduced spectroscopic moments which have been employed to correlate and predict intensity changes and wavelength shifts in a large number of benzene derivatives. Doub and Vandenbelt [55] have studied the absorption spectra of several mono- and di-substituted benzene derivatives and have correlated the position of the absorption maximum of the 200 mμ band ($A_{ig} \rightarrow B_{iu}$ "Primary" band) of benzene, with the electrical properties of substituents. The results clearly show the importance of resonance interaction in determining the wavelength-shifts due to substitution. Goodman and Shull [56] have summarized the empirical regularities in the ultraviolet absorption spectra of substituted benzenes. The correlations of the positions of the absorption maxima in monosubstituted and *para*-disubstituted benzenes with the Hammett reactivity constants and resonance parameters of the substituents were proposed by Rao [57,58]. The limitations and the applicability of these correlations could not be determined because of the lack of reliable data. In recent years, Forbes and coworkers [59-69] have published data on the ultraviolet absorption spectra of several series of disubstituted benzenes. We have now carried out the statistical evaluation of the various linear correlations of the λ_{max} of the "primary" band (corresponding to the 200 mμ band of benzene) of *para*- and *meta*-disubstituted benzene derivatives with the substituent constants and resonance parameters. The linear relations are of the form

$$\lambda = \lambda_0 + \sigma_i \ \rho_i$$

where λ is the absorption maximum of the "primary" band in mμ of the substituted derivative, λ_0 the intercept, σ_i the substituent constant employed for the correlation and ρ_i the slope of the line. The results of the least square treatment of the linear correlations are expressed in terms of the correlation coefficient r, standard deviation, s and the number of points employed in the correlation, n.

The results of the statistical evaluation of the correlations of *para*- and *meta*-disubstituted benzene derivatives with σ and σ^+ substituent constants and of the *para*-derivatives alone with the σ and σ^+ constants and with the σ_R and σ_R^+ resonance parameters have been summarized in Table 6. It can be seen that for *para*- and *meta*-disubstituted benzenes,

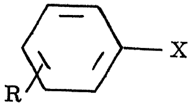

where X is the invariant group in a series and R is the *meta*- or *para*-substituent, the correlation coefficients with σ^+ values are considerably higher (r_{ave}, 0.85) than those with σ values (r_{ave}, 0.78), when X is a strongly electron-withdrawing group as in nitrobenzenes or acetophenones. In the series of benzene derivatives where X is strongly electron-donating in nature, the correlations are better (r_{ave}, 0.68) with the combination of σ and σ^- constants than with σ^+ and σ^- constants (r_{ave}, 0.57). This kind of dependence of the type of substituent constants to be employed on the nature of X is understandable. When X is strongly electron-withdrawing as in the case of nitrobenzenes or acetophenones, the absorption process will be akin to electrophilic reactions and the σ^+ constants for the electron-donating groups should be more suitable. Similarly, σ^- constants of electron-withdrawing groups should better describe the substituent effects when X is strongly electron-donating. The correlations are particularly poor when the invariant groups interact weakly as in the case of toluenes (r, 0.51), or fluorobenzenes (r, 0.47). With a view to decrease the deviations, correlations were carried out for the *para* derivatives alone and they are also not very satisfactory (Table 6). However, they show small improvements in correlation coefficients when σ^+ constants are used for the

Table 6

Correlations of Ultraviolet Absorption Spectra of *p*- and *m*- Disubstituted Benzenes with the σ and σ^+ Substituent Constants and Resonance Parameters

Series	Solvent*	*para* and *meta*-derivatives						Only *para*-derivatives											
		σ			σ^+			σ_{para}			σ^+_{para}			$\sigma_{R\ para}$			$\sigma^+_{R\ para}$		
		n	r	s	n	r	s	n	r	s	n	r	s	n	r	s	n	r	s
Nitrobenzenes[59] †	Et, Me	19	0.911	16	19	0.943	13	12	0.899	26	12	0.939	5	12	0.818	21	12	0.882	17
Benzoic acids[60] ‡	Et	17	0.82	10	17	0.844	9	9	0.758	13	9	0.791	12	9	0.746	13	9	0.784	12
Acetophenones[60,69]	Et	13	0.74	16	13	0.848	12	8	0.848	15	8	0.88	13	8	0.809	16	8	0.873	13
Benzaldehydes[61]	C or H	19	0.646	12	19	0.764	10	13	0.589	13	11	0.694	12	11	0.680	12	11	0.745	11
Average ⟶			0.779	13		0.850	11		0.773	17		0.826	10		0.763	16		0.821	13
Anilines[62] #	C or E	18	0.739	18	17	0.654	17	11	0.853	15	11	0.754	19	11	0.812	17	11	0.700	21
Phenols[63] #	C	17	0.577	17	17	0.416	19	11	0.747	17	11	0.612	20	11	0.696	18	11	0.532	21
Anisoles[64] #	C	23	0.579	17	21	0.511	18	12	0.825	15	12	0.739	17	12	0.820	15	12	0.720	18
Acetanilides[70] #	Et	17	0.825	11	17	0.715	13	9	0.91	10	9	0.816	15	9	0.860	13	9	0.756	17
Average ⟶			0.680	16		0.574	17		0.817	14		0.730	18		0.797	16		0.677	19
Toluenes[59,60,62-68]	C, H or O	20	0.512	14	--	--	--	11	0.641	14	--	--	--	--	--	--	--	--	--
Fluorobenzenes[65]	C	22	0.469	14	20	0.314	15	12	0.524	14	12	0.415	15	12	0.402	15	12	0.32	16

*Et, Ethanol; C, Cyclohexane; H, n-Hexane; E, Ether; Me, Methanol; O, isoOctane. †m-NH_2 group omitted. ‡p- and m-NO_2 groups omitted. #The σ^- values of the electron-withdrawing groups (NO_2, $COCH_3$, etc.) were used in all the correlations, since correlations with σ values were very poor.

series with an electron-withdrawing invariant group and when the combination of σ and σ^- constants is used for the series with an electron-donating invariant group. The use of resonance parameters also show these preferences of substituent constants depending on the nature of the invariant group, but the correlations are, once again, not satisfactory. In general, it may be said that the correlations are poor with any set of substituent constants or with resonance parameters either for *para-* and *meta*-derivatives together or for *para*-derivatives alone, the correlation coefficients varying between 0.42 and 0.94 (Figure 4). These correlations (Table 6) are poor probably because the magnitude of the interaction of the substituents with the benzene nucleus does not vary linearly with the substituent constants of groups, unless the two substituents possess opposite electrical properties.

One would expect some correspondence between the λ_{max} of disubstituted benzenes and the electrical properties of substituents only when there is strong resonance interaction involving

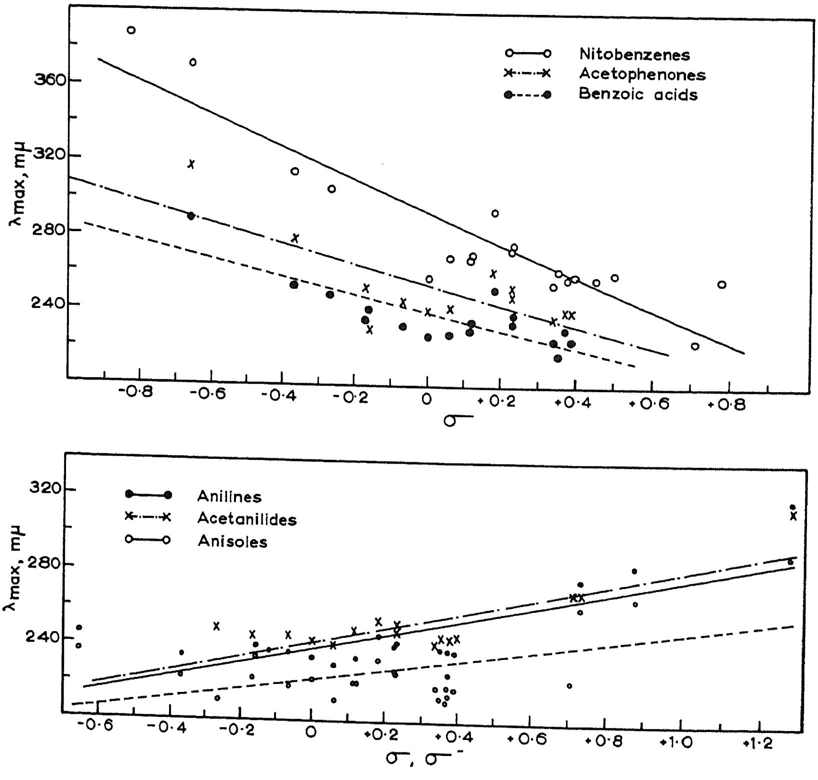

Figure 4. Correlation of the absorption maxima of *para-* and *meta-* disubstituted benzene derivatives with substituent constants.

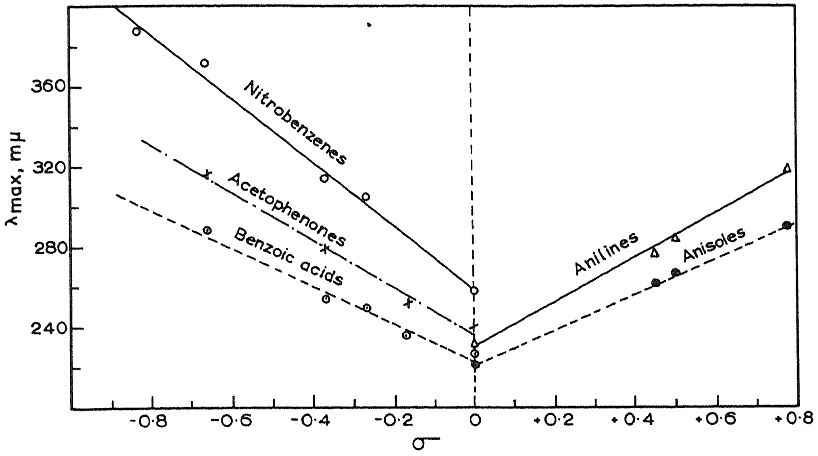

Figure 5. Correlation of the absorption maxima of *para*-complimentarily disubstituted benzene derivatives with Hammett σ constants.

dipolar resonance structures. The results of the statistical evaluation of correlations for complimentarily disubstituted benzenes with the substituent constants and resonance parameters are given in Table 7. The term complimentary disubstitution necessarily means that the two substituents should have opposite signs for the substituent constants. The data for halogen-substituted derivatives were not included because of their anomalous behaviour. The halogen anomaly will be discussed later in this paper. From the results in Table 7 it can be seen that the correlations are much improved. This is particularly true when only the *para*-groups are included for the correlations and the correlation coefficients are very high (0.945 to 1.0) (Figure 5). This is to be expected since dipolar resonance structures assume importance only in the *para* derivatives. Unfortunately, for the correlations with complimentarily *para*-disubstituted benzene derivatives, the number of available points is very small and it would be very difficult to obtain any more points. The use of the σ_R parameters has been found to be unsatisfactory (r, 0.68-0.95), thus indicating the importance of the induction term in determining wavelength shifts due to substitution.

Encouraged by the success of substituent effect correlations with the complimentarily disubstituted benzenes, it was considered interesting to attempt generalized correlations including the data for all these derivatives. Such correlations were carried out by plotting the λ_{max} against the difference of the σ values (absolute value) of the two substituents. This may be expressed by the relation

Table 7

Correlations of the Ultraviolet Absorption Spectra of Complimentarily Disubstituted Benzenes with the Substituent Constants and Resonance Parameters*

Series	Solvent†	n	r	s	n	r	s	n	r	s	n	r	s	n	r	s	n	r	s
			σ			σ, σ^+			σ_{para}			σ^+_{para}			$\sigma_{R(para)}$			$\sigma^+_{R(para)}$	
Nitrobenzenes[59]	Et, Me	6	0.942	23	6	0.969	17	5	0.996	6	5	0.978	13	4	0.910	22	4	0.903	24
Benzoic acids[60]	Et	7	0.988	3	7	0.930	8	5	0.988	4	5	0.945	9	5	0.895	12	5	0.879	22
Acetophenones[60,69]	Et	6	0.948	11	6	0.966	9	4	0.995	4	4	0.979	8	4	0.952	13	4	0.947	13
Average ⟶			0.92	12		0.955	11		0.993	5		0.967	10		0.919	16		0.910	20
			σ			σ, σ^-			σ_{para}			σ^-_{para}			$\sigma_{R(para)}$			$\sigma^-_{R(para)}$	
Anilines[62]	C or E	5	0.832	24	5	0.940	15	4	0.996	4	4	0.993	5	3	0.680	45	4	0.916	17
Anisoles[64]	C	7	0.543	29	8	0.872	17	4	0.999	1	5	0.992	7	3	0.728	34	4	0.917	20
Average ⟶			0.688	27		0.906	16		0.998	2		0.992	6		0.704	40		0.916	19

*Data on halogen-substituted derivatives not included.

†Et, Ethanol; E, Ether; C, Cyclohexane; Me, Methanol.

$$\lambda = \lambda_o + |\,\sigma' - \sigma''|\,\rho$$

where σ' and σ'' are the substituent constants of the two *para*- or *meta*-substituents. In these correlations, combinations of σ and σ^+ and σ and σ^- constants have both been tried. That is, if the σ constants are used for electron-withdrawing groups, σ^+ constants are used for electron-donating groups. Similarly, if σ constants are used for electron-donating groups, σ^- constants are used for electron-withdrawing groups. The results of the statistical evaluation show that the σ σ^- combination is much better than the σ σ^+ combination (Table 8). The highest correlation coefficient obtained is only 0.86 which is not completely disheartening compared to the results obtained with the different series of disubstituted benzenes (Table 6).

Table 8

Generalized Correlations of the Ultraviolet Absorption Spectra of Complimentarly Disubstituted Benzene Derivatives(a)

Correlation	λ_o	ρ	r	s	n
σ , σ^+ (p, m)	209.6	56.4	0.779	23.0	19
σ , σ^- (p, m)	202.0	68.4	0.857	19.0	19
σ , σ^+ (p)	182.3	76.5	0.759	23.0	12
σ , σ^- (p)	177.6	85.7	0.815	20.0	12
σ , σ^+ (p) with halogens	179.3	72.1	0.780	22.0	29
σ , σ^- (p) with halogens	174.2	80.9	0.932	12.0	30
σ , σ^+ (p) with halogens and alkyl groups	190.5	65.5	0.756	21.0	38
σ , σ^- (p) with halogens and alkyl groups	175.1	78.9	0.929	11.0	39

(a)All the data in ethanol.

The Halogen Anomaly

The absorption maxima of *para*-halogen substituted benzene derivatives are in the order I > Br ≥ Cl > F (Figure 6) [65-68]. This is exactly in the reverse order to the normally accepted trend of the resonance parameters of the halogens, F > Cl > Br > I. Schubert and coworkers [71] have studied the 200 mμ band in *para*-halonitrobenzenes, -acetophenones, -phenols, -anisoles and -anilines in different solvents and have interpreted the results in terms of the polarizability of the halogen substituent and the solvent orientation and solvent polarization effects. Baliah and Uma [72] have pointed out the importance of the expansion of valency shells of chlorine, bromine and iodine in determining the λ_{max}. We have obtained the *para*-σ and σ^+ values for the four halogens by interpolation using the data for *para*-complimentarily

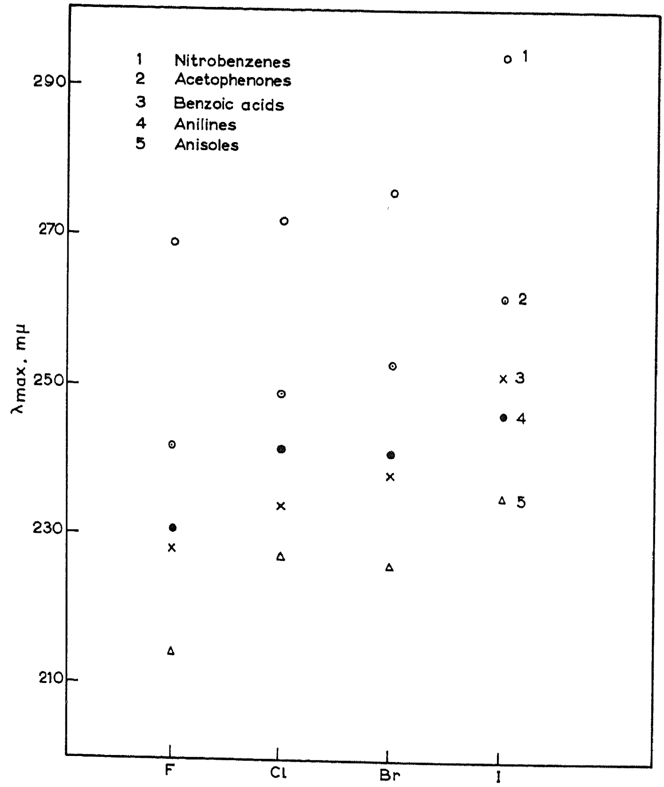

Figure 6. Absorption maxima of a few series of *para*-halogen substituted benzene derivatives.

disubstituted nitrobenzenes, acetophenones and benzoic acids. The *para* σ and σ^- values for the halogens have been obtained using the data for *para*-complimentarily disubstituted anilines and anisoles. The average values of these derived constants are summarized in Table 9. It is interesting to note that the signs of the derived substituent constants depend on the electrical property of the invariant group X. They are all negative when X is electron-withdrawing and positive when X is electron-donating. This implies that halogen substituents in *para*-disubstituted benzene derivatives can act as electron-donating or -accepting groups depending on the nature of the other *para*-substituent. The magnitude of the electron-donating or -accepting ability of the *para*-halogen substituents vary in the order I > Br > Cl > F.

Table 9

Values of Substituent Constants (σ, σ^+, σ^-) for Halogens Derived from the Correlations of Ultraviolet Absorption Spectra of *p*-Complimentarily Disubstituted Benzenes

	F	Cl	Br	I
X, Electron withdrawing:				
Interpolated σ (average)	-0.05	-0.11	-0.14	-0.25
Interpolated σ^+(average)	-0.15	-0.25	-0.33	-0.56
X, Electron donating:				
Interpolated σ (average)	+0.03	+0.11	+0.11	+0.15
Interpolated σ^-(average)	+0.05	+0.19	+0.19	+0.26

When X is an electron-withdrawing group, the $\Delta\sigma$ values (σ derived - σ Hammett) are negative indicating that a term involving electron donation has to be added to the Hammett σ value. The same is true of the σ^+ values. When X is an electron-donating group, the $\Delta\sigma$ values are still negative, but smaller in magnitude to those found when X is electron-withdrawing. It is possible that the polarizabilities of C-halogen bonds and the participation of inner orbitals are both responsible for the observed effects. The resonance picture involving inner-orbital participation, however, seems to be more important. The extent of electron-donation by halogens through resonance interaction should be greater when the other *para*-substituent, X, is electron-withdrawing than when it is electron-donating in nature. This is exactly what is observed. These results clearly show that the values of the *para*-halogen substituent constants normally used with kinetic or equilibrium data are not satisfactory to explain the observed trends in electronic absorption spectra and that it is necessary to add an additional term involving electron donation to the Hammett σ values.

By using the derived σ, σ^+ and σ^- constants of *para*-halogens, the generalized correlations of *para*-complimentarily disubstituted benzenes (n = 30) were found to be considerably improved, the correlation coefficient with the combination of *para*- σ and σ^- values being 0.93 (Table 8).

Alkyl Groups

The effect of alkyl substituents on the electronic absorption spectra of benzene derivatives has been a subject of some controversy. Schubert and coworkers [73] have discussed the absorption spectra of *para*-alkyl substituted-nitrobenzenes and -acetophenones in terms of steric hindrance to solvation. They point out that hyperconjugation may not be an important mode of electron release in these derivatives. We have derived the σ and σ^+ values for the methyl, ethyl, i-propyl and t-butyl groups making use of the correlations of *para*-complimentarily disubstituted nitrobenzenes and acetophenones (Table 7 and Figure 3) employing the data of Schubert, *et al.* The results in Table 10 clearly show that the derived values are quite close to the normally accepted values of the substituent constants for these groups.

Table 10

Values of Substituent Constants σ, σ^+ for Alkyl Groups Derived from the Correlations of Ultraviolet Absorption Data of *p*-Substituted Nitrobenzenes and Acetophenones

	CH_3	C_2H_5	i - C_3H_7	t - C_4H_9
Interpolated σ (average)	-0.107	-0.111	-0.112	-0.112
$\Delta\sigma$ = σ (average) - σ (Hammett)	+0.063	+0.040	+0.039	+0.085
Interpolated σ^+ (average)	-0.280	-0.289	-0.291	-0.290
$\Delta\sigma$ = σ^+ (average) - σ^+ (Brown.....)	+0.031	+0.006	-0.011	-0.034

Generalizations

The available data (n = 39) on *para*-complimentarily disubstituted benzene derivatives (including halogens and alkyl groups) give a satisfactory correlation of the λ_{max} with the combination of σ and σ^- constants of groups, the correlation coefficient is about 0.93, with a standard deviation of 11 mμ (Figure 7). This correlation is considered to be quite acceptable and it is heartening to find that substituent constants can satisfactorily correlate the electronic absorption spectra of benzene derivatives.

An interesting feature is found in the correlations with *para*-complimentarily disubstituted benzene derivatives (Table 7). Not only the sign but also the magnitude of the slope, ρ, varies systematically with the electrical property of the invariant group X. This can be clearly seen from the data below. This trend is similar to that reported in the correlations of the infrared spectra of related groups of organic molecules with substituent constants (Table 4).

Series	Hammett σ Value of the Invariant Group, X	ρ
Nitrobenzenes	0.78	-159.4
Acetophenones	0.50	-118.2
Benzoic acids	0.45	-93.7
Anisoles	-0.27	89.5
Anilines	-0.66	109.9

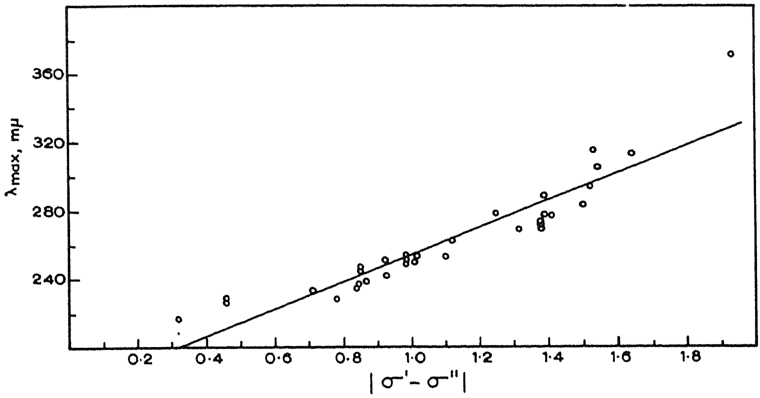

Figure 7. Generalized correlation of the absorption maxima of *para*-complimentarily disubstituted benzene derivatives with substituent constants.

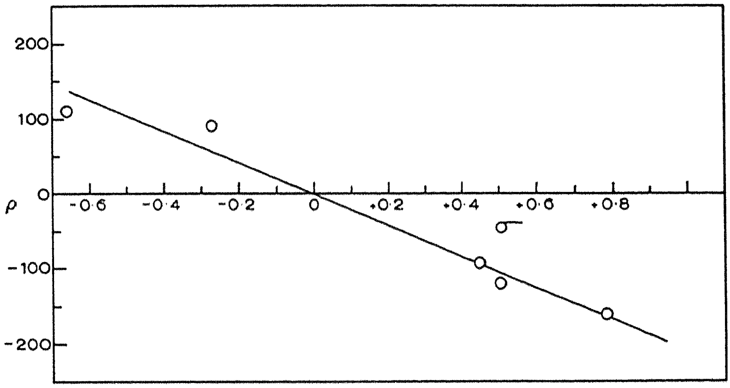

Figure 8. Relation between the ρ value and the substituent constant of the invariant group in *para*-complimentarily disubstituted benzene derivatives.

The ρ value is a measure of the sensitivity of the transition to change in electron density due to the substituents. The ρ is negative when the invariant group is electron-withdrawing and positive when it is electron-donating. The algebraic value of ρ increases with the increasing electron-donating ability of the invariant group X and the plot of ρ versus the σ value of X is nearly linear (Figure 8).

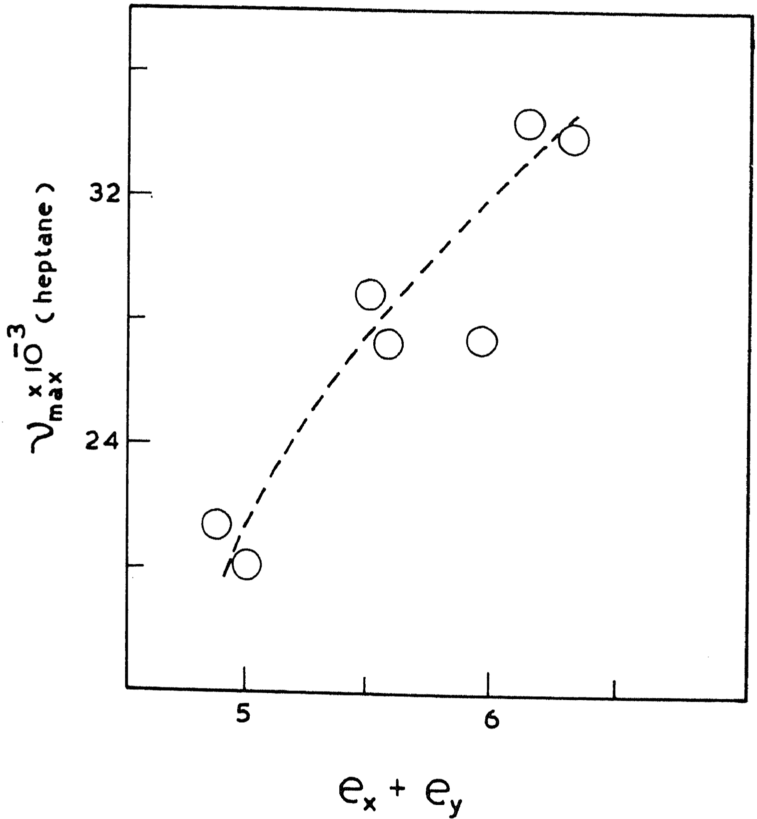

Figure 9. Plot of the $\underline{n} \rightarrow \pi^*$ frequency (ν_{max}) of the thiocarbonyl group against the sum of the electronegativities ($e_x + e_y$) of the elements directly linked to the C=S group.

SUBSTITUENT EFFECTS ON $n \rightarrow \pi^*$ TRANSITIONS OF CHROMOPHORES

The position of the $n \rightarrow \pi^*$ absorption band [50] of a carbonyl group is greatly affected by substitution. Substitution with auxochromic groups such as NH_2, OH and halogens shift the $n \rightarrow \pi^*$ band to shorter wavelengths. This is because these groups donate electrons by resonance interaction and raise the energy of the excited state relative to the ground state [74]. In addition, these groups withdraw electrons by inductive effect and lower the energy of the ground state. Thus, both resonance and inductive interactions of auxochromes shift the $n \rightarrow \pi^*$ transition to higher energy.

Although the $n \rightarrow \pi^*$ transitions of both carbonyl and thiocarbonyl groups were predicted around the same time [75], systematic investigation of the electronic absorption spectra of the thiocarbonyl group has not been carried out till recently [76,77]. The $n \rightarrow \pi^*$ frequency of the thiocarbonyl group has been found to increase with the increasing electronegativity of the elements linked to the thiocarbonyl group Figure 9. To be more precise, the frequency increases with the increasing electron-donating ability (by resonance) of the elements, *viz.* N > O > S. This is similar to the observations of Nagakura [74] on the substituent effects on the $n \rightarrow \pi^*$ frequency of the carbonyl group.

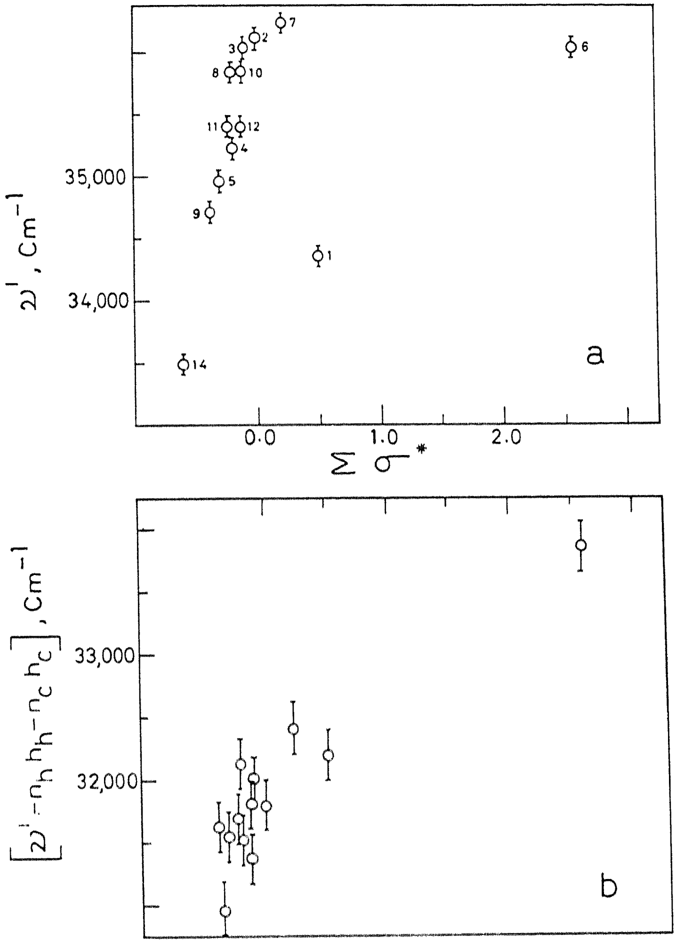

Figure 10. (a) Plot of the $n \rightarrow \pi^*$ transition frequencies (ν') in aliphatic carbonyl derivatives against the polar substituent constants of Taft, $\Sigma\sigma^*$. (b) Plot of ($\nu' - n_h h_h - n_c h_c$) against $\Sigma\sigma^*$. The maximum limits of uncertainty on the frequencies have been shown.

The effect of alkyl substituents on the $n \rightarrow \pi^*$ transitions of the C=O, NO_2 and C=S groups have been investigated in detail [78-80]. The $n \rightarrow \pi^*$ frequencies in the alkyl substituted derivatives are always in the Baker-Nathan order, $CH_3 > C_2H_5 > i\text{-}C_3H_7 > t\text{-}C_4H_9$. This trend is maintained in solvents of varying degree of polarity or/and proton-donating ability. It has been possible to quantitatively correlate the observed $n \rightarrow \pi^*$ frequencies with the inductive and hyperconjugative contributions of the alkyl substituents. The expression of is of the form

$$\nu' = \nu_o' + (\Sigma\sigma^*)\,\rho^* + n_h h_h + n_c h_c$$

where ν' is the observed $n \rightarrow \pi^*$ frequency in cm^{-1}, ν_o' and ρ^* are constants, σ is the Taft-aliphatic polar substituent constant, n_h and n_c are the number of α-hydrogens and carbons respectively available for C-H and C-C hyperconjugation and h_h and h_c are the C-H and C-C hyperconjugation constants respectively. Mere inductive effects and C-H hyperconjugation alone could not explain the data quantitatively. However the expression above yields very satisfactory correlations. The correlation coefficients in the case of aliphatic carbonyl derivatives and nitro compounds are about 0.92 and 0.99 respectively (Figure 10). These studies provide clear evidence for the importance of hyperconjugation in the electronically excited states of molecules. The evidence is particularly convincing because (a) the molecules studied are aliphatic and no other type of resonance interaction can occur, (b) the infrared carbonyl and nitro group stretching frequencies in these molecules are proportional to Taft-aliphatic polar parameters of groups, thus indicating that hyperconjugation may be unimportant in the ground electronic states, (c) $n \rightarrow \pi^*$ transitions are very sensitive to change in structure and solvent and (d) similar trends of the $n \rightarrow \pi^*$ frequencies are found in solvents of varying degree of polarity or/and proton-donating ability.

SUBSTITUENT EFFECTS ON SOLUTE-SOLVENT HYDROGEN BONDING:

We have investigated the effects of various non-polar, polar and proton donor solvents on the $n \rightarrow \pi^*$ transitions of C=O, C=S, NO_2 and N=N chromophores [81]. The shifts of the absorption maxima in non-polar and polar solvents can be satisfactorily related to the electrostatic interactions between the solute and solvent molecules, by the use of the theoretical expression derived by McRae [82]. Very large blue-shifts of the $n \rightarrow \pi^*$ transitions are observed in proton donor solvents and the shifts are much greater in magnitude than expected on the basis of the solvent dielectric constants. These large shifts can only be due to hydrogen bonding between the solute and solvent molecules.

Indeed, isobestic points are found in the $n \rightarrow \pi^*$ band of ethylenetrithiocarbonate in alcohol-hydrocarbon and chloroform-hydrocarbon solvent systems indicating the existence of equilibria between the hydrogen bonded and free species of the solute.

The $n \rightarrow \pi^*$ blue-shifts have been determined in a number of hydroxylic solvents in order to study the effect of substituents on the OH group, in determining the ability of alcohols to donate protons. Alcohols investigated are 2,2,2-trifluoroethanol, methanol, ethanol, *i*-propanol and *t*-butanol. The blue-shifts for all the chromophores in alcohols decreases in the above order Figure 11. The blue-shift in trifluoroethanol is very nearly equal to that in water for all the chromophores. The hydrogen bond energies for the different donor-acceptor systems have been

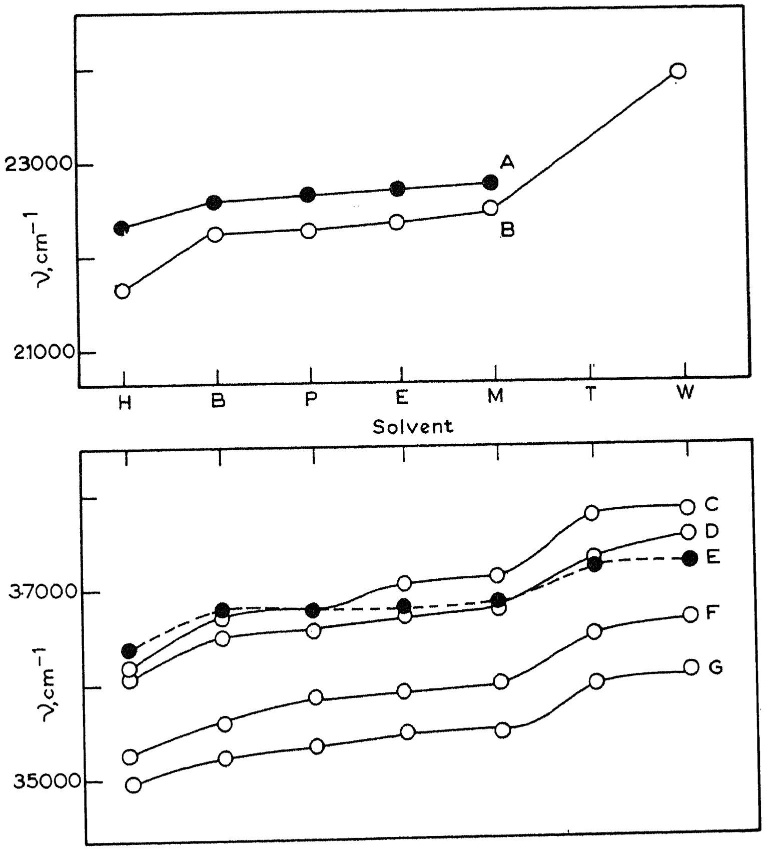

Figure 11. Effect of hydroxylic solvents on $n \rightarrow \pi^*$ transitions: A, azobenzene; B, ethylenetrithiocarbonate; C, acetone; D, methyl ethyl ketone; E, nitromethane; F, methyl *i*-propyl ketone and G, methyl *t*-butyl ketone. Solvent: H, heptane; B, *t*-butanol; P, *i*-propanol; E, ethanol; M, methanol; T, trifluoroethanol and W, water.

evaluated (i) assuming that the solvent blue-shift is entirely due to hydrogen bonding, and (ii) by subtracting the contribution due to the dielectric constant of the solvent from the observed blue-shift, by making use of the McRae-expression [81]. Either way, the hydrogen bond energies for all the donor system studied decrease in the order: water, trifluoroethanol, methanol, ethanol, *i*-propanol and *t*-butanol. It should however be pointed out that the hydrogen bond energies estimated by us may not represent the energy of one hydrogen bond. Since we are only interested in relative values, comparison of the values for a series of alcohols will probably be valid. The average hydrogen bond energies found for these different alcohols (ROH), are plotted against Taft's σ^* constant of the alkyl group, R, in Figure 12a. The plot is seen to be fairly linear. Apparently, the ability of alcohols to donate protons increases with the increasing electronegativity of the alkyl group. This trend is consistent with the concept of acidities of these alcohols. The proton-donating ability (acidity) decreases while going from trifluoroethanol to *t*-butanol. At the same time, it should be noted that the self-association of alcohols (basicity) increases in the same order [83,84]. Our conclusions based on the $n \rightarrow \pi^*$ blue-shifts with regard to proton donating ability of alcohols are in agreement with the recent infrared studies of Becker [85], who finds that the equilibrium constant for the 1:1 complex formation decreases in the order; methanol, ethanol, *i*-propanol and *t*-butanol.

In the case of the C=O and NO_2 chromophores, the effect of different alkyl substituents (methyl, ethyl, *i*-propyl and *t*-butyl) on the $n \rightarrow \pi^*$ solvent blue-shifts have been investigated. The blue-shifts (and therefore the hydrogen bond energies) with the different alcohols are found to decrease with the electron-withdrawing ability of the alkyl group (Figure 12b and c). This conclusion is further supported by the fact that benzophenone gives higher hydrogen bond energies than acetone. According to this interpretation, trifluoro or perfluoroacetone should be a powerful proton acceptor. It is indeed known that electron-withdrawing groups are generally found to promote the hydration of the carbonyl group [86].

We have assumed that stabilization of the electronic ground states of molecules through hydrogen bonding is more prominent. This seems reasonable because, in $n \rightarrow \pi^*$ transitions, one electron is removed from the *n*-orbital and the hydrogen bonded complex should be destabilized in the excited state. Accordingly, an approximately linear relationship has been found between the infrared frequencies reported by Bellamy and Rogasch [44] and our $n \rightarrow \pi^*$ data of ethylenetrithiocarbonate in different solvents.

From these investigations, we conclude that electron-withdrawing groups render the chromophores better proton ac-

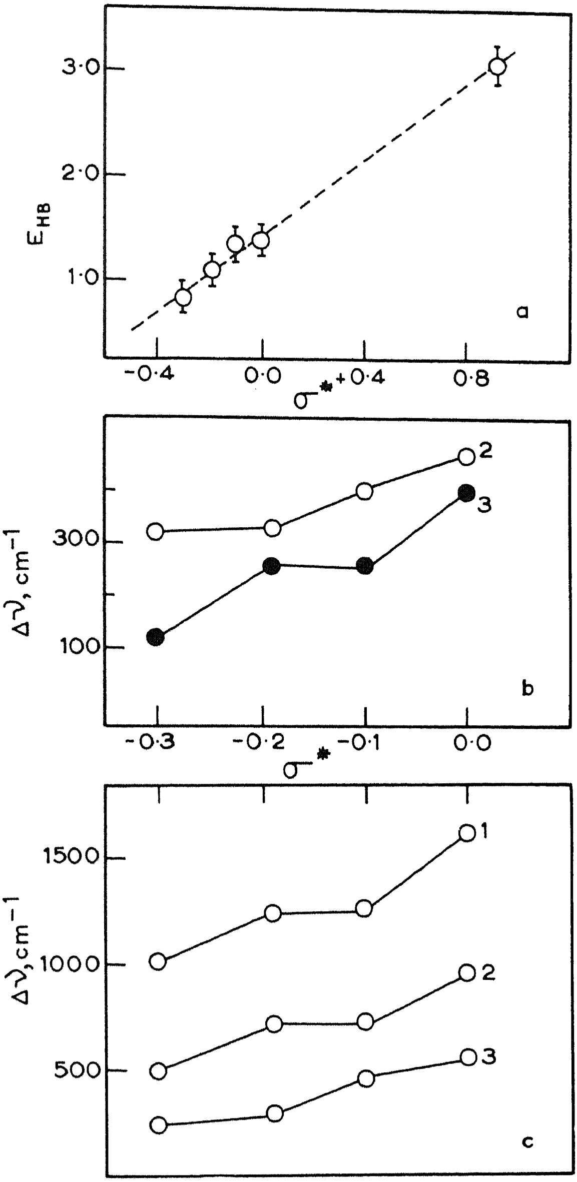

Figure 12. Correlations of $n \rightarrow \pi^*$ blue-shifts and hydrogen bond energies with Taft $-\sigma^*$ constants of the alkyl substituents.

a: Average hydrogen bond energies of aliphatic ketones in different alcohols, ROH, versus Taft $-\sigma^*$ constant of R.

b: Solvent blue-shifts in different alcohols of aliphatic nitrocompounds, RNO_2, versus Taft σ^* constants of R.

c: Solvent blue-shifts in different alcohols of aliphatic ketones, $RCOCH_3$, versus Taft σ^* constant R. 1, trifluoroethanol; 2, ethanol; 3, *t*-butanol.

ceptors and the alcohols, better proton donors. Interestingly enough, the extent of self-association of a good proton donor alcohol like trifluoroethanol, is relatively small [84].

ACKNOWLEDGMENTS

The senior author (C.N.R. Rao) is extremely thankful to the organizers of the X International Conference of Spectroscopy, Maryland, 1962, for their kind invitation and financial assistance. The authors are thankful to the Indian Institute of Science for the facilities and for the awards of Research Scholarships (R. Venkataraghavan, K. R. Bhaskar and A. Balasubramanian).

REFERENCES

1. L. P. Hammett, Physical Organic Chemistry, McGraw-Hill Book Co., Inc., New York, 1940 Chap. VII.
2. H. H. Jaffe, Chem. Revs., 53, 191 (1953).
3. D. H. McDaniel and H. C. Brown, J. Org. Chem., 23, 420 (1958).
4. Y. Okamoto and H. C. Brown, J. Org. Chem., 22, 485 (1957).
5. H. C. Brown and Y. Okamoto, J. Am. Chem. Soc., 80, 4979 (1958).
6. R. W. Taft, Jr., in "Steric Effects in Organic Chemistry," Ed. by M. S. Newman, John Wiley and Sons, Inc., New York, 1956, Chap. 13.
7. C. N. R. Rao, J. Sci. Ind. Res. (India), 20A, 24 (1961).
8. H. W. Thompson, R. W. Needham and D. Jameson, Spectrochim. Acta, 9, 208 (1957).
9. T. L. Brown, Chem. Revs., 58, 581 (1958).
10. P. J. Krueger and H. W. Thompson, Proc. Roy. Soc., A250, 22 (1959).
11. H. W. Thompson, Spectrochim. Acta, 14, 145 (1959).
12. H. W. Thompson and D. A. Jameson, Spectrochim. Acta, 13, 236 (1958).
13. C. N. R. Rao, Chem. Ind., 891 (1958).
14. C. N. R. Rao, W. H. Wahl and E. J. Williams, Can. J. Chem., 35, 1575 (1957).
15. O. Exner, Coll. Czech Chem. Comm., 25, 642 (1960).
16. C. N. R. Rao and R. Venkataraghavan, Can. J. Chem., 39, 1757 (1961).
17. C. N. R. Rao and G. B. Silverman, Curr. Sci. (India), 26, 375 (1957).
18. G. K. Goldman, H. Lehman and C. N. R. Rao, Can. J. Chem., 38, 171 (1960).

19. K. B. Whetsel, W. E. Roberson and M. W. Krell, Anal. Chem., 30, 1598 (1958).
20. T. L. Brown, J. Phys. Chem., 64, 1798 (1960).
21. W. J. Orville-Thomas, A. E. Parsons and C. P. Ogden, J. Chem. Soc., 1047 (1958).
22. G. L. Caldow and H. W. Thompson, Spectrochim. Acta, 13, 212 (1958).
23. C. N. R. Rao and R. Venkataraghavan, Tetrahedron, 18, 531 (1962).
24. D. G. O'Sullivan and P. W. Sadler, Spectrochim. Acta, 16, 742 (1960).
25. P. J. Stone and H. W. Thompson, Spectrochim. Acta, 10, 17 (1957).
26. M. St. C. Flett, Trans. Faraday Soc., 44, 767 (1948).
27. R. N. Jones, W. F. Forbes and W. A. Mueller, Can. J. Chem., 35, 504 (1957).
28. P. J. Krueger and H. W. Thompson, Proc. Roy. Soc., A243, 143 (1957).
29. R. D. Kross and V. A. Fassel, J. Am. Chem. Soc., 78, 4225 (1956).
30. M. R. Mander and H. W. Thompson, Trans. Faraday Soc., 53, 1402 (1957).
31. C. N. R. Rao, G. K. Goldman and C. Lurie, J. Phys. Chem., 63, 1311 (1959).
32. D. G. O'Sullivan and P. W. Sadler, J. Chem. Soc., 4144 (1957).
33. T. L. Brown, J. F. Regan, R. D. Schultz and J. C. Steenberg, J. Phys. Chem., 63, 1324 (1959).
34. J. D. S. Goulden, Spectrochim. Acta, 6, 129 (1954).
35. R. N. Haszeldine, J. Chem. Soc., 2525 (1953).
36. J. Mason and J. Dunderdale, J. Chem. Soc., 759 (1956).
37. J. P. Jessen and H. W. Thompson, Spectrochim. Acta, 13, 217 (1958).
38. T. L. Brown, J. Am. Chem. Soc., 80, 794 (1958).
39. L. J. Bellamy, "The Infrared Spectra of Complex Molecules," Methuen, London (1958).
40. C. N. R. Rao and R. Venkataraghavan, Spectrochim. Acta, 18, 541 (1962).
41. E. Spinner, Spectrochim. Acta, 15, 95 (1959).
42. B. Bak, L. Hasen-Nygaard and C. Pedersen, Acta Chem. Scand., 12, 1451 (1958).
43. N. Lozach and G. Guillouzo, Bull. Soc. Chem. France, 1221 (1957).
44. L. J. Bellamy and P. E. Rogasch, J. Chem. Soc., 2218 (1960).
45. T. Miyazawa, T. Shimanouchi and S. Mizushima, J. Chem. Phys., 29, 611 (1958).
46. C. L. Angell, P. J. Krueger, R. Lauzon, L. C. Leitch, K. Noack, R. J. D. Smith and R. N. Jones, Spectrochim. Acta, 926 (1959).

47. T. Miyazawa, J. Mol. Spec., 4, 168 (1960).
48. M. Tsuboi, Bull. Soc. Chem., Japan, 22, 255 (1949).
49. C. N. R. Rao and R. Venkataraghavan, Spectrochim. Acta, 18, 273 (1962).
50. C. N. R. Rao in "Ultraviolet and Visible Spectroscopy-Chemical Applications," Butterworths, London, 1961.
51. R. B. Woodward, J. Am. Chem. Soc., 63, 1123 (1941); 64, 72, 76 (1942).
52. A. L. Sklar, J. Chem. Phys., 7, 339, 353 (1937); 10, 135 (1942).
53. F. A. Matsen and coworkers, J. Am. Chem. Soc., 72, 5243, 5248, 5250, 5252, 5256, 5260 (1950).
54. J. R. Platt, J. Chem. Phys., 19, 263 (1951).
55. L. Doub and J. M. Vandenbelt, J. Am. Chem. Soc., 69, 2714 (1947); 71, 2414 (1949).
56. L. Goodman and H. Shull, J. Chem. Phys., 27, 1388 (1957).
57. C. N. R. Rao, J. Sci. Ind. Research (India), 17B, 56, (1958); Curr. Sci. (India), 26, 276 (1957).
58. C. N. R. Rao, Chem. & Ind. (London), 666 (1956); 1239 (1957).
59. W. F. Forbes, Can. J. Chem., 36, 1350 (1958).
60. W. F. Forbes, W. A. Mueller, A. S. Ralph and J. F. Templeton, Can. J. Chem., 35, 1049 (1957).
61. J. C. Dearden and W. F. Forbes, Can. J. Chem., 36, 1362 (1958).
62. W. F. Forbes and I. R. Leckie, Can. J. Chem., 36, 1371 (1958).
63. J. C. Dearden and W. F. Forbes, Can. J. Chem., 37, 1294 (1959).
64. J. C. Dearden and W. F. Forbes, Can. J. Chem., 37, 1305 (1959).
65. W. F. Forbes, Can. J. Chem., 37, 1977 (1959).
66. W. F. Forbes, Can. J. Chem., 39, 1131 (1961).
67. W. F. Forbes, Can. J. Chem., 39, 2295 (1961).
68. W. F. Forbes, Can. J. Chem., 38, 1104 (1960).
69. W. F. Forbes and J. C. Dearden, Can. J. Chem., 38, 896 (1960).
70. H. E. Ungnade, J. Am. Chem. Soc., 76, 5133 (1954).
71. W. M. Schubert, J. M. Craven and H. Steadly, J. Am. Chem. Soc., 81, 2695 (1959); 82, 1353 (1960); 82, 1357 (1960).
72. V. Baliah and M. Uma, Naturwiss., 45, 512 (1958).
73. W. M. Schubert, Janis-Robins and J. L. Haun, J. Am. Chem. Soc., 79, 910 (1957).
74. S. Nagakura, Bull. Chem. Soc. Japan, 25, 164 (1952).
75. R. S. Mulliken, J. Chem. Phys., 3, 564 (1935).
76. M. J. Janssen, Recueil, 79, 454, 464, 1066 (1960).
77. C. N. R. Rao, A. Balasubramanian and J. Ramachandran, J. Sci. Ind. Res. (India), 20B, 382 (1961).

78. C. N. R. Rao, G. K. Goldman and A. Balasubramanian, Can. J. Chem., 38, 2508 (1960).
79. A. Balasubramanian and C. N. R. Rao, Chem. & Ind. (London), 1025 (1960).
80. M. J. Janssen, A. Balasubramanian and C. N. R. Rao, J. Sci. Ind. Res. (India), 20B, 349 (1961).
81. A. Balasubramanian and C. N. R. Rao, Spectrochim. Acta (In press), 18 (1962).
82. E. G. McRae, J. Phys., Chem., 61, 563 (1957).
83. U. Liddel and E. D. Becker, Spectrochim. Acta, 10, 70 (1957).
84. B. D. N. Rao, P. Venkateswarlu, A. S. N. Murthy and C. N. R. Rao, Canad. J. Chem., 40, 387 (1962).
85. E. D. Becker, Spectrochim. Acta, 17, 436 (1961).
86. R. P. Bell and A. O. McDougall, Trans. Faraday Soc., 56, 1281 (1960).

THE DONOR CHARACTERISTICS OF THE CARBONYL GROUP

III. BF_3 COMPLEXES.

Denys Cook
Dow Chemical of Canada, Ltd.
Sarnia, Ontario, Canada

INTRODUCTION

Perturbations of X-H stretching vibrations in hydrogen-bonded interactions have been used previously to determine the donor characteristics of functional groups in molecules, particularly effectively in a wide range of compounds containing the carbonyl group [1]. It was found that these easily measured perturbations were related to the carbonyl frequency, ν_{CO}, with certain reservations [2], and the ionization potential, IP, of the carbonyl compound. The latter is a measure of the energy required to remove one of the lone pair electrons from the oxygen atom, and should also be a measure of the availability of the lone pair electrons in hydrogen-bond formation or in donor-acceptor complex formation. The latter function, particularly with BF_3 as the acceptor is considered in this paper.

Some structural details of a few BF_3 donor-acceptor complexes have been reported, chiefly of amines [3-5], acetonitrile [6] and pyridine [7], table 1 showing some of these. The BF_3 molecule, originally planar in the gas phase, assumed a nearly tetrahedral disposition in the solid complexes, three bonds being to the F atoms, the other to the donor atom in the organic molecule. Figure 1 shows how the stretching frequency of the BF bonds in the complex $F_3B\ldots X$ varies with the BF and BX distances. The BX distance in donor-acceptor complexes should bear an inverse proportionality to the strength of the interaction, which is a property fundamental to the discussion of donor-acceptor, or Lewis acid-base interactions. This property is usually measured thermochemically, and requires elaborate and painstaking procedures for its accurate determination. Other quantitative methods

Table 1

BF Stretching Frequencies for Some Nitrogen Base:BF_3 Complexes

	$^{10}\nu^{as}_{BF}$	$^{11}\nu^{as}_{BF}$	r_{BX}, Å	r_{BF}, Å
CH_3CN	1264	1206	1.635 ± 0.02[6]	1.33[6]
NH_3	1206	1160	1.60[3]	1.38[3]
CH_3NH_2	1196	1155	1.57 ± 0.02[4]	1.39[4]
$(CH_3)_3N$	1171	1133	1.585 ± 0.03[5]	1.39[5]
C_5H_5N	1165[16]	1125[16]	1.53[7]	1.41[7]
BF_4^-	(1090)	1041[9]	1.43[17]	1.43[17]

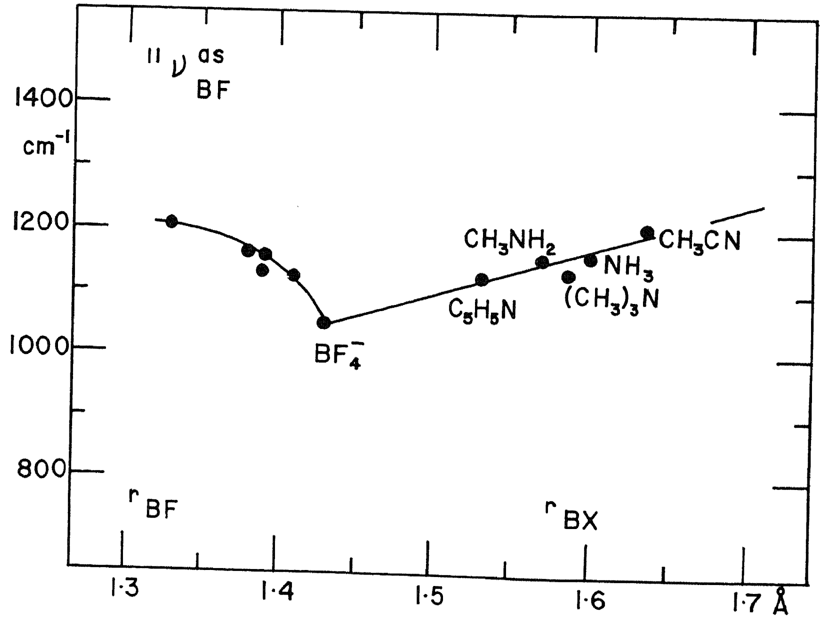

Figure 1. Variation of ν_{BF} with r_{BX} and r_{BF}.

of evaluation of this interaction energy are therefore valuable. In view of the relationship between the BX and BF bond lengths, and the BF stretching frequency, it was determined to measure the vibrational spectra of several BF_3 complexes. Those of BF_3 complexes of carbonyl compounds are reported at this time, since a wealth of experimental data on the pure compounds exists. Some BF_3 complexes of amines have been studied in a similar way and the results are similar to those for carbonyl compounds.

RESULTS

The bands assigned to the asymmetric stretching frequencies of the BF bond have been abstracted from the spectra and are shown in tables 1 and 2. Table 2 also includes the IP of the organic molecule, if known, or, in parentheses, an estimate from the known value of similar molecules. Figure 2 shows the spectrum of a typical complex, that of the 2,6-dimethyl-4-pyrone:BF_3 complex. Figures 3 and 4 show graphs of the IP plotted against the BF stretching frequencies.

Table 2

BF Stretching Frequencies for Some Carbonyl:BF_3 Complexes

	IP, ev[18]	$^{11}\nu^{as}_{BF}$	$^{10}\nu^{as}_{BF}$	$^{11}\nu^{as}_{BF}$	$^{10}\nu^{as}_{BF}$
		A'		A''	
$HCOOCH_3$	10.82	1162		1195	1212
$CH_3COOC_2H_5$	10.11	1156		1185	1235
$(CH_3)_2CO$	9.69	1175[20]	1210[20]	1175[20]	1210[20]
$HCOC_6H_5$	9.53	1136		1179	
$(C_2H_5)_2CO$	9.32	1155	1192	1155	1192
$CH_3COC_6H_5$	9.27	1138[21]		1165[21]	1190[21]
$(nC_3H_7)_2CO$	(9.20)	1165[20]	1200[20]	1165[20]	1200[20]
$HCON(CH_3)_2$	9.12	1112		1142	1170
$(C_6H_5)_2CO$	9.00[19]	1131[21]	1160[21]	1131[21]	1160[21]
$CH_3CON(C_6H_{11})_2$	(8.50)	1104		1143	1187
2,6-dimethyl-4-pyrone	(8.36)	1112	1139	1112	1139

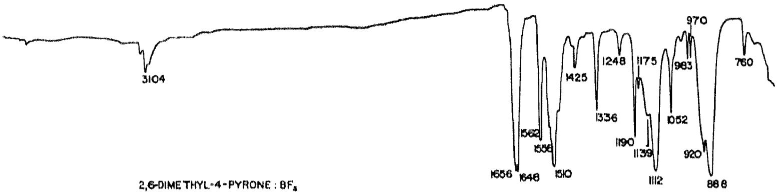

Figure 2. Infrared spectrum of the 2,6-dimethyl-4-pyrone:BF_3 complex.

DISCUSSION

The assignments of gaseous BF_3 [8] are shown in table 3, and are therein related to those of the BF_4^- anion [9], and a hypothetical model BF_3X which is similar to, but has higher symmetry than the BF_3 complexes with carbonyl compounds. An

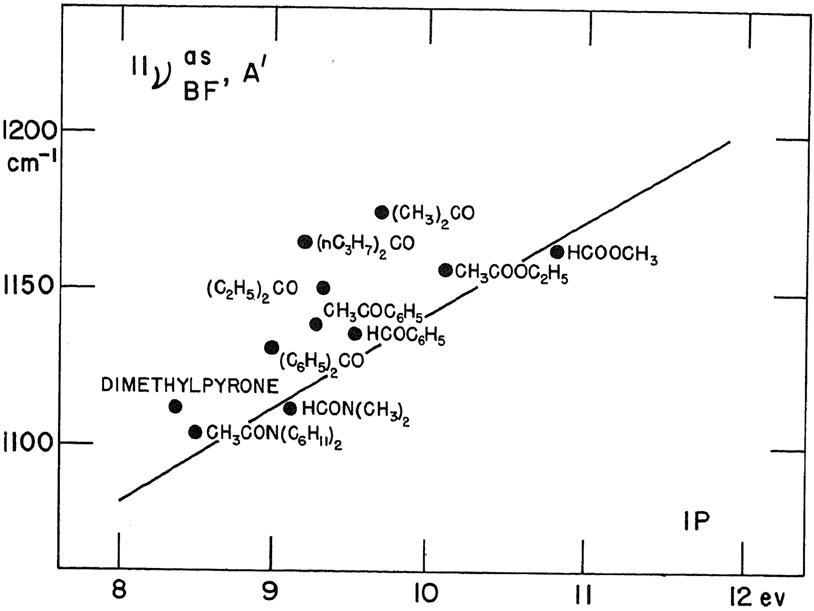

Figure 3. Variation of ${}^{11}\nu^{as}_{BF}$ A' with IP.

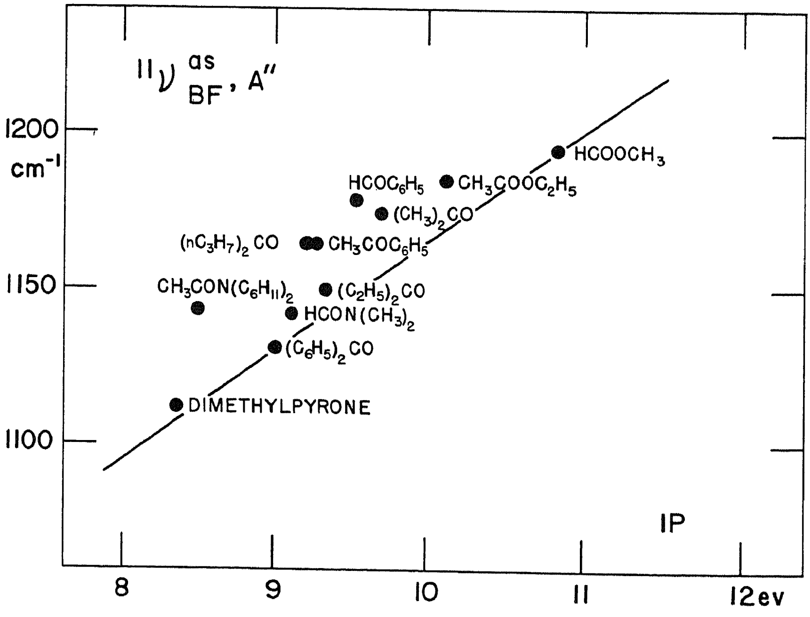

Figure 4. Variation of ${}^{11}\nu^{as}_{BF}$, A" with IP.

example of this type is BF_3Cl^-, and the assignments [10] for this ion are also shown.

When the coordinating species is other than a monatomic anion or a linear molecule coordinated along the threefold axis, the point group for the complex becomes C_s. The doubly degenerate vibrations of E species of the C_{3v} model should therefore be split in the C_s model, and the vibration under consideration, the asymmetric BF stretching mode, should have an A' and an A'' component. In addition to this splitting there should also be a doubling of each absorption band due to a vibration involving movement of the B atom, because of the presence of the two isotopes ^{10}B and ^{11}B in the ratio 1:4. A high frequency satellite of each band should appear, of about one fourth the intensity and with a separation of about 30-50 cm^{-1}.

In several complexes it has been possible to observe the splitting of the BF asymmetric stretching vibration, though the $^{10}\nu^{as}_{BF}$, A' band could not be measured since it was probably obscured by the $^{11}\nu^{as}_{BF}$, A'' band. (It has not been possible experimentally to distinguish the species of the components in the BF asymmetric stretching vibration; the lower frequency has been arbitrarily assigned to the A' species.) In many complexes this splitting has not been observed; and the carbonyl compounds in these complexes were those having C_{2v} symmetry, for example, symmetrical ketones and 4-pyrones.

Table 3

BF_3 [8]	BF_4^- [9]	BF_3X	BF_3X'
D_{3h}	T_d	C_{3v}	C_s
A_1' (ν_1 = 888)	A_1 (ν_1 = 774)	A_1 (ν_1 = 845)[10]	A' (ν_2 = 888)
A_2'' (ν_2 = 720)	E (ν_2 = 353)	E (ν_6 =)	A' (ν_6 =)
			A'' (ν_9 =)
E' (ν_3 = 1497)	F_2 (ν_3 = 1035)	A_1 (ν_2 = 625)	A' (ν_3 =)
		E (ν_4 = 1037)	A' (ν_1 = 1112)
			A'' (ν_7 = 1143)
E' (ν_4 = 482)	F_2 (ν_4 = 519)	A_1 (ν_3 = 456)	A' (ν_5 =)
		E (ν_5 = 520)	A' (ν_4 =)
			A'' (ν_8 =)

The graphs in Figures 3 and 4 show the relationship between IP and $^{11}\nu_{BF}^{as}$ for the A' and A'' species respectively. The trend to lower frequencies as the IP decreases is unmistakable, and affords support for the view advanced in the introduction that the BF stretching frequencies can be a useful measure of the donor ability of the carbonyl compound in the complex, and also of the interaction energy, and strengthens the use of the IP for the same purpose.

Further information can however be derived from these graphs, in particular from the data in Figure 3. The observation that the compounds close to the line were those with an H atom attached to the CO group prompted an explanation for those points which deviated from the curve. All these, in Figure 3, (with one exception in Figure 4) have substituents much bulkier than an H atom. It is believed that the curve denotes a true relationship between IP and $^{11}\nu_{BF}^{as}$, but because of bulky substituents some carbonyl compounds prevent the closest approach of the BF_3 molecule to the extent governed by the IP. Hence r_{BX} is larger than it should be, r_{BF} must therefore be smaller, and it follows that $^{11}\nu_{BF}^{as}$ would be larger than the value derived from the curve.

The deviations from the curve in Figure 3 in terms of ν_{BF} and $\Delta\nu_{BF}$ have been calculated, and lead to the following generalisation. The mean deviations for compounds whose least bulky group is methyl, ethyl and n-propyl are 19, 33 and 47 cm^{-1}, respectively. These figures call for some comment, for although individual values may show some scatter, particularly when Figure 4 is considered too, the orders of magnitude seem acceptable. In acetone, and other compounds whose least bulky substituent is a methyl group, only restricted rotation about the CC bond is possible, which would not grossly affect the hindrance to the BF_3 molecule. In 3-pentanone, however, a variety of configurations are possible. In the gas phase an extended, zigzag, symmetrical configuration was proposed from electron diffraction experiments [11]. In the liquid phase Jones and Noack [12] regarded an equilibrium of II and III as most likely, but conceded that the solid form could be either II, or less probably, I. These latter views are quite in accord with the conclusion that since $\Delta\nu_{BF}$ for the 3-pentanone:BF_3 complex is of the same order of magnitude as for compounds with a methyl group, a similar hindering agency is present. Conformation II or IV would provide such an agency (IV being unlikely, due to interference between the terminal methyl groups), while III could also be satisfactory provided the degree of skewness was large enough.

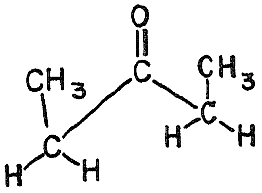

I

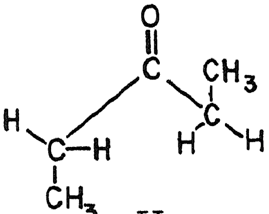

II

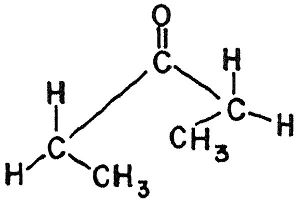

III

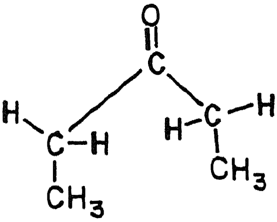

IV

In principle, all that has just been said of 3-pentanone should pertain to 4-heptanone. The magnitude of $\Delta\nu_{BF}$ for the 4-heptanone:BF_3 complex suggests however that the solid may contain the ketone in conformation I, the more symmetrical state being dictated by packing considerations.

$\Delta\nu_{BF}$ for the phenyl group is similar in size to that of the methyl group. This is understandable since it is known that in benzophenone derivatives the CO and C_6H_5 groups are not coplanar, but that the rings are rotated out of this plane: the figures for this rotation are 38° and 24° for 4,4'-dimethoxybenzophenone [13], and 29° for 4,4'-dichlorobenzophenone [14]. Rough calculations and trials with molecular models reveal hindering agencies comparable in size to the methyl group.

Efforts have been made to try to relate the spectroscopic values derived from the present results to some other independent measure of the strength of the interaction between BF_3 and carbonyl compounds. The literature is remarkably sparse, and while some data exist for the thermochemically derived heats of formation of some BF_3 complexes of nitrogen bases [15], none was found for carbonyl compounds.

Although these accurate data are lacking, the mere physical behaviour of the complexes on exposure to atmospheric moisture parallels the stability as defined by ν_{BF}. The complexes with the esters, aldehydes, aliphatic and aromatic ketones are all hygroscopic and fume in moist air. The complexes with carbonyl compounds having low IP, such as 2,6-dimethyl-4-pyrone, N,N-dimethylformamide and N,N-dicyclohexylacetamide are much more stable in moist air. A further example of such stability is the xanthone:BF_3 complex. The value of ${}^{11}\nu^{as}_{BF}$ is 1130 cm^{-1}. No IP has been measured for xanthone so it was not included in table 2 or Figures 3 and 4. However, it belongs to the 4-pyrone species, but with two benzene groups fused to the 2,3 and 5,6 bonds. The effect of these on the IP is unknown, but to a first approximation, because of increased conjugation, it would be lower than that of 2,6-dimethyl-4-pyrone. Even assuming the same value of IP as the pyrone, 8.36 ev, the calculated ν_{BF} is 1093 cm^{-1}, which leads to a value of $\Delta\nu_{BF}$ of 37 cm^{-1}, comparable to an ethyl group, which has a spatial arrangement very similar to that in xanthone. Too much weight must not be placed on this agreement however in view of the assumptions involved.

A reasonable conclusion from the foregoing is that the spectroscopically determined value of ν_{BF} seem to give a plausible, and self-consistent set of values of the strength of interaction: a strict comparison will have to wait till carefully determined energies of complex formation are available. The fact that the weaker complexes probably have appreciable vapour pressures may facilitate this task.

Some preliminary, unpublished results from studies of BF_3 complexes with amines have shown that a similar correlation with IP is possible, though not with the same parametric relation as for carbonyl compounds. Little or no interference with complex formation has been observed for aliphatic amines having a hydrogen atom on the carbon atom attached to the nitrogen atom. These are the analogues of aldehydes etc. in the carbonyl series. Tertiary butylamine, which has no such hydrogen atom is highly hindered, $\Delta\nu_{BF}$ being about 66 cm^{-1}. Simple models show that the terminal methyl group in the amine approaches the F atom much more closely than, for example, the methyl group in a ketone due to the differences in the angles.

EXPERIMENTAL

The Spectra. These were recorded on a Perkin-Elmer Model 221 prism-grating spectrometer. Emulsions of the solids in nujol and fluorolube were used.

The Compounds. Solutions of the compounds in an inert solvent like CCl_4 or Freon 113 were cooled by ice, or solid CO_2 and treated with BF_3. The solids so formed were filtered and prepared for spectral recording in a dry box, since for the most part they were hygroscopic. Small portions were put into sealed tubes for melting point determination at the same time.

ACKNOWLEDGEMENT

The author wishes to thank Miss C. D. Anderson for technical assistance, and Professor K. Watanabe for much information on the ionization potential of organic molecules.

REFERENCES

1. D. Cook, J. Amer. Chem. Soc. 80, 49 (1958).
2. D. Cook, Can. J. Chem. 39, 31 (1961).
3. J. L. Hoard, S. Geller, and W. M. Cashin, Acta Cryst. 4, 396 (1951).
4. S. Geller and J. L. Hoard, Acta Cryst. 3, 121 (1950).
5. S. Geller and J. L. Hoard, Acta Cryst. 4, 399 (1951).
6. J. L. Hoard, T. B. Owen, A. Buzzell and O. N. Salmon, Acta Cryst. 3, 130 (1950).
7. Z. V. Zvonkova, Kristallografiya. 1, 73 (1956). C. A. 51, 34 (1957).
8. G. Herzberg, Infrared and Raman Spectra. D. Van. Nostrand, Inc., New York, 1945, p. 299.
9. A. P. Altschuler, J. Amer. Chem. Soc. 77, 6187 (1955).
10. T. C. Waddington and F. Klanberg, J. Chem. Soc. 2339 (1960).
11. C. Romers and J. E. G. Creuzberg. Rec. Trav. Chim. 75, 331 (1956).
12. R.N. Jones and K. Noack, Can. J. Chem. 39, 2214 (1961).
13. I. L. Karle, H. Hauptman, J. Karle and A. B. Wing. Acta Cryst. 11, 257 (1958).
14. J. Toussaint, Bull. Soc. Sci. Liège. 17, 10 (1948).
15. H. C. Brown and R. R. Holmes. J. Amer. Chem. Soc. 78, 2173 (1956) and earlier papers.
16. A. R. Katritzky. J. Chem. Soc. 2049 (1959).
17. D. Pendred and R. E. Richards. Trans. Faraday Soc. 51, 468 (1955).
18. K. Watanabe, T. Nakayama and J. Mottl. Final Report on Ionization Potential of Molecules by a Photoionization Method. University of Hawaii, Honolulu, Hawaii. (1959).
19. Private Communication. Dr. K. U. Ingold. National Research Council, Ottawa.
20. P. Chalandon and B. P. Susz. Helv. Chim. Acta. 41, 697 (1958).
21. B. P. Susz and P. Chalandon. Helv. Chim. Acta. 41, 1332 (1958).

SOME HIGH RESOLUTION STUDIES IN THE INFRARED

J. H. Jaffe
The Weizmann Institute of Science
Rehovoth, Israel

INTRODUCTION

Infrared spectroscopy has been a common tool of the chemist for the last fifteen years though up to about 1950 the infrared was thought of as a very poor region optically and certainly inferior to the visible and near ultraviolet. By 1950, however, the basic needs with respect to instruments had been satisfied for those spectroscopists working with liquids and solids. On the other hand since the spectra of gases and particularly gases at low pressures consist of extremely sharp lines it is necessary to strive for very high resolution indeed, and high resolution infrared spectroscopy was in difficulties because of inadequate spectrometers. During the last decade there have been developments both in instrumentation and in method and it is the purpose of this lecture to describe some of them.

Today the near infrared region (1 to 5 μ) is in many respects a better region to work in than the visible. This has come about because of two great advances in instrumentation.

The first is the development of photoconductive detectors [1]. Efforts during the second world war produced lead sulphide, lead telluride and lead selenide detectors. These are several orders of magnitude more sensitive than the thermal devices that were the only detectors in general use before the war. In addition to being sensitive these photoconductive detectors are fast and this has made possible the construction of very stable and compact electronic equipment for amplifying and recording their responses.

The second advance is the development of improved diffraction gratings. Manufacture of gratings has been the achievement almost solely of Americans and it is certainly not for a foreigner to lecture to an American audience on the history of the development of gratings. Rowland, Wood, Strong at the Johns Hopkins University, Michelson and Gale at University of Chicago, paved the way [2]. In 1947 on the initiative of George Monk, Michelson's two great ruling engines were reactivated. One went to Bausch and Lomb Inc. and the other to the Massachusetts Institute of Technology. At Bausch and Lomb, David Richardson has ruled nearly 800 gratings, some of them the excellent 8 x 5 inch blazed plane gratings that have proved to be so good for the near infrared. Replica techniques have been perfected. Production of these gratings continues and according to Richardson the B & L - Michelson engine is steadily improving with age.

The second Michelson engine at the Massachusetts Institute of Technology under the direction of G.R. Harrison is producing outstanding rulings. The aim of the M.I.T. ruling program is to manufacture larger gratings. By using sophisticated methods of controlling the line spacing [3] beautiful plane rulings of ten inches and more have been made.

Using the new gratings and detectors and with unbelievable skill, D.H. Rank has been able to measure wavelengths of absorption lines in the near infrared with an accuracy of one part in several million [4]. Thus for example, in a recent paper [5] Rank lists the lines of bands of HCl^{35} and DCl^{35} quoting frequencies in wave number units to four figures after the decimal point. From this work it has been possible to obtain values of the magnetic moments of HCl and DCl. By combining the rotational constants of DCl determined from this work and from microwave data, a value for the velocity of light was obtained, 299,793.1 ± 0.65 km/sec, that is as reliable a value as any obtained to date.

Rank has given highly precise frequency standards for the entire 1-5 μ region [4]. Plyler and others have studied the spectra of many molecules in considerable detail. Even a molecule as complicated as H_2O has been tackled! [6]

LINE INTENSITIES AND LINE WIDTHS

In addition to line frequency measurements, there are two other features of a spectrum that can be fruitfully studied. (a) Intensities—and since we have in mind high resolution, we have in mind in addition to band intensities, the intensities of individual lines, and (b) Widths and shapes of lines.

The intensity S_m of an individual spectral line m in a band is defined as the area under the plot of the absorption coefficient $k(\nu)$ *versus* frequency ν thus

$$S_m = \int_{\text{line}} k(\nu)\, d\nu$$

It can be shown that [7]

$$S_m = S_{band} \frac{\nu_m |m| \exp(-E(J)/kT)}{\bar{\nu} Z} \times F_m$$

where m = -J for the P branch and J + 1 for the R branch. Z is the rotational partition function; $\bar{\nu}$ is the "effective" vibrational frequency; F_m is the vibration-rotation interaction factor and the S_{band} is the strength of the entire band [8]:

$$S_{band} = \sum_m S_m = \frac{8\pi^3}{3hc} N_v \bar{\nu} |R^{vv'}|^2$$

Here $R^{vv'}$ is a matrix element of the dipole moment function [9] $M = M_o + M_1(r-r_e) + M_2(r-r_e)^2 + \ldots$ where r is the instantaneous interatomic distance, r_e is the equilibrium interatomic distance and where it is assumed that M can be expanded in a power series about r_e. Measurement of line intensities gives therefore information about the temperature of the system, the interaction between vibration and rotation and the dipole moment function. M_o is approximately equal to the permanent dipole moment; M_1 is approximately the effective charge on the vibrating atom and M_2, M_3 . . . express what is called "electrical anharmonicity."

One of the most important stimuli to modern studies of line intensities was a remarkable contribution—now a classic—by Herman and Wallis to the theory of vibration-rotation interaction [10]. Even on the most naive assumptions one must take account of vibration-rotation interactions. The most elementary model of a vibrator is that of a harmonic oscillator and the simplest model rotor is a rigid rotor. Clearly these two models cannot be reconciled. An oscillating rotor cannot be rigid! Vibration-rotation interactions have been discussed for about forty years but Herman and his associates produced a detailed theory that transforms vibration-rotation interaction effects from a dull correction into an exciting observable leading to important new information about the electrical properties of molecules. Qualitatively the important result of Herman may be explained as follows. For a diatomic molecule in vibration the intensity of absorption depends mainly on M_1. In rotation the intensity depends mainly on M_o. The vibration-rotation interaction depends on the ratio M_o/M_1. Theory shows that if this ratio is positive the effect of vibration-rotation interaction on the intensity is to depress the R branch and enhance the P branch. The reverse is the case if M_o/M_1 is negative. Whereas only the absolute value of M_1 is obtainable from band intensities, a study of vibration-rotation interaction makes it possible to obtain the sign of M_1.

Experimental measurement of the absolute intensities of individual lines in a band remains a relatively difficult matter. They are extremely sharp and even with the best resolution available, instrumental corrections must still be made. These are often complicated and unreliable. A basic contribution to the experimental problem was made in 1956 by Benedict, Herman, Moore and Silverman [7,11]. These workers showed in detail and with wonderful care and precision how to determine line intensities and widths by the so-called curve of growth method. Although an observed line is a smeared out version of the true line, the area above the transmission curve depends only upon the amount of energy removed from the incident beam by absorption. This must surely be independent of instrumental factors. This area is given by $\int (1 - T(\nu))d\nu$ and it does not matter whether $T^{obs}_{(\nu)}$ or $T^{real}_{(\nu)}$ is put in the integrand. By determining this area for a series of sample lengths (and assuming a definite line shape) it is possible to determine absolute line intensity and the line width. Benedict *et al.* applied the curve of growth method to bands of HCl and DCl and subsequently more work has been done on HCl, on CO, CO_2 and other gases.

REFRACTION SPECTRUM

In our laboratory the approach to the line intensity problem has been somewhat different. When infrared spectroscopists speak about a "spectrum" they usually mean an absorption spectrum—a plot of absorption *versus* frequency but there also exists the refraction spectrum, that is a plot of refractive index *versus* frequency. Where there are sharp lines in the absorption spectrum, there are sharp wrinkles in the refraction spectrum. The intensity of an absorption line is given by the area under it and if the line shape is known it is proportional to the product of the peak absorption and the half-width. It turns out that the intensity of a line in the refraction spectrum is proportional to the product of its amplitude and the frequency interval between the peak and the trough. This latter is numerically equal to the half-width of the corresponding absorption line. In fact the refraction spectrum in every way gives the same information as the absorption spectrum. It can be shown that if the refraction spectrum is known over the entire frequency range, then the absorption spectrum may be calculated from it—and *vice-versa* [12]. Theoretically then, there is nothing to choose between the two. In practice however it has been found that in some cases determinations of intensities and widths are much better with the refraction spectrum.

Refraction spectra of gases in the infrared have been determined for many years notably by Rollefson and his collaborators [13], but recently very sensitive refractometers have been combined with spectrometers of very high resolution and this has made possible the study of individual refraction lines. Several types of refractometers have been devised. Legay in Paris used an interferometer while we in Israel have used a simple hollow prism. The instrument is shown schematically in Figure 1. The optical system is shown in more detail in Figure 2.

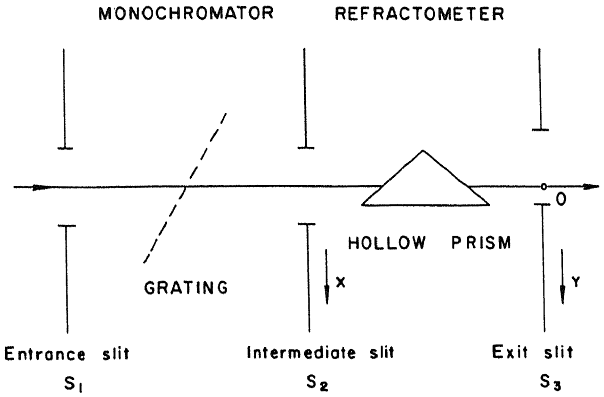

Figure 1. Schematic arrangement for measurement of refraction spectra of gases.

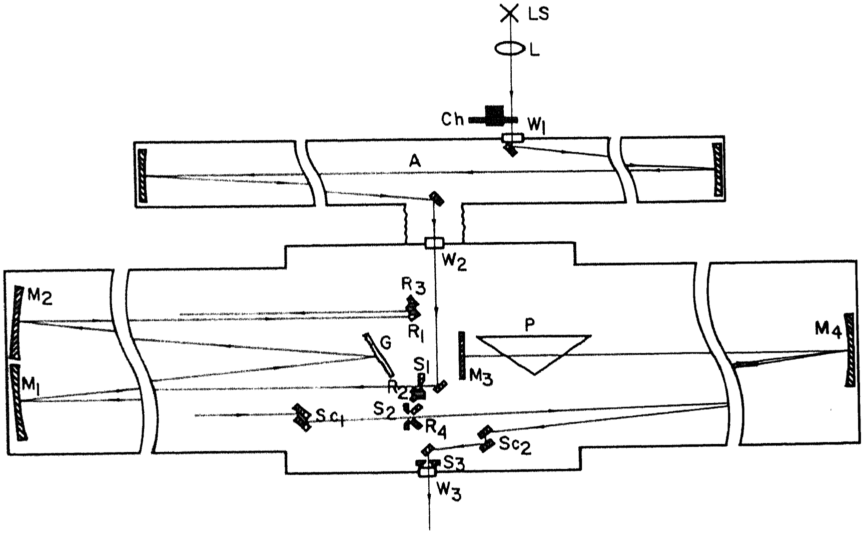

Figure 2. Optical system of the Rehovoth spectrometer-refractometer.

Just as for absorption lines, instrumental effects cause distortion of refraction lines. This situation is shown in Figure 3. The dotted curve is a true line and the full curves are those to be expected with three different instrumental settings. Curves *b* and *c* show peaks depressed and tails lifted just as in the case of absorption lines. Curve *a* corresponds to very narrow slits and here there is a curious effect—the peak is enhanced. This is actually observed and there is a simple physical explanation for it. Note that in the wings the correction is small and in practice it is found to be fairly easy to make a good line intensity determination from the wings alone. This is one of the advantages of the refraction spectrum. The second main advantage is that of background. A constant background does not interfere with determinations of line intensity or line width. A detailed method of making the instrumental corrections has been worked out taking into account the effects of both finite slit widths and of diffraction within the instrument [14]. Knowing the instrumental settings, trial values of the line intensity are fed into a computer until the predicted and observed curves correspond in the wings to the observed line. In the example shown in Figure 4 a value of $S^\circ = 0.063\ \text{cm}^{-1}\ \text{atm}^{-1}$ was obtained for the intensity of the line R(7) in the 2-0 band of HCl^{35}. Using this value, different values of the half width γ are tried out until the computer fits the calculated curve to the observed curve in the neighbourhood of the peak and trough. Note that the amplitude of the line depends on γ. The shape of the wings also depends weakly on γ and it is possible to obtain a second approximation for S° by refitting in the wings, and then proceed to compute a second approximation for γ° by refitting at the peak and trough and so on. In the example such an iteration was not found necessary. The width was found to be $\gamma^\circ = 0.30\ \text{cm}^{-1}$. Figure 5 shows the same line observed with wider slits and although it looks quite different, the same values for S° and γ° were obtained from it. In this way the intensities of lines of several bands have been determined.

In a recent study the intensities of the lines in the 001-000 band of hydrogen cyanide have been measured by the refraction method. This work led us to an investigation of vibration-rotation interactions in linear molecules and a theory for the general linear molecule has now been elaborated [15]. A vibration-rotation interaction factor is calculated for each normal vibration. In general each factor contains one term due to the interaction of the molecular rotation with the vibrations and a second term due to the interaction of the Coriolis motion with the vibration.

An example of line width determination is given in Figure 6 where the widths of lines in the HCl 2-0 band, obtained by refraction, are compared with other determinations.

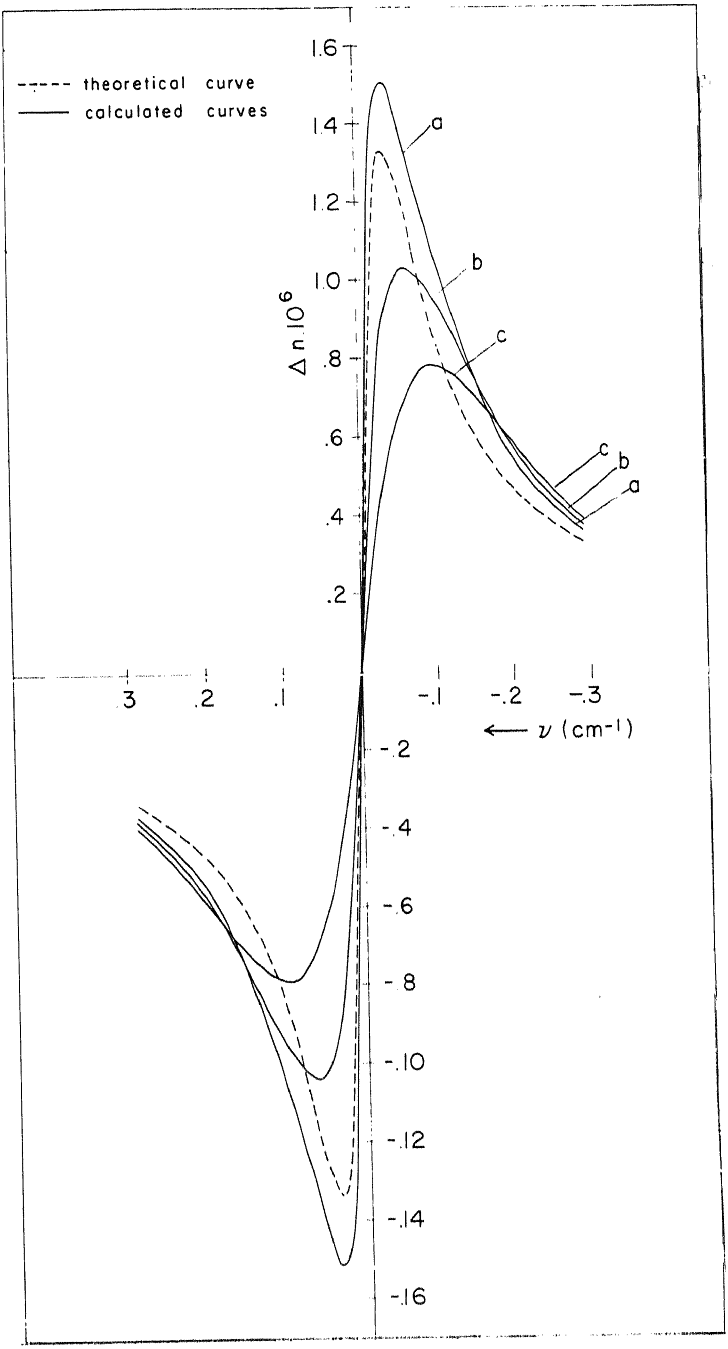

Figure 3. A theoretical refraction line (intensity 0.0226 cm^{-2} and half width 0.074 cm^{-1}) compared with three calculated curves corresponding to those expected with three different instrumental settings.

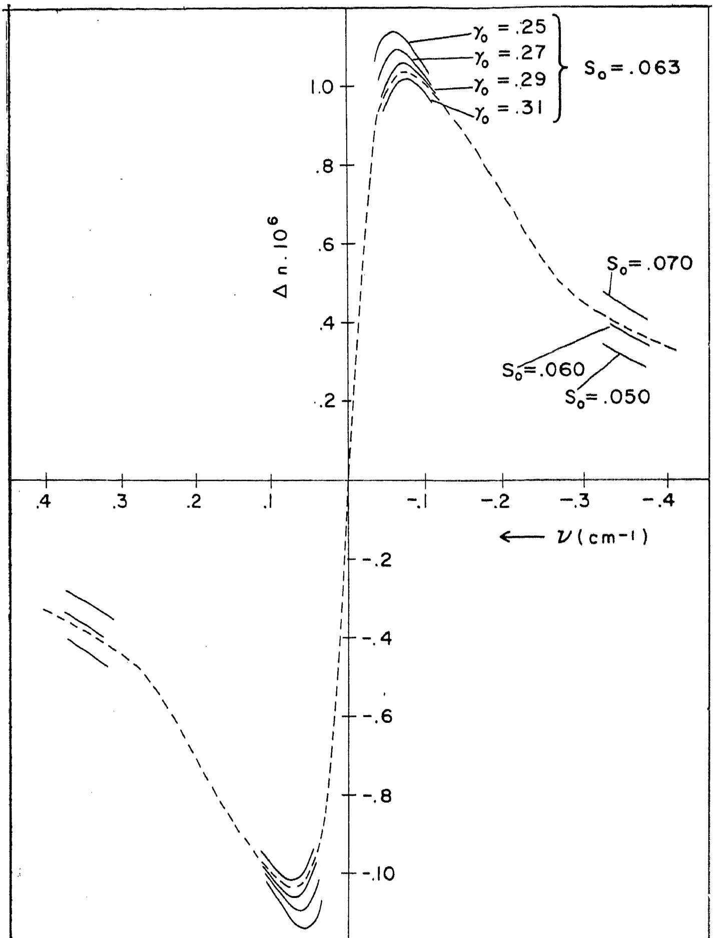

Figure 4. Sample calculation of line strength and the half width from the refraction spectrum. The dotted curve is the observed line.

The most interesting feature of these results is that the line widths are not all the same; they depend on the rotational quantum number of J. This effect was first observed by Herzberg and Spinks [16] in an overtone band of HCN.

Line width depends in the main on intermolecular forces. The absorbing molecule in a gas is being constantly disturbed by collisions with other molecules. The very first theories [17] predicted that the width of a spectral line should be proportional to the number of collisions suffered by the absorber in unit time; that is, proportional to pressure. At a given pressure wide lines

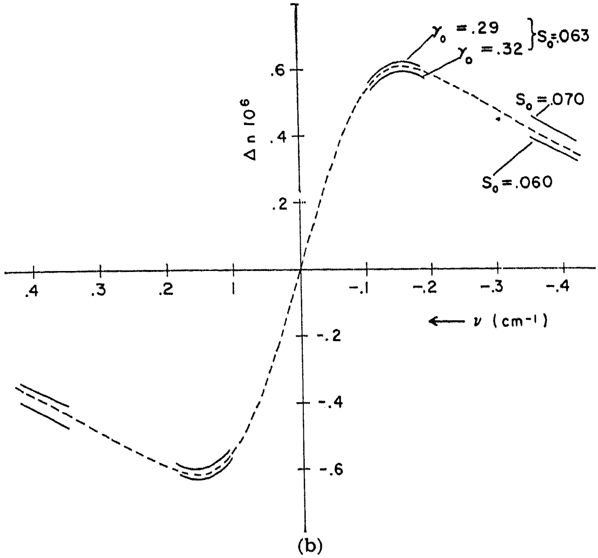

Figure 5. The same refraction line as that shown in Figure 4, but with wider spectrometer slits.

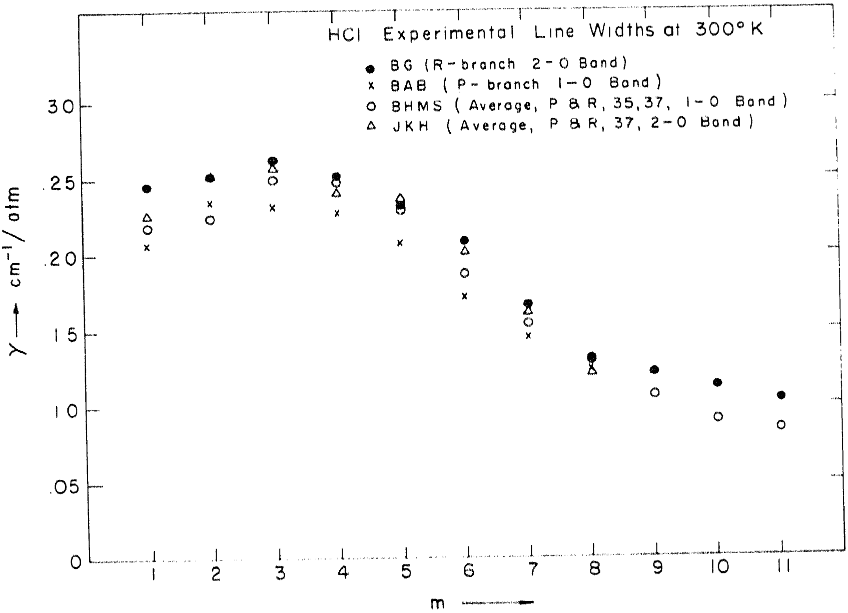

Figure 6. Widths of lines in absorption bands of HCl.

mean strong intermolecular forces and narrow lines mean weak ones. When the individual lines in a band all have different widths it means that molecules in certain states interact with neighbours more strongly than others. The J-dependence of width yields new information about intermolecular forces.

PRESSURE INDUCED SHIFTS

I should like now to report on a slightly different though closely related phenomenon that also yields information about intermolecular forces. This is termed pressure "shifting." When the pressure of a sample is increased, not only are the lines in its spectrum broadened. They are also slightly shifted. There exist numerous discussions of this phenomenon in the literature [18], but it must be confessed that originally our approach to it was made in ignorance of previous work. Most of you are familiar with the phenomenon of band shifts in liquids due to solvent effects. Leaving aside chemical effects, these shifts are due to the polarisability of the solvent, that is, they are a function of the dielectric constant (or refractive index) of the solvent. Figure 7 shows the absorption of hexane in three solvents and the shifts are seen to be quite large [19]. Since the refractive index of a gas at atmospheric pressure differs from unity only by a few parts in ten thousand, this "solvent" effect in

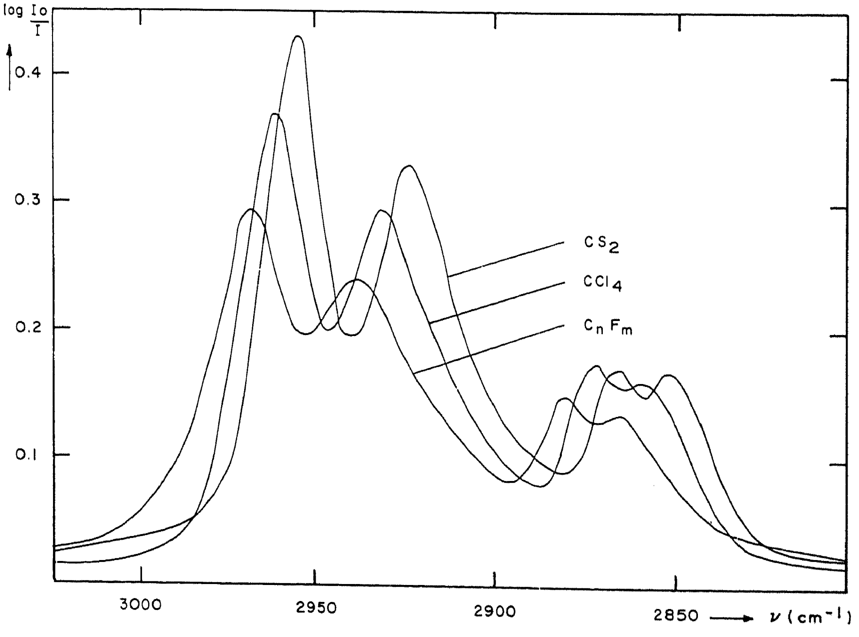

Figure 7. Absorption of n-hexane in three different solvents.

gases must be very small. But it was the suggestion of S. Kimel that it should nevertheless be detected. It was estimated that if a line in the spectrum of HCl be observed in two samples differing in pressure by one atmosphere, then a shift of about 0.01 cm^{-1} should be detected. When the experiment was made it was found that each individual line of a band was shifted differently. It was also found that the shifts were different for different bands. Finally the effect was found to display a marked temperature dependence [20]. These results were considered to be too hard to interpret at the time, and a simpler situation was next studied, namely pressure shifts of HCl lines due to noble gases [21]. That is, the positions of lines with a sample of HCl at low pressure were compared with the positions of lines of the same sample with the addition of a quantity of a noble gas. Figure 8 shows the line shifts in the 2-0 band of HCl due to five noble gases.

Since both the lines themselves and the instrumental slit function were found to be symmetrical, no instrumental corrections were necessary, and in spite of the smallness of the effect it could nevertheless be reliably measured. Pressure shifts certainly offer a wealth of information on intermolecular forces—though it must be admitted that up to the time of writing the theoretical interpretation is proving to be a very tough proposition [20,21].

CONCLUSION

Summing up it may be stated that developments of the last decade have transformed the near infrared into one of the best regions of optical spectroscopy. In addition to the highly precise wavelength measurements, successful work has been done on the intensities, widths and shifts of individual rotational lines. It may be confidently expected that studies in this region will furnish much additional information about molecular structure and intermolecular forces.

REFERENCES

1. R. A. Smith, Advances in Physics 2, 321 (1953).
2. G. R. Harrison, Physics Today 3, No. 9, 6 (1950).
3. G. R. Harrison and G. W. Stroke, J. Opt. Am. 45, 112 (1955).
4. D. H. Rank, Bull. Am. Phys. Soc. Series II 7, No. 1, Part 1, 81 (1962).
5. D. H. Rank, D. P. Eastman, B. S. Rao and T. A. Wiggins, J. Opt. Soc. Am. 52, 1 (1962).

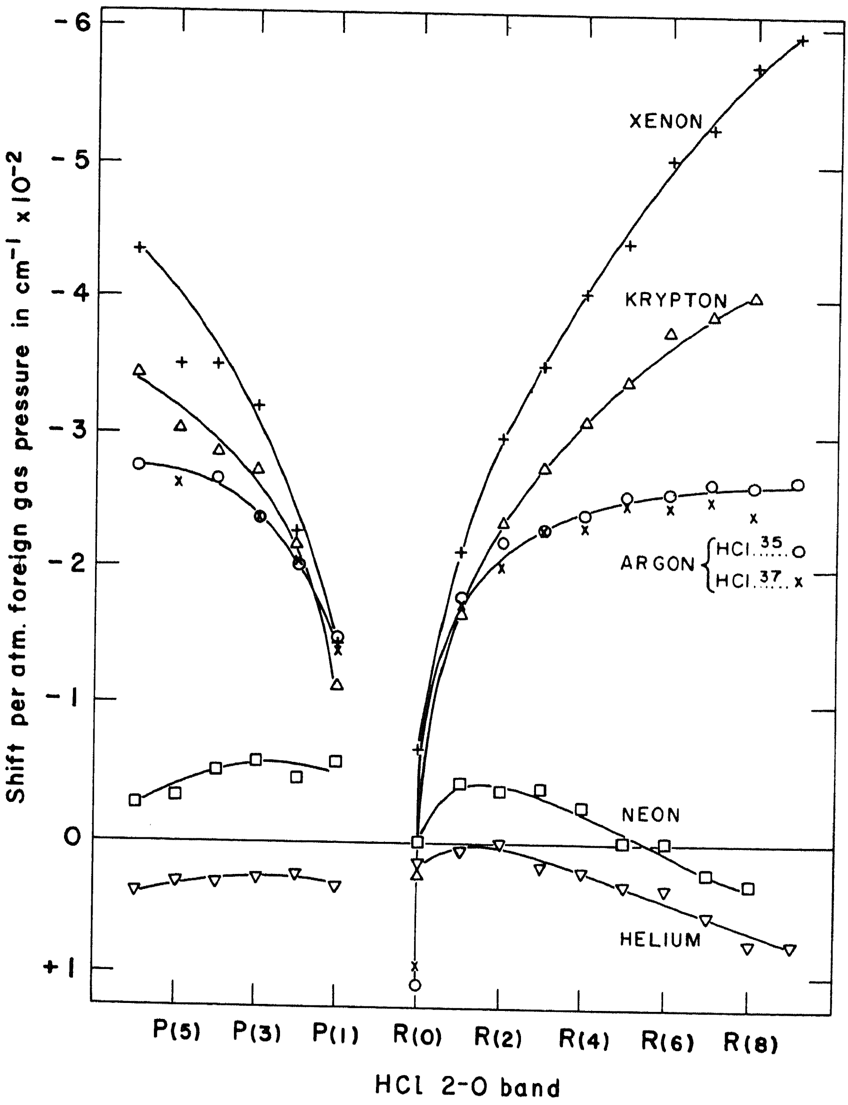

Figure 8. Pressure induced shifts of lines in the 2-0 band of HCl due to noble gases (297°K)

6. W. S. Benedict, N. Gailer and E. K. Plyler, J. Chem. Phys. 24, 1139 (1956).
7. W. S. Benedict, R. Herman, G. E. Moore and S. Silverman, Canad. J. Phys. 34, 850 (1956).
8. G. Herzberg, Spectra of Diatomic Molecules (van Nostrad Co. New York 1950).

9. R. S. Mulliken, J. Chem. Phys. 2, 400 (1934).
10. R. Herman and R. F. Wallis, J. Chem. Phys. 23, 637 (1955).
11. W. S. Benedict, R. Herman, G. E. Moore and S. Silverman, Canad. J. Phys. 34, 830 (1956).
12. R. de L. Kronig, J. Opt. Soc. Amer. 12, 547 (1926).
13. J. H. Jaffe, Advances in Spectroscopy Vol. 2 (Interscience, New York 1961).
14. J. H. Jaffe, J. Meiron and N. Jacobi, J. Opt. Soc. Am. 52, 8 (1962).
15. N. Jacobi and J. H. Jaffe, In Press.
16. G. Herzberg and J. W. T. Spinks, Proc. Roy. Soc. 147A, 434 (1934).
17. H. A. Lorentz, Proc. Roy. Acad. Sci. (Amsterdam) 8, 591 (1906).
18. H. M. Foley, Phys. Rev. 69, 616, 628 (1946).
19. J. H. Jaffe and S. Kimel, J. Chem. Phys. 25, 374 (1956).
20. S. Kimel, M. A. Hirshfeld and J. H. Jaffe, J. Chem. Phys. 31, 81 (1959).
21. A. Ben-Reuven, S. Kimel, M. A. Hirshfeld, and J. H. Jaffe, J. Chem. Phys. 35, 955 (1961).
22. H. Margenau, In Press.
23. A. D. Buckingham, Trans. Farad. Soc. 58, 449 (1962).

INFRA-RED DISPERSION STUDIES

W. H. Prichard and W. J. Orville-Thomas
The Edward Davies Chemical Laboratories
University College of Wales
Aberystwyth, Wales, United Kingdom

INTRODUCTION

The variation of refractive index with wave length is known as dispersion and in general the refractive index decreases with increasing wave length. Cauchy showed that the variation of refractive index with wave length could be represented by the equation

$$n = A + B/\lambda^2 + C/\lambda^4$$

where A, B, and C are constants characteristic of the medium.

When refractive index measurements are extended into the infra-red region the dispersion curve shows marked deviations from the Cauchy equation in the region of absorption bands. As λ tends to λ_j (the centre of an absorption band) the refractive index decreases more and more rapidly whilst beyond the region of absorption the refractive index has a larger value than for certain shorter wave lengths. This phenomenon is known as anomalous dispersion because in the neighbourhood of an absorption band the longer wave lengths have a higher value of the refractive index.

This is illustrated in figure 1 which shows how the refractive index varies with wave length. As one approaches a region of absorption the dispersion curve exhibits a region of anomalous dispersion. It is clear therefore that the processes which occur in molecules and which give rise to absorption bands are directly linked to those which give rise to changes in refractive index in the vicinity of an absorption band.

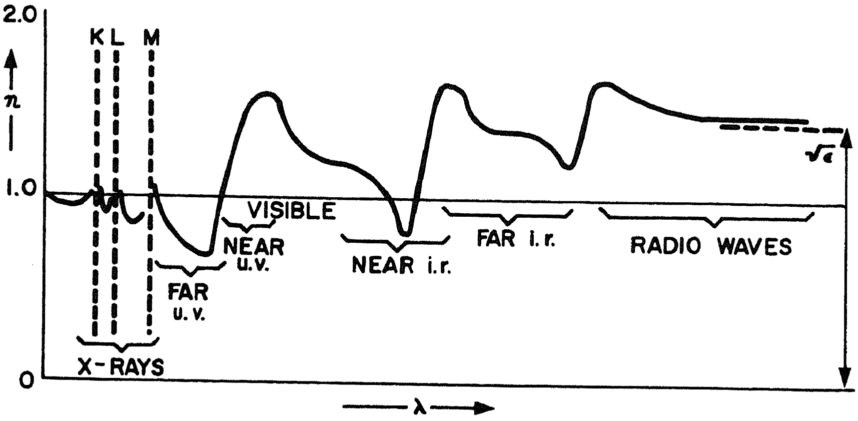

Figure 1. Schematic Dispersion Curve for a substance transparent in the visible region.

EXPERIMENTAL

The use of interferometers for the measurement of refractive index in the visible region of the spectrum is well-established. In the past the measurement of refractive index in the infra-red region has been relatively neglected since the techniques were difficult. The position has now changed owing to the pioneering work of Jaffé, Legay, Fahrenfort, and the introduction of the germanium Fabry-Perot etalon by Kagarise. Using such an interferometer, constructed by Dr. Tadayon of the Limit Research Corporation, we have carried out dispersion measurements on a number of halogenated methanes and ethylenes to an accuracy of ±0.001.

Our results for dibromoethylene are given in figure 2 and table 1.

ANALYSIS OF RESULTS—INTENSITIES

Having got our numbers the question now arises as to the possible uses of dispersion data.

The Cauchy equation is not capable of representing the dispersion curve in regions of anomalous dispersion. Sellmeier assuming that the medium contained oscillators of natural frequencies, ν_j , derived an equation of the form,

$$n^2 - 1 = \sum \frac{A_j \lambda^2}{\lambda^2 - \lambda_j^2}.$$

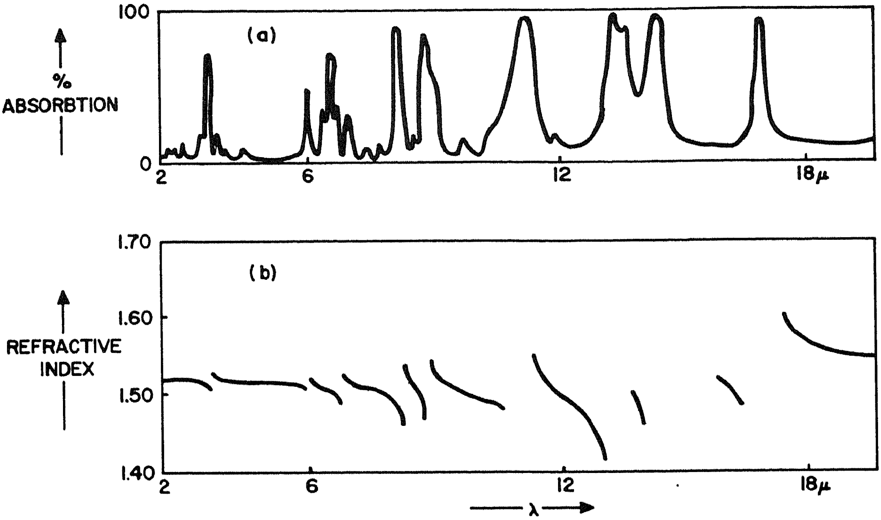

Figure 2. Cis and Trans-Dibromoethylene (film 0.1 mm thick).
(a) Absorption Spectrum; (b) Dispersion Curve.

He argued that the radiation passing through the medium exerted a periodic force on the oscillators causing them to undergo forced vibrations. As ν tends one of the natural frequencies of the system, the amplitude of the forced vibration increases and becomes very large when the resonance condition $\lambda = \lambda_j$ is reached. According to Sellmeier's equation the refractive index tends to plus or minus infinity as the wave length of the incident radiation approaches one of the resonant wave lengths λ_j, from the long wave length and short wave length sides respectively. The defect with Sellmeier's relation is that it does not take into account the absorption of energy by the system from the wave as the wave length goes through a resonant value.

Taking this factor into account Schatz and Kagarise have obtained relations connecting the variation of refractive index with the intensities of absorption bands. These relations can be used to compute band intensities from dispersion data. In this way it is possible to avoid the difficulties involved in the direct measurement of band intensities in the liquid phase.

The absolute intensities obtained from dispersion data for some methylene halides are given in table 2.

For the stretching vibrations we see that for the $\nu_a(CH_2)$ mode the band intensity is greatest for the dibromo-compound — there is no regular change in intensity for this vibration. The CH stretching frequencies do not vary greatly in the methylene halides. This indicates that the CH bond-stretching force

Table 1

Refractive Indices of cis and trans Dibromoethylene Corrected to 20°C

Wave-length, μ	Refractive Index	Wave-length, μ	Refractive Index	Wave-length, μ	Refractive Index
2.009	1.522	5.422	1.516	8.784	1.545
2.109	1.522	5.505	1.514	8.907	1.526
2.206	1.522	5.681	1.512	9.103	1.519
2.359	1.521	5.804	1.518	9.323	1.514
2.615	1.521	5.887	1.513	9.824	1.506
2.810	1.521	6.201	1.510	10.083	1.501
2.931	1.520	6.294	1.504	10.353	1.494
3.089	1.519	6.397	1.500	10.623	1.485
3.145	1.518	6.471	1.488	11.416	1.545
3.174	1.517	6.613	1.521	11.632	1.521
3.200	1.515	6.750	1.522	11.926	1.506
3.226	1.513	6.853	1.514	12.270	1.494
3.298	1.532	6.990	1.513	12.593	1.477
3.318	1.526	7.593	1.507	12.877	1.452
3.346	1.524	7.725	1.498	13.088	1.417
3.409	1.522	7.858	1.489	13.912	1.506
3.513	1.521	7.931	1.467	14.127	1.466
3.664	1.520	8.108	1.536	16.04	1.523
3.918	1.520	8.216	1.519	16.54	1.496
4.159	1.519	8.358	1.508	17.70	1.601
4.572	1.517	8.505	1.496	18.28	1.569
5.172	1.516	8.578	1.470	19.10	1.555

Table 2

Absolute Intensities, A, for the Antisymmetrical CH_2 Stretching Band

Molecule	Absolute Intensity (10^3 darks)					
	Liquid, A_l	Frequency, cm^{-1}	Gas, A_g	Frequency, cm^{-1}	Solution, A_s	Frequency, cm^{-1}
Dichloromethane	0.46	3048	0.36	3048	--	--
Dibromomethane	1.92	3065	0.11	3040	--	--
Diiodomethane	1.66	3049	0.28	3049	--	--
Hydrocarbons	--	--	--	--	7.63	~2900
-CO × CH_2 - group	--	--	--	--	1.00	~2900

constants, and hence the normal coordinates describing the vibrations, are sensibly the same as we go from one member of the series to another. Since the intensities of the bands associated with CH stretching do vary, however, it seems that the ionic character of the CH bonds must differ in the various molecules. This appears most plausible if one takes into account the inductive and dipolar field effects of the carbon-halogen bonds on the CH_2 groups.

COMPARISON OF INTENSITIES IN THE LIQUID AND VAPOUR PHASES

Experimentally, the measurement of intensities in the liquid phase is simpler than gas phase measurements. It would be helpful, then, if we could predict vapour phase intensities from liquid state measurements.

The change in intensity of a vibration band in the liquid, A_1, as compared with the value, A_g, found for the same band in the gaseous phase depends upon a large number of factors. They include (i) inter-molecular interaction, (ii) the dielectric constant of the medium, (iii) the shape of the molecules, and a variety of other effects of lesser importance.

Debye and Onsager have both attempted to calculate the dielectric effect and have obtained relations which differ widely in their predictions for the ratio A_l/A_g. This marked discrepancy has been resolved by Polo and Wilson who have corrected the Onsager expression and deduced an expression identical to that derived from Debye's theory.

Using band intensities calculated from dispersion data and the values available in the literature for gaseous intensities we have tested the Debye-Polo-Wilson relation in a large number of cases.

In table 3 the ratios predicted for A_l/A_g are compared with those obtained experimentally for methyl iodide. Agreement is seen to be poor. It should be remembered, however, that the theory applies ideally to non-polar substances and hence it is not surprizing that an expression which has not been modified to take the polar character of the molecules into account breaks down.

Table 3

Tests of the Polo-Wilson Equation for Methyl Iodide[a]

Vibration	Frequency (cm^{-1}), Liquid	Liquid Intensity, A_1	Gas Intensity, A_g	Frequency (cm^{-1}), Gas	A_1/A_g Experimental	A_1/A_g Theoretical
$\nu_{as}(CH_3)$ e	3050	1.28	1.32	3060.3	0.97	1.35
$\nu_s(CH_3)$ a_1	2950			2969.8		
$2b_{as}(CH_3)$ A_1+E	2841	0.17	0.16	2861	1.06	1.35
$2b_s(CH_3)$ A_1	2475	0.17	---	---	---	---
$b_{as}(CH_3)$ e	1429	2.27	1.06	1440.3	2.14	1.34
$b_s(CH_3)$ a_1	1242	2.78	2.07	1251.5	1.34	1.35
$b(H_3$-C-I) e	887	2.14	0.89	880.1	2.40	1.35
ν (C-I) a_1	522	1.20	0.19	532.8	6.32	1.35

[a] All intensity values are quoted in units of 10^3 darks.

INFRA-RED SOLVENT SHIFTS AND MOLECULAR INTERACTIONS

Part 3. Studies in Liquid Bromine and Halogen-Atom Interactions.

H. E. Hallam and T. C. Ray
Department of Chemistry
University College of Swansea
Swansea, Wales, Great Britain

During our systematic investigations of the effect of solvent environment on infra-red—active group frequencies we have had cause to employ a wide range of solvents rarely found, let alone used, in an infra-red laboratory. Whereas, on the one hand, we always utilize the most "inert" solvent, that solubility and background absorptions will allow, when examining a solute vibrational frequency, on the other hand we never cease to search for more "active" solvents which will interact strongly with the particular group dipole. The aim is first, to provide a challenge for the interpretation of the observed spectral changes, *viz.* solvent shifts, intensities and band shapes; and second, to extend our knowledge of intermolecular interactions. Further, to provide another tool for the identification of group frequencies and therefore for structural diagnosis.

Solvents such as antimony trichloride, hydrogen cyanide and bromine can provide valuable information if one is prepared to face the numerous experimental difficulties their use entails. We have singled out bromine to illustrate these since it embraces halogen-atom interactions which have been receiving most of our attention of late, some aspects of which we should also like to discuss. A homonuclear diatomic, bromine fulfills the ideal for an infra-red solvent; it dissolves most common compounds in sufficient concentrations to yield a spectrum with a 1 to 5 mm cell, but suffers from the considerable disadvantage of its chemical reactivity. Our interest in bromine arose during our search for solvents to displace carbonyl frequencies when we saw Pullin's [1] report of $\nu(C = 0)$ of acetone at 1689 cm^{-1} in liquid bromine, a (ν vap.-ν soln.) shift of 48 cm^{-1} which is almost double the shift observed in strong proton-donating solvents such as trifluoroethanol.

EXPERIMENTAL

Spectra were measured with a Grubb-Parsons G.S.2 double-beam grating spectrometer. The cells used were of a conventional type with the exception that the spacers and filler tubes and caps were manufactured from teflon. All solution preparation and cell filling was performed in an adequate fumes cupboard before seating the cells in the standard spectrometer housing. The radiation-unit casing, however, was replaced by a funnel, fitted with double open windows for the optical beams, and connected direct to a high-extract fan fitted on the outside wall of the building. Although somewhat elementary it is necessary to stress that such an arrangement is absolutely essential as even minute traces of bromine vapour rapidly attack the spectrometer parts not to mention the operator!

Bromine purified by the standard method of drying with conc. H_2SO_4 followed by distillation, has an infra-red spectrum (Figure 1) which indicates the persistence of traces of strongly-absorbing halogenated impurities. Several methods for preparing "Spectroscopic" bromine were tried and the following procedure finally adopted. Small batches (~25 ml) were frozen at -20°C using a cardice/chloroform freezing mixture and the excess liquid decanted and discarded. The solid was then warmed slightly and the liquid layer again removed. The solid was then completely melted, shaken with P_2O_5 and allowed to stand for 12 hours and then fractionally distilled, the second fraction being collected. This procedure was repeated twice to yield a product,

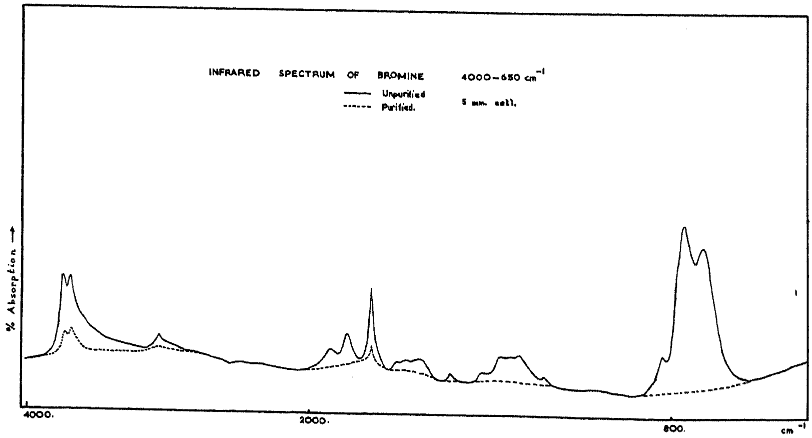

Figure 1. Infra-red spectrum of liquid bromine.

b. pt. 58.5°C, almost free from water and completely free from other impurities (Figure 1).

The solutes and other solvents were all distilled prior to use until their boiling-points agreed with literature values, and all were rigorously dried. Frequency values of the (X-H) bands have a precision of ±1.5 cm^{-1} and those of (C-Hal), ±1 cm^{-1} .

RESULTS

We have examined numerous carbonyl compounds, such as amides and urethanes, which are less susceptible to bromination than acetone, and in each case found an extremely low ν(C = 0). There is considerable doubt, however, as to whether these are real "solvent shifts" as the spectral changes we observe elsewhere makes it almost certain that reaction occurs too rapidly for us to record the true ν(C=0) in bromine solution. Pullin himself expressed some doubt about his acetone value but considered reaction not too great in pure dry bromine since the ν(C=0) was recorded within 1/2 minute of making up the solution. We have repeated his measurement and feel convinced that the low value arises from brominated species.

We then turned our attention to saturated hydrocarbon and halogenated-hydrocarbon solutes where bromination problems are small. Some typical results of these are shown in Table 1 together with the relative frequency shifts, $10^3\ \Delta\nu/\nu$, calculated on the basis of the vapour-state frequencies.

Table 1

Solute Frequencies in Liquid Bromine

Solute	cm^{-1} ν (C - H)	$10^3 \cdot \Delta\nu/\nu$	cm^{-1} ν (C - Cl)	$10^3 \cdot \Delta\nu/\nu$
Methyl Chloride	3025 2952	6.0 (mean)	705	36.9
Methylene Chloride	3043 2974	5.7*	738 702.5	29.1 (mean)
Chloroform	3007	8.6	756.5	20.7
Water	ν (O - H) 3662 3578	22.5 (mean)	δ (O - H) 1592	

*For the lower band referred to the vapour frequency of 3007 cm^{-1} .

DISCUSSION

Frequency Shifts and Solvent Pattern

(X-H) Bonds: In bromine solution (X-H) links display relative shifts of the same order as in solution in substituted benzenes [2]. This indicates that the Br atom lone-pair electrons interact with the solute proton quite as strongly as aromatic π-electrons.

(C-Hal) Bonds: The solvent-dependency of (C-Hal) dipoles has recently been established and was reported by us at the Amsterdam European Molecular Spectroscopy Meeting last year. Since it is now in press [3] it will suffice here to mention only the salient features so that some time can be spent discussing the possible modes of interactions, particularly those of bromine.

As might be anticipated, the solvent response of $(\mathrm{C}\text{-}\overset{\delta-}{\mathrm{Hal}})$ dipoles is closely similar to that of $(\mathrm{X}{=}\overset{\delta-}{0})$ dipoles [4]. The relative shifts plot sensibly against the corresponding shifts of any ν(X=0), but for internal consistency and to obtain further insight into the mechanism of the shifts, it is preferable to use a ν(C-Hal) as a reference. Normally we choose cis-dichloroethylene since its asymmetric ν(C-Cl) occurs at 857 cm^{-1}, a region relatively unhindered by solvent absorptions, which allows it to be followed in the most representative range of solvents. This, however, excludes bromine on account of its reaction with the double-bond, so since the aim of this paper is to discuss interactions in this solvent we shall here use methylene chloride as a reference for BHW plots (Figure 2).

Strong proton-donating solvents such as trichloroethanol, in the few instances when solvent background allows their use, cause the largest ν(C-Hal) displacements. Significant lowerings are also exhibited in electron-donating solvents such as dimethyl formamide and dimethyl sulphoxide; bromine interactions are but slightly less and are comparable with those of acetone and acetonitrile. The band-widths at half-absorbance and the band intensities show an enhancement which parallels $\Delta\nu$ but the effect is not nearly so dramatic as found with ν(X-H) frequencies. We shall not be able to discuss these other than to say that in the case of ν(C-Cl) asym. of $CHCl_3$ they have been fairly successfully fitted [5] to Buckingham's relationship for the solvent-dependency of solute intensities.

INTERACTION MECHANISMS

From the way in which ν(C-Hal) shifts follow the simple dielectric function [6] of Kirkwood, Bauer and Magat and from our detailed analysis [3] following Buckingham it seems clear

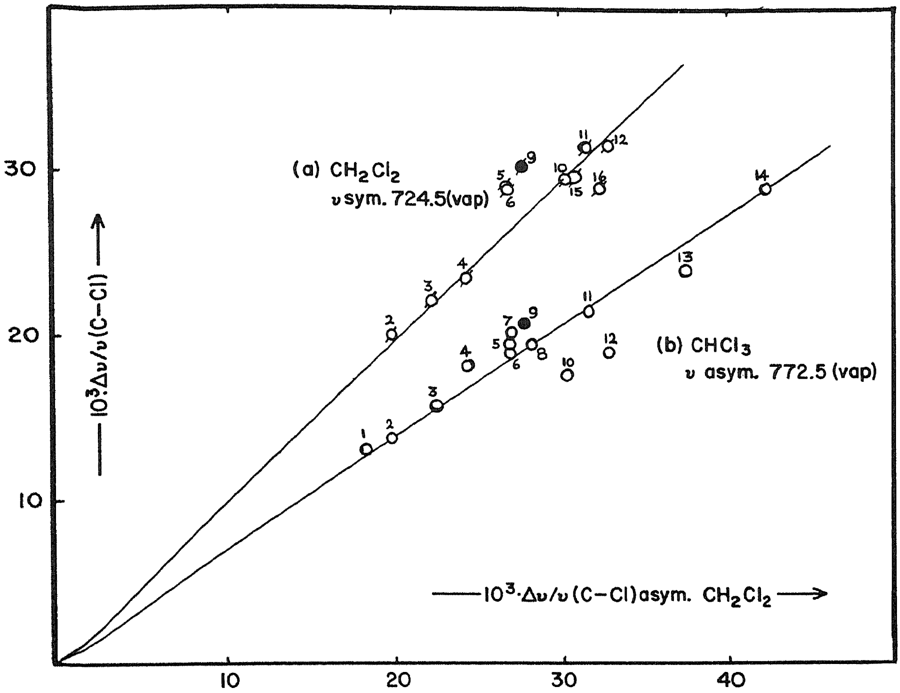

Figure 2. Plots of the relative frequency shifts of (a) ν(C–Cl) sym. of methylene chloride, and (b) the ν(C–Cl) asym. of chloroform plotted against the corresponding shifts for ν(C–Cl) asym. of methylene chloride. Solvents: (1) n-hexane; (2) cyclohexane; (3) cyclohexene; (4) carbon disulphide; (5) methyl iodide; (6) methylene bromide; (7) bromoform; (8) benzene; (9) bromine; (10) nitromethane; (11) acetone; (12) dioxane; (13) dimethyl formamide; (14) dimethyl sulphoxide; (15) acetonitrile; (16) ethylene dibromide.

that dielectric factors play a greater role in determining ν(C-Hal) shifts than they do with any other frequencies which so far have been examined.

This is borne out by mixed solvent studies in which the ν(C-Hal) band moves progressively to lower frequency with increasing proportion of polar solvent and in no instance can two absorption peaks, due to competing specific interactions, be resolved. Such interactions are undoubtedly present but are masked by the bulk dielectric shift. They are clearly indicated in Buckingham - KBM plots (Figure 3) by well-defined groups of related solvents which lie off the line:

(I) π-electron systems such as aromatics, olefines, carbon disulphide; (II) dioxane; (III) bromine; (IV) X=0 electron donors; and (V) proton-donors.

The interactions of proton-donating solvents are readily classified as $(\text{C-}\overset{\delta-}{\text{Hal}} \ldots . \overset{\delta+}{\text{H}}\text{-X})$ dipolar associations; in fact,

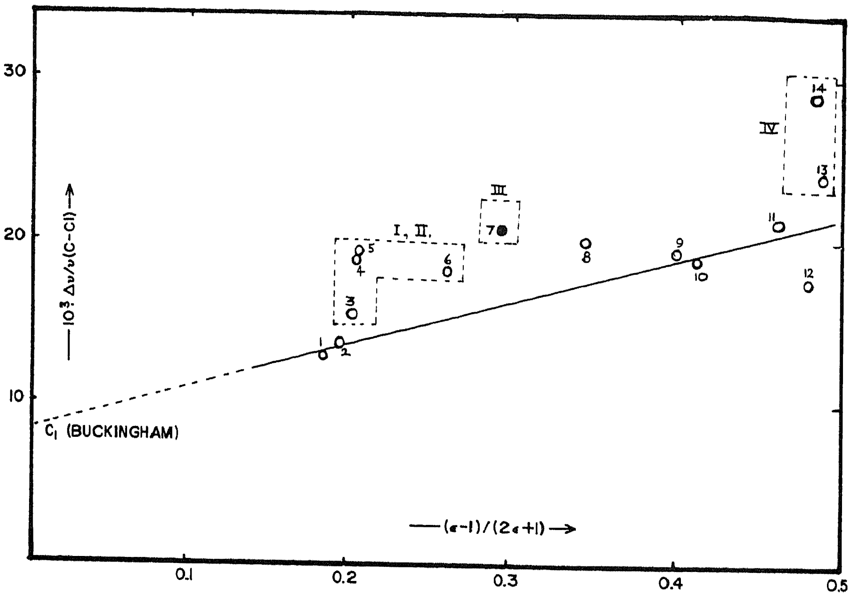

Figure 3. Relative frequency shifts of ν(C-Cl) asym. of chloroform in dilute solution as a function of the dielectric constant of the solvent. Solvents: (1) n-hexane; (2) cyclohexane; (3) cyclohexene; (4) dioxane; (5) benzene; (6) carbon disulphide; (7) bromine; (8) bromoform; (9) methyl iodide; (10) methylene dibromide; (11) acetone; (12) nitromethane; (13) dimethyl formamide; (14) dimethyl sulphoxide.

weak hydrogen-bonds. Those listed (I) to (IV) are all potential electron-donors (D_e) and on the simple basis of the dipolar-association theory of solvent-shifts [2] would not be expected to interact strongly with dipoles possessing a negative end-atom. Quadrupole or contra-association ($^{+}_{-}{}^{-}_{+}$) would be a possible mechanism, but for steric factors which must prevent this in many cases. In the case of Br and I atoms a plausible mechanism may be based on an overlap of non-bonding d-orbitals with vacant anti-bonding orbitals on the solvent molecules, e.g., Figure 4. All of these specific interactions probably give rise to at least half of the total shift observed [3] in each instance.

It is of interest to consider the numerous studies which have been made on charge-transfer complexes, between halogens and interhalogens and aromatic compounds, particularly those of Br_2, ICl and ICN. Person et al. [7] have drawn attention to the fact that the frequencies of these complexes closely parallel the frequency values of ν(O-H) in the corresponding solvents, and suggest that Br_2 . . . . D_e, ICl . . . . D_e, etc., charge-transfer interactions are fundamentally not different from (O-H . . . . D_e) hydrogen-bonded interactions, which charge-transfer theory includes as a special case. It has also been suggested by Bellamy

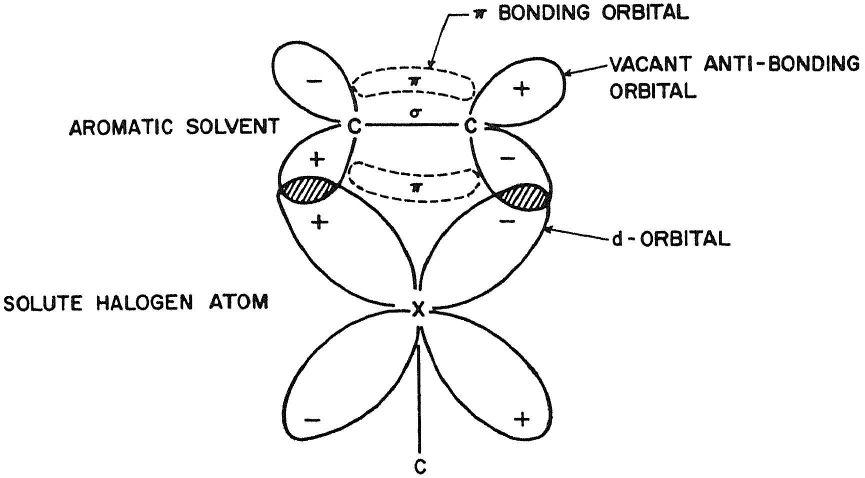

Figure 4. Schematic representation of halogen-atom specific interaction.

et al. [4] that the very weak dipolar interactions as found for example with ν(X-H) in carbon-tetrachloride, X-$\overset{\delta+}{\text{H}}$ . . . . $\overset{\delta-}{\text{Cl}}$-C—, differ only in the magnitude of the interaction energy rather than the nature, from true or accepted H-bonds. With the hope of embracing all these specific molecular interactions under one generalized scheme we have attempted to relate our ν(C-Hal) shifts with the corresponding charge-transfer frequencies. There is a similarity as far as average shifts are concerned but with the strong complexes the charge-transfer frequency difference far exceeds a "normal" ν(C-Hal) shift. However, the similarities are sufficient to suggest that a charge-transfer mechanism may also play some part in determining the halogen shifts that we observe. The same phenomenon may also account for the large carbonyl shifts observed in bromine solution if indeed chemical reaction can be ruled out.

ACKNOWLEDGMENTS

We are grateful to the Hydrocarbon Research Group of the Institute of Petroleum for a studentship (T. C. R.) and for financial support.

REFERENCES

1. A. D. E. Pullin, Spectrochim. Acta 16 (1960) 12.
2. L. J. Bellamy, H. E. Hallam, and R. L. Williams, Trans. Faraday Soc., 54 (1958) 1120.

3. H. E. Hallam and T. C. Ray, Trans. Faraday Soc., 58 (1962) 1299.
4. L. J. Bellamy and R. L. Williams, Trans. Faraday Soc., 55 (1959) 14.
5. H. E. Hallam, Proceedings of the Institute of Petroleum Hydrocarbon Research Group Third Conference, London (1962) 245.
6. H. E. Hallam and T. C. Ray, Nature, 189 (1961) 915.
7. W. B. Person, R. E. Humphrey, W. A. Deskin, and A. I. Popov, J. Amer. Chem. Soc., 80 (1958) 2049; 81 (1959) 273; 82 (1960) 29.

RECORDING THE INFRA-RED SPECTRA OF GAS-CHROMATOGRAPHY FRACTIONS

A. R. Philpotts
The Distillers Company Limited
Great Burgh
Epsom, Surrey, England

The use of gas-chromatography to separate components of mixtures which were then identified by infra-red spectroscopy started about 1955 [1]. The value of the combination was soon recognised particularly in the essential oil field. In 1959 at least forty papers appeared which showed how a wide range of chemical problems had been solved this way. Most of the early work was done with large chromatographic columns separating grams of material. This short review is mainly concerned with the principles of reducing sample size and does not include the elegant apparatus which is used for automatic, sequential and multiple fraction-collection.

The convenience and greater separating power of small analytical columns soon led to working with milligram samples. After all, Blout [2] was already doing infra-red in the microgram range, although not with gas-chromatography fractions. Anderson [3, 4] described the trapping of milligram samples followed by re-evaporation into an evacuated gas-cell, and modifications of this approach have been published [5, 6]. However, better optical use of the sample is made at a focus, rather than with a straight gas-cell, so interest changed to examining the trapped fractions as pure liquids, solutions or in bromide discs.

A number of simple traps for the milligram range have been described in the literature and produced by the instrument manufacturers. Some of these are based on the conventional concentric-tube trap. These have the advantages that the inner tube can be a hypodermic needle and that a liquid sample can be collected together by centrifuging. Other traps are some variation of the U-tube.

The routine method used in our laboratory is one example of these methods. A simple U-tube as shown in the figure has a small well under the entry limb. The effluent from the column passes along a heated tube, through the connecting joint and into the cooled trap. Liquid condensed on the walls can sometimes be shaken into the well, or else driven down by distillation, under vacuum if necessary. The sample can then be dissolved in a few microlitres of solvent in the well and transferred by hypodermic needle to a micro-cell or on to potassium bromide for pressing into a disc. Alternative transfer methods are

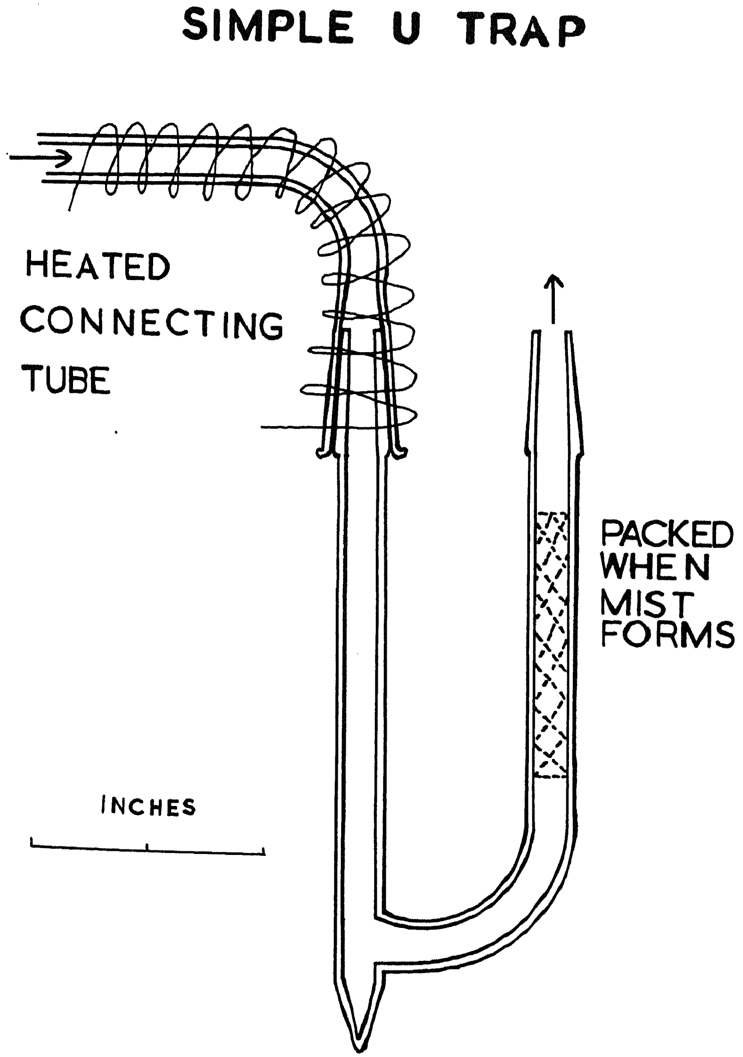

described, using a stoppered or detachable well [7], or capillary [8, 9, 10] or by fitting the micro cell in place of the well [11]. Normal spectroscopic techniques can be used at these levels, without beam-condenser or scale-expansion.

Various opinions have been given about the efficiency of simple traps, varying from complete trust to positive disapproval. In our experience the simple trap has been effective down to 500 μg with more than half the compounds tried (boiling between 50° and 250°C.) and sometimes to 200 μg. Failure of the trap has usually been due to mist formation. This can be counteracted to some extent by choosing a refrigerant such that the temperature is not reduced unnecessarily, by using a connecting tube with a temperature gradient when possible and by packing the outlet limb of the U-tube with glass wool or ballotini. Sometimes a sintered-glass disc has been sealed into this limb. Vacuum distillation is then essential to collect the sample together. About 25% of failures were still found, even with the packed tube.

Although the system is often efficient at the 500 μg level, it is almost useless for 50 μg. If the developments in infra-red methods are to be fully used, the trapping and transfer technique must be greatly improved or some effort made to record the spectrum of the fraction without condensing it.

The principles of improving trapping and dealing with mist formation have been discussed [12]. Reducing the vapour pressure of the condensed material by using an absorbent [13], adsorbent [14], solvent [15] or reagent makes trapping more efficient. Adding a solvent to the gas stream as a vapour is sometimes better still [16]. Whether these expedients can be used or not depends on the particular application. A more general method is the centrifugal freezing trap, but the sample size is rather large [17]. The electrostatic precipitator also offers a general method of collecting fog particles. Again, the published fraction-collectors [18, 19] are designed for rather large samples but one microgram amounts of radioactive components have been quantitatively recovered this way [20]. The alternate refrigeration and re-heating of the gas stream gives good recovery under fog-forming conditions [21, 22] and a micro-version has recently been successfully used by Dr. Swoboda [23]. This consists of a coiled, stainless steel capillary with a part of each turn in liquid nitrogen and another part in hot air; 10 μg samples have been condensed. Another capillary condensing system has been described, using a solvent-coated tube [24].

Transferring these small amounts is difficult and micromethods must be used. Soluble, involatile compounds can be handled in solution in the way already established for paper chromatography fractions [25]. When the sample is trapped on potassium bromide [26] or other adsorbent [14] transfer is easier.

Infra-red techniques for microgram samples are well established, and there are several recent reviews of micro and semi-micro methods [25, 27, 28, 29, 30]. In one recent development potassium bromide powder is charged to a 1 mm. blind hole drilled in the face of a standard potassium bromide disc [31]. Sample is transferred in solution, then the disc is re-pressed and so acts as mould and support for a micro disc. A reduction of sample size by a factor of ten or so can often be achieved by using scale-expansion (we have recorded good spectra at the 20 μg level without a beam-condenser). Scale-expansion may not be possible if the incident intensity has already been attenuated by sample holder, beam-condenser or multi-reflection.

The direct examination of fractions in the vapour phase is very attractive, if a suitable gas-cell can be made [32, 33]. A higher ratio of pathlength to cell volume than that used by Anderson [4] is essential and White [33] raised this to about 5 cms. per ml. (by using the multi-reflection method). The equivalent cross section is 20 sq. mm., about the same as for the normal (liquid) micro-cell without beam-condenser. The minimum sample is then about 200 μg, with the possibility of reducing it to 20 μg by scale-expansion. The ideal gas cell must have a length to volume ratio of at least 5 cm^{-2} and a volume of 100 mls. It should be equipped with heaters and preferably be of such a shape that fractions are swept through the cell by carrier gas flow. Our efforts to produce a useful cell have so far been unsuccessful and no further results using the White cell have appeared in the literature.

The limiting sample sizes given in this paper have been calculated assuming that 5 μ moles are needed per sq. cm. of beam cross-section, and a molecular weight of 200 has been used to convert to μgs. The amount required obviously varies with the extinction coefficients, but this value is suggested as a representative figure for the amount required when identifying organic compounds.

To sum up, then, 200 μg represents the lowest limit working with simple trapping methods and ordinary infra-red techniques. 1-10 μg samples can be used when one of the improved trapping methods is successful and infra-red micro-techniques are available. The use of samples as small as 20 μg is feasible with an ideal gas cell (using scale-expansion) but no results have been reported.

REFERENCES

1. E. F. Williams. Appl. Spectroscopy, 10, 221, 1956.
2. E. R. Blout and G. R. Bird. J. Opt. Soc. Amer., 41, 547, 1951.
3. D. M. W. Anderson and J. L. Duncan. Chem. and Ind. (London), 50, 1662, 1958.
4. D. M. W. Anderson. Analyst, 84, 50, 1959.
5. J. Haslam, A. R. Jeffs and H. A. Willis. Analyst, 86, 44, 1961.
6. S. S. Chang, C. E. Ireland and H. Tai. Anal. Chem., 33, 479, 1961.
7. G. J. Frisone. Chemist-Analyst, 48, 47, 1959.
8. B. M. Mitzner and M. H. Jacobs. Chemist-Analyst, 48, 104, 1959.
9. H. J. Gold. Chemist-Analyst, 49, 112, 1960.
10. A. Kreuchunas. Chemist-Analyst, 49, 82, 1960.
11. P. A. Wilks and C. W. Warren. Connecticut Instr. Corp. Newsletter, 6, 1, 1960.
12. A. Klinkenberg. In "Vapour Phase Chromatography," ed. Desty. Butterworth (London), p. 211, 1956.
13. C. M. Drew, J. R. McNesby, S. R. Smith and A. S. Gordon. Anal. Chem. 28, 979, 1956.
14. H. Szymanski, R. Povinelli, D. Stamires and G. Lynch. Anal. Chem. 31, 2110, 1959.
15. W. J. Zubyk and A. Z. Connor. Anal. Chem. 32, 912, 1960.
16. J. H. Jones and C. D. Ritchie. J. Assoc. Offic. Agr. Chem., 41, 753, 1959.
17. A. Wehrli and E. Kovats. J. Chromatog., 3, 313, 1960.
18. P. Kratz, M. Jacobs and B. M. Mitzner. Analyst, 84, 671, 1959.
19. A. E. Thompson. J. Chromatog., 6, 454, 1961.
20. J. N. A. Ridyard. Private communication.
21. F. Van der Craats. In "Vapour Phase Chromatography," ed. Desty. Butterworth (London), p. 96, 1956.
22. H. de Vries. Appl. Sci. Res. Hague, B5, 387, 1956.
23. P. A. T. Swoboda. In "Fourth International Gas Chromatography Symposium 1962," ed. van Swaay. Butterworth (London), in press.
24. R. Self. Nature, 189, 223, 1961.
25. A. F. Krivis, G. E. Bronson, W. A. Struck and J. L. Johnson, in "Submicrogram Experimentation," ed. Cheronis. Interscience (New York), p. 277, 1961.
26. H. W. Leggon. Anal. Chem., 33, 1295, 1961.
27. J. U. White, S. Weiner, N. L. Alpert and W. M. Ward. Anal. Chem., 30, 1694, 1958.
28. J. E. Stewart, R. O. Brace, T. Johns and W. F. Ulrich. Nature, 186, 628, 1960.

29. W. B. Mason. In "Submicrogram Experimentation," ed. Cheronis. Interscience (New York), p. 293, 1961.
30. M. Sparagana and W. B. Mason. Anal. Chem. 34, 242, 1962.
31. A. F. Machin. Private communication.
32. M. Feldstein. J. Forensic Sci., 5, 266, 1960.
33. J. U. White, N. L. Alpert, W. M. Ward and W. S. Galloway. Anal. Chem., 31, 1267, 1959.

OPTICAL SPECTRA OF GASEOUS FREE RADICALS*

D. A. Ramsay
Division of Pure Physics
National Research Council
Ottawa, Canada

INTRODUCTION

Considerable advances have been made in the last decade in our knowledge of the optical spectra of polyatomic free radicals. More than fifty free radical spectra have been observed in the region between 1000 and 10,000 Å and high resolution studies have been carried out for approximately fifteen of these spectra.

The information which is derived may be briefly summarized as follows:

1. Electronic Energy Levels
2. Symmetry Species of the Electronic Eigenfunctions
3. Vibrational Constants
4. Rotational Constants
5. Bond Lengths and Bond Angles
6. Dissociation Energies and Predissociation Phenomena

A knowledge of the electronic energy levels and of the symmetry species of the electronic eigenfunctions provides extensive data which must be explained by any acceptable theory of electronic structure. The vibrational and rotational constants characterise the internal motions of the free radicals and are also essential to the calculation of thermodynamic functions. Geometrical parameters may frequently be deduced from the rotational constants and provide interesting information concerning the change of molecular shape with electronic excitation. One dissociation limit (for HNO[8]) and two ionisation potentials (for CH_2[15] and CH_3[16]) have so far been determined from optical studies but further values can be expected from future work.

---

*Issued as N.R.C. No. 0000

Finally the study of the optical spectra of free radicals has provided some interesting information concerning the interaction of electronic and vibrational motions in degenerate electronic states of linear molecules, a phenomenon known as the Renner effect [37].

A summary of the main developments in this field up to the beginning of 1959 has been given by the author [35] in an earlier review article. The principal aim of the present paper is to discuss some of the more recent developments.

TECHNIQUES

One new technique has emerged in the last few years, the technique of flash pyrolysis [Lundberg, Kuebler and Nelson 27, 30, 31, 32]. This method is similar in many respects to the technique of flash photolysis, except that the radiation from the "photolysis" flash lamp is used to heat finely divided particles suspended in a gas or gas mixture, rather than to photolyse the gas directly. Free radicals are then produced by heterogeneous decomposition of the gas molecules on the hot particles. For example, Nelson [30] has observed the absorption band of the methyl radical at 2160 Å following the flash pyrolysis of methane containing finely divided carbon particles. Similarly, he has observed absorption bands of CF_2 following the flash pyrolysis of carbon tetrafluoride on carbon particles. The technique can thus be used with gases which are not amenable to flash photolysis. So far the technique has not achieved the repetition rates (~1 per minute) which are frequently used in high resolution flash photolysis studies, but nevertheless the method has interesting potentialities.

The method of flash photolysis continues to be the main technique for most high resolution studies. Johns and Ramsay [23] have recently built an apparatus in which a 600 μF condenser bank, charged to 7 kV, is discharged through two 1 meter flash tubes in series in ~30 μs. The lamps irradiate a reaction cell which is 2 meters long and which is fitted with multiple reflection mirrors. Using this apparatus with absorption path lengths up to 120 meters, Johns and Ramsay have obtained spectra with much greater absorption intensities than in earlier work. For example, in the flash photolysis of acetaldehyde, the HCO absorption bands are sufficiently intense that two bands of $H^{13}CO$ in natural abundance are seen. Claesson [7] and coworkers have recently discharged a very large condenser bank (1008 μF, 18 kV, 160,000 J) through a 6 meter quartz flash tube in ~150 μs. Such an apparatus has considerable potentialities for the spectroscopic study of radicals with lifetimes greater than ~100 μs. For radicals with very short lifetimes e.g., ~1 μs, it is advantageous to use an apparatus in which the maximum energy is discharged through the photolysis flash lamp in a time not exceeding a few microseconds. In this connection it is interesting to note that Claesson [7] and his colleagues have discharged 900 joules of energy through a short flash lamp (10 cm) in 2 μs.

NEW SPECTRA AND RESULTS

CH_2

Two transitions of the CH_2 radical have been observed in absorption during the flash photolysis of diazomethane (Herzberg and Shoosmith [19], Herzberg [16]). The first system lies in the vacuum ultraviolet region near 1415 Å and consists of a few bands which are diffuse due to predissociation of the molecule in the excited state. For CHD and CD_2, however, and even for $^{13}CH_2$, the bands exhibit discrete rotational fine structures, although for $^{13}CH_2$ the lines are still distinctly broad. The bands have the appearance of a Σ-Σ transition of a linear molecule and an alternation in the intensities of successive rotational lines is observed for $^{13}CH_2$ and for CD_2 but not for CHD. Herzberg has concluded that the bands are due to a $^3\Sigma_u^- - {}^3\Sigma_g^-$ transition, though the triplet structure is not resolved, and has obtained the following values for the rotational constants and bond lengths:

CD_2: $B_o'' = 3.95_0$ cm^{-1}, $B_o' = 3.59_5$ cm^{-1}; $r_o'' = 1.029$ Å, $r_o' = 1.079$ Å.

CHD: $B_o'' = 5.33_3$ cm^{-1}, $B_o' = 4.80_8$ cm^{-1}; $r_o'' = 1.034$ Å, $r_o' = 1.089$ Å.

$^{13}CH_2$: $B_o'' = 7.79$ cm^{-1}, $B_o' = 6.89$ cm^{-1}; $r_o'' = 1.03_6$ Å, $r_o' = 1.10_2$ Å.

The molecule is assumed to be linear in both states.

The second transition lies in the region from 6000 to 9000 Å and consists of bands which are very similar in structure to the well known α-bands of NH_2. The bands have been assigned by Herzberg to a $^1B_1 \leftarrow {}^1A_1$ transition and involve a lower state in which the molecule is bent ($r_o'' = 1.12$ Å, $\theta'' = 103._2$°) and an upper state in which the molecule is linear ($r_o' = 1.0_4$ Å, $\theta' = 180$°).

Since the triplet and singlet bands are both observed in absorption it is clear that there cannot be any large separation in energy between the lowest triplet ($^3\Sigma_g^-$) and the lowest singlet

($^1A_1$) state. From indirect evidence based on the behaviour of the two band systems when the initial diazomethane is mixed with various ratios of inert gas, Herzberg concluded that the "observations point rather definitely to $^3\Sigma_g^-$ as the lowest state." This conclusion is in agreement with the recent valence-bond calculations of Jordan and Longuet-Higgins [25]. To obtain an experimental value for the energy separation between the lowest singlet and triplet states it will be necessary to obtain (i) an intercombination system, which unfortunately is likely to be extremely weak, (ii) mutual perturbations of the rotational levels of a singlet and a triplet state—cf. the recent determination [2] of the ground state of the C_2 molecule, or (iii) Rydberg series of singlet and triplet terms to a common ionisation limit. It is interesting to note that Herzberg [15] has recently reported a Rydberg series of CH_2 converging to an ionisation limit at 83851 cm^{-1} (≡ 10.396 ev), the first member of the series being the 1415 Å band discussed above.

NH_2

The earlier analysis by Dressler and Ramsay [13] of the well-known α-bands of NH_2 and ND_2 has been extended recently by Eaton, Johns and Ramsay [14], particular emphasis being given to the long wavelength end of the band system. The transition involves the ground state in which the molecule is bent ($r_o'' = 1.024$ Å, $\theta_o'' = 103.3°$) and a low lying excited state in which the molecule is linear ($r_o' = 0.97_5$ Å, $\theta_o' = 180°$). The relation between these states is indicated by the potential energy diagram given in Figure 1b. The spectrum consists of a long progression $(0,v_2',0) \leftarrow (0,0,0)$ of the bending vibration ν_2' in the excited state

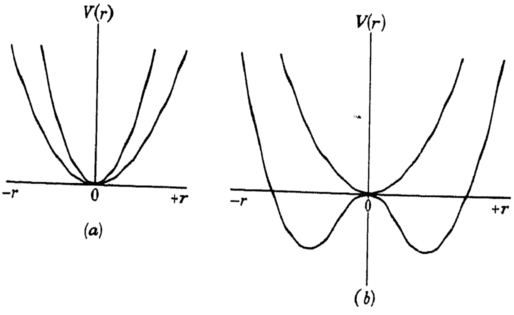

Figure 1. Potential curves for (a) small Renner effect, (b) large Renner effect. The coordinate r is the normal coordinate of the bending vibration.

and a subsidiary progression $(1,v'_2,0) \leftarrow (0,0,0)$ in which one quantum of the symmetric N-H stretching vibration is also excited. In the recent work weak bands have also been observed in absorption from the (0,1,0) level of the ground state ($\nu''_2 = 1497.3$ cm^{-1} for NH_2). Furthermore the principal progression has been extended to the first member at the long wavelength end of the spectrum which is found to be the $(0,1,0) \leftarrow (0,0,0)$ band and not the $(0,0,0) \leftarrow (0,0,0)$ band as may have been expected. The reason for the absence of the $(0,0,0) \leftarrow (0,0,0)$ band is rather involved but has been discussed in detail by Dressler and Ramsay.

One of the principal reasons for the continuing study of the NH_2 spectrum is that it affords extensive information concerning the coupling of electronic and vibrational motions. The theory of this coupling in NH_2 has been discussed by Pople and Longuet-Higgins [34] and in the recent experimental work many more vibronic levels have been identified so that altogether 56 vibronic levels of NH_2 and 47 vibronic levels of ND_2 have been characterized experimentally. In particular *all* the predicted low lying vibronic levels for NH_2 with $v'_2 = 1, 2, \ldots 5$ have now been observed.

CH_3

The earlier work by Herzberg and Shoosmith [18] on the absorption spectrum of CH_3 has been considerably extended by Herzberg [16]. A much stronger source of the spectrum has been obtained by the flash photolysis of a mixture of diazomethane and hydrogen and altogether 12 bands of CH_3 and 24 bands of CD_3 have been reported. The bands fall into three Rydberg series, designated β, γ and δ by Herzberg, all converging to a limit at 79392 ± 5 cm^{-1} (9.843 ev) for CH_3 and 79315 ± 5 cm^{-1} (9.833 ev) for CD_3. Three of the band groups for CD_3 at 2144, 1500 and 1385 Å and one of the CH_3 bands at 1500 Å show discrete rotational fine structure, while the other bands are diffuse. The sharp bands all display a slight alternation in the intensities of successive rotational "lines" consistent with the assignment of a planar or nearly planar structure to at least one of the two combining states. Since each electronic transition consists of only one strong band, it is clear that there is no appreciable change in geometric structure in any of the observed transitions, i.e., the molecule is either planar or very nearly planar in all observed states. Herzberg estimates that the maximum departure from planarity consistent with the spectroscopic observations is ~10°, corresponding to a pyramid height of 0.18 Å.

By rotational analysis, Herzberg has shown that the 2144 Å band (β_1-X) of CD_3 and the 1500 Å bands of CH_3 and CD_3 (δ_1-X) are all parallel type bands. The 1383 and 1385 Å bands of CD_3 (δ_2-X and γ_2-X) appear to be parallel and perpendicular type bands respectively but no detailed analyses have yet been carried out. The rotational constants which have been obtained, correspond to the moment of inertia of the methyl radical about an axis perpendicular to the three-fold axis of symmetry and are:

	CH_3	CD_3
X	9.57 cm^{-1}	4.79_3 cm^{-1}
β_1	-	4.41_5 cm^{-1}
δ_1	10.72 cm^{-1}	5.13_7 cm^{-1}

If the molecule is assumed to be planar in each of the three states the corresponding bond lengths are:

	CH_3	CD_3
X	1.08_0 Å	1.079_0 Å
β_1	-	1.124 Å
δ_1	1.020 Å	1.042 Å

From simple theoretical considerations the ground state of the molecule, if planar, is expected to be a $^2A_2''$ state, and this indeed is in agreement with the "sign" of the observed intensity alternation. The three principal series have been assigned by Herzberg as follows:

β series: $(a_1')^2(a_1')^2(e')^4(nsa_1')$, $^2A_1' \leftarrow (a_1')^2(a_1')^2(e')^4(a_2'')$, $^2A_2''$

γ series: $(a_1')^2(a_1')^2(e')^4(nde'')$, $^2E'' \leftarrow (a_1')^2(a_1')^2(e')^4(a_2'')$, $^2A_2''$

δ series: $(a_1')^2(a_1')^2(e')^4(nda_1')$, $^2A_1' \leftarrow (a_1')^2(a_1')^2(e')^4(a_2'')$, $^2A_2''$

It is interesting to note that none of the other Rydberg states formed by the excitation of the a_2'' electron to *np* and *nd* orbitals has an allowed transition with the ground state.

HCO

The measurements on the 4500-7500 Å absorption system of HCO, first investigated by Herzberg and Ramsay [17], have been recently extended by Johns and Ramsay [23]. The transition involves the excitation of the radical from the ground state in which it has a bent configuration ($\theta''_0 = 119.5°$) to an excited state in which the equilibrium configuration is linear. The spectrum thus consists principally of a long progression of the bending vibration in the excited state $(0,v'_2,0) \leftarrow (0,0,0)$. The main aim of the recent work was to attempt to decide experimentally whether the electronic transition is $^2\Sigma^+$ - $^2A''$ as postulated by Herzberg and Ramsay or $^2A''$ - $^2A'$ as predicted by Walsh [38]. In an earlier review article the author [35] suggested that HCO might afford an example of the Renner effect in the same way as for NH_2. Thus the two combining states of HCO may be regarded as being derived from a $^2\Pi$ state. On bending, the potential energy increases if the lone π electron remains perpendicular to the plane of bending, but the potential energy decreases if the lone π electron lies in the plane of bending. In the latter case the molecule is eventually stabilised in a bent configuration (see Figure 1b). The upper state of the molecule is thus only "half a Π state" and the transition may be designated $^2A''\Pi \leftarrow {}^2A'$.

In the recent work Johns and Ramsay have been able to extend the main progression to lower quantum numbers (to $v'_2 = 3$ for HCO and $v'_2 = 5$ for DCO). They have also been able to observe weak transitions to levels involving v'_1 and v'_3 in addition to "hot" bands involving one quantum of v''_2. By extrapolating the principal progressions of HCO and DCO to their origins, Johns and Ramsay have shown that the isotope shifts between the extrapolated (000)-(000) bands can only be explained if the assignment for the transition is $^2A''\Pi \leftarrow {}^2A'$ and *not* $^2\Sigma^+ \leftarrow {}^2A''$. It should be noted that the revised assignment also necessitates that the values for v'_2 given by Herzberg and Ramsay be reduced by one. Little direct information concerning the presence or absence of a Renner effect has been obtained since all of the vibronic levels in the upper state, except the Σ levels, are predissociated and give rise to diffuse bands.

It is interesting to note that the assignment of the ground state as a $^2A'$ state receives independent support from the recent electron spin resonance measurements of Adrian, Cochran and Bowers [1]. These results cannot be explained on the basis of the alternative assignment.

HNO

Further work has been carried out both on the emission [8] and absorption [3] spectrum of HNO in the 5500 to 10,000 Å region. The emission spectrum was excited by the reaction of hydrogen (or deuterium) atoms with nitric oxide and twelve bands of HNO and eighteen bands of DNO were observed. Two of the HNO bands and three of the DNO bands show a sharp breaking-off in the K-rotational structure due to predissociation of the molecule in the excited state (see Figure 2). These results provide the first example of the breaking-off in the rotational structure in the emission spectrum of a polyatomic molecule and afford upper limits for the energies of the reactions H + NO → HNO ($D_0 \leq$ 17,000 cm^{-1}) and D + NO → DNO ($D_0 \leq 17{,}190$ cm^{-1}). Clyne and Thrush [9] have shown that the activation energies for these recombination reactions are very small hence the limits quoted above will correspond quite closely to the true dissociation energies.

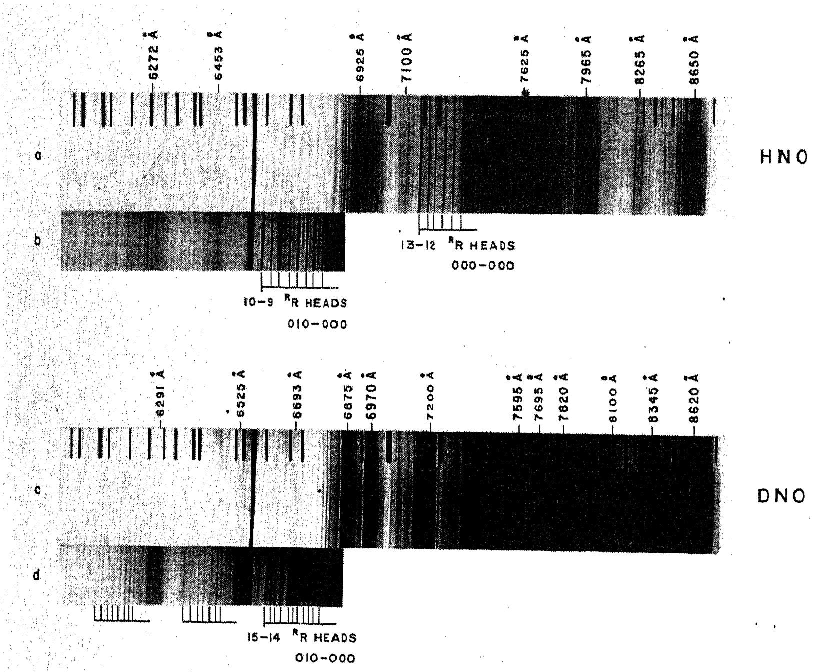

Figure 2. Emission bands of HNO and DNO produced by reacting H (or D) atoms with NO. The bands were photographed with a three-prism glass spectrograph, f/10 camera and hypersensitized I-N plates. The exposure times are (a) 20 min, (b) 2 hr, (c) 20 min, (d) 3 hr. A neon lamp was used to provide the reference spectrum. [Reproduced from a paper by M. J. Y. Clement and D. A. Ramsay, Can. J. Phys. 39, 205 (1961), by kind permission of the Journal.]

A potential energy diagram for HNO showing the known states and their probable dissociation products is given in Figure 3. It is assumed that the four states arising from the combination $H(^2S) + NO(^2\Pi)$ give rise initially to repulsive potential surfaces. When any one of these surfaces meets a potential surface of one of the stable states having the same symmetry species (A' or A") and the same multiplicity, there will be a strongly "avoided crossing." In addition there may be weak interactions between states of different multiplicity. The predissociation in the $^1A''$ state at ~17,000 cm^{-1} is thus caused either by the repulsive $^1A''$ state or by one of the triplet states $^3A'$ or $^3A''$.

In an attempt to determine the strength of the predissociation, the absorption spectrum was reinvestigated by Bancroft, Hollas and Ramsay [3] using much longer absorption paths than in the earlier work of Dalby [10]. Seven new bands of HNO and six new bands of DNO were found but in only one band, viz. the (101)-(000) band of HNO, was any evidence of diffuseness found. The rotational lines of this band were found to be slightly diffuse, the

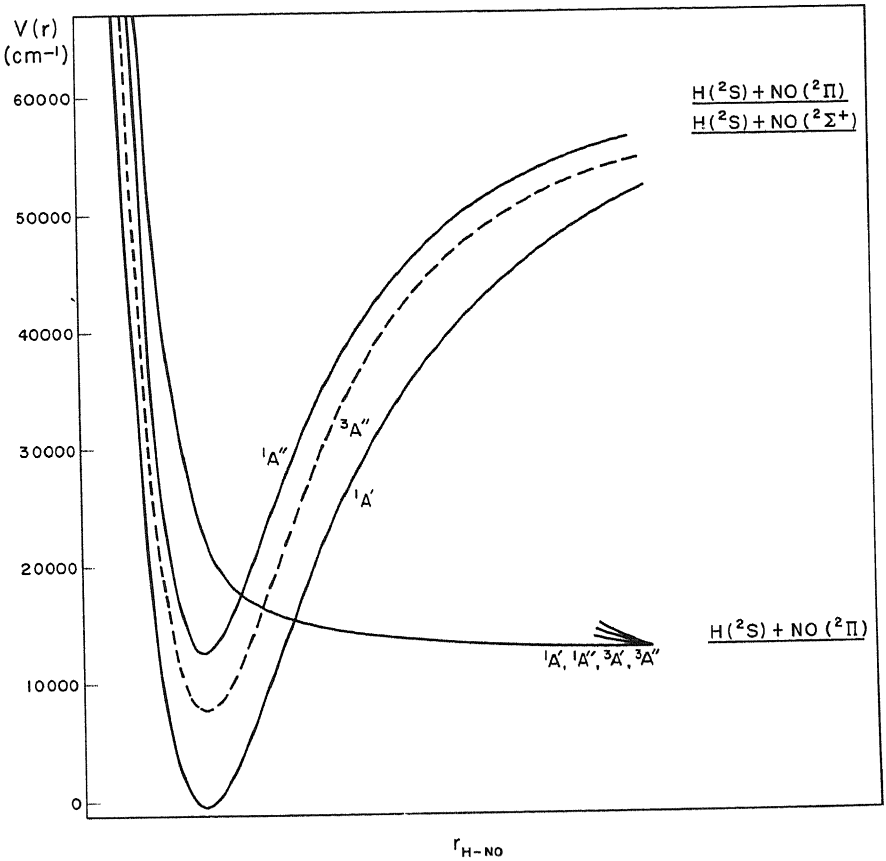

Figure 3. Potential energy diagram for HNO. The $^3A''$ state is predicted theoretically but has not been characterized experimentally. There are some avoided crossings which are discussed in the text but are not shown in the diagram. [Reproduced from a paper by J. L. Bancroft, J. M. Hollas and D. A. Ramsay, Can. J. Phys. 40, 322 (1962), by kind permission of the Journal.]

maximum observed line width being ~0.7 cm^{-1}. This observation gives a value for the lifetime of the molecule in the excited state, viz. $\tau \sim 7.6 \times 10^{-12}$ sec, which corresponds to ~650 N-H stretching vibrations. The predissociation is therefore weak, though it is not possible to decide whether the predissociation is in fact allowed and caused by the $^1A''$ state or spin forbidden and caused by one of the triplet states $^3A'$ or $^3A''$.

BO_2, NCO and N_2O^+

These three species, in addition to CO_2^+ and CS_2^+ which have been studied earlier, form an interesting class of molecules of the general type ABC (or AB_2) with 15 valence electrons. According to molecular orbital theory the ground states should have the configuration

$$\ldots (\sigma_u)^2(\pi_u)^4(\pi_g)^3, \quad {}^2\Pi_g(i)$$

while the first two excited states may be written

$$\ldots (\sigma_u)^2(\pi_u)^3(\pi_g)^4, \quad {}^2\Pi_u(i)$$

$$\ldots (\sigma_u)\ (\pi_u)^4(\pi_g)^4, \quad {}^2\Sigma_u^+$$

The transitions $^2\Pi_u$ - $^2\Pi_g$ and $^2\Sigma_u^+$ - $^2\Pi_g$ are allowed while the transition $^2\Sigma_u^+$ - $^2\Pi_u$ is forbidden. The *g* and *u* symbols should of course be deleted if the molecule does not have a center of symmetry. Both transitions [4,29] have been observed for CO_2^+ but only the $^2\Sigma_u^+$ - $^2\Pi_g$ transition [5] has so far been analysed for CS_2^+.

In the more recent work, Dixon [11,12] has observed both transitions in absorption for NCO and Johns [22] has likewise observed both transitions for BO_2. In the former experiments the NCO radicals were produced by the flash photolysis of HNCO or C_2H_5NCO, while in the latter experiments the bands were observed following the flash photolysis of mixtures of BCl_3 and O_2. For N_2O^+, the spectrum was observed in emission by Callomon[6] using a hollow cathode discharge lamp and bands of the $^2\Sigma^+$ - $X^2\Pi$ system were investigated. For all the above systems detailed rotational and vibrational analyses were carried out. In all observed states the molecules are linear.

An interesting result which emerges from the analysis of the NCO and BO_2 bands concerns the Renner effect. Both molecules exhibit small Renner effects (see Figure 1a) in their ground states ($\varepsilon = -0.18$ for NCO, $\varepsilon = -0.20$ for BO_2) while even smaller

Renner splittings are found in the A $^2\Pi_u$ state of BO$_2$ ($\varepsilon = -0.027$). For both molecules the splittings produced by the coupling of the electron spin to the axis of the molecule are comparable to the splittings produced by the coupling of electronic and vibrational angular momenta. A theory which treats the coupling of Λ, ℓ and S has been given by Pople [33] and gives a satisfactory interpretation of the observed levels. In the $^2\Sigma$ vibronic levels unusually large splittings of the rotational levels are found, such that the spin splitting constant γ may be comparable to or even larger than the rotational constant B. Hougen [20] has shown theoretically that this phenomenon is a natural consequence of the Renner effect.

NO$_3$

The blue color which is formed when NO$_2$ is treated with ozonised oxygen has been attributed to the NO$_3$ molecule. The absorption spectrum was first studied in detail by Jones and Wulf [24] and has recently been reinvestigated by Ramsay [36] at high dispersion. Approximately 20 bands were observed in the

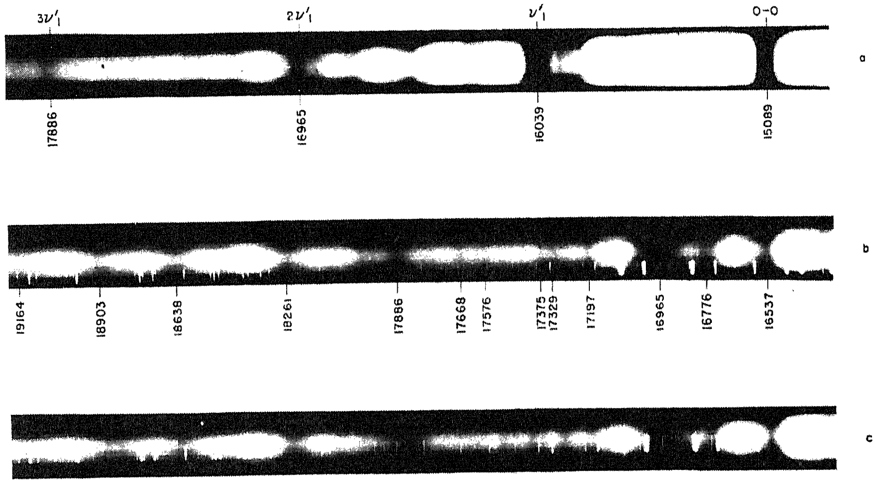

Figure 4. Absorption bands of NO$_3$ formed by reacting NO$_2$ with ozonized oxygen. The bands were photographed using a Hilger E 1 spectrograph with glass optics and absorption path lengths of several meters. The strongest bands in the spectrum of N^{14}O$_3$ are shown in (a). Some of the weaker bands, photographed with a longer absorption path are shown in (b). For comparison purposes, a similar region in the spectrum of N^{15}O$_3$ is shown in (c). The reference lines in (b) and (c) are provided by an iron hollow cathode lamp. The numbers below the bands are vacuum wave numbers.

region 6650 to 5000 Å (see Figure 4), all of which were found to be diffuse under the resolution afforded by a 21 ft. concave grating spectrograph. The observation of diffuseness indicates predissociation of the molecule in the excited state and gives an upper limit for the dissociation energy of the molecule, viz. $D_o \leq 15100\ \text{cm}^{-1} \equiv 43.2$ kcal/mole $\equiv 1.87$ ev). A small isotope shift was observed when $N^{15}O_2$ was used as the starting material (see Figure 4c), proving that the molecule responsible for the spectrum does indeed contain one or more N atoms. The shift however is too small to permit a determination of the number of N atoms present by the use of mixed isotopes. The assignment of the spectrum to the NO_3 molecule is thus based largely on circumstantial evidence but nevertheless this assignment appears plausible and will be adopted for the present discussion.

The strong band at the long wavelength end is undoubtedly the (0-0) band, and the bands at 16039, 16965 and 17886 cm^{-1} presumably form a short progression in the symmetric stretching vibration ν_1'. The spectrum has been assigned by Walsh [39] to the transition

$$\ldots (e')^3(a_2')^2, \quad {}^2E' \leftarrow \ldots (e')^4(a_2'), \quad {}^2A_2'$$

in which an electron is excited from an e' to an a_2' orbital. Since both of these orbitals are predominantly non-bonding between the N and O atoms, no large change in N-O bond length is expected to accompany the transition. Since the a_2' orbital is $0 \longleftrightarrow 0$ antibonding and the e' orbital is $0 \longleftrightarrow 0$ bonding a small increase in bond length is expected in the excited state. These considerations are in accord with the short progression observed for ν_1'. Walsh assumed that the molecule has a planar configuration in both states, hence no excitation of the symmetrical bending vibration ν_2' is expected on the basis of the Franck-Condon principle. Moreover such transitions are forbidden by the vibronic selection rules viz. $E' \cdot a_2'' = E''$, $A_2' \cdot a_1' = A_2'$, $E'' \longleftrightarrow A_2'$.

It is tempting to conclude that the remaining unassigned bands in the NO_3 spectrum are due to transitions involving the excitation of ν_3' or ν_4' or both, and combinations of these vibrations with ν_1' and ν_2'. If the upper state has E' symmetry, a distortion of the molecule from a symmetrical configuration is expected on account of the Jahn-Teller theorem [21]. Such a distortion, however, can only be small since no long progressions involving ν_3' or ν_4' are observed. For small distortions, theory predicts (see Longuet-Higgins, Öpik, Pryce and Sack [26], Moffitt and Thorson [28]) that progressions of the antisymmetric vibrations should be characterised by vibrational intervals of the type large, small, large ---. For example if we assume that $k^2 = 0.2$, where k^2 is a parameter denoting the distortion of the molecule from the symmetrical configuration, then successive vibrational intervals are predicted to be in the ratio 1:0.769:0.949, etc. Moreover the intensity falls off rapidly with increasing vibrational quantum number. The high density of weak unassigned bands and the general diffuseness of these bands does not permit unique vibrational assignments. Hence no definite conclusions can be reached concerning the presence or absence of a Jahn-Teller effect in the NO_3 molecule.

CONCLUDING REMARKS

It is worthwhile to consider the advantages and limitations of electronic spectroscopy as a means for studying polyatomic free radicals. It is clear from the above discussion that a large amount of detailed information can be obtained from high resolution studies of the spectra of small polyatomic free radicals. Indeed the only precise information concerning the structures of free radicals has been derived from a study of their electronic spectra. With larger free radicals the spectra are more complex, the analyses are more difficult, and data on several isotopic species are necessary for complete structural determinations. It should not be too difficult, however, to obtain very accurate values (± 0.003 ev) for the ionisation potentials of many of these radicals by the study of Rydberg series in the vacuum ultraviolet.

REFERENCES

1. Adrian, F., Cochran, E. L., and Bowers, V. A., J. Chem. Phys. 36, 1661 (1962).
2. Ballik, E. A., and Ramsay, D. A., J. Chem. Phys., 31, 1128 (1959): Astrophys. J. In Press.
3. Bancroft, J. L., Hollas, J. M., and Ramsay, D. A., Can. J. Phys. 40, 322 (1962).
4. Bueso-Sanllehi, F., Phys. Rev., 60, 556 (1941).
5. Callomon, J. H., Proc. Roy. Soc. (London), A, 244, 220 (1958).
6. Callomon, J. H., Proc. Chem. Soc., 313 (1959).
7. Claesson, S., Introduction to the Papers presented at the Fifth International Symposium on Free Radicals held at the Institute of Physical Chemistry, University of Uppsala, Sweden, July 6-7, 1961. Published by Almqvist and Wiksell, Stockholm, Sweden.
8. Clement, M. J. Y., and Ramsay, D. A., Can. J. Phys., 39, 205 (1961).
9. Clyne, M. A. A., and Thrush, B. A., Trans. Faraday Soc. 57, 1305 (1961).

10. Dalby, F. W., Can. J. Phys., 36, 1336 (1958).
11. Dixon, R. N., Can. J. Phys., 38, 10 (1960).
12. Dixon, R. N., Phil. Trans. Roy. Soc. (London), Ser. A, 252, 165 (1960).
13. Dressler, K., and Ramsay, D. A., Phil. Trans. Roy. Soc. (London), Ser. A, 251, 553 (1959).
14. Eaton, D. R., Johns, J. W. C., and Ramsay, D. A. (Unpublished results).
15. Herzberg, G., Can. J. Phys., 39, 1511 (1961).
16. Herzberg, G., Proc. Roy. Soc. (London) A262, 291 (1961).
17. Herzberg, G., and Ramsay, D. A., Proc. Roy. Soc. (London), A, 233, 34 (1955).
18. Herzberg, G., and Shoosmith, J., Can. J. Phys., 34, 523 (1956).
19. Herzberg, G., and Shoosmith, J., Nature, 183, 1801 (1959).
20. Hougen, J. H., J. Chem. Phys. 36, 519 (1962).
21. Jahn, H. A., and Teller, E., Proc. Roy. Soc. (London), A, 161, 220 (1937).
22. Johns, J. W. C., Can. J. Phys., 39, 1738 (1961).
23. Johns, J. W. C., and Ramsay, D. A., (Unpublished data).
24. Jones, E. J., and Wulf, O. R., J. Chem. Phys., 5, 873 (1937).
25. Jordan, P. C. H., and Longuet-Higgins, H. C., Mol. Phys., 5, 121 (1962).
26. Longuet-Higgins, H. C., Öpik, U., Pryce, M. H. L., and Sack, R. A., Proc. Roy. Soc. (London), A, 244, 1 (1958).
27. Lundberg, J. L. and Nelson, L. S., Nature, 179, 367 (1957).
28. Moffitt, W., and Thorson, W., Phys. Rev., 108, 1251 (1957).
29. Mrozowski, S., Phys. Rev., 60, 730 (1941); 62, 270 (1942); 72, 682, 691 (1947).
30. Nelson, L. S., J. Chem. Phys., In Press.
31. Nelson, L. S., and Kuebler, N. A., J. Chem. Phys., 33, 610 (1960).
32. Nelson, L. S., and Lundberg, J. L., J. Phys. Chem. 63, 433 (1959).
33. Pople, J. A., Mol. Phys., 3, 16 (1960).
34. Pople, J. A., and Longuet-Higgins, H. C., Mol. Phys., 1, 372 (1958).
35. Ramsay, D. A., Advances in Spectroscopy, 1, 1 (1959).
36. Ramsay, D. A., Unpublished results first reported here.
37. Renner, R., Z. Physik, 92, 172 (1934).
38. Walsh, A. D., J. Chem. Soc., 2292 (1953).
39. Walsh, A. D., J. Chem. Soc., 2306 (1953).

FEATURES AND REGULARITIES IN RESEARCH OF DIATOMIC MOLECULAR SPECTRA

Rafael Grinfeld
Department of Physics
University of La Plata
La Plata, Argentina

The band spectra of some 380 neutral diatomic molecules and about 30 ionized ones are known at the present time, out of a possible total of about 5000. In the list, oxides come first with known spectra of 69; then homonuclear ones with 46; chlorides, hydrides, bromides and fluorides with 35 to 40; sulfides with 24; iodides with 28; nitrides with 14.

About half of those molecular spectra have no rotational analysis; about one-third of the total have even no vibrational analysis; and perhaps 15 percent are of uncertain identification. Less than 10 percent of the spectra include 6 or more known band systems. About 40 spectra of isotopic diatomic species are known. See Bibliography at the end of the paper.

The simple statistics given above are obviously insufficient information. The author wanted to know what oxides, what hydrides, and so forth, have been spectroscopically studied. With this aim we constructed a graph in which we locate the molecules, spectra of which are known, as a function of the atomic number Z of the two components.

This graph, given in Figure 1, shows interesting features, suggesting besides, many new research problems. In Figures 2 through 10 we give each of the 9 combinations quoted before as a function of the atomic number of the elements combining with the principal one.

OXIDES

Figures 1 and 2 show that no spectra of the following oxides were found: a) the alkali metals; b) the actinides, except those of Th and U.; c) of Au, in spite of the fact that those of the oxides

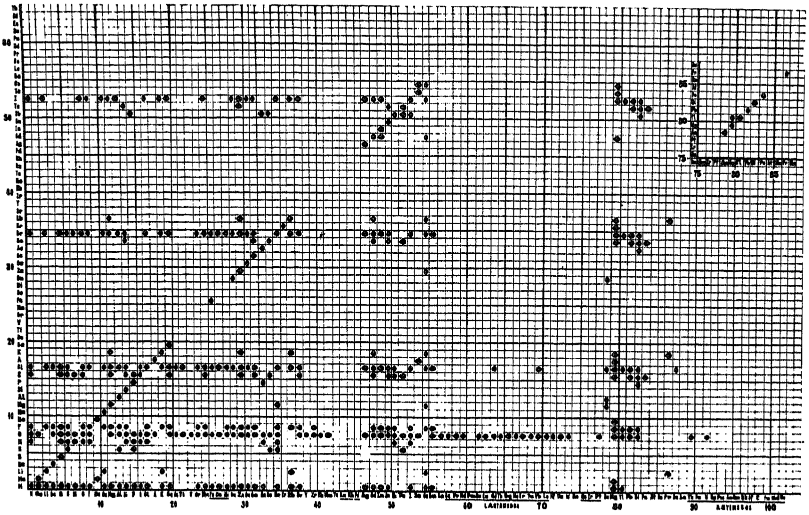

Figure 1. In this graph each black circle represents a diatomic molecule for which band spectra are known, located as a function of the atomic numbers of the component atoms.

of Cu and Ag are known; d) of Ru, Rh, Pd; Os and Ir; of Ne, Kr, and Rn.

HYDRIDES

a) Up to date no spectra of the hydrides of the lanthanides and actinides are known; b) neither of the elements similar to Sc, Ti and V; c) in the literature one does not find spectra belonging to the hydrides of the following elements Pb; Sb; Se, Te and Po; d) no spectra are known of the hydrides of Ru, Rh, Pd; Os, Ir and Pt; and so forth. See Figure 3.

HOMONUCLEAR MOLECULES

a) No spectra were identified as produced by Sr_2, Ba_2, Ra_2 while spectra of Ca_2 are known; b) except that of Fe_2, up to the present time no spectra have been found of the homonuclear diatomic molecules whose component atoms belong to the groups in process of filling-up the 3d, 4d, and 5d shells; c) the same is true for the lanthanides (4f) and the actinides (5f); and so forth. See Figure 4.

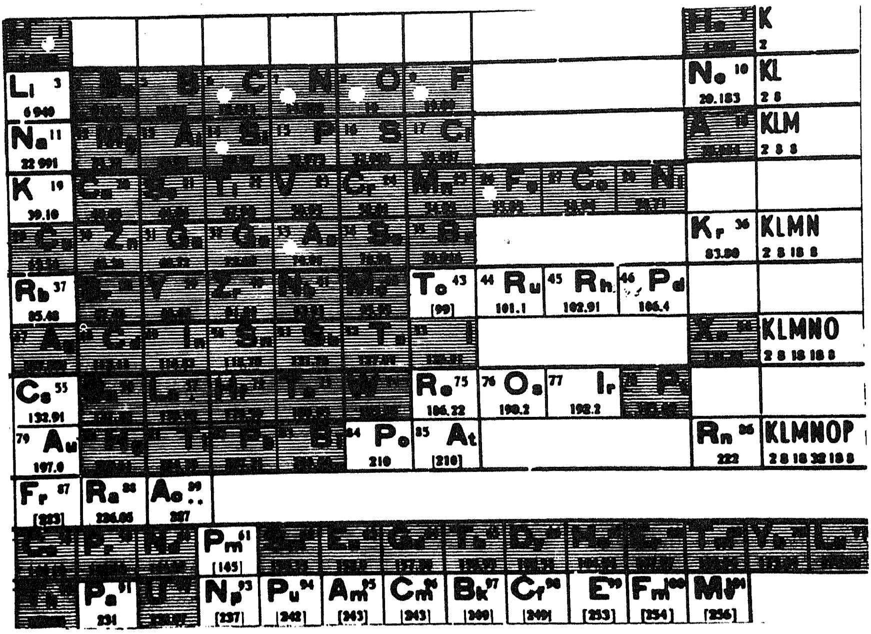

Figure 2. The dark rectangles correspond to the elements for which oxide band spectra are known. The white circles represent ionized species.

HALIDES

There are about 40 binary combinations of each of the following elements F, Cl, Br and I whose band spectra are known. Looking into the Figures 5, 6, 7, and 8 one sees a few interesting differences; for example: a) the number of spectra of the iodides is only about 2/3 of the known spectra of any one of the other halides; b) the spectra of NF and NCl are known, but not that of NBr; c) we do not know spectra of NF, PF, AsF while those of SbF and BiF were registered; and so forth.

SULFIDES AND NITRIDES

The number of spectra of these combinations are very few. Observing Figures 9 and 10 the reader can draw many interesting conclusions.

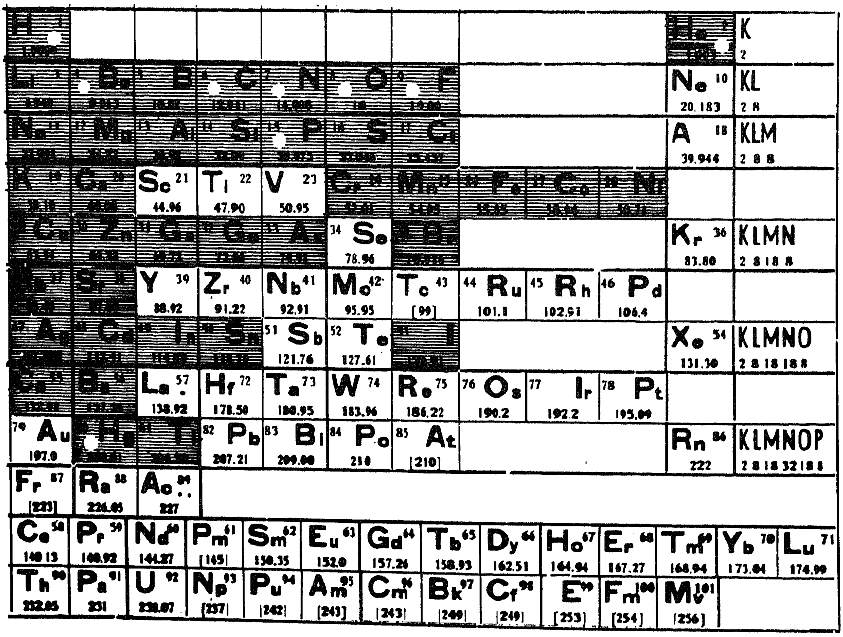

Figure 3. The dark rectangles correspond to the elements for which hydride band spectra are known.

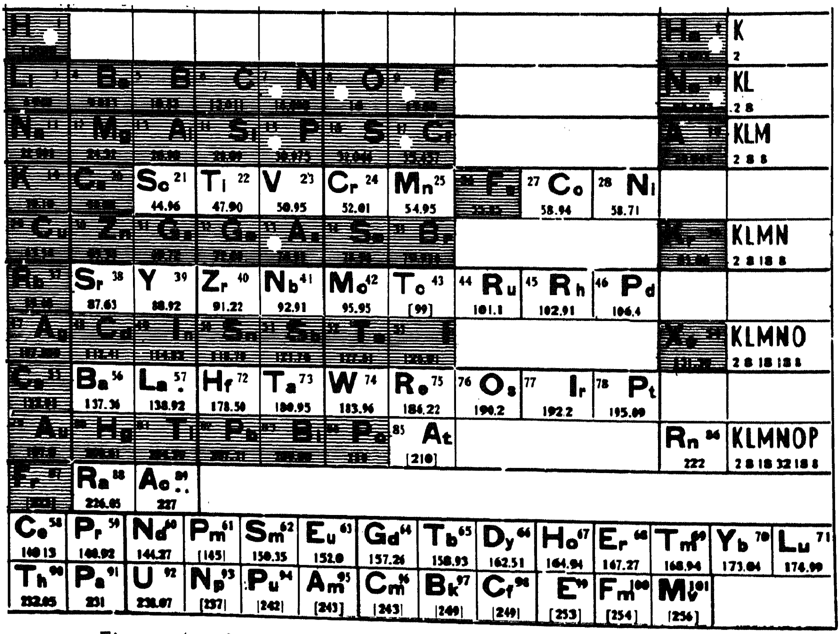

Figure 4. The dark rectangles represent the corresponding homonuclear molecules for which band spectra are found.

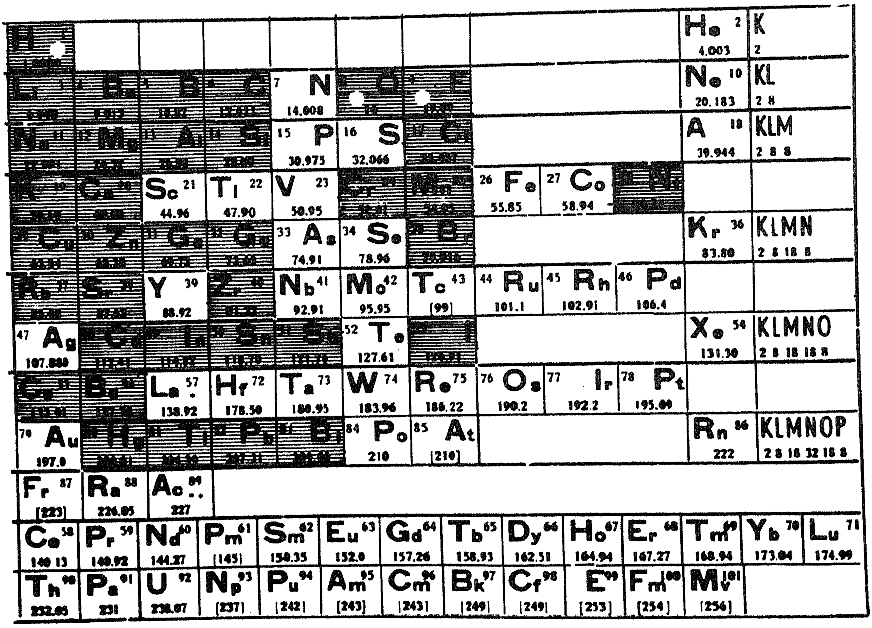

Figure 5. The dark rectangles correspond to the elements for which fluoride band spectra are known.

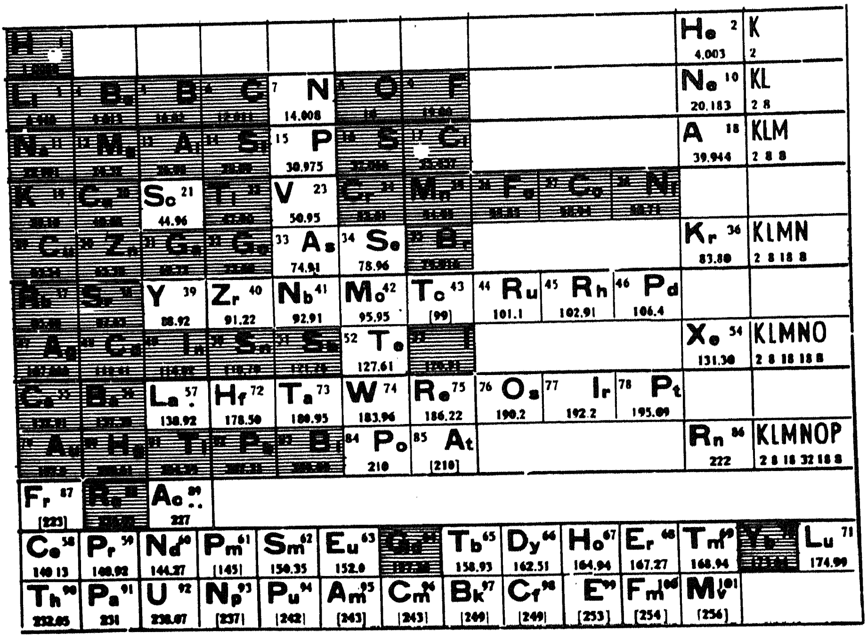

Figure 6. The dark rectangles correspond to the elements for which chloride band spectra are known.

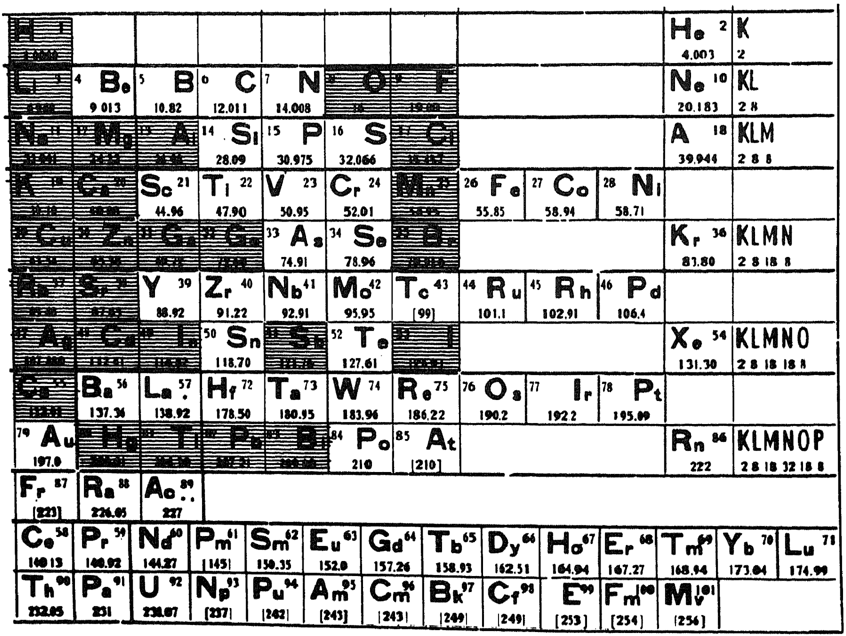
H 1 He 2 K
Li 3 Be 4 B 5 C 6 N 7 O 8 F 9 Ne 10 KL
Na 11 Mg 12 Al 13 Si 14 P 15 S 16 Cl 17 A 18 KLM
K 19 Ca 20 Sc 21 Ti 22 V 23 Cr 24 Mn 25 Fe 26 Co 27 Ni 28
Cu 29 Zn 30 Ga 31 Ge 32 As 33 Se 34 Br 35 Kr 36 KLMN
Rb 37 Sr 38 Y 39 Zr 40 Nb 41 Mo 42 Tc 43 Ru 44 Rh 45 Pd 46
Ag 47 Cd 48 In 49 Sn 50 Sb 51 Te 52 I 53 Xe 54 KLMNO
Cs 55 Ba 56 La 57 Hf 72 Ta 73 W 74 Re 75 Os 76 Ir 77 Pt 78
Au 79 Hg 80 Tl 81 Pb 82 Bi 83 Po 84 At 85 Rn 86 KLMNOP
Fr 87 Ra 88 Ac 89
Ce 58 Pr 59 Nd 60 Pm 61 Sm 62 Eu 63 Gd 64 Tb 65 Dy 66 Ho 67 Er 68 Tm 69 Yb 70 Lu 71
Th 90 Pa 91 U 92 Np 93 Pu 94 Am 95 Cm 96 Bk 97 Cf 98 E 99 Fm 100 Mv 101

Figure 7. The dark rectangles correspond to the elements for which bromide band spectra are known.

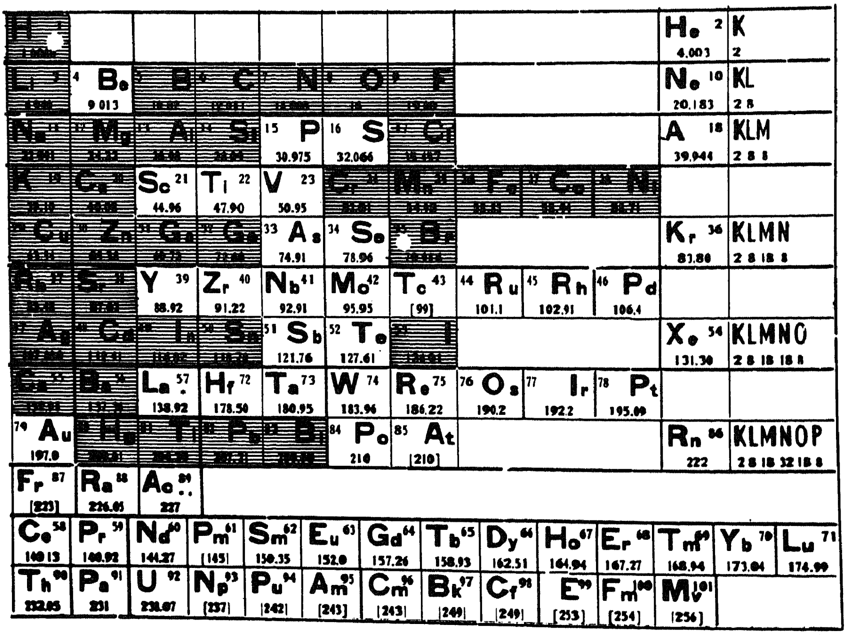
H 1 He 2 K
Li 3 Be 4 B 5 C 6 N 7 O 8 F 9 Ne 10 KL
Na 11 Mg 12 Al 13 Si 14 P 15 S 16 Cl 17 A 18 KLM
K 19 Ca 20 Sc 21 Ti 22 V 23 Cr 24 Mn 25 Fe 26 Co 27 Ni 28
Cu 29 Zn 30 Ga 31 Ge 32 As 33 Se 34 Br 35 Kr 36 KLMN
Rb 37 Sr 38 Y 39 Zr 40 Nb 41 Mo 42 Tc 43 Ru 44 Rh 45 Pd 46
Ag 47 Cd 48 In 49 Sn 50 Sb 51 Te 52 I 53 Xe 54 KLMNO
Cs 55 Ba 56 La 57 Hf 72 Ta 73 W 74 Re 75 Os 76 Ir 77 Pt 78
Au 79 Hg 80 Tl 81 Pb 82 Bi 83 Po 84 At 85 Rn 86 KLMNOP
Fr 87 Ra 88 Ac 89
Ce 58 Pr 59 Nd 60 Pm 61 Sm 62 Eu 63 Gd 64 Tb 65 Dy 66 Ho 67 Er 68 Tm 69 Yb 70 Lu 71
Th 90 Pa 91 U 92 Np 93 Pu 94 Am 95 Cm 96 Bk 97 Cf 98 E 99 Fm 100 Mv 101

Figure 8. The dark rectangles represent elements for which iodide band spectra are known.

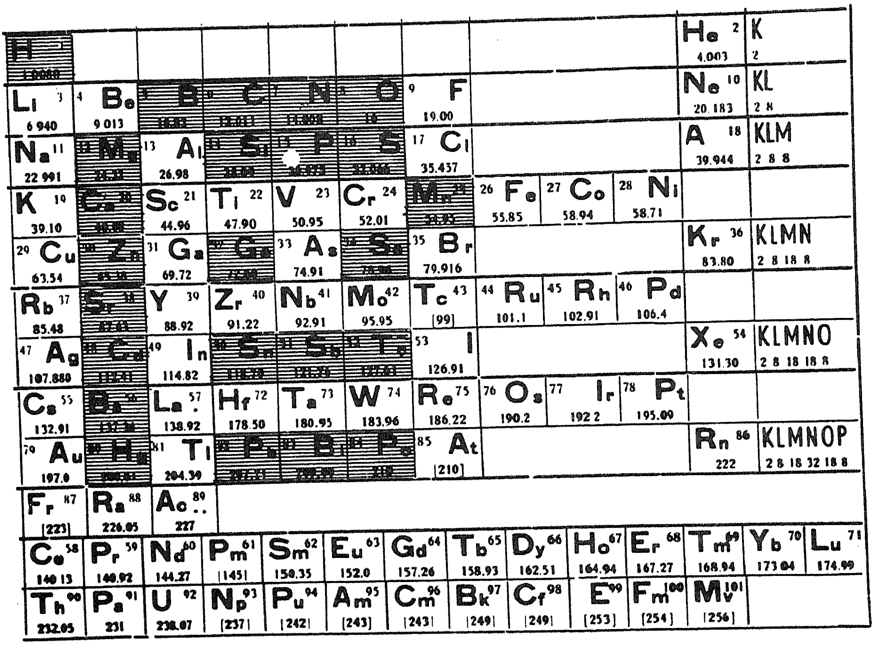

Figure 9. The dark rectangles represent elements for which nitride band spectra are known.

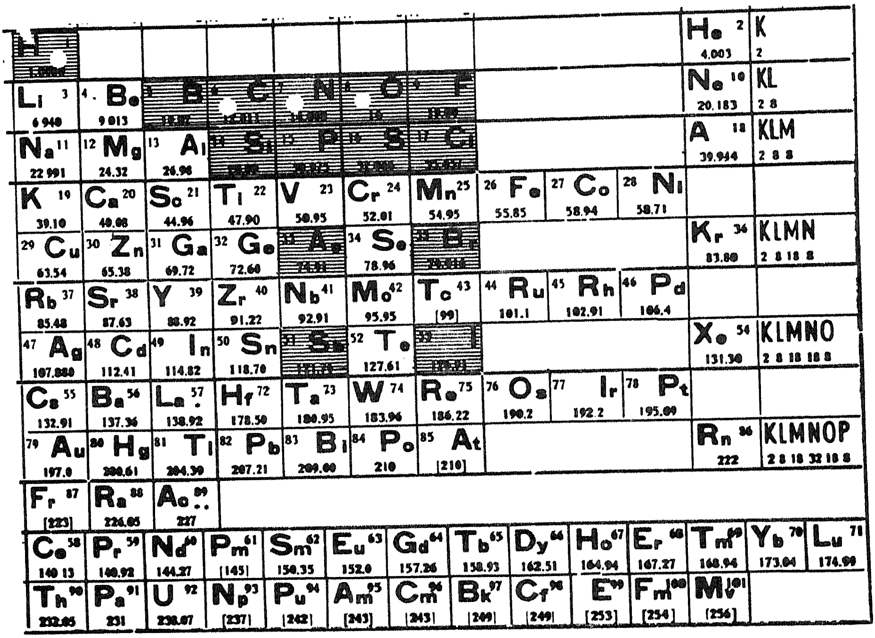

Figure 10. The dark rectangles represent elements for which sulfide band spectra are known.

IONIZED MOLECULES

On each of the given figures, we put a white circle on the square of the elements of which the spectra of the ionized combination are known. The number is too small to draw general conclusions. The same is true in the case of spectra of *isotopic species.*

CONCLUSIONS

a) It seems logical to expect that many new spectra of neutral diatomic molecules can be excited using sources and conditions analogous to those successfully employed with molecules composed of like atoms, as pointed out above; b) the previous statement appears applicable to isotopic species and to ionized molecules; c) Figure 1 suggests that a systematic study of those problems will be fruitful; d) the attack on the problem of exciting spectra of the hydrides and halides of the lanthanides looks to be of real importance. We in La Plata have started this with the hydrides, and with systematics of rotational and vibrational constants.

ACKNOWLEDGMENT

The author wants to state his gratitude to Professor S. P. Davis for reading and correcting the manuscript.

REFERENCES

G. Herzberg, Molecular Spectra and Molecular Structure, Prentice-Hall, New York, 1939.

B. Rosen, Tables des Données Spectroscopiques, Herrmann, Paris, 1952.

R. W. Pearse and A. G. Gaydon, The Identification of Molecular Spectra, Chapman & Hall, London, 1941.

R. W. Pearse, J. Opt. Soc. Am. 41, 148 (1951).

R. W. Pearse, J. Opt. Soc. Am. 43, 416 (1953).

P. Swings, J. Opt. Soc. Am. 41, 153 (1951).

Berkeley News Letters, 1960, 1961, 1962.

G. Herzberg and L. L. Howe, Bibliography of Spectra of Diatomic Molecules, 1950-1960; and Addenda and Errata, Ottawa, 1961.

THE METHODOLOGY OF THE MEASUREMENT AND REPRESENTATION OF FLUORESCENCE SPECTRA

Giorgio Nebbia
Istituto di Merceologia
Università di Bari
Bari, Italy

The availability in the recent years of commercial instruments for spectrofluorimetric measurements has broadened the interest in the use of fluorescence spectra in physical chemistry and in analytical chemistry.

The spectral distribution of the fluorescence emission radiation is a physical and absolute characteristic of a given substance. The fluorescence emission intensity at a given wavelength depends, on the contrary, on many features such as the intensity and the spectral distribution of the exciting radiation, the geometry of the path of the exciting and emitted fluorescence radiation, the characteristics of the detector, the concentration of the substance and the nature of the solvent, and the quantum yield of the solution. A fluorescence emission spectrum, therefore, is useful for qualitative considerations; its use for quantitative analysis is possible only for an operator with a given instrument. For physico-chemical purposes the qualitative aspect of spectrofluorimetry is generally sufficient; for the analytical chemist there is an interest in obtaining fluorescence emission spectra which are the same on different instruments. In this paper an attempt is made to give a contribution to this problem, developing the results presented in a previous paper [1].

The goal of this work is to advance fluorescence spectroscopy to the position in which absorption spectroscopy is to-day. The problem is, however, difficult because there are many variables in fluorescence spectroscopy which cause great errors in the fluorescence emission spectra; this does not happen in absorption spectroscopy which depends simply on the measurement of the ratios of two light intensities, but it must not be forgotten that absorption spectroscopy itself was born as a semiquantitative technique when the photographic method was used. Fluorescence spectroscopy can become much more accurate than at the present.

The present suggestion is based on the measurement and representation of the fluorescence emission spectrum of a given substance "*against*" the fluorescence emission spectrum of some reference compound.

The suggestion of using a comparison between the intensities of the fluorescence at a given wavelength of a compound and the fluorescence of quinine sulphate at the same wavelength was presented in a paper by Kortüm and Finckh as early as in 1941, using a photographic technique. For the comparison of fluorescence emission spectra of different compounds and for obtaining, therefore, reproducible fluorescence spectra, it is necessary to measure in the same experimental conditions and at the same time the fluorescence emission spectra of a given solution of the compound under examination and of a solution of the reference compound at a known concentration, and to express and compare the results in arbitrary units, for instance as energy per unit wavelength interval or as quanta per unit frequency interval. Both the spectra must be corrected, following the same procedure, in order to take into account the different sensitivity of the detector to radiation of different wavelengths and other variables. The comparison between the intensities of the fluorescence at given wavelengths may give the concentration of the compound under analysis if a specific fluorescence intensity ratio has been obtained in preliminary trials. If the method proves reliable it is possible to express the fluorescence intensity of a compound at a given wavelength in terms of the fluorescence intensity of the reference compound at the same or at another wavelength.

The experimental data so far available show that there are many sources of errors and discrepancies between the results of different workers using different instruments, even though the spectra have been corrected and presented in absolute units. The main sources of discrepancies seem to be the impurity of the exciting radiation, the self-absorption of the fluorescence, varying band widths in the analyzing monochromator, and the difficulty of obtaining a precise correction curve. Most fluorescence emission spectra which appear in the literature are not corrected at all and it is the opinion of the writer that fluorescence spectroscopy can make some progress only through an accurate preparation, comparison and representation of the spectra which are measured with the various compounds. For obtaining this purpose in every spectrofluorimetric measurement the elements to be kept into account have been recently reviewed [3] and are the following: (a) the experimental measurement conditions, (b) the correction procedure and (c) the characteristics of the reference compound.

The following experimental conditions must be kept into account and possibly stated together with every fluorescence emission spectrum: (1) The nature and purity of the exciting radiation. It is necessary to state the source of radiation (if a xenon or mercury lamp is used) and its spectral distribution; if filters are used their transmission characteristics; if a monochromator is used to isolate the exciting radiation the band width, or half band width, of such radiation must be noted. A great amount of work has been done using the 366 mμ (2.73 μ^{-1}) radiation; the popularity of this exciting radiation is due to the fact that at this wavelength a very intense line exists in the mercury spectrum, that this line can be readily isolated, and that many compounds emit fluorescence radiation at a wavelength greater than 366 mμ. For comparison purposes the same source must be used for the compound under analysis and for the reference substance. The purity of the exciting radiation is undoubtedly a very important point, especially when substances with different absorption characteristics are compared. (2) The type of analyzing monochromator and the band widths at a given appropriate wavelength. (3) The geometry of the cell containing the solution and of the light beam and whether right angle or frontal illumination is used. It is convenient to specify the path length of the fluorescence excitation and emission radiation through the liquid, from the point from which the fluorescence is viewed. (4) The substances under examination must be characterized by their purity and concentration, the purity of the solvents, the optical density of the solutions at the excitation and fluorescence wavelengths and the temperature.

The measurements are usually carried out by causing the fluorescence emission radiation to enter the analyzing monochromator, fixing an exit slit which allows to pass a portion of the fluorescence emission spectrum of a stated band width at a given wavelength, and measuring the amount of radiation received by the detector (if a usual spectrophotometer is used the readings on the transmittance scale are taken) which represent in arbitrary units the energy per unit wavelength interval. This is the *apparent* fluorescence emission spectrum. In order to obtain the *true* fluorescence emission spectrum the apparent one must be corrected. Such correction is necessary because, usually, with constant exciting radiation intensity, the analyzing monochromator is scanned at constant slit width; the correction takes into account the changes of the detector sensitivity with frequency of the incident radiation and therefore of its electrical response, and the band width and the transmission of the analyzing monochromator.

A procedure for the correction of the fluorescence emission spectra has been indicated by Kortüm and Finckh [2] in 1941 and has more recently received further development by other authors [4,5,6]; the present status of the problem has been recently reviewed by Parker and Rees [3]. The correction can be done essentially in three ways: (a) by using a tungsten lamp which emits radiation of known spectral distribution; (b) by using a calibrated detector and (c) by comparing the apparent fluorescence emission spectrum of a given compound with the accurately corrected spectrum of the same compound.

In all these methods a series of coefficients, at the various wavelengths, are obtained; by multiplying the apparent spectrum by these coefficients the corrected spectrum, in arbitrary units, is obtained. The first method is the most largely followed and the third one has been recently suggested by Lippert and coworkers [7] and by Melhuish [8]. If the correction curve is prepared using a tungsten lamp it is necessary to keep into account the type, color temperature, and filament characteristics, and on the basis of these data it is possible to calculate fairly well the spectral emission curve of the source, from the laws of the black-body emission radiation. Usually, at a given slit width of the analyzing monochromator, the response of the detector to the tungsten lamp radiation is recorded and the values of the correction factors f are obtained by dividing, at each wavelength, the spectral emission curve of tungsten at the color temperature of the lamp by the detector response to the tungsten lamp radiation. It must be noted that this correction procedure applies only in the visible range. It is thus possible to obtain a series of coefficients f_λ; by multiplying the apparent fluorescence emission intensity of a substance at a given wavelength by the corresponding correction coefficient one obtains the corrected fluorescence emission intensity in energy per unit wavelength interval.

Parker and Rees [3,6] have suggested that to be of maximum value the spectra should be reported in terms of quanta per unit frequency interval (arbitrary units) and this is obtained by multiplying the fluorescence intensity, in energy per unit wavelength interval, by λ^3. As a convenient frequency unit the "reciprocal micron" (μ^{-1}) can be used.

The third point for obtaining quantitative fluorescence emission spectra refers to the reference compound or compounds. The requirements for an ideal reference compound include: it must possess absorption and fluorescence spectra which are structureless and cover as wide a frequency range as possible. Since the fluorescence of a reference compound is inevitably restricted to a comparatively narrow range, more than one standard is required. The reference compound must be a solid which can be readily and cheaply prepared in a pure state of precisely known composition. It should be stable to air and light both as a solid and in solution; it should be soluble in water (acid or alkaline); it must have high fluorescence efficiency and little absorption-fluorescence overlap. The composition of the fluorescent reference solution should be checked by recording the optical density at the wavelength for excitation. The major part of the work has been done so far using as fluorescence standards acid solutions of quinine sulphate, although this compound is far from possessing all the ideal requirements.

Generally, as a starting material, quinine bisulphate is used, $C_{20}H_{24}O_2N_2 \cdot H_2SO_4 \cdot 7H_2O$, mol. w. 548.6. The absorption of such compound in 0.1 N H_2SO_4 is shown in Figure 1. It presents two maxima, one at 346 mμ ($E_{1\,cm}^{1\%}$ 100) and one at 248 mμ ($E_{1\,cm}^{1\%}$ 555). The value $E_{1\,cm}^{1\%}$ at 366 mμ is 62 and such value is in good agreement with the one given by Parker and Rees [6]. Melhuish [8] in

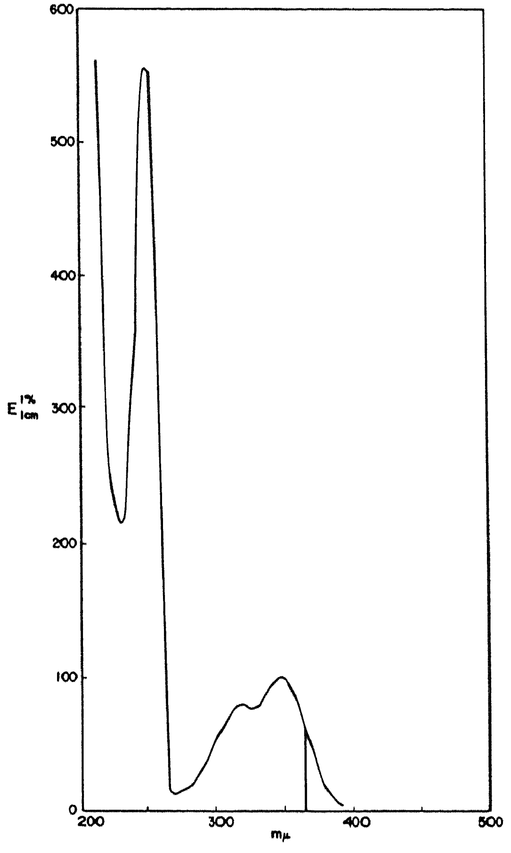

Figure 1. Absorption spectrum of quinine sulphate in 0.1 N H_2SO_4.

his work on the preparation of a corrected spectrum of quinine sulphate used quinine bisulphate dried at 100°C; Lippert and co-workers [7] started from quinine base. Lippert and co-workers [7] have extended the range of possible fluorescent reference compounds by suggesting four other compounds: 4-dimethylamino-4'-nitro-stilbene to be used in o-dichlorobenzene solution; m-dimethyl-amino-nitrobenzene in a solvent mixture (v/v) of 70% hexane and 30% benzene; 3-amino-phthalimide in 0.1 N H_2SO_4; and β-naphthol in 0.1 molar standard acetate buffer Merck. β-Naphthol, however, requires an exciting radiation at 313 mμ (3.18 μ^{-1}). In their paper, Lippert and coworkers give directions for the preparation and purification of the suggested compounds.

In the present paper a comparison is presented between two different correction procedures and then an attempt is made to obtain "quantitative" fluorescence emission spectra with anthracene, m-dimethylamino-nitrobenzene and riboflavine, against the spectra of quinine sulphate, measured with the same experimental conditions. The failure or success in obtaining the solution of the problem will give some information on the line to follow in future work.

Spectrophotometer

A Beckman DU Spectrophotometer with a line-operated power supply and 1P28 photomultiplier tube has been used.

Spectral Fluorescence Attachment

The fluorescence emission spectra have been obtained using the Beckman 22850 Spectral fluorescence attachment illustrated in Figure 2. The radiation from a Beckman 2260 mercury vapor

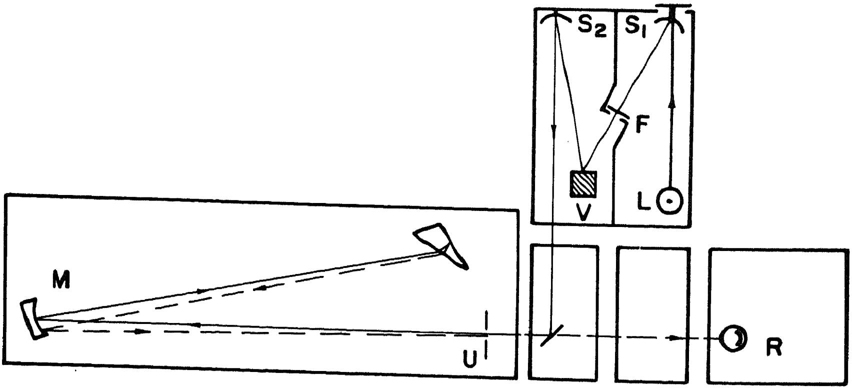

Figure 2. Geometry of the apparatus for the measurement of fluorescence emission spectra.

lamp (L) is filtered through a Corning Glass Filter No. 5840 (F) and reaches, with an incidence angle of about 20°, the silica cell (V) 1.0 cm. deep containing the fluorescent sample. The reflected fluorescence emission radiation enters the monochromator and, after having passed through the prism, its spectrum is projected against the slit U and a narrow band reaches the photomultiplier R. The band width vs. the slit width at various wavelengths for the apparatus is shown in Figure 3, which has been prepared on the basis of the data supplied by the manufacturer. The photomultiplier response is read on the transmittance scale. The maximum response is regulated by the width of the slit.

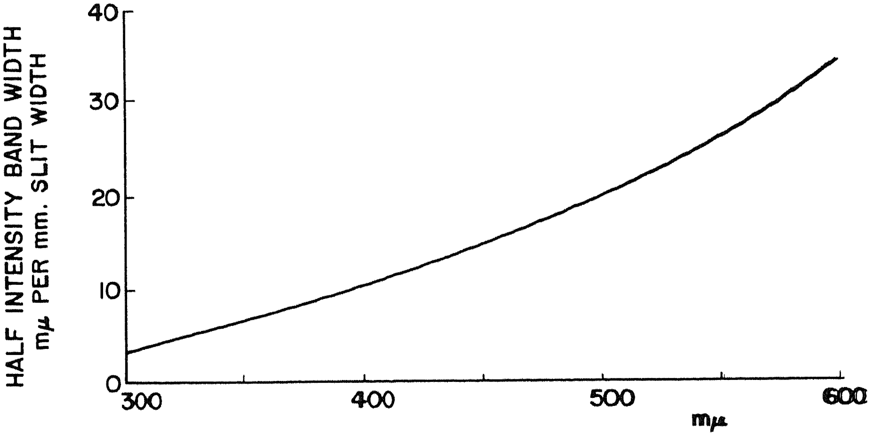

Figure 3. Dispersion of the monochromator of the Beckman DU Spectrophotometer: from data supplied by the manufacturer.

Purity of the Exciting Radiation

The purity of the exciting radiation has been determined by filling the cell (V) with distilled water and collecting the reflected light at various slit openings of the analyzing monochromator.

Balancing the spectrophotometer circuit with the same conditions in which the fluorescence measurements are made, the energy response has been measured on the transmission scale. The results are contained in Figure 4 and show that, with the lamp-filter combination used, no appreciable radiation is observed at wavelengths greater than 400 mμ, even with the largest slit width used, 1.5 mm, corresponding to a half-band width of 150 mμ at 400 mμ.

Calibration for Spectral Response

It has been previously discussed that the response of the photomultiplier to an equal-energy spectrum is a function of the

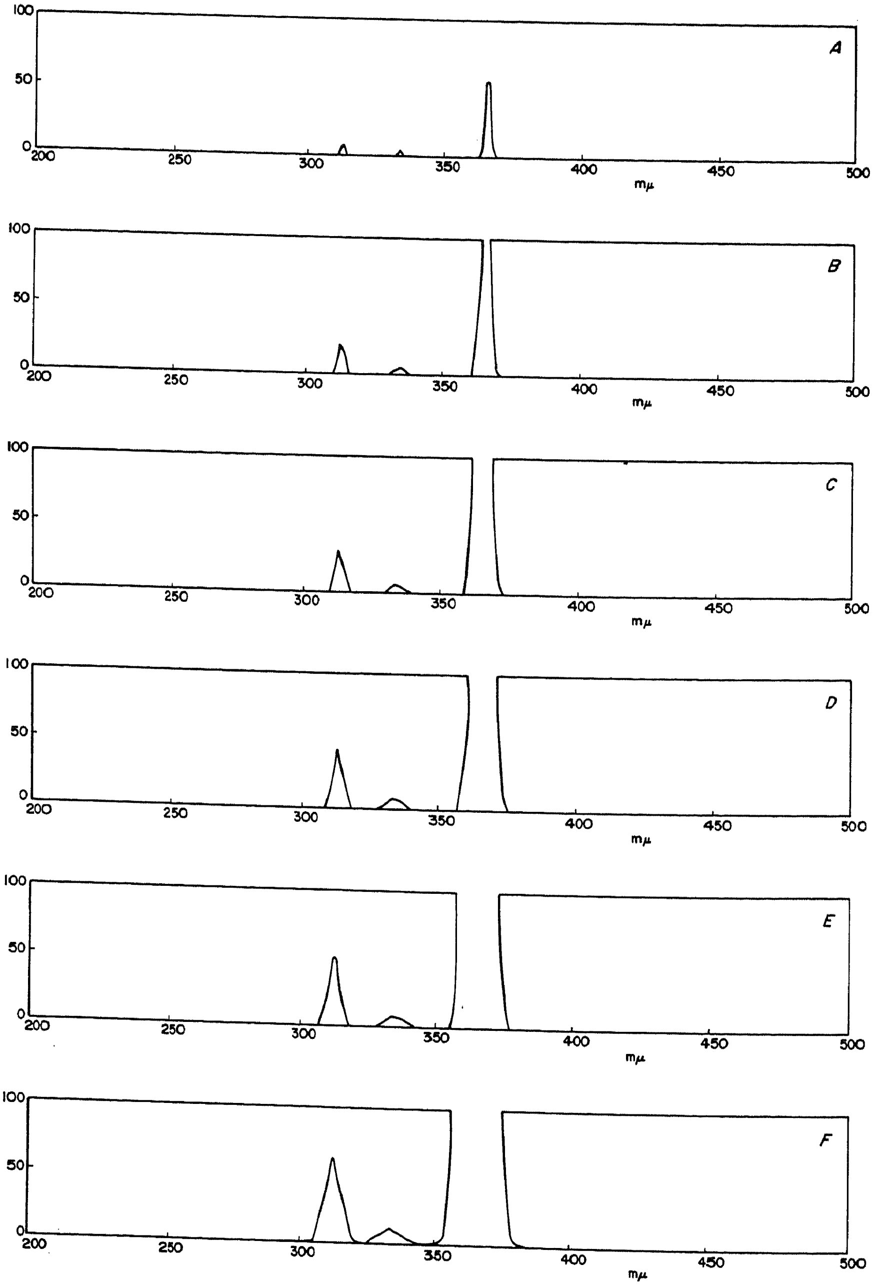

Figure 4. Purity of the exciting radiation at various slit widths of the analyzing monochromator. Half band widths, mμ @ 400 mμ: A 2.5; B 5.0; C 7.5; D 10.0; E 12.0; F 15.0.

spectral transmission of the monochromator and of the spectral response of the cathode of the photomultiplier. For correction of the apparent emission spectra two procedures have been followed: (a) the observed spectral response of the instrument to a tungsten filament lamp operated at a known colour temperature was compared with the calculated energy distribution of the lamp spectrum; (b) the observed spectral response of the instrument with reference compounds has been compared with the corrected fluorescence spectra of the same compounds, reported in the literature. For the first procedure, the light of the tungsten lamp of the Beckman DU Spectrophotometer, operated at 6 volts, was used in conjunction with the fluorescence attachment shown in Figure 2. It has been assumed that the tungsten lamp gives a black-body radiation at a color temperature of 2800°K. The spectral distribution of such radiation is indicated as E_λ and is shown in Figure 5.

The light of the lamp was reflected by the cell *V* filled with distilled water and placed in the same position in which, during the fluorescence measurements, the cells containing the fluorescent solutions are placed. The reflected light follows the same light path followed by the fluorescent emission light and this enables the spectrophotometer to be calibrated at a light intensity level comparable to that generated by the fluorescent compounds. If I_λ is the measured response of the photomultiplier to the reflected tungsten radiation at the various wavelengths, a calibration factor f can be defined as

$$f_\lambda = \frac{E_\lambda}{I_\lambda}.$$

These figures were, for convenience sake, all corrected to f = 1 at 520 mμ and are contained in Figure 5. The second correction procedure consisted of the comparison of apparent fluorescence spectra of some reference compounds with the corrected spectra of the same compounds. Lippert and coworkers [7] have reported a number of corrected fluorescence spectra and have kindly made available the reference compounds. The fluorescence emission spectra of quinine sulphate in 0.1 N H_2SO_4, of 3-amino-phthalimide in 0.1 N H_2SO_4, and of m-dimethylamino-nitrobenzene in 70% hexane and 30% benzene (v/v) have been measured. The photomultiplier response on the transmittance scale gives the energy per unit wavelength interval (in arbitrary units); such figures have been converted to quanta per unit frequency interval (uncorrected) by multiplying by λ^3. The data so obtained, represented as Q/Q_{max}, together with the corrected spectra reported by Lippert and coworkers [7] and by Melhuish [8], are represented in Figures 6, 7, 8.

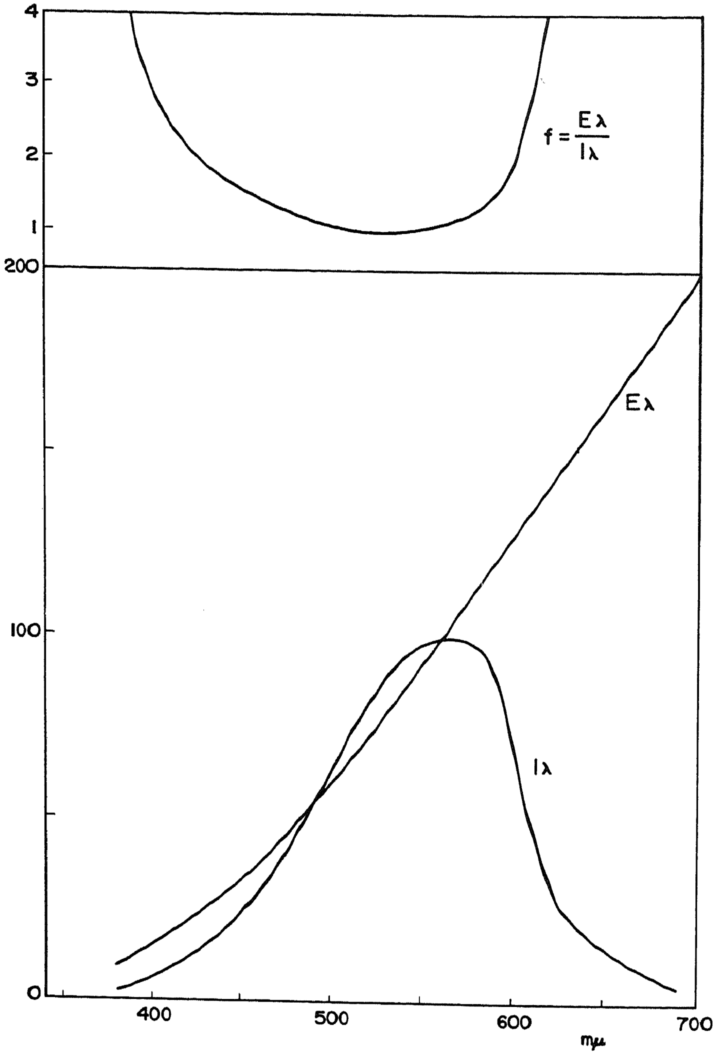

Figure 5. Preparation of the correction coefficients f_λ. I_λ are the spectral responses of the photomultiplier to the radiation of a tungsten lamp, reflected by the cell filled with distilled water. E_λ are the values of the spectral distribution of the energy from a tungsten lamp, calculated by the black-body radiation laws for a color temperature of 2800°K.

The values obtained for quinine sulphate by Lippert and coworkers [7] were identical with the data of Melhuish [8], who also had suggested this compound as a fluorescent standard and presented a corrected fluorescence spectrum. The values of the corrected spectra have been divided, wavelength by wavelength,

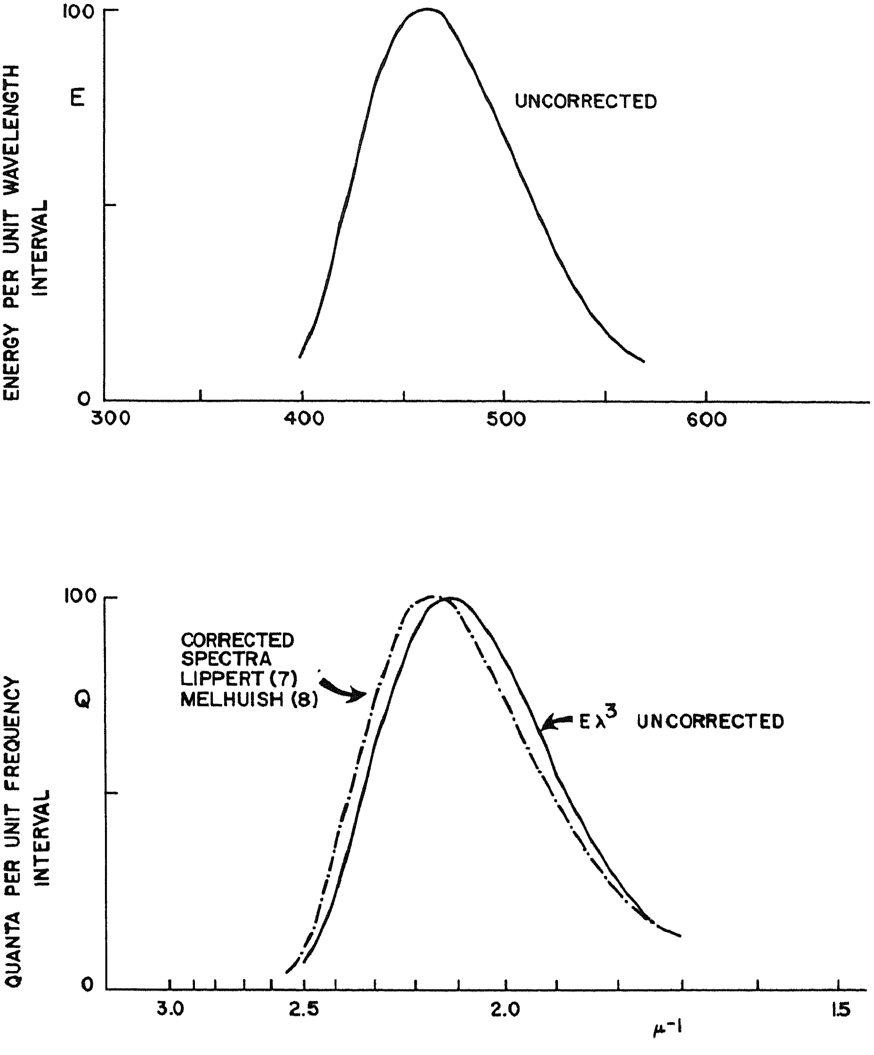

Figure 6. Fluorescence emission spectra of quinine sulphate in 0.1 N H_2SO_4. Upper graph: uncorrected spectra at concentrations between 20 and 2 μg/ml (average figures). Lower graph: comparision between the uncorrected average spectrum and the corrected spectrum, both expressed as quanta per unit frequency interval.

by the uncorrected values obtained in the present measurements; it has thus been possible to obtain a series of correction coefficients f. Such coefficients are somewhat different between themselves and from the ones obtained with the tungsten lamp, especially in the violet region, and are presented in Figure 9. The differences may be caused by some uncertainty in the part of the

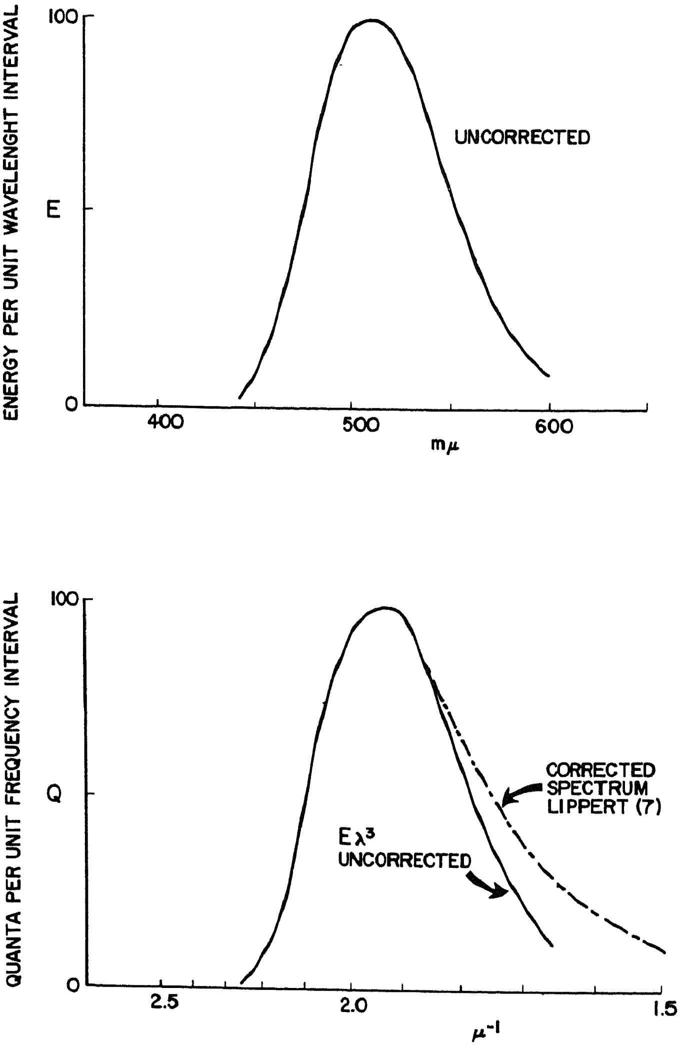

Figure 7. Fluorescence emission spectra of 3-aminophthalimde in 0.1 N H_2SO_4. Upper graph: uncorrected spectra at concentrations between 100 and 5 μg/ml (average figures). Lower graph: comparison between the uncorrected average spectrum and the corrected spectrum, both expressed as quanta per unit frequency interval.

fluorescence spectra which present energy less than 30% of the maximum. In the measurements here described the correction coefficients obtained with the tungsten lamp have been used.

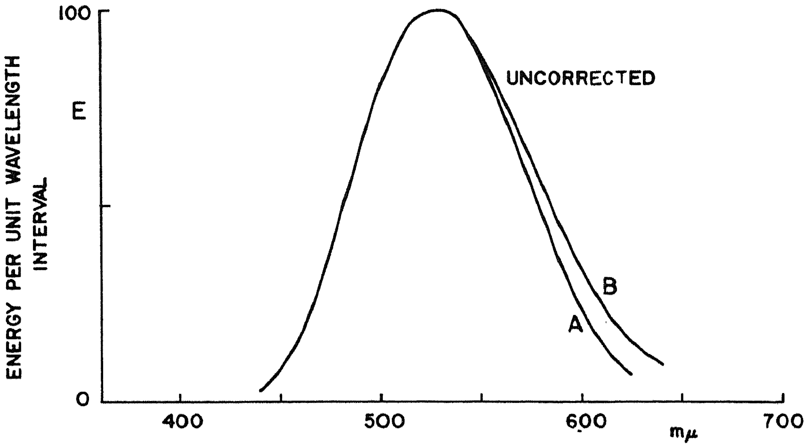

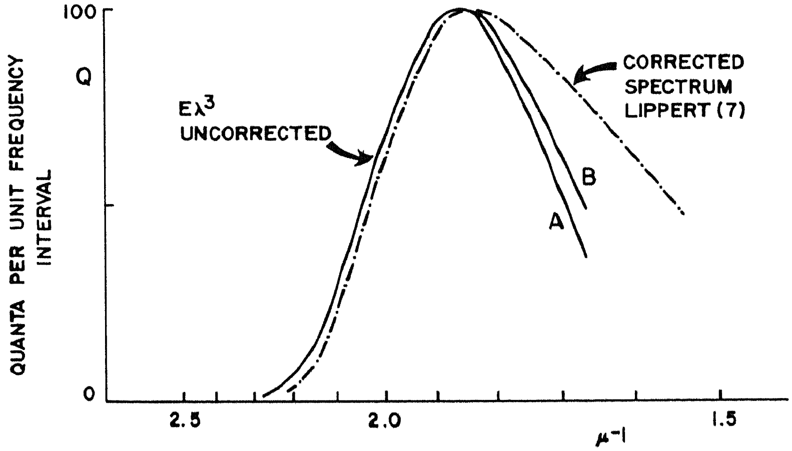

Figure 8. Fluorescence emission spectra of m-dimethyl-amino-nitrobenzene in 70% hexane-30% benzene. Upper graph: uncorrected spectra at concentrations between 200 and 100μg/ml at slit widths of 1.0 mm. (A), and 2.0 mm (B) (average figures). Lower graph: comparison between the uncorrected average spectra and the corrected spectrum; both expressed as quanta per unit frequency interval.

Fluorescence Emission Spectra of Anthracene

As a contribution to the possibility of applying the procedure here proposed for obtaining quantitative fluorescence spectra to practical problems, the fluorescence emission spectra of

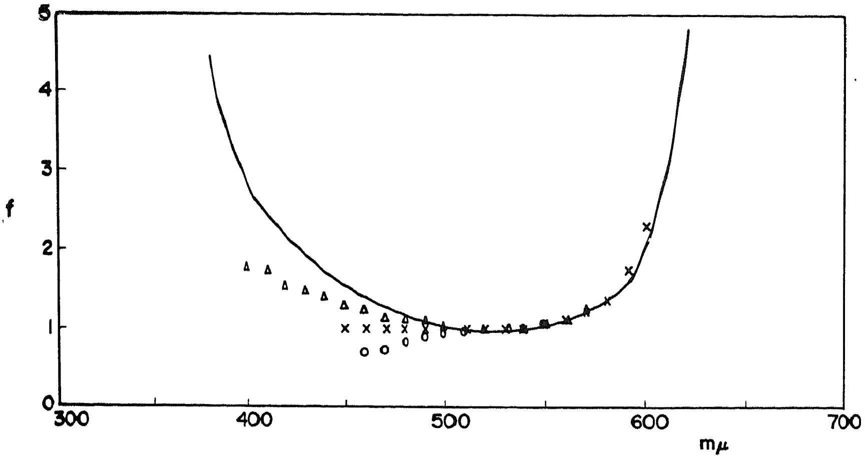

Figure 9. Correction coefficients f. Continuous line: calculated from the tungsten lamp radiation. Δ: calculated from quinine sulphate spectra (Figure 6). X: calculated from 3-amino-phthalimide spectra (Figure 7). O: calculated from m-dimethylamino-nitrobenzene spectra (Figure 8).

anthracene have been studied. The anthracene was an analytically pure sample and its solutions in ethyl alcohol have been subjected to measurements. The absorption spectrum of the substance is shown in Figure 10. Solutions with concentrations between 50 and 10 μg/ml have been measured and compared with solutions of equal concentrations of quinine sulphate in 0.1 N H_2SO_4, measured with the same experimental conditions. Each pair of apparent fluorescence spectra has been corrected by multiplying by the f coefficients and has been represented in quanta per unit frequency interval by multiplying by λ^3. The fluorescence intensity of quinine sulphate solutions has been put equal to 100 at 2.17 μ^{-1} (460 mμ) and the fluorescence spectra of anthracene at equal concentration have been correspondingly shifted.

The results are contained in Figure 11 and show some interesting facts. The best-resolved anthracene spectra are those obtained at high concentrations and small band width in the analyzing monochromator. At these high concentrations, however, a strong inner filter effect is observed. At lower concentrations it is necessary to operate with large band widths in the analyzing monochromator and this brings a much poorer resolution of the maxima and the loss of the first fluorescence band, corresponding to the 0-0 transition, at 2.64 μ^{-1} (380 mμ).

The present results can be compared with those of Parker and Rees [6]; placing the fluorescence intensity (corrected) of quinine sulphate equal to 1.00 at their maximum at 2.21 μ^{-1} (450 mμ), the fluorescence intensities (in quanta per unit frequency interval) of anthracene in their work are:

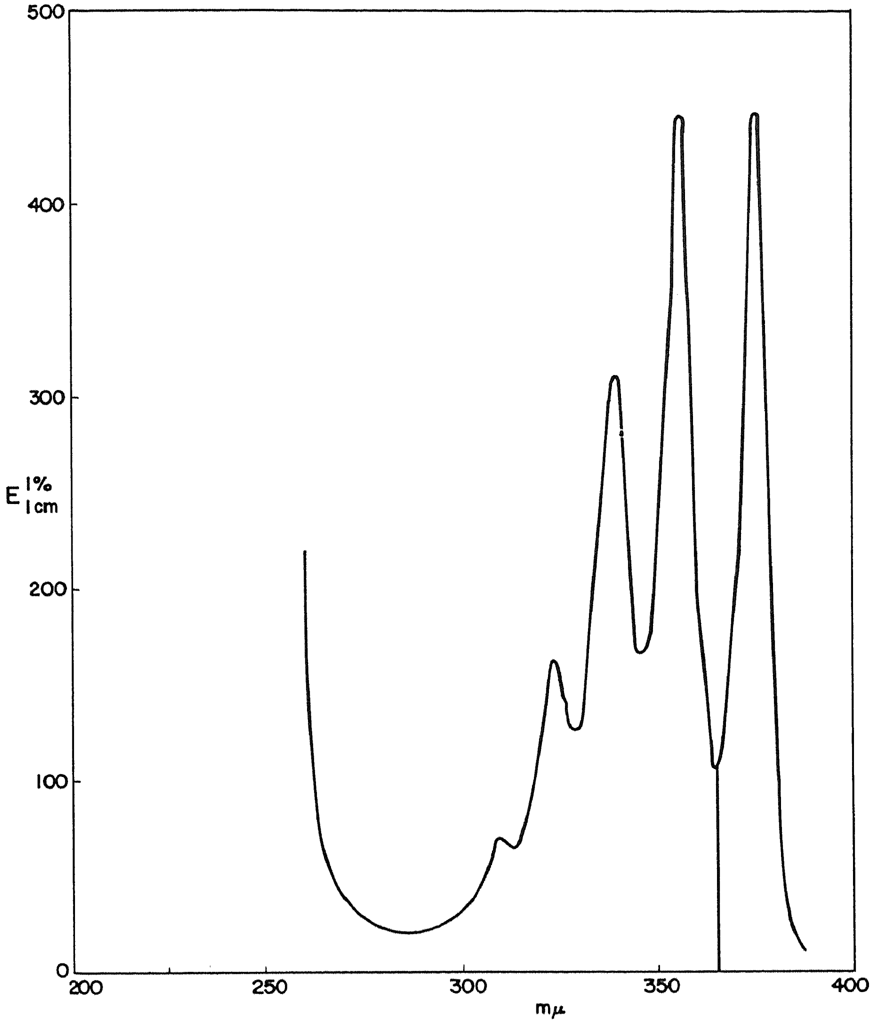

Figure 10. Absorption spectrum of anthracene in ethyl alcohol.

2.64 μ^{-1} (380 mμ)	1.56
2.50 μ^{-1} (400 mμ)	1.60
2.37 μ^{-1} (420 mμ)	0.88
2.26 μ^{-1} (440 mμ)	0.29

It may be interesting also to compare the present relative heights (corrected) of maxima of anthracene fluorescence spectra (in quanta per unit wavelength interval) with those reported in the literature, placing the maximum at 2.50 μ^{-1} (400 mμ) equal to 100.

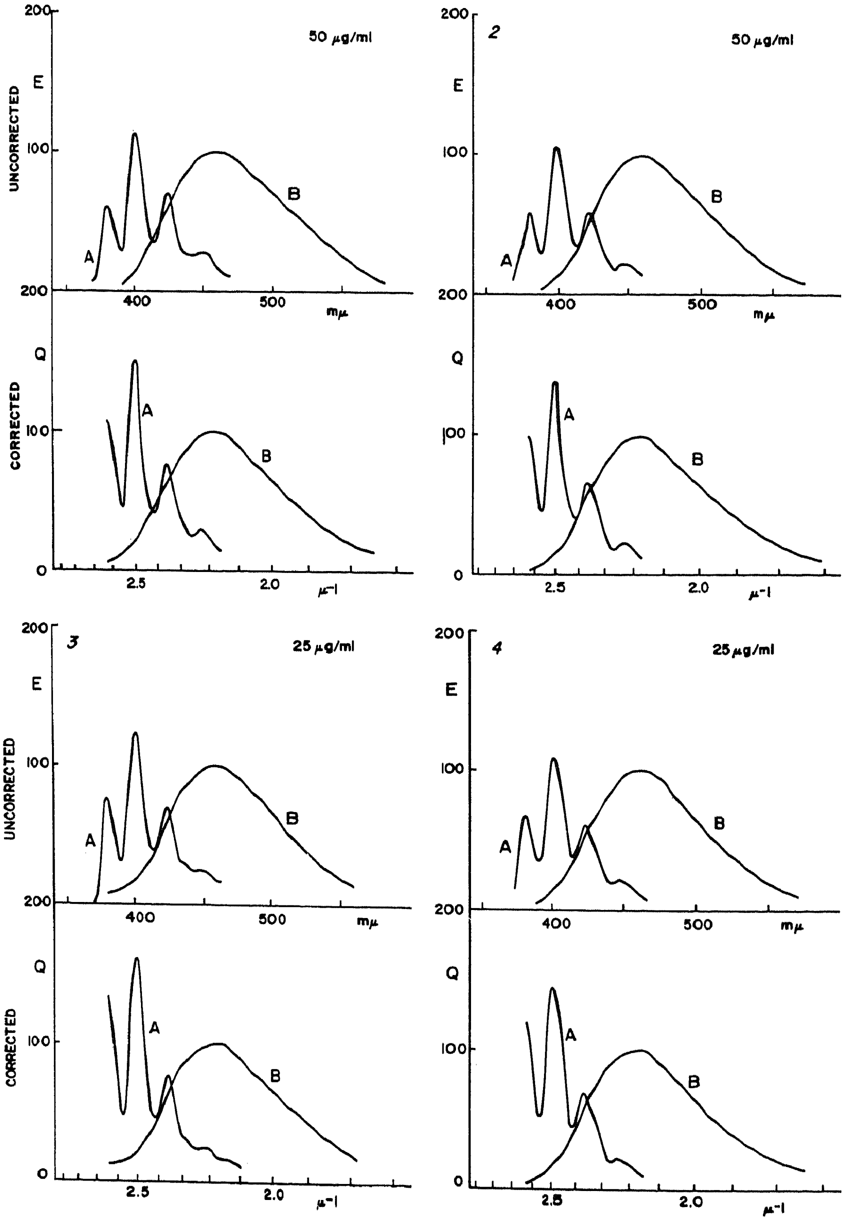

Figure 11. Uncorrected and corrected fluorescence emission spectra of anthracene (A) in ethyl alcohol against quinine sulphate (B) in 0.1 N H_2SO_4. Fluorescence intensities: E, energy per unit wavelength interval; Q, quanta per unit frequency interval.

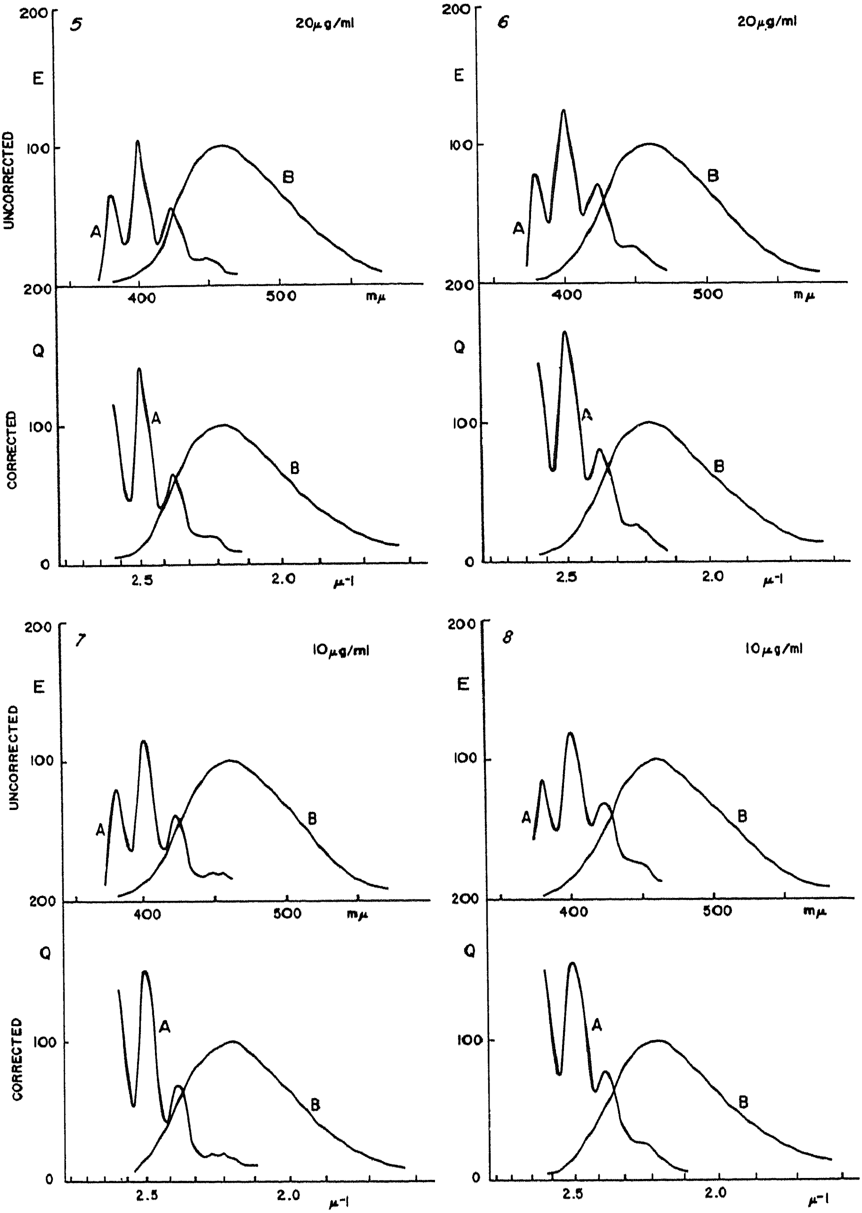

Figure 11. Uncorrected and corrected fluorescence emission spectra of anthracene (A) in ethyl alcohol against quinine sulphate (B) in 0.1 N H_2SO_4. Fluorescence intensities: E, energy per unit wavelength interval; Q, quanta per unit frequency interval. (Continued)

	Kortüm & Finckh [2]	Parker & Rees [6]	Lippert et al. [7]	Melhuish [8]
2.64 μ^{-1} (380 mμ)	81	98	(72)	74
2.50 μ^{-1} (400 mμ)	100	100	100	100
2.37 μ^{-1} (420 mμ)	53	55	52	53
2.26 μ^{-1} (440 mμ)	18	18	18	20

The discrepancies might be due to oxygen quenching; Parker and Rees [6] and Melhuish [8] have deareated their solutions, while in the present work the solutions were not oxygen-free. Another source of difference might be due to different resolving powers of the optical systems, to self-absorption, and to inaccuracies in the correction curves due to the fact that the intensity of the light emitted by the tungsten lamp in the violet region is more sensitive to the precise temperature at which the lamp is operated. The widest discrepancies occur in the 2.64 μ^{-1} (380 mμ) band where inner filter effect may have a great role, especially at high concentrations. Parker and Rees [6] have shown that with a viewing depth of 0.5 cm. a concentration of 17 μg/ml is sufficient to reduce the fluorescent intensity of the first vibration band of anthracene by about one third.

Fluorescence Emission Spectra of 3-Amino-Phthalimide

3-aminophthalimide was kindly supplied by Dr. Lippert. The product has been used in solution in 0.1 N H_2SO_4.

The fluorescence emission spectra (uncorrected and expressed in energy per unit wavelength interval) of solutions containing between 100 and 5 μg/ml, compared with those of quinine sulphate in 0.1 N H_2SO_4 at the same concentrations are shown in Figure 12 and clearly show the inner filter effect. The relative fluorescence intensity increases with the lowering of the concentration and this prevents obtaining a quantitative comparison in the concentration limits in which measurements have been carried out.

Fluorescence Emission Spectra of Riboflavine

Riboflavine offers an example of how quantitative fluorescence emission spectra can be obtained. Riboflavine and riboflavine phosphate $C_{17}H_{20}N_4O_9PNa.2H_2O$, mol. w. 514.4, have been used and their water solutions have been analyzed. The absorption spectrum of riboflavine in water is shown in Figure 13.

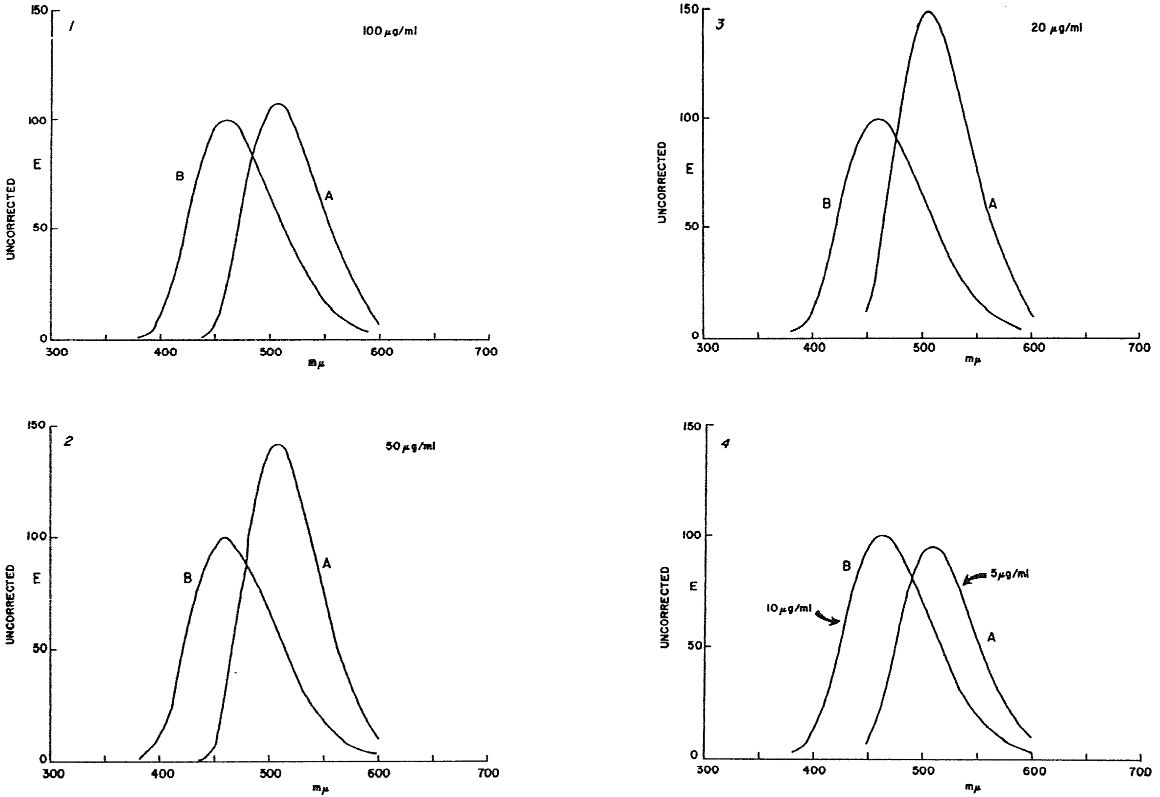

Figure 12. Uncorrected fluorescence emission spectra of 3-amino-phthalimide (A) in 0.1 N H_2SO_4 against quinine sulphate (B) in 0.1 N H_2SO_4. Fluorescence intensities E in energy per unit wavelength interval.

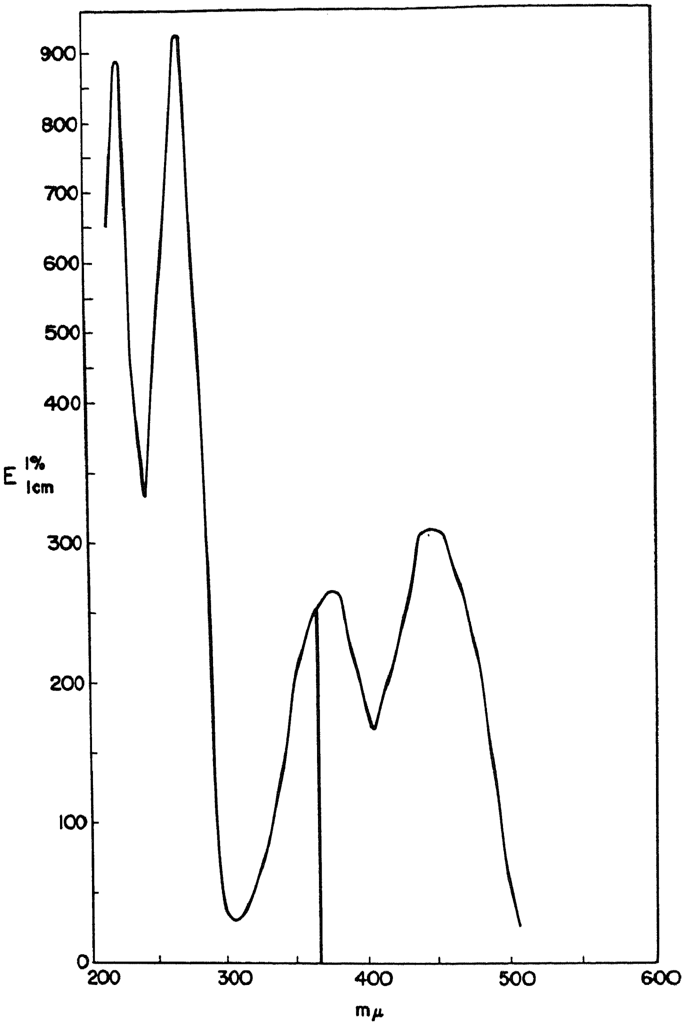

Figure 13. Absorption spectrum of riboflavine in water.

Figure 14 shows the uncorrected fluorescence emission spectra of riboflavin in water and of quinine sulphate in 0.1 N H_2SO_4 at equal concentrations between 20 and 2 μg/ml. (in energy per unit wavelength interval). Figure 15 shows the uncorrected fluorescence emission spectra of riboflavine phosphate in water and of quinine sulphate in 0.1 N H_2SO_4 at equal concentrations between 20 and 2 μg/ml (in energy per unit wavelength interval). The shape of the spectra of riboflavine and riboflavine phosphate are identical.

In Figure 16 the upper graph (1) shows the average of data of Figure 14 at concentrations between 10 and 2 μg/ml; the central

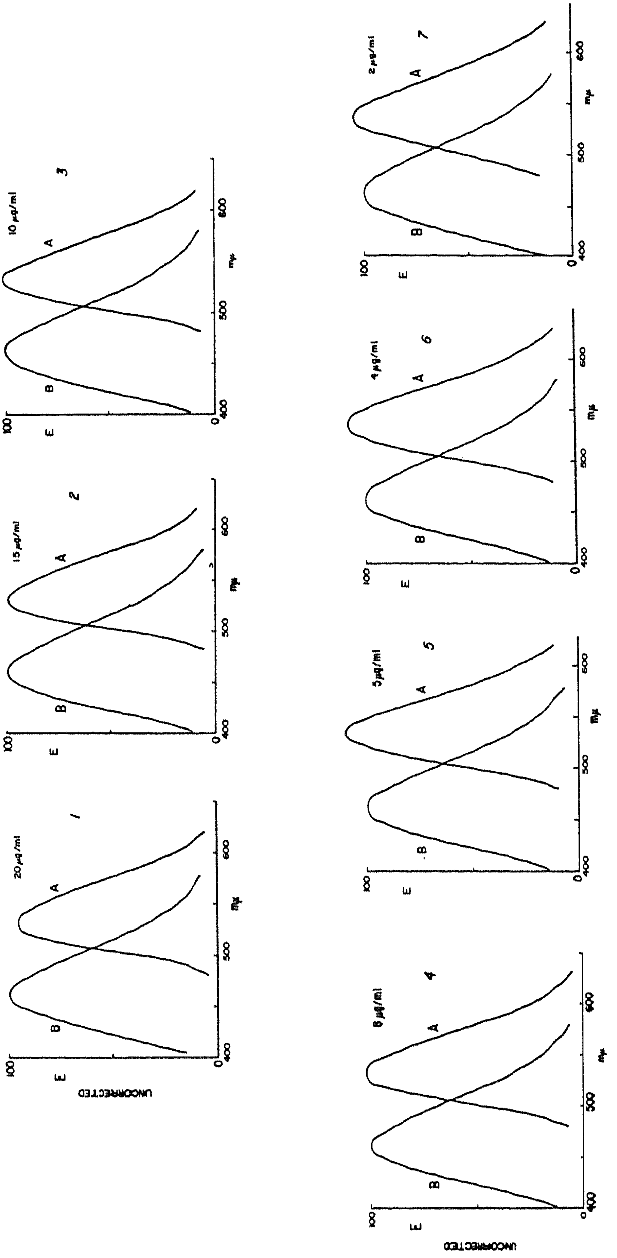

Figure 14. Uncorrected fluorescence emission spectra of riboflavin (A) in water against quinine sulphate (B) in 0.1 N H_2SO_4. Fluorescence intensities E in energy per unit wavelength interval.

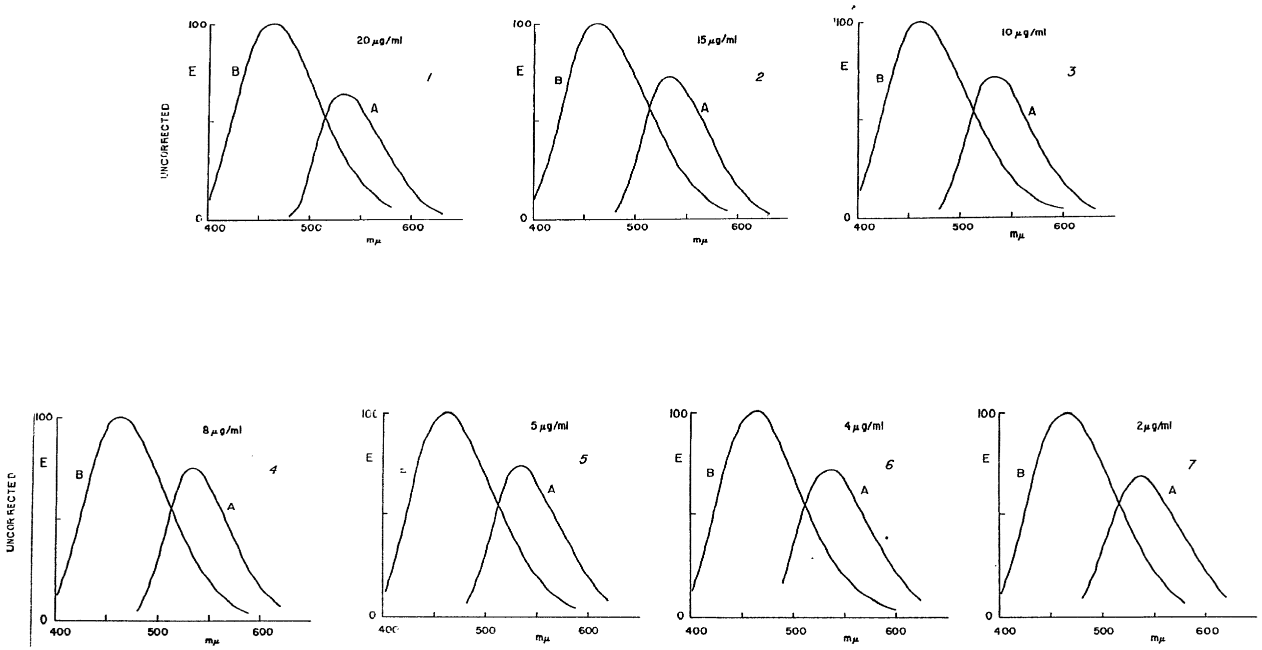

Figure 15. Uncorrected fluorescence emission spectra of riboflavin phosphate (A) in water against quinine sulphate (B) in 0.1 N H_2SO_4. Fluorescence intensities E in energy per unit wavelength interval.

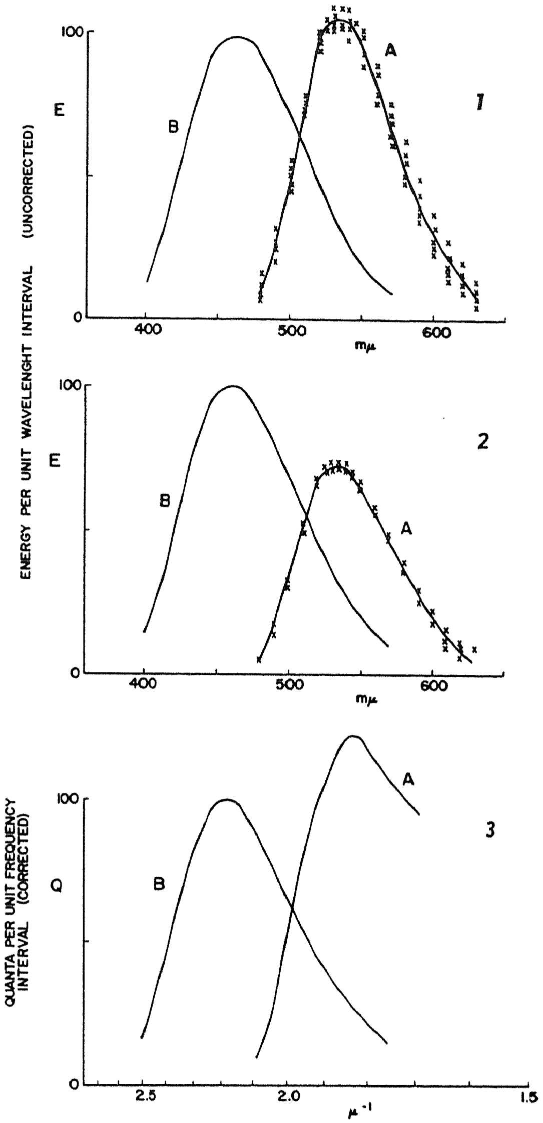

Figure 16. Graph 1. Uncorrected fluorescence emission spectrum of riboflavine (A) against quinine sulphate (B): average of the figures of Figure 14. Graph 2. Uncorrected fluorescence emission spectrum of riboflavine phosphate (A) against quinine sulphate (B): average of the figures of Figure 15. Graph 3: Corrected fluorescence emission spectrum of riboflavine in water (A) against quinine sulphate (B) in 0.1 N H_2SO_4, both expressed as Q, quanta per unit frequency interval.

graph (2) shows the average of the data of Figure 15 at concentrations between 15 and 2 μg/ml. The average relative (to quinine sulphate) uncorrected fluorescence intensities at their maxima for riboflavine and riboflavine phosphate are 105 and 73, very near to the reciprocal ratio of their molecular weights, 376 and 514.4, respectively. This demonstrates that in riboflavine phosphate the riboflavine group only is responsible for the fluorescence and that the esterification does not change at all the fluorescence shape and intensity. The fluorescence emission spectrum of riboflavine alone therefore presents interest and this spectrum (Figure 16-1) has been corrected with the described procedure.

The corrected fluorescence spectrum, relative to quinine sulphate, is shown in Figure 16-3, represented in quanta per unit wavelength interval. The fluorescence intensity at the maximum at 1.83 μ^{-1} (545 mμ) is 1.22 times the fluorescence intensity at 2.17 μ^{-1} (460 mμ) of a solution of equal concentration of quinine sulphate in 0.1 N H_2SO_4. This means that the concentration of a solution of riboflavine in water can be obtained with the following procedure:

(a) determination of the fluorescence emission spectra of the solution and, with the same conditions, of a solution of quinine sulphate in 0.1 N H_2SO_4 at the concentration c, using the exciting radiation at 2.73 μ^{-1} (366 mμ);

(b) correction of the fluorescence emission spectra;

(c) if the fluorescence intensity (corrected and in quanta per unit frequency interval) of the quinine sulphate solution is A at 2.17 μ^{-1} (460 mμ) and the corresponding fluorescence intensity of the riboflavine solution is B at 1.83 μ^{-1} (545 mμ), the concentration x of the riboflavine solution is given by

$$\underline{x} = \frac{\underline{c}\,\underline{A}}{\underline{B}}\,1.22$$

if the same units are chosen for c and x and for A and B.

ACKNOWLEDGMENTS

This work has been made possible by the financial support of Consiglio Nazionale delle Ricerche, Roma. Thanks are due to Dr. Lippert and Dr. Melhuish for samples of their reference compounds and to Dr. Parker and Dr. Chapman for their valuable comments.

Finally, it is a pleasure to acknowledge the assistance rendered by Dr. Notarnicola and Dr. Mastrorilli in the experimental work and for helping to carry out the large number of calculations needed to evaluate the results.

REFERENCES

1. G. Nebbia, Boll. Sci. Fac. Chim. Ind., 18, 35 (1960).
2. G. Kortüm and B. Finckh, Spectrochim. Acta, 2, 137 (1941).
3. C. A. Parker and W. T. Rees, Analyst, 87, 83 (1962).
4. R. A. Burdett and L. C. Jones, Jr., J. Opt. Soc. Am., 37, 554 (1947).
5. C. A. Parker and W. J. Barnes, Analyst, 82, 606 (1957).
6. C. A. Parker and W. T. Rees, Analyst, 85, 587 (1960).
7. E. Lippert, W. Nägele, I. Seibold-Blankenstein, U. Staiger and W. Voss, Z. Anal. Chem., 170, 1 (1959).
8. W. H. Melhuish, J. Phys. Chem., 64, 762 (1960).

TOTAL LUMINESCENCE OF ORGANIC MOLECULES OF PETROCHEMICAL INTEREST

I. NAPHTHALENE, PHENANTHRENE AND 1,2,4,5–TETRAMETHYLBENZENE

S. P. McGlynn, B. T. Neely, and W. C. Neely
Coates Chemical Laboratories
Louisiana State University
Baton Rouge 3, Louisiana, U.S.A.

INTRODUCTION

The use of phosphorimetry as an analytical tool was first suggested and applied by Keirs, Britt and Wentworth [1]. The work of these authors demonstrated the feasibility of using spectroscopic resolution of phosphorescence and the time discrimination of a phosphoroscope to identify and quantify the components of various binary mixtures. No published work has thus far utilized selective excitation techniques (i.e., variation of the exciting wavelength) in conjunction with phosphorimetry to similarly identify and quantify components of a mixture; nor has any attempt been made to compare the sensitivities of room temperature fluorescence (35°C), low temperature fluorescence (-195.8°C), low temperature phosphorescence (-195.8°C) and room temperature absorption (35°C) with regard to their identification and quantification capabilities. Such is the aim of the present work.

It is well at this time to point out a prejudice of the authors: they regard low temperature fluorimetry and phosphorimetry as being mutually complementary rather than independent techniques. They believe that maximum usefulness results from quantification of both the fluorescence, phosphorescence, and excitation spectra of the pure components, and that any mixture of these luminescent species may then be readily analyzed and quantified. Only in the rare event that *all spectra* of two substances are completely superposable would their mutual analysis in a mixture be rendered impossible by this method, and in this case time-resolution of the phosphorescence should generally suffice to make it possible again.

In this investigation the fluorescence (at 77°K in a glass matrix and at 35°C in a liquid solution) and the phosphorescence of naphthalene, phenanthrene and 1,2,4,5-tetramethylbenzene have been studied. The quantification data so obtained have then been applied to analysis of a blend in which the ratio by weight of these three components was 1:1:1.

EXPERIMENTAL

Apparatus

An Aminco-Keirs Spectrophosphorimeter and an Aminco-Bowman Spectrophotofluorometer in combination with an X-Y recorder and an RCA 1P-28 photomultiplier tube were used to obtain spectra and decay curves. The sample geometry for both 77°K and 35°C experimentation is shown in Figure 1. The cylindrical quartz tubes employed at the former temperature were of 2 mm internal diameter, while those used at 35°C were 1 cm square quartz cells. Ultraviolet absorption spectra were obtained at room temperature using a Cary-14 Spectrophotometer with both 1 and 0.1 cm quartz cells.

Materials

The low temperature glass matrix consisted of EPA obtained from the American Instrument Company.* The background luminescence of this glass was observable only at the most sensitive settings of the luminescence metering systems. The room temperature solvent was a Harleco fluorometric grade *n*-heptane;† there was no observable luminescence and only slight scatter from this solvent at room temperature when using the slits employed throughout this work.

Procedure

Excitation and emission spectra, both fluorescence and phosphorescence were obtained at 77°K for each of the three compounds and suitable excitation and emission wavelengths were chosen. A series of solutions of varying concentrations in EPA mixed solvent was then prepared for each of the compounds.

---

*The American Instrument Company, 8030 Georgia Avenue, Silver Spring, Maryland.

†Hartmann-Leddon Company, Philadelphia, Pennsylvania.

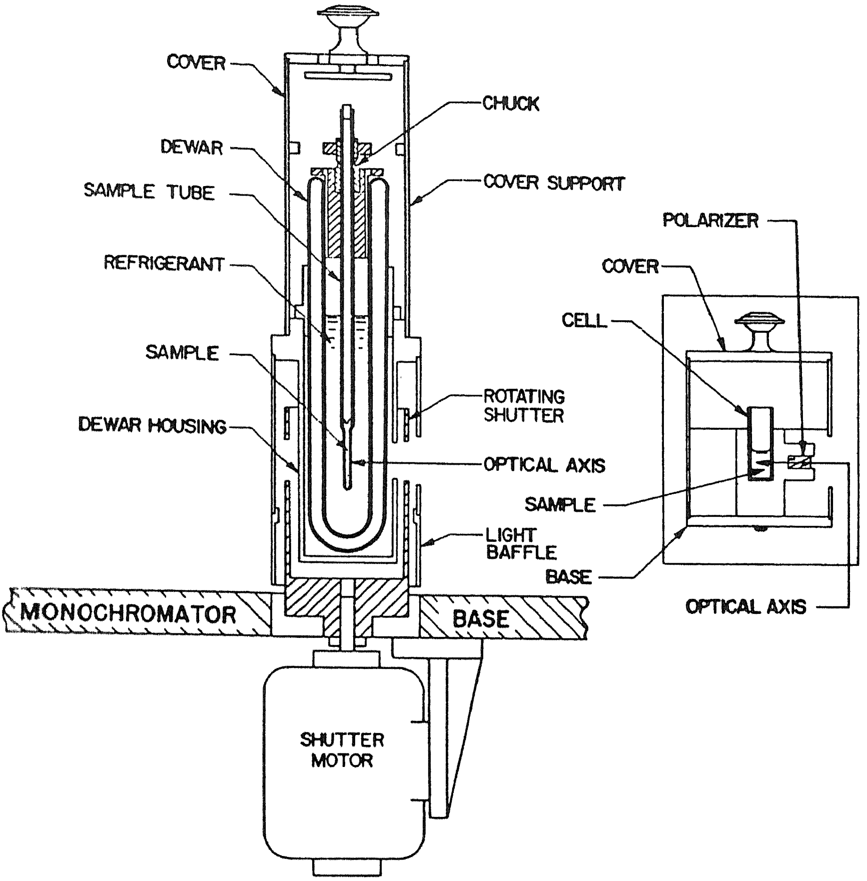

Figure 1, Left: Sample geometry for phosphorescence at 77°K. This same geometry, with the rotating shutter removed, was used for fluorescence at 77°K. The diagram is self-explanatory. Right: Sample geometry for fluorescence at 35°C. The use of polarizers enables one to eliminate scatter; they were not used, nor was such use necessary, in the present work.

The intensity of emission at the optimum wavelengths was measured for the individual solutions. To obtain easily reproducible and accurate results, it was found necessary to remove the cover from the sample compartment of the instrument, and, having provided suitable shielding from stray room light, to manually rotate the chuck which holds the sample tube until a maximum intensity reading was obtained.

A series of solutions of varying concentration in *n*-heptane was prepared for each compound and emission intensities were measured at room temperature (35°C) for the solutions. No difficulties were encountered in the placement of the 1 cm.^{2} cell.

RESULTS

The phosphorescence decays of the three compounds in EPA at 77°K are shown in Figure 2. The lifetimes are tabulated in Table 1. Since all three lifetimes are relatively long and not too different, no significant discrimination may be effected by variation of phosphoroscope speed.

The various emission and excitation spectra of the pure aromatics are shown in Figures 3, 4 and 5. The wavelengths of the maxima of intensities are tabulated in Table 1. A reproducible linear relationship between emitted radiant intensity and concentration was found for each of the three compounds. The maximum and minimum concentrations which may be accurately determined under the conditions of the experiment are shown in

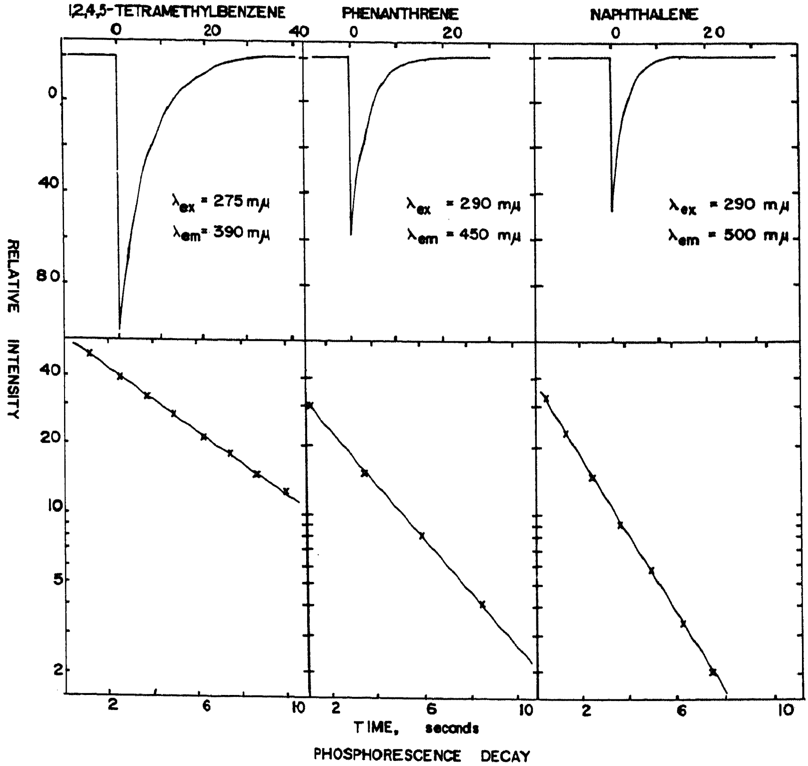

Figure 2. The phosphorescent decay of naphthalene (right), phenanthrene (middle), and 1,2,4,5-tetramethylbenzene (left).

Table 1

Phosphorescence Lifetimes and Vibronic Peaks[a]

Compound	$\tau_{1/2}$	LTF[b]	LTP[c]	LTE[d]
Naphthalene	1.75 sec	314mμ 327mμ 335mμ 342mμ	463mμ 474mμ 497mμ 580mμ	221mμ 267mμ 275mμ 282mμ
Phenanthrene	2.6 sec	348mμ 354mμ 363mμ 382mμ 405mμ	462mμ 470mμ 498mμ 538mμ	305mμ 325mμ 332mμ 340mμ
Tetramethylbenzene	4.5 sec	310mμ	375mμ 387mμ 392mμ	225mμ 275mμ

[a] Underlined wavelengths are the most intense, and therefore most sensitive analytically.

[b] Low temperature fluorescence (77°K).

[c] Low temperature phosphorescence (77°K).

[d] Low temperature excitation (77°K).

Table 2, and the working curves are given in Figures 6-8, inclusive. It is possible to conclude from the data of Table 2 that phosphorimetry (1) is of comparable sensitivity to any of the other techniques, and (2) may be used to higher concentrations than fluorimetry, presumably because of less self-absorption. It is further evident from Figures 3, 4 and 5 that the phosphorescence spectrum contains more *apparent* resolution than the fluorescence spectrum, and that it should, if anything, be a better characterization spectrum than fluorescence.

Analysis of the previously specified blend was attempted. It is clear from Figures 3, 4 and 5 that 340mμ excitation should produce only phenanthrene emission since neither of the other two components absorb in this region. That such is the case is very clearly illustrated in Figure 9, and the resulting phosphoroscopic analysis for phenanthrene is shown in Table 3. Excitation at 275mμ enables one to excite the tetramethylbenzene luminescence, and to spectrally distinguish the phosphorescence. Excitation at 275mμ maximizes the naphthalene fluorescence which is spectrally quite distinct (see excitation at 290mμ in Figure 9). There should then be no difficulty in determining any component of the ternary solution; an effort to do such resulted in the data of Table 4. At concentrations above 0.01

Table 2

A Comparison of Methods of Determination[a]

Compound	1,2,4,5-Tetramethylbenzene	Naphthalene	Phenanthrene
Low Temperature Phosphorescence SLITS:[b] 5 -2 -2 -4 -3	λ ex = 275mμ λ em = 392mμ MAX. = 1.34 mg/ml. MIN. = 0.0018 mg/ml.	λ ex = 310mμ λ em = 475mμ MAX. = 1.4 mg/ml. MIN. = 0.0007 mg/ml.	λ ex = 340mμ λ em = 465mμ MAX. = 0.5 mg/ml. MIN. = 0.001 mg/ml.
Low Temperature Fluorescence SLITS:[b] 3 -2 -2 -1 - 0.5	λ ex = 225mμ λ em = 285mμ MAX. = 1.00 mg/ml. MIN. = 0.0007 mg/ml.	λ ex = 275mμ λ em = 320mμ MAX. = 0.100 mg/ml. MIN. = 0.00058 mg/ml.	λ ex = 300mμ λ em = 340mμ MAX. = 0.03 mg/ml. MIN. = .0002 mg/ml.
Room Temperature Fluorescence SLITS:[c] 5 -2 -2 -2 - 2 -3 -2	λ ex = 260mμ λ em = 298mμ MAX. = 0.50 mg/ml. MIN. = 0.001 mg/ml.	λ ex = 310mμ λ em = 335mμ MAX. = 0.100 mg/ml. MIN. = 0.005 mg/ml.	λ ex = 325mμ λ em = 368mμ MAX. = 0.500 mg/ml. MIN. = 0.0015 mg/ml.
Ultraviolet Absorption 275mμ Using 1cm. and .1cm cells only	MAX. = 0.6 mg/ml. MIN. = 0.01 mg/ml.	MAX. = 0.400 mg/ml. MIN. = 0.0007 mg/ml.	MAX. = 0.100 mg/ml. MIN. = 0.0015 mg/ml.

[a] The phosphorescence results for the three compounds are intercomparable, as are both sets of fluorescence results. However, one set is not strictly comparable with another set since different slit-widths were used. However, in a practical sense the use of larger slit widths should not have significantly increased the sensitivity of either method, since there are background scatter and spurious emission effects to be contended with. It is implied then that the three sets of data (i.e., phosphorescence, fluorescence and room temperature fluorescence) are indeed truly comparable.

[b] The order of slits is A, B, C, D and E; the numbers quoted are slit widths in mm; the positions of these slits is described in the operating instructions for the Aminco-Keirs Spectrophosphorimeter.

[c] The order of slits is 1, 2, 3, 4, 5, 6, 7; the numbers quoted are slit widths in mm; the positions of these slits is described in the operating instructions for the Aminco-Bowman Spectrophotofluorometer.

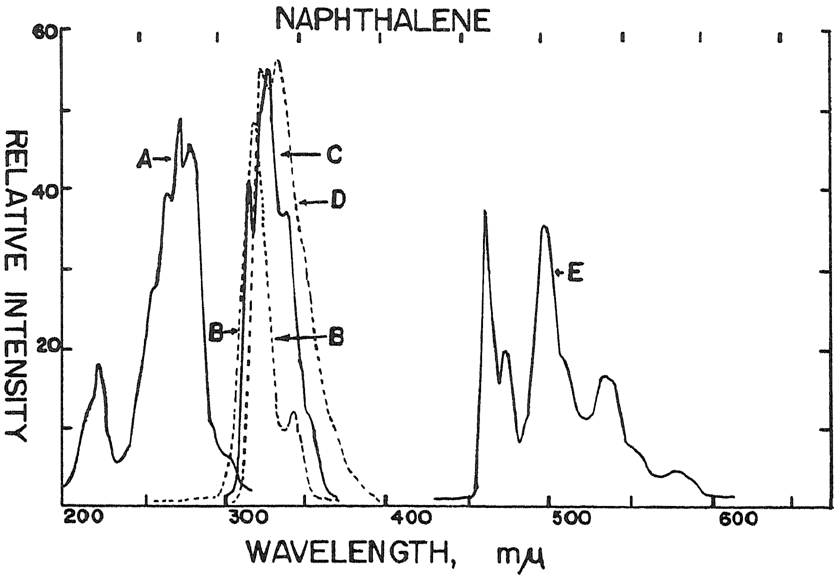

Figure 3. The fluorescence excitation spectrum (A), the fluorescence spectrum (C) and the phosphorescence spectrum (E) of naphthalene at 77°K in EPA; the fluorescence excitation spectrum (B) and fluorescence spectrum (D) of naphthalene in *n*-heptane at 35°C. It is not intended that this diagram reflect true relative intensities and the spectra are presented merely to show the spectral discrimination which is possible. Quantitative data are available from Fig. 6 and Table 2.

Table 3

Determination of Phenanthrene in a Three Component Mixture of 1 Part Phenanthrene: 1 Part Naphthalene: 1 Part 1,2,4,5-Tetramethylbenzene[a]

Known Concentration (mg/ml.)	Concentration as Determined From Working Curve (mg/ml.)
0.010	0.010
0.0010	0.0011
0.0005	0.0007
0.0001[b]	0.0002

[a] $\lambda_{ex} = 340 m\mu$; $\lambda_{em} = 460 m\mu$.

[b] Smaller than minimum amount that may be determined under the given conditions.

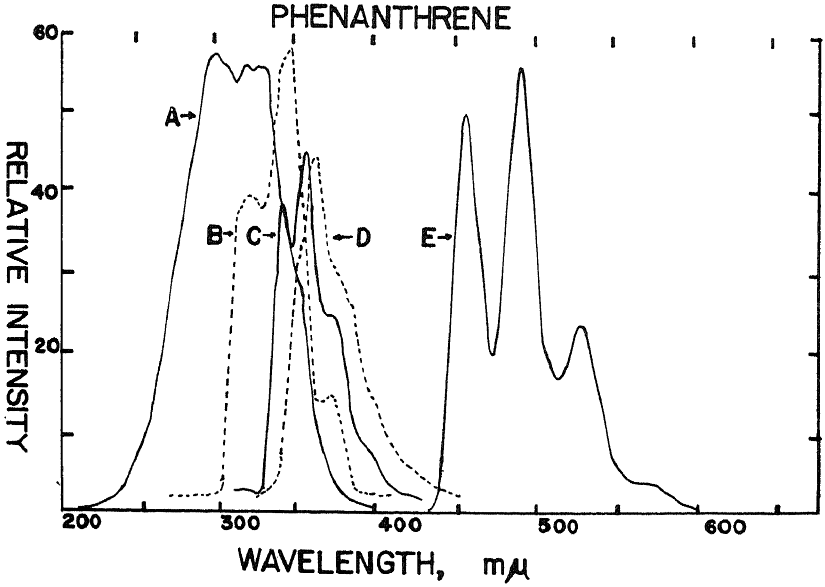

Figure 4. Fluorescence excitation spectrum (A), fluorescence spectrum (C) and phosphorescence spectrum (E) of phenanthrene at 77°K in EPA; fluorescence excitation spectrum (B) and fluorescence spectrum (D) of phenanthrene in *n*-heptane at 35°C. It is not intended that this diagram reflect true relative intensities and the spectra are presented merely to show the spectral discrimination which is possible. Quantitative data are available from Fig. 7 and Table 2.

Table 4

Determination of Phenanthrene, Naphthalene and 1,2,4,5-Tetramethylbenzene in the Blend

Component	Naphthalene	Phenanthrene	Tetramethylbenzene
Technique	Fluorescence	Phosphorescence	Phosphorescence
λ_{ex} (mμ)	375	340	275
λ_{em} (mμ)	320	460	392
Introduced (mg/ml.)	0.01	0.01	0.01
Measured (mg/ml.)	0.006	0.01	0.007

mg/ml competitive absorption processes made estimation of both naphthalene and tetramethylbenzene impossible, while at concentrations much below 0.01 mg/ml the sensitivity decrease renders accuracy poor.

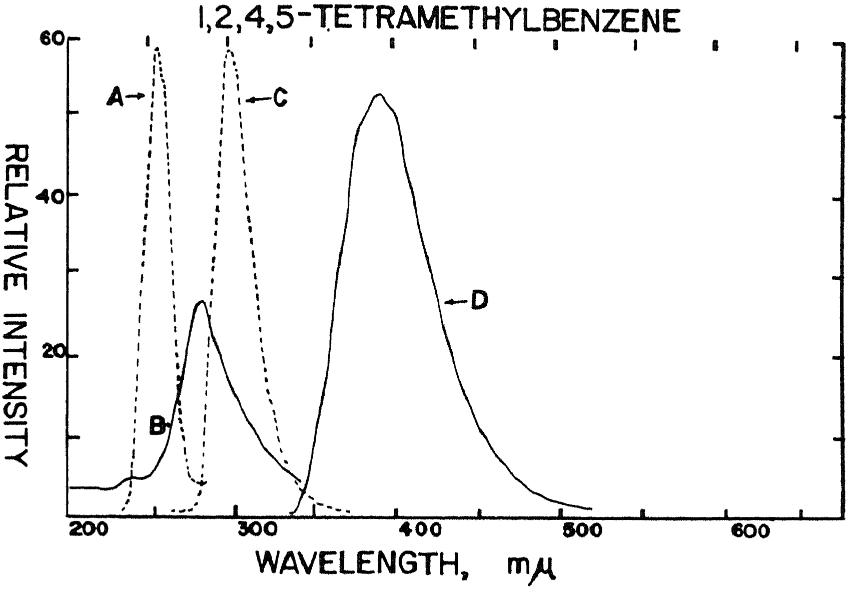

Figure 5. Phosphorescence excitation spectrum (B) and phosphorescence spectrum (D) of 1,2,4,5-tetramethylbenzene in EPA at 77°K; fluorescence excitation spectrum (A) and fluorescence spectrum (C) of 1,2,4,5-tetramethylbenzene in *n*-pentane at 35°C. It is not intended that this diagram reflect true relative intensities and the spectra are presented merely to show the spectral discrimination which is possible. Quantitative data are available from Fig. 8 and Table 2.

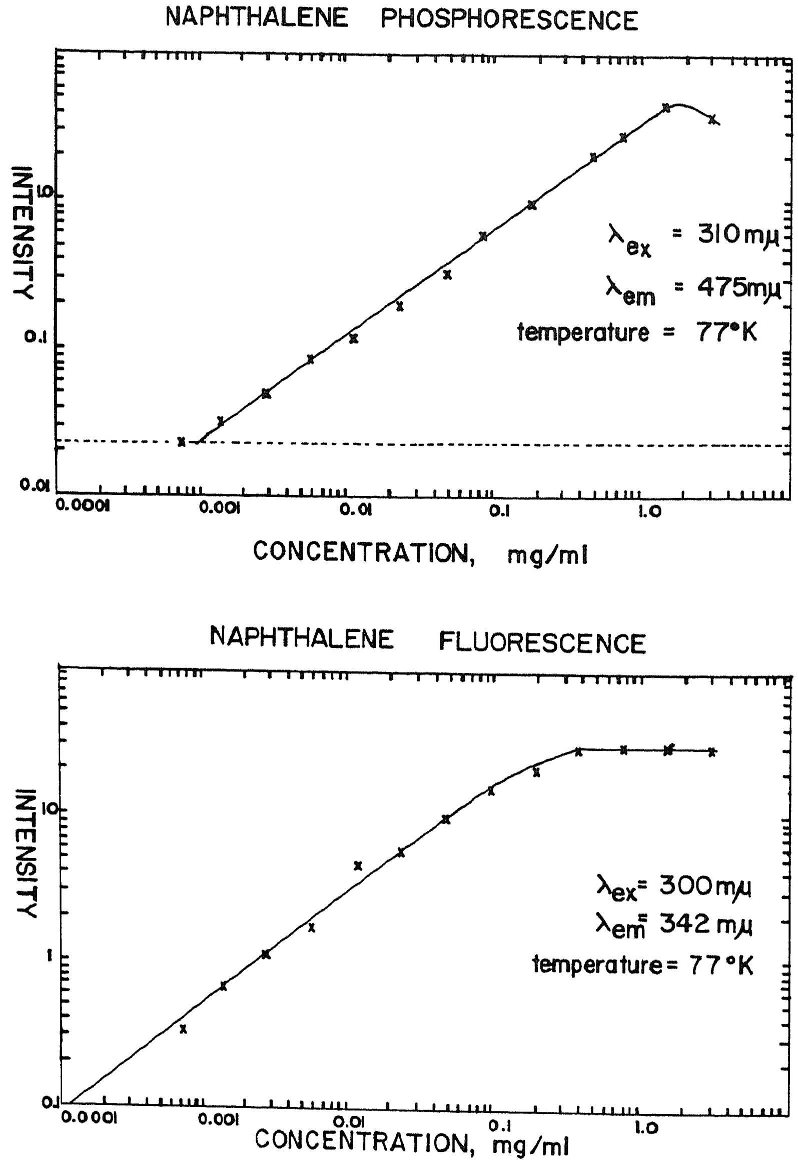

Figure 6. Working curves for naphthalene. A – phosphorescence at 77°K, B – fluorescence at 77°K.

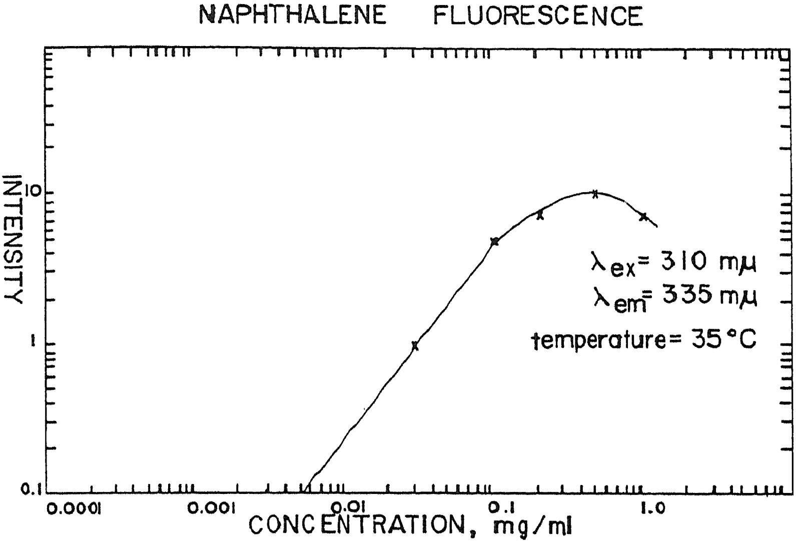

Figure 6. Working curves for naphthalene. C - fluorescence at 35°C. The slits used are specified in Table 2.

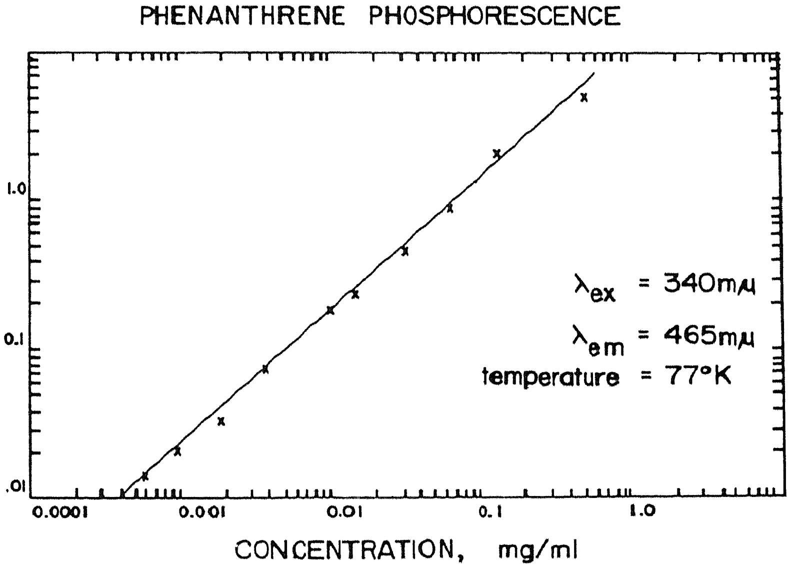

Figure 7. Working curves for phenanthrene. A - phosphorescence at 77°K.

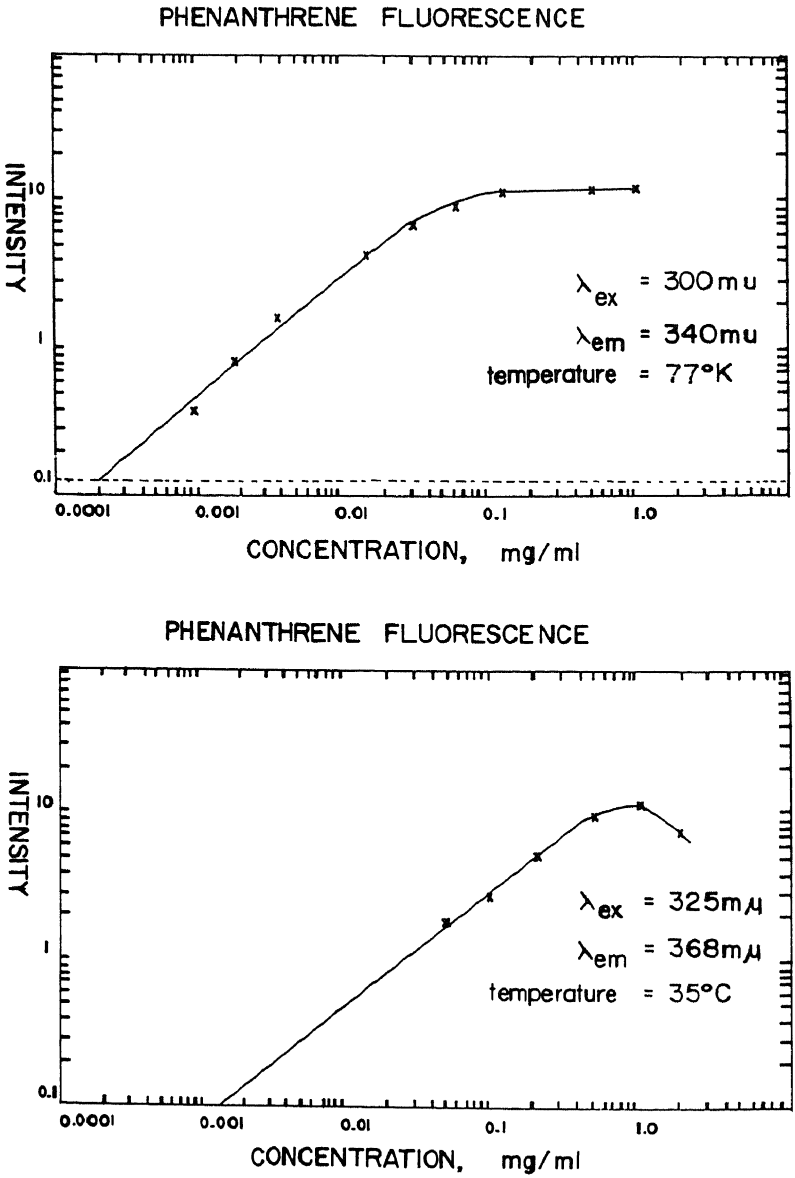

Figure 7. Working curves for phenanthrene. B – fluorescence at 77°K, C – Fluorescence at 35°C. The slits used are specified in Table 2.

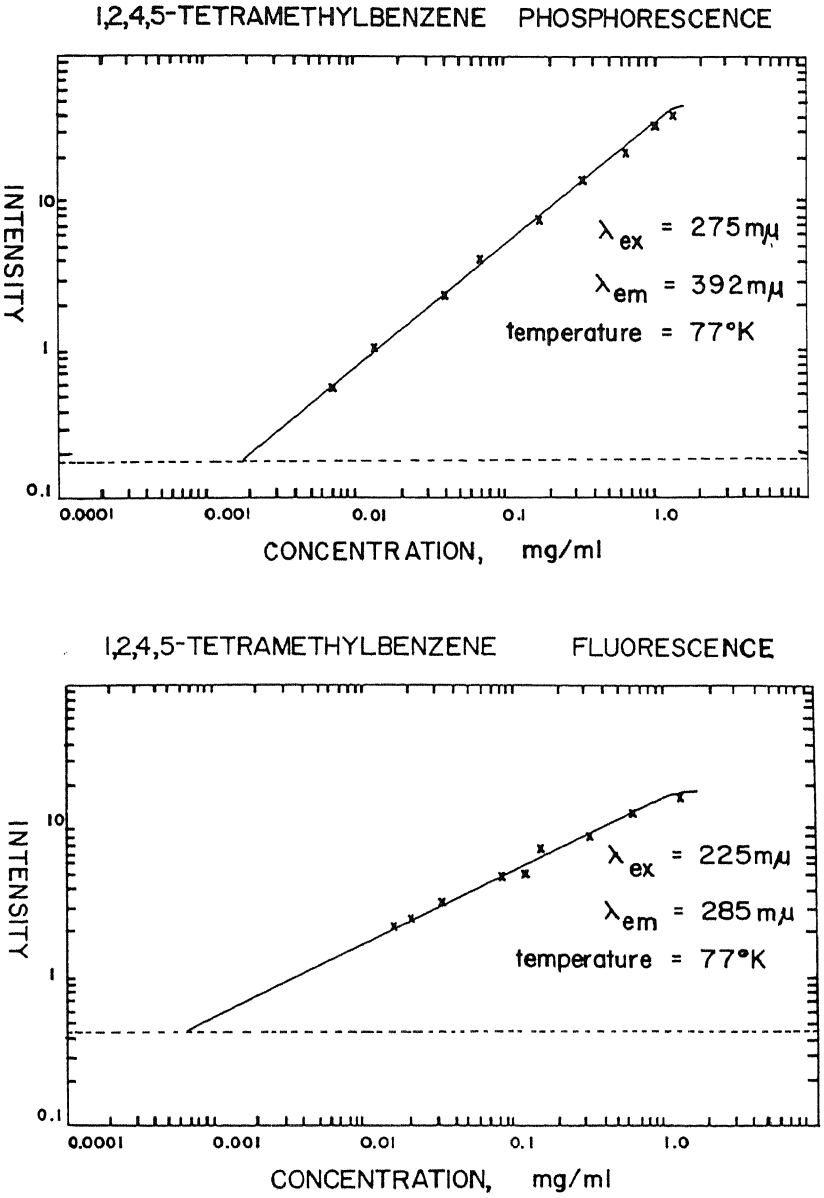

Figure 8. Working curves for 1,2,4,5-tetramethylbenzene. A - phosphorescence at 77°K, B - fluorescence at 77°K.

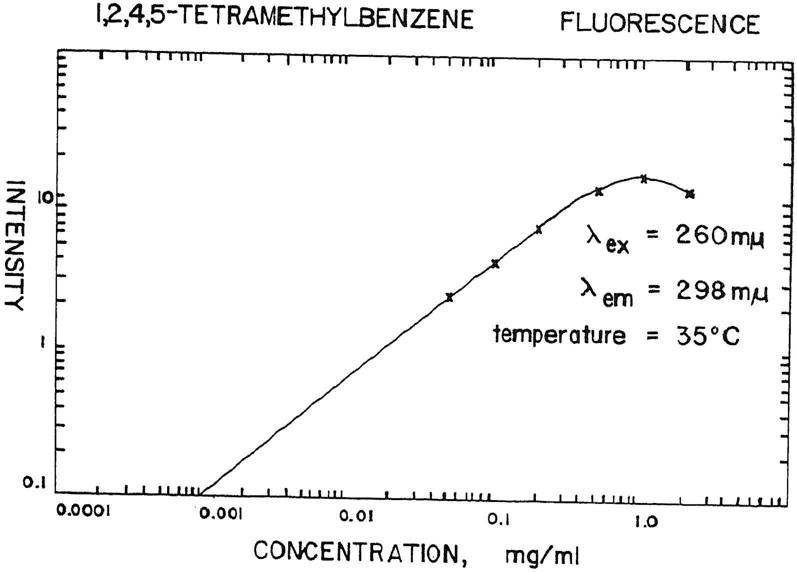

Figure 8. Working curves for 1,2,4,5-tetramethylbenzene. C - fluorescence at 35°C. The slits used are specified in Table 2.

ACKNOWLEDGMENT

The authors wish to thank the American Instrument Company for their support of this work. They also thank Dr. Friedel and Dr. Blaustein for their gift of a very pure phenanthrene sample.

REFERENCE

1. R. J. Keirs, R. D. Britt, Jr., and W. E. Wentworth, Anal. Chem. 29, 202 (1957).

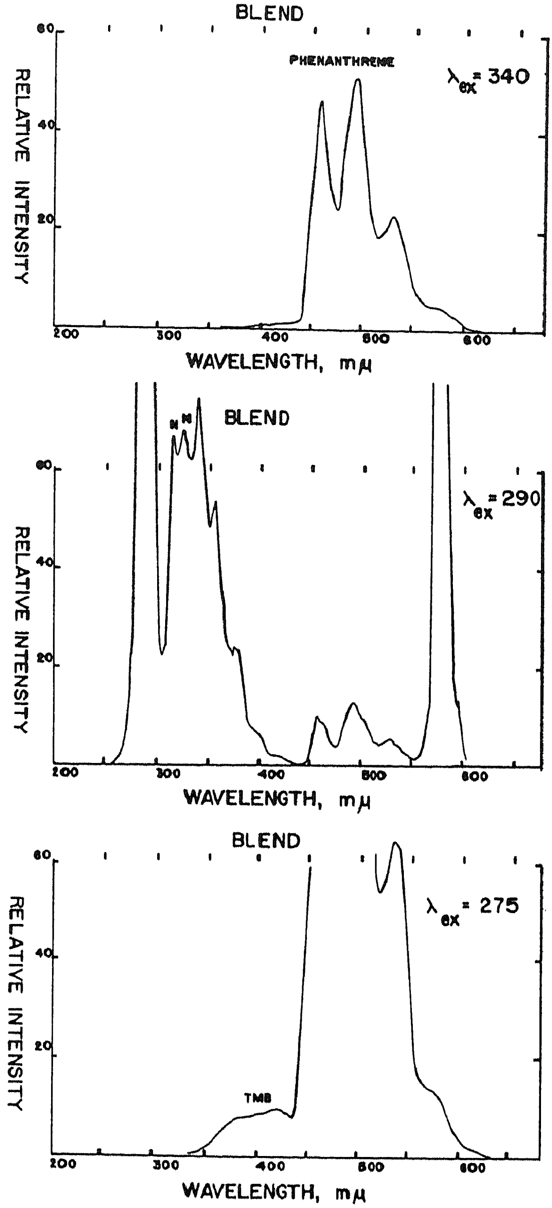

Figure 9. Phosphorescence of blend excited at 340mμ (top), phosphorescence of blend excited at 275mμ (bottom) and total emission of blend excited at 290mμ (middle). It is to be noted that the top spectrum is the phosphorescence of phenanthrene only, that the bottom spectrum contains the phosphorescence of 1,2,4,5-tetramethylbenzene well-resolved spectrally and that the fluorescence of naphthalene (denoted N) is quite distinct, spectrally, on the middle spectrum.

CHEMICAL APPLICATIONS OF NUCLEAR MAGNETIC RESONANCE

R. E. Richards
Physical Chemistry Laboratory
South Park Road
Oxford, England

When a nucleus of spin quantum number, I, is placed in a strong uniform magnetic field, H, a number of energy levels become available to it by virtue of the interaction between the nuclear moment and the field, H. There are (2I + 1) energy levels, corresponding to different allowed orientations of the nuclear magnet with respect to the applied field, H, and when transitions of the nuclei are induced among these energy levels by radiofrequency radiation a nuclear resonance spectrum may be observed.

The frequency of radiation required to induce magnetic resonance is ν_o, where

$$\nu_o = \frac{\mu H}{Ih}, \tag{1}$$

μ is the magnetic moment of the particle and h is Planck's constant.

These spectra are often complex and contain a wealth of information which can frequently be of great help to the chemist.

The properties of the nuclear resonance spectrum depend on interactions between the extra-nuclear electrons and the applied magnetic field, on mutual interactions between the magnetic moments in the sample, which may be transmitted in a number of ways, and on interactions between *electric* field gradients at the nucleus and the nuclear *electric* quadrupole moment. These effects will be considered in turn and their usefulness to the chemist will be discussed.

The magnetic field, H, in equation (1) is the field actually experienced by the nucleus; this often differs from the field of the laboratory magnet, H_0, because of interactions between the applied field and the extranuclear electrons, so that we write

$$H = H_0(1 - \sigma) .$$

The applied field, H_0, induces diamagnetic moments in the extranuclear electrons which oppose H_0 and are proportional to it, and these are represented by the factor σ. The different electron distributions about a given nucleus characteristic of different chemical environments are associated with different values of σ, and it is these variations which are responsible for the so-called "chemical shifts" in nuclear resonance spectra. The range of values of σ varies from one atom to another; in proton resonance spectra σ varies over about 20 p.p.m. whereas cobalt resonances show shifts of as much as 2%. The detailed theory has been given by Ramsey [1] but this cannot be applied rigorously to complex molecules. Attempts to apply M.O. and V.B. theories have had only limited success and the chemical applications of these effects rest on semi-empirical theories.

The applications of chemical shifts to the study of molecular structures and chemical equilibria and rate processes are now well known [2]. From the practical point of view the chemical applications are limited by (a) the line width in relation to the chemical shift and (b) the signal to noise ratio. The line width is governed by interactions between the magnetic nuclei and the signal to noise by various fundamental parameters and by the Boltzman distribution of the population of the nuclear energy levels.

We must now consider how the magnetic interactions influence the magnetic resonance spectra. Two magnetic moments close to one another each experience a magnetic field due to the other, and the interaction transmitted by these magnetic fields is known as magnetic dipolar coupling. In a crystal, the nuclei find themselves in a magnetic field, H, due to the laboratory magnet, modified by these dipolar interactions. Each nucleus may therefore experience a range of magnetic fields on either side of the mean value, H; the range of the fields depends on the strength of the local fields set up by neighbouring moments and these depend on μ/r^3 where μ is the strength of the magnetic moment and r is the distance. Nuclear resonances of crystals are therefore usually broad, and the broadening can sometimes be used to measure the mean distances between the nuclei in simple crystals [3]. The proton has a strong magnetic moment, and because of its small size, interproton distances in crystals are often small. Proton resonances in crystals are therefore broad, and in a typical organic substance the mean square width may be about 40 Kc/s., or about 10 gauss. Since proton chemical shifts range over only 20 p.p.m. it is clearly impossible to observe chemical shifts in solids where these very broad (~ 1000 p.p.m.) lines occur. On the other hand, other nuclei with weaker magnetic moments and larger atoms experience much smaller dipolar interactions of this kind, which may be as little as 0.1 gauss. If the chemical shifts are large then in this case they may be observed in the solid. For example the thallium resonance in solid Tl_2Cl_3 has two shifted components with intensities in the ratio of 3 : 1 in accordance with the structure [4].

$$\overset{\text{III}}{Tl^{I}_{3}\,[Tl\,Cl_6]}$$

If there is molecular motion in the crystal, the local fields will fluctuate with the same frequency spectrum as the molecular motion. If the fluctuations occur rapidly enough the nuclear moment may not be able to experience the local fields of its neighbours long enough to notice any deviation from H, with the result that a narrower line is obtained. The careful study of changes of line width due to molecular motion can often be of great value, especially in the study of polymeric substances [5]. When the substance is changed into the liquid state by melting or dissolving in a solvent, the molecular motion is very vigorous, and all that remains of the dipole-dipole interaction is a range of magnetic fields fluctuating with the frequency spectrum of the molecular motion of the liquid. Dipolar broadening is now completely removed and the line widths are determined only by the Heisenberg uncertainty principle. This may be expressed approximately in the form

$$\Delta E \times t = \frac{h}{2\pi} = h\Delta\nu$$
$$\Delta\nu = \frac{1}{2\pi t} \tag{2}$$

where ΔE is the uncertainty of the energy level, $\Delta\nu$ is the line width, t is the lifetime of the nucleus in the energy level and h is Planck's constant.

For nuclei with $I = 1/2$ and a zero electric quadrupole moment, t may be very long so that the nuclear resonance lines are then very narrow.

The effects of the fluctuating dipolar interactions will be discussed later; it is convenient now to discuss the greater detail in the nuclear resonance spectrum which is revealed by the very narrow lines obtained from liquid samples. Line widths of 1 in 10^8 are common for nuclei with no electric quadrupole moment, and this permits the spectra to be studied under very high resolving power. Chemical shifts in proton resonances as well as of other nuclei can now be measured with some accuracy, and the results applied to chemical problems [2].

Although the "static" component of the direct dipole-dipole coupling is averaged to zero by the molecular motion in a liquid, there often remains a further dipole coupling which is unaffected by this motion. This is the so-called "spin-spin" coupling which is transmitted via the spins of the electrons in chemical bonds joining the nuclei together. The theory of this scalar coupling has been given by Ramsey [6], but again this theory can be applied rigorously only to the simplest molecules. Valence Bond methods have, however, been applied successfully by Karplus and his collaborators [7] to the spin-spin coupling between protons in organic molecules. Not only can coupling constants be calculated to a correct order of magnitude, but their dependence on molecular geometry can be correctly predicted.

Coupling constants between protons are usually less than 20 c/s. and between flourine nuclei less than 500 c/s. It is therefore clearly possible to observe this effect only in liquids since in solids the line widths are of the order of 50 Kc/s. Spin-spin coupling among heavier nuclei is often much greater. For example in the solid thallous halides the spin-spin coupling between the two nearly equally abundant thallium isotopes is of the order of several Kc/s. and is largely responsible for the observed line width [4].

According to the theory of Karplus, the spin-spin coupling is transmitted predominantly by the electrons involved in σ-bonds between the nuclei; electrons in π orbitals make a negligible contribution except over large distances. This conclusion may not be correct, however, for nuclei other than hydrogen. For example, in the course of a study of platinum and phosphorus resonances in platinum complexes, a marked correlation has been found by Pidcock and Richards [8] between the Pt - P coupling constant and the extent of π-*bonding* between these two atoms. In *trans*-$(PBu_3)_2PtCl_2$ the Pt - P coupling constant is 2.46 Kc/s. but in the *cis* isomer it is 3.62 Kc/s., where there is good reason [8] to believe that the π-bonding is stronger. Furthermore in $[P(OEt)_3]_2PtCl_2$, where π-bonding between Pt and P is expected to be still stronger, the coupling constant is found to be 5.70 Kc/s.

There is considerable theoretical interest in the signs of the spin-spin coupling constants. The relative signs can often be found by detailed analysis of the complex high resolution spectra which are observed when the chemical shifts are comparable with the coupling constants. In other cases the signs can be found by elegant double nuclear resonance experiments [9] or by the observation of double quantum jumps in suitable cases [10].

The great importance of the line width in nuclear resonance spectra cannot be overstressed. When very narrow lines occur, the fine effects of chemical shifts and spin-spin coupling can be measured accurately; when the lines are broad these may become obscured and at the same time the resonance becomes more difficult to observe because of the reduced signal to noise ratio.

The broad lines in solids arise from direct dipolar coupling between the nuclei (and sometimes from electric quadrupolar interactions, see later). The line widths in liquids are governed approximately by equation (2). The lifetime of a nucleus in a particular energy level may be expressed in terms of two "relaxation times." The "spin-lattice" relaxation time, T_1, is a measure of the time taken for a nucleus to exchange energy with the thermal motion of the molecules around it; the spin-spin relaxation time, T_2, is a measure of the time taken for two nuclei to exchange a quantum of energy, one falling from an upper to a lower energy level and the other using the quantum to raise it from a lower to an upper energy level. Spin-lattice relaxation is the process by which the nuclear spin system heats up or cools down to the temperature of the "lattice" (which may be a solid or liquid). Spin-spin relaxation is an adiabatic process in which energy is passed through the spin system but not exchanged with other forms of energy. In liquids, T_1 and T_2 are frequently equal, so for the purposes of this lecture I shall consider only the factors which determine T_1, since similar considerations apply to T_2 in liquids.

For nuclear spins the coefficient of spontaneous emission is vanishingly small so that nuclei can exchange their energy levels only when stimulated to do so by some external agency.

If the nuclei have a spin $I = 1/2$, so that they have no electric quadrupole moment, the only mechanism by which they may change their energy levels is by transitions stimulated by a magnetic field which fluctuates at a frequency close to the Larmor frequency $\nu_o = \mu H/Ih$. In a liquid the dipolar interactions are fluctuating at the frequencies of the molecular motion, and field fluctuations are set up by the magnetic nuclei in the molecules which are in thermal motion. It is the components of these field fluctuations near the Larmor frequency which induce transitions of the nuclei among their energy levels and so permit spin-lattice relaxation.

In liquids the molecular motion is characterised by a correlation frequency near 10^{12} c/s. so the field fluctuations set up by the molecular motion near the very much lower Larmor frequency of about 10^7 c/s. are extremely weak. Spin-lattice relaxation is therefore very inefficient, T_1 is long (many seconds) and the nuclear resonance line is very narrow. If the nuclei are in a large rigid molecule, for which the molecular correlation frequency is much lower, then the component of field fluctuations near 10^7 c/s. is increased, so that spin lattice relaxation is more efficient. T_1 is indeed found to be much shorter for nuclei in large rigid molecules than in small ones. For example Bovey, Tiers, and Filipovich [11] have described how the proton resonance of a protein in the rigid helical structure is broad because of the short T_1. When the protein is dissolved in trifluoroacetic acid, the rigid structure is broken down so that much segmental motion can occur. The correlation frequency rises, T_1 becomes longer and the proton resonances are sharper.

If one adds a paramagnetic substance to a diamagnetic solution, dramatic changes occur in the nuclear resonance line width. The unpaired electron in the paramagnetic solute has a magnetic moment of the order of 10^3 times those of the nuclei, so that although the correlation spectrum of field fluctuations may remain unchanged, the total intensity is much greater from the unpaired electrons. Once again spin-lattice relaxation is made more effective and line broadening occurs in the nuclear resonance spectra.

A rather fascinating example of these effects has been described recently by Eisinger, Shulman and Szymanski [12]. When ferric ions are dissolved in water, the electronic moments cause effective spin-lattice relaxation and T_1 is short. If to this solution a small amount of D.N.A. is added, the T_1 of the protons in the water is increased, almost back to its value in pure water. This is interpreted [12] as due to coördination of the ferric ions by the D.N.A. on internal sites, so that the D.N.A. "wraps up" the ions and prevents the water molecules from gaining access to them. The T_1 of the protons is therefore no longer affected by the iron atoms. When cupric ions are dissolved in water, the proton T_1 is also reduced. When D.N.A. is added to this solution, however, the spin-lattice relaxation time is reduced still further in contrast to the effect on the ferric solution. The reason for this is that the cupric ions must be coordinated by the D.N.A. on *external* sites, so that the water molecules can gain access to the paramagnetic ion just as well as when it is in its normal hydrated state. However, because it is now attached to a large rigid molecule, the correlation frequency of the copper ion is greatly reduced, and the component of field fluctuations it produces near the nuclear Larmor frequency becomes more intense. Its effect on the proton T_1 is therefore even greater than in the absence of the D.N.A.

The dipolar interaction between magnetic moments can be split up into six terms [13] and some of these interactions can bring about simultaneous changes in energy level in two nuclei, or in a nucleus and electron together. One of these interactions can cause a nucleus to rise from a lower energy level to an upper one when an electron (with spin = 1/2) falls from the upper to the lower energy level. The energy given out by the electron is much greater than that required by the nucleus (because the magnetic moment of the electron is so much greater) so the excess energy is dissipated as thermal motion of the molecules. If in such a solution, the electron resonance is strongly excited so as to produce a continuous flow of electrons down from the upper to the lower energy level, many nuclei will be simultaneously flipped into their upper energy level. The effect is to pump nuclei from one energy level to another and so greatly to modify the distribution of the nuclear population. This change has a direct effect on the intensity of the nuclear resonance. As the rate of excitation of electrons is slowly increased, the nuclear resonance signal is decreased in intensity until it vanishes when the nuclear energy levels are equally populated. Further increase in the electron excitation causes the nuclear resonance to reappear with reversed sign and then to grow in intensity until it reaches a value which may be as great as $\gamma_e/2\gamma_N$ times the original signal, where γ_e and γ_N are the magnetogyric ratios of the electron and of the nucleus. The improvement is clearly limited when the electron energy levels are equally populated, i.e., when the electron resonance is saturated. This is one form of the so-called Overhauser Effect [14]. The effect offers many possibilities for the chemist. Increases in signal to noise ratio are always most welcome and the sensitivity of the effect to molecular interactions in solution offers the possibility of studying them in some detail.

Richards and White [15] have studied the Overhauser Effect in solutions of various radicals in a variety of solvents and in the presence of various solutes. For example the proton resonances of water, ammonia, and dimethyl formamide are reversed and increased in intensity by about 20 fold when a solution of the p-ditert-butyl-semiquinone radical in each of them is irradiated with a certain microwave power at the electron resonance frequency. The increase in intensity of the dimethyl formamide resonance would have been expected to have been less than for the water because its proton spin-lattice relaxation time is shorter. If p-semiquinone radical is used instead, the proton resonance of the dimethyl formamide is much more strongly affected than that of the water, in spite of its short relaxation time. Now amides have been shown by Hatton and Richards [16], using high resolution proton resonances, to associate strongly with aromatic substances unless they contain bulky substituents which provide steric hindrance. The stronger enhancement of the amide resonance is no doubt concerned with its close association with the semiquinone, and less close association with the t-butyl semiquinone. Quantitative studies of this effect are being made which can give an indication of the mean distance of approach of the radical and solvent.

A more striking effect may be observed [17] in solutions of a semiquinone radical in water containing sodium trifluoroacetate. The proton resonance is reversed in the usual manner when the electron resonance is excited, but the fluorine resonance is actually *enhanced.* Since there can be no scalar coupling between the radical and the CF_3COO^- ions this must mean that the radicals are coupled to the protons but *not* to the fluorines and that the protons and fluorines are coupled together. The electrons pump the protons into a reversed population distribution and the relaxation of the protons pumps the fluorines into an enhanced population distribution. This is no doubt associated with the similar negative charges on the CF_3COO^- and semiquinone ions which are therefore unlikely to make frequent encounters.

The final interaction to consider is of the greatest importance in determining nuclear resonance line widths. Nuclei with spins greater than 1/2 usually have an aspherical distribution of charge which can be expressed as an electric quadrupole moment. This moment can couple strongly with any electric field gradient set up at the nucleus by the electrons distributed around it. If the molecule is tumbling over in a liquid this electric quadrupole coupling tends to "drag" the nucleus over with the molecule, causing it to reorient itself into another energy level. The effect of this is to reduce the nuclear spin-lattice relaxation time according to an equation of the form

$$\frac{1}{T_1} \propto (\mathrm{eq\ Q})^2 \tau_c$$

where eq Q is the quadrupole coupling constant and τ_c is the molecular correlation time. By treating the molecule as a sphere turning in a medium of viscosity η we find

$$\frac{1}{T_1} \propto (\mathrm{eq\ Q})^2\ \eta/T,$$

where T is the temperature. The broadening produced by this relaxation is the greatest limitation to the study of nuclei affected by it, because the broadening is often so great as to make the signal undetectable.

The effect can often be turned to good account, however. When glycerol is added to dimethyl formamide and $1/T_1$ of the nitrogen resonance is plotted against viscosity, a straight line is obtained [18] the slope of which is a measure of the quadrupole coupling at the nitrogen. Protonation of the amide with a strong acid could occur at the nitrogen or at the oxygen; the former would make the electric field round the nitrogen more symmetrical and reduce the quadrupole coupling and the latter would increase the π bonding at the nitrogen and also the quadrupole coupling. The slope of the plot of $1/T_1$ for the nitrogen resonance against viscosity is greater in CF_3COOH than without it, providing strong evidence that the proton is added mainly to the oxygen of the amide.

Measurements have been made recently by Richards and Yorke of $1/T_1$ of the bromine resonance in bromide solutions as a function of viscosity. The plots are linear and indicate that the quadrupole coupling is independent of concentration even in the saturated solutions. The same is true of the sodium resonances. Ion-Ion interaction cannot be very important therefore for this effect.

The quadrupole coupling is, however, very sensitive to the solvent medium and depends on its dielectric constant. This result has been confirmed for a wide variety of solvent mixtures and strongly suggests that the quadrupole coupling is determined largely by ion-solvent interactions.

REFERENCES

1. Ramsey, N. F., Phys. Rev., 78, 699 (1950).
2. Pople, J., Berstein, H., and Schneider, W. G., "High Resolution Nuclear Magnetic Resonance," McGraw-Hill (1959).
3. Richards, R. E., "Physical Methods of Organic Chemistry," Vol. 2, ed. Phillips & Nachod., A.P., 1962.
4. Freeman, R., Gasser, R. P. H., and Richards, R. E., Mol. Phys., 2, 301 (1959).
5. Richards, R. E., "Determination of Organic Structures by Physical Methods" by F. C. Nachod and W. P. Phillips., Vol. 2., A. P. New York 1962. p 554.
6. Ramsey, N. F., Phys. Rev., 91, 303 (1953).
7. Karplus, M., J. Chem. Phys., 30, 11 (1959); 33, 841, 1842 (1960). Karplus, M., Anderson, D. H., Farrar, T. C., and Gutowsky, H. S., J. Chem. Phys., 27, 597 (1957).
8. Pidcock, A., and Richards, R. E., Proc. Chem. Soc., 1962, 184.
9. Freeman, R., Mol. Phys., 4, 385 (1961).
10. McLauchlan, K. A. and Whiffen, D. H., Proc. Chem. Soc., 1962, 144.
11. Bovey, F. A., Tiers, G. V. D., and Filipovich, G., J. Polymer. Sci., 38, 73 (1959).

12. Eisinger, J., Shulman, R. G., and Szymanski, B. M., J. Chem. Phys., 36, 1721 (1962).
13. Bloembergen, N., Purcell, E. M., and Pound, R. V., Phys. Rev., 73, 679 (1948).
14. Overhauser, A. W., Phys. Rev., 91, 476 (1953).
15. Richards, R. E. and White, J. W., Proc. Roy. Soc., in press.
16. Hatton, J. V. and Richards, R. E., Mol. Phys., 5, 139 (1962).
17. Richards, R. E. and White, J. W., Proc. Chem. Soc., 1962, 119.
18. Herbison-Evans, D. and Richards, R. E., Trans. Faraday Soc., 58, 845 (1962).

RECENT APPLICATIONS OF HIGH RESOLUTION NUCLEAR MAGNETIC RESONANCE TO CHEMICAL PROBLEMS

J. N. Shoolery
Varian Associates
Palo Alto, Calif.

INTRODUCTION

High resolution NMR has been used for about 10 years to study molecular structure, hydrogen bonding, and kinetics of certain types of reactions, particularly those involving proton exchange. Due to its strong magnetic moment, high abundance, and widespread distribution in organic substances, the hydrogen nucleus, or proton, has been employed most frequently. The main difficulties which have been encountered are the small chemical shift for protons compared to other nuclei such as F^{19} or P^{31}, the signal-to-noise problem when very small or insoluble samples are involved, and the complexities due to spin-spin coupling between neighboring nuclei in complicated molecules. The recent history of high resolution NMR is mostly concerned with the alleviation of these difficulties through advances in instrumentation, experimental techniques, and better theoretical understanding of the relationship between the chemical shift and spin-spin coupling parameters, δ, and J, and the observed spectrum.

THE CHEMICAL SHIFT PROBLEM

Since the chemical shift is a field dependent effect it can be increased by working at higher magnetic field strengths. The field cannot be increased indefinitely, however, due to the power and size requirements in the magnet and the need to maintain a homogeneous field. The radio frequency must be increased in proportion to the field and this results in some electronic sophistication at the highest frequencies employed, i.e., 100 mc/sec for protons in a field of 23,490 oersteds.

The advantages of working at high field strengths are well illustrated in Figure 1 by the spectrum of 1,2-dibromobutane. The upper trace shows the spectrum at 60 mc/sec and the lower trace shows the effect of raising the frequency to 100 mc/sec. Better separation of the various multiplets is achieved, since the spin-spin splittings remain constant in magnitude. A more important aspect of the high field spectrum is that it more nearly approximates a "first-order" spectrum, i.e., spacings and intensities predicted on the basis of simple empirical rules rather than complex quantum mechanical calculations, although in this

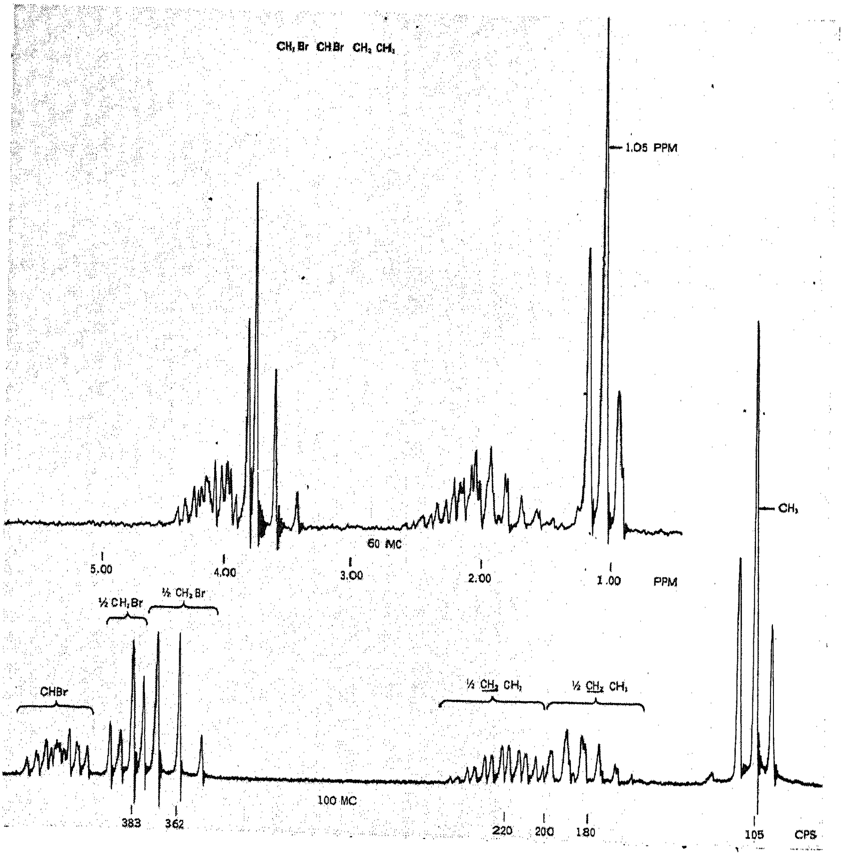

Figure 1. Upper: High Resolution NMR Spectrum of 1,2-dibromobutane at 60 mc/sec. Lower: High Resolution NMR Spectrum of 1,2-dibromobutane at 100 mc/sec.

case considerable perturbations must still be taken into account. At 60 mc it is not at all clear which line spacings are significant and which lines may have diminished in intensity to the point of becoming lost in the noise.

It is interesting that the two CH_2 groups in the molecule both show a relative chemical shift of the two protons on the same carbon atom, the effect being much clearer at 100 mc/sec due to the small chemical shift difference compared to the spin-spin coupling between the protons. This comes about from a difference in the depth of the three potential minima in the rotation about the bond joining C_1 and C_2 and also C_2 and C_3.

The importance of having the largest possible chemical shifts increases with the complexity of the compounds being studied, due to the greater probability of overlapping and interference. Work at 100 mc/sec is resolving a number of problems in natural product chemistry which were marginal, or, if not impossible, at least beyond present interpretational techniques.

THE SENSITIVITY PROBLEM

Since 1955 there has been a steady improvement, not only in field strength, but also in the stability of high resolution spectrometers. Furthermore, the input circuitry and coil configuration surrounding the sample have undergone steady improvement. The result is that the combination of the signal dependence on the square of the frequency, the noise dependence upon the reciprocal square root of the bandwidth, and the improved filling factor and noise figure yields better overall sensitivity by an order of magnitude.

A technique has been developed recently especially for small samples. Two plastic plugs, with hemispherical cavities, can be placed facing one another in a precision glass cell. The resulting spherical cavity can be filled by means of an axial hole through one of the plugs. This "microcell" technique increases the sensitivity of a high resolution instrument by a factor of 5 without significant loss of resolution, by concentrating the sample where it can couple to the receiver coil in an optimum way. It has been found invaluable with samples of a few milligrams down to samples as small as the 100 μgram sample of an alkaloid shown in Figure 2.

SPIN-SPIN DECOUPLING

It has been known for some time [1,2] that the spectral complexity due to a nucleus or group of equivalent nuclei coupling

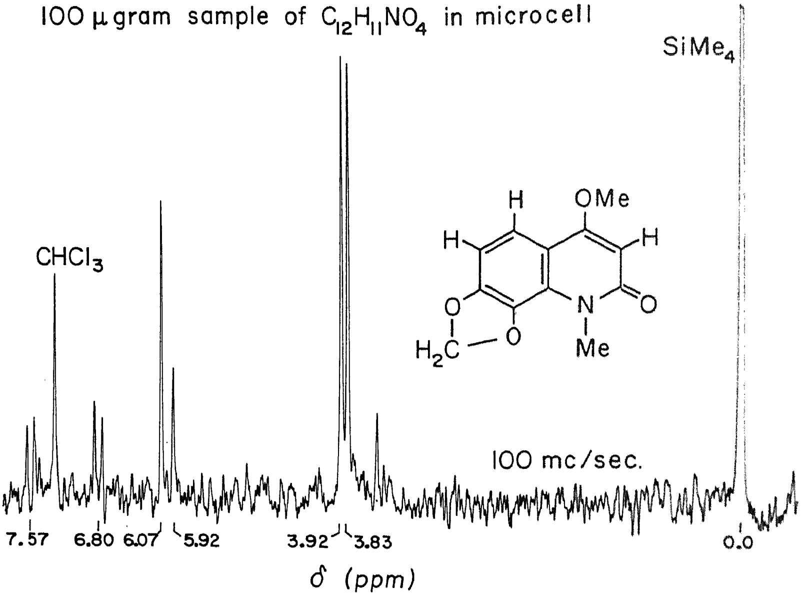

Figure 2. 100 mc/sec spectrum of 100 µgrams of casimiroin, $C_{12}H_{11}NO_4$, taken with sample in 25 µliters of $CDCl_3$ in a microcell.

their spins to other nuclei in a molecule could often be reduced by strongly irradiating the offending nuclei at their resonance frequency while studying the remaining ones in the usual manner. The problem is experimentally more complex for proton-proton couplings since the small chemical shifts result in frequencies which are very close together.

We have found quite recently that a minor modification of the Varian NMR integrator, Model V-3521, allows it to be used as a rather effective and quite flexible spin decoupler. Since the device already uses two kilocycle modulation and phase sensitive detection, it is relatively simple to introduce strong irradiating fields at one or more nearby frequencies without undue interference. This allows the coupling of one or more other groups of nuclei to be effectively wiped out during the observation of a multiplet which would be hopelessly complex in their presence. As an example, consider Figure 3, the 100 mc/sec spectrum of 1,2-dibromobutane, shown undecoupled in Figure 1, with the decoupling frequency set 216 cps above the observing frequency. The resonance of the proton on C_2, unequally coupled to all four neighbors is simplified to the four line pattern typical of the X part of an ABX system of nuclei.

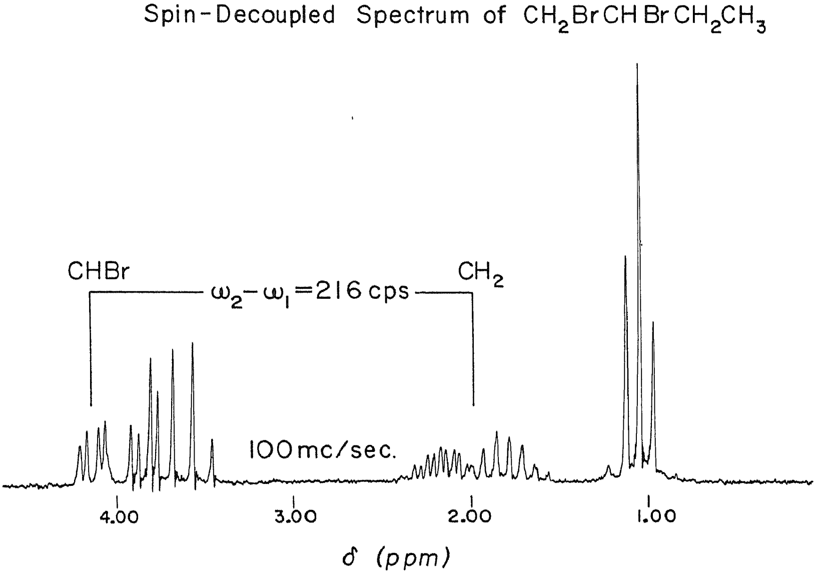

Figure 3. Spin-decoupled spectrum of 1,2-dibromobutane at 100 mc/sec. Decoupling frequency 216 cps above observing frequency.

MOLECULAR CONFORMATION STUDIES

The dependence of the coupling between vicinal protons upon the dihedral angle between the CH bonds makes a large number of molecular conformation problems susceptible to study [3]. An example in which structurally useful information was forthcoming is the following problem. A dithiol was prepared [4] via a chemical path which could lead either to I or II.

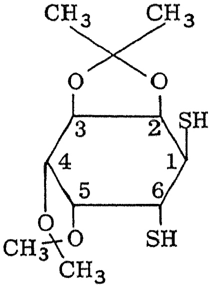

I

or

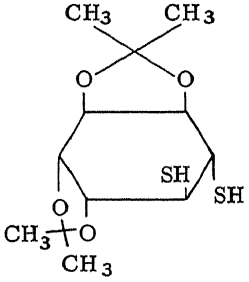

II

The spectrum of the dithiol is shown in Figure 4. In addition to the two strong peaks at $\delta = 1.33$ and $\delta = 1.45$ (δ = ppm from $SiMe_4$) due to the CH_3 groups, a strong line at $\delta = 4.52$ is found which results from accidental near-equivalence of the chemical shifts for the protons on C_2, C_3, C_4 and C_5. The sharpness and lack of structure of this line shows that the couplings J_{12} and J_{56} between the protons on the corresponding carbon atoms must be quite small; i.e., 1 cps or less. The remaining four protons represent an A_2B_2 group of spins; the A nuclei being the SH protons at $\delta = 2.13$ and the B nuclei being the C_1 and C_6 protons.

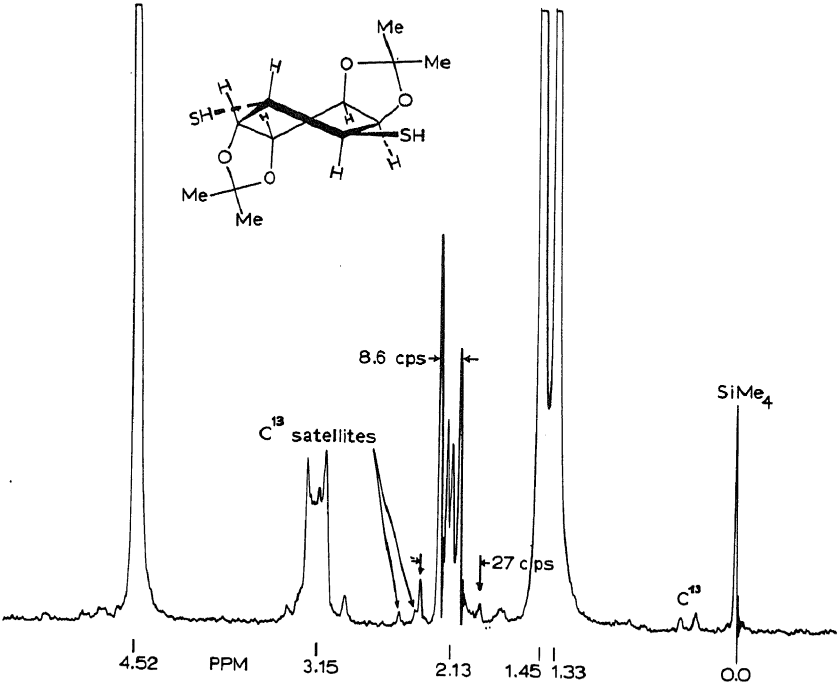

Figure 4. 60 mc/sec spectrum of the 1,2,3,4-di-isopropylidene ketal of 5,6-dimercapto-1,2,3,4-cyclohexane-tetrol in $CDCl_3$.

Analysis of the A_2B_2 pattern by the usual techniques [5] reveals that J_{16} is 12 cps and J_{AB} is 8.6 cps. Now structures I and II can each exist in two conformations. The value of 12 cps for J_{16} shows that we need only be concerned with the conformations in which these protons are in a trans-diaxial configuration. In the case of structure II, the protons on C_2 and C_5 also bear a trans-diaxial relationship to those on C_1 and C_6. The lack of an appreciable coupling constant, J_{12} or J_{56}, precludes this possibility and leaves us with structure I as the only alternative.

QUANTITATIVE MEASUREMENTS

Since the transition probability is not affected appreciably by the small perturbation of the magnetic field which is called the chemical shift, the integrated intensity of each multiplet in the spectrum is proportional to the number of nuclei in the sample with that particular chemical or structural environment. Under proper experimental conditions [6] this relationship is obeyed precisely and the relative numbers of nuclei in different functional groups can be determined. Figure 5 shows the spectrum of an indole alkaloid with its integral recorded as an ascending step function. Groups of protons can be distinguished with the step size ratios of 1:4:1:5:5:6. The sum of these numbers is 22, the total number of hydrogen atoms in the molecule.

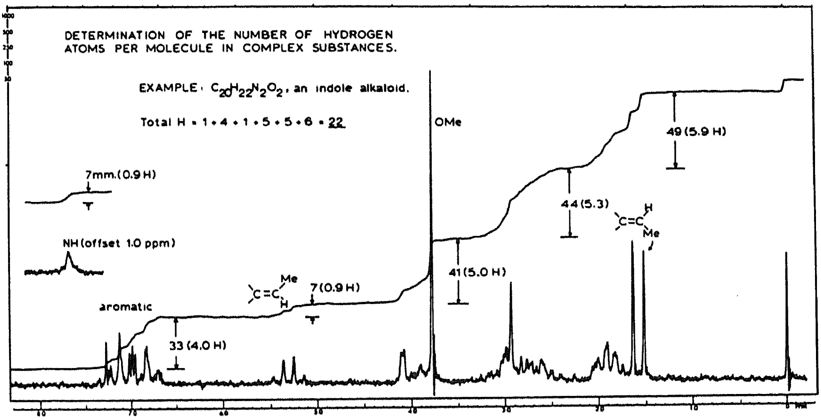

Figure 5. 60 mc/sec spectrum of an indole alkaloid, $C_{20}H_{22}N_2O_2$, with integral trace on the same chart.

In the case of mixtures a quantitative analysis can be made in the same way if the number of protons per molecule corresponding to a selected analytical peak for each component is known.

CONCLUSIONS

The recent development of techniques for obtaining additional parameters from NMR spectra, namely, high field studies, decoupling, and integrating, has resulted in a steadily increasing number of chemical problems for which sufficient parameters can be measured to determine a unique solution. This has greatly increased the utility of the method for the chemist.

REFERENCES

1. W. A. Anderson, Phys. Rev. 102, 151 (1956).
2. A. L. Bloom and J. N. Shoolery, Phys. Rev. 97, 1261 (1955).
3. M. Karplus, J. Chem. Phys. 30, 11 (1959).
4. Sample provided by Dr. G. E. McCasland, University of San Francisco. This work will be described in detail in a forthcoming publication.
5. J. A. Pople, H. J. Bernstein, and W. G. Schneider, High Resolution Nuclear Magnetic Resonance, McGraw-Hill, 1959, pp. 139-143.
6. Varian Associates Staff, NMR and EPR Spectroscopy, Pergamon Press, 1960, Chapter 8.

SPIN DENSITY DISTRIBUTIONS IN CONJUGATED MOLECULES BY NMR CONTACT SHIFTS*

D. R. Eaton, W. D. Phillips, R. E. Benson and A. D. Josey
Central Research Department, Experimental Station,
E. I. duPont de Nemours and Company,
Wilmington 98, Delaware, U.S.A.

INTRODUCTION

The concept of a spin density distribution in an organic free radical arose from the observation and interpretation of the hyperfine structure in the EPR spectra of such species[1]. This hyperfine structure was attributed to isotropic hyperfine contact interactions between the unpaired electron and atoms in the molecule possessing a nuclear moment, most commonly hydrogen. Since such an interaction demands a finite probability of finding the electron at the nucleus in question, it was apparent that the unpaired electron could not be regarded as being localized on one atomic orbital but must be assumed to be distributed over the whole molecule. The theoretical work of McConnell and Chesnut [2] placed this concept on a quantitative basis for aromatic molecules and showed how the spin densities could be derived from observed proton hyperfine coupling constants. Thus, a rather precise experimental method was made available for examining in detail the wave function governing the distribution of the odd electron. Further experimental and theoretical work showed that this orbital containing the unpaired electron could not be treated in isolation but that exchange interactions with electrons in lower filled orbitals had to be considered. In particular, such effects, termed correlation effects, lead to negative spin densities[3] in certain odd-alternant and non-alternant radicals.

---

*Contribution No. 802 from the Central Research Department, Experimental Station, E. I. duPont de Nemours and Company, Wilmington 98, Delaware.

In the EPR experiment, transitions between electron spin states are observed, and contact interactions are manifested in the magnetic resonance spectrum by hyperfine structure. An alternative procedure for obtaining contact interactions is via the NMR approach which is concerned with transitions between nuclear spin states. Here, nucleus-electron contact interactions produce internal fields at the resonating nuclei which either add to or subtract from the external field and thereby lead to resonance field shifts. This NMR approach to contact shifts has several attractive features, but it possesses also a number of limitations. In the EPR experiment, the complexity of the spectrum (hyperfine components) increases very rapidly with the number of coupling constants, and analysis usually becomes prohibitively difficult if more than three or four different coupling constants are involved. In the NMR experiment, on the other hand, each nonequivalent proton gives rise to a single resonance, accompanied in some instances by nuclear I·I structure. However, since the contact shifts are usually very large compared to the spin-spin coupling constants, simple first order spectra result and the I·I structure is an invaluable aid to spectral analysis. Compounds with molecular weights approaching 1000 and involving as many as twelve different contact constants have been analyzed, and there is no reason to believe that a limiting complexity has yet been approached.

Further, small hyperfine couplings in EPR will not be detected if they give rise to splittings less than the line widths, which are at best a few hundredths of a gauss. In NMR no difficulty in this respect is experienced, providing the contact shifts are not small compared with the normal chemical shifts in the molecule. In proton magnetic resonance, chemical shifts are never more than a few parts/million, and consequently, spin densities of the order 10^{-5} have been measured with some certainty.

Finally, NMR contact shifts yield the sign of the spin density since protons attached to sp^2 carbon atoms which sense a positive spin on carbon are shifted to high field while those protons which sense a negative spin on carbon are moved to low field. EPR experiments can only rarely give information about the signs of the spin densities at individual atoms.

To offset these advantages of NMR over EPR for spin density determinations, there are certain limitations to the application of the NMR method. These limitations are associated with the relaxation times of nuclear and electron spins in paramagnetic species. Thus, nucleus-electron dipolar interactions and contact interactions may lead to short relaxation times for the nuclei which in turn will result in such broadening of the nuclear resonances that determinations of contact constants become impossible.

Contact interaction constants normally are not manifested in the NMR spectra of organic free radicals in solution because of the relatively long electronic relaxation times of these species. For observation of contact shifts in NMR, either or both of the inequalities

$$T_1^{-1} \gg a$$

$$T_e^{-1} \gg a$$

must be satisfied. Here T_1 is the electronic relaxation time, T_e is the characteristic exchange time between paramagnetic species, and a is the hyperfine contact interaction constant. Brown, Anderson and Gutowsky [4] and Anderson, Pake and Tuttle [5] have observed contact shifts of organic radicals in the solid state where T_e is greatly shortened over the solution value. In these studies the resonances were very broad because of the magnetic dipolar interactions operating in the solid. A perhaps more esthetically satisfying approach to contact shifts is to examine systems with a T_1 sufficiently short that solution studies, where magnetic dipolar interactions are largely absent, are possible.

The above considerations suggest transition metal compounds as a fruitful area for observation of NMR contact shifts. Here, electronic relaxation times for many transition metals are sufficiently short that the condition

$$T_1^{-1} \gg a$$

is satisfied. The earlier EPR work of Owen and Stevens [6] and Tinkham [7] had shown that with suitable types of chemical bonding, d-electrons can be partially delocalized from a metal atom to the surrounding ligands. It is, therefore, a desirable objective to search for a combination of a paramagnetic metal with a short electronic relaxation time and a ligand with an extended π-electron system bonded together in such a fashion that the unpaired electron will spend an appreciable time on the ligand. Results have been reported on some acetylacetonates [8] and metallocenes [9] where these conditions are sufficiently well satisfied to allow observation of NMR contact shifts for the ligand protons.

DISCUSSION

We have recently examined in this laboratory [10,11] a metal chelate system which satisfies the above conditions rather well. This system comprises the nickel (II) aminotroponeimineates possessing the structure I below.

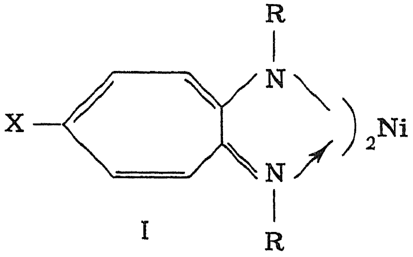

I

In this chelate system, it appears that the short electronic relaxation time is produced by the rapid interconversion of two geometrically different forms, the two forms possessing different magnetic characteristics [12]. The d^8 configuration of nickel (II) gives rise to both singlet and triplet electronic states, the former corresponding to a square planar geometry for the chelate and the latter, in this case, to a tetrahedral configuration. It would appear that interconversion occurs via a torsional vibration and is sufficiently rapid to reduce the NMR line widths to 1-2 cps. in the most favorable cases, and 20-30 cps. in the least favorable. For many of these chelates, the component resonances of the NMR spectra appear as simple multiplets which are due to nuclear spin-spin coupling. This structure is of considerable aid in analyses of the NMR spectra. In the tetrahedral paramagnetic form, the unpaired electrons of nickel reside in the d_{xy}, d_{xz} and d_{yz} orbitals. These metal orbitals have the correct symmetry to form a bond with the filled pπ orbital on the nitrogen. This π-bonding has the effect of partly removing an electron of β (negative) spin from the nitrogen atoms to the nickel atom, leaving an excess of α (positive) spin at nitrogen. Here the direction of α, or positive, spin polarization is taken to be that of the unpaired electrons of the nickel (II) atom. The fractional unpaired electron on nitrogen can then be further delocalized by contributions from resonance structures such as III and IV.

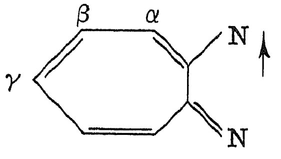

II

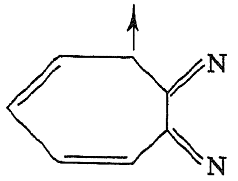

III

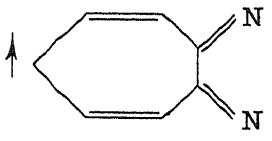

IV

These structures place positive spin densities in the pπ orbitals centered on the α and γ carbon atoms. By the π-σ polarization mechanism, positive carbon pπ spin densities lead to high field shifts of protons attached to these carbon atoms.

Negative spin density is placed at the β-carbon atom as a result of electron correlation effects and gives rise to a low field contact shift for the H_β proton. Proton contact shifts of up to 12,000 cps. at 60 Mc/sec. have been observed in these chelates. Spin density can be delocalized onto aryl groups attached to the nitrogen atoms in a similar manner. Inspection of the contributing valence bond structures shows that in the case of a phenyl group, positive spin densities will be observed at the ortho and para positions and a negative spin density will appear at the meta position. A spectrum of one of these nickel (II) aminotroponeimineates, typical of the class, is shown in Figure 1.

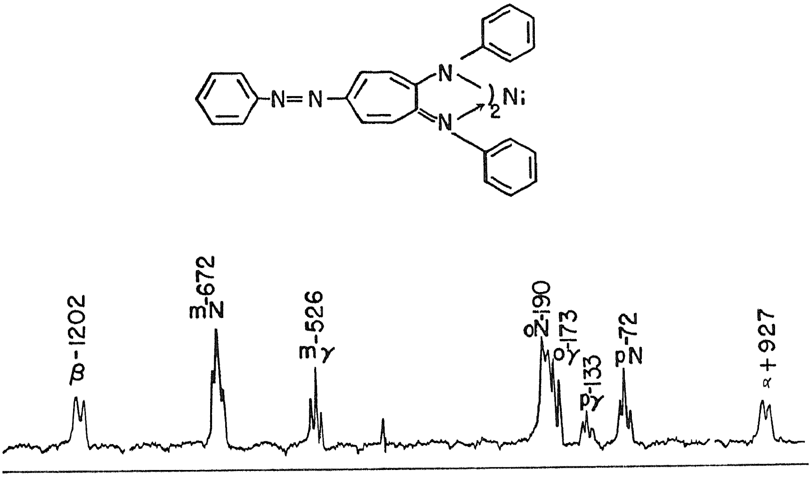

Figure 1. Proton nuclear magnetic resonance spectrum of nickel (II) γ-phenylazo-N,N'-diphenylaminotroponeimineate, determined at 60 Mc/sec. in deuteriochloroform and internally referenced to tetramethylsilane.

Contact shifts, Δf_i, are defined as the differences in resonance frequencies between corresponding protons in the nickel (II) chelate and the diamagnetic zinc (II) chelate or ligand. Spin densities, ρ_{C_i}, may be calculated using the equations

$$\left(\frac{\Delta f}{f}\right)_i = -a_i \frac{\gamma_e}{\gamma_H} \frac{g\beta S(S+1)}{2SkT(e^{\Delta F/kT}+3)} \qquad (1)$$

and

$$a_i = Q_{CH}\,\rho_{C_i} \qquad (2)$$

In Eq. 1, γ_e and γ_H are the magnetogyric ratios of the electron and proton, respectively, and ΔF is the free energy change for the diamagnetic ⇌ paramagnetic equilibrium. The free energy may be obtained from temperature dependence of the contact shifts or of the magnetic susceptibility. In Eq. 2, Q_{CH} is a proportionality constant for which a value of ~-22.5 gauss has been established by theoretical and experimental EPR studies [2].

In this chelate system, $d\pi$-$p\pi$ nickel-nitrogen bonding has imparted to the aminotroponeimineate ligand the desirable characteristics of a free radical without giving it the undesirable long relaxation time characteristic (undesirable from the NMR viewpoint) of organic free radicals. The spin density distributions within the ligands may be treated by exactly the same theoretical techniques used for aromatic free radicals, with the exception that less than one unpaired electron will reside on the ligand. Chelates possess an added advantage in that unlike most free radicals, they generally are relatively stable entities. The basic aminotroponeimineate structure, I, may be modified by introducing different groups at R and X using rather straight-forward synthetic methods [13]. The possibility is open, therefore, for tailoring "free radicals" to test specific points dealing with conjugation and electron delocalization.

Thus, with a view to assessing the conjugative ability of various linking groups, contact shifts have been determined [14] in a number of molecules with nitrogen substituents of the type

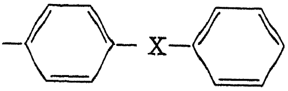

The observed spin density distributions for the two examples where X = -CH=CH- and -NH- are shown in Figure 2. It is apparent that if X is a conjugating group so that the π-systems of the two phenyl groups are linked, spin may be expected to be transferred onto the second ring. The magnitude of spin density reaching this second ring may be taken as a measure of the conjugative ability of X. Thus, the CH=CH link provides an example of classical conjugation. The structure

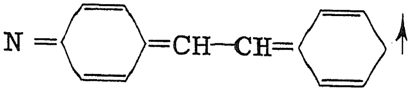

places spin at the para position of the second ring. Dative conjugation is exemplified by the NH linkage.

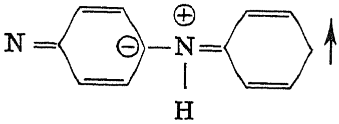

Spin Density Distributions

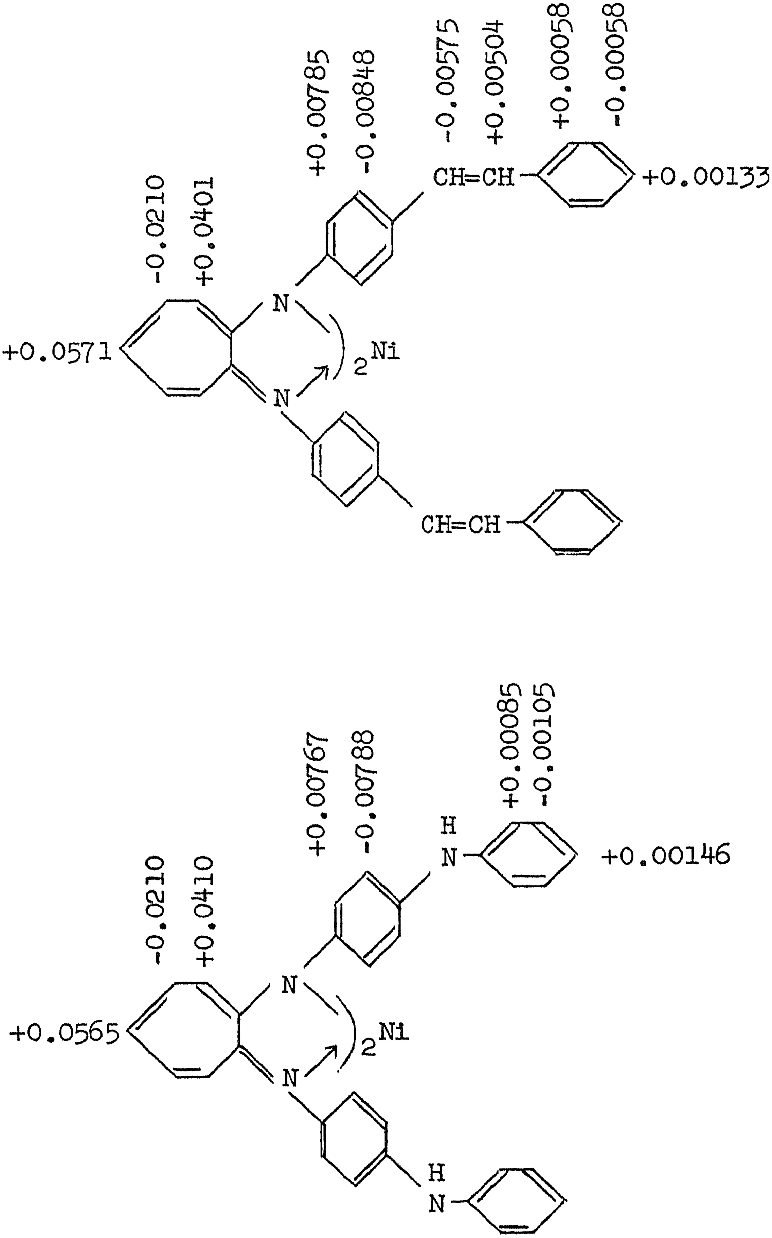

Figure 2

Dative conjugation is found to proceed much more efficiently with the NH group than with the oxygen or sulfur atoms as conjugative linkages. For fluorine in fluoroaromatics, dative conjugation is also possible and a rather more detailed treatment can be made[15,16]. F^{19} has a nuclear spin of 1/2 so the NMR characteristics are favorable for observing contact shifts. A parameter Q_{CF}, analogous to the similar quantity for the C-H bond defined in Eq. 2, may be obtained from these measurements. It is found, though, that Q_{CF} differs from Q_{CH} in two respects. Q_{CF} is positive and its numerical value depends on the position of fluorine substitution. Analysis of the data from a number of fluorine substituted nickel (II) aminotroponeimineates has led to the conclusion that Q_{CF} is composed of a negative contribution from the σ-π spin polarization mechanism for spin density centered on carbon and a positive contribution arising from spin density centered on fluorine. The latter contribution is a manifestation of C-F double bonding in fluoroaromatics.

Hyperconjugation has been studied in a number of tolyl derivatives [14,16] and in the compound with R=2-fluorenyl. Direct evidence for the existence of the hyperconjugative effect is found in the direction (high or low resonance field) of the contact shifts. A proton senses the spin in an adjacent $p\pi$ orbital by the polarization mechanism indicated in Figure 3a. Thus a positive spin in the $p\pi$ orbital places a negative spin at the proton and gives rise to the negative sign of Q_{CH} in Eq. 2. If, however, the hyperconjugation mechanism is operative, direct overlap of the hydrogen 1s atomic orbitals with the $p\pi$ orbital of sp^2 carbon places a positive spin density at the proton. Consistent with this hyperconjugative mechanism, contact shifts of protons of CH_3 groups bound to sp^2 carbon always are found to be shifted in a direction opposite to that of hydrogen bound to the same carbon atom.

Delocalization of spin density is not necessarily confined to π systems, and by studying a series of compounds with R = alkyl we have obtained evidence for transmission of spin density through σ bonds. In table 1 the relative shifts in the methyl, ethyl, n-propyl and n-butyl groups are shown. There is seen to be a fairly rapid attenuation of spin density along the alkyl chain, and preliminary calculations employing the LCBO (linear combination of bond orbitals) procedure have indicated that the results are consistent with delocalization in the σ system.

Spin densities in the π systems of these molecules can be calculated by any of the theoretical methods previously developed to interpret EPR results [17]. Since large negative spin densities are observed, only calculation schemes which take into account electron correlation are likely to be successful. One such theoretical approach is the valence bond procedure [18,19]. In table 2,

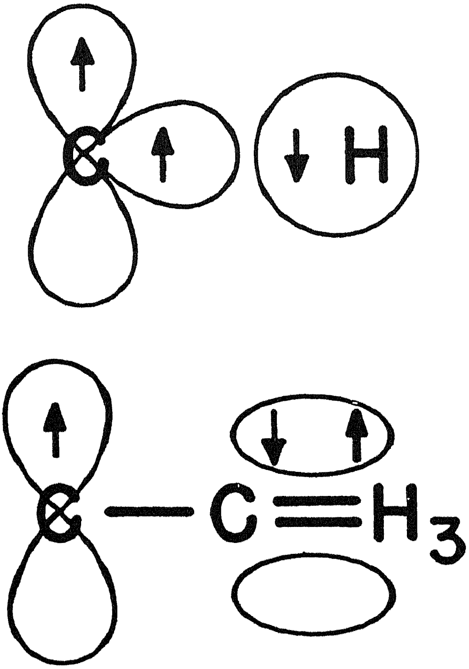

Figure 3. Models for nucleus-electron interaction in (a) a ·C-H fragment and (b) a ·C-CH_3 fragment.

Table 1

Relative Contact Shifts of Ni (II) N,N'-Alkyl Aminotroponeimineate

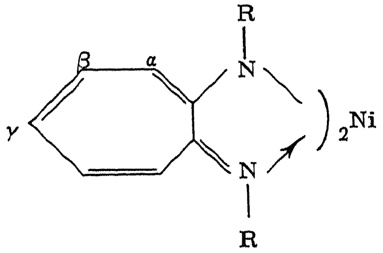

R	H_α	H_β	H_γ	CH_2 (CH_3)*	CH_2 (CH_3)*	CH_2 (CH_3)*	CH_3
Methyl	-1.839	+1.000	-2.568	+3.358*			
Ethyl	-1.949	+1.000	-2.678	+3.239	+0.213*		
n-Propyl	-1.964	+1.000	-2.632	+3.440	+0.235	+0.123*	
n-Butyl	-1.958	+1.000	-2.617	+3.502	+0.230	+0.142	+0.070

Table 2

Comparison of Experimental and Calculated Spin Densities

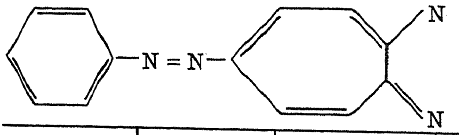

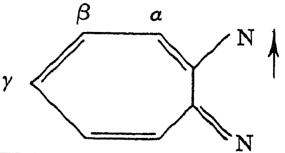

Position	Calc.^{a}	Expt.	Position	Calc.^{b}	Expt.
α	+0.0344	+0.0383	α	+0.0424	+0.0429
β	-0.0210	-0.0210	β	-0.0241	-0.0220
ortho	+0.00702	+0.00756	γ	+0.0490	+0.0589
meta	-0.00353	-0.00263			
para	+0.00586	+0.00872			

^{a}Normalization Factor 10.7
15 Structures in Calculation
^{b}Normalization Factor 10.5
8 Structures in Calculation

experimental spin densities are compared with the results of valence bond calculations for the aminotroponeimineate ring and for the nickel (II) γ-(phenylazo)-aminotroponeimineate. Calculations were carried out [20] assuming that one unpaired electron was transferred from nickel to the aminotroponeimine ring. Calculated spin densities were then reduced by a suitable factor to give best agreement with experiment. By this combination of theory and experiment, it was shown that approximately 1/10 of an electron is delocalized to each aminotroponeimineate ligand as a result of dπ-pπ bonding. This result constitutes a measure of the extent of such bonding in these nickel (II) chelates.

The above examples indicate ways in which determinations of spin density distributions in paramagnetic nickel (II) aminotroponeimineates by NMR contact shifts can be used to elucidate problems of conjugation and chemical bonding. This approach, using nickel (II) aminotroponeimineates or other paramagnetic chelates, promises to give rather detailed information about the electronic structure of large molecules for which other physical techniques are often unduly cumbersome or inapplicable.

REFERENCES

1. For a recent review, see S. I. Weissman, Ann. Rev. Phys. Chem. 12, 151 (1961).
2. H. M. McConnell and D. B. Chesnut, J. Chem. Phys. 28, 107 (1958).
3. H. M. McConnell and D. B. Chesnut, J. Chem. Phys. 27, 984 (1957).
4. T. H. Brown, D. H. Anderson and H. S. Gutowsky, J. Chem. Phys. 33, 720 (1960).
5. M. E. Anderson, G. E. Pake and T. R. Tuttle, Jr., J. Chem. Phys. 33, 1581 (1960).
6. J. Owen and K. W. H. Stevens, Nature 171, 836 (1953); J. Owen, Disc. Faraday Soc. 19, 127 (1955).
7. M. Tinkham, Proc. Roy. Soc. A236, 535 (1956).
8. A. Forman, J. N. Murrell and L. E. Orgel, J. Chem. Phys. 31, 1129 (1959).
9. H. M. McConnell and C. H. Holm, J. Chem. Phys. 27, 314 (1957); ibid., 28, 749 (1958).
10. W. D. Phillips and R. E. Benson, J. Chem. Phys. 33, 607 (1960).
11. R. E. Benson, D. R. Eaton, A. D. Josey and W. D. Phillips, J. Am. Chem. Soc. 83, 3714 (1961).
12. D. R. Eaton, W. D. Phillips and D. J. Caldwell, to be published.
13. W. R. Brasen, H. E. Holmquist and R. E. Benson, J. Am. Chem. Soc. 83, 3125 (1961).
14. D. R. Eaton, A. D. Josey, W. D. Phillips and R. E. Benson, J. Chem. Phys. 37, 347 (1962).
15. D. R. Eaton, A. D. Josey, W. D. Phillips and R. E. Benson, Mol. Phys. 5, 407 (1962).
16. D. R. Eaton, A. D. Josey, R. E. Benson, W. D. Phillips and T. L. Cairns, to be published.
17. A. D. McLachlan, Mol. Phys. 3, 233 (1960).
18. P. Brovetto and S. Ferroni, Nuovo Cimento 5, 142 (1957).
19. H. M. McConnell and H. H. Dearman, J. Chem. Phys. 28, 51 (1958).
20. D. R. Eaton, Y. K. Kim and W. D. Phillips, to be published.

UNSTEADY MODES OF THE SPIN GENERATOR

K. V. Vladimirsky and B. A. Labzov
P. N. Lebedev Institute of Physics
Academy of Sciences of USSR
Moscow, USSR

The topic of the present paper is closely connected with the problem of the frequency scale stability in high-resolution nuclear magnetic resonance. There is a very good progress in this field in recent years, but still in most cases the long time stability does not correspond to the minimum line width.

The only choice in this respect is to stabilize nuclear magnetic resonance by nuclear magnetic resonance. There are several ways to do this. In our laboratory we investigated the possibilities of the simple proton stabilizer in high-resolution NMR. A very elegant solution was given by Varian in A-60. But still the problems remain to be overcome because of the field strength difference between two samples used. It should be emphasized also that the second control sample necessarily would be located in a field with homogeneity not so good as that at the sample under study.

I believe the best solution must be a single sample spectrometer. In our laboratory we constructed and tested such a spectrometer [1] based on the idea of the Schmelzer spin generator. Both for the spectrum study and for the precise stabilization, a single sample is used. The strongest of the lines is the control one. The rest of the lines are recorded by using a double modulation. The synchronous detection of the signals proceeds in our case by means of the two succeeding ring modulators because of the necessity to obtain the reference frequency following the unstable polarizing field H_0. Spectrum sweeping proceeds by changing slowly the second modulating frequency. Frequency marks are obtained by means of the crystal calibrator. Some nonlinear effects are possible in such a spectrometer because of the presence of two signals in one and the same circuit, but they are small when the control signal is strong enough and do not prevent precise chemical shift measurements. The reproducibility of such measurements is very promising, better than 10^{-8}. In this way we measured the relative chemical shift of the two important substances: tetramethyl silane, widely used as a reference compound, and its heavier homolog tetramethyl germanium [3]. The last of the two may be more convenient in some cases because of its higher boiling point.

But a lot of problems still remain connected with the use of the spin generator as an element of high resolution nuclear magnetic resonance spectrometer.

Most of the troubles are connected with the stability of the amplitude of the spin generator oscillations. The theory describing the spin generator with linear feedback circuit is identical with that of the nuclear maser as given by Combrisson [4]. The basic result of this treatment is the stability of the amplitude of the oscillations at all values of the feedback. This cannot be applied to the spin generator operating with the narrow line sample. The steady oscillations can be obtained experimentally in this case in very narrow limits of the parameters of the generator only. There are many points in common in this respect between masers and maser-type n.m.r. apparatus.

A very considerable improvement of the oscillation stability was obtained in our case by using a noninerted non-linearity, a limiting amplifier, in the feedback loop [1]. This is equivalent to the amplitude of the feedback signal being fixed. At the same time the frequency follows that of the signal induced by the sample. The theory of such a spin generator is similar to that of the linear case. The corresponding equations can be derived from Bloch equations [5]

$$\frac{dm}{dt} + \frac{1}{T_2}\,m = k\gamma\mu_2$$

$$\frac{d\varphi}{dt} + \gamma H_o = 0 \tag{1}$$

$$\frac{d\mu_z}{dt} = -k\gamma m + \frac{\mu_z \qquad \mu_o}{T_s},$$

where $\omega_{x+i}\ \omega_y = m_e{}^{i\varphi}$, k = coefficient characterizing the amplitude of the feedback. It was assumed by deriving the equations (1) that the polarizing field H_o is homogeneous and that the phase changes in the feedback circuit can be neglected. The solution of these equations gives at any $k\mu > 0$ the self excitement proceeding to the stationary sinusoidal oscillations. At

$$0 < k\gamma < \frac{1}{2}\left(\frac{1}{T_2} - \frac{1}{T_1}\right)$$

the small perturbations decay exponentially, outside of this interval the transients are oscillatory.

Experiments performed with our spectrometer show, that the use of this limit gives good amplitude stability in the absence of saturation only. At higher values of the r.f. field the oscillations become unstable with periodic abrupt changes of the amplitude. The most important indication of the origin of this instability is the small change of the frequency of oscillations which always accompany the instability of the amplitude. These changes of the frequency are very small, less than the technical line width dependent on the inhomogeneity of the polarizing field H_0. Nevertheless they are very essential as it is the only change of the signal penetrating through the limiting amplifier. For the detailed study of these frequency change special experiments with enlarged specimens (17 mm in diameter) were carried out. In these experiments we observed easily measurable changes of the frequency without violation of the general character of the instability. In this way it was stated that the frequency of oscillations of the spin generator in an unstable mode of operation is a monotonic function of the time with abrupt changes (of saw-tooth type). The frequency deviation is small when the amplitude of the r.f. field is just beyond the limits of stable operation. By increasing the amplitude of the r.f. field one obtains the frequency deviation corresponding to the inhomogeneity of the polarizing field H_0.

For the explanation of these phenomena it must be mentioned that as the result of the field inhomogeneity the signal controlling the frequency is created not in the sample as a whole. Simple evaluations show that even in the best high-resolution spectrometers the polarizing field inhomogeneity exceeds by much the natural line width. So the r.f. field excites the nuclear moment transitions in a small fraction of the volume of the sample only. The saturation begins in this same fraction of the volume when the amplitude of the r.f. field is increased. The resonance curve of the sample as a whole becomes then a bell-shaped curve with a notch [6]. Such local saturation in the sample becomes the cause of the instability. The resonance area moves from the saturated parts of the sample to the fresh ones, which is accompanied by the corresponding change of the frequency. The monotonic character of the frequency changes agrees well with such a concept of the origin of the instability. The order of magnitude of the rate of such a "self-sweeping" may be evaluated assuming that the frequency change for the time interval sufficient for the partial saturation is equal to the natural line width, which gives

$$\frac{d\omega}{dt} \sim \frac{\gamma H_1}{T_2} .$$

This equation agrees with the magnitude and the field strength dependence of the sweep rate observed.

It should be emphasized that these effects are to be studied in more detail in the future.

REFERENCES

1. K. V. Vladimirsky and B. A. Labzov, Nucl. Instr. & Methods, 14, 94 (1961); Pribory i tehnika experimenta USSR, 1962, No. 2, p. 103.
2. Ch. Schmelzer, Lectures on the theory and design of an alternating gradient proton-synchrotron, CERN (1953).
3. K. V. Vladimirsky, G. Ya. Zueva and B. A. Labzov, Optika i spektroscopia, 12, 522 (1962).
4. J. Combrisson "Quantum electronics" N.Y., 1960, p. 167.
5. F. Bloch, Phys. Rev. 70, 460 (1946).
6. N. Bloembergen, E. M. Purcell, R. V. Pound, Phys. Rev. 73, 679 (1948).

THE APPLICATION OF ELECTRON MAGNETIC RESONANCE TECHNIQUES TO THE STUDY OF THE PHOSPHORESCENCE OF ORGANIC MOLECULES

Clyde A. Hutchison, Jr.
Department of Chemistry and Enrico Fermi
Institute for Nuclear Studies
University of Chicago
Chicago, Illinois

RELATIONSHIP BETWEEN PHOSPHORESCENCE OF ORGANIC MOLECULES AND ELECTRON MAGNETIC RESONANCE SPECTRA

Introduction

This talk will summarize the work done in various laboratories, and reported during the past several years, on the application of paramagnetic resonance techniques to the study of the photoexcited triplet states of organic molecules. This work links two fields of interest to spectroscopists; phosphorescence of organic molecules and paramagnetic resonance.

Lewis mechanism for phosphorescence

As a result of a series of brilliant experiments on the spectroscopy of phosphorescing organic systems G. N. Lewis proposed in 1944 a new mechanism for their phosphorescence. Figure 1 illustrates the energy levels and states involved in his mechanism. He postulated the populating of metastable excited states via radiationless transitions from the excited singlet states of nearly the same energy. These singlet states are responsible for the visible and ultraviolet absorptions of aromatic conjugated ring systems. This radiationless process was assumed to be followed by loss of vibrational energy to the rigid medium in which the phosphor was dissolved, thus trapping the molecules

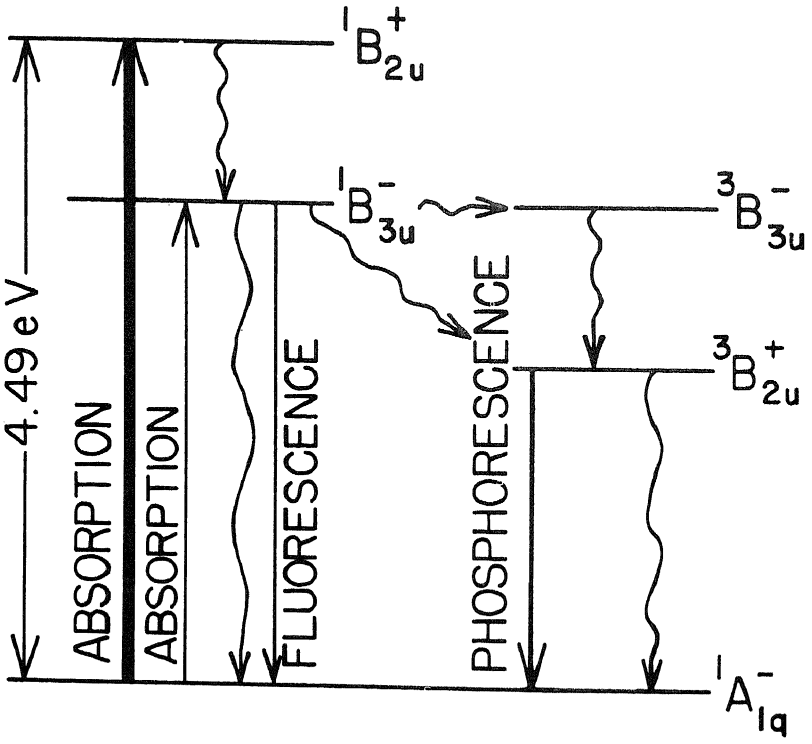

Figure 1.

in the lowest vibrational level of the lowest metastable excited state. The metastable states were assumed to be triplet states with spin 1, one electron having been flipped over during the radiationless transition so that the molecules contained two unpaired electrons.

The strong forbiddenness of singlet-triplet transitions was held to be responsible for the relatively long phosphorescence lifetimes, several seconds or minutes. Spin-orbit coupling, which is a magnetic perturbation capable of flipping spins, was believed to be the main source of phosphorescence transitions back to the ground state.

Figure 1 shows the situation in the case of naphthalene with energy levels given approximately to scale.

Paramagnetism of triplet states

Lewis pointed out that this mechanism implied the occurrence of photomagnetism and with Calvin and Kasha performed the first experiments proving that paramagnetism accompanied such phosphorescence.

Figure 2 represents the 5 filled bonding π-orbitals and 5 antibonding orbitals of naphthalene with its 10 C atoms. The numerical values given in Figure 2 are those of Moffitt and Gouterman. 2 excitations of low energy are indicated. These both have the same symmetry, namely the symmetry which the paramagnetic resonance results demonstrate to be the case for the lowest triplet. In the excited state the 5 and 5' or 4 and 4' electrons may have their spins parallel since they occupy different orbitals. It is such a paramagnetic state with 2 unpaired spins which was postulated as responsible for the long-lived phosphorescence observed in aromatic molecules.

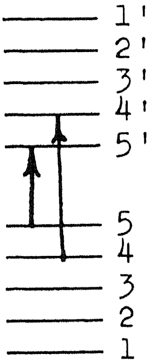

$$L_a = \sin\Phi\,(5,5') + \cos\Phi\,(4,4')$$

$$\Phi = 1.01\ (58°)$$

$$D/hc = +0.104\ \mathrm{cm}^{-1}$$

$$E/hc = -0.0136\ \mathrm{cm}^{-1}$$

Figure 2.

CHARACTERISTICS OF TRIPLET STATE PARAMAGNETIC RESONANCE SPECTRA

Analogy with Ni^{+2}

These triplet states with $S = 1$ of course differ markedly in the nature of their paramagnetic resonance spectra from the doublet states of organic free radicals and free radical ions with $S = 1/2$. The triplet states are analogous to the ground states of the much studied Ni^{+2} ion in crystals, where there is essentially no orbital degeneracy, and the paramagnetic resonance spectra arise from a ground manifold of 3 states associated with the spin of 1.

Magnetic dipole-dipole interaction

One of the main differences of these triplet state spectra from those of the free radicals arises from the removal of degeneracy in the absence of a magnetic field in the case of the triplet states.

The magnetic dipole-dipole interaction between the moments of the 2 unpaired electrons has as a result the removal of the triplet electronic degeneracy even in the absence of any external magnetic field. In the case of the doublet states there is of course the 2-fold electronic degeneracy in the absence of a magnetic field. This triplet degeneracy removal occurs because of the dipole-dipole correlation as the electrons are constrained to move in the π-systems of the very flattened planar aromatic structures.

The energy required to turn over one bar magnet of moment β in the presence of another of the same strength which is one aromatic C-C distance away, corresponds to 0.16 cm^{-1}. This is about as close as the 2 electrons can get because there is only one p orbital on each C, the spins are parallel, and they must not violate the Pauli principle. Because we are dealing with a triplet state the spin part of which is symmetric, the spacial part of the state must be antisymmetric and this gives a strong correlation of the electrons' position in space, keeping them apart. We therefore expect to find zero field splittings a little less but of the same order as the 0.16 cm^{-1} just mentioned.

Anisotropy of spectra

We will also expect a strong anisotropy in our paramagnetic resonance spectra of triplet states in contrast to free radical spectra which occur at almost $h\nu/\beta H = 2$ regardless of direction of the magnetic field. Since the resultant splitting is a combination of the splitting produced within the molecule by the dipole-dipole interaction and the splitting produced by the laboratory magnet, the angle between the lab field and the aromatic plane will be important because the two splittings are comparable in magnitude. In the usual microwave experiments the splittings produced by the laboratory magnet are of order 0.3 cm^{-1}. In other words when we average the dipole-dipole interaction over the distribution of the 2 electrons in the flat aromatic structure it makes quite a difference to the result as to whether the lab field is holding the spin in some direction in the aromatic plane or in a direction perpendicular to the plane.

Energy level diagrams

The effects of the magnetic dipole-dipole interaction on the paramagnetic resonance spectra are easily seen from an inspection of diagrams in which the triplet state energy is plotted versus the magnitude of the magnetic field, $|\mathbf{H}|$. We use the axis system shown in Figure 3. In the upper left corner of Figure 4 the energy level situation is shown for the triplet in the absence of any

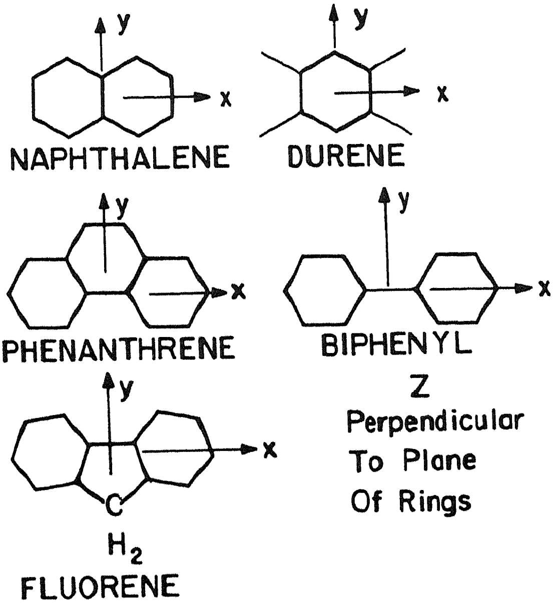

Figure 3.

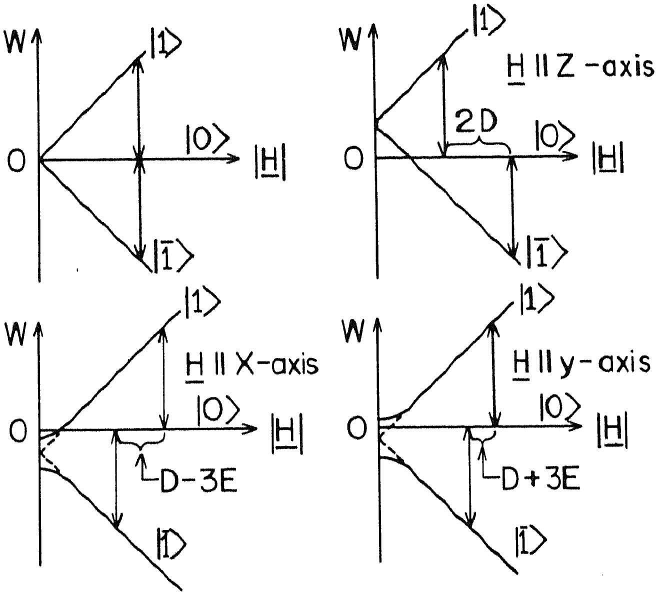

Figure 4.

dipole-dipole interaction (or other interaction resulting in zero field splitting). The states corresponding to the $2S+1 = 3$ orientations of a spin angular momentum, $S = 1$, in an external field are labelled by $|1\rangle$, $|0\rangle$ and $|\bar{1}\rangle$. The microwave quantum is assumed to have the size indicated by the arrows and therefore the resonance will occur at the single field strength shown. This is the same field strength at which the resonance would occur for the doublet S = 1/2 state of a free radical.

Now suppose that we consider the dipole-dipole interaction between the 2 electrons with parallel spin in the triplet S = 1 state. When the field **H** is applied along the z-axis the diagram in the upper right of Figure 4 describes the result. We see that now resonance for fixed microwave frequency will occur at 2 different field strengths. Moreover for each different orientation of **H** with respect to the molecule we will in general find a different such energy level situation. 2 others along the remaining principal magnetic axes of the molecule are given in the lower half of Figure 4. The separations of the 2 absorptions and the position of the absorptions in field vary with the direction of **H** in the molecular axis system. In naphthalene the range of the absorption is approximately 2100 gauss. The experiment is done at about 3000 gauss and the anisotropy is very great.

For randomly oriented molecules the absorptions are therefore very broad. For oriented molecules the absorptions vary with direction of **H** as shown in Figures 5 and 6. In these figures the values of the magnitudes of field |**H**| at which resonance absorptions are observed for photoexcited naphthalenes are plotted on the horizontal axis and the dial readings (arbitrary scale proportional to angle) on the magnet are plotted on the vertical scale. The magnet was rotated and the crystal remained stationary.

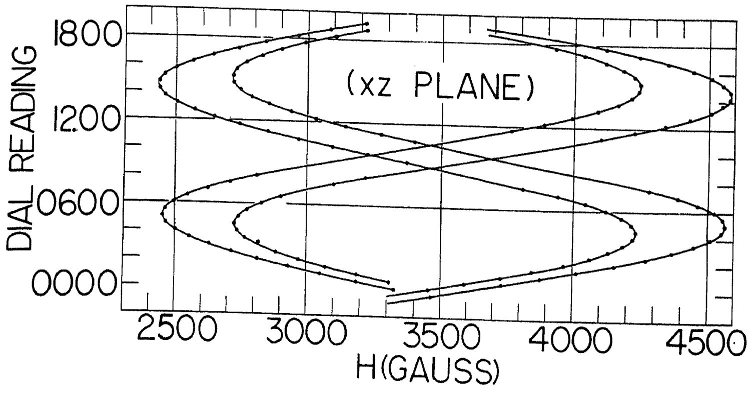

Figure 5.

There are in general 4 absorptions for each orientation of **H**. This is because the naphthalenes are held in a durene crystal and in this crystal they occur in 2 and only 2 orientations with respect to the crystallographic axes. Each molecule gives 2 absorptions,

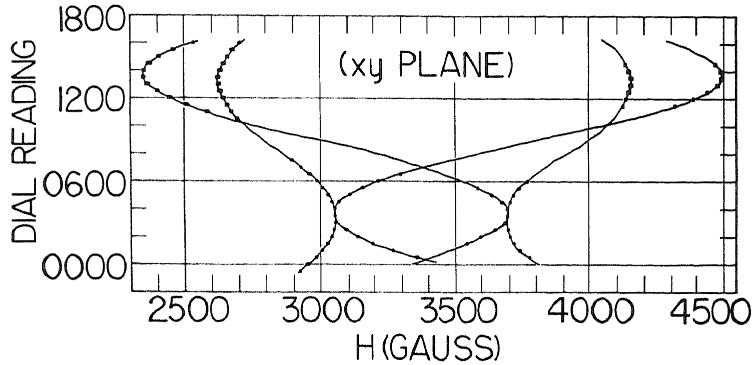

Figure 6.

as we have seen, for each orientation. The stationary points in the variation of $|\mathbf{H}|$ for resonance absorption with angle occur $\pi/2$ apart on the angle scale. In Figures 5 and 6 $\mathbf{H}$ is being moved in principal magnetic planes of a naphthalene molecule. Hence the maximum and minimum in the $|\mathbf{H}|$ for resonance will occur at the values of angle where we pass through the x, y or z-axes of the molecule. In the case shown in Figure 5 the two types of naphthalene molecule are oriented with aromatic planes almost perpendicular to each other and y-axes almost parallel to each other so that as we go around in the xz-plane of one type we are also moving approximately in the xz-plane of the second type, but are $\pi/2$ out of phase. We have 2 almost identical patterns, one shifted $\pi/2$ from the other. The larger peak separation in Figure 5 corresponds to $\mathbf{H} \parallel$ z-axis and the smaller to $\mathbf{H} \parallel$ x-axis. In Figure 6 we are moving in the xy-plane. The y-axes are nearly parallel in the crystal. At the angle where $\mathbf{H}$ is parallel to the y-axis of one molecule it is almost parallel to the y-axis of the other and here we therefore have only 2 peaks instead of the usual 4. In Figure 7 we show a similar diagram for a case in which oriented phenanthrene and naphthalene molecules occurred together in a biphenyl crystal.

Spin-hamiltonian

Such experimental results are very simply described by means of the operator

$$\mathcal{H} \equiv \mathbf{S}\cdot\mathbf{T}\cdot\mathbf{S} + |\beta|\,\mathbf{H}\cdot\mathbf{g}\cdot\mathbf{S};\quad S = 1.$$

This is a Hamiltonian operator which, when diagonalized within the manifold of the 3 states $|1\rangle$, $|0\rangle$ and $|\bar{1}\rangle$ of $S = 1$ (these are the states in the absence of dipole-dipole or magnetic field perturbations) gives the 3 possible values of the energy of the

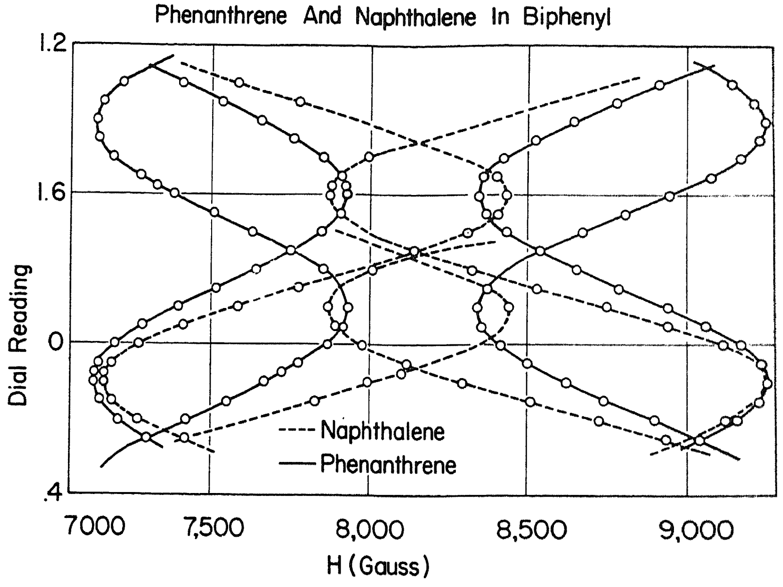

Figure 7.

triplet state system. The linear combinations of $|1\rangle$, $|0\rangle$ and $|\bar{1}\rangle$ which diagonalize the operator are the states of the system in the presence of the perturbations described by the 2 terms of this operator.

Details of states and energies

The first term $\mathbf{S}\cdot\mathbf{T}\cdot\mathbf{S}$ describes the spin-spin (magnetic dipole-dipole) interactions. The second term $|\beta|\, \mathbf{H}\cdot\mathbf{g}\cdot\mathbf{S}$ describes the interaction of the spin with the laboratory magnetic field, **H**. β is the Bohr magneton. Since both **S** and **H** are vectors the 2 proportionality constants T and g must be second rank tensors. It may be shown that when T is put into diagonal form for S = 1 we may give the principal values as $T_{zz} = D$, $T_{xx} = E$ and $T_{yy} = -E$, i.e., the principal value T_{zz} has a magnitude different from the equal magnitudes of the other 2 and the values of T_{xx} and T_{yy} are opposite in sign. It is also the case that the g-tensor is nearly isotropic. This is observed experimentally and expected theoretically. Hence it may be considered approximately as a single scalar. We therefore write:

$$\mathcal{H} = DS_z^2 + E(S_x^2 - S_y^2) + |\beta|\, g\{H_zS_z + H_xS_x + H_yS_y\}.$$

All of the experimental results such as those shown in Figures 5 and 6 may be correlated in terms of the 3 parameters D, E and

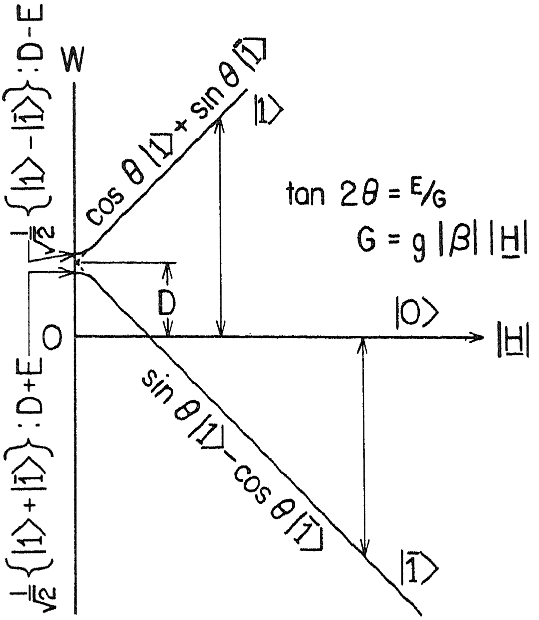
W
$\frac{1}{\sqrt{2}}\{|1\rangle - |\bar{1}\rangle\}$: D-E
$\cos\theta|1\rangle + \sin\theta|\bar{1}\rangle$
$|1\rangle$
$\tan 2\theta = E/G$
$G = g|\beta||H|$
D
$|0\rangle$
0
$|H|$
$\frac{1}{\sqrt{2}}\{|1\rangle + |\bar{1}\rangle\}$: D+E
$\sin\theta|1\rangle - \cos\theta|\bar{1}\rangle$
$|\bar{1}\rangle$

Figure 8.

g. Values of these may be found such that the diagonalized operator gives energy level separation versus angle in agreement with the experimental ones within the error of the measurements. If $|\mathbf{H}| = 0$ we have $\mathcal{H} = DS_z^2 + E(S_z^2 - S_y^2) + |\beta|\, g\{H_zS_z + H_xS_x + H_yS_y\}$.

When in addition $E = 0$ the operator DS_z^2 remains which gives 2 energy levels separated by D, one having 2-fold degeneracy and the other being nondegenerate. The 2-fold level is above the single one when D is + and is below it when D is -. $E = 0$ for molecules with a 3-fold axis perpendicular to the aromatic plane such as triphenylene and with a 6-fold axis such as benzene or coronene. If $E \neq 0$ then diagonalization leads to 3 levels, all nondegenerate. Two of the levels are separated by 2E. The mean of these 2 levels is separated from the third by D. The 3 energies are 0, D+E and D-E. This situation is described at the $|\mathbf{H}| = 0$ side (left side) of Figure 8 (for D positive and E negative). The states here are $|0\rangle$ (same state as in the absence of zero field splitting) and the symmetric and antisymmetric linear combination of $|1\rangle$ and $|\bar{1}\rangle$. When $D = E = 0$ we have just the magnetic interaction $|\beta|g\{H_zS_z + H_xS_x + H_yS_y\}$. If we make $\mathbf{H}$ parallel to the z-axis we then have just $|\beta|g|\mathbf{H}|S_z$ and this gives the 3 energy levels $|\beta|g|\mathbf{H}|$, 0 and $-|\beta|g|\mathbf{H}|$ with the corresponding states $|1\rangle$, $|0\rangle$ and $|\bar{1}\rangle$.

In the presence of both the dipole-dipole interaction and the laboratory field the energies are 0, $D + \{G^2 + E^2\}^{1/2}$ and $D - \{G^2 + E^2\}^{1/2}$

where $G = |\beta| g |\mathbf{H}|$. In Figure 8 these three levels are shown plotted against $|\mathbf{H}|$ for $\mathbf{H}$ parallel to the z-axis. The states are $\cos\theta\,|1\rangle + \sin\theta\,|\bar{1}\rangle$, $|0\rangle$ and $\sin\theta\,|1\rangle - \cos\theta\,|\bar{1}\rangle$ where $2\theta = \tan^{-1}(E/G)$. In very strong fields where the molecular splitting is negligible compared with the splitting produced by $\mathbf{H}$ these states become $|1\rangle$, $|0\rangle$ and $|\bar{1}\rangle$ respectively.

In this talk crystal field effects have been ignored and only intramolecular fields and laboratory fields have been considered. In molecular crystals of aromatic molecules crystal field effects are measurable but are very small indeed relative to the effects considered above.

Zero field spectra

In constrast to the case for free radicals, $S = 1/2$, in which removal of the laboratory field leaves only the splitting produced by weak local magnetic fields, such as those of magnetic nuclei in the molecule, we have for the case of triplets, $S = 1$, a splitting even when $|\mathbf{H}| = 0$ which is of the same order of magnitude as that produced by $|\mathbf{H}|$'s of several thousand gauss. As a result we may still see intense magnetic resonance absorptions when $|\mathbf{H}| = 0$ because energy separations are relatively large and the Boltzmann distribution between magnetic states is still favorable for observation of transitions. 3 transitions may be observed at zero field for naphthalene and other molecules of similar and lower symmetry since there are 3 levels. These transitions correspond to microwave quanta of magnitudes $D+E$, $D-E$ and $2E$. At zero field there is of course no longer any anistropy of field position for which magnetic resonance is observed at fixed frequency. However there is an anisotropy of intensity, i.e. the various transitions are polarized in different directions, the one of size $D+E$ being polarized along the x-axis, the one of size $D-E$ along the y-axis and the one of size $2E$ along the z-axis as shown in Figure 9. It will also be noticed that inasmuch as the zero field states are either (a) the state $|0\rangle$ or (b) one of the states with mixtures of equal amounts of $|1\rangle$ and $|\bar{1}\rangle$, namely, $|1\rangle + |\bar{1}\rangle$ or $|1\rangle - |\bar{1}\rangle$, the hyperfine interaction with magnetic nuclei in the molecule, or dipole-dipole interaction with neighboring magnetic species in the crystal, will largely disappear.

Summary

The chief differences between the electron magnetic resonance spectra of free radicals and the magnetic spectra of phosphorescing molecules are seen to arise from: (a) the degeneracy removal by intramolecular magnetic dipole-dipole interactions

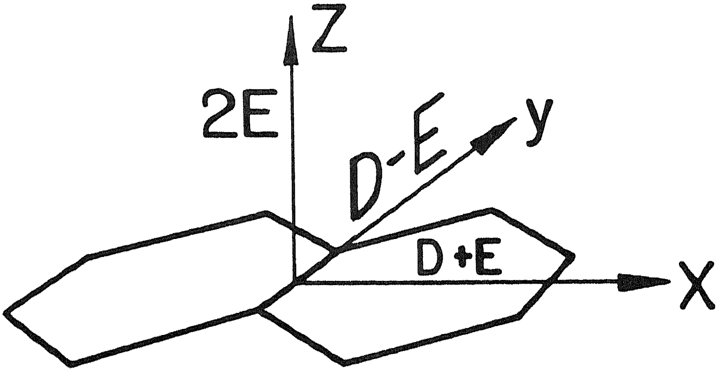

Figure 9.

in the absence of an external magnetic field; (b) the anisotropy of the resonance spectrum with respect to the orientation of the external magnetic field in the molecular axis system; (c) the existence of splittings in the microwave region in the absence of a laboratory field; and (d) the absence of hyperfine interaction in zero external field.

TECHNIQUES FOR THE INVESTIGATION OF THE PARAMAGNETIC RESONANCE SPECTRA OF TRIPLET STATE MOLECULES

Single crystal measurements

In order to eliminate all effects of the anisotropy of the paramagnetic resonance spectra of phosphorescing organic molecules it is necessary to orient the molecules in a single or in a small discrete number of directions in the external magnetic field. Inasmuch as the spectra are not observed in pure crystals of the molecules because of the high mobility of the triplet excitation in such crystals it is necessary to incorporate the phosphor in a host which will fix the direction of the molecular axes of the molecule being examined. The host must of course have suitable transmission of light in the wavelength region required for the photoexcitation of the guest. Such an orientation of naphthalene in durene is illustrated in Figure 10. Such crystals were used for the measurements described in Figures 5 and 6. Another host crystal which has proved convenient for the orientation of phenanthrene or naphthalene is the biphenyl crystal described in Figure 11. This crystal was used for the measurements described in Figure 7. In such crystals intense sharp line spectra are observed and precise information on the fine structure (values of D and E) and the hyperfine interaction with magnetic nuclei is obtainable.

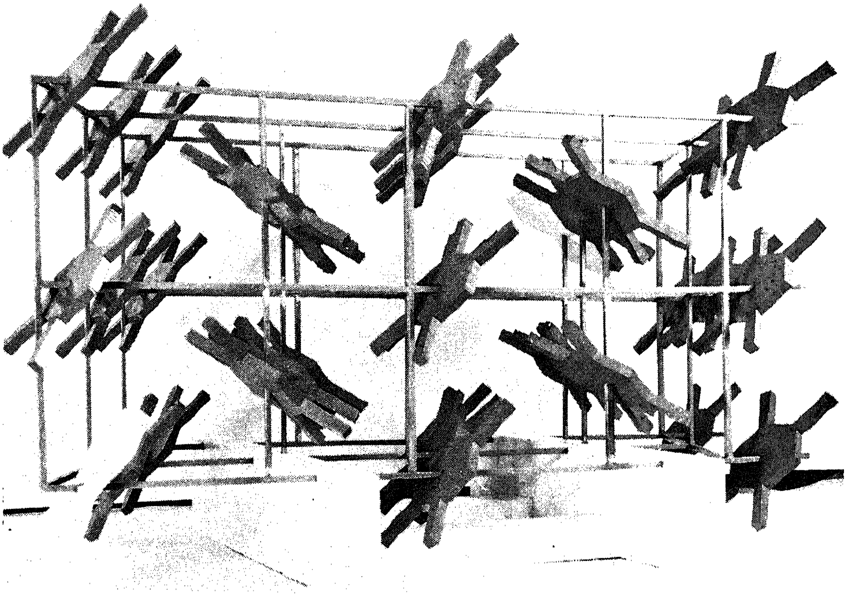

Figure 10.

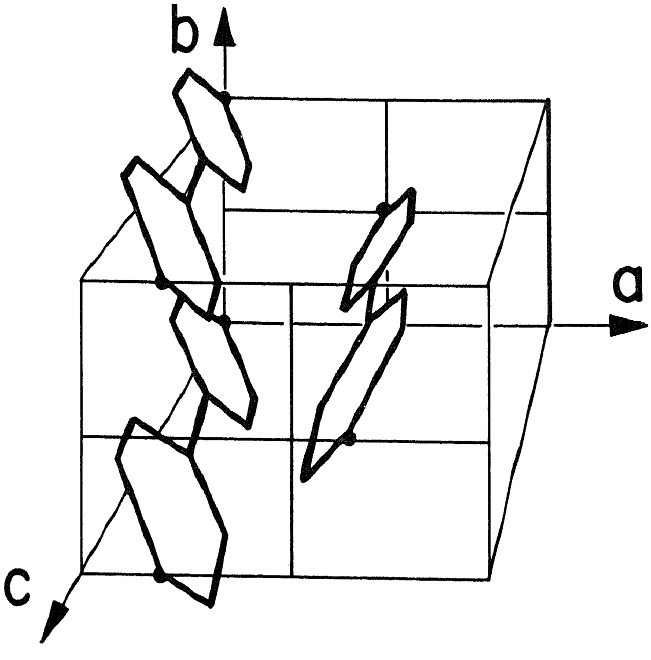

Figure 11.

Randomly oriented molecules

$\Delta M = 2$ transitions

Van der Waals and de Groot have studied the paramagnetic resonance of photoexcited triplet state molecules by observation of the transition from the state which for very large $|\mathbf{H}|$ becomes $|1\rangle$ to the one which for large fields becomes $|\bar{1}\rangle$. As shown in Figure 8, when $\mathbf{H}$ is parallel to the z-axis the 3 states are $\cos\theta\,|1\rangle + \sin\theta\,|\bar{1}\rangle$, $|0\rangle$ and $\sin\theta\,|1\rangle - \cos\theta\,|\bar{1}\rangle$. When the microwave field, H_M, is perpendicular to the external magnetic field, $\mathbf{H}$, and $\mathbf{H}$ is parallel to the z-axis, only the transitions $\cos\theta\,|1\rangle + \sin\theta\,|\bar{1}\rangle \rightarrow |0\rangle$ and $|0\rangle \rightarrow \sin\theta\,|1\rangle - \cos\theta\,|\bar{1}\rangle$ are observable because only these involve the normal perpendicular Zeeman transitions with changes of 1 in M, the strong field quantum number ($|M\rangle$). These are the transitions described in Figures 4, 5, 6, 7, and 8'. If H_M is parallel to $\mathbf{H}$, however, the selection rule is $\Delta M = 0$, and the transition $\cos\theta\,|1\rangle + \sin\theta\,|\bar{1}\rangle \rightarrow \sin\theta\,|1\rangle - \cos\theta\,|\bar{1}\rangle$ may be observed. These 2 states are the ones which in strong field become $|1\rangle$ and $|\bar{1}\rangle$ and this transition is therefore called a $\Delta M = 2$ transition. When $\mathbf{H}$ is not along a principal magentic axis all three states of the triplet molecule are linear combinations of all three states $|1\rangle$, $|0\rangle$ and $|\bar{1}\rangle$. Hence all 3 possible transitions may be seen. The $\Delta M = 2$ transitions are less anisotropic than the $\Delta M = 1$ transition. The $\Delta M = 2$ transitions are sufficiently isotropic that they may be observed in randomly oriented molecules e.g., in solutions of organic phosphors in a glass. This permits the study of many of these systems without the necessity of finding suitable host crystals in which the molecule may be incorporated as an oriented species and greatly extends the scope of possible investigations.

$\Delta M = 1$ transitions

It has recently been observed by Wasserman that the $\Delta M = 1$ transition shown in Figures 5 and 6 may also be observed in glasses containing randomly oriented phosphor molecules. There is a sufficiently larger number of the randomly oriented molecules with orientations such that they give resonances at fields near the stationary points of the patterns shown in Figures 5 and 6 than there is of molecules giving peaks at other fields, that signals in the vicinity of these turning points can be observed.

Zero field transitions

Because of the fact that, as explained earlier, the magnetic resonance absorptions of these triplet state molecules are intense at zero magnetic field, the spectra of randomly oriented molecules of such phosphors in glasses may be observed in zero field. Because of the absence of line broadening due to hyperfine interaction and dipole-dipole interaction with neighboring paramagnetic species we may expect these spectra to consist of sharp intense lines. This provides a very useful technique of considerable sensitivity for the investigation of randomly oriented phosphor molecules.

RESULTS OF THE INVESTIGATIONS OF TRIPLET STATE SPECTRA

Spin-hamiltonian parameters and zero field splittings

Tables I, II and III list some results of measurements of parameters in the spin-hamiltonian. These results were obtained at the boiling point of liquid N_2 and at both ~ 10,000 mc sec^{-1} and ~ 23,000 mc sec^{-1} microwave frequency. The magnetic resonance spectra were observed during continuous irradiation of the crystals with light from a high pressure Hg arc. Table I gives g values for naphthalene. It will be seen that g is nearly isotropic. Tables II and III give values of D/hc and E/hc for naphthalene and phenanthrene respectively. D and E have opposite signs and Klein has shown that D is +. The values labelled low field were obtained from transition frequencies measured at fields from 4 to 50 or 75 gauss and represent extrapolations to zero field. At 4 gauss the measured frequencies are equal to the true zero field frequencies to within a few units in the sixth decimal place.

Table I

HIGH FIELD RESONANCE

$$\mathcal{H} = \underline{H}g\underline{S} + DS_z^2 + E(S_x^2 - S_y^2)$$

	g_{xx}	g_{yy}	g_{zz}	D/hc cm^{-1}	E/hc cm^{-1}
H	2.0030 ±0.0004	2.0030 ±0.0012	2.0029 ±0.0004	±0.1003 ±0.0001	∓0.0137 ±0.0002
D	2.0030 ±0.0004	2.0031 ±0.0003	2.0023 ±0.0006	±0.1010 ±0.0002	∓0.0134 ±0.0001

Table II

NAPHTHALENE

UNIT CM^{-1}		PROTO		DEUTERO
		DURENE	BIPHENYL	D-DURENE
HIGH FIELD	D E	+0.1003 -0.0137	+0.0994 -0.0154	+0.1010 -0.0134
LOW FIELD	D E	+0.10118 -0.01408	+0.09920 -0.01545	+0.10134 -0.01393

Table III

PHENANTHRENE

UNIT CM^{-1}		BIPHENYL	FLUORENE
High Field	D/hc E/hc	+0.1008 -0.0467	+0.1005 -0.0445
Low Field	$\frac{D+E}{hc}$	+0.05387 ±0.00002	———
	$\frac{D-E}{hc}$	+0.14701 ±0.00002	
	$\frac{2E}{hc}$	-0.09315 ±0.00003	-0.09045 ±0.00003
	$\frac{D}{hc}$	+0.10044 ±0.00002	———
	$\frac{E}{hc}$	-0.04657 ±0.00002	-0.04528 ±0.00002

The values found for the spin-Hamiltonian parameters are in excellent agreement with those calculated as mentioned previously by Moffitt and Gouterman and others and show that the origin of the zero field splitting is indeed the magnetic dipole-dipole interaction between the 2 electrons with parallel spins in the triplet state.

It should be noted that although crystal field effects are small the effect of the medium in which the phosphor is held can be observed and measured. The effect of deuterium substitution on the values of the parameters can also be seen. The effect of temperature has been measured and in the vicinity of the boiling point of liquid N_2 the temperature coefficient of (D-E)/hc for naphthalene in biphenyl was found to be -1.3×10^{-5} cm^{-1} deg^{-1}.

These experiments on the fine structure of organic phosphors oriented in host crystals have proved

A. the triplet character of the states associated with the phosphorescence of these molecules;

B. the origin of the zero field splitting in the magnetic dipole-dipole interactions of the 2 triplet state electrons;

C. the orientation of phosphor molecules in the host crystal with principal magnetic axes parallel to those of the host;

D. the small effects of crystal fields.

Hyperfine structure

The theory of the observed isotropic and anisotropic hyperfine interactions of π-electrons with protons attached to aromatic rings in organic free radicals is now quite well understood. In the case of the organic phosphors oriented in host crystals we have the opportunity of investigating the anisotropic hyperfine interaction in photoexcited triplet states.

The magnitudes of both the isotropic and anisotropic components of the proton hyperfine interactions in such systems are very accurately proportional to the normalized electron spin density on the C atom to which the H in question is attached. A C atom of an aromatic ring with attached H is described in Figure 12. The A-axis is along the C-H bond, the B-axis is normal to the plane of the aromatic ring and along the axis of the p orbital on the C atom and the C-axis is a third mutually perpendicular axis. The isotropic plus anisotropic proton hyperfine splittings per unit spin density on adjacent C atom are approximately 30, 60 and 90 mc sec^{-1} along the A, B and C-axes respectively. We may regard our triplet state molecule as a collection of such C-H fragments. Figure 13 shows such a collection of 8 fragments in the case of the naphthalene molecule. There are of course only 2 types of structurally inequivalent C-H fragments in this particular molecule, the 4 α fragments which are located next to the hydrogenless bond at the center of the molecule and the 4 β fragments. One ABC system for an α fragment and one ABC system for a β fragment are shown in Figure 13. Now suppose that the laboratory field $\mathbf{H}$ is along the x-axis of the naphthalene

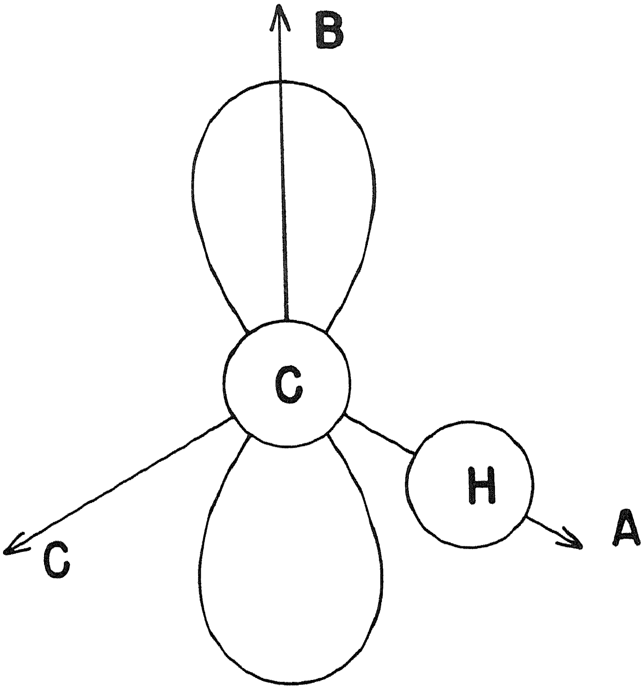

Figure 12.

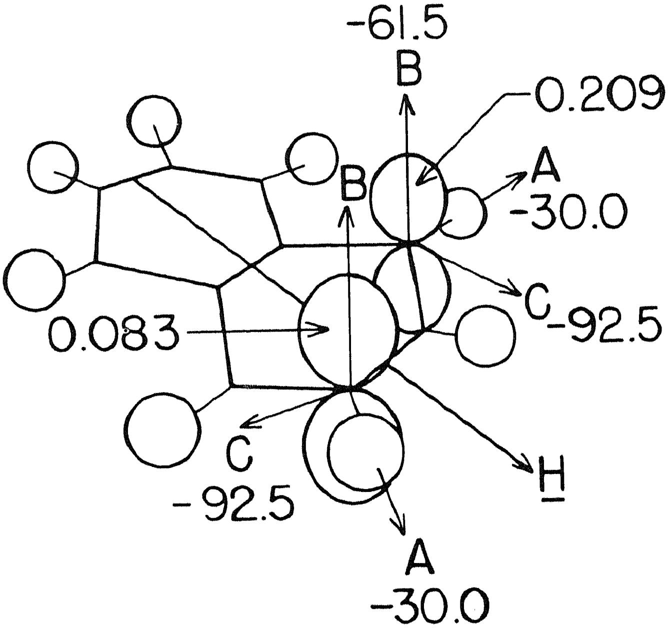

Figure 13.

molecule. In this orientation **H** is close to parallel to the C-axis of the α fragments, i.e., to the direction of largest hyperfine interaction. The α C atom is the one with largest spin density, the numerical values of the spin densities being 0.209 and 0.083 for the α and β C's respectively (and presumably having a small negative value for the central C's). The total spin density of the molecule must be normalized to 1, not 2. On the other hand for the β fragments **H** is close to the A-axis, i.e., to the direction of smallest hyperfine interaction. The β C's are also the ones with the smallest spin density and hence the contribution of the β fragments to the hyperfine splitting is very small compared with that of the α fragments. The 4 equivalent α interactions therefore give a 5 peak pattern, each proton having spin 1/2. Each of these 5 peaks is further split by a smaller amount into 5 peaks giving the total of 25 peaks expected for 2 sets of 4 equivalent spins each. The splittings of the β's have not at the present time been resolved. With **H** in the direction of the x-axis of naphthalene the 5 peak pattern shown in Figure 14 is observed (first

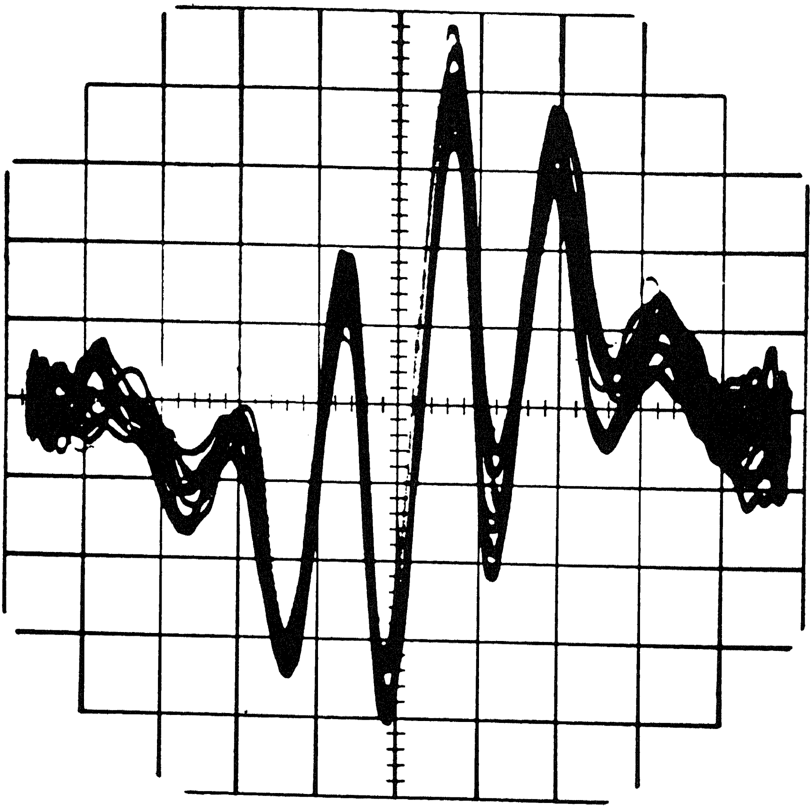

Figure 14.

derivative of the absorption). If now a D atom is substituted for an α H atom it will produce only a very small hyperfine interaction because of its much smaller gyromagnetic ratio. We now have only 3 α H's and a 4 peak pattern is observed. With substitution of a second D the 3 peak pattern of Figure 15 is the result when **H** is parallel to the x-axis of naphthalene. Thus we see that the hyperfine patterns which we observe may be understood in terms of the conventional theories of the hyperfine interaction and afford very detailed insight into the electronic structures of the triplet state systems. With **H** parallel to the z-axis and with the substitution of one β D only, the pattern shown in Figure 16 is observed.

These investigations of the hyperfine patterns of the triplet state spectra of ordinary light naphthalene and of the D substituted species have proved that

A. the chemical species responsible for the phosphorescence and paramagnetic resonance absorption is the naphthalene molecule;

B. the orientation of the naphthalene molecule is such that not only are its principal axes parallel to those of durene but also the x, y and z-axes of naphthalene are parallel respectively to the x, y and z-axes of durene;

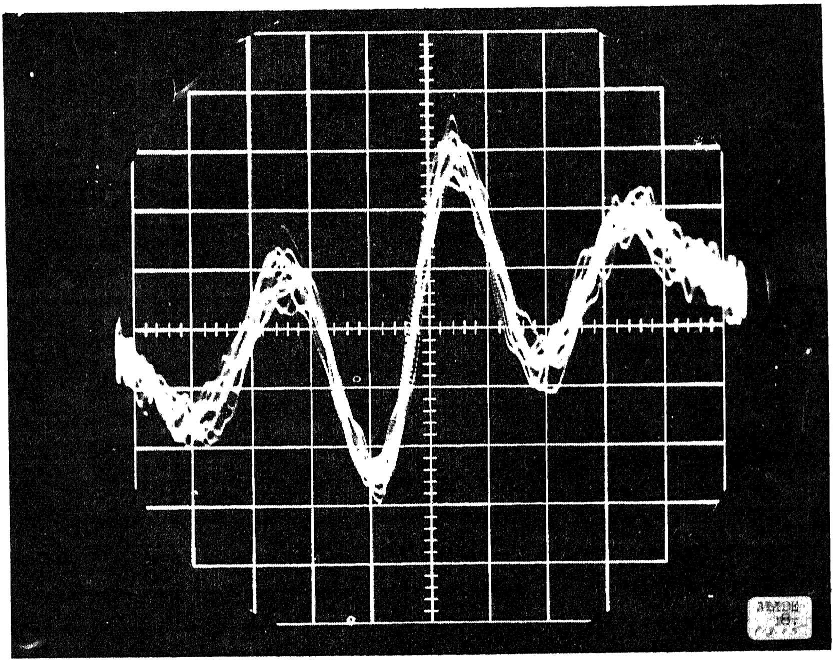

Figure 15.

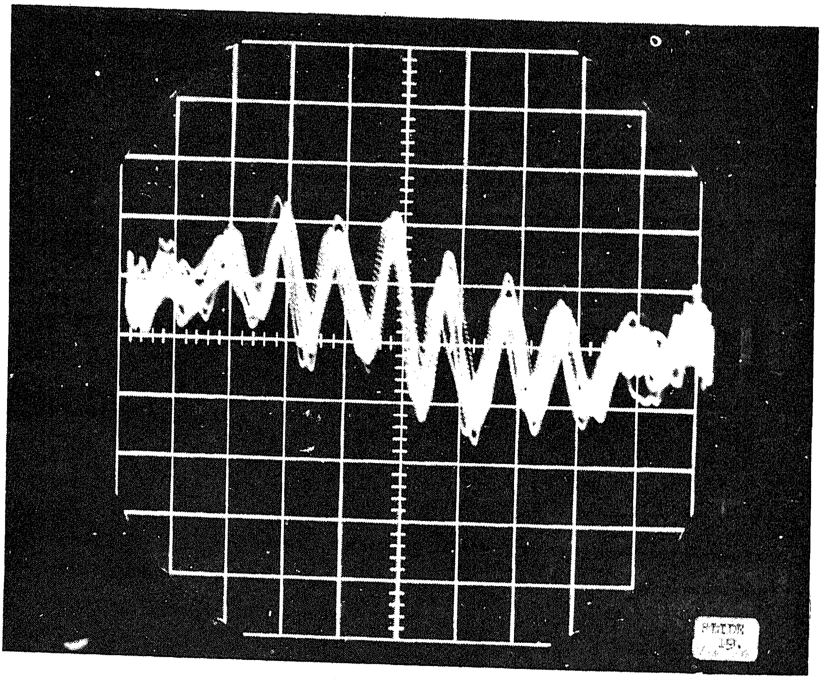

Figure 16.

C. the electronic state responsible for the phosphorescence and the magnetic spectrum is $^3B^+_{2u}$ and not $^3B^+_{3u}$ as has been claimed, or some state of other symmetry.

Isotope effect on lifetimes

If 8 D's are substituted for the 8 H's of naphthalene the absorption peak shown in Figure 17 is observed. This absorption is much more intense than those shown on previous slides and this accounts for the much increased signal to noise ratio. When the lifetime of this absorption after cessation of irradiation was measured it was found to be ~ 17 sec compared with the measured 2.1 sec for ordinary light naphthalene. The increased signal intensity is due to the higher concentration of triplet states resulting from the slower decay rate. It has been shown that ~0.80 of the naphthalene molecules which reach the triplet state leave it by radiationless transition to excited vibrational levels of the ground singlet state rather than by phosphorescence emission. The 2.1 sec lifetime for the light naphthalene is therefore largely determined by this radiationless decay rate. The introduction of D alters the density of vibrational states, because of the different zero point energy, in such a way as to reduce the amount of radiationless decay and the decay occurs then largely by

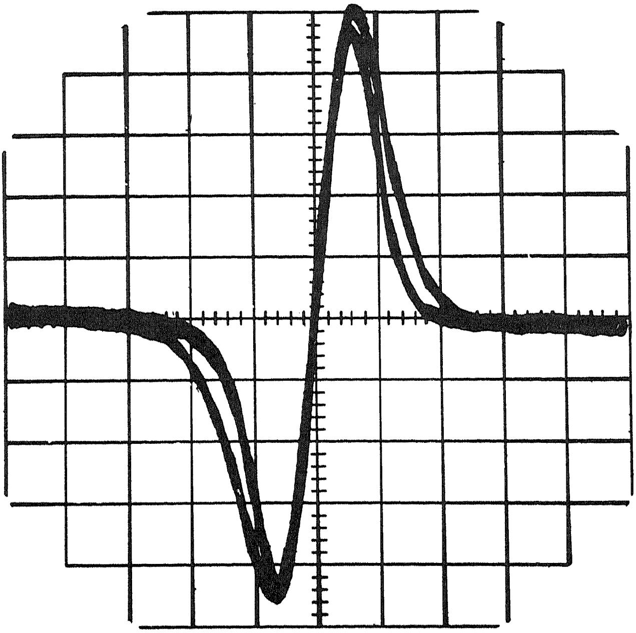

Figure 17.

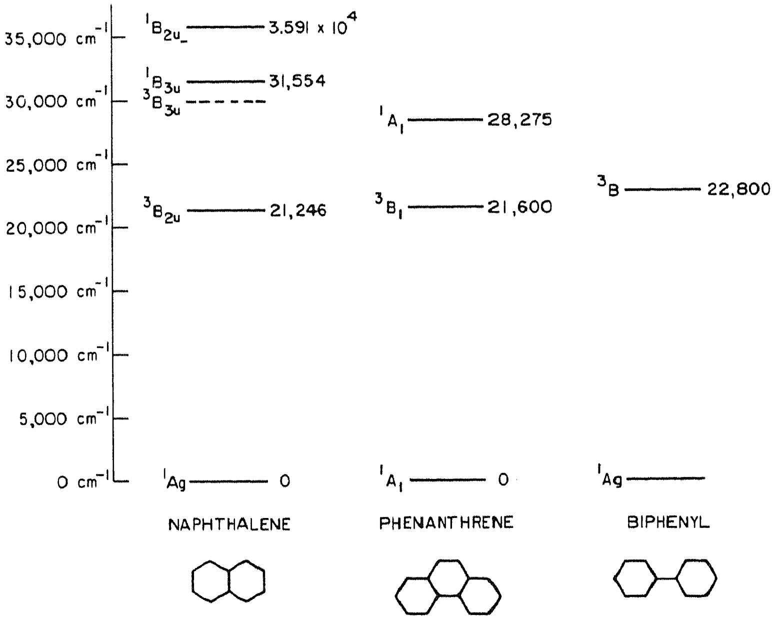

Figure 18.

phosphorescence which has the longer lifetime. D has the effect in general, for aromatic molecules, of lengthening the lifetimes. This effect was first observed by study of the paramagnetic resonance spectrum.

Energy transfer in organic crystals

Paramagnetic resonance absorption has been employed to investigate the transfer of triplet excitations from one molecular species to another in a rigid medium e.g., the transfer of triplet excitation from phenanthrene to naphthalene when both molecules are oriented in the same biphenyl crystal has been observed at the boiling point of liquid N_2. Figure 18 shows the lower energy levels of naphthalene, phenanthrene and biphenyl. When such a biphenyl crystal containing naphthalene and phenanthrene was irradiated the results described in Table IV were obtained. The third column lists the species whose resonance was observed. The filter mentioned in the slide was a solution of naphthalene in isooctane placed between the Hg arc and the biphenyl crystal and which of course removed all light absorbable by naphthalene. We observed the ratios of (a) the intensities of the resonance signals of the crystalline solutions in the presence of this high frequency cutoff filter between the light source and the crystalline solution to (b) the intensities in the absence of such a filter.

Comparison of the ratios in Table IV shows the following: (1) The filter annihilates the naphthalene magnetic resonance signal when only naphthalene is present as solute in the biphenyl crystal. (2) The filter reduces the phenanthrene magnetic resonance signal to approximately one-half its value whether naphthalene is present in the biphenyl crystal or not. This is very close to the factor by which the light energy available in the α-absorption band of phenanthrene is reduced by the absorption of light in the filter. (3) The filter does not annihilate the naphthalene magnetic resonance signal when phenanthrene is also present. In fact the naphthalene magnetic signal is attenuated by only 1.3 to 1.6 times the factor by which the phenanthrene signal is reduced. The triplet states of naphthalenes are clearly excited in case (3) by transfer of energy from phenanthrene molecules. This transfer does not appreciably reduce the steady state concentration of triplet phenanthrene.

The observed anisotropies of the fine structures and the measured spin-Hamiltonian parameters of both the naphthalene and phenanthrene spectra show that both molecular species occur as oriented molecules. Both solute molecules have entered the structure substitutionally for biphenyl whether added individually or together to the solvent crystal. The principal magnetic axes of both the naphthalene and phenanthrene molecules are respectively parallel to those of biphenyl molecules.

In Table IV we have summarized the observed values of the parameters D and E for naphthalene and phenanthrene in biphenyl and other solvents. These measurements serve, of course, to identify the orientations described above. Inspection of Table IV shows that whereas a change of solvent from biphenyl to durene or fluorene produces changes in transition frequencies which are from 25 to 150 times as large as the experimental uncertainties, the transistion frequencies of both naphthalene and phenanthrene are independent, within experimental error, of the presence or absence of the other in the biphenyl crystal. This indicates that the environment of a solute molecule of one species is the same whether or not the other species is present in the biphenyl crystal. One might therefore conclude that (a) complex formation between phenanthrene and naphthalene or (b) some type of molecular association or juxtaposition in the crystal structure did not occur to an observable extent.

These results indicate the possibility of the transfer of triplet state energy between the two solutes by means of the biphenyl structure.

Ground state triplets

A related subject of interest which is not included under the title of this talk is the investigation of stable triplet ground state organic molecules. Such states have recently been observed by Wasserman and in our own laboratory together with Closs and Brandon. We have observed stable triplet states produced by irradiation of diphenyldiazomethane with visible light in a benzophenone crystal. We believe that the stable species is diphenylmethylene described in Figure 19 together with the host species, benzophenone. The species which we observe is a triplet state

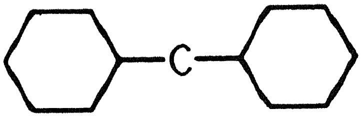

DIPHENYLMETHYLENE

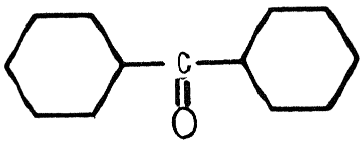

BENZOPHENONE

Figure 19.

Table IV

Solvent	Solute	Magnetic Resonance	$\frac{\text{Intensity with Filter}}{\text{Intensity without Filter}}$		$\frac{D+E}{hc}$ cm^{-1}	$\frac{D-E}{hc}$ cm^{-1}	$-\frac{2E}{hc}$ cm^{-1}
			Value at Low Field	Value at High Field			
Biphenyl	Naphthalene Phenanthrene	Naphthalene	0.290 ±0.015	0.35 ±0.04	0.08373 ±0.00003	0.11469 ±0.00003	(0.03096)[a]
Biphenyl	Naphthalene	Naphthalene	<0.011	<0.076	---	0.11476 ±0.00002	---
Biphenyl	Naphthalene Phenanthrene	Phenanthrene	0.530 ±0.008	0.44 ±0.07	0.05385 ±0.00002	0.14700 ±0.00001	(0.09315)[a]
Biphenyl	Phenanthrene	Phenanthrene	0.491 ±0.006	0.46 ±0.04	0.05387 ±0.00002	0.14701 ±0.00002	0.09315 ±0.00003
Durene	Naphthalene	Naphthalene	---	---	0.08708	0.11529	(0.02821)[a]
Fluorene	Phenanthrene	Phenanthrene	---	---	---	---	0.09045 ±0.00003

[a] Calculated from other entries in the row.

molecule produced by the irradiation with visible light, which does not decay when irradiation ceases, provided the temperature remains at the boiling point of N_2, showing it to be in its ground state. Also the zero field splittings which we observe are much larger than those which we find for photoexcited triplet states of aromatic rings indicating that the 2 triplet electrons get much closer together than in the previously investigated phosphors. This is of course possible on the central C of diphenylmethylene where 2 orthogonal p orbitals are available for simultaneous occupancy by these electrons.

ACKNOWLEDGMENTS

The research on photoexcited triplet states at the University of Chicago which has led to many of the results described in this talk has been the result of the efforts of R. W. Brandon, R. E. Gerkin, W. M. Huo, B. W. Mangum and P. Palmer. E. Bartal, J. S. D. Danielson and C. Davoust have assisted in the construction of the apparatus which was used. The work has been supported by the United States Atomic Energy Commission.

HIGH RESOLUTION ELECTRON SPIN RESONANCE

K. H. Hausser
Max-Planck-Institut
Heidelberg, Germany

Magnetic spin resonance is a comparatively new branch of spectroscopy. The quantization of the spatial orientation of the spins of electrons or nuclei with respect to a static magnetic field results in discrete energy levels. Between these energy levels magnetic dipolar transitions may be induced by a radio frequency electromagnetic field, provided its frequency fulfills the resonance condition:

$$h\nu = \Delta E = g\mu_B H_o .$$

In contrast to other branches of spectroscopy, where the frequency is the fundamental quantity to be measured, in magnetic spin resonance the frequency is proportional to the applied field, and the factor of proportionality, the g-value, is the simplest basic quantity characteristic of any particular system.

However, ESR renders much more detailed information by virtue of the interaction of the electronic spin with neighbouring nuclei. The splitting of the ESR-absorption line into individual components by this interaction is termed hyperfine structure (HFS). The energy of the hyperfine interaction with one nucleus is usually expressed in the form of a Hamiltonian $\mathcal{H}_{HFS}$, the subscript indicating that the other terms of the spin-Hamiltonian have been omitted:

$$\mathcal{H}_{HFS} = g_\ell \, g_N \, \mu_B \, \mu_N \left[\frac{\vec{S}\cdot\vec{I}}{|\vec{r}_{\ell,N}|^3} - \frac{3(\vec{S}\cdot\vec{r})(\vec{I}\cdot\vec{r})}{|\vec{r}_{\ell,N}|^5} - \frac{8\pi}{3}\,\psi^2(\vec{S}\cdot\vec{I}) \right].$$

For more than one nucleus this expression has to be extended to a sum over all nuclei.

The first two terms originate from the direct magnetic dipolar interaction; this direction-dependent anisotropic part of the HFS can be studied in single crystals. We are here concerned with the anisotropic HFS only in so far as it causes broad lines in randomly oriented material. Consequently, high resolution ESR is restricted for the same reason as high resolution NMR to solutions, in which the anisotropic broadening of the absorption lines is averaged out by the fast tumbling of the molecules due to the thermal motion.

The third term, usually called the "Fermi" or "contact-term," is proportional to the square of the wave function ψ^2 of the unpaired electron at the nucleus. This "isotropic" HFS provides a means of measuring the extension of the orbital of the unpaired electron, or in the language of valence bond theory, the statistical weight of the mesomer resonance structures. A well resolved HFS-pattern is a "fingerprint" suitable to identify the paramagnetic substance from which it originates.

The amount of information obtainable in ESR as in any spectroscopy obviously increases with increasing resolution. However, the conditions under which the best possible resolution occurs have not been studied as systematically in ESR as in NMR, where in the last 10 years high resolution has been established as a routine method. The main reason for this difference is probably the different origin of the line width. While in HR-NMR the obtainable resolution is primarily determined by the technique, in particular the homogeneity and stability of the magnetic field, the linewidth of the individual HFS-components in ESR originates from physical events within the sample itself, that is, from the relaxation phenomena. Therefore, HR-ESR requires the study of relaxation mechanisms.

It is convenient to distinguish two relaxation phenomena. The first maintains temperature equilibrium between the spin system and its surroundings; the rate of energy transfer between the spin system and the "lattice" is measured by the spin lattice relaxation time T_1. The second part comprises all processes in which the energy of the spin system remains constant; the rate of change of the entropy of the spin system due to spin-spin interactions is measured by the spin-spin relaxation time T_2'. Finally the reciprocal width of the ESR absorption line is usually expressed in terms of a third relaxation time T_2, to which both T_1 and T_2' contribute in the general form

$$\Delta\nu \approx \frac{1}{T_2} = \frac{C_1}{T_1} + \frac{C_2}{T_2'} ,$$

where C_1 and C_2 are constants whose value depends on the particular relaxation mechanisms which occur in a given sample.

A theoretical treatment of the origin of the linewidth of the HFS-components has been given by Kivelson [1] and others. The three most important mechanisms by which relaxation occurs are:

1. Magnetic dipolar interaction.
2. Exchange interaction.
3. Interactions involving spin-orbit coupling.

1. The magnetic dipolar interaction is always present; its description is based on the theory of Bloembergen, Purcell and Pound [2]. Following these authors one has to consider the magnetic noise spectrum as a function of the frequency. The Fourier component in the Larmor frequency induces transitions between the energy levels and therewith contributes to T_1; its intensity depends on the correlation frequency, i.e., the viscosity of the solvent. On the other hand, the quasi-static "near zero" frequencies determine the spin-spin relaxation time T_2'. Both depend on the temperature; the resulting line width could be shown to decrease with decreasing viscosity and increasing temperature respectively. At higher concentrations the dominating interaction is the one between the electronic spins because of their much bigger magnetic moment, while at lower concentrations the interaction between the electronic spin and the neighbouring nuclei becomes more important. Consequently, the linewidth originating from magnetic dipolar interaction should be concentration-dependent at high concentration and level off at lower concentrations.

2. The contribution of the exchange interaction both to T_1 and T_2' depends on the exchange frequency f_{ex}, which is in a liquid proportional to the number of collisions per unit time [3], and consequently to the concentration and temperature:

$$f_{ex} \sim ckT/\eta.$$

The linewidth of the individual HFS-components due to exchange phenomena increases with increasing concentration and with increasing temperature.

3. The relaxation mechanisms involving spin-orbit coupling are somewhat more complicated. The anisotropy of the g-value increases with the square of the spin-orbit coupling parameter λ. This effect leads to a static term which contributes to T_2' and is dominating at high viscosity, and leads as well to a term contributing to T_1 which becomes more important at lower viscosity. The linewidth due to this type of interaction is proportional to the applied magnetic field H_o and could hence be distinguished from another mechanism to

be described as follows: The spin-orbit interaction couples the spin S, which is oriented with respect to the external magnetic field, to the orbital momentum, L, which has a fixed orientation within the framework of the molecule. The angle, θ, between the molecular axis and the magnetic field varies due to the tumbling of the molecules in solution. The variation of θ causes a time dependent perturbation of the Spin-Hamiltonian which contributes to the relaxation. The relevant frequency for this interaction is the rotational correlation frequency ($\tau_{c,\,rot}$), for which the rather poor approximation $\tau_{c,rot} = 4\pi\nu a^3/3kT$ is usually used. (a = radius of the molecule, η = viscosity.) Without going into details I would like to point out that all interactions based on spin-orbit coupling do not depend on concentration in contrast to the other relaxation mechanisms mentioned above. Relaxation *via* spin-orbit coupling is the dominating mechanism for paramagnetic ions and for metal chelate compounds containing heavy elements, but less important for free radicals containing first row elements only.

I would like to illustrate this theoretical reasoning by some examples. The sandwich-dibenzene complexes of chromium, molybdenum and tungsten are suitable examples for case 3, relaxation *via* spin orbit coupling. These three compounds have the same structure and outer electronic configuration, but increasing atomic numbers Z and therewith increasing spin orbit coupling parameter λ. Their spectra in ethanol at different temperatures are given in Figure 1 in the sequence Cr, Mo and W from top to bottom.

At room temperature the HFS of the Cr-complex is partially resolved while it is smeared out in the Mo-complex by the shorter T_1 originating from the larger spin orbit coupling. In the W-complex the line is so broad as a result of the still larger spin-orbit coupling that it cannot be detected. With increasing temperature the Brownian motion is slowed down and the intensity of the Fourier component at the Larmor frequency is reduced, with the result that at -80°C the HFS of the Cr-complex is fully resolved, the one of the Mo-complex is partially resolved and the absorption of the W-complex becomes observable, but without structure. At -100°C the anisotropy of the g-value is only partially averaged out by the reorientation of the molecules with the result that all structure disappears. Finally, at -140°C the linewidth of the Cr and Mo-compound are determined primarily by the magnetic dipolar interaction which is almost the same for both compounds. Hence the resolution of the Mo-complex is better due to the larger coupling constant of 4.8 gauss instead of 3.5 of the Cr-complex. Some structure appears also in the spectrum of the W-complex, but its linewidth is still considerably larger due to a contribution of the

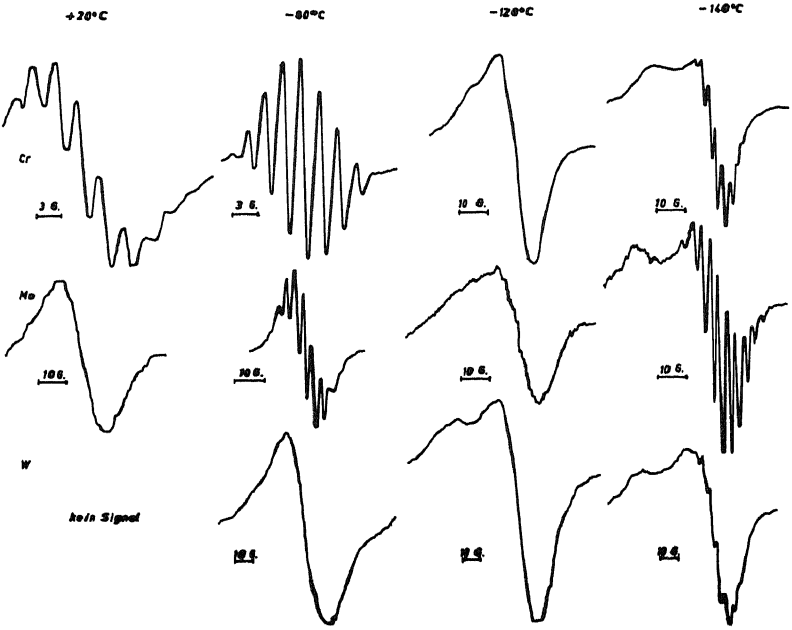

Figure 1. ESR spectra of the dibenzene-iodides of Cr, Mo and W in ethanol at different temperatures.

spin-orbit interaction. It is obvious that such systems with large spin-orbit coupling are not suitable for HR-ESR.

Solutions of free radicals possessing a small spin-orbit coupling parameter λ at medium and high concentrations are useful to illustrate the exchange effects since their linewidth is almost entirely determined by exchange interactions. Figure 2 shows the temperature dependence of the ESR spectrum of bis-diphenylene-phenyl-allyl in toluene, at a concentration 10^{-2} mol/l. The hyperfine structure disappears with increasing temperature, which increases the exchange frequency, until finally the remaining single line in the center of the absorption becomes narrower by the effect known as exchange narrowing, which we do not want to discuss further since it occurs only at high concentrations and definitely excludes high resolution.

Following the arguments and examples given so far, a well resolved HFS pattern would be expected for dilute solutions of free radicals containing first row elements only. In many cases, however, such solutions do not exhibit any structure but show only one single broad absorption. In these cases the broadening is due to the interaction with the dissolved paramagnetic molecular oxygen. The effect of the dissolved oxygen may be illustrated by Figure 3 which shows the ESR spectrum of 2,4,6-triphenyl-phenoxyl, at a concentration ca.10^{-4} mol/l., in benzene.

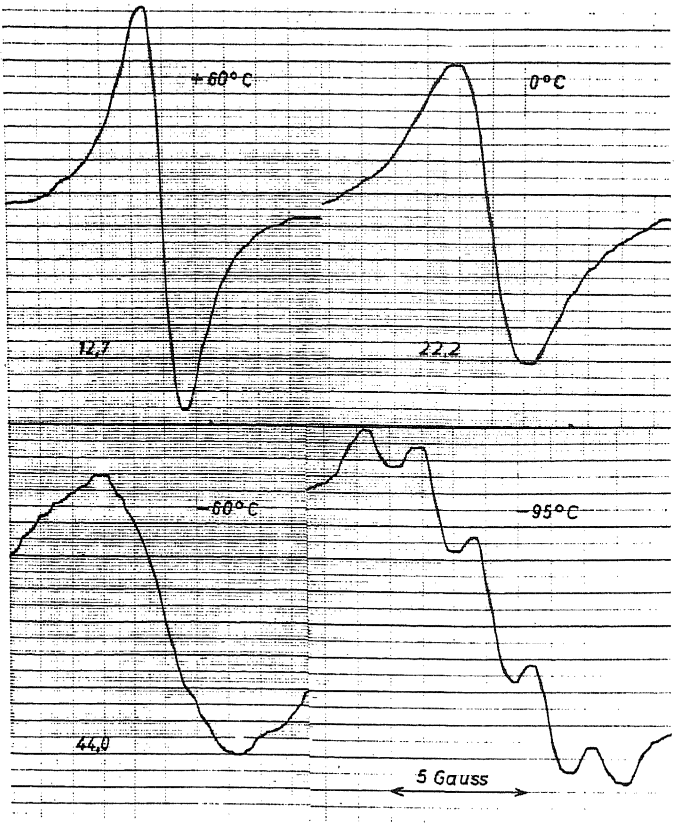

Figure 2. ESR spectra of 1,3-bisdiphenylene-phenyl-allyl in toluene, concentration 10^{-2} mol/l, at different temperatures.

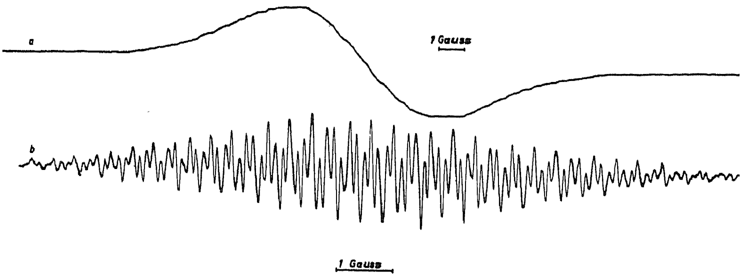

Figure 3. ESR spectrum of the 2,4,6-triphenyl-phenoxyl in benzene, concentration about 10^{-4} mol/l. Above: saturated with air, below: oxygen-free.

The upper spectrum is taken with a solution saturated with air, while the lower spectrum results from the same solution after the oxygen has been carefully removed.

Another example of the effect of the dissolved oxygen is the spectrum of Wursters Blue, the central part of which is given in Figure 4, saturated with air and after the exclusion of the oxygen. It is tempting to attribute the additional splitting to a third small coupling constant of 0.28 gauss originating from the two equivalent nitrogen atoms, since the two bigger splittings present in the spectrum had been shown previously [4] to be due to the methyl- and ring-protons respectively. I have actually given this incorrect interpretation in an earlier paper [5], but a more careful reexamination of the spectrum has shown that it can be much better accounted for in terms of a coupling constant of 7.02 G for the nitrogen together with the two other coupling constants of 6.74 G for the methyl protons and 1.98 G for the ring protons. The observed and the theoretical spectrum based on these constants are given in Figure 5, the excellent agreement leaving little doubt about the correctness of this interpretation. The nitrogen splitting of the order of 7 G is also in better agreement with theory and with the observed splittings in similar molecules.

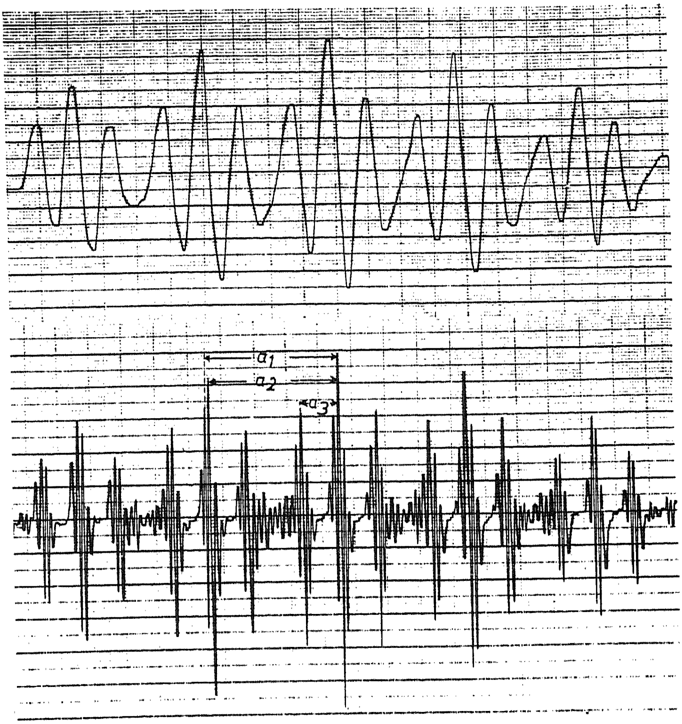

Figure 4. Central part of the ESR spectrum of Wursters blue.

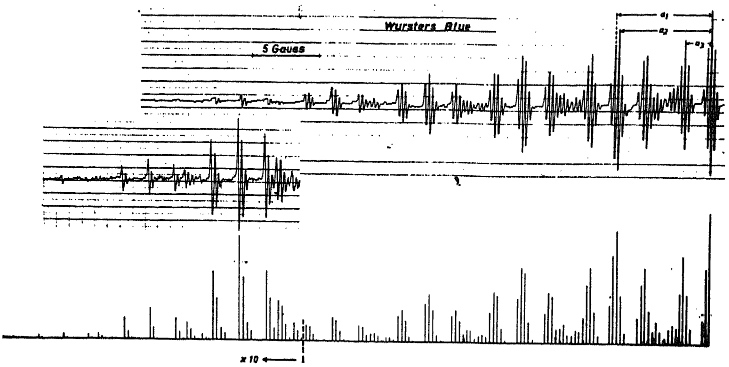

Figure 5. ESR spectrum of Wursters blue together with the theoretical reconstruction based on the coupling constants $a_N = 7.02$ G, $a_{H,met} = 6.74$ G and $a_{H,ring} = 1.98$ G.

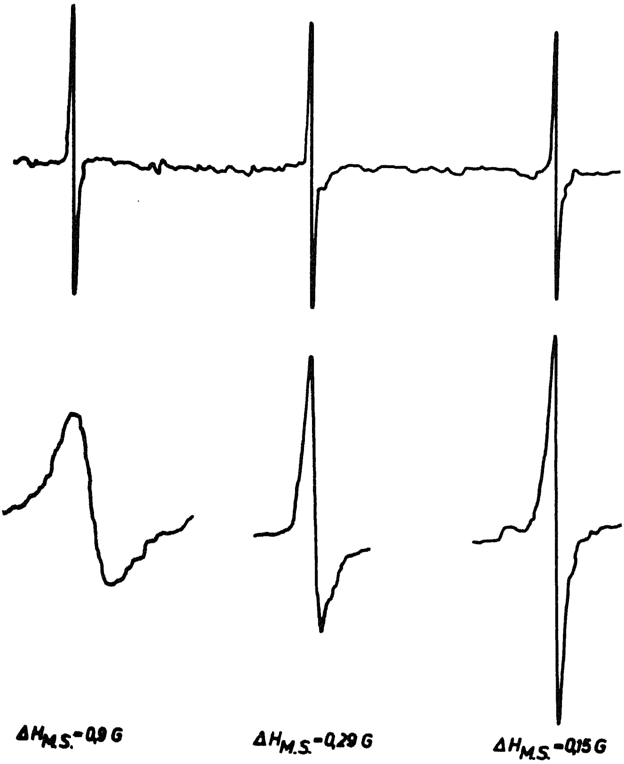

Figure 6. ESR spectrum of $K_2(SO_3)_2NO$ in water. Above, the complete spectrum, and below, the central line, from left to right, saturated with pure oxygen, saturated with air, and oxygen-free.

Figure 6 demonstrates the oxygen effect with a single line, the center line of the triplet due to the interaction with the spin $I = 1$ of the nitrogen of the peroxyl-amine disulfonate ion. The linewidth of a solution saturated with pure oxygen was found to be 0.90 G, the width of an air-saturated solution 0.29 G and without oxygen 0.15 G, the remaining width probably being due to spin orbit interaction since the radical contains sulfur.

The effect of the paramagnetic oxygen is not surprising if one remembers that its concentration in most air-saturated organic solvents is of the order of $1 - 2 \cdot 10^{-3}$ mol/l. $\approx 10^{18}$ spins/cm^3. I do not want to go into details on the mechanism of the interaction of the radical spin with the oxygen, which involves exchange interactions as well as lifetime T_1 broadening, since this is a somewhat more complicated matter, but it should be clearly understood that this interaction is a physical phenomenon and that these radicals are not chemically sensitive to oxygen. In any case, the given examples demonstrate that a careful exclusion of oxygen is necessary for obtaining well resolved ESR spectra.

With this precaution, a linewidth of the order of 70 milligauss could be readily obtained in a number of radicals. The present limit of resolution is shown in Figure 7 with the spectrum of the 1,3-bisdiphenylene-allyl in very dilute solution in CS_2, the concentration of spins being about 10^{-5} mol/l. The spectrum is divided into two identical parts due to a large splitting of 13.2 G. The first of these is shown above and the second below in the figure. A little over 400 HFS components with a separation of 60 milligauss could be fully resolved and accounted for in terms of 5 coupling constants. The largest of these, mentioned above, originates from interaction with the central proton,

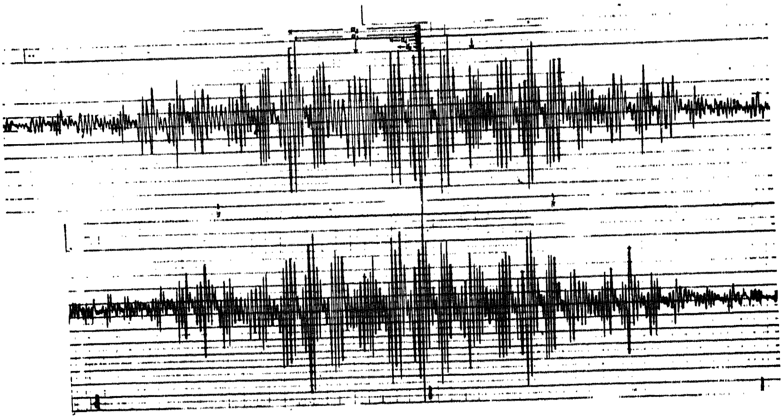

Figure 7. ESR spectrum of 1,3-bisdiphenylene-allyl in CS_2, concentration about 10^{-5} mol/l.

whereas the 4 others all results from a group of 4 equivalent protons as expected from the symmetry of the molecule. Their values are $a_1 = 13.2$ G, $a_2 = 1.92$ G, $a_3 = 1.86$ G, $a_4 = 0.48$ G and $a_5 = 0.36$ G. The theoretical reconstruction based on these constants is given in Figure 8 for comparison with the experimental spectrum. It should be emphasized that the individual components should be equidistant, the apparent deviations being caused by experimental effects to be discussed below.

The observed linewidth in Figure 7 is about 30 milligauss. In Figure 9 the central groups of Figure 7 are given again, taken under somewhat different technical conditions with the purpose of minimizing the linewidth at the expense of the signal to noise ratio. The obtained linewidth is 17±1 milligauss, corresponding to about 50 kc.

Is this the limit of resolution of ESR or could one possibly expect still narrower HFS lines? This question is closely related to another question, namely "what causes the residual linewidth of 17 milligauss?" It should be easy to find the answer by varying some parameters such as concentration and temperature. In practice, however, a further reduction in concentration is impossible because of the insufficient signal to noise ratio. Since this

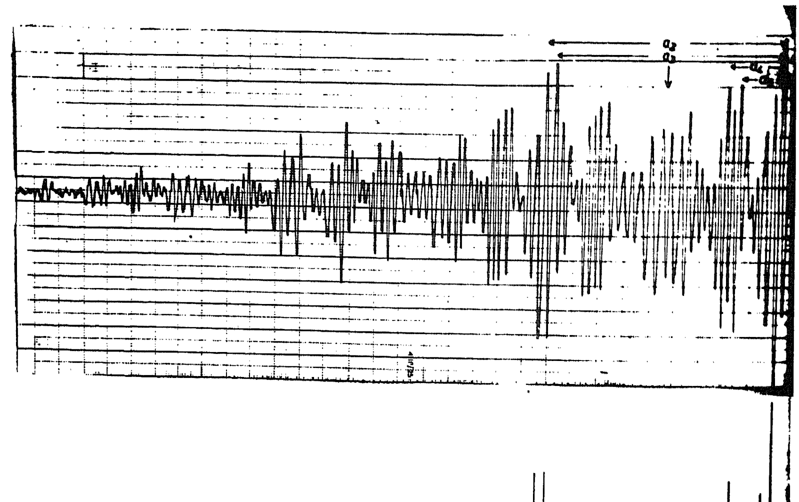

Figure 8. ESR spectrum of 1,3-bisdiphenylene-allyl together with the theoretical reconstruction based on the coupling constants: $a_1 = 13.2$ G, $a_2 = 1.92$ G, $a_3 = 1.86$ G, $a_4 = 0.48$ G and $a_5 = 0.36$ G.

introduces a more technical aspect, it might be useful to discuss the technical requirements of an ESR spectrometer for high resolution work.

The homogeneity and stability of the magnetic field as well as the frequency stability of the microwave oscillator has to be better than 1 in 10^6. Since the time taken for recording the spectrum of Figure 7 is of the order of 15 hours, the required stability should be a long time stability. This was not the case in the spectrum shown in Figure 7, where differences in the spacing of the lines indicated by arrows seem to be due to non-linearities in the field scanning.

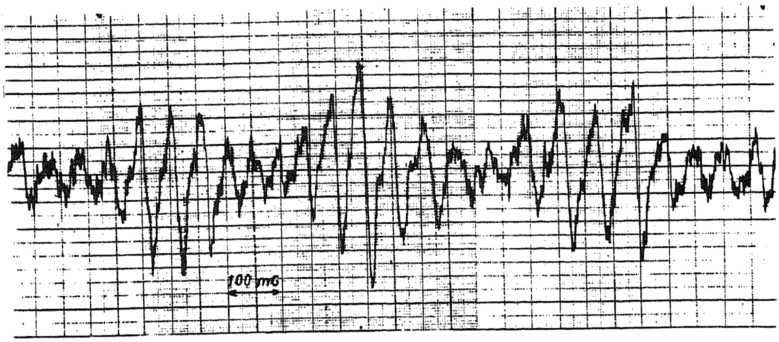

Figure 9. Central part of the spectrum of Figure 7, recorded under technical conditions to minimize linewidth.

High resolution requires low concentrations and low microwave fields; the power incident into the cavity in our measurements was about 10^{-5} watts corresponding to a H_1 field of the order of 5 milligauss. Both these requirements lead to small signal amplitudes. In addition, the total intensity is distributed to hundreds of HFS components. Consequently, the most critical property of a spectrometer is its sensitivity. This excludes low frequency modulation because of the high noise level of the crystal detector. Since high frequency modulation cannot be used because of the modulation broadening, a superhet system seems to be most suitable for high resolution ESR. In the future, parametric amplifiers might possibly be useful.

Returning to the question of the origin of the residual linewidth, it seems that dipolar interactions are negligible. The neutral CH-radical, 1,3-bisdiphenylene-allyl, g-value 2.0028± 0.0001, is an extreme case of very small spin orbit interaction. We believe that the measured linewidth of 17 milligauss is predominately due to exchange interactions, particularly since the order of magnitude is in agreement with what one would expect from extrapolating the experimental results obtained at higher concentrations.

On the other hand, the linewidth obtained with Wursters blue is about a factor of 5 larger at comparable concentrations. Since Wursters blue contains nitrogen, the spin-orbit coupling is larger than in a CH-radical $[(\lambda_N/\lambda_C)^2 \approx 4.3]$. Furthermore, in an ionic solution the Coulomb repulsion and the shell of solvated solvent molecules keep the radical ions farther apart and hence will reduce the exchange interactions. The anisotropic magnetic dipolar interaction, and the static part of the g-value anisotrophy seem to be less important since fairly narrow lines of the order of 40 milligauss have been obtained in highly viscous solvents. From these results and arguments we conclude that for radical ions containing other elements than C and H the dominating relaxation mechanism is the spin-orbit interaction. Intermediate cases, i.e., CH-radical ions and neutral radicals containing other elements, require further investigation.

Let me conclude with a few general remarks. The resolution of ESR depends on the sample investigated. The same resolution is not to be expected with different substances. We believe the 17 milligauss shown in Figure 9 to be near the limit. In the most favorable case, a CH-radical with not too many HFS components, it may be possible to reduce the linewidth by another factor of two or so. There is no theoretical limit, but we believe the practical limit of high resolution ESR in the foreseeable future to be at a linewidth of the order of 10 milligauss.

REFERENCES

1. D. Kivelson, J. Chem. Phys. 33, 1094 (1960).
2. N. Bloembergen, E. M. Purcell and R. V. Pound, Phys. Rev. 73, 679 (1948).
3. G. E. Pake and T. R. Tuttle, Phys. Rev. Lett. 3, 423 (1959).
4. K. H. Hausser, Z. Naturforsch. 14a, 425 (1959).
5. K. H. Hausser, Naturwiss. 47, 251 (1960).

ELECTRON SPIN RESONANCE IN ORIENTED RADICALS

D. H. Whiffen
Basic Physics Division, National Physical Laboratory,
Teddington, Middlesex, England

INTRODUCTION

Although single crystals have been used for many years in the electron spin resonance study of transition and rare earth metal ions, corresponding study of organic free radicals is of recent growth. Following the initial paper of Uebersfeld and Erb [1] in 1956, the power of such work was not appreciated until 1958 [2,3,4], but the balance is now redressed and over fifty publications have appeared since then. The most important finding common to these studies is that radicals produced in crystals by radiation damage have just as precise alignments in the crystal as do the undamaged molecules. Consequently if the spectrum of a single crystal is observed all radicals have the same spectra which is a function of the angle of the crystal with respect to the magnetic field. This is in contrast to the spectrum of an irradiated powder in which each grain makes a different angle with the magnetic field and the resultant lines, if identifiable, are very broad being in fact due to the superposition of lines at different positions. Similar difficulties apply to radicals trapped in glassy matrices. Parts of the theory of detailed interpretation of these anisotropic spectra are somewhat specialised; since the theory has been well described in the literature [5-9] it will not be repeated in this account devoted to the applications. These can be roughly divided into three classes, not always distinct, according as the information obtained relates to the host material, the radiation chemistry or the detailed structure of the free radical. The majority of the work refers to radicals formed by radiation damage which are normally too unstable to exist as more than the most transient species in solution.

INFORMATION ABOUT HOST MATERIAL

It was implied above that all radicals were parallel but this is not strictly true in most crystal lattices for which there may be several possible sites related to each other by the space group symmetry operations of the crystal. If the sites are related by translation or inversion only one radical orientation is apparent in the spectrum since these operations leave the spectrum unchanged. Symmetry planes on the other hand affect the direction of principal axes of the hyperfine coupling tensors. Consequently a doubling of the spectra is found with the spectra from two chemically equivalent radicals in distinguishable orientations. For monoclinic crystals there is normally such a plane perpendicular to the *b* axis and two superposed spectra are observed as in glycine [3]. However, in other cases only one radical can be identified and this must occupy a special site such as a plane perpendicular to *b*. This is exemplified by the radical in lithium glycollate monohydrate [10]. Another possibility is a site with a twofold axis parallel to *b* since a twofold rotation axis plus inversion is not distinguishable from a plane of symmetry. Here CO_2^- trapped in the site of a formate, HCO_2^-, ion is an example [11] and the result is consistent with the known crystal structure in which the formate ion has a twofold symmetry axis. Although it is unlikely to be an important tool in X-ray crystallography, it may happen that in some cases such information is more readily obtained than by standard methods. A recent example from these laboratories is fumaric acid where serious multiple twinning makes X-ray studies more difficult. Despite this twinning, the spin resonance of results strongly suggest that the fumaric acid skeleton lies perpendicular to the *b* axis of the monoclinic cell and retains its twofold symmetry axis. There is one case in which the spin resonance and X-ray studies are in slight disagreement; this is glutaric acid [12]. In this the radical appeared unexpectedly to have two unrelated orientations and it was suggested that an apparent twofold axis shown by X-rays to lie through the central carbon of the glutaric acid was in fact an artefact due to a random disorder.

The principal directions of the hyperfine coupling tensors, indicate the direction of certain links in the radical and may suggest the molecular orientation in the crystal. There are also interesting experiments on the anisotropy of the spectra in stretched polymers. For polyethylene it has been shown [13,14] that the C-H link of the $-CH_2-CH-CH_2-$ chain radical lies perpendicular to the direction of stretch.

RADIATION DAMAGE

In almost every case of simple organic molecules studied the spectra in single crystals have indicated unambiuously the nature of the trapped radical. Table 1 shows a selection of the type of damage observed. There have been no well substantiated cases of differences between the action of γ-rays, X-rays, fast electrons, etc. although ultraviolet light may be more specific. In general Table 1 refers to radicals observed at room temperature a few hours after the radiation has ceased. Although a number of cases had been proved by chemical means and by interpretation of the electron spin resonance spectra of powders and of polymers, Table 1 certainly shows that the single crystal studies have demonstrated the presence of over thirty otherwise unknown free radicals.

In the radiation studies it is not usually possible to determine the fate of the missing fragment. The predominance of hydrogen removal shown by the extent of Table 1a suggests that a particularly favourable feature may be the escape of the hydrogen atom from the crystal or its reaction with a molecule to form H_2 and a second radical of the same kind. For heavier fragments such motion is more difficult and self healing may be important. However, there is growing evidence that the radicals observed at room temperature may not be those formed in the primary process. The temperature of irradiation may influence the relative proportion of the radicals formed when more than one chemical species is observed in the same crystal. Also irradiation at liquid nitrogen temperatures may lead to different spectra or at least different proportions of the several products [50-54]. Many irreversible changes occur on warming from 77°K to 293°K and until this aspect is more fully documented it will not be possible to rely on the observed radicals being primary products.

RADICAL STRUCTURE

Besides identifying the free radical through the hyperfine coupling pattern, information may be obtained about the electronic and geometrical structure from an interpretation of the numerical values of the hyperfine coupling information.

One of the most common couplings is that to a hydrogen atom attached directly to a free radical carbon atom. The isotropic coupling in such a case is about -57 Mc/s. This corresponds to the observed coupling in solution and to the trace or diagonal sum of the coupling tensor observed for radicals rigidly held in a solid. The principal tensor elements are commonly about -29, -55 and -87 Mc/s and the anisotropy is in good

Table 1

Radicals Produced by Radiation Damage

(a) One $\underline{H}$ removed to form radical (Reference in parenthesis)

$C\underline{H}_2(COOH)_2$	(6)	$C\underline{H}_2NH_3^+(CO_2)^-$	(3)
$C\underline{H}_2(COOH)CO_2^-$	(15)	$CH_3CONHC\underline{H}_2COOH$	(29,30)
$(C\underline{H}_2COOH)_2$	(16,17)	$NH_3^+CH_2CONHC\underline{H}_2CO_2^-$	(30,31,32)
$(CH_2)\ C\underline{H}_2CH(COOH)_2$	(12)	$CH_3CONHC\underline{H}(CH_3)COOH$	(30)
$(CH_2C\underline{H}_2COOH)_2$	(18)	$C\underline{H}_3NHCONH_2$	(33)
$CH_3\ C\underline{H}\ (COOH)_2$	(19)	$CH_3\ C\underline{H}_2\ NH\ CONH_2$	(33)
$CH_3\ CH_2\ C\underline{H}(COOH)_2$	(20)	$C\underline{H}_2(SO_3)_2^{=}$	(34)
$CH_3\ CH_2\ CH_2\ C\underline{H}(COOH)_2$	(21)	$C\underline{H}O_2^-$	(11)
$(CH_3)_2C\underline{H}\ CH(COOH)_2$	(21)	$\underline{H}PO_3^{=}$	(35)
$C\underline{H}_2(OH)COOH$	(5)	$\underline{H}_2PO_2^-$	(36)
$C\underline{H}_2(OH)CO_2^-$	(10,22)	$N\underline{H}(SO_3)_2^{=}$	(34)
$CH_3OC\underline{H}_2\ CO_2^-$	(23)	$N\underline{H}_3^+\ SO_3^-$	(37)
$O(C\underline{H}_2\ COOH)_2$	(24)	$N\underline{H}_2\ SO_3^-$	(21)
$(C\underline{H}(OH)COOH)_2$	(25)	$N\underline{H}_4^+$	(47,48)
$(C\underline{H}(OH)CO_2)_2^{=}$	(26)	$\underline{H}_2O$	(49)
$C\underline{H}_2Cl(COOH)$	(27)		
$S(C\underline{H}_2\ COOH)_2$	(28)		

(b) C - C bond broken to form radical

$CH_2(COOH)_2 \longrightarrow CH_2(COOH)$	(38,39)
$CH_3CH(COOH)_2 \longrightarrow CH_3CH(COOH)$	(19)

(c) C - N bond broken to form radical

$NH_3^+CH(CH_3)CO_2^- \longrightarrow CH_3\ CH\ CO_2^-$	(40,41)
$(CH_3)_2\ C(NH_3^+)CO_2^- \longrightarrow (CH_3)_2\ C\ CO_2^-$	(42)
$CH(COOH)NH_3^+CH_2\ COOH \longrightarrow CH(CO_2H)CH_2\ COOH$	(43)
$CH_3\ CH_2 - C(NH_3^+)\ (CH_3)COOH \longrightarrow CH_3\ CH_2\ C(CH_3)COOH$	(44)

(d) C - S bond broken to form radical

$CH_2(SO_3)_2 \longrightarrow SO_3^-$	(45)

Table 1—Continued

(e) N - S bond broken to form radical

$NH_3^+ SO_3^- \longrightarrow SO_3^-$ (45)

$NH(SO_3)_2^= \longrightarrow SO_3^-$ (45)

$NH_2(SO_3)^- \longrightarrow SO_3^-$ (45)

(f) S - S bond broken to form radical

$((COOH)\ CH(NH_3^+)CH_2\ S)_2 \longrightarrow COOH\ CH(NH_3^+)CH_2\ S\cdot$ (46)

$S_2O_6^= \longrightarrow SO_3^-$ (45)

(g) Cl - O bond broken to form radical

$ClO_4^- \longrightarrow ClO_3$ (47)

agreement with the values calculated [55] for a Slater 2p wave function for the unpaired electron on the carbon atom. A recent tabulation [56] of such couplings shows that there is a surprisingly small departure from these numbers between different radicals. An interesting use of the directions for which the principal couplings occur is possible for radicals of the form $RCH_2\cdot$. The angle between appropriate tensor elements for the separate H atoms is the HCH angle. With CH_2COOH the value 116° was obtained [39] while for $CH_2NHCONH_2$ the HCH angle came [33] to 117°.

Another fairly constant group of hyperfine couplings is those to the hydrogens of a methyl group attached to the free radical centre. At room temperature there is free rotation about the CH_3-C bond all these are three equivalent hydrogen atoms with an isotropic coupling close to +69 Mc/s, a value which is slightly reduced to nearer +65 Mc/s if two methyl groups are attached to the same carbon atom [19,40-42,44]. The anisotropy is small but not quite zero [41,42].

If the methyl group is substituted it can no longer rotate freely and the remaining hydrogens may have any value of isotropic coupling up to +130 Mc/s. The value appears to be a strong function of molecular geometry as is shown most plainly for the radical $CH_3CHCOOH$ trapped in α-alanine. If the measurements are made at 77°K each hydrogen of the methyl group has a different isotropic coupling [57,58,59] the values being 120, 76 and 14 Mc/s. At this temperature the methyl group is no longer rotating and the three hydrogen atoms are in non-equivalent positions. If the CH bond and the free radical 2p orbital are projected on the plane perpendicular to the C-C bond and make an angle θ with each other the coupling may be written $B_o + B_2 \cos^2\theta$. B_o is certainly very small, less [57] than 10 Mc/s and B_2 is 120-160 Mc/s but the factors influencing the exact values are not yet certain [16,17,20,57] and may depend on the nature of the substituents. The couplings of this paragraph also show fairly small anisotropies in agreement with their larger distance from the unpaired electron.

More distant hydrogens, that is those separated by two carbons from the free radical centre do not usually give resolved hyperfine coupling. However, if one of two intermediate atoms is oxygen [23,24] or sulphur [28] a small coupling of less than 15 Mc/s is common. Under favourable circumstances it is also possible to see coupling to a hydrogen nucleus in the host lattice. In the two cases studied in detail [34] this coupling is purely anisotropic and of the magnitude to be expected from the known crystal structure. It is probable that in other crystals unresolved coupling to nuclei in the host molecules is the major factor controlling line widths and their variation with crystal orientation.

Information about electron distribution obtained from hydrogen couplings is a little indirect since the major electron distribution is elsewhere. If, as in substituted methyl radicals, the unpaired electron is in predominantly a 2p state on a carbon atom the anisotropy of the coupling to this carbon is large. It is also a better measure of the degree to which the odd electron is located on this atom. Such studies require complete ^{13}C coupling tensors which are not easily observed in natural abundance unless the crystal structure and line widths are favourable. Table 2 indicates the available data for π electron radicals; the spin populations refer to the 2p wave function with a radical distribution determined by a SCF treatment for the neutral atom.

Table 2

Anisotropy and 2p Spin Populations in π Electron Free Radicals

Radical	Nucleus	Tensor Components	2p Spin Population
$^{13}CH(COOH)_2$ (60)	^{13}C	213, 42, 23 Mc/s	0.69
$^{13}CH(SO_3)_2^{=}$ (34)	^{13}C	260, 62, 55 Mc/s	0.75
$N(SO_3)_2^{=}$ (34)	^{14}N	106, 6, 0 Mc/s	0.73

CONCLUSIONS

The study of oriented free radicals is still quite young and it is interesting to examine what lies in the future. Two matters mentioned above clearly require further study; namely the extension of measurements to low temperatures without intermediate warm up and, secondly, the further study of the coupling of hydrogen attached to a carbon atom itself attached to the free radical centre. Only one paper [61] has referred to zero field measurements and only one [62] to Endor spectra of such systems although such measurements are well known elsewhere in electron spin resonance. They are likely to provide more accurate hyperfine coupling constants and might prove especially valuable for nuclei with electric quadrupole moments. Where electric quadrupole coupling is large enough to affect the spectra [27,34] these prove difficult to interpret accurately. Often more than one radical is trapped in a lattice and the separate chemical species may show different thermal stabilities or even interconvert [63]. A fuller study of radical chemistry, reaction rates, diffusion rates, etc. is certainly possible. So is a more serious study of relative radiation yields under different conditions. There are many crystals which have not yet been examined, including some very simple substances which are normally liquids or gases at room temperature. Many cases could also be usefully studied again with emphasis on the coupling to ^{13}C, ^{17}O, ^{33}S and in general to nuclei of non-zero spin of elements whose dominant isotope has zero spin.

Another field which is opening up is the ultraviolet spectroscopy of these radicals [45,64], especially when the direction of the transmission moment can be found [65] using polarized ultraviolet radiation in association with spin resonance measurements to measure the concentration and orientation of the radicals. Besides the usual interest in ultraviolet spectroscopy, the work with oriented free radicals is of special interest in connection with the g-factors of the resonance spectrum. The conditions under which the g-factor may be significantly above or below the free spin value, 2.0023, are now understood [66] and semiquantitative agreement obtained [11,65] with the theoretical values derived from the wave functions and the excitation energies. Occasionally g-factors may be both above and below the free spin value for different directions in the same radical [11].

Also of interest is the study of rates of rotation in the solid. The radical $CH_3CHCOOH$ is the best example. From the change of spectrum as regards line width and position, it has been shown that the reorientation rate of the methyl group is about 10^8 per second at 160°K when trapped in α-alanine [58,59] but the rate is at least 10^9 per second for the same radical in a methyl malonic acid host crystal [19] at 4°K. There is rotation, which is possibly internal or possibly overall rotation, about the N-S direction of $\overset{+}{N}H_2\ SO_3^-$ trapped in sulphamic acid [37] which is slowing to about 10^8 per sec at about 80°K.

The very large amount of information that is now available about so many radicals, most of which have only been studied trapped in crystals, shows that electron spin resonance spectroscopy is an even more powerful tool than was realised when most applications were to metallic ions or aromatic compounds in solution.

REFERENCES

1. J. Uebersfeld and E. Erb, Comptes Rendues, 1956, 242, 478.
2. D. K. Ghosh and D. H. Whiffen, Chemical Society Symposia, Bristol, 1958, p. 168. Chemical Society, London.
3. D. K. Ghosh and D. H. Whiffen, Molecular Physics, 1959, 2, 285.
4. I. Miyagawa and W. Gordy, J. Chem. Phys., 1959, 30, 1590.
5. N. M. Atherton and D. H. Whiffen, Molecular Physics, 1960, 3,1.
6. H. M. McConnell, C. Heller, T. Cole and R. W. Fessenden, J. Amer. Chem. Soc., 1960, 82, 766.
7. I. Miyagawa and W. Gordy, J. Chem. Phys., 1960, 32, 255.
8. H. Zeldes, G. T. Trammell, R. Livingston and R. W. Holmberg, J. Chem. Phys., 1960, 32, 618.
9. D. H. Whiffen, Free Radicals in Biological Systems (Ed. M. S. Blois), 1961 Academic Press, p. 227.
10. D. Pooley and D. H. Whiffen, Trans. Faraday Soc., 1961, 57, 1445.
11. D. W. Ovenall and D. H. Whiffen, Molecular Physics, 1961, 4, 135.
12. A. Horsfield, J. R. Morton and D. H. Whiffen, Molecular Physics, 1961, 4, 169.
13. D. Libby and M. G. Ormerod, J. Phys. Chem. Solids, 1961, 18, 316.
14. M. Kashiwagi, J. Chem. Phys., 1962, 36, 575.
15. W. C. Lin and C. A. McDowell, Molecular Physics, 1961, 4, 343.
16. C. Heller and H. M. McConnell, J. Chem. Phys., 1960, 32, 1535.

This work forms part of the program of the Basic Physics Division, National Physical Laboratory, Teddington, England, and is published by permission of the Director.

17. D. Pooley and D. H. Whiffen, Molecular Physics, 1961, 4, 81.
18. J. R. Morton and A. Horsfield, Molecular Physics, 1961, 4, 219.
19. C. Heller, J. Chem. Phys., 1961, 36, 175.
20. J. R. Rowlands and D. H. Whiffen, Molecular Physics, 1961, 4, 349.
21. J. R. Rowlands. Personal communication.
22. N. M. Atherton and D. H. Whiffen, Molecular Physics, 1960, 3, 103.
23. A. Horsfield and J. R. Morton, Trans Faraday Soc., 1962, 58, 470.
24. Y. Kurita, J. Chem. Phys., 1962, 36, 560.
25. D. V. G. L. N. Rao and W. Gordy, J. Chem. Phys., 1962, 36, 1143.
26. G. C. Moulton and W. G. Moulton, J. Chem. Phys., 1961, 35, 208.
27. D. Pooley and D. H. Whiffen, Spect. Acta., 1962, 18, 291.
28. Y. Kurita and W. Gordy, J. Chem. Phys., 1961, 34, 1285.
29. I. Miyagawa, Y. Kurita and W. Gordy, J. Chem. Phys., 1960, 33, 1599.
30. H. C. Box, H. G. Freund and K. Lilga, Free Radicals in Biological Systems (Ed. M. S. Blois), Academic Press 1961, p. 239.
31. M. Katayama and W. Gordy, J. Chem. Phys., 1961, 35, 117.
32. W. C. Lin and C. A. McDowell, Molecular Physics, 1961, 4, 333.
33. T. S. Jaseja and R. S. Anderson, J. Chem. Phys., 1961, 35, 2192.
34. A. Horsfield, J. R. Morton, J. R. Rowlands and D. H. Whiffen, Molecular Physics, 1962, 5, 241.
35. A. Horsfield, J. R. Morton and D. H. Whiffen, Molecular Physics, 1961, 4, 475.
36. J. R. Morton, Molecular Physics, 1962, 5, 217.
37. J. R. Rowlands and D. H. Whiffen, Nature, 1962, 193, 61.
38. H. M. McConnell and C. R. Giulano, J. Chem. Phys., 1961, 35, 1910.
39. A. Horsfield, J. R. Morton and D. H. Whiffen, Molecular Physics, 1961, 4, 327.
40. I. Miyagawa and W. Gordy, J. Chem. Phys., 1960, 32, 255.
41. J. R. Morton and A. Horsfield, J. Chem. Phys., 1961, 35, 1142.
42. A. Horsfield, J. R. Morton and D. H. Whiffen, Trans. Faraday Soc., 1961, 57, 1657.
43. J. R. Rowlands, J. Chem. Soc., 1961, p. 4264.
44. T. S. Jaseja and R. S. Anderson, J. Chem. Phys., 1962, 36, 1098.
45. G. W. Chantry, A. Horsfield, J. R. Morton, J. R. Rowlands and D. H. Whiffen, Molecular Physics, 1962, 5, 233.

46. Y. Kurita and W. Gordy, J. Chem. Phys., 1961, 34, 282.
47. T. Cole, J. Chem. Phys., 1961, 35, 1169.
48. J. S. Hyde and E. S. Freeman, J. Phys. Chem., 1961, 65, 1636.
49. J. A. McMillan, M. S. Matheson and R. Smaller, J. Chem. Phys., 1960, 33, 609.
50. F. Patten and W. Gordy, Proc. Nat. Acad. Sci., 1960, 64, 1137.
51. I. Miyagawa and W. Gordy, J. Amer. Chem. Soc., 1961, 83, 1036.
52. Yu N. Molin, I. I. Chkheidze, N. Ya. Buben, and V. V. Voevodskii, Zhur. Strukt. Khim., 1961, 2, 293.
53. T. Henriksen, J. Chem. Phys., 1962, 36, 1258.
54. D. Pooley and D. H. Whiffen, J. Chem. Soc., 1962, p. 366.
55. H. M. McConnell and J. Strathdee, Molecular Physics, 1959, 2, 129.
56. D. H. Whiffen, Pure and Applied Chemistry, 1962, 4, 185.
57. A. Horsfield, J. R. Morton and D. H. Whiffen, Molecular Physics, 1961, 4, 425.
58. I. Miyagawa and K. Itoh, J. Chem. Phys., 1962, 36, 2157.
59. A. Horsfield, J. R. Morton and D. H. Whiffen, Molecular Physics, 1962, 5, 115.
60. T. Cole and C. Heller, J. Chem. Phys., 1961, 34, 1085.
61. H. M. McConnell, D. D. Thompson and R. W. Fessenden, Proc. Nat. Acad. Sci., 1959, 45, 1600.
62. T. Cole, C. Heller and J. Lambe, J. Chem. Phys., 1961, 34, 1447.
63. D. K. Ghosh and D. H. Whiffen, J. Chem. Soc., 1960, p. 1869.
64. G. W. Chantry and D. H. Whiffen, Spectrochimica Acta, 1961, 17, 367.
65. G. W. Chantry and D. H. Whiffen, Molecular Physics, 1962, 5, 189.
66. H. M. McConnell and R. E. Robertson, J. Phys. Chem., 1957, 61, 1018.

LOW FREQUENCY TO NEAR MICROWAVE SPECTRUM SPECTROSCOPY

Herbert A. Elion and Louis Shapiro
Elion Instruments, Inc.
Burlington, New Jersey

This paper concerns some of the unique features to be found in the low to near microwave portion of the electron spin resonance spectrum as compared with the microwave portion. The low radio frequency spectroscopy is treated from a theoretical and experimental point of view. Emphasis is placed on fundamental advantages of basic investigation under low frequency-weak magnetic field conditions. A survey is made of the important quantum mechanical relationships involved. The complete Hamiltonian is reviewed and an example is discussed utilizing the Breit-Rabi formula for fields of arbitrary strength. Zero field absorption is considered. Additional evaluation is made of factors such as applicability to aqueous solutions, skin effect and general instrumental conditions. Matters of equipment sensitivity, simplicity, reliability and cost are reviewed. Commercial applications are discussed and an example given for fluid catalytic cracking.

GENERAL CONCEPTS

The unique features of the radio frequency, or "rf," approach to paramagnetic absorption spectroscopy fall into two main categories, namely, those of interest to the scientific community and those of interest to industry at large.

We may first recall the fact that basic physical relationships existing between the frequency of paramagnetic absorption spectra and the intensity of the unidirectional magnetic field in which lattice elements of the test specimen find themselves, imply that low intensity magnetic fields give rise to low frequency spectra while high intensity magnetic fields give rise to high frequency spectra. In the particularly simple case of a free electron the relationship reduces to

$$\nu \text{ (megacycles)} = 2.8026 \text{ B (gauss)}.$$

In general we may consider the dividing line between low and high frequency paramagnetic spectroscopy as lying in the neighborhood of 1000 megacycles. Above this frequency formal microwave techniques tend to take over from a lumped constant or modified lumped constant-transmission line approach. For convenience we may refer to the low frequency approach as radio frequency or "rf" paramagnetic spectroscopy and to the high frequency approach as microwave paramagnetic spectroscopy.

The purpose of this paper is to present a survey of some of the important features of low frequency or "rf" approach.

LOW FIELD VERSUS HIGH FIELD SPECTROSCOPY

Returning to the factors of interest to the scientific community we note that we deal here with the use of rf paramagnetic spectroscopy as a tool in fundamental research.

In most general terms, a magnetic field of appropriate intensity is applied to a paramagnetic material and the resulting spectra studied for determination of the geometric, force field and energy structure of the material involved.

Where this investigation is carried out in the high frequency, or microwave, region magnetic fields utilized are quite intense being of the order of several thousand gauss or higher. The result, necessarily, is that the normal field environment and resulting energy structure of the constituent atoms or molecules are altered to the corresponding extent. Thus, although much interesting spectra may be obtained, other spectra perhaps of equal or greater interest may be obscured or lost entirely. Such concealed or destroyed spectra may deal with the many subtle and delicate factors involved in energy coupling mechanisms, both within the atoms or molecules themselves and with lattice forces present on a periodic basis in the individual lattice cells.

Time does not permit - nor is it the purpose of this paper - to go into such matters in detail. Interested parties are referred to the literature which includes basic treatments by Bleaney and Stevens [1] and by Wertz [2]. A few general remarks may be in order, however.

In the simple case of a one electron atom with the electron subject to a spherically symmetrical central field only, the energy levels are given by

$$W = - \frac{2 \pi^2 m e^4 Z^2}{h^2 n^2}.$$

Only the principle quantum number, n, appears in this expression - leading to degeneracy when the other quantum numbers assume different values for a given n. Thus, for each value of the angular momentum quantum number, ℓ, the energy is $(2\ell + 1)$ degenerate. This condition follows from the fact that the projection of ℓ, which is m_ℓ, may have $(2\ell + 1)$ values.

Further degeneracy follows when the two values of the spin projection, $m_s = \pm 1/2$, are taken into account.

In the more general case where the electron no longer sees a simple spherically symmetrical electric field, the "ℓ" degeneracy is partially or fully lifted and different values of ℓ may lead to different energy levels.

In a similar manner, the presence of a magnetic field provides a frame of reference for the magnetic projection or the m_ℓ quantum number, and new energy levels appear which, for a weak field at least, are in accordance with the standard equation

$$W = W_0 - \mu_a B ,$$

where W_0 is the energy before application of the field, B, and μ_a is the magnetic moment component of the particular particle involved. Spin degeneracy is also lifted in this manner.

Mention will briefly be made of spin-orbit coupling; this is a factor which plays an increasingly important role as the atomic number of the sample under test increases.

The behavior of the complete atom in its lattice environment is described by Bleaney and Stevens in terms of a composite Hamiltonian:

$$H = H_{\substack{\text{coulomb}\\ \text{field}\\ \text{(a)}}} + H_{\substack{\text{magnetic}\\ \text{spin-orbit}\\ \text{(b)}}} + H_{\substack{\text{external}\\ \text{magnetic}\\ \text{field}\\ \text{(c)}}} + H_{\substack{\text{nuclear-}\\ \text{electron}\\ \text{spin-spin-}\\ \text{orbit}\\ \text{(d)}}}$$

$$+ H_{\substack{\text{nuclear}\\ \text{quadrupole}\\ \text{(e)}}} + H_{\substack{\text{nuclear with}\\ \text{external}\\ \text{magnetic}\\ \text{field}\\ \text{(f)}}} + H_{\substack{\text{spin-spin}\\ \text{(g)}}} + H_{\substack{\text{exchange}\\ \text{(h)}}}$$

The first term, (a) specifies the behavior of the electron as a result of the surrounding electric field of the nucleus and other electrons. The (b) term evaluates the effect of spin-orbit coupling of the electron concerned. The (c) term is responsible for the basic Zeeman effect leading to the phenomenon of paramagnetic resonance absorption which is the subject of this paper. The (d) term described the interaction of the spin and orbital magnetic moments of the electron with the moment of the nucleus. The (e) term deals with the electrostatic attraction between the nucleon structure of the nucleus and the orbital electrons giving rise to quadrupole and higher order effects. The (f) term describes the interaction of the nucleus directly with an external magnetic field. In this respect it corresponds to the (c) term for the electron.

The last two terms have been added since the original Bleaney-Stevens formulation. The (g) term separates out the electron spin-spin (or dipole-dipole) interaction which originally was included as part of the (b) term while the (h) term describes the electron-electron exchange interaction.

It is of extreme interest now to compare the spectra available from paramagnetic materials under conditions of different impressed magnetic field intensities. Qualitatively we may speak of "weak" fields and "huge" fields. The simpler case is that of the "huge" field. Here, the ultimate consequence is that the impressed field tends to overpower the effects of the various local fields and their associated coupling mechanisms. Spins and orbits align themselves separately and energy levels follow a particularly simple pattern. The relationship is [3]:

$$W = W_o + (M + 2\,m_s)\,\mu_e\,B\,,$$

where M is the total magnetic quantum number of the particle involved and μ_e is the Bohr magneton.

It is obvious that much valuable structural information may be lost under these conditions.

At the opposite extreme we have the weak magnetic field where existing energy and coupling relationships are maintained intact and the effect of the field is more in the nature of a superimposed perturbation. It is under these conditions, for example, that (for the lighter elements at least) the "L" and "S" quantum numbers combine to give a "J" resultant with physical significance. This condition corresponds to the well-known Russell-Saunders Coupling System.

For the heavier elements account is immediately taken of the much stronger spin-orbit coupling and quantum numbers, n, ℓ, j, m are assigned on an individual electron basis to describe the coupling structure involved. This type of coupling is identified as "jj" coupling.

Energy transitions take place in the usual manner on a quantum level in accordance with permitted changes in the relevant quantum numbers. Where different numbers apply due to different values of impressed magnetic field, the resulting transitions will necessarily follow the applicable quantum number structure. As a result spectra will differ depending upon the effectiveness of applied fields in producing different quantum number structures.

It is in this respect, for example, that we meet up with expressions like "good" quantum numbers and "bad" quantum numbers in accordance with their applicability to the energy transition structure in effect at any given time.

For intermediate applied magnetic field intensity conditions there may be two or more quantum mechanisms in operation simultaneously as internal and external fields compete for axes of precession.

The energy levels as a general function of magnetic field intensity are given by the Breit-Rabi formula [4]:

$$W = \frac{h\Delta\nu}{2(2I+1)} + g_I \mu_e M H_z \pm \frac{h\Delta\nu}{2}\left(1 + \frac{4Mx}{2I+1} + x^2\right)^{1/2},$$

where $h\Delta\nu$ is the usual zero field separation of energy levels, g_I is the nuclear hyperfine splitting factor, and

$$x = (g - g_I)\frac{\mu_e H_z}{h\Delta\nu}.$$

An interesting example of this type of change in quantum number structure is shown in the following energy level diagram from the recent book METHODS OF EXPERIMENTAL PHYSICS, Vol. 3, MOLECULAR PHYSICS (Academic Press 1962), page 452. See Figure 1.

We note that, with total magnetic quantum number $J = 1/2$ and nuclear magnetic quantum number $I = 3/2$ we have, in the absence of any applied magnetic field, available resultants, F, as follows:

$$F = I \pm J = 3/2 \pm 1/2 = 2,\ 1.$$

The application of a weak magnetic field, quantizes the magnetic projection of F at once following the rules

$$M_F = F,\quad F-1,\quad ---0---,\quad -(F-1),\quad -F,$$

leading to the splitting as shown. F and M_F are here valid weak field quantum numbers. As the applied magnetic field is increased, however, the pattern changes drastically as the I, J coupling is broken and J quantizes separately as

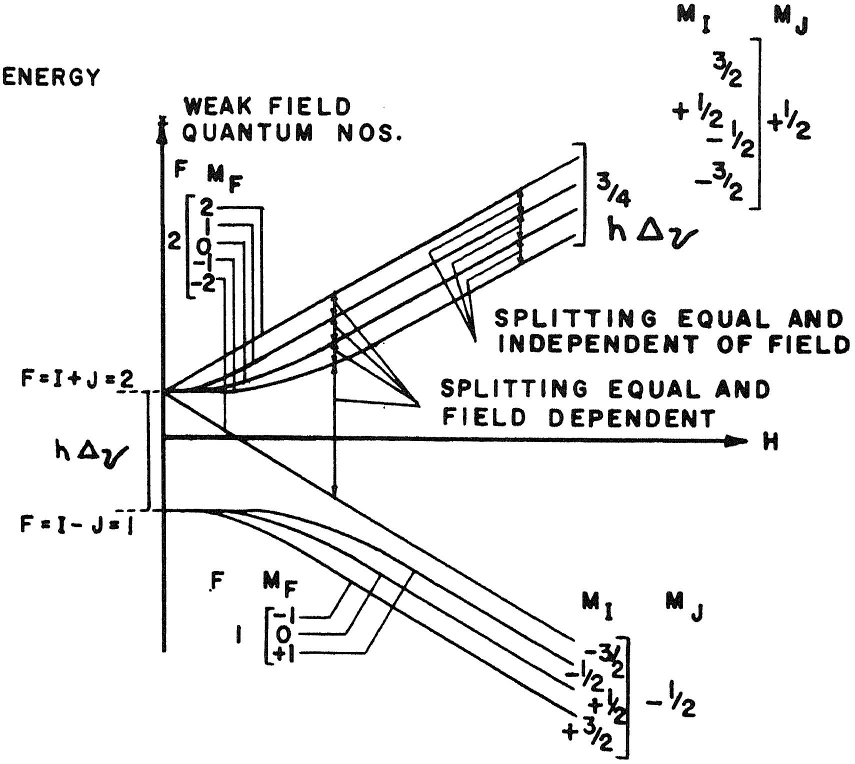

Figure 1. Breit-Rabi Diagram of Energy Levels of an Atom, Having J = 1/2 and I = 3/2, in a Magnetic Field. (After R. S. Anderson.)

$$M_J = J\ ,\quad J - 1\ ,\quad ---0---\ ,\quad -\ (J - 1)\ ,\quad -J\ ,$$

leading in this case (J = 1/2) to values of M_J of +1/2 and -1/2. Similarly, the I quantum number projects out separately as

$$M_I = I\ ,\quad I - 1\ ,\quad ---0---\ ,\quad -\ (I - 1)\ ,\quad -I$$

leading to values of 3/2, 1/2, -1/2 and -3/2.

Due to the unequal energy intervals involved, the M_J's become the dominant branches while the M_I's form perturbations or hyperfine structure on each such branch.

It is important to note that study and accumulation of the strong field spectra alone would give little or no indication of conditions existing in the original lattice state. Hence, it is primarily by a knowledge of the weak field spectra that the original coupling scheme can be reconstructed and the original interplay of forces determined.

ZERO FIELD ABSORPTION

In certain cases of great interest actual splitting of energy levels into fine and hyperfine spectral structures takes place with no applied magnetic field. Magnetic resonance experiments carried out under these conditions lead to determination of energy levels in their natural (or zero field) condition.

This procedure is of basic importance in certain approaches to achievement of very low temperatures by paramagnetic means. The object here is for the magnetic moment-bearing particles - upon removal of the impressed magnetic field - to align themselves in accordance with an appropriate pre-existing energy transition structure of the correct range of values. In this manner there is achieved a maximum removal of residual phonons from the lattice structure since agreement then exists between the energy values of residual phonons and available energy transitions for the magnetic moment-bearing particles.

The necessity for an accurate determination of these zero field energy levels for selection of an appropriate paramagnetic salt for the above application is obvious. A general treatment of the problem is given by Ingram [5] in which reference is made to earlier work by Bleaney.

As an aside to experimental techniques in determination of zero field spectra it may be pointed out that it is usually convenient to use a fixed low value of rf in accordance with anticipated spectra and then apply small incremental magnetic fields until such spectra are actually obtained. This method remains valid so long as the incremental field acts as a perturbation only on the pre-existing energy level structure. In practice this limitation is not experimentally embarrassing.

To sum up this portion of the paper, accumulation and interpretation of zero field or weak field spectra may often provide invaluable information - not otherwise available - for determination of important physical parameters of the atomic or molecular or lattice structure of the material under investigation.

AQUEOUS SOLUTIONS

A number of more mundane matters which may be of interest for both basic research and industrial applications in evaluating the advisability of the "rf" as against the microwave approach to paramagnetic spectroscopy will now be considered. The first of these is the matter of aqueous solutions.

It is well known that the interaction of water's large dipole moment with a microwave electric field results in a large non-resonant absorption. This phenomenon seriously embarrasses attempts to study aqueous solutions at these high frequencies, particularly in large volumes. Important advantages accrue, however, from use of the lower frequencies of "rf" paramagnetic spectroscopy in these cases. For one thing, use of a lower frequency - together with the greater volume of specimen available for analysis due to changed equipment configurations as well as reduced dipole absorption - provides the basic conditions for an overall increase in sensitivity despite the general reduction in available paramagnetic absorption per unit specimen mass due to the lowering of frequency per se.

However, more important, the great flexibility of component design in the rf range permits the development of rf sample holders - such as have been produced by Elion, Inc. - in which the entire electric field is excluded from the region of the sample, thus bypassing this problem of electric dipole moment absorption completely.

Needless to say, this factor should be of extreme interest to all workers concerned with the life sciences as well as to those working with industrial processes.

SKIN EFFECT

Another matter of importance is the question of skin effect at high frequencies, particularly for conductors. It is obvious, of course, that paramagnetic absorption spectra can only be obtained when penetration of the specimen by the rf or microwave field is achieved.

The concept of "skin depth" is a convenient measure of the above penetration and corresponds to the depth (or penetration) of the specimen that a uniform current of magnitude equal to that actually existing on the surface of the conductor would need to have in order to produce the same metal losses. Analytically, the expression [6] is:

$$\delta = \sqrt{\frac{2}{\omega \mu \sigma}} \qquad \text{Meters} ,$$

where ω = circular frequency of the applied field; $\mu = \mu_0$ = permeability free space value 1.257×10^{-6}, henry per meter; and σ = conductivity, mhos per meter.

Insertion of the value of $\sigma = 5.80 \times 10^7$ mhos per meter for copper and conversion of the result to units of thousandths of an inch gives the results shown in Table 1 for the frequencies indicated.

Taking values of metallic conductivity ranging from 6.17×10^7 for silver to $.71 \times 10^7$ for solder we note that the range is within a factor of nine — leading to a skin depth factor of 3 after the

Table 1

Frequency (Mc/Sec)	Skin Depth (Mils)
1	2.60
10	0.82
100	0.26
1000	0.082
10000	0.026

square root is taken. The skin depth value, then, can be correspondingly increased when materials of conductivity lower than copper are analyzed.

The significant advantage in the use of rf paramagnetic spectroscopy in the case of conductors is thus very apparent with the increased penetration of rf fields at the lower frequencies. It no longer becomes necessary, for instance, to resort to such fine powdering techniques to obtain particle dispersion, with the possible resultant loss of extended macroscopic domain properties or general changes in characteristics due to the powdering process itself.

GENERAL INSTRUMENTAL CONSIDERATIONS

Another factor of great interest and importance in rf paramagnetic spectroscopy is the great flexibility in equipment configurations due on the one hand to the weaker d.c. magnetic field employed and on the other hand to the lumped constant or quasi-lumped constant approach. Thus, without the requirement for extremely intense magnetic fields it becomes possible to use air type multicoil arrangements allowing for large volumes of great magnetic homogeneity in the interior of fairly small coils. Such a system is presently undergoing test at Elion Instruments, Inc. Test data will be announced in the near future.

Another important factor of an open coil system is the general accessibility of the sample area. It may be reached directly from either end of the common coil axis as well as from 360° about the equatorial plane of the system. There is ample room, for example, for insertion of a variety of cryostat equipment - with no embarrassment whatsoever to the instrumental configuration.

Regarding the rf volume in which the specimen is normally placed we have here, in the simplest case, merely a coil of the proper frequency characteristic. Access to the coil is direct and may be from either end of its own axis.

More sophisticated rf specimen holders are now under development at Elion Instruments, Inc. which represent a meeting ground for the various requirements leading to optimum operation of such a device. These include provision for maximum volume or quantity of sample (or, alternately, maximum number of available spins), maximum "Q" for optimum instrumental sensitivity, and shielding from electric fields where such would react adversely with the specimen.

Considering in turn, the unrestricted array of both thermal and solid state detection systems and devices available at rf frequencies there is good reason to believe that high sensitivities, will indeed, be achieved. We may mention just in passing, for example, that we are here in the region of commercial radio communications as well as FM and television - and hence in a region where instrumental techniques have reached a very high state of perfection and where much is known about factors such as precision and reliability.

It should be emphasized that, although it is recognized that intensity of spectral paramagnetic absorption varies as the square of the rf or microwave frequency utilized, it is expected that this inherent signal advantage of the microwave region will, to a large measure, be overcome as the basic advantages of operation in the more amenable rf region are realized.

In general, for example, the equipment is simpler, cheaper and much more reliable than its microwave counterpart. We have only to think, for example, of the marvel of the present commercial television receiver with all of its sensitivity and complexity - as well as its relatively trouble-free operation for periods of many months at a time - for the cost of only a few hundred dollars.

Even allowing for the advantage of production techniques it is confidently believed that the rf paramagnetic spectrograph will develop into a simple, rugged trouble-free device with extremely high sensitivity - and yet within a reasonable cost figure.

APPLICATIONS

An area where large economies can be realized in industrial monitoring of products is the chemical engineering of process control. Figure 2 shows how the simple coil configurations of rf sensors can be applied to batch or on-stream processes. Petroleum products, petrochemicals, and a variety of other chemicals lend themselves to practical product control, including observation and timing of a reaction. Entire rf sensors and their associates coils can be subjected to varying environmental conditions such as temperature, pressure, or nuclear radiation with controlled effects, homogeneous magnetic fields and reasonable product volume statistics at locations remote from the main console of the spectrograph.

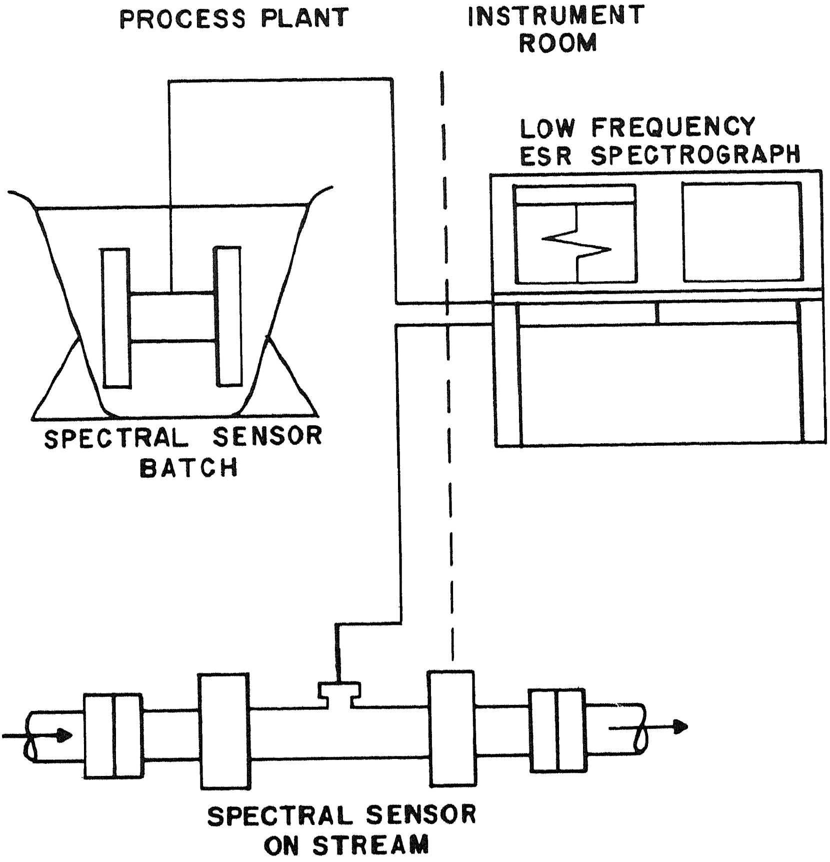

Figure 2. ESR Measurement in Batch Processes and On-Stream.

A typical use potential is illustrated in Figure 3 for fluid catalytic cracking. The system illustrated shows how the rf paramagnetic spectrograph can monitor several critical locations in a catalytic cracker from metallic poisoning such as vanadium (2) present in a crude oil; degree of catalyst contamination, deposited carbon and pyrolized constituents (1); degree of catalyst regeneration (3); to final product (4). Figure 4 is illustrative of the results obtained on a laboratory sample at 74 mc/s of a typical hydrogenation catalyst taken from a reactor.

CONCLUSION

To summarize, one finds that the radio frequency approach to paramagnetic absorption spectroscopy provides unique features of major scientific importance in the investigation of the

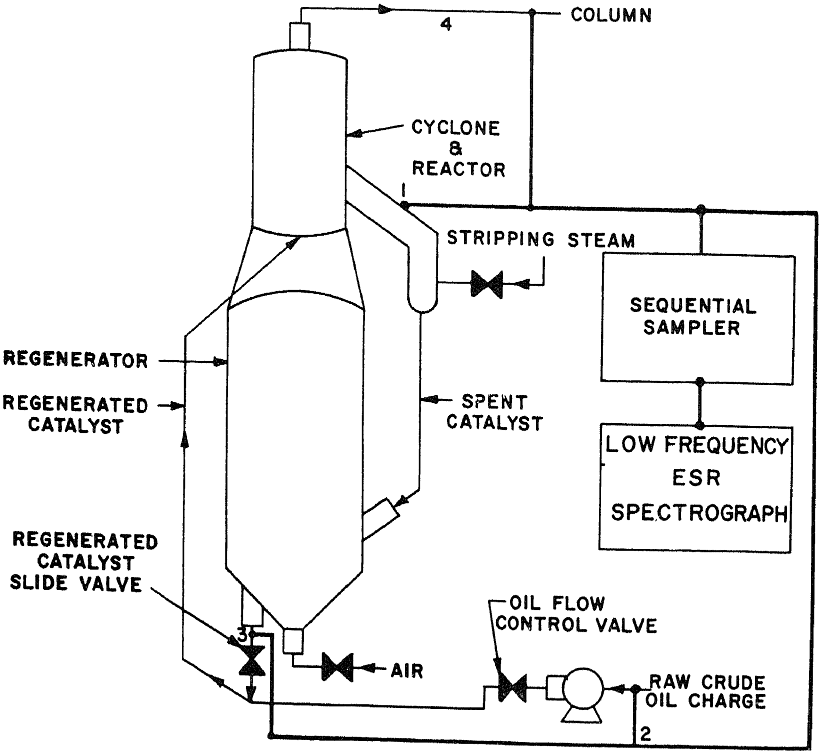

Figure 3. Measurement and Control of Catalyst Contamination (1, 3), Poisoning Content of Crude Oil (2), and Product (4).

structure of materials. It also provides the practical essentials for utilization of paramagnetic absorption in the measurement of physical-chemical properties of chemical compounds, and automation procedures for analytical chemistry [7, 8].

REFERENCES

1. B. Bleaney and K. W. H. Stevens, Repts. Prog. in Phys. 16, 108 (1953).
2. J. E. Wertz, Chem. Revs. 55, No. 5 (1955).
3. Richtmyer, Kennard, and Lauritsen, Introduction to Modern Physics, McGraw-Hill, New York, 1955, p. 290.
4. G. Breit and I. I. Rabi, Phys. Rev. 38, 2082 (1931).
5. D. J. E. Ingram, Spectroscopy at Radio and Microwave Frequencies, Butterworth, London, 1955.
6. Montgomery, Dicke, and Purcell, Principles of Microwave Circuits, McGraw-Hill, New York, 1948, pp. 46-7.

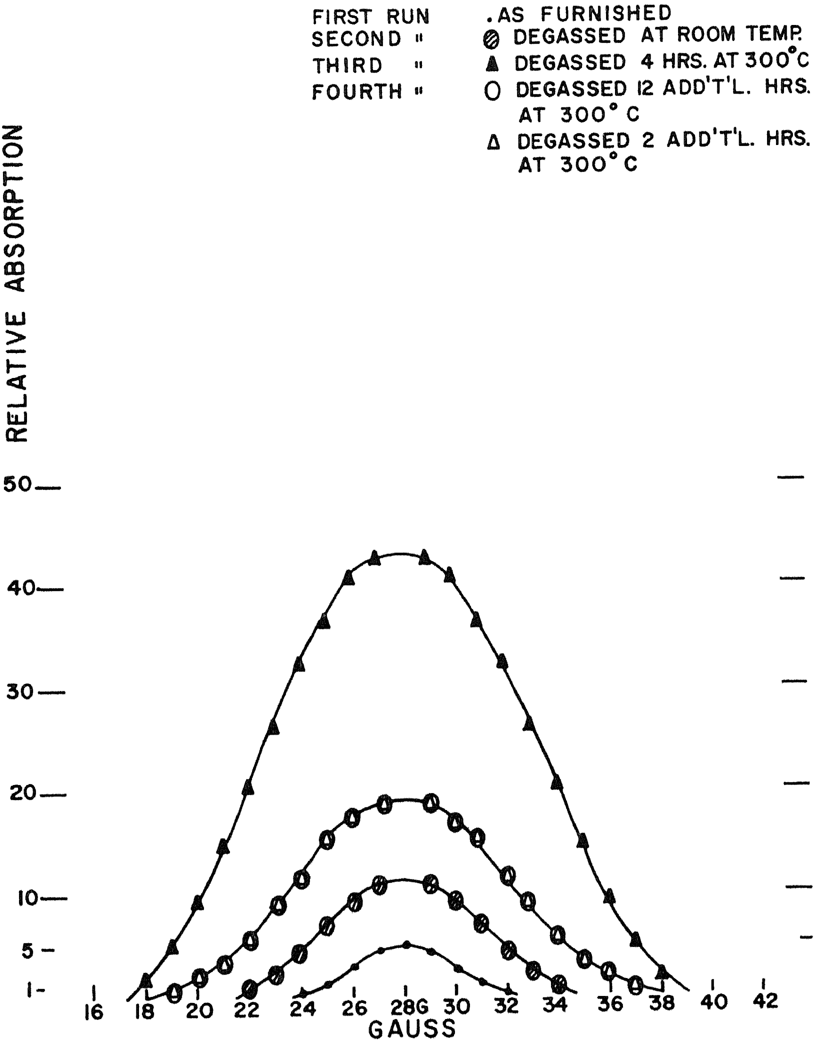

Figure 4. Hydrogenation Catalyst Poisoned by Metals, Pyrolized Material and Carbon Deposits.

7. H. A. Elion, Design Features and Process Applications of the Electron Spin Resonance Analyzer, Instrument Society of America, Paper 83-NY60 (1960).

8. H. A. Elion and L. Shapiro, Applications of Electron Spin Resonance Spectroscopy to Organic and Inorganic Chemistry, Progress in Nuclear Energy, Series IX, Analytical Chemistry, Vol. 2, Pergamon Press, New York (1961).

CORRELATION OF MASS SPECTRA WITH MOLECULAR STRUCTURE

J. H. Beynon
Imperial Chemical Industries Ltd.
Dyestuffs Division
Manchester, England

Mass spectra of organic compounds are usually produced by bombarding the vapour of the substance being investigated, at a pressure of the order 10^{-6} mm. mercury, with a stream of electrons of 50-100 eV energy. Since it requires only about 10 eV to ionize an organic molecule or to break a covalent bond, a variety of fragments will generally be formed, both charged and uncharged. The positively charged ions are drawn out of the ionization chamber, accelerated by a voltage (E) and enter via a slit a magnetic field (H) at right angles to their direction of motion, in which they are deflected according to their mass-to-charge ratio. An ion of mass m and charge e will follow a path of radius R given by [1]

$$R = \left(\frac{2E}{H^2} \cdot \frac{m}{e}\right)^{1/2} . \qquad (1)$$

An electrode behind a resolving slit collects ions which have traversed the magnetic field in a circular orbit of the correct radius. A mass spectrum is a recording of the ion currents falling on the collector as either E or H is varied causing the ions of different mass-to-charge ratio to be collected in succession.

That such a spectrum can be used to identify the substance from which it is produced may be illustrated by a simple example. Consider the mass spectrum of Figure 1. It is usually the case that the ion of greatest mass-to-charge ratio is formed by removal of a single electron from the sample molecule to give the so-called "parent" or "molecular" ion. It is assumed that

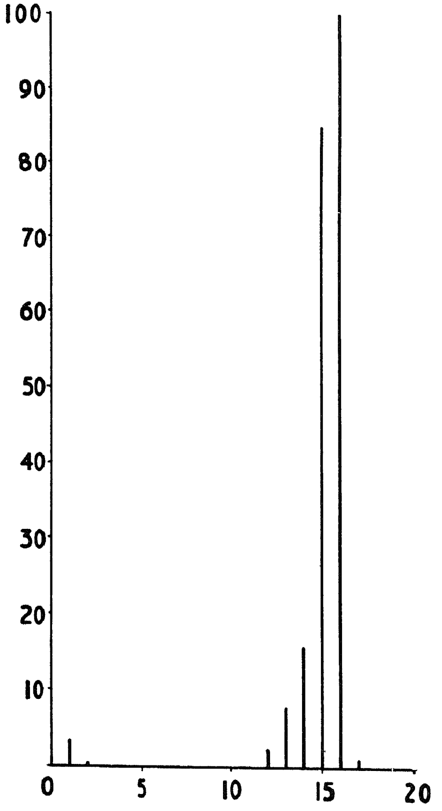

Figure 1. The mass spectrum of methane.

the pressure within the ionization chamber is so low that collisions between ions and neutral molecules are rare and can be neglected. (Examples in which this is not so are discussed later.) Thus, it would be inferred that the molecular weight of the substance considered here is 16, the peaks at masses 17 and 18 being due to molecules containing heavy isotopes. The difference in mass between adjacent isotopic peaks is known to be unity and it can thus be confirmed that the ion at m/e = 16 carries only a single positive charge. Peaks at masses 15, 14, 13 and 12 show the possibility of successive loss of mass 1, 2, 3 and 4 from the molecular ion and must correspond to the presence in it of 4 hydrogen atoms. The remaining fragment of mass 12 can only be a carbon atom and the unknown is identified as methane.

Similar arguments may be applied to the more complicated mass spectrum shown in Figure 2. A molecular weight of 84 would be assumed and this would immediately restrict the number of possible formulae for the unknown. If one limits one's considerations to compounds containing only atoms of C, H, N and O, the only possible molecular formulae are those shown in the left-hand column of Table 1.

It will be noted that only combinations containing an even number of nitrogen atoms are listed. This is an example of the so-called "nitrogen rule" which states that if the molecular weight, calculated on the basis of the most abundant isotope of each element, is even so is the number of nitrogen atoms. If one excludes from consideration the rare earths and metals which can exist in valency states differing by unity, then every

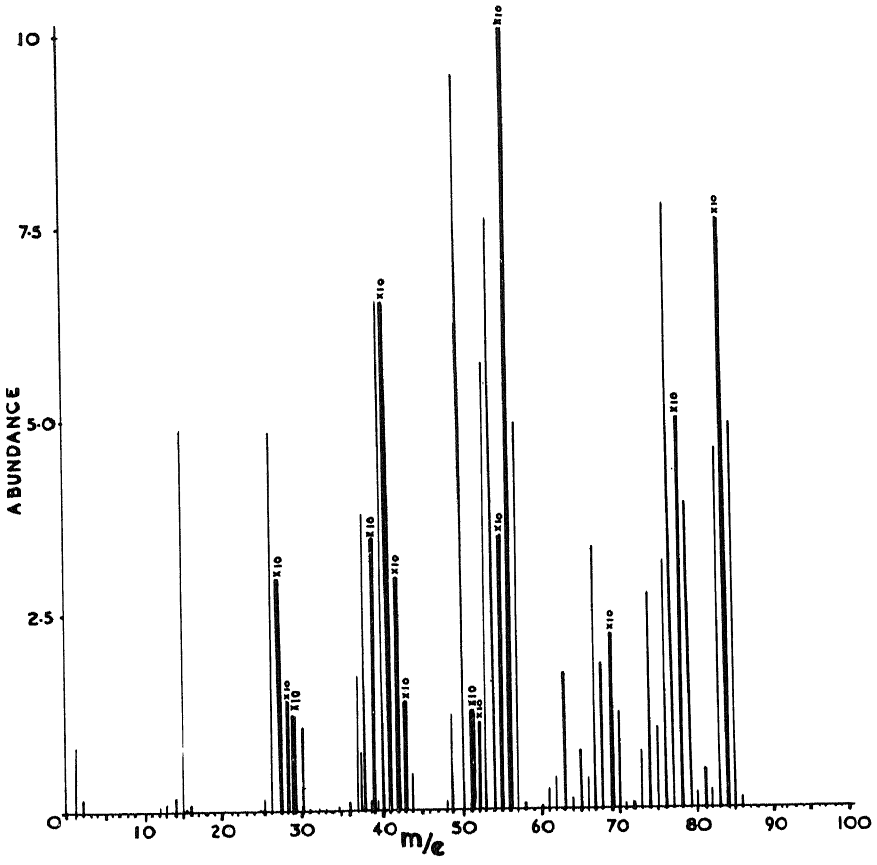

Figure 2. The mass spectrum of a mixture of cyclohexane and benzene. The peaks marked "x 10" have been scaled down by a factor of 10.

element obeys this rule with the exception of Be (atomic weight of most abundant isotope = 9, valency = 2) and Pt (atomic weight of most abundant isotope = 195, valency = 2 or 4). One must take care in applying the rule to organo-metallic compounds containing Cr, Co, Cu, Ir, Fe, Mn, Hg, Mo, Ni, Os, Re, Rh, Ru, Ti, W and V since all these exhibit alternative valency states differing by unity.

The fact that a mass spectrometer can give a molecular weight with such accuracy leads, in fact, to other arithmetical rules which can be used to check formulae of organic compounds. One of these is that if the nominal molecular weight of a C,H,N,O compound is even so is the number of hydrogen atoms it contains;

Table 1

Possible Molecular Formulae Corresponding to a Nominal Molecular Weight of 84. p, p+1, p+2 Represent the Relative Peak Heights to be Expected at Masses 84, 85 and 86 Due to the Presence of Heavy Isotopes at Natural Abundance, but Neglecting any Contributions from Peaks at Lower Masses

Formula	Mass*	$\frac{p+1}{p} \times 100$	$\frac{p+2}{p} \times 1000$
$C_2H_4N_4$	84.043594 u.	3.751	0.558
$C_3H_4N_2O$	84.032360 u.	4.108	2.659
$C_4H_4O_2$	84.021127 u.	4.465	4.772
$C_4H_8N_2$	84.068745 u.	5.213	1.111
C_5H_8O	84.057511 u.	5.570	3.264
C_6H_{12}	84.093896 u.	6.676	1.878

*Throughout this paper accurate masses are based on the mass reference $^{12}C = 12.0000$ u.

if the molecular weight is divisible by 4 the number of hydrogen atoms is also divisible by this number

In order to distinguish between the possible molecular formulae shown in Table 1, it is necessary to measure accurately the mass of the parent ion or the isotopic abundances at masses 84, 85 and 86 due to this ion. The masses of the various atomic combinations shown are known to about 1 part in 10^7; in order to distinguish between them an accuracy of measurement of only 1 in 2×10^4 will suffice. The abundances of the heavy isotopes of C, H, N and O show natural variations and there would be an uncertainty of the order 0.1 - 0.2 in the value of $100\ (p + 1)/p$ and $1000\ (p + 2)/p$ from this cause. Measurement to about this accuracy might be needed at mass 84 to distinguish possible formulae.

As one proceeds to higher molecular weight materials the number of possible molecular formulae becomes greater [2] and it is correspondingly more difficult to distinguish between them. However, two molecular ions difficult to distinguish by mass measurement are not necessarily difficult to distinguish by abundance measurement and if any other information is available concerning the unknown this might provide a further basis for selection. The situation is illustrated in Figure 3. The bottom curve shows the masses of all possible molecules of C, H, N and O arranged in ascending order of mass. The difficulty of distinguishing between adjacent compounds depends on the

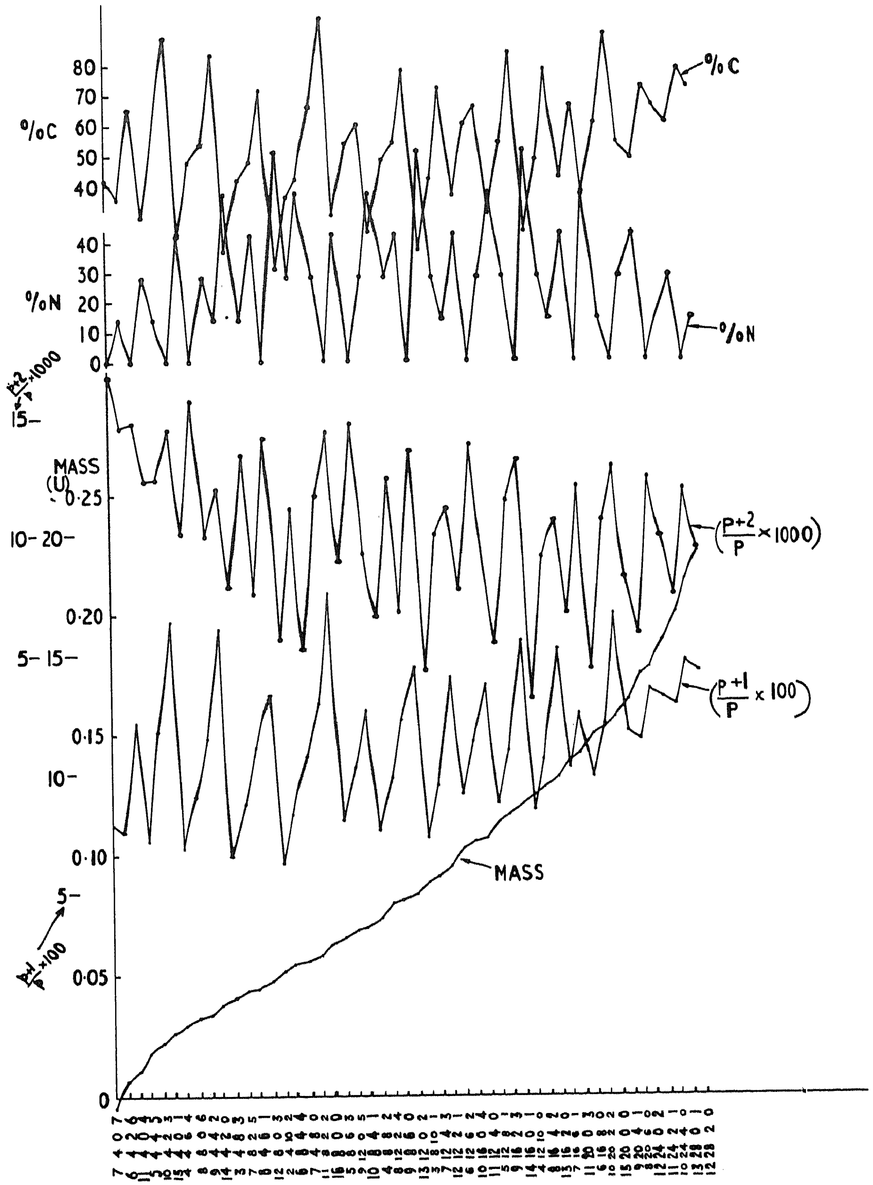

Figure 3. Means of distinguishing between molecular formulae at a mass number of 200. The bottom curve shows the accurate masses of the various atomic combinations, the other curves show respectively the abundances of the first and second isotopes and the percentages of carbon and nitrogen in the molecules. The numbers along the abscissa indicate the number of C, H, N and O atoms. Thus, 8,4,6,1 represents the formula $C_8H_4N_6O$.

slope of the line joining adjacent points. When the values of 100 (p + 1)/p and 1000 (p + 2)/p are plotted in the corresponding order, it is seen that it is very seldom that a small slope on the mass graph coincides with small slopes on the abundance graphs. When further information about the molecules is plotted (for example the other two graphs show the % N and C in the compounds) it becomes easily possible to distinguish any combination from any other.

Before one can carry out the necessary measurements on a parent peak in a mass spectrum one must be able to distinguish a parent peak from a fragment peak. Evidence concerning parent ions can be assembled in many ways. For example,

(i) The formula corresponding to this ion will obey the nitrogen rule referred to above. Generally speaking fragment ions do not obey this rule unless they have been formed by a multiple fragmentation from different parts of the molecule or have been formed in a re-arrangement reaction.

(ii) If a fragment ion appears in the spectrum of a pure compound at an unusual mass interval (e.g. 7-12 or 20-24) below the peak due to ions of greatest mass this is evidence that the latter ion species is itself a fragment.

(iii) If reduction of the electron-bombarding energy to a value in the region of the expected ionization potential of an organic compound causes a particular peak to disappear when other peaks still remain, the peak which disappears must be due to a fragment. Unfortunately, the converse is not always true and some fragment ions tend to persist even at very low electron-bombarding energies.

(iv) It can be confirmed that the rate of diffusion of sample from the sample reservoir agrees with a molecular weight equal to the mass of the heaviest observed ion.

(v) If the sample pressure is increased above the value usually employed, peaks sometimes appear due to reactions between ions and neutral molecules in the ionization chamber. These peaks can be recognized from the fact that their absolute intensity varies as the square of the sample pressure, and also from the way in which their abundance varies relative to peaks arising from unimolecular decomposition of molecular ions as a function of electron energy. Almost all compounds containing a nitrogen or oxygen atom exhibit this phenomenon. The most abundant ion-molecule peak occurs at a mass of (p + 1) and can be used to deduce the parent mass. Such peaks appear even in spectra of compounds such as adiponitrile in which there is a complete absence of parent peaks.

(vi) If the general class to which the unknown compound belongs is known (e.g. paraffin, aliphatic alcohol, etc.) the total abundance of all ions in the spectra per unit volume of sample vapour introduced is a smooth function of molecular weight and does not vary within a group of isomers. This "total ionization" can be used to give a rough guide to molecular weight.

(vii) A peak in a mass spectrum of a pure compound cannot be due to molecular ions if it can be shown to be composed of two or more ionic species of the same nominal mass. At a sufficiently high resolving power, fine structure will be apparent in such a peak.

If the molecular ion can be distinguished and its chemical formula deduced by mass and abundance measurement a very important preliminary step towards determining the molecular structure has been made. The method is unique in leading to exact values for the numbers of C, H, N, O, etc., atoms in the molecule rather than ratios of these; once the molecular formula is known the structure to be determined is limited to a definite number of possibilities. If the formula is denoted by $C_w H_x N_y O_z$, the total number of rings and double bonds is immediately obvious, being given by $(2w + 2 - x + y)$. Another powerful advantage of this method of molecular formula determination is that the measurement is usually unaffected by the presence of impurities, and when a mixture is examined, the mass spectrometer can often give a formula for more than one component. Indeed in favourable cases, formulae can be deduced for impurities present to only about 0.01%.

The accuracy of mass measurement necessary in the region of mass 200 can be estimated from Figure 3. A mass measurement to 1 in 10^5 restricts the number of possible formulae to a maximum of 3 and is adequate, when coupled with abundance measurements, to give the formula of any organic compound in this mass region. The presence of atoms in addition to C, H, N and O, for example, Cl, Br, S, Si is easy to deduce from the unusual isotopic patterns of these elements and these and other elements such as P, F, I are also detectable from the unusual mass differences which they produce between some fragment ions in the spectra.

Re-writing equation (1) as

$$mE = \frac{R^2 H^2 e}{2} \qquad (2)$$

or

$$mE = \text{const. (at const. H)} \qquad (3)$$

it can be seen that mass comparisons can be carried out between known and unknown masses merely by measuring the accelerating voltages at which they appear at constant magnetic field. In this way, using a 6" radius single-focussing mass spectrometer of resolving power 300, it has been found possible to carry out mass measurements to about 1 in 2×10^4, the limitation being due to the difficulty of determining the exact position of the maximum of a mass peak. Although we have not yet considered in detail the fragment ions in a mass spectrum, it can be mentioned here that some of these may be formed with kinetic energy. If this is so, they will enter the accelerating field with a non-zero velocity and be deflected in the magnetic field along the same circular path as a heavier ion formed with zero kinetic energy. This difficulty may be overcome by using a so-called double-focussing mass spectrometer which corrects for this kinetic energy effect. One method by which this may be accomplished is to use an energy selector preceding the magnetic field [3]; a schematic diagram of a recent commercial instrument built to this design is shown in Figure 4.

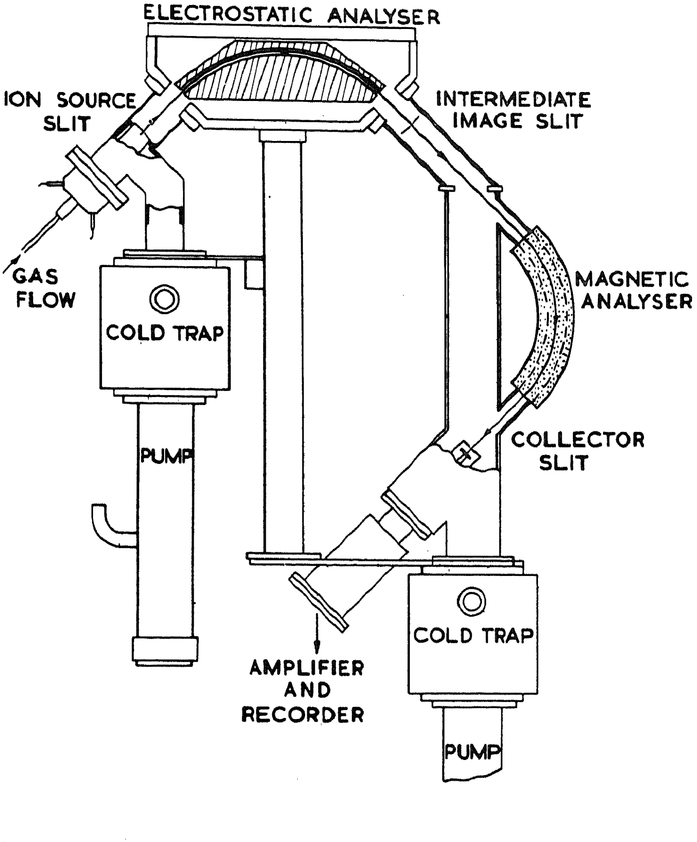

Figure 4. Schematic diagram of the M.S.8 mass spectrometer manufactured by Associated Electrical Industries Ltd., Manchester, England.

The introduction of such equipment for the study of organic structures led to several other advantages. The improved focus enabled entrance and exit slits to be narrowed with a corresponding increase in resolving power. With a 6" radius of curvature in the magnetic field, resolving power of about 10,000 could be achieved in day-to-day operation [4]. This enabled the maxima of peaks to be located with greater accuracy, and the accuracy of mass measurement to be increased. Using at the same time the elegant peak-matching technique [5], accuracy of 1 in 2×10^5 could be attained over a mass range of 2%. But an equally powerful advantage of the use of high resolution double-focussing instruments is that it enables fine structure to be distinguished in peaks consisting of several different species of ion, all of the same nominal mass number. A tracing of a mass multiplet at mass 44 plotted at a resolving power of 3900 is shown in Figure 5. Five different components can be distinguished and their origins are shown.

In order to separate all multiplets which can be formed in C, H, N, O compounds, an extremely high resolving power is

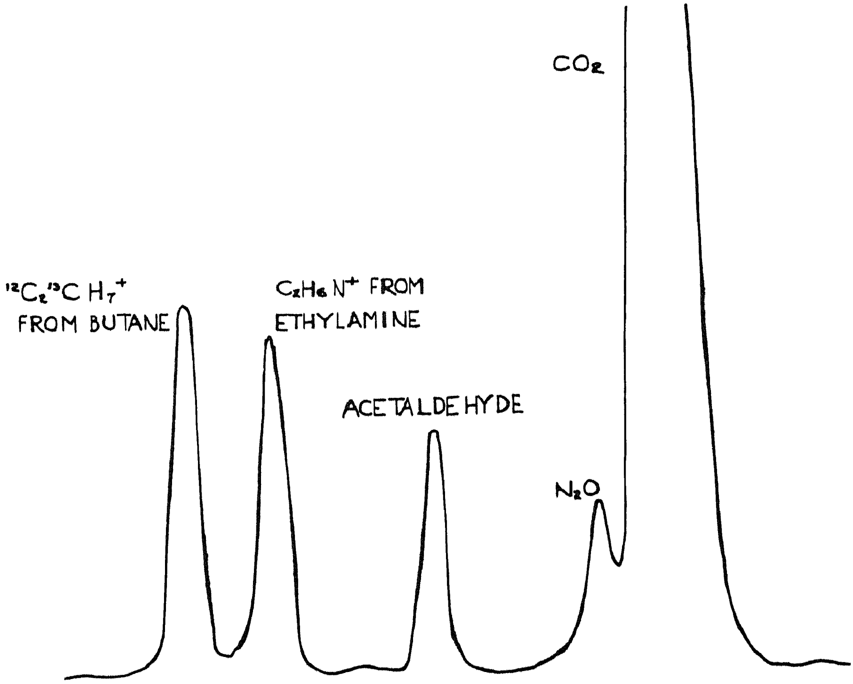

Figure 5. High resolution plot of a multiplet at a nominal mass of 44.

necessary. For example, if it were required to separate two peaks due to ions differing in formulae only from the fact that one contained two hydrogen atoms and the other a single deuterium atom, this would require at mass 400 a resolving power of about 250,000. This is beyond the present practicable limit for apparatus to be used in routine qualitative analysis. However, if one neglects doublets containing a heavy isotope, the only doublet which cannot be resolved at a resolving power of 100,000 at mass 400 is the rather uncommon combination CH_4—H_4O_4. The common doublets CH_2—N, CH_4—O, NH_2—O and N_2—CO can all be resolved up to mass 400 with an available resolution of 36,000 and evidence of multiplet structure obtained at half this resolution. A resolution of 36,000 enables the important heavy isotope doublet CH—^{13}C to be resolved up to mass 161 and useful measurements to be obtained to mass 300 on partially resolved multiplets based on this mass difference. The CH—^{13}C doublet will surely become of great importance in tracer work at high resolution.

A resolving power of over 10,000 has been achieved with our M.S.8 spectrometer which has a 6" radius magnetic sector, and as larger instruments become available the attainable performance should increase still further. Figures 6 and 7 show the performance of a prototype machine of 12" radius magnetic sector.

The arrangement of the atoms within the molecule which gives the structural formula can only be deduced from a knowledge of the formulae and abundances of the fragment ions in the spectrum and an understanding of the factors which govern this fragmentation pattern.

In favourable cases it is possible to deduce that some of the peaks in a spectrum are not fragments from the heaviest ions in the spectrum. Thus, in Figure 2, if we are dealing with a compound of molecular weight 84, it is extremely unlikely that fragmentation would occur with high probability leading to loss of six hydrogen atoms when 1, 2, 3, 4 or 5 hydrogens are not eliminated readily. It would then be deduced that the spectrum is in fact that of a mixture. Under conditions of high resolution, ions due to a second component might also be detected on the basis of their formula if this was sufficiently different from that of the first component. It should be emphasized that the presence of an impurity is unlikely to interfere with a mass and formula determination of the major component. Indeed, the reverse is also true and formulae of impurities can often be deduced, even when they are present to as little as 0.01%.

By far the most generally useful proposal to explain the mass spectrometric "cracking pattern" of an organic compound has been the "quasi-equilibrium" theory [6]. This assumes that

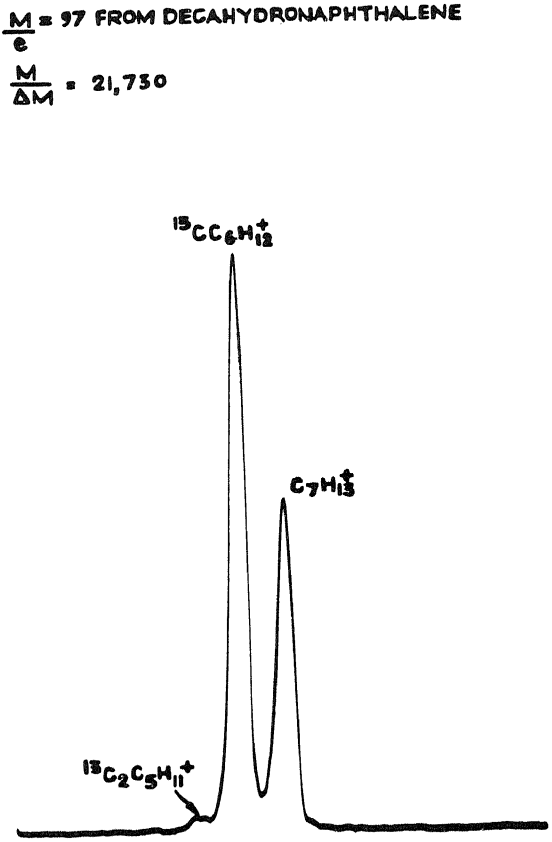

Figure 6. The doublet at m/e = 97 in the mass spectrum of decalin.

in its passage through a sample molecule the bombarding electron can repel any valence shell electron near which it passes in a "vertical" ionization to give a parent ion in an electronically excited state. According to the theory the excitation energy does not remain concentrated in the bond from which the electron has been removed but can distribute itself over the molecule ion in random fashion. Fragmentation occurs when sufficient time has elapsed for energy greater than the dissociation energy to accumulate in one degree of freedom. The fragment ion formed may itself be excited and dissociate further. Recent work has shown anomalies in the quantitative aspects of the theory and it seems that the theory is invalid in the vicinity of the ionization threshold.

A great deal of effort has been concentrated into the study of the mass spectra of large numbers of compounds in a single

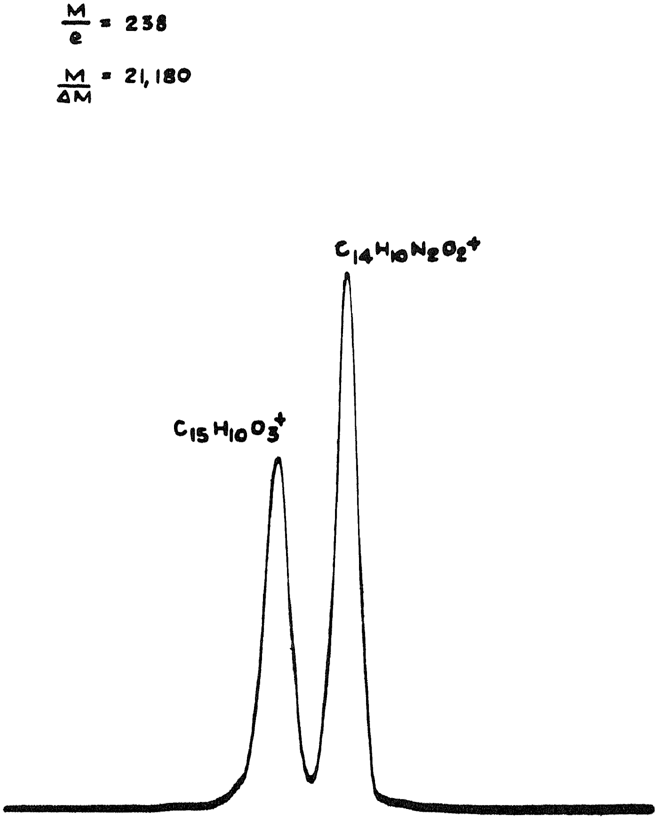

Figure 7. The doublet at m/e= 238 formed by the molecular ions of methoxy anthraquinone and di-amino anthraquinone.

chemical class, e.g., ethers, ketones, nitriles, etc. By this means, empirical rules can be deduced so that once a compound is known to be of a particular chemical type its complete structure can be deduced. Correlations carried out to date have been listed in reviews [7].

Many of the ions in mass spectra are difficult to explain by any simple theory, and involve, for example, re-arrangement of the atoms during fragmentation. Naturally, the discovery of these re-arrangement ions at first cast doubts upon whether the mass spectrometer would prove useful for detailed structural investigation, but it is becoming clear that when enough is known about the structures of ions, and the factors important in determining the localization of charge and thus bond strengths, the steric configuration of the atoms as compared with those in the

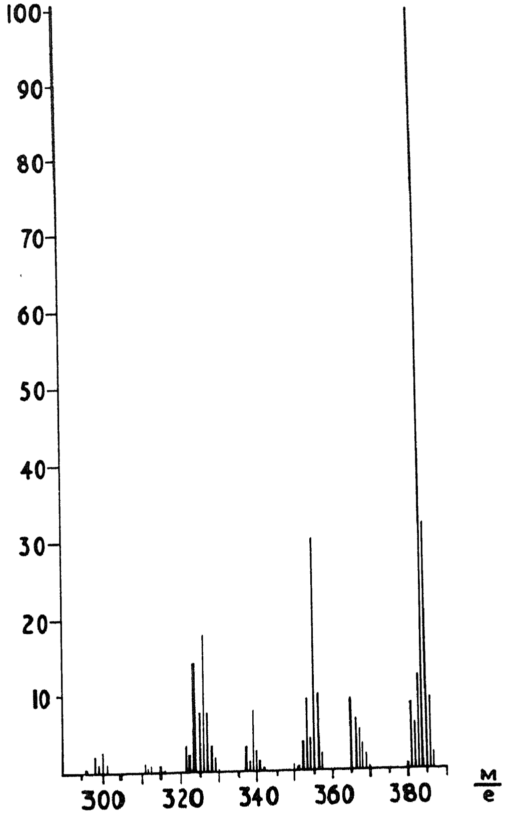

Figure 8. The partial mass spectrum of 9:9' dianthraquinone.

neutral molecule, the effect of the total stability of products in producing the "driving force" for fragmentation along a particular path, the structures of the transition complexes formed during fragmentation, and so on, one may be able to use such rearrangements to deduce subtle features of the structure. Special mention should be made of the work of McLafferty [8] and Meyerson [9] who by the use of the concepts of physical-organic chemistry, sometimes coupled with the use of isotopic labelling, have added greatly to our detailed knowledge of fragmentation processes in various classes of organic compound.

The so-called "meta-stable" ion peaks in the mass spectrum are often valuable in determining the detailed path of fragmentation. These peaks are formed by ions of mass m_1 sufficiently stable to have been accelerated by the electric field in a mass spectrometer, but which have undergone fragmentation into ions of mass m_2 in the vicinity of the entrance slit before deflection in the magnetic field. Such ions will produce a diffuse peak at an effective mass m^* in the spectrum, where $m^* = m_2^2/m_1$.

As an example of their use, it is known that esters of formula

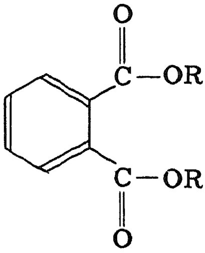

give a large peak in their mass spectra at a mass of 149, corresponding to loss of (OR_2—1) from the parent ion. A meta-stable ion peak in the di-butyl ester at mass 108.3 corresponds to the transition: $205^+ \rightarrow 149^+ + 56$ and shows the sequence of events to be: $p^+ \rightarrow 205^+ + 73 \rightarrow 149^+ + 56 + 73$, suggesting the detailed path

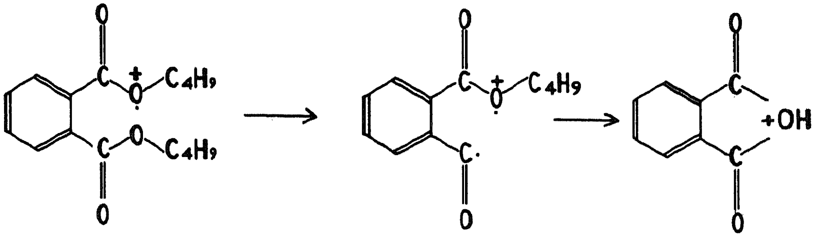

Hydrogen atoms can move over considerable distances to take part in re-arrangements as is illustrated in the following example. Anthraquinone has been shown by accurate mass measurement of fragments and by study of meta-stable peaks to fragment according to the scheme:

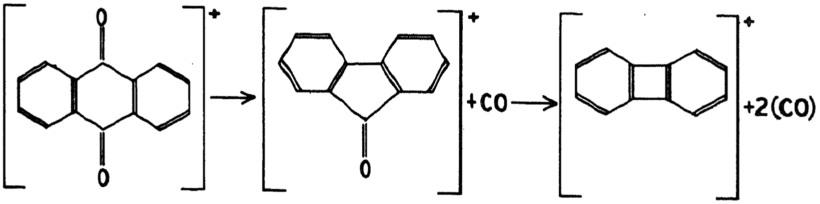

9:9'-dianthraquinone (the partial mass spectrum of which is shown in Figure 8) does not break with loss of CO, but instead loses either CHO, CH_3O or CH_5O and this is followed by a second step in which hydrogen is again included in the neutral fragment eliminated.

Now the molecule of 9:9'-dianthraquinone is not planar and it can gain stability by eliminating hydrogen from the 4 and 5 positions on the rings. It is thought that by localization of charge on the oxygen atoms they acquire some degree of trivalency and a transition state can be visualized which we may represent by:

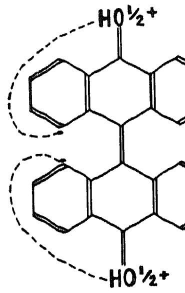

leading initially to fragmentation into

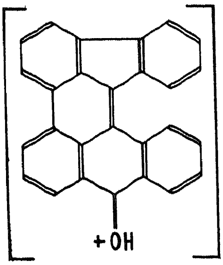

$+ CHO$ or

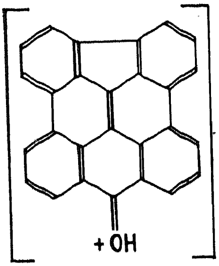

$+ CHO + H_2$

and finally into

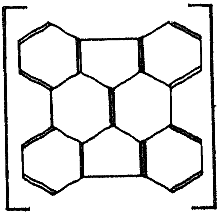

$+ 2CHO + H_2$

the ion gaining in stability by the formation of extra bonds, and by increased resonance stabilization.

Similar behaviour occurs with hydrocarbons and can be used as an aid in structure determination. Thus, 9:9'-dianthracene [10] readily loses pairs of hydrogen atoms to give prominent ions of even mass in its spectrum. Another hydrocarbon of this type known to give abundant (p - 4)+ ions is 4,5-dimethylphenanthrene, and here, too, the possibility of formation of an extra ring is evident

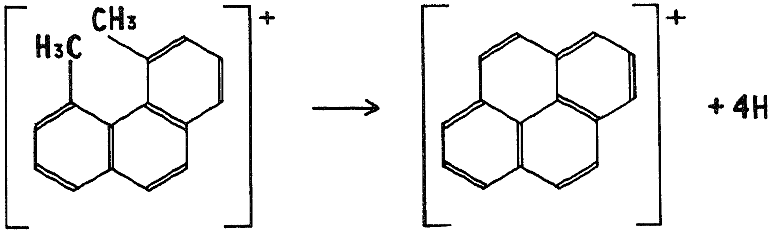

This is typical of the behaviour of fused ring compounds having methyl substituents in similar positions. That this is not, however, the only factor important in giving rise to (p - 4)$^+$ ions is shown by the fact that 9,10-dimethyl 1,2-benzanthracene

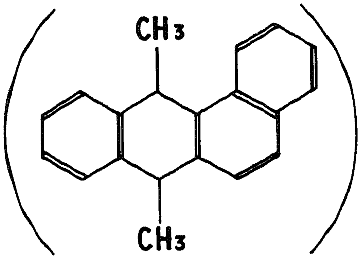

and 1,2,5,6 dibenzanthracene

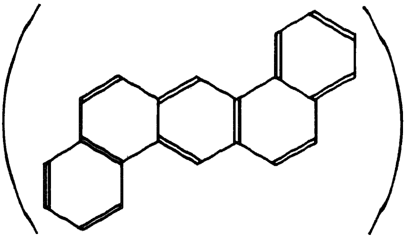

can also lose four hydrogens from their molecular ions with moderate probability.

It is not possible in a short article of this nature to point out more than one or two of the semi-empirical methods used by mass spectroscopists to arrive at structural formulae, but an overall idea of the power and limitations of the method can perhaps be gained from the following examples, each of which has been chosen to illustrate that the use of a different mode of argument may be appropriate in different cases.

The first example concerns the identification of a reaction product formed from known starting materials, and illustrates the great advantage gained from the exact molecular weight as given by the mass spectrometer. It was one of the constituents formed when cyclopentanone (C_5H_8O, M.W. 84) was reacted with n-butylamine ($C_4H_{11}N$, M.W. = 73) in a sealed tube [11]. The heaviest ion species in the mass spectrum, excluding heavy isotopes, was at mass 201 and was assumed to be due to the parent ion.

The reaction which had taken place to give this product can be written in one of the following ways (cyclopentanone is represented merely by its molecular weight of 84 and n-butylamine by 73):

$$\begin{aligned} &3 \times 73 &&\rightarrow 201 + 18 \\ &2 \times 73 + 1 \times 84 &&\rightarrow 201 + 29 \\ &1 \times 73 + 2 \times 84 &&\rightarrow 201 + 40 \end{aligned}$$

Reaction of cyclopentanone alone is not possible since the odd molecular weight shows the product to contain nitrogen. For the same reason, in the first example shown, the mass 18 must be of formula CH_6 so as to retain an odd number of nitrogens in the product. By similar arguments, the reactions can be rewritten:

$$\begin{aligned} &3(C_4H_{11}N) &&\rightarrow C_{11}H_{27}N_3 + CH_6 \\ &2(C_4H_{11}N) + C_5H_8O &&\rightarrow C_{12}H_{27}NO + CH_3N \\ &C_4H_{11}N + 2(C_5H_8O) &&\rightarrow C_{11}H_{23}NO_2 + C_3H_4 \\ &\qquad\qquad\qquad\text{or} &&\rightarrow C_{12}H_{27}NO + C_2O \\ &\qquad\qquad\qquad\text{or} &&\rightarrow C_{14}H_{19}N + H_8O_2 \end{aligned}$$

An obvious method of attempting to distinguish between the possibilities is to measure accurately the mass of the "201" ions. This was done, using a mercury isotope as reference mass and a value 201.151 u. was obtained. The only possible formulae to satisfy this mass are found by reference to a mass table such as is referred to earlier and found to be $C_{14}H_{19}N$, $C_9H_{19}N_3O_2$ and $C_{10}H_{19}NO_3$. Only the first of these satisfies any of the reaction possibilities. Reactions are known in cyclopentanone which eliminate water to give 2-cyclopentylidene cyclopentanone and between cyclopentanone and n-butylamine to eliminate the same substance and give N-cyclopentylidene n-butylamine. A combined reaction eliminating H_8O_2 (i.e. $2H_2O + 4H$) might thus be expected to give a dehydrogenation product of

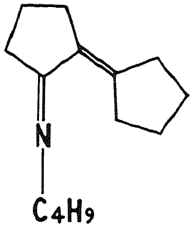

which one would expect to take the form

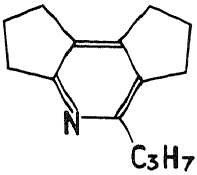

This then is the postulated structural formula suggested almost entirely by an arithmetic method.

The second example is one which is greatly assisted by a correlation study published in the literature. From its spectrum, shown in Figure 9, the compound is thought to have a molecular weight of 118 and it can be seen from the unusual isotope pattern in this region ($(p+2)/p \sim 4.5\%$) that it contains a sulphur atom. An accurate mass measurement shows its formula to be $C_6H_{14}S$ and thus that it contains no rings or double bonds in its structure. It is thus either a thiol or a sulphide and correlation studies have been carried out for both these compound types [12]. From these studies it can be seen that the

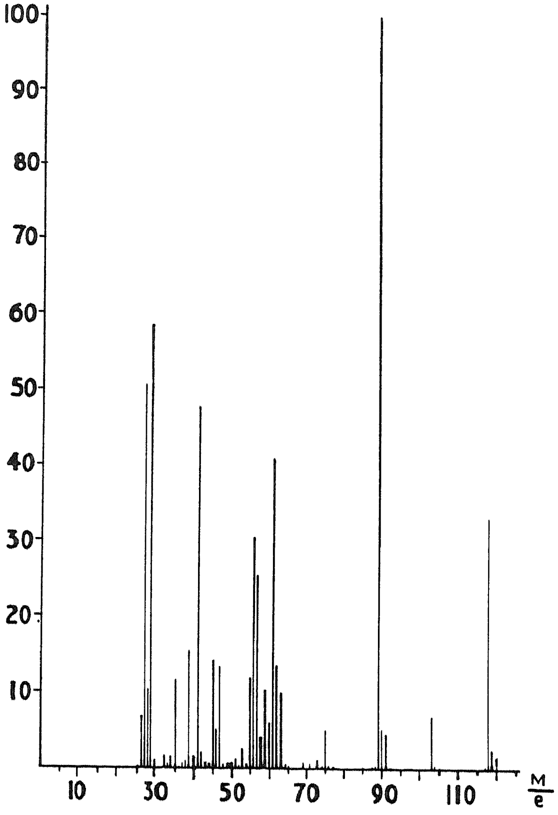

Figure 9. The mass spectrum of a compound for identification. (It can be shown to be ethyl, sec-butyl sulphide.)

absence of a large peak at either mass 84 or 85 [(p - SH_2) and (p - SH)] shows the compound is not a thiol. The largest peaks in the re-arrangement series $(RSH)^+$ and $(RSH_2)^+$ are at masses 62 and 63 and show that the smaller radical attached to the sulphur atom is of mass 29 and thus is ethyl. The compound is, therefore, an ethyl butyl sulphide. Fragmentation of the longer radical would take place at bonds β to the sulphur atom and there are large peaks corresponding to loss of both CH_3 and C_2H_5. The butyl radical is, thus, sec-butyl and the complete formula is:

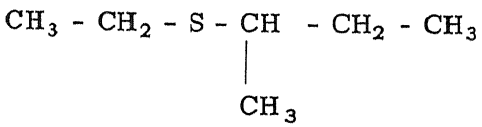

$$CH_3 - CH_2 - S - \underset{\displaystyle CH_3}{\underset{|}{CH}} - CH_2 - CH_3$$

A more complex spectrum which illustrates how apparently contradictory information maybe reconciled with a single structure is that shown in Figure 10. A large number of odd-mass fragments suggests an even mass molecular weight. The heaviest-mass ion is at 198, so it is reasonable to suppose that this is the mass of the complete molecule. If the molecular weight is 198, then measurement of the exact parent mass (by comparison with the ^{198}Hg isotope) leads to the molecular formula $C_{12}H_{22}O_2$. Fragmentation takes place with low probability to lose masses 15, 29 or 43 and this suggests a straight hydrocarbon chain; branches would be indicated by a higher probability of fragmentation. There is a much larger peak corresponding to loss of mass 55 than mass 57, the next member of the series. This suggests a re-arrangement process with transfer of 2 hydrogens such as occurs sometimes in esters.

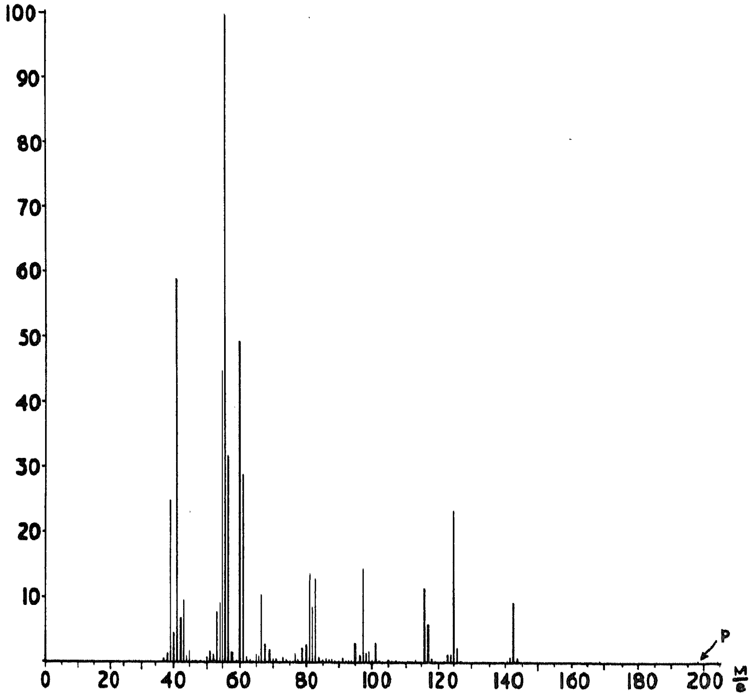

Figure 10. The mass spectrum of a compound for identification. (It can be shown to be the n-butyl ester of cyclohexylacetic acid.)

Thus

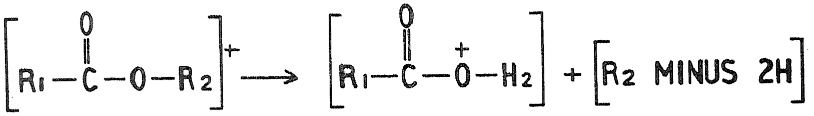

$$\left[R_1-\overset{\overset{\displaystyle O}{\|}}{C}-O-R_2\right]^+ \longrightarrow \left[R_1-\overset{\overset{\displaystyle O}{\|}}{C}-\overset{+}{O}-H_2\right] + \left[R_2 \text{ MINUS } 2H\right]$$

so that R_2 is n-butyl in this case.

According to a correlation study made between spectra and structure in esters [13] this is the most intense kind of re-arrangement in formates, acetates, etc., leading to ions of masses 47, 61, etc.

Since the re-arrangement here is to mass 143, we can assume, by analogy that R_1 has a mass of (143 - 47 + 1) = 97.

Confirmation that we are dealing with a n-butyl ester is obtained from the fragment peak at mass 125 which corresponds to loss of $-OC_4H_9$ without re-arrangement, and the peak at mass 97 due to loss of $-COOC_4H_9$. A meta-stable peak at mass 75.4 corresponds to the transition

$$\left[P \text{ MINUS } - OC_4H_9\right]^+ \longrightarrow \left[P \text{ MINUS } - COOC_4H_9\right]^+ + CO$$

and shows that the further loss of mass 28 occurs in a single step.

The peaks at masses 117, 116 and 101 cannot be part of this chain fragmentation process and must correspond to bond cleavage from a different part of the molecule. They correspond respectively to loss of mass 81, 82 and 97 from the parent ion and there do not appear to be any fragments of higher mass which correspond to this series. There are, however, also peaks in the spectrum at masses 97, 82, 81 which are probably due to fragmentation at the same bonds in the molecule, the positive charge remaining on the alternative fragment. We know from the molecular formula that the entire fragment (R_1) can contain only carbon and hydrogen and thus must be of formula C_7H_{13} and contain a single ring or double bond. A C_6 ring would seem most likely to explain why the smallest fragment lost is of mass 81 (C_6H_9) and indeed this fragmentation and also that which gives loss of mass 82 must be accompanied by re-arrangement.

Thus one must postulate a structural formula

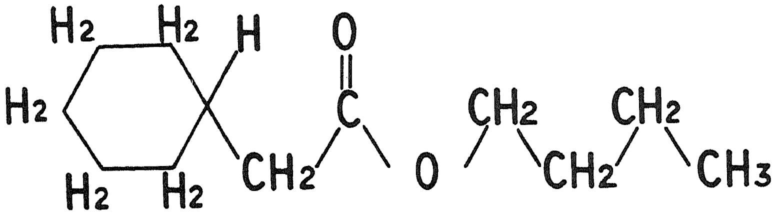

to satisfy the spectrum.

It now remains to study the peaks in the spectrum which have not been used in the identification to see whether they fit in with the proposed structure. Peaks at masses 39 to 43 and 53 to 57 and at 83 are due to hydrocarbon fragments of the ends of the molecule, that at mass 83 confirming the pendant cyclohexyl group.

Re-arrangement peaks at masses 60 and 61 due to ions $C_2H_4O_2^+$ and $C_2H_5O_2^+$ would be expected from an acetate. They are quite unexpected from the present compound, but previous correlations (which have not included any esters of cyclohexyl acetic acid) suggest that mass 60 is to be expected only from fatty acids or butanoates. Obviously neither of these compound types explains the majority of the peaks in the spectrum and must be rejected.

The peak at mass 95 corresponds to fragmentation of R_1 with loss of a further two hydrogen atoms. This is unexpected but not so surprising as to throw doubt on the proposed structure.

Peaks at masses 67, 68 and 69 cannot be explained on the above hypothesis except by fragmentation of $-OR_2$ followed by loss of up to 6 hydrogen atoms. Nevertheless the spectrum discussed has, in fact, been published and is that of the n-butyl ester of cyclohexylacetic acid.

The fourth example concerns the identification of a fungal derivative prepared by Dr. G. M. Blackburn of Cambridge University, the partial mass spectrum of which is shown in Figure 11. The prominent ion at a nominal mass of 422 is assumed to be the molecular ion. Its measured mass of 422.223 ± 0.004 u. and isotope peaks at masses 423 and 424 of measured abundance 32.62% and 6.05% of that of the peak at mass 422 fit only the formula $C_{30}H_{30}O_2$ of mass 422.224 u. and isotope abundances 32.97% and 5.66% respectively.

The major fragmentations are to peaks of masses (p-57) and (p-114) where p represents the parent mass. These suggest the presence of two amyl groups on an aromatic nucleus. These side chains are not branched, otherwise fragments corresponding to cleavage at the branches would be seen.

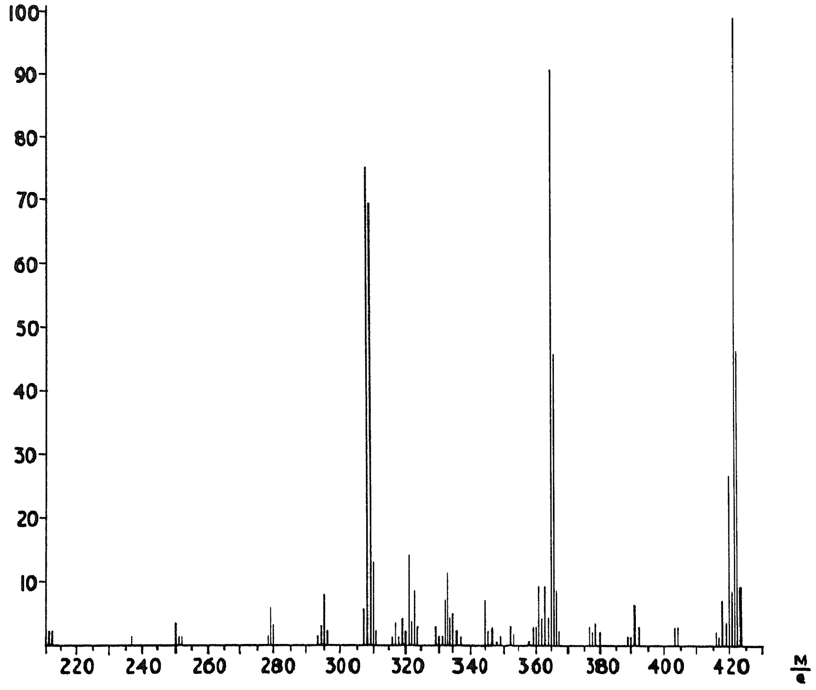

Figure 11. The partial mass spectrum of a fungal derivative.

The nucleus itself is thus of formula $C_{20}H_{10}O_2$ and therefore contains a total of 16 rings and double bonds. Unless the structure contains several fused five membered rings, the structure will be a 6 fused ring system with ether oxygens as shown below. There are other peroxide structures to fit the formula but the fragmentation pattern best fits the system shown:

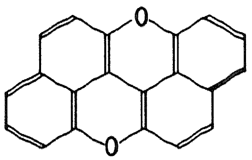

We have run the mass spectrum of this nucleus (perixanthenoxanthene) and find it is characterised by loss of mass 29 and mass 58. This represents loss of (COH) and $(COH)_2$ to more highly fused structures.

All peaks other than (p-57) and (p-114) in the mass spectrum of the fungal derivative compound are small and occur at (p-19); (p-29) to (p-33) with an outstanding (p-31); (p-46) to (p-52); (p-70); (p-76); (p-77); (p-87) to (p-93) with an outstanding (p-89); (p-99) to (p-106) with an outstanding (p-101); (p-127); (p-143) and (p-172).

Now, if the fragmentation takes place in several steps, the first steps could be loss of the partial side chains, i.e.

$$p^+ \rightarrow (p-57)^+ + C_4H_9 \rightarrow (p-114)^+ + 2C_4H_9 .$$

The remaining nucleus would then be expected to break exactly like peri-xanthenoxanthene, i.e.

$$(p-114)^+ \rightarrow (p-143)^+ + COH \rightarrow (p-172)^+ + 2COH .$$

Both these reactions are seen and are evidence that the nucleus is as expected. Further evidence for a strong nucleus comes from a large doubly-charged ion of $(p-114)^{++}$ in the spectrum.

The peaks in the region of (p-52) and (p-77) are probably from fragmentation of benzene rings.

It remains to explain how the amyl side chains can prevent loss of (CHO) from the parent molecule. Now there are many known examples of fragmentation patterns of a particular group being modified by the presence of adjacent groups which can themselves take part in the fragmentation reaction to increase the overall stability of the resultant ion by forming additional rings or bonds. Suppose one postulates amyl groups in the positions shown, then replacement re-arrangement reactions of the form illustrated could occur. The positive charge probably lies mainly in the position shown:

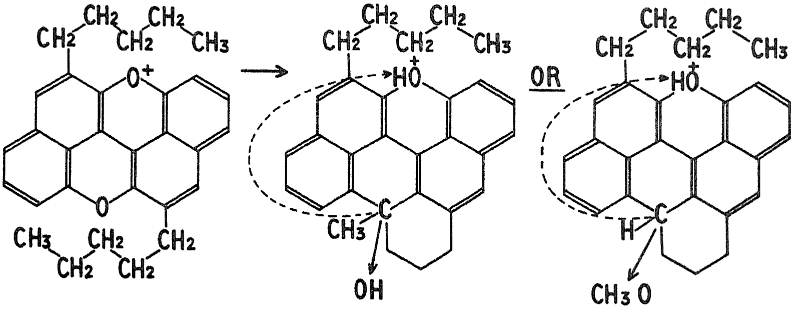

and extra stability can be gained by further elimination of H_2 groups to unsaturate the new ring formed. Thus, there is elimination of H_3O, (p-19); CH_5O, (p-33); elimination of C_4H_9 from one side chain followed by H_3O, (p-76) or CH_3O, (p-88). (There are no methoxy groups present in the original compound, since these would lead to loss of CH_3 very readily, and this is not observed.)

There is also a small possibility of a n-amyl side chain breaking to lose C_5H_{10} with transfer of a hydrogen. Thus we have (p-70), and can also see (p-89), which is formed by loss of a further H_3O and (p-101) formed by alternative loss of a further CH_3O. There is loss of 57 from one amyl group and 70 from the other: (p-127), but there is *never* loss of fragments of both side chains together with loss of H_3O and CH_3O and it is clear why this is so. Thus every peak (and lack of peak) is explained on the above hypothesis. If we assume the isomer to be:

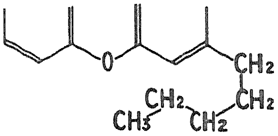

we should expect to see loss of CH_3 or CH_5 and this does not occur.

The migration of a hydrogen to the trivalent $\overset{+}{O}$ is again over a very long path, as in the case of 9:9' dianthraquinone.

REFERENCES

1. A. J. Dempster. Phys. Rev. 11, 316 (1918).
2. J. H. Beynon. "Mass Spectrometry and its Applications to Organic Chemistry." D. Van Nostrand Company, Inc., Princeton, N.J. (1960).
3. R. F. K. Herzog. Z. Physik. 89, 447 (1934).
4. J. Mattauch and R. F. K. Herzog. Z. Physik. 89, 786 (1934). J. H. Beynon in Symposium on Mass Spectrometry, Oxford, 1961. Pergamon Press Ltd., Oxford, 1962. M. K. Elliott, Ed.
5. C. F. Giese and T. L. Collins. Phys. Rev. 96, 823 (1954). K. S. Quisenberry, T. T. Scolman and A. O. Nier. Phys. Rev. 102, 1071 (1956).
6. See for example, review by H. M. Rosenstock in Symposium on Mass Spectrometry, Oxford, 1961. Pergamon Press Ltd., Oxford, 1962. M. K. Elliott, Ed.
7. F. W. McLafferty in "Determination of Organic Structures by Physical Methods," Vol. 2, 1962. Academic Press Inc. New York, N.Y.

8. See for example F. W. McLafferty. Appl. Spectroscopy, 11, 148 (1957).
9. See for example P. N. Rylander and S. Meyerson. J. Amer. Chem. Soc., 78, 5799 (1956). P. N. Rylander, S. Meyerson and H. M. Grubb. J. Amer. Chem. Soc., 79, 842 (1957).
10. American Petroleum Institute, Research Project 44, Mass Spectral Data Sheet No. 1440.
11. O. B. Edgar and D. H. Johnson. J. Chem. Soc., 3925 (1958).
12. E. J. Levy and W. A. Stahl. 5th Annual Meeting, A.S.T.M. Committee E-14, New York, 1957.
13. A. G. Sharkey, J. L. Shultz and R. A. Friedel. Anal. Chem., 31, 87 (1959).
14. American Petroleum Institute, Research Project 44, Mass Spectral Data Sheet No. 1442.

VACUUM SPARK MASS SPECTROGRAPHIC ANALYSIS OF SOLIDS AND LIQUIDS

A. J. Ahearn
Bell Telephone Laboratories, Incorporated
Murray Hill, New Jersey, U.S.A.

INTRODUCTION

Mass spectroscopy has been employed in recent years with increasing frequency in the analysis of solids. This is largely to meet the need to detect increasingly lower concentrations of impurities in solids. Heretofore the emission spectrograph has led the field in this work. However, it generally cannot detect impurities at concentrations below one part per million (1 ppm) and for many elements the sensitivity is substantially poorer than 1 ppm. Consequently there are many problems for which the emission spectrograph is not adequate. For example, impurities of one part per billion (1 ppb) are of great importance in semiconductors.

The mass spectrograph is an instrument that reveals the composition of a sample of material by disclosing the ratio mass/charge of the constituent atoms and molecules after they have been ionized.

For general purposes, the vacuum spark is probably the best positive ion source for mass spectroscopic analysis of solids. This source was first employed for this purpose by A. J. Dempster in 1935 [1]. He eventually demonstrated that the sensitivity of this technique was at least as high as one part per million. His work clearly suggested the potential usefulness of the method without, however, firmly establishing its broad scope.

Gorman, Jones and Hipple [2] promoted the usefulness of the vacuum spark as a positive ion source for general analytical work by verifying the composition of a series of stainless steel standard samples. Using electrical recording they determined concentrations as low as 0.25% with a high degree of accuracy and precision.

Several years ago N. B. Hannay [3] designed and built a mass spectrograph for the detection of low concentrations of impurities in solids. On the basis of the experience of Dempster and Gorman et al., he chose the vacuum spark as the most suitable ion source for general analytical purposes.

This source employs a high frequency voltage between two closely spaced electrodes of the sample to form the spark. This ion source enjoys several advantages over other ion sources such as the vaporization electron bombardment and the thermal ionization sources. Not only can it be used for all elements, but with it all elements are detected with about the same sensitivity, as will be shown later. This ion source is relatively free from the serious problem of contamination. However, since the ions from the spark source are very inhomogeneous in energy, it can be used only with a double focusing instrument wherein both direction and velocity focusing is provided. Moreover, the ion current from a vacuum spark fluctuates seriously. This disadvantage is most easily circumvented by employing photographic detection.

For these reasons Hannay chose the Mattauch geometry [4] double focusing design [5] with which ions of all masses are simultaneously in focus on a given plane.

INSTRUMENTAL DETAILS

This Mattauch geometry double focusing design is sketched in Figure 1. Positive ions from the vacuum spark are accelerated by an applied voltage of ten to twenty KV. The ions from the spark are limited by a series of apertures to a beam of an appropriately small angular divergence. This inhomogeneous beam of ions passes into the electric analyzer with $\Phi_e = 31°50'$. Here velocity dispersion takes place and appropriate apertures limit the emergent beam to an appropriately small energy band of singly charged ions and integral multiples of this band for multiply charged ions. Figure 1 sketches two emergent ion beams corresponding to the upper and lower end of this energy band. The 90° sector magnetic field just compensates for this dispersion in energy and at the same time provides mass separation.

Figure 2 shows a plan view of the Bell Telephone Laboratory mass spectrograph. The commercial instruments now on the market are basically like Figure 2. They use a vacuum spark ion source; they employ the Mattauch geometry double focusing and at present use principally photographic detection.

Some typical mass spectra are reproduced in Figure 3. Here a mass range of about 15 to 1 can be covered in a single exposure and the particular range desired can be obtained by an appropriate setting of the magnetic field. Mass spectra of a high

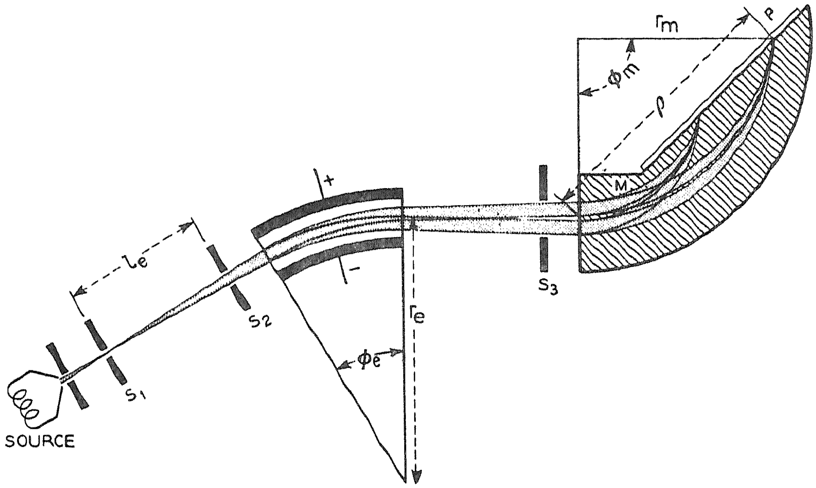

Figure 1. Double focusing [10] in a Mattauch geometry mass spectrograph.

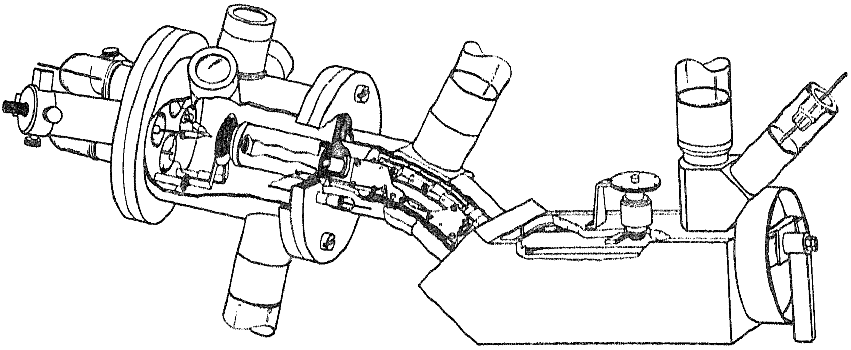

Figure 2. Plan view of Bell Telephone Laboratory Mattauch geometry double focusing mass spectrograph [3].

purity lead sample, a high purity germanium sample containing six parts per million of added antimony and an antimony sample containing one hundred parts per million of arsenic are shown.

CALIBRATION, SENSITIVITY AND RESOLUTION

Figure 4 presents [7] a calibration and sensitivity determination for the instrument shown in Figure 2. A series of high purity silicon crystals that contained varying amounts of added boron served as standard samples. The concentration of the boron was derived from electrical measurements on these semiconductors. Similar data with standard samples of germanium doped with antimony [7] demonstrate that (a) this impurity concentration determination is directly proportional to the known impurity

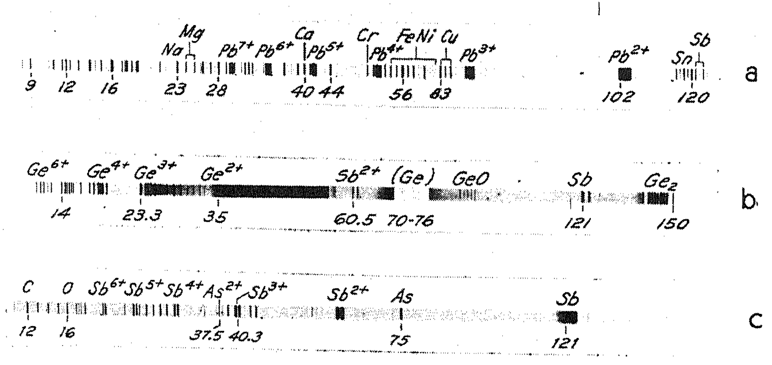

Figure 3. Typical Mass Spectra [14]. (a) "High purity" lead, (b) germanium with 6 ppm added antimony, (c) antimony containing 100 ppm arsenic.

concentration over several decades and (b) impurity concentrations below 100 parts per billion (ppb) are detectible by this technique, (c) an impurity concentration can be determined to within a factor of two. Elliott [5] (et al.) in recent work reports that concentration measurements can be made with an accuracy of the order of 20% provided suitable calibration standards are used.

The scattering of residual gas atoms by the ions enroute through the instrument produces a diffuse darkening of the photographic plate that may be the most important factor limiting the sensitivity of this type of analytical instrument. Table 1 presents data by Brown [8] et al. on the detection sensitivity for a large number of elements in gallium phosphide. Similar data by Perkins [9] et al. indicate that these values are typical for today's commercial instruments. This improvement in detection sensitivity down to a few ppb or even less is probably largely the result of less ion scattering because of better vacuum conditions achieved.

High mass resolution is extremely desirable in this type of solids analysis. Background lines such as carbon, nitrogen, oxygen etc., hinder the detection of other elements having the same nominal mass unless sufficient resolution is available to separate such mass lines. The detection of silicon against the background lines of the nitrogen molecular ion or of carbon monoxide and the detection of sulfur against the oxygen background line are typical cases in point. High resolution is also needed when the impurity element has the same nominal mass as that of an ion of a major component as for instance, the case of aluminum in iron. The theoretical resolving power of the Mattauch double focusing geometry is

$$\frac{m}{\Delta m} = \frac{r_e}{C S_1}$$

where Δm is the minimum mass difference that can be resolved, C is the number of mass line widths used as the criterion to define resolution and S_1 and r_e are as designated in Figure 1.

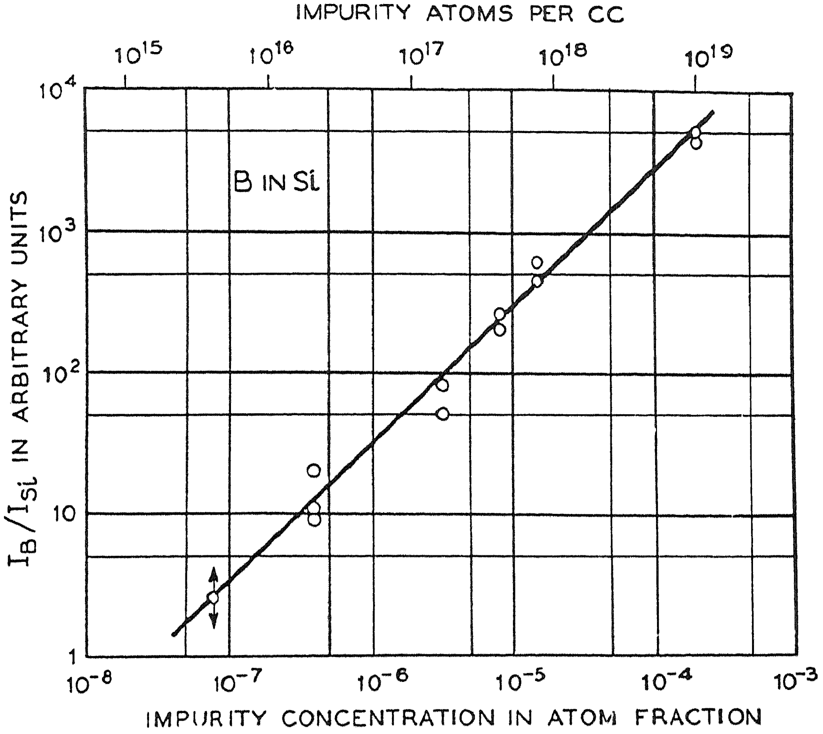

Figure 4. Boron in Silicon Determination [7].

The microphotometer tracing in Figure 5 obtained by Robinson et al. [17] with $S_1 = 2 \times 10^{-3}$ inches and $r_e = 25$ inches shows the mass line separation achieved between the zirconium molecule and the hafnium atom where the mass difference is 1 in 1310. This tracing indicates that mass differences substantially smaller than 1 in 1300 should be resolvable.

This mass spectrographic technique already is being used for a wide variety of analytical problems some of which are fairly straightforward and others of which require special techniques. These typical problems will be outlined in the succeeding sections.

ANALYSIS OF METALS AND SEMICONDUCTORS

The analysis of metals and semiconductors requires no special technique. A wide variety of these materials have been

Table 1

Tungsten

Impurity	Concentration		
	Original Material		Zone Melted
	IV A		IV B
	Emission Spectroscopy	Mass Spectroscopy	Mass Spectroscopy
Iron	< 50 ppm	10-100 ppm	0.1-1 ppm
Nickel	< 50	10-100	0.1-1
Molybdenum	N.D.*	10-100	1-10
Chromium	< 50	1-10	0.1-1
Potassium	No test	10-100	1-10
Calcium	< 50	10-100	0.1-1
Germanium	N.D.*	10-100	1-10
Cobalt	N.D.*	1-10	1-10
Silicon	< 10	10-100	1-10
Aluminum	N.D.*	0.1-1	0.1-1
Magnesium	< 10	1-10	0.1-1
Titanium	N.D.*	No test	No test

*Not detected.

studied and apparently any metal or semiconductor can be so analyzed. Table 1 shows the results of such an analysis of tungsten [11] before and after zone melting in vacuum along with emission spectroscopic data. The zone melted sample was taken from the starting end of a single pass zone melted sample. The mass spectrographic data shows that a marked improvement in purity is achieved in tungsten by zone melting in vacuum.

ANALYSIS OF INSULATORS

The analysis of solid insulators was first [7] undertaken with the aid of two short metal tubes that were completely filled with the insulator after the latter had been ground up into a powder. The mass spectrum of the insulator along with that of the metal was recorded when a vacuum spark between the tube ends was formed. The spectrum of the insulator could be isolated from that of the metal by suitable control tests.

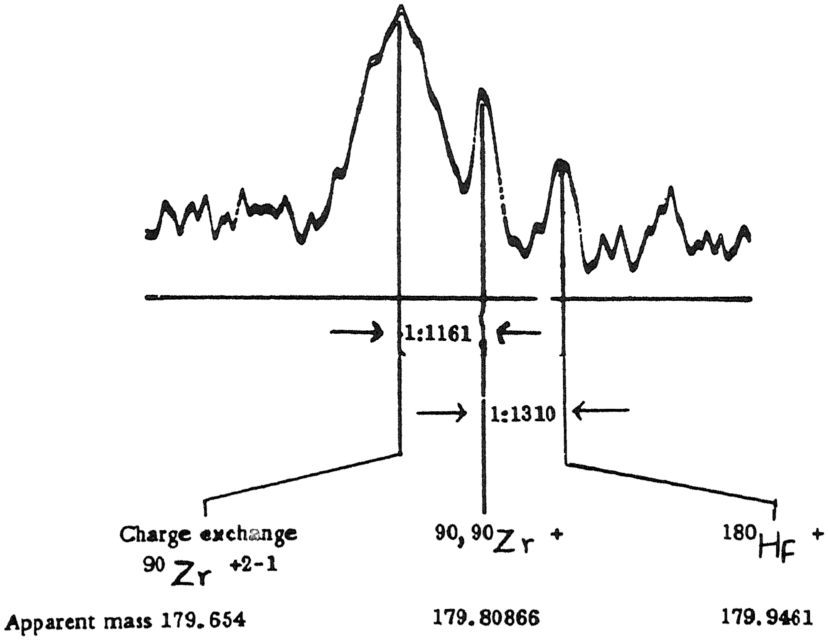

Figure 5. Microphotometer tracing of triplet in mass spectrum of zircalloy [17].

This method of analyzing powdered insulator has three limitations: a) the danger of contamination of the sample during the powdering process is great in cases where the sample must be ground up, b) surface contamination cannot be distinguished from bulk impurities, and c) the contribution of the powder to the spark, and therefore to the spectrum, is erratic—it varies appreciably with time. This limitation means that the sensitivity with which trace impurities in the powder are detected would vary erratically.

The above limitations inherent in this powder technique for analyzing insulators led to the methods [12] sketched in Figure 6. When the conductor electrode is brought near the insulator with the usual spark voltage applied a vacuum spark between the two is produced. Its mass spectrum is a mixture of the conductor and the insulator. By means of the electrode positioners, a spark can also be formed between the two conductor electrodes in order to obtain the spectrum of the conductor alone along with the background characteristic of the instrument. The difference between these spectra yields the spectrum of the insulator.

The presence of impurities in the conductor would hinder the detection of the same impurities in the insulator. Therefore a metal whose impurity content is too low in concentration to be detected should if possible be used. For this reason the

Table 2

Detection Limits of Impurities in Gallium Phosphide[8]
(ppm atomic)

Element	Detection Limit	Element	Detection Limit	Element	Detection Limit
Uranium	0.001	Neodymium	0.008	Arsenic	0.01
Thorium	0.001	Praseodymium	0.001	Germanium	0.03
Bismuth	0.001	Cerium	0.01	Zinc	0.006
Lead	0.002	Lanthanum	0.003	Copper	0.005
Thallium	0.005	Barium	0.2	Nickel	0.005
Mercury	0.003	Cesium	0.01	Cobalt	0.003
Gold	0.001	Iodine	0.01	Iron	0.003
Platinum	0.003	Tellurium	0.03	Manganese	0.003
Iridium	0.002	Antimony	0.002	Chromium	0.01
Osmium	0.002	Tin	0.003	Vanadium	0.01
Rhenium	0.002	Indium	0.001	Titanium	0.01
Tungsten	0.003	Cadmium	0.003	Scandium	0.01
Tantalum	0.001	Silver	0.002	Calcium	0.01
Hafnium	0.003	Palladium	0.004	Potassium	0.01
Lutecium	0.001	Rhodium	0.001	Chlorine	0.01
Ytterbium	0.003	Ruthenium	0.005	Sulphur	0.03
Thulium	0.001	Molybdenum	0.004	Silicon	0.03
Erbium	0.003	Niobium	0.3	Aluminum	0.003
Holmium	0.001	Zirconium	0.006	Magnesium	0.003
Dysprosium	0.004	Yttrium	0.001	Sodium	3
Terbium	0.001	Strontium	0.001	Fluorine	0.003
Gadolinium	0.004	Rubidium	0.05	Boron	0.001
Europium	0.002	Bromine	0.02	Beryllium	0.001
Samarium	0.004	Selenium	0.02	Lithium	0.003

conductor electrodes were cut from high-resistivity silicon semiconductor in which the impurity concentration was too low to detect.

Figure 7 presents photographs of typical mass spectra obtained for steatite using the geometry of Figure 6a. The Figure

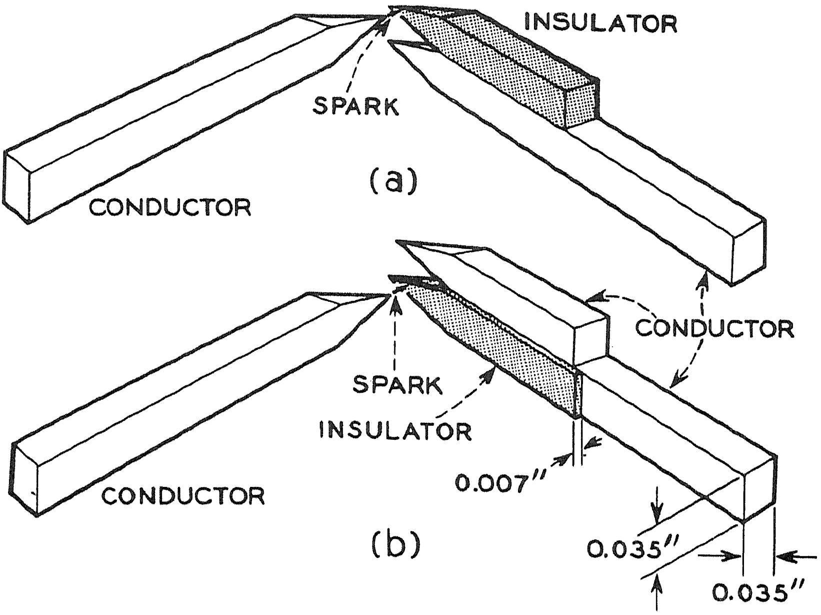

Figure 6. Electrodes for vacuum spark positive ion source for mass spectrographic studies of insulators [12].

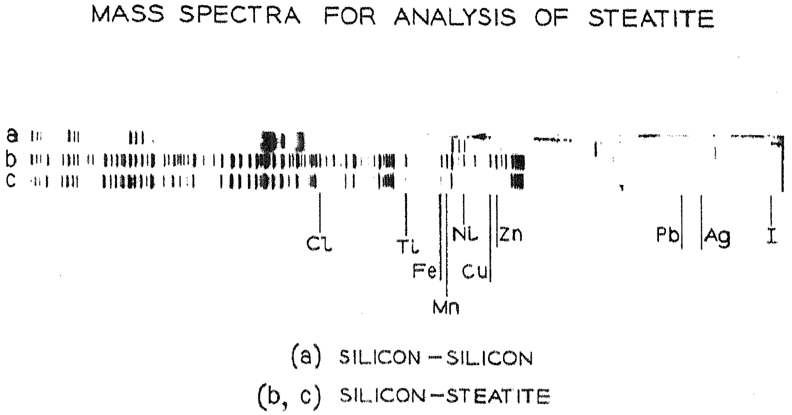

Figure 7. Mass spectra for analysis of steatite [12]. (a) Vacuum spark between silicon electrodes, (b) initial vacuum spark between silicon and steatite, (c) subsequent vacuum spark between silicon and steatite.

7a spectrum was obtained from the spark between the two high-purity silicon electrodes. Only silicon mass lines and the usual background lines of carbon, nitrogen, oxygen, etc. appear in this spectrum. The (b) spectrum was recorded when the spark was first passed between the steatite and the silicon. The (c) spectrum was recorded immediately after the (b) one. In all three, the total number of ions to the photographic plate was the same.

The major components of this particular steatite were barium oxide (16%), magnesium oxide (26%) silicon oxide (40%), and aluminum oxide (8%). The sum of all other components was less than 1% of the mixture.

The seven isotopes of barium with positive charges ranging up to seven electronic units, along with similar multiply charged ions of the aluminum and the three isotopes of silicon, magnesium, and oxygen, account for most but not all of the many lines in the (b) spectrum. The remaining lines of the (b) spectrum reveal the presence of iodine, silver, lead, zinc, copper, nickel, manganese, iron, titanium, chlorine, sodium, potassium, calcium and strontium.

The spectra of Figure 7 were part of a study of the efficiency of different chemical treatments in cleaning steatite that had been heavily contaminated with perspiration. Before the (b) spectrum was recorded, the steatite had been treated successively in petroleum ether, ammonium hydroxide, distilled water and ethyl alcohol.

In the absence of standard samples of steatite containing impurities at known concentrations, the sensitivity for the detection of bulk impurities remains unknown. However since the contribution of the insulator to the spectrum is large, the sensitivity is probably comparable to that for semiconductors where impurities at concentrations below 10^{-7} atom fraction are detected.

Figure 6b sketches the geometry used in the analysis of a natural crystal of Brazilian quartz. Impurities in this quartz revealed by the mass spectra recorded included phosphorus, sulfur, magnesium, aluminum, iron, fluorine, nickel, calcium and copper.

In the analysis of insulators, the vacuum spark source used by James and Williams [13] employed auxiliary conducting electrodes each of which had a piece of the insulator sample in contact with its sparked end. This method has been used in analyzing synthetic silica and fused quartz. James and Williams [13] also report preliminary examination of unknown powder samples such as hard metal powders. Here they use carbon as the conducting electrode since its surface is sufficiently rough for some of the powdered sample to adhere. Quite satisfactory spectra of lithium fluoride, etc., have been obtained in this way.

SURFACE CONTAMINATION

The vacuum spark source enables the mass spectrograph to distinguish between bulk impurities homogeneously distributed through the sample and those impurities that are present largely as contamination on the surface of the sample electrode. This differentiation arises since the vacuum spark first samples the surface of the electrodes before it consumes the interior of the sample. Consequently, impurity mass lines due to surface contamination decay in intensity as the spark erodes into the electrode, whereas bulk impurity mass lines do not decrease.

This is illustrated in Figure 8. Three successive photographs [14] of the mass spectrum from nickel electrodes were made. The photographic plate received the same number of ions from the spark in each case. A, B, and C are density records of the aluminum doubly charged ion mass line obtained, A being that from the initial sparking of the electrodes. These data indicate that the aluminum is present in the nickel as a bulk impurity

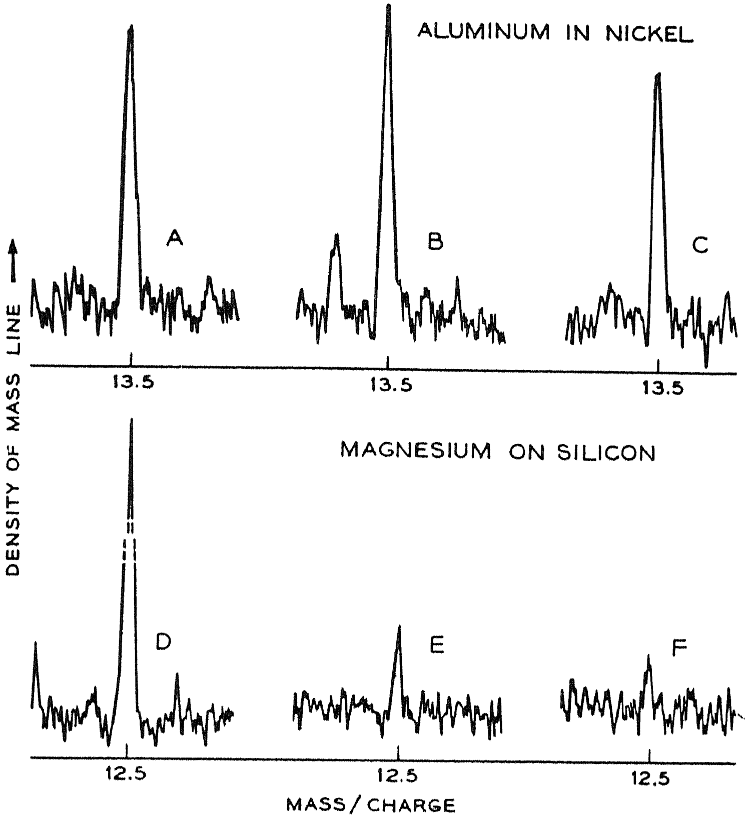

Figure 8. Microphotometer tracings of mass line of bulk impurity versus surface contaminant [16].

A,B,C: Aluminum as bulk impurity in nickel. Mass line 13.5 (Al^{2+}) in successive spectra.

D,E,F: Magnesium as surface contaminant on silicon. Mass line 12.5 (Mg^{2+}) in successive spectra.

since the density (A) of the aluminum line during the initial sparking of the nickel electrodes is no greater than that subsequently obtained (B and C).

In Figure 8, D, E, and F are density records of a magnesium doubly charged ion mass line that appeared in the spectrum of silicon. This data indicates that the magnesium is present as a surface contaminant on the silicon since the density of the magnesium line during the initial sparking (D) of the silicon electrodes is about 10 times greater than that subsequently obtained (E), which in turn is greater than (F).

In the early work with this instrument, with the use of a pair of pointed electrodes, surface contaminants were detected and identified when they were equivalent to 0.1 monolayer. The film thickness that can be detected by this means clearly is determined by the surface area that the vacuum spark explores. Figure 9 illustrates a simple way to increase the area scanned by the spark. The pair of pointed electrodes referred to above and ordinarily used for bulk impurity studies was replaced by one pointed and one wedge shaped electrode. The electrode positioners enable the operator to move the pointed electrode along the entire two mm. width of this wedge.

By evaporation in vacuum, a single monolayer of indium was deposited on such a pair of point-wedge electrodes of germanium. Figure 10 presents the microphotometer tracing of the mass lines for the two isotopes of indium from the spectrum photographed during the initial sparking of the electrodes.

Since the mass 113 indium isotope is 4% abundant, the mass 113 line is the response* from the equivalent of 0.04 monolayer of indium.

In Figure 7 many of the lines not assignable to steatite are stronger in the (b) spectrum than in the succeeding (c) spectrum. This indicates that the chlorine, titanium, iron, manganese, nickel, copper, zinc, lead, silver and iodine are present as surface contaminants on the steatite.

This technique for detecting and identifying surface contaminants was also employed to detect and identify boron from a borosilicate glass [16] vacuum system as the acceptor in deleterious p layers grown on vacuum heated silicon.

ANALYSIS OF LIQUIDS

This surface contamination sensing ability of the vacuum spark has been employed to study trace impurities in liquids.

---

*The density ratio of the two indium lines does not reflect the true abundance ratio because the mass 115 line is overexposed.

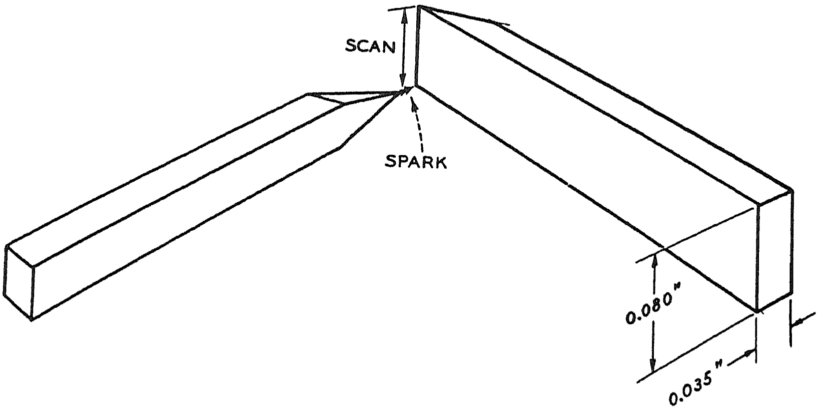

Figure 9. Electrodes for surface contamination [16] studies in which area explored by spark is increased by manual scanning.

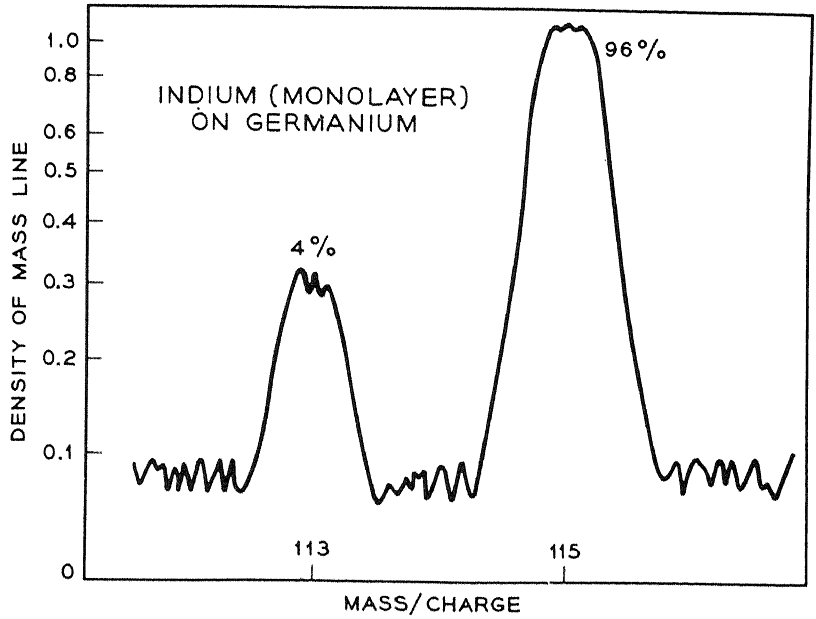

Figure 10. Microphotometer tracings of indium mass lines from one monatomic layer [16] deposited on germanium surface.

This is done by exposing a suitable surface to the liquid and its impurities in one of a number of ways. It is best done with high purity electrode material the surface of which is initially clean. Control tests justify the assignment of detected surface contamination to the liquid in question.

Experiments reported elsewhere [14] were made in which electrode surfaces were contaminated merely by dipping into a sodium hydroxide solution. Surface contaminants subsequently detected and identified included boron, sulfur, sodium, magnesium, aluminum, copper, zinc, nickel, iron, chromium, calcium and chlorine.

Other experiments [16] demonstrated that impurities in low conductivity water could be detected by contamination of suitable electrodes by an electroplating technique.

These experiments suggested that impurities at very low concentrations might be detected if a mass of liquid was deposited on an electrode surface and allowed to evaporate. The impurities in the liquid would be left contaminating the surface provided the liquid evaporated more rapidly than the impurities. Such experiments with pure water [16] subsequently doped with specific impurities at known concentrations have been made. Since the spark can sample only the tips of electrodes such as those shown in Figure 9, this is where the residue from the evaporation must be deposited in order to be subsequently detected. But drops of water placed on the tips of these electrodes would spread out over the surface and most of the residue would be inaccessible to the spark.

This difficulty was circumvented by means of specially shaped electrodes shown in the photograph in Figure 11. Originally this electrode was square in cross section throughout its length, this cross section being about 1 mm ^{2}. Over a length of several millimeters, this cross section was decreased as shown but at the extreme tip it flared out to the original dimensions.

If the mass of a drop of water is the maximum that the tip can support, the drop will hang from the tip. Larger ones fall off, and smaller ones creep up the electrode. However by applying the electric field indicated in Figure 11, these smaller drops can be pulled down toward the tip. With the flared end the integrated contact force increases as the drop is pulled down. Consequently by increasing the field the drop can be pulled well down to the tip without pulling it off. As the evaporation proceeds the remaining drop can be held at the tip by appropriately increasing the electric field, the needed value of which may reach several kilovolts per centimeter.

This localization of a water drop is illustrated by the photographs of Figure 12. In (A) with zero electric field the drop, being less than the critical mass, has crept up the electrode. By applying an appropriate electric field it was pulled down to the tip as shown in (B). (C), (D), (E), and (F) show the remaining drop held in position by progressive increase in the voltage as the water evaporated.

A deionized water sample was doped simultaneously with beryllium, sulfur, chromium, copper, arsenic, silver and lead. One drop of this multiply doped water was dried on an electrode as shown in Figure 12. All were detected in the mass spectrum subsequently recorded. Table 3 lists the concentration of a specific isotope of each of these doped impurities along with the density of the corresponding mass line used for detection of this impurity. The density of the doubly charged mass line of lead suggests that the singly charged ion would be detected at about 1 x 10^{-9} atom fraction if the latter were recorded. Similarly the density of the sulfur triply charged line suggests that if the singly charged line were resolved from the oxygen background line it

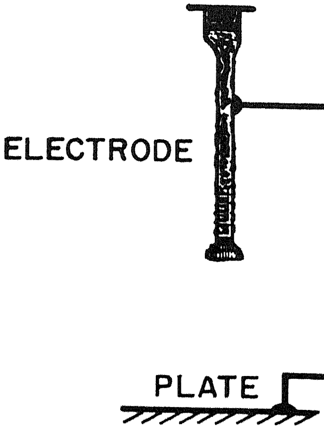

Figure 11. Electrode tip on which water drop can be confined by electric field [16].

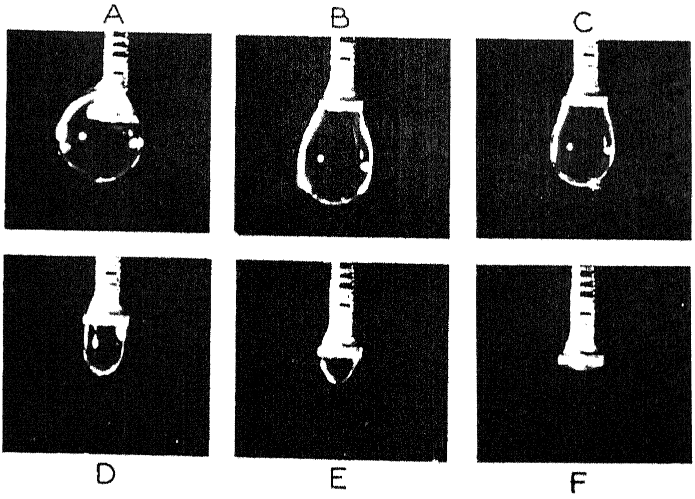

Figure 12. Evaporation of water drop confined to electrode tip by electric field [16].

too could be detected at about 1 x 10^{-9} atom fraction. Thus the data of Table 3 indicates that impurities in water can be detected at or below concentrations of 10^{-9}.

Table 3

Mass Spectrographic Detection of Impurities Introduced into Deionized Water[16]

Impurity	Isotope	Mass Line m/e	Density of Mass Line	Concentration, Atom Fraction
Beryllium	9	9	0.44	1.1×10^{-9}
Chromium	53	53	0.12	1.0×10^{-9}
Copper	65	65	0.06	0.9×10^{-9}
Arsenic	75	75	0.33	1.0×10^{-9}
Silver	107	107	< 0.02	1.2×10^{-9}
Lead	207	103.5	0.04	5.8×10^{-9}
Sulfur	32	10.67	0.11	22.0×10^{-9}

The single drop of water about 3 mm in diameter that was used contained about 10^{-11} gm of beryllium and 10^{-10} gm of silver. These small quantities needed for detection by this mass spectrographic technique compare favorably with the quantity of about 10^{-7} gm needed by spectrophotometric methods at optimum sensitivity.

This method of detecting impurities is not limited to the case of water but should be applicable to any liquid that evaporates more rapidly than do the impurities in solution in the liquid. The analysis of body fluids, the detection of nuclear fragmentation by-products in water, the identification of inorganic impurities in air by dissolving in a suitable solvent are examples that indicate the wide range of studies to which this technique should be applicable.

ANALYSIS OF LIQUID GALLIUM

When a clean electrode of high purity silicon is dipped into liquid gallium, a little of the latter adheres to the end of the electrode by wetting it. When a vacuum spark is formed between two such gallium tipped silicon electrodes, gallium and silicon are major constituents in the mass spectrum recorded. This use of silicon electrodes precludes the detection of silicon as an impurity in the gallium. This limitation can be circumvented by using high purity germanium electrodes. In this case it is necessary to use supersonic agitation of the electrode to get the gallium to wet the germanium.

Using high purity silicon electrodes, mass spectra of a gallium sample from the tail end and from the seed end of a supply of zone refined gallium were recorded. Figure 13 displaying mass line densities shows the principal differences that appeared. Sulfur, boron, aluminum, magnesium, phosphorus, chlorine, potassium and calcium appeared in the tail end but were either not detected or were substantially weaker in the seed end sample of this zone refined gallium. In addition to these elements, copper, iron, lead, zinc, indium and tin were detected in each sample at about the same concentration indicating that little or no segregation of these elements was achieved in gallium.

Brown [8] et al. have analyzed gallium by supporting it on the end of high purity graphite electrodes.

ANALYSIS OF MICROSAMPLES

Sometimes the total amount of sample available for analysis is so small that conventional methods of analysis even for major components becomes difficult or even impossible. The higher sensitivity available in this mass spectrographic technique fills an important gap in the analysis of such "microsamples."

Figure 14 shows a short (0.10 inch) piece of 0.001 inch diameter gold wire mounted on a heavier support post. The composition of the free end of the gold wire was needed—particularly regarding III and/or V elements in the periodic table. Because this fine wire was so flexible and because it was difficult to see their relative positions it was not possible to form a satisfactory spark between the ends of such wires; the necessary control could not be achieved and they fused together as soon as the spark was started. This difficulty was circumvented by forming the spark between one gold wire and a large cross section high purity silicon electrode as shown in Figure 14. Boron, aluminum and gallium were detected. The concentrations ranged from 10 to 1000 ppm.

Small crystals of diodes or other semiconductor devices could not be analyzed satisfactorily "in situ" because the spark could not be completely confined to the crystal. This limitation was avoided by removing the minute crystal in question and mounting it in a suitable holder. In addition to certain limitations of size and geometry imposed by the instrument itself, this holder must be of sufficiently pure material so that the detected impurities can be unambiguously assigned to the crystal itself.

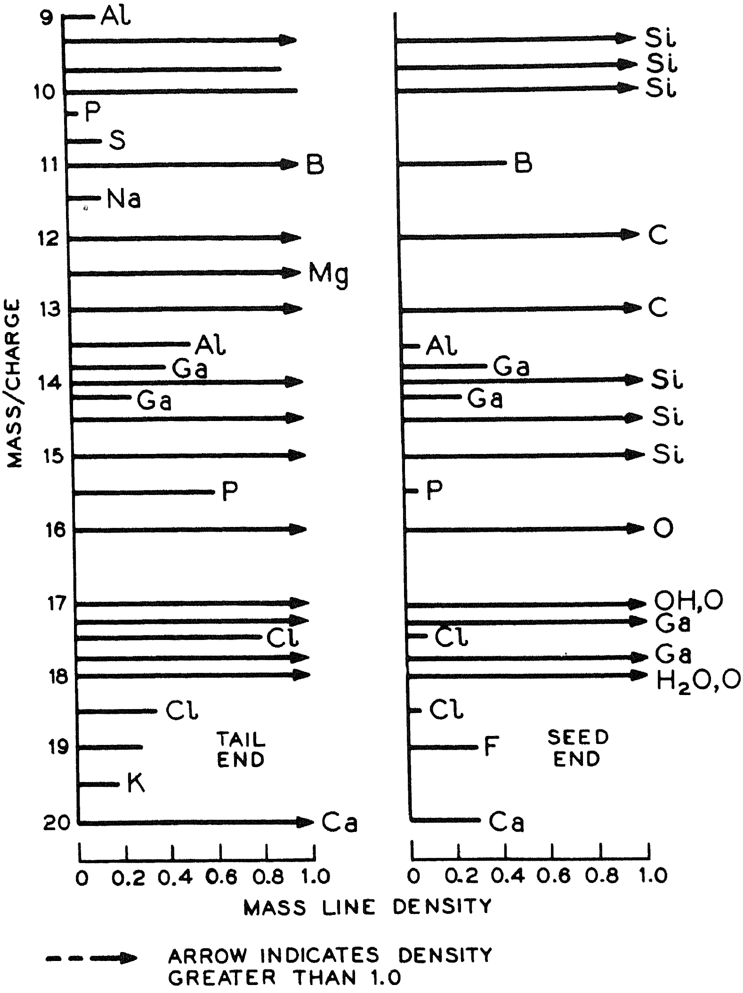

Figure 13. Comparison of mass spectra of zone refined gallium.

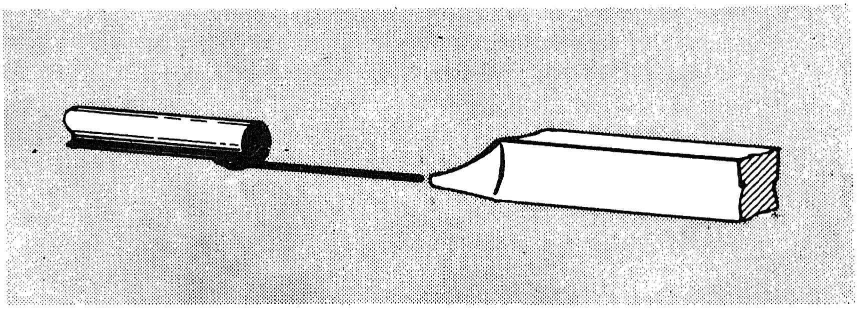

Figure 14. Electrodes for vacuum spark to fine wire.

Figure 15 contains photographs showing two views of a holder meeting these requirements. Since the crystal it holds is silicon, the holder is made of high purity silicon. The two pieces comprising the holder and the crystal are held together in position by platinum wire. The unit is mounted in the standard pin vise ordinarily used to hold an electrode of a sample like those of Figure 6.

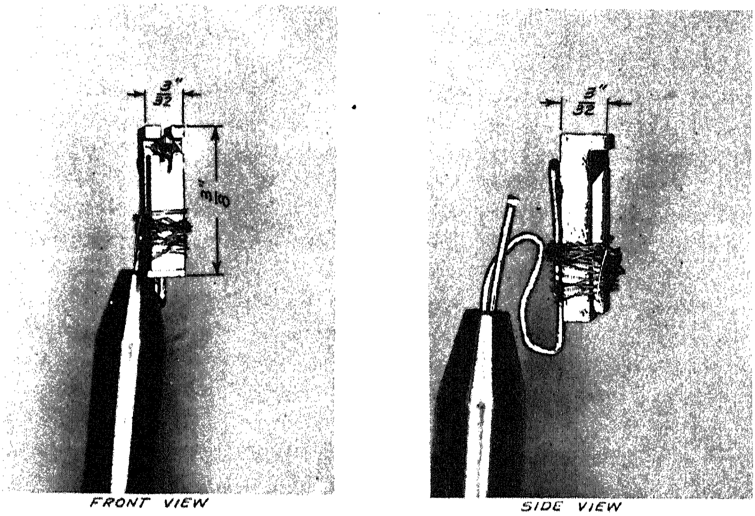

FRONT VIEW SIDE VIEW

Figure 15. Silicon holder for vacuum spark to small sample.

The mass spectrum of the crystal is obtained by running a vacuum spark between it and a high purity electrode of the same element—silicon in this case. For the analysis of a germanium crystal a holder and second electrode of high purity germanium would be used.

For some materials, it might not be feasible to make the holder and second electrode of the same material as the sample. This difficulty could be circumvented by two analyses, one with silicon holder and second electrode followed by one with a germanium holder, etc. The first would test for all elements but silicon and the second would test for all but germanium.

Donor and/or acceptor impurities detected in silicon crystals from a number of semiconductor devices included boron, arsenic, aluminum, gallium, antimony and indium in concentrations ranging from 1 to 1000 ppm.

The sample holder of Figure 15 is not limited to holding square or rectangular shaped samples. It could be used to hold a wide variety of irregularly shaped small samples.

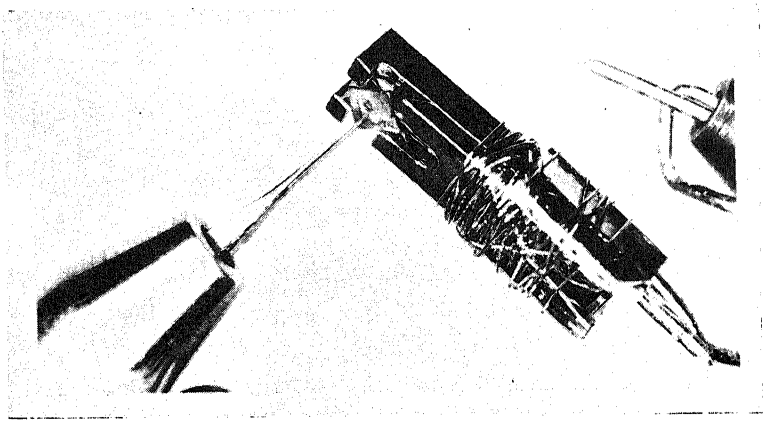

Figure 16. Pointed electrode for confining vacuum spark to specific area sample.

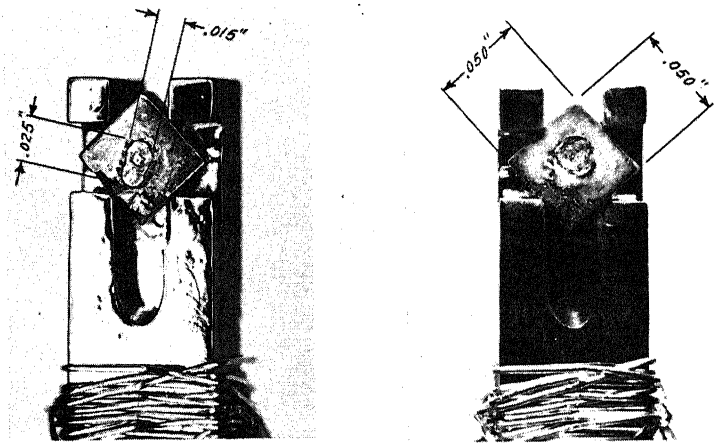

BEFORE AFTER

Figure 17. Photographs showing area of sample explored by spark using pointed electrode.

Brown [8] et al. have analyzed small samples by inserting them into a split electrode of high purity graphite. Using this technique they have successfully analyzed a single radar diode which weighed only two milligrams, showing the doping element and its approximate concentration. They have also examined individual crystals of cadmium sulfide for photocells by this technique.

Sometimes even with small samples of Figure 15, the region of interest comprises only a fraction of the crystal. In this instance it is very desirable to localize the spark as much as possible. For this purpose a second electrode needle—like in shape as shown in Figure 16 has been used. The photographs of Figure 17 illustrate the degree with which the spark can be localized by this simple technique.

Donor and acceptor impurities in silicon detected by this technique consisted of boron, aluminum, gallium and arsenic in concentrations ranging from 1 to 100 ppm. Gold, silver and copper were also detected in concentrations ranging from 1 to 1000 ppm.

CONCLUSIONS

The Mattauch geometry double focusing mass spectrograph with the vacuum spark positive ion source is proving to be quite a versatile instrument for analytical studies. This technique complements that of emission spectroscopy by extending this general analytical capability to lower impurity concentrations.

Now that satisfactory techniques are at hand for testing almost any insulator, this instrument can test for most impurities in almost any solid of a wide variety of sizes and shapes.

Since the vacuum spark initially samples the surface of a solid, surface contaminants can be distinguished from bulk impurities. This surface sensing ability has added greatly to the usefulness of the instrument. Not only has it been used to study surface contamination per se, but this surface sensing ability can be employed to study liquids. Here the surface of a suitable solid is deliberately contaminated with the liquid after which the resulting surface impurities are picked up in the mass spectrum recorded.

The techniques now available for handling and analyzing microsamples opens up yet another field where the high sensitivity of this mass spectrographic method can be profitably used.

REFERENCES

1. A. J. Dempster, Proc. Am. Phil. Soc., 75, 755, (1935); A. J. Dempster, AEC Paper MDDC - 370, (1946).
2. J. G. Gorman, E. J. Jones, and J. A. Hipple, Anal. Chem., 23, 438, 1951; J. A. Hipple and J. G. Gorman, ASTM Special Technical Publication No. 149, (1943).
3. N. B. Hannay, Rev. Sci. Instr., 25, 644, (1954).
4. R. Herzog, Z. Physik., 89, 447, (1934); J. Mattauch and R. Herzog, Z. Physik., 89, 786, (1934); J. Mattauch, Phys. Rev., 50, 617, (1936).
5. R. M. Elliott, R. D. Craig, G. A. Errock, Proceedings of Fifth International Instruments and Measurements Conference, Sept. 13-16, 1960, Stockholm, Sweden.

6. A. E. Shaw and W. Rall (Rev. Sci. Instr., 18, 278, (1947) described a Mattauch geometry double focusing instrument but no results were reported.
7. N. B. Hannay and A. J. Ahearn, Anal. Chem., 26, 1056, (1954).
8. R. Brown, R. D. Craig, J. A. James, and C. M. Wilson, Conference on Ultrapurification of Semiconductor Materials, Boston, April 1961.
9. G. D. Perkins, C. F. Robinson and R. K. Willardson (private communication).
10. N. B. Hannay, Science 134, 1220, (1961).
11. E. Buehler, Transactions of the Metallurgical Society of AIME, 212, 5, 694, (1958).
12. A. J. Ahearn, J. Appl. Phys., 32, 1195, (1961).
13. J. A. James, and J. L. Williams, Advances in Mass Spectrometry edited by J. D. Waldron (Pergamon Press, New York, 1959).
14. A. J. Ahearn, Sixth National Symposium on Vacuum Technology, Transactions Pergamon Press, New York, 1960.
15. F. G. Allen, T. M. Buck, and J. T. Law, J. Appl. Phys., 31, 979, (1960).
16. A. J. Ahearn, J. Appl. Phys., 32, 1197, (1961).
17. C. F. Robinson, G. D. Perkins, and N. W. Bell, Eastern Analytical Symposium, New York City, Nov. 5, 1959.

THE TEACHING OF SPECTROSCOPY

A. C. Menzies
Hilger & Watts Ltd.
London, England

This is a very wide subject, and unless some limits are set to it the article would become so diffuse as to be worthless. I have therefore considered particularly the education of operators, the technicians on whose findings the scientists may have to rely. Much of what I write will have a wider application than this. In this first paper in our discussion, it is permissible and necessary to make some definitions. First, spectroscopist. The derivation is helpful, and I find less well known than it deserves to be. The "spectro" part is obvious, but the "scopist" part is derived from a verb used by the Greeks in philosophy, to mean *apprehend* rather than to see visually—i.e., to see with the mind. Thus, *spectroscopist* should mean one who studies and understands the spectrum.

Next I consider the types one has to educate, depending upon their respective duties. A spectroscopic team consists of

(a) a leading scientist
(b) assistant scientist(s)
(c) technicians.

(a) and (b) will have had a university education or its equivalent, some may have commenced as technicians. (c) may be at any lower stage of experience: they may have just started, or may have worked as such for some years, and attended technical college classes in the evenings or by some form of day release.

Later in the discussion my colleagues will be talking about the education of (a) and (b). I will speak about (c), whom I believe to be the more difficult type to educate—if a man is suitable for university training as a scientist, he is easier material with which to deal than the man who is less gifted but must be trained to employ complicated equipment.

Technicians

Lord Cherwell, speaking of the trained technician, distinguished him thus from the technologist:-

"The word 'technician' is used to mean a man who has been trained to carry out established techniques which may be complex, and require a high degree of skill, or to work in a prescribed field under instruction; whereas by a 'technologist' is meant a man, who, as a result of broadly based studies and wide practical experience, has acquired a real understanding of scientific principles and can apply them to the development of industrial processes in diverse fields. It may sometimes be difficult to draw a sharp line of demarcation between the technician on the one hand and the scientist or the technologist on the other."

The Supply and the Intelligence Level

We have to share in the national supply of technician material, and this fixes the level of intelligence possessed by recruits.

J. F. Coales [1] has discussed this supply in connection with education for automation, and has concluded that for the supply of technicians we must depend on an I. Q. down to 107—only slightly above the average. The range of I. Q. for the university population, which supplies the scientists, begins approximately at 120, and has the largest number around 125. Our supply of technicians is sufficient, if we can devise training methods for them bearing in mind the relatively low I. Q.

How Are We to Select Recruits?

The personal qualities which appeal to me are

(a) Conscientiousness.
(b) Interest in little things.
(c) Enthusiasm for this job.

(a) is of first importance since consistency is all-important for securing accurate results. G. Carlsson of Stockholm said that he made analyses of steel photographically with 1% coefficient of variation, only if he performed all the steps—including sample preparation—himself. The chief scientist of a steelworks in the Ruhr told me that slag analyses made in his laboratory with x-ray fluorescence were excellent if he watched the sample preparation or did it himself.

(b) is common to all successful scientists and technicians—Sir Francis Bacon wrote:-

> "Rare and notable things cannot be understood, much less new things brought to light, unless the sense of common things and their causes be duly examined and brought out."

An interest in little things usually indicates good powers of observation.

(c) is meant to connote an enthusiasm for working with instruments—not just enthusiasm for the higher pay which may go with the job.

Training the Recruit

This recruit—what is he like? Possibly a young man 17 years of age or more, whose acquaintance with science has been through exposure to instruction in elementary science while at school. A vacancy occurs for an operator, and he has been selected. He reports to the spectroscopy lab, where everyone is busy with their own jobs, and he has to be useful and pick things up. At first he will have the fetch and carry jobs, and be initiated first into sample preparation.

He has to be trained, but he must be useful while being trained. To reconcile these requirements, it pays to give him two kinds of training—first what might be called preliminary training, followed up more leisurely by the main training.

Preliminary Training

It is possible for operators to be successfully working with quite sophisticated instruments only days after beginning, provided nothing out of the ordinary occurs, for which greater experience or knowledge is needed.

As an example from another field, that of the manufacture of precise optical parts, consider the Twyman-Green interferometer. The university physics student knows enough to understand how it works when he has reached the second year. Girls are taught in two weeks to use it to check the perfection or otherwise of a prism or lens, and after four weeks can safely be left to deduce which are high spots and which low. They are shown how to put in the optical piece to be tested, and how to tweak gently a bar supporting the eye-lens so that the fringes move—towards the high spot. Later they can learn something about interference; the preliminary training whets the appetite and makes them almost immediately useful.

Main Training

It would be good if all our technicians could attend courses in physics and chemistry, electronics and engineering. Some will do so, who have the ability and urge to advance. It is not necessary for all to do so, and remembering the I. Q. limitation only a few should be encouraged to attend such courses.

What is needed is a special course, covering those parts of the sciences necessary for understanding the operations of applied spectroscopy. It does not need to be basic, in the sense that every statement is proved, but so that it may be apprehended, reasons must be given, and facts related to one another. This last requirement is important, because the pupil needs to remember, permanently, what he has learned, and it is easier to remember a whole system of interlocking ideas than a few haphazard unconnected ones. What we need for our technicians is a system of interlocking ideas, but their intelligence level is not high enough to give them the complete physical description of all that is relevant. This requires a book to be written, on what I call "Plausible Spectroscopy."

An example of the interlocking of ideas is the treatment of the luminosity of spectrographs and spectrometers, normally treated separately on the grounds that the former are photographic while the latter are photoelectric. Separate treatments are given, considering intensity of illumination at the photographic plate, and total flux at the exit slit, respectively. Let us see how these can be linked. In reality, both are photoelectric—the only basic difference lies in the extreme smallness of the detector residing in the photographic plate. This is so, because each grain is an isolated detector—what happens in one scarcely affects what happens in a neighbouring one. It follows that both types of instrument can be treated as photoelectric, and conclusions drawn for the spectrograph by considering the dimensions of the detector to be very small. This applies particularly to the *height* of the grain (in the direction of the slit) for in both types of instrument the slit will be narrow. To be definite, the normal consideration of the spectrometer used with a continuous source gives for the power issuing from the exit slit

$$PDs^2TAH/F \text{ watts,}$$

where P is the power radiated by each unit area of the source through unit solid angle for unit band-width,
D is the angular dispersion of the system
s is the spectral band-width
T is the transmission of the instrument
A, F are the area and focal length of the telescope lens, and
H is the height of the entrance slit.

This has been calculated for photoelectric instruments. If we make H the average diameter of the grain, it applies directly to photographic instruments, and one may deduce all the consequences for the design of a luminous spectrograph.

In the same way, this formula deduced for a continuous source, includes the result for a line source, if we make the band-width suitably narrow.

Practical Work

The technician gets practice in his work with the firm's equipment, but this is the routine upon which it is the business of technical classes to shed light. On the continent of Europe, demonstrations by the instructor are more stressed than individual practical work by the pupil. With us the reverse is true—we have a "do it yourself" mentality. Recent enquiries have suggested that both extremes are wrong, and we are being advised to introduce more demonstrations by the teacher, while the continentals are being urged to arrange more individual work.

As in all scientific practical work, each experiment should have a limited aim which must be carefully defined, and the apparatus must be chosen so that the aim can be achieved without distraction. If, for example, the experiment is on the functioning of a spectroscope, the instrument must be capable of being taken apart; but if the aim of the experiment is to apply the spectroscope to some task, it must not be in danger of falling to pieces. Put another way, subordinate parts of the apparatus should not need to be "babied"—the only difficulties should be directly connected with the main intention. I remember the great C.T.R. Wilson of cloud-chamber fame used to provide students with a sensitive galvanometer having no levelling screws—one was provided with paper of thickness varying from postcard to cigarette-paper which one tore up and inserted beneath it. The aim here was to learn to be patient!

These thoughts suggest that two kinds of apparatus are needed for the technical courses,

(a) instruments to apply to spectroscopic experiments; they need to be robust, simple and preferably cheap.

(b) apparatus capable of acting as instruments when complete, but which can easily be taken apart to study the functioning of component parts. This type should, if possible, be able to be set up in various ways, like Meccano.

Many instruments of class (a) already exist, for one may afford the cheaper instruments made by various manufacturers. Conscious effort to provide simple and cheap equipment for the purpose is being made in various countries.

There is less choice in class (b); it is interesting to recall that so long ago as 1924 William Taylor, founder of Taylor, Taylor and Hobson of Leicester, England, copyrighted a constructional kit of optics, and called it Koptor—it was made at Southbridge, Mass. by the Koptor Company. It did not become popular, being somewhat clumsy and easy to knock over.

More modern constructional kits for the teaching of optics are now produced in Sweden, Western Germany and Great Britain, and a kit for teaching spectroscopy especially is being developed in Great Britain.

REFERENCE

1. J. F. Coales, "Education for Automation," Bull. Inst. Phys. 11, 94 (1960).

INDEX

absorption spectra
  atomic spectra, *see* atomic absorption spectra
  of condensed gases in vacuum ultraviolet, 233
  of gases in vacuum ultraviolet, 230-233
  of solids in vacuum ultraviolet, 235-241
  see also X-ray absorption spectra
alkyl groups, substituent effects and, 525-526
3-amino-phthalimide, fluorescence spectra of, 616, 622
anistrophy, of paramagnetic resonance spectra, 685, 690, 696
anomalous dispersion, 567
anthracene, fluorescence spectra of, 617-622
antimony, analytical curves in flame spectroscopy, 195
  flame spectroscopy detection sensitivity, 182
  flame spectrum of, 176, 189
archeology, electron microprobe applications in, 369-371
argon, energy levels of, 64, 67, 70
  vacuum ultraviolet spectrum, 257
  wavelengths, infrared, 66, 69
aromatic molecules, 683
arsenic, analytical curves in flame spectroscopy, 195
  flame spectroscopy detection sensitivity, 182
  flame spectrum, 176, 189
astronomical spectra, interstellar absorption, 20
astrophysics, spectroscopy in, 1-35
  see also solar spectra; stellar spectra
as X NO_2 stretching vibration, 500-501
atomic absorption spectra, by flash heating, 83-90
  time-resolved, *see* time-resolved spectra
atomic absorption spectroscopy, 127-141
  apparatus for, 131-132
  applications of, 134
  cathodic sputtering in, 137
atomic absorption spectroscopy—Cont.
  comparison with emission spectroscopy, 128
  crucible furnace for, 140
  isotopic analysis in, 141
  line profiles in, 141
  oscillator strength determination in, 140
  scope and limitations of, 133
  sensitivity of detection in, 135
  of tungsten, 83-90
atomic energy levels, 60
atomic spectra, 1-4 μ
  Doppler broadening in, 168-169
  isotopic shifts in, 73-81
ATR, *see* attenuated total reflection
attenuated total reflection, infrared spectra and, 445-460
  Kramers-Kronig relations and, 456-458
  micromethod in, 458
  optical constants determination in, 453-455
  optical density and, 453
  phase shifts in, 458
  reflection accessory in, 450-451

band intensities, infrared, 510-511
  substituent effects and, 506
barium, sensitivity of detection by atomic spectra, 135
  wavelength, infrared, 59
benzene, absorption spectrum in vacuum ultraviolet, 234
benzenoid derivatives, substituent effects and, 517-523
benzophenone, electron magnetic resonance spectrum of, 703
beryllium, analytical curves in flame spectroscopy, 196
  flame spectroscopy detection sensitivity of, 182, 185
  flame spectrum of, 177-178
BF_3 complexes, 540
biological and medical applications, of electron microprobe, 371-379
biphenyl, 685
1,3-bisdiphenylene-phenyl-allyl, electron spin resonance spectra of, 712, 715-716

bismuth, analytical curves in flame spectroscopy, 195
  flame spectroscopy detection sensitivity of, 185
  flame spectrum of, 176, 190
Bleaney-Stevens formulation, 732
BO_2 spectrum, 600
Bohr magneton, 732
Boltzmann equation, 16
boron, flame spectrum of, 187
Breit-Rabi formula, 733-734
bromide band spectra, 602
bromine, energy levels of, 61
  infrared spectrum of, 570
  as solvent, 569
Buckingham-KBM plots, 573
cadmium, analytical curves in flame spectroscopy, 194
  flame spectroscopy detection sensitivity, 182-185
  flame spectrum of, 177-186
  sensitivity of detection by atomic spectra, 135
  wavelength, infrared, 60
calcium, energy levels of, 62
sensitivity of detection by atomic spectra, 135
carbon, flame spectrum of, 187
  sensitive emission lines, 225
carbon dioxide, absorption spectrum in vacuum ultraviolet, 231-232
carbon disulfide, Raman spectra intensities of, 469-473
carborundum, *see* silicon carbide
  carbonyl frequencies, 488-500
carbonyl group, donor characteristics of, 539-546
  frequency shifts and, 498
  polarity changes in, 498
cesium, flame spectrum of, 180
  sensitivity of detection by atomic spectra, 135
  wavelength, infrared, 59
CH_3 gaseous spectra, 587
charge-transfer complexes, 574
chemical bond, effect of on X-ray spectra, 307-318
chemical shifts, nuclear magnetic resonance and, 648-678, 657-659
chemiluminescence, *see* flame spectroscopy
chloride band spectra, 601
chlorine, energy levels, 61, 63
chloroform, Raman spectra intensities of, 469
chromium, flame spectrum of, 175-182
chromophores, n →π* transitions of, 528-534
comets, spectra of, 17
composite Hamiltonian, 731
contact interaction, in nuclear magnetic resonance, 666-667
contact shifts, 669-673
copper, flame spectroscopy detection sensitivity of, 182
  flame spectrum of, 175, 186
  sensitivity of detection by atomic spectra, 135
  wavelength, infrared, 59
correlation effects, in nuclear magnetic resonance, 669
coupling constants, 650
coupling systems, 732
critical angle, in attenuated total reflection, 446
crystal field effects, 696
crystals, nuclear resonance of, 648
  radiation damage in, 719, 721
C=S stretching frequency, 514-515

dative conjugation, 670
Debye-Polo-Wilson relation, 566
deuterium substitution, 696
diamagnetic moments, 648
diatomic molecular spectrum, 597-604
dibenzene-iodides, electron spin spectrum of, 711
dibromoethylene, refractive indices of, 567
dichloromethane, absolute intensities of, 567
diffraction gratings, 549
diphenylmethyl, electron magnetic resonance spectra and, 703
dipole-dipole coupling, 650
dipole-dipole interaction, 649, 688-689, 734
D.N.A., spin-lattice relaxation and, 652
donor-acceptor complexes, 539
Doppler broadening, in flames, 168-169
double modulation, 677
double nuclear resonance, 650
durene, 685
dysprosium, isotopic shifts in spectra of, 73-81

education, 791-796
  equipment for, 795
electron distribution, hydrogen couplings and, 724
electronegativity, group frequencies and, 489, 498
  infrared spectra and, 487
  Pauling, 502

electronic spectra, of gaseous free radicals, 583-595
  substituent effects of organic molecules in, 505-537
electron magnetic resonance, 681-705
electron microprobe, design of, 358
  electron back-scattering and, 358-362
  for light elements, 364-367
sample holder, 385, 393
  scanning, 357-380
  as X-ray microprobe, 394-396
electron microprobe analysis, 357-380
  analysis of radioactive materials, 383-388
    of thin films, 391-397
  applications in biology, 371-379
    in medicine, 371-379
    in metallurgy, 362-365
    in mineralogy, 367-369
  archeological applications, 369-371
electron spin resonance, 666, 707-718
  line width in, 717-718
  low-frequency to near microwave, 729-741
  in oriented radicals, 719-726
electrostatic precipitation, 579
electric quadrupole moments, 654, 725
elements, origin of, 28
emission spectra, X-ray, *see* X-ray emission spectroscopy
EMR, *see* electron magnetic resonance
Endor spectra, 725
energy levels, argon, 64, 67, 70
  calcium, 62
  chlorine, 61, 63
  germanium, 61, 65
  iodine, 61
ESR, *see* electron spin resonance
exchange interactions, in electron spin resonance, 709, 717
exploding wires, time-resolved spectra of, 108
extreme ultraviolet, *see* vacuum ultraviolet

Fermi resonance, substituent effects of, 515-516
field effects, 487
  of substituents, 505
flames, chemical excitation in, 157-160
  chemiluminescence in, 165-168
  deviations from equilibrium in, 149, 160-161
  equilibrium in, 144
  excitation in, 143-169
excitation mechanism in, 154
flames, chemical excitation—Cont.
  inelastic collisions in, 154-157
  ionization in, 154
  non-equilibrium excitation in, 160-161
  OH emission from, 151
  relatation times in, 150
  resonance fluorescence in, 161
  self-absorption in, 145
flame photometry, *see* flame spectroscopy
flame spectra, detection sensitivity (table), 189
  Doppler broadening in, 168-169
  table of, 175-177, 180
flame spectroscopy, with air-hydrogen flame, 174-176
  analytical curves, 193-196
  analytical process in, 192-193
  chemiluminescence in, 171-211
    mechanism of, 203-208
  detection sensitivity in, 182-184, 191-192
  excitation in, 143-169
  fuel-rich flame, 177
  hydrogen-oxygen-acetylene flames, 199-203
  interferences in, 195-196
  ionization in flames, 208-212
  with optical maser, 413
  oxidant mixtures, 197-199
  solvent effect, 195
flash heating, atomic absorption spectra with, 83-90
flash pyrolysis, 584
fluorene, 685
fluorescence, apparent vs. true, 607
  of atoms in flames, 161-165
  bandwidths in, 606-607
  intensity of, 605, 608
  reference compound in, 608
fluorescence spectra, 605-629
  excited by optical maser, 408-410
  intensity of, 618, 628
  of organic molecules, 631-645
  purity of exciting radiation, 611-612
  standard and corrected spectra, 614
fluoride band spectra, 601
fluoride, sensitive emission lines of, 225
fragmentation patterns, mass spectra and, 755-766
Franck-Condon principle, 594
free radicals, electron magnetic resonance and, 690
  electron spin resonance in, 719
  nuclear magnetic resonance and, 670
  radiation damage and, 721-722
  structure of, 721

free-radical spectra, 583
  nuclear magnetic resonance and, 665
frequency shifts, solvent pattern and, 572
  see also group frequency

gallium, liquid, mass spectroscopy of, 784-785
gas chromatography, infrared spectra and, 577
gaseous atoms, absorption spectra of, 83-90
gaseous free radicals, optical spectra of, 583-595
gases, refraction spectra of, 553
germanium, analytical curves in flame spectroscopy, 194
  energy levels, 61, 65
  flame spectroscopy detection sensitivity, 182
  flame spectrum, 177, 187
  reflection spectra in vacuum ultraviolet, 238
  wavelengths, infrared, 65
g-factor, resonance spectrum and, 725
g-value, 707
glasses, electron magnetic resonance spectra and, 693
gold, sensitivity of detection by atomic spectra, 135
gratings, diffraction, 549-550
group frequencies, infrared, 508-509
  infrared solvent shifts and molecular interactions, 569-575
  intensity correlations and, 514
  non-bonded interactions and, 487
  relations to Hammett σ and Taft σ^* values, 487
  substituent effects of organic molecules and, 507-509
group frequency shifts, 487
  CH_3X symmetric deformation frequencies and, 491-493
  Hammett σ and Taft σ^* relations, 497-498
  resonance and inductive effects, 494
  XH stretching frequencies and, 489-490
halides, diatomic molecular spectra of, 599
halogen anomaly, substituent effects and, 523-525
Hammett σ and Taft σ^* values, 497-498, 506
HCO, spectrum of, 588
helium, vacuum ultraviolet spectrum of, 248, 254
  wavelengths, infrared, 59
HFS, *see* hyperfine structure
high-resolution studies, 549-559
HNO, spectrum of, 589
homonuclear molecules, 598
homonuclear spectra, 600
hydride band spectrum, 600
hydrides, diatomic molecular spectra of, 598
hydrogen, infrared wavelengths of, 59
hyperconjugation, 672
hyperfine components, 665-666
hyperfine coupling tensors, 720-721
hyperfine spectral structure, 734-735
hyperfine structure, 707
  isotropic and anisotropic reactions and, 696

inductive effects, of substituents in infrared and electronic spectra, 505
infrared reflection spectroscopy, attenuated total reflection and, 437-460
  strongly absorbing substances, 460
  see also attenuated total reflection
infrared spectra, attenuated total reflection and, 445-460
  dispersion formula, 439
  dispersion studies and, 563
  gas-chromatography and, 577-580
  group frequencies of, 487-505
  Hammett σ and Taft σ^* values in, 537
  high-resolution studies and, 549-559
  integrated absorption coefficient, 440
  interaction mechanisms and, 572-575
  Kramers-Kronig relation and, 437, 444
  line intensities and widths in, 550-552
  oblique incidence in, 441
  origins of group frequency shifts in, 487-501
  pressure-induced shifts, 558-559
  reflection vs. absorption in, 442-446
  reflection spectra and, 438-445
  solvent shifts and molecular interations in, 569-575
  of steroids, 477-484
  substituent effects of organic molecules, 505-534
  transmission technique, 437-438
infrared spectroscopy, 461-485
  see also attenuated total reflection
inhomogeneity, of polarizing field,
insulators, mass spectroscopy of, 775
interferences, in determinations with flames, 196

iodide band spectra, 602
iodine, energy levels of, 61
ionization potentials, 488
ion-solvent interactions, 655
iron, flame spectroscopy detection sensitivity, 182
  flame spectrum of, 175, 186
isomers, rotational, 497, 499
isotopic analysis, by atomic absorption spectroscopy, 141
isotopic coupling values, 723
isotopic shifts, atomic spectra and, 73-81

Jahn-Teller theorem, 594

Kramer-Kronig relations, 437, 444, 456-458
krypton, wavelengths, infrared, 71

Larmor frequency, 651
laser, *see* optical maser
lead, analytical curves in flame spectroscopy, 194
  flame spectroscopy detection sensitivity, 182, 185
  flame spectrum, 175, 188
light sources, vacuum ultraviolet, 219
line profiles, by atomic absorption spectroscopy, 141
line width, in nuclear magnetic resonance, 651, 677
  refraction spectra and, 556
lipids, Raman spectra intensities and, 474
liquids, mass spectroscopy of, 780-784
lithium, sensitivity of detection by atomic absorption, 135
  wavelength, infrared, 59
luminescence, of organic molecules, 631-645
  see also phosphorescence

magnesium, sensitivity of detection by atomic spectra, 135
  wavelength, infrared, 59
magnesium fluoride, reflection spectra in vacuum ultraviolet, 236
magnetic dipolar interaction, 709
magnetic field, nuclear magnetic resonance and, 647-655
  unidirectional, 729
magnetic interactions, 648
magnetic resonance, nuclear, *see* nuclear magnetic resonance; *see also* electron magnetic resonance
magnetic susceptibility, 670
magnetogyric ratios, 653, 669
magneton, Bohr's, 732
maser, nuclear, 678
  optical, *see* optical maser
mass spectra, accuracy of mass measurements with, 749
  correlation with molecular structure, 743
  empirical correlations, 753
  fragmentation processes and, 754-766
  identification of parent ions in, 750
  meta-stable peaks and, 755-766
  nitrogen rule in, 744
  quasi-equilibrium theory and, 748
mass spectrometer, double-focusing, 752, 789
    design of, 770
    resolution with, 772
  sensitivity with spark source, 771
mass spectroscopy, 743-789
  of insulators, 775-778
  of liquids with spark source, 780-784
  of metals and semiconductors, 773-775
  of microsamples, 785-789
  of solids, 769-789
  with spark source, 769-789
  of surface contaminants, 778-780
m-dimethylaminonitrobenzene, spectra of, 613, 617
mercury, analytical curves in flame spectroscopy, 194
  flame spectroscopy detection sensitivity, 183
  flame spectrum of, 177, 187
  sensitivity of detection by atomic spectra, 135
  vacuum ultraviolet absorption spectrum, 234
  wavelength, infrared, 60
mesomeric effects, 505
meta-stable excited states, 681
meta-stable peaks, mass spectra and, 755-766
methanol, absorption spectrum in vacuum ultraviolet, 232
methyl iodide, Polo-Wilson equation for, 568
methyl laurate derivatives, 474
microcell technique, nuclear magnetic resonance, 659
microprobe, electron, *see* electron microprobe
microsamples, mass spectroscopy of, 785-789

molybdenum, flame spectroscopy detection sensitivity of, 183
  flame spectrum of, 184

naphthalene, electron magnetic resonance of, 682
  phosphorescence of, 639-644
  spectrum of, 681
  triplet states and, 685
NCO, spectrum of, 592
-N-C=S bands, 514-515
neon, vacuum ultraviolet spectrum of, 248, 256
NH_2, gaseous spectrum of, 586
nickel, flame spectroscopy detection sensitivity of, 183
  flame spectrum, 175, 186
nickel (II) aminotroponeimineates, 667, 674
nitride band spectra, 603
nitrides, diatomic molecular spectra of, 599-604
nitrogen, absorption spectrum in vacuum ultraviolet, 230
  analytical curves in flame spectroscopy, 194
  flame spectrum of, 176, 189
  sensitive emission lines of, 225
  vacuum ultraviolet spectrum of, 255
NMR, *see* nuclear magnetic resonance
N_2O^+ spectrum, 592
$NO_3^{\cdot}$ spectrum, 593
non-bonded reactions, group frequencies and, 487-488, 491-493, 495, 498, 502
$\underline{n} \rightarrow \pi^*$ transitions, substituent effects on, 528-534
nuclear magnetic resonance, 647-655
  applications to chemical problems, 657-663
  high-resolution, 657-665, 677
  interactions affecting, 647-648
  molecular conformation studies and, 661-662
  quantitative measurements in, 663
  sensitivity problem in, 659
  spin-density distributions in conjugate molecules, 665-674
  spin-generation modes, 677-680
nuclear maser, 678
nucleus-electron interactions, 673

optical constants, determination of, 453-455
optical maser, apparatus of,
  available types, 399-401
  crystal defects in, 432
  emission mode patterns in, 421-436
optical maser, apparatus of—Cont.
  emission spectra, 403-407
  for fluorescence excitation, 408-410
  formation of flames with, 413
  high-speed photography of, 421-436
  power output of, 401
  for Raman spectroscopy, 410-412
  as Raman source, 417-420
  scattering in crystals, 432
  spectroscopic applications of, 408-418
  spectroscopic studies with, 399-415
  temperature dependence of emission in, 403-407
organic compounds, mass spectra of, 743
organic free radicals, electron spin resonance in, 719
organic molecules, luminescence, fluorescence, and phosphorescence of, 631-645,
  radiation damage to, 721
  stable triplet ground state, 703
  substituent effects of, on infrared spectra, 509-538
oscillator strengths, *see* transition probabilities
Overhauser Effect, 653
oxides, diatomic molecular spectra of, 597-604

paramagnetic absorption spectroscopy, 729
paramagnetic resonance, 681-691
  investigation techniques, 691-694
paramagnetic spectroscopy, 681-694, 730
  aqueous solutions and, 735-736
  skin effect and, 736-737
Pauling electronegativities, 502
phenanthrene, electron magnetic resonance spectra of, 695
  phosphorescence of, 631-644
  triplet states and, 685
phosphorescence, electron magnetic resonance spectra and, 696
  of organic molecules, 631-635,
phosphorecence lifetimes, 605
phosphorus, analytical curves in flame spectroscopy, 195
  flame spectroscopy detection sensitivity, 183, 185
  flame spectrum, 182, 189
phosphorus compounds, X-ray spectra of, 313-314
phosphoryl frequencies, 501
photoconductive detectors, 549
photomultiplier detectors, 226-227
π-bonding, 650

π-electron radicals, 724
π-systems, 684
Planck function, 16
Planck's constant, 649
plutonium, X-ray absorption spectra, 330, 339
  X-ray spectrum, 325, 339
  emission, 331-333
polar group, inductive effect of, 501-502
polarizer, Raman, 463
polarizing field inhomogeneity, 679
polonium, X-ray emission spectra, 324
Polo-Wilson equation, 568
potassium, sensitivity of detection by atomic spectra, 135
  wavelength, infrared, 59
pulsed light source, 250-253
predissociation, 590-591
pressure-induced shifts, in infrared spectra, 558-560
proton stabilizer, 677
pyrolysis, flash, 584

quadrupole coupling, 655
quadrupole interactions, 651
quadrupole moment, 654, 725
quartz, X-ray spectrum of, 317
quinine sulfate, spectrum of, 610, 613, 615

radiation damage, to organic molecules, 719-721
radicals, *see* free radicals
radioactive elements, X-ray spectra of, 321-339
  experimental methods of, 334
radioactive materials, analysis of with electron microprobel, 383-388
radio-frequency paramagnetic spectroscopy, 730
Roman intensity scale, 464-469
Raman polarizers, 463
Raman source, optical maser as, 417-420
Raman spectra, band intensities in, 464, 469-477
  of lipids, 474-476
  optical maser stimulation of, 410-412
  refractive index effect, 466-467
  of solids, 468-469
  of steroids, 477-484
Raman spectrophotometry, semimicro, 462
  group frequency studies in, 461-485
redox potentials, of infrared spectra, 487
reflection, absorption and, in infrared spectra, 438-440
reflection accessory, in attenuated total reflection, 450-451
reflection spectra, 438
  oblique and normal incidence in, 441-444
  of solids in vacuum ultraviolet, 235-241
refraction spectra, 552-558
refractive index, variation of with wavelength, 563
refractometers, 552
relaxation mechanisms, 708, 718
Renner effect, 583
resonance, nuclear magnetic, *see* nuclear
  magnetic resonance
resonance effects, of organic molecules, 506
resonance field shifts, 666
rhenium, flame spectroscopy detection sensitivity, 183
  flame spectrum of, 177, 185
rhodium, flame spectrum of, 186
riboflavin, fluorescence spectra of, 622-624, 626
rubidium, sensitivity of detection by atomic spectra, 135
  wavelength, infrared, 59
Russell-Saunders Coupling System, 732

samarium, isotopic shifts in spectra of, 73-81
Schmelzer spin generator, 677
selenium, absorption spectrum in vacuum ultraviolet, 239
  flame spectrum of, 191
semiconductors, mass spectroscopy of, 773-774
silicon, analytical curves in flame spectroscopy, 196
  flame spectroscopy detection sensitivity, 183, 185
  flame spectrum, 177, 187
  reflection spectra in vacuum ultraviolet, 237
silicon carbide, X-ray spectrum of, 314
silicon compounds, X-ray spectra of, 315
silicon oxides, X-ray spectra of, 316
silver, sensitivity of detection by atomic spectra, 135
  wavelength, infrared, 59
singlet-triplet transitions, 681

skin depth, concept of, 736
skin effect, 736
sodium, sensitivity of detection by atomic spectra, 135
  wavelength, infrared, 59
solar spectra, atomic and molecular species in, 10-13
  composition analysis of, 24
  ionization in, 22
  line broadening in, 23
solids, mass spectroscopy of, 769-789
  Raman spectroscopy of, 468-469
solid sample, in attenuated total reflection, 448
spark discharges, afterglow of, 107
  ionization in, 107, 108
  order of appearance of lines in, 105
  relaxation times, 106
  temperature of, 105, 108
  time-resolved spectra of, 105
  vapor jets in, 109
spark sources, for vacuum ultraviolet, 219
spectra, atomic, *see* atomic spectra
  mass, *see* mass spectra, etc.
  X-ray, *see* X-ray spectra, etc.
spectrographs, for vacuum ultraviolet, 226-227, 241
spectrometer, double-beam, 450
  double-focusing, 750, 770, 789
  X-ray, 330, 338
spectrometer-refractometer, 553
spectrophotometer, 610
spectroscopy, atomic absorption, *see* atomic
    absorption spectroscopy
  flame, *see* flame spectroscopy
  low-field vs. high-field, 730-734
  mass, see mass spectroscopy
  teaching of, 791-796
spin-density, negative, 669
spin-density distributions, 671-673
  nuclear magnetic resonance and, 665-674
spin generator, Schmelzer, 677
spin-lattice relaxation, 651-652, 654
spin-orbit coupling, 681, 709, 731
spin-orbit reaction, 718
spin-spin coupling, 650
  constants for, 666
spin-spin decoupling, 659-660
spin-spin reactions, 688, 732
spin-spin relaxation, 651, 709
spin-splitting constant, 592
stellar envelopes, 7-9
stellar spectra, atomic and molecular species in, 10-13
  composition analysis in, 24
stellar spectra, atomic—Cont.
  ionization in, 22
  line broadening in, 23
  non-equilibrium condition in, 17
  specific physical conditions of excitation, 14
steroids, Raman and infrared spectra of, 477-484
stretching vibrations, 500-501
strontium, sensitivity of detection by atomic spectra, 135
substituent constants, 513
substituent effects, benzenoid derivatives and, 517-523
  empirical correlations of, 516-517
  Fermi resonance and, 515-516
  on $n \rightarrow \pi^*$ transitions, 528-534
sulfide band spectra, 603
sulfides, diatomic molecular spectra, 599-604
sulfur, analytical curves in flame spectroscopy, 196
  flame spectroscopy detection sensitivity, 183, 185
  flame spectrum of, 180, 190
  X-ray spectrum of, 309-312
surface contamination, mass spectroscopy of, 778-780

Taft σ^* values, 487-488, 497-498, 502, 511, 532
teaching, of spectroscopy, 791-796
technicians, training of, 793
tellurium, flame spectroscopy detection sensitivity of, 183
  flame spectrum of, 176, 191
1,2,4,5-tetranethylbenzene, phosphorescence of, 631-644
tetramethyl germanium, 678
thallium, resonance of, 649
  wavelength, infrared, 60
thin films, analysis of with electron microprobe, 391-397
time-resolved spectra, in absorption, 111
  applications in analysis, 112-115
  of exploding wires, 108
  improvement in sensitivity of detection, 116
  limits on resolution, 101, 118
  methods of, 91-101
  performance of, 101
  of sparks, 105
  studies with, 105
  of vacuum sparks, 108
tin, analytical curves in flame spectroscopy, 194
  flame spectroscopy detection sensitivity, 184

tin—Cont.
  flame spectrum of, 175, 177, 187
training, in spectrometry, 792-794
transition metals, 667
transition probabilities, 140
  availability of, 38-43
  calculation of, 46, 52-53
  conversion factors, 44
  measurement by anomalous dispersion, 51
    from arc spectra, 46, 54
    from furnace absorption spectra, 49
    from lifetimes, 50
  present status, 37
triplet-state molecules, paramagnetic resonance spectra and, 691-694
triplet states, 681, 683-691
tungsten, atomic absorption spectra of, 83-90

uranium, X-ray absorption spectrum of, 336
Urey-Bradley Force Field, 491, 495

vacuum-spark mass spectroscopy, 769-789
vacuum sparks, in time-resolved spectra, 108
vacuum-ultraviolet spectrographs, 241-243
vacuum ultraviolet spectroscopy, 217-243
  absorption spectra of condensed gases, 233
    of gases, 230-233
    of solids, 235-241
  analytical applications of, 223-224
  of argon, 257
  detectors for, 222-223, 247
  elimination of overlapping orders, 220-222
  of helium, 248, 258
  light sources in, 219, 220, 247-260
  of neon, 248, 256
  of nitrogen, 255
  photoelectric detectors in, 222-223
  reflection spectra of solids in, 235-241
  sensitive emission lines (table), 225
  spectrographs in, 226-229
  window materials in, 222
vanadium, analytical curves in flame spectroscopy, 196
  flame spectroscopy detection sensitivity, 184, 185

vanadium—Cont.
  flame spectrum of, 177, 181
vibration-rotation interactions, 551
vinyl and vinylidene CH_2 wagging mode, 493-498
vinyl esters, group frequency shifts in, 496

wavelengths, infrared, 59-60
  argon, 66, 69
  germanium, 65
  krypton, 71
wavelength standards, infrared, 65
Wursters blue, electron spin resonance spectrum of, 714

X-ray absorption spectra, 271-275, 330
  plutonium, 330, 339
  uranium, 336
X-ray emission spectrography, light element and long wavelength, 341-356
X-ray microprobe, 282
  interelement effects, 293
  see also electron microprobe
X-ray spectra, absorption, *see* X-ray absorption spectra
  effect of on chemical bond, 307-318
  emission of polonium, 324
  emission theory, 264
  excitation, 276-278
    with radioactive sources, 279-282
  interelement effects, 291-293
    correction of, 297-308
  of phosphorus compounds, 313-314
  of plutonium, 325, 331-333, 339
  of quartz, 317
  of radioactive elements, 321-339
    experimental methods of, 322, 323, 334
  of silicon carbide, 314-315
  of silicon compounds, 315
  of silicon oxides, 316
  sulfur, effect of on chemical bond, 309-312
  theory of, 299
X-rays, atmospheric absorption of at long wavelengths, 343
  detectors for long wavelengths, 345, 355-356
  diffraction crystals for long wavelengths, 346
  light elements, direct excitation of, 354
    indirect methods, 351
  long wavelength detectors, 345, 355-356
    interelement effects, 351-353
    tube targets, 347-350

X-ray—Cont.
  microprobe, *see* electron microprobe
  window materials at long wavelengths, 343
X-ray spectrometers, 265-271, 326, 334
  crystal, 267
  detectors for, 267
  with electronic discrimination, 267, 282

X-ray—Cont.

zero-field absorption, 735
zinc, flame spectroscopy detection sensitivity, 184
  flame spectrum of, 186
  sensitivity of detection by atomic spectra, 135
  wavelength, infrared, 60
zinc sulfide, X-ray spectrum of, 312